frontiers | Research Topics

Tumor microenvironment and cancer therapy, 2nd Edition

Edited by
Shaoquan Zheng, Pranav Gupta and Zhe-Sheng Chen

Published in
Frontiers in Oncology
Frontiers in Cell and Developmental Biology

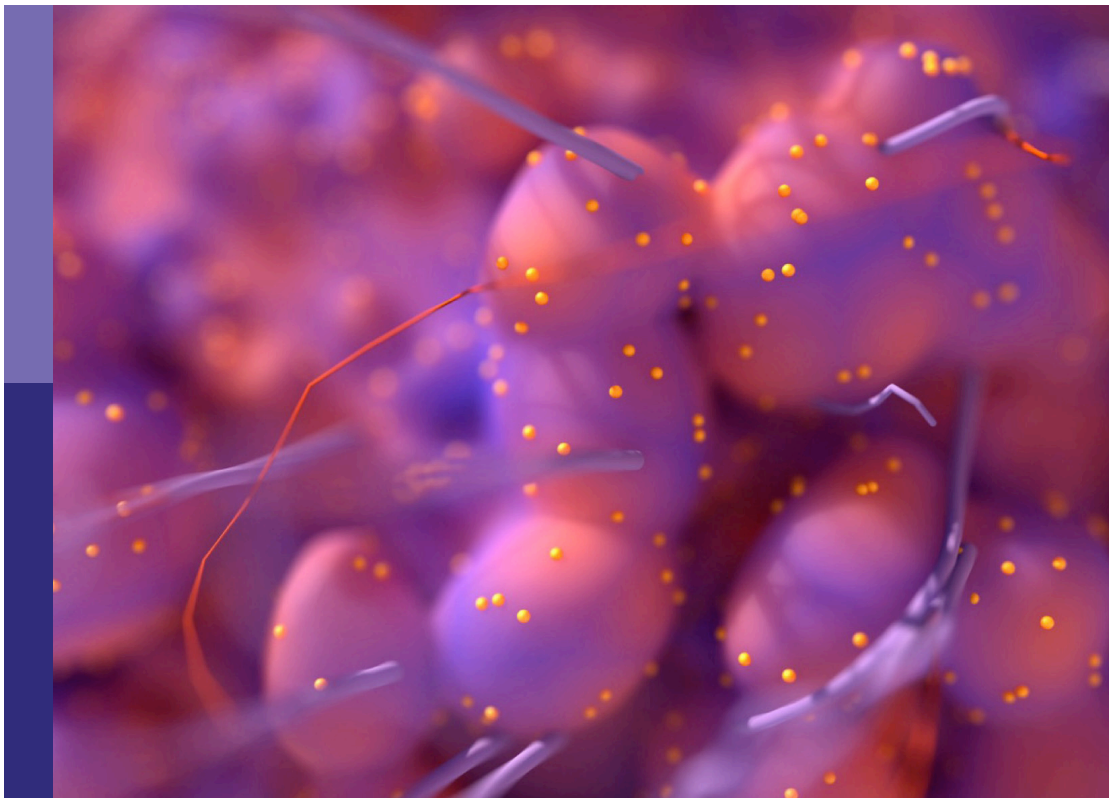

FRONTIERS EBOOK COPYRIGHT STATEMENT

The copyright in the text of individual articles in this ebook is the property of their respective authors or their respective institutions or funders. The copyright in graphics and images within each article may be subject to copyright of other parties. In both cases this is subject to a license granted to Frontiers.

The compilation of articles constituting this ebook is the property of Frontiers.

Each article within this ebook, and the ebook itself, are published under the most recent version of the Creative Commons CC-BY licence. The version current at the date of publication of this ebook is CC-BY 4.0. If the CC-BY licence is updated, the licence granted by Frontiers is automatically updated to the new version.

When exercising any right under the CC-BY licence, Frontiers must be attributed as the original publisher of the article or ebook, as applicable.

Authors have the responsibility of ensuring that any graphics or other materials which are the property of others may be included in the CC-BY licence, but this should be checked before relying on the CC-BY licence to reproduce those materials. Any copyright notices relating to those materials must be complied with.

Copyright and source acknowledgement notices may not be removed and must be displayed in any copy, derivative work or partial copy which includes the elements in question.

All copyright, and all rights therein, are protected by national and international copyright laws. The above represents a summary only. For further information please read Frontiers' Conditions for Website Use and Copyright Statement, and the applicable CC-BY licence.

ISSN 1664-8714
ISBN 978-2-8325-3655-1
DOI 10.3389/978-2-8325-3655-1

About Frontiers

Frontiers is more than just an open access publisher of scholarly articles: it is a pioneering approach to the world of academia, radically improving the way scholarly research is managed. The grand vision of Frontiers is a world where all people have an equal opportunity to seek, share and generate knowledge. Frontiers provides immediate and permanent online open access to all its publications, but this alone is not enough to realize our grand goals.

Frontiers journal series

The Frontiers journal series is a multi-tier and interdisciplinary set of open-access, online journals, promising a paradigm shift from the current review, selection and dissemination processes in academic publishing. All Frontiers journals are driven by researchers for researchers; therefore, they constitute a service to the scholarly community. At the same time, the *Frontiers journal series* operates on a revolutionary invention, the tiered publishing system, initially addressing specific communities of scholars, and gradually climbing up to broader public understanding, thus serving the interests of the lay society, too.

Dedication to quality

Each Frontiers article is a landmark of the highest quality, thanks to genuinely collaborative interactions between authors and review editors, who include some of the world's best academicians. Research must be certified by peers before entering a stream of knowledge that may eventually reach the public - and shape society; therefore, Frontiers only applies the most rigorous and unbiased reviews. Frontiers revolutionizes research publishing by freely delivering the most outstanding research, evaluated with no bias from both the academic and social point of view. By applying the most advanced information technologies, Frontiers is catapulting scholarly publishing into a new generation.

What are Frontiers Research Topics?

Frontiers Research Topics are very popular trademarks of the *Frontiers journals series*: they are collections of at least ten articles, all centered on a particular subject. With their unique mix of varied contributions from Original Research to Review Articles, Frontiers Research Topics unify the most influential researchers, the latest key findings and historical advances in a hot research area.

Find out more on how to host your own Frontiers Research Topic or contribute to one as an author by contacting the Frontiers editorial office: frontiersin.org/about/contact

Tumor microenvironment and cancer therapy, 2nd Edition

Topic editors

Shaoquan Zheng — The First Affiliated Hospital of Sun Yat-sen University, China
Pranav Gupta — Albert Einstein College of Medicine, United States
Zhe-Sheng Chen — St. John's University, United States

Citation

Zheng, S., Gupta, P., Chen, Z.-S., eds. (2023). *Tumor microenvironment and cancer therapy, 2nd Edition*. Lausanne: Frontiers Media SA.
doi: 10.3389/978-2-8325-3655-1

Publisher's note: In this 2nd edition, the following article has been updated: Xie Y, Xie J, Gupta P, Chen Z-S and Zheng S (2023) Editorial: Tumor microenvironment and cancer therapy. Front. Cell Dev. Biol. 11:1290456. doi: 10.3389/fcell.2023.1290456

Table of contents

07 Editorial: Tumor microenvironment and cancer therapy
Yi Xie, Jindong Xie, Pranav Gupta, Zhe-Sheng Chen and Shaoquan Zheng

09 Identification of Key Pathways and Genes Related to Immunotherapy Resistance of LUAD Based on WGCNA Analysis
Weina Yu, Fengsen Liu, Qingyang Lei, Peng Wu, Li Yang and Yi Zhang

23 Links Between N^6-Methyladenosine and Tumor Microenvironments in Colorectal Cancer
Yundi Zhang, Ke Zhang, Haoming Gong, Qin Li, Lajie Man, Qingchang Jin, Lin Zhang and Song Li

37 HSPA6 is Correlated With the Malignant Progression and Immune Microenvironment of Gliomas
Xiang Zhou, Qiankun Ji, Qin Li, Peng Wang, Guowen Hu, Feng Xiao, Minhua Ye, Li Lin, Min Luo, Yun Guo, Weijun Wu, Kai Huang and Hua Guo

51 Nasopharyngeal Carcinoma and Its Microenvironment: Past, Current, and Future Perspectives
Zhi Yi Su, Pui Yan Siak, Chee-Onn Leong and Shiau-Chuen Cheah

71 Bioinformatics Analysis Combined With Experiments Predicts PUDP as a Potential Prognostic Biomarker for Hepatocellular Carcinoma Through Its Interaction With Tumor Microenvironment
Jiahao Yu, Weirui Zhang, Dawei Ding, Yinan Hu, Guanya Guo, Jingbo Wang and Ying Han

87 Identify the Prognostic and Immune Profile of VSIR in the Tumor Microenvironment: A Pan-Cancer Analysis
Yuanyuan Liu, Jingwei Zhang, Zeyu Wang, Xun Zhang, Ziyu Dai, Wantao Wu, Nan Zhang, Zaoqu Liu, Jian Zhang, Peng Luo, Zhipeng Wen, Jing Yu, Hao Zhang, Tubao Yang and Quan Cheng

104 Integrative Analysis Constructs an Extracellular Matrix-Associated Gene Signature for the Prediction of Survival and Tumor Immunity in Lung Adenocarcinoma
Lingyan Xiao, Qian Li, Yongbiao Huang, Zhijie Fan, Wan Qin, Bo Liu and Xianglin Yuan

119 Integrative Dissection of Novel Lactate Metabolism-Related Signature in the Tumor Immune Microenvironment and Prognostic Prediction in Breast Cancer
Lu Yang, Peixin Tan, Hengwen Sun, Zijun Zeng and Yi Pan

134 OAS3 is a Co-Immune Biomarker Associated With Tumour Microenvironment, Disease Staging, Prognosis, and Treatment Response in Multiple Cancer Types
Xin-yu Li, Lei Hou, Lu-yu Zhang, Liming Zhang, Deming Wang, Zhenfeng Wang, Ming-Zhe Wen and Xi-tao Yang

149 Low CRIM1 Levels Predict Poor Prognosis in Breast Cancer Patients
Wei Wen, Baohong Jiang, Xi Cao, Liming Xie, Xiaoli Zhang, Yuehua Li and Rongfang He

160 Development and Validation of a Risk Prediction Model for Breast Cancer Prognosis Based on Depression-Related Genes
Xuan Wang, Neng Wang, Linda L. D. Zhong, Kexin Su, Shengqi Wang, Yifeng Zheng, Bowen Yang, Juping Zhang, Bo Pan, Wei Yang and Zhiyu Wang

173 Identification of LSM Family Members as Novel Unfavorable Biomarkers in Hepatocellular Carcinoma
Hongkai Zhuang, Bo Chen, Chenwei Tang, Xinming Chen, Wenliang Tan, Lei Yang, Zhiqin Xie, Xiaowu Ma, Qingbin Wang, Chuanzhao Zhang, Changzhen Shang and Yajin Chen

185 The Role of miRNAs in the Resistance of Anthracyclines in Breast Cancer: A Systematic Review
Zihan Si, Yan Zhong, Sixian Lao, Yufeng Wu, Guoping Zhong and Weiwei Zeng

195 Characterization of the Estrogen Response Helps to Predict Prognosis and Identify Potential Therapeutic Targets in Cholangiocarcinoma
Chenglin Lu, Ji Miao, Minhuan Li, Qisi Zheng, Feng Xu, Yiming Pan, Yizhou Wang, Zhi Yang, Xuefeng Xia, Hao Zhu, Jie Chen and Shanhua Bao

211 Necroptosis-Related LncRNAs Signature and Subtypes for Predicting Prognosis and Revealing the Immune Microenvironment in Breast Cancer
Yuhao Xu, Qinghui Zheng, Tao Zhou, Buyun Ye, Qiuran Xu and Xuli Meng

224 Comprehensive Analyses of MELK-Associated ceRNA Networks Reveal a Potential Biomarker for Predicting Poor Prognosis and Immunotherapy Efficacy in Hepatocellular Carcinoma
Yu Liu, Rongkuan Li, Xiaobo Wang, Zuguang Xue, Xiaozhou Yang and Bo Tang

238 Analysis of Omics Data Reveals Nucleotide Excision Repair-Related Genes Signature in Highly-Grade Serous Ovarian Cancer to Predict Prognosis
Danian Dai, Qiang Li, Pengfei Zhou, Jianjiang Huang, Hongkai Zhuang, Hongmei Wu and Bo Chen

253 Tumor Microenvironment Characterization in Breast Cancer and an Immune Cell Infiltration Score Development, Validation, and Application
Lang Li

267 Glia Maturation Factor β as a Novel Independent Prognostic Biomarker and Potential Therapeutic Target of Kidney Renal Clear Cell Carcinoma
Tong Zhu, Tianyu Wang, Zijun Feng, Furong Gao, Jieping Zhang, Caixia Jin, Haibin Tian, Jingying Xu, Hao Chen, Qingjian Ou, Juan Wang, Guotong Xu and Lixia Lu

287 Immune Characteristics and Prognosis Analysis of the Proteasome 20S Subunit Beta 9 in Lower-Grade Gliomas
Junzhe Liu, Xinyu Yang, Qiankun Ji, Lufei Yang, Jingying Li, Xiaoyan Long, Minhua Ye, Kai Huang and Xingen Zhu

302 Effect of Pyroptosis-Related Genes on the Prognosis of Breast Cancer
Ying Zhou, Jianfeng Zheng, Mengru Bai, Yuzhen Gao and Nengming Lin

316 Comprehensive analysis of the endoplasmic reticulum stress-related long non-coding RNA in bladder cancer
Zhenyu Wu, Yue Wang, Mengxin Yan, Quan Liang, Bin Li, Guoliang Hou, Taolin Xia, Zhe Lin and Wenfeng Xu

328 Advances in the study of HSP70 inhibitors to enhance the sensitivity of tumor cells to radiotherapy
Sihan Du, Ying Liu, Yuan Yuan, Yuran Wang, Yanfang Chen, Shuai Wang and Yuhua Chi

344 Matricellular protein tenascin C: Implications in glioma progression, gliomagenesis, and treatment
Zaixiang Fu, Ganggui Zhu, Chao Luo, Zihang Chen, Zhangqi Dou, Yike Chen, Chen Zhong, Sheng Su and Fuyi Liu

361 HMOX1 promotes lung adenocarcinoma metastasis by affecting macrophages and mitochondrion complexes
Bo Chen, Liyang Zhang, Hongshu Zhou, Wenrui Ye, Cong Luo, Liting Yang, Ning Fang and Anliu Tang

380 Roles of tumor-associated neutrophils in tumor metastasis and its clinical applications
Man Yan, Minying Zheng, Rui Niu, Xiaohui Yang, Shifeng Tian, Linlin Fan, Yuwei Li and Shiwu Zhang

396 Circ0038632 modulates MiR-186/DNMT3A axis to promote proliferation and metastasis in osteosarcoma
Xinyu Tan, Canjun Zeng, Haomiao Li, Yeru Tan and Hongbo Zhu

404 Radiation-induced FAP + fibroblasts are involved in keloid recurrence after radiotherapy
Yan Gao, Xue Hou, Yuyin Dai, Ting Yang and Kexin Chen

415 Dissecting a hypoxia-related angiogenic gene signature for predicting prognosis and immune status in hepatocellular carcinoma
Guixiong Zhang, Yitai Xiao, Xiaokai Zhang, Wenzhe Fan, Yue Zhao, Yanqin Wu, Hongyu Wang and Jiaping Li

428 Quantification of ferroptosis pathway status revealed heterogeneity in breast cancer patients with distinct immune microenvironment
Yuying Li, Tianfu Li, Duanyang Zhai, Chuanbo Xie, Xiaying Kuang, Ying Lin and Nan Shao

441 The immune escape signature predicts the prognosis and immunotherapy sensitivity for pancreatic ductal adenocarcinoma
Hao Lu, Li-Yan Zheng, Ling-Yan Wu, Jun Chen, Na Xu and Sui-Cai Mi

453 Neddylation pattern indicates tumor microenvironment characterization and predicts prognosis in lung adenocarcinoma
Yuan Cui, Zhike Chen, Bin Pan, Tong Chen, Hao Ding, Qifan Li, Li Wan, Gaomeng Luo, Lang Sun, Cheng Ding, Jian Yang, Xin Tong and Jun Zhao

470 Establishment of lactate-metabolism-related signature to predict prognosis and immunotherapy response in patients with colon adenocarcinoma
Zhengrong Zou, Yongjie Chai, Qi Li, Xuan Lin, Qingfang He and Qiusheng Xiong

483 A pro-oxidant combination of resveratrol and copper down-regulates hallmarks of cancer and immune checkpoints in patients with advanced oral cancer: Results of an exploratory study (RESCU 004)
Aishwarya Pilankar, Hitesh Singhavi, Gorantla V. Raghuram, Sophiya Siddiqui, Naveen Kumar Khare, Vishalkumar Jadhav, Harshali Tandel, Kavita Pal, Atanu Bhattacharjee, Pankaj Chaturvedi and Indraneel Mittra

492 Role of hypoxia in the tumor microenvironment and targeted therapy
Gaoqi Chen, Kaiwen Wu, Hao Li, Demeng Xia and Tianlin He

505 Heparin binding epidermal growth factor–like growth factor is a prognostic marker correlated with levels of macrophages infiltrated in lung adenocarcinoma
Nguyen Van Hiep, Wei-Lun Sun, Po-Hao Feng, Cheng-Wei Lin, Kuan-Yuan Chen, Ching-Shan Luo, Le Ngoc Dung, Hoang Van Quyet, Sheng-Ming Wu and Kang-Yun Lee

520 A pyroptosis-related gene signature for prognostic and immunological evaluation in breast cancer
Yue Zhong, Fu Peng, Xiaoru Luo, Xuan Wang, Bowen Yang, Xinglinzi Tang, Zheng Xu, Linlin Ren, Zhiyu Wang, Cheng Peng and Neng Wang

frontiers | Frontiers in Cell and Developmental Biology

TYPE Editorial
PUBLISHED 22 September 2023
DOI 10.3389/fcell.2023.1290456

Check for updates

OPEN ACCESS

EDITED AND REVIEWED BY
Shyamala Maheswaran,
Massachusetts General Hospital and Harvard Medical School, United States

*CORRESPONDENCE
Shaoquan Zheng,
zhengshq3@mail2.sysu.edu.cn

RECEIVED 07 September 2023
ACCEPTED 08 September 2023
PUBLISHED 22 September 2023

CITATION
Xie Y, Xie J, Gupta P, Chen Z-S and Zheng S (2023), Editorial: Tumor microenvironment and cancer therapy. *Front. Cell Dev. Biol.* 11:1290456. doi: 10.3389/fcell.2023.1290456

COPYRIGHT
© 2023 Xie, Xie, Gupta, Chen and Zheng. This is an open-access article distributed under the terms of the Creative Commons Attribution License (CC BY). The use, distribution or reproduction in other forums is permitted, provided the original author(s) and the copyright owner(s) are credited and that the original publication in this journal is cited, in accordance with accepted academic practice. No use, distribution or reproduction is permitted which does not comply with these terms.

Editorial: Tumor microenvironment and cancer therapy

Yi Xie[1], Jindong Xie[1], Pranav Gupta[2], Zhe-Sheng Chen[2] and Shaoquan Zheng[3]*

[1]State Key Laboratory of Oncology in South China, Sun Yat-sen University Cancer Center, Guangzhou, China, [2]Department of Pharmaceutical Sciences, College of Pharmacy and Health Sciences, St. John's University, New York, NY, United States, [3]Department of Breast Surgery, Breast Disease Center, The First Affiliated Hospital, Sun Yat-sen University, Guangzhou, China

KEYWORDS

tumor microenvironment, cancer therapy, oncology, immune, bioinformatics

Editorial on the Research Topic
Tumor microenvironment and cancer therapy

The tumor microenvironment (TME), an integral part of tumor, is comprised of all the non-cancerous host cells in the tumor, including fibroblasts, endothelial cells, neurons, adipocytes, adaptive, and innate immune cells. It also consists of non-cellular components, including the extracellular matrix (ECM) and soluble products such as chemokines, cytokines, growth factors, and extracellular vesicles (Bejarano et al., 2021). Accumulating evidence indicates that cellular and acellular constituents in TME play a pivotal role in reprogramming tumor initiation, growth, invasion, metastasis and response to therapies (Park et al., 2023; Zhang et al., 2023). Although considerable progress has been made in TME-targeted cancer therapy, such as immune checkpoint blockade (ICB), chimeric antigen receptor (CAR) T-cell therapy and oncolytic virus therapy, the clinical efficacy of therapeutic strategies targeting TME, especially the specific cells or pathways of TME, remains unsatisfactory. It is imperative to identify new targets and biomarkers that could improve the clinical efficacy and precision in specific patients. The current Research Topic, "*Tumor microenvironment and cancer therapy*", brings together researchers at the forefront of the much-anticipated field with a series of authoritative reviews and exciting original articles to provide a timely update on our current understanding of biology of the TME and therapies to target it.

Anticancer drug resistance presents a substantial barrier to cancer treatment (Sun et al., 2022). Although many approaches have been employed to study drug resistance, its mechanisms still remain poorly understood. Si et al. provided an overview that microRNAs, a large family of post-transcriptional regulators of gene expression, play a significant role in regulating the resistance of anthracyclines in breast cancer therapy and demonstrate the potential as prognostic biomarkers. TME has emerged as a critical factor in both drug efficacy and chemoresistance in recent years, impelling the development of novel therapeutic strategies. Chen et al. submitted a comprehensive review on the roles of hypoxia in the tumor microenvironment and targeted therapy. They observed immunosuppression and metabolic reprogramming in TME under the condition of hypoxia. Immunosuppressive cells such as MDSCs, TAM and Tregs were recruited to the hypoxic parts to facilitate the escape of tumor cells and resistance to anticancer drug. The metabolic reprogramming of

tumor cells was conducive to obtaining energy in a hypoxic environment while maintaining an acidic microenvironment. Apart from chemotherapy resistance, immunotherapy resistance also attracts much attention. Yu et al. identified nine hub genes (*COL1A1, COL1A2, COL3A1, COL5A1, COL5A2, COL6A3, EMILIN1, MMP2,* and *THY1*) as potential predictors for implying cancer stemness and immunotherapy resistance to lung adenocarcinoma (LUAD) by Weighted Gene Co-Expression Networks Analysis (WGCNA) and protein-protein interaction (PPI) network analysis and found that *THY1* might serve as a prognostic marker.

Although immune checkpoint blockade has brought new hope for many cancers, it has not yet provided substantial benefit to patients with glioma. Utilizing a range of analyses involving protein networks, survival, clinical correlation and function, Zhou et al. demonstrated that the levels of specific ligands (PDL1/PDL2 and CD80/CD86) were significantly higher in the subgroup of glioma patients with high expression levels of *HSAP6*, which might provide new insights into immunotherapy for glioma patients with a deeper understanding of the correlation between *HSPA6* and immunity. Additionally, the ECM is a dynamic and complex meshwork consisting of various multi-domain macromolecules that are continually synthesized and secreted by surrounding cells. On this subject, Fu et al. emphasized that Tenascin C (TNC), a non-structural protein in the ECM, was implicated in the malignant progression of glioma, including proliferation, neovascularization, invasiveness, and immunomodulation. Thorough research on TNC, particularly on the different domains and critical targets of the signaling pathway, may provide new therapeutic strategies for glioma treatment.

Metastasis, a primary cause of death in patients with malignancies and a challenge for cancer therapy, is promoted by intrinsic changes in both tumor and non-malignant cells in the TME. Yan et al. focused their study on the roles of tumor-associated neutrophils (TANs) in tumor metastasis, which can be a potential target of cancer treatment. In another study, Tan et al. analyzed the role of *circPLK1* in cancer cell proliferation and metastasis. They demonstrated that *circPLK1* could sponge miR-186, which upregulated the downstream *DNMT3A* expression and triggered the DNA hypermethylation of *APCDD1* promoter, leading to *APCDD1* downregulation and promoting the cell invasion and metastasis in osteosarcoma.

Prognostic biomarkers for various types of cancer were also investigated based on the signature of TME. Li et al. identified *OAS3* as a prognostic and immunotherapeutic biomarker that was associated with unfavorable survival outcomes. Yu et al. investigated the role of *PUDP* in hepatocellular carcinoma (HCC) and showed that *PUDP* was highly expressed in most cancers and high expression of *PUDP* indicated a poor prognosis and lower response rates to immunotherapy in HCC.

Fibroblasts play an essential role in TME. Gao et al. discovered the underlying mechanism of keloid scars (KS) recurrence. The authors focused on FAP + fibroblasts, which are crucial for KS recurrence after surgical resection and radiation therapy. Their findings revealed that irradiation promoted cell cycle progression in FAP + fibroblasts due to the ATP production, upregulation of Cyclin D1 and downregulation of the CKIs p53, p21, and p16, which was associated with cell proliferation and delayed cellular senescence.

In conclusion, TME is a complicated and highly heterogeneous circumstance that can affect almost every aspect of cancer biology. It brings therapeutic targets for cancer treatment, which still needs further discussion and validation. In addition, TME is the inevitable part of tumor bulk and understanding the complexity of it lays a solid foundation for the development of more effective biomarkers and therapies for cancer. We hope that the findings in this Research Topic can inspire further innovations and look forward to an exciting future in this field.

Author contributions

YX: Methodology, Validation, Writing–original draft. JX: Writing–original draft. PG: Conceptualization, Supervision, Writing–review and editing. Z-SC: Supervision, Writing–review and editing. SZ: Conceptualization, Supervision, Writing–review and editing.

Acknowledgments

We would like to thank all authors and reviewers for their contributions to this Research Topic. Their efforts help us to communicate current knowledge under this Research Topic to a worldwide audience.

Conflict of interest

The authors declare that the research was conducted in the absence of any commercial or financial relationships that could be construed as a potential conflict of interest.

Publisher's note

All claims expressed in this article are solely those of the authors and do not necessarily represent those of their affiliated organizations, or those of the publisher, the editors and the reviewers. Any product that may be evaluated in this article, or claim that may be made by its manufacturer, is not guaranteed or endorsed by the publisher.

References

Bejarano, L., Jordão, M. J. C., and Joyce, J. A. (2021). Therapeutic targeting of the tumor microenvironment. *Cancer Discov.* 11, 933–959. doi:10.1158/2159-8290.CD-20-1808

Park, J., Hsueh, P-C., Li, Z., and Ho, P-C. (2023). Microenvironment-driven metabolic adaptations guiding CD8+ T cell anti-tumor immunity. *Immunity* 56, 32–42. doi:10.1016/j.immuni.2022.12.008

Sun, L., Gao, L., Zhao, Y., Wang, Y., Xu, Q., Zheng, Y., et al. (2022). Understanding and targeting the epigenetic regulation to overcome EGFR-TKIs resistance in human cancer. *Recent Pat. Anticancer Drug Discov.* 18, 506–516. doi:10.2174/1574892818666221201145810

Zhang, C., Zhang, C., and Wang, H. (2023). Immune-checkpoint inhibitor resistance in cancer treatment: current progress and future directions. *Cancer Lett.* 562, 216182. doi:10.1016/j.canlet.2023.216182

frontiers in Oncology

ORIGINAL RESEARCH
published: 06 January 2022
doi: 10.3389/fonc.2021.814014

Identification of Key Pathways and Genes Related to Immunotherapy Resistance of LUAD Based on WGCNA Analysis

Weina Yu[1,2,3†], *Fengsen Liu*[1,2,3†], *Qingyang Lei*[1,2,3], *Peng Wu*[1,2,3], *Li Yang*[1,2,3*] *and Yi Zhang*[1,2,3,4*]

[1] Biotherapy Center and Cancer Center, The First Affiliated Hospital of Zhengzhou University, Zhengzhou, China, [2] Henan Key Laboratory for Tumor Immunology and Biotherapy, Zhengzhou University, Zhengzhou, China, [3] State Key Laboratory of Esophageal Cancer Prevention and Treatment, Zhengzhou University, Zhengzhou, China, [4] School of Life Sciences, Zhengzhou University, Zhengzhou, China

OPEN ACCESS

Edited by:
Zhe-Sheng Chen,
St. John's University, United States

Reviewed by:
Lihua Liu,
Fourth Hospital of Hebei Medical University, China
Jingting Jiang,
First People's Hospital of Changzhou, China

***Correspondence:**
Yi Zhang
yizhang@zzu.edu.cn
Li Yang
fccyangl1@zzu.edu.cn

[†]These authors have contributed equally to this work

Specialty section:
This article was submitted to Molecular and Cellular Oncology, a section of the journal Frontiers in Oncology

Received: 12 November 2021
Accepted: 06 December 2021
Published: 06 January 2022

Citation:
Yu W, Liu F, Lei Q, Wu P, Yang L and Zhang Y (2022) Identification of Key Pathways and Genes Related to Immunotherapy Resistance of LUAD Based on WGCNA Analysis. Front. Oncol. 11:814014. doi: 10.3389/fonc.2021.814014

Immunotherapy resistance is a major barrier in the application of immune checkpoint inhibitors (ICI) in lung adenocarcinoma (LUAD) patients. Although recent studies have found several mechanisms and potential genes responsible for immunotherapy resistance, ways to solve this problem are still lacking. Tumor immune dysfunction and exclusion (TIDE) algorithm is a newly developed method to calculate potential regulators and indicators of ICI resistance. In this article, we combined TIDE and weighted gene co-expression network analysis (WGCNA) to screen potential modules and hub genes that are highly associated with immunotherapy resistance using the Cancer Genome Atlas (TCGA) dataset of LUAD patients. We identified 45 gene co-expression modules, and the pink module was most correlated with TIDE score and other immunosuppressive features. After considering the potential factors in immunotherapy resistance, we found that the pink module was also highly related to cancer stemness. Further analysis showed enriched immunosuppressive cells in the extracellular matrix (ECM), immunotherapy resistance indicators, and common cancer-related signaling pathways in the pink module. Seven hub genes in the pink module were shown to be significantly upregulated in tumor tissues compared with normal lung tissue, and were related to poor survival of LUAD patients. Among them, THY1 was the gene most associated with TIDE score, a gene highly related to suppressive immune states, and was shown to be strongly expressed in late-stage patients. Immunohistochemistry (IHC) results demonstrated that THY1 level was higher in the progressive disease (PD) group of LUAD patients receiving a PD-1 monoclonal antibody (mAb) and positively correlated with SOX9. Collectively, we identified that THY1 could be a critical biomarker in predicting ICI efficiency and a potential target for avoiding tumor immunotherapy resistance.

Keywords: LUAD, WGCNA, TIDE, immunotherapy resistance, cancer stem cell

INTRODUCTION

Chemotherapy, radiotherapy, and surgery have dominated the cancer treatment field for years and did acquire considerable effects. However, these traditional therapies have noticeable limitations in treating patients with late-stage or metastatic malignant tumors and often cause severe side effects. To solve current problems, immunotherapies are emerging as promising methods by rebuilding immunosurveillance and stimulating tumor immune elimination (1). T cells are primary participants in tumor-associated immune response. Their infiltration, ratio, and functions influence antitumor immune response (2). Immune checkpoints [cytotoxic T lymphocyte-associated antigen-4 (CTLA-4), programmed cell death protein 1 (PD-1)] and immune checkpoint-related ligands [immune checkpoint-related ligands such as programmed cell death ligand 1 (PD-L1)] are critical parts in this process that promote or inhibit T-cell activity (3). As a result, ICIs are considered a promising strategy in reactivating antitumor immune responses by blocking immune checkpoints/immune checkpoint ligands. In recent decades, ICI therapy has been shown to be effective in patients with refractory tumors, especially for those late-stage patients who were unresponsive to traditional treatments (4). The United States Food and Drug Administration approved its application in solid tumors in 2011 (5). Anti-PD-1/PD-L1 therapy increased the overall survival to 40–50% at 5 years in advanced melanoma patients and is also becoming a promising method for non-small-cell lung cancer (NSCLC) patients (6, 7). The KEYNOTE-042 study indicated that in NSCLC patients whose PD-L1 tumor proportion score was ≥1%, pembrolizumab monotherapy prolonged their survival for longer than with traditional chemotherapy (8). In addition, dual blockage of PD-1 and CTLA-4 using nivolumab and ipilimumab also showed better effects compared with chemotherapy (9).

However, ICI did not show the same effects in all malignant tumor patients, and its response rate in an unselected population as single agent is below 20% (7, 10). More than one-half of patients are either unresponsive, or they relapse after a period of response, which seriously limits the effectiveness of ICI (11). ICI resistance can be generally divided into two sorts: primary resistance in which patients experience no significant effect in the initial period of ICI treatment; and secondary resistance (acquired drug resistance) in which initially, ICI can slow tumor progression, but patients later develop treatment failure (12). Two primary reasons for ICI resistance are the dysfunction of tumor infiltrating cytotoxic T cells and immunosuppressive factors, which hinder T cells from entering the tumor microenvironment (TME) (13, 14). Although many mechanisms were reported to be accountable for ICI resistance, there is still not an efficient method to predict it. Therefore, identification of predictive biomarkers for ICI response is crucial for determining appropriate patients for and predicting efficacy of ICI. TIDE is a computational method developed by Jiang et al. and is used for forming a tumor immune evasion model and calculating potential regulators and indicators in ICI resistance through integrating the expression features of T cell dysfunction and T cell exclusion, as well as pre-treatment tumor profiles (15). To identify potential biomarkers associated with immunotherapy, especially ICI resistance, WGCNA was also adopted in this study. WGCNA is a newly developed bioinformatics method to process medical data. Various researchers have utilized this method to analyze the gene expressions in different samples, depict correlations, and identify potential co-expressed genes or targets (16–18).

Self-renewal capacity and long-term persistence are critical properties of cancer stem cells (CSCs), and help them to maintain immune evasion, epithelial-mesenchymal transition (EMT), signaling pathway regulation, multidrug resistance, and pro-tumor immunity (19). CSCs express low levels of cancer-associated antigens, immune stimulatory molecules (CD86, CD40, and MHC II), and high levels of immune checkpoint proteins (20). Recent studies put forward that cancer cell stemness could be represented by clusters of core genes (21–23). Based on these gene sets, Miranda et al. found pervasive negative associations between cancer cell stemness and anticancer immunity (24). They showed that stemness led to higher intratumoral heterogeneity and restrained antitumor immune response, which result in poor outcome for malignant tumor patients. Research showed that complex interactions between CSCs and immune cells in the TME-induced immunotherapy resistance by promoting anti-apoptotic pathways, inducing EMT, and enhancing immune tolerance (25–27).

After taking into consideration both TIDE score and stemness index, we identified a potential gene module (pink) which was highly related to T cell dysfunction and cancer cell stemness. Further analysis revealed strong enrichment of ECM remodeling, EMT, tumor invasion, tumor growth, and a positive relationship to immunosuppressive markers in the pink module. According to the gene significance of TIDE (GS.TIDE), we selected nine genes and observed their higher levels in tumor tissues and LUAD patients with poorer survival. Among them, THY1 (Thy-1 cell surface antigen) was selected as the key gene and was shown to be related to tumor stage, survival, and immune states of LUAD patients. Analysis of clinical samples showed a positive correlation between THY1 and classical cancer stemness marker SOX9. Moreover, the highest levels of THY1 were found in the PD group of PD-1 mAb-treated LUAD patients. These results provide the fundamental basis for further research of immunotherapy resistance and the discovery of new therapeutic target to refine ICI treatments of LUAD patients.

MATERIALS AND METHODS

Data Processing

We obtained gene expression data (FPKM format) and relevant clinical characteristics of 526 LUAD samples from the Cancer Genome Atlas (TCGA) database (https://www.cancer.gov/tcga). After excluding patients that lacked key clinical information, 513 patients were retained. TPM format conversion was performed for gene expression data in FPKM format for further analysis. We also obtained data for gene expression and survival of LUAD patients (GSE72094) from Gene Expression Omnibus (https://

www.ncbi.nlm.nih.gov/geo/). A total of 398 samples with complete clinical information were utilized in further analysis.

Immunotherapy Response Prediction and Stemness Index

TIDE score was shown to be more effective and accurate than current methods in predicting the immunotherapy response of melanoma and lung cancer patients. We downloaded LUAD patient-related TIDE scores from (http://tide.dfci.harvard.edu) (15). To bring cancer stemness into analysis, we used single-sample gene set enrichment analysis (ssGSEA) to process stemness-related gene sets (Benporath_ES1, Benporath_ES2, Bhattacharya_hESC, Shats_iPSC, Shats_Consensus, Benporath_Sox2, Kim_Myc, Smith_Human. Epithelial_ASC, Palmer_2012, Proliferative_Ben_Porath, Curated_genes) in malignant tumors obtained from previous articles (21–23, 28–32). The above data were included in the WGCNA analysis according to a previous report (33).

Constructing Weighted Gene Co-Expression Networks and Identifying Modules Associated With Immunotherapy Resistance Score and Stemness Score of LUAD Patients

WGCNA is used to group correlated genes pairwise into a model or network according to their similar expression profiles (34). In this article, WGCNA was adopted to identify the modules correlated with immunotherapy resistance and cancer stemness. Further filtration of 513 LUAD patients found that six patients lacked TIDE values or were outliers according to the original clustering tree at a height of 150,000. As a result, we ultimately included 507 samples in the WGCNA analysis. We chose the soft threshold $\beta = 4$ (scale free $R^2 = 0.88$) to construct a co-expression network. We then transformed the adjacency matrix into a topological overlap matrix to quantitatively describe the similarity. Next, we used cutreeDynamic function to perform the gene hierarchical clustering dendrograms and identify various co-expression modules. Correlations between modules and TIDE scores or other characteristics were assessed by Spearman test.

Identification of Hub Genes

GS and module membership (MM) were adopted to filter hub genes in the pink module. GS stands for the level of correlation between gene expression and designated features. MM stands for the correlation of the module eigengene and the gene expression profile. GS.TIDE represents the relevance of each module to the TIDE score. Among all the modules, the pink module had the highest GS.TIDE, which means the highest correlation with immune evasion. Therefore, we selected top 20 genes according to GS.TIDE for protein-protein interaction (PPI) network analysis and nine genes for further analysis. Among them, THY1 was the gene most associated with TIDE score in the pink module.

Protein-Protein Interaction Analysis of Top 20 Hub Genes

We performed a PPI analysis with top 20 hub genes using GeneMANIA website (https://genemania.org/search/homo-sapiens/) to depict their relationship in Co-expression, Physical Interactions, Co-localization, and Pathways.

Gene Ontology and Kyoto Encyclopedia of Genes and Genomes Enrichment Analysis

Clusterprofiler R package was adopted in Gene Ontology (GO) and Kyoto Encyclopedia of Genes and Genomes (KEGG) enrichment analysis using genes in the pink module. We used "adjusted $p < 0.05$" to identify significant GO terms and KEGG terms.

Cell Infiltration Analysis

xCell (http://xcell.ucsf.edu/) was used to obtain the relative expression level of 64 types of cells in the tumor microenvironment of LUAD patients using mRANseq data (TPM format) from TGCA in R software.

Pathway Enrichment of the Pink Module

Four gene set lists were downloaded from the nanoString website (https://www.nanostring.com/): the nCounter PanCancer Pathways panel, the nCounter® PanCancer Immune Profiling panel, the nCounter PanCancer Progression panel, and the nCounter® PanCancer IO 360™ Panel. These panels include detailed listings of genes, corresponding pathways, and immune types. ssGSEA and heatmap packages were used to analyze these four panels and displayed the results by LUAD patients.

Kaplan-Meier Survival Analysis

Gene expression data and corresponding clinical information from GSE72094 dataset were used to analyze the survival rate of each gene. We utilized Kaplan-Meier curve and log-rank test to estimate the prognostic significance of nine hub genes. We divided each gene into two groups according to the best cut point method using "surv_cutpoint" algorithm of the survminer R package.

Immune Subtypes and Clinical Characteristics Analysis

According to the research of Thorsson et al., the intratumor immune states could be divided into six subtypes: C1 (wound healing), C2 (IFN-γ dominant), C3 (inflammatory), C4 (lymphocyte depleted), C5 (immunologically quiet), and C6 (TGF-β dominant) (35). C1 has higher expression of angiogenic genes and Th2-type adaptive immune infiltration. C2 shows high M1/M2 macrophage polarization and activated function of antitumor T cells. C3 is related to Th17 and Th1 cells and could suppress tumor cell proliferation. C4 displays a prominent M2 macrophage signature and suppressed Th1. C5 exhibits the lowest lymphocyte and highest M2 responses. The highest TGF-β signature is the feature of C6. We evaluated the expression level of THY1 on these six subtypes. We also assessed THY1 expression in different clinical stages of LUAD patients using gene expression data and clinical information from the TCGA dataset. Wilcoxon test was adopted to compare differences between groups.

Clinical Samples

Human LUAD tumor tissues were acquired from the First Affiliated Hospital of Zhengzhou University in 2020. All patients were pathologically diagnosed with LUAD through surgery or percutaneous pulmonary biopsy and failed chemotherapy or targeted therapy. All patients had a lung computerized tomography (CT) scan before receiving at least three cycles of

PD-1 mAb treatment (baseline). Lung CT scan was also used to evaluate the therapeutic effects after using PD-1 mAb (first/second). The clinical information of the patients is shown in **Table 1**.

Immunohistochemistry

All patients agreed to informed consent before specimen collection. Tissues were fixed with 4% paraformaldehyde and embedded in paraffin. IHC was performed according to previous research (36). Tumor tissue slides were incubated with anti-human THY1 (ABCAM, Rabbit mAb, CAT: ab133350, 1:50) and anti-human SOX9 (ABCAM, Rabbit mAb, CAT: ab185966, 1:1,000) at 4°C for overnight. Then, the slides were incubated with horseradish peroxidase-conjugated anti-rabbit/mouse antibody (ZSGB-BIO, SP-9000) for 30 min at room temperature. Subsequently, diaminobenzidine (ZSGB-BIO, ZLI-9018) and hematoxylin were used to visualize the protein and cell nucleus. Vectra Polaris Multispectral Imaging and Whole Slide Scanning System (PerkinElmer, Vectra) was used to screen the slides. IHC staining score of each protein was evaluated by imageJ software using IHC toolbox.

Statistical Analysis

Wilcoxon test is used to compare the differences between groups of classified variable. Spearman analysis is used to calculate the correlation between continuous variables. The above collected data was analyzed using R software version 3.6.1 (https://www.r-project.org). Differences between groups were analyzed using t test. Pearson's correlation analysis was used to calculate correlation coefficients (r) using Graphpad Prism 7. With all statistical methods, $p < 0.05$ was considered statistically significant.

RESULT

WCGNA Analysis and Modules Significance Calculation

The gene expression matrix of 7,298 preprocessed genes derived from LUAD patients in the TCGA dataset was used for WGCNA with R package. After excluding patients that lacked critical characteristics, 507 samples were utilized for further analysis. Sample dendrogram and trait heatmap are displayed in **Figure 1A**. To ensure high-scale independence (near 0.9), we set $\beta = 4$ in this analysis (**Figure 1B**). After obtaining the β value, we constructed an adjacency matrix and topological overlap matrix (**Figures 1C, D**). On the basis of average hierarchical clustering and dynamic tree clipping, we obtained 45 modules in total (**Figure 2A**). Then, we calculated the correlation coefficients between each module and the sample characteristics related to TIDE, cancer stemness markers, and various immune-related characteristics (**Figures 2B, C**). According to GS.TIDE, we found that the pink module had the highest correlation with TIDE (cor = 0.56; p = 2e-43). In addition, the pink module showed a strong correlation with various cancer stemness markers and immunosuppressive features, such as Exclusion (cor = 0.55; p = 4e-42) and cancer-associated fibroblast (CAF) (cor = 0.9; p = 3e-189) (**Figure 2B**). As a result, this module was selected as a critical module for the possible relationship between cancer stemness and immunotherapy resistance. GS.TIDE was used to filter the top 20 hub genes in the pink module (**Table 2**). We adopted the PPI network with top 20 hub genes using GeneMANIA and found a strong relationship in expression, physical interaction, and pathways between hub genes (**Figure 2D**).

TABLE 1 | The summary clinical information of the samples.

Characteristics	LUAD Patients (n = 6)
Age, year *(mean ± SD)*	63.50 ± 8.12
Male, *n (%)*	2 (*33.3*)
Female, *n (%)*	4 (*66.7*)
TNM stage, *n (%)*	
I	0 (*0*)
II	1 (*16.7*)
III	3 (*50*)
IV	2 (*33.3*)
Outcome, *n*	
PD	2
SD	2
PR	2

SD, standard deviation; LUAD, lung adenocarcinoma; PD, progressive disease; SD, stable disease; PR, partial response.

Functional Annotation of Genes in the Pink Module

The pink module contains 274 genes. The results of the GO enrichment analysis and KEGG enrichment analysis of these 274 genes are shown in **Figures 3A, B**. Results showed that genes in the pink module were strongly enriched in the ECM organization. Enriched items in the cellular component were also related to the ingredients of ECM and focal adhesion (**Figure 3A**). Results from KEGG analysis showed a similar conclusion (**Figure 3B**). Top 15 GO items of the hub genes in the pink module are shown in **Table 3**.

To further investigate the characteristics of these genes, we utilized gene set lists downloaded from nanoString and identified higher enrichment of genes in the immunosuppressive items and tumor-associated pathways and functions (**Figures 3C–F**). For example, the pink module was associated with senescence, adhesion, and transporter functions and was also enriched with tumor intrinsic factors and stromal factors. A cluster of cancer-related pathways were involved, such as JAK-STAT, Wnt, PI3K, MAPK, and RAS. More importantly, the enrichment of metastasis, cancer metabolism, ECM remodeling, EMT, tumor invasion, tumor growth, angiogenesis, and ECM layers was heightened in the pink module. Highly positive correlations were found between the pink module and cancer stemness markers, such as Benporath-Nanog (Cor = 0.468, p = 0e+00), Palmer_2012 (Cor = 0.331, p = 2.452e-14), and Curated_genes (Cor = 0.326, p = 7.074e-14) (**Figure 4A**).

It has been reported that the occurrence of immunotherapy resistance is associated with the upregulation of suppressive characteristics in TME and downregulation of immune stimulators (37). To support the hypothesis that the pink module is associated with immune evasion, we performed a correlation analysis between the pink module and immunosuppressive markers

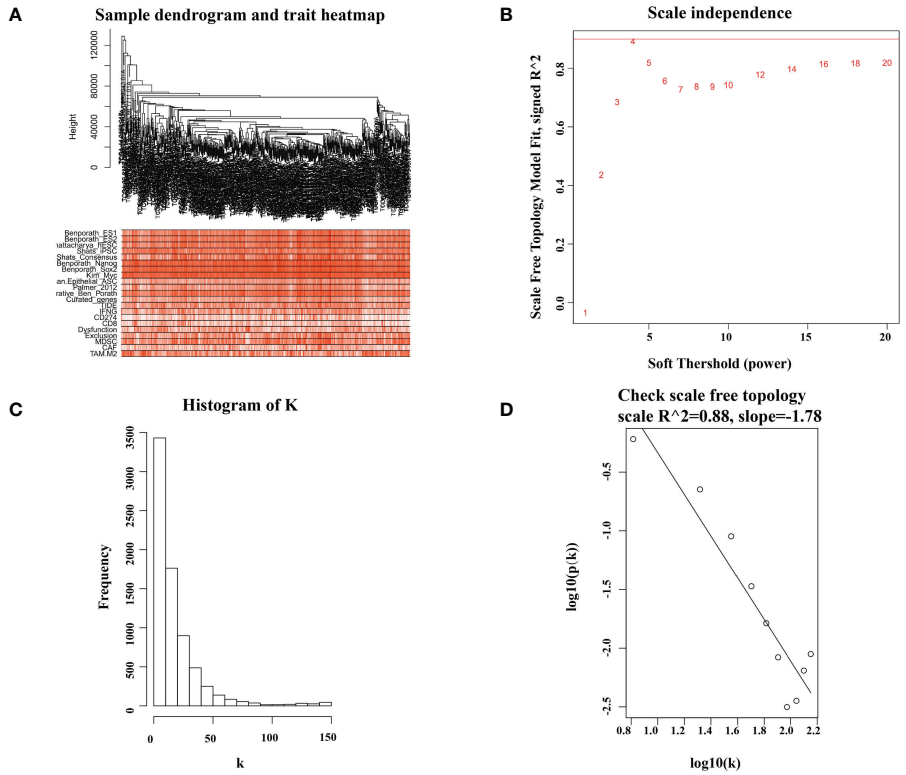

FIGURE 1 | Sample dendrogram and soft-thresholding values estimation. **(A)** Sample dendrogram and trait heatmap of 507 samples. The upper 12 traits are representative marker of cancer stemness, and the lower 9 traits are common evaluation index of immunotherapy. **(B)** Analysis of the scale-free index for various soft-threshold powers (β). **(C, D)** The scale free topology when β = 4.

or immunostimulatory makers. We found that pink module genes are positively correlated with immunosuppressive markers and cells, such as Tr1, Th2, iTreg, CAF, and CD274 (**Figure 4B**). Correspondingly, immune-stimulating cells and markers, like Th17, effector-memory and Gamma-delta T cells, and neutrophils, were negatively correlated with the pink module (**Figure 4C**). These results demonstrated that the pink module is a set of genes that potently correlated with cancer stemness and immunosuppressive characteristics.

Identification and Validation of Hub Genes

In *WCGNA Analysis and Modules Significance Calculation* we filtered the top 20 hub genes in the pink module according to GS.TIDE. To shrink the range, we ranked genes on the base of GS.TIDE and selected nine genes from them (*THY1*, *COL5A1*, *COL1A2*, *COL3A1*, *COL1A1*, *COL5A2*, *MMP2*, *COL6A3*, *EMILIN1*). The expression levels and clinical information of these nine genes were obtained from the TCGA and GEO database. Higher expression levels were found in the tumor tissues than in the corresponding normal tissues, except for *EMILIN1* and *MMP2* (**Figure 5A**). We then used a Kaplan-Meier plotter to analyze patient survival and found that *THY1*, *COL5A1*, *COL1A2*, *COL3A1*, *COL1A1*, *COL5A2*, *COL6A3* exhibited excellent diagnostic efficiency in LUAD patients (**Figure 5B**). These results indicated the strong clinical significance of *THY1*, *COL5A1*, *COL1A2*, *COL3A1*, *COL1A1*, *COL5A2*, *COL6A3*.

Clinical Characteristics of THY1

To find a more targeted gene, we filtered these hub genes according to GS.TIDE, expression levels in cancer, and survival probability, and selected THY1 as the key gene in the pink module. We then analyzed THY1 based on the theory of Thorsson et al. and observed that THY1 was highly expressed in the wound-healing subtype (C1) and TGF-βdominant subtype (C6) (**Figure 6A**), which means that THY1 is an immunosuppressive participant in malignant tumors. Moreover, clinical characteristics analysis showed that tumor stages were highly associated with THY1 expressions, which were highest in LUAD patients in stage iii (**Figure 6B**). Correlation analysis revealed that THY1 had a strong positive correlation with cancer stemness markers, as well as immunosuppressive markers and cells, especially with the TIDE score (Cor = 0.578, p = 4.293e-50) (**Figures 6C, D**). The negative correlation between THY1 and immune stimulators were also apparent (**Figure 6E**). These results implied that THY1 mediates immunotherapy resistance by enhancing immunosuppressive function as well as limiting the antitumor effects of immune stimulators.

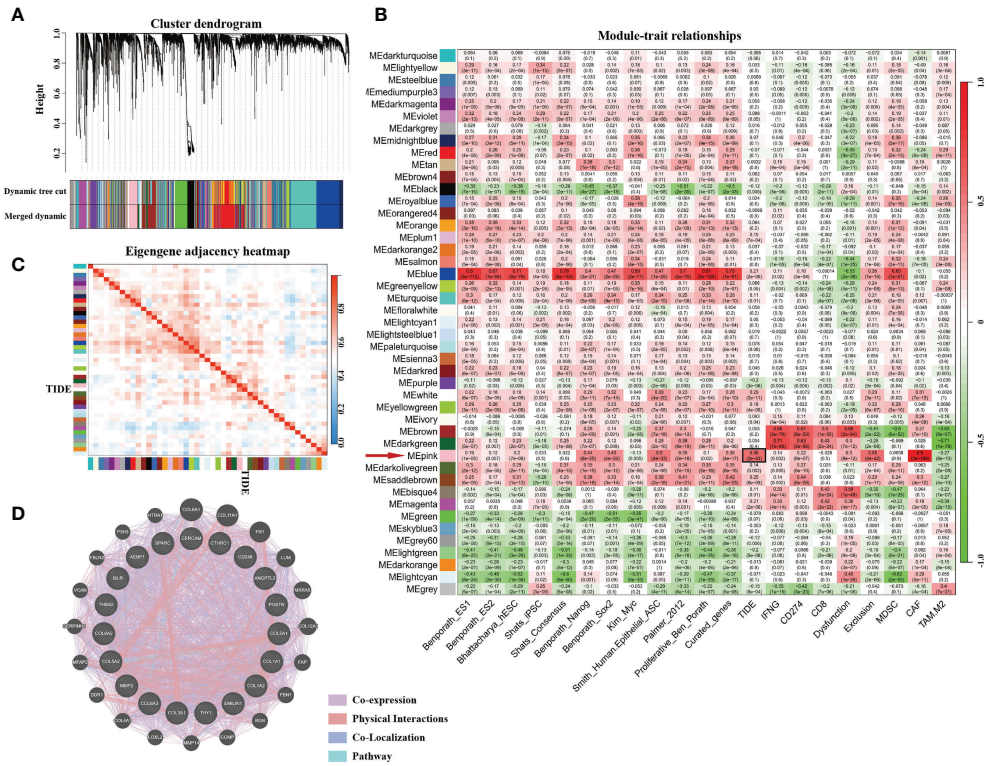

FIGURE 2 | The genes enrichment and module identification. **(A)** Hierarchical clustering dendrogram of co-expressed genes in LUAD patients. A total of 45 modules were identified, and each colored row stands for a module with a cluster of highly connected genes. **(B)** Correlation coefficient between consensus module eigengenes and TIDE score, cancer stemness, or other immune-related characteristics. **(C)** Heatmap plot of the adjacent modules. **(D)** Protein–protein interactions of top 20 hub genes. The strength of the relationship is associated with the thickness of the colorful lines.

TABLE 2 | The top 20 hub genes in pink module.

Gene symbol	Module color	GS.TIDE	p.GS.TIDE	MM.PINK	p.MM.pink
THY1	pink	0.565112	4.07E-44	0.863729	2.10E-152
COL5A1	pink	0.561903	1.56E-43	0.909754	6.08E-195
COL1A2	pink	0.545879	1.03E-40	0.900204	1.86E-184
COL3A1	pink	0.53608	4.63E-39	0.871879	1.08E-158
COL1A1	pink	0.536067	4.65E-39	0.85819	2.33E-148
COL5A2	pink	0.535168	6.55E-39	0.894479	1.14E-178
MMP2	pink	0.528323	8.60E-38	0.870475	1.40E-157
COL6A3	pink	0.52624	1.86E-37	0.880475	8.24E-166
EMILIN1	pink	0.520856	1.34E-36	0.828496	2.91E-129
CTHRC1	pink	0.519758	1.99E-36	0.714135	2.97E-80
CERCAM	pink	0.519243	2.40E-36	0.686384	7.24E-72
SPARC	pink	0.517456	4.56E-36	0.898107	2.69E-182
POSTN	pink	0.516439	6.56E-36	0.803405	8.62E-116
ANGPTL2	pink	0.51307	2.17E-35	0.835944	1.09E-133
COL6A2	pink	0.511227	4.16E-35	0.794625	1.57E-111
AEBP1	pink	0.508668	1.02E-34	0.884474	2.60E-169
THBS2	pink	0.506547	2.13E-34	0.877036	6.73E-163
ISLR	pink	0.504474	4.35E-34	0.794421	1.96E-111
CD248	pink	0.499077	2.74E-33	0.719266	6.47E-82
BGN	pink	0.498091	3.81E-33	0.854806	5.69E-146

GS, gene significance; MM, module membership.

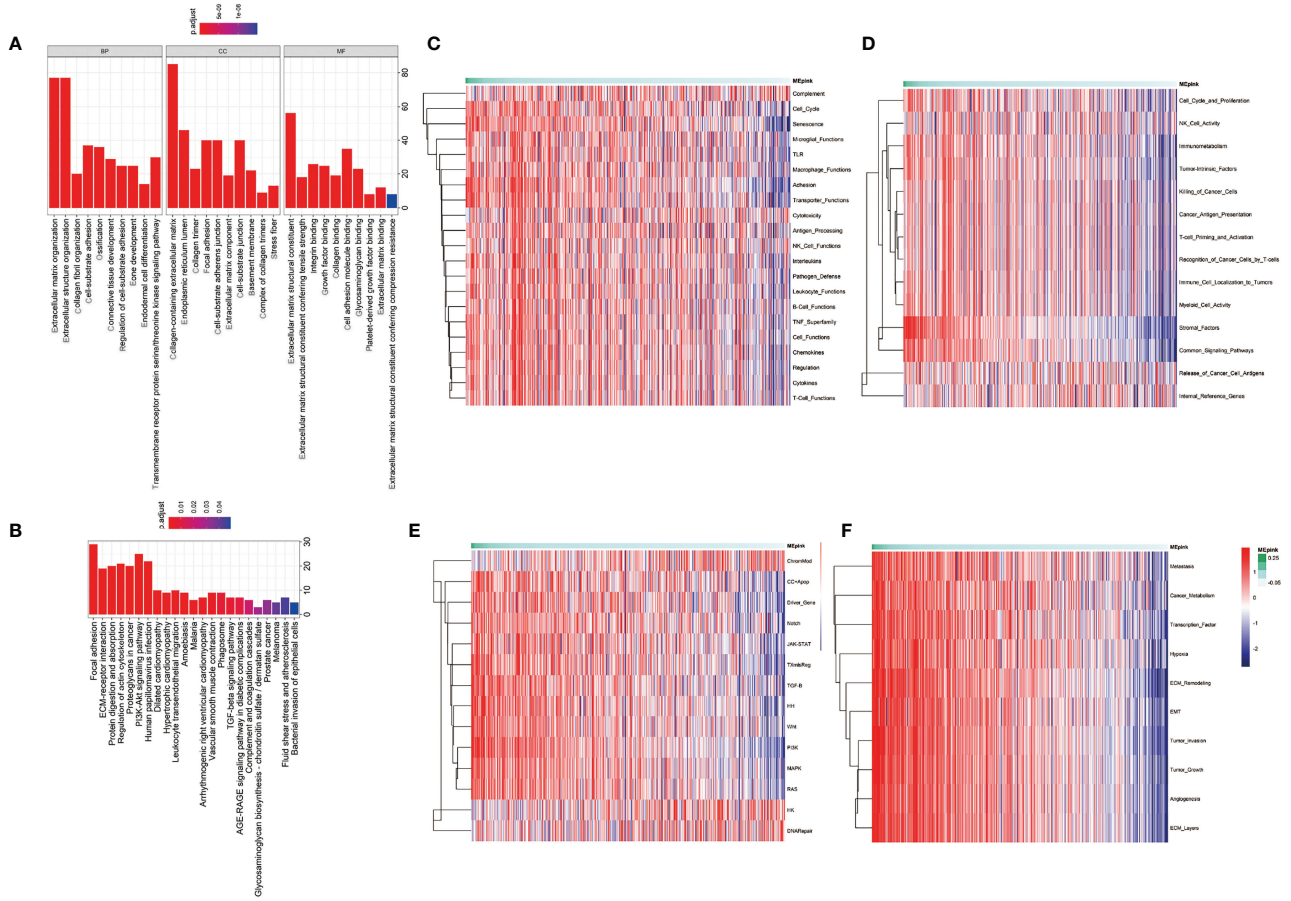

FIGURE 3 | Enrichment analysis of the significant genes in the pink module. **(A)** Gene ontology enrichment including biological process (BP), cellular component (CC), and molecular function (MF). **(B)** KEGG enrichment of significant genes in pink module. **(C–F)** Pathway enrichment of significant genes in pink module. **(C)** is the pathways that participate in immune profiling. **(D)** is the pathways in IO.unity. **(E)** is the common pathways in human physiological process. **(F)** is the pathways of cancer progression.

Clinical Validation of THY1 and SOX9 in LUAD Patients

In order to validate the hypothesis that THY1 is related to cancer stemness and immunotherapy resistance, we performed IHC staining on six tissue samples of LUAD patients who received at least three cycles of PD-1 mAb treatments using THY1 and SOX9 antibodies. The clinicopathological data are presented in **Table 1**. Lung CT examination was used to evaluate the efficacy of PD-1 mAb therapy, and the result prior to the first dose was used as the baseline. The results of the CT scan showed that two patients displayed PD, two patients displayed stable disease (SD), and the remaining two patients acquired partial response (PR) (**Figure 7C**). IHC results proved that THY1 expression was highest in the PD group and lowest in the PR group. Moreover, THY1 expression was positively related to the level of SOX9, a classical biomarker of cancer stemness (38) (**Figures 7A, B**). However, the IHC scores of THY1 and SOX9 between PR group and SD group showed no statistical difference. These results indicated a strong relationship between THY1 and the therapeutic resistance of PD-1 mAb, which was consistent with the above analysis. Furthermore, THY1 levels also positively correlated with cancer stemness. This means that THY1 could be used as a possible biomarker in predicting the efficacy of PD-1 mAb.

DISCUSSION

The fact that ICI treatments are ineffective for some malignant tumor patients prompts research for the underlying molecular mechanisms and ways to refine it. As a newly developed computational method, TIDE has been used to model tumor immune evasion by evaluating the interactions between candidate genes and the characteristics of T cells in LUAD and melanoma (15). A higher TIDE score is related to a higher likelihood of immune escape by tumors and lower response rate to ICI treatment. As a result, TIDE score is now becoming a more reasonable and accurate method in assessing the outcome of

TABLE 3 | The top 15 GO items of genes in the pink module.

GO-ID	*p*-value	Description	Genes in the test list
5578	3.30E-20	Proteinaceous extracellular matrix	*POSTN|SPARC|LUM|MMP2|BGN|COL1A1|ADAMTS2|COL3A1|VCAN|COL1A2|COL5A1|COL5A2|TIMP2|COL6A3|ANGPTL2|EMILIN1|FBN1*
31012	7.25E-20	Extracellular matrix	*POSTN|SPARC|LUM|MMP2|BGN|COL1A1|ADAMTS2|COL3A1|VCAN|COL1A2|COL5A1|COL5A2|TIMP2|COL6A3|ANGPTL2|EMILIN1|FBN1*
44421	3.67E-15	Extracellular region part	*POSTN|SPARC|LUM|MMP2|BGN|AEBP1|INHBA|COL1A1|ADAMTS2|COL3A1|VCAN|COL1A2|COL5A1|COL5A2|TIMP2|COL6A3|ANGPTL2|EMILIN1|FBN1*
44420	2.27E-13	Extracellular matrix part	*COL1A1|COL3A1|SPARC|COL1A2|COL5A1|LUM|COL5A2|TIMP2|COL6A3|FBN1*
5583	3.82E-13	Fibrillar collagen	*COL1A1|COL3A1|COL1A2|COL5A1|LUM|COL5A2*
5201	6.99E-13	Extracellular matrix structural constituent	*COL1A1|COL3A1|COL1A2|COL5A1|LUM|COL5A2|BGN|EMILIN1|FBN1*
30199	1.47E-12	Collagen fibril organization	*COL1A1|ADAMTS2|COL3A1|COL1A2|COL5A1|LUM|COL5A2*
48856	1.86E-12	Anatomical structure development	*PDGFRB|TAGLN|POSTN|SPARC|UNC5B|MMP2|BGN|AEBP1|THY1|INHBA|ANTXR1|COL1A1|ACTA2|ADAMTS2|COL3A1|VCAN|COL1A2|COL5A1|COL5A2|ITGA11|TIMP2|COL6A3|FBN1*
5576	2.27E-12	Extracellular region	*POSTN|SPARC|LUM|MMP2|BGN|AEBP1|INHBA|THBS2|COL1A1|ADAMTS2|COL3A1|VCAN|COL1A2|COL5A1|COL5A2|TIMP2|COL6A3|ANGPTL2|EMILIN1|MXRA5|FBN1*
30198	3.94E-12	Extracellular matrix organization	*COL1A1|ADAMTS2|POSTN|COL3A1|COL1A2|COL5A1|LUM|COL5A2|EMILIN1*
32502	5.15E-12	Developmental process	*PDGFRB|TAGLN|POSTN|SPARC|UNC5B|MMP2|BGN|AEBP1|THY1|INHBA|ANTXR1|COL1A1|ACTA2|ADAMTS2|COL3A1|VCAN|COL1A2|COL5A1|COL5A2|ITGA11|TIMP2|COL6A3|ANGPTL2|FBN1*
5581	5.15E-12	Collagen	*COL1A1|COL3A1|COL1A2|COL5A1|LUM|COL5A2|COL6A3*
7275	1.35E-11	Multicellular organismal development	*PDGFRB|TAGLN|POSTN|SPARC|UNC5B|MMP2|BGN|AEBP1|THY1|INHBA|COL1A1|ACTA2|ADAMTS2|COL3A1|VCAN|COL1A2|COL5A1|COL5A2|ITGA11|TIMP2|COL6A3|ANGPTL2|FBN1*
48731	5.21E-11	System development	*PDGFRB|TAGLN|POSTN|SPARC|UNC5B|MMP2|BGN|AEBP1|THY1|INHBA|COL1A1|ADAMTS2|COL3A1|VCAN|COL1A2|COL5A1|COL5A2|ITGA11|TIMP2|COL6A3|FBN1*
43062	1.49E-10	Extracellular structure organization	*COL1A1|ADAMTS2|POSTN|COL3A1|COL1A2|COL5A1|LUM|COL5A2|EMILIN1*

immunotherapy and prognosis of patients compared with the single evaluation of PD-L1 levels, tumor mutational burden, or IFN-γ signature (39). To figure out which cluster of genes is potentially responsible for ICI resistance in LUAD patients, WGCNA was adopted to build a co-expression module and illuminate the complicated correlation between candidate genes and phenotypes. Highly co-expressed genes formed a module that can be used to assess the depth of the association with selected characteristics. Based on these concepts, we used the TIDE score and WGCNA to identify genes associated with immunotherapy resistance in LUAD patients, and picked the pink modules (274 genes), which was highly associated with the TIDE score. In addition, we introduced a cluster of cancer stemness markers (ES1/2, hESC, iPSC, Nanog, Sox2, Myc, et. al) into WGCNA analysis, and observed that these markers were positively correlated with the pink module (24) (**Figure 2B**). These results were in line with previous reports that CSCs mediate resistance to antitumor therapy, such as chemotherapy and radiotherapy, as well as immunotherapy (40–42).

In the exploration of immunotherapy resistance mechanism, cancer stemness has been a focus for years. Maccalli et al. proposed that one main reason for ICI treatment failure might be the immune-resistant ability of CSCs. Although few in number, CSCs remain in the tumor after treatment, reforming the tumor mass and promoting tumor progression (43). In the research by Miranda et al., they found that $CD8^+$ T cells, natural killer (NK) cells, and B cells showed a strongly negative correlation with stemness for most cancer (24). These results proposed an association between stemness and suppressed antitumor immune response, which indicates worse clinical outcomes with malignant tumors. Complicated interactions between CSCs and other stromal cells, such as immune cells and fibroblasts, can lead to malignant biological properties such as EMT and result in immune evasion (44). In our analysis, top 15 GO enrichment items of these genes showed a concentration on the organization and regulation of ECM, including EMT (**Figures 3A, B**).

The relationship between ECM remodeling and cancer stemness has already been reported. Elevated collagen-induced stiff ECM triggers cancer cell stem-like programming and metastatic dissemination *in vivo*. Suppression of collagen deposition could increase expression of lung differentiation markers (45). Liang et al. proposed that CD44, a transmembrane receptor for hyaluronic acid and many other ECM components, was a critical marker and regulator of cancer stemness (46). Furthermore, macrophage-derived glycoprotein non-metastatic B facilitates the expansion of CSCs through CD44/IL-33 axis and promote metastasis in mouse tumor models (17). Moreover, ECM could facilitate immune evasion in CSCs by activating PI3K/AKT and recruiting immunosuppressive cells like tumor associated macrophages and Tregs (47–49). The relationship between tumor ECM, drug resistance, and immune suppression has been reported (50).

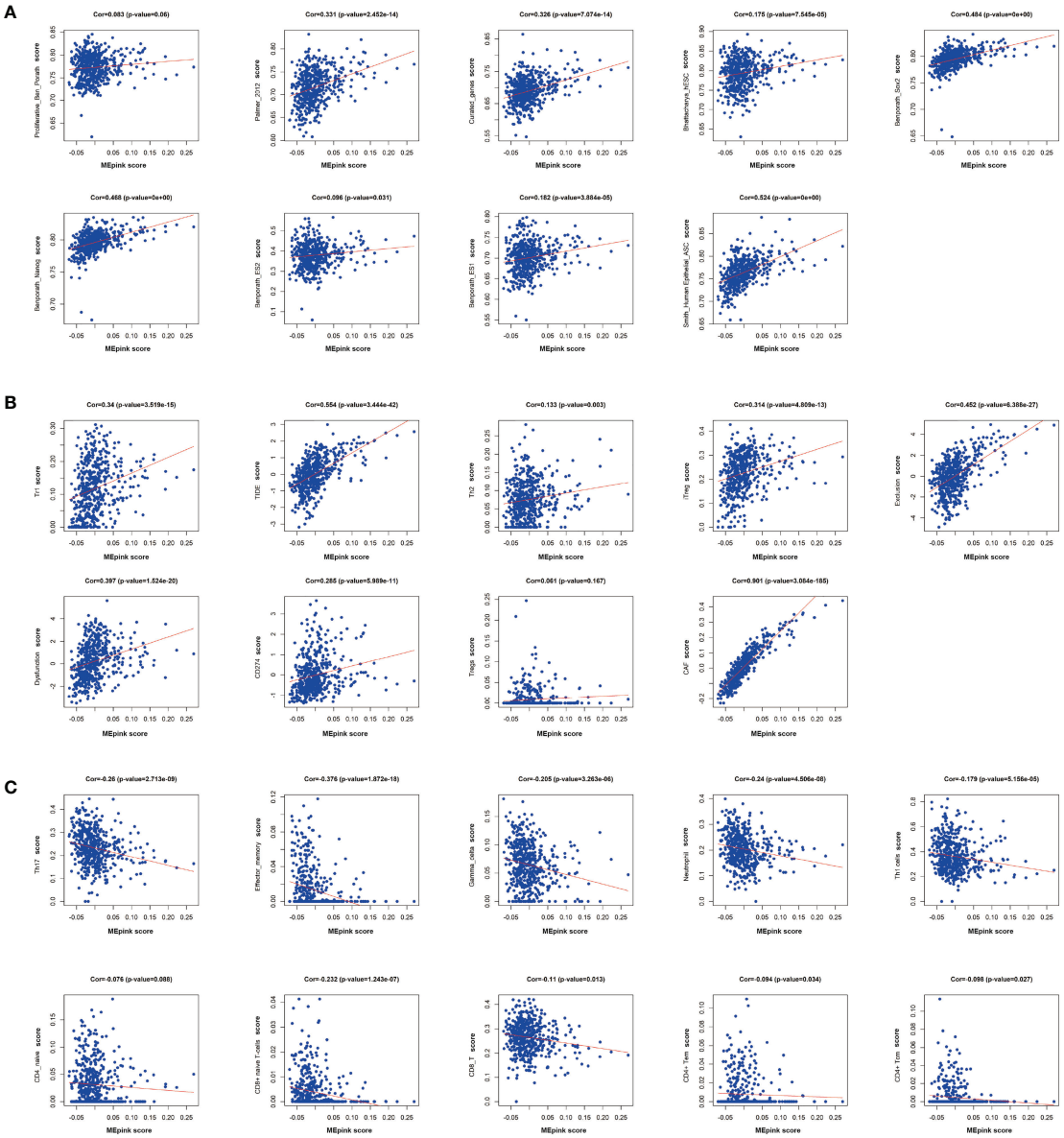

FIGURE 4 | Correlation of significant genes in pink modules with stemness and immunotherapy resistance. **(A)** Correlation analysis of pink modules with markers of cancer stemness. **(B)** Correlation analysis of pink modules with immune suppressive markers. **(C)** Correlation analysis of pink modules with immune stimulative markers. Cor, correlation.

ECM can damage the activation and proliferation of T cells, thus facilitating CSCs survival and inducing immunotherapy resistance (51). Peng et al. demonstrated that LAIR1-SHP-1 pathway regulated the increased collagen levels and exhausted $CD8^+$ T cell subpopulations in lung tumor tissues, and mediated the resistance to PD-1/PD-L1 blockade (50). EMT increases tumor initiation and potential for metastasis, as well as resistance to several treatments (52). EMT-associated gene signatures were collectively described as features of intrinsic anti-PD-1 resistance (53). Some studies linked PD-L1 upregulation with EMT, which is also a feature closely related to CSCs (54, 55). Positive correlations were found between EMT-related genes and inhibitory immune molecules (e.g., PD-L1/2, PD-1, CTLA-4) and Tregs in LUAD patients (56, 57). A transcriptomic meta-analysis of breast cancer patients showed that PD-L1 regulated the expression of OCT4A, Nanog, and BMI1 through AKT signaling (58). Thus, EMT is considered to be a potential mechanism in immune escape.

Pathway enrichment analysis in signaling pathways pointed out that genes in the pink module were en1riched in MAPK, JAK-STAT, PI3K, RAS, Notch, Wnt signaling pathways (**Figure 3E**). These pathways have been reported to be activated in immunotherapy resistance. For example,

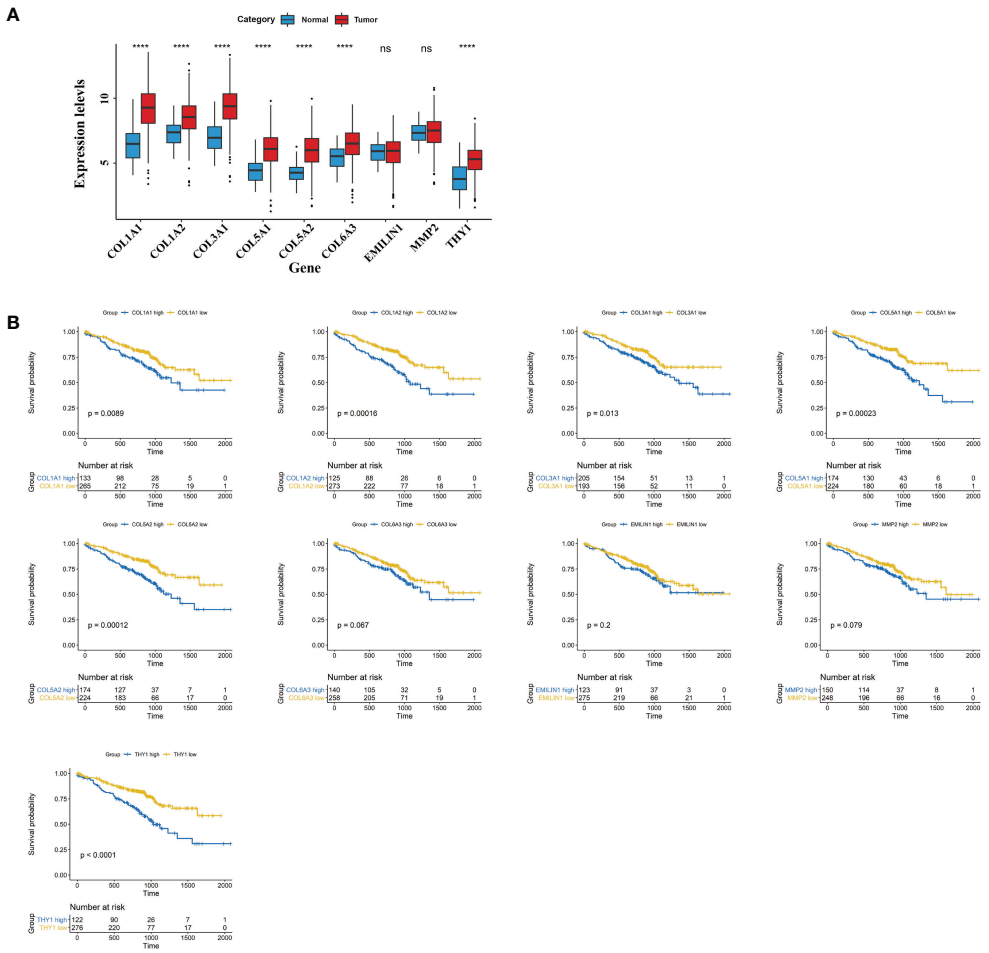

FIGURE 5 | Clinical characteristics of hub genes in pink module. **(A)** mRNA expressions of nine hub genes in cancer tissues of LUAD and normal lung tissues. **(B)** Survival plots of the significant genes by Kaplan Meier test. The data were obtained from the GEO website. ns, no significance; ****$p < 0.001$.

dysregulation of MAPK pathways has been linked with immune-silencing phenotypes in breast cancer and is associated with treatment resistance (59). Activation of the JAK-STAT signaling pathway inhibits cytotoxic T lymphocytes and counteracts the antitumor effects of anti-PD-1 immunotherapy in pancreatic cancer (60). RAS-related oncogenesis could increase the level of PD-L1, eliminate antigen presentation, and alter the expressions of cytokines, thus leading to immune evasion and immunotherapy resistance (61). The research implies a close relationship between immunotherapy resistance and cancer stemness. Further analysis on the immune infiltration patterns of the pink module also confirms these hypotheses. We found that genes in the pink module were positively related with immune suppressive cells (Tregs, Tr1, Tr2, CAF), molecules (CD274), and two critical characteristics in immune evasion (Exclusion and Dysfunction) (**Figure 4B**). Meanwhile, the immune-activated cells and markers, such as antitumor T cells, neutrophils, Th1 cells, and gamma-delta T cells, were downregulated in the pink module (**Figure 4C**). These results support the hypothesis that the genes in the pink module can be used as potential markers or targets in identifying and eliminating malignant tumors.

To ascertain specific genes involved in ICI resistance, we selected nine genes (*COL1A1*, *COL1A2*, *COL3A1*, *COL5A1*, *COL5A2*, *COL6A3*, *EMILIN1*, *MMP2*, *THY1*) for further analysis. These genes are stemness-related and were predicted to be associated with the clinical outcomes of LUAD patients receiving immunotherapy. Expression analysis showed that these genes were more highly expressed in LUAD tumor tissues compared with normal tissues (**Figure 5A**) except for *EMILIN1* and *MMP2*. Moreover, *COL1A1*, *COL1A2*, *COL3A1*, *COL5A1*, *COL5A2*, *THY1* exhibited a more promising outcome in more lowly expressed group (**Figure 5B**). Among them, *THY1* ranked first based on GS.TIDE. THY1 (CD90) is a glycosylphosphatidylinositol-anchored glycoprotein and is mainly expressed on blood stem cells, activated microvascular endothelial cells (ECs), and fibroblasts (62). It could be used as a biomarker in stem cell isolation. THY1 is an important protein in

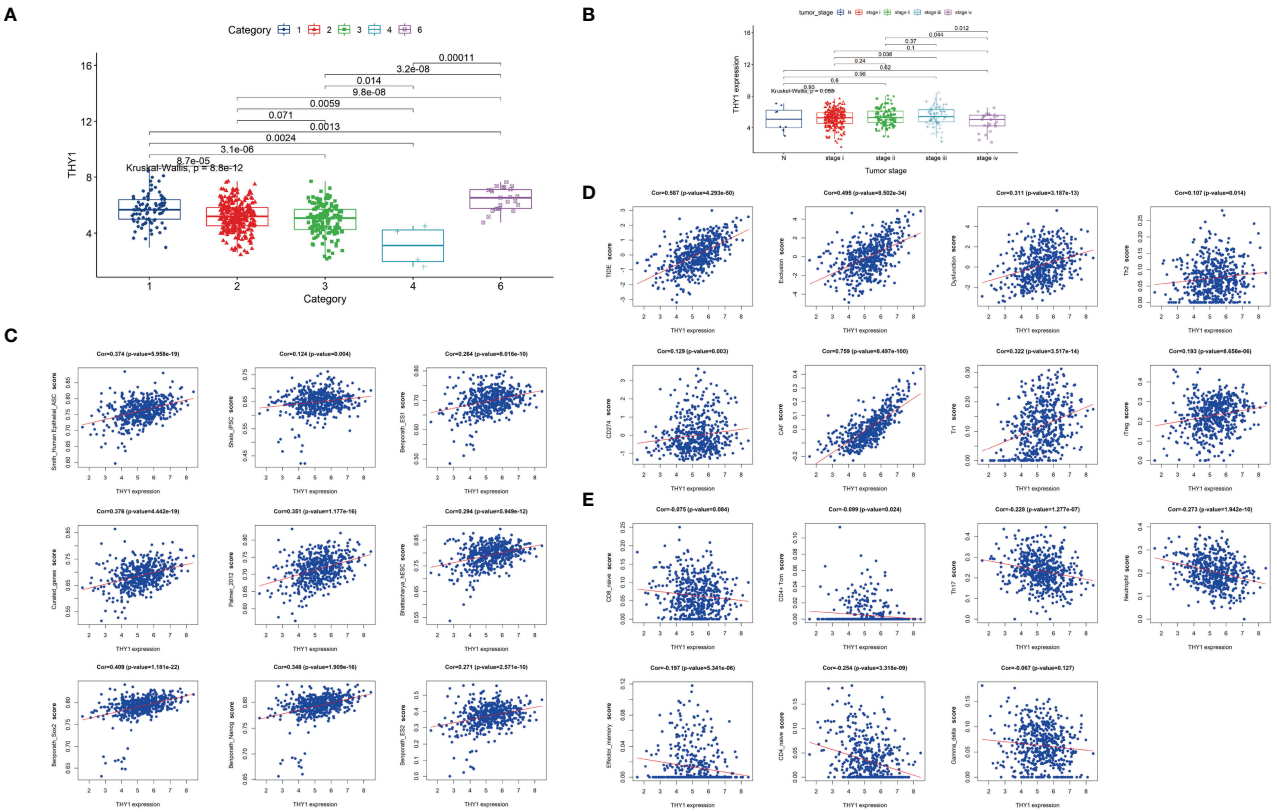

FIGURE 6 | Characteristics of THY1 in LUAD patients. **(A)** THY1 expression of LUAD patients in six immune subtypes: C1, wound healing; C2, IFN-γ dominant; C3, inflammatory; C4, lymphocyte depleted; and C6. TGF-b dominant. **(B)** mRNA expression levels of THY1 in different tumor clinical stages (N and stage i-iv) of LUAD patients. **(C)** Correlation analysis of THY1 and various cancer stemness features. **(D)** Correlation analysis of THY1 with immunosuppressive markers. **(E)** Correlation analysis of THY1 with immunoactivating markers. Cor, correlation.

malignant tumors and is considered a candidate marker of CSCs with highly tumorigenic and metastatic potential due to its regulation of cell-cell interactions, cell-matrix interactions, cellular adhesion, and migration (63, 64). Transcriptional analysis of mRNA profiles in $CD90^+$ esophageal CSCs showed that CD90-mediated metastasis occurs at least partially *via* the dysregulation of EMT and matrix metalloproteins (64). Strong correlations between THY1 and stemness markers were also found in LUAD according to our research (**Figure 6C**). Except for tumor cells, THY1 has also been observed in stromal cells, like ECs and CAFs, but not $CD45^+$ cells (65, 66). Co-localization of THY1 and CD31 implies a possibility that CSCs may reside in the endothelial niche, facilitate vascular formation, and receive supportive signals *via* direct contacts with ECs (67–69). THY1 can influence tumor-infiltrating immune cells. For example, physical interactions between tumor-associated macrophages and CSCs are associated with EMT and could be regulated by CD90 and EphA4 (48). Similarly, THY1 was observed to be positively correlated with immunosuppressive markers, especially TIDE score and T cell exclusion and dysfunction (**Figure 6D**). However, research on THY1 in LUAD is limited. High expressions of THY1 and CD44 influence the relapse-free survival in LUAD patients (70). In our analysis, THY1 was highly expressed in the wound-healing subtype and TGF-β-dominant subtype in LUAD patient (**Figure 6A**). These two subtypes are related to the immunosuppressive phenotype and poor prognosis. Furthermore, THY1 was associated with tumor metastasis, tumor category, and tumor stage in LUAD, which implies that THY1 has an immunosuppressive role in TME and might be responsible for immunotherapy resistance (**Figure 6C**). To verify this hypothesis, we detected the expression of THY1 in LUAD patients who received PD-1 mAb. THY1 was highly correlated with the effectiveness of PD-1 mAb (**Figure 7**). Patients in PD group had the highest expression of THY1 and SOX9, a marker of cancer stemness. These results are consistent with above analysis and strongly support the hypothesis that THY1 might be a predictive marker of immunotherapy resistance and inhibiting it may improve the effects of ICI.

However, there are still some limitations in the current research. Analysis based on a public dataset cannot confirm this result, and the number of LUAD patients receiving PD-1 mAb included in the analysis is small. Moreover, underlying mechanisms of this phenomenon need further research. Therefore, large sample size verification and well-designed biological studies are needed to further confirm our findings.

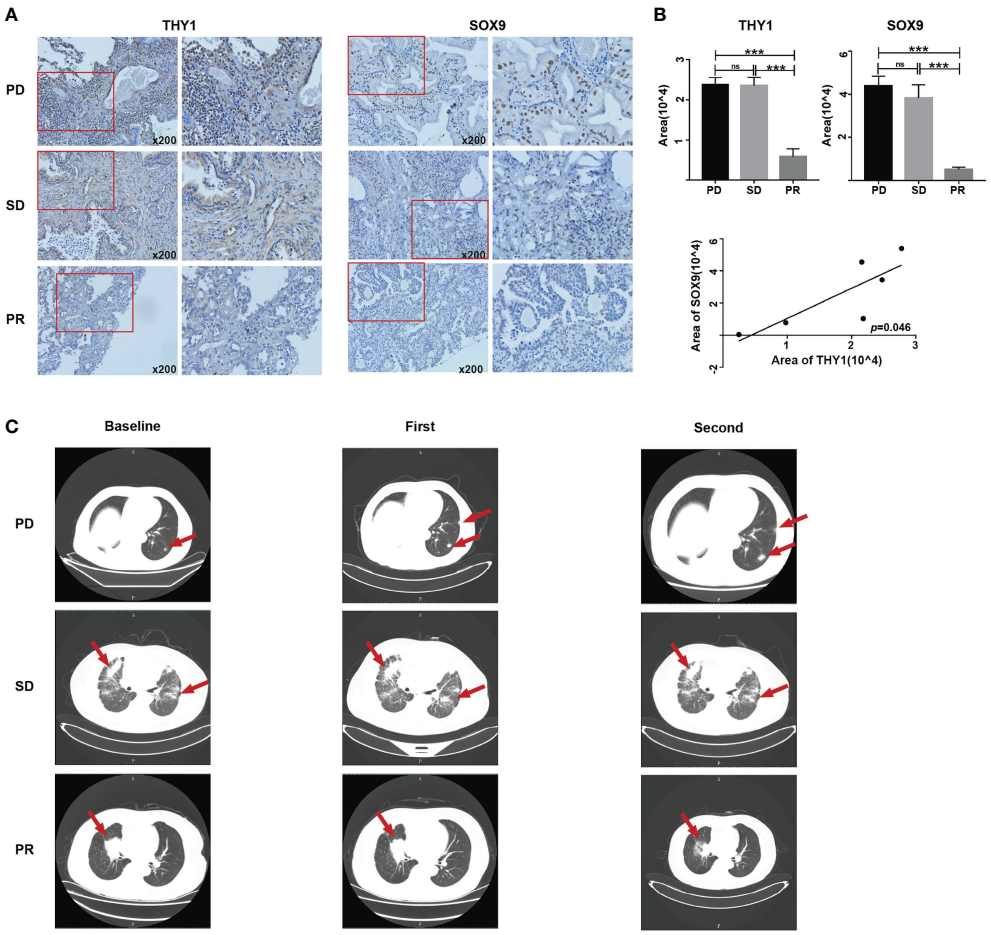

FIGURE 7 | The expression levels of THY1 are significantly associated with SOX9 and efficiency of PD-1 mAb treated LUAD patients. **(A)** Representative immunohistochemical staining of THY1 and SOX9 on tumor tissues of LUAD patient receiving PD-1 mAb treatment. Original magnification, 200×. **(B)** Statistic analysis of immunohistochemical staining score of THY1 and SOX9. Correlation analysis of the immunohistochemical staining score of THY1 and SOX9. ns, no significance; ***$p < 0.001$. **(C)** Representative CT results of LUAD patients before and after receiving PD-1 mAb treatment. PD, progressive disease; SD, stable disease; PR, partial response.

CONCLUSION

In summary, we identified nine hub genes (*COL1A1*, *COL1A2*, *COL3A1*, *COL5A1*, *COL5A2*, *COL6A3*, *EMILIN1*, *MMP2*, *THY1*) as potential participants in implying cancer stemness and immunotherapy resistance. Among them, THY1, which was verified in clinical samples, was associated with the resistance of ICI treatment and co-expressed with familiar CSCs markers. As a result, THY1 may be used as a prognostic LUAD marker; and therapy targeting THY1 may be a promising avenue in eliminating LUAD and enhancing immunotherapy.

DATA AVAILABILITY STATEMENT

Publicly available datasets were analyzed in this study. This data can be found here: https://www.cancer.gov/tcga and https://www.ncbi.nlm.nih.gov/geo/.

ETHICS STATEMENT

The studies involving human participants were reviewed and approved by the Ethics Committee of the First Affiliated Hospital of Zhengzhou University. The patients/participants provided their written informed consent to participate in this study. Written informed consent was obtained from the individual(s) for the publication of any potentially identifiable images or data included in this article.

AUTHOR CONTRIBUTIONS

YZ and LY designed the study and drafted the manuscript. WY and FL prepared the tables and figures and drafted the manuscript. All authors participated in revising the manuscript. All authors contributed to the article and approved the submitted version.

FUNDING

This work was supported by grants from the National Natural Science Foundation of China (Nos. 91942314, U1804281, 82072578), the State's Key Project of Research and Development Plan (No. 2021YFE0110600), the major public welfare projects in Henan Province (201300310400), and the outstanding young talents in science and technology innovation in Henan Province (YXK2020027).

REFERENCES

1. Dunn GP, Bruce AT, Ikeda H, Old LJ, Schreiber RD. Cancer Immunoediting: From Immunosurveillance to Tumor Escape. *Nat Immunol* (2002) 3:991–8. doi: 10.1038/ni1102-991
2. van der Woude LL, Gorris MAJ, Halilovic A, Figdor CG, de Vries IJM. Migrating Into the Tumor: A Roadmap for T Cells. *Trends Cancer* (2017) 3:797–808. doi: 10.1016/j.trecan.2017.09.006
3. Marin-Acevedo JA, Kimbrough EO, Lou Y. Next Generation of Immune Checkpoint Inhibitors and Beyond. *J Hematol Oncol* (2021) 14:45. doi: 10.1186/s13045-021-01056-8
4. Ribas A, Wolchok JD. Cancer Immunotherapy Using Checkpoint Blockade. *Science* (2018) 359:1350–55. doi: 10.1126/science.aar4060
5. Larkin J, Chiarion-Sileni V, Gonzalez R, Grob JJ, Cowey CL, Lao CD, et al. Combined Nivolumab and Ipilimumab or Monotherapy in Untreated Melanoma. *N Engl J Med* (2015) 373:23–34. doi: 10.1056/NEJMoa1504030
6. Larkin J, Chiarion-Sileni V, Gonzalez R, Grob JJ, Rutkowski P, Lao CD, et al. Five-Year Survival With Combined Nivolumab and Ipilimumab in Advanced Melanoma. *N Engl J Med* (2019) 381:1535–46. doi: 10.1056/NEJMoa1910836
7. Reck M, Rodriguez-Abreu D, Robinson AG, Hui R, Csoszi T, Fulop A, et al. Pembrolizumab Versus Chemotherapy for PD-L1-Positive Non-Small-Cell Lung Cancer. *N Engl J Med* (2016) 375:1823–33. doi: 10.1056/NEJMoa1606774
8. Mok TSK, Wu YL, Kudaba I, Kowalski DM, Cho BC, Turna HZ, et al. Pembrolizumab Versus Chemotherapy for Previously Untreated, PD-L1-Expressing, Locally Advanced or Metastatic non-Small-Cell Lung Cancer (KEYNOTE-042): A Randomised, Open-Label, Controlled, Phase 3 Trial. *Lancet* (2019) 393:1819–30. doi: 10.1016/S0140-6736(18)32409-7
9. Hellmann MD, Paz-Ares L, Bernabe Caro R, Zurawski B, Kim SW, Carcereny Costa E, et al. Nivolumab Plus Ipilimumab in Advanced Non-Small-Cell Lung Cancer. *N Engl J Med* (2019) 381(21):2020–31. doi: 10.1056/NEJMoa1910231
10. Anichini A, Perotti VE, Sgambelluri F, Mortarini R. Immune Escape Mechanisms in Non Small Cell Lung Cancer. *Cancers (Basel)* (2020) 12 (12):3605. doi: 10.3390/cancers12123605
11. Nowicki TS, Hu-Lieskovan S, Ribas A. Mechanisms of Resistance to PD-1 and PD-L1 Blockade. *Cancer J* (2018) 24:47–53. doi: 10.1097/PPO.0000000000000303
12. Lim SY, Rizos H. Immune Cell Profiling in the Age of Immune Checkpoint Inhibitors: Implications for Biomarker Discovery and Understanding of Resistance Mechanisms. *Mamm Genome* (2018) 29:866–78. doi: 10.1007/s00335-018-9757-4
13. Joyce JA, Fearon DT. T Cell Exclusion, Immune Privilege, and the Tumor Microenvironment. *Science* (2015) 348:74–80. doi: 10.1126/science.aaa6204
14. Spranger S, Gajewski TF. Tumor-Intrinsic Oncogene Pathways Mediating Immune Avoidance. *Oncoimmunology* (2016) 5:e1086862. doi: 10.1080/2162402X.2015.1086862
15. Jiang P, Gu S, Pan D, Fu J, Sahu A, Hu X, et al. Signatures of T Cell Dysfunction and Exclusion Predict Cancer Immunotherapy Response. *Nat Med* (2018) 24:1550–58. doi: 10.1038/s41591-018-0136-1
16. Presson AP, Yoon NK, Bagryanova L, Mah V, Alavi M, Maresh EL, et al. Protein Expression Based Multimarker Analysis of Breast Cancer Samples. *BMC Cancer* (2011) 11:230. doi: 10.1186/1471-2407-11-230
17. Liguori M, Digifico E, Vacchini A, Avigni R, Colombo FS, Borroni EM, et al. The Soluble Glycoprotein NMB (GPNMB) Produced by Macrophages Induces Cancer Stemness and Metastasis *via* CD44 and IL-33. *Cell Mol Immunol* (2021) 18:711–22. doi: 10.1038/s41423-020-0501-0
18. Wang C, Yang Y, Yin L, Wei N, Hong T, Sun Z, et al. Novel Potential Biomarkers Associated With Epithelial to Mesenchymal Transition and Bladder Cancer Prognosis Identified by Integrated Bioinformatic Analysis. *Front Oncol* (2020) 10:931. doi: 10.3389/fonc.2020.00931
19. Weygant N, Ge Y, Westphalen CB, Ma WW, Vega KJ. Role of the Microenvironment in Gastrointestinal Tumors. *J Oncol* (2019) 2019:2153413. doi: 10.1155/2019/2153413
20. Wei J, Barr J, Kong LY, Wang Y, Wu A, Sharma AK, et al. Glioblastoma Cancer-Initiating Cells Inhibit T-Cell Proliferation and Effector Responses by the Signal Transducers and Activators of Transcription 3 Pathway. *Mol Cancer Ther* (2010) 9:67–78. doi: 10.1158/1535-7163.MCT-09-0734
21. Smith BA, Balanis NG, Nanjundiah A, Sheu KM, Tsai BL, Zhang Q, et al. A Human Adult Stem Cell Signature Marks Aggressive Variants Across Epithelial Cancers. *Cell Rep* (2018) 24:3353–66.e5. doi: 10.1016/j.celrep.2018.08.062
22. Malta TM, Sokolov A, Gentles AJ, Burzykowski T, Poisson L, Weinstein JN, et al. Machine Learning Identifies Stemness Features Associated With Oncogenic Dedifferentiation. *Cell* (2018) 173:338–54.e15. doi: 10.1016/j.cell.2018.03.034
23. Palmer NP, Schmid PR, Berger B, Kohane IS. A Gene Expression Profile of Stem Cell Pluripotentiality and Differentiation is Conserved Across Diverse Solid and Hematopoietic Cancers. *Genome Biol* (2012) 13:R71. doi: 10.1186/gb-2012-13-8-r71
24. Miranda A, Hamilton PT, Zhang AW, Pattnaik S, Becht E, Mezheyeuski A, et al. Cancer Stemness, Intratumoral Heterogeneity, and Immune Response Across Cancers. *Proc Natl Acad Sci U.S.A.* (2019) 116:9020–29. doi: 10.1073/pnas.1818210116
25. Wu YC, Tang SJ, Sun GH, Sun KH. CXCR7 Mediates TGFbeta1-Promoted EMT and Tumor-Initiating Features in Lung Cancer. *Oncogene* (2016) 35:2123–32. doi: 10.1038/onc.2015.274
26. Saha S, Mukherjee S, Khan P, Kajal K, Mazumdar M, Manna A, et al. Aspirin Suppresses the Acquisition of Chemoresistance in Breast Cancer by Disrupting an NFkappaB-IL6 Signaling Axis Responsible for the Generation of Cancer Stem Cells. *Cancer Res* (2016) 76:2000–12. doi: 10.1158/0008-5472.CAN-15-1360
27. Singh SP, Singh R, Gupta OP, Gupta S, Brahma Bhatt ML. Immunotherapy: Newer Therapeutic Armamentarium Against Cancer Stem Cells. *J Oncol* (2020) 2020:3963561. doi: 10.1155/2020/3963561
28. Chen H, He X. The Convergent Cancer Evolution Toward a Single Cellular Destination. *Mol Biol Evol* (2016) 33:4–12. doi: 10.1093/molbev/msv212
29. Shats I, Gatza ML, Chang JT, Mori S, Wang J, Rich J, et al. Using a Stem Cell-Based Signature to Guide Therapeutic Selection in Cancer. *Cancer Res* (2011) 71:1772–80. doi: 10.1158/0008-5472.CAN-10-1735
30. Ben-Porath I, Thomson MW, Carey VJ, Ge R, Bell GW, Regev A, et al. An Embryonic Stem Cell-Like Gene Expression Signature in Poorly Differentiated Aggressive Human Tumors. *Nat Genet* (2008) 40:499–507. doi: 10.1038/ng.127
31. Bhattacharya B, Miura T, Brandenberger R, Mejido J, Luo Y, Yang AX, et al. Gene Expression in Human Embryonic Stem Cell Lines: Unique Molecular Signature. *Blood* (2004) 103:2956–64. doi: 10.1182/blood-2003-09-3314
32. Almeida LG, Sakabe NJ, deOliveira AR, Silva MC, Mundstein AS, Cohen T, et al. CTdatabase: A Knowledge-Base of High-Throughput and Curated Data on Cancer-Testis Antigens. *Nucleic Acids Res* (2009) 37:D816–9. doi: 10.1093/nar/gkn673
33. Langfelder P, Horvath S. WGCNA: An R Package for Weighted Correlation Network Analysis. *BMC Bioinf* (2008) 9:559. doi: 10.1186/1471-2105-9-559
34. Yin L, Cai Z, Zhu B, Xu C. Identification of Key Pathways and Genes in the Dynamic Progression of HCC Based on WGCNA. *Genes (Basel)* (2018) 9 (2):92. doi: 10.3390/genes9020092
35. Thorsson V, Gibbs DL, Brown SD, Wolf D, Bortone DS, Ou Yang TH, et al. The Immune Landscape of Cancer. *Immunity* (2018) 48:812–30.e14. doi: 10.1016/j.immuni.2018.03.023
36. Yang L, Li A, Liu F, Zhao Q, Ji S, Zhu W, et al. Immune Profiling Reveals Molecular Classification and Characteristic in Urothelial Bladder Cancer. *Front Cell Dev Biol* (2021) 9:596484. doi: 10.3389/fcell.2021.596484

37. Saleh R, Elkord E. Acquired Resistance to Cancer Immunotherapy: Role of Tumor-Mediated Immunosuppression. *Semin Cancer Biol* (2020) 65:13–27. doi: 10.1016/j.semcancer.2019.07.017
38. Christin JR, Wang C, Chung CY, Liu Y, Dravis C, Tang W, et al. Stem Cell Determinant SOX9 Promotes Lineage Plasticity and Progression in Basal-Like Breast Cancer. *Cell Rep* (2020) 31:107742. doi: 10.1016/j.celrep.2020.107742
39. Killock D. Signatures IMPRES and Might Turn the TIDE in Predicting Responses. *Nat Rev Clin Oncol* (2018) 15:654. doi: 10.1038/s41571-018-0088-x
40. Bao S, Wu Q, McLendon RE, Hao Y, Shi Q, Hjelmeland AB, et al. Glioma Stem Cells Promote Radioresistance by Preferential Activation of the DNA Damage Response. *Nature* (2006) 444:756–60. doi: 10.1038/nature05236
41. Diehn M, Clarke MF. Cancer Stem Cells and Radiotherapy: New Insights Into Tumor Radioresistance. *J Natl Cancer Inst* (2006) 98:1755–7. doi: 10.1093/jnci/djj505
42. Irvin DK, Jouanneau E, Duvall G, Zhang XX, Zhai Y, Sarayba D, et al. T Cells Enhance Stem-Like Properties and Conditional Malignancy in Gliomas. *PloS One* (2010) 5:e10974. doi: 10.1371/journal.pone.0010974
43. Maccalli C, Parmiani G, Ferrone S. Immunomodulating and Immunoresistance Properties of Cancer-Initiating Cells: Implications for the Clinical Success of Immunotherapy. *Immunol Invest* (2017) 46:221–38. doi: 10.1080/08820139.2017.1280051
44. Mani SA, Guo W, Liao MJ, Eaton EN, Ayyanan A, Zhou AY, et al. The Epithelial-Mesenchymal Transition Generates Cells With Properties of Stem Cells. *Cell* (2008) 133:704–15. doi: 10.1016/j.cell.2008.03.027
45. Pankova D, Jiang Y, Chatzifrangkeskou M, Vendrell I, Buzzelli J, Ryan A, et al. RASSF1A Controls Tissue Stiffness and Cancer Stem-Like Cells in Lung Adenocarcinoma. *EMBO J* (2019) 38:e100532. doi: 10.15252/embj.2018100532
46. Wang L, Zuo X, Xie K, Wei D. The Role of CD44 and Cancer Stem Cells. *Methods Mol Biol* (2018) 1692:31–42. doi: 10.1007/978-1-4939-7401-6_3
47. Dituri F, Mazzocca A, Giannelli G, Antonaci S. PI3K Functions in Cancer Progression, Anticancer Immunity and Immune Evasion by Tumors. *Clin Dev Immunol* (2011) 2011:947858. doi: 10.1155/2011/947858
48. Lu H, Clauser KR, Tam WL, Frose J, Ye X, Eaton EN, et al. A Breast Cancer Stem Cell Niche Supported by Juxtacrine Signalling From Monocytes and Macrophages. *Nat Cell Biol* (2014) 16:1105–17. doi: 10.1038/ncb3041
49. Bollyky PL, Wu RP, Falk BA, Lord JD, Long SA, Preisinger A, et al. ECM Components Guide IL-10 Producing Regulatory T-Cell (TR1) Induction From Effector Memory T-Cell Precursors. *Proc Natl Acad Sci USA* (2011) 108:7938–43. doi: 10.1073/pnas.1017360108
50. Peng DH, Rodriguez BL, Diao L, Chen L, Wang J, Byers LA, et al. Collagen Promotes Anti-PD-1/PD-L1 Resistance in Cancer Through LAIR1-Dependent CD8(+) T Cell Exhaustion. *Nat Commun* (2020) 11:4520. doi: 10.1038/s41467-020-18298-8
51. Di Tomaso T, Mazzoleni S, Wang E, Sovena G, Clavenna D, Franzin A, et al. Immunobiological Characterization of Cancer Stem Cells Isolated From Glioblastoma Patients. *Clin Cancer Res* (2010) 16:800–13. doi: 10.1158/1078-0432.CCR-09-2730
52. Dongre A, Weinberg RA. New Insights Into the Mechanisms of Epithelial-Mesenchymal Transition and Implications for Cancer. *Nat Rev Mol Cell Biol* (2019) 20:69–84. doi: 10.1038/s41580-018-0080-4
53. Hugo W, Zaretsky JM, Sun L, Song C, Moreno BH, Hu-Lieskovan S, et al. Genomic and Transcriptomic Features of Response to Anti-PD-1 Therapy in Metastatic Melanoma. *Cell* (2016) 165:35–44. doi: 10.1016/j.cell.2016.02.065
54. Zhi Y, Mou Z, Chen J, He Y, Dong H, Fu X, et al. B7H1 Expression and Epithelial-To-Mesenchymal Transition Phenotypes on Colorectal Cancer Stem-Like Cells. *PloS One* (2015) 10:e0135528. doi: 10.1371/journal.pone.0135528
55. Lee Y, Shin JH, Longmire M, Wang H, Kohrt HE, Chang HY, et al. CD44+ Cells in Head and Neck Squamous Cell Carcinoma Suppress T-Cell-Mediated Immunity by Selective Constitutive and Inducible Expression of PD-L1. *Clin Cancer Res* (2016) 22:3571–81. doi: 10.1158/1078-0432.CCR-15-2665
56. Chen L, Gibbons DL, Goswami S, Cortez MA, Ahn YH, Byers LA, et al. Metastasis is Regulated *via* microRNA-200/ZEB1 Axis Control of Tumour Cell PD-L1 Expression and Intratumoral Immunosuppression. *Nat Commun* (2014) 5:5241. doi: 10.1038/ncomms6241
57. Lou Y, Diao L, Cuentas ER, Denning WL, Chen L, Fan YH, et al. Epithelial-Mesenchymal Transition Is Associated With a Distinct Tumor Microenvironment Including Elevation of Inflammatory Signals and Multiple Immune Checkpoints in Lung Adenocarcinoma. *Clin Cancer Res* (2016) 22:3630–42. doi: 10.1158/1078-0432.CCR-15-1434
58. Almozyan S, Colak D, Mansour F, Alaiya A, Al-Harazi O, Qattan A, et al. PD-L1 Promotes OCT4 and Nanog Expression in Breast Cancer Stem Cells by Sustaining PI3K/AKT Pathway Activation. *Int J Cancer* (2017) 141:1402–12. doi: 10.1002/ijc.30834
59. Bedognetti D, Roelands J, Decock J, Wang E, Hendrickx W. The MAPK Hypothesis: Immune-Regulatory Effects of MAPK-Pathway Genetic Dysregulations and Implications for Breast Cancer Immunotherapy. *Emerg Top Life Sci* (2017) 1:429–45. doi: 10.1042/ETLS20170142
60. Lu C, Talukder A, Savage NM, Singh N, Liu K. JAK-STAT-Mediated Chronic Inflammation Impairs Cytotoxic T Lymphocyte Activation to Decrease Anti-PD-1 Immunotherapy Efficacy in Pancreatic Cancer. *Oncoimmunology* (2017) 6:e1291106. doi: 10.1080/2162402X.2017.1291106
61. Ward AB, Keeton AB, Chen X, Mattox TE, Coley AB, Maxuitenko YY, et al. Enhancing Anticancer Activity of Checkpoint Immunotherapy by Targeting RAS. *MedComm (Beijing)* (2020) 1:121–28. doi: 10.1002/mco2.10
62. Dennis JE, Esterly K, Awadallah A, Parrish CR, Poynter GM, Goltry KL. Clinical-Scale Expansion of a Mixed Population of Bone-Marrow-Derived Stem and Progenitor Cells for Potential Use in Bone-Tissue Regeneration. *Stem Cells* (2007) 25:2575–82. doi: 10.1634/stemcells.2007-0204
63. Yang ZF, Ho DW, Ng MN, Lau CK, Yu WC, Ngai P, et al. Significance of CD90+ Cancer Stem Cells in Human Liver Cancer. *Cancer Cell* (2008) 13:153–66. doi: 10.1016/j.ccr.2008.01.013
64. Tang KH, Dai YD, Tong M, Chan YP, Kwan PS, Fu L, et al. A CD90(+) Tumor-Initiating Cell Population With an Aggressive Signature and Metastatic Capacity in Esophageal Cancer. *Cancer Res* (2013) 73:2322–32. doi: 10.1158/0008-5472.CAN-12-2991
65. Sukowati CH, Anfuso B, Torre G, Francalanci P, Croce LS, Tiribelli C. The Expression of CD90/Thy-1 in Hepatocellular Carcinoma: An In Vivo and *In Vitro* Study. *PloS One* (2013) 8:e76830. doi: 10.1371/journal.pone.0076830
66. Samaniego R, Estecha A, Relloso M, Longo N, Escat JL, Longo-Imedio I, et al. Mesenchymal Contribution to Recruitment, Infiltration, and Positioning of Leukocytes in Human Melanoma Tissues. *J Invest Dermatol* (2013) 133:2255–64. doi: 10.1038/jid.2013.88
67. He J, Liu Y, Zhu T, Zhu J, Dimeco F, Vescovi AL, et al. CD90 is Identified as a Candidate Marker for Cancer Stem Cells in Primary High-Grade Gliomas Using Tissue Microarrays. *Mol Cell Proteomics* (2012) 11:M111 010744. doi: 10.1074/mcp.M111.010744
68. Zhu J, Thakolwiboon S, Liu X, Zhang M, Lubman DM. Overexpression of CD90 (Thy-1) in Pancreatic Adenocarcinoma Present in the Tumor Microenvironment. *PloS One* (2014) 9:e115507. doi: 10.1371/journal.pone.0115507
69. Lasorella A, Benezra R, Iavarone A. The ID Proteins: Master Regulators of Cancer Stem Cells and Tumour Aggressiveness. *Nat Rev Cancer* (2014) 14:77–91. doi: 10.1038/nrc3638
70. Mehta K, Moravcikova E, McFall D, Luketich JD, Pennathur A, Donnenberg AD, et al. The Mesenchymal State Predicts Poor Disease-Free Survival in Resectable Non-Small Cell Lung Cancer. *Ann Thorac Surg* (2017) 104:321–28. doi: 10.1016/j.athoracsur.2017.01.091

Conflict of Interest: The authors declare that the research was conducted in the absence of any commercial or financial relationships that could be construed as a potential conflict of interest.

Publisher's Note: All claims expressed in this article are solely those of the authors and do not necessarily represent those of their affiliated organizations, or those of the publisher, the editors and the reviewers. Any product that may be evaluated in this article, or claim that may be made by its manufacturer, is not guaranteed or endorsed by the publisher.

Copyright © 2022 Yu, Liu, Lei, Wu, Yang and Zhang. This is an open-access article distributed under the terms of the Creative Commons Attribution License (CC BY). The use, distribution or reproduction in other forums is permitted, provided the original author(s) and the copyright owner(s) are credited and that the original publication in this journal is cited, in accordance with accepted academic practice. No use, distribution or reproduction is permitted which does not comply with these terms.

frontiers in Cell and Developmental Biology

ORIGINAL RESEARCH
published: 10 February 2022
doi: 10.3389/fcell.2022.807129

Links Between N^6-Methyladenosine and Tumor Microenvironments in Colorectal Cancer

Yundi Zhang[1†], Ke Zhang[2†], Haoming Gong[3], Qin Li[4], Lajie Man[3], Qingchang Jin[3], Lin Zhang[5] and Song Li[6*]*

[1]National Cancer Center/Cancer Hospital, Chinese Academy of Medical Sciences and Peking Union Medical College, Beijing, China, [2]Department of General Practice, Qilu Hospital, Cheeloo College of Medicine, Shandong University, Jinan, China, [3]Department of Physiology, School of Basic Medical Sciences, Cheeloo College of Medicine, Shandong University, Jinan, China, [4]Department of General Surgery, Qilu Hospital, Cheeloo College of Medicine, Shandong University, Jinan, China, [5]Department of Radiation Oncology, Qilu Hospital, Cheeloo College of Medicine, Shandong University, Jinan, China, [6]Department of Medical Oncology, Qilu Hospital, Cheeloo College of Medicine, Shandong University, Jinan, China

OPEN ACCESS

Edited by:
Shaoquan Zheng,
Sun Yat-sen University Cancer Center (SYSUCC), China

Reviewed by:
Alice Hsu,
National Cancer Institute (NIH), United States
Min Xiao,
Third Affiliated Hospital of Sun Yat-sen University, China
Hongyu Li,
Sun Yat-sen University, China

***Correspondence:**
Lin Zhang
linzhangsdu@163.com
Song Li
songli@sdu.edu.cn

[†]These authors have contributed equally to this work

Specialty section:
This article was submitted to Molecular and Cellular Oncology, a section of the journal Frontiers in Cell and Developmental Biology

Received: 01 December 2021
Accepted: 19 January 2022
Published: 10 February 2022

Citation:
Zhang Y, Zhang K, Gong H, Li Q, Man L, Jin Q, Zhang L and Li S (2022) Links Between N^6-Methyladenosine and Tumor Microenvironments in Colorectal Cancer. Front. Cell Dev. Biol. 10:807129. doi: 10.3389/fcell.2022.807129

N^6-methyladenosine (m^6A) is a critical epigenetic modification for tumor malignancies, but its role in regulating the tumor microenvironments (TMEs) has not been fully studied. By integrating multiple data sets and multi-omics data, we comprehensively evaluated the m^6A "writers," "erasers," and "readers" in colorectal cancer and their association with TME characteristics. The m^6A regulator genes showed specific patterns in co-mutation, copy number variation, and expression. Based on the transcriptomic data of the m^6A regulators and their correlated genes, two types of subtyping systems, m^6A_{reg}Cluster and m^6A_{sig}Cluster, were developed. The clusters were distinct in pathways (metabolism/inflammation/extracellular matrix and interaction), immune phenotypes (immune-excluded/immune-inflamed/immune-suppressive), TME cell composition (lack immune and stromal cells/activated immune cells/stromal and immune-suppressive cells), stroma activities, and survival outcomes. We also established an m^6Ascore associated with molecular subgroups, microsatellite instability, DNA repair status, mutation burdens, and survival and predicted immunotherapy outcomes. In conclusion, our work revealed a close association between m^6A modification and TME formation. Evaluating m^6A in cancer has helped us comprehend the TME status, and targeting m^6A in tumor cells might help modulate the TME and improve tumor therapy and immunotherapy.

Keywords: colorectal cancer, immunotherapy, N^6-methyladenosine, tumor microenvironments, molecular classification

INTRODUCTION

Colorectal cancer (CRC) is a major cause of cancer-related death worldwide (Siegel et al., 2020). Limited by treatment strategies, late-stage CRC has a 5-year survival rate of approximately 10% (Kuipers et al., 2015). In recent years, the therapeutic targets shifted from tumor cells to the tumor microenvironment (TME), consisting of a heterogeneous complex of immune cells, stromal cells, and extracellular matrix (Joyce and Pollard, 2009; Quail and Joyce, 2013). The anti-TME strategies, such as anti-angiogenetic drugs, immune checkpoint inhibitors (ICIs), and their combinations (*e.g.*, ICI plus angiogenesis or chemotherapy), were beneficial to only a part of patients (Tapia Rico and Price, 2018; Eng et al., 2019; Bourhis et al., 2021). It is essential to understand and evaluate the

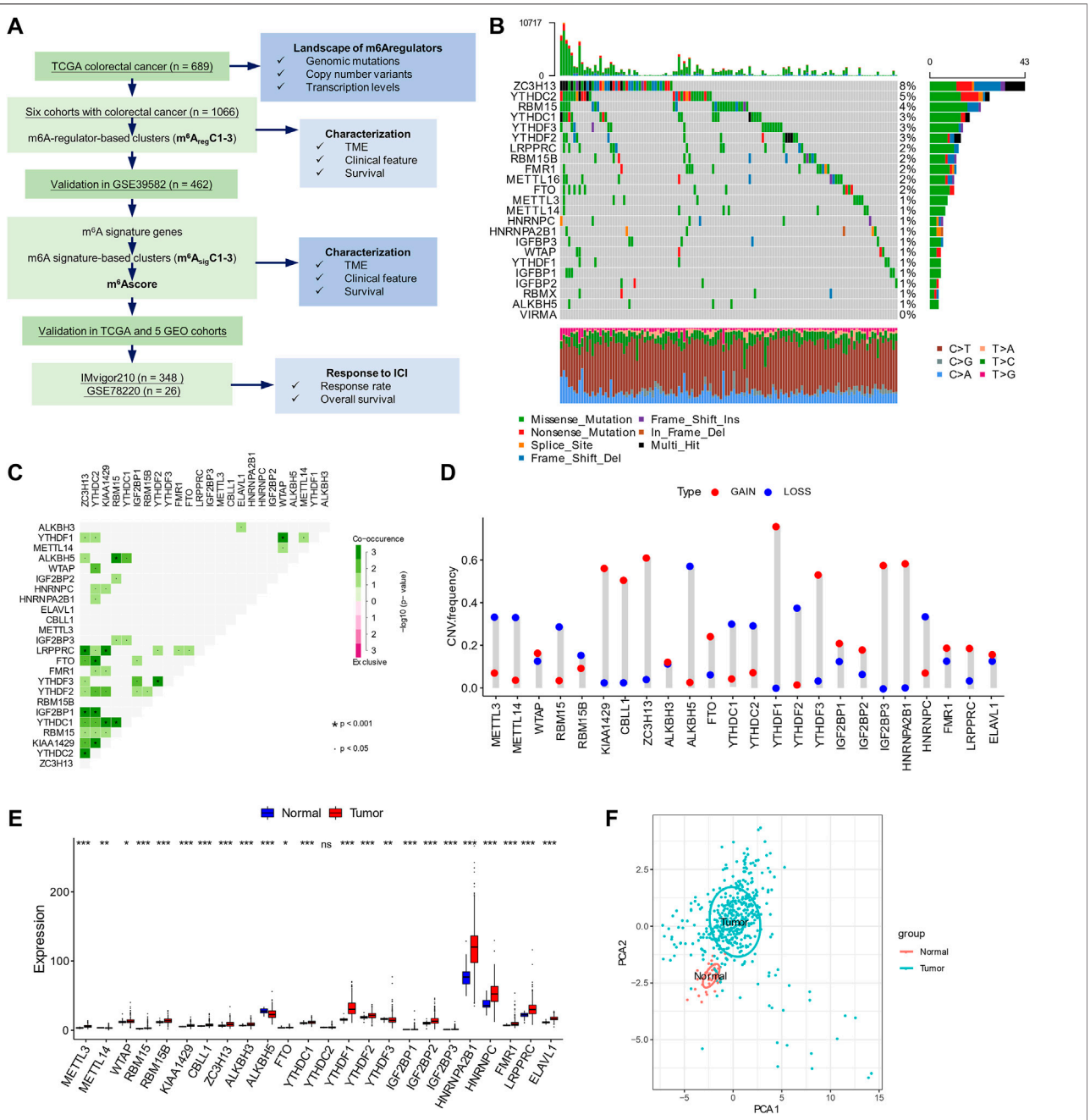

FIGURE 1 | Workflow and landscapes of m^{6}A regulators. **(A)** Workflow chart of this study with the main process. Cohorts used in this study are underlined. **(B)** Mutation rates of m^{6}A regulators in The Cancer Genome Atlas (TCGA) data set. **(C)** Mutation co-occurrence analysis of m^{6}A regulators in the TCGA data set. Co-occurrences with statistical significance ($p < 0.05$ and <0.001) are shown. **(D)** Copy number variants in the TCGA data set. **(E)** Expression levels of m^{6}A regulators in normal and tumor tissues. **(F)** Principal component analysis for RNA level of 24 m^{6}A regulators in the TCGA data set. *$p < 0.05$; **$p < 0.01$; ***$p < 0.001$.

composition and activities of TMEs to guide clinical practice when using these treatments. A case in point in CRC is the immunoscore, which is calculated based on the TME cells and helps predict responses to chemotherapy or ICIs (Angell et al., 2020; Bruni et al., 2020).

N^6-Methyladenosine (m^{6}A) is the most frequent epigenetic modification of RNA in eukaryotic cells (Frye et al., 2018). This process was reversibly regulated by its "writers," "erasers," and "readers." It has multifaceted effects in deciding RNA fates, such as RNA transcription, splicing, structure, and translation, and participates in almost all physiological and pathological bioprocesses, including cancer development (Gaikwad et al., 2020). A connection between the m^{6}A and TME is also present in some cancers. Based on multi-omics data, two

studies evaluated the landscape of m^6A modulators and found they were associated with immune cell infiltration in the TME and efficacies of ICIs in gastric cancer and renal carcinoma (Zhang et al., 2020a; Zhong et al., 2021). Recently, a specific study focusing on "writers" of four types of RNA modification and their relationship with immunotherapy efficacy was conducted in CRC (Chen et al., 2021a). However, a comprehensive study of three kinds of m^6A regulators, including "writers," "erasers," and "readers," in CRC has not been reported.

In the present study, we integrated the multi-omics and clinical data of seven CRC cohorts to evaluate the m^6A modification patterns, TME characteristics, and their associations.

MATERIALS AND METHODS

Data Sets

Level 3 data from The Cancer Genome Atlas (TCGA), including expression, mutation, copy number variations, and clinical annotation, were downloaded from the TCGA database (https://tcga-data.nci.nih.gov/tcga/). The expression data and clinical information from six CRC cohorts (GSE17536, GSE29621, GSE33113, GSE37892, GSE38832, and GSE39582) were downloaded from the Gene Expression Omnibus (GEO) database (https://www.ncbi.nlm.nih.gov/geo). The GEO data were merged by R package "dplyr" and batch normalized by R package "sva." The data from the two cohorts with ICI treatment, IMvigor210 and GSE78220, were obtained from the IMvigor210CoreBiologies package and GEO website, respectively. The study design and workflow are outlined in **Figure 1A**.

Clustering According to *N*^{6}-Methyladenosine Regulators

The gene expression data of m^6A regulators, including eight "writers" (*METTL3*, *METTL14*, *RBM15*, *RBM15B*, *WTAP*, *KIAA1429*, *CBLL1*, and *ZC3H13*), three "erasers" (*ALKBH3*, *ALKBH5*, and *FTO*), and 13 "readers" (*YTHDC1*, *YTHDC2*, *YTHDF1*, *YTHDF2*, *YTHDF3*, *IGF2BP1*, *IGF2BP2*, *IGF2BP3*, *HNRNPA2B1*, *HNRNPC*, *FMR1*, *LRPPRC*, and *ELAVL1*) were used for unsupervised clustering analysis. Cluster number determination and the following clustering were performed using the R package "ConsensusClusterPlus," with 1000 times repetition. This method was used for clustering of m^6A_{reg}Clusters in the meta-GEO cohort, single GEO cohorts, and the TCGA cohort.

Enrichment Analysis

Single-sample gene-set enrichment analysis and gene set variation analysis (GSVA) were used to quantify cell composition, immune checkpoints, $CD8^+$ T-effector signature, epithelial–mesenchymal transition (EMT), angiogenesis, pan-fibroblast TGF^2 response signature (Pan-F-TBRS), WNT targets, DNA damage repair, mismatch repair, nucleotide excision repair, DNA replication, and antigen processing and presentation. The gene sets were derived from previous studies (Rosenberg et al., 2016; Şenbabaoğlu et al., 2016; Charoentong et al., 2017; Mariathasan et al., 2018) and have been summarized in a previous paper (Zhang et al., 2020a). The gene signatures of KEGG analysis were downloaded from the Molecular Signatures Database (http://www.gsea-msigdb.org/gsea/msigdb). The R package "gsea" was used.

N^6-Methyladenosine Gene Signatures and m^6A_{sig}Clusters

The differentially expressed genes (DEGs) were identified by pairwise comparisons of three m^6A_{reg}Clusters by the "limma" R package. The overlapped genes among them were defined as m^6A gene signatures. Tumors were unsupervised and clustered into three m^6A_{sig}Clusters by the R package "ConsensusClusterPlus" according to the expression levels of the m^6A signature genes.

Immune Cell Estimation

An abundance of 22 types of infiltrated immune cells were estimated by the software CIBERSORT (Newman et al., 2015) from the transcriptome data of CRC cohorts.

Generation of m^6Ascore

The m^6Ascore was developed as follows: first, univariate Cox regression was performed for each m^6A signature gene. Second, the dimensionality of the significant genes was reduced to two by principal component analysis (PCA) using the prcomp function in R. Third, PCA1 and PCA2 were summed up to get the m^6Ascore for each patient.

Survival Analysis

Survival outcomes were compared by log-rank regression and univariable COX regression. Confounding factors of survival prognosis were analyzed by multivariable COX regression. The Kaplan–Meier method and log-rank tests were performed by the R package "survminer." The function "surv-cutpoint" was used for the determination of cut-off values in the cohorts.

Statistical Analysis

The categorical variables were compared by Chi-square or Fisher's exact tests. The continuous variables between the two groups were compared by t-test. The continuous variables among multiple groups were compared by one-way ANOVA or Kruskal–Wallis tests. The Benjamini–Hochberg methods were used to correct *p*-values for multiple testing. The survival distributions were compared by log-rank regression and COX regression. Correlations were calculated by linear regressions. The data were analyzed with the R (version 3.6.3) and R Bioconductor packages. A p-value < 0.05 was considered statistically significant.

RESULTS

Landscape of *N*^{6}-Methyladenosine Regulator Gene Mutation, Copy Number, and Expression in Colorectal Cancer

According to previous reports, a total of 24 m^6A regulators, including eight "writers" (*METTL3*, *METTL14*, *WTAP*, *RBM15*,

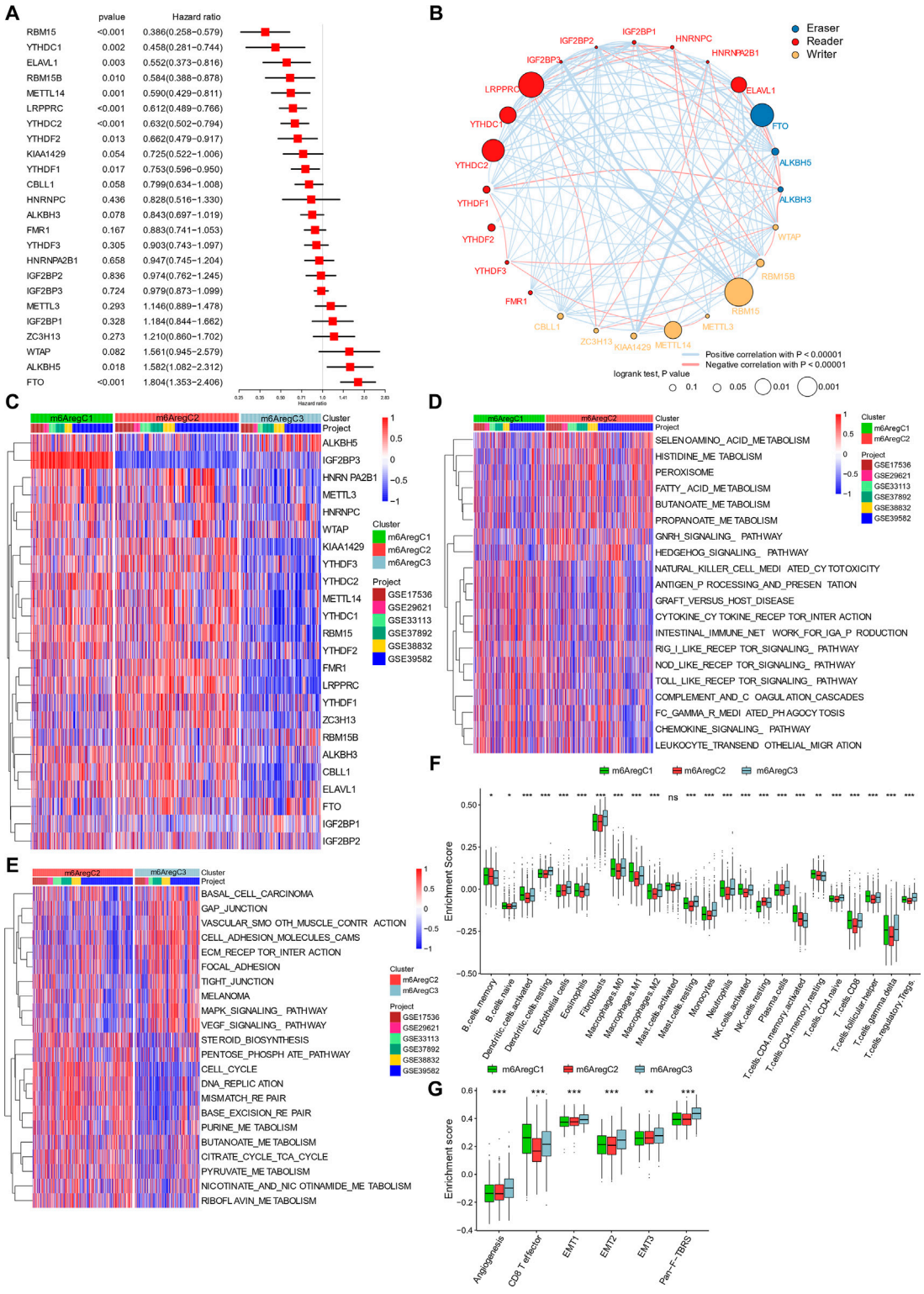

FIGURE 2 | Clustering of m^{6}A regulator–based subtypes in meta-data of six Gene Expression Omnibus cohorts. **(A)** Hazard ratio of m^{6}A regulators in predicting survivals in CRC patients. **(B)** Interaction among m^{6}A regulators in colorectal cancer. Line colors represent positive or negative correlation, and thickness represents correlation strength. Colored circles indicate the types of m^{6}A regulators, and circle sizes indicate prognostic ability. **(C)** Unsupervised clustering based on 24 m^{6}A regulators. Three clusters, termed m^{6}A$_{reg}$C1–3, were defined. **(D–E)** Differential biological pathways between m^{6}A regulator–based clusters. The pathways were quantified by gene set variation analysis enrichment and compared between C1 and C2 **(D)** and C2 and C3 **(E)**. **(F)** Abundance of tumor-infiltrating cells in three subtypes. **(G)** Enrichment of stroma-activated pathways in three subtypes. One-way ANOVA tests compared the three groups in **(F,G)**. *p < 0.05; **p < 0.01; ***p < 0.001.

RBM15B, *KIAA1429*, *CBLL1*, and *ZC3H13*), three "erasers" (*ALKBH3*, *ALKBH5*, and *FTO*), and 13 "readers" (*YTHDC1-2*, *YTHDF1-3*, *IGF2BP1-3*, *HNRNPA2B1*, *HNRNPC*, *FMR1*, *LRPPRC*, and *ELAVL1*) were included for analysis in this study (**Figure 1B**). A frequency of 24.11% had at least one mutation on the m^6A regulators. The "readers" such as *ZC3H13*, *YTHDC2*, *YTHDC1*, *YTHDF3*, and *YTHDF2* were the most frequently mutated genes, while most "writers" (except *RBM15*) and "erasers" were less mutated (**Figure 1B**). High percentages of mutation co-occurrences between 11 pairs of genes were detected ($p < 0.001$; **Figure 1C**). Most of these were "reader–writer" and "reader–eraser" co-mutations (**Figure 1C**). No mutation co-occurrence between "writers" or "erasers" was found (**Figure 1C**).

Copy number variations were significant in some m^6A regulators (**Figure 1D**, **Supplementary Figure S1**). Changes of *YTHDF1/3*, *HNRNPA2B1*, *IGF2BP2/3*, *CBLL1*, *KIAA1429*, *ZC3H13*, and *FTO* were dominantly gains, while those of *YTHDF2*, *ALKBH5*, *RBM15*, *METTL14*, *YTHDC1*, *HNRNPC*, *METTL3*, and *YTHDC2* were dominantly losses (**Figure 1D**).

The RNA levels of most m^6A regulators were significantly different between normal and tumor samples, with 22 genes upregulated and ALKBH5 downregulated in tumor tissues (**Figure 1E**). The PCA of RNA expression distinctly distinguished tumor from normal samples (**Figure 1F**).

Clustering Colorectal Cancer by *N*^{6}-Methyladenosine Regulators

A total of six GEO data sets (GSE17536, GSE29621, GSE33113, GSE37892, GSE38832, and GSE39582), including 1066 CRC patients, were pooled for survival analysis. About 11 of the 24 m^6A regulators had prognostic roles in patients by univariate Cox regression (**Figure 2A**). Among them, the "erasers" ALKBH5 and FTO had a significantly high hazard ratio of death, while nine "readers" and "writers" were associated with better survival (**Figure 2A**).

Based on prognostic values of m^6A regulator RNA levels and their intercorrelations, a correlation network was constructed (**Figure 2B**). Positive correlations were prevalent among m^6A regulators. The highest correlations were found between RBM15B and IGF2BP3, KIAA1429 and FTO, and YTHDC2 and IGF2BP1 (**Figure 2B**). Negative correlations also occurred among the three groups (**Figure 2B**). These indicated a cross talk between the m^6A regulators.

Under unsupervised clustering, the patients were classified into three subgroups with different m^6A regulator expression patterns, named m^6A regulator–based Cluster 1–3 ($m^6A_{Reg}C1$-3) (**Figure 2C** and **Supplementary Figure S2**). C1 was characterized with high expression of IGF2BP3, and C3 was characterized with overexpression of ALKBH5 and FTO and downregulation of the other regulators (**Figure 2C**, **Supplementary Figure S3**). C2 was characterized by the low expression of ALKBH5, and high levels of some readers, including FMR1, LRPPRC, HNRNPA2B1, and YTHDF1 and 3 (**Figure 2C**, **Supplementary Figure S3**). The three clusters showed different survivals, C1 and C2 showing better outcomes than C3 (**Supplementary Figure S4**).

N^6-Methyladenosine Regulator–Based Subtypes Are Different in Tumor Microenvironment Composition

Activation of pathways within the three m^6A regulator–based subtypes was analyzed by GSVA. Comparing C1 and C2, C1 was characterized by the inflammation pathways, including pattern recognition (RIG I, NOD-like, and Toll-like receptor pathways), cytotoxicity (NK cell–mediated cytotoxicity and FCγ-mediated phagocytosis), and chemokines (chemokine signaling pathway, cytokine–cytokine receptor interaction, and leukocyte transendothelial migration; **Figure 2D**), while C2 was characterized by metabolism (selenoamino acid metabolism, histidine metabolism, fatty acid metabolism, butanoate metabolism, and propanoate metabolism) (**Figure 2D**). When we compared cluster C2 and C3, C2 was still enriched in metabolic pathways (pentose phosphate pathway, purine metabolism, butanoate metabolism, citrate cycle–TCA cycle, pyruvate metabolism, and riboflavin metabolism), while C3 was characterized with cell–extracellular matrix and cell–cell connections (gap junction, focal adhesion, and tight junction; **Figure 2E**).

Due to the prominent differences in inflammation and ECM connections, we then used CIBERSORT to evaluate the TME composition in these subtypes. Like immune inflamed cancer, C1 showed activated DC cells, M1 macrophage, activated NK cells, activated $CD4^+$ T memory cells, $CD8^+$ cells, and follicular T helper cells (**Figure 2F**). C3 was highly infiltrated with stroma cells (endothelial cells, fibroblasts), resting cells (monocytes, M0 macrophages, resting DC cells, resting NK cells), and immune suppressive cells (M2 macrophages and regulatory T cells), representing an excluded immunity (**Figure 2F**). Further GSVA showed an enhanced stromal activity in C3, including signatures of angiogenesis, EMT 1–3, and pan-fibroblast TGFβ responses (**Figure 2G**). By contrast, C1 had the highest $CD8^+$ T-effector signature (**Figure 2G**). C2 was likely immune-ignored cancer due to a lack of all types of immune and stromal cells (**Figure 2G**).

N^6-Methyladenosine Regulator–Based Subtypes Are Related to Clinical Features

To validate and further explore the clinical features of the three subtypes, we used the GSE39582 cohort with detailed clinical and molecular information for further analyses. Unsupervised clustering with m^6A regulators showed an optimal reclassification of the three subgroups (**Figures 3A,B**). C1 had more CpG island methylator phenotype (CIMP) status (**Figure 3C**). C3 had less microsatellite instability (MSI) status and more chromosomal instability (CIN) status than the other two subgroups (**Figure 3B**). The mutation rates of BRAF, KRAS, and TP53 were similar among C1–3 (**Figure 3B**). With another molecular subtype system, the Cartes d'Identité des Tumeurs classification system, C1 patients were characterized with more dMMR and fewer CIN patients, while C2 had the most CIN subtypes (**Figure 3C**). In addition, Kaplan–Meier revealed survival differences among the three subtypes, with $m^6A_{reg}C3$

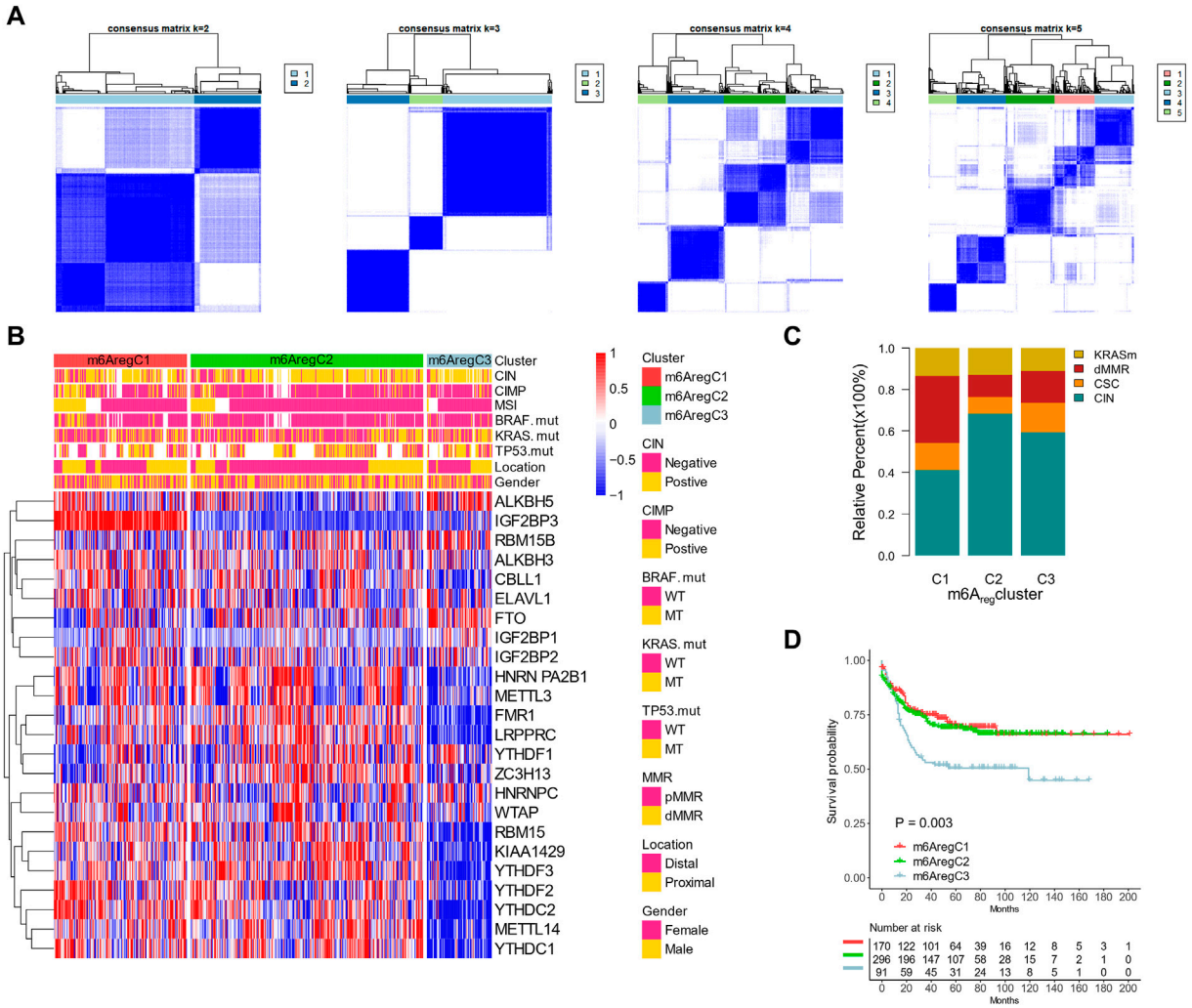

FIGURE 3 | Association between m^{6}A regulator–based subtypes and tumor microenvironment composition. **(A)** Unsupervised clustering based on m^{6}A regulators with n = 2 to 5 in the GSE39582 data set. **(B)** Clustering m^{6}A regulators into three subtypes. Distribution of molecular subtypes (chromosomal instability, CpG island methylator phenotype, and microsatellite instability) and driver mutations (KRAS, RBAF, and TP53) were provided. **(C)** Distribution of genetic change types in three m^{6}A regulator–based subtypes. **(D)** Kaplan–Meier curves of the three m^{6}A regulator–based subtypes.

with an inferior prognosis (**Figure 3D**). The validation was also performed on TCGA, which was also divided into three clusters with survival differences (**Supplementary Figure S5A** and **Supplementary Figure S5B**).

Generation of *N*^{6}-Methyladenosine–Related Gene Signatures and Signature-Based Clusters

To define a gene signature related to the m^{6}A regulators, we examined the DEGs among them. In total, 738 genes were shared among the DEGs by pairwise comparisons of three m^{6}A$_{reg}$Clusters, which were termed m^{6}A-related gene signatures (**Figure 4A**). The signature genes were enriched in pathways related to RNA metabolism, validating the roles of the m^{6}A regulators on RNA fates. They were also enriched in terms related to immunity (tumor necrosis factor, T-cell receptor signaling, innate immune responses, and antigen processing and presentation), DNA damage responses (signal transduction in response to DNA damage, regulation of responses to DNA damage stimulus, DNA recombination, nucleotide–excision repair complex, and DNA damage checkpoint), and cell cycle (e.g., cell cycle checkpoint, cell cycle arrest, and metaphase/anaphase transition of cell cycles; **Figure 4B**). These indicated that immunity, DNA damage responses, and cell cycles might be regulated by m^{6}A modification.

To further evaluate this m^{6}A regular–related signature, we performed further unsupervised clustering and got three m^{6}A signature–based clusters (m^{6}A$_{sig}$C1–3; **Figure 4C**, **Supplementary Figure S6**). The three signature-based subgroups overlapped with the m^{6}A regulator–based subgroups well (**Figures 4C,D**) and showed

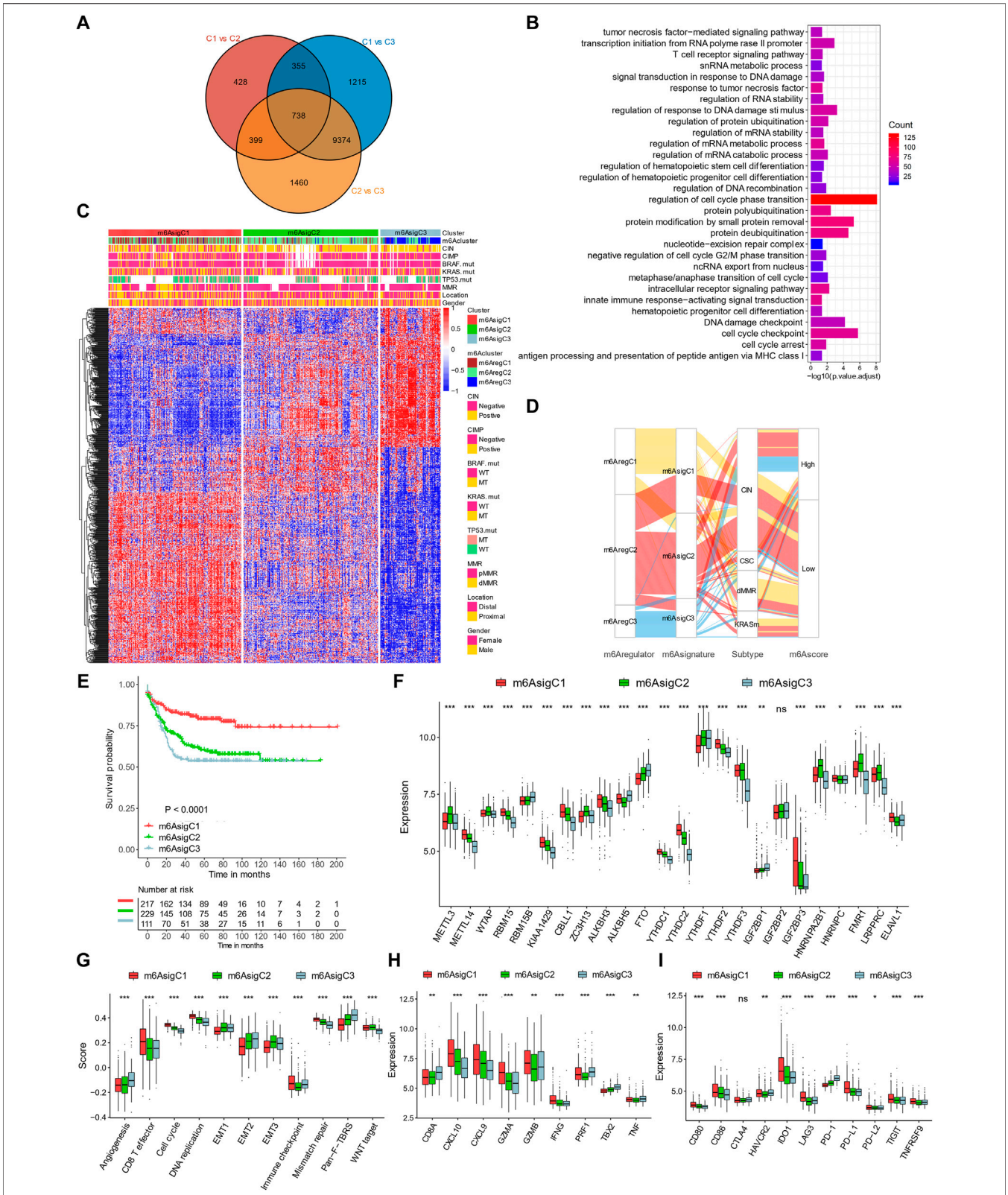

FIGURE 4 | Construction of m^{6}A signature–based clusters. **(A)** Overlaps of differential expression genes among the three m^{6}A regulator–based subtypes. **(B)** Gene Ontology enrichment of the m^{6}A signature genes. **(C)** Clustering patients based on m^{6}A signature genes into three subtypes termed m^{6}A$_{sig}$C1–3. **(D)** Alluvial diagram connecting m^{6}A$_{reg}$Clusters, m^{6}A$_{sig}$Clusters, gene mutation subtypes, and m^{6}Ascores. **(E)** Kaplan–Meier curves of the three m^{6}A signature–based subtypes. **(F)** Expression levels of m^{6}A regulators in three m^{6}A signature–based subtypes. **(G–I)** Signatures of stromal activation **(G)**, immune activation **(H)**, and immune checkpoints **(I)** in three m^{6}A signature–based subtypes. *p < 0.05; **p < 0.01; ***p < 0.001.

similar clinical features (**Figures 4C,D**). The $m^6A_{sig}C1$ showed superior survival outcomes than $m^6A_{sig}C2$ and C3 (**Figure 4E**). In addition, they had different expression levels of 23/24 m^6A regulators (**Figure 4F**).

By evaluating pre-defined signatures, we found the $m^6A_{sig}C1$ was characterized with immune activation, with high $CD8^+$ effector T cells (**Figure 4G**), transcripts of immune activation (**Figure 4H**), and immune checkpoints (**Figure 4I**). By contrast, C3 was characterized with stromal components, including angiogenesis and Pan-F-TBRS (**Figure 4G**).

Generation of *N*^{6}-Methyladenosine Score and Its Predictive Ability of Tumor Microenvironment and Clinical Feature

To quantify m^6A modification patterns, we defined an m^6Ascore based on the m^6A signature genes. The majority of $m^6A_{reg}C1$ and $m^6A_{sig}C1$ had a low m^6Ascore, while patients with high scores were mainly $m^6A_{reg}C2/3$ or $m^6A_{sig}C2/3$ (**Figure 4D**). Correspondingly, $m^6A_{reg}C1$ and $m^6A_{sig}C1$ both showed a lower median m^6Ascore than the other two groups (**Figures 5A,B**). The m^6Ascore positively correlated with stromal signatures, including endothelial cells, angiogenesis, EMT 1/2/3, Pan-F-TBRS, and fibroblasts. We found an inverse correlation with signatures of immune activation ($CD8^+$ T, antigen processing, immune checkpoints) and DNA damage responses (DNA replication, mismatch repair, nucleotide excision repair, homologous recombination, DNA damage repair, and Fanconi anemia), suggesting that a low m^6Ascore was linked with immune activation, while a high m^6Ascore was linked with stromal activation (**Figure 5C**). Consistent with this, patients with a high m^6Ascore had a low $CD8^+$ T score but enhanced activation of the stromal pathways (**Figure 5D**).

In addition, most dMMR patients had a low m^6Ascore (**Figure 4D**) and a lower median m^6Ascore than the other groups (**Figure 5E**). By contrast, the CSC-subtype patients had the highest m^6Ascore (**Figure 5E**). The m^6Ascore was also associated with many clinical features; younger patients (age <65 years), high AJCC stages, distal location, and pMMR were significantly associated with a higher m^6Ascore (**Figure 5F**). By univariate analysis, patients with a low m^6Ascore showed a remarkably superior survival than the m^6Ascore-high group, with a hazard ratio of death of 0.2474 (95% CI, 0.172–0.3561) and p-value < 0.001 (**Figure 5G**). A multivariate cox regression model was also used to exclude the confounding factors for patients' survival, including chemotherapy, gender, age, stage, tumor location, MMR status, and molecular subtype (**Figure 5H**). The results also showed that m^6Ascore is still an independent prognostic biomarker for evaluating patient outcomes, with a hazard ratio of death of 3.95 (95% CI, 2.71–5.70 and p-value < 0.001; **Figure 5H**).

Validation of *N*^{6}-Methyladenosine Score in The Cancer Genome Atlas and Five Gene Expression Omnibus Data Sets

We then validated the prognostic value of m^6Ascore in the TCGA data set. When stratifying patients by molecular subtypes, the MSI/CIMP patients showed the lowest m^6Ascore, and CIN patients showed the highest m^6Ascore (**Figure 6A**). The m^6Ascore was also associated with the MSI status and tumor stages; the MSI-H and stage I/II patients had a low m^6Ascore (**Figure 6B**).

The mutation landscapes were compared between low-m^6Ascore and high-m^6Ascore patients (**Figure 6C**). Frequencies of the top 20 mutations were similar, except of *KRAS*, which occurred more frequently in the m^6Ascore-high patients (44.7 vs. 32.6%; **Figure 6C**). The m^6Ascore and TMB were negatively correlated (**Figure 6D**), with higher TMB in low-m^6Ascore tumors than in m^6Ascore-high tumors (**Figure 6E**). Patients with a low m^6Ascore also showed prolonged survival compared to patients with a high m^6Ascore, with a hazard ratio of death of 0.5345 (95% CI, 0.3137–0.9109) and p-value 0.014 (**Figure 6F**).

We further evaluated the prognostic ability of the m^6Ascore in TCGA and the other cohorts (GSE17536, GSE29621, GSE33113, GSE37892, and GSE38832; **Figures 7A–G**) to validate its stability. The low-m^6Ascore was associated with more prolonged relapse-free survival (**Figure 7A**) and overall survival (**Figure 7B**) in the combined cohorts. The area under the curve to predict 3-year and 5-year survivals was 0.719 and 0.733, respectively (**Figures 7H,I**).

Prediction of Immunotherapy Outcomes by *N*^{6}-Methyladenosine Score

Due to the close association between the m^6A status and immunotherapy biomarkers (MSI, DDR, TMB, immune checkpoints, and stromal scores), we evaluated the ability of the m^6Ascore to predict responses to ICIs, using two cohorts (IMvigor210 and GSE78220), with ICI treatment. The IMvigor210 cohort included 310 PD-L1–treated patients, who were classified into three immune subgroups, including "ignored," "excluded," and "inflamed" (Rosenberg et al., 2016). In accordance with the former study, patients with a low m^6Ascore showed higher expression of PD-L1 (**Figure 8A**) and lower expression of stromal signatures (angiogenesis, EMT 1/2/3, and Pan-F-TBRS; **Figure 8B**) than patients with a high m^6Ascore. The "inflamed" patients showed a significantly higher m^6Ascore than the other two subtypes (**Figure 8C**). Clinically, patients with a low m^6Ascore exhibited more prolonged survival (hazard ratio, 0.58; 95% CI, 0.40–0.83; p-value = 0.003; **Figure 8D**) and a higher response rate (29.56 vs. 8.42%, **Figure 8E**) than patients with a high m^6Ascore. Correspondingly, the patients with complete and partial responses showed a significantly lower m^6Ascore than patients with stable or progressing disease (**Figure 8F**). The prognostic value of the m^6Ascore in ICI-treated patients was also validated in GSE78220, although the differences were not statistically significant due to limited sample sizes (**Figures 8G–I**).

DISCUSSION

m^6A is a critical epigenetic mechanism for regulating tumor malignancies by promoting proliferation, migration, stemness,

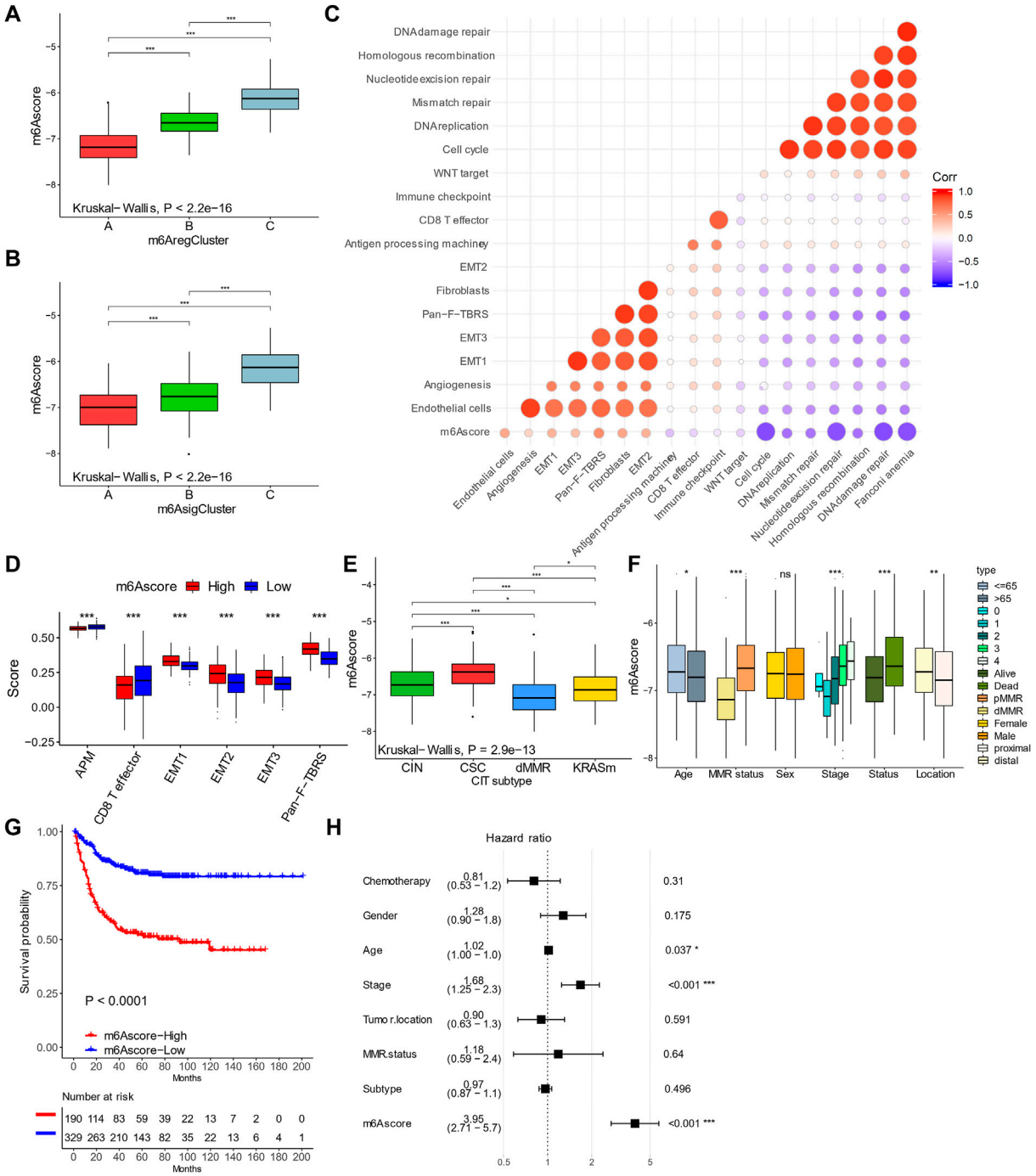

FIGURE 5 | Characteristics of m^{6}Ascore in colorectal cancer. **(A,B)** m^{6}Ascores in m^{6}A regulator–based **(A)** and signature–based **(B)** clusters. **(C)** Correlations between m^{6}Ascores and gene signatures in colorectal cancer. **(D)** Levels of stromal activity in patients with high and low m^{6}Ascores. **(E,F)** Distribution of m^{6}Ascores in patients with different genomic change subtypes and clinical features. **(G)** Kaplan–Meier curves of patients with high and low m^{6}Ascores. **(H)** Forest plot showing multivariable COX results of m^{6}Ascore and clinical features in predicting death. *p < 0.05; **p < 0.01; ***p < 0.001.

drug sensitivity, and resistance (Lan et al., 2021). Nonetheless, its role in TME regulation has been less studied. This needs a comprehensive analysis of both m^{6}A and TME components simultaneously. In this study with multi-omics data, we revealed a specific pattern in co-mutation, copy number variation, and expression of m^{6}A "writers", "erasers", and "readers" in the CRC samples. Molecular differences between colon and rectal cancers were not seen. In unsupervised clustering, two types of subtyping methods—m^{6}A$_{reg}$Cluster and m^{6}A$_{sig}$Cluster—were distinct in the pathways, TME cell

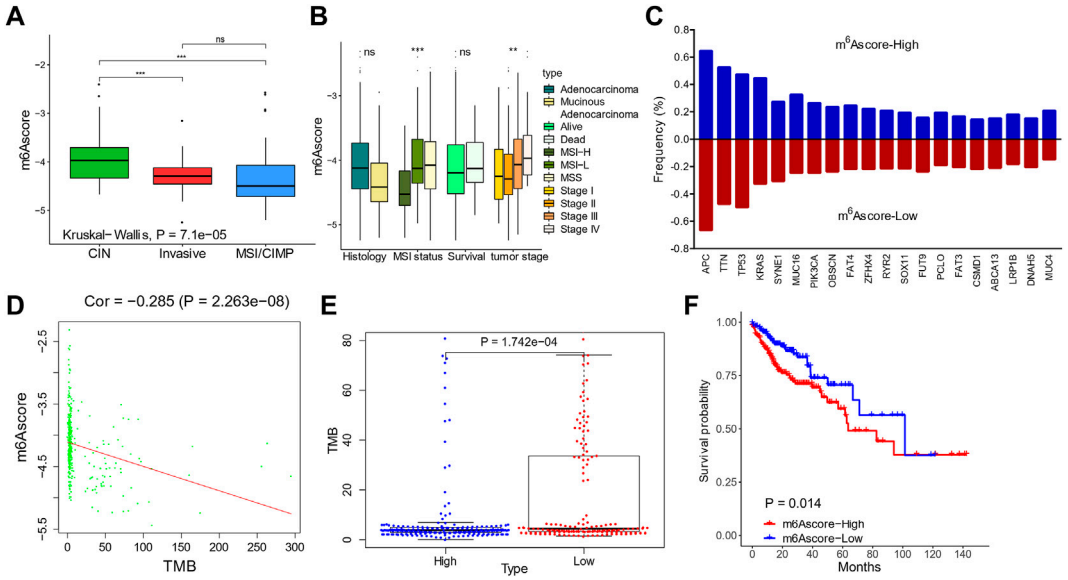

FIGURE 6 | Validation of m^{6}Ascores in The Cancer Genome Atlas (TCGA) cohorts. **(A,B)** m^{6}Ascores in patients with different molecular subtypes **(A)** and clinical features **(B)**. **(C)** Genomic mutation rates of the top 20 genes in patients with high and low m^{6}Ascores. **(D)** Correlation between m^{6}Ascores and tumor mutation burdens. **(E)** Tumor mutation burdens in patients with high and low m^{6}Ascores. **(F)** Kaplan–Meier curves of m^{6}Ascores.

composition, immune phenotypes, stroma activities, and survival outcomes (**Figure 8J**). Based on the m^{6}A regulator–related signatures, we also established an m^{6}Ascore associated with molecular subtyping, MSI and DNA repair status, tumor mutation burdens, survival, and responses to immunotherapy. These results indicated a close relationship between m^{6}A modification and anti-tumor immunity in CRC, shedding light on a future direction to evaluate and modulate TME by targeting m^{6}A.

This connection was not unique in CRC, since such phenomenon was also found in other types of cancers, such as gastric cancer (Zhang et al., 2020a). Pan-cancer analyses also showed that the m^{6}A regulators, mainly "writers" and "erasers," were differentially expressed in different TME subtypes (Zhu et al., 2020). Recently, a study focusing on "readers" of RNA modification and their relationship with TME was conducted in CRC (Chen et al., 2021a). Indeed, our study found a genetic pattern of m^{6}A regulators, especially the "readers." For example, "reader-writer" and "reader-eraser" co-mutations were frequent, while "writer-eraser" co-mutation was not found, suggesting an important role of "readers" in tumorigenesis and potential driving ability of "writer-reader" or "eraser-reader" communications. Consistent with this, many studies revealed that "writers" or "erasers" regulate tumor malignancies in a "reader"-dependent manner (Li et al., 2019). Copy numbers of two main "erasers," *ALKBH5* (loss) and *FTO* (gain), were inversely related. Accordingly, their relative expression levels compared to normal tissue were also inversely related (ALKBH5 down and FTO up). The different targets and functions between them have been reported by previous studies (Wei et al., 2018). This imbalance of "erasers" might be another mechanism in CRC tumorigenesis and targeted by specific inhibitors, such as meclofenamic acid (Huang et al., 2015). In this study, we found ALKBH5 and FTO had parallel values in predicting outcomes of patients and were both highly expressed in m^{6}AregC3, suggesting these two erasers cooperate in shaping the RNA modification patterns and impacting patients' survival.

Despite the genetic patterns that were different from normal tissues, heterogeneity of m^{6}A regulator expressions was found among patients. By clustering with m^{6}A regulators or m^{6}A signature genes, three clusters were obtained. The heterogeneity has also been observed by other groups. For example, Ogino and Goel (2008), De Sousa E Melo et al. (2013), Sadanandam et al. (2013), Marisa et al. (2013), and Roepman et al. (2014) provided their classification systems to divide the CRC patients into three to six subtypes, yet being different in methodology, inclusion criteria, and interpretations (Singh et al., 2021). In 2015, a consensus of molecular subtypes of CRC was raised based on large patient cohorts and CRC was categorized into five subtypes (Guinney et al., 2015). Different from these previous subtyping methods, which mainly used mutation and epigenetics data (Singh et al., 2021), our subtyping method was based on the transcriptomic data of limited genes (22 or 738). Our method had a strong ability to predict survival outcomes, was reliable across multiple cohorts, and overlapped with other classification systems well. These findings suggest that subtyping by m^{6}A regulators or m^{6}A signatures was meaningful and clinically feasible.

In this era of immunotherapy, exploring immune TME is becoming a hot issue these days. The initial work on ICI in CRC showed limited success (Topalian et al., 2012). The following studies discriminate the dMMR/MSI-H patients with high responses to ICI

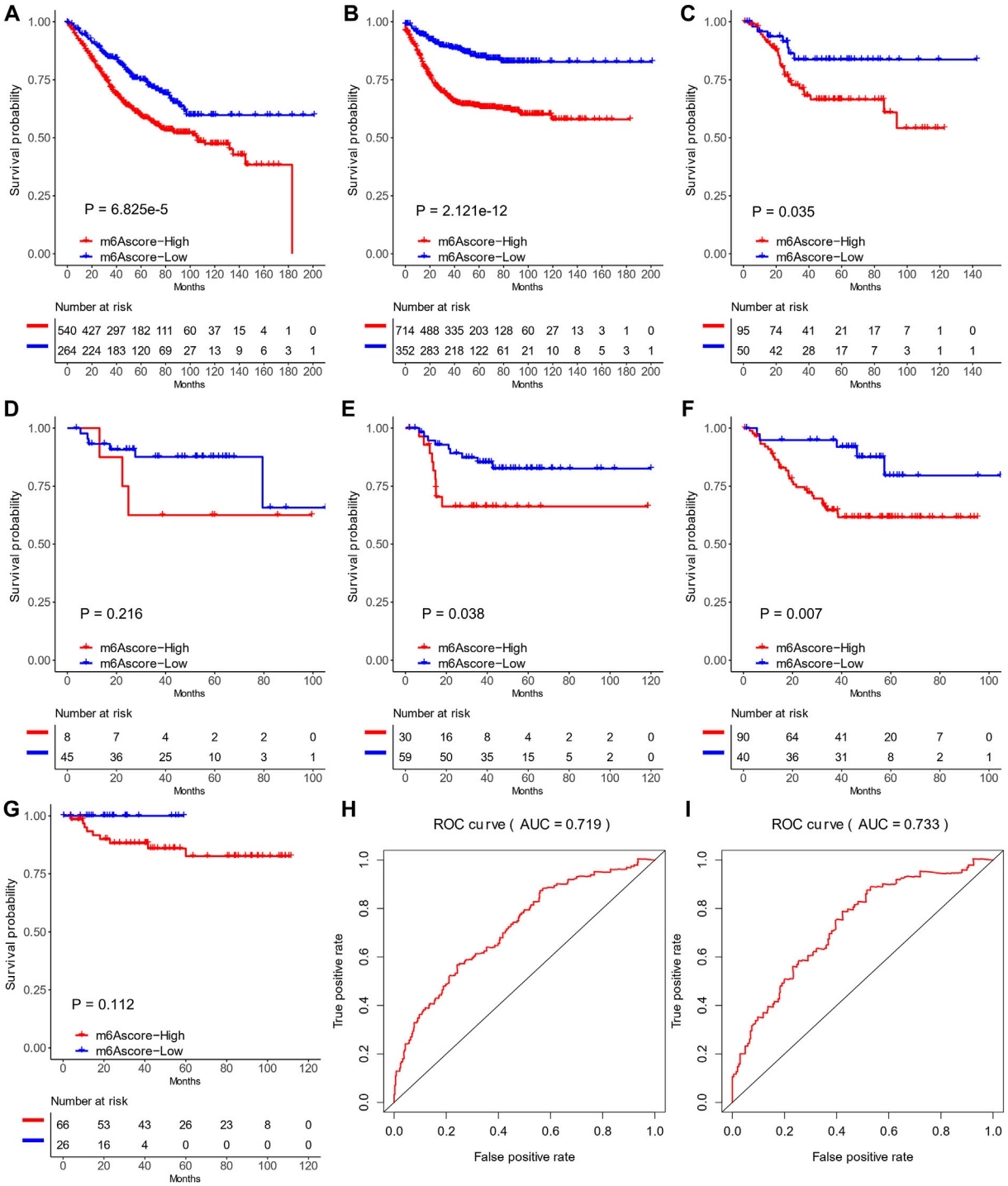

FIGURE 7 | Prediction values of m^{6}Ascores in six Gene Expression Omnibus data sets. **(A,B)** Recurrence-free survival **(A)** and overall survival **(B)** of patients with high and low m^{6}Ascores in six data sets. **(C–G)** Kaplan–Meier curves of patients with high and low m^{6}Ascores in GSE17536 **(C)**, GSE29621 **(D)**, GSE33113 **(E)**, GSE37892 **(F)**, and GSE38832 **(G)**. **(H,I)** ROC curves of recurrence-free survival **(H)** and overall survival **(I)** in six data sets.

(Chung et al., 2010; Overman et al., 2018). Combination with other therapeutic regimens, such as regorafenib, FOLFOX, or cetuximab, was also beneficial to a part of microsatellite stable (MSS) patients (Tapia Rico and Price, 2018; Eng et al., 2019; Bourhis et al., 2021). Therefore, subtyping CRC in the aspect of immune activity or TME is important for identifying "hot" tumors that may benefit from immunotherapy in MSS CRC. Becht et al. (2016) characterized the immune and stromal features of 1,388 CRC and found that

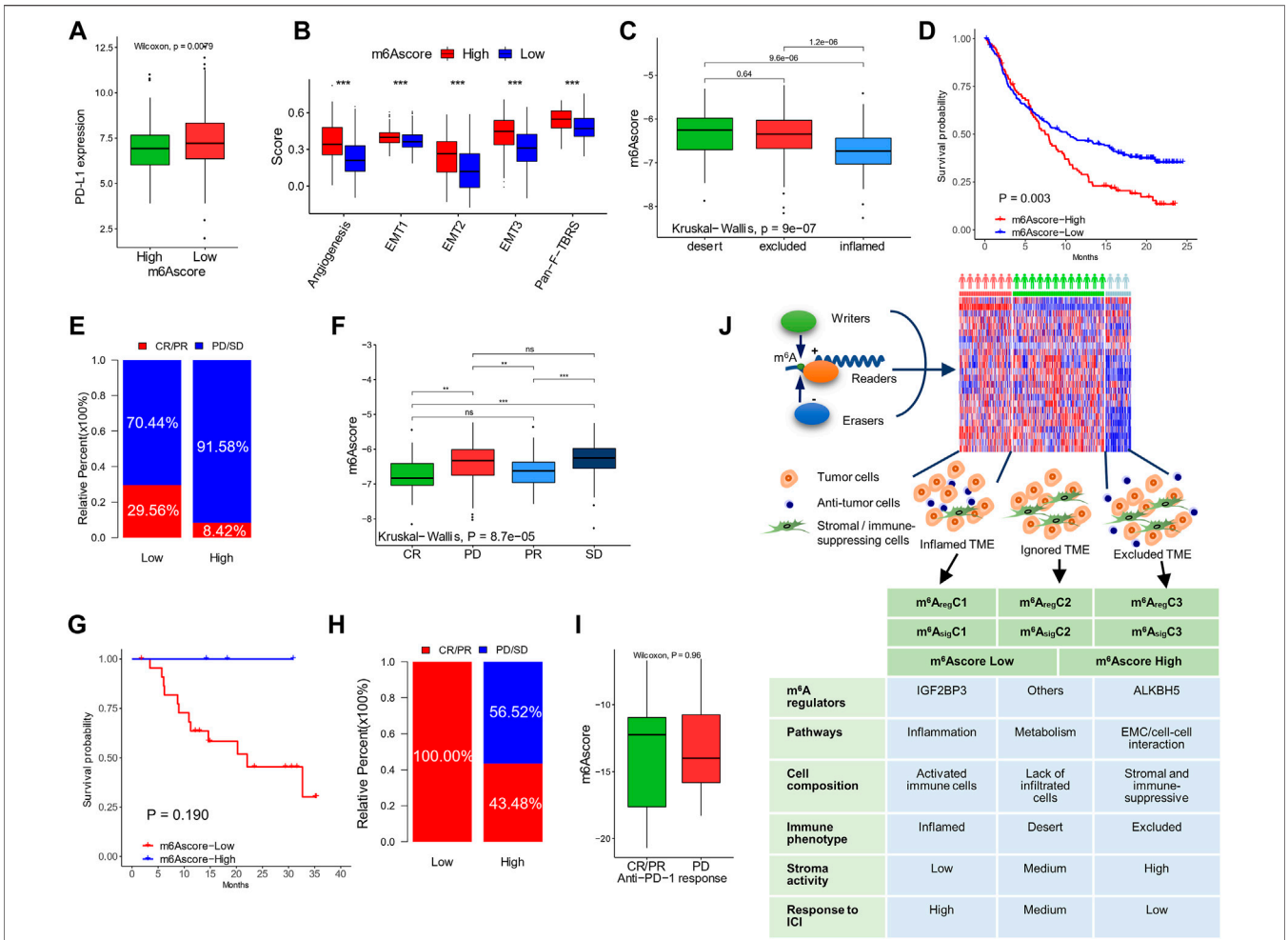

FIGURE 8 | The ability of m^{6}Ascore to predict responses to ICI. **(A)** PD-L1 expression in patients with high and low m^{6}Ascores in the IMvigor210 cohort. **(B)** Stromal activation signatures in patients with high and low m^{6}Ascores. **(C)** m^{6}Ascores in the ignored, excluded, and inflamed types of tumors. **(D,E)** Kaplan–Meier curves **(D)** and response rates **(E)** in patients with high and low m^{6}Ascores after treatment of ICI. **(F)** m^{6}Ascores in patients with different responses to ICI. Data of **(A–F)** were from the IMvigor210 cohort. **(G,H)** Kaplan–Meier curves **(G)** and response rates **(H)** to ICI in patients with high and low m^{6}Ascores after treatment of ICI in the GSE78220 cohort. **(I)** m^{6}Ascores in patients with different responses to ICI in the GSE78220 cohort. **(J)** Graphic abstract of this study (top) and characteristics of the subtypes (bottom). *$p < 0.05$; **$p < 0.01$; ***$p < 0.001$.

they were highly correlated with the CRC subtypes. Our subgroups also have a potent ability to differentiate immune orientations. The m^{6}A$_{reg}$C1 and m^{6}A$_{sig}$C1 were likely "hot" tumors, characterized by the activation of inflammation pathways, the infiltration of active immune cells, and a lack of stromal components. This subtype represents an inflammatory type of cancer that responds well to immunotherapy. The m^{6}A$_{reg}$C3 and m^{6}A$_{sig}$C3 were characterized by high stroma activity, immune-suppressive cells, and resting immune cells, which might represent the immune-exclusive type and respond to immunotherapy only in case of immunity inducers, such as chemotherapy, radiation, or target therapy (Chen and Mellman, 2017). The third subtype was characterized by metabolism pathways and a lack of immune cells, thus representing the immune-ignored tumors, which might not benefit from immunotherapy and should be treated with cytotoxic and targeting medicines (Chen and Mellman, 2017). These results provide information for personalized therapy.

Besides subtyping, a scoring system to describe CRC features and guide treatment is also an interesting issue. For example, the immunoscore is a prognostic marker in CRC based on quantifying the lymphocyte populations at tumor centers and invasive margins (Bruni et al., 2020). This score correlates with neoantigen load, WNT/β-catenin signaling pathways, gut microbiota, and, most importantly, response to ICIs (Angell et al., 2020). Our m^{6}Ascore also has a similar ability. A low m^{6}Ascore indicated defected DNA response, high CD8$^+$ T cells, low stromal activity, high mutation burdens, and prolonged survival. Although we do not have CRC cohorts treated with ICI, in two cohorts beyond CRC, the m^{6}Ascore showed a prognostic value in terms of objective response, progression-free survival, and overall survival. Our m^{6}Ascore might be used for clinical decisions as immunoscore, MSI, or RAS mutation. Signatures that predict the immune status or response to immunotherapy were also found in previous studies for CRC. For example, a STING-related prognostic score (Chen et al.,

2021b) or an immune-related gene signature (Zhang et al., 2020b) has been shown to provide insights into immunotherapy. They were derived from existing gene pools. Unlike them, our m^{6}Ascore was derived from m^{6}A modulator–related genes. Some studies also utilized m^{6}A regulators for signature construction. Zhang et al. (2020c) used two m6A readers, YTHDC2 and IGF2BP3, to construct a prognostic model in CRC. Jiang et al. (2021) found that an m^{6}A-related lncRNA-based signature was associated with tumor-infiltrating immune cells. Chong et al. (2021) used a similar method to ours to construct an m^{6}Ascore, but their study was confined to colon cancer and used fewer cohorts. These studies support our result of a close link between m^{6}A and immune TME. Unfortunately, all these signatures were only studied by association to indirect factors favoring immunotherapy, but none were validated in the CRC-ICI cohorts.

This study also has several limitations. First, the m^{6}A regulators were based on known genes with functions related to m^{6}A modification. Clustering with a more comprehensive range of m^{6}A regulators or signatures may result in better clinical values. Second, the subtyping and scoring systems were based on transcriptomic data. Methods based on PCR or immunostaining would be more feasible in clinical practice. Third, this study is retrospectively based on published cohorts. A prospective study is needed for medical translation in the future. Last, because there were no transcriptomic data from a CRC cohort with ICI treatment, we used two non-CRC cohorts for validation of m^{6}Ascore in predicting responses to immunotherapy. Such an investigation in CRC patients would be of greater value.

In conclusion, we established a connection between m^{6}A modification and the TME status in CRC. The m^{6}A-based subtyping and scoring systems stratified CRC patients with different tumor immunity, molecular features, and clinical outcomes and have potential clinical implications in clinical decisions.

DATA AVAILABILITY STATEMENT

The datasets presented in this study can be found in online repositories. The names of the repository/repositories and accession number(s) can be found in the article/ **Supplementary Material**.

AUTHOR CONTRIBUTIONS

All authors contributed to the article and approved the submission. SL and LZ designed this study. YZ and KZ performed the main parts of the analysis and wrote the manuscript. HG, QL, LM, and QJ helped with data collection and analysis. LZ revised the manuscript.

FUNDING

This work was supported by the Foundation of Shandong University Clinical Research Center (2020SDUCRCC011).

SUPPLEMENTARY MATERIAL

The Supplementary Material for this article can be found online at: https://www.frontiersin.org/articles/10.3389/fcell.2022.807129/full#supplementary-material

REFERENCES

Angell, H. K., Bruni, D., Barrett, J. C., Herbst, R., and Galon, J. (2020). The Immunoscore: Colon Cancer and beyond. *Clin. Cancer Res.* 26 (2), 332–339. doi:10.1158/1078-0432.CCR-18-1851

Becht, E., de Reyniès, A., Giraldo, N. A., Pilati, C., Buttard, B., Lacroix, L., et al. (2016). Immune and Stromal Classification of Colorectal Cancer Is Associated with Molecular Subtypes and Relevant for Precision Immunotherapy. *Clin. Cancer Res.* 22 (16), 4057–4066. doi:10.1158/1078-0432.CCR-15-2879

Bourhis, J., Stein, A., Paul de Boer, J., Van Den Eynde, M., Gold, K. A., Stintzing, S., et al. (2021). Avelumab and Cetuximab as a Therapeutic Combination: An Overview of Scientific Rationale and Current Clinical Trials in Cancer. *Cancer Treat. Rev.* 97, 102172. doi:10.1016/j.ctrv.2021.102172

Bruni, D., Angell, H. K., and Galon, J. (2020). The Immune Contexture and Immunoscore in Cancer Prognosis and Therapeutic Efficacy. *Nat. Rev. Cancer* 20 (11), 662–680. doi:10.1038/s41568-020-0285-7

Charoentong, P., Finotello, F., Angelova, M., Mayer, C., Efremova, M., Rieder, D., et al. (2017). Pan-cancer Immunogenomic Analyses Reveal Genotype-Immunophenotype Relationships and Predictors of Response to Checkpoint Blockade. *Cel Rep.* 18 (1), 248–262. doi:10.1016/j.celrep.2016.12.019

Chen, D. S., and Mellman, I. (2017). Elements of Cancer Immunity and the Cancer-Immune Set point. *Nature* 541 (7637), 321–330. doi:10.1038/nature21349

Chen, H., Yao, J., Bao, R., Dong, Y., Zhang, T., Du, Y., et al. (2021). Cross-talk of Four Types of RNA Modification Writers Defines Tumor Microenvironment and Pharmacogenomic Landscape in Colorectal Cancer. *Mol. Cancer* 20 (1), 29. doi:10.1186/s12943-021-01322-w

Chen, S.-Y., Chen, S., Feng, W., Li, Z., Luo, Y., and Zhu, X. (2021). A STING-Related Prognostic Score Predicts High-Risk Patients of Colorectal Cancer and Provides Insights into Immunotherapy. *Ann. Transl Med.* 9 (1), 14. doi:10.21037/atm-20-2430

Chong, W., Shang, L., Liu, J., Fang, Z., Du, F., Wu, H., et al. (2021). m6A Regulator-Based Methylation Modification Patterns Characterized by Distinct Tumor Microenvironment Immune Profiles in colon cancerA Regulator-Based Methylation Modification Patterns Characterized by Distinct Tumor Microenvironment Immune Profiles in colon Cancer. *Theranostics* 11 (5), 2201–2217. doi:10.7150/thno.52717

Chung, K. Y., Gore, I., Fong, L., Venook, A., Beck, S. B., Dorazio, P., et al. (2010). Phase II Study of the Anti-cytotoxic T-Lymphocyte-Associated Antigen 4 Monoclonal Antibody, Tremelimumab, in Patients with Refractory Metastatic Colorectal Cancer. *Jco* 28 (21), 3485–3490. doi:10.1200/JCO.2010.28.3994

De Sousa E Melo, F., Wang, X., Jansen, M., Fessler, E., Trinh, A., de Rooij, L. P. M. H., et al. (2013). Poor-prognosis colon Cancer Is Defined by a Molecularly Distinct Subtype and Develops from Serrated Precursor Lesions. *Nat. Med.* 19 (5), 614–618. doi:10.1038/nm.3174

Eng, C., Kim, T. W., Bendell, J., Argilés, G., Tebbutt, N. C., Di Bartolomeo, M., et al. (2019). Atezolizumab with or without Cobimetinib versus Regorafenib in Previously Treated Metastatic Colorectal Cancer (IMblaze370): a Multicentre, Open-Label, Phase 3, Randomised, Controlled Trial. *Lancet Oncol.* 20 (6), 849–861. doi:10.1016/S1470-2045(19)30027-0

Frye, M., Harada, B. T., Behm, M., and He, C. (2018). RNA Modifications Modulate Gene Expression during Development. *Science* 361 (6409), 1346–1349. doi:10.1126/science.aau1646

Gaikwad, S. M., Phyo, Z., Arteaga, A. Q., Gorjifard, S., Calabrese, D. R., Connors, D., et al. (2020). A Small Molecule Stabilizer of the MYC G4-Quadruplex

Induces Endoplasmic Reticulum Stress, Senescence and Pyroptosis in Multiple Myeloma. *Cancers* 12 (10), 2952. doi:10.3390/cancers12102952

Guinney, J., Dienstmann, R., Wang, X., de Reyniès, A., Schlicker, A., Soneson, C., et al. (2015). The Consensus Molecular Subtypes of Colorectal Cancer. *Nat. Med.* 21 (11), 1350–1356. doi:10.1038/nm.3967

Huang, Y., Yan, J., Li, Q., Li, J., Gong, S., Zhou, H., et al. (2015). Meclofenamic Acid Selectively Inhibits FTO Demethylation of m6A over ALKBH5. *Nucleic Acids Res.* 43 (1), 373–384. doi:10.1093/nar/gku1276

Jiang, Z., Zhang, Y., Chen, K., Yang, X., and Liu, J. (2021). Integrated Analysis of the Immune Infiltrates and PD-L1 Expression of N6-Methyladenosine-Related Long Non-coding RNAs in Colorectal Cancer. *Ijgm* 14, 5017–5028. doi:10.2147/IJGM.S327765

Joyce, J. A., and Pollard, J. W. (2009). Microenvironmental Regulation of Metastasis. *Nat. Rev. Cancer* 9 (4), 239–252. doi:10.1038/nrc2618

Kuipers, E. J., Grady, W. M., Lieberman, D., Seufferlein, T., Sung, J. J., Boelens, P. G., et al. (2015). Colorectal Cancer. *Nat. Rev. Dis. Primers* 1, 15065. doi:10.1038/nrdp.2015.65

Lan, Q., Liu, P. Y., Bell, J. L., Wang, J. Y., Hüttelmaier, S., Zhang, X. D., et al. (2021). The Emerging Roles of RNA m6A Methylation and Demethylation as Critical Regulators of Tumorigenesis, Drug Sensitivity, and Resistance. *Cancer Res.* 81 (13), 3431–3440. doi:10.1158/0008-5472.CAN-20-4107

Li, T., Hu, P.-S., Zuo, Z., Lin, J.-F., Li, X., Wu, Q.-N., et al. (2019). METTL3 Facilitates Tumor Progression via an m6A-igf2bp2-dependent Mechanism in Colorectal Carcinoma. *Mol. Cancer* 18 (1), 112. doi:10.1186/s12943-019-1038-7

Mariathasan, S., Turley, S. J., Nickles, D., Castiglioni, A., Yuen, K., Wang, Y., et al. (2018). TGFβ Attenuates Tumour Response to PD-L1 Blockade by Contributing to Exclusion of T Cells. *Nature* 554 (7693), 544–548. doi:10.1038/nature25501

Marisa, L., de Reyniès, A., Duval, A., Selves, J., Gaub, M. P., Vescovo, L., et al. (2013). Gene Expression Classification of colon Cancer into Molecular Subtypes: Characterization, Validation, and Prognostic Value. *Plos Med.* 10 (5), e1001453. doi:10.1371/journal.pmed.1001453

Newman, A. M., Liu, C. L., Green, M. R., Gentles, A. J., Feng, W., Xu, Y., et al. (2015). Robust Enumeration of Cell Subsets from Tissue Expression Profiles. *Nat. Methods* 12 (5), 453–457. doi:10.1038/nmeth.3337

Ogino, S., and Goel, A. (2008). Molecular Classification and Correlates in Colorectal Cancer. *J. Mol. Diagn.* 10 (1), 13–27. doi:10.2353/jmoldx.2008.070082

Overman, M. J., Lonardi, S., Wong, K. Y. M., Lenz, H.-J., Gelsomino, F., Aglietta, M., et al. (2018). Durable Clinical Benefit with Nivolumab Plus Ipilimumab in DNA Mismatch Repair-Deficient/Microsatellite Instability-High Metastatic Colorectal Cancer. *Jco* 36 (8), 773–779. doi:10.1200/JCO.2017.76.9901

Quail, D. F., and Joyce, J. A. (2013). Microenvironmental Regulation of Tumor Progression and Metastasis. *Nat. Med.* 19 (11), 1423–1437. doi:10.1038/nm.3394

Roepman, P., Schlicker, A., Tabernero, J., Majewski, I., Tian, S., Moreno, V., et al. (2014). Colorectal Cancer Intrinsic Subtypes Predict Chemotherapy Benefit, Deficient Mismatch Repair and Epithelial-to-mesenchymal Transition. *Int. J. Cancer* 134 (3), 552–562. doi:10.1002/ijc.28387

Rosenberg, J. E., Hoffman-Censits, J., Powles, T., van der Heijden, M. S., Balar, A. V., Necchi, A., et al. (2016). Atezolizumab in Patients with Locally Advanced and Metastatic Urothelial Carcinoma Who Have Progressed Following Treatment with Platinum-Based Chemotherapy: a Single-Arm, Multicentre, Phase 2 Trial. *The Lancet* 387 (10031), 1909–1920. doi:10.1016/S0140-6736(16)00561-4

Sadanandam, A., Lyssiotis, C. A., Homicsko, K., Collisson, E. A., Gibb, W. J., Wullschleger, S., et al. (2013). A Colorectal Cancer Classification System that Associates Cellular Phenotype and Responses to Therapy. *Nat. Med.* 19 (5), 619–625. doi:10.1038/nm.3175

Şenbabaoğlu, Y., Gejman, R. S., Winer, A. G., Liu, M., Van Allen, E. M., de Velasco, G., et al. (2016). Tumor Immune Microenvironment Characterization in clear Cell Renal Cell Carcinoma Identifies Prognostic and Immunotherapeutically Relevant Messenger RNA Signatures. *Genome Biol.* 17 (1), 231. doi:10.1186/s13059-016-1092-z

Siegel, R. L., Miller, K. D., and Jemal, A. (2020). Cancer Statistics, 2020. *CA A. Cancer J. Clin.* 70 (1), 7–30. doi:10.3322/caac.21590

Singh, M. P., Rai, S., Pandey, A., Singh, N. K., and Srivastava, S. (2021). Molecular Subtypes of Colorectal Cancer: An Emerging Therapeutic Opportunity for Personalized Medicine. *Genes Dis.* 8 (2), 133–145. doi:10.1016/j.gendis.2019.10.013

Tapia Rico, G., and Price, T. J. (2018). Atezolizumab for the Treatment of Colorectal Cancer: the Latest Evidence and Clinical Potential. *Expert Opin. Biol. Ther.* 18 (4), 449–457. doi:10.1080/14712598.2018.1444024

Topalian, S. L., Hodi, F. S., Brahmer, J. R., Gettinger, S. N., Smith, D. C., McDermott, D. F., et al. (2012). Safety, Activity, and Immune Correlates of Anti-PD-1 Antibody in Cancer. *N. Engl. J. Med.* 366 (26), 2443–2454. doi:10.1056/NEJMoa1200690

Wei, J., Liu, F., Lu, Z., Fei, Q., Ai, Y., He, P. C., et al. (2018). Differential m6A, m6Am, and m1A Demethylation Mediated by FTO in the Cell Nucleus and Cytoplasm. *Mol. Cel* 71 (6), 973–985. doi:10.1016/j.molcel.2018.08.011

Zhang, B., Wu, Q., Li, B., Wang, D., Wang, L., and Zhou, Y. L. (2020). m6A Regulator-Mediated Methylation Modification Patterns and Tumor Microenvironment Infiltration Characterization in Gastric cancerA Regulator-Mediated Methylation Modification Patterns and Tumor Microenvironment Infiltration Characterization in Gastric Cancer. *Mol. Cancer* 19 (1), 53. doi:10.1186/s12943-020-01170-0

Zhang, J., Cheng, X., Wang, J., Huang, Y., Yuan, J., and Guo, D. (2020). Gene Signature and Prognostic merit of M6a Regulators in Colorectal Cancer. *Exp. Biol. Med. (Maywood)* 245 (15), 1344–1354. doi:10.1177/1535370220936145

Zhang, X., Zhao, H., Shi, X., Jia, X., and Yang, Y. (2020). Identification and Validation of an Immune-Related Gene Signature Predictive of Overall Survival in colon Cancer. *Aging* 12 (24), 26095–26120. doi:10.18632/aging.202317

Zhong, J., Liu, Z., Cai, C., Duan, X., Deng, T., and Zeng, G. (2021). m6A Modification Patterns and Tumor Immune Landscape in clear Cell Renal Carcinoma. *J. Immunother. Cancer* 9 (2), e001646. doi:10.1136/jitc-2020-001646

Zhu, J., Xiao, J., Wang, M., and Hu, D. (2020). Pan-Cancer Molecular Characterization of m6A Regulators and Immunogenomic Perspective on the Tumor Microenvironment. *Front. Oncol.* 10, 618374. doi:10.3389/fonc.2020.618374

Conflict of Interest: The authors declare that the research was conducted in the absence of any commercial or financial relationships that could be construed as a potential conflict of interest.

Publisher's Note: All claims expressed in this article are solely those of the authors and do not necessarily represent those of their affiliated organizations, or those of the publisher, the editors, and the reviewers. Any product that may be evaluated in this article, or claim that may be made by its manufacturer, is not guaranteed or endorsed by the publisher.

Copyright © 2022 Zhang, Zhang, Gong, Li, Man, Jin, Zhang and Li. This is an open-access article distributed under the terms of the Creative Commons Attribution License (CC BY). The use, distribution or reproduction in other forums is permitted, provided the original author(s) and the copyright owner(s) are credited and that the original publication in this journal is cited, in accordance with accepted academic practice. No use, distribution or reproduction is permitted which does not comply with these terms.

frontiers in Cell and Developmental Biology

ORIGINAL RESEARCH
published: 23 February 2022
doi: 10.3389/fcell.2022.833938

HSPA6 is Correlated With the Malignant Progression and Immune Microenvironment of Gliomas

Xiang Zhou[1,2†], Qiankun Ji[1†], Qin Li[3†], Peng Wang[1], Guowen Hu[1], Feng Xiao[1], Minhua Ye[1], Li Lin[1], Min Luo[1], Yun Guo[1], Weijun Wu[1], Kai Huang[1,4] and Hua Guo[1,5*]*

[1]Departments of Neurosurgery, The Second Affiliated Hospital of Nanchang University, Nanchang, China, [2]Departments of Neurosurgery, The Fifth Affiliated Hospital of Nanchang University, Fuzhou, China, [3]Departments of General Practice, The Fifth Affiliated Hospital of Nanchang University, Fuzhou, China, [4]Institute of Neuroscience, Nanchang University, Nanchang, China, [5]Jiangxi Key Laboratory of Neurological Tumors and Cerebrovascular Diseases, Nanchang, China

OPEN ACCESS

Edited by:
Pranav Gupta,
Albert Einstein College of Medicine, United States

Reviewed by:
Swapna Chaudhuri,
Chittaranjan National Cancer Institute, India
Regina M. Graham,
University of Miami Health System, United States
Hui Cao,
Second People's Hospital of Hunan Province, China

***Correspondence:**
Hua Guo
ndefy02014@ncu.edu.cn
Kai Huang
kaihuang@ncu.edu.cn

†These authors have contributed equally to this work

Specialty section:
This article was submitted to Cancer Cell Biology, a section of the journal Frontiers in Cell and Developmental Biology

Received: *12 December 2021*
Accepted: *09 February 2022*
Published: *23 February 2022*

Citation:
Zhou X, Ji Q, Li Q, Wang P, Hu G, Xiao F, Ye M, Lin L, Luo M, Guo Y, Wu W, Huang K and Guo H (2022) HSPA6 is Correlated With the Malignant Progression and Immune Microenvironment of Gliomas. Front. Cell Dev. Biol. 10:833938. doi: 10.3389/fcell.2022.833938

Gliomas are primary intracranial space lesions with a high mortality rate. Current treatments for glioma are very limited. Recently, immunotargeted therapy of the glioma microenvironment has been developed. Members of the 70 kDa heat shock protein (HSP70) family are involved in the development of many tumors and immunity. HSPA6 protein belongs to the HSP70 family; However, the biological function of this protein in gliomas has yet to be evaluated. In the present study, a range of analyses, involving protein networks, survival, clinical correlation, and function, revealed that the expression of HSPA6 was negatively correlated with clinical prognosis and closely associated with immunity, invasion, and angiogenesis. Quantitative protein analysis confirmed that HSPA6 was expressed at high levels in patients with glioblastoma. Vitro experiments further verified that HSPA6 enhanced the malignant progression of glioma cells by promoting proliferation, invasion and anti-apoptosis. We also found that HSPA6 was closely correlated with genomic variations and tumor microenvironment. Collectively, we demonstrated that HSPA6 may represent a new therapeutic target to improve the prognosis of patients with gliomas.

Keywords: gliomas, heat shock protein family A member 6 (HSPA6), malignancy, experimental validation, tumor immune microenvironment

INTRODUCTION

Gliomas are derived from a group of neuroepithelial tumors that are collectively known as brain gliomas and account for the vast majority of primary brain tumors, the most common form of primary intracranial tumors (Ostrom et al., 2014). The grading system developed by the World Health Organization (WHO) classifies gliomas from grade I (the least malignant and associated with the best prognosis) to grade IV (the most malignant and associated with the worst prognosis); of these, glioblastoma has the highest degree of malignancy and mortality (Weller et al., 2015; Jiang et al., 2016; Zhang et al., 2019). Currently, the most dominant treatments include surgery, temozolomide-targeted chemotherapy, and radiotherapy; however, the clinical prognosis of undergoing treatment for patients with these modalities is not satisfactory (Stupp et al., 2017). The investigation of gene/protein regulatory networks and immunopathological mechanisms may identify novel molecular targeting and immunotherapeutic methods for glioma (Eckel-Passow et al., 2015). Therefore,

the discovery of new and effective treatments for glioma still remains an unprecedented challenge.

When heat shock proteins (HSPs) were first discovered in the salivary gland cells of *drosophila* in 1962 (Ritossa, 1962), they represent a widely distributed and highly conserved family of proteins that are usually expressed under a variety of physiological and stressful conditions, including carcinogenesis. According to molecular weight, the superfamily of HSPs can be divided into HSP110, HSP90, HSP70, HSP60, HSP40, and a family of small HSPs (Carper et al., 1987; Lindquist and Craig, 1988). Particularly, the ability of the HSP70 family to protect cells against stress (Beere and Green, 2001; Daugaard et al., 2007; Yang et al., 2012) is so efficient that they represent the most prominently conserved family (Oehler et al., 2000). Among humans, a total of 15 members of the HSP70 family have been detected at different sites, thus suggesting a range of biological functions that are location-specific (Daugaard et al., 2007; Rosenzweig et al., 2019). HSP70s are highly expressed in many tumors and promote the progression of malignancy by inhibiting apoptosis, evading cellular senescence-mechanisms, disturbing immunity, and promoting angiogenesis (Albakova et al., 2020). HSP70 proteins are highly expressed in a wide range of malignant cancers and are negatively correlated with a poor clinical prognosis (Calderwood et al., 2006). Beaman et al. (Beaman et al., 2014) proved that the expression of HSP70 genes and proteins were positively correlated with glioma grade. However, the mechanisms that mediate the effects of HSP70 family members on glioma remain unknown.

While investigating potential prognostic markers for human glioma, Sun et al. (Sun et al., 2020a) constructed a protein-protein interaction (PPI) network and found that nine heat shock proteins (DNAJA4, DNAJC6, DNAJC12, HSPA6, HSP90B1, DNAJB1, DNAJB6, DNAJC10, and SERPINH1) were differentially expressed; of these, only HSPA6 belonged to the HSP70 family. Other studies indicated that HSPA6 may have an inhibitory effect on bladder cancer (Shin et al., 2017), lung cancer (Wang et al., 2020a), and triple-negative breast cancer (Hahm et al., 2021; Shen et al., 2021), while may be relevant to the early recurrence of human hepatocellular carcinoma (Yang et al., 2015). However, the functional effect of HSPA6 in the progression of glioma remains unclear. In another study, Wang et al. confirmed that the expression of RAB34 conferred a poor prognosis in high-grade glioma patients; furthermore, HSPA6 was positively correlated with the expression of RAB34 (Wang et al., 2015). Therefore, we hypothesized that HSPA6 may be a reliable prognostic biomarker for gliomas.

In this study, we reconfirmed the core role of HSPA6, a member of the HSP70 family, by constructing a PPI network. To further predict the prognostic significance of HSPA6 in gliomas, bioinformatics analysis was performed on three different independent cohorts, including The Cancer Genome Atlas (TCGA), the Chinese Glioma Genome Atlas (CGGA), and the GSE16011 dataset. Survival analysis showed that the subgroup of patients of high levels of HSPA6 expression had a shorter survival time. This result indicated that HSPA6 may represent a biomarker of poor prognosis for patients with glioma and was further confirmed by analysis of time-dependent receiver operating characteristic (ROC) curves and area under the curve (AUC) values. By analyzing the clinical data, we detected relationships between HSPA6 expression and isocitrate dehydrogenase (IDH) mutations, 1p19q co-deletion, grade, gender, and age. These clinically relevant indicators were significant in both univariate cox regression analysis and multivariate cox regression analysis. Gene Ontology-Biological Process (GO-BP) analysis, Kyoto Encyclopedia of Genes and Genomes (KEGG) enrichment analysis, and Gene Set Variation Analysis (GSVA), further suggested that HSPA6 was mainly correlated with immunity, invasion, and angiogenesis. Compared with para-carcinoma tissues, HSPA6 protein was highly expressed in clinical samples of glioma. Furthermore, functional *in vitro* experiments verified the effect of HSPA6 in glioma cells and its possible pathway mechanism. Finally, comprehensive analyses revealed significant differences in genomic variation, tumor-infiltrating immune cells (TIICs), different tumor microenvironments (TMEs), immune checkpoint (ICP) expression levels, when compared between patients with low and high expression levels of HSPA6.

METHODS

Figure 1 depicts a flow diagram that describes the overall research process.

Dataset Acquisition and Pre-Processing

We downloaded all databases featuring patients with gliomas from the TCGA (https://portal.gdc.cancer.gov/) and CGGA (www.cgga.org.cn/) databases. We also downloaded information from a microarray dataset (GSE16011) from the Gene Expression Omnibus (GEO; www.ncbi.nlm.nih.gov/geo/) database. The inclusion criteria for glioma samples were as follows: 1) patients with WHO grade II, III, or IV glioma, 2) patients diagnosed with glioma with OS of more than 30 days, 3) patients with expression data, and 4) patients with primary glioma. After filtering, we acquired 1810 glioma samples (TCGA, n = 608; CGGA, n = 965; GSE16011, n = 237). The clinical classifications for the 1810 patients with glioma are shown in **Supplementary Table S1**. We transformed the transcripts per kilobase million (TPM) values from RNA-sequencing data, and robust multichip averaging analysis (RMA)-processed values from the GSE16011, by log2 to allow easier comparison. In addition, somatic mutations and frequency data were processed by the maftools package within R (www.r-project.org/). The GISTIC algorithm was taken to process amplification and deletion of copy number variation (CNV) data (Mermel et al., 2011). In total, 29 immune-associated gene sets, and 28 key ICPs, as based on the methods described by Auslander (Auslander et al., 2018).

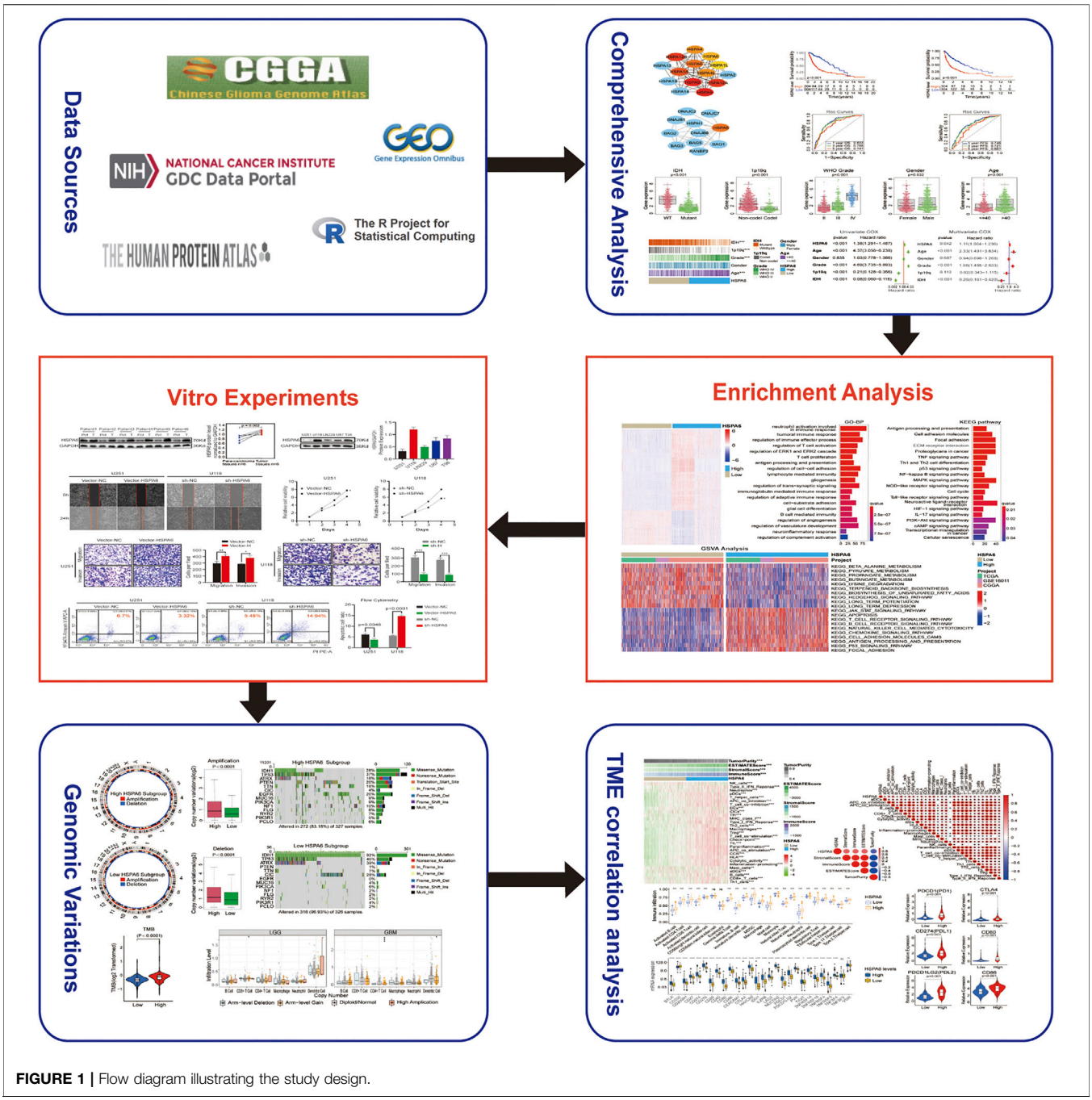

FIGURE 1 | Flow diagram illustrating the study design.

Six paired frozen specimens, along with para-carcinoma tissues, were acquired from surgical patients with gliomas at The Second Affiliated Hospital of Nanchang University between 2016 and 2021.

Protein Network Construction

We generated a protein-protein interaction (PPI) network for the HSP superfamily; this network featured 182 members (**Supplementary Table S2**). Next, we analyzed the HSP70 family, and HSPA6, by applying STRING version 11.5 and Cytoscape software (Otasek et al., 2019). To further investigate the core role of HSPA6 within the HSP70 family, we calculated the top 10 networks through using CytoHubba tool in Cytoscape; these were ranked by the MCC method.

Clinicopathological Characteristics

On the grounds of the median expression level of HSPA6 in the three cohorts, patients with gliomas were separated into groups exhibiting low and high of HSPA6 expression levels.

The Kaplan-Meier method was used to perform survival analysis and evaluate the outcomes of patients with gliomas in both the low and high expression subgroups; two parameters were generated: overall survival (OS) and progression-free survival (PFS; only for the TCGA cohort). ROC curves and AUC values were utilized to evaluate the predictive accuracy of HSPA6 expression across the three cohorts. Next, we exploited the survival package in R to perform univariate Cox regression analysis of five clinical factors (age, gender, grade, 1p19q co-deletion, IDH mutations), and HSPA6 expression, to identify key factors related to survival. Meanwhile, multivariate Cox regression analysis was utilized to differentiate the independent factors of prognosis.

Functional Enrichment Analysis

The limma package in R was utilized to distinguish differentially expressed genes (DEGs) between the glioma patients showing low and high expression levels of HSPA6 expression; DEGs were defined by a log2 (fold change) >1 and $p < 0.05$ (Ritchie et al., 2015). GO-BP and KEGG enrichment analyses (based on $p < 0.05$ and $q < 0.05$) were then carried out on the DEGs using the clusterProfiler, enrichplot, and ggplot2 packages in R (Yu et al., 2012). In order to identify significantly enriched pathways in the patients' subgroups showing low and high of HSPA6 expression, we performed GSVA in the R environment, incorporating—data from c2.cp. kegg. v6.2. symbols in the Molecular Signatures Database (MSigDB) database (www.gsea-msigdb.org/gsea/msigdb/) (Hänzelmann et al., 2013). KEGG analysis identified significant pathways between the two groups of patients on the basis of an adjusted $p < 0.05$, a log2 (fold change) >0.1, and a false discovery rate (FDR) < 0.05.

Ethical Approval

The research protocol was approved by the medical ethics committee of the Second Affiliated Hospital of Nanchang University. We got written informed consent from all the patients with glioma.

Cell Culture and Plasmid Transfection

Several human glioma cell lines (U251, U87, U118, LN229, and T98) were purchased from the Shanghai Institute of Biosciences and Cell Resources Center (Shanghai, China). These cell lines were cultured with Dulbecco's modified Eagle medium (DMEM, ATCC) and 10% fetal bovine serum (Gibco, United States) at 37°C and 5% CO_2. When the cell density reached 70–90%, we performed transfection using Lipofectamine 3000 (Thermo Fisher, L3000075, United States). Cells were then separated into an overexpressed group, a knockdown transfection group, a negative control (NC) group, and an untreated group. The primers used to create the HSPA6 overexpression plasmid were as follows: forward, 5′-TACCGGACTCAGATCTCGAGCGCCACC ATGCAGGCCCCACGGGAGCTC-3′; reverse, 5′-GATCCC GGGCCCGCGGTACCGTATCAACCTCCTCAATGATGG GGC-3′. The HSPA6 siRNA sequence was: 5′-GCCCGCCTA TTTCAATGACTC-3′.

Western Blotting

Proteins from cells and tissues lysates were extracted with radioimmunoprecipitation (RIP) assay buffer (Solarbio, Beijing, China) containing proteinase inhibitors. The primary antibodies were HSPA6 (1:1000, DF8465 affinity Biosciences Ltd., China), the PI3K (1:2000, 67071-1-Ig, Proteintech, China), AKT1 (1:1000, 10176-2-AP, Proteintech), pAKT1-S473 (1:2000, 66444-1-Ig, Proteintech), pAKT1-T308 (1:1000, #4056S, Cell Signaling Technology, United States), and glyceraldehyde-3-phosphate dehydrogenase (GAPDH) (1:20000, 60004-1-lg, Proteintech, Wuhan, China). Then, 10% sodium dodecyl sulfate polyacrylamide gel electrophoresis (SDS-PAGE) was utilized to separate the proteins which were then transferred onto a 0.22 μm PVDF membrane (Millipore, MA, United States). Next, the membranes were blocked with 5% skimmed milk. Subsequently, the membranes were incubated with primary antibodies overnight at 4°C followed by appropriate secondary antibodies (anti-rabbit antibody, 1:5000, SA00001-2; anti-mouse antibody, 1:5000, SA00001-1; Proteintech, Wuhan, China). Finally, the membranes were incubated with enhanced chemiluminescence (ECL) substrate (Thermo Fisher Scientific, MA, United States) and developed with GV6000M imaging system (GelView 6000pro).

Quantitative Real-Time PCR and RNA-seq

Total RNA was extracted from cells with the Simply P Total RNA Extraction Kit (Bioflux, Beijing, China) and reverse-transcribed to synthesize cDNA with HiScript III-RT SuperMix for qPCR (Vazyme, Nanjing, China). The ChamQ Universal SYBR qPCR Master Mix (Vazyme, Nanjing, China) was used for qPCR. The primer sequences were as follows: the forward HSPA6 primer was 5′-CGTGCCCGCCTATTTCAATG-3′, the reverse HSPA6 primer was 5′-AAAAATGAGCACGTTGCGCT-3′; the forward GAPDH primer was 5′- GAACGGGAAGCTCAC TGG-3′, and the reverse GAPDH primer was 5′- GCCTGC TTCACCACCTTCT-3′. RNA samples were sequenced and analyzed by Shanghai Majorbio Biotechnology Co., Ltd. and Shanghai Jiayin Biotechnology Co.; Ltd. RNA-seq transcriptome library was prepared following TruSeqTM RNA sample preparation Kit from Illumina (San Diego, CA, United States) using 1 μg of total RNA.

Wound-Healing Assay

5×10^5 cells were cultivated per well on six-well plates using the medium described above; the plates were covered and incubated overnight. The following morning, the cells were scratched in the middle of the cell plate with the tip of a 200 μl sterile spear to form artificial wounds. After washing with phosphate-buffered saline, the medium was replaced with a serum-free medium. At 0 and 24 h, images of the wound-healing process were photographed with an inverted Leica microscope with a ×10 objective lens. The width of the scratch edge was compared at different time points.

Cell Proliferation Assays

Cell Counting Kit-8 (CCK-8) assays were used to detect cell proliferation. In total, 5×10^3 viable cells were cultivated per well on 96-well plates in a final volume of 100 μl DMEM containing 10% FBS. After 1–4 days of incubation, 10 μl of CCK8 (Beyotime, C0037, China) was added and incubated for 4 h. Then, the absorbance values of the plates were measured at a wavelength of 450 nm.

Transwell Migration and Invasion Assays

Transwell chambers (Corning, United States) were used to execute migration and invasion assays. First, the chambers were covered with 500 μg/ml of Matrigel (Corning, 356234 United States). Then, 5×10^5 cells were added to each well and cultured with 200 μl of serum-free medium. Then, the lower chamber of the Transwell was covered with 600 μl of DEME with 10% fetal bovine serum. After 24 h of incubation, the non-invasive cells on the upper surface of the chambers were wiped away with a cotton swab. The chambers were then fixed with 4% paraformaldehyde (Solarbio, P1110, China) for 30 min, dyed with Crystal Violet stain (Solarbio, G1075, China) 30 min, and then imaged with a Leica Microsystems D-35578 microscope (five random 200 × fields per well). The migration assay was performed in the same ways as the invasion assay, except that the bottom of the chamber did not contain Matrigel.

Flow Cytometry

A YF 647A-Annexin V and PI Apoptosis Kit (Yuheng Biotechnology Co., Ltd., Suzhou, China) was used for flow cytometry. First, the medium was gathered in a 15 ml centrifuge tube. Then, the cells were digested in trypsin-free EDTA, centrifuged with the retained medium at 300 g for 5 min at 4°C, and the supernatant was discarded. Next, the cells were resuspended and centrifuged twice with PBS under the same conditions. The supernatant was then got rid of and the cells were gently resuspended in 100 μl of binding buffer. Then, 5 μl of YF647A-Annexin V and 5 μl of PI were mixed to each tube and incubated at 24°C in the dark for 15 min. At last, the experiment was detected with a CytoFLEX LX system (Beckman Coulter, United States); data were analyzed with CytExpert software.

A Comparison of CNV and TMB Between Patients With Low and High Expression Levels of HSPA6

The RCircos tool was used to identify and visualize meaningful genomic amplifications and deletions (Zhang et al., 2013). Maftools and GenVisR were used to calculate and compare mutation categories, and the frequencies of mutant genes, between groups of patients with low and high expression levels of HSPA6 (Skidmore et al., 2016; Mayakonda et al., 2018). Considering that this is a newly developing biomarker for immunotherapy, we compared the tumor mutational burden (TMB) between the two different subgroups of HSPA6 expression. In addition, the correlations between CNV for HSPA6 and six TIICs were investigated employing the Tumor Immune Estimation Resource (TIMER).

Single Sample Gene Set Enrichment Analysis

The enrichment of 29 TIICs in the tumor microenvironment (TME) was quantitatively analyzed by single sample gene set enrichment analysis (ssGSEA). To further detect the association between HSPA6, TME, and TIICs, we used the corrplot package. The ssGSEA algorithm was then exploited to estimate the abundance of each TIIC.

Immune Checkpoint Analysis

We identified 28 immune checkpoints (ICPs) from the existing literature (Auslander et al., 2018). To investigate the correlations between the expression of HSPA6 and these 28 ICPs, we used Sanger box (http://sangerbox.com/Tool). In addition, we investigated the correlation between paired immune checkpoints (PD1, CD274, PDL2; CTLA4, CD80, and CD86) and HSPA6 expression.

Statistical Analysis

Comparisons between two groups were calculated by the student's t-test. Comparisons between three or more groups were computed by the Kruskal–Wallis test. Clinicopathological correlation analysis was performed with Pearson's Chi-squared test. Kaplan-Meier analysis and Cox regression were performed for univariate and multivariate prognosis analyses, respectively. Two-sided tests were used for all statistical analyses and all analyses were carried out with GraphPad Prism 8 (GraphPad Software, Inc.), SPSS Statistics, version 25 (IBM, United States), and R programming, version 4.0.3. $p < 0.05$ was regarded as being statistical significance. All the vitro experiments were performed independently and in triplicate.

RESULTS

HSPA6 may be a Poor Prognostic Biomarker for Patients With Glioma

A total of 182 members of the HSP superfamily exist in the human genome. We employed Cytoscape to construct a PPI network for members of the HSP superfamily and found that HSPA6 is directly or indirectly associated with 47 family proteins (**Supplementary Figure S1A**). According to the correlation score (**Supplementary Table S3**), the core network map showed that the core function of HSPA6 protein ranked sixth in the HSP70 family (**Figure 2A**). We also found several chaperone proteins of the BAG family that were associated with HSPA6 (**Figure 2B**). Patients with gliomas were split into low and high subgroups based on their median expression level of HSPA6 in the TCGA. Survival analyses showed that HSPA6 may be a poor prognostic biomarker for OS and PFS (**Figures 2C,E**). Similar trends were identified for the CGGA and GSE16011 cohorts (**Supplementary Figures S1B,D**). Furthermore, the AUCs for 1-, 3-, and 5-year OS were 0.803, 0.788, and 0.747, respectively; while the AUCs for 1-,

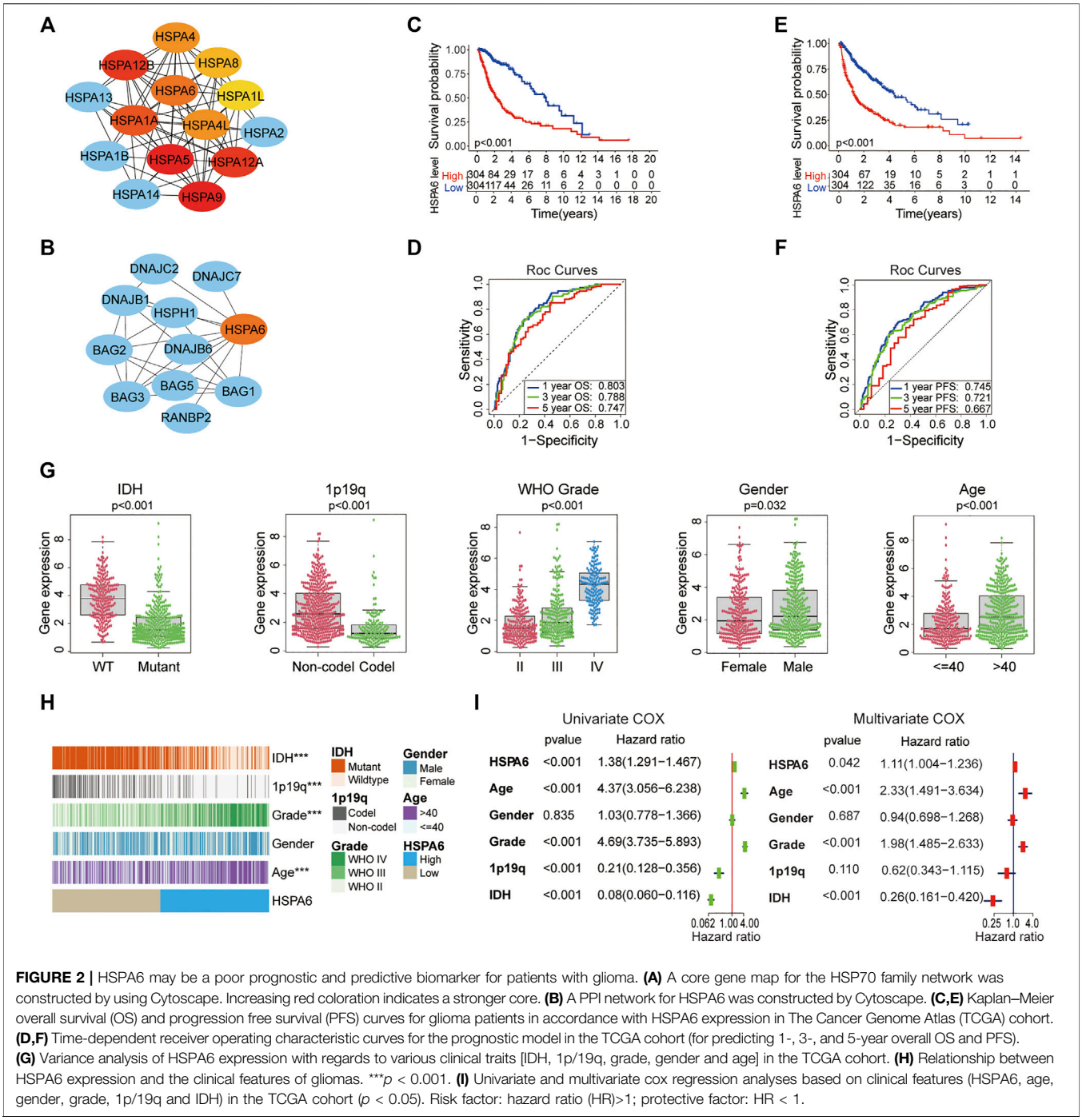

FIGURE 2 | HSPA6 may be a poor prognostic and predictive biomarker for patients with glioma. **(A)** A core gene map for the HSP70 family network was constructed by using Cytoscape. Increasing red coloration indicates a stronger core. **(B)** A PPI network for HSPA6 was constructed by Cytoscape. **(C,E)** Kaplan–Meier overall survival (OS) and progression free survival (PFS) curves for glioma patients in accordance with HSPA6 expression in The Cancer Genome Atlas (TCGA) cohort. **(D,F)** Time-dependent receiver operating characteristic curves for the prognostic model in the TCGA cohort (for predicting 1-, 3-, and 5-year overall OS and PFS). **(G)** Variance analysis of HSPA6 expression with regards to various clinical traits [IDH, 1p/19q, grade, gender and age] in the TCGA cohort. **(H)** Relationship between HSPA6 expression and the clinical features of gliomas. ***$p < 0.001$. **(I)** Univariate and multivariate cox regression analyses based on clinical features (HSPA6, age, gender, grade, 1p/19q and IDH) in the TCGA cohort ($p < 0.05$). Risk factor: hazard ratio (HR)>1; protective factor: HR < 1.

3-, and 5-year PFS were 0.745, 0.721 and 0.667, respectively ($p < 0.01$ for all) (**Figures 2D,F**). In the CGGA cohort, the AUCs for 1-, 3-, and 5-year OS were 0.714, 0.765, and 0.768, respectively. In the GSE16011 dataset, the AUCs for 1-, 3-, and 5-year OS were 0.751, 0.817, and 0.738 (**Supplementary Figures S1C,E**).

Therefore, the correlation between HSPA6 expression and clinical factors (IDH, 1p/19q, grade, gender, and age) were investigated in the three cohorts. As shown in **Figures 2G,H**, in the TCGA cohort, the clinical traits differed significantly between patients with high levels of HSPA6 expression and patients with low levels of HSPA6 expression ($p < 0.001$), except for gender in the TCGA cohort. Similar presentations were also obtained in the CGGA and GSE16011 cohorts (**Supplementary Figures S2A,B,E,F**).

Moreover, Univariate and multivariate Cox regression analyses displayed that HSPA6 was meaningfully statistical significance ($p < 0.05$) which was associated with clinical outcome in patients with gliomas in the three cohorts

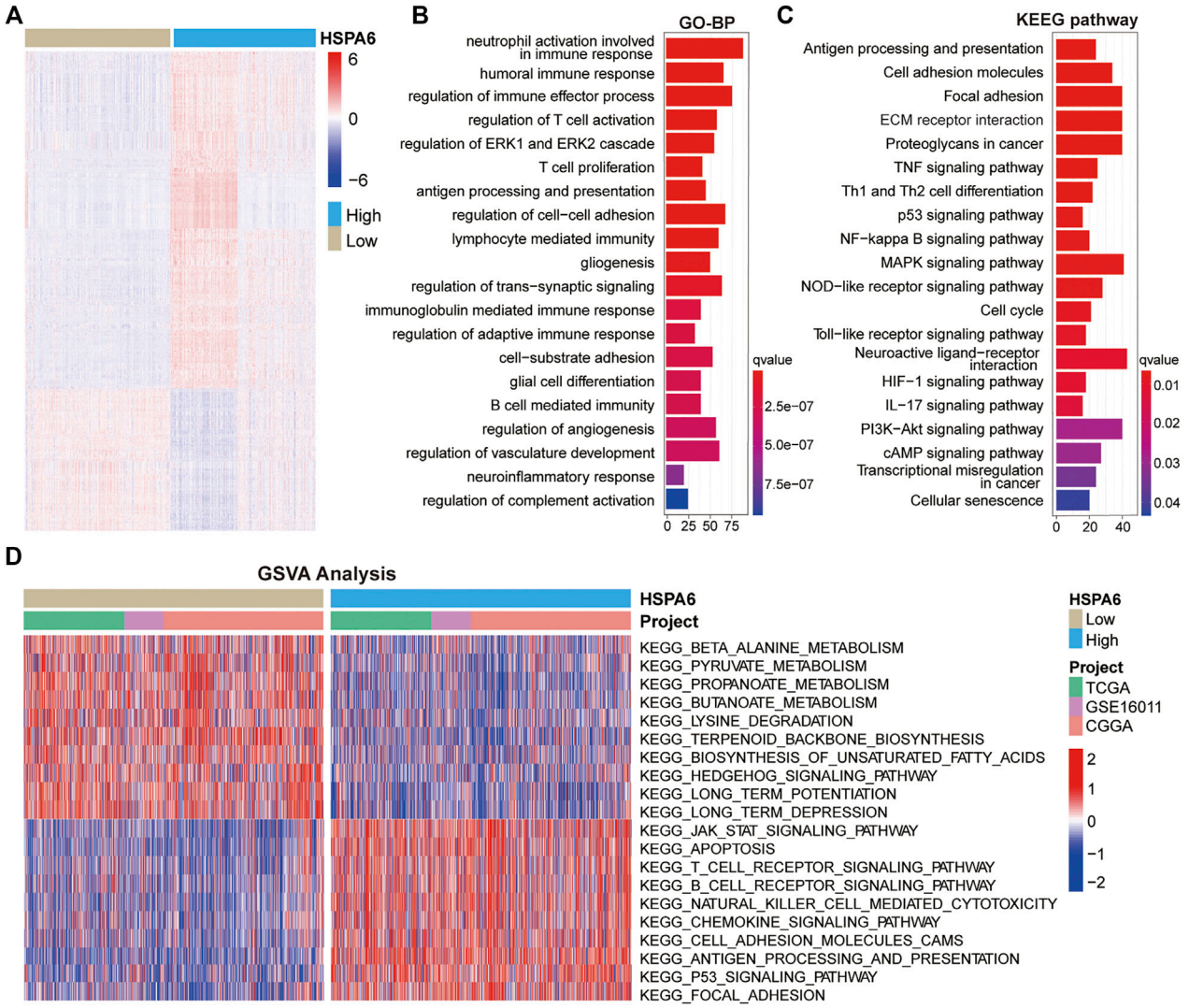

FIGURE 3 | Functional annotation of subgroups with high and low expression levels of HSPA6. **(A)** Differentially expressed genes (DEGs) between the subgroups of patients with low and high HSPA6 expression were identified by the Wilcoxon rank sum test in the TCGA cohort (FDR < 0.05 and log2Fold Change >1) cohort. **(B,C)** GO (Gene Ontology) and KEGG (Kyoto Encyclopedia of Genes and Genomes) enrichment analysis for DEGs ($p < 0.05$ and $q < 0.05$). There were 1669 DEGs in the TCGA cohort. **(D)** GSVA (Gene Set Variation Analysis) in the TCGA cohort, Chinese Glioma Genome Atlas (CGGA) cohort, and GSE16011 cohort, as determined by Gene Expression Omnibus (red = high score, blue = low score).

(**Figure 2I** and **Supplementary Figures S2C,F**). Collectively, these results suggested that HSPA6 may be an independent but poor prognostic biomarker for patients with glioma.

Function Annotation of HSPA6-Related Genes

To further investigate the mechanisms undergoing how HSPA6 may be associated with the outcome of patients with glioma, we identified DEGs by comparing subgroups with low and high expression levels of HSPA6 in the three cohorts (FDR <0.05 and log2Fold Change >1) using the Wilcoxon rank sum test. We identified 1669 DEGs in the TCGA cohort (**Supplementary Table S4**), 1114 in the CGGA cohort (**Supplementary Table S5**), and 581 in the GSE16011 cohort (**Supplementary Table S6**). All significant DEGs are shown in the heatmap in **Figure 3A**. GO enrichment analysis showed that these DEGs were closely associated with immune regulation, cell adhesion, and angiogenesis (**Figure 3B**). Similarly, KEGG enrichment analysis identified pathways associated with immune pathways, adhesion, and tumorigeneses, such as antigen processing and presentation, ECM receptor interaction, and the p53 signaling

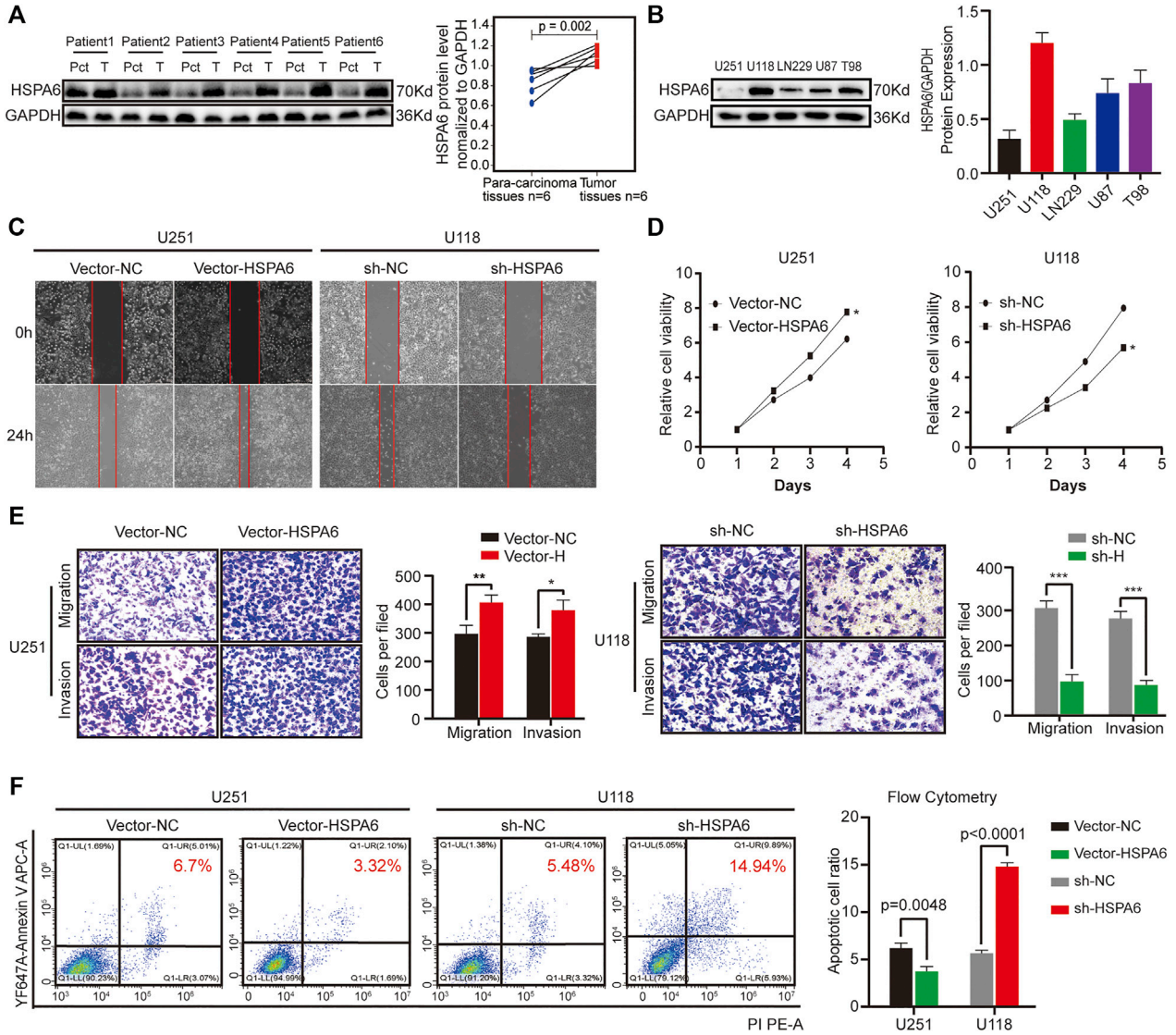

FIGURE 4 | Expression verification of HSPA6 in clinical brain tissues and different glioma cell lines and experimental validation of HSPA6 in U251 and U118 cells. **(A)** Western blot showing HSPA6 expression in six paired glioma tissues and matched para-carcinoma tissues from the same patient. HSPA6 protein expression levels were quantified by ImageJ software. **(B)** Western blot of HSPA6 expression in different glioma cell lines. HSPA6 protein expression levels were quantified by ImageJ software. **(C)** Cell scratch test to detect the migration ability of U251 and U118 cells which had been transfected with Vector-NC or Vector-HSPA6 and the sh-NC or sh-HSPA6 plasmids. The width of the wound was photographed under a microscope (magnification, 100x). **(D)** Cell Counting Kit-8 (CCK-8) assays were used to detect the proliferation of U251 and U118 cells which had been transfected with Vector-NC or Vector-HSPA6 and the sh-NC or sh-HSPA6 plasmids. **(E)** Transwell assays of U251 and U118 cells which had been transfected with Vector-NC or Vector-HSPA6 and sh-NC or sh-HSPA6 plasmids. Representative photographs (magnification, 200×) of migratory or invading cells on the membrane coated with or without Matrigel. Quantitative analysis of Transwell assays was performed by ImageJ software. **(F)** Flow cytometry detection of apoptosis in U251 and U118 cells which had been transfected with Vector-NC or Vector-HSPA6 and sh-NC or sh-HSPA6 plasmids. The proportion of apoptotic cells was equal to the sum of the proportion of early and late apoptosis. Data are expressed as the mean ± SEM from three independent experiments, $^{*}p < 0.05$, $^{**}p < 0.01$, $^{***}p < 0.001$.

pathway (**Figure 3C**). Similar functional annotations were also verified in the TCGA and GSE16011 cohorts (**Supplementary Figures S3A,B**).

In addition, we conducted GSVA to investigate the potential pathways associated with the low and high subgroups of HSPA6 expression in patients with gliomas. When comparing the three cohorts, we found that the subgroup with low expression levels of HSPA6 was closely related with tumor metabolism-related mechanisms, such as beta-alanine, pyruvate and propanoate metabolism. The subgroup with high expression levels was associated mainly with the development of tumors, cancer-related signaling pathways, and immune responses, such as apoptosis and focal adhesion, antigen processing and presentation, and the Jak-Stat and P53-signaling pathways

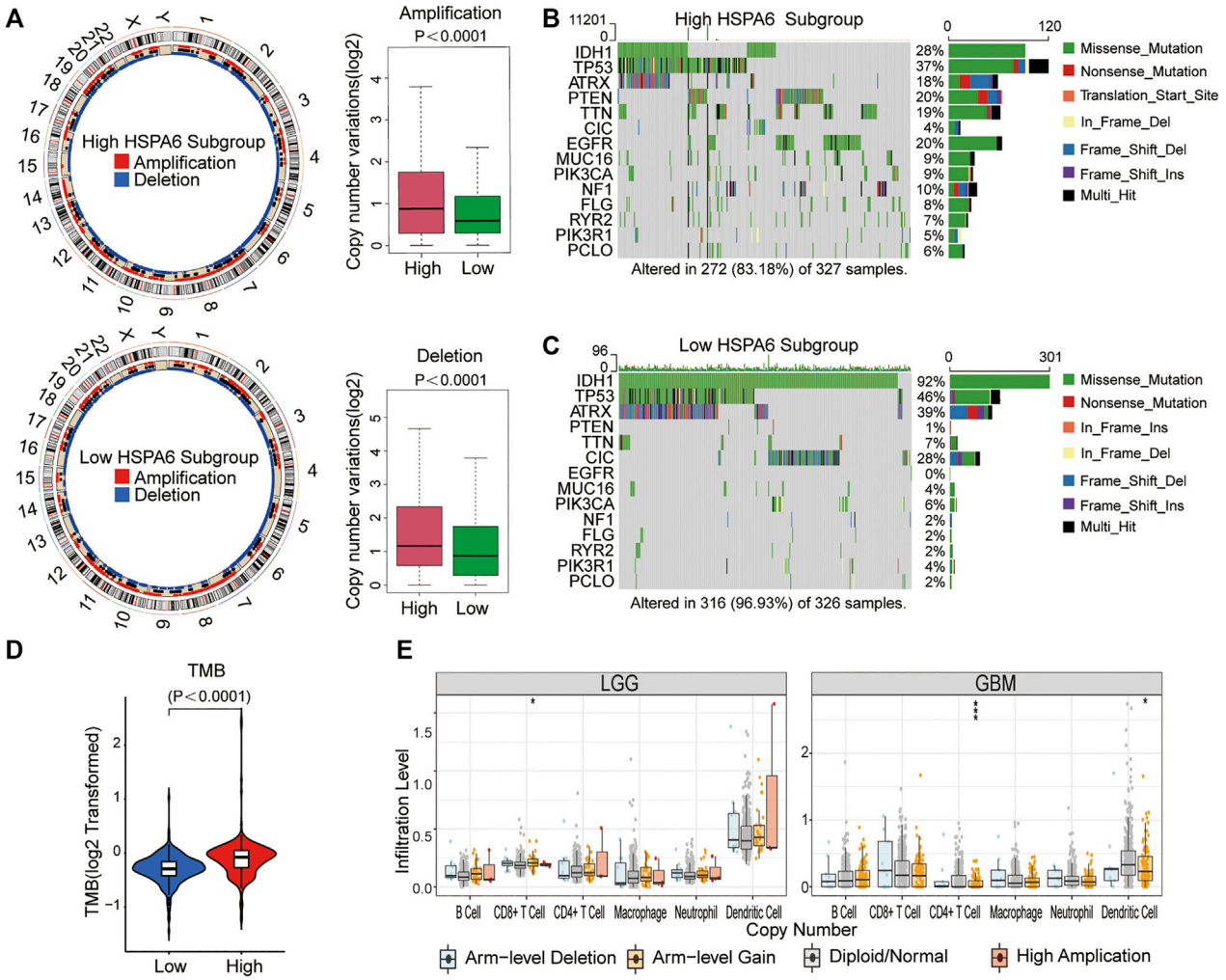

FIGURE 5 | Genomic variations of subgroups with low and high HSPA6 expression and associations between HSPA expression and tumor-infiltrating immune cells (TIICs). **(A)** Left: Circos plots illustrating amplification and deletion in the two subgroups. Right: A significant difference was detected in copy number variation (CNV) frequencies between two subgroups. **(B,C)** Waterfall plots illustrating the somatic mutations of 14 genes in tumors from the two subgroups. **(D)** Differential tumor mutational burden (TMB) between the two subgroups. **(E)** Associations of HSPA6 CNV with six types of TIICs. *$p < 0.05$; ***$p < 0.001$.

(**Figure 3D**). These results indicated that HSPA6 is closely related to immune regulation in patients with glioma.

In Vitro Investigations of HSPA6

We acquired glioma samples from six patients undergoing surgery in the Second Affiliated Hospital of Nanchang University. The expression levels of HSPA6 proteins were much higher in the glioma tissues compared with matched para-cancerous tissue. (**Figure 4A**). To further verify the association between HSPA6 expression and the malignant progression of glioma, we inspected the differential expression of HSPA6 in these glioma cell lines. We found that HSPA6 expression was the lowest in U251 cells and the highest in U118 cells (**Figure 4B**). To further investigate the function of HSPA6 in U251 and U118 cells, we constructed plasmids to overexpress and knockdown HSPA6 in U251 and U118 cells, respectively. Q-PCR and western blotting (WB) confirmed that HSPA6 expression in U251 cells transfected with the overexpression plasmid was significantly higher than in the control and untreated cell groups ($p < 0.05$, **Supplementary Figures S4A,B**). The same methods also proved that HSPA6 expression in U118 cells transfected with the knock-down plasmid was significantly lower than in the control and untreated cell groups ($p < 0.05$, **Supplementary Figures S4C,D**).

Next, a range of functional experiments were undertaken to investigate the connection between HSPA6 expression and the degree of malignancy in glioma cells from different treatment groups. Wound healing assays revealed that the migration capacity of the U251 Vector-HSPA6 group was significantly enhanced and the ability of the U118 sh-HSPA6 group was significantly reduced when compared to the control group (**Figure 4C**). CCK-8 assays further showed that the

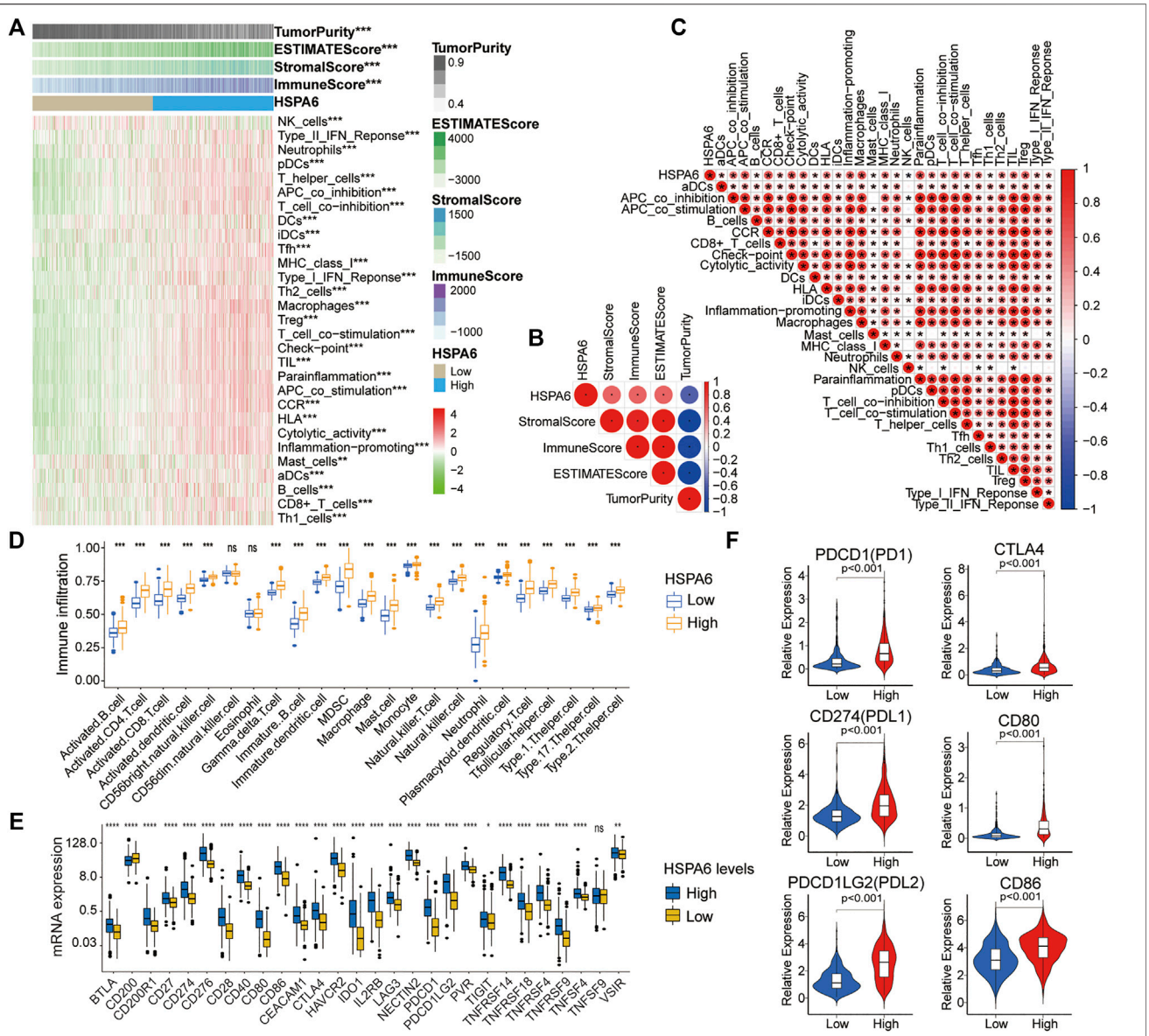

FIGURE 6 | Different tumor microenvironment (TME) characteristics of the two subgroups in the TCGA cohort. **(A–C)** Correlations of HSPA6 expression with 29 immune-associated gene sets, immune score, stromal score, ESTIMATE score, and tumor purity. **(D)** Different abundances of TIICs when compared between subgroups of patients with low and high expression levels of HSPA6. **(E)** Differential analysis of several immune checkpoint (ICP) expression levels between patients with low and high HSPA6 expression levels. **(F)** Differential expression of different immune checkpoint receptors and ligands between the two subgroups. Correlation analysis was performed by Pearson's correlation analysis. ns, $p > 0.05$, $^{*}p < 0.05$, $^{**}p < 0.01$, $^{***}p < 0.001$, $^{****}p < 0.0001$.

proliferative capacity of the U251 Vector-HSPA6 group was significantly promoted while the proliferative capacity of the U118 sh-HSPA6 group was significantly reduced when compared to the control group ($p < 0.05$, **Figure 4D**). Transwell assays showed that those capacities of the U251 Vector-HSPA6 group were significantly improved and that the migration and invasion capacities of the U118 sh-HSPA6 group were significantly reduced when compared to the control group ($^{*}p < 0.05$, $^{**}p < 0.01$, $^{***}p < 0.001$, **Figure 4E**). Flow cytometry analyses also disclosed the apoptotic cell ratio of the U251 Vector-HSPA6 group was significantly declined and that the apoptotic cell ratio of the U118 sh-HSPA6 group was significantly ascended when compared to the control group ($p < 0.005$, **Figure 4F**).

In order to further study the related pathway mechanism of HSPA6 in glioma cell lines, the differential gene pathway enrichment was analyzed by RNA sequencing after HSPA6 overexpression in the U251 cell line. The result also indicated that HSPA6 was closely related to tumor cell immunity, proliferation, and apoptosis, such as antigen processing and

presentation and PI3K-AKT signaling pathways (only top ten, **Supplementary Figure S4E**). It is often known that PI3K activates or inhibits a series of downstream substrates such as apoptosis-related proteins (Bad and Caspase9) after phosphorylation of AKT, thus regulating cell proliferation, differentiation, apoptosis, migration, and other phenotypes. Western blotting confirmed that the expression of PI3K and pAKT (Ser473 and Thr308) in the HSPA6 overexpressed U251 cell group were significantly higher than those in the control group, while the total protein expression of AKT basically changed little (**Supplementary Figure S4F**). Collectively, these results indicated that HSPA6 may influence the degree of malignancy in glioma cells by interacting with PI3K-AKT signaling pathway.

Differences in Genomic Variation Between the Two Subgroups

In view of the obligatory function of genomic variation in immune cell infiltration and tumor immunoregulation, CNV and somatic mutation were used to identify distinguishing genomic alterations in the subgroups showing differential HSPA6 expression. Both the amplification and deletion frequency of CNV was significantly higher in the subgroup with high expression levels when compared to the subgroup with low expression levels. (**Figure 5A**). Next, we created a "waterfall" map of somatic mutations; this revealed that each subgroup possessed genes with different mutations. The proportions of patients in the subgroup with high expression levels of HSPA6 with mutations in IDH1 (28%), ATRX (18%), PTEN (20%), TTN (19%), and EGFR (20%) was significantly different from those in the subgroup with low expression levels of HSPA6. ($p < 0.01$), whereas the frequency of TP53 was similar between the two subgroups. (**Figures 5B,C**). In addition, the subgroup with high expression levels of HSPA6 tended to have a significantly higher TMB ($p < 0.0001$, **Figure 5D**). Finally, three of the six types of TIIC were found to be associated with HSPA6 CNV in patients with low grade gliomas (LGGs) and glioblastoma (GBM) (**Figure 5E**). Collectively, these results implied that patients with gliomas with high expression levels of HSPA6 exhibited a special immunological reaction.

The Role of HSPA6 in Immune Cell Infiltration and Potential Responses to Immunotherapy

Significant correlations of HSPA6 expression with 29 immune-associated signatures and immune correlation scores, were determined for the TCGA cohort (**$p < 0.01$, ***$p < 0.001$, **Figures 6A,C**). HSPA6 expression was positively associated with immune score, stromal score, and ESTIMATE score, but negatively correlated with tumor purity (**Figure 6B**). To investigate the correlation between immune infiltration and HSPA6 expression, we used the ssGSEA algorithm to determine the enrichment of the 23 signatures with immune. There was a significantly greater number of immune-related signatures (***$p < 0.001$, **Figure 6D**) in the subgroup of patients with high HSPA6 expression levels than in the subgroup with low expression levels. Next, we investigated the differences in expression of diverse immune checkpoints between the subgroups of glioma patients with low and high HSPA6 expression. We found that the majority of immune checkpoints differed significantly between the two subgroups (**Figure 6E**). Similar results were also acquired from the CGGA and GSE16011 cohorts (**Supplementary Figures S5, S6**). **Figure 6F** shows that the relative expression levels of immune checkpoint receptors and ligands in the subgroup of patients with high expression levels of HSPA6 were significantly higher than those in the subgroup with low expression levels ($p < 0.001$). These results imply that HSPA6 may be closely related to the immune microenvironment.

DISCUSSION

Gliomas are intracranial neoplasms that stem from neuroglial progenitor cells (Cheng et al., 2020). Despite different combinations of surgery, temozolomide targeted-chemotherapy, and radiotherapy, patients with glioma still have a poor quality of life and a short survival time, especially those with high-grade gliomas (Touat et al., 2017). Traditional treatments are often ineffective for patients with glioma; consequently, there is a clear need to identify effective prognostic and therapeutic agents for patients with gliomas. In our study, we explored the specific value of HSPA6 in glioma.

First, we constructed a PPI network for members of the HSP superfamily; this showed that HSPA6 is directly or indirectly associated with 47 proteins in the HSP family. This also showed that HSPA6 had complex and extensive connections with other members of the HSP superfamily. This network also identified proteins that are directly related to HSPA6, including those in the HSP superfamily, and others in the BCL-2 associated athanogene (BAG) family, including BAG1, BAG2, BAG3, and BAG5. One previous study reported that the modular structure of the BAG family members enables interaction with a variety of proteins to exert pro-tumorigenic roles (Mariotto et al., 2020). Analysis of OS and PFS analyses indicated that the subgroup of patients with high expression levels of HSPA6 had a poor prognosis when compared with patients with low expression levels of HSPA6 in the TCGA cohort. ROC curve analyses were conducted to calculate the predictive accuracy of the prognostic model in patients with gliomas. This led to the question as to what controls the expression of HSPA6 protein in patients with glioma. The association between HSPA6 expression and relevant clinical factors in patients with glioma further indicated that there were significant differences in certain clinical traits, including IDH, 1p/19q, grade, and age. Moreover, univariate and multivariate Cox regression analysis showed that HSPA6 may represent a poor but independent prognostic biomarker for glioma. These results were further verified in both the CGGA and GSE16011 cohorts.

GO and KEGG analysis of DEGs showed that HSPA6 expression was closely associated with immune regulation, cell adhesion, and angiogenesis across all three cohorts. In addition, GSVA analysis revealed that the subgroup of patients with low expression levels of HSPA6 were mainly associated with metabolism-related mechanisms, while the subgroup of

patients with high expression levels of HSPA6 were mainly associated with cancer-related signaling pathways and immune responses. These results were also in line with the cancer-promoting mechanism of HSP70s, including the regulation of apoptosis pathways, tumor immunity, and the induction of angiogenesis (Albakova et al., 2020).

In recent years, there are more and more studies on HSPA6 protein in different tumors. However, the signaling pathway and mechanism of HSPA6 are still unclear in the field of cancer research. Shin et al. (Shin et al., 2017) found that HSPA6 induces phosphorylation of MAPK and AKT signals in bladder cancer cells and inhibits transcription factor related MMP-9 regulation to act on garlic extract, thus enhancing its mediated inhibition of bladder cancer cell proliferation, migration, and invasion; Meanwhile, Wang et al. (Wang et al., 2020b) showed that the expression of ARHGEF10L can stimulate gastric cancer by promoting RhoA-Rock1-phosphorylation-ERM signal transduction, inducing epithelial-mesenchymal cell transformation (EMT) and increasing HSPA6 expression.

We also verified that HSPA6 protein was expressed at significantly higher levels in clinical glioma specimens than in matched para-cancerous tissues. Next, we further verified the relationship between HSPA6 and the malignant progression of glioma cell lines *in vitro*. Interestingly, we found that the overexpression of HSPA6 accelerated the migration, proliferation, and invasion abilities of glioma cells. However, the opposite effect was observed following the knockdown of HSPA6 in glioma cells. The PI3K-AKT pathway is a critical regulatory pathway for cell proliferation and metabolism and is closely related to tumorigenesis and development (Janku et al., 2018). When receptor tyrosine kinases and G protein-coupled receptors are activated, PI3K phosphorylates phosphatidylinositol 3,4-diphosphate to produce 3,4,5-triphosphate phosphatidylinositol (PIP3). Activated PIP3 recruits and activates AKT in the cytoplasm, which in turn affects the level of related transcription factors involved in EMT to promote cell invasion and metastasis (Wu et al., 2015). In our study, we preliminarily explored that HSPA6 may affect the malignant degree of glioma cells through interaction with the PI3K-AKT signaling pathway. These results manifested that HSPA6 may be a potentially reliable therapeutic target for patients with glioma.

A growing body of research indicates that the TME is essential for the growth and aggressive nature of gliomas (Chang et al., 2016; Qian et al., 2018; Meng et al., 2019). Over the past few years, immunotherapeutic strategies targeting ICPs has achieved promising results in multiple forms of human cancer (Boussiotis and Charest, 2018; Sun et al., 2020b). Genomic alterations can predict disease classification and the prognosis of patients with gliomas (McNulty et al., 2019). Both amplification and deletion showed that the frequency of variants in the subgroup with high HSPA6 expression levels was significantly higher than that in the subgroup with low expression levels. Furthermore, the frequency of several types of common somatic gene mutations varied in the subgroups showing low and high expression levels of HSPA6. The loss of PTEN is known to lead to metabolic abnormalities in the lipid product of PI-Kinase (PIP3), thus directly antagonizing the activation of the carcinogenic PI3K/AKT/mTOR signaling network (Álvarez-Garcia et al., 2019). When applied for clinical targeted therapy, the EGFR is usually mutated in patients with glioma (Oh et al., 2021). EGFR has been shown to be implicated in tumorigenesis as an oncogene. EGFR signaling leads to the activation of the MAPK pathway intracellularly, signaling of PI3K and src kinase and activation of STAT transcription factor (Yarden and Pines, 2012). The results indicate that the higher the expression of HSPA6, the more the number of genomic alterations, and the higher the degree of malignancy. However, glioma patients with IDH1 mutant tumors are known to have a better prognosis than those with the wild-type IDH gene (Yan et al., 2009). We also found that patients in the subgroup with higher HSPA6 levels possessed a higher TMB than those in the subgroup with low expression levels. Other researchers have already proven that some tumor patients can benefit from immunotherapy and that TMB can be used as a marker to predict the clinical response to immunotherapy (Cristescu et al., 2018).

Three of the six types of TIIC were found to be associated with HSPA6 CNV in patients with LGGs and GBMs. Previous studies showed that the degree of stromal and immune cell infiltration has a prominent effect on the prognosis of patients with tumors (Winslow et al., 2016). We generated an immune heat map that identified statistically significant correlations between HSPA6 expression and 29 immune-associated signatures and immune correlation scores, across the three cohorts. The higher the expression level of HSPA6, the higher the immune score, stromal score, and ESTIMATE score; the opposite effect was observed for tumor purity. Infiltrating immune cells are composed of microglia/macrophages, MDSCs, $CD4^+$ T cells, regulatory T cells (Tregs), and granulocytes in the TME of gliomas. Infiltrating immune cells in the TME of gliomas consist of microglia/macrophages, $CD4^+$ T cells, MDSCs, regulatory T cells (Tregs) and granulocytes; microglia and MDSCs are the most common factors (Gieryng et al., 2017); the presence of these factors is responsible for the inefficacious immune response in patients with glioblastoma (Marvel and Gabrilovich, 2015). HSPA6 was found to be involved in the development of cervical squamous cell carcinoma as an antigen processing and presentation gene (Qin et al., 2021). Zhang Peng et al. (Peng et al., 2021) also found HSPA6 as part of an immune signature in esophageal cancer (ESCA). Our results showed that various types of immune-associated cells had been produced in patients with glioma and that most of the immune checkpoints were significantly higher in the subgroup of patients with high expression levels of HSPA6.

Over recent years, immune checkpoint block (ICB) therapy has become a novel and effective form of treatment for various tumors (Pitt et al., 2016), particularly with regards to certain receptor molecules (CTLA-4 and PD-1). Our analyses showed that the levels of corresponding ligands (PDL1/PDL2 and CD80/CD86) were also significantly higher in the subgroup of patients with high expression levels of HSAP6. Therefore, it follows that a gaining a more enhanced understanding of the correlation between HSPA6 and immunity will inevitably yield new concepts for immunotherapy in patients with glioma.

CONCLUSION

Herein, we described the biological functionality of HSPA6 in patients with glioma for the first time and verified our findings by performing *in vitro* experiments. However, our study had some limitations that need to be considered. Future research should investigate the precise immune and cellular functional mechanisms of HSPA6, both *in vivo* and *in vitro*. Whether HSPA6 can be regarded as an effective target-therapeutic agent for glioma needs to be investigated further.

DATA AVAILABILITY STATEMENT

The datasets presented in this study can be found in online repositories. The names of the repository/repositories and accession number(s) can be found in the article/ **Supplementary Material**.

ETHICS STATEMENT

The studies involving human participants were reviewed and approved by The medical ethics committee of the Second Affiliated Hospital of Nanchang University. The patients/ participants provided their written informed consent to participate in this study.

AUTHOR CONTRIBUTIONS

HG and KH designed the research. XZ, QJ, and QL took the lead in doing experiments and writing the manuscript, figures, and tables. GH, MY, and WW contributed to the collect the brain tissue samples and matching clinical data. PW, FX, LL, ML, and YG made important revisions to the paper. All authors contributed to the article and approved the submitted version.

FUNDING

The present study was supported by The National Natural Sciences Foundations of China (No. 81960457).

ACKNOWLEDGMENTS

We thank all the participants who were involved in this study.

SUPPLEMENTARY MATERIAL

The Supplementary Material for this article can be found online at: https://www.frontiersin.org/articles/10.3389/fcell.2022.833938/full#supplementary-material

REFERENCES

Albakova, Z., Armeev, G. A., Kanevskiy, L. M., Kovalenko, E. I., and Sapozhnikov, A. M. (2020). HSP70 Multi-Functionality in Cancer. *Cells* 9. doi:10.3390/cells9030587

Álvarez-Garcia, V., Tawil, Y., Wise, H. M., and Leslie, N. R. (2019). Mechanisms of PTEN Loss in Cancer: It's All about Diversity. *Semin. Cancer Biol.* 59, 66–79. doi:10.1016/j.semcancer.2019.02.001

Auslander, N., Zhang, G., Lee, J. S., Frederick, D. T., Miao, B., Moll, T., et al. (2018). Robust Prediction of Response to Immune Checkpoint Blockade Therapy in Metastatic Melanoma. *Nat. Med.* 24, 1545–1549. doi:10.1038/s41591-018-0157-9

Beaman, G. M., Dennison, S. R., Chatfield, L. K., and Phoenix, D. A. (2014). Reliability of HSP70 (HSPA) Expression as a Prognostic Marker in Glioma. *Mol. Cel Biochem* 393, 301–307. doi:10.1007/s11010-014-2074-7

Beere, H., and Green, D. R. (2001). Stress Management - Heat Shock Protein-70 and the Regulation of Apoptosis. *Trends Cel Biol.* 11, 6–10. doi:10.1016/s0962-8924(00)01874-2

Boussiotis, V. A., and Charest, A. (2018). Immunotherapies for Malignant Glioma. *Oncogene* 37, 1121–1141. doi:10.1038/s41388-017-0024-z

Calderwood, S. K., Khaleque, M. A., Sawyer, D. B., and Ciocca, D. R. (2006). Heat Shock Proteins in Cancer: Chaperones of Tumorigenesis. *Trends Biochem. Sci.* 31, 164–172. doi:10.1016/j.tibs.2006.01.006

Carper, S. W., Duffy, J. J., and Gerner, E. W. (1987). Heat Shock Proteins in Thermotolerance and Other Cellular Processes. *Cancer Res.* 47, 5249–5255.

Chang, A. L., Miska, J., Wainwright, D. A., Dey, M., Rivetta, C. V., Yu, D., et al. (2016). CCL2 Produced by the Glioma Microenvironment Is Essential for the Recruitment of Regulatory T Cells and Myeloid-Derived Suppressor Cells. *Cancer Res.* 76, 5671–5682. doi:10.1158/0008-5472.can-16-0144

Cheng, J., Meng, J., Zhu, L., and Peng, Y. (2020). Exosomal Noncoding RNAs in Glioma: Biological Functions and Potential Clinical Applications. *Mol. Cancer* 19, 66. doi:10.1186/s12943-020-01189-3

Cristescu, R., Mogg, R., Ayers, M., Albright, A., Murphy, E., Yearley, J., et al. (2018). Pan-tumor Genomic Biomarkers for PD-1 Checkpoint Blockade-Based Immunotherapy. *Science* 362, eaar3593. doi:10.1126/science.aar3593

Daugaard, M., Rohde, M., and Jäättelä, M. (2007). The Heat Shock Protein 70 Family: Highly Homologous Proteins with Overlapping and Distinct Functions. *FEBS Lett.* 581, 3702–3710. doi:10.1016/j.febslet.2007.05.039

Eckel-Passow, J. E., Lachance, D. H., Molinaro, A. M., Walsh, K. M., Decker, P. A., Sicotte, H., et al. (2015). Glioma Groups Based on 1p/19q,IDH, andTERTPromoter Mutations in Tumors. *N. Engl. J. Med.* 372, 2499–2508. doi:10.1056/nejmoa1407279

Gieryng, A., Pszczolkowska, D., Walentynowicz, K. A., Rajan, W. D., and Kaminska, B. (2017). Immune Microenvironment of Gliomas. *Lab. Invest.* 97, 498–518. doi:10.1038/labinvest.2017.19

Hahm, E. R., Kim, S. H., Singh, K. B., and Singh, S. V. (2021). RNA-Seq Reveals Novel Cancer-selective and Disease Subtype-independent Mechanistic Targets of Withaferin A in Human Breast Cancer Cells. *Mol. Carcinogenesis* 60, 3–14. doi:10.1002/mc.23266

Hänzelmann, S., Castelo, R., and Guinney, J. (2013). GSVA: Gene Set Variation Analysis for Microarray and RNA-Seq Data. *BMC Bioinformatics* 14, 7. doi:10.1186/1471-2105-14-7

Janku, F., Yap, T. A., and Meric-Bernstam, F. (2018). Targeting the PI3K Pathway in Cancer: Are We Making Headway? *Nat. Rev. Clin. Oncol.* 15, 273–291. doi:10.1038/nrclinonc.2018.28

Jiang, T., Mao, Y., Ma, W., Mao, Q., You, Y., Yang, X., et al. (2016). CGCG Clinical Practice Guidelines for the Management of Adult Diffuse Gliomas. *Cancer Lett.* 375, 263–273. doi:10.1016/j.canlet.2016.01.024

Lindquist, S., and Craig, E. A. (1988). The Heat-Shock Proteins. *Annu. Rev. Genet.* 22, 631–677. doi:10.1146/annurev.ge.22.120188.003215

Mariotto, E., Viola, G., Zanon, C., and Aveic, S. (2020). A BAG's Life: Every Connection Matters in Cancer. *Pharmacol. Ther.* 209, 107498. doi:10.1016/j.pharmthera.2020.107498

Marvel, D., and Gabrilovich, D. I. (2015). Myeloid-derived Suppressor Cells in the Tumor Microenvironment: Expect the Unexpected. *J. Clin. Invest.* 125, 3356–3364. doi:10.1172/jci80005

Mayakonda, A., Lin, D.-C., Assenov, Y., Plass, C., and Koeffler, H. P. (2018). Maftools: Efficient and Comprehensive Analysis of Somatic Variants in Cancer. *Genome Res.* 28, 1747–1756. doi:10.1101/gr.239244.118

McNulty, S. N., Cottrell, C. E., Vigh-Conrad, K. A., Carter, J. H., Heusel, J. W., Ansstas, G., et al. (2019). Beyond Sequence Variation: Assessment of Copy Number Variation in Adult Glioblastoma through Targeted Tumor Somatic Profiling. *Hum. Pathol.* 86, 170–181. doi:10.1016/j.humpath.2018.12.004

Meng, X., Duan, C., Pang, H., Chen, Q., Han, B., Zha, C., et al. (2019). DNA Damage Repair Alterations Modulate M2 Polarization of Microglia to Remodel the Tumor Microenvironment via the P53-Mediated MDK Expression in Glioma. *EBioMedicine* 41, 185–199. doi:10.1016/j.ebiom.2019.01.067

Mermel, C. H., Schumacher, S. E., Hill, B., Meyerson, M. L., Beroukhim, R., and Getz, G. (2011). GISTIC2.0 Facilitates Sensitive and Confident Localization of the Targets of Focal Somatic Copy-Number Alteration in Human Cancers. *Genome Biol.* 12, R41. doi:10.1186/gb-2011-12-4-r41

Oehler, R., Schmierer, B., Zellner, M., Prohaska, R., and Roth, E. (2000). Endothelial Cells Downregulate Expression of the 70 kDa Heat Shock Protein during Hypoxia. *Biochem. Biophysical Res. Commun.* 274, 542–547. doi:10.1006/bbrc.2000.3184

Oh, H., Hwang, I., Jang, J.-Y., Wu, L., Cao, D., Yao, J., et al. (2021). Therapy-Induced Transdifferentiation Promotes Glioma Growth Independent of EGFR Signaling. *Cancer Res.* 81, 1528–1539. doi:10.1158/0008-5472.can-20-1810

Ostrom, Q. T., Bauchet, L., Davis, F. G., Deltour, I., Fisher, J. L., Langer, C. E., et al. (2014). The Epidemiology of Glioma in Adults: a "State of the Science" Review. *Neuro-Oncology* 16, 896–913. doi:10.1093/neuonc/nou087

Otasek, D., Morris, J. H., Bouças, J., Pico, A. R., and Demchak, B. (2019). Cytoscape Automation: Empowering Workflow-Based Network Analysis. *Genome Biol.* 20, 185. doi:10.1186/s13059-019-1758-4

Peng, Z., Liu, X.-Y., Cheng, Z., Kai, W., and Song, Z. (2021). Comprehensive Analysis of a New Immune-Related Prognostic Signature for Esophageal Cancer and its Correlation with Infiltrating Immune Cells and Target Genes. *Ann. Transl Med.* 9, 1576. doi:10.21037/atm-21-4756

Pitt, J. M., Marabelle, A., Eggermont, A., Soria, J.-C., Kroemer, G., and Zitvogel, L. (2016). Targeting the Tumor Microenvironment: Removing Obstruction to Anticancer Immune Responses and Immunotherapy. *Ann. Oncol.* 27, 1482–1492. doi:10.1093/annonc/mdw168

Qian, J., Wang, C., Wang, B., Yang, J., Wang, Y., Luo, F., et al. (2018). The IFN-Γ/pd-L1 axis between T Cells and Tumor Microenvironment: Hints for Glioma Anti-PD-1/pd-L1 Therapy. *J. Neuroinflammation* 15, 290. doi:10.1186/s12974-018-1330-2

Qin, K., Jian, D., Xue, Y., Cheng, Y., Zhang, P., Wei, Y., et al. (2021). DDX41 Regulates the Expression and Alternative Splicing of Genes Involved in Tumorigenesis and Immune Response. *Oncol. Rep.* 45, 1213–1225. doi:10.3892/or.2021.7951

Ritchie, M. E., Phipson, B., Wu, D., Hu, Y., Law, C. W., Shi, W., et al. (2015). Limma powers Differential Expression Analyses for RNA-Sequencing and Microarray Studies. *Nucleic Acids Res.* 43, e47. doi:10.1093/nar/gkv007

Ritossa, F. (1962). A New Puffing Pattern Induced by Temperature Shock and DNP in drosophila. *Experientia* 18, 571–573. doi:10.1007/bf02172188

Rosenzweig, R., Nillegoda, N. B., Mayer, M. P., and Bukau, B. (2019). The Hsp70 Chaperone Network. *Nat. Rev. Mol. Cel Biol* 20, 665–680. doi:10.1038/s41580-019-0133-3

Shen, S., Wei, C., and Fu, J. (2021). RNA-sequencing Reveals Heat Shock 70-kDa Protein 6 (HSPA6) as a Novel Thymoquinone-Upregulated Gene that Inhibits Growth, Migration, and Invasion of Triple-Negative Breast Cancer Cells. *Front. Oncol.* 11, 667995. doi:10.3389/fonc.2021.667995

Shin, S.-S., Song, J.-H., Hwang, B., Noh, D.-H., Park, S. L., Kim, W. T., et al. (2017). HSPA6 Augments Garlic Extract-Induced Inhibition of Proliferation, Migration, and Invasion of Bladder Cancer EJ Cells; Implication for Cell Cycle Dysregulation, Signaling Pathway Alteration, and Transcription Factor-Associated MMP-9 Regulation. *PLoS One* 12, e0171860. doi:10.1371/journal.pone.0171860

Skidmore, Z. L., Wagner, A. H., Lesurf, R., Campbell, K. M., Kunisaki, J., Griffith, O. L., et al. (2016). GenVisR: Genomic Visualizations in R. *Bioinformatics* 32, 3012–3014. doi:10.1093/bioinformatics/btw325

Stupp, R., Taillibert, S., Kanner, A., Read, W., Steinberg, D. M., Lhermitte, B., et al. (2017). Effect of Tumor-Treating Fields Plus Maintenance Temozolomide vs Maintenance Temozolomide Alone on Survival in Patients with Glioblastoma. *JAMA* 318, 2306–2316. doi:10.1001/jama.2017.18718

Sun, H., Zou, H.-Y., Cai, X.-Y., Zhou, H.-F., Li, X.-Q., Xie, W.-J., et al. (2020). Network Analyses of the Differential Expression of Heat Shock Proteins in Glioma. *DNA Cel Biol.* 39, 1228–1242. doi:10.1089/dna.2020.5425

Sun, J., Zhang, Z., Bao, S., Yan, C., Hou, P., Wu, N., et al. (2020). Identification of Tumor Immune Infiltration-Associated lncRNAs for Improving Prognosis and Immunotherapy Response of Patients with Non-small Cell Lung Cancer. *J. Immunother. Cancer* 8, e000110. doi:10.1136/jitc-2019-000110

Touat, M., Idbaih, A., Sanson, M., and Ligon, K. L. (2017). Glioblastoma Targeted Therapy: Updated Approaches from Recent Biological Insights. *Ann. Oncol.* 28, 1457–1472. doi:10.1093/annonc/mdx106

Wang, D.-w., Tang, J.-y., Zhang, G.-q., and Chang, X.-t. (2020). ARHGEF10L Expression Regulates Cell Proliferation and Migration in Gastric Tumorigenesis. *Biosci. Biotechnol. Biochem.* 84, 1362–1372. doi:10.1080/09168451.2020.1737503

Wang, H.-j., Gao, Y., Chen, L., Li, Y.-l., and Jiang, C.-l. (2015). RAB34 Was a Progression- and Prognosis-Associated Biomarker in Gliomas. *Tumor Biol.* 36, 1573–1578. doi:10.1007/s13277-014-2732-0

Wang, L., Hou, J., Wang, J., Zhu, Z., Zhang, W., Zhang, X., et al. (2020). Regulatory Roles of HSPA6 in Actinidia Chinensis Planch. Root Extract (acRoots)-Inhibited Lung Cancer Proliferation. *Clin. Transl Med.* 10, e46. doi:10.1002/ctm2.46

Weller, M., Wick, W., Aldape, K., Brada, M., Berger, M., Pfister, S. M., et al. (2015). Glioma. *Nat. Rev. Dis. Primers* 1, 15017. doi:10.1038/nrdp.2015.17

Winslow, S., Lindquist, K. E., Edsjö, A., and Larsson, C. (2016). The Expression Pattern of Matrix-Producing Tumor Stroma Is of Prognostic Importance in Breast Cancer. *BMC Cancer* 16, 841. doi:10.1186/s12885-016-2864-2

Wu, Y.-J., Neoh, C.-A., Tsao, C.-Y., Su, J.-H., and Li, H.-H. (2015). Sinulariolide Suppresses Human Hepatocellular Carcinoma Cell Migration and Invasion by Inhibiting Matrix Metalloproteinase-2/-9 through MAPKs and PI3K/Akt Signaling Pathways. *Ijms* 16, 16469–16482. doi:10.3390/ijms160716469

Yan, H., Parsons, D. W., Jin, G., McLendon, R., Rasheed, B. A., Yuan, W., et al. (2009). IDH1andIDH2Mutations in Gliomas. *N. Engl. J. Med.* 360, 765–773. doi:10.1056/nejmoa0808710

Yang, X., Wang, J., Zhou, Y., Wang, Y., Wang, S., and Zhang, W. (2012). Hsp70 Promotes Chemoresistance by Blocking Bax Mitochondrial Translocation in Ovarian Cancer Cells. *Cancer Lett.* 321, 137–143. doi:10.1016/j.canlet.2012.01.030

Yang, Z., Zhuang, L., Szatmary, P., Wen, L., Sun, H., Lu, Y., et al. (2015). Upregulation of Heat Shock Proteins (HSPA12A, HSP90B1, HSPA4, HSPA5 and HSPA6) in Tumour Tissues Is Associated with Poor Outcomes from HBV-Related Early-Stage Hepatocellular Carcinoma. *Int. J. Med. Sci.* 12, 256–263. doi:10.7150/ijms.10735

Yarden, Y., and Pines, G. (2012). The ERBB Network: at Last, Cancer Therapy Meets Systems Biology. *Nat. Rev. Cancer* 12, 553–563. doi:10.1038/nrc3309

Yu, G., Wang, L.-G., Han, Y., and He, Q.-Y. (2012). clusterProfiler: an R Package for Comparing Biological Themes Among Gene Clusters. *OMICS: A J. Integr. Biol.* 16, 284–287. doi:10.1089/omi.2011.0118

Zhang, H., Meltzer, P., and Davis, S. (2013). RCircos: an R Package for Circos 2D Track Plots. *BMC Bioinformatics* 14, 244. doi:10.1186/1471-2105-14-244

Zhang, H., Wang, R., Yu, Y., Liu, J., Luo, T., and Fan, F. (2019). Glioblastoma Treatment Modalities besides Surgery. *J. Cancer* 10, 4793–4806. doi:10.7150/jca.32475

Conflict of Interest: The authors declare that the research was conducted in the absence of any commercial or financial relationships that could be construed as a potential conflict of interest.

Publisher's Note: All claims expressed in this article are solely those of the authors and do not necessarily represent those of their affiliated organizations, or those of the publisher, the editors and the reviewers. Any product that may be evaluated in this article, or claim that may be made by its manufacturer, is not guaranteed or endorsed by the publisher.

Copyright © 2022 Zhou, Ji, Li, Wang, Hu, Xiao, Ye, Lin, Luo, Guo, Wu, Huang and Guo. This is an open-access article distributed under the terms of the Creative Commons Attribution License (CC BY). The use, distribution or reproduction in other forums is permitted, provided the original author(s) and the copyright owner(s) are credited and that the original publication in this journal is cited, in accordance with accepted academic practice. No use, distribution or reproduction is permitted which does not comply with these terms.

frontiers in Oncology

REVIEW
published: 02 March 2022
doi: 10.3389/fonc.2022.840467

Nasopharyngeal Carcinoma and Its Microenvironment: Past, Current, and Future Perspectives

Zhi Yi Su[1], *Pui Yan Siak*[1], *Chee-Onn Leong*[2,3] *and Shiau-Chuen Cheah*[1]*

[1] Faculty of Medicine and Health Sciences, UCSI University, Kuala Lumpur, Malaysia, [2] Centre of Cancer and Stem Cells Research, International Medical University, Kuala Lumpur, Malaysia, [3] Institute for Research, Development and Innovation, International Medical University, Kuala Lumpur, Malaysia

Nasopharyngeal carcinoma (NPC) is an epithelial malignancy that raises public health concerns in endemic countries. Despite breakthroughs in therapeutic strategies, late diagnosis and drug resistance often lead to unsatisfactory clinical outcomes in NPC patients. The tumor microenvironment (TME) is a complex niche consisting of tumor-associated cells, such as fibroblasts, endothelial cells, leukocytes, that influences tumor initiation, progression, invasion, and metastasis. Cells in the TME communicate through various mechanisms, of note, exosomes, ligand-receptor interactions, cytokines and chemokines are active players in the construction of TME, characterized by an abundance of immune infiltrates with suppressed immune activities. The NPC microenvironment serves as a target-rich niche for the discovery of potential promising predictive or diagnostic biomarkers and the development of therapeutic strategies. Thus, huge efforts have been made to exploit the role of the NPC microenvironment. The whole picture of the NPC microenvironment remains to be portrayed to understand the mechanisms underlying tumor biology and implement research into clinical practice. The current review discusses the recent insights into the role of TME in the development and progression of NPC which results in different clinical outcomes of patients. Clinical interventions with the use of TME components as potential biomarkers or therapeutic targets, their challenges, and future perspectives will be introduced. This review anticipates to provide insights to the researchers for future preclinical, translational and clinical research on the NPC microenvironment.

Keywords: nasopharyngeal carcinoma, tumor microenvironment, Epstein-Barr virus, immunotherapy, exosomes

OPEN ACCESS

Edited by:
Pranav Gupta,
Albert Einstein College of Medicine, United States

Reviewed by:
Olivier Morales, CNRS, France
Weiren Luo, The Second Affiliated hospital of Southern University of Science and Technology, China

***Correspondence:**
Shiau-Chuen Cheah
cheahsc@ucsiuniversity.edu.my

Specialty section:
This article was submitted to Molecular and Cellular Oncology, a section of the journal Frontiers in Oncology

Received: *21 December 2021*
Accepted: *11 February 2022*
Published: *02 March 2022*

Citation:
Su ZY, Siak PY, Leong C-O and Cheah S-C (2022) Nasopharyngeal Carcinoma and Its Microenvironment: Past, Current, and Future Perspectives. Front. Oncol. 12:840467. doi: 10.3389/fonc.2022.840467

INTRODUCTION

Nasopharyngeal carcinoma (NPC) is a squamous cell neoplasm that originated from the nasopharyngeal mucosal lining, commonly found at the fossa of Rosenmüller (1, 2). In 2020, the International Agency for Research on Cancer (IARC) reported 133,354 incidences of NPC globally, which accounted for 0.7% of all cancers diagnosed (**Figure 1A**) (4). Intriguingly, NPC demonstrated a remarkable geographical distribution, where over 77% of NPC incidences were found in Eastern and South-Eastern Asia (**Figure 1B**). In South-Eastern Asia, NPC ranked the 10th most common

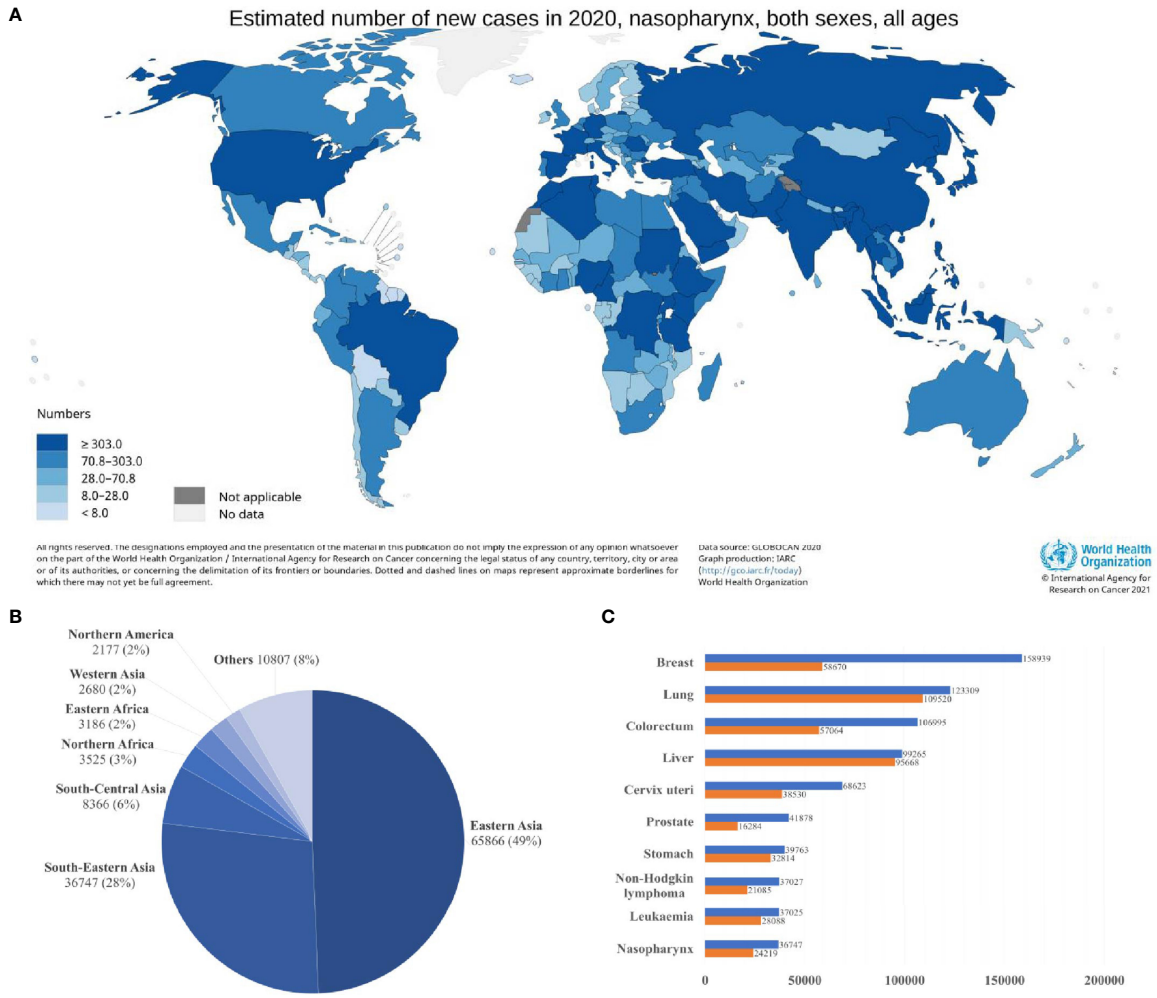

FIGURE 1 | Global distribution of nasopharyngeal carcinoma **(A)** Estimated age-standardized incidence rate (ASR; world) **(B)** Estimated number of new cases in different world areas. **(C)** Estimated number of incident cases and deaths in South-Eastern Asia. Data source: GLOBOCAN 2020 (3).

cancer among the entire population (**Figure 1C**) (3). Brunei had the highest age-standardized incidence rate of NPC (13.35 per 100,000 in males; 6.44 per 100,000 in females), followed by Maldives (10.67 per 100,000 in males; 3.3 per 100,000 in females), Indonesia (10.71 per 100,000 in males; 3.03 per 100,000 in females), Malaysia (9.53 per 100,000 in males; 3.05 per 100,000 in females) and Vietnam (8.12 per 100,000 in males; 2.79 per 100,000 in females) (5, 6). China had an age-standardized rate of 3.0 per 100,000, whereby the incidences are more prevalent among the Cantonese-speaking population which resided in southern China, including Guangzhou province (13.9 per 100,000 in males; 5.2 per 100,000 in females) and Hong Kong (12.8 per 100,000 in males; 4.0 per 100,000 in females).

The incidence of NPC is higher in males (96,371) than in females (36,983), with a ratio of about 2 to 3:1 (4). This phenomenon can be explained by the inheritance of genetic susceptibility associated with X chromosomes, leading to male predominance in the incidence of NPC (7). Sex hormones, such as estrogen, may play a protective role against NPC in females (8). Viral infection with Epstein-Barr virus (EBV) is the most common aetiologic factor in NPC, 100% of non-keratinizing NPCs are detected with EBV infection. Several environmental factors, including dietary consumption of preserved food, and social practice such as tobacco smoking and alcohol consumption, are associated with increased risk of NPC (1, 2, 9). Taken together, EBV infection, genetic and environmental factors contribute to the pathogenesis of NPC.

The application of intensity-modulated radiotherapy (IMRT) alone or with chemotherapy for treatment of NPC significantly improves the clinical outcome of NPC patients. NPC patients diagnosed with early-stage (stage I to II) have a 5-year overall survival (OS) as high as 94% (10–12). Tragically, despite the advances in medical treatment, over 60% of newly diagnosed patients have poor clinical outcomes as they are often diagnosed at late-stage, due to non-specific clinical presentation and lack of biomarkers for early detection (12). Early manifestations of NPC,

such as headache, cervical mass, nasal obstruction, and epistaxis, are non-specific, leading to a misdiagnosis rate of approximately 43%, which ultimately results in delay in treatment and poor prognosis (10). When patients are diagnosed with late-stage (stage III-IV) NPC, the 5-year survival rate declines drastically, which is lower than 80% (10). The mortality risk of patients who were diagnosed with stage IV NPC is 3.41-fold higher in comparison with those diagnosed at early-stage (13). Other challenges include locoregional or distant recurrence, which affects 20 to 30% of patients, and therapeutic resistance (1, 12). Thus, it is imperative for the development of high specificity, high sensitivity, and non-invasive laboratory tests for the diagnosis and prognosis of NPC and the development of new therapeutic strategies to reduce morbidity and mortality of the disease.

The tumor microenvironment (TME) is a specialized niche made up of resident malignant and infiltrated cells, metabolites, and extracellular matrix, characterized by its heterogeneity and complexity (**Figure 2**). Stephen Paget's "seed and soil" theory suggested the preference of tumor cells (the "seed") to grow in a favourable microenvironment (the "soil") (14). The Tissue Organization Field Theory supported the above hypothesis by suggesting that communication between the microenvironment and cell through biophysical and biochemical cues drives phenotypic transformation of cells, which eventually leads to cancer (15). The heterogenous TME further contributes to the progression of cancer by facilitating the acquisition of a series of hallmark capabilities, including [1] sustained proliferative signaling; [2] evasion of growth suppressors; [3] apoptotic resistance; [4] immortal replication; [5] angiogenesis; [6] invasion and metastasis; [7] reprogramming energy metabolism and [8] evasion from immune surveillance, as enumerated by Hanahan and Weinberg (16). These theories open a door towards a new era of medical research targeting the TME. Since the last few decades, several efforts have been made to explore the NPC microenvironment by immunohistological analysis of NPC biopsies. With the advancement of technologies, researchers can delineate the complex TME and cellular crosstalk at single-cell

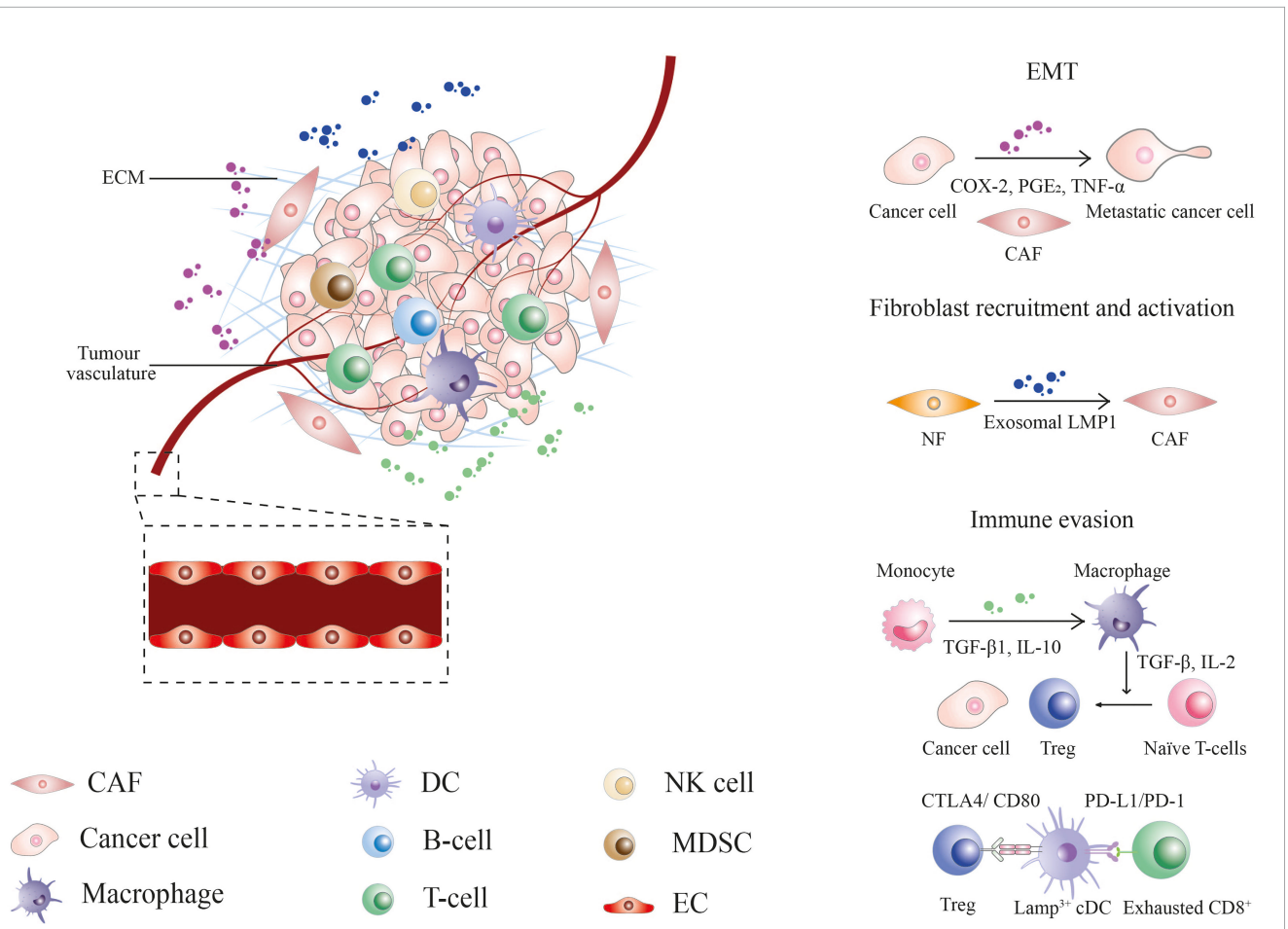

FIGURE 2 | The nasopharyngeal carcinoma tumor microenvironment. CAF, cancer-associated fibroblast; COX-2, cyclooxygenase-2; CTLA4, cytotoxic T-lymphocyte associated protein 4; DC, dendritic cell; EC, endothelial cell; ECM, extracellular matrix; EMT, epithelial-mesenchymal transition; Exo-LMP, exosome-packaged latent membrane protein; IL, interleukin; MDSCs, myeloid-derived suppressor cells; NF, normal fibroblast; NK, natural killer; PD-1, programmed cell death protein 1; PD-L1, programmed death-ligand 1; PGE_2, prostaglandin E2; TGF, tumor growth factor; TNF, tumor necrosis factor; Treg, regulatory T-cell.

resolution, thereby facilitating the development of diagnostic, prognostic, and therapeutic tools against NPC (17–21).

As a requisite in tumor initiation, progression, and metastasis, the TME components and their interplay with cancer cells offer a variety of promising targets for the development of anti-cancer therapy against NPC. This review introduces the cellular and acellular players, their roles in the NPC microenvironment, current and potential biomarkers, and therapeutic strategies targeting TME.

COMPONENTS IN TUMOR MICROENVIRONMENT

The NPC microenvironment is complex and highly heterogeneous, its components can be classified into cellular and acellular components. Cellular components include [1] tumor endothelial cells (TECs), which forms blood and lymphatic vascular networks for transportation of nutrients and oxygen, [2] cancer-associated fibroblasts (CAFs), which support tumor growth, survival, invasion, and migration, and [3] immune cells, which are involved in immune reactions in the TME (22–25). On the other hand, acellular components include the extracellular matrix (ECM), which facilitates tumor development, progression, and metastasis (26, 27).

Tumor-Infiltrating Immune Cells

The NPC microenvironment is characterized by the intense filtration of tumor-infiltrating immune cells (TIICs), which constitute 40 – 50% of the tumor mass in NPC, with EBV-negative $CD3^+$ T-lymphocytes as the commonest infiltrate (28–30). Despite its abundance, lack of effective immune response, and the presence of immunosuppressive infiltrates such as regulatory T-cells (Tregs), M2 macrophages, and myeloid-derived suppressor cells (MDSCs) leads to immunotolerance, promoting tumor progression. TIICs can be further classified based on lymphoid and myeloid lineage. Tumor-infiltrating lymphocytes (TILs), including T-cells and B-cells, are abundant in the NPC microenvironment as a result of an immune response against EBV. On the other hand, tumor-infiltrating myeloid cells (TIMs) consist of various cell types, including mature mast cells, monocytes and macrophages, dendritic cells (DCs), and pathologically activated immature MDSCs (17, 31, 32).

Tumor-Infiltrating Lymphocytes

TILs, including T-cells and B-cells, are most predominant in the NPC microenvironment. Tumor-associated T-cells consisted of several subpopulations, namely naïve T-cells, cytotoxic T-cells (CTLs), exhausted T-cells, and Tregs (17–21). $CD3^+$ T-lymphocytes, which are comprised of $CD4^+$ T-helper cells and $CD8^+$ T-suppressor cells, is the predominant lymphocytes infiltrating the NPC microenvironment. The majority of these lymphocytes express the activation marker OKT10, however, restriction on human leukocyte antigen (HLA) and T-cell receptor gene expression might contribute to tumor evasion from immune surveillance (29, 30, 33, 34). Consistent with these findings, transcriptomic studies reported that $CD4^+$ and $CD8^+$ T-cells clusters in NPC are highly activated and exhausted, as they co-express exhaustion markers (*LAG3*, *TIGIT*, *PDCD1*, *HAVCR2*, *CTLA4*, *TOX*) and effector molecules (*GZMB*, *GZMK*, *INFG*, *NKG7*, *GNLY*, and *IL2*) (17–21). Exhausted T-cell clusters display intermediate-to-high cytotoxic activity, implying a dynamic transitional process from activated T-cells to exhausted T-cells (17). Both intrinsic and extrinsic mechanisms are involved in the exhaustion or dysfunction of T-cells. The intrinsic mechanisms include [1] expression of inhibitory receptors, including programmed cell death protein 1 (PD-1), cytotoxic T-lymphocyte-associated protein 4 (CTLA-4), T-cell immunoglobulin and mucin-domain containing-3 (TIM-3), lymphocyte activation gene (LAG-3), B and T lymphocyte attenuator (BTLA) and T-cell immunoglobulin and ITIM domain (TIGIT), [2] decreased cytokine signaling pathways which suppresses the production of interleukin (IL)-2, tumor necrosis factor (TNF)-α, interferon (IFN)-γ and granzyme B (GzmB) in a hierarchical manner, and [3] transcription factors such as the nuclear factor of activated T-cells 1 (NFATC1) (20, 35). Extrinsic mechanisms, on the other hand, include [1] inhibitory effects exerted by regulatory cells including Treg cells, DCs, tumor-associated macrophages (TAMs), MDSCs, [2] immunosuppressive cytokines, such as transforming growth factor (TGF)-β and IL-10, and [3] interaction with major histocompatibility complex (MHC) class II-expressing NPC cells (18, 35).

Tregs are immunosuppressive cells expressing $CD4^+CD25^{high}$ $Foxp3^+$ markers (18, 36). Tregs mediate tumor escape from immune surveillance by [1] involvement of immune checkpoint molecules, such as PD-1 and CTLA-4, [2] secretion of cytokines, for instance, IL-10 and TGF-β, which elicits inhibitory effects on immunoreactive cell proliferation, [3] induction of T-cells apoptosis through secretion of cytotoxic perforin and GzmB or ligand-receptor interaction through Fas/FasL, [4] cell contact-dependent suppression of naïve T-cells proliferation, [5] metabolic modulation through enhancing immunosuppressive metabolites, such as indoleamine 2,3-dioxygenase (IDO), in the TME (37–39). Studies revealed enhanced expression level of *LGALS1* in NPC-derived Tregs, which was reported to mediate immunosuppression by upregulation of cell-surface programmed death-ligand 1 (PD-L1) and galectin-9 (Gal-9) in head and neck cancer (18, 40). Physical or pharmacologic depletion of Tregs targeting drugs removes their suppression effect and restores EBV-specific $CD8^+$ T-cells (41).

NK cells are the first line of defense against viral infections and neoplasms. Studies reported diminished expression of inhibitory surface receptors of NK cells, including NK group 2, member D (NKG2D), NKp30, and NKp46 as a mechanism for immune evasion. Expression of *metastasis-associated in colon cancer-1* (*MACC1*) gene on NPC cells and enhanced level of soluble MHC class I chain-related molecular A (MICA) is correlated with the downregulation of NKG2D surface expression on NK cells, contributing to tumor progression (42–44). Moreover, the expression of inhibitory receptors such as IL-18-induced PD-1 also mitigates the anti-tumor effect of NK cells (45). Paradoxically, in a recent transcriptomic study of

NPC-infiltrating cells, Gong et al. reported expression of cytotoxic genes and chemokine encoding genes in NK cells of the NPC microenvironment, indicating their role as a positive regulator of the immune response against the malignancy (17).

B-cells represent the second largest and most diverse cells in the NPC microenvironment. In particular, EBV positivity is correlated with an increase in B-cell abundance and diversity. The various phenotypes of tumor-infiltrating B-cells include memory B-cells, germinal center B-cells, plasmablast-like cells and plasma cells. B-cells are recruited into tertiary lymphoid structures by tumor-derived PD-1$^+$ exhausted CD4$^+$ T- cells through the CXCL13/CXCR5 axis (20, 46, 47). CD19$^+$ B-cells positively correlated with better prognosis in EBV-positive NPC patients (48). Consistent with this finding, higher expression of B-cell-associated gene signatures such as *CD79A*, *MS4A1*, *IGHD* and *FCRL4* favored the survival in NPC patients, suggesting potential anti-NPC immunity by NPC-infiltrating B-cells (17). In contrast, IL-10$^+$ B-cells are immunosuppressive B-cells induced by NPC-derived miRNA-21 (49).

Tumor-Infiltrating Myeloid Cells

MDSCs, macrophages and DCs are the three major myeloid-lineage subtypes in the NPC microenvironment. Under the influence of tumors, alteration of myelopoiesis and impairment of progenitor cells differentiation leads to accumulation of MDSCs. Metabolic alteration by EBV-encoded latent membrane protein (LMP)1 enhances the secretion of IL-1β, IL-16 and GM-CSF through NLRP3 inflammasome, cyclooxygenase-2 (COX-2) and P-p65, which subsequently activates signal transducer and activator of transcription (STAT)-3 signaling pathway to induce MDSCs accumulation (50, 51). Many signature genes of MDSCs are associated with exhaustion and cell cycle arrest of immune cells, implying their role in the induction of immunosuppression through inhibition of T-cell proliferation, promotion of T-cell anergy, and induction of T-cell apoptosis (17, 51). Other than that, MDSCs directly promote NPC cell migration, invasion, and metastasis *via* contact-dependent induction of epithelial-mesenchymal transition (EMT) in NPC cells *in vitro* through upregulation of *COX-2* expression and activation of *β-catenin/TCF4* pathway. Clinically, HLA-DR$^-$CD33$^+$ MDSCs and *COX-2* predict poor disease-free survival (DFS) in NPC patients (32).

Monocytes and macrophages are the most predominant cell types in TIMs, which account for around 50% of TIMs in NPC (52). Macrophages may replace T-lymphocytes in anti-tumor immune response and preventing lymphatic spread (53). Macrophages demonstrate a high degree of plasticity when exposed to signals from the TME (52). They can be classically polarized into inflammatory M1 macrophages or activated into immunosuppressive M2 macrophages (54). NPC cells induce polarization of CD163$^+$ M2 macrophages *via* TGF-β1 and IL-10, which subsequently recruits Foxp3$^+$ Tregs through induction of conversion from naïve T-cells, *via* TGF-β and IL-2, and chemotaxis, leading to immune escape. Tregs, in return, secrete TGF-β1 and IL-10 to promote M2 macrophage differentiation, forming a positive feedback loop that favors immune escape in NPC (55). Single-cell transcriptomic analysis *via* RNA sequencing reported co-expression of M1 and M2 gene signatures in NPC-derived TAMs, suggesting an M1-M2 coupled activation pattern in TMEs which gives rise to a unique phenotype that exhibits both pro-inflammatory and pro-tumoral functions (18). The potential anti-tumor capacity of NPC-derived macrophage is exhibited by its high expression of CXC chemokine ligands CXCL9 and CXCL10 which recruit CXCR3$^+$ NK cells and CD8$^+$ T-cells into the TME (20). In contrast, pro-tumorigenic TAMs display expression of angiogenic signature *SPP1*, which is typically associated with poor prognosis (31). Furthermore, exosomal miR-18a derived from M2 macrophages promote NPC progression, invasion, and tumor growth in *in vitro* and *in vivo* animal models *via* TGF-β signaling pathway by repression of transforming growth factor-beta III receptor (TGFBR3) (56).

DCs initiate antigen-specific immune responses by recognition and presentation of antigen to T-cells. Early studies reported the presence of T-zone histiocytes such as DCs in about half of NPC tissues, their densities significantly correlates with favorable prognosis in NPC patients, implying their role in anti-tumor immunity (57, 58). Tumor-infiltrating DCs can be immunogenic or regulatory, depending on the environmental signals. Different subtypes of DCs are present in the TME, for instance, classical dendritic cells (cDCs) and plasmacytoid dendritic cells (pDCs). The proportion of pDCs is high in NPC compared to other malignancies. pDCs are associated with favorable prognostic value, which implies their potential roles in the induction of anti-tumor immune response. Consistent with this finding, *GZMB*, a gene that encodes pro-apoptotic enzyme GzmB, is highly expressed in pDCs (20). On the other hand, cDCs can be further divided into three distinct subsets, including classical *CLEC9A*$^+$ cDC1s and *CDC1C*$^+$ cDC2s and a mature phenotype *LAMP3*$^+$ cDCs. *LAMP3*$^+$ cDCs can be derived from both cDC1s and cDC2s, resulting in *LAMP3*$^+$ cDCs with different transcriptomic properties and might exhibit diverse functions. *LAMP3*$^+$ cDCs represent a group of regulatory DCs demonstrating a high level of differentiation and apoptosis but low antigen presentation, with elevated expression of immune-suppressive related genes, such as *CD274* (PD-L1), *PDCD1LG2* (PD-L2), *IDO1*, and *CD200*. These cells potentially exert regulatory activities *via* recruitment of Tregs, secretion of immunosuppressive molecules, and ligand-receptor inhibition of T-cell activities (21, 31).

Intercellular interactions among LAMP3$^+$ DCs, Treg cells, exhausted CD8$^+$ T-cells, and malignant cells nurture an immunosuppressive NPC microenvironment. LAMP3$^+$ DCs potentially recruit peripheral Tregs through C-C motif chemokine ligand (CCL)/C-C motif chemokine receptor (CCR) interactions such as the CCL17/CCR4 and CCL22/CCR4 signalling pathways. Furthermore, LAMP3$^+$ DCs elicit suppressive activities on CD8$^+$ T-cells *via* CD200/CD200R signalling and PD-L1/PD-1, leading to the exhaustion of CD8$^+$ T-cells. On the other hand, Treg cells expressing CTLA-4 interacts with CD80/CD86 on LAMP3$^+$ DCs, whereby the interaction might restrain the antigen presentation of DCs and promote their secretion of IDO1 to induce the proliferation of Treg cells (21).

The proportion of mast cells is relatively higher in NPC when compared to other malignancies. NPC-derived mast cells have a high anti-tumor *TNF* to angiogenic *VEGFA* ratio, implying high anti-tumor capacity, whereas mast cells in other malignancies are generally pro-tumorigenic. Hence, mast cells are correlated with a survival advantage in NPC. The anti-tumor phenotype of mast cells is possibly driven by the presence of $IL1B^+$ macrophages *via* IL1B/ADRB2 ligand-receptor interaction (31, 59).

Cancer-Associated Fibroblasts

CAFs, also termed tumor-associated fibroblasts, are found abundantly in the cancer stroma. CAFs have elongated spindle morphology, displayed mesenchymal biomarkers, such as alpha-smooth muscle actin (α-SMA), platelet-derived growth factor receptors (PDGFRs), vimentin and fibroblast activation protein (FAP), and lack of genetic mutations (60, 61). The CAFs predecessors are recruited from diverse origins, which include resident tissue fibroblasts, peri-tumoral adipocytes, endothelial cells through endothelial-mesenchymal transition (EndMT), epithelial cells through EMT, bone-marrow-derived mesenchymal stem cells and haematopoietic stem cells (25, 60, 62). In NPC, extracellular vesicle-packaged EBV-encoded LMP1 can promote the activation of normal fibroblasts into CAFs *via* the nuclear factor-kappa B (NF-κB) p65 pathway (63). α-SMA expression in CAFs predicted an adverse prognosis in patients with NPC. A high density of CAFs is correlated with shorter OS and lower 5-year survival rates, suggesting CAF density as an independent prognostic factor for NPC patients, suggesting their role in tumorigenesis (64). Consistent with this finding, several studies reported that CAFs promote neoangiogenesis, metastasis, and therapeutic resistance in NPC (65–67).

CAFs stimulate neoangiogenesis in NPC. Genes correlated with endothelial cells abundance were highly expressed by fibroblasts, implying their potential roles in endothelial cell recruitment and angiogenesis (18). The immunohistochemical method revealed high expression of α-SMA fibroblasts in NPC stroma, together with increased intensities of the chemokine stroma-derived factor-1 (SDF-1, also known as CXCL12), a mediator of the recruitment of endothelial progenitor cells, and its receptor CXCR4 in NPC cells. Vascular endothelial growth factor (VEGF) was detected in both cancer and stromal cells, indicating secretion of a significant amount of VEGF in these cells. Prominin 1 (PROM 1, or CD133) and VEGF receptor (VEGFR)-2 double-positive endothelial progenitor cells or CD34 positive cells were observed in the stroma, suggesting tumor-associated neoangiogenesis. Statistical analyses revealed a positive correlation between α-SMA and endothelial antigens CD34, suggesting that CAFs and NPC tumor cells may enhance neoangiogenesis in a VEGF- and SDF-1-dependent manner by the recruitment endothelial progenitor cells from the bone marrow into the tumor stroma (65).

CAFs support tumor metastasis in NPC. Increased density of α-SMA-expressing CAFs at metastatic sites of NPC compared with primary sites, along with upregulation of COX-2 or prostaglandin-endoperoxide synthase (PTGS2) in CAFs, indicated the involvement of fibroblasts and COX-2 in NPC metastasis. High expression of COX-2 catalysed CAF-secreted prostaglandin E2 (PGE2), which induces EMT, thereby promoting NPC cell migration and invasiveness *in vitro*. Furthermore, COX-2 in host fibroblasts promotes lung metastasis and correlated with the expression of TNF-α expression in mouse models, suggesting that high expression of COX-2 in fibroblasts promotes NPC metastasis through the COX-2-PGE2-TNF-α axis. Consistent with this finding, the expression of COX-2 in CAF was positively correlated with N stage, relapse, and poor survival in patients with NPC (66).

CAFs promote therapeutic resistance and immune evasion. CAFs induced the formation of radioresistance and promoted NPC cell survival following irradiation *via* the IL-8/NF-κB pathway to reduce irradiation-induced DNA damage. Moreover, CAFs express immunosuppressive factor *IDO1*, which encodes the enzyme IDO. IDO catalyses the production of L-kynurenine (Kyn), which subsequently promote the generation or differentiation of tolerogenic immune cells by interacting with aryl hydrocarbon receptors on immune cells. High expression of IDO is inversely correlated with the density of $CD3^+$ T-cells and predicted poor survival outcomes in NPC patients. Hence, CAFs may promote immune suppression in NPC by the expression of IDO (18, 68).

CAFs exhibit a supportive role in tumor progression through the remodeling of the ECM (25). NPC-derived fibroblasts express genes that encode ECM components, including *COL1A1*, *COL1A2*, *LUM*, *FN1*. This suggests the complexity of ECM in the NPC microenvironment and the possible interaction with tumors and stromal cells *via* integrin signaling, indicating integrin receptors on tumor and immune cells as potential therapeutic targets for disruption of ECM-dependent tumor progression and suppressive immunomodulation (17). Increased production and crosslinking of collagen, such as COL1A1, increase the stiffness of ECM, leading to the promotion of tumor progression through increased integrin signaling (25, 27). On the other hand, fibronectin 1 (FN1) is shown to increase migration and invasion of NPC cells by upregulation of matrix metalloproteinase 9 (MMP9) and MMP2, which are ECM-digesting enzymes mainly produced by CAFs. FN1 also suppresses NPC cell apoptosis *via* the NF-κB pathway by upregulation of the expression of BCL2 and P65 (25, 69). CAFs mediated directional migration of cancer cells by assembling a fibronectin-rich ECM with anisotropic fiber orientation through increased non-muscle myosin II- and PDGFRα-mediated contractility and traction forces (62, 70).

Angiogenesis, Tumor Endothelial Cells and Hypoxia

Angiogenesis, the formation of blood vessels from existing vasculature in response to a hypoxic condition, is one of the hallmarks of cancer that contributes to tumor growth, development and metastases (71). The vascular niche is associated with stem cell-like NPC at the invasive front (72). The tumor vasculature is lined internally by TECs and surrounded externally by perivascular cells. TECs are characterized by their genetic instability, which contributes to the development of distinct phenotypes that promote therapeutic resistance, tumor progression and metastasis. TECs also interact

with tumor cells by secretion of angiocrine factors, contributing to tumor migration and metastasis (73, 74). Drug-resistant human microvasculature endothelial cells (HMECs) are reported to promote progression, EMT and chemoresistance in NPC through secretion of exosomes (75). In NPC, TECs demonstrated enhanced capacity to recruit CTLs and Tregs *via* CXCL9–CXCR3 and CXCL10–CXCR3 while simultaneously inhibiting CTLs through PDL2–PD1 interaction, suggesting their role in the mediation of an immunosuppressive niche in the NPC microenvironment (18).

Hypoxia was detected in over 80% of NPC tumors as a result of the high requirement of oxygen due to increased proliferation and metabolism. It was reported to play an important role in NPC by regulating its apoptotic activity, metastasis, angiogenesis, metabolic adaptation, and therapeutic resistance, thereby representing a potential target for the treatment of NPC. Hypoxic stress prevents cell survival by inducing the upregulation of anti-apoptotic proteins such as growth arrest and DNA-damage-inducible beta (Gadd45β) and immediate early response 3 (IER3) (76). Hypoxia promotes tumor cell migration by EMT stimulation and ECM remodeling through Notch signaling (27). Lysyl oxidase (LOX), an extracellular matrix-remodeling enzyme, was significantly upregulated in hypoxic conditions and predicted poor prognosis in patients with NPC (76, 77). In addition, hypoxia induces the upregulation of VEGF, which is responsible for neoangiogenesis. Furthermore, hypoxia mediates metabolic adaptation and acidosis in NPC (76). A metabolic shift in NPC infiltrating lymphocytes was reported to induce the exhausted phenotype of T-cells through overexpression of miR-24. miR-24 overexpression suppresses the expression of MYC and FG11 in TILs and disrupts MFN1-mediated mitochondrial fusion, thereby inducing T-cell exhaustion (78).

Various molecular signals and tumor-derived factors are involved in angiogenesis. VEGF is a pro-angiogenic factor that activates and stimulates proliferation and migration in VEGFR expressing endothelial cells. VEGF also alters vascular permeability by loosening the junctions between endothelial cells, favouring tumor intravasation (79). Besides hypoxia, increased VEGF production can be induced by EBV-encoded LMP1 through COX-2 expression in NPC cells (80). High expression of tissue VEGF is associated with reduced OS and DFS in NPC patients (81).

INTERCELLULAR COMMUNICATIONS IN NASOPHARYNGEAL CARCINOMA MICROENVIRONMENT

Intercellular communication between malignant and stromal cells in the NPC microenvironment is established *via* paracrine mechanisms involving cytokines and chemokines, extracellular vesicles including exosomes and ligand-receptor interactions. The NPC microenvironment is primarily comprised of heavy immune infiltrates, with $CD3^+$ T-lymphocytes as the most abundant lymphocyte infiltrates in NPC biopsies (37, 82). EBV-encoded proteins, such as LMP1, initiate immune cell recruitment by the regulation of multiple signalling pathways associated with cytokine and chemokine secretion from tumor and immune cells. Immunosuppression, mediated by cytokines and regulatory cells, facilitates malignant cells to escape from anti-tumor immune response and promotes tumor growth and progression. Tumor-derived exosomes, carrying viral proteins and immunosuppressive substances, and ligand-receptor interactions, such as PD-1/PD-L1 signalling pathway, also contribute to the construction of an immunosuppressive TME (28, 83).

Chemokines and Cytokines

EBV-infected nasopharyngeal epithelial cells construct the NPC microenvironment, which is characterized by heavy infiltration of immune cells with suppressed immune activities, by secretion of EBV-encoded products that activate several inflammatory-associated signalling pathways. A variety of cytokines, such as IL-6, IL-8, interferon-inducible protein 10 (IP-10), TNF-α, VEGF, and macrophage inflammatory protein (MIP)-3α are elevated in NPC patients (84). LMP1 recruit immune cells into the tumor site by upregulating several cytokines through NF-κB and STAT3 signaling pathways (82, 85). These include regulatory cells with immunosuppressive influence in the TME. NPC cells induce polarization of macrophage into immunosuppressive M2-like phenotype through secretion of interferon-stimulated gene 15 (ISG15) (18). EBV nuclear antigen 1 (EBNA1) induce the production of CCL20, or MIP-3α to promote chemotaxis of Tregs to the tumor site (86, 87). In addition, EBV-encoded small RNAs (EBERs) activates the toll-like receptor 3 (TLR3) pathway to produce inflammatory cytokines such as CXCL8 which recruit and activate TAMs. The inflammatory responses in NPC cells are amplified by a positive feedback loop consisting of EBER, LMP1 and NF-κB (88). Metabolic reprogramming by LMP1 leads to alteration in Nod-like receptor family protein 3 (NLRP3) inflammasome, COX-2 and P-p65 signaling pathways, which results in the release of cytokines, including IL-1β, IL-6 and granulocyte-macrophage colony-stimulating factor (GM-CSF), contributing to the expansion of MDSCs (50). Stromal cells, including TECs, can attract CTLs and Tregs *via* chemokine-receptor interactions such as CXCL9/CXCR3 and CXCL10/CXCR3, however, cytotoxic activities of CTLs are inhibited by PD-L2/PD1 interaction (18).

Chemokines and cytokines facilitate tumor elusion from immune surveillance. EBER, LMP1 and EBV lytic transactivator, Zta, are positively correlated with the production of IL-10. BCRF1, or viral IL-10, share immunosuppressive properties with human IL-10. IL-10 induces immunosuppressive activities by inhibition of antigen-specific T-cell proliferation, induction of T-cell apoptosis and inhibition of IFN-γ secretion from NK cells. LMP1 upregulates IL-18 and IP-10 (CXCL10), which take part in the recruitment and immunosuppression of $CXCR3^+$ NK cells and T-cells (45, 82, 85, 89). IL-6 and TNF-α mediate the expression of IDO, which demonstrates an immunosuppressive role by suppression of T-cell proliferation and impairment of $CD8^+$ T-cells cytotoxic activities. Pre-treatment serum levels of IL-6 and TNF-α are negatively correlated with the 2-year survival rate in

NPC patients (90, 91). Increased levels of IL-18 in NPC induces NK cells exhaustion *via* upregulation of expression of PD-1 on NK cells (45).

Furthermore, chemokines induce metastasis and promote tumor progression. IL-8 induce EMT by activating AKT signalling, enhancing migration and invasion of NPC cells. Enhanced level of IL-8 predicts adverse OS, DFS, and DMFS of NPC patients (92).

Exosomes

Exosomes are small (30-100 nm) extracellular vesicles that originated from the plasma membrane. They are often involved in the intercellular interactions in the TME, influencing various cellular processes, including cell growth, angiogenesis, EMT, metastasis, immune tolerance, and therapeutic resistance (93). Exosomes may play a significant role in the formation of a premetastatic milieu by acting as a vehicle for tumor-derived factors that modulate pre-metastatic sites (15). Exosome contents include transcription factors, enzymes, ECM proteins, lipids, and nucleic acids, such as DNA, mRNA, and non-coding RNA. Based on their parental cells, exosomes in NPC can be classified into nasopharyngeal carcinoma-derived exosomes (NPC-Exo) and EBV-related exosomes (94–96).

NPC-Derived Exosomes

NPC-derived exosomes (NPC-Exos) [1] mediate the tumor immune microenvironment, [2] enhance angiogenesis, [3] induce EMT and [4] promotes resistance towards chemoradiotherapy as summarized in **Tables 1** and **2**. NPC-Exo facilitates tumor progression by promoting tumor evasion from immune surveillance. NPC-Exo carries clusters of microRNAs (miRNAs) associated with the downregulation of the MARK1 signaling pathway, including miR-24-3p, miR-891a, miR-106a-5p, miR-20a-5p, and miR-1908, leading to altered T-cell proliferation and differentiation. Hypoxia-induced exosomal miR-24-3p modulates the phosphorylation of ERK and STAT protein by repression of FG11 expression, leading to impeded T-cell proliferation, induction of $Foxp3^+$ Tregs differentiation and inhibition of Th1 and Th17 differentiation. Low levels of exosomal serum miR-24-3p and high FGF11 expression predicts favorable DFS in NPC patients and may serve as potential prognostic biomarkers in NPC. Furthermore, NPC-Exo enhances the levels of pro-inflammatory cytokines IL-1β, IL-6 and IL-10 and reduce the levels of IFN-γ, IL-2 and IL-17 in $CD4^+$ and $CD8^+$ T-cells (113, 114, 125). Exosome-packaged CCL20 expands the Tregs population by promoting Tregs recruitment and conversion of conventional T-cells into inhibitory Tregs in the TME. CCL20 also enhances the suppressive effect of Tregs by inducing the overexpression of *TNFRSF4*, *SELL*, *ICAM1*, *TBX21*, *CCR6*, *TNF*, *GZMB*, *TGFB1*, *IL10*, *IL2* and *IL15*, which are associated with Treg phenotype, properties, and recruitment capacity (107, 113). Moreover, exosomes also transport Gal-9, which is associated with myeloid lineage-mediated immunosuppression through regulation of the expression of pro-inflammatory cytokines for the expansion of MDSCs by attenuating STING signaling (100).

Exosomes mediate angiogenesis by the transportation of pro-angiogenic and angiogenic-suppressive proteins and miRNAs, which mediate multiple angiogenesis-associated pathways (99). miR-17-5p and miR-23a are angiogenesis promoters, targeting BAMBI and testis-specific gene antigen (TSGA10) respectively (108, 109). In contrast, miR-9 inhibits angiogenesis by downregulating MDK and regulating PDK/Akt pathway.

Exosomes are also involved in the promotion of tumor invasion and metastasis. For instance, miR-301a-3p, which targets B-cell translocation gene 1 (*BTG1*) mRNA, promotes proliferation, migration, invasion and EMT of NPC (115). Under hypoxic condition, exosomes containing MMP13promotes metastasis by inducing EMT of malignant cells or mediating the TME by interacting with stromal fibroblasts and endothelial cells, hence promoting tumor invasion (105, 106).

Exosomes contributed to the development of resistance towards chemotherapy and radiotherapy. Taxol-resistant NPC cells can transfer dead-box helicase 53 (DDX53) into normal NPC cells to promote resistance to Taxol through upregulation

TABLE 1 | Exosomal content and their functions.

Class	Exosomal content	Function	Ref
Protein	HAX-1	Tumor growth, angiogenesis	(97)
	HMGB3	Angiogenesis, metastasis	(98)
	ICAM-1, CD44v5	Angiogenesis	(99)
	Gal-9	Immunosuppression	(100)
	HIF-1α	Metastasis	(101)
	DDX53	Chemoresistance	
lncRNA	CCAT2	Angiogenesis	(102)
circRNA	circMYC	Radio-resistance, cell proliferation	(103)
Enzyme	PFKFB3	Angiogenesis, tumor proliferation and metastasis	(104)
	MMP13	Invasion and metastasis	(105, 106)
Chemokine	CCL20	Immunosuppression	(107)
miRNA	miR-17-5p, miR-23a, miR-BART-10-5p, miR-18a, miR-144	Pro-angiogenesis	(108–111)
	miR-9	Anti-angiogenesis	(112)
	miR-24-3p, miR-891a, miR-106a-5p, miR-20a-5p, miR-1908	Immune regulation	(113, 114)
	miR-301a-3p	Metastasis	(115)
	miR-34c, miR-433-3p		(116, 117)

TABLE 2 | Clinical studies targeting NPC microenvironment.

Target	Ref	Study	Conditions	Phases
Immunotherapy				
CTLA-4 & PD-1	NCT04220307	AK104	Metastatic NPC	II
	NCT04945421	IBI310 & Siltilimab	Anti-PD-1/PD-L1 Resistance R/M NPC	I/II
	NCT02834013	Ipilimumab & nivolumab	Rare tumors, including NPC	II
	NCT03097939			
EBV	NCT03648697	EBV-TCR-T (YT-E001) cells	EBV-positive R/M NPC	II
	NCT02287311	LMP, BARF1 & EBNA1 Specific CTL	R/M NPC	I
	NCT02578641 (118)	EBV-specific CTL & Chemotherapy	Advanced NPC	III
LMP2	NCT03925896	LMP2 Antigen-specific TCR T-cell Therapy	R/M NPC	I
PD-1	NCT03707509	Camrelizumab & Chemotherapy	R/M NPC	III
	NCT04944914	Camrelizumab & Stereotactic Body RT	R/M NPC	III
	NCT04978012	Camrelizumab & Fluzoparib	NPC	II
	NCT04833257	Chemotherapy & Tislelizumab	LA-NPC	II
	NCT04447612	Durvalumab & chemoradiation	R/M, platinum-resistant NPC	II
	NCT02339558 (119)	Nivolumab	R/M NPC	II
	NCT03267498	Nivolumab & Chemoradiation	Stage II - IVB NPC	II
	NCT03544099	Pembrolizumab	NPC	II
	NCT03734809	Pembrolizumab & Chemoradiation	NPC	II
	NCT04736810	Penpulimab Combination Therapy	NPC	II
	NCT03558191	SHR-1210	R/M NPC	II
	NCT04917770	Sintilimab & Multimodal RT	NPC	II
	NCT04376866	Toripalimab	Recurrent NPC	III
	NCT03925090	Toripalimab & CCRT	NPC	II
	NCT04534855	Treprilimab	Recurrent NPC	II
	NCT04421469	Triprilimab (JS001) & Chemotherapy	NPC	II
PD-1 & EBV	NCT03044743	PD-1 knockout EBV-CTLs	Advanced EBV-associated malignancies	I/II
PD-L1	NCT04282070	SHR-1701	R/M NPC	I
PD-L1 & VEGFR-2	NCT05020925	SHR-1701 & Famitinib	NPC	I/II
TGF-β	NCT02065362	TGF-β Resistant CTLs	EBV-positive NPC	I
TIM-3	NCT02817633	TSR-022 (combolimab)	Advanced solid tumors	I
T-cells	NCT04476641	DC-CIK Immunotherapy	Solid tumors, including NPC	II
Anti-angiogenic therapy				
VEGF	NCT00408694 (120)	Bevacizumab & Chemoradiation	LA NPC	II
VEGF/VEGFR signaling	NCT02636231	Endostar	Recurrent NPC	II
	NCT04447326 (121)	Endostar & Chemotherapy	LA-NPC	II
	NCT03932266		NPC	II
VEGFR	NCT03639467	Anlotinib & Gemcitabine/Cisplatin	R/M NPC	Ib/II
	NCT01462474 (122)	Famitinib & chemoradiation	LA NPC	I
	NCT00454142 (123)	Pazopanib	R/M NPC	II
	NCT00747799 (124)	Sorafenib & chemotherapy	R/M NPC	II
VEGFR & PD-L1	NCT04562441	Axitinib & Avelumab	R/M NPC	II

R/M, recurrent/metastatic; LA, locally advance.

of multidrug resistance 1 (MDR1) (126). circMYC is a circulating exosomal circular RNA (circRNA) associated with cell survival from radiotherapy. circMYC could sponge tumor suppressing miR-20b-5p and let-7e-5p, hence influencing their downstream targets, argonaute RISC component 1 (AGO1) and cryptochrome circadian regulator 2 (CRY2), affecting tumor progression (103).

EBV-Related Exosomes

EBV-infected NPC cells promote tumor growth by transferring viral oncoprotein such as LMP1, signal transduction molecules, and virus-encoded miRNA through exosomes (127). It is reported that recipient cells internalized exosomes derived from EBV-infected cells *via* caveola-dependent endocytosis (128).

LMP1 is an EBV-encoded gene product that is detected in almost all primary NPC specimens. A small amount of LMP1 facilitates tumor progression, whereas high LMP1 expression induced growth inhibition and cell apoptosis. LMP1 exerts its oncogenic activity by activating several signaling cascades including NF-κB, PI3K-AKT, ERK-MAPK, JNK, JAK-STAT and p38/MAPK signaling pathways. Activation of NF-κB and STAT3 pathway results in increase secretion of immunomodulatory molecules, for instance, IL-18 and IP-10, which recruit and suppress $CXCR3^+$ T-cells and macrophages. LMP1 and IFN-γ upregulate immune checkpoint PD-1/PD-L1 synergistically, leading to suppression of anti-tumor activities. Furthermore, LMP1 induce the Warburg effect in NPC through upregulation of hypoxia-inducible factor (HIF)-1α and hexokinase 2, leading to enhance malignant transformation, tumor progression and resistance to radiotherapy. In addition, LMP1 facilitates metastasis by inducing EMT, through upregulation of Twist, Snail and SatB1 pathways, and remodeling of ECM, by induction of MMP9. LMP1 also promote angiogenesis, cell growth and cell survival through induction of pro-angiogenic

factors, growth factors and anti-apoptotic proteins (85, 129). LMP-1 activated NF-κB induces cellular proliferation, EMT and metastasis by inhibition of tumor suppressing miR-203 (130).

EBNA1 promotes immunosuppression by converting naïve T-cells into Treg cells and promotes chemotactic migration of Treg cells by upregulating TGF-β1. Upregulation of the TGF-β1-SMAD3-PI3K-AKT-c-JUN axis induces the production of CXCL12 which recruit Treg cells by binding to CXCR4. On the other hand, TGF-β1 downregulates miR-200a, a negative regulator of CXCL12 by enhancing the SMAD3/c-Jun complex. CXCL12 also exerts an inhibitory effect on miR-200a *via* the c-Jun-miR-200a-CXCL12-c-JUN feedback loop (36). Enhanced CCL20 production in EBNA1-expressed tumor cells increased Tregs migration. Polarized-M2 macrophages by EBNA1 expression cells converted naïve T-cells into Tregs (86).

EBV non-coding RNAs (ncRNAs) include EBERs and miRNAs. EBERs mediate inflammatory response through interferon regulatory factor 3 (IRF3) and NF-κB signaling pathways by targeting RIG-I, leading to tumor progression. EBERs trigger MCP-1 and M-CSF which recruit macrophages into the TME and promote their differentiation into pro-tumorigenic TAMs (131, 132). EBER-1 expression was upregulated in NPC tissues, a high level of EBER-1 correlated with better prognosis in NPC patients (133). The EBV miRNA precursors are clustered in two main regions, which are Bam HI fragment H rightward open reading frame 1 (BHRF1) and Bam HI-A region rightward transcript (BART). EBV-miRNAs assist NPC progression by promotion of immune evasion, cell proliferation, inhibition of apoptosis and promotion of invasion and metastasis (134, 135).

TARGETING TUMOR MICROENVIRONMENT IN NASOPHARYNGEAL CARCINOMA: CURRENT AND FUTURE PERSPECTIVES

Immunotherapy: Boosting T-Cell Immunity

NPC is a promising candidate for immunotherapy owing to its immunosuppressive property and expression of immunogenic EBV antigen. Several approaches which include immune checkpoint inhibitors and cellular-based immunotherapy have been employed to reinvigorate the exhausted immune cells in the NPC microenvironment (83) (**Table 2**). PD-1/PD-L1 axis has been exploited as a potential therapeutic target for reversing T-cells exhaustion and restoration of their anti-tumor function (136, 137). PD-1 is an immune checkpoint encoded by the *PDCD1* gene and expressed on the T-cell surface, whereas PD-L1 is expressed on tumor cells and immune cells. Studies reported expression of PD-L1 in approximately 70 - 90% of NPC tissues and its prognostic significance. The difference in interpretational methods leads to inconsistency of results, suggesting the need for further large-scale study (138–141).

PD-1/PD-L1 blockade therapies with anti-PD-1 antibodies, such as nivolumab, pembrolizumab, cemiplimab and anti-PD-L1 antibodies, including atezolizumab, avelumab and duravulumab have been implicated in immunotherapy against various neoplasms (136, 137). Anti-PD-1 and anti-PD-L1 therapies are generally safer than chemotherapy, with a lower incidence of treatment-related adverse events (142, 143). Single-agent studies involving PD-L1 antibodies showed lower overall response rate (ORR), OS and progression-free survival (PFS) when compared with studies with PD-1 antibodies, likely due to alternative binding of PD-1 to PD-L2 following blockade of PD-L1. Combination therapy of chemoradiation and PD-1/PD-L1 promote a synergistic anti-tumor immunity by enhancing host recognition, elimination of tumor cells and preventing T-cell apoptosis. For instance, a phase I trial investigating anti-PD1 antibody camrelizumab achieved an ORR of 34%, whereas a combination trial of camrelizumab with gemcitabine and cisplatin achieved an ORR of 91%. In spite of that, combination therapy exhibited a higher incidence of treatment-related adverse events when compared with anti-PD-1 monotherapy, suggesting synergistic toxicity (142, 143). There is also limited anti-tumor response rate towards PD-1/PD-L1 blockade therapy. Resistance to PD-1/PD-L1 therapy involves multiple mechanisms, including low tumor immunogenicity, T-cell dysfunction by other immune checkpoint receptors and modulation by noncoding RNAs.

Strategies to overcome the challenge include the incorporation of PD-L1/PD-1 inhibitors with other anti-tumor therapy. Ongoing clinical trials propose the combination of PD-1/PD-L1 blockade with other immune checkpoint inhibitors such as anti-CTLA-4 or anti-angiogenic agents such as anti-VEGFR inhibitors as potential therapeutic strategies for NPC (144, 145). Besides that, the identification of predictive biomarkers of PD-1 inhibitors will allow the selection of appropriate patients for PD-1/PD-L1 targeted treatment (136). Other immune regulatory checkpoints, for instance, the Gal-9/TIM-3 (HAVCR2) interaction represents a promising alternative as they are prominently expressed in recurrent NPC (20, 146).

Two approaches of cellular-based immunotherapy include adoptive immunotherapy, which is the infusion of *ex vivo* generated activated effector cells, such as EBV-specific CTLs, chimeric antigen receptor (CAR) engineered T-cells and cytokine-induced killer cells (CIKs) (147–150). An increase in the frequency of MDSCs, and immunosuppressive cytokines, such as CCL2 and CXCL10, underlie the development of resistance towards adoptive immunotherapy. Chemotherapeutic agents, such as gemcitabine and carboplatin may alleviate the resistance by limiting the expansion of MDSCs, secretion of pro-inflammatory cytokines and depletion of immune checkpoint molecules (151). A phase II study combining chemotherapy with adoptive immunotherapy using engineered EBV-specific CTLs as first-line treatment for metastatic or recurrent NPC patients yield a satisfactory result, with a 2-year OS of 62.9% (118). On the other hand, active immunotherapy or tumor vaccines aim to enhance recognition by the immune system by the delivery of tumor-specific antigens through antigen-presenting cells or viral vectors. These include LMP2 expressing DCs and recombinant modified vaccinia Ankara vaccine (MVA-EL), which has been proved to be safe and well-tolerated (152, 153). Besides targeting EBV-encoded

oncoproteins, a peptide vaccine targeting non-EBV associated tumor specific antigen, four-jointed box 1 (FJX1), was also designed in a preclinical setting (154).

Further research should consider [1] large-scale studies for the evaluation of clinical efficacy and the optimization of dosage for the above therapy; [2] combination of therapies to augment the clinical responses, for example, combining immune checkpoint blockade with adoptive T-cell therapy (155–157); [3] development of personalized immunotherapy targeting neoantigens (158); and [4] localization of NPC-specific CTLs at the malignant site, for example, *via* chemokine-receptor interactions (159). Other alternatives, for example, CAR-NK, an emerging cellular immunotherapy strategy for cancer, should be evaluated in NPC, given its promising clinical efficacy in other settings (160).

Tumor Infiltrating Immune Cells as Prognostic Markers

Immune score, established based upon the density of lymphocyte populations, is predictive of disease progression and distant metastases. High immune scores predict better OS, DFS and distant-metastasis free survival (DMFS) of NPC patients (37). Among TILs, $CD3^+$, $CD4^+$, and $CD8^+$ T-cells as well as $CD56^+$ NK cells are good prognostic factors for NPC patients (161–163). Despite its immunosuppressive role, high $Foxp3^+$ T-cells to $CD8^+$ T-cells ratio was associated with favorable PFS in early-stage NPC patients (164). Similarly, Ooft et al. reported Foxp3 as an independent predictor for better OS in NPC patients (165). On the other hand, CD68+ TAM density predicted favorable DFS, whereas stromal $CD163^+$ M2-like TAMs correlated with poor OS and PFS in NPC patients (20, 166, 167).

Nonetheless, there are discrepancies among studies investigating the prognostic significance for different TIICs, due to different methodologies used. Thus, further studies should consider the development of a standardized method for the evaluation of TIICs as an indicator or predictor for the progression and therapeutic response of NPC patients.

Anti-angiogenic Therapy

Angiogenesis is important to meet the huge demand for oxygen and nutrients by tumor cells, thus, anti-angiogenic therapy using angiogenic inhibitors is a promising anti-cancer therapeutic strategy. Conventional chemotherapeutic agents, for instance, epirubicin, elicits inhibitory activity on angiogenesis by inducing non-specific vascular toxicity (168). On the other hand, hypericin-mediated photodynamic therapy exerts its antitumor activity by targeting the tumor vasculature (169). Several small-molecule inhibitors of VEGFR such as apatinib are employed in angiogenesis-targeting therapy for NPC patients (170, 171). The inhibition of angiogenesis could enhance the effectiveness of standard chemoradiotherapy against NPC. Combination of VEGF inhibitor bevacizumab with chemotherapy promoted microvasculature maturation, enhanced immune infiltration and exhibited promising tumor response (172). Combination therapy of apatinib with cisplatin showed a synergistic effect in inhibition of tumor growth, repression of VEGFR-2 expression and reduction in microvascular density in preclinical models (173). On the other hand, combining apatinib and radiation enhances the anti-angiogenic effect and increases hypoxia in tumor tissues, leading to an anti-tumor effect (174). Endostatin, an endogenous angiogenesis inhibitor is another anti-tumor agent tested in clinical trials. Endostar, a recombinant endostatin, sensitized NPC towards radiation therapy by induction of endothelial cell and tumor cell apoptosis and repression of radiation-induced pro-angiogenic factors (175). Phase II multicentre randomized controlled combining Endostar therapy with standard chemoradiation reported an improved remission rate of cervical lymph node metastasis, with a slight improvement in objective response rate (121). To sum, anti-angiogenic agents targeting VEGF and VEGFR can enhance the effectiveness of chemoradiotherapy through inhibition of blood vessels formation, normalization of blood vessels, which restore vascular function, improve tumor perfusion, and drug delivery, and activation of immune response (176).

Currently, anti-angiogenic therapy faces the challenge of the development of resistance, which leads to limited survival benefits. The resistance is likely due to hypoxic events as a consequence of vascular depletion, resulting in the promotion of cancer invasion and metastasis, activation of alternative pro-angiogenic signalling pathways, VEGF-independent vascular mimicry, and increased recruitment of pro-angiogenic cells (176, 177). Studies unveiled upregulation of several proangiogenic factors, including VEGF, TNF-α, IFN-α, and basic fibroblast growth factor (bFGF), following hypericin-mediated photodynamic therapy. This indicates the need of combination therapies such as photodynamic therapies with angiogenesis inhibitors to enhance the efficacy of treatment (169, 178). Other challenges include toxicity effects, which include haemorrhage, hypertension, and thrombosis (79). Several strategies direct targeting the tumor vessels are introduced to increase the effectiveness of the therapy and minimise the side effects. Nanoparticles might serve as vectors for the delivery of anti-angiogenic drugs to the target site (79). Given the high effectivity for DNA enzyme (DNAzyme) to cleave targeted sequence with high specificity, DNAzyme also serves as a potential therapeutic agent for anti-angiogenic therapy. DNAzyme targeting VEGFR-1 mRNA significantly downregulated VEGFR-1, inhibited angiogenesis and altered the vascular permeability. No toxicity effect was observed *in vivo*, indicating anti-VEGFR-1 DNAzyme as potential drug candidates for further clinical evaluation (179).

Targeting Hypoxic Condition in Nasopharyngeal Carcinoma

The increased oxygen demand by the highly proliferative and metabolically active tumor cells with inadequate oxygen supply from the impaired vasculature leads to hypoxia, a condition that mediates tumor progression, metastasis, and therapeutic resistance. This tumor-specific event has been studied extensively for the development of anti-tumor therapy. Several strategies targeting hypoxia are employed, which include a

cytotoxic approach with hypoxic selectivity. In the hypoxic TME, hypoxia-activated prodrugs such as tirapazamine are preferentially activated into cytotoxic drugs and eliminate hypoxic tumor cells with high selectivity. The second approach direct inhibits hypoxia-inducible proteins. HIF-1α siRNA and PX-478 directly target HIF-1α and elicit anti-tumor activity. Hypoxia-modifying therapy improves the hypoxic condition in tumors by increasing the blood oxygen level through blood transfusion, carbogen, and nicotinamide treatment (76).

The combination of hypoxia-targeting therapy and radiotherapy exhibited a synergistic effect. Topotecan is reported to enhance the radiosensitivity of tumors by inhibiting topoisomerase I and subsequently downregulating the expression of HIF-1α target genes (180, 181). Nanotechnology is also employed to enhance the therapeutic efficacy of hypoxia-targeting therapy. In a preclinical study, nanoparticle delivering siRNA targeting HIF-1α significantly suppressed tumor growth in *in vivo* animal models of NPC (182). In recent studies, hypoxia-responsive nanoparticles have been designed for the selective release of drugs in the hypoxic tumor environment, thereby prolonging the bioavailability and improving the effectiveness of the drug (183). These nanomedicines are still in the early phase, their mechanism, delivery efficacy and safety in human bodies remain to be studied.

Targeting Chemokines and Cytokines

Chemokines and cytokines are potential targets for the development of diagnostic biomarkers or therapeutic strategies. CCL5, also known as RANTES (regulated upon activation, normal T-cell expressed and presumably secreted), is a pro-angiogenic chemokine that can be detected in NPC patients' plasma with 90.07% sensitivity and 56.34% specificity. Increased screening efficacy was observed when combining CCL5 with EBV viral capsid antigen (VCA-IgA) or EBV DNA assay. Inhibition of the CCL5 receptor, CCR5 with its antagonist maraviroc could suppress CCL5-associated migration of NPC cells (184, 185). Leukaemia inhibitory factor (LIF), a member of the IL-6 type cytokine family, is remarkably increased in the TME and NPC patients' serum. Secreted by tumor cells and inflammatory infiltrates, LIF mediates the mTOR pathway in NPC, which leads to tumor growth and enhanced radioresistance. Elevated serum LIF in NPC patients is predictive of local recurrence and radiosensitivity. The blockade of the LIF signalling pathway through a LIF antagonist, soluble LIF receptor, or mTOR inhibitor, rapamycin, could sensitize NPC towards irradiation (186, 187).

The development of anti-tumor therapeutics targeting chemokines or their receptors need to consider [1] the optimal dosage of drugs with concern on their safety and efficacy; [2] evaluation of synergism effect when combined with conventional therapy and immunotherapy; [3] development of drugs with high affinity and high specificity; and [4] identification of tumor-specific targets, with minimal effects on non-tumor-associated cells.

Clinical Applications of Exosomes

Tumor-derived exosomes are involved in a wide range of biological and pathological processes as well as intercellular crosstalk and thus are promising targets for the development of biomarkers and anti-cancer therapies. Exosomes are highly stable and can be detected in patients' body fluids, such as urine, saliva, cerebrospinal fluid, and serum, and hence can be used in liquid biopsies as non-invasive biomarkers (96). Sera exosome concentrations have clinical significance and prognostic value in NPC patients, whereby a positive correlation between tumor lymph node metastasis and shorter disease-free survival was observed in NPC patients.

Nasopharyngeal brush or swab is a less invasive alternative for the collection of tumor tissue samples when compared to the conventional biopsy method. Elevation of EBV miRNAs, including mir-BART1-5p, mir-BART5, mir-BART6-5p, mir-BART17-5p, were reported in nasopharyngeal brush samples from NPC patients. miR-BART1-5p shows potential as a diagnostic indicator of NPC, with 93.5% sensitivity and 100% specificity, its expression level positively correlated with tumor progression (188).

In addition, miR-BART7 and miR-BART13 are significantly elevated in plasma specimens from NPC patients, the combination of both markers offers a 90% prediction of NPC. Furthermore, the level of miR-BART7 is associated with metastatic progression. Diminished levels of miR-BART7 and miR-BART13 were reported after radiotherapy, suggesting their potential as biomarkers for the monitoring of therapeutic efficacy (189). Post-treatment detection of circulating miR-BART17-5p is a potential biomarker of a poor prognosis (190). Plasma EBV-miR-BART7-3p showed 96.1% sensitivity and 96.7% specificity, whereas miR-BART13-3p has a sensitivity of 97.9% and specificity of 96.7% for the detection of NPC. miR-BART7-3p is a potential prognostic biomarker, whereby prominent levels of pre-treatment miR-BART7-3p in plasma indicated a higher risk of distant metastasis whereas post-treatment miR-BART7-3p is associated with short DMFS and OS (191, 192). Significant upregulation of miR-1301-3p was detected in the exosomes from early-stage NPC patients' plasma, indicating their potential application as diagnostic biomarkers in early-stage NPC (193).

Upregulation of circulating exosomal circRNA circMYC is correlated with increase cell proliferation and resistance to radiotherapy in NPC patients. Circulating circMYC is a potential biomarker for the differentiation of radiosensitive and radioresistant patients with 90.24% sensitivity and 94.51% specificity (103). The detection of exosomal cyclophilin A (CYPA) combined with EBV VCA-IgA could increase the accuracy of diagnosis, indicating the utility of exosomal CYPA as a potential non-invasive biomarker for the diagnosis of NPC (194).

Besides serving as biomarkers, exosomes are potential vehicles for the delivery of cancer drugs to the target molecules. iRGD-tagged exosomes targeting αvβ3 integrin-positive NPC cells containing antagomir-BART10-5p and antagomir-18a showed remarkable anti-angiogenic efficacy in *in vitro* and *in vivo* NPC models (110). Exosomes are also employed as vehicles for tumor antigen in cancer vaccines, however, to our knowledge, exosome vaccines have not been tested specifically in NPC yet (195).

While exploiting exosomes as therapeutic and diagnostic tools, there are some challenges that need to be addressed. These include [1] time and cost consumption; [2] unsatisfactory yield, purity, and quality, which could affect [3] the sensitivity and specificity of assays, [4] absence of endogenous control for miRNA quantification, and [5] limited sample size in current studies, which affect the reliability of these studies (196, 197). On the other hand, several problems need to be considered when using exosomes as therapeutic vehicles or targets: [1] enhancing the specificity of therapy to prevent undesirable adverse events; [2] prolonging the half-life of exosomes after administration into the body; [3] effective and safe therapeutic dose of exosomes; [4] effective drug loading into the exosomes; [5] cost and time effectiveness in the production of bioengineered exosomes (93, 196).

Overall, exosomes play a pivotal role in the interplay communication between EBV-infected NPC cells and stromal cells, which contribute to the construction of the TME that favours tumor progression, development, invasion, and metastasis. Further investigations should consider [1] understanding the mechanisms underlying cellular crosstalk *via* exosomes, including the biogenesis and internalization of exosomes; [2] development of standard methods for scalable isolation and purification of exosomes; [3] large-scale clinical studies for the evaluation of exosome as reliable cancer biomarkers.

Cancer-Associated Fibroblasts

The vast influence of CAFs on tumor development and progression made them promising therapeutic targets. Several strategies for CAF-directed anti-cancer therapies have been tested in preclinical settings, but only a few studies are focusing on CAFs in NPC (198). Disulfiram/copper exhibited anti-tumor activity by targeting both cancer cells and CAFs. It could induce apoptosis and inactivate CAFs by inhibiting the expression of α-SMA (199). Treatment with CAF inhibitor, for instance, Tranilast, inhibits CAFs from activating the NF-κB pathway, thus sensitizing NPC cells to irradiation (67). The targeting of CAFs is challenging as they demonstrate complexity in intercellular signaling, phenotype and source and lack of specific surface marker (198). Thus, further understanding of CAFs, with regards to their different phenotype and respective protumorigenic or tumor suppressive properties in TME is required for CAF-targeting therapies.

NF-κB Signaling Pathway

The NF-κB signaling pathway is constitutively activated in 90% of EBV-associated NPC by EBV oncoproteins and genetic mutations. This pathway plays a pivotal role in the intercellular communication and regulation of immune cells in the TME, which renders it a promising target for anti-cancer therapy against NPC (200–202). Strategies targeting the NF-κB signaling pathway include anti-inflammatory compounds such as aspirin, inhibition of IκB kinase (IKK) and proteasome inhibition (130, 203, 204). Acting as an NF-κB inhibitor, aspirin reverses LMP1-induced EMT by suppressing NF-κB-exosomal secretion of LMP1 and promoting miR-203 expression (130). Inhibition of lung metastasis by aspirin is also observed in mouse models. PS1145, an inhibitor of IKK, could abrogate the NF-κB signaling pathway and subsequently inhibit the production of pro-inflammatory cytokine and cell proliferation. PS1145 significantly inhibits the tumor growth of NPC in *in vitro* cell lines and *in vivo* xenograft models (203). Bortezomib, a proteasome inhibitor, targeting STAT1 and NF-κB, could relieve the immune tolerance in NPC (204). Vitexin, a natural flavonoid glycoside targeting NF-κB, displayed promising anti-tumor activity against NPC in preclinical studies (205). Restoration of Ras-like estrogen-regulated growth inhibitor (RERG), an NF-κB inhibitor, by 5-Aza-2'-deoxycytidine and trichostatin A attenuated ERK/NF-κB signaling pathway, resulting in the inhibition of tumor growth and angiogenesis *in vivo*. Therefore, RERG might be employed as a target molecule in cancer therapy (206).

Whilst translating these bench findings into bedside application, several issues need to be addressed. As the NF-κB signaling pathway regulates multiple physiological processes, the development of therapeutic tools should consider developing drug delivery strategies with high specificity to prevent undesirable adverse events. It is reported that the NF-κB complex p50/p50/Bcl3 is prevalent in NPC but seldom found in a normal cell. Thus, Bcl3 inhibitors may represent promising therapeutic agents against NPC (202, 207). Other than that, the route of administration and dosage of NF-κB inhibitors should consider their bioavailability and safety.

CONCLUDING THOUGHTS

The advances in multi-omics technology allow researchers to unravel the complex intercellular communication in the NPC microenvironment, which contributes to the growth, development, progression, and metastasis of this malignancy. Nevertheless, there is a lack of thorough studies on the players in the NPC microenvironment, particularly, B-cells, NK cells, cancer stem cells and the ECM. Of note, spindle-shaped NPC cells predominantly located at the invasive margin of the tumor site display stem cell-like properties and are significantly associated with EMT. Further studies targeting these neoplastic spindle cells might shed light on the understanding of the mechanism underlying tumor cell dissemination, and thus facilitating future development of predictive biomarker and preventive medicine for NPC metastasis (72, 208, 209). Other than that, it is suggested that future studies look into the spatial heterogeneity of the NPC microenvironment to gain further insights into tumor heterogeneity and discover new opportunities for the development of theragnostic tools (210).

Several anti-cancer drugs targeting TME have been tested in clinical trials, however, several pre-clinical and clinical barriers remain to be overcome. Preclinically, models for cancer drugs are inadequate to visualize the complexity of TME. Cell and tissue-engineered models with 3-dimensional co-culture systems could be utilized to recapitulate the cellular organization, growth kinetics, cellular heterogeneity, intra- and intercellular interactions *in vitro* to improve translation and reduce animal

testing (211). Clinically, given the inter-patient heterogeneity in genetic and epigenetic factors, responses towards drugs are highly variable among individuals. Thus, an optimal combination of therapeutic strategies should be designed based on the integration of individual information on TME landscape, genomic and molecular profile to ensure precision, safety, and effectiveness of cancer therapies, which ensure better health outcomes of NPC patients. Moreover, to reduce the adverse events of therapeutic and enhance therapeutic efficacy, strategies to improve specificity in targeting, delivery, and release of drugs against TME should be considered. These include the engineering of nanoparticles or exosomes with specific ligands as vehicles for the delivery of drugs into the target cells. Several delivery systems which could enhance the effectiveness of delivery have been developed, which include arginine-modified hydroxyapatite nanoparticles and fusion-based NPC-specific lipid nanoparticles (212, 213).

On the other hand, there is a need for the discovery of tumor-specific molecules as targets for the specific delivery of therapeutic agents or disease diagnosis *via* liquid biopsy. The biomarker should have high specificity, sensitivity, accuracy, precision, and reliability, inexpensive and timely. While diagnostic biomarkers allow the early detection of NPC, prognostic biomarkers will predict the disease progression of patients and facilitate the development of prophylactic drugs. Advancement in molecular technologies, together with enormous databases integrating molecular and clinical data sets, will accelerate the research findings and their translation into clinical use.

In conclusion, the NPC microenvironment consists of cellular and acellular players which serve as targets for the development of therapeutic, diagnostic, and prognostic tools. Despite that, most of them are only tested in preclinical or early phases of clinical studies. Hence, large-scale clinical studies should be considered to evaluate the reliability of TME components as diagnostic tools, and guidelines or standards should be developed to ensure safe clinical use of therapeutic tools.

AUTHOR CONTRIBUTIONS

ZS, PS, and S-CC were involved in the conceptualization and design of the content. ZS wrote and revised the manuscript. PS, C-OL, and S-CC reviewed and revised the manuscript. All authors have read and agreed to the published version of the manuscript.

FUNDING

This study was supported by grant from the Ministry of Higher Education (MOHE) through Fundamental Research Grant Scheme (FGRS/1/2020/SKK0/UCSI/02/2) and UCSI University Research Excellence and Innovation (REIG-FMS-2020/009).

REFERENCES

1. Chen YP, Chan ATC, Le QT, Blanchard P, Sun Y, Ma J. Nasopharyngeal Carcinoma. *Lancet* (2019) 394(10192):64–80. doi: 10.1016/S0140-6736(19)30956-0
2. Chua MLK, Wee JTS, Hui EP, Chan ATC. Nasopharyngeal Carcinoma. *Lancet* (2016) 387(10022):1012–24. doi: 10.1016/S0140-6736(15)00055-0
3. Ferlay J, Ervik M, Lam F, Colombet M, Mery L, Piñeros M, et al. *Global Cancer Observatory: Cancer Today* (2020). Available at: https://gco.iarc.fr/today/home.
4. Sung H, Ferlay J, Soerjomataram I, Siegel RL, Bray F, Jemal A. Global Cancer Statistics 2020: GLOBOCAN Estimates of Incidence and Mortality Worldwide for 36 Cancers in 185 Countries. *CA Cancer J Clin* (2021) 71(1):7–33. doi: 10.3322/caac.21660
5. Bray F, Colombet M, Mery L, Pineros M, Znaor A, Zanetti R, et al. *Cancer Incidence in Five Continents Volume Xi*. Lyon: World Health Organization (2021).
6. Chang ET, Ye W, Zeng Y-X, Adami H-O. The Evolving Epidemiology of Nasopharyngeal Carcinoma. *Cancer Epidemiol Biomark Prev* (2021) 30(6):1035–47. doi: 10.1158/1055-9965.EPI-20-1702
7. Zuo X-Y, Feng Q-S, Sun J, Wei P-P, Chin Y-M, Guo Y-M, et al. X-Chromosome Association Study Reveals Genetic Susceptibility Loci of Nasopharyngeal Carcinoma. *Biol Sex Differ* (2019) 10(1):13–24. doi: 10.1186/s13293-019-0227-9
8. Xie SH, Yu ITS, Tse LA, Mang OWK, Yue L. Sex Difference in the Incidence of Nasopharyngeal Carcinoma in Hong Kong 1983-2008: Suggestion of a Potential Protective Role of Oestrogen. *Eur J Cancer* (2013) 49(1):150–5. doi: 10.1016/j.ejca.2012.07.004
9. Linton RE, Daker M, Khoo AS-B, Chung YCD, Viljoen M, Neilsen PM. Nasopharyngeal Carcinoma Among the Bidayuh of Sarawak, Malaysia: History and Risk Factors (Review). *Oncol Lett* (2021) 22(1):514–36. doi: 10.3892/ol.2021.12775
10. Wu Z-X, Xiang L, Rong J-F, He H-L, Li D. Nasopharyngeal Carcinoma With Headaches as the Main Symptom: A Potential Diagnostic Pitfall. *J Cancer Res Ther* (2016) 12(1):209–14. doi: 10.4103/0973-1482.157334
11. Jen C-W, Tsai Y-C, Wu J-S, Chen P-L, Yen J-H, Chuang W-K, et al. Prognostic Classification for Patients With Nasopharyngeal Carcinoma Based on American Joint Committee on Cancer Staging System T and N Categories. *Ther Radiol Oncol* (2020) 4(0):2–13. doi: 10.21037/tro.2020.02.01
12. Pok MH, Lung HL, Wu M, Tsang CM, Wong K-L, Mak NK, et al. Targeting Epstein-Barr Virus in Nasopharyngeal Carcinoma. *Front Oncol* (2020) 10:600. doi: 10.3389/fonc.2020.00600
13. Siti-Azrin AH, Norsa'adah B, Naing NN. Prognostic Factors of Nasopharyngeal Carcinoma Patients in a Tertiary Referral Hospital: A Retrospective Cohort Study. *BMC Res Notes* (2017) 10(1):705–12. doi: 10.1186/s13104-017-2990-1
14. Langley RR, Fidler IJ. The Seed and Soil Hypothesis Revisited-The Role of Tumor-Stroma Interactions in Metastasis to Different Organs. *Int J Cancer* (2011) 128(11):2527–35. doi: 10.1002/ijc.26031
15. Smythies J. Intercellular Signaling in Cancer-The SMT and TOFT Hypotheses, Exosomes, Telocytes and Metastases: Is the Messenger in the Message? *J Cancer* (2015) 6(7):604–9. doi: 10.7150/jca.12372
16. Hanahan D, Weinberg RA. Hallmarks of Cancer: The Next Generation. *Cell* (2011) 144(5):646–74. doi: 10.1016/j.cell.2011.02.013
17. Gong L, Lai-Wan Kwong D, Dai W, Wu P, Li S, Yan Q, et al. Comprehensive Single-Cell Sequencing Reveals the Stromal Dynamics and Tumor-Specific Characteristics in the Microenvironment of Nasopharyngeal Carcinoma. *Nat Commun* (2021) 12(1):1540–58. doi: 10.1038/s41467-021-21795-z
18. Jin S, Li R, Chen MY, Yu C, Tang LQ, Liu YM, et al. Single-Cell Transcriptomic Analysis Defines the Interplay Between Tumor Cells, Viral Infection, and the Microenvironment in Nasopharyngeal Carcinoma. *Cell Res* (2020) 30(11):950–65. doi: 10.1038/s41422-020-00402-8
19. Zhao J, Guo C, Xiong F, Yu J, Ge J, Wang H, et al. Single Cell RNA-Seq Reveals the Landscape of Tumor and Infiltrating Immune Cells in Nasopharyngeal Carcinoma. *Cancer Lett* (2020) 477:131–43. doi: 10.1016/j.canlet.2020.02.010
20. Chen Y-P, Yin J-H, Li W-F, Li H-J, Chen D-P, Zhang C-J, et al. Single-Cell Transcriptomics Reveals Regulators Underlying Immune Cell Diversity and

Immune Subtypes Associated With Prognosis in Nasopharyngeal Carcinoma. *Cell Res* (2020) 30(11):1024–42. doi: 10.1038/s41422-020-0374-x
21. Liu Y, He S, Wang X-L, Peng W, Chen Q-Y, Chi D-M, et al. Tumour Heterogeneity and Intercellular Networks of Nasopharyngeal Carcinoma at Single Cell Resolution. *Nat Commun* (2021) 12(1):741–59. doi: 10.1038/s41467-021-21043-4
22. Wang M, Zhao J, Zhang L, Wei F, Lian Y, Wu Y, et al. Role of Tumor Microenvironment in Tumorigenesis. *J Cancer* (2017) 8(5):761–73. doi: 10.7150/jca.17648
23. Arneth B. Tumor Microenvironment. *Medicina* (2020) 56(1):15–36. doi: 10.3390/medicina56010015
24. Tao L, Huang G, Song H, Chen Y, Chen L. Cancer Associated Fibroblasts: An Essential Role in the Tumor Microenvironment (Review). *Oncol Lett* (2017) 14(3):2611–20. doi: 10.3892/ol.2017.6497
25. Liu T, Zhou L, Li D, Andl T, Zhang Y. Cancer-Associated Fibroblasts Build and Secure the Tumor Microenvironment. *Front Cell Dev Biol* (2019) 7:60–74. doi: 10.3389/fcell.2019.00060
26. Eble JA, Niland S. The Extracellular Matrix in Tumor Progression and Metastasis. *Clin Exp Metastasis* (2019) 36(3):171–98. doi: 10.1007/s10585-019-09966-1
27. Spill F, Reynolds DS, Kamm RD, Zaman MH. Impact of the Physical Microenvironment on Tumor Progression and Metastasis. *Curr Opin Biotechnol* (2016) 40:41–8. doi: 10.1016/j.copbio.2016.02.007
28. Gourzones C, Barjon C, Busson P. Host-Tumor Interactions in Nasopharyngeal Carcinomas. *Semin Cancer Biol* (2012) 22(2):127–36. doi: 10.1016/j.semcancer.2012.01.002
29. Lai M-M, Cheng PNM, Tsao SY, Lai KN. Immunohistological Characteristics of the Infiltrating Lymphoid Cells and Expression of HLA Class I and II Antigens in Nasopharyngeal Carcinoma. *Virchows Arch A Pathol Anat* (1990) 417(4):347–52. doi: 10.1007/BF01605787
30. Chong PY, Chew CT, Chan KC, Ow CK. Tumour Infiltrating Lymphocytes in Nasopharyngeal Carcinoma. *Ann Acad Med Singapore* (1988) 17(2):238–42.
31. Cheng S, Li Z, Gao R, Xing B, Gao Y, Yang Y, et al. A Pan-Cancer Single-Cell Transcriptional Atlas of Tumor Infiltrating Myeloid Cells. *Cell* (2021) 184 (3):792–809.e23. doi: 10.1016/j.cell.2021.01.010
32. Li Z-L, Ye S-B, Ouyang L-Y, Zhang H, Chen Y-S, He J, et al. COX-2 Promotes Metastasis in Nasopharyngeal Carcinoma by Mediating Interactions Between Cancer Cells and Myeloid-Derived Suppressor Cells. *Oncoimmunology* (2015) 4(11):e1044712. doi: 10.1080/2162402X.2015.1044712
33. Chen Y, Chew CT, Chan SH. T-Cell Receptor Gene Expression in Tumour-Infiltrating Lymphocytes and Peripheral Blood Lymphocytes of Patients With Nasopharyngeal Carcinoma. *Br J Cancer* (1995) 72(1):117–22. doi: 10.1038/bjc.1995.286
34. Herait P, Ganem G, Lipinski M, Carlu C, Micheau C, Schwaab G, et al. Lymphocyte Subsets in Tumour of Patients With Undifferentiated Nasopharyngeal Carcinoma: Presence of Lymphocytes With the Phenotype of Activated T Cells. *Br J Cancer* (1987) 55(2):135–9. doi: 10.1038/bjc.1987.28
35. Jiang Y, Li Y, Zhu B. T-Cell Exhaustion in the Tumor Microenvironment. *Cell Death Dis* (2015) 6(6):e1792. doi: 10.1038/cddis.2015.162
36. Huo S, Luo Y, Deng R, Liu X, Wang J, Wang L, et al. EBV-EBNA1 Constructs an Immunosuppressive Microenvironment for Nasopharyngeal Carcinoma by Promoting the Chemoattraction of Treg Cells. *J Immunother Cancer* (2020) 8(2):e001588. doi: 10.1136/jitc-2020-001588
37. Yang L, Liu G, Li Y, Pan Y. The Emergence of Tumor-Infiltrating Lymphocytes in Nasopharyngeal Carcinoma: Predictive Value and Immunotherapy Implications. *Genes Dis* (2021). doi: 10.1016/j.gendis.2021.07.002
38. Ohue Y, Nishikawa H. Regulatory T (Treg) Cells in Cancer: Can Treg Cells be a New Therapeutic Target? *Cancer Sci* (2019) 110(7):2080–9. doi: 10.1111/cas.14069
39. Li J, Huang Z-F, Xiong G, Mo H-Y, Mai H-Q, Chen Q-Y, et al. Distribution, Characterization, and Induction of CD8 + Regulatory T Cells and IL-17-Producing CD8 + T Cells in Nasopharyngeal Carcinoma. *J Transl Med* (2011) 9:189. doi: 10.1186/1479-5876-9-189
40. Nambiar DK, Aguilera T, Cao H, Kwok S, Kong C, Bloomstein J, et al. Galectin-1-Driven T Cell Exclusion in the Tumor Endothelium Promotes Immunotherapy Resistance. *J Clin Invest* (2019) 129(12):5553–67. doi: 10.1172/JCI129025
41. Fogg M, Murphy JR, Lorch J, Posner M, Wang F. Therapeutic Targeting of Regulatory T Cells Enhances Tumor-Specific CD8+ T Cell Responses in Epstein–Barr Virus Associated Nasopharyngeal Carcinoma. *Virology* (2013) 441(2):107–13. doi: 10.1016/j.virol.2013.03.016
42. Zhao C, Liu Y, Liang Z, Feng H, Xu S, Xu E. MACC1 Facilitates the Escape of Nasopharyngeal Carcinoma Cells From Killing by Natural Killer Cells MACC1 Facilitates the Escape of Nasopharyngeal Carcinoma Cells From Killing by Natural Killer Cells. *Biotechnol Biotechnol Equip* (2019) 33 (1):579–88. doi: 10.1080/13102818.2019.1596041
43. Xu Y, Zhou R, Huang C, Zhang M, Li J, Zong J, et al. Analysis of the Expression of Surface Receptors on NK Cells and NKG2D on Immunocytes in Peripheral Blood of Patients With Nasopharyngeal Carcinoma. *Asian Pac J Cancer Prev* (2018) 19(3):661–5. doi: 10.22034/APJCP.2018.19.3.661
44. Arij BC, Nesrine O, Hayet D, Fayza A, Hajer A, Tesnim M, et al. Soluble MICA and Anti-MICA Antibodies as Biomarkers of Nasopharyngeal Carcinoma Disease. *Immunol Invest* (2019) 49(5):498–509. doi: 10.1080/08820139.2019.1690506
45. Liou AK-F, Soon G, Tan L, Peng Y, Meng Cher B, Cher Goh B, et al. Elevated IL18 Levels in Nasopharyngeal Carcinoma Induced PD-1 Expression on NK Cells in TILS Leading to Poor Prognosis. *Oral Oncol* (2020) 104:104616. doi: 10.1016/j.oraloncology.2020.104616
46. Li J-P, Wu C-Y, Chen M-Y, Liu S-X, Yan S-M, Kang Y-F, et al. PD-1 + CXCR5 – CD4 + Th-CXCL13 Cell Subset Drives B Cells Into Tertiary Lymphoid Structures of Nasopharyngeal Carcinoma. *J Immunother Cancer* (2021) 9(7):2101. doi: 10.1136/jitc-2020-002101
47. Selitsky SR, Marron D, Mose LE, Parker JS, Dittmer DP. Epstein-Barr Virus-Positive Cancers Show Altered B-Cell Clonality. *mSystems* (2018) 3(5): e00081–18. doi: 10.1128/mSystems.00081-18
48. Xu T, Huang Z, Su B, Wang S, Wang D, Wang C, et al. Prognostic Significance of Circulating CD19+ B Lymphocytes in EBV-Associated Nasopharyngeal Carcinoma. *Med Oncol* (2014) 31(10):198. doi: 10.1007/s12032-014-0198-y
49. Miao B-P, Zhang R-S, Li M, Fu Y-T, Zhao M, Liu Z-G, et al. Nasopharyngeal Cancer-Derived microRNA-21 Promotes Immune Suppressive B Cells. *Cell Mol Immunol* (2015) 12(6):750–6. doi: 10.1038/cmi.2014.129
50. Cai T-T, Ye S-B, Liu Y-N, He J, Chen Q-Y, Mai H-Q, et al. LMP1-Mediated Glycolysis Induces Myeloid-Derived Suppressor Cell Expansion in Nasopharyngeal Carcinoma. *PloS Pathog* (2017) 13(7):e1006503. doi: 10.1371/journal.ppat.1006503
51. Groth C, Hu X, Weber R, Fleming V, Altevogt P, Utikal J, et al. Immunosuppression Mediated by Myeloid-Derived Suppressor Cells (MDSCs) During Tumour Progression. *Br J Cancer* (2019) 120(1):16–25. doi: 10.1038/s41416-018-0333-1
52. Kim J, Bae JS. Tumor-Associated Macrophages and Neutrophils in Tumor Microenvironment. *Mediators Inflamm* (2016) 2016:6058147. doi: 10.1155/2016/6058147
53. Chen HC, Kawamura A, Murata M, Hamajima K, Osono M. A Histopathological Study of Lymphoid Tissue Reaction to Metastatic Nasopharyngeal Carcinoma in Nude Mice. *IARC Sci Publ* (1978) 20:65–84.
54. Hinshaw DC, Shevde LA. The Tumor Microenvironment Innately Modulates Cancer Progression. *Cancer Res* (2019) 79(18):4557–67. doi: 10.1158/0008-5472.CAN-18-3962
55. Wang J, Huang H, Lu J, Bi P, Wang F, Liu X, et al. Tumor Cells Induced-M2 Macrophage Favors Accumulation of Treg in Nasopharyngeal Carcinoma. *Int J Clin Exp Pathol* (2017) 10(8):8389–401.
56. Peng Y, Li X, Liu H, Deng X, She C, Liu C, et al. microRNA-18a From M2 Macrophages Inhibits TGFBR3 to Promote Nasopharyngeal Carcinoma Progression and Tumor Growth *via* TGF-β Signaling Pathway. *Nanoscale Res Lett* (2020) 15(1):196. doi: 10.1186/s11671-020-03416-8
57. Gallo O, Bianchi S, Giannini A, Gallina E, Libonati GA, Gini-Storchi O. Correlations Between Histopathological and Biological Findings in Nasopharyngeal Carcinoma and Its Prognostic Significance. *Laryngoscope* (1991) 101(5):487–93. doi: 10.1288/00005537-199105000-00008
58. Nomori H, Watanabe S, Nakajima T, Shimosato Y, Kameya T. Histiocytes in Nasopharyngeal Carcinoma in Relation to Prognosis. *Cancer* (1986) 57

(1):100–5. doi: 10.1002/1097-0142(19860101)57:1<100::AID-CNCR2820570121>3.0.CO;2-X
59. Lu J, Chen XM, Huang HR, Zhao FP, Wang F, Liu X, et al. Detailed Analysis of Inflammatory Cell Infiltration and the Prognostic Impact on Nasopharyngeal Carcinoma. *Head Neck* (2018) 40(6):1245–53. doi: 10.1002/hed.25104
60. Ping Q, Yan R, Cheng X, Wang W, Zhong Y, Hou Z, et al. Cancer-Associated Fibroblasts: Overview, Progress, Challenges, and Directions. *Cancer Gene Ther* (2021) 28(9):984–99. doi: 10.1038/s41417-021-00318-4
61. Nurmik M, Ullmann P, Rodriguez F, Haan S, Letellier E. In Search of Definitions: Cancer-Associated Fibroblasts and Their Markers. *Int J Cancer* (2019) 146(4):895–905. doi: 10.1002/ijc.32193
62. Liao Z, Tan ZW, Zhu P, Tan NS. Cancer-Associated Fibroblasts in Tumor Microenvironment – Accomplices in Tumor Malignancy. *Cell Immunol* (2019) 343:103729. doi: 10.1016/j.cellimm.2017.12.003
63. Wu X, Zhou Z, Xu S, Liao C, Chen X, Li B, et al. Extracellular Vesicle Packaged LMP1-Activated Fibroblasts Promote Tumor Progression *via* Autophagy and Stroma-Tumor Metabolism Coupling. *Cancer Lett* (2020) 478:93–106. doi: 10.1016/j.canlet.2020.03.004
64. Chen J, Yang P, Xiao Y, Zhang Y, Liu J, Xie D, et al. Overexpression of α-Sma-Positive Fibroblasts (CAFs) in Nasopharyngeal Carcinoma Predicts Poor Prognosis. *J Cancer* (2017) 8(18):3897–902. doi: 10.7150/jca.20324
65. Wang S, Ma N, Kawanishi S, Hiraku Y, Oikawa S, Xie Y, et al. Relationships of Alpha-SMA-Positive Fibroblasts and SDF-1-Positive Tumor Cells With Neoangiogenesis in Nasopharyngeal Carcinoma. *BioMed Res Int* (2014) 2014:507353. doi: 10.1155/2014/507353
66. Zhu Y, Shi C, Zeng L, Liu G, Jiang W, Zhang X, et al. High COX-2 Expression in Cancer-Associated Fibiroblasts Contributes to Poor Survival and Promotes Migration and Invasiveness in Nasopharyngeal Carcinoma. *Mol Med* (2019) 59(3):265–80. doi: 10.1002/mc.23150
67. Huang W, Zhang L, Yang M, Wu X, Wang X, Huang W, et al. Cancer-Associated Fibroblasts Promote the Survival of Irradiated Nasopharyngeal Carcinoma Cells *via* the NF-κb Pathway. *J Exp Clin Cancer Res* (2021) 40 (1):87–101. doi: 10.1186/s13046-021-01878-x
68. Ben-Haj-Ayed A, Moussa A, Ghedira R, Gabbouj S, Miled S, Bouzid N, et al. Prognostic Value of Indoleamine 2,3-Dioxygenase Activity and Expression in Nasopharyngeal Carcinoma. *Immunol Lett* (2016) 169:23–32. doi: 10.1016/j.imlet.2015.11.012
69. Wang J, Deng L, Huang J, Cai R, Zhu X, Liu F, et al. High Expression of Fibronectin 1 Suppresses Apoptosis Through the NF-κb Pathway and Is Associated With Migration in Nasopharyngeal Carcinoma. *Am J Transl Res* (2017) 9(10):4502–11.
70. Erdogan B, Ao M, White LM, Means AL, Brewer BM, Yang L, et al. Cancer-Associated Fibroblasts Promote Directional Cancer Cell Migration by Aligning Fibronectin. *J Cell Biol* (2017) 216(11):3799–817. doi: 10.1083/jcb.201704053
71. Wakisaka N, Wen Q-H, Yoshizaki T, Nishimura T, Furukawa M, Kawahara E, et al. Association of Vascular Endothelial Growth Factor Expression With Angiogenesis and Lymph Node Metastasis in Nasopharyngeal Carcinoma From the Department of Otolaryngology. *Laryngoscope* (1999) 109(5):810–4. doi: 10.1097/00005537-199905000-00024
72. Luo W, Li S, Peng B, Ye Y, Deng X. Embryonic Stem Cells Markers SOX2, OCT4 and Nanog Expression and Their Correlations With Epithelial-Mesenchymal Transition in Nasopharyngeal Carcinoma. *PloS One* (2013) 8(2):56324. doi: 10.1371/journal.pone.0056324
73. Maishi N, Hida K. Tumor Endothelial Cells Accelerate Tumor Metastasis. *Cancer Sci* (2017) 108(10):1921–6. doi: 10.1111/cas.13336
74. Hida K, Maishi N, Annan DA, Hida Y. Contribution of Tumor Endothelial Cells in Cancer Progression. *Int J Mol Sci* (2018) 19(5):1272–84. doi: 10.3390/ijms19051272
75. Huang L, Hu C, Chao H, Zhang Y, Li Y, Hou J, et al. Drug-Resistant Endothelial Cells Facilitate Progression, EMT and Chemoresistance in Nasopharyngeal Carcinoma *via* Exosomes. *Cell Signal* (2019) 63:109385. doi: 10.1016/j.cellsig.2019.109385
76. Hong B, Lui VWY, Hashiguchi M, Hui EP, Chan AT-C. Targeting Tumor Hypoxia in Nasopharyngeal Carcinoma. *Head Neck* (2011) 35(1):133–45. doi: 10.1002/hed.21877
77. Hua YJ, Wang HY, Tang LQ, Chen QY, Shao JY, Mai HQ. LOX Expression in Primary Nasopharyngeal Carcinoma: Correlation With Prognostic Parameters and Outcome. *Oncotarget* (2016) 7(7):8200–7. doi: 10.18632/oncotarget.6996
78. Liu YN, Yang JF, Huang DJ, Ni HH, Zhang CX, Zhang L, et al. Hypoxia Induces Mitochondrial Defect That Promotes T Cell Exhaustion in Tumor Microenvironment Through MYC-Regulated Pathways. *Front Immunol* (2020) 11:1906. doi: 10.3389/fimmu.2020.01906
79. Mukherjee A, Madamsetty VS, Paul MK, Mukherjee S. Recent Advancements of Nanomedicine Towards Antiangiogenic Therapy in Cancer. *Int J Mol Sci* (2019) 21(2):455–82. doi: 10.3390/ijms21020455
80. Murono S, Inoue H, Tanabe T, Joab I, Yoshizaki T, Furukawa M, et al. Induction of Cyclooxygenase-2 by Epstein-Barr Virus Latent Membrane Protein 1 is Involved in Vascular Endothelial Growth Factor Production in Nasopharyngeal Carcinoma Cells. *Proc Natl Acad Sci USA* (2001) 98 (12):6905–10. doi: 10.1073/pnas.121016998
81. Liu X, Wang F, Peng L, Wang Y. A Meta-Analysis of Vascular Endothelial Growth Factor for Nasopharyngeal Cancer Prognosis. *Front Oncol* (2018) 8:486. doi: 10.3389/fonc.2018.00486
82. Chor S, Huang M, Tsao SW, Tsang CM. Interplay of Viral Infection, Host Cell Factors and Tumor Microenvironment in the Pathogenesis of Nasopharyngeal Carcinoma. *Cancers (Basel)* (2018) 10(4):106. doi: 10.3390/cancers10040106
83. Renaud S, Lefebvre A, Mordon S, Moralès O, Delhem N. Novel Therapies Boosting T Cell Immunity in Epstein Barr Virus-Associated Nasopharyngeal Carcinoma. *Int J Mol Sci* (2020) 21(12):4292. doi: 10.3390/ijms21124292
84. Chang KP, Chang YT, Wu CC, Liu YL, Chen MC, Tsang NM, et al. Multiplexed Immunobead-Based Profiling of Cytokine Markers for Detection of Nasopharyngeal Carcinoma and Prognosis of Patient Survival. *Head Neck* (2011) 33(6):886–97. doi: 10.1002/hed.21557
85. Kwok-Fung Lo A, Dawson CW, Lok Lung H, Wong K-L, Young LS. The Role of EBV-Encoded LMP1 in the NPC Tumor Microenvironment: From Function to Therapy. *Front Oncol* (2021) 11:640207. doi: 10.3389/fonc.2021.640207
86. Wang J, Luo Y, Bi P, Lu J, Wang F, Liu X, et al. Mechanisms of Epstein-Barr Virus Nuclear Antigen 1 Favor Tregs Accumulation in Nasopharyngeal Carcinoma. *Cancer Med* (2020) 9(15):5598–608. doi: 10.1002/cam4.3213
87. Tang M, Ou N, Li C, Lu A, Li J, Ma L, et al. Expression and Prognostic Significance of Macrophage Inflammatory Protein-3 Alpha and Cystatin A in Nasopharyngeal Carcinoma. *BioMed Res Int* (2015) 2015:617143. doi: 10.1155/2015/617143
88. Li Z, Duan Y, Cheng S, Chen Y, Hu Y, Zhang L, et al. EBV-Encoded RNA *via* TLR3 Induces Inflammation in Nasopharyngeal Carcinoma. *Oncotarget* (2015) 6(27):24291–303. doi: 10.18632/oncotarget.4552
89. Lee C-H, Yeh T-H, Lai H-C, Wu S-Y, Su I-J, Takada K, et al. Epstein-Barr Virus Zta-Induced Immunomodulators From Nasopharyngeal Carcinoma Cells Upregulate Interleukin-10 Production From Monocytes. *J Virol* (2011) 85(14):7333–42. doi: 10.1128/JVI.00182-11
90. Adel FA-K, Omminea AA, Mamdouh ZA, Manal MH, Mohamed FS, Dalia M, et al. Pre-Treatment Serum Inflammatory Cytokines as Survival Predictors of Patients With Nasopharyngeal Carcinoma Receiving Chemoradiotherapy. *Mol Clin Oncol* (2016) 5(6):811–6. doi: 10.3892/mco.2016.1041
91. Liu W, Lin Y, Xiao H, Xing S, Chen H, Chi P, et al. Epstein-Barr Virus Infection Induces Indoleamine 2,3-Dioxygenase Expression in Human Monocyte-Derived Macrophages Through P38/Mitogen-Activated Protein Kinase and NF-κb Pathways: Impairment in T Cell Functions. *J Virol* (2014) 88(12):6660–71. doi: 10.1128/JVI.03678-13
92. Li X-J, Peng L-X, Shao J-Y, Lu W-H, Zhang J-X, Chen S, et al. As an Independent Unfavorable Prognostic Factor, IL-8 Promotes Metastasis of Nasopharyngeal Carcinoma Through Induction of Epithelial-Mesenchymal Transition and Activation of AKT Signaling. *Carcinogenesis* (2012) 33 (7):1302–9. doi: 10.1093/carcin/bgs181
93. Luo H, Yi B. The Role of Exosomes in the Pathogenesis of Nasopharyngeal Carcinoma and the Involved Clinical Application. *Int J Biol Sci* (2021) 17 (9):2147–56. doi: 10.7150/ijbs.59688
94. Mashouri L, Yousefi H, Reza Aref A, mohammad Ahadi A, Molaei F, Alahari SK. Exosomes: Composition, Biogenesis, and Mechanisms in Cancer Metastasis and Drug Resistance. *Mol Cancer* (2019) 18(1):75–89. doi: 10.1186/s12943-019-0991-5

95. Li I, Nabet BY. Exosomes in the Tumor Microenvironment as Mediators of Cancer Therapy Resistance. *Mol Cancer* (2019) 18(1):32–42. doi: 10.1186/s12943-019-0975-5
96. Zhou Y, Xia L, Lin J, Wang H, Oyang L, Tan S, et al. Exosomes in Nasopharyngeal Carcinoma. *J Cancer* (2018) 9(5):767–77. doi: 10.7150/jca.22505
97. You B, Cao X, Shao X, Ni H, Shi S, Shan Y, et al. Clinical and Biological Significance of HAX-1 Overexpression in Nasopharyngeal Carcinoma. *Oncotarget* (2016) 7(11):12505–24. doi: 10.18632/oncotarget.7274
98. Zhang K, Liu D, Zhao J, Shi S, He X, Da P, et al. Nuclear Exosome HMGB3 Secreted by Nasopharyngeal Carcinoma Cells Promotes Tumour Metastasis by Inducing Angiogenesis. *Cell Death Dis* (2021) 12(6):554. doi: 10.1038/s41419-021-03845-y
99. Chan Y-K, Zhang H, Liu P, Tsao S-W, Li Lung M, Mak N-K, et al. Proteomic Analysis of Exosomes From Nasopharyngeal Carcinoma Cell Identifies Intercellular Transfer of Angiogenic Proteins. *UICC Int J Cancer IJC* (2015) 137(8):1830–41. doi: 10.1002/ijc.29562
100. Zhang C, Huang D, Baloche V, Zhang L, Xu J, Li B, et al. Galectin-9 Promotes a Suppressive Microenvironment in Human Cancer by Enhancing STING Degradation. *Oncogenesis* (2020) 9(7):65. doi: 10.1038/s41389-020-00248-0
101. Aga M, Bentz GL, Raffa S, Torrisi MR, Kondo S, Wakisaka N, et al. Exosomal Hif1α Supports Invasive Potential of Nasopharyngeal Carcinoma-Associated LMP1-Positive Exosomes. *Oncogene* (2014) 33(37):4613–22. doi: 10.1038/onc.2014.66
102. Zhou SK, Gao F, Zhong ZS, Yao H. Long Non-Coding RNA Colon Cancer Associated Transcript-2 From Nasopharyngeal Carcinoma-Derived Exosomes Promotes Angiogenesis. *Chin J Otorhinolaryngol Head Neck Surg* (2020) 55(10):944–51. doi: 10.3760/cma.j.cn115330-20200423-00322
103. Luo Y, Ma J, Liu F, Guo J, Gui R. Diagnostic Value of Exosomal circMYC in Radioresistant Nasopharyngeal Carcinoma. *Head Neck* (2020) 42(12):3702–11. doi: 10.1002/hed.26441
104. Gu M, Li L, Zhang Z, Chen J, Zhang W, Zhang J, et al. PFKFB3 Promotes Proliferation, Migration and Angiogenesis in Nasopharyngeal Carcinoma. *J Cancer* (2017) 8(18):3887–96. doi: 10.7150/jca.19112
105. You Y, Shan Y, Chen J, Yue H, You B, Shi S, et al. Matrix Metalloproteinase 13-Containing Exosomes Promote Nasopharyngeal Carcinoma Metastasis. *Cancer Sci* (2015) 106(12):1669–77. doi: 10.1111/cas.12818
106. Shan Y, You B, Shi S, Shi W, Zhang Z, Zhang Q, et al. Hypoxia-Induced Matrix Metalloproteinase-13 Expression in Exosomes From Nasopharyngeal Carcinoma Enhances Metastases. *Cell Death Dis* (2018) 9(3):382. doi: 10.1038/s41419-018-0425-0
107. Mrizak D, Martin N, Barjon C, Jimenez-Pailhes A-S, Mustapha R, Niki T, et al. Effect of Nasopharyngeal Carcinoma-Derived Exosomes on Human Regulatory T Cells. *J Natl Cancer Inst* (2015) 107(1):363. doi: 10.1093/jnci/dju363
108. Duan B, Shi S, Yue H, You B, Shan Y, Zhu Z, et al. Exosomal miR-17-5p Promotes Angiogenesis in Nasopharyngeal Carcinoma *via* Targeting BAMBI. *J Cancer* (2019) 10(26):6681–92. doi: 10.7150/jca.30757
109. Bao L, You B, Shi S, Shan Y, Zhang Q, Yue H, et al. Metastasis-Associated miR-23a From Nasopharyngeal Carcinoma-Derived Exosomes Mediates Angiogenesis by Repressing a Novel Target Gene TSGA10. *Oncogene* (2018) 37(21):2873–89. doi: 10.1038/s41388-018-0183-6
110. Wang J, Jiang Q, Faleti OD, Tsang CM, Zhao M, Wu G, et al. Exosomal Delivery of AntagomiRs Targeting Viral and Cellular MicroRNAs Synergistically Inhibits Cancer Angiogenesis. *Mol Ther - Nucleic Acids* (2020) 22:153–65. doi: 10.1016/j.omtn.2020.08.017
111. Tian X, Liu Y, Wang Z, Wu S. miR-144 Delivered by Nasopharyngeal Carcinoma-Derived EVs Stimulates Angiogenesis Through the FBXW7/HIF-1α/VEGF-A Axis. *Mol Ther - Nucleic Acids* (2021) 24:1000–11. doi: 10.1016/j.omtn.2021.03.016
112. Lu J, Liu QH, Wang F, Tan JJ, Deng YQ, Peng XH, et al. Exosomal miR-9 Inhibits Angiogenesis by Targeting MDK and Regulating PDK/AKT Pathway in Nasopharyngeal Carcinoma. *J Exp Clin Cancer Res* (2018) 37(1):147. doi: 10.1186/s13046-018-0814-3
113. Ye S-B, Li Z-L, Luo D-H, Huang B-J, Chen Y-S, Zhang X-S, et al. Tumor-Derived Exosomes Promote Tumor Progression and T-Cell Dysfunction Through the Regulation of Enriched Exosomal microRNAs in Human Nasopharyngeal Carcinoma. *Oncotarget* (2014) 5:5439–52. doi: 10.18632/oncotarget.2118
114. Ye S-B, Zhang H, Cai T-T, Liu Y-N, Ni J-J, He J, et al. Exosomal miR-24-3p Impedes T-Cell Function by Targeting FGF11 and Serves as a Potential Prognostic Biomarker for Nasopharyngeal Carcinoma. *J Pathol* (2016) 240(3):329–40. doi: 10.1002/path.4781
115. Cheng Q, Li Q, Xu L, Jiang H. Exosomal microRNA-301a-3p Promotes the Proliferation and Invasion of Nasopharyngeal Carcinoma Cells by Targeting BTG1 mRNA. *Mol Med Rep* (2021) 23(5):328. doi: 10.3892/mmr.2021.11967
116. Wan F-Z, Chen K-H, Sun Y-C, Chen X-C, Liang R-B, Chen L, et al. Exosomes Overexpressing miR-34c Inhibit Malignant Behavior and Reverse the Radioresistance of Nasopharyngeal Carcinoma. *J Transl Med* (2020) 18(1):12. doi: 10.1186/s12967-019-02203-z
117. Yin H, Qiu X, Shan Y, You B, Xie L, Zhang P, et al. HIF-1α Downregulation of miR-433-3p in Adipocyte-Derived Exosomes Contributes to NPC Progression via Targeting SCD1. *Cancer Sci* (2021) 2021(112):1457–70. doi: 10.1111/cas.14829
118. Chia WK, Teo M, Wang WW, Lee B, Ang SF, Tai WM, et al. Adoptive T-Cell Transfer and Chemotherapy in the First-Line Treatment of Metastatic and/or Locally Recurrent Nasopharyngeal Carcinoma. *Mol Ther* (2014) 22(1):132–9. doi: 10.1038/mt.2013.242
119. Ma BBY, Lim W-T, Goh B-C, Hui EP, Lo K-W, Pettinger A, et al. Antitumor Activity of Nivolumab in Recurrent and Metastatic Nasopharyngeal Carcinoma: An International, Multicenter Study of the Mayo Clinic Phase 2 Consortium (NCI-9742). *J Clin Oncol* (2018) 36(14):1412–8. doi: 10.1200/JCO.2017.77.0388
120. Lee NY, Zhang E, Pfister DG, Kim J, Garden AS, Mechalakos J, et al. Phase II Study of the Addition of Bevacizumab to Standard Chemoradiation for Loco-Regionally Advanced Nasopharyngeal Carcinoma: Radiation Therapy Oncology Group (RTOG) Trial 0615. *Lancet Oncol* (2012) 13(2):172. doi: 10.1016/S1470-2045(11)70303-5
121. Li Y, Tian Y, JIn F, Wu W, Long J, Ouyang J, et al. A Phase II Multicenter Randomized Controlled Trial to Compare Standard Chemoradiation With or Without Recombinant Human Endostatin Injection (Endostar) Therapy for the Treatment of Locally Advanced Nasopharyngeal Carcinoma: Long-Term Outcomes Update. *Curr Probl Cancer* (2020) 44(1):100492. doi: 10.1016/j.currproblcancer.2019.06.007
122. Chen Q, Tang L, Liu N, Han F, Guo L, Guo S, et al. Famitinib in Combination With Concurrent Chemoradiotherapy in Patients With Locoregionally Advanced Nasopharyngeal Carcinoma: A Phase 1, Open-Label, Dose-Escalation Study. *Cancer Commun* (2018) 38(1):66. doi: 10.1186/s40880-018-0330-z
123. Lim W-T, Ng Q-S, Ivy P, Leong S-S, Singh O, Chowbay B, et al. A Phase II Study of Pazopanib in Asian Patients With Recurrent/Metastatic Nasopharyngeal Carcinoma. *Clin Cancer Res* (2011) 17(16):5481–9. doi: 10.1158/1078-0432.CCR-10-3409
124. Xue C, Huang Y, Huang PY, Yu QT, Pan JJ, Liu LZ, et al. Phase II Study of Sorafenib in Combination With Cisplatin and 5-Fluorouracil to Treat Recurrent or Metastatic Nasopharyngeal Carcinoma. *Ann Oncol* (2013) 24(4):1055–61. doi: 10.1093/annonc/mds581
125. Wang X, Xiang Z, Tsao GSW, Tu W. Exosomes Derived From Nasopharyngeal Carcinoma Cells Induce IL-6 Production From Macrophages to Promote Tumorigenesis. *Cell Mol Immunol* (2021) 18(2):501–3. doi: 10.1038/s41423-020-0420-0
126. Yuan F, Zhou Z-F. Exosomes Derived From Taxol-Resistant Nasopharyngeal Carcinoma (NPC) Cells Transferred DDX53 to NPC Cells and Promoted Cancer Resistance to Taxol. *Eur Rev Med Pharmacol Sci* (2021) 25(1):127–38. doi: 10.26355/eurrev_202101_24375
127. Meckes DG, Shair KHY, Marquitz AR, Kung C-P, Edwards RH, Raab-Traub N. Human Tumor Virus Utilizes Exosomes for Intercellular Communication. *Proc Natl Acad Sci USA* (2010) 107(47):20370–5. doi: 10.1073/pnas.1014194107
128. Nanbo A, Kawanishi E, Yoshida R, Yoshiyama H. Exosomes Derived From Epstein-Barr Virus-Infected Cells Are Internalized via Caveola-Dependent Endocytosis and Promote Phenotypic Modulation in Target Cells. *J Virol* (2013) 87(18):19334–47. doi: 10.1128/JVI.01310-13
129. Yoshizaki T, Kondo S, Endo K, Nakanishi Y, Hatano M, Ueno T, et al. Modulation of the Tumor Microenvironment by Epstein-Barr Virus Latent

Membrane Protein 1 in Nasopharyngeal Carcinoma. *Cancer Sci* (2017) 109 (2):272–8. doi: 10.1111/cas.13473
130. Zuo L, Xie Y, Tang J, Xin S, Liu L, Zhang S, et al. Targeting Exosomal EBV-LMP1 Transfer and miR-203 Expression via the NF-κb Pathway: The Therapeutic Role of Aspirin in NPC. *Mol Ther - Nucleic Acids* (2019) :17:175–84. doi: 10.1016/j.omtn.2019.05.023
131. Duan Y, Li Z, Cheng S, Chen Y, Zhang L, He J, et al. Nasopharyngeal Carcinoma Progression is Mediated by EBER-Triggered Inflammation via the RIG-I Pathway. *Cancer Lett* (2015) 361(1):67–74. doi: 10.1016/j.canlet.2015.02.037
132. Takada K. Role of EBER and BARF1 in Nasopharyngeal Carcinoma (NPC) Tumorigenesis. *Semin Cancer Biol* (2012) 22(2):162–5. doi: 10.1016/j.semcancer.2011.12.007
133. Zeng Z, Fan S, Zhang X, Li S, Zhou M, Xiong W, et al. Epstein-Barr Virus-Encoded Small RNA 1 (EBER-1) Could Predict Good Prognosis in Nasopharyngeal Carcinoma. *Clin Transl Oncol* (2016) 18(2):206–11. doi: 10.1007/s12094-015-1354-3
134. Fan C, Tang Y, Wang J, Guo C, Wang Y, Xiang B, et al. The Emerging Role of Epstein-Barr Virus Encoded microRNAs in Nasopharyngeal Carcinoma. *J Cancer* (2018) 9(16):2852–64. doi: 10.7150/jca.25460
135. Michiel Pegtel D, Cosmopoulos K, Thorley-Lawson DA, Van Eijndhoven MAJ, Hopmans ES, Lindenberg JL, et al. Functional Delivery of Viral miRNAs via Exosomes. *Proc Natl Acad Sci USA* (2010) 107(14):6328–33. doi: 10.1073/pnas.0914843107
136. Hamanishi J, Masaki M, Noriomi M, Abiko K, Baba T, Konishi I. PD-1/PD-L1 Blockade in Cancer Treatment: Perspectives and Issues. *Int J Clin Oncol* (2016) 21(3):462–73. doi: 10.1007/s10147-016-0959-z
137. Jiang Y, Chen M, Nie H, Yuan Y. PD-1 and PD-L1 in Cancer Immunotherapy: Clinical Implications and Future Considerations. *Hum Vaccin Immunother* (2019) 15(5):1111–22. doi: 10.1080/21645515.2019.1571892
138. Hsu C, Lee S-H, Ejadi S, Even C, Cohen RB, Le TC, et al. Safety and Antitumor Activity of Pembrolizumab in Patients With Programmed Death-Ligand 1–Positive Nasopharyngeal Carcinoma: Results of the KEYNOTE-028 Study. *J Clin Oncol* (2017) 35(36):4050–6. doi: 10.1200/JCO.2017.73.3675
139. Li Y, Ding J, Liao L, Zhang Z, Liao S, Wu Y, et al. Expression of Programmed Death Ligand-1 Predicts Poor Outcome in Nasopharyngeal Carcinoma. *Mol Clin Oncol* (2017) 7(3):378–82. doi: 10.3892/mco.2017.1318/abstract
140. Huang Z-L, Liu S, Wang G-N, Zheng S-H, Ding S-R, Tao Y-L, et al. The Prognostic Significance of PD-L1 and PD-1 Expression in Patients With Nasopharyngeal Carcinoma: A Systematic Review and Meta-Analysis. *Cancer Cell Int* (2019) 19:141. doi: 10.1186/s12935-019-0863-5
141. Zhu Q, Cai MY, Chen CL, Hu H, Lin HX, Li M, et al. Tumor Cells PD-L1 Expression as a Favorable Prognosis Factor in Nasopharyngeal Carcinoma Patients With Pre-Existing Intratumor-Infiltrating Lymphocytes. *Oncoimmunology* (2017) 6(5):e1312240. doi: 10.1080/2162402X.2017.1312240
142. Lv J-W, Li J-Y, Luo L-N, Wang Z-X, Chen Y-P. Comparative Safety and Efficacy of Anti-PD-1 Monotherapy, Chemotherapy Alone, and Their Combination Therapy in Advanced Nasopharyngeal Carcinoma: Findings From Recent Advances in Landmark Trials. *J Immunother Cancer* (2019) 7 (1):159. doi: 10.1186/s40425-019-0636-7
143. Dong H, De L, Cruz-Merino L, Inman BA, Du J, Huang Y-F, et al. Comparative Safety of PD-1/PD-L1 Inhibitors for Cancer Patients: Systematic Review and Network Meta-Analysis. *Front Oncol* (2019) 9:972. doi: 10.3389/fonc.2019.00972
144. Masterson L, Howard J, Gonzalez-Cruz J, Jackson C, Barnett C, Overton L, et al. Immune Checkpoint Inhibitors in Advanced Nasopharyngeal Carcinoma: Beyond an Era of Chemoradiation? *Int J Cancer* (2020) 146 (8):2305–14. doi: 10.1002/ijc.32869
145. Johnson D, Ma BBY. Targeting the PD-1/PD-L1 Interaction in Nasopharyngeal Carcinoma. *Oral Oncol* (2021) 113:105127. doi: 10.1016/j.oraloncology.2020.105127
146. Chen T-C, Chen C-H, Wang C-P, Lin P-H, Yang T-L, Lou P-J, et al. The Immunologic Advantage of Recurrent Nasopharyngeal Carcinoma From the Viewpoint of Galectin-9/Tim-3-Related Changes in the Tumour Microenvironment. *Sci Rep* (2017) 7(1):10349. doi: 10.1038/s41598-017-10386-y
147. Huang J, Fogg M, Wirth LJ, Daley H, Ritz J, Posner MR, et al. Epstein-Barr Virus-Specific Adoptive Immunotherapy for Recurrent, Metastatic Nasopharyngeal Carcinoma. *Cancer* (2017) 123(14):2642–50. doi: 10.1002/cncr.30541
148. Tang X, Zhou Y, Li W, Tang Q, Chen R, Zhu J, et al. T Cells Expressing a LMP1-Specific Chimeric Antigen Receptor Mediate Antitumor Effects Against LMP1-Positive Nasopharyngeal Carcinoma Cells *In Vitro* and *In Vivo*. *J BioMed Res* (2014) 28(6):468–75. doi: 10.7555/JBR.28.20140066
149. Zhu Q, Zhao G, Li Y, Talakatta G, Mai H, Le Q, et al. Advances in Pathogenesis and Precision Medicine for Nasopharyngeal Carcinoma. *MedComm* (2021) 2(2):175–206. doi: 10.1002/mco2.32
150. Li Y, Pan K, Liu L, Li Y, Gu M, Zhang H, et al. Sequential Cytokine-Induced Killer Cell Immunotherapy Enhances the Efficacy of the Gemcitabine Plus Cisplatin Chemotherapy Regimen for Metastatic Nasopharyngeal Carcinoma. *PloS One* (2015) 10(6):e0130620. doi: 10.1371/journal.pone.0130620
151. Hopkins R, Xiang W, Marlier D, Au VB, Ching Q, Wu LX, et al. Monocytic Myeloid-Derived Suppressor Cells Underpin Resistance to Adoptive T Cell Therapy in Nasopharyngeal Carcinoma. *Mol Ther* (2021) 29(2):734–43. doi: 10.1016/j.ymthe.2020.09.040
152. Taylor GS, Jia H, Harrington K, Lee LW, Turner J, Ladell K, et al. A Recombinant Modified Vaccinia Ankara Vaccine Encoding Epstein-Barr Virus (EBV) Target Antigens: A Phase I Trial in UK Patients With EBV-Positive Cancer. *Clin Cancer Res* (2014) 20(19):5009–22. doi: 10.1158/1078-0432.CCR-14-1122-T
153. Zeng Y, Si YF, Lan GP, Wang Z, Zhou L, Tang MZ, et al. LMP2-DC Vaccine Elicits Specific EBV-LMP2 Response to Effectively Improve Immunotherapy in Patients With Nasopharyngeal Cancer. *BioMed Environ Sci* (2020) 33 (11):849–56. doi: 10.3967/bes2020.115
154. Jiun Chai S, Yeow Yap Y, Ching Foo Y, Fah Yap L, Ponniah S, Hwang Teo S, et al. Identification of Four-Jointed Box 1 (FJX1)-Specific Peptides for Immunotherapy of Nasopharyngeal Carcinoma. *PloS One* (2015) 10(11): e0130464. doi: 10.1371/journal.pone.0130464
155. Smith C, McGrath M, Neller MA, Matthews KK, Crooks P, Le Texier L, et al. Complete Response to PD-1 Blockade Following EBV-Specific T-Cell Therapy in Metastatic Nasopharyngeal Carcinoma. *Precis Oncol* (2021) 5 (1):24. doi: 10.1038/s41698-021-00162-7
156. Duraiswamy J, Kaluza KM, Freeman GJ, Coukos G. Dual Blockade of PD-1 and CTLA-4 Combined With Tumor Vaccine Effectively Restores T-Cell Rejection Function in Tumors. *Cancer Res* (2013) 73(12):3591–603. doi: 10.1158/0008-5472.CAN-12-4100
157. Foy SP, Sennino B, dela Cruz T, Cote JJ, Gordon EJ, Kemp F, et al. Poxvirus-Based Active Immunotherapy With PD-1 and LAG-3 Dual Immune Checkpoint Inhibition Overcomes Compensatory Immune Regulation, Yielding Complete Tumor Regression in Mice. *PloS One* (2016) 11 (2):150084. doi: 10.1371/journal.pone.0150084
158. Lin M, Zhang X-L, You R, Yang Q, Zou X, Yu K, et al. Neoantigen Landscape in Metastatic Nasopharyngeal Carcinoma. *Theranostics* (2021) 11(13):6427–44. doi: 10.7150/thno.53229
159. Parsonage G, MacHado LR, Hui JWY, McLarnon A, Schmaler T, Balasothy M, et al. CXCR6 and CCR5 Localize T Lymphocyte Subsets in Nasopharyngeal Carcinoma. *Am J Pathol* (2012) 180(3):1215–22. doi: 10.1016/j.ajpath.2011.11.032
160. Xie G, Dong H, Liang Y, Ham JD, Rizwan R, Chen J. CAR-NK Cells: A Promising Cellular Immunotherapy for Cancer. *EBioMedicine* (2020) 59:102975. doi: 10.1016/j.ebiom.2020.102975
161. Liu W, Chen G, Zhang C, Liao X, Xie J, Liang T, et al. Prognostic Significance of Tumor-Infiltrating Lymphocytes and Macrophages in Nasopharyngeal Carcinoma: A Systematic Review and Meta-Analysis. *Eur Arch Oto-Rhino-Laryngol* (2021) 279(1):25–35. doi: 10.1007/s00405-021-06879-2
162. Al-Rajhi N, Soudy H, Ahmed SA, Elhassan T, Mohammed SF, Khoja HA, et al. Cd3+T-Lymphocyte Infiltration is an Independent Prognostic Factor for Advanced Nasopharyngeal Carcinoma. *BMC Cancer* (2020) 20):240–53. doi: 10.1186/s12885-020-06757-w
163. Ooft ML, Van Ipenburg JA, Braunius WW, Zuur CI, Koljenovic S, Koljenovic K, et al. Prognostic Role of Tumor Infiltrating Lymphocytes in EBV Positive and EBV Negative Nasopharyngeal Carcinoma. *Oral Oncol* (2017) 71:16–25. doi: 10.1016/j.oraloncology.2017.05.015
164. Zhang Y-L, Li J, Mo H-Y, Zheng L-M, Qian C-N, Zeng Y-X. Different Subsets of Tumor Infiltrating Lymphocytes Correlate With NPC Progression in Different Ways. *Mol Cancer* (2010) 9:4. doi: 10.1186/1476-4598-9-4

165. Ooft ML, van Ipenburg JA, Sanders ME, Kranendonk M, Hofland I, de Bree R, et al. Prognostic Role of Tumour-Associated Macrophages and Regulatory T Cells in EBV-Positive and EBV-Negative Nasopharyngeal Carcinoma. *J Clin Pathol* (2018) 71(3):267–74. doi: 10.1136/jclinpath-2017-204664
166. Chen Y-L. Prognostic Significance of Tumor-Associated Macrophages in Patients With Nasopharyngeal Carcinoma A Meta-Analysis. *Med* (2020) 99 (39):e21999. doi: 10.1097/MD.0000000000021999
167. Huang H, Liu X, Zhao F, Lu J, Zhang B, Peng X, et al. M2-Polarized Tumour-Associated Macrophages in Stroma Correlate With Poor Prognosis and Epstein–Barr Viral Infection in Nasopharyngeal Carcinoma. *Acta Otolaryngol* (2017) 137(8):888–94. doi: 10.1080/00016489.2017.1296585
168. Zhang X-S, Zhu X-F, Gao J-S, Ye Y-L, Feng Q-S, Liu Z-C, et al. Variable Sensitivity of Endothelial Cells to Epirubicin in Xenografts of Human Nasopharyngeal Carcinoma CNE-2 Cells. *Cancer Biol Ther* (2002) 1 (3):263–5. doi: 10.4161/cbt.78
169. Bhuvaneswari R, Gan YYY, Yee KKL, Soo KC, Olivo M. Effect of Hypericin-Mediated Photodynamic Therapy on the Expression of Vascular Endothelial Growth Factor in Human Nasopharyngeal Carcinoma. *Int J Mol Med* (2007) 20(4):421–8. doi: 10.3892/ijmm.20.4.421/abstract
170. Li L, Kong F, Zhang L, Li X, Fu X, Wang X, et al. Apatinib, a Novel VEGFR-2 Tyrosine Kinase Inhibitor, for Relapsed and Refractory Nasopharyngeal Carcinoma: Data From an Open-Label, Single-Arm, Exploratory Study. *Invest New Drugs* (2020) 38(6):1847–53. doi: 10.1007/s10637-020-00925-2
171. Ruan X, Liang J-H, Pan Y, Cai R, Zhang RJ, He Z, et al. Apatinib for the Treatment of Metastatic or Locoregionally Recurrent Nasopharyngeal Carcinoma After Failure of Chemotherapy: A Multicenter, Single-Arm, Prospective Phase 2 Study. *Cancer* (2021) 127(17):3163–71. doi: 10.1002/cncr.33626
172. Chong WQ, CMi L, AK S, CS T, Chan GHJ, Huang Y, et al. Integration of Antiangiogenic Therapy With Cisplatin and Gemcitabine Chemotherapy in Patients With Nasopharyngeal Carcinoma. *Clin Cancer Res* (2020) 26 (20):5320–8. doi: 10.1158/1078-0432.CCR-20-1727
173. Peng Q-X, Han Y-W, Zhang Y-L, Hu J, Fan J, Fu S-Z, et al. Apatinib Inhibits VEGFR-2 and Angiogenesis in an *In Vivo* Murine Model of Nasopharyngeal Carcinoma. *Oncotarget* (2017) 8(32):52813–22. doi: 10.18632/oncotarget.17264
174. Liu S, Wu F, Zhang Y, Qin R, Zhu N, Li Y, et al. Apatinib Combined With Radiotherapy Enhances Antitumor Effects in an *In Vivo* Nasopharyngeal Carcinoma Model. *Cancer Control* (2020) 27(1):1073274820922553. doi: 10.1177/1073274820922553
175. Wen Q-L, Meng M-B, Yang B, Tu L-L, Jia L, Zhou L, et al. Endostar, a Recombined Humanized Endostatin, Enhances the Radioresponse for Human Nasopharyngeal Carcinoma and Human Lung Adenocarcinoma Xenografts in Mice. *Cancer Sci* (2009) 100(8):1510–9. doi: 10.1111/j.1349-7006.2009.01193.x
176. Lugano R, Mohanraj R, Dimberg A. Tumor Angiogenesis: Causes, Consequences, Challenges and Opportunities. *Cell Mol Life Sci* (2020) 77 (9):1745–70. doi: 10.1007/s00018-019-03351-7
177. Xiang T, Lin Y-X, Ma W, Zhang H-J, Chen K-M, He G-P, et al. Vasculogenic Mimicry Formation in EBV-Associated Epithelial Malignancies. *Nat Commun* (2018) 9(1):5009. doi: 10.1038/s41467-018-07308-5
178. Bhuvaneswari R, Gan YY, Lucky SS, Chin WW, Ali SM, Soo KC, et al. Molecular Profiling of Angiogenesis in Hypericin Mediated Photodynamic Therapy (2008). Available at: http://www.molecular-cancer.com/content/7/1/56.
179. Shen L, Zhou Q, Wang Y, Liao W, Chen Y, Xu Z, et al. Antiangiogenic and Antitumoral Effects Mediated by a Vascular Endothelial Growth Factor Receptor 1 (VEGFR-1)- Targeted DNAzyme. *Mol Med* (2013) 19(1):377–86. doi: 10.2119/molmed.2013.00090
180. Guérin E, Raffelsberger W, Pencreach E, Maier A, Neuville A, Schneider A, et al. *In Vivo* Topoisomerase I Inhibition Attenuates the Expression of Hypoxia-Inducible Factor 1α Target Genes and Decreases Tumor Angiogenesis. *Mol Med* (2012) 181. 2011 Oct 1918(1):83–94. doi: 10.2119/molmed.2011.00120
181. Zhang Y, Chen X, Ren P, Su Z, Cao H, Zhou J, et al. Synergistic Effect of Combination Topotecan and Chronomodulated Radiation Therapy on Xenografted Human Nasopharyngeal Carcinoma. *Int J Radiat Oncol Biol Phys* (2013) 87(2):356–62. doi: 10.1016/j.ijrobp.2013.05.047
182. Chen Y, Xu G, Zheng Y, Yan M, Li Z, Zhou Y, et al. Nanoformulation of D-α-Tocopheryl Polyethylene Glycol 1000 Succinate-B-Poly(ϵ-Caprolactone-Ran- Glycolide) Diblock Copolymer for sirNa Targeting hIF-1α for Nasopharyngeal Carcinoma Therapy. *Int J Nanomed* (2015) 10:1375–86. doi: 10.2147/IJN.S76092
183. Li Y, Ding J, Xu X, Shi R, Saw PE, Wang J, et al. Dual Hypoxia-Targeting RNAi Nanomedicine for Precision Cancer Therapy. *Nano Lett* (2020) 20 (7):4857–63. doi: 10.1021/acs.nanolett.0c00757
184. Ma W, Feng L, Zhang S, Zhang H, Zhang X, Qi X, et al. Induction of Chemokine (C-C Motif) Ligand 5 by Epstein-Barr Virus Infection Enhances Tumor Angiogenesis in Nasopharyngeal Carcinoma. *Cancer Sci* (2018) 109 (5):1710–22. doi: 10.1111/cas.13584
185. Lin SJ, Chang KP, Hsu CW, Chi LM, Chien KY, Liang Y, et al. Low-Molecular-Mass Secretome Profiling Identifies C-C Motif Chemokine 5 as a Potential Plasma Biomarker and Therapeutic Target for Nasopharyngeal Carcinoma. *J Proteom* (2013) 94:186–201. doi: 10.1016/j.jprot.2013.09.013
186. Liu S-C, Chang Y-S. Role of Leukemia Inhibitory Factor in Nasopharyngeal Carcinogenesis. *Mol Cell Oncol* (2014) 1(1):e29900. doi: 10.4161/mco.29900
187. Liu S-C, Tsang N-M, Chiang W-C, Chang K-P, Hsueh C, Liang Y, et al. Leukemia Inhibitory Factor Promotes Nasopharyngeal Carcinoma Progression and Radioresistance. *J Clin Invest* (2013) 123(12):5269–83. doi: 10.1172/JCI63428
188. Zheng X-H, Lu L-X, Cui C, Chen M-Y, Li X-Z, Jia W-H. Epstein-Barr Virus Mir-Bart1-5p Detection via Nasopharyngeal Brush Sampling is Effective for Diagnosing Nasopharyngeal Carcinoma. *Oncotarget* (2015) 7(4):4972–80. doi: 10.18632/oncotarget.6649
189. Zhang G, Zong J, Lin S, Verhoeven RJA, Tong S, Chen Y, et al. Circulating Epstein-Barr Virus microRNAs miR-BART7 and miR-BART13 as Biomarkers for Nasopharyngeal Carcinoma Diagnosis and Treatment. *Authors Int J Cancer* (2015) 136(5):E301–12. doi: 10.1002/ijc.29206
190. Hirai N, Wakisaka N, Kondo S, Aga M, Moriyama-Kita M, Ueno T, et al. Potential Interest in Circulating miR-BART17-5p As a Post-Treatment Biomarker for Prediction of Recurrence in Epstein-Barr Virus-Related Nasopharyngeal Carcinoma. *PloS One* (2016) 11(9):e0163609. doi: 10.1371/journal.pone.0163609
191. Lu T, Guo Q, Lin K, Chen H, Chen Y, Xu Y, et al. Circulating Epstein-Barr Virus microRNAs BART7-3p and BART13-3p as Novel Biomarkers in Nasopharyngeal Carcinoma. *Cancer Sci* (2020) 111(5):1711–23. doi: 10.1111/cas.14381
192. Siak PY, Khoo AS-B, Leong CO, Hoh B-P, Cheah S-C. Current Status and Future Perspectives About Molecular Biomarkers of Nasopharyngeal Carcinoma. *Cancers (Basel)* (2021) 13(14):3490. doi: 10.3390/cancers13143490
193. Zheng W, Ye W, Wu Z, Huang X, Xu Y, Chen Q, et al. Identification of Potential Plasma Biomarkers in Early-Stage Nasopharyngeal Carcinoma-Derived Exosomes Based on RNA Sequencing. *Cancer Cell Int* (2021) 21 (1):185. doi: 10.1186/s12935-021-01881-4
194. Liu L, Zuo L, Yang J, Xin S, Zhang J, Zhou J, et al. Exosomal Cyclophilin A as a Novel Noninvasive Biomarker for Epstein-Barr Virus Associated Nasopharyngeal Carcinoma. *Cancer Med* (2019) 8(6):3142–51. doi: 10.1002/cam4.2185
195. Xu Z, Zeng S, Gong Z, Yan Y. Exosome-Based Immunotherapy: A Promising Approach for Cancer Treatment. *Mol Cancer* (2020) 19:160. doi: 10.1186/s12943-020-01278-3
196. Patel GK, Khan MA, Zubair H, Srivastava SK, Khushman M, Singh S, et al. Comparative Analysis of Exosome Isolation Methods Using Culture Supernatant for Optimum Yield, Purity and Downstream Applications. *Sci Rep* (2019) 9(1):5335. doi: 10.1038/s41598-019-41800-2
197. Ludwig N, Whiteside TL, Reichert TE. Challenges in Exosome Isolation and Analysis in Health and Disease. *Int J Mol Sci* (2019) 20(19):4684. doi: 10.3390/ijms20194684
198. Chen X, Song E. Turning Foes to Friends: Targeting Cancer-Associated Fibroblasts. *Nat Rev Drug Discov* (2019) 18(2):99–115. doi: 10.1038/s41573-018-0004-1
199. Li Y, Chen F, Chen J, Chan S, He Y, Liu W, et al. Disulfiram/Copper Induces Antitumor Activity Against Both Nasopharyngeal Cancer Cells and Cancer-Associated Fibroblasts Through ROS/MAPK and Ferroptosis Pathways. *Cancers (Basel)* (2020) 12(1):138. doi: 10.3390/cancers12010138
200. Bruce JP, To K-F Y, Lui VW, Y Chung GT, Chan Y-Y, Man Tsang C, et al. Whole-Genome Profiling of Nasopharyngeal Carcinoma Reveals Viral-Host

Co-Operation in Inflammatory NF-κb Activation and Immune Escape. *Nat Commun* (2021) 12(1):4193. doi: 10.1038/s41467-021-24348-6
201. Li YY, Chung GTY, Lui VWY, To K-F, Ma BBY, Woo JKS, et al. Exome and Genome Sequencing of Nasopharynx Cancer Identifies NF-kB Pathway Activating Mutations. *Nat Commun* (2017) 8:14121. doi: 10.1038/ncomms14121
202. Chung GTY, Lou WPK, Chow C, To KF, Choy KW, Leung AWC, et al. Constitutive Activation of Distinct NF-κb Signals in EBV-Associated Nasopharyngeal Carcinoma. *J Pathol* (2013) 231(3):311–22. doi: 10.1002/path.4239
203. Lung HL, Kan R, Yin Chau W, Man Y, Mak K, Fong CH, et al. The Anti-Tumor Function of the iKK Inhibitor PS1145 and High Levels of P65 and KLF4 are Associated With the Drug Resistance in Nasopharyngeal Carcinoma Cells. *Sci Rep* (2019) 9(1):12064. doi: 10.1038/s41598-019-48590-7
204. Jiang G-M, Wang H-S, Du J, Ma W-F, Wang H, Qiu Y, et al. Bortezomib Relieves Immune Tolerance in Nasopharyngeal Carcinoma via STAT1 Suppression and Indoleamine 2,3-Dioxygenase Downregulation. *Cancer Immunol Res* (2017) 5(1):42–51. doi: 10.1158/2326-6066.CIR-16-0102
205. Wang W, Cheng H, Gu X, Yin X. The Natural Flavonoid Glycoside Vitexin Displays Preclinical Antitumor Activity by Suppressing NF-κb Signaling in Nasopharyngeal Carcinoma. *Onco Targets Ther* (2019) 12:4461–8. doi: 10.2147/OTT.S210077
206. Zhao W, Ma N, Wang S, Mo Y, Zhang Z, Huang G, et al. RERG Suppresses Cell Proliferation, Migration and Angiogenesis Through ERK/NF-κb Signaling Pathway in Nasopharyngeal Carcinoma. *J Exp Clin Cancer Res* (2017) 36(1):88. doi: 10.1186/s13046-017-0554-9
207. Soukupová J, Bordoni C, Turnham DJ, Yang WW, Seaton G, Gruca A, et al. The Discovery of a Novel Antimetastatic Bcl3 Inhibitor. *Mol Cancer Ther* (2021) 20(5):775–86. doi: 10.1158/1535-7163.MCT-20-0283
208. Luo WR, Chen XY, Li SY, Wu AB, Yao KT. Neoplastic Spindle Cells in Nasopharyngeal Carcinoma Show Features of Epithelial-Mesenchymal Transition. *Histopathology* (2012) 61(1):113–22. doi: 10.1111/j.1365-2559.2012.04205.x
209. Luo W, Yao K. Molecular Characterization and Clinical Implications of Spindle Cells in Nasopharyngeal Carcinoma: A Novel Molecule-Morphology Model of Tumor Progression Proposed. *PloS One* (2013) 8(12):e83135. doi: 10.1371/journal.pone.0083135
210. Yuan Y. Spatial Heterogeneity in the Tumor Microenvironment. *Cold Spring Harb Perspect Med* (2016) 6(8):a026583. doi: 10.1101/cshperspect.a026583
211. Roma-Rodrigues C, Mendes R, Baptista PV, Fernandes AR. Targeting Tumor Microenvironment for Cancer Therapy. *Int J Mol Sci* (2019) 20(4):840–71. doi: 10.3390/ijms20040840
212. Luo H, Lu L, Yang F, Wang L, Yang X, Luo Q, et al. Nasopharyngeal Cancer-Specific Therapy Based on Fusion Peptide- Functionalized Lipid Nanoparticles. *ACS Nano* (2014) 8(5):4334–47. doi: 10.1021/nn405989n
213. Chen Y, Yang L, Huang S, Li Z, Zhan L, He J, et al. Delivery System for DNAzymes Using Arginine-Modified Hydroxyapatite Nanoparticles for Therapeutic Application in a Nasopharyngeal Carcinoma Model. *Int J Nanomed* (2013) 8:3107–18. doi: 10.2147/IJN.S48321

Conflict of Interest: The authors declare that the research was conducted in the absence of any commercial or financial relationships that could be construed as a potential conflict of interest.

Publisher's Note: All claims expressed in this article are solely those of the authors and do not necessarily represent those of their affiliated organizations, or those of the publisher, the editors and the reviewers. Any product that may be evaluated in this article, or claim that may be made by its manufacturer, is not guaranteed or endorsed by the publisher.

Copyright © 2022 Su, Siak, Leong and Cheah. This is an open-access article distributed under the terms of the Creative Commons Attribution License (CC BY). The use, distribution or reproduction in other forums is permitted, provided the original author(s) and the copyright owner(s) are credited and that the original publication in this journal is cited, in accordance with accepted academic practice. No use, distribution or reproduction is permitted which does not comply with these terms.

frontiers in Oncology

ORIGINAL RESEARCH
published: 08 March 2022
doi: 10.3389/fonc.2022.830174

Bioinformatics Analysis Combined With Experiments Predicts PUDP as a Potential Prognostic Biomarker for Hepatocellular Carcinoma Through Its Interaction With Tumor Microenvironment

Jiahao Yu[1†], Weirui Zhang[2†], Dawei Ding[1†], Yinan Hu[1†], Guanya Guo[1], Jingbo Wang[1*] and Ying Han[1*]*

[1] State Key Laboratory of Cancer Biology, Xijing Hospital of Digestive Diseases, The Fourth Military Medical University, Xi'an, China, [2] Department of Biomedical Engineering, The Fourth Military Medical University, Xi'an, China

OPEN ACCESS

Edited by:
Pranav Gupta, Albert Einstein College of Medicine, United States

Reviewed by:
Siyuan Sun, Tianjin Medical University General Hospital, China
Kangkang Yu, Huashan Hospital, China

***Correspondence:**
Ying Han
hanying1@fmmu.edu.cn
Jingbo Wang
jimberw@163.com
Guanya Guo
guoguanya@126.com

[†]These authors have contributed equally to this work

Specialty section:
This article was submitted to Molecular and Cellular Oncology, a section of the journal Frontiers in Oncology

Received: *06 December 2021*
Accepted: *15 February 2022*
Published: *08 March 2022*

Citation:
Yu J, Zhang W, Ding D, Hu Y, Guo G, Wang J and Han Y (2022) Bioinformatics Analysis Combined With Experiments Predicts PUDP as a Potential Prognostic Biomarker for Hepatocellular Carcinoma Through Its Interaction With Tumor Microenvironment. Front. Oncol. 12:830174. doi: 10.3389/fonc.2022.830174

Hepatocellular carcinoma (HCC) is one of the deadliest tumors in the world and is notorious for poor prognosis. There is mounting evidence that pseudouridine performs key functions in the initiation and progression of several cancers. A previous study demonstrated that Pseudouridine 5'-phosphatase (PUDP) may be a novel prognostic biomarker in colorectal cancer. However, in the past, we have paid little attention to PUDP and we are still not clear about its function and role in cancer. In this study, a pan-cancer analysis of PUDP expression and prognosis was performed firstly using The Cancer Genome Atlas (TCGA) and Genotype-Tissue Expression (GTEx) data and we found that PUDP may be a potential oncogene for HCC. Then the most potential upstream microRNA contributing to PUDP was identified as let-7c-5p through expression analysis, correlation analysis, and survival analysis. Subsequently, the result of single cell RNA sequencing (scRNA-seq) demonstrated that PUDP was significantly highly expressed on malignant cells. In addition, there are significantly positive correlations between PUDP and tumor immune cell infiltration, biomarkers of immune cells, and immune checkpoint expression, especially with tumor-promoting immune cells such as T cell regulatory (Treg), Myeloid-derived suppressor cell (MDSC), cancer-associated fibroblast (CAF). Moreover, we found the methylation level of three loci was positively correlated with PUDP expression and four loci were negatively correlated. 15 pairs of HCC and normal adjacent tissues from HCC patients who were treated at our center were used to verify the results of the bioinformatics analysis and the results of experiments are similar to the bioinformatics analysis. Our study demonstrated that HCC patients with high PUDP expression are less likely to benefit from immunotherapy, and in addition, we explored the relationship between PUDP and anticancer drugs. Finally, we explored the clinical relevance of PUDP, identified PUDP as an independent risk factor for HCC patients and constructed a prognostic model, used International Cancer Genome Consortium

(ICGC) data to do external validation. Collectively, our study demonstrated that high expression of PUDP suggested a poor prognosis and low response to immunotherapy, providing new insight into the treatment and prognosis of HCC.

Keywords: HCC, PUDP, bioinformatics, prognosis, tumor microenvironment

INTRODUCTION

Hepatocellular carcinoma(HCC) is a highly aggressive and inflammation-associated cancer, accounts for 70%-85% of the total liver cancer burden (1). The incidence and the mortality of HCC respectively ranks 6th, 3rd worldwide and the new cases of HCC were estimated that up to 906,000 and 830,000 related deaths occur each year (2). The initiation and progression of HCC depend on lots of risk factors, such as alcohol abuse, hepatitis B virus infection, obesity, and immune microenvironment (2–5). In recent years, significant advances have been made in the diagnosis, treatment, and prognosis of HCC, such as the PD-L1 inhibitor atezolizumab, combined with the anti-angiogenic agent bevacizumab, which has achieved success in the first-line treatment of advanced HCC, however, treatment outcomes for HCC patients remain unsatisfactory (6). Therefore, it is necessary for us to find new and effective prognostic biomarkers.

Pseudouridine 5'-phosphatase (PUDP), also called HDHD1 or HDHD1A, encodes a member of the haloacid dehalogenase-like (HAD) hydrolase superfamily, was a phosphatase specifically involved in dephosphorylation of pseudouridine 5'-phosphate (7). Pseudouridylation, the most common type of RNA epigenetic modification in biosome, and was discovered to play a critical role in the translation control of stem cells with implications for development and disease (8). According to the latest findings, Pseudouridylation alters splicing, while genes that control essential processes, such as metabolism, cell proliferation and apoptosis, are globally altered in HCC through alternative splicing (9, 10). Furthermore, pseudouridine was reported may be a potential biomarker for kidney disease, which is characterized by a decline in kidney function and the occurrence of chronic kidney disease (11). Some pseudouridine metabolism-related enzymes, such as dyskerin pseudouridine synthase 1(DKC1), have been reported that correlate with the prognosis of HCC patients (12). Past researches revealed that the expression level of PUDP may be a prognostic biomarker for colorectal cancer and demonstrated that the overexpression of PUDP conferred 2-deoxyglucose(2DG) resistance in HeLa cells, suggesting that it may be a conserved regulator of 2DG resistance and could interfere 2DG-based chemotherapies (13, 14). However, the biological function of PUDP remains poorly understood and a thorough study on the expression, prognosis, and mechanism of PUDP in HCC is absent.

In this study, the expression level of PUDP in pan-cancer was analyzed firstly. According to the results of survival analysis and expression analysis, PUDP was identified to be linked with the prognosis of HCC patients. Then, we incorporated 711 HCC samples and 475 normal tissues from The Cancer Genome Atlas (TCGA) database, GSE39791 and GSE25097 to analyze the differential expression of PUDP in HCC patients. And we verified the differential expression of PUDP by using qPCR, it was also validated in the level of protein using the HPA database. Next, the regulation of microRNAs(miRNAs) with PUDP was explored in HCC. We also did the mutation and correlation analysis between PUDP and common immune checkpoint in HCC. In addition, we analyze the response of immunotherapy for high PUDP expression patients and low PUDP expression patients. Subsequently, we demonstrated the correlation between PUDP expression and immune infiltration, clinical staging, clinical prognosis, and sensitivity to anticancer drugs. Finally, the prognostic model was constructed using data from the TCGA database and was validated using data from the International Cancer Genome Consortium (ICGC). In summary, our findings suggest that PUDP is an independent risk factor and may be a novel prognostic biomarker for HCC patients.

MATERIALS AND METHODS

Ethics Statement

Tumor samples were collected from the tumor tissue bank of Xijing Hospital. The samples were stored in liquid nitrogen before use and were collected in accordance with the ethical standards of the 1964 Declaration of Helsinki. This study was approved by The Xijing Hospital's Ethics Committee.

Data Download, Process, and Analysis

The mRNA expression data of 33 cancer types were downloaded from TCGA official website (https://portal.gdc.cancer.gov/) and then were used to perform the differential expression analysis for PUDP in 33 cancer types by using R package "limma" (15). HCC RNA sequencing data (GSE25097 and GSE39791) came from Gene Expression Omnibus(GEO) database and were used to analyze the differential expression of PUDP in HCC patients after normalization. GSE25097 includes the data of 268 HCC tumor tissues and 243 normal tissues. GSE39791 includes the 72 HCC tumor tissues and paired adjacent non-tumor tissues. The baseline information of HCC patients in the TCGA database is shown in **Table 1**.

Differential Expression and Survival Analysis

Besides the differential expression analysis for PUDP in 33 cancer types using the data from the TCGA database, we also analyzed the expression level of PUDP in pan-cancer by using TIMER2.0 (http://timer.cistrome.org/), ONCOMINE (https://

TABLE 1 | Baseline information of HCC patients from the TCGA database.

Characteristic	levels	Overall
n		374
T stage, n (%)	T1	183 (49.3%)
	T2	95 (25.6%)
	T3	80 (21.6%)
	T4	13 (3.5%)
N stage, n (%)	N0	254 (98.4%)
	N1	4 (1.6%)
M stage, n (%)	M0	268 (98.5%)
	M1	4 (1.5%)
Pathologic stage, n (%)	Stage I	173 (49.4%)
	Stage II	87 (24.9%)
	Stage III	85 (24.3%)
	Stage IV	5 (1.4%)
Tumor status, n (%)	Tumor free	202 (56.9%)
	With tumor	153 (43.1%)
Gender, n (%)	Female	121 (32.4%)
	Male	253 (67.6%)
Age, n (%)	<=60	177 (47.5%)
	>60	196 (52.5%)
Histologic grade, n (%)	G1	55 (14.9%)
	G2	178 (48.2%)
	G3	124 (33.6%)
	G4	12 (3.3%)
AFP(ng/ml), n (%)	<=400	215 (76.8%)
	>400	65 (23.2%)
OS event, n (%)	Alive	244 (65.2%)
	Dead	130 (34.8%)
Age, median (IQR)		61 (52, 69)

www.oncomine.org/resource/main.html) and GEPIA (http://gepia.cancer-pku.cn/). Kaplan-Meier(K-M) survival analysis was performed by using the R package "survminer" (https://cran.r-project.org/web/packages/survminer/index.html) and R package "survival" (https://cran.r-project.org/web/packages/survival/index.html). We then summarized the results of the K-M analysis and did separate K-M analyses for HCC and Pancreatic adenocarcinoma (PAAD).

The Protein Expression Level for PUDP in HCC Patients

The Human Protein Atlas (HPA, https://www.proteinatlas.org/), a Swedish-based program, aims to figure all the human proteins. Data from the HPA database is freely available for all researchers and we downloaded the immunohistochemistry images of PUDP expression from the HPA database.

qPCR

In accordance with the manufacturer's protocol, we extracted total RNA from HCC samples with the TRIzol reagent (Ambion). β-Actin was used as an internal control to normalize mRNA expression. The primer sequences for PUDP were GCAATGACAACTGATAAAGCGAGATG (Forward primer 5'-3'), GCTAACAAGGAGTGCTCATCAAAAAC (Reverse primer 5'-3') and the primer sequences for β-actin were CTCCATCC TGGCCTCGCTGT (Forward primer 5'-3'), GCTGTCA CCTTCACCGTTCC (Reverse primer 5'-3'). The pathological stage for most HCC samples were stage II and stage III.

Identification of Differentially Expressed Genes

According to the expression of PUDP in HCC patients, high and low PUDP expression groups were divided based on median value. Then we analyzed the significantly differentially expressed genes(DEGs) between the high and low expression groups by using the R package "DESeq2" (16). The results were displayed in the form of a volcano map and heat map. The threshold value for significant DEGs was adjust *P-value*<0.05 and $|Log\ fold\ change\ (FC)| \geq 2.0$.

Enrichment Analysis of PUDP

We used the "clusterprofiler" package to do Gene Ontology(GO) enrichment and Kyoto Encyclopedia of Genes and Genomes (KEGG) analysis (17). The threshold values were identified with corrected $P<0.01$ and a false discovery rate(FDR) <0.05. Gene set enrichment analysis (GSEA) was performed using the gene set "c2.cp.v7.2.symbols.gmt" which were downloaded from the Molecular Signatures Database (MSigDB, http://software.broadinstitute.org/gsea/msigdb/index.jsp).

ScRNA-Seq Analysis

Single-cell RNA sequencing (scRNA-seq) demonstrated the distribution and expression of PUDP in HCC patients. Data of scRNA sequencing were obtained from GSE125449 and Tumor Immune Single-cell Hub (TISCH) was used to perform analysis (18).

Mutation and Correlation Analysis of PUDP With Common Immune Checkpoints

We analyzed the mutation status and correlation of PUDP with common immune checkpoints in HCC using cBioPortal for Cancer Genomics (http://www.cbioportal.org) (19, 20). The results of the correlation analysis between PUDP and four common immune checkpoints of HCC are presented in the form of scatter plots.

Correlation of PUDP With the Infiltration of Immune Cells

We used the Timer2.0 website to analyze the infiltration relationship between PUDP and 6 types of immune cells (21). Besides, we explored the immune infiltration distribution between different somatic copy number variations(sCNA) status of the PUDP with T cell regulatory.

Prediction of the Immunotherapeutic Response

Tumor Immune Dysfunction and Exclusion (TIDE) algorithm was used to predict the potential immunotherapeutic response using TCGA RNA sequencing data and the corresponding clinical information of HCC patients (22).

Candidate MiRNA Prediction

StarBase (http://starbase.sysu.edu.cn/), an open-source database, identifies millions of miRNA-ncRNA, miRNA-mRNA, RBP-RNA,

and RNA-RNA interactions from multi-dimensional sequencing data (23). StarBase predicts miRNA-mRNA interactions by multiple prediction tools such as PITA, RNA22, miRmap, DIANA-microT, miRanda, PicTar and TargetScan. Those that meet the screening of more than two prediction tools are considered as potential upstream regulatory miRNAs of PUDP.

DNA Methylation Analysis

We estimated and visualized DNA methylation of PUDP in HCC by using the MEXPRESS web server (https://mexpress.be) (24, 25). MEXPRESS focuses on correlation analysis and visualization using information such as gene expression profiles, DNA methylation sites, and clinical data from the TCGA database. The predesignated methylation probes for each gene were taken into consideration.

Correlations of the Expression Levels of PUDP With Anticancer Drug Sensitivity and Clinical Stage

The CellMiner database (https://discover.nci.nih.gov/cellminer/home.do) which is an open database, was performed to analyze the relationship between 23,101 chemical compounds, including 218 drugs approved by FDA and 574 drugs tested by clinical trials, and the expression level of PUDP (26). R package limma and R package impute (http://www.bioconductor.org/packages/release/bioc/html/impute.html) were used in the analysis (27).

Establishment and Validation of the Clinical Prognostic Model

The clinical information of 337 HCC patients such as sex, age, clinical stage, and the expression level of PUDP were downloaded from the UCSC Xena website (http://xena.ucsc.edu/) to establish the prognostic model. The LIRI-JP cohort data which were downloaded from the ICGC database (https://dcc.icgc.org/) were used to perform external validation.

Risk score of HCC patients was performed by Cox regression analysis and R package "rms", R package "survival" were used to construct the nomogram. Harrell's concordance index(C-index) and calibration curve were used to do internal validation of the prognostic model.

Statistical Analysis

For K-M survival analysis, the log-rank test was utilized. The receiver operating characteristic (ROC) curve and the area under the curve (AUC) were conducted using R package "survival ROC" and "pROC" (28, 29). In calculating the relationship between immune cells, co-expressed genes, and the expression level of PUDP, we used the Spearman statistical method. All statistical analyses were performed by R software, version 4.1.0.

RESULTS

PUDP Expression Profiles in Pan-Cancer

We first analyzed the differential expression of PUDP between tumor and adjacent non-tumor tissues in pan-cancer and used different data sources and databases to ensure the reliability of the results that we analyzed. In a pan-cancer analysis using the Timer2.0 database, we found that PUDP was significantly up-regulated expressed in 11 types of tumors (**Figure 1A**). We then used the Oncomine database to perform differential expression analysis of PUDP in tumor and normal tissues (**Figure 1B**). In addition to using the database analysis, we downloaded RNAseq data from TCGA and GTEx and transformed them into the form of log2, and the results are shown in **Figure 1C**. We finally used the GEPIA database to do an interactive bodymap on the expression of PUDP in various human organs. Red represents expression in tumor tissues, green represents expression in normal tissues, and the shade of color represents the degree of expression (**Figure 1D**). The results of the analysis showed that PUDP is differentially expressed in most tumors and adjacent non-tumor tissues, but whether they all have a prognostic value according to the expression level of PUDP remains unknown.

Relationship Between PUDP Expression and Prognosis in Pan-Caner

Using gene expression and clinical data from the TCGA, survival analysis was performed to analyze the relationship between PUDP expression and prognosis. We summarized the results of analyses and found that PUDP had a significant prognostic value in PAAD and HCC, with a p-value less than 0.001 in both (**Figure 2A**). Employing OS, DSS, and PFI as outcome endpoints, we determined the predictive value of PUDP in HCC and PAAD (**Figures 2B–G**). The results demonstrated that PUDP had a significant prognostic value in HCC regardless of which of OS, DSS, PFI was used as the outcome endpoint, while hazard ratio (HR) value greater than 1 suggested that it was a risk factor. Our findings demonstrated that high PUDP expression correlates a poor prognosis of HCC patients.

The Analysis of Differential Expression of PUDP in HCC

In our previous analysis, we found that PUDP may be a novel prognostic biomarker for HCC. Then, we used two datasets, GSE39791 and GSE25097, as well as the HPA database, to re-identify the differences of PUDP expression between HCC tissues with adjacent non-tumor tissues at the mRNA and protein levels. The results demonstrated that PUDP has a significant differential expression on the level of mRNA and protein between HCC tissues and adjacent non-tumor tissues (**Figures 3A–D**). Finally, we collected tumor and paired adjacent non-tumor tissues from 15 HCC patients from the tumor tissue bank of Xijing Hospital for qPCR assay, and again verified this differential expression on mRNA level (**Figure 3E**). All the above analyses suggested that there was a significant difference in the expression of PUDP in HCC tissues and adjacent non-tumor tissues.

Identification of DEGs Associated With PUDP Expression in HCC

According to the expression profile of PUDP, we separated HCC patients into two groups: high PUDP expression and low PUDP

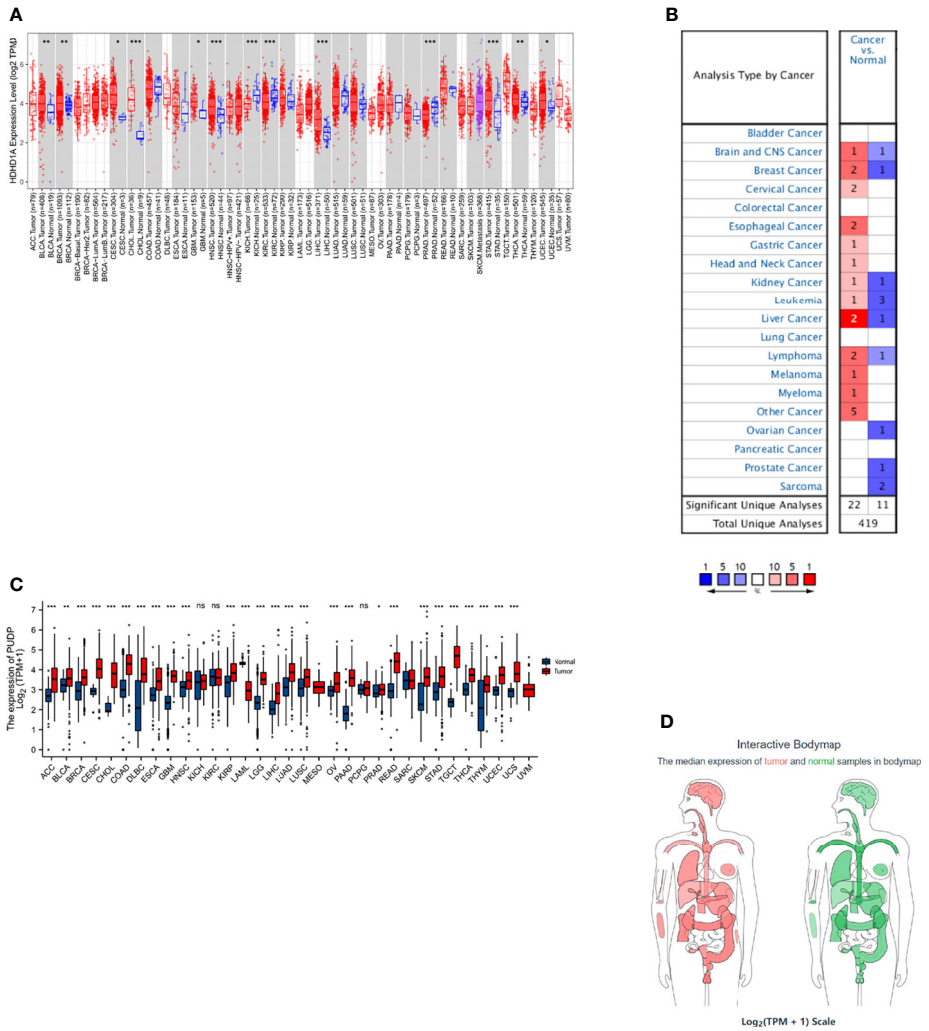

FIGURE 1 | The differential expression of PUDP in Pan-Cancer. We used Timer2.0, Oncomine database to identify the differential expression of PUDP in Pan-Cancer, and performed differential expression analysis using data from TCGA and GTEx, and finally used the GEPIA database to show an interactive bodymap of PUDP expression in humans. **(A)** Using Timer2.0 database to identify the differential expression of PUDP; **(B)** Using Oncomine database to identify the differential expression of PUDP; **(C)** Using data from TCGA and GTEx to identify the differential expression analysis of PUDP; **(D)** An interactive bodymap of PUDP in human using GEPIA database. *P < 0.05, **P < 0.01, ***P < 0.001; ns, no significant difference in statistics.

expression, with the low PUDP expression group serving as the reference group for DEGs analysis. We found that 453 genes were upregulated and 48 genes were downregulated with a strict cut-off of $p<0.05$ and $|Log\ fold\ change(FC)|\geq 2.0$ (**Figure 4A**). We took the top 5 up-regulated and down-regulated genes according to the size of LogFC values and plotted the correlation heat map (**Figure 4B**). We then analyzed the correlation of PUDP with Wnt7B and SMR3A in patients with HCC (**Figures 4C, D**). The results suggested that PUDP had a strong positive correlation with Wnt7B, while a strong negative correlation with SMR3A.

Enrichment Analysis of PUDP in HCC

We performed a functional enrichment analysis of the PUDP. The results of the molecular function of GO analysis demonstrated that PUDP was closely associated with substrate-specific channel activity, channel activity, passive transmembrane transporter activity, and antigen binding. And GO analysis showed that the PUDP was closely associated with biological processes such as protein activation cascade, complement activation, humoral immune response mediated by circulating immunoglobulin and complement activation, classical pathway (**Figures 5A, B**). The results of KEGG functional analysis suggested that PUDP mainly affects the neuroactive ligand-receptor interaction, bile secretion (**Figures 5C, D**).

Furthermore, the GSEA of DEGs revealed that the enrichment of DEGs were correlated with the NABA MATRISOME, REACTOME CELL CYCLE CHECKPOINTS, REACTOME CELL CYCLE MITOTIC, REACTOME CELL CYCLE, AND REACTOME M PHASE (**Supplementary Figures 1A, B**).

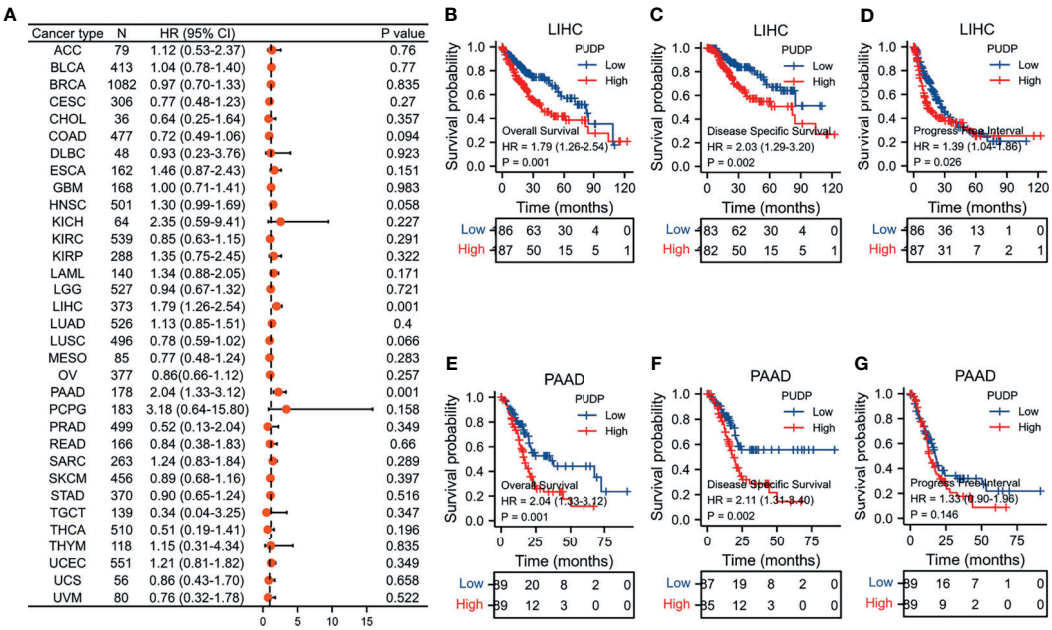

FIGURE 2 | Survival analysis in Pan-Cancer and exploring the prognostic value in PAAD and HCC of PUDP. **(A)** The prognostic value of PUDP in Pan-Cancer; **(B–D)** Prognosis analysis of PUDP in HCC; **(E–G)** Prognosis analysis of PUDP in PAAD.

ScRNA Analysis of PUDP Expression on Different Cells of HCC

We utilized the HCC scRNA sequencing results from the GSE125449 dataset to investigate the expression of PUDP in different cells of HCC. Our work indicated that in HCC, PUDP was expressed in exhausted CD8 T cells (CD8Tex), monocytes or macrophages, endothelial cells, fibroblasts, malignant cells, hepatic progenitor cells, and especially in malignant cells with significantly high expression (**Supplementary Figure 2**). The findings suggested that PUDP expression is related to the tumor microenvironment in HCC.

Immune Infiltration and Drug Sensitivity Analysis of PUDP

In recent years, with the advancement of research, it has become a consensus that the tumor immune microenvironment affects tumor progression. We analyzed the tumor purity of PUDP in HCC and its correlation with multiple immune cells. We found that PUDP showed a strong positive association with B cell, T cells regulatory (Tregs), CD8+ T cell, CD4+ T cell, Myeloid-derived suppressor cell (MDSC), macrophage, neutrophil, dendritic cell and cancer associated fibroblast (CAF) (**Figures 6A–D**). Surprisingly, there is a strong positive correlation between PUDP and Tregs, MDSC, and other immune cells that promote tumor progression. The sCNA information was derived from copy number segmentation profiles at the gene level. The alteration status for reference is high amplification. The results showed that the distribution of Tregs infiltration differed depending on the PUDP's sCNA status (**Figure 6E**).

Moreover, we used the CellMiner database to investigate the relationship between PUDP and sensitivity to various anticancer chemotherapeutic drugs (**Supplementary Figure 3**). The results revealed a significant positive correlation between PUDP expression and sensitivity to tic10, nelarabine. It could shed new light on the clinical treatment of HCC.

Correlation of PUDP Expression With Immunotherapy Response and Immune Checkpoints

In recent years, with the progression of immunotherapy, the prognosis of HCC patients has been improved, but some patients do not benefit from immunotherapy, so how to accurately distinguish which patients can benefit from immunotherapy is an urgent problem. Two distinct mechanisms of tumor immune escape: tumor-infiltrating cytotoxic T lymphocyte (CTL) dysfunction and CTL rejection by immunosuppressive factors were assessed by TIDE employing a set of gene expression markers. High TIDE scores are related with poor immune checkpoint blockade therapy (ICB) efficacy and short survival after ICB therapy. We used the TIDE algorithm to assess the responsiveness of the different PUDP expression groups to immunotherapy. The group with high PUDP expression had higher scores, suggesting that high PUDP expression patients with HCC may be less responsive to immunotherapy and not benefit from immunotherapy (**Supplementary Figure 4**).

In addition, we analyzed the molecular subtypes and immune subtypes of PUDP in HCC, and the results suggested that in HCC, the molecular subtypes of PUDP were mainly concentrated in

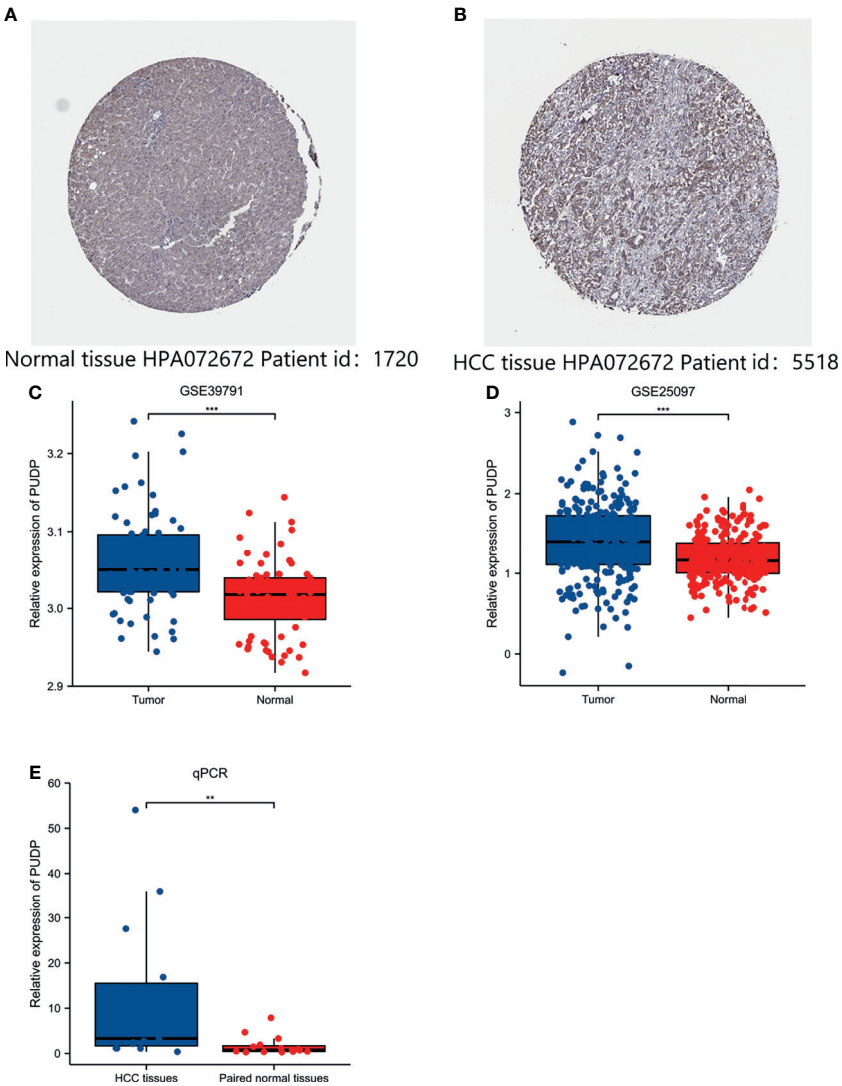

FIGURE 3 | Exploring the expression of PUDP in HCC. **(A)** The expression of PUDP in normal liver tissues on the level of protein; **(B)** The expression of PUDP in HCC tissues on the level of protein; **(C)** Expression analysis of PUDP using GSE39791; **(D)** Expression analysis of PUDP using GSE25097; **(E)** The result of qPCR. *P < 0.05, **P < 0.01, ***P < 0.001.

iCluster:3, and the immune subtypes were mainly C1, C2, C3, C4 (**Supplementary Figure 5**).

We also explored the correlation between PUDP and immune checkpoints mutation in HCC. The general landscape of PUDP and immune checkpoint alteration in HCC was compactly visualized, including inframe mutation, missense mutation, amplification, and deep deletion (**Figure 7A**). The detailed relationship between PUDP and common immune checkpoints in HCC was individually presented as indicated in **Figures 7B–E**.

Analysis of PUDP Expression With Clinical Correlation and Methylation Modifications

We explored the clinical relevance of PUDP expression in HCC and found that the degree of PUDP expression was clinically significantly correlated with patient gender, and its prevalence was seen in primary HCC compared to the recurrent tumor and solid tissue normal. Meanwhile, we found that the methylation level of three loci on the X chromosome was positively correlated with PUDP expression, with probe ID: cg10858432, cg17878951, and cg26547788, respectively. And there were four loci on the X chromosome whose methylation levels were significantly and negatively correlated with the expression levels of PUDP, whose probe IDs were cg20214316, cg11024551, cg03043405, cg19788004 (**Figure 8**). Subsequently, we incorporated common clinical indicators and performed a logistic regression analysis with PUDP as the independent variable, PUDP low expression as the reference, and the detailed results are shown in **Table 2**. We also did subgroup K-M analysis in an attempt to find the detailed

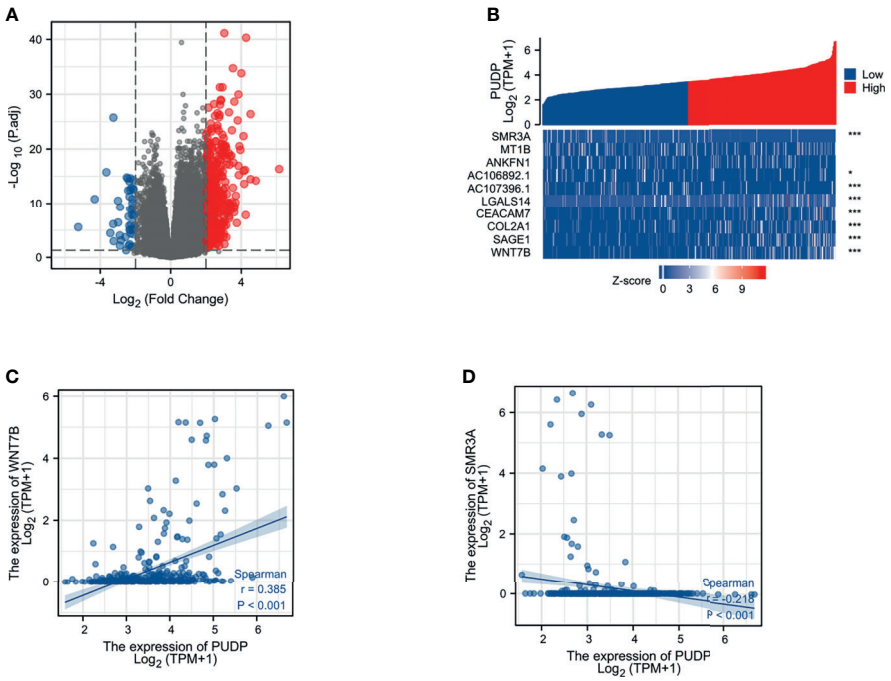

FIGURE 4 | Identification of the DEGs between PUDP high and low expression groups in HCC. **(A)** Volcano map of DEGs that 453 genes were upregulated and 48 genes were downregulated; **(B)** Correlation heat map of the top 5 up- and down-regulated genes with PUDP; **(C)** Correlation of PUDP and Wnt7B in patients with HCC; **(D)** Correlation of PUDP and SMR3A in patients with HCC. (*p < 0.05, ***p < 0.001).

correlations between PUDP expression and clinical indicators. The results demonstrated that the association between high PUDP expression and prognosis was more pronounced in male than in female, while high PUDP expression indicates the poor prognosis in the early stage of HCC, and in addition, the association between elevated PUDP and prognosis was more statistically significant in patients without vascular invasion (**Supplementary Figure 6**).

Exploring Predicted Upstream MiRNAs of PUDP

There are widely accepted that miRNAs perform an important function in the regulation of gene expression and the development of malignancies. To determine whether PUDP was regulated by miRNAs, upstream miRNAs were predicted firstly and eventually we discovered 19 miRNAs that may potentially bind to PUDP. Using the cytoscape software, a miRNA-PUDP regulatory network was created to better visualization (**Figure 9A**). In HCC, PUDP was most strongly connected with let-7c-5p and miR-106a-5p, as shown in **Figure 9B**. Based on the mechanism of effect of miRNA in the regulation of target gene expression, let-7c-5p may be the promising candidate. Subsequently, the expression correlation analysis and survival analysis of let-7c-5p were performed. Let-7c-5p was significantly downregulated in HCC, as shown in **Figures 9C, D**, and its expression had significant correlation with patients' prognosis. Finally, let-7c-5p expression and prognostic value in HCC were identified. All of these studies indicate let-7c-5p as the most promising PUDP regulatory miRNA in HCC.

Clinical Staging and Cox Regression Analysis

As the tumor progresses, whether there are differences in PUDP expression between patients with different clinical stages remains unknown, so we further explored the correlation between the expression of PUDP with different clinical stages, and the results showed that the expression of PUDP was significantly correlated with the pathologic stage and histologic grade (**Figures 10A, B**). It indicates that PUDP was significantly higher in patients with early-stage HCC and PUDP was differentially expressed in different staging HCC patients, suggesting that it may be a prognostic biomarker. To further explore the impact of the expression of the PUDP on HCC patient prognosis, Cox regression analyses were used and we found that the PUDP was an independent risk factor in HCC patients (P =0.031) (**Figures 10C, D**).

Development of a Prognostic Model Based on PUDP Expression Profile

We incorporated the risk score and OS into the model to plot the risk factor diagram (**Figure 11A**). Then we constructed the nomogram to predict HCC patients' OS (**Figure 11C**). C-index and the calibration curves were used as internal validation for the nomogram and C-index was performed to assess the discriminatory power of the nomogram (PUDP: 0.696 (0.668-0.724). Furthermore, the results of the calibration curves showed a good fit between the nomogram-predicted 1-, 3-, and 5-OS and the actual observed values (**Figure 11D**). We also used the ROC curve for evaluation, with an AUC value of 0.788 (**Figure 11B**).

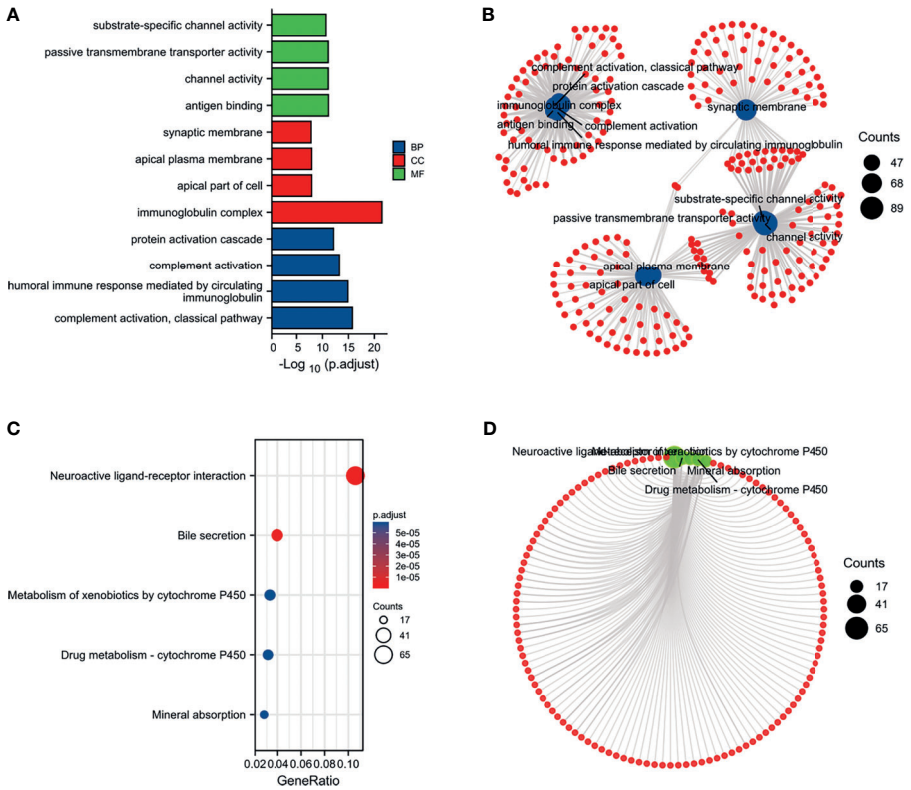

FIGURE 5 | Enrichment analysis of PUDP. **(A, B)** The results of GO analysis; **(C, D)** The results of KEGG analysis.

In addition, ICGC-JP dataset was employed as an external validation to assess the prognostic model's accuracy and stability (**Supplementary Figure 6**).

DISCUSSION

HCC is one of the most prevalent malignancies in the world, and the vast majority of patients with HCC do not have a good prognosis. The results of a randomized study that included 600 untreated HCC patients showed that the overall median survival was 9 months, and the principal cause of death was tumor progression (30). Thus, it is urgent for us to find new and effective prognostic biomarkers.

In recent years, RNA modifications have gradually become the new frontier of cancer research. Common RNA modifications include N6-Methyladenosine, m6A methyltransferases, 5-Methylcytosine, Pseudouridine, etc (31). Pseudouridylation, in particular, is known to be the most abundant modification in total RNA from human cells, but the effect of Pseudouridylation is still poorly understood. Previous studies have shown that RNA pseudouridine modification could affect the prognosis of glioma patients by enriching tumour-infiltrating immune cells such as macrophages M0 and Tregs (32). Dyskerin pseudouridine synthase 1 (DKC1), a gene located on the X chromosome, is associated with the progression of multiple diseases (33–36). A previous study demonstrated that elevated levels of reactive oxygen species (ROS) in HCC regulate cytoplasmic protein-disulfide isomerase-associated 3 (PDIA3) levels, leading to HCC cell survival through upregulation of DKC1. Similar to DKC1, PUDP is also involved in the pseudouridine process and is located on the X chromosome. However, we are still unclear about the biological function of PUDP. In the present study, we systematically investigated the possible mechanisms and biological functions of PUDP in the development of HCC.

Pan-cancer expression analyses of PUDP were performed firstly and we found that PUDP was significantly highly expressed in most tumor tissues. It suggested that PUDP may be involved in the development of tumors. Investigations of the correlation between PUDP expression level and tumor patients' prognosis were explored and the results demonstrated PUDP was significantly negatively correlated with OS in patients with HCC and PAAD. Especially in HCC patients, high PUDP expression was strongly negatively correlated with OS, DSS, and PFI of patients. For exploring the expression of PUDP in HCC patients, we included two GEO datasets (GSE39791, GSE25097) to perform expression analysis and tumor tissues with paired non-tumor tissues from 15 HCC patients from the tumor tissues bank of Xijing Hospital for qPCR to detect their RNA expression levels, and finally used the HPA database to identify the protein expression of PUDP in HCC patients. All of the results showed that the expression level of PUDP was significantly increased in HCC tissues compared with normal tissues.

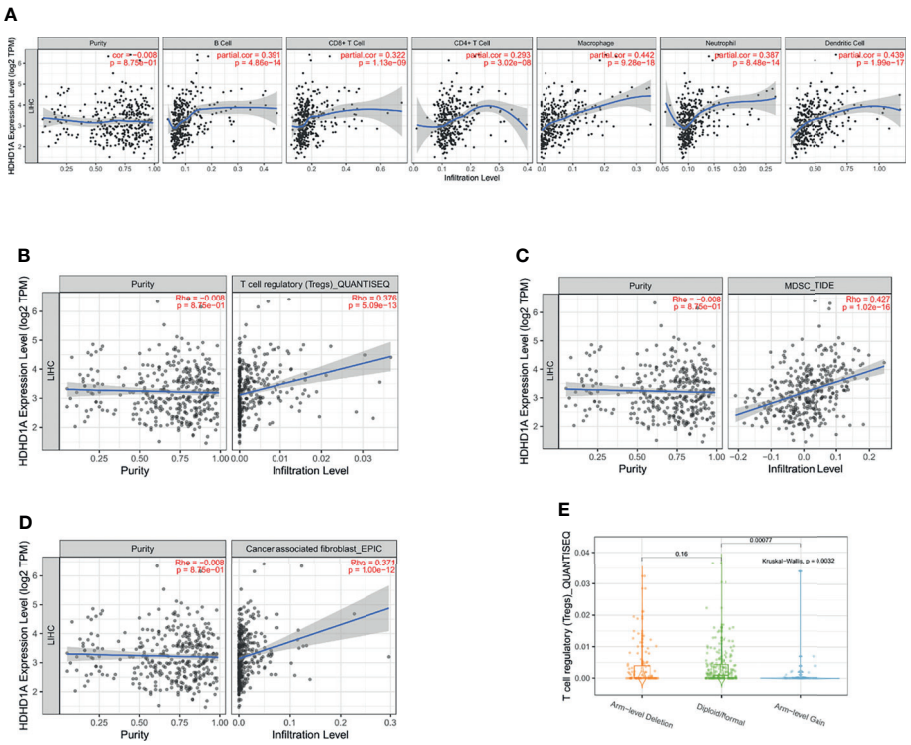

FIGURE 6 | Exploring the relationship between the expression of PUDP and immune infiltration in HCC. **(A)** The correlation of PUDP and 6 common types of immune cells in HCC; **(B)** The correlation of PUDP and Tregs in HCC; **(C)** The correlation of PUDP and MDSC in HCC; **(D)** The correlation of PUDP and cancer associated fibroblast; **(E)** Tregs infiltration distribution between different sCNA status of the PUDP.

To further investigate the role of PUDP in HCC, we divided the HCC patients into PUDP high expression group and PUDP low expression group, and identify the DEGs between the two groups. Co-expression genes are involved in the development of multiple cancers, for example, high expression of SMR3A suggests poor prognosis in patients with head and neck squamous cell carcinoma, and WNT7B promotes gastric cancer progression and metastasis (37, 38). We also found that co-expression genes are mainly involved in antigen binding, neuroactive ligand-receptor interaction, bile secretion pathways.

In recent years, with in-depth research, it has become a consensus that the tumor immune microenvironment is involved in tumor progression. In order to investigate the relationship between PUDP and tumor immune microenvironment, we analyzed the correlation between PUDP and common immune cells in HCC. First, we analyzed the scRNA sequencing data of HCC patients (GSE125449), which showed that PUDP was expressed on CD8Tex, Mono/macrophages, endothelial, fibroblasts, malignant, hepatic progenitor cells, especially on malignant cells with significantly high expression.

Then, we explored the correlation between the expression level of PUDP and various immune cells such as Tregs, CD8+ T cells, MDSCs, CD4+ T cells, macrophages, and CAFs et al. Interestingly, we found that the expression of PUDP was significantly positively correlated with the expression of Tregs, MDSCs, CAFs. Tregs, one subset of T lymphocytes that regulate the immune response according to suppressing the effector T lymphocytes (39, 40). Tregs have been shown to promote tumor development, for example, in non-alcoholic steatohepatitis (NASH) -associated HCC, Tregs interact with neutrophil extracellular traps (NETs) to inhibit immune surveillance to exert oncogenic effects in the early stage of NASH, while in HBV-associated HCC, specifically blocking the infiltration of Tregs could enhance the anti-tumor immunity and Tregs expression correlated with sorafenib resistance and HBV load titers (41, 42). In cancer, the differentiation of myeloid cells is often altered, producing a cohort of immature myeloid cells called MDSCs that have strong immunosuppressive activity and impaired function as antigen-presenting cells (APCs) (43). MDSCs impede dendritic cell function, inhibit T-cell tumor invasion, and reduce the efficacy of current immune checkpoint treatments. Drug-resistant HCC cells have been found to perform the cancer stem cell (CSC) characteristics, which can boost MDSC proliferation and immunosuppressive activity by preferentially secreting IL-6 (44). In the HCC tumor microenvironment, activated hepatic stellate cells (HSCs) are the major source of CAFs and the crosstalk between activated HSC/CAF and tumor cells is associated with tumor cell proliferation, migration, metastasis, and chemoresistance (45). Given that more than 80% of HCC tumors develop in the setting of cirrhosis, which in turn is associated with a large number of activated fibroblasts due to the presence of chronic inflammation, CAFs are known to be critical to the development and progression of HCC and have a significant impact on the clinical outcome of patients (46). According

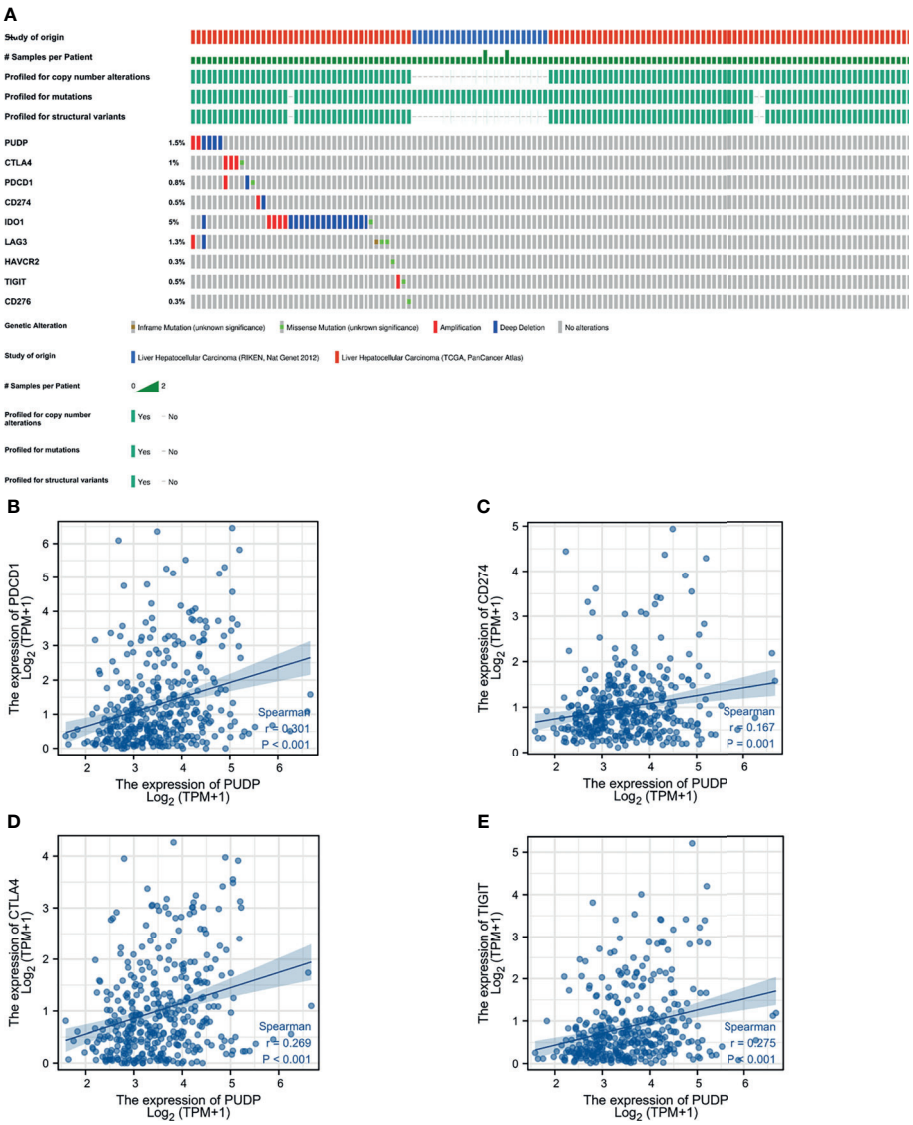

FIGURE 7 | The relationship between PUDP and immune checkpoint genes. **(A)** Mutations in PUDP and common immune checkpoint genes in HCC. **(B–E)** Correlation analysis of PUDP with PD-1, PD-L1, CTLA-4, TIGIT respectively.

to our findings, PUDP is strongly and positively correlated with a range of tumor-promoting immune cells such as Tregs, MDSCs, and CAFs, suggesting that PUDP may influence the progression and prognosis of patients with HCC by interacting with immunosuppressive cells in the tumor microenvironment. For the mutation of PUDP in HCC patients, we have studied, and the results showed that the mutation form of PUDP in HCC patients existed mainly in amplification, deep deletion.

Furthermore, immunotherapy success is dependent not only on sufficient immune cell infiltration in the TME, but also on enough expression of immune checkpoints. Therefore, the relationship between PUDP and immune checkpoints was analyzed and the results showed that PUDP was significantly and positively correlated with the expression of TIGIT, PD-1, PD-L1, CTLA-4, and other immune checkpoint genes, and the highest correlation was with the expression of the PD-1 gene (*r=0.301, p <0.001*). Despite the remarkable clinical success of immune checkpoint blockade therapy, most patients do not benefit from immunotherapy (47–49). It is, therefore, crucial to accurately distinguish which patients can benefit from immunotherapy. Using the TIDE algorithm, we found that patients with high PUDP expression were less likely to benefit from ICB. For the first time, we analyzed the correlation between PUDP and therapeutic sensitivity to anticancer drugs. The expression of the PUDP gene was significantly positive with tic10, Nelarabine and negative with AZD-1480, Dovitinib, ITRI-260. Previous studies demonstrated that Dovitinib inhibits the metastasis and invasion of HCC through the antiangiogenic mechanism, and overcomes sorafenib resistance (50, 51).



FIGURE 8 | Correlations between PUDP expression and methylation modifications and the correlation of PUDP with clinical indicators.

TABLE 2 | The relationship between PUDP and clinical indicators.

Characteristics	Total (N)	Odds Ratio (OR)	P value
Age (>60 vs. <=60)	373	0.731 (0.486-1.099)	0.132
Gender (Male vs. Female)	374	0.137 (0.080-0.226)	<0.001
T stage (T3&T4 vs. T1&T2)	371	1.855 (1.154-3.015)	0.011
N stage (N1 vs. N0)	258	2.817 (0.355-57.360)	0.373
M stage (M1 vs. M0)	272	3.000 (0.379-61.068)	0.344
Pathologic stage (Stage III&Stage IV vs. Stage I&Stage II)	350	2.144 (1.316-3.539)	0.002
AFP(ng/ml) (>400 vs. <=400)	280	4.811 (2.597-9.370)	<0.001
Tumor status (With tumor vs. Tumor free)	355	1.485 (0.975-2.269)	0.066
Histologic grade (G3&G4 vs. G1&G2)	369	2.489 (1.615-3.870)	<0.001
Albumin(g/dl) (>=3.5 vs. <3.5)	300	1.009 (0.589-1.733)	0.974
Vascular invasion (Yes vs. No)	318	1.252 (0.788-1.992)	0.341

It has been well documented that miRNAs were involved in the regulation of gene expression (52–54). PITA, RNA22, miRmap, microT, miRanda, PicTar, and TargetScan were used to predict the upstream regulatory miRNAs of PUDP. 19 miRNAs were finally obtained. In HCC, the majority of miRNAs have been found to function as tumor suppressor, for example, upregulated let-7a-5p could prevent HCC progression (55). In the end, the most potential upstream tumor suppressor miRNA for PUDP was identified as let-7c-5p after correlation analysis, expression analysis, and survival analysis. Previous studies demonstrated that sponging let-7c-5p could promote proliferation and migration of HCC (56, 57).

In addition, the relationship between the expression of PUDP and clinical indicators in HCC patients was analyzed using the MEXPRSS database and TCGA HCC cohort. The results revealed that high PUDP expression was common in primary HCC, and there were gender differences. The results of subgroup K-M analysis showed that high PUDP expression in male compared to female was more significant in the prognosis of patients with HCC. We also performed a subgroup K-M analysis for clinical staging and clinical-grade. The results demonstrated high expression of PUDP in the early stage of HCC could indicate a poor prognosis. By incorporating PUDP expression with common clinical indicators, Cox regression analyses were performed, identifying high PUDP expression was an independent risk factor for HCC patients.

This study still has some areas for improvement. First, we lack a prospective clinical cohort study to explore the detailed correlation between PUDP expression and the prognosis and clinical stage of patients with HCC. Second, although based on the previous studies, we can speculate that PUDP expression in serology is consistent with changes in expression in tissues, however, we lack serological data to validate. Finally, the prevalence of COVID-19 has made access to the laboratory very difficult, thus lacking validation of the detailed mechanisms of PUDP *in vitro* and *vivo*.

CONCLUSION

In summary, our findings suggested that PUDP was highly expressed in most tumors and high expression of PUDP indicated the poor prognosis and low response to

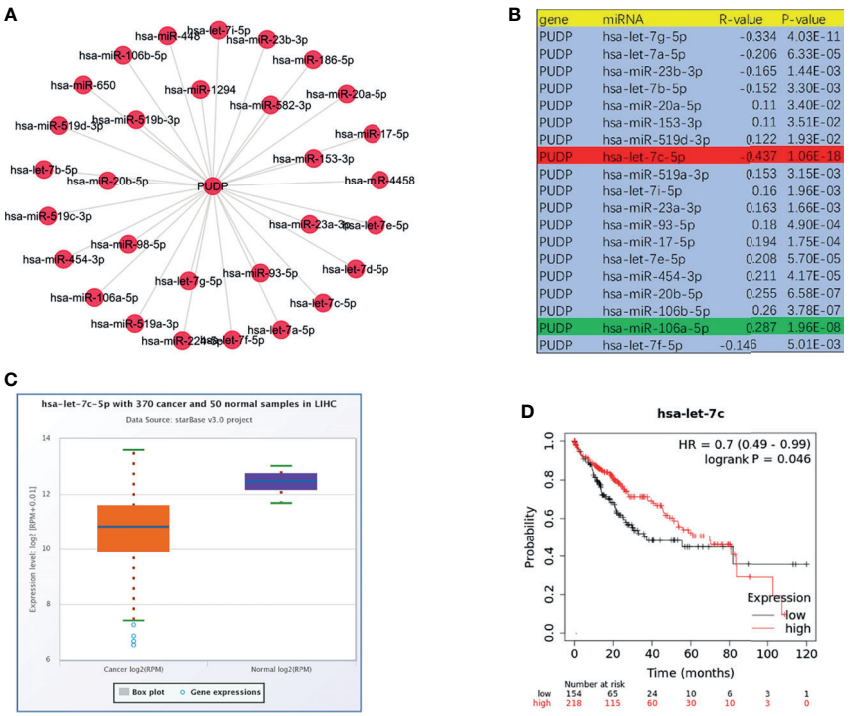

gene	miRNA	R-value	P-value
PUDP	hsa-let-7g-5p	-0.334	4.03E-11
PUDP	hsa-let-7a-5p	-0.206	6.33E-05
PUDP	hsa-miR-23b-3p	-0.165	1.44E-03
PUDP	hsa-let-7b-5p	-0.152	3.30E-03
PUDP	hsa-miR-20a-5p	0.11	3.40E-02
PUDP	hsa-miR-153-3p	0.11	3.51E-02
PUDP	hsa-miR-519d-3p	0.122	1.93E-02
PUDP	hsa-let-7c-5p	-0.437	1.06E-18
PUDP	hsa-miR-519a-3p	0.153	3.15E-03
PUDP	hsa-let-7i-5p	0.16	1.96E-03
PUDP	hsa-miR-23a-3p	0.163	1.66E-03
PUDP	hsa-miR-93-5p	0.18	4.90E-04
PUDP	hsa-miR-17-5p	0.194	1.75E-04
PUDP	hsa-let-7e-5p	0.208	5.70E-05
PUDP	hsa-miR-454-3p	0.211	4.17E-05
PUDP	hsa-miR-20b-5p	0.255	6.58E-07
PUDP	hsa-miR-106b-5p	0.26	3.78E-07
PUDP	hsa-miR-106a-5p	0.287	1.96E-08
PUDP	hsa-let-7f-5p	-0.145	5.01E-03

FIGURE 9 | Prediction and analysis of upstream miRNAs of PUDP. **(A, B)** Potential upstream miRNAs that regulate the expression of PUDP; **(C)** Expression analysis of let-7c-5p in HCC; **(D)** Correlation analysis of let-7c-5p expression and prognosis of HCC patients.

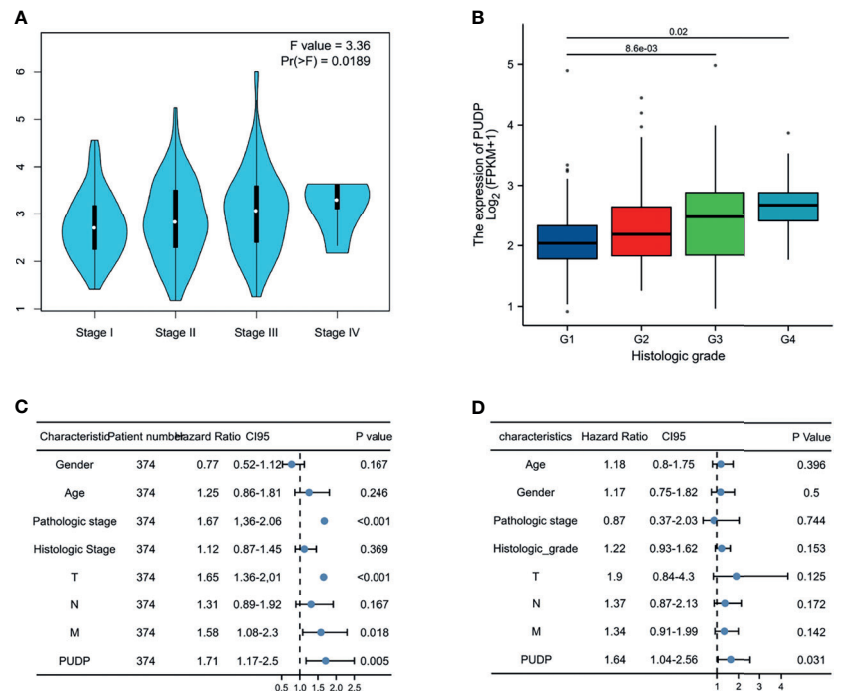

FIGURE 10 | Expression of PUDP in different clinical stages and Cox regression analysis. **(A)** The expression of PUDP in different pathologic stages; **(B)** The expression of PUDP in different histologic grades; **(C, D)** Univariate and multivariate Cox regression analysis.

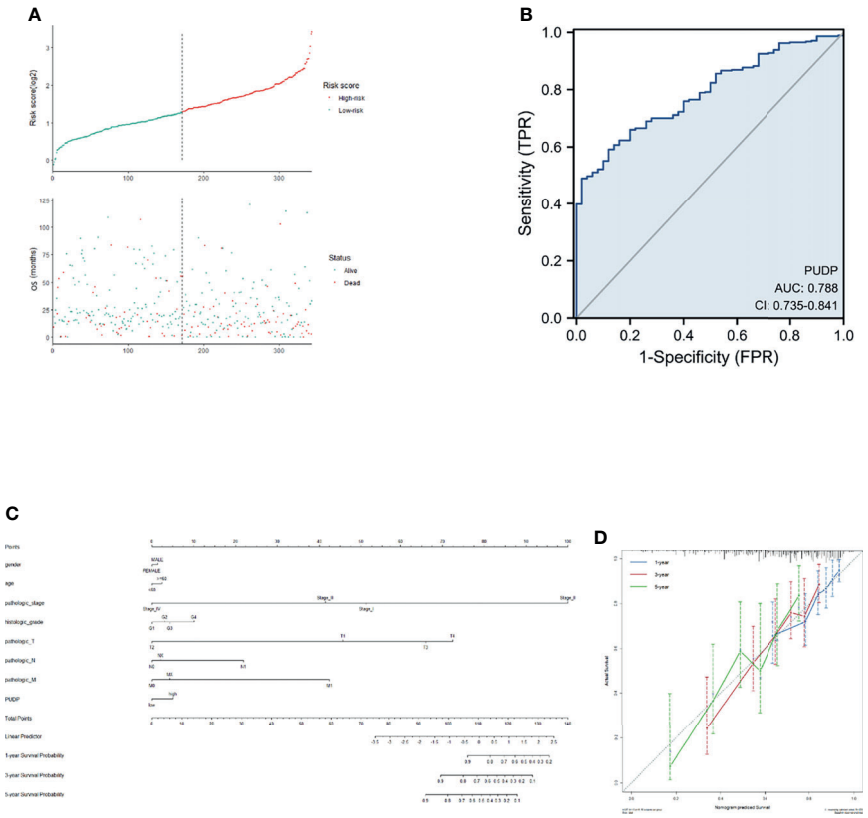

FIGURE 11 | Construction of a prognostic model for HCC patients. **(A).** Risk factor correlation diagram; **(B)** ROC curve analysis; **(C)** A nomogram combining common clinical indicators with PUDP expression to predict 1-, 3-, and 5-prognosis survival; **(D)** Calibration curves of the nomogram, each curve was repeated 1000 times.

immunotherapy in HCC. The most potential upstream miRNA of PUDP was identified as let-7c-5p. Mechanistically, we found that PUDP has a strong positive correlation with tumor-promoting immune cells such as Tregs, MDSCs, CAFs. Moreover, there are significantly positive correlations between the PUDP expression and immune checkpoint. These findings enhanced our understanding of PUDP and suggested that PUDP may exert oncogenic effects by the enrichment of tumor immune cell infiltration and expression of immune checkpoints. Finally, the prognostic model was constructed by the data from TCGA and validated by the data from ICGC.

DATA AVAILABILITY STATEMENT

The original contributions presented in the study are included in the article/**Supplementary Material**. Further inquiries can be directed to the corresponding authors.

ETHICS STATEMENT

The studies involving human participants were reviewed and approved by Xijing Hospital's Ethics Committee. The patients/participants provided their written informed consent to participate in this study.

AUTHOR CONTRIBUTIONS

Conceived and designed the experiments, YH, JW, and GG. Collected the data, WZ, JY, and YNH. Analyzed the data, JY, YNH, DD, and WZ. Drafted the manuscript, JY, YNH, WZ, and DD. All authors contributed to the article and approved the submitted version.

FUNDING

The study was funded by National Key Research and Development Program of China (2020YFA0710803, 2017YFA0105704), National Natural Science Foundation of China (81900502, 81820108005, 81870421, 81873562 and 81870398), Key Research and Development Projects of Shaanxi Province, 2021ZDLSF02-07.

SUPPLEMENTARY MATERIAL

The Supplementary Material for this article can be found online at: https://www.frontiersin.org/articles/10.3389/fonc.2022.830174/full#supplementary-material

REFERENCES

1. El-Serag HB. Hepatocellular Carcinoma. *New Engl J Med* (2011) 365 (12):1118–27. doi: 10.1056/NEJMra1001683
2. Sung H, Ferlay J, Siegel RL, Laversanne M, Soerjomataram I, Jemal A, et al. Global Cancer Statistics 2020: GLOBOCAN Estimates of Incidence and Mortality Worldwide for 36 Cancers in 185 Countries. *CA Cancer J Clin* (2021) 71(3):209–49. doi: 10.3322/caac.21660
3. Vandenbulcke H, Moreno C, Colle I, Knebel JF, Francque S, Sersté T, et al. Alcohol Intake Increases the Risk of HCC in Hepatitis C Virus-Related Compensated Cirrhosis: A Prospective Study. *J Hepatol* (2016) 65(3):543–51. doi: 10.1016/j.jhep.2016.04.031
4. Chen Y, Tian Z. HBV-Induced Immune Imbalance in the Development of HCC. *Front Immunol* (2019) 10:2048. doi: 10.3389/fimmu.2019.02048
5. Huang DQ, El-Serag HB, Loomba R. Global Epidemiology of NAFLD-Related HCC: Trends, Predictions, Risk Factors and Prevention. *Nat Rev Gastroenterol Hepatol* (2021) 18(4):223–38. doi: 10.1038/s41575-020-00381-6
6. Finn RS, Qin S, Ikeda M, Galle PR, Ducreux M, Kim TY, et al. Atezolizumab Plus Bevacizumab in Unresectable Hepatocellular Carcinoma. *N Engl J Med* (2020) 382(20):1894–905. doi: 10.1056/NEJMoa1915745
7. Preumont A, Rzem R, Vertommen D, Van Schaftingen E. HDHD1, Which Is Often Deleted in X-Linked Ichthyosis, Encodes a Pseudouridine-5'-Phosphatase. *Biochem J* (2010) 431(2):237–44. doi: 10.1042/BJ20100174
8. Guzzi N, Cieśla M, Ngoc PCT, Lang S, Arora S, Dimitriou M, et al. Pseudouridylation of tRNA-Derived Fragments Steers Translational Control in Stem Cells. *Cell* (2018) 173(5):1204–16.e26. doi: 10.1016/j.cell.2018.03.008
9. Zlotorynski E. Pseudouridylation Alters Splicing. *Nat Rev Mol Cell Biol* (2022). doi: 10.1038/s41580-022-00458-x
10. Lee SE, Alcedo KP, Kim HJ, Snider NT. Alternative Splicing in Hepatocellular Carcinoma. *Cell Mol Gastroenterol Hepatol* (2020) 10(4):699–712. doi: 10.1016/j.jcmgh.2020.04.018
11. Sekula P, Goek ON, Quaye L, Barrios C, Levey AS, Römisch-Margl W, et al. A Metabolome-Wide Association Study of Kidney Function and Disease in the General Population. *J Am Soc Nephrol JASN* (2016) 27(4):1175–88. doi: 10.1681/ASN.2014111099
12. Ko E, Kim JS, Ju S, Seo HW, Chang Y, Kang JA, et al. Oxidatively Modified Protein-Disulfide Isomerase-Associated 3 Promotes Dyskerin Pseudouridine Synthase 1-Mediated Malignancy and Survival of Hepatocellular Carcinoma Cells. *Hepatology* (2018) 68(5):1851–64. doi: 10.1002/hep.30039
13. Defenouillère Q, Verraes A, Laussel C, Friedrich A, Schacherer J, Léon S. The Induction of HAD-Like Phosphatases by Multiple Signaling Pathways Confers Resistance to the Metabolic Inhibitor 2-Deoxyglucose. *Sci Signaling* (2019) 12(597). doi: 10.1126/scisignal.aaw8000
14. Kurokawa T, Kohno K, Nagai K, Chiba M, Pak S, Murata S, et al. Antisense RNA Transcripts in the Blood May Be Novel Diagnostic Markers for Colorectal Cancer. *Oncol Lett* (2017) 14(3):3487–93. doi: 10.3892/ol.2017.6572
15. Smyth GK, Michaud J, Scott HS. Use of Within-Array Replicate Spots for Assessing Differential Expression in Microarray Experiments. *Bioinf (Oxford England)* (2005) 21(9):2067–75. doi: 10.1093/bioinformatics/bti270
16. Love MI, Huber W, Anders S. Moderated Estimation of Fold Change and Dispersion for RNA-Seq Data With Deseq2. *Genome Biol* (2014) 15(12):550. doi: 10.1186/s13059-014-0550-8
17. Yu G, Wang LG, Han Y, He QY. Clusterprofiler: An R Package for Comparing Biological Themes Among Gene Clusters. *Omics J Integr Biol* (2012) 16 (5):284–7. doi: 10.1089/omi.2011.0118
18. Sun D, Wang J, Han Y, Dong X, Ge J, Zheng R, et al. TISCH: A Comprehensive Web Resource Enabling Interactive Single-Cell Transcriptome Visualization of Tumor Microenvironment. *Nucleic Acids Res* (2021) 49(D1):D1420–d30. doi: 10.1093/nar/gkaa1020
19. Cerami E, Gao J, Dogrusoz U, Gross BE, Sumer SO, Aksoy BA, et al. The Cbio Cancer Genomics Portal: An Open Platform for Exploring Multidimensional Cancer Genomics Data. *Cancer Discovery* (2012) 2(5):401–4. doi: 10.1158/2159-8290.CD-12-0095
20. Gao J, Aksoy BA, Dogrusoz U, Dresdner G, Gross B, Sumer SO, et al. Integrative Analysis of Complex Cancer Genomics and Clinical Profiles Using the Cbioportal. *Sci Signaling* (2013) 6(269):pl1. doi: 10.1126/scisignal.2004088
21. Li T, Fu J, Zeng Z, Cohen D, Li J, Chen Q, et al. TIMER2.0 for Analysis of Tumor-Infiltrating Immune Cells. *Nucleic Acids Res* (2020) 48(W1):W509–w14. doi: 10.1093/nar/gkaa407
22. Jiang P, Gu S, Pan D, Fu J, Sahu A, Hu X, et al. Signatures of T Cell Dysfunction and Exclusion Predict Cancer Immunotherapy Response. *Nat Med* (2018) 24(10):1550–8. doi: 10.1038/s41591-018-0136-1
23. Li JH, Liu S, Zhou H, Qu LH, Yang JH. Starbase V2.0: Decoding miRNA-ceRNA, miRNA-ncRNA and Protein-RNA Interaction Networks From Large-Scale CLIP-Seq Data. *Nucleic Acids Res* (2014) 42(Database issue): D92–7. doi: 10.1093/nar/gkt1248
24. Koch A, De Meyer T, Jeschke J, Van Criekinge W. MEXPRESS: Visualizing Expression, DNA Methylation and Clinical TCGA Data. *BMC Genomics* (2015) 16(1):636. doi: 10.1186/s12864-015-1847-z
25. Koch A, Jeschke J, Van Criekinge W, van Engeland M, De Meyer T. MEXPRESS Update 2019. *Nucleic Acids Res* (2019) 47(W1):W561–w5. doi: 10.1093/nar/gkz445
26. Reinhold WC, Sunshine M, Liu H, Varma S, Kohn KW, Morris J, et al. CellMiner: A Web-Based Suite of Genomic and Pharmacologic Tools to Explore Transcript and Drug Patterns in the NCI-60 Cell Line Set. *Cancer Res* (2012) 72(14):3499–511. doi: 10.1158/0008-5472.CAN-12-1370
27. Ritchie ME, Phipson B, Wu D, Hu Y, Law CW, Shi W, et al. Limma Powers Differential Expression Analyses for RNA-Sequencing and Microarray Studies. *Nucleic Acids Res* (2015) 43(7):e47. doi: 10.1093/nar/gkv007
28. Rizvi AA, Karaesmen E, Morgan M, Preus L, Wang J, Sovic M, et al. Gwasurvivr: An R Package for Genome-Wide Survival Analysis. *Bioinf (Oxford England)* (2019) 35(11):1968–70. doi: 10.1093/bioinformatics/bty920
29. Robin X, Turck N, Hainard A, Tiberti N, Lisacek F, Sanchez JC, et al. pROC: An Open-Source Package for R and S+ to Analyze and Compare ROC Curves. *BMC Bioinf* (2011) 12:77. doi: 10.1186/1471-2105-12-77
30. Giannini E, Farinati F, Ciccarese F, Pecorelli A, Rapaccini G, Di Marco M, et al. Prognosis of Untreated Hepatocellular Carcinoma. *Hepatol (Baltimore Md)* (2015) 61(1):184–90. doi: 10.1002/hep.27443
31. Barbieri I, Kouzarides T. Role of RNA Modifications in Cancer. *Nat Rev Cancer* (2020) 20(6):303–22. doi: 10.1038/s41568-020-0253-2
32. Wang LJ, Lv P, Lou Y, Ye J. Gene Expression-Based Predication of RNA Pseudouridine Modification in Tumor Microenvironment and Prognosis of Glioma Patients. *Front Cell Dev Biol* (2021) 9:727595. doi: 10.3389/fcell.2021.727595
33. Heiss NS, Knight SW, Vulliamy TJ, Klauck SM, Wiemann S, Mason PJ, et al. X-Linked Dyskeratosis Congenita Is Caused by Mutations in a Highly Conserved Gene With Putative Nucleolar Functions. *Nat Genet* (1998) 19 (1):32–8. doi: 10.1038/ng0598-32
34. Ruggero D, Grisendi S, Piazza F, Rego E, Mari F, Rao PH, et al. Dyskeratosis Congenita and Cancer in Mice Deficient in Ribosomal RNA Modification. *Sci (New York NY)* (2003) 299(5604):259–62. doi: 10.1126/science.1079447
35. Penzo M, Casoli L, Ceccarelli C, Trerè D, Ludovini V, Crinò L, et al. DKC1 Gene Mutations in Human Sporadic Cancer. *Histol Histopathol* (2013) 28 (3):365–72. doi: 10.14670/HH-28.365
36. Miao FA, Chu K, Chen HR, Zhang M, Shi PC, Bai J, et al. Increased DKC1 Expression in Glioma and Its Significance in Tumor Cell Proliferation, Migration and Invasion. *Invest New Drugs* (2019) 37(6):1177–86. doi: 10.1007/s10637-019-00748-w
37. Gao Q, Yang L, Shen A, Li Y, Li Y, Hu S, et al. A WNT7B-M(6)A-TCF7L2 Positive Feedback Loop Promotes Gastric Cancer Progression and Metastasis. *Signal Transduction Targeted Ther* (2021) 6(1):43. doi: 10.1038/s41392-020-00397-z
38. Grünow J, Rong C, Hischmann J, Zaoui K, Flechtenmacher C, Weber KJ, et al. Regulation of Submaxillary Gland Androgen-Regulated Protein 3A *via* Estrogen Receptor 2 in Radioresistant Head and Neck Squamous Cell Carcinoma Cells. *J Exp Clin Cancer Res CR* (2017) 36(1):25. doi: 10.1186/s13046-017-0496-2
39. Thornton AM, Shevach EM. CD4+CD25+ Immunoregulatory T Cells Suppress Polyclonal T Cell Activation *In Vitro* by Inhibiting Interleukin 2 Production. *J Exp Med* (1998) 188(2):287–96. doi: 10.1084/jem.188.2.287
40. Ng WF, Duggan PJ, Ponchel F, Matarese G, Lombardi G, Edwards AD, et al. Human CD4(+)CD25(+) Cells: A Naturally Occurring Population of Regulatory T Cells. *Blood* (2001) 98(9):2736–44. doi: 10.1182/blood.V98.9.2736

41. Wang H, Zhang H, Wang Y, Brown ZJ, Xia Y, Huang Z, et al. Regulatory T-Cell and Neutrophil Extracellular Trap Interaction Contributes to Carcinogenesis in Non-Alcoholic Steatohepatitis. *J Hepatol* (2021) 75 (6):1271–83. doi: 10.1016/j.jhep.2021.07.032
42. Gao Y, You M, Fu J, Tian M, Zhong X, Du C, et al. Intratumoral Stem-Like CCR4+ Regulatory T Cells Orchestrate the Immunosuppressive Microenvironment in HCC Associated With Hepatitis B. *J Hepatol* (2021) 76(1):148–59. doi: 10.1016/j.jhep.2021.08.029
43. Lu C, Rong D, Zhang B, Zheng W, Wang X, Chen Z, et al. Current Perspectives on the Immunosuppressive Tumor Microenvironment in Hepatocellular Carcinoma: Challenges and Opportunities. *Mol Cancer* (2019) 18(1):130. doi: 10.1186/s12943-019-1047-6
44. Xu M, Zhao Z, Song J, Lan X, Lu S, Chen M, et al. Interactions Between Interleukin-6 and Myeloid-Derived Suppressor Cells Drive the Chemoresistant Phenotype of Hepatocellular Cancer. *Exp Cell Res* (2017) 351(2):142–9. doi: 10.1016/j.yexcr.2017.01.008
45. Ezhilarasan D. Hepatic Stellate Cells in the Injured Liver: Perspectives Beyond Hepatic Fibrosis. *J Cell Physiol* (2022) 237(1):436–49. doi: 10.1002/jcp.30582
46. Tarao K, Nozaki A, Ikeda T, Sato A, Komatsu H, Komatsu T, et al. Real Impact of Liver Cirrhosis on the Development of Hepatocellular Carcinoma in Various Liver Diseases-Meta-Analytic Assessment. *Cancer Med* (2019) 8 (3):1054–65. doi: 10.1002/cam4.1998
47. Zaretsky JM, Garcia-Diaz A, Shin DS, Escuin-Ordinas H, Hugo W, Hu-Lieskovan S, et al. Mutations Associated With Acquired Resistance to PD-1 Blockade in Melanoma. *New Engl J Med* (2016) 375(9):819–29. doi: 10.1056/NEJMoa1604958
48. Gao J, Shi LZ, Zhao H, Chen J, Xiong L, He Q, et al. Loss of IFN-γ Pathway Genes in Tumor Cells as a Mechanism of Resistance to Anti-CTLA-4 Therapy. *Cell* (2016) 167(2):397–404.e9. doi: 10.1016/j.cell.2016.08.069
49. Sade-Feldman M, Jiao YJ, Chen JH, Rooney MS, Barzily-Rokni M, Eliane JP, et al. Resistance to Checkpoint Blockade Therapy Through Inactivation of Antigen Presentation. *Nat Commun* (2017) 8(1):1136. doi: 10.1038/s41467-017-01062-w
50. Chen ZY, Shi M, Peng LX, Wei W, Li XJ, Guo ZX, et al. Dovitinib Preferentially Targets Endothelial Cells Rather Than Cancer Cells for the Inhibition of Hepatocellular Carcinoma Growth and Metastasis. *J Trans Med* (2012) 10:245. doi: 10.1186/1479-5876-10-245
51. Tai WT, Cheng AL, Shiau CW, Liu CY, Ko CH, Lin MW, et al. Dovitinib Induces Apoptosis and Overcomes Sorafenib Resistance in Hepatocellular Carcinoma Through SHP-1-Mediated Inhibition of STAT3. *Mol Cancer Ther* (2012) 11(2):452–63. doi: 10.1158/1535-7163.MCT-11-0412
52. Lou W, Ding B, Wang J, Xu Y. The Involvement of the Hsa_Circ_0088494-miR-876-3p-CTNNB1/CCND1 Axis in Carcinogenesis and Progression of Papillary Thyroid Carcinoma. *Front Cell Dev Biol* (2020) 8:605940. doi: 10.3389/fcell.2020.605940
53. Gao S, Ding B, Lou W. microRNA-Dependent Modulation of Genes Contributes to ESR1's Effect on Erα Positive Breast Cancer. *Front Oncol* (2020) 10:753. doi: 10.3389/fonc.2020.00753
54. Razavi ZS, Tajiknia V, Majidi S, Ghandali M, Mirzaei HR, Rahimian N, et al. Gynecologic Cancers and Non-Coding RNAs: Epigenetic Regulators With Emerging Roles. *Crit Rev Oncol/Hematol* (2021) 157:103192. doi: 10.1016/j.critrevonc.2020.103192
55. Yang L, Si H, Ma M, Fang Y, Jiang Y, Wang J, et al. LINC00221 Silencing Prevents the Progression of Hepatocellular Carcinoma Through Let-7a-5p-Targeted Inhibition of MMP11. *Cancer Cell Int* (2021) 21(1):202. doi: 10.1186/s12935-021-01819-w
56. Chen S, Xie C, Hu X. lncRNA SNHG6 Functions as a ceRNA to Up-Regulate C-Myc Expression *via* Sponging Let-7c-5p in Hepatocellular Carcinoma. *Biochem Biophys Res Commun* (2019) 519(4):901–8. doi: 10.1016/j.bbrc.2019.09.091
57. Huang Y, Xiang B, Liu Y, Wang Y, Kan H. LncRNA CDKN2B-AS1 Promotes Tumor Growth and Metastasis of Human Hepatocellular Carcinoma by Targeting Let-7c-5p/NAP1L1 Axis. *Cancer Lett* (2018) 437:56–66. doi: 10.1016/j.canlet.2018.08.024

Conflict of Interest: The authors declare that the research was conducted in the absence of any commercial or financial relationships that could be construed as a potential conflict of interest.

Publisher's Note: All claims expressed in this article are solely those of the authors and do not necessarily represent those of their affiliated organizations, or those of the publisher, the editors and the reviewers. Any product that may be evaluated in this article, or claim that may be made by its manufacturer, is not guaranteed or endorsed by the publisher.

Copyright © 2022 Yu, Zhang, Ding, Hu, Guo, Wang and Han. This is an open-access article distributed under the terms of the Creative Commons Attribution License (CC BY). The use, distribution or reproduction in other forums is permitted, provided the original author(s) and the copyright owner(s) are credited and that the original publication in this journal is cited, in accordance with accepted academic practice. No use, distribution or reproduction is permitted which does not comply with these terms.

frontiers | Frontiers in Cell and Developmental Biology

ORIGINAL RESEARCH
published: 12 April 2022
doi: 10.3389/fcell.2022.821649

Identify the Prognostic and Immune Profile of VSIR in the Tumor Microenvironment: A Pan-Cancer Analysis

Yuanyuan Liu[1,2†], Jingwei Zhang[2,3†], Zeyu Wang[2,3], Xun Zhang[2,3], Ziyu Dai[2,3], Wantao Wu[2,4], Nan Zhang[5], Zaoqu Liu[6], Jian Zhang[7], Peng Luo[7], Zhipeng Wen[8], Jing Yu[9], Hao Zhang[2,3], Tubao Yang[1,2]* and Quan Cheng[2,3,10]**

[1]Department of Epidemiology and Health Statistics, Xiangya School of Public Health, Central South University, Changsha, China, [2]National Clinical Research Center for Geriatric Disorders, Changsha, China, [3]Department of Neurosurgery, Xiangya Hospital, Central South University, Changsha, China, [4]Department of Oncology, Xiangya Hospital, Central South University, Changsha, China, [5]One-third Lab, College of Bioinformatics Science and Technology, Harbin Medical University, Harbin, China, [6]Department of Interventional Radiology, The First Affiliated Hospital of Zhengzhou University, Zhengzhou, China, [7]Department of Oncology, Zhujiang Hospital, Southern Medical University, Guangzhou, China, [8]Department of Pharmacy, The Affiliated Hospital of Guizhou Medical University, Guizhou Medical University, Guiyang, China, [9]Department of Clinical Pharmacology, Xiangya Hospital, Central South University, Changsha, China, [10]Clinical Diagnosis and Therapy Center for Glioma of Xiangya Hospital, Central South University, Changsha, China

VSIR is a critical immunomodulatory receptor that inhibits T cell effector function and maintains peripheral tolerance. However, the mechanism by which VSIR participates in tumor immunity in the pan-cancer tumor microenvironment remains unclear. This study systematically explored the prognostic and immune profile of VSIR in the tumor microenvironment of 33 cancers. We compared the expression patterns and molecular features of VSIR in the normal and cancer samples both from the public databases and tumor chips. VSIR level was significantly related to patients' prognosis and could be a promising predictor in many tumor types, such as GBM, KIRC, SKCM, READ, and PRAD. Elevated VSIR was closely correlated with infiltrated inflammatory cells, neoantigens expression, MSI, TMB, and classical immune checkpoints in the tumor microenvironment. Enrichment signaling pathways analysis indicated VSIR was involved in several immune-related pathways such as activation, proliferation, and migration of fibroblast, T cell, mast cell, macrophages, and foam cell. In addition, VSIR was found to widely express on cancer cells, fibroblasts, macrophages, and T cells in many tumor types based on the single-cell sequencing analysis and co-express with M2 macrophage markers CD68, CD163 based on the immunofluorescence staining. Finally, we predicted the sensitive drugs targeting VSIR and the immunotherapeutic value of VSIR. In sum, VSIR levels strongly correlated with the clinical outcome and tumor immunity in multiple cancer types. Therefore, therapeutic strategies targeting VSIR in the tumor microenvironment may be valuable tools for cancer immunotherapy.

Keywords: VSIR, immunotherapy, macrophages, t cells, tumor microenvironment

OPEN ACCESS

Edited by:
Pranav Gupta,
Albert Einstein College of Medicine, United States

Reviewed by:
Wenli Li,
Yuebei People's Hospital, China
Sohini Chakraborty,
NYU Grossman School of Medicine, United States

***Correspondence:**
Quan Cheng
chengquan@csu.edu.cn
Tubao Yang
yangtb@csu.edu.cn
Hao Zhang
haozhang@csu.edu.cn

†These authors have contributed equally to this work

Specialty section:
This article was submitted to Molecular and Cellular Oncology, a section of the journal Frontiers in Cell and Developmental Biology

Received: *24 November 2021*
Accepted: *02 March 2022*
Published: *12 April 2022*

Citation:
Liu Y, Zhang J, Wang Z, Zhang X, Dai Z, Wu W, Zhang N, Liu Z, Zhang J, Luo P, Wen Z, Yu J, Zhang H, Yang T and Cheng Q (2022) Identify the Prognostic and Immune Profile of VSIR in the Tumor Microenvironment: A Pan-Cancer Analysis. Front. Cell Dev. Biol. 10:821649. doi: 10.3389/fcell.2022.821649

INTRODUCTION

The emergence of new diagnostic methods and therapeutic strategies over the past few decades has significantly improved the quality of life and survival in patients with advanced cancers (Davis et al., 2017; Arnold et al., 2019). The 5 year relative survival was more than 60% for all cancers combined based on the global cancer epidemiological survey calculated by the National Cancer Control Indicators. Cancer mortality has steadily declined from its peak in 1991–2018, with an overall decrease of more than 30% (Siegel et al., 2020). However, the prognosis in patients with malignant cancers remains far from satisfactory. For example, the 5-year survival rate was high for cancer of the prostate (95%), melanoma (92%), and female breast cancer (91%). In comparison, it was low for cancers of the pancreas (11%), lung cancer (19%), liver cancer (20%), and central nervous system (CNS) tumors (22%) (Bach et al., 2020). In addition, the number of new diagnostic cancer cases and cancer-related deaths are still high. For example, a recent study indicated that there would be more than 1.8 million new cancer cases and nearly 600,000 million cancer deaths expected in the United States in 2021 (Siegel et al., 2021).

Cancer cells are located in a complex and dynamic ecosystem called the tumor microenvironment (TME). TME consists of cancer cells, non-malignant cells, blood vessels, extracellular matrix (ECM), various cytokines, and growth factors (Baghban et al., 2020; Yang et al., 2022). Both factors decided the tumor formation and development, including genetic variation and the rearrangement of the components of the TME through interconnections (Jahanban-Esfahlan et al., 2017). Increasing evidence revealed that tumor immunity regulated by infiltrated inflammatory cells in the TME plays an essential role in the whole process of tumorigenesis and metastasis (Vitale et al., 2019; Lim et al., 2020; Sahai et al., 2020; Zhang et al., 2021c; Ping et al., 2021). Significantly, the specific antibodies that block immune checkpoints secreted by immune infiltrates have become a novel weapon in fighting cancer and have achieved good results in preclinical studies (Dyck and Mills, 2017; Zhang et al., 2018; He and Xu, 2020). For example, programmed death 1 (PD-1) and the cytotoxic T-lymphocyte-associated antigen 4 (CTLA-4) are the top two crucial immune checkpoints that are mainly produced by activated T cells in the TME (Gao et al., 2020; Zhang et al., 2021a). Both play an essential role in negatively mediating T cell immune function during different stages of T-cell activation in tumor immunity. The regulation of PD-1 and CTLA-4 levels in the TME has significantly affected the immunotherapy response and therapeutic effect (Qin et al., 2019). Therefore, discovering and understanding the in-depth mechanisms of new immune checkpoints could prolong the survival time of cancer patients and improve their quality of life.

V-Set Immunoregulatory Receptor (VSIR), also known as VISTA, C10orf54, PD-1H, B7H5, GI24, PP2135, SISP1, is a type 1 transmembrane protein that comes from the immunoglobulin superfamily (Yoon et al., 2015). Two potential protein kinase C binding sites and proline docking residues construct the VSIR cytoplasmic tail domain, indicating that VSIR can act as a receptor or ligand in cellular progress (Le Mercier et al., 2015). Multiple cell types can express VSIR, such as cancer cells, neutrophils, monocytes, macrophages, dendritic cells (D.C.s), and T cells in humans and mice (Flies et al., 2011; Lines et al., 2014). Previous studies have found that VSIR is widely involved in various physiological and pathological processes, including regulating peripheral tolerance, inducing T cell activation and differentiation, and mediating tumor immunity (ElTanbouly et al., 2019; Hosseinkhani et al., 2021). Thus, growing evidence indicated that VSIR might be a promising target for tumor immunotherapeutic intervention in the TME.

To date, most evidence has focused on the suppressive effect role of VSIR in the immune system and the ability to regulate antitumor immunity. However, the mechanisms of VSIR in tumor immunity regulation remain controversial. There are also compelling studies that do not support the value of VSIR as an immunotherapy target. VSIR plays both negative and positive roles in tumor immunity. Upregulated VSIR on the tumor-infiltrating myeloid cells has been found to promote tumor growth through suppressing T cell immunity (Mulati et al., 2019). The specific antibody that neutralizes VSIR can effectively suppress tumor growth in mouse models (Le Mercier et al., 2014). A previous study indicated that higher VSIR levels are related to better clinical prognosis in epithelioid mesothelioma cancer (Muller et al., 2020), non-small-cell lung cancer (Villarroel-Espindola et al., 2018), and esophageal adenocarcinoma (Villarroel-Espindola et al., 2018). However, Lawrence F. Kuklinski et al. found that increased VSIR was associated with unfavorable DSS in primary cutaneous melanoma (Kuklinski et al., 2018).

Therefore, in this study, we systematically investigated the predictive value of VSIR in pan-cancer using large-scale RNA-sequencing (RNA-seq) data from the public databases. We also explored the relationship between VSIR and immune infiltration in different cancer TME. Meanwhile, the co-expression of VSIR on infiltrated inflammatory cells was studied from both online databases and tumor chip data. In addition, we evaluated the immunotherapy value of VSIR in pan-cancer from various immunotherapy cohorts. Finally, we predicted many sensitive small molecule drugs based on VSIR expression from the public databases.

MATERIALS AND METHODS

Data Collection and Collation

We obtained the RNA-seq data from the TCGA (pan-cancer) (https://portal.gdc.cancer.gov/), GETX (normal control) (https://gtexportal.org/home/), and CCLE (cancer cell lines) (https://sites.broadinstitute.org/ccle/) datasets. In addition, the single-cell sequencing data were downloaded from the GEO database (https://www.ncbi.nlm.nih.gov/geo/), including invasive breast carcinoma (BRCA, GSE75688, and GSE118389), cholangiocarcinoma (CHOL, GSE125449), colon adenocarcinoma (COAD, GSE81861), head and neck squamous cell carcinoma (HNSC, GSE103322), liver hepatocellular carcinoma (LIHC, GSE125449), bladder cancer (BLCA, GSE145137), kidney renal

clear cell carcinoma (KIRC, GSE121636 and GSE171306), ovarian serous cystadenocarcinoma (OV, GSE118828), prostate adenocarcinoma (PRAD, GSE137829), skin cutaneous melanoma (SKCM, GSE72056), stomach adenocarcinoma (STAD, GSE183904). Besides, the single-cell sequencing data of glioblastoma multiforme (GBM, SCP50, and SCP393) was downloaded from the Single Cell Portal platform (http://singlecell.broadinstitute.org); the single-cell sequencing dataset of LUAD was downloaded from the BioProject (PRJNA591860).

Identification of Relevant Features

The mutant genetic aspects of VSIR were analyzed by the GSCA(Liu et al., 2018) (http://bioinfo.life.hust.edu.cn/GSCA/) and CBIOPORTAL (https://www.cbioportal.org/) databases. The Kaplan-Meier (KM) analysis with log-rank test was used to calculate the disease-specific survival (DSS) and overall survival (OS) of pan-cancer patients (Lanczky and Gyorffy, 2021). We explored the immune characteristics of VSIR through TIMER 2.0 (Li et al., 2017) (https://cistrome.shinyapps.io/timer/) and R package (immunedeconv). The gene set variation analysis (GSVA) based on Gene Ontology (GO) terms and the gene set enrichment analysis (GSEA) based on Kyoto Encyclopedia of Genes and Genomes (KEGG) and HALLMARK gene sets were used to identify the enriched signaling pathways related to VSIR. The TIDE (http://tide.dfci.harvard.edu) and TISMO (http://tismo.cistrome.org) websites were selected to evaluate the immunotherapy value of VSIR. The involvement of VSIR in diseases and aid systematic drug target identification and prioritization was identified from the OPEN TARGET platform (https://www.targetvalidation.org/). The GSCA database was used to predict sensitive drugs based on VSIR expression. The GSCA data contains over 750 small-molecule drugs from GDSC and CTRP for 10,000 genomic data across 33 cancer types.

Single-Cell Sequencing Analysis

The single-cell sequencing data of BRCA was integrated using the R package Seurat. Quality control was conducted by the R package (Seurat) (Butler et al., 2018). Principal component analysis (PCA) was used for dimension reduction. FindClusters function was used to cluster cells. The R package, infercnv, and copykat were applied to explore the identification of tumor cells. The UMAP function was used for the visualization of dimensionality reduction. Vlnplot, Dimplot, and Featureplot were used for visualizing VSIR expression.

Immunofluorescence Staining

We obtained the tissue microarray from the Outdo Biotech company (HOrg-C110PT-01, total number of cases: 69 cases, total points: 110 points, Shanghai, China). The tissue microarray was approved by the Ethics Committee. Each tumor/normal tissue has three to eight cores (diameter 1.5 mm). The primary Abs were VSIR (Rabbit, 1:200, Proteintech, China), CD68 (Rabbit, 1:3000, AiFang biological, China), CD163 (Rabbit, 1:3000, Proteintech, China), CD8 (Mouse, 1:3000, Proteintech, China). The secondary antibody was horseradish peroxidase-conjugated secondary antibody incubation (GB23301, GB23303, Servicebio, China), and the tyramide signal amplification was TSA (FITC-TSA, CY3-TSA, 594-TSA, and 647-TSA (Servicebio, China)). Multispectral images were analyzed, and positive cells were quantified at single-cell levels by Caseviewer (CV 2.3, CV 2.0) and Pannoramic viewer (PV 1.15.3) image analysis software. Negative control procedures included the omission of the primary antibody.

Statistical Analysis

We calculated the optimal cutoff of VSIR using the R package (survminer). Student's t-test and Kruskal-Walli's test were performed to compare VSIR expression in the tumor and normal samples. In addition, the log-rank test was used to explore the survival differences between VSIR-high and VSIR-low groups regarding OS and DSS. All tests were two-sided, and $p < 0.05$ was statistically significant.

RESULTS

VSIR Expression and Mutation Characteristics in Normal and Cancer Samples

First, to comprehensively describe the expression profile of VSIR in normal and cancer specimens, we download the RNA-seq data from three public databases. It was found that VSIR is expressed in 31 normal tissues in the GTEx database, among which the top five tissues with the highest VSIR content are blood, spleen, nerve, lung, and adipose tissue (**Figure 1A**). Results from the CCLE database showed the differential expression profile of VSIR in 38 tumor cell lines, among which the top three cell lines enriched by VSIR are AML, giant cell tumor, and upper aerodigestive (**Figure 1B**). We also compared the VSIR levels in the tumor samples and counterparts based on the GTEx and TCGA databases (**Figure 1C**). VSIR is significantly upregulated in the tumor than normal samples in GBM, STAD, CHOL, LIHC, pancreatic adenocarcinoma (PAAD), brain lower-grade glioma (LGG), kidney renal clear cell carcinoma (KIRC), and acute myeloid leukemia (LAML) ($P < 0.001$). On the contrary, VSIR is significantly decreased ($P < 0.001$) in the tumor than normal samples in OV, THYM, SKCM, PRAD, BRCA, esophageal carcinoma (ESCA), cervical squamous cell carcinoma (CESC), uterine corpus endometrial carcinoma (UCEC), bladder urothelial carcinoma (BLCA), lymphoid neoplasm diffuse large B-cell lymphoma (DLBC), lung adenocarcinoma (LUAD), kidney chromophobe (KICH), thyroid carcinoma (THCA), lung squamous cell carcinoma (LUSC), rectum adenocarcinoma (READ), and uterine carcinosarcoma (UCS) ($P < 0.001$). These results were also verified through immunofluorescence staining (**Figure 1D**). In addition, we found that VSIR levels in the normal samples were higher than in cancer samples in upper tract urothelial cancer (UTUC) and Penile squamous cell carcinoma (PSCC), while laryngeal squamous cell carcinoma (LSCC) samples had higher VSIR expression than normal samples. Interestingly, PRAD samples with higher Gleason scores 8) have more

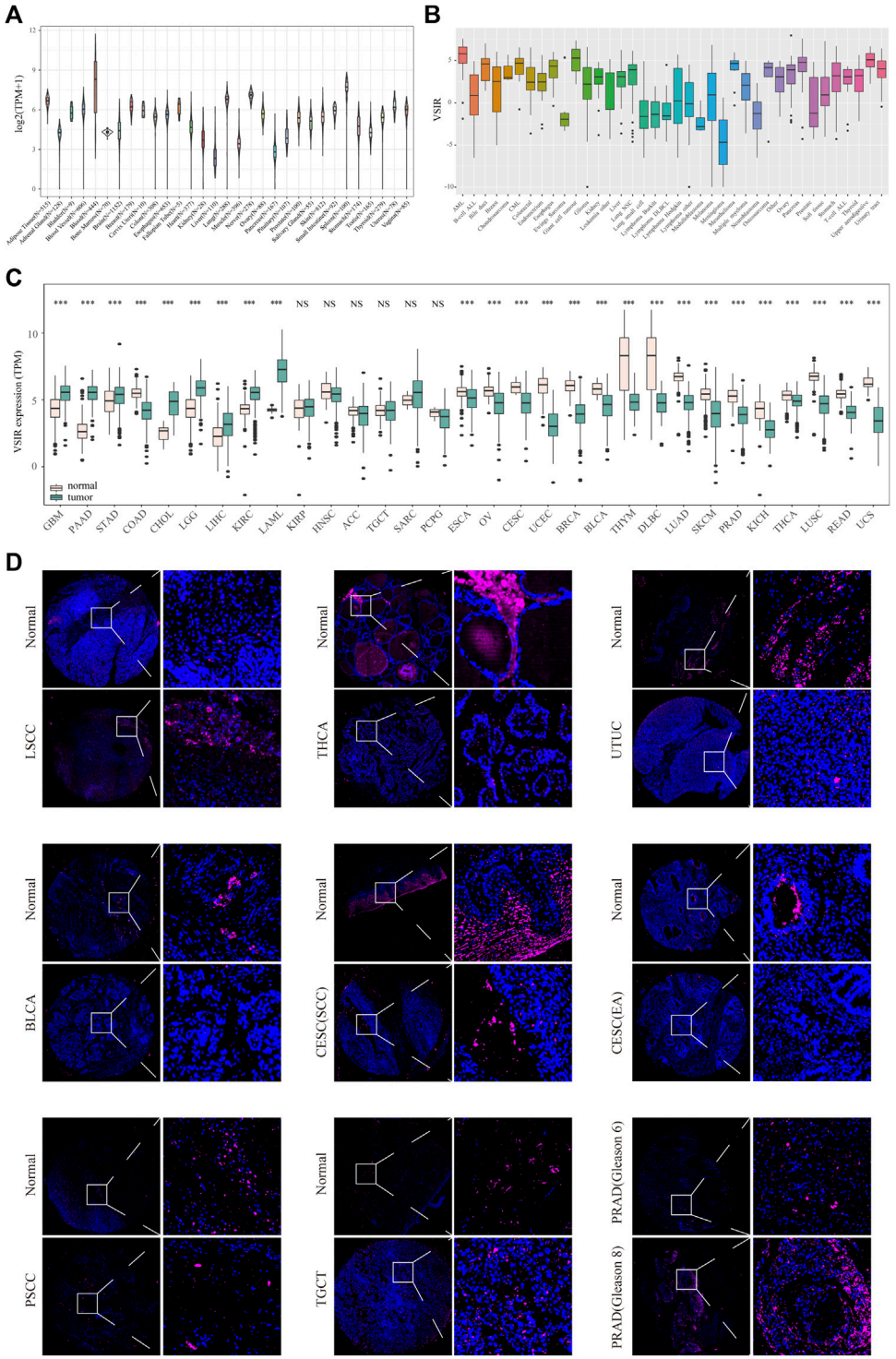

FIGURE 1 | Expression profiles of VSIR in the normal and tumor tissues. VSIR levels in the 31 human tissues **(A)** and tumor cell lines **(B)**. VSIR levels in the tumor and normal samples were analyzed by the R language **(C)**. VSIR expression was revealed by immunofluorescence staining **(D)**. ***$p < 0.001$, NS: no significant differences.

VSIR than lower Gleason scores (6). Together with previous studies, these results help to illustrate the variable role of VSIR in different cancer types.

Meanwhile, we analyzed the mutation profiles of VSIR in pan-cancer using the cBioportal and GSCA datasets (**Supplementary Figure S1**). The results indicated that the top two cancers with the

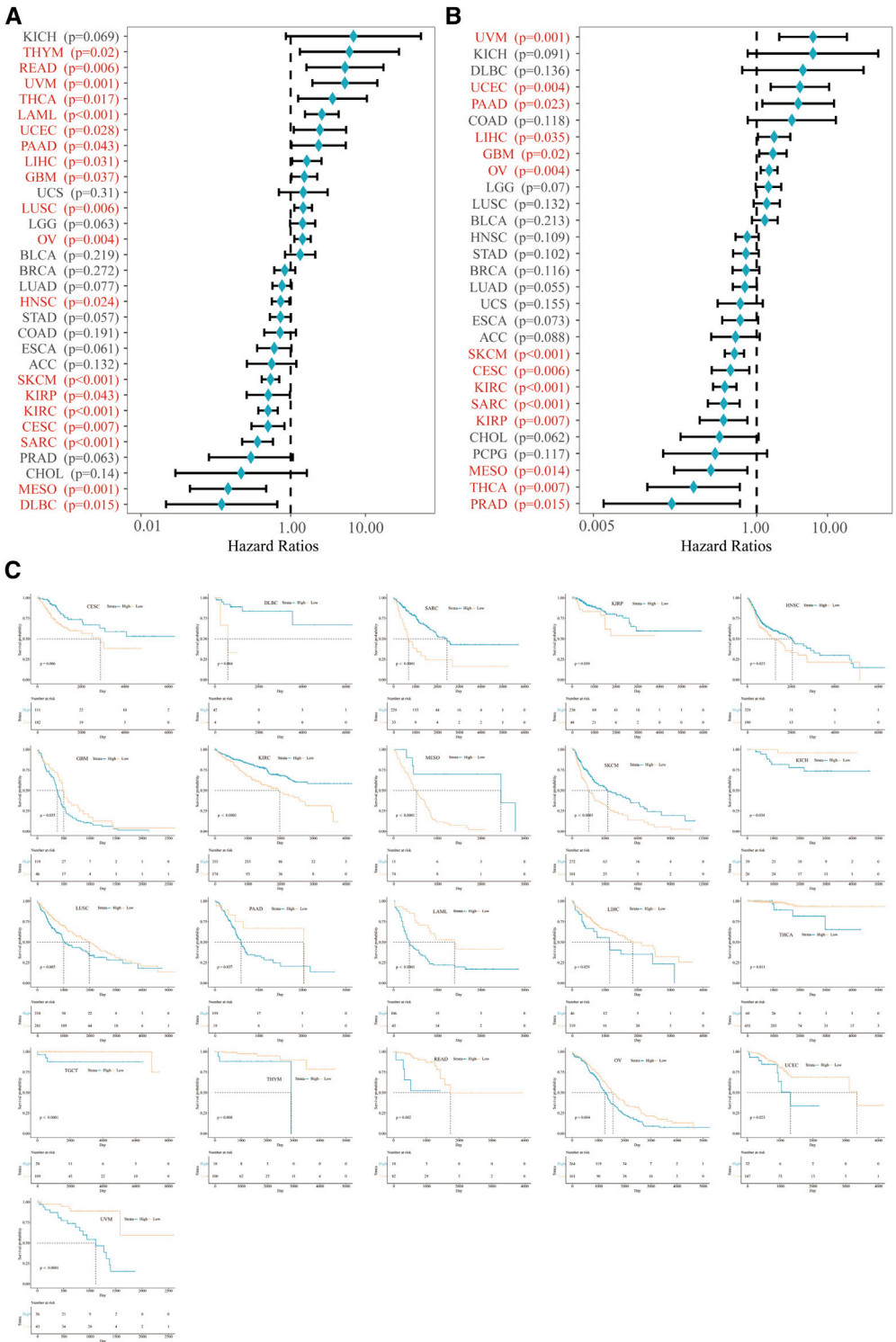

FIGURE 2 | Prognostic value of VSIR in pan-cancer. Survival analysis of VSIR on OS **(A)** and DSS **(B)** in pan-cancer described by the forest plot. K. M. analysis of VSIR on OS **(C)**.

highest mutation levels are SKCM and STAD, with a mutation frequency above 4% (**Supplementary Figures S1A, B**). A total of 90 mutation sites (including seventy-five missenses, nine truncating, three splices, two fusions, and one inflame) were detected between amino acids 0 and 311 (**Supplementary Figure S1C**). We also summarized the survival profile between gene set copy number

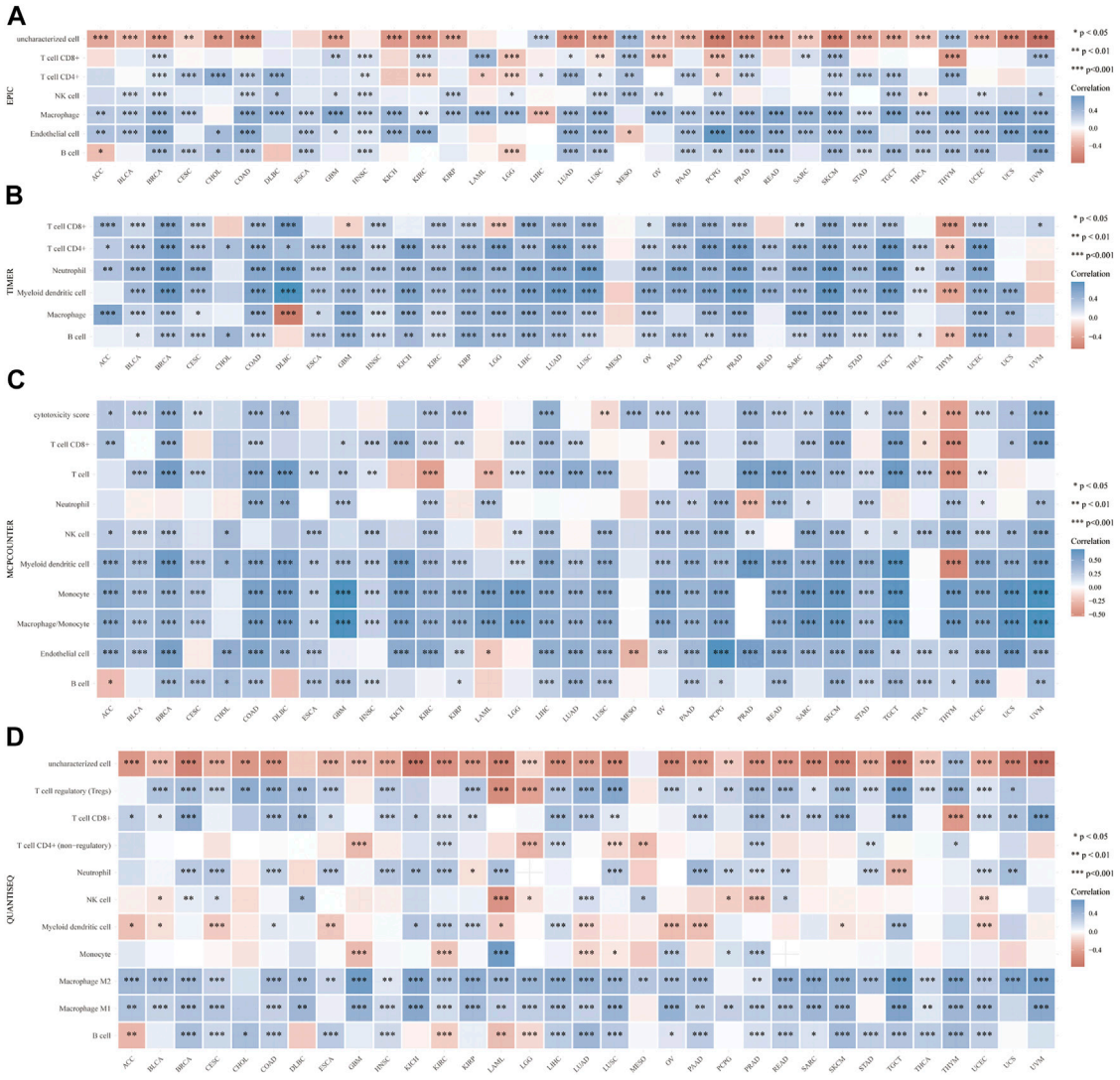

FIGURE 3 | Correlation between VSIR and infiltrated inflammatory cells analyzed by the immunedeconv algorithm. Immune cell infiltration analyzed by the EPIC **(A)**, TIMER **(B)**, MCP-counter **(C)**, quanTIseq **(D)** algorithms. *$p < 0.05$, **$p < 0.01$, ***$p < 0.001$.

variation (CNV) groups in pan-cancer (**Supplementary Figure S1D**; **Supplementary Table S1**). There is a significant correlation between the survival time of LGG patients and gene set CNV ($P < 0.0001$). The survival difference between gene set mutant (deleterious) and broad type in pan-cancer was also revealed in **Supplementary Figure S1E**; **Supplementary Table S2**.

Prognostic Value of VSIR in Pan-Cancer

Next, we clarified the predictive value of VSIR in pan-cancer based on the KM analysis. VSIR was closely related to OS (**Figure 2A**) and DSS (**Figure 2B**) of multiple cancers. High VSIR levels are associated with longer OS than low VSIR levels in CESC, DLBC, SARC, kidney renal papillary cell carcinoma (KIRP), HNSC, KIRC, mesothelioma (MESO), and SKCM (**Figure 2C**; $P < 0.05$). High VSIR expression, however, is related to shorter OS than low VSIR levels in GBM, KICH, LUSC, PAAD, LAML, LIHC, THCA, testicular germ cell tumor (TGCT), THYM, READ, OV, uveal melanoma (UVM), and UCEC (**Figure 2C**; $P < 0.05$). In addition, we also found that elevated VSIR is associated with longer DSS in CHOL, KIRC, KIRP, MESO, PRAD, SARC, SKCM, and THCA (**Supplementary Figure S2**; $P < 0.05$). On the contrary, elevated VSIR is related to shorter DSS in GBM, LIHC, OV, PAAD, TGCT, UCEC, and UVM (**Supplementary Figure S2**; $P < 0.05$).

Immune Characteristics of VSIR in Pan-Cancer TME

Then, we explored the immune features of VSIR in the tumor microenvironment among these cancers. We found that VSIR

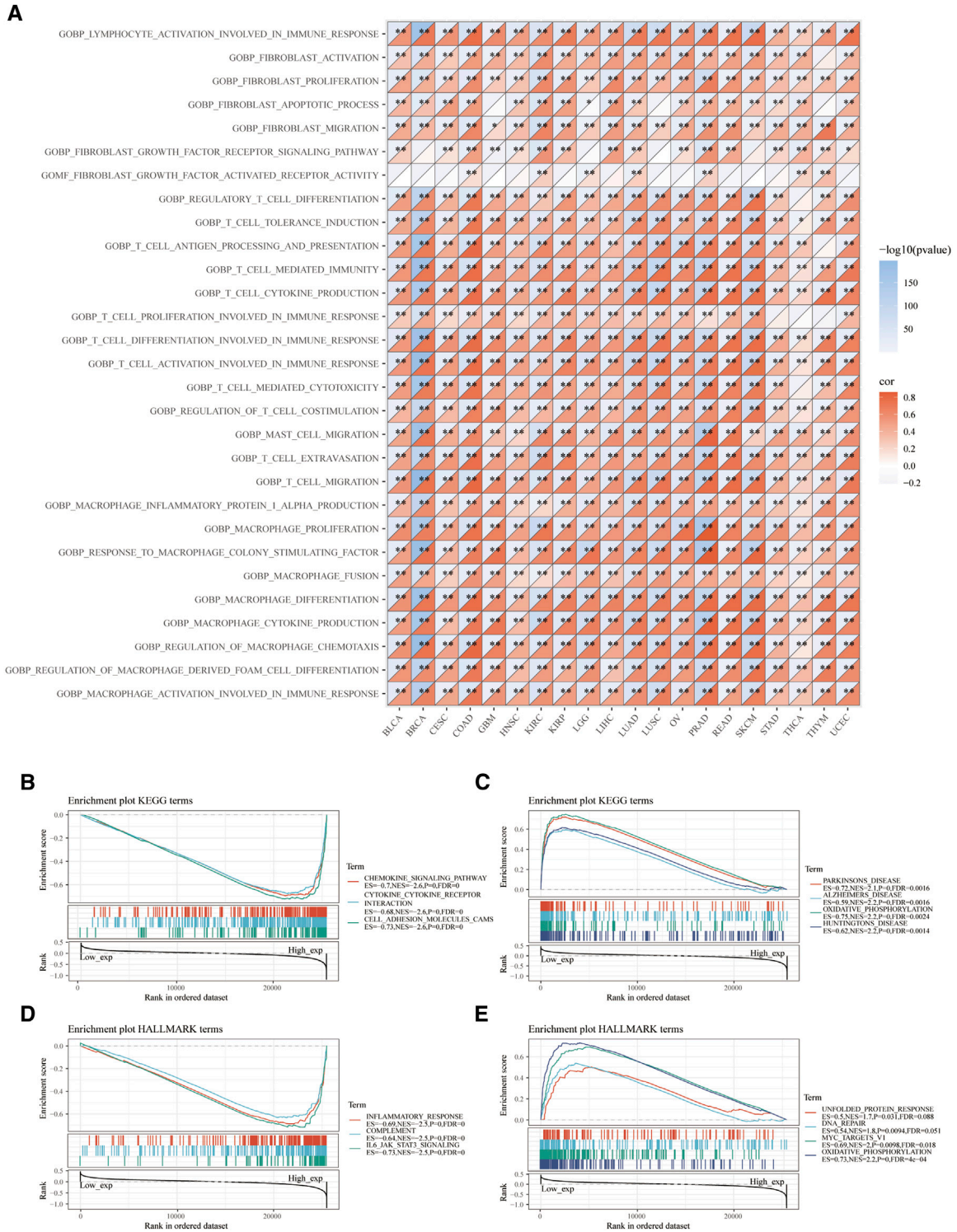

FIGURE 4 | Functional pathways analysis of VSIR in pan-cancer. Enrichment pathways analysis of VSIR from the GSVA algorithm **(A)**. Top three negative **(B)** and top four positive **(C)** enrichment pathways of VSIR from the KEGG terms. Top three negative **(D)** and top four positive **(E)** enrichment pathways of VSIR from the HALLMARK terms.

levels are positively related to immune score (**Supplementary Figure S3**), estimate score (**Supplementary Figure S4**), and stromal score (**Supplementary Figure S5**) in almost all cancers. Especially BLCA, BRCA, and CESC are the top three cancers most related to immune and estimate scores ($P < 0.001$); BLCA, BRCA, and COAD are the top three cancers most related to stromal score ($P < 0.001$). Furthermore, it was found that VSIR expression is most positively correlated with immune infiltrates (B cell, $CD4^+$, and $CD8^+$ T cells, DCs, macrophages, and neutrophils) in ACC, BRCA, and CHOL (**Supplementary Figure S6A**; $P < 0.05$). In addition, we also studied the relationship between VSIR expression and other infiltrated inflammatory cells in pan-cancer using six latest algorithms, including EPIC (**Figure 3A**), TIMER (**Figure 3B**), MCP-counter (**Figure 3C**), quanTIseq (**Figure 3D**), CIBERSORT (**Supplementary Figure S6B**), and xCell (**Supplementary Figure S6C**). VSIR expression was positively related to various infiltrated inflammatory cells in most cancer types. Increased VSIR kept a significant correlation with B cell, T cell, macrophages, neutrophils, NK Cells and monocytes in BLCA, BRCA, COAD, CESC, LGG, GBM, HNSC, KICH, KIRC, LIHC, LUAD, PAAD, PCPG, READ, SKCM, STAD, TGCT, and UCEC ($P < 0.05$).

Moreover, we demonstrated signaling pathways related to VSIR expression based on GOBP terms. A series of immune-related signaling pathways closely related to VSIR were discovered in pan-cancer, such as activation of lymphocytes involved in immune response, infiltrated inflammatory cells (fibroblast, T cell, mast cell, macrophages, and foam cell) activation, proliferation, and migration (**Figure 4A**; $P < 0.05$). Based on the KEGG gene set, the top three negative enriched pathways were chemokine signaling, cytokine-cytokine receptor interaction, and cell adhesion molecules CAMs (**Figure 4B**; $P < 0.001$); the top four positive enriched pathways were Parkinson's disease, Alzheimer's disease, oxidative phosphorylation, and Huntington's disease (**Figure 4C**; $P < 0.001$). This result indicated that VSIR might play a crucial role in CNS diseases through various immune-related pathways. Based on the HALLMARK gene set, the top three negative enriched pathways were inflammatory response, complement, and IL-6/JAK/STAT3 signaling (**Figure 4D**; $P < 0.001$); the top four positive enriched pathways were unfolded protein response, DNA repair, MYC targets V1, and oxidative phosphorylation (**Figure 4E**; $P < 0.001$).

Meanwhile, we calculated the relationship between VSIR expression and other immune checkpoints using Sangerbox (**Supplementary Figure S7A**) and immunedeconv (**Supplementary Figure S7B**) algorithms. Results indicated that VSIR levels significantly positively correlated with these immune checkpoints in many cancers, especially in BRCA, COAD, LIHC, SKCM, PRAD, TGCT, and UVM ($P < 0.05$). SIGLEC15, IDO1, CD274, HAVCR2, PDCD1, CTLA-4, LAG3, and PDCD1LG2 are transcripts related to immune checkpoints. We found that VSIR was closely correlated with these markers in most cancers, especially in BRCA, COAD, LUAD, LUSC, PAAD, PRAD, and SKCM ($P < 0.05$). VSIR levels in COAD are positively correlated with microsatellite instability (MSI) ($P < 0.0001$), while negatively related to MSI in HNSC, LUSC, MESO, PCPG, READ, PRAD, SKCM, STAD, and TGCT (**Supplementary Figures S8A, C**; $P < 0.05$). VSIR levels are positively correlated with tumor mutation burden (TMB) in COAD, SARC, UVM, and THYM($P < 0.01$), while negatively related to TMB in DLBC, GBM, LAML, LIHC, LUAD, LUSC, PRAD, SARC, SKCM, STAD, and THCA (**Supplementary Figures S8B, D**; $P < 0.05$). VSIR levels are closely related to expressions of mismatch repair system genes (MMRs) in many cancers, such as BRCA, KIRC, LGG, and LIHC (**Supplementary Figure S8E**; $P < 0.01$). VSIR was associated with neoantigen numbers in BRCA, STAD, THCA, BLCA, and PRAD (**Supplementary Figure S9**; $P < 0.05$).

Furthermore, to comprehensively clarify the predictive value of VSIR in pan-cancer, we merged all the cancer datasets we used in this study and divided them into two groups regarding VSIR expression, prognostic role, and association with tumor immunity (**Figure 5**; **Supplementary Figures S10**). Results showed that low expression of VSIR correlates with longer OS and predicts a better prognosis in pan-cancer (**Figure 5A**; $P < 0.001$). In the group with high VSIR expression, high immune score (**Figure 5B**; $P < 0.001$), estimate score (**Figure 5C**; $P < 0.001$) and stromal score (**Figure 5D**; $P < 0.001$) indicate poor outcome in pan-cancer. We also explored the immune infiltrates in the TME based on VSIR levels in pan-cancer. A large number of immune cell types were found to upregulate in the VSIR high expression group, such as activated B cell, T cells, eosinophil, mast cell, macrophage, monocyte, NK cell and neutrophil (**Figure 5E**; $P < 0.0001$). High scores are also associated with unfavorable prognosis in LGG (**Figure 5F**; $P < 0.01$), favorable prognosis in KIRC (**Figure 5G**; $P < 0.05$), unfavorable prognosis in TGCT (**Figure 5H**; $P < 0.05$), unfavorable prognosis in UVM (**Figure 5I**; $P < 0.05$). These results revealed that the extent to which VSIR correlates with immune cell infiltration can be used to explain prognostic outcomes.

Co-Expression of VSIR With Tumor and Inflammatory Cells

To fully clarify the role of VSIR in the TME in pan-cancer, we used single-cell sequencing analysis to observe the co-expression of VSIR with tumor and inflammatory cells in BLCA (**Figure 6A**), CHOL (**Figure 6B**), HNSC (**Figure 6C**), KIRC (**Figure 6D**), LUAD (**Figure 6E**), GBM (**Figure 7A**), BRCA (**Supplementary Figure S11A**), COAD (**Supplementary Figure S11B**), LIHC (**Supplementary Figure S11C**), and STAD (**Supplementary Figure S11D**). VSIR was found to co-expression with cancer cells and various inflammatory cells, such as T cells, B cells, regulatory T cells (Tregs), macrophages, M2 macrophages, cancer-associated fibroblasts (CAFs), monocytes, microglial cells, and astrocytes. Our previous enrichment pathway analysis indicated that VSIR might play an important role in CNS diseases, so we focused on the part of VSIR in BGM (**Figure 7**). We performed and defined three cell states using pseudotime trajectory analysis, in which VSIR expression increased as pseudotime increased (**Figure 7B**). VSIR was most expressed in state three compared with states 1 and 2 (**Figure 7C**). G.O. enrichment analysis revealed that as pseudotime increased, the top 10 signaling

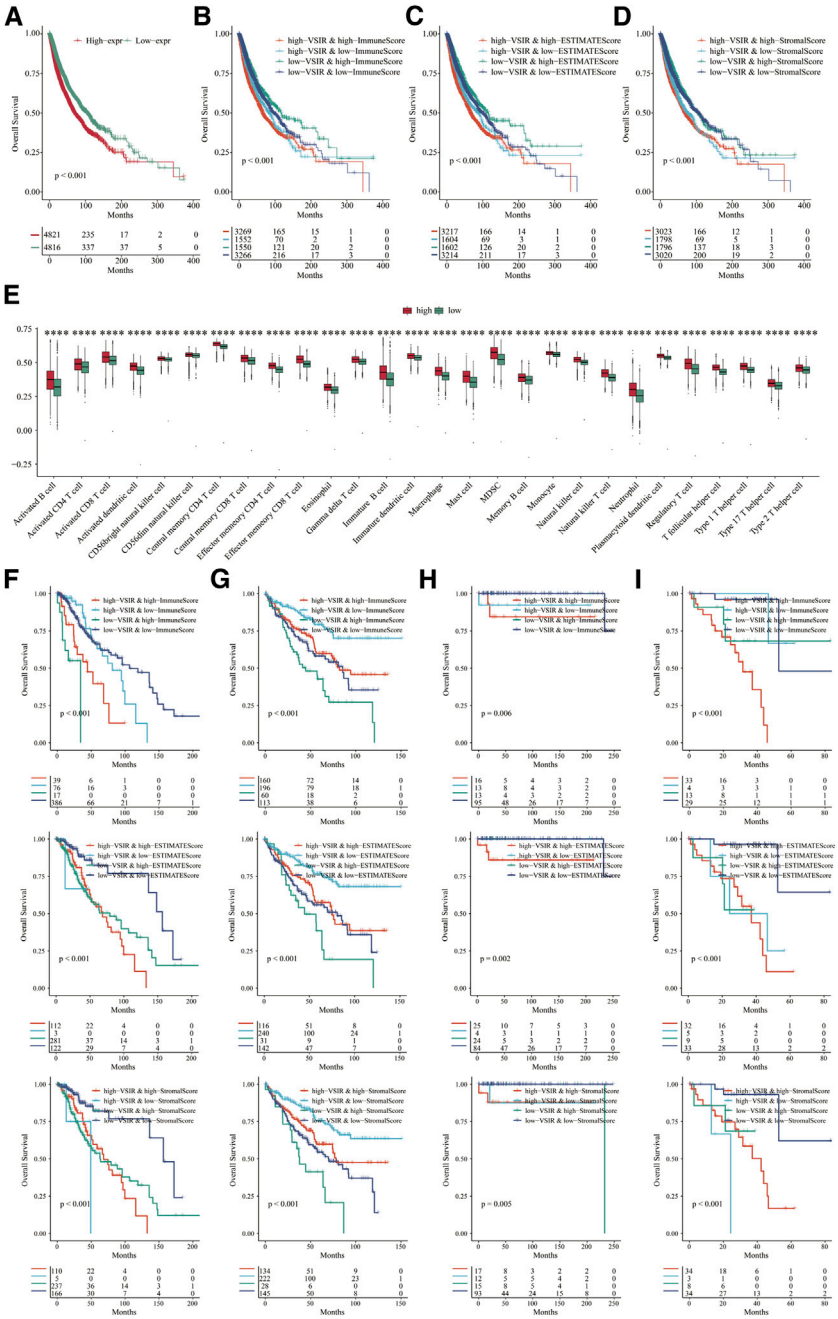

FIGURE 5 | Role of VSIR in pan-cancer regarding VSIR expression, prognostic role, and association with tumor immunity. Survival analysis of VSIR in pan-cancer based on VSIR levels **(A)**, immune score **(B)**, estimate score **(C)**, stromal score **(D)**. Immune infiltrates in pan-cancer based on VSIR levels **(E)**. Survival analysis of VSIR regarding expression and score in LGG **(F)**, KIRC **(G)**, TGCT **(H)** and UVM **(I)**. ****$p < 0.0001$.

pathways enriched by upregulated genes are shown in **Figure 7D**. The top 10 signaling pathways enriched by downregulated genes are shown in **Figure 7E**. The top 100 downregulated and upregulated genes with the increase in pseudotime are shown in **Figure 7F**.

We also observed the co-expression of VSIR with T cells (CD8), macrophages (CD68), and M2 macrophages (CD163) in GBM (**Figure 8A**), LSCC (**Figure 8B**), THCA (**Figure 8C**), UTUC (**Figure 8D**), BLCA (**Figure 8E**), CESC (**Figures 8F,G**), PSCC (**Figure 8H**), and TGCT (**Figure 8I**) using multiplex immunofluorescence staining (**Figure 8J**). VSIR was found to co-expression with $CD163^{+}$ cells in these cancers, including GBM, LSCC, BLCA, CESC, PSCC, and TGCT. In addition,

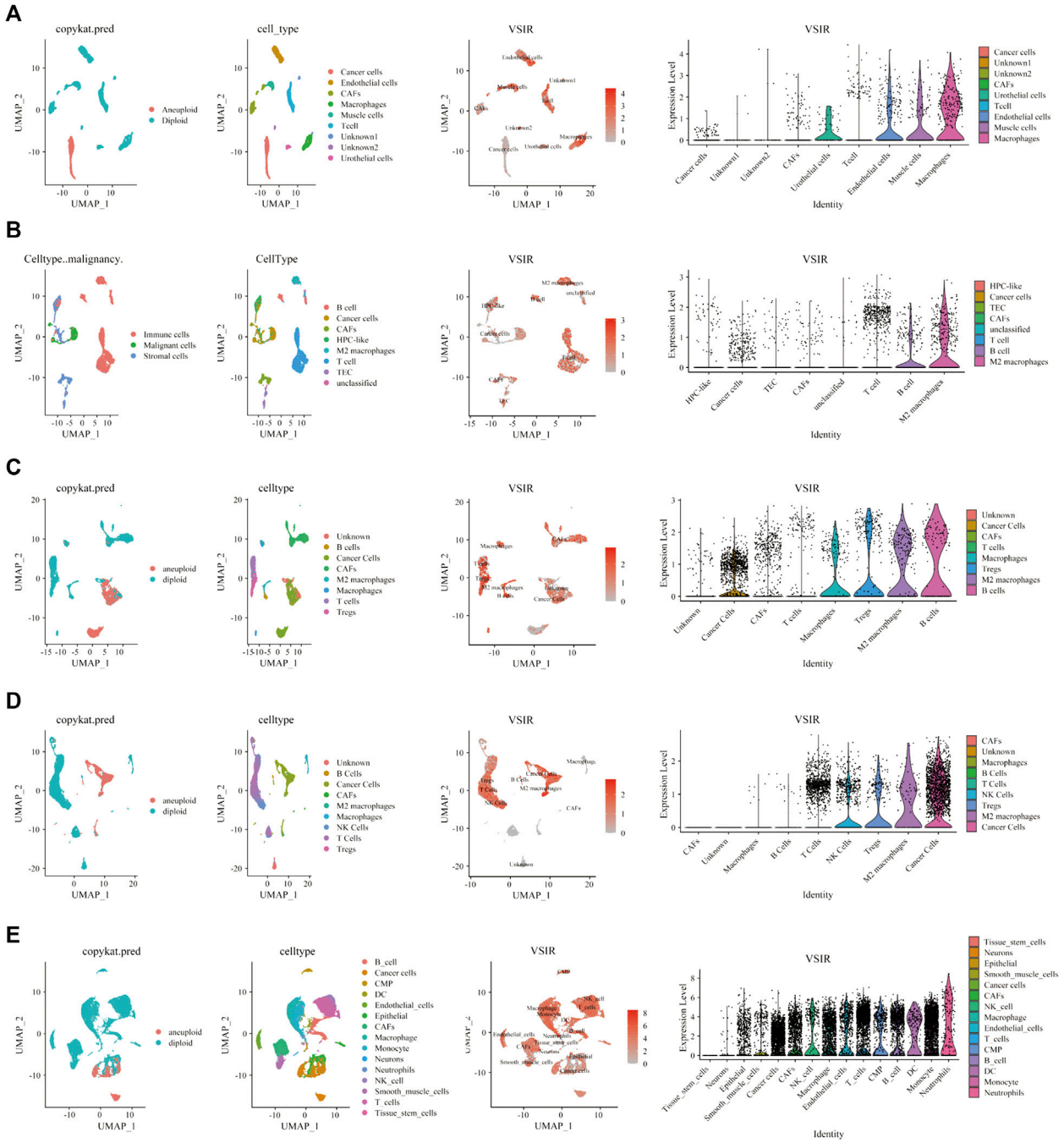

FIGURE 6 | Single-cell sequencing analysis of VSIR in the TME. The relationship between VSIR levels and cancer cells and stromal cells in BLCA **(A)**, CHOL (B), HNSC **(C)**, KIRC **(D)**, LUAD **(E)**.

VSIR was found to co-expression with $CD8^+$ in LSCC and PSCC.

Immunotherapy Value of VSIR in Pan-Cancer

Finally, we predicted the immunotherapy value of VSIR in pan-cancer based on the public databases. Biomarker relevance of VSIR was calculated by comparing it with standardized biomarkers based on their predictive power of response outcomes and OS of human immunotherapy cohorts. VSIR alone had an AUC of more than 0.5 in seven of 25 immunotherapy cohorts (**Figure 9A**). VSIR has the similar predictive value with B. Clonality (AUC >0.5 in seven immunotherapy cohorts). However, the predictive value of VSIR was lower than the MSI score, CD274, TIDE, IFNG, and CD8, which respectively gave AUC values above 0.5 in 13, 21, 18, 17, 18

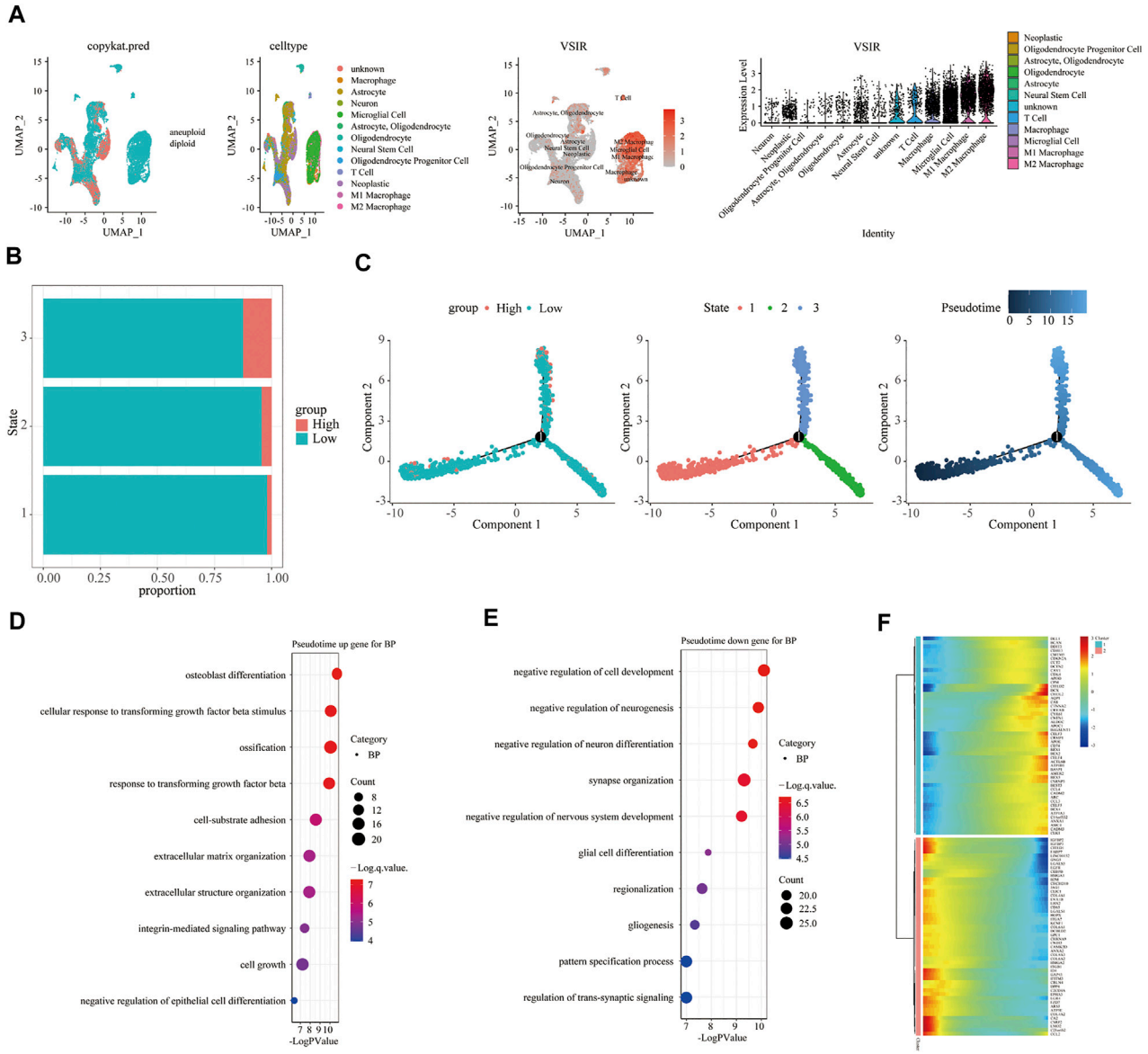

FIGURE 7 | Immune characteristics of VSIR in the TME in GBM. Immune features of VSIR in the TME were explored by the single-cell sequencing analysis **(A)** and pseudotime trajectory analysis **(B, C)**. GO enrichment analysis revealed pathways based on the upregulated genes **(D)** and downregulated genes **(E)**. In addition, the top 100 downregulated and upregulated genes increase pseudotime **(F)**.

immunotherapy cohorts. Interestingly, VSIR was found to significantly predict immunotherapy response in 15 murine immunotherapy cohorts based on *in vivo* studies (**Figure 9B**) and five murine cytokine treatment cohorts based on *in vitro* studies (**Figure 9C**). We then predicted sensitive small molecules and drugs based on VSIR levels through the public databases. The expression of each gene in the gene set was performed by Spearman correlation analysis with the small molecule/drug sensitivity (IC50). The positive correlation means that the gene is resistant to the drug and the negative correlation means that the gene is sensitive to the drug. Many sensitive drugs negatively correlated with VSIR expression were found based on the GDSC database. The top three drugs are sunitinib, WZ-1-84, and gefitinib (**Figure 9D** and **Supplementary Table S3**; $p < 0.0001$). Many resistant drugs positively correlated with VSIR expression were found based on the CTRP database. The top three drugs are belinostat, necrosulfonamide, and marinopyrrole A (**Figure 9E** and **Supplementary Table S4**; $p < 0.0001$).

DISCUSSION

In this paper, we discussed the expression profile and prognostic value of VSIR in pan-cancer. VSIR levels are higher in the tumor

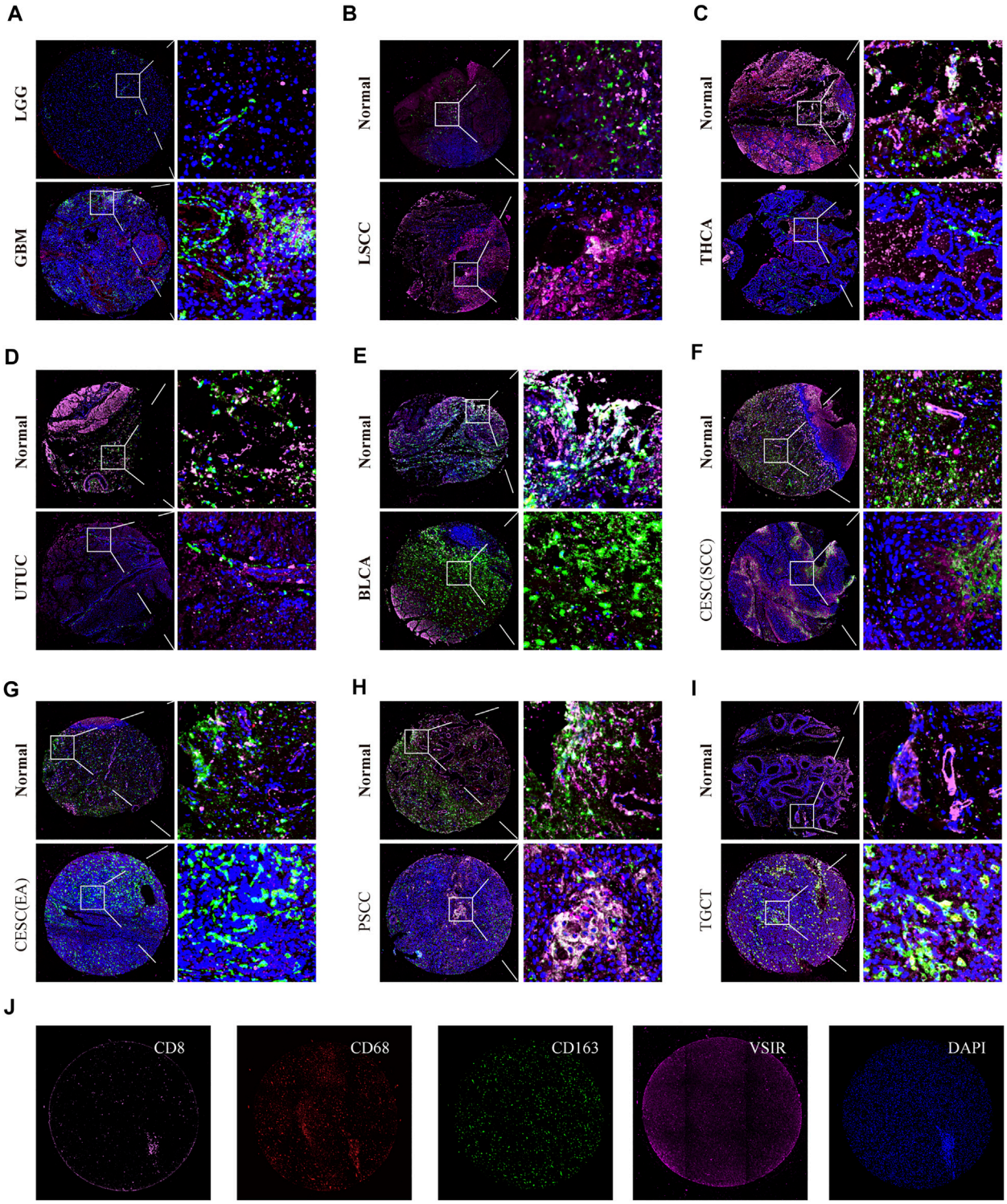

FIGURE 8 | Triple immunofluorescence analyzes the co-expression of VSIR on T cells, macrophage, and M2 macrophage. The co-expression of VSIR with $CD8^+$, $CD68^+$, and CD163 + cells in LGG and GBM **(A)**, LSCC **(B)**, THCA **(C)**, UTUC **(D)**, BLCA **(E)**, CESC **(F, G)**, PSCC **(H)**, TGCT **(I)**. Immunofluorescence staining of CD8, CD68, CD163, VSIR and DAPI **(J)**.

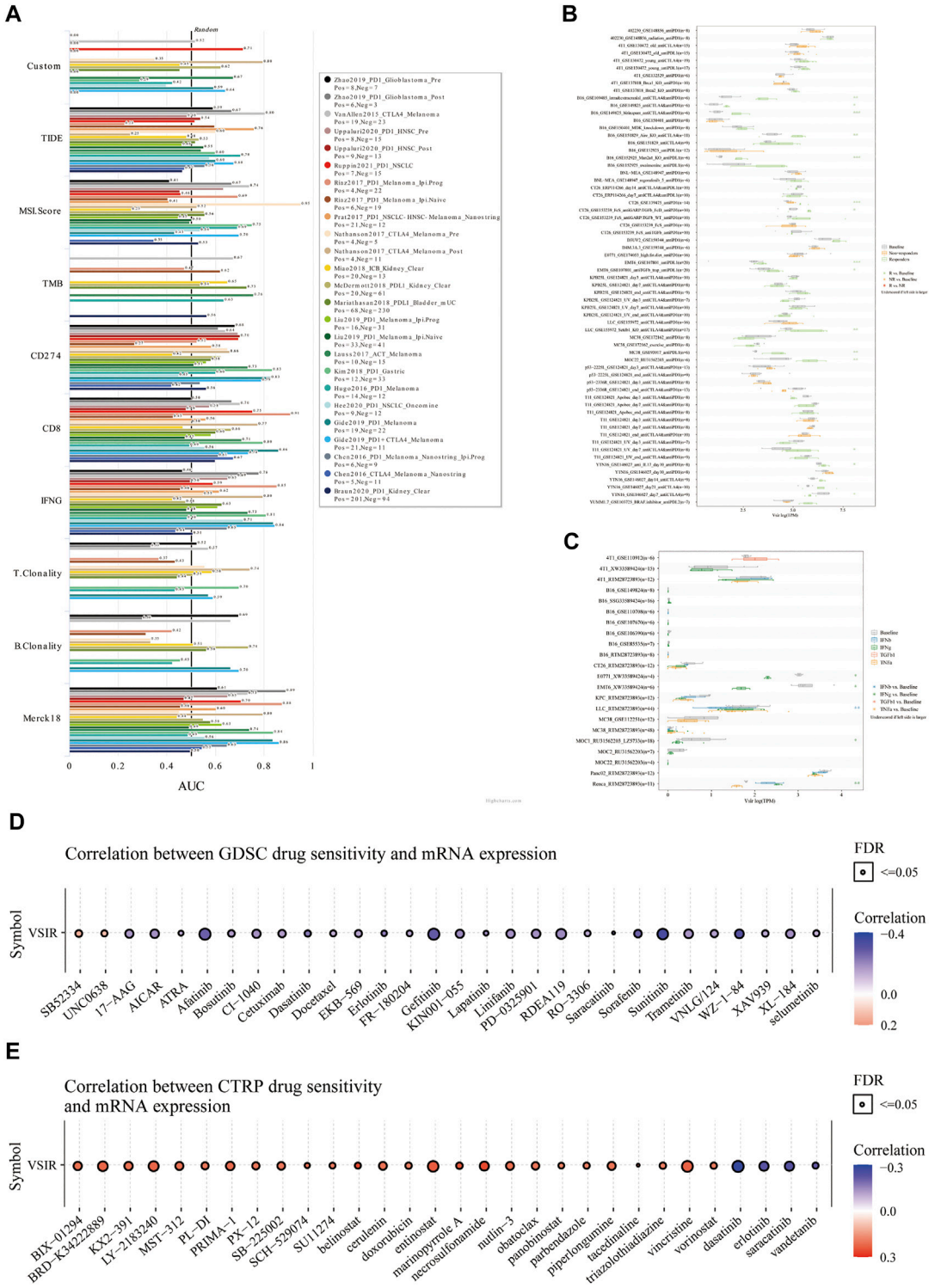

FIGURE 9 | Immunotherapeutic value of VAIR in pan-cancer. The predictive value of VSIR in 25 immunotherapy cohorts **(A)**. Immunotherapy response of VSIR in murine immunotherapy cohorts based on *in vivo* studies **(B)** and *in vitro* studies **(C)**. Correlation between VSIR expression and drug sensitivity from the GDSC **(D)** and CTRP **(E)** datasets.

than normal samples in GBM, STAD, CHOL, LIHC, PAAD, LGG, KIRC, and LAML, while being lower in OV, THYM, SKCM, PRAD, BRCA, ESCA, CESC, UCEC, BLCA, DLBC, LUAD, KICH, THCA, LUSC, READ, UCS. Meanwhile, we found that VSIR has an excellent predictive value in these cancers, which will provide new directions for future research on the function of VSIR in tumor immunity in these cancers.

Tumor-infiltrating inflammatory cells play a vital role in the progress of tumor formation, growth, metastasis, and recurrence. For example, As an indispensable component for mediating immune homeostasis, Tregs play essential roles in tumor immunity by inhibiting the activation and differentiation of $CD4^+$ helper T cells and $CD8^+$ cytotoxic T cells (Newton et al., 2016). In the progress of tumor immune response, Tregs differentiated from ordinary T cells can secrete TGF-β, IL-10, and IL-35, which suppress antitumor immunity and promote the formation and progression of tumors (Li et al., 2020). Recently, attempts to target CAFs for benefit have become a promising way to improve cancer therapy. CAFs regulate cancer metastasis through a series of complex mechanisms, including rebuilding the ECM, inducing growth factors, influencing drug resistance and immunotherapy response, remodeling the interactions with cancer cells, and infiltrating inflammatory cells (Sahai et al., 2020). In this study, we clarified the correlation between VSIR expression and infiltrated immune cells in the TME among these cancers through public databases, single-cell sequencing analysis, and multiplex immunofluorescence staining. Tumor-associated macrophages (TAMs) regulate inflammation and initiate, facilitate, or inhibit cancer development by affecting other immune cells and producing various factors, including nitric oxide, VEGF, EGF, and TGF-β(Zhang et al., 2021b; Duan and Luo, 2021; Zhang N. et al., 2021). VSIR plays a key role in reprogram and restrain macrophage inflammatory differentiation by regulating factors that mediate macrophage tolerance and inflammation during immune response. Anti-VSIR antibody treatment was found to induce mediators involved in both M2 macrophages polarization (up-regulated IL-10, miR-221, A20 and IRG1) and suppress mediators of M1 macrophages polarization (down-regulated IRF5 and IRF8) (ElTanbouly et al., 2020). scRNA-seq technology analysis indicated that macrophages derived from $VSIR^{-/-}$ mice and macrophages derived from WT mice exhibit heterogeneity in certain subtypes and have different functions. Especially, the expression levels of Hspb1, Cebpb, Gm8797, Bag3 and interferon-stimulated gene Ifit1 were upregulated in the macrophages from $VSIR^{-/-}$ mice skin lesions compared to WT controls (Qie et al., 2020). Increasing studies have found that according to different subtypes (anti-tumorigenic neutrophils and pro-tumorigenic neutrophils), tumor-associated neutrophils (TANs) play diametrically opposite effects in tumor immunity (Galli et al., 2020). It was found that VSIR maintains a close relationship with these inflammatory cells in most cancers, especially with T cells, CAFs, macrophages, M2 macrophages, Tregs, neutrophils, monocytes, microglial cells, and astrocytes. VSIR was found to engage in several immune-related signaling pathways, such as regulating the activation, proliferation, and migration of fibroblast, T cell, mast cell, macrophages, and foam cell. In addition, the co-expression of VSIR on M2 macrophages and T cells was also detected in our tumor chip.

The B7 protein is expressed on activated antigen-presenting cells and can bind to classical immune checkpoints on T cells, such as CD28, PD-L1, and CTLA-4 (Chaudhri et al., 2018; Du et al., 2018). Structural analysis revealed similar functional domains between VSIR and B7 family members, containing a conserved IGV-like fold. Phylogeny and protein sequence analysis show that VSIR is also partially homologous to PD-1 and CTLA-4 (Nowak et al., 2017). Thus, the VSIR signaling pathway has increasingly become a promising immunotherapy target in anti-cancer treatment in recent years. Although the VSIR antagonist's monotherapy did not show any effect based on preclinical studies, the combination of VSIR and CTLA-4 or PD-1 significantly reduced the number of tumor-recruiting T cells, thereby inducing antitumor responses against squamous cell carcinoma (Kondo et al., 2016). In addition, studies have found that patients who show resistance to PD-1/CTLA-4-targeting therapies may benefit from VSIR blockade (Kong et al., 2021). Moreover, CA-170, an orally administered dual inhibitor of VISTA and PD-L1, has shown clinical efficacy in phase I and II clinical trials in several advanced solid tumor types (Sasikumar et al., 2021). This paper comprehensively explored the relationship between VSIR and other immune checkpoints. We found that VSIR exhibited a close positive correlation with these immune checkpoints in most cancers, especially with LAIR1, HAVCR2, SIGLEC15, IDO1, CD274, HAVCR2, PDCD1, CTLA-4, LAG3, and PDCD1LG2. In addition, we discovered that VSIR expression is positively associated with the immune score, estimate score, and stromal score in these cancers. In addition, to fully clarify the immune aspects of VSIR in pan-cancer, we merged all the samples we used in this study and divided them into two groups based on VSIR levels and scores. We detected increased expression of a large number of infiltrating immune cells in the VSIR high expression group, including activated B cells, T cells, eosinophils, mast cells, macrophages, monocytes, NK cells and neutrophils. In the high VSIR expression group, patients with high immune, estimate and stromal score had poorer outcome in pan-cancer, especially in LGG, TGCT, and UVM. These results re-emphasize that irrespective of the difference in levels of its expression, VSIR is significantly associated with tumor immunity across different cancers. MMRs are a group of particular genes that identify genetic error pairs and initiate repair (Tamura et al., 2019). We found that VSIR levels are closely related to mutations of mismatch repair system genes (MMRs) in several cancers, such as BRCA, KIRC, LGG, and LIHC. Tumor neoantigens, including antigens produced by cancer cells and antigens produced by mutant proteins, have been considered a new approach to cancer immunotherapy (Zhang Z. et al., 2021). VSIR was associated with neoantigen numbers in BRCA, STAD, THCA, BLCA, and PRAD. Taking these data together, we speculate that VSIR plays a pivotal role in tumor immunity by affecting the functions of many inflammatory cells and can be used as a novel immunotherapy target in the process of tumor treatment in the future.

The past few decades have witnessed exciting breakthroughs that help us understand tumor immunity's specific mechanisms and pathways (Ventola, 2017). However, even with these advances, cancer immunotherapy still has limitations. For example, obstacles such as the inability to predict immunotherapy efficacy and patient response, the lack of sensitive drugs and development of treatment resistance, and the difficulty in finding the optimal biomarkers are still the main factors hindering the benefit of cancer patients. Therefore, in the last of this paper, we identified the therapeutic value of VSIR in 25 immunotherapy cohorts through the public databases. We found that VSIR alone had predictive value in seven of 25 immunotherapy cohorts. Furthermore, in several immunotherapy cohorts, VSIR has the similar predictive value with B. Clonality. However, the predictive value of VSIR was lower than the MSI score, CD274, TIDE, IFNG, and CD8 in more than 10 immunotherapy cohorts. Of note, we found VSIR can predict immunotherapy response in 15 murine immunotherapy cohorts based on *in vivo* studies and five murine immunotherapy cohorts based on *in vitro* studies. Furthermore, a series of sensitive small molecules and drugs were found based on the GDSC and CTRP database, further increasing the benefits of targeting the highly expressed VSIR in the TME in tumor immunotherapy. The top five sensitive drugs were sunitinib, WZ-1-84, gefitinib, afatinib, and sorafenib based on the VSIR expression from the GDSC database. The top three drugs positively correlated with VSIR expression were LY-2183240, vincristine, and entinostat, which means VSIR is resistant to these drugs. For example, afatinib, gefitinib, and sunitinib are EGFR inhibitors, which have been confirmed by many clinical trials, which can significantly inhibit the growth, metastasis and angiogenesis of various cancers, and increase the apoptosis of tumor cells. Especially for patients with the NSCL, HNSC, MESO, KIRC, leukemia, and KIRC, these drugs can significantly benefit them and prolong the time of tumor recurrence (George et al., 2009; Bang et al., 2011; Rizzo and Porta, 2017; Deeks and Keating, 2018). Excitingly, our results indicated that elevated VSIR levels are associated with better outcome than low VSIR levels in CESC, DLBC, SARC, KIRP, HNSC, KIRC, MESO, and SKCM. These data provide a new perspective for us to expand the therapeutic range of these drugs and develop new targeted drugs for those tumors whose prognosis is correlated with VSIR expression.

It should be noted that in cancer types with high infiltration of M2 macrophages and high expression of VSIR, patients with the corresponding cancers were associated with decreased survival, which might also partly explain the observation that VSIR behaves similarly in some cancers. Likewise, in cancer types with weakened activation of immune response and high expression of VSIR, patients with the corresponding cancers were almost uniformly associated with decreased survival. Notably, in cancer types with the negative correlation between VSIR and TMB, patients with the corresponding cancers were also associated with decreased survival. Taken together, VSIR was likely to induce an immune suppressive microenvironment in some cancers, which could lead to the tumor progression and decreased survival of patients.

DATA AVAILABILITY STATEMENT

The datasets presented in this study can be found in online repositories. The names of the repository/repositories and accession number(s) can be found in the article/ **Supplementary Material**.

AUTHOR CONTRIBUTIONS

Writing—Original Draft, Methodology, Validation, Visualization: YL and JZ Data Curation, Validation: ZYW and XZ Investigation: NZ, ZD, JY, ZPW, ZL, JZ, PL, and WW Conceptualization, Methodology, Supervision, Project Administration and Funding Acquisition: TY, HZ, and QC.

FUNDING

This study is supported by the National Nature Science Foundation of China (NO. 82073893, 81703622, 82060667, 81903725); the China Postdoctoral Science Foundation (NO. 2018M633002); the Natural Science Foundation of Hunan Province (NO. 2018JJ3838); the Hunan Provincial Health and Health Committee Foundation of China (C2019186); Xiangya Hospital Central South University postdoctoral foundation.

SUPPLEMENTARY MATERIAL

The Supplementary Material for this article can be found online at: https://www.frontiersin.org/articles/10.3389/fcell.2022.821649/full#supplementary-material

REFERENCES

Arnold, M., Rutherford, M. J., Bardot, A., Ferlay, J., Andersson, T. M.-L., Myklebust, T. Å., et al. (2019). Progress in Cancer Survival, Mortality, and Incidence in Seven High-Income Countries 1995-2014 (ICBP SURVMARK-2): a Population-Based Study. *Lancet Oncol.* 20 (11), 1493–1505. doi:10.1016/S1470-2045(19)30456-5

Bach, A. C., Lo, K. S., Pathirana, T., Glasziou, P. P., Barratt, A. L., Jones, M. A., et al. (2020). Is the Risk of Cancer in Australia Overstated? the Importance of Competing Mortality for Estimating Lifetime Risk. *Med. J. Aust.* 212 (1), 17–22. doi:10.5694/mja2.50376

Baghban, R., Roshangar, L., Jahanban-Esfahlan, R., Seidi, K., Ebrahimi-Kalan, A., Jaymand, M., et al. (2020). Tumor Microenvironment Complexity and Therapeutic Implications at a Glance. *Cell Commun Signal* 18 (1), 59. doi:10.1186/s12964-020-0530-4

Bang, Y.-J., Kang, Y.-K., Kang, W. K., Boku, N., Chung, H. C., Chen, J.-S., et al. (2011). Phase II Study of Sunitinib as Second-Line Treatment for Advanced Gastric Cancer. *Invest. New Drugs* 29 (6), 1449–1458. doi:10.1007/s10637-010-9438-y

Butler, A., Hoffman, P., Smibert, P., Papalexi, E., and Satija, R. (2018). Integrating Single-Cell Transcriptomic Data across Different Conditions, Technologies, and Species. *Nat. Biotechnol.* 36 (5), 411–420. doi:10.1038/nbt.4096

Chaudhri, A., Xiao, Y., Klee, A. N., Wang, X., Zhu, B., and Freeman, G. J. (2018). PD-L1 Binds to B7-1 Only in Cis on the Same Cell Surface. *Cancer Immunol. Res.* 6 (8), 921–929. doi:10.1158/2326-6066.CIR-17-0316

Davis, C., Naci, H., Gurpinar, E., Poplavska, E., Pinto, A., and Aggarwal, A. (2017). Availability of Evidence of Benefits on Overall Survival and Quality of Life of Cancer Drugs Approved by European Medicines Agency: Retrospective Cohort Study of Drug Approvals 2009-13. *BMJ* 359, j4530. doi:10.1136/bmj.j4530

Deeks, E. D., and Keating, G. M. (2018). Afatinib in Advanced NSCLC: a Profile of its Use. *Drugs Ther. Perspect.* 34 (3), 89–98. doi:10.1007/s40267-018-0482-6

Du, X., Tang, F., Liu, M., Su, J., Zhang, Y., Wu, W., et al. (2018). A Reappraisal of CTLA-4 Checkpoint Blockade in Cancer Immunotherapy. *Cell Res* 28 (4), 416–432. doi:10.1038/s41422-018-0011-0

Duan, Z., and Luo, Y. (2021). Targeting Macrophages in Cancer Immunotherapy. *Sig Transduct Target. Ther.* 6 (1), 127. doi:10.1038/s41392-021-00506-6

Dyck, L., and Mills, K. H. G. (2017). Immune Checkpoints and Their Inhibition in Cancer and Infectious Diseases. *Eur. J. Immunol.* 47 (5), 765–779. doi:10.1002/eji.201646875

ElTanbouly, M. A., Croteau, W., Noelle, R. J., and Lines, J. L. (2019). VISTA: a Novel Immunotherapy Target for Normalizing Innate and Adaptive Immunity. *Semin. Immunol.* 42, 101308. doi:10.1016/j.smim.2019.101308

ElTanbouly, M. A., Schaafsma, E., Smits, N. C., Shah, P., Cheng, C., Burns, C., et al. (2020). VISTA Re-programs Macrophage Biology through the Combined Regulation of Tolerance and Anti-inflammatory Pathways. *Front. Immunol.* 11, 580187. doi:10.3389/fimmu.2020.580187

Flies, D. B., Wang, S., Xu, H., and Chen, L. (2011). Cutting Edge: A Monoclonal Antibody Specific for the Programmed Death-1 Homolog Prevents Graft-Versus-Host Disease in Mouse Models. *J.I.* 187 (4), 1537–1541. doi:10.4049/jimmunol.1100660

Galli, F., Aguilera, J. V., Palermo, B., Markovic, S. N., Nisticò, P., and Signore, A. (2020). Relevance of Immune Cell and Tumor Microenvironment Imaging in the new era of Immunotherapy. *J. Exp. Clin. Cancer Res.* 39 (1), 89. doi:10.1186/s13046-020-01586-y

Gao, J., Navai, N., Alhalabi, O., Siefker-Radtke, A., Campbell, M. T., Tidwell, R. S., et al. (2020). Neoadjuvant PD-L1 Plus CTLA-4 Blockade in Patients with Cisplatin-Ineligible Operable High-Risk Urothelial Carcinoma. *Nat. Med.* 26 (12), 1845–1851. doi:10.1038/s41591-020-1086-y

George, S., Merriam, P., Maki, R. G., Van den Abbeele, A. D., Yap, J. T., Akhurst, T., et al. (2009). Multicenter Phase II Trial of Sunitinib in the Treatment of Nongastrointestinal Stromal Tumor Sarcomas. *Jco* 27 (19), 3154–3160. doi:10.1200/JCO.2008.20.9890

He, X., and Xu, C. (2020). Immune Checkpoint Signaling and Cancer Immunotherapy. *Cel Res* 30 (8), 660–669. doi:10.1038/s41422-020-0343-4

Hosseinkhani, N., Derakhshani, A., Shadbad, M. A., Argentiero, A., Racanelli, V., Kazemi, T., et al. (2021). The Role of V-Domain Ig Suppressor of T Cell Activation (VISTA) in Cancer Therapy: Lessons Learned and the Road Ahead. *Front. Immunol.* 12, 676181. doi:10.3389/fimmu.2021.676181

Jahanban-Esfahlan, R., Seidi, K., Monhemi, H., Adli, A. D. F., Minofar, B., Zare, P., et al. (2017). RGD Delivery of Truncated Coagulase to Tumor Vasculature Affords Local Thrombotic Activity to Induce Infarction of Tumors in Mice. *Sci. Rep.* 7 (1), 8126. doi:10.1038/s41598-017-05326-9

Kondo, Y., Ohno, T., Nishii, N., Harada, K., Yagita, H., and Azuma, M. (2016). Differential Contribution of Three Immune Checkpoint (VISTA, CTLA-4, PD-1) Pathways to Antitumor Responses against Squamous Cell Carcinoma. *Oral Oncol.* 57, 54–60. doi:10.1016/j.oraloncology.2016.04.005

Kong, X., Lu, P., Liu, C., Guo, Y., Yang, Y., Peng, Y., et al. (2021). A Combination of PD-1/PD-L1 I-nhibitors: The prospect of O-vercoming the W-eakness of T-umor I-mmunotherapy (Review). *Mol. Med. Rep.* 23 (5). doi:10.3892/mmr.2021.12001

Kuklinski, L. F., Yan, S., Li, Z., Fisher, J. L., Cheng, C., Noelle, R. J., et al. (2018). VISTA Expression on Tumor-Infiltrating Inflammatory Cells in Primary Cutaneous Melanoma Correlates with Poor Disease-specific Survival. *Cancer Immunol. Immunother.* 67 (7), 1113–1121. doi:10.1007/s00262-018-2169-1

Lánczky, A., and Győrffy, B. (2021). Web-Based Survival Analysis Tool Tailored for Medical Research (KMplot): Development and Implementation. *Med. Internet Res.* 23 (7), e27633. doi:10.2196/27633

Le Mercier, I., Chen, W., Lines, J. L., Day, M., Li, J., Sergent, P., et al. (2014). VISTA Regulates the Development of Protective Antitumor Immunity. *Cancer Res.* 74 (7), 1933–1944. doi:10.1158/0008-5472.CAN-13-1506

Le Mercier, I., Lines, J. L., and Noelle, R. J. (2015). Beyond CTLA-4 and PD-1, the Generation Z of Negative Checkpoint Regulators. *Front. Immunol.* 6, 418. doi:10.3389/fimmu.2015.00418

Li, C., Jiang, P., Wei, S., Xu, X., and Wang, J. (2020). Regulatory T Cells in Tumor Microenvironment: New Mechanisms, Potential Therapeutic Strategies and Future Prospects. *Mol. Cancer* 19 (1), 116. doi:10.1186/s12943-020-01234-1

Li, T., Fan, J., Wang, B., Traugh, N., Chen, Q., Liu, J. S., et al. (2017). TIMER: A Web Server for Comprehensive Analysis of Tumor-Infiltrating Immune Cells. *Cancer Res.* 77 (21), e108–e110. doi:10.1158/0008-5472.CAN-17-0307

Lim, A. R., Rathmell, W. K., and Rathmell, J. C. (2020). The Tumor Microenvironment as a Metabolic Barrier to Effector T Cells and Immunotherapy. *Elife* 9. doi:10.7554/eLife.55185

Lines, J. L., Pantazi, E., Mak, J., Sempere, L. F., Wang, L., O'Connell, S., et al. (2014). VISTA Is an Immune Checkpoint Molecule for Human T Cells. *Cancer Res.* 74 (7), 1924–1932. doi:10.1158/0008-5472.CAN-13-1504

Liu, C.-J., Hu, F.-F., Xia, M.-X., Han, L., Zhang, Q., and Guo, A.-Y. (2018). GSCALite: a Web Server for Gene Set Cancer Analysis. *Bioinformatics* 34 (21), 3771–3772. doi:10.1093/bioinformatics/bty411

Mulati, K., Hamanishi, J., Matsumura, N., Chamoto, K., Mise, N., Abiko, K., et al. (2019). VISTA Expressed in Tumour Cells Regulates T Cell Function. *Br. J. Cancer* 120 (1), 115–127. doi:10.1038/s41416-018-0313-5

Muller, S., Victoria Lai, W., Adusumilli, P. S., Desmeules, P., Frosina, D., Jungbluth, A., et al. (2020). V-domain Ig-Containing Suppressor of T-Cell Activation (VISTA), a Potentially Targetable Immune Checkpoint Molecule, Is Highly Expressed in Epithelioid Malignant Pleural Mesothelioma. *Mod. Pathol.* 33 (2), 303–311. doi:10.1038/s41379-019-0364-z

Newton, R., Priyadharshini, B., and Turka, L. A. (2016). Immunometabolism of Regulatory T Cells. *Nat. Immunol.* 17 (6), 618–625. doi:10.1038/ni.3466

Nowak, E. C., Lines, J. L., Varn, F. S., Deng, J., Sarde, A., Mabaera, R., et al. (2017). Immunoregulatory Functions of VISTA. *Immunol. Rev.* 276 (1), 66–79. doi:10.1111/imr.12525

Ping, Q., Yan, R., Cheng, X., Wang, W., Zhong, Y., Hou, Z., et al. (2021). Correction: Cancer-Associated Fibroblasts: Overview, Progress, Challenges, and Directions. *Cancer Gene Ther.* 28 (9), 1074. doi:10.1038/s41417-021-00343-3

Qie, C., Jiang, J., Liu, W., Hu, X., Chen, W., Xie, X., et al. (2020). Single-cell RNA-Seq Reveals the Transcriptional Landscape and Heterogeneity of Skin Macrophages in Vsir-/- Murine Psoriasis. *Theranostics* 10 (23), 10483–10497. doi:10.7150/thno.45614

Qin, S., Xu, L., Yi, M., Yu, S., Wu, K., and Luo, S. (2019). Novel Immune Checkpoint Targets: Moving beyond PD-1 and CTLA-4. *Mol. Cancer* 18 (1), 155. doi:10.1186/s12943-019-1091-2

Rizzo, M., and Porta, C. (2017). Sunitinib in the Treatment of Renal Cell Carcinoma: an Update on Recent Evidence. *Ther. Adv. Urol.* 9 (8), 195–207. doi:10.1177/1756287217713902

Sahai, E., Astsaturov, I., Cukierman, E., DeNardo, D. G., Egeblad, M., Evans, R. M., et al. (2020). A Framework for Advancing Our Understanding of Cancer-Associated Fibroblasts. *Nat. Rev. Cancer* 20 (3), 174–186. doi:10.1038/s41568-019-0238-1

Sasikumar, P. G., Sudarshan, N. S., Adurthi, S., Ramachandra, R. K., Samiulla, D. S., Lakshminarasimhan, A., et al. (2021). PD-1 Derived CA-170 Is an Oral Immune Checkpoint Inhibitor that Exhibits Preclinical Anti-tumor Efficacy. *Commun. Biol.* 4 (1), 699. doi:10.1038/s42003-021-02191-1

Siegel, R. L., Miller, K. D., Fuchs, H. E., and Jemal, A. (2021). Cancer Statistics, 2021. *CA A. Cancer J. Clin.* 71 (1), 7–33. doi:10.3322/caac.21654

Siegel, R. L., Miller, K. D., and Jemal, A. (2020). Cancer Statistics, 2020. *CA A. Cancer J. Clin.* 70 (1), 7–30. doi:10.3322/caac.21590

Tamura, K., Kaneda, M., Futagawa, M., Takeshita, M., Kim, S., Nakama, M., et al. (2019). Genetic and Genomic Basis of the Mismatch Repair System Involved in Lynch Syndrome. *Int. J. Clin. Oncol.* 24 (9), 999–1011. doi:10.1007/s10147-019-01494-y

Ventola, C. L. (2017). Cancer Immunotherapy, Part 3: Challenges and Future Trends. *P T* 42 (8), 514–521.

Villarroel-Espindola, F., Yu, X., Datar, I., Mani, N., Sanmamed, M., Velcheti, V., et al. (2018). Spatially Resolved and Quantitative Analysis of VISTA/PD-1H as a Novel Immunotherapy Target in Human Non-small Cell Lung Cancer. *Clin. Cancer Res.* 24 (7), 1562–1573. doi:10.1158/1078-0432.CCR-17-2542

Vitale, I., Manic, G., Coussens, L. M., Kroemer, G., and Galluzzi, L. (2019). Macrophages and Metabolism in the Tumor Microenvironment. *Cel Metab.* 30 (1), 36–50. doi:10.1016/j.cmet.2019.06.001

Yang, K., Wu, Z., Zhang, H., Zhang, N., Wu, W., Wang, Z., et al. (2022). Glioma Targeted Therapy: Insight into Future of Molecular Approaches. *Mol. Cancer* 21 (1), 39. doi:10.1186/s12943-022-01513-z

Yoon, K. W., Byun, S., Kwon, E., Hwang, S.-Y., Chu, K., Hiraki, M., et al. (2015). Control of Signaling-Mediated Clearance of Apoptotic Cells by the Tumor Suppressor P53. *Science* 349 (6247), 1261669. doi:10.1126/science.1261669

Zhang, H., Dai, Z., Wu, W., Wang, Z., Zhang, N., Zhang, L., et al. (2021a). Regulatory Mechanisms of Immune Checkpoints PD-L1 and CTLA-4 in Cancer. *J. Exp. Clin. Cancer Res.* 40 (1), 184. doi:10.1186/s13046-021-01987-7

Zhang, H., Luo, Y.-B., Wu, W., Zhang, L., Wang, Z., Dai, Z., et al. (2021b). The Molecular Feature of Macrophages in Tumor Immune Microenvironment of Glioma Patients. *Comput. Struct. Biotechnol. J.* 19, 4603–4618. doi:10.1016/j.csbj.2021.08.019

Zhang, H., Wang, Z., Dai, Z., Wu, W., Cao, H., Li, S., et al. (2021c). Novel Immune Infiltrating Cell Signature Based on Cell Pair Algorithm Is a Prognostic Marker in Cancer. *Front. Immunol.* 12, 694490. doi:10.3389/fimmu.2021.694490

Zhang, J.-c., Chen, W.-d., Alvarez, J. B., Jia, K., Shi, L., Wang, Q., et al. (2018). Cancer Immune Checkpoint Blockade Therapy and its Associated Autoimmune Cardiotoxicity. *Acta Pharmacol. Sin* 39 (11), 1693–1698. doi:10.1038/s41401-018-0062-2

Zhang, N., Zhang, H., Wang, Z., Dai, Z., Zhang, X., Cheng, Q., et al. (2021d). Immune Infiltrating Cells-Derived Risk Signature Based on Large-Scale Analysis Defines Immune Landscape and Predicts Immunotherapy Responses in Glioma Tumor Microenvironment. *Front. Immunol.* 12, 691811. doi:10.3389/fimmu.2021.691811

Zhang, Z., Lu, M., Qin, Y., Gao, W., Tao, L., Su, W., et al. (2021e). Neoantigen: A New Breakthrough in Tumor Immunotherapy. *Front. Immunol.* 12, 672356. doi:10.3389/fimmu.2021.672356

Conflict of Interest: The authors declare that the research was conducted in the absence of any commercial or financial relationships that could be construed as a potential conflict of interest.

Publisher's Note: All claims expressed in this article are solely those of the authors and do not necessarily represent those of their affiliated organizations, or those of the publisher, the editors and the reviewers. Any product that may be evaluated in this article, or claim that may be made by its manufacturer, is not guaranteed or endorsed by the publisher

Copyright © 2022 Liu, Zhang, Wang, Zhang, Dai, Wu, Zhang, Liu, Zhang, Luo, Wen, Yu, Zhang, Yang and Cheng. This is an open-access article distributed under the terms of the Creative Commons Attribution License (CC BY). The use, distribution or reproduction in other forums is permitted, provided the original author(s) and the copyright owner(s) are credited and that the original publication in this journal is cited, in accordance with accepted academic practice. No use, distribution or reproduction is permitted which does not comply with these terms.

frontiers | Frontiers in Cell and Developmental Biology

ORIGINAL RESEARCH
published: 26 April 2022
doi: 10.3389/fcell.2022.835043

Integrative Analysis Constructs an Extracellular Matrix-Associated Gene Signature for the Prediction of Survival and Tumor Immunity in Lung Adenocarcinoma

Lingyan Xiao[1†], Qian Li[2†], Yongbiao Huang[1], Zhijie Fan[1], Wan Qin[1], Bo Liu[1] and Xianglin Yuan[1*]*

[1]Department of Oncology, Tongji Hospital, Tongji Medical College, Huazhong University of Science and Technology, Wuhan, China, [2]Department of Pathophysiology, School of Basic Medicine, Tongji Medical College, Huazhong University of Science and Technology, Wuhan, China

OPEN ACCESS

Edited by:
Shaoquan Zheng,
Sun Yat-sen University Cancer Center, China

Reviewed by:
Shu-Heng Jiang,
Shanghai Cancer Institute, China
Gaofeng Xiong,
University of Kentucky, United States
Pankaj Kumar Ahluwalia,
Augusta University, United States

***Correspondence:**
Bo Liu
boliu888@hotmail.com
Xianglin Yuan
yuanxianglin@hust.edu.cn

†These authors have contributed equally to this work and share first authorship

Specialty section:
This article was submitted to Cancer Cell Biology, a section of the journal Frontiers in Cell and Developmental Biology

Received: 14 December 2021
Accepted: 06 April 2022
Published: 26 April 2022

Citation:
Xiao L, Li Q, Huang Y, Fan Z, Qin W, Liu B and Yuan X (2022) Integrative Analysis Constructs an Extracellular Matrix-Associated Gene Signature for the Prediction of Survival and Tumor Immunity in Lung Adenocarcinoma. Front. Cell Dev. Biol. 10:835043. doi: 10.3389/fcell.2022.835043

Background: Lung adenocarcinoma (LUAD) accounts for the majority of lung cancers, and the survival of patients with advanced LUAD is poor. The extracellular matrix (ECM) is a fundamental component of the tumor microenvironment (TME) that determines the oncogenesis and antitumor immunity of solid tumors. However, the prognostic value of extracellular matrix-related genes (ERGs) in LUAD remains unexplored. Therefore, this study is aimed to explore the prognostic value of ERGs in LUAD and establish a classification system to predict the survival of patients with LUAD.

Methods: LUAD samples from The Cancer Genome Atlas (TCGA) and GSE37745 were used as discovery and validation cohorts, respectively. Prognostic ERGs were identified by univariate Cox analysis and used to construct a prognostic signature by Least Absolute Shrinkage and Selection Operator (LASSO) regression analysis. The extracellular matrix-related score (ECMRS) of each patient was calculated according to the prognostic signature and used to classify patients into high- and low-risk groups. The prognostic performance of the signature was evaluated using Kaplan–Meier curves, Cox regression analyses, and ROC curves. The relationship between ECMRS and tumor immunity was determined using stepwise analyses. A nomogram based on the signature was established for the convenience of use in the clinical practice. The prognostic genes were validated in multiple databases and clinical specimens by qRT-PCR.

Results: A prognostic signature based on eight ERGs (*FERMT1*, *CTSV*, *CPS1*, *ENTPD2*, *SERPINB5*, *ITGA8*, *ADAMTS8*, and *LYPD3*) was constructed. Patients with higher ECMRS had poorer survival, lower immune scores, and higher tumor purity in both the discovery and

Abbreviations: ECM, extracellular matrix; LUAD, lung adenocarcinoma; TME, tumor microenvironment; ERG, extracellular matrix-related gene; TCGA, The Cancer Genome Atlas; LASSO, Least Absolute Shrinkage and Selection Operator; GEO, Gene Expression Omnibus; CI, confidence interval; HPA, Human Protein Atlas; ECMRS, extracellular matrix-related score; FDR, false discovery rate; OS, overall survival; DC, dendritic cell; HR, hazard ratio; CI, confidence interval.

validation cohorts. The predictive power of the signature was independent of the clinicopathological parameters, and the nomogram could also predict survival precisely.

Conclusions: We constructed an ECM-related gene signature which can be used to predict survival and tumor immunity in patients with LUAD. This signature can serve as a novel prognostic indicator and therapeutic target in LUAD.

Keywords: lung adenocarcinoma, extracellar matrix, prognostic signature, tumor micoenvironment, immunotharapy

INTRODUCTION

With approximately 1.8 million new cases diagnosed annually, lung cancer remains the primary cause of cancer-related death globally (Ferlay et al., 2015). Non-small-cell lung carcinoma is the main histological type of lung cancer, and LUAD is the most common subtype. The reported 5-years survival rate of non-small-cell lung cancer patients across all stages of the disease is 26% (American Cancer Society, 2017). The rising incidence of lung cancer and poor survival of patients call for robust biomarkers to predict patient outcomes.

The extracellular matrix (ECM) is defined as the acellular component of tissues that can provide biochemical and biophysical support for cells. ECM genes can be broadly divided into core- and matrisome-related molecules. The major components of the ECM include collagens, glycoproteins, proteoglycans, and other molecules, such as hyaluronan and galectin. As a fundamental component of organisms, the ECM is essential for organ development and cell communication. The ECM is also an important constituent of solid tumors and can be altered through time and space to create a microenvironment that facilitates oncogenesis and progression (Peng et al., 2017; Pearce et al., 2018; Mierke, 2019; Cox, 2021). Alterations in the components or organization of the ECM can modulate a series of signaling pathways that regulate cell proliferation, differentiation, migration, and other behaviors (Nebuloni et al., 2016; Peng et al., 2017; Fattet et al., 2020). Some studies have revealed the prognostic role of ECM-related genes in cancer. An ECM-associated gene signature has been found to correlate with patient outcomes in early-stage non-small-cell lung cancer (Lim et al., 2017). Downregulation of lumican and decorin has been shown to be related to poor prognosis in breast malignancies (Troup et al., 2003).

Immunotherapy is an emerging and effective therapy for lung cancer, but the main challenge in immunotherapy is the low response rate of patients. Recent years have seen explosive growth in studies exploring approaches to predicting and augmenting the response to immunotherapy. Pancancer analysis has revealed that transforming growth factor (TGF)-β-associated ECM genes are reliable predictors of immunotherapy response (Chakravarthy et al., 2018).

Although ECM is significant in tumorigenesis and can be a potent indicator of survival, no attempt has been made to comprehensively explore the prognostic role of ECM-associated genes in LUAD. Therefore, this study aimed to explore the prognostic value of ERGs in LUAD and develop a classification system, based on the expression level of ERGs, to predict the survival of patients with LUAD.

MATERIALS AND METHODS

Data Acquisition and Differential Analysis

Transcriptional data were obtained from TCGA-LUAD dataset, GSE37745, GSE32863, and GSE43458. ERGs were identified from the Gene Ontology website (http://geneontology.org/) with the key word "extracellular matrix." The list of ERGs is provided in **Supplementary Table 1**. The package "edgeR" was used to preprocess the expression data in TCGA (Robinson et al., 2010; McCarthy et al., 2012; Chen et al., 2016), including discarding genes with expression less than five in all samples and normalizing the expression data. Genes that met the filtering criteria of adjusted p value (false discovery rate) < 0.05 and $|\log_2$ fold change$| > 2.0$ were considered dysregulated ERGs.

Identification of Prognostic Extracellular Matrix-Related Genes and Construction of a Prognostic Signature

To screen prognostic genes from the differentially expressed ERGs, univariate Cox regression analysis was conducted with the "survival" package (Therneau et al., 2000). As a common machine learning method, LASSO Cox regression analysis can properly handle multicollinearity and is frequently applied to construct prognostic signatures (Gui and Li, 2005; Wang and Liu, 2020). Thus, LASSO regression analysis was performed with the "glmnet" package to screen prognostic genes further and create a prognostic signature that was presented as a formula (Friedman et al., 2010). The ECMRS of each sample was calculated using regression coefficients and mRNA levels of prognostic ERGs in the formula. The classification of patients into high-risk and low-risk groups was based on the median ECMRS.

Validation of the Prognostic Signature

The discovery cohort was randomly divided into two subsets (N1 = 240, N2 = 239) to test the prognostic potential of the signature. The prognostic performance of the signature was further evaluated in the entire discovery cohort (N = 479) and external testing cohort (GSE37745, N = 196). Kaplan–Meier

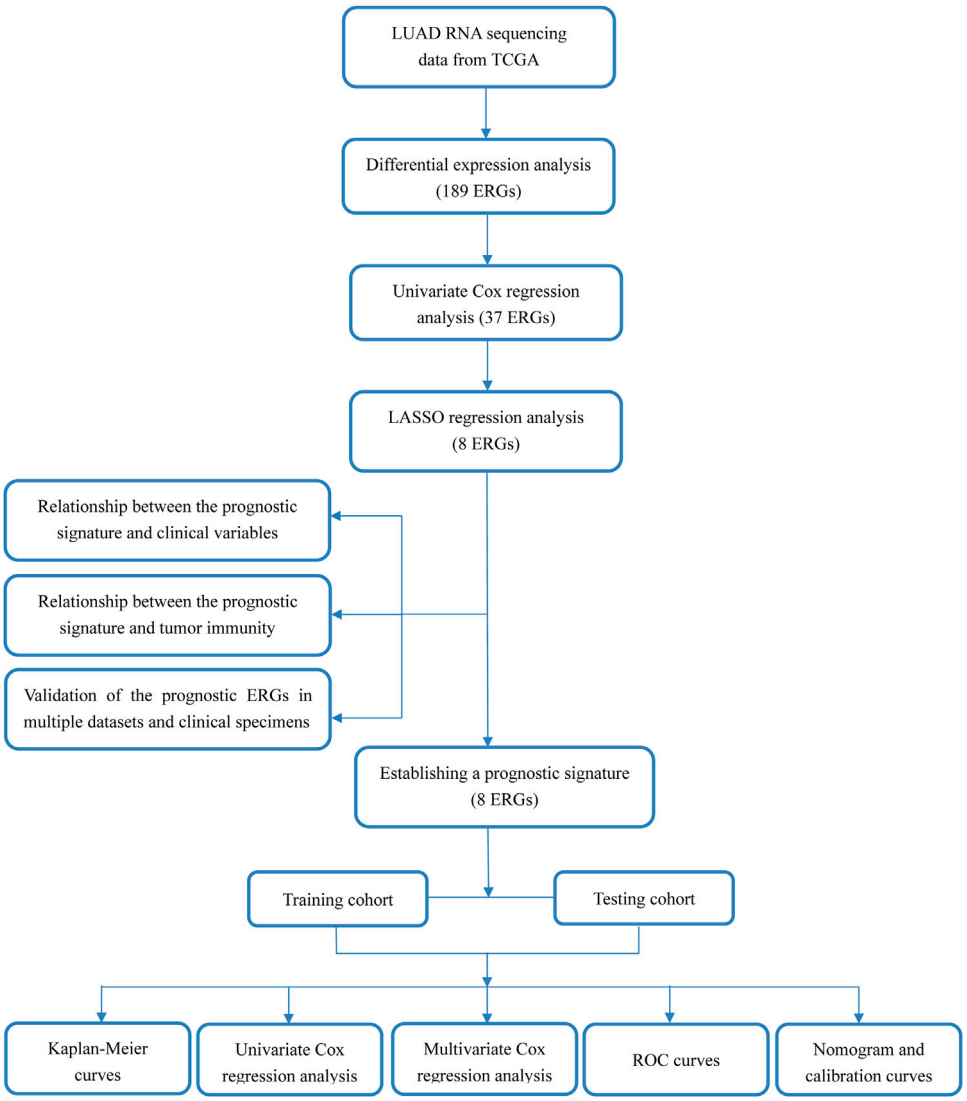

FIGURE 1 | Work flow of this study.

survival curves were generated to compare overall survival (OS) between the high- and low-risk patients based on the log-rank test. Next, univariate and multivariate Cox regression analyses were conducted to assess the effects of ECMRS on OS by using the "survival" packages (Therneau et al., 2000). ROC curves were created to evaluate the power of the signature in OS prediction with the "timeROC" package (Blanche et al., 2013).

Evaluation of Association Between ECMRS and Clinicopathological Variables

The difference in ECMRS among patients stratified by clinical parameters was evaluated to elucidate the effect of ECMRS on cancer progression. Moreover, the survival probability of LUAD patients stratified by clinicopathological variables was assessed using Kaplan–Meier curves to explore whether the prognostic value of our signature changed with clinical parameters.

Assessment of the Relationship Between ECMRS and Immunophenotypes

ESTIMATE is an algorithmic tool that can calculate tumor purity and the abundance of cells in the TME, including immune cells and stromal cells (Yoshihara et al., 2013). Here, the ESTIMATE algorithm was run to obtain the immune score, stromal score, and ESTIMATE score of each patient with the "estimate" package. Immune cells infiltrating the TME of TCGA-LUAD were identified from TIMER (Li

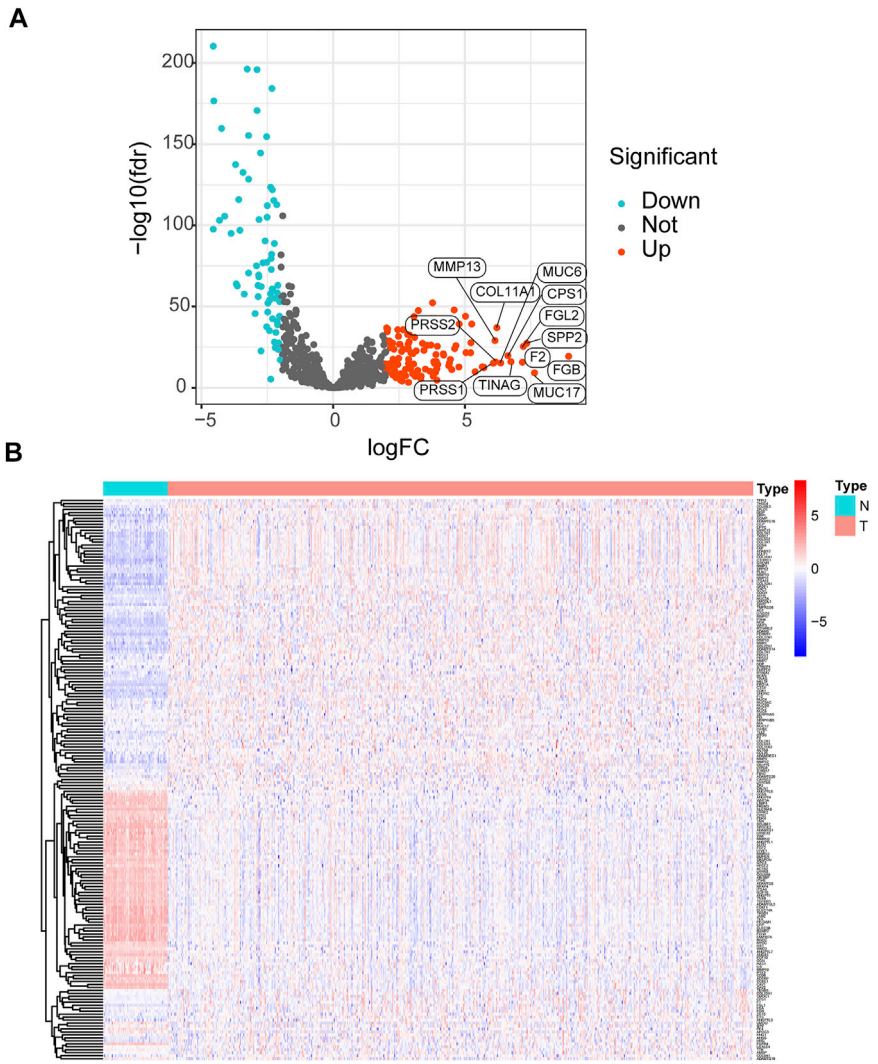

FIGURE 2 | Analysis of differentially expressed ERGs **(A)** Volcano plot of differentially expressed ERGs, showing the FDR and log2-fold change of each gene **(B)** The heatmap shows the distribution of 189 differentially expressed ERGs between LUAD and normal lung tissues. ERGs = extracellular matrix-related genes; FDR = false discovery rate; LUAD = lung adenocarcinoma.

et al., 2016; Li et al., 2020a) (http://timer.comp-genomics.org/). ssGSEA was performed using the R package "GSVA" to further identify the related immune processes of the signature in both TCGA and GEO cohorts (Subramanian et al., 2005; Hänzelmann et al., 2013). The relationship between the prognostic signature and immune checkpoint gene expression was also explored. Comparison of all these results between the low- and high-risk patients was done using Wilcox test.

Visualization of the Prognostic Signature

To visualize our prognostic signature, a nomogram was established based on ECMRS for survival prediction by using the "rms package." Additionally, calibration curves at 3 and 5 years were created to show the predictive accuracy of the nomogram.

Validation of the Prognostic Extracellular Matrix-Related Genes

Differential expression analysis was performed in GSE43458 [N (Normal) = 30, N (Tumor) = 80] and GSE32863 [N (Normal) = 58, N (Tumor) = 58] with the "limma" package to verify whether the ERGs in the signature were also differentially expressed in other datasets (Ritchie et al., 2015; Phipson et al., 2016). The Human Protein Atlas (HPA) database is a tool developed to map the proteome of human tissues and cancers (https://www.proteinatlas.org/) (Uhlén et al., 2015; Uhlen et al., 2017). Immunohistochemistry images of LUAD and normal lung tissues were acquired from the HPA database to validate the protein expression of the prognostic ERGs. The effects of these ERGs on the survival of patients with LUAD were validated

TABLE 1 | Results of univariate cox regression analysis in the TCGA cohort.

Gene	HR	95% CI	Pvalue
ADAM12	1.054	1.009–1.101	0.019
ADAM8	1.012	1.000–1.024	0.050
ADAMTS8	0.771	0.655–0.908	0.002
AHSG	1.728	1.298–2.299	<0.001
APOC3	1.046	1.009–1.085	0.015
BCAN	1.049	1.000–1.101	0.050
CAV1	1.003	1.000–1.005	0.021
CAV2	1.016	1.005–1.026	0.003
CDK1	1.024	1.008–1.041	0.004
CLEC14A	0.973	0.948–0.998	0.036
COCH	1.043	1.004–1.083	0.029
COL22A1	1.106	1.025–1.194	0.010
COL6A6	0.751	0.609–0.926	0.008
COL7A1	1.027	1.001–1.054	0.043
COL9A1	1.916	1.184–3.101	0.008
CPS1	1.003	1.001–1.005	0.001
CTSV	1.024	1.006–1.043	0.010
ENTPD2	1.100	1.043–1.161	<0.001
F12	1.109	1.030–1.194	0.006
FAM107A	0.935	0.878–0.996	0.037
FBN2	1.037	1.018–1.055	<0.001
FERMT1	1.041	1.020–1.062	<0.001
FGA	1.000	1.000–1.001	0.039
FGF2	1.227	1.062–1.417	0.005
FOXF1	0.890	0.800–0.990	0.032
GDF10	0.887	0.794–0.990	0.033
HPSE2	0.416	0.206–0.840	0.014
ITGA8	0.860	0.780–0.949	0.003
JAM2	0.829	0.716–0.960	0.012
LYPD3	1.013	1.006–1.020	<0.001
MFAP4	0.993	0.988–0.998	0.006
RGCC	0.992	0.986–0.999	0.024
SERPINB5	1.024	1.011–1.036	<0.001
SMOC1	1.016	1.006–1.027	0.002
TEK	0.893	0.808–0.988	0.028
TINAG	1.144	1.052–1.245	0.002
ZG16	1.174	1.016–1.355	0.029

TCGA, the cancer genome atlas; HR, hazard ratio; CI, confidence interval.

using Kaplan–Meier plotter (http://kmplot.com/analysis/) (Győrffy, 2021).

Clinical Specimen Collection

Human lung adenocarcinoma tissues and paired peritumoral lung tissues were collected from 12 patients who underwent surgical resection at the Thoracic Surgery Department of Wuhan Tongji Hospital between March 2021 and August 2021. Written informed consent was obtained from all the 12 patients. All patients were histopathologically diagnosed with LUAD and had not received any antitumor therapy before surgery.

RNA Extraction and qRT–PCR

Fresh LUAD tissues and peritumoral lung tissues were frozen in liquid nitrogen and stored at -80°C until RNA extraction. After thawing the tissues, total RNA was extracted using TRIzol reagent (Takara, Otsu, Japan) according to the manufacturer's protocol. cDNA was synthesized using Hiscript@ Q RT SuperMix (Vazyme, Nanjing, China) and used for quantitative polymerase chain reaction detection with SYBR Green SuperMix (Vazyme, Nanjing, China). Quantitative reverse transcription polymerase chain reaction was performed under the following conditions: 95°C for 60 s, 40 cycles of 95°C for 5 s, and 50°C–60°C for 15 s mRNA levels were normalized to the expression of endogenous GAPDH. The primer sequences are provided in **Supplementary Table 2**.

TABLE 2 | Clinicopathological parameters of TCGA cohort and GEO cohort.

Characteristics	TCGA cohort (n = 479)	GEO cohort (n = 196)
Age (years), n (%) <65 ≥ 65	213 (44.47) 266 (55.53)	94 (47.96) 102 (52.04)
Gender, n(%)		
Male	219 (45.72)	107 (54.59)
Female	260 (54.28)	89 (45.41)
Stage, n (%)		
I	259 (54.07)	130 (66.33)
II	117 (24.43)	35 (17.86)
III	78 (16.28)	27 (13.78)
IV	25 (5.22)	4 (2.04)
Survival status, n (%)		
Dead	177 (36.95)	51 (26.02)
Alive	302 (63.05)	145 (73.98)

TCGA, the cancer genome atlas; GEO, gene expression omnibus.

RESULTS

Dysregulated Extracellular Matrix-Related Genes of Lung Adenocarcinoma

The workflow of the study is displayed in **Figure 1**. The expression data of 539 LUAD tissues and 59 normal lung tissues were downloaded and analyzed. A total of 189 dysregulated ERGs were identified in LUAD from 953 ERGs, with 119 upregulated genes and 70 downregulated genes (**Figures 2A, B**).

Construction of a Prognostic Signature

The differentially expressed ERGs were subjected to univariate Cox regression analysis to obtain 37 prognostic genes (**Table 1**). The prognostic ERGs were further screened by LASSO regression analysis, and a prognostic signature was constructed based on these prognostic ERGs. The final signature was fit with eight key prognostic genes (*FERMT1*, *CTSV*, *CPS1*, *ENTPD2*, *SERPINB5*, *ITGA8*, *ADAMTS8*, and *LYPD3*). Among these prognostic genes, *FERMT1* (hazard ratio (HR) = 1.041, $p < 0.001$), *CTSV* (HR = 1.024, $p = 0.010$), *CPS1* (HR = 1.003, $p = 0.001$), *ENTPD2* (HR = 1.100, $p < 0.001$), *SERPINB5* (HR = 1.024, $p < 0.001$), and *LYPD3* (HR = 1.013, $p < 0.001$) were indicators of poor prognosis, whereas survival was positively affected by ITGA8 (HR = 0.860, $p = 0.003$) and *ADAMTS8* (HR = 0.771, $p = 0.002$) (**Table 1**). The predictive signature was created as a formula, and the ECMRS of each patient was estimated with regression co-efficient and mRNA levels of the prognostic ERGs in the formula (**Supplementary Table 3**). The median ECMRS was set as the threshold to classify patients into high and low-risk groups (**Supplementary Table 4-5**).

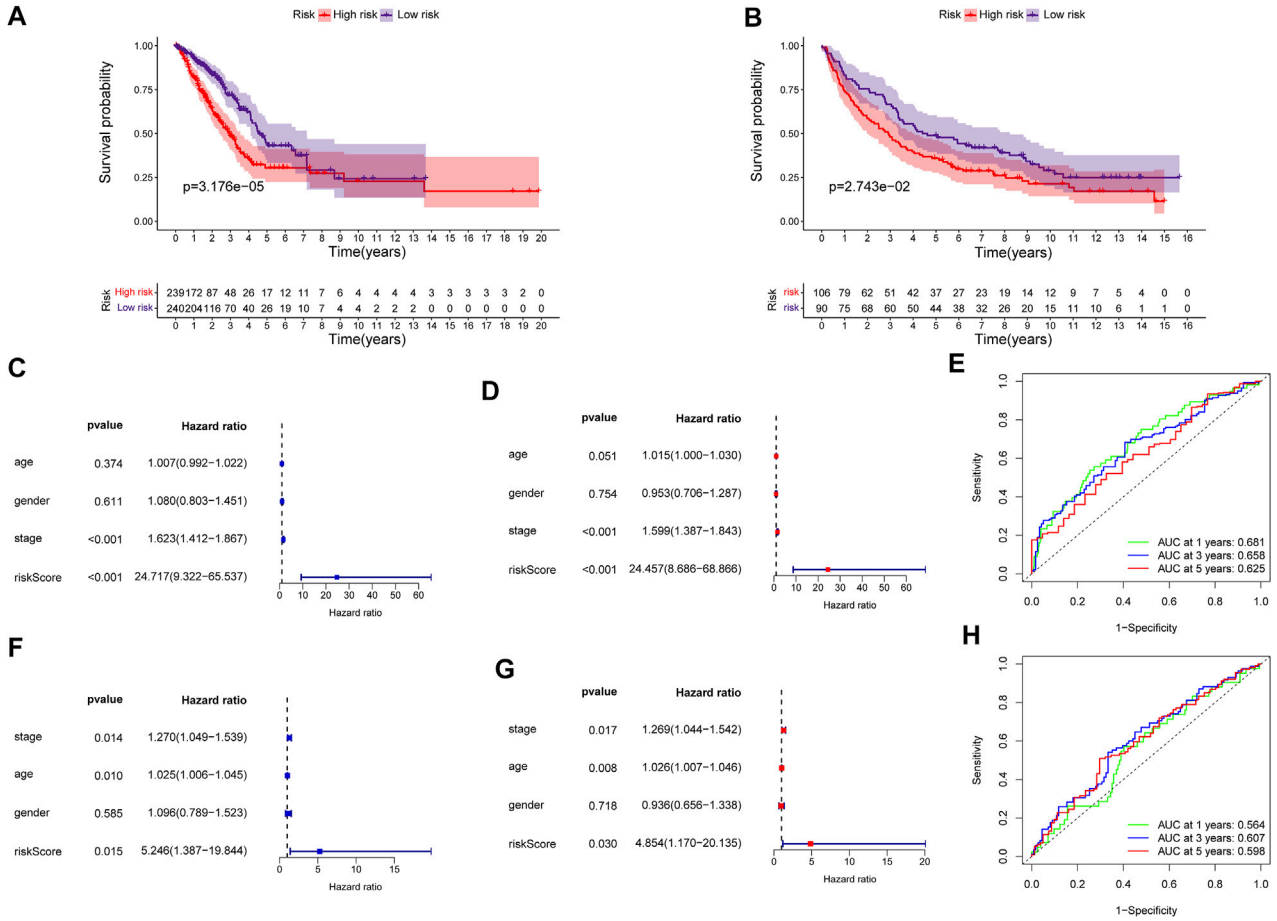

FIGURE 3 | Validation of the prognostic signature in the entire TCGA and GEO cohorts **(A)** Kaplan–Meier survival curve of the high- and low-risk groups in the entire TCGA cohort **(B)** Kaplan–Meier survival curve of the high- and low-risk groups in the GEO cohort **(C)** Univariate Cox regression analysis of clinicopathological variables and ECMRS in the entire TCGA cohort **(D)** Multivariate Cox regression analysis of clinicopathological variables and ECMRS in the entire TCGA cohort **(E)** ROC curves of one-, three- and five- years in the entire TCGA cohort indicating the predictive ability of ECMRS **(F)** Univariate Cox regression analysis of ECMRS and clinicopathological variables in the GEO cohort **(G)** Multivariate Cox regression analysis of ECMRS and clinicopathological variables in the GEO cohort **(H)** ROC curves of one-, three- and five- years in the GEO cohort indicating the predictive ability of ECMRS. TCGA = The Cancer Genome Atlas; GEO = Gene Expression Omnibus; ECMRS = extracellular matrix-related score.

Validation of the Prognostic Signature in The Cancer Genome Atlas and Gene Expression Omnibus

The predictive power of the ECMRS was verified in the discovery cohort and GSE37745. **Table 2** presents the clinical characteristics of the discovery cohort and GSE37745. Patients with low ECMRS were likely to live longer in both the discovery cohort (**Figure 3A**) and GSE37745 (**Figure 3B**). The results of univariate Cox regression analysis demonstrated that survival was adversely affected by ECMRS in the TCGA cohort (HR = 24.717, $p < 0.001$) (**Figure 3C**) and GSE37745 (HR = 5.246, $p = 0.015$) (**Figure 3F**). Consistent with the univariate Cox regression analysis, the results of multivariate Cox regression analysis also suggested that the adverse impact of ECMRS on prognosis in the discovery cohort (HR = 24.457, p value <0.001) (**Figure 3D**) and GSE37745 (HR = 4.854, $p = 0.030$) (**Figure 3G**) was independent of age, sex, and disease stage. ROC curves for 1, 3, and 5 years were plotted to evaluate the predictive power of our signature. The areas under the curve (AUCs) for 1, 3, and 5 years were 0.681, 0.658, and 0.625, respectively, in the TCGA cohort (**Figure 3E**). The AUCs for 1, 3, and 5 years were 0.564, 0.607, and 0.598, respectively, in the GEO cohort (**Figure 3H**). The results of Kaplan–Meier curves and Cox regression analysis in the two subsets of the TCGA cohort (**Figure 4**) were consistent with these results in the entire discovery cohort and GSE37745. 95% Confidence interval (CI) of the AUCs in the TCGA and GEO cohorts are displayed in **Supplementary Figure 1.**

The Extracellular Matrix-Related Score Was Related to Clinical Variables

The difference in ECMRS in patients stratified by clinicopathological features was evaluated to show the connection between the prognostic signature and progression

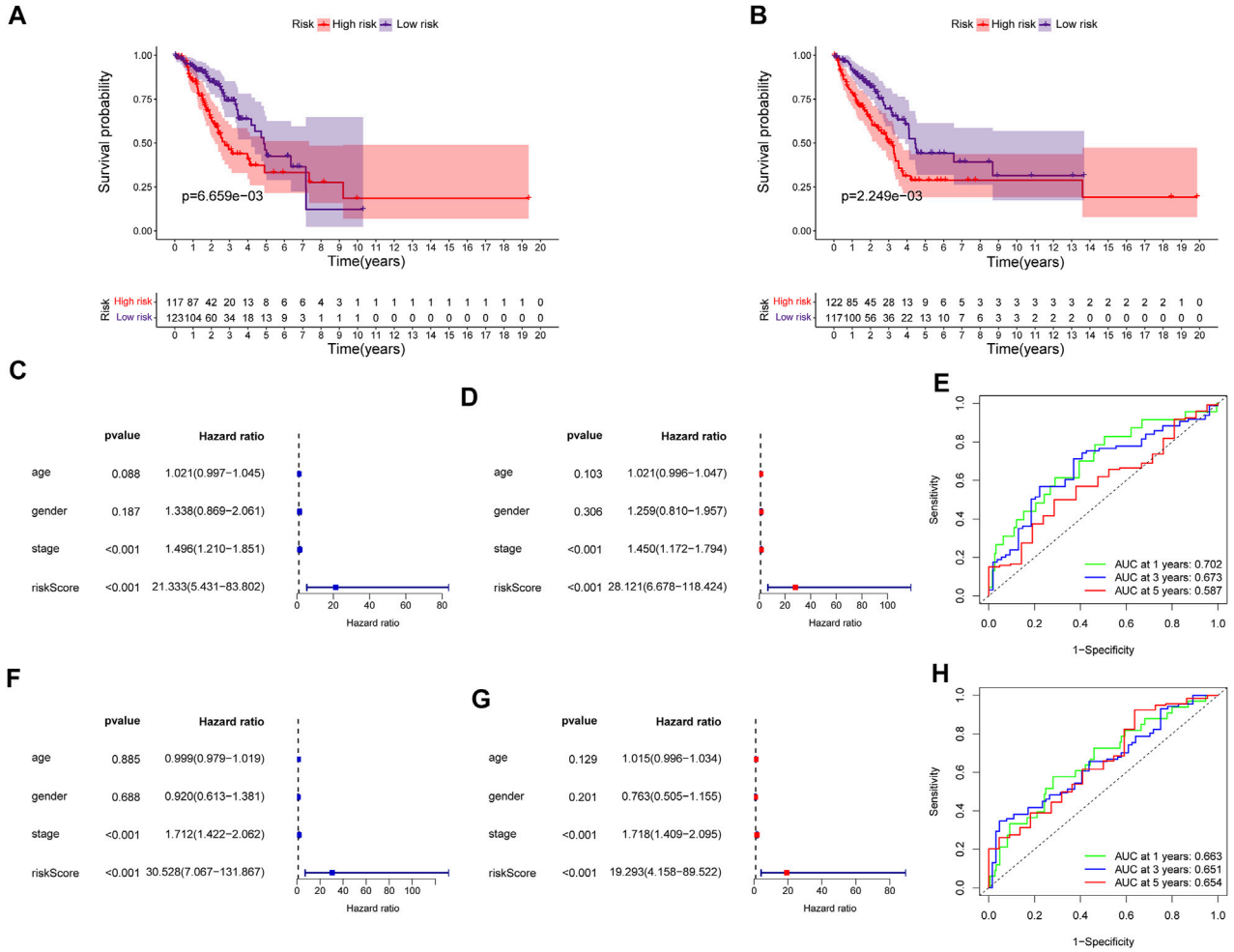

FIGURE 4 | Validation of the prognostic signature in the two subsets of the TCGA cohort **(A)** Kaplan–Meier survival curve of the high- and low-risk groups in subset one of the TCGA cohort **(B)** Kaplan–Meier survival curve of the high- and low-risk groups in subset two of the TCGA cohort **(C)** Univariate Cox regression analysis of clinicopathological variables and ECMRS in subset one of the TCGA cohort **(D)** Multivariate Cox regression analysis of clinicopathological variables and ECMRS in subset one of the TCGA cohort **(E)** ROC curves of one-, three- and five- years in subset one of the TCGA cohort indicating the predictive ability of ECMRS **(F)** Univariate Cox regression analysis of ECMRS and clinicopathological variables in subset two of the TCGA cohort **(G)** Multivariate Cox regression analysis of ECMRS and clinicopathological variables in subset two of the TCGA cohort **(H)** ROC curves of one-, three- and five- years in subset two of the TCGA cohort indicating the predictive ability of ECMRS. TCGA = The Cancer Genome Atlas; GEO = Gene Expression Omnibus; ECMRS = extracellular matrix-related score.

of LUAD (**Figure 5**). The results demonstrated that ECMRS was related to sex ($p < 0.001$), T stage ($p < 0.001$), N stage ($p = 0.0073$), and M stage ($p = 0.027$). Male patients and patients in the advanced tumor, node, and metastasis (TNM) stage had higher ECMRS. Survival curves of patients stratified by clinicopathologic features suggested that survival time was longer in patients with low ECMRS than in those with high ECMRS, and the prognostic value of the signature was not affected by clinical parameters (**Figure 6**).

The Prognostic Signature can Affect Tumor Immunity

The ECM is a vital determinant of antitumor immunity in solid tumors. Here, we speculated that our prognostic signature was associated with tumor immunity in patients with LUAD. To verify this speculation, we obtained the immune score, stromal score, and ESTIMATE score of each patient and found that the low-risk patients had significantly higher ESTIMATE score ($p < 0.001$) (**Figure 7A**), immune score ($p < 0.001$) (**Figure 7B**), and stromal score ($p < 0.001$) (**Figure 7C**) than the high-risk patients, which meant that the low-risk patients had higher degree of infiltration of antitumor immune cells and lower tumor purity in the TME than high-risk patients. Although the immune score was higher in patients with low ECMRS than in those with high ECMRS, the fraction of each immune component between the two groups remains unknown. Therefore, fractions of tumor-infiltrating immune cells in patients with LUAD were acquired from TIMER to evaluate their relationship with ECMRS. Patients with low

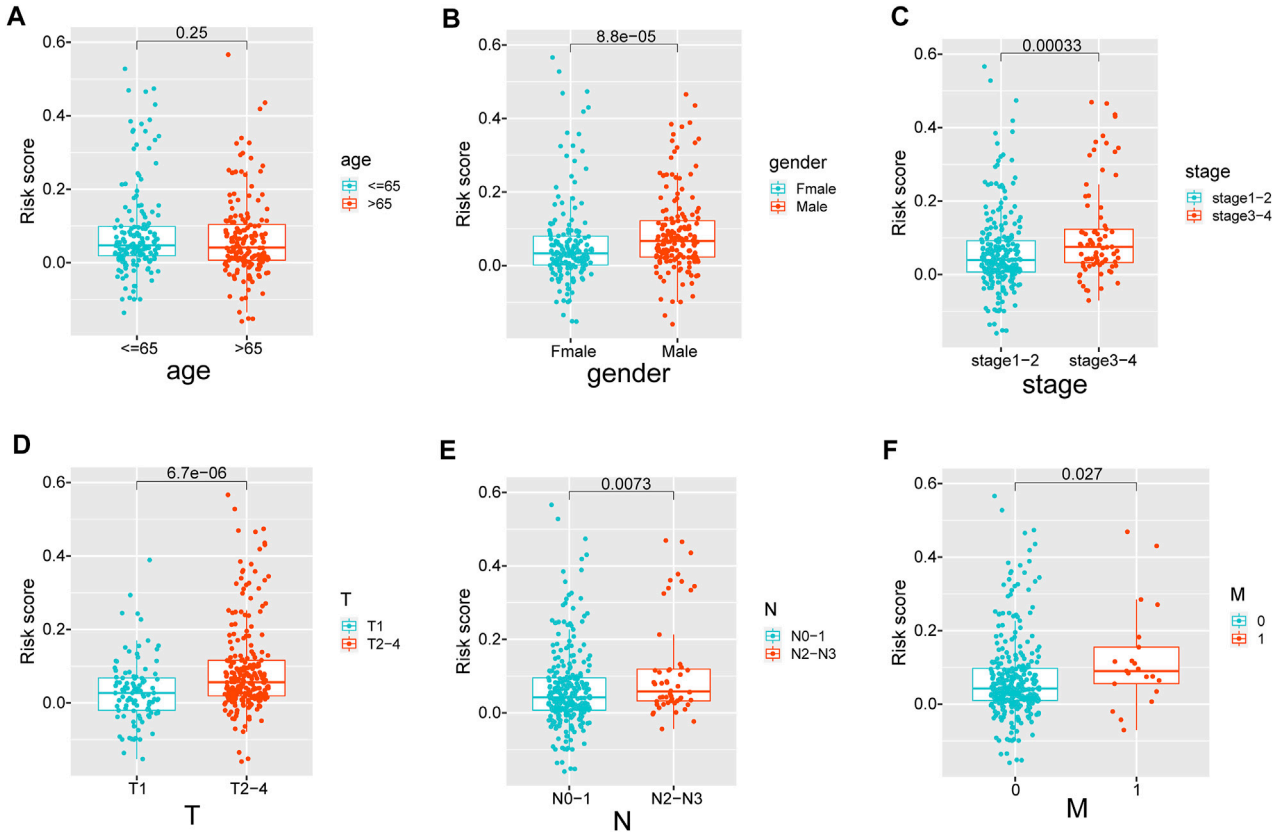

FIGURE 5 | (A–F) The difference in ECMRS between patients stratified by clinicopathological variables. ECMRS = extracellular matrix-related score.

ECMRS had higher degree of infiltration of $CD8^+$ T cells ($p < 0.001$), $CD4^+$ T cells ($p < 0.001$), B cells ($p < 0.001$), neutrophils ($p < 0.001$), macrophages ($p < 0.001$), and dendritic cells (DCs) ($p < 0.001$) than those with high ECMRS (**Figure 7D**). Next, to confirm the difference in immune cells present in the TME between the low- and high-risk patients and to identify the immune processes involved in the prognostic signature, ssGSEA was conducted in TCGA and GSE37745. The ssGSEA results suggested that patients with low ECMRS had more B cells, dendritic cells, macrophages, neutrophils, and mast cells in the TME than those with high ECMRS in both the TGGA (**Figure 7E**) and GEO cohorts (**Figure 7G**). The low-risk patients also had higher expression of chemokine receptors and human leukocyte antigen, and stronger response to antigen-presenting cell co-stimulation and interferon than the high-risk patients in both the TCGA cohort (**Figure 7F**) and GSE37745 (**Figure 7H**).

We also illustrated the relationship between ECMRS and the expression of key immune checkpoint genes. Patients with low ECMRS had higher expression of PD-L1, CTLA4, TIM3, and BTLA (**Figures 8A, B, D**) than those with low ECMRS, whereas no significant difference was observed in the expression of PD-1 between the two groups (**Figure 8C**). Among the immune checkpoint genes that were associated with ECMRS, the expressions of BTLA (HR = 0.852, $p = 0.0232$) (**Figure 8E**), CD47 (HR = 0.874, $p = 0.0535$) (**Figure 8F**), and CTLA4 (HR = 0.845, $p = 0.0178$) (**Figure 8G**) were associated with survival. High expression of CTLA4, BTLA, and CD47 was observed in low-risk patients and was positively related to survival duration, which confirmed our finding that ECMRS is an indicator of poor survival in patients with LUAD.

Establishment of a Nomogram

A nomogram was constructed to visualize the prognostic signature, providing a reference for clinical applications (**Figure 9A**). Calibration curves at 3 and 5 years indicated that the nomogram could accurately predict OS (**Figures 9B,C**).

Validation of the Prognostic Extracellular Matrix-Related Genes in Clinical Specimens and Multiple Databases

To assess the differential expression of the prognostic ERGs, polymerase chain reaction was conducted in 12 paired LUAD and peritumoral lung tissues collected at our institute. *ITGA8* and *ADAMTS8* were downregulated in tumor tissues, whereas *FERMT1*, *CTSV*, *CPS1*, *ENTPD2*, *SERPINB5*, and *LYPD3* were upregulated in tumor tissues (**Figure 10**).

Differential expression of the prognostic ERGs was also validated in the GSM43458 and GSM32863 datasets

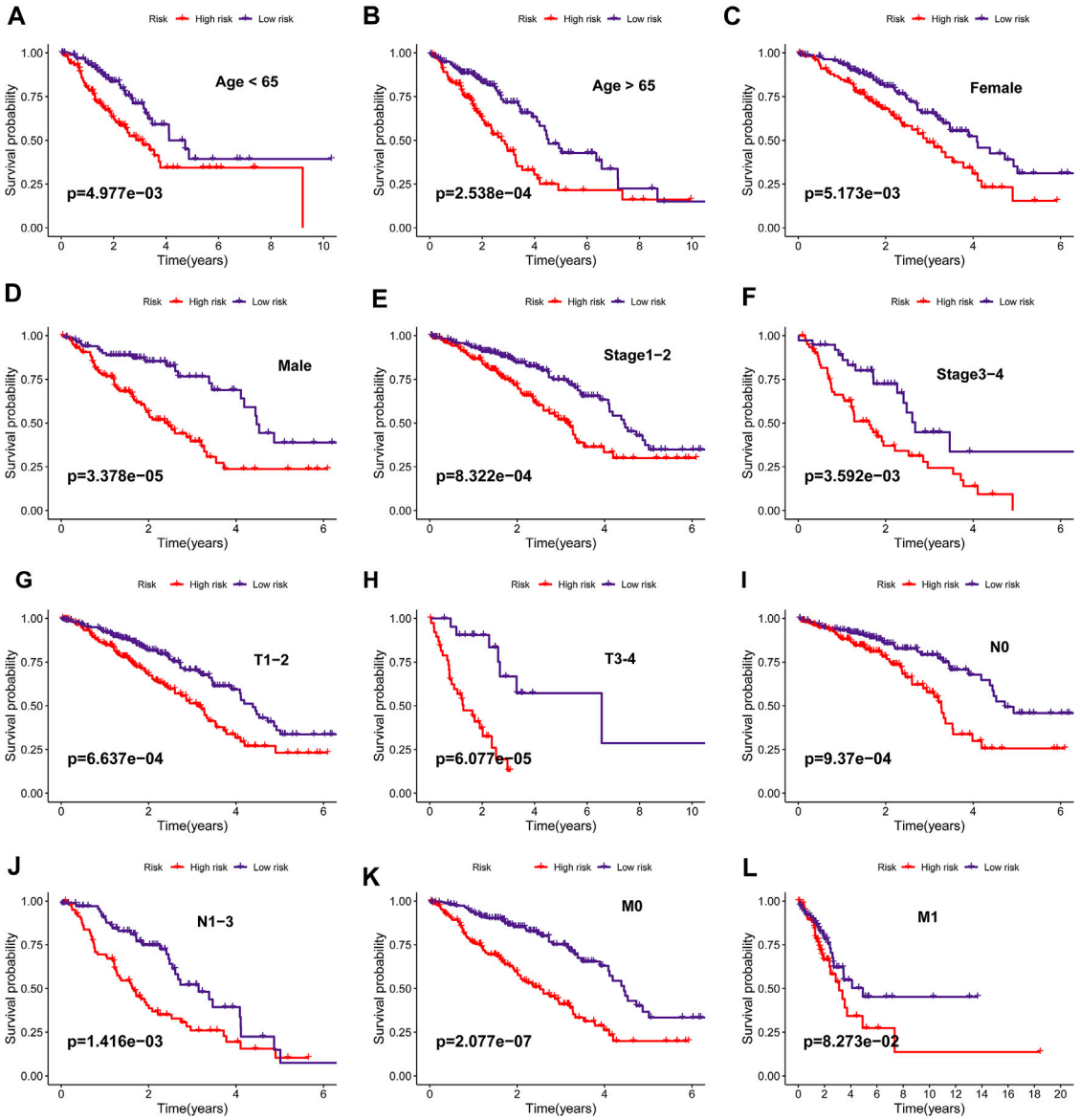

FIGURE 6 | (A–L) Kaplan–Meier survival curves of overall survival between high- and low-risk groups in patients stratified by clinicopathological variables (age, sex, stage, T stage, N stage, M stage).

(**Supplementary Figure 2**), which is consistent with the polymerase chain reaction results. The immunohistochemistry images of *ENDPT2* , *FERMT1* , *SERPINB5*, *ITGA8*, *ADAMTS8* and *CPS1* were collected from HPA, which further verified differential expression of these prognostic genes between LUAD and normal lung tissues **(Supplementary Figure 3)**. However, ADAMTS8 were not detected in both LUAD and normal lung tissues, which may be attributed to its low expression. The prognostic value of the eight genes was validated using the Kaplan–Meier plotter. Patients with high expression of *ITGA8* or *ADAMTS8* survived longer than those with low expression of *ITGA8* or *ADAMTS8*, whereas high expression of *FERMT1*, *CTSV*, *CPS1*, *ENTPD2*, *SERPINB5*, and *LYPD3* was associated with shorter survival duration (**Supplementary Figure 4**).

DISCUSSION

The ECM is a fundamental component of the TME, and its alterations can affect the phenotypes and immune environment of cancer cells. Perturbation of the biochemical and mechanical properties of the ECM can affect cell behavior through transmembrane receptors, such as integrins and syndecans. Desmoplastic response is common in solid tumors and is characterized by excessive deposition of ECM proteins, which

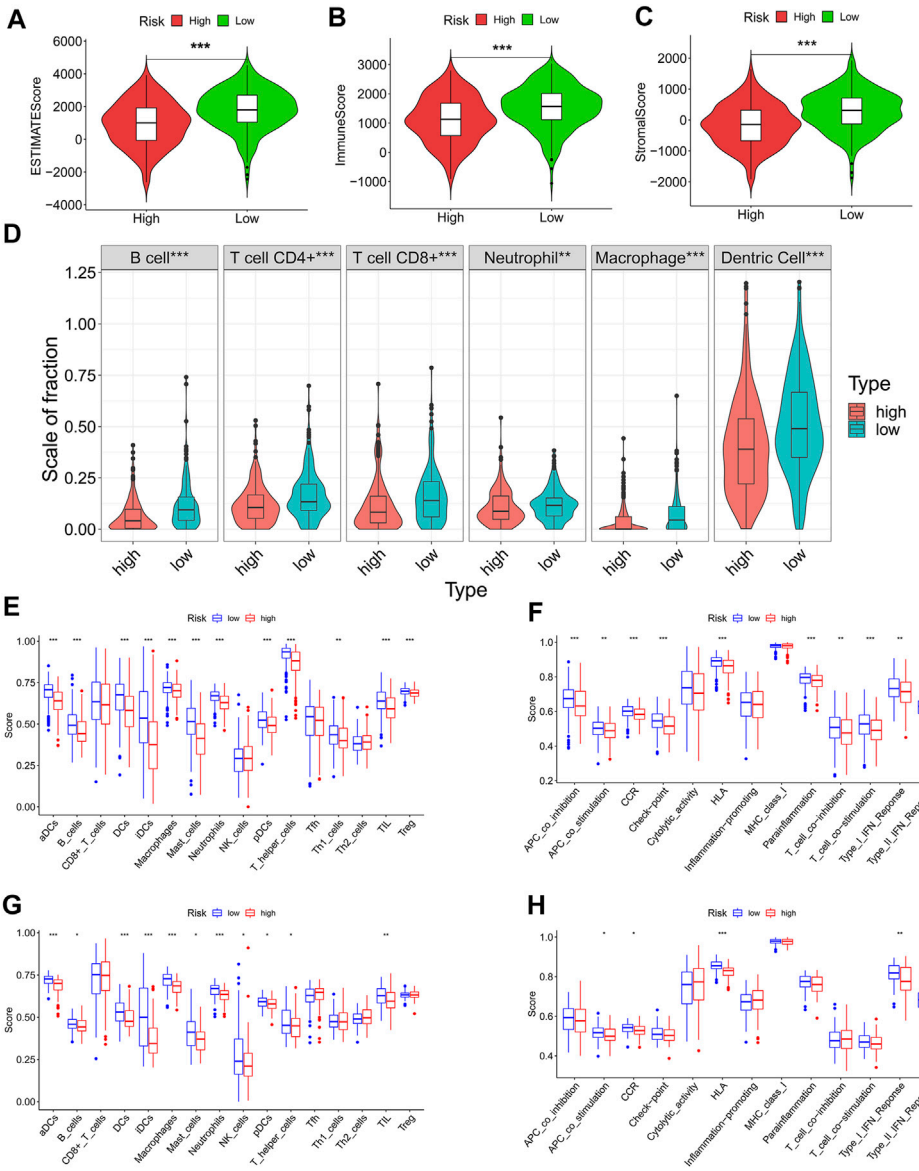

FIGURE 7 | Differences in immune cells and immune functions between the high- and low-risk groups **(A-C)** ESTIMATE score, immune score, and stromal score between the high- and low-risk groups **(D)** Infiltration degree of immune cells between the high- and low-risk groups in TCGA cohort based on TIMER **(E)** Fraction of immune cells between the high- and low-risk groups based on ssGSEA in the TCGA cohort **(F)** Immune functions between the high- and low-risk groups based on ssGSEA in the TCGA cohort **(G)** Fraction of immune cells between the high- and low-risk groups based on ssGSEA in the GEO cohort **(H)** Immune functions between the high- and low-risk groups based on ssGSEA in the GEO cohort. TCGA = The Cancer Genome Atlas; GEO = Gene Expression Omnibus; $^{*}p < 0.05$; $^{**}p < 0.01$; $^{***}p < 0.001$.

has been suggested to be a feature of poor prognosis (Sundqvist et al., 2020). Cancer cells have to migrate through the ECM to spread to other parts of the body; therefore, metastasis can be affected if the biophysical properties of the ECM, such as deformability or stiffness, are changed. Remodeled and stiffened ECM has been shown to promote the dissemination of cancer cells (Han et al., 2016; Miroshnikova et al., 2017). Furthermore, the ECM is a reservoir for cytokines and controls their distribution and interaction with cells (Huleihel et al., 2016). In addition, ECM can serve as a protective shield against host antitumor immunity in solid tumors, thereby impeding the infiltration of lymphocytes and reducing the efficacy of immunotherapy. Changes in TME and tumor behavior can be fully reflected by perturbations in the ECM. Thus, ECM-related biomarkers have enormous potential for prognostication.

In this study, eight key prognostic ERGs (*FERMT1*, *CTSV*, *CPS1*, *ENTPD2*, *SERPINB5*, *ITGA8*, *ADAMTS8*, and *LYPD3*) were identified by stepwise statistical analyses to construct a prognostic signature for patients with LUAD. Among these genes, *ITGA8* and *ADAMTS8* were downregulated in LUAD

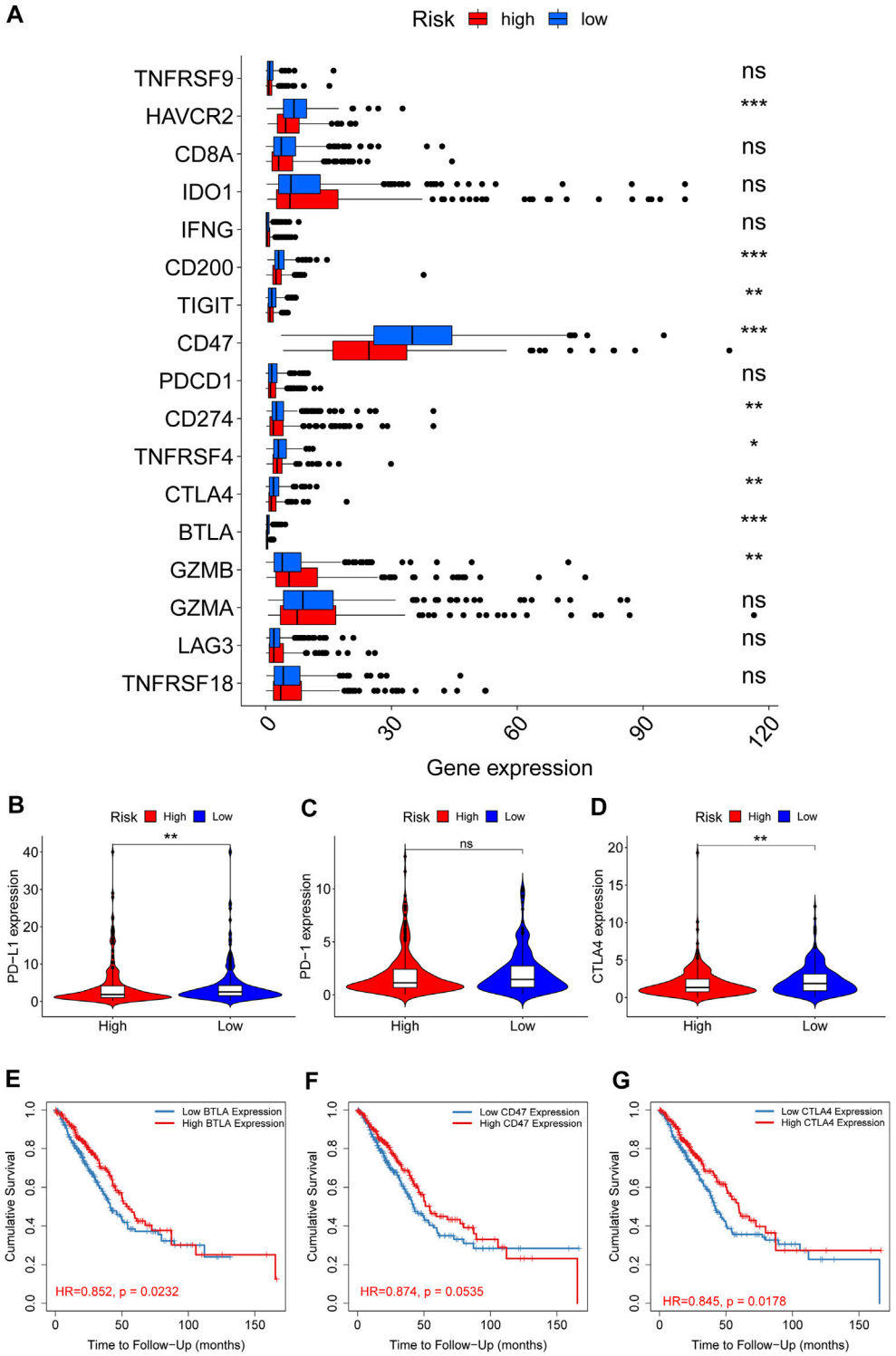

FIGURE 8 | Differences in the expression of immune checkpoint genes between the high- and low-risk groups **(A)** Box plots show the difference in the expression of immune checkpoint genes between the high- and low-risk group **(B–D)** Violin plots show the difference in the expression of PD-L1, PD-1, and CTLA4 between the high- and low-risk groups **(E–G)** Survival curves of BTLA, CD47, and CTLA4 in TIMER. *$p < 0.05$; **$p < 0.01$; ***$p < 0.001$.

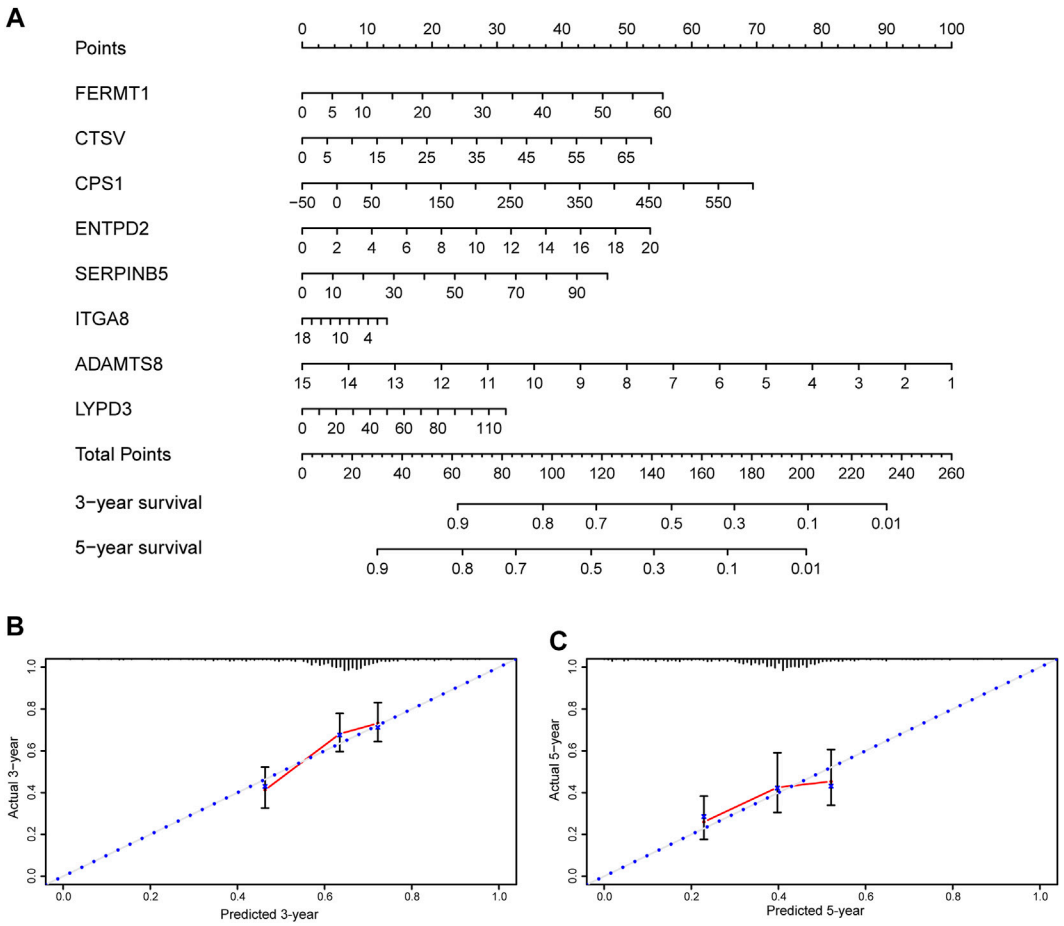

FIGURE 9 | Nomogram and calibration plots of the prognostic signature **(A)** Nomogram based on eight prognostic ERGs predicting the overall survival probability of patients with lung adenocarcinoma **(B,C)** The three- and five-years calibration plots of the nomogram. ERGs = extracellular matrix-related genes.

tissues and functioned as tumor suppressor genes, whereas the remaining genes were oncogenes. Although only few studies have highlighted the functions of these eight genes in the development of LUAD, their vital function in other cancers has been delineated by numerous studies. *FERMT1* encodes the kindlin-1 protein, which mediates integrin activation and cell adhesion. Evidence has shown that kindlin-1 facilitates integrin-mediated TGF-β activation (Rognoni et al., 2014). Upregulation of *FERMT1* promotes the progression of gastric cancer (Fan et al., 2020). Liu et al. found that *FERMT1* was overexpressed in colon adenocarcinoma, promoting epithelial-mesenchymal transition and metastasis (Liu et al., 2017). Yan et al. found that *FERMT1* is overexpressed in esophageal cancer and facilitates the proliferation of cancer cells (Yan et al., 2019). Cathepsin V (*CTSV*/*CTSL2*) is a cysteine proteinase that can degrade some constituents of the ECM and has been found to be related to the malignancy of tumor cells and the prognosis of patients with breast cancer (Toss et al., 2020; Wang et al., 2020). Carbamoyl-phosphate synthetase 1 (*CPS1*) not only serves as a crucial catalyst in the urea cycle but also functions in the progression of cancer. Studies have demonstrated that *CPS1* is downregulated in hepatocellular carcinoma and that its decline could lead to poor survival (Ridder et al., 2021). *CPS1* has also been identified as a biomarker of progression in colorectal cancer (Palaniappan et al., 2016). *ENTPD2* was found to be elevated in hepatocellular carcinoma, indicating an unfavorable prognosis for patients. Additionally, *ENTPD2* has been proven to impede the differentiation of myeloid-derived suppressor cells, which can induce immunosuppression in hepatocellular carcinoma. Inhibition of *ENTPD2* could augment the efficacy of immunotherapy (Chiu et al., 2017). A disintegrin and metalloproteinase with thrombospondin motifs 8 (*ADAMTS8*) is a secreted protein that functions in the degradation of the ECM. Similar to matrix metalloproteinases, adamalysins are enzymes that can cause degradation and crosslinking of the ECM. *SERPINB5* belongs to the serpin superfamily which can regulate degradation of structural elements of the ECM such as collagens and hyaluronan. *SERPINB5* has been reported to mediate invasion of cancer cell and identified as an oncogene in multiple tumors (Chang et al., 2018; Atay, 2020). *ADAMTS8* has been reported to function as a tumor suppressor gene in various solid tumors (Zhao et al., 2018;

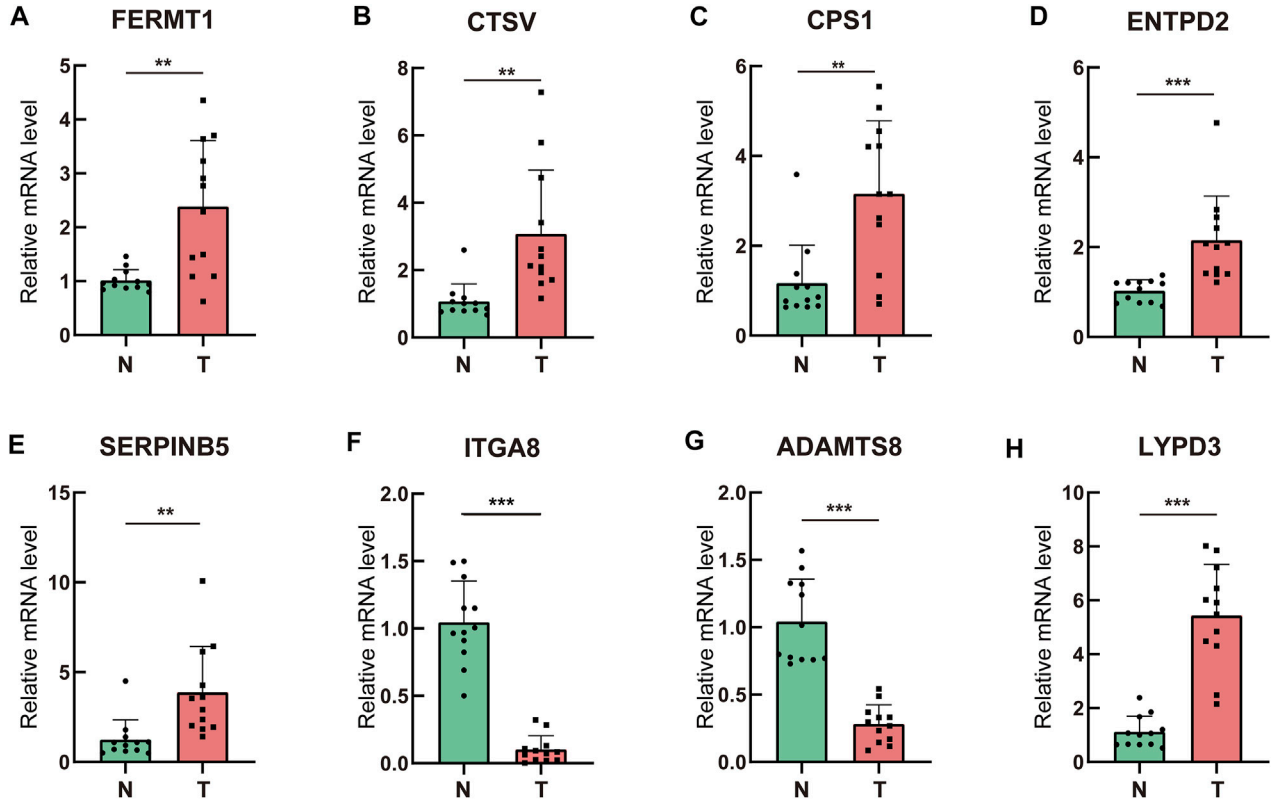

FIGURE 10 | Validation of the prognostic ERGs in clinical specimens by qRT-PCR **(A–H)** Differential expression of the prognostic ERGs between lung adenocarcinoma tissues and paired adjacent normal lung tissues.ERGs = extracellular matrix-related genes; * $p < 0.05$; ** $p < 0.01$; *** $p < 0.001$.

Li et al., 2020b; Wu et al., 2020). In our study, *ADAMTS8* was downregulated in LUAD tissues and correlated with favorable outcomes, which is consistent with previous findings. ITGA8 belongs to the ITGA subfamily of integrins. Apart from mediating cell-cell and cell-ECM adhesion, integrins also play a pivotal role in signal transduction and modulate various cellular processes (Zhang and Wang, 2012). *ITGA8* has been proven to be correlated with favorable outcomes in patients with basal-like and HER2+ breast cancer and colon cancer (Gong et al., 2019; Rojas et al., 2021).

The effect of the prognostic signature developed in this study on survival was independent of age and disease stage. Although age, disease stage, and ECMRS are all contributing factors to OS, the HR of ECMRS in univariate and multivariate Cox regression analysis was far greater than that of age and disease stage, which indicated the superiority of ECMRS as a stratification tool for survival in LUAD. Till date, the TNM staging system is the major tool used for prediction of the survival of patients with LUAD. However, with in-depth understanding of tumor behavior and updating of antitumor treatment, the TNM staging system is unable to meet clinical demands. The prognostic signature developed in this study may therefore be applicable as a supplement to the TNM staging system.

Immune checkpoint inhibitors (ICIs) are effective antitumor therapies. However, only 40–45% of non-small-cell lung carcinoma patients achieve remission after administration of ICIs (Borghaei et al., 2015; Garon et al., 2015; Larkin et al., 2015), indicating that most patients cannot benefit from ICIs. In solid tumors, dense ECM can serve as a protective shield against host antitumor immunity. Excessive matrix crosslinking can prevent immune cells and immunotherapeutic drugs from reaching the TME (Henke et al., 2019). Therefore, the expression of ERGs may affect tumor immunity to some extent. Indeed, the prognostic signature developed in our study was shown to predict tumor immunity in LUAD. Patients with low ECMRS had higher degree of immune cell infiltration, including $CD8^+$ T cells, $CD4^+$ T cells, and macrophages. Thus, our prognostic signature can serve as a useful tool to predict tumor immunity, and targeting the genes in the signature may collaborate with ICIs to exert antitumor efficacy.

Our research has a few limitations. First, the prognostic signature was retrospectively constructed and validated in TCGA and GEO databases; therefore, a prospective cohort study is needed to verify our findings. Second, the mechanism underlying the signature has not been explored, and *in vivo* and *in vitro* experiments should be conducted to elucidate the

mechanism of the prognostic ERGs in oncogenesis and tumor immunity.

In conclusion, we constructed a gene signature and developed a scoring system based on the expression of prognostic ERGs which can predict the survival and tumor immunity of patients with LUAD. Our study contributes to dissection of the ECM in LUAD and identifies promising prognostic indicators and potential therapeutic targets for patients with LUAD.

DATA AVAILABILITY STATEMENT

The datasets presented in this study can be found in online repositories. The names of the repository/repositories and accession number(s) can be found in the article/ **Supplementary Material**.

ETHICS STATEMENT

The studies involving human participants were reviewed and approved by The Medical Ethics Committee of Tongji Hospital, Tongji Medical College, Huazhong University of Science and Technology. The patients/participants provided their written informed consent to participate in this study.

AUTHOR CONTRIBUTIONS

Conceptualization: LX, QL, BL and XY; Design and methodology: LX, QL, YH, WQ, ZF, and BL; Data analysis and figure plotting: LX, QL, YH and WQ; Writing–original draft: LX, QL and BL; Writing–review and editing: BL and XY; Supervision: BL and XY.

FUNDING

This work was supported by grants from the National Natural Science Foundation of China (grant numbers 82130092 and 81902619), and National Natural Science Foundation of Hubei Province (2020CFB591).

ACKNOWLEDGMENTS

We acknowledge TCGA and GEO databases for providing their platforms and contributors for uploading their meaningful datasets.

SUPPLEMENTARY MATERIAL

The Supplementary Material for this article can be found online at: https://www.frontiersin.org/articles/10.3389/fcell.2022.835043/full#supplementary-material

REFERENCES

American Cancer Society (2017). *American Cancer Society*. https://www.cancer.org/cancer/lung-cancer/detection-diagnosis-staging/survival-rates.html

Atay, S. (2020). Integrated Transcriptome Meta-Analysis of Pancreatic Ductal Adenocarcinoma and Matched Adjacent Pancreatic Tissues. *PeerJ* 8, e10141. doi:10.7717/peerj.10141

Blanche, P., Dartigues, J.-F., and Jacqmin-Gadda, H. (2013). Estimating and Comparing Time-dependent Areas under Receiver Operating Characteristic Curves for Censored Event Times with Competing Risks. *Statist. Med.* 32, 5381–5397. doi:10.1002/sim.5958

Borghaei, H., Paz-Ares, L., Horn, L., Spigel, D. R., Steins, M., Ready, N. E., et al. (2015). Nivolumab versus Docetaxel in Advanced Nonsquamous Non-small-cell Lung Cancer. *N. Engl. J. Med.* 373, 1627–1639. doi:10.1056/NEJMoa1507643

Chakravarthy, A., Khan, L., Bensler, N. P., Bose, P., and De Carvalho, D. D. (2018). TGF-β-associated Extracellular Matrix Genes Link Cancer-Associated Fibroblasts to Immune Evasion and Immunotherapy Failure. *Nat. Commun.* 9, 4692. doi:10.1038/s41467-018-06654-8

Chang, I.-W., Liu, K.-W., Ragunanan, M., He, H.-L., Shiue, Y.-L., and Yu, S.-C. (2018). SERPINB5 Expression: Association with CCRT Response and Prognostic Value in Rectal Cancer. *Int. J. Med. Sci.* 15, 376–384. doi:10.7150/ijms.22823

Chen, Y., Lun, A. T. L., and Smyth, G. K. (2016). From Reads to Genes to Pathways: Differential Expression Analysis of RNA-Seq Experiments Using Rsubread and the edgeR Quasi-Likelihood Pipeline. *F1000Res* 5, 1438. doi:10.12688/f1000research.8987.1

Chiu, D. K.-C., Tse, A. P.-W., Xu, I. M.-J., Di Cui, J., Lai, R. K.-H., Li, L. L., et al. (2017). Hypoxia Inducible Factor HIF-1 Promotes Myeloid-Derived Suppressor Cells Accumulation through ENTPD2/CD39L1 in Hepatocellular Carcinoma. *Nat. Commun.* 8, 517. doi:10.1038/s41467-017-00530-7

Cox, T. R. (2021). The Matrix in Cancer. *Nat. Rev. Cancer* 21, 217–238. doi:10.1038/s41568-020-00329-7

Fan, H., Zhang, S., Zhang, Y., Liang, W., and Cao, B. (2020). FERMT1 Promotes Gastric Cancer Progression by Activating the NF-Kb Pathway and Predicts Poor Prognosis. *Cancer Biol. Ther.* 21, 815–825. doi:10.1080/15384047.2020.1792218

Fattet, L., Jung, H.-Y., Matsumoto, M. W., Aubol, B. E., Kumar, A., Adams, J. A., et al. (2020). Matrix Rigidity Controls Epithelial-Mesenchymal Plasticity and Tumor Metastasis via a Mechanoresponsive EPHA2/LYN Complex. *Developmental Cel.* 54, 302e307. doi:10.1016/j.devcel.2020.05.031

Ferlay, J., Soerjomataram, I., Dikshit, R., Eser, S., Mathers, C., Rebelo, M., et al. (2015). Cancer Incidence and Mortality Worldwide: Sources, Methods and Major Patterns in GLOBOCAN 2012. *Int. J. Cancer* 136, E359–E386. doi:10.1002/ijc.29210

Friedman, J., Hastie, T., and Tibshirani, R. (2010). Regularization Paths for Generalized Linear Models via Coordinate Descent. *J. Stat. Softw.* 33, 1–22. doi:10.18637/jss.v033.i01

Garon, E. B., Rizvi, N. A., Hui, R., Leighl, N., Balmanoukian, A. S., Eder, J. P., et al. (2015). Pembrolizumab for the Treatment of Non-small-cell Lung Cancer. *N. Engl. J. Med.* 372, 2018–2028. doi:10.1056/NEJMoa1501824

Gong, Y. Z., Ruan, G. T., Liao, X. W., Wang, X. K., Liao, C., Wang, S., et al. (2019). Diagnostic and Prognostic Values of Integrin α Subfamily mRNA Expression in colon Adenocarcinoma. *Oncol. Rep.* 42, 923–936. doi:10.3892/or.2019.7216

Gui, J., and Li, H. (2005). Penalized Cox Regression Analysis in the High-Dimensional and Low-Sample Size Settings, with Applications to Microarray Gene Expression Data. *Bioinformatics* 21, 3001–3008. doi:10.1093/bioinformatics/bti422

Győrffy, B. (2021). Survival Analysis across the Entire Transcriptome Identifies Biomarkers with the Highest Prognostic Power in Breast Cancer. *Comput. Struct. Biotechnol. J.* 19, 4101–4109. doi:10.1016/j.csbj.2021.07.014

Han, W., Chen, S., Yuan, W., Fan, Q., Tian, J., Wang, X., et al. (2016). Oriented Collagen Fibers Direct Tumor Cell Intravasation. *Proc. Natl. Acad. Sci. U.S.A.* 113, 11208–11213. doi:10.1073/pnas.1610347113

Hänzelmann, S., Castelo, R., and Guinney, J. (2013). GSVA: Gene Set Variation Analysis for Microarray and RNA-Seq Data. *BMC bioinformatics* 14, 7. doi:10.1186/1471-2105-14-7

Henke, E., Nandigama, R., and Ergün, S. (2019). Extracellular Matrix in the Tumor Microenvironment and its Impact on Cancer Therapy. *Front. Mol. Biosci.* 6, 160. doi:10.3389/fmolb.2019.00160

Huleihel, L., Hussey, G. S., Naranjo, J. D., Zhang, L., Dziki, J. L., Turner, N. J., et al. (2016). Matrix-bound Nanovesicles within ECM Bioscaffolds. *Sci. Adv.* 2, e1600502. doi:10.1126/sciadv.1600502

Larkin, J., Chiarion-Sileni, V., Gonzalez, R., Grob, J. J., Cowey, C. L., Lao, C. D., et al. (2015). Combined Nivolumab and Ipilimumab or Monotherapy in Untreated Melanoma. *N. Engl. J. Med.* 373, 23–34. doi:10.1056/NEJMoa1504030

Li, B., Severson, E., Pignon, J.-C., Zhao, H., Li, T., Novak, J., et al. (2016). Comprehensive Analyses of Tumor Immunity: Implications for Cancer Immunotherapy. *Genome Biol.* 17, 174. doi:10.1186/s13059-016-1028-7

Li, L., Yuan, S., Zhao, X., and Luo, T. (2020). ADAMTS8 Is Frequently Down-Regulated in Colorectal Cancer and Functions as a Tumor Suppressor. *Biochem. biophysical Res. Commun.* 524, 663–671. doi:10.1016/j.bbrc.2020.01.020

Li, T., Fu, J., Zeng, Z., Cohen, D., Li, J., Chen, Q., et al. (2020). TIMER2.0 for Analysis of Tumor-Infiltrating Immune Cells. *Nucleic Acids Res.* 48, W509–w514. doi:10.1093/nar/gkaa407

Lim, S. B., Tan, S. J., Lim, W.-T., and Lim, C. T. (2017). An Extracellular Matrix-Related Prognostic and Predictive Indicator for Early-Stage Non-small Cell Lung Cancer. *Nat. Commun.* 8, 1734. doi:10.1038/s41467-017-01430-6

Liu, C.-C., Cai, D.-L., Sun, F., Wu, Z.-H., Yue, B., Zhao, S.-L., et al. (2017). FERMT1 Mediates Epithelial-Mesenchymal Transition to Promote colon Cancer Metastasis via Modulation of β-catenin Transcriptional Activity. *Oncogene* 36, 1779–1792. doi:10.1038/onc.2016.339

McCarthy, D. J., Chen, Y., and Smyth, G. K. (2012). Differential Expression Analysis of Multifactor RNA-Seq Experiments with Respect to Biological Variation. *Nucleic Acids Res.* 40, 4288–4297. doi:10.1093/nar/gks042

Mierke, C. T. (2019). The Matrix Environmental and Cell Mechanical Properties Regulate Cell Migration and Contribute to the Invasive Phenotype of Cancer Cells. *Rep. Prog. Phys.* 82, 064602. doi:10.1088/1361-6633/ab1628

Miroshnikova, Y. A., Rozenberg, G. I., Cassereau, L., Pickup, M., Mouw, J. K., Ou, G., et al. (2017). α5β1-Integrin Promotes Tension-dependent Mammary Epithelial Cell Invasion by Engaging the Fibronectin Synergy Site. *MBoC* 28, 2958–2977. doi:10.1091/mbc.E17-02-0126

Nebuloni, M., Albarello, L., Andolfo, A., Magagnotti, C., Genovese, L., Locatelli, I., et al. (2016). Insight on Colorectal Carcinoma Infiltration by Studying Perilesional Extracellular Matrix. *Sci. Rep.* 6, 22522. doi:10.1038/srep22522

Palaniappan, A., Ramar, K., and Ramalingam, S. (2016). Computational Identification of Novel Stage-specific Biomarkers in Colorectal Cancer Progression. *PLoS One* 11, e0156665. doi:10.1371/journal.pone.0156665

Pearce, O. M. T., Delaine-Smith, R. M., Maniati, E., Nichols, S., Wang, J., Böhm, S., et al. (2018). Deconstruction of a Metastatic Tumor Microenvironment Reveals a Common Matrix Response in Human Cancers. *Cancer Discov.* 8, 304–319. doi:10.1158/2159-8290.Cd-17-0284

Peng, D. H., Ungewiss, C., Tong, P., Byers, L. A., Wang, J., Canales, J. R., et al. (2017). ZEB1 Induces LOXL2-Mediated Collagen Stabilization and Deposition in the Extracellular Matrix to Drive Lung Cancer Invasion and Metastasis. *Oncogene* 36, 1925–1938. doi:10.1038/onc.2016.358

Phipson, B., Lee, S., Majewski, I. J., Alexander, W. S., and Smyth, G. K. (2016). Robust Hypermeter Estimation Protects Against Hypervariable Genes Aand Improves Power To Detect Differential Expression. *Ann. Appl. Stat.* 10, 946–963. doi:10.1214/16-aoas920

Ridder, D. A., Schindeldecker, M., Weinmann, A., Berndt, K., Urbansky, L., Witzel, H. R., et al. (2021). Key Enzymes in Pyrimidine Synthesis, CAD and CPS1, Predict Prognosis in Hepatocellular Carcinoma. *Cancers* 13, 744. doi:10.3390/cancers13040744

Ritchie, M. E., Phipson, B., Wu, D., Hu, Y., Law, C. W., Shi, W., et al. (2015). Limma powers Differential Expression Analyses for RNA-Sequencing and Microarray Studies. *Nucleic Acids Res.* 43, e47. doi:10.1093/nar/gkv007

Robinson, M. D., McCarthy, D. J., and Smyth, G. K. (2010). edgeR: a Bioconductor Package for Differential Expression Analysis of Digital Gene Expression Data. *Bioinformatics* 26, 139–140. doi:10.1093/bioinformatics/btp616

Rognoni, E., Widmaier, M., Jakobson, M., Ruppert, R., Ussar, S., Katsougkri, D., et al. (2014). Kindlin-1 Controls Wnt and TGF-β Availability to Regulate Cutaneous Stem Cell Proliferation. *Nat. Med.* 20, 350–359. doi:10.1038/nm.3490

Rojas, K., Baliu-Piqué, M., Manzano, A., Saiz-Ladera, C., García-Barberán, V., Cimas, F. J., et al. (2021). In Silico transcriptomic Mapping of Integrins and Immune Activation in Basal-like and HER2+ Breast Cancer. *Cell Oncol.* 44, 569–580. doi:10.1007/s13402-020-00583-9

Subramanian, A., Tamayo, P., Mootha, V. K., Mukherjee, S., Ebert, B. L., Gillette, M. A., et al. (2005). Gene Set Enrichment Analysis: a Knowledge-Based Approach for Interpreting Genome-wide Expression Profiles. *Proc. Natl. Acad. Sci. U.S.A.* 102, 15545–15550. doi:10.1073/pnas.0506580102

Sundqvist, A., Vasilaki, E., Voytyuk, O., Bai, Y., Morikawa, M., Moustakas, A., et al. (2020). TGFβ and EGF Signaling Orchestrates the AP-1- and P63 Transcriptional Regulation of Breast Cancer Invasiveness. *Oncogene* 39, 4436–4449. doi:10.1038/s41388-020-1299-z

Therneau, T. M., Grambsch, P. M., and SpringerLink (2000). *Modeling Survival Data: Extending the Cox Model*. New York: Springer.

Toss, M., Miligy, I., Gorringe, K., Mittal, K., Aneja, R., Ellis, I., et al. (2020). Prognostic Significance of Cathepsin V (CTSV/CTSL2) in Breast Ductal Carcinoma *In Situ*. *J. Clin. Pathol.* 73, 76–82. doi:10.1136/jclinpath-2019-205939

Troup, S., Njue, C., Kliewer, E. V., Parisien, M., Roskelley, C., Chakravarti, S., et al. (2003). Reduced Expression of the Small Leucine-Rich Proteoglycans, Lumican, and Decorin Is Associated with Poor Outcome in Node-Negative Invasive Breast Cancer. *Clin. Cancer Res.* 9, 207–214.

Uhlén, M., Fagerberg, L., Hallström, B. M., Lindskog, C., Oksvold, P., Mardinoglu, A., et al. (2015). Tissue-based Map of the Human Proteome. *Science* 347, 1260419. doi:10.1126/science.1260419

Uhlen, M., Zhang, C., Lee, S., Sjöstedt, E., Fagerberg, L., Bidkhori, G., et al. (2017). A Pathology Atlas of the Human Cancer Transcriptome. *Science* 357, e2507. doi:10.1126/science.aan2507

Wang, C.-H., Wang, L.-K., Wu, C.-C., Chen, M.-L., Kuo, C.-Y., Shyu, R.-Y., et al. (2020). Cathepsin V Mediates the Tazarotene-Induced Gene 1-induced Reduction in Invasion in Colorectal Cancer Cells. *Cell Biochem Biophys* 78, 483–494. doi:10.1007/s12013-020-00940-3

Wang, W., and Liu, W. (2020). Integration of Gene Interaction Information into a Reweighted Lasso-Cox Model for Accurate Survival Prediction. *Bioinformatics* 36, 5405–5414. doi:10.1093/bioinformatics/btaa1046

Wu, Z., Shi, Y., Ren, S., Ju, Y., Hu, Y., and Wu, J. (2020). ADAMTS8 Inhibits Progression of Esophageal Squamous Cell Carcinoma. *DNA Cell Biol.* 39, 2300–2307. doi:10.1089/dna.2020.6053

Yan, Q., Chen, T., Yang, H., Yu, H., Zheng, Y., He, T., et al. (2019). The Effect of FERMT1 Regulated by miR-24 on the Growth and Radiation Resistance of Esophageal Cancer. *J Biomed. Nanotechnol* 15, 621–631. doi:10.1166/jbn.2019.2711

Yoshihara, K., Shahmoradgoli, M., Martínez, E., Vegesna, R., Kim, H., Torres-Garcia, W., et al. (2013). Inferring Tumour Purity and Stromal and Immune Cell Admixture from Expression Data. *Nat. Commun.* 4, 2612. doi:10.1038/ncomms3612

Zhang, Y., and Wang, H. (2012). Integrin Signalling and Function in Immune Cells. *Immunology* 135, 268–275. doi:10.1111/j.1365-2567.2011.03549.x

Zhao, X., Yang, C., Wu, J., and Nan, Y. (2018). ADAMTS8 Targets ERK to Suppress Cell Proliferation, Invasion, and Metastasis of Hepatocellular Carcinoma. *Ott*, 11, 7569–7578. doi:10.2147/ott.S173360

Conflict of Interest: The authors declare that the research was conducted in the absence of any commercial or financial relationships that could be construed as a potential conflict of interest.

Publisher's Note: All claims expressed in this article are solely those of the authors and do not necessarily represent those of their affiliated organizations, or those of the publisher, the editors and the reviewers. Any product that may be evaluated in this article, or claim that may be made by its manufacturer, is not guaranteed or endorsed by the publisher.

Copyright © 2022 Xiao, Li, Huang, Fan, Qin, Liu and Yuan. This is an open-access article distributed under the terms of the Creative Commons Attribution License (CC BY). The use, distribution or reproduction in other forums is permitted, provided the original author(s) and the copyright owner(s) are credited and that the original publication in this journal is cited, in accordance with accepted academic practice. No use, distribution or reproduction is permitted which does not comply with these terms.

frontiers | Frontiers in Oncology

ORIGINAL RESEARCH
published: 27 April 2022
doi: 10.3389/fonc.2022.874731

Integrative Dissection of Novel Lactate Metabolism-Related Signature in the Tumor Immune Microenvironment and Prognostic Prediction in Breast Cancer

Lu Yang[†], *Peixin Tan*[†], *Hengwen Sun*[†], *Zijun Zeng*[*] *and Yi Pan*[*]

Department of Radiation Oncology, Guangdong Provincial People's Hospital, Guangdong Academy of Medical Sciences, Guangzhou, China

OPEN ACCESS

Edited by:
Pranav Gupta, Albert Einstein College of Medicine, United States

Reviewed by:
Xiaofang Guo, University of South Florida, United States
Zhiyu Wang, Guangzhou University of Chinese Medicine, China

***Correspondence:**
Yi Pan
panyiff01@163.com
Zijun Zeng
zzj49@hotmail.com

[†]*These authors have contributed equally to this work and share first authorship*

Specialty section:
This article was submitted to Molecular and Cellular Oncology, a section of the journal Frontiers in Oncology

Received: *12 February 2022*
Accepted: *24 March 2022*
Published: *27 April 2022*

Citation:
Yang L, Tan P, Sun H, Zeng Z and Pan Y (2022) Integrative Dissection of Novel Lactate Metabolism-Related Signature in the Tumor Immune Microenvironment and Prognostic Prediction in Breast Cancer. Front. Oncol. 12:874731. doi: 10.3389/fonc.2022.874731

The outcomes of some breast cancer patients remain poor due to being susceptible to recurrence, metastasis and drug resistance, and lactate metabolism has been described as a hallmark of cancer and a contributor to cancer progression and immune escape. Hence, it is worthy of seeking potentially novel biomarkers from lactate metabolism relevant perspectives for this particular cohort of patients. In this context, 205 available lactate metabolism-related genes (LMGs) were obtained by a search of multiple genesets, and the landscape of somatic mutation, copy number variation, and mRNA expression levels was investigated among these genes. Crucially, 9 overall survival-related LMGs were identified through univariate Cox regression analysis in The Cancer Genome Atlas (TCGA) and Molecular Taxonomy of Breast Cancer International Consortium (METABRIC) databases. Subsequently, a prognostic signature, defined as Lactate Metabolism Index (LMI), was established with 5 OS-related LMGs using Least Absolute Shrinkage and Selection Operator (LASSO) Cox hazard regression analysis in TCGA training set, and then validated in two external cohorts (METABRIC and GSE96058). From the comprehensive results, breast cancer patients with high LMI had considerably poorer survival probability across all cohorts, and the degree of clinical features tended to be more severe as the LMI value increased. Furthermore, a prognostic nomogram incorporating LMI, age, and AJCC stage was constructed and demonstrated great prediction performance for OS of breast cancer patients, which was evaluated by the calibration plot and the decision curve analysis. Moreover, the potential effect of different LMI values on levels of immune checkpoints, tumor-infiltrating immune cells, and cytokines were explored ultimately, and patients with higher LMI values might gain an immunosuppressive tumor microenvironment that contributed to immune escape of breast cancer and inferior prognosis. Collectively, all findings in the study indicated the potential prognostic value of LMI in breast cancer, providing further implications for the

role of lactate metabolism in breast cancer prognosis, tumor immune microenvironment, and immunotherapy.

Keywords: lactate metabolism, breast cancer, prognostic signature, tumor immune microenvironment, immunotherapy

INTRODUCTION

Owing to high morbidity and corresponding mortality in women, breast cancer (BC) has consistently received extensive attention worldwide (1). Also, with the development of comprehensive therapy strategies, outcomes for patients with breast cancer have extremely improved. However, the outcomes of some patients are still poor due to being susceptible to recurrence, metastasis, and drug resistance (2). Thus, there is still a need to find novel and effective biomarkers to identify this subgroup of patients with breast cancer.

In recent years, it is becoming increasingly evident that lactate metabolism plays a critical role in tumor progression and has been a hallmark of cancer (3). Previous studies have shown that lactate has prognostic and predictive utility in several cancer types. For example, a higher lactate level was correlated with worse outcomes in cervical cancer (4). In head and neck squamous cell carcinoma, lactate was found to be inversely correlated with overall and disease-free patient survival and positively correlated with radioresistance (5, 6). For breast cancer, it has been reported that elevated intratumoral lactate levels were an adverse prognostic factor in breast cancer (7). Furthermore, raised intratumoural lactate levels were related to HER2 addiction status and trastuzumab susceptibility in HER2-positive breast cancer (8). Despite this, a comprehensive review of the influence of lactate on breast cancer was still lacking.

It is commonly accepted that the tumor microenvironment (TME), which included not only the surrounding stromal and immune cells but also the changes of metabolites and signaling molecules, has emerged as a major regulator to drive cancer development and progression (9). Lactate, produced by cancer cells, was secreted into the extracellular space and then functioned as a contributor to facilitating tumor immune escape (10). Specifically, lactate accumulation could directly inhibit the cytotoxic functions of T cells and innate lymphocytes such as natural killer (NK) and natural killer T (NKT) cells (11–13), induce a tolerogenic DC phenotype promoting regulatory T-cell (Treg) polarization (14), and cause accumulation and polarization of myeloidderived suppressor cells (MDSCs) and M2-tumor-associated macrophages (TAMs) (10, 15). Because of this immunosuppressive role, lactate played a negative role in the efficacies of immunotherapy. High lactate dehydrogenase (LDH) level was identified as an independent biomarker for predicting therapeutic response to immune checkpoint inhibitors (ICIs), including anti-PD-1 and anti-CTLA-4 therapy, in patients with melanoma, non-small cell lung cancer, and esophageal squamous cell carcinoma (16–18). However, a 2020 meta-analysis of ICIs in metastatic breast cancer did not find a utility for LDH in predicting response to these treatments (19). To further explore the immune-related role of lactate metabolism in breast cancer, a landscape assessment of the relationship between lactate metabolism and TME and ICIs therapy remains necessary.

In the current study, we aimed to screen out prognostic lactate metabolism-related genes (LMGs) and identify a prognostic signature based on LMGs for predicting the outcomes of patients with BC. In addition, the utility of the signature applied in the clinic was completely evaluated. Subsequently, the potential correlation between the signature and the landscape of TME was systematically dissected. The comprehensive analysis might provide more detailed insights into the cancer research about lactate metabolism and immunotherapy.

MATERIALS AND METHODS

Data Collection and Acquisition of Lactate Metabolism-Related Genes

The public transcriptome expression matrices and detailed clinical data of BC were collected from The Cancer Genome Atlas (TCGA) database[1] (113 normal breast samples and 1,109 BC samples), the Molecular Taxonomy of Breast Cancer International Consortium (METABRIC) database[2] (1,904 BC samples), and GSE96058 in the Gene Expression Omnibus (GEO) database[3] (3,409 BC samples), respectively. Besides, 1,082 BC patients of TCGA were selected as the training set, while 1,903 BC samples of METABRIC and 3,409 BC patients were chosen as external validation sets after excluding patients without overall survival information. In total, 284 lactate metabolism-related genes were acquired from the Molecular Signature Database v7.5.1 (MSigDB)[4]. Furthermore, 205 overlapping LMGs were screened out for further analyses after intersecting the above 284 LMGs with the total genes in TCGA-BRCA, METABRIC, and GSE96058 datasets (**Supplementary Figure S1**).

Investigation of Somatic Mutation, Copy Number Variation Frequency and Differentially Expressed Genes Among LMGs

We obtained the information on the somatic mutation and copy number variation (CNV) of BC from TCGA-BRCA in the UCSC Xena database[5]. The somatic mutation frequency of 205 LMGs was analyzed by the R package "maftools" (20) and visualized in an

[1] https://portal.gdc.cancer.gov/repository
[2] http://www.cbioportal.org/
[3] https://www.ncbi.nlm.nih.gov/geo/
[4] http://www.gsea-msigdb.org/gsea/msigdb/index.jsp
[5] https://xenabrowser.net/datapages/

oncoplot waterfall plot. Additionally, the CNV frequency of LMGs was calculated and visualized in a bi-directional column chart. The differentially expressed genes (DEGs) of LMGs were identified after comparing the normal breast samples and BC samples in TCGA-BRCA dataset with the threshold set to |log2FC| >1 and false-discovery rate (FDR) <0.05 using the "edgR" R package (21). A heatmap and a volcano plot of these significant DEGs were shown subsequently.

Identification of Overall Survival-Associated LMGs

To elucidate the underlying prognostic significance of 205 LMGs in BC, overall survival (OS)-associated LMGs were identified through univariate Cox hazard regression analysis with $p < 0.05$ in the TCGA-BRCA (n = 1,082) and METABRIC (n = 1,903) cohorts, respectively (**Supplementary Tables S1, S2**). Moreover, the overlapping OS-associated LMGs were extracted to further research. Meanwhile, the expression levels and the location on chromosomes of those eligible LMGs were illustrated by the "RCircos" R package (22), and the correlation characteristics among these LMGs were demonstrated in a correlation matrix plot.

Construction and Validation of Lactate Metabolism-Correlated Prognostic Signature

Least Absolute Shrinkage and Selection Operator (LASSO) Cox regression analysis was performed in the training cohort to construct the statistical prognostic signature utilizing the candidate OS-related LMGs. Next, 5 optimal LMGs were dug out to establish the prognostic model for BC patients, while the expression levels and prognostic significance of each signature-contained LMG were depicted, respectively. In according with the predictive prognostic signature, Lactate Metabolism Index (LMI) could be calculated for each BC patient by employing the following formula:

$$LMI = \sum Expression\ of\ Each\ LMG\ *\ Corresponding\ Regression\ Coefficient$$

To make data and plots more intuitionistic, a linear transformation was carried out to adjust the LMI in each dataset using the following formula:

$$adj.LMI = \frac{LMI - min\ (LMI)}{\max(LMI) - \min(LMI)}$$

Afterwards the BC patients in each cohort could be separated into the high- and low-LMI groups by the cutoff of the median LMI value. Principal component analysis (PCA) was carried out to evaluate the classification accuracy of the signature. To discover the feasibility of the signature, a K-M analysis of OS was executed between the high- and low-LMI groups in three datasets separately.

Integrated Dissection of LMI and Clinical Parameters in Patients With BC

To decipher the availability of LMI applied in actual clinical issues further, boxplots with the Kruskal test were exhibited to compare the distribution of adjusted LMI value in various degrees of diverse clinicopathologic parameters available in the three datasets. Besides, heatmaps were shown to unveil the relevance between each signature-included LMGs' expression level and several clinical indicators, comprising of LMI, T stage, N stage, AJCC stage, PAM50 subtypes, and survival status in the training set in addition to LMI, tumor size, positive nodes, PAM50 subtypes, AJCC stage, and survival status in two validation datasets.

Establishment and Evaluation of Lactate Metabolism-Correlated Clinical Nomogram

Subsequently, it was delineated whether the LMI was an independent prognostic predictor in BC by univariate and multivariate Cox regression analyses. Based on the results above, a lactate metabolism-correlated clinical nomogram that integrated LMI, age, and AJCC stage in TCGA-BRCA was established through the "rms" and "regplot" R packages (23). To assess the satisfactory predictive discrimination of nomogram, the calibration curve (24) and the decision curve analysis (DCA) plot were portrayed for BC patients.

Clarification of Different Biological Functions Within Two LMI Groups

"GSVA" R package (25) was employed to clarify the different biological functions and signaling pathways between high- and low-LMI groups in the training set. "c2.cp.kegg.v7.5.1.symbols.gmt" [KEGG] was retrieved from MSigDB as the reference molecular signature database and the pathways with adjusted p-values <0.05 were considered significant. Ultimately, the most significant pathways were displayed in a heatmap.

Potential Implications for Immunotherapy and Tumor-Immune Microenvironment Landscape Estimation Based on LMI

To verify the potential implications for immunotherapy based on LMI, the expression levels of several immunologic checkpoints, comprising PD-1, PD-L1, CTLA4, CD96, VSIR, and TIGIT, were compared between the high- and low-LMI groups using the Wilcox test.

To dissect the TME landscape between the two LMI subgroups, the ESTIMATE algorithm (26) was implemented to calculate the estimate scores, immune scores, and stromal scores for further predicting tumor purity and analyzing the TME. Moreover, the CIBERSORT deconvolution algorithm (27) was utilized to estimate the abundance of 22 tumor immune-infiltrating cell types in the training set.

Likewise, to investigate the correlation between LMI signature and cytokines in TME, several essential cytokines were picked out to make a comparison between high- and low LMI subgroups in expression levels, including IL-1B, IL-2, IL-6, IL-10, IL-18, TNF, IFNG, GZMA, and GZMB.

Cell Lines and Cell Culture

Human breast cancer cell lines were purchased from the American Type Culture Collection. All cell lines were cultured

following standard guidelines. All cell lines were maintained without antibiotics in an atmosphere of 5% CO_2 and 99% relative humidity at 37°C. Cell lines were passaged for fewer than 6 months and were authenticated by short tandem repeat analysis. No mycoplasma infection was found for all cell lines.

RNA Isolation and Quantitative Real-Time PCR Analysis

Total RNA of cells was obtained with RNA-Quick Purification Kit (ES-RN001, Shanghai Yishan Biotechnology Co., Shanghai, China). The quantitative real-time PCR (qRT-PCR) plate was employed from NEST (402301, Wuxi NEST Biotechnology Co., Jiangsu, China). The primer sequences are shown in **Supplementary Table S3**. RNA levels were determined by qRT-PCR in triplicate on a Bio-Rad CFX96 using the SYBR Green method (RR420A, Takara, Mountain View, CA, USA). The RNA levels were normalized against β-actin RNA using the comparative Ct method.

Statistical Analysis

All statistical analyses were completed *via* R software (Version 4.0.2, http://www.R-project.org). The discrepancy in the expression level of signature-encompassed LMGs in normal breast and BC samples, ESTIMATE algorithm-calculated scores, checkpoints, and cytokines in the low- and high-LMI groups were detected by the Wilcox test. The comparison of each Kaplan–Meier (KM) curve that occurred in this study was accomplished by the log-rank test. Also, Kruskal tests were performed to discover the differences in adjusted LMI values in various clinical parameters. Univariate and multivariate Cox regression analyses were employed to screen out the OS-related LMGs and the independent prognostic indicators of OS for BC. The correlation matrix plot was portrayed under Spearman's correlation test. Statistical significance was confirmed as p-value <0.05, and all p-values were bilateral.

RESULTS

Identification of Prognostic Lactate Metabolism-Related Genes in Breast Cancer

Initially, we assessed the global alterations of 205 LMGs in somatic mutation and copy number variation (CNV). As shown in **Figure 1A**, the top 10 genes with the highest somatic mutation rates were included in the heatmap, with the highest mutation frequency distributed in TP53. For frequency of CNV, the result showed that there were common CNV mutations among LMGs, and the top 20 genes in amplified and deleted CNV status separately were displayed in **Figure 1B**. Additionally, to investigate the differential expression of these LMGs, we compared their mRNA expression levels between 1082 tumor samples and 113 normal breast samples with the threshold of |log2FC| > 1 and FDR <0.05, and the results were demonstrated through a heatmap (**Figure 1C**) and a volcano plot (**Figure 1D**). Furthermore, to identify prognostic LMGs in breast cancer for the following research, the univariate Cox regression analyses were conducted to screen out OS-related genes in both TCGA and METABRIC datasets (**Figure 1E**). In total, 25 and 79 significant OS-related genes were obtained respectively and 9 overlapping genes (RPS14, MECP2, OCRL, RRM2B, GOT2, AIFM1, SDHA, SLC19A1, and CYC1) were included for further analysis after taking intersecting of the results above (**Figure 1F**). Moreover, the location of chromosomes and expression level of the 9 genes were illustrated by a Circos plot (**Figure 1G**). Finally, a correlation network plot was used to unravel the correlation features among 9 eligible FMGs (**Figure 1H**).

Construction and Validation of Lactate Metabolism-Relevant Prognostic Signature for Patients With Breast Cancer

By performing the LASSO Cox regression analysis with 9 candidate genes in breast cancer patients of TCGA-BRCA training dataset, 5 pivotal genes were unearthed to establish the prognostic signature, Lactate Metabolism Index, namely LMI (**Figures 2A, B**), including RPS14, SLC19A1, CYC1, RRM2B, OCRL. Besides, the investigation of expression levels and survival capability of every signature-contained gene was further conducted by boxplots (**Figure 2C**) of mRNA expression levels and KM survival curves of OS (**Figure 2D**). From the results, we found that mRNA expressions of SLC19A1, CYC1, RRM2B, and OCRL were clearly elevated in breast cancer, while RPS14 expression was considerably decreased. Additionally, the RNA expression levels of SLC19A1 and RPS14 were validated in human breast cancer cell lines (**Supplementary Figure S2**), the result of which demonstrated that SLC19A1 was significantly promoted in breast cancer cell lines including MDA-MB-231, T47D, and SK-BR-3 while RPS14 declined significantly in BC cell lines comparing with breast epithelial cell line MCF10A. And for the survival analyses of OS, high expressions of SLC19A1, CYC1, RRM2B, and OCRL and downregulation of RPS14 were significantly related to more unfavorable OS in breast cancer, which further confirmed the validity of selected genes. Eventually, the prognostic signature was established as follows: LMI = Expression of SLC19A1 * 0.010382 − Expression of RPS14 * 0.000045 + Expression of CYC1 * 0.000408 + Expression of RRM2B * 0.000005 + Expression of OCRL * 0.006258.

Validation of Signature Based on 5 LMGs

To further verify the prognostic value of LMI in breast cancer, patients of the TCGA-BRCA training set and two validation sets (METABRIC and GSE96058) were then independently segregated into high-LMI and low-LMI subgroups according to the median value of LMI in each dataset (**Figure 3A**). As expected, we found that the number of deaths increased with LMI increasing in both the training and validation cohorts (**Figure 3B**). Meanwhile, PCA was applied to demonstrate the distribution patterns of the two subgroups in two-dimensional graphs (**Figure 3C**). Finally, the KM curves for the OS of breast cancer patients showed that patients with high LMI had considerably poorer survival probability across all cohorts

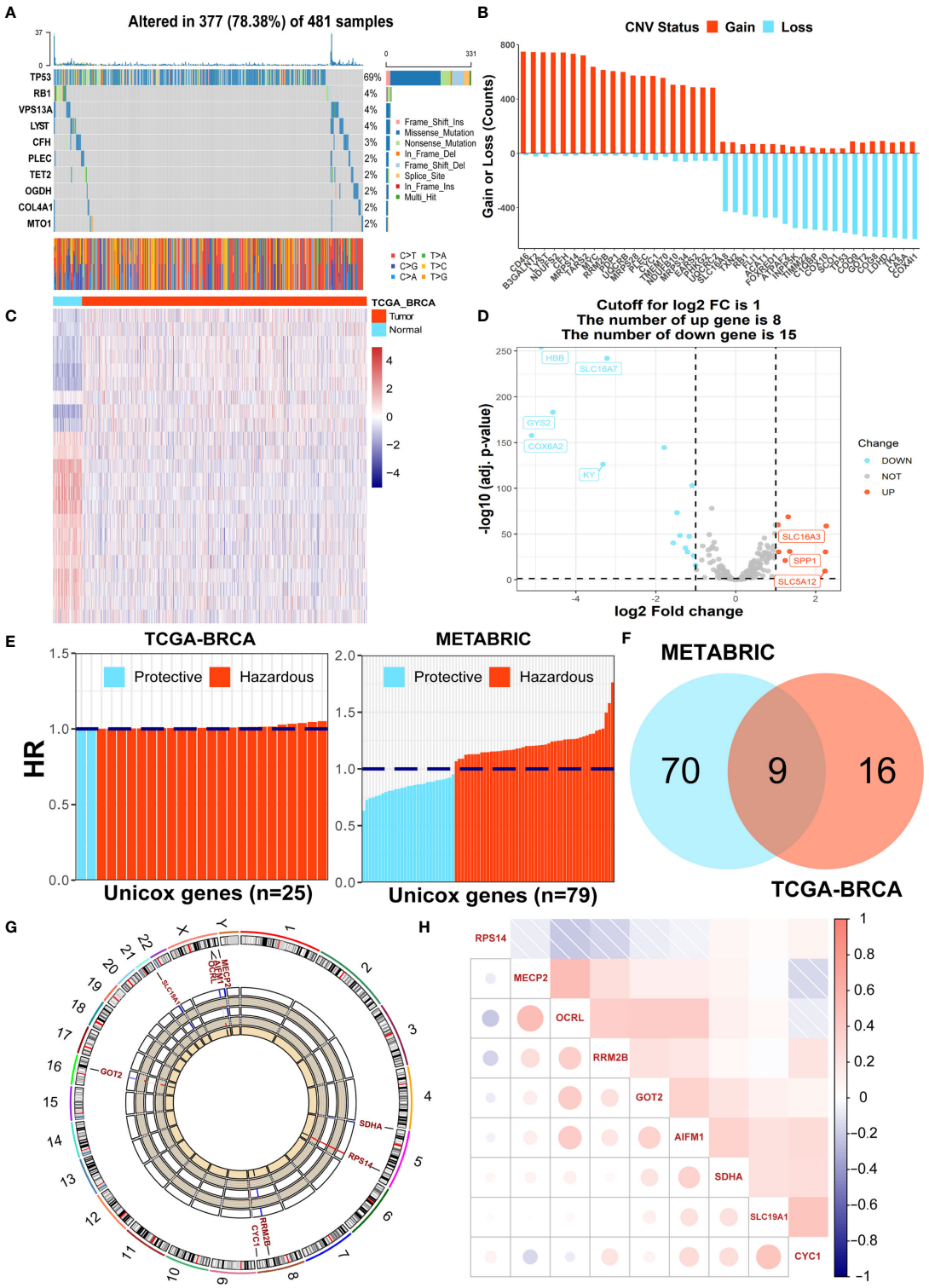

FIGURE 1 | Identification of prognostic LMGs in BC patients. **(A)** The somatic mutation frequency of LMGs in the TCGA-BRCA cohort. **(B)** The prevalent CNV frequency of LMGs in the TCGA-BRCA cohort. **(C)** Heatmap of differentially expressed genes among LMGs. **(D)** Volcano plot exhibiting DEGs in LMGs. **(E)** OS-related LMGs in TCGA-BRCA and METABRIC datasets, respectively. **(F)** The Veen diagram to detect 9 common prognostic LMGs. **(G)** The Circos plot illustrating the locations on chromosomes and expression levels of the 9 candidate LMGs. **(H)** The correlation matrix plot containing 9 prognostic LMGs.

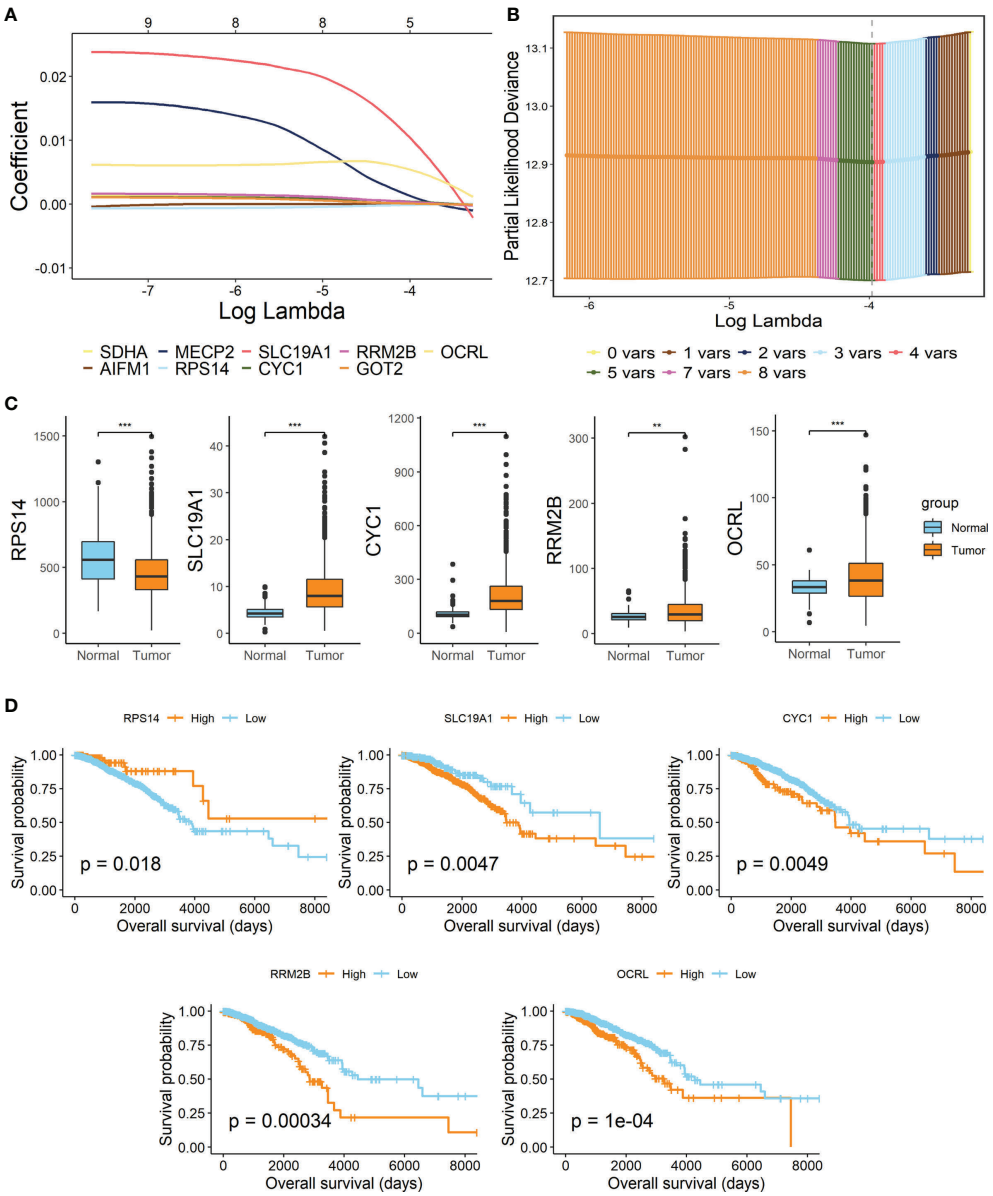

FIGURE 2 | Establishment of lactate metabolism-related signature in BC. **(A)** LASSO Cox regression analysis. **(B)** Partial likelihood deviance for the LASSO regression to screen out 5 optimal prognostic LMGs. **(C)** Boxplots showing the mRNA expression levels of 5 signature-contained LMGs in the training cohort. **(D)** KM survival curves of OS based on expression levels of 5 LMGs in the training cohort. **p < 0.01; ***p < 0.001.

(**Figure 3D**), which proved the predictive accuracy of LMI in the prognoses of breast cancer.

Assessment of the Correlation Between LMI and Clinicopathological Characteristics in BC Patients

Further evaluation of the relationship between LMI and various clinicopathological factors in breast cancer patients was also conducted. In the TCGA-BRCA training cohort (**Figure 4A**), prominent discrepancies were found between LMI and clinical characteristics, including survival status, T, N, AJCC stage, and PAM50 subtypes. Similarly, conspicuous differences were also observed in validation cohorts, containing survival status, tumor size, positive nodes, stage, and PAM50 subtypes in the METABRIC set (**Figure 4B**) and survival status, tumor size, positive nodes, and PAM50 subtypes in the GSE96058 set (**Figure 4C**). Notably, as the LMI levels were higher, the degree of clinical features tended to become more severe, which was displayed in both the training and validation sets and reconfirmed the predictive value of LMI in breast cancer. Meanwhile, heatmaps were used to demonstrate the correlation analyses between LMI-contained genes and clinicopathological

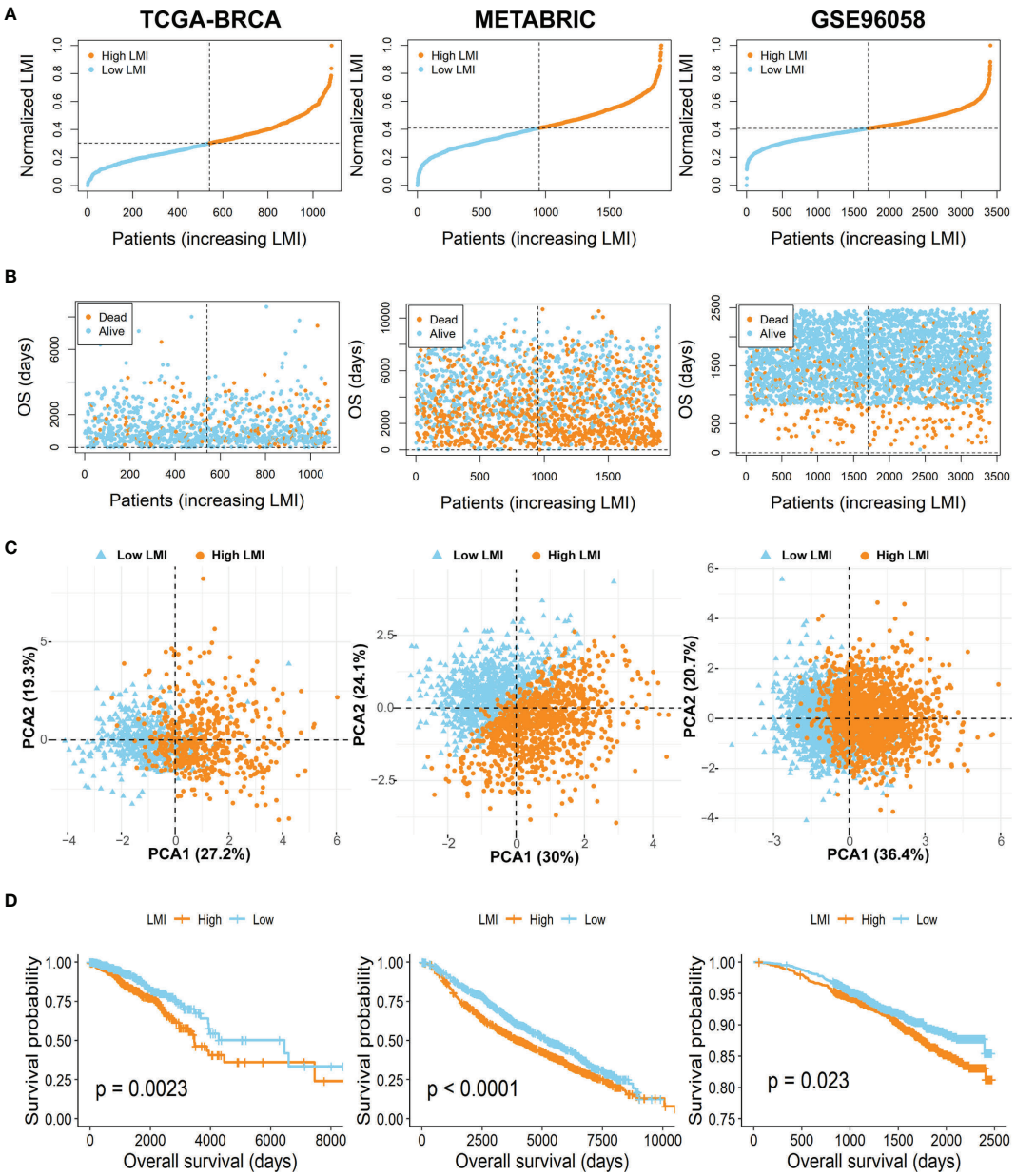

FIGURE 3 | Evaluation and validation of the feasibility of LMI in training set and validation sets. **(A)** Distribution of the patients' adjusted LMI score. **(B)** BC patients' OS time along with their LMI score. **(C)** PCA analyses of high- and low-LMI groups. **(D)** KM curves for the OS of BC patients between high- and low-LMI groups.

features in TCGA-BRCA (**Figure 4D**), METABRIC (**Figure 4E**), and GSE96058 (**Figure 4F**) sets.

Development and Validation of a Prognostic Nomogram Based on LMI Signature

Concerning whether LMI signature could be an independent prognostic predictor for breast cancer patients, univariate and multivariate Cox regression analyses were performed in the TCGA dataset. And the results illuminated that age, T stage, N stage, AJCC stage and LMI were significantly linked to OS in the univariate Cox analysis (**Figure 5A**), while only age, AJCC stage and LMI were still independent prognostic factors in the multivariate Cox analysis (**Figure 5B**). Next, a clinicopathologic nomogram, which contained LMI, age and AJCC stage, was developed to predict individual OS of 2-, 3- and 5-years (**Figure 5C**). Moreover, the calibration plot was portrayed to confirm the predictive consistency of the nomogram, which displayed great fitness (**Figure 5D**). And decision curve analysis (DCA) showed that the nomogram attained a greater

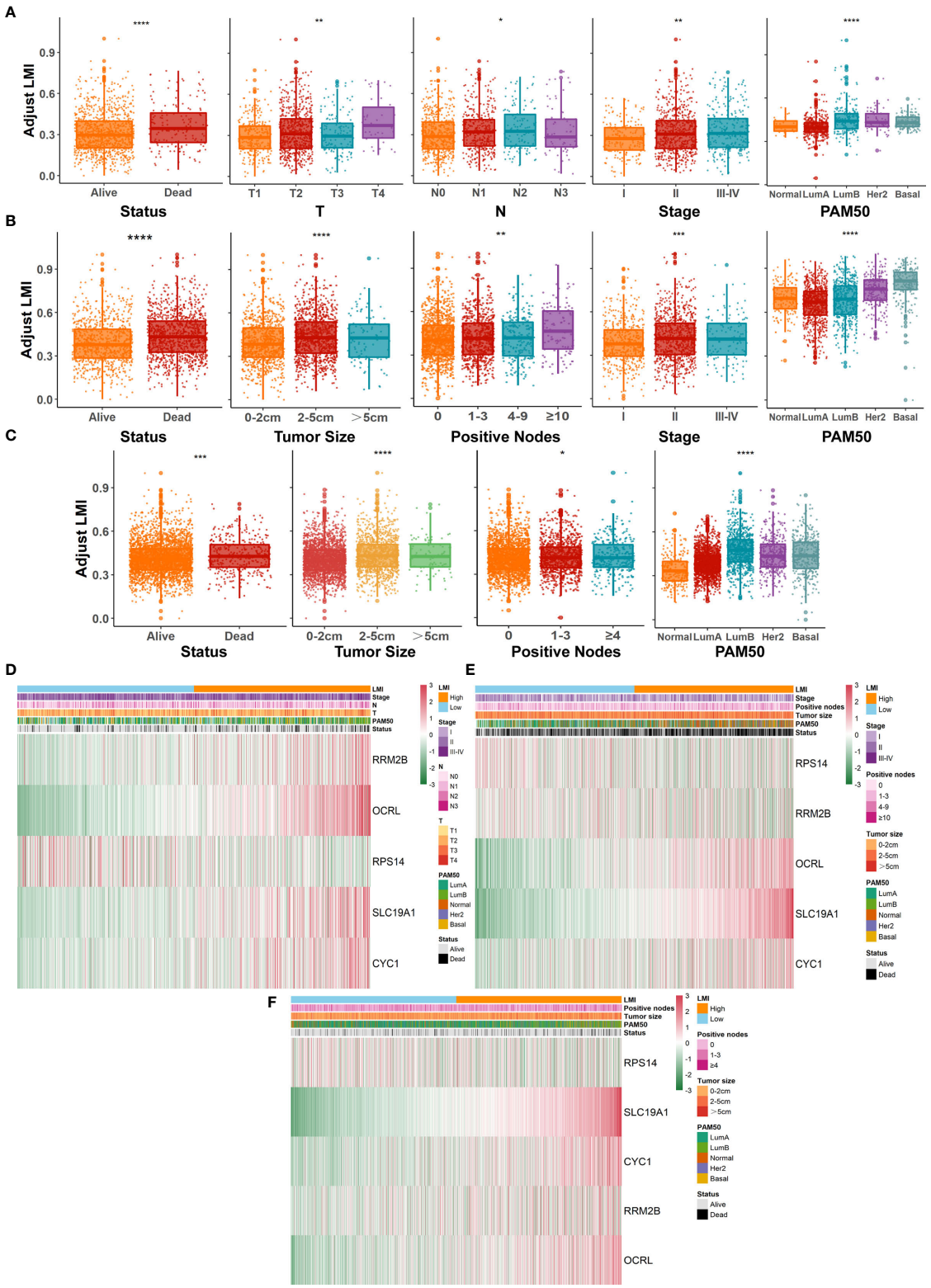

FIGURE 4 | Systematic dissection of LMI and clinical parameters in BC patients. The boxplots to illustrate the correlation between LMI and different clinicopathological characteristics of BC patients in TCGA-BRCA **(A)**, METABRIC **(B)** and GSE96058 **(C)**, respectively. Correlation heatmaps of signature-included LMGs and clinicopathological features in datasets of TCGA-BRCA **(D)**, METABRIC **(E)** and GSE96058 **(F)** separately. *p < 0.05; **p < 0.01; ***p < 0.001; ****p < 0.0001.

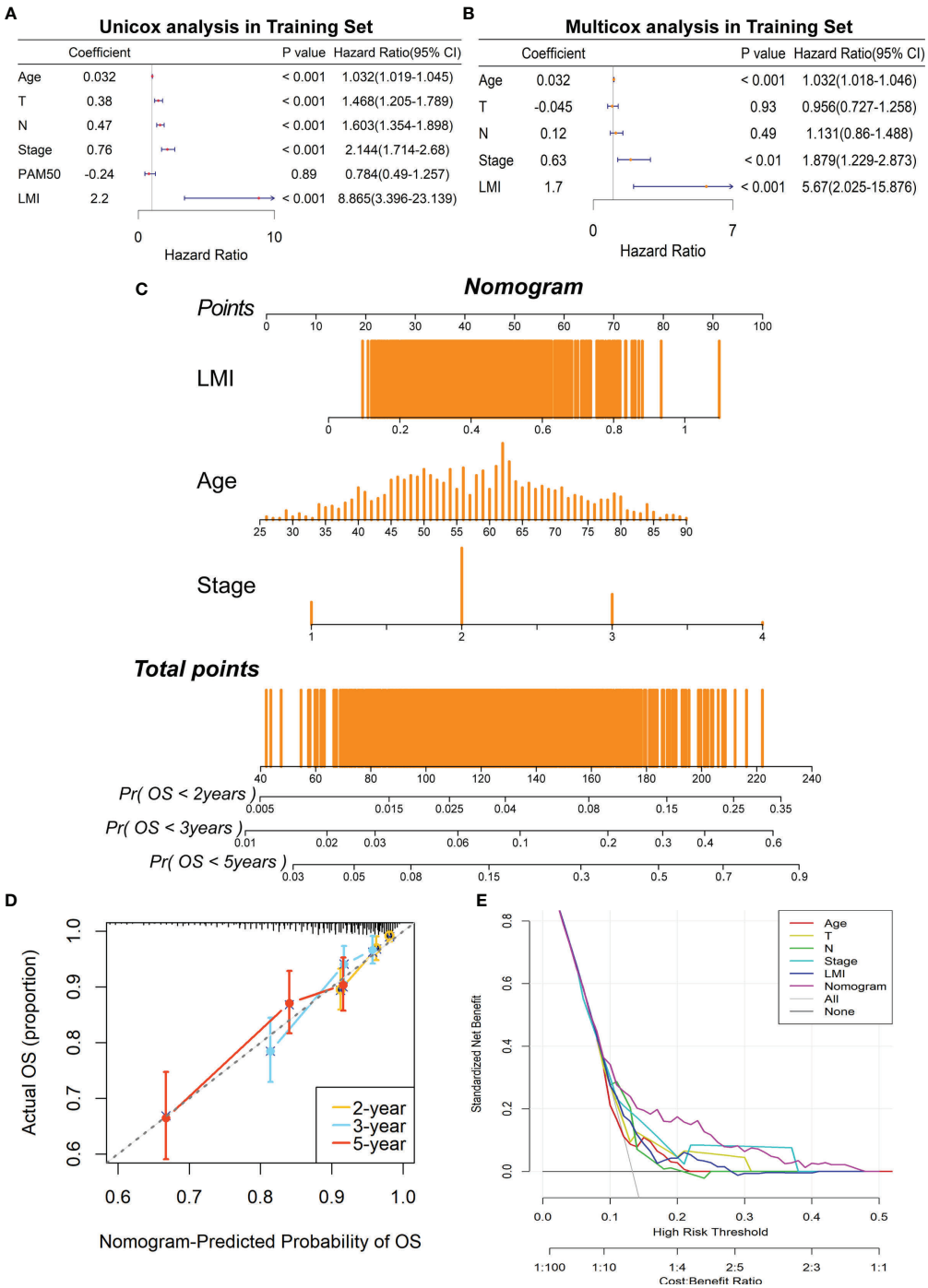

FIGURE 5 | Construction of a prognostic nomogram containing LMI signature in the training set. **(A)** Univariate Cox regression analysis of age, T stage, N stage, AJCC stage, PAM50 subtypes, and LMI for OS. **(B)** Multivariate Cox regression analysis of age, T stage, N stage, AJCC stage, and LMI for OS. **(C)** Nomogram for the prediction of 2-, 3-, and 5-year survival probability. **(D)** The calibration plot to assess the consistency of predicted and actual OS based on the nomogram. **(E)** Decision curve analysis (DCA) for evaluating clinical utility of the nomogram.

clinical net benefit than any single clinical feature (**Figure 5E**). Collectively, the prognostic nomogram based on LMI signature has excellent prediction performance for OS of breast cancer patients.

Verification of Different Biological Functions Between Two LMI Groups

To clarify the different biological functions and signaling pathways between high- and low-LMI groups in the training set, "GSVA"

enrichment analysis was exploited to detect that there are substantial differences in the metabolic pathways and immune-related pathways in the two LMI subgroups of BC (**Figure 6A**). For instance, ether lipid metabolism, cytokine cytokine-receptor interaction, and arachidonic acid metabolism were primarily enriched in the high-LMI group, while selenoamino acid metabolism, pyrimidine metabolism, B-cell receptor signaling pathway, T-cell receptor signaling pathway, and natural killer cell-mediated cytotoxicity were considerably enriched in the low-LMI group.

Underlying Implications for Immunotherapy and TME Landscape Estimation Based on LMI

As the aforementioned result unveiled the immune-related pathways with significant differences between the high- and low-LMI groups, considerable attention was paid to the TME landscape and characteristics of the two LMI subgroups. ESTIMATE algorithm was utilized to calculate the stromal score, immune score, and ESTIMATE score to evaluate and quantify the TME, the results of which unraveled that the low-LMI group of BC obtained the higher ESTIMATE score, stromal score, and immune score together with the diminished tumor purity than the high-LMI group (**Figure 6B**). Furthermore, the comparison of expression levels of the candidate immune checkpoints within the two LMI groups manifested that PD-1, CTLA4, CD96, VSIR, TIGIT except PD-L1 were significantly augmented in the low-LMI group (**Figure 6C**), which hinted that BC patients with lower LMI might acquire a more enhanced response to immunotherapy targeting the checkpoints above. Aiming to estimate the distribution of immune infiltrating cells in the TME of BC in various LMI groups, the CIBERSORT algorithm was performed to disclose that CD8+ T cells, gamma delta T cells, resting NK cells, resting dendritic cells, and neutrophils were notably enriched in TME of the low-LMI group while macrophages M0 and M2 were markedly strengthened in the high-LMI group (**Figure 6D**). Collectively, the results above shed light on that BC patients of the lower LMI could attain an immune-activated TME, while BC patients of the higher LMI might gain an immunosuppressive TME that contributed to the immune escape of tumor cells and a worse prognosis.

Additionally, it is well established that cytokines play a crucial role in the immune TME. Therefore, the boxplots in TCGA-BRCA dataset show that the expression levels of IL-2, IL-6, IL-18, TNF, IFNG, GZMA, and GZMB were promoted in the low-LMI group (**Figure 7A**). Likewise, in the METABRIC dataset, IL-1B, IL-6, IFNG, and GZMA were enhanced in the low-LMI group (**Figure 7B**). Meanwhile, IL-1B, IL-2, IL-6, IL-10, IL-18, IFNG, GZMA, and GZMB were elevated in BC patients of the low-LMI group (**Figure 7C**).

DISCUSSION

Despite great improvement in breast cancer treatment, some patients still have inferior outcomes after systemic therapy measures. In order to distinguish this target population, the identification of novel and valid biomarkers is needed. As considerable studies reveal that lactate has a vital role in tumorigenesis and progression, lactate metabolism has drawn increasing attention in recent years (3). For breast cancer, tumor lactate has been indicated as an unfavorable biomarker and was related to HER2 status and trastuzumab susceptibility (7, 8). However, additional data and more studies were required to support this conclusion. To provide more direct evidence for the important finding, our study integrated mRNA expression profiles of lactate metabolism-related genes and clinical variables of breast cancer patients from three independent databases to construct a predictive signature and then validate its efficacy.

In search of the most effective LMGs to establish the signature, we initially performed univariate Cox regression analyses of OS in breast cancer patients of both TCGA and METABRIC databases. Nine obtained genes were then further optimized with LASSO Cox regression analysis in TCGA-BRCA, and 5 pivotal genes were enrolled to establish the prognostic signature, namely LMI, including RPS14, SLC19A1, CYC1, RRM2B, and OCRL. The ribosomal protein S14 (RPS14), which was identified to be associated with the cancer-prone 5q-syndrome, was also found to negate c-Myc functions and promotes the proliferation and metastasis of estrogen receptor-positive breast cancer cells (28, 29). However, the result diverged from the findings shown in **Figure 2**, which may have resulted from different subtypes of breast cancer. Solute carrier family 19 member 1(SLC19A1), as the first known transporter of cGAMP and other CDNs (30), has been suggested to exert influence on cancer immunotherapy (31). Our study indicated that high expression of SLC19A1 was related to poorer survival in breast cancer, and therefore, the effects and potential functions of SLC19A1 on breast cancer initiation and progression warrant further investigation. Cytochrome c1 (CYC1), an important subunit of mitochondrial complex III, was found to be upregulated in breast cancer and might be a predictive factor assisting future patient diagnosis (32, 33), which was consistent with the results of our study. Ribonucleotide reductase M2B (RRM2B), also known as p53R2, was believed to play essential roles in DNA repair, mtDNA synthesis, and protection against oxidative stress (34) and has been reported to be associated with tumorigenesis of several cancer types, including colorectal cancer (35), hepatocellular carcinoma (36), esophageal squamous cell carcinoma (37), and breast cancer (38). As an unfavorable factor indicated in the present study, we suggested intensive research on the role of RRM2B in breast cancer. As for OCRL, the role in cancer remained to be further elucidated by experiments.

Based on the above five selected genes, a prognostic signature was established and was named LMI. To explore the prognostic value and clinical relevance of LMI, we proceeded with the following investigation. From the result of survival analyses, high LMI levels were confirmed to predict worse overall survival probability in breast cancer patients of three datasets independently. Besides, patients of each dataset were clarified into subgroups according to different clinical features, including

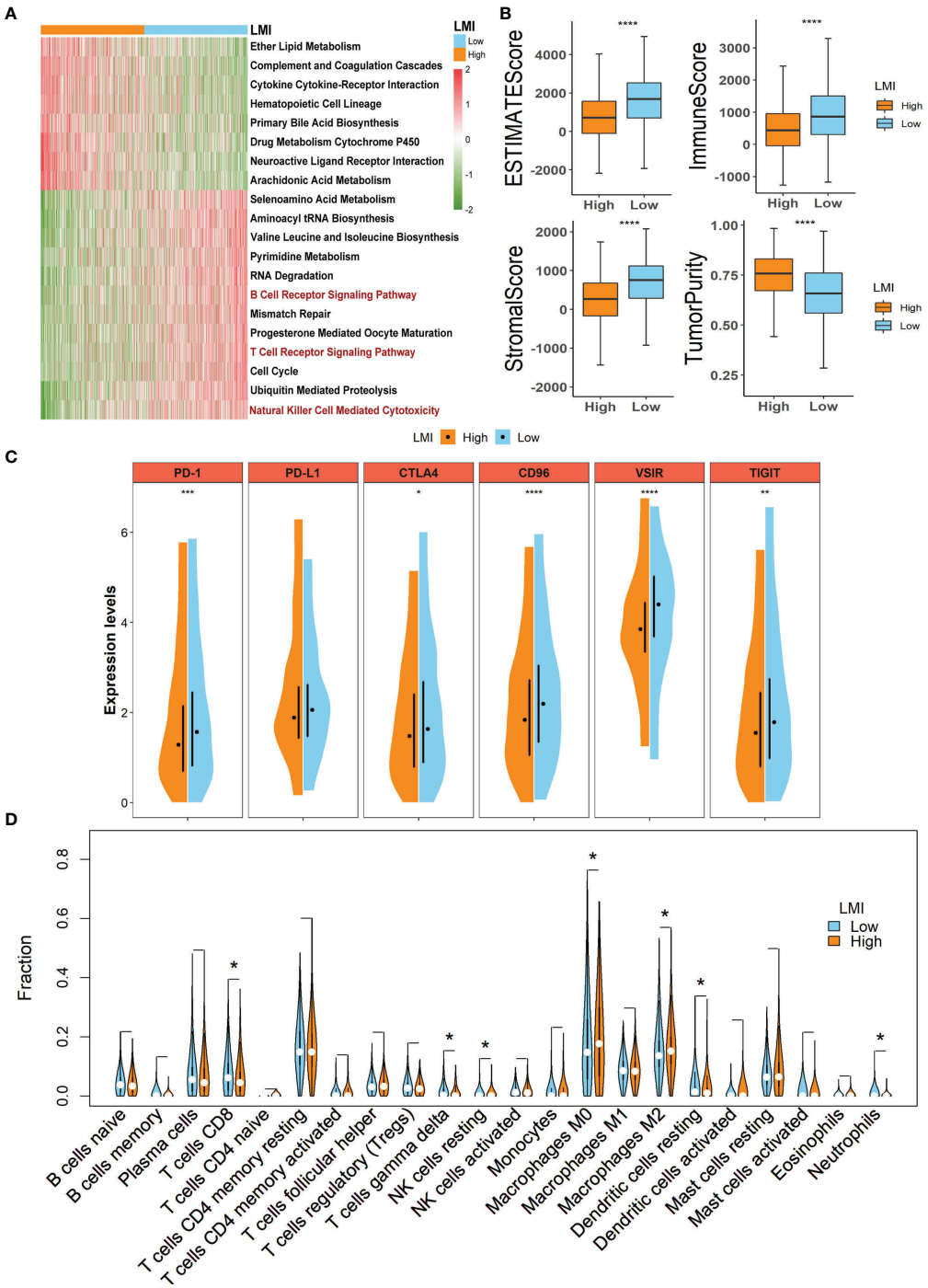

FIGURE 6 | Potential implications for immunotherapy and TME landscape estimation between the high- and low-LMI groups. **(A)** Results of GSVA in TCGA-BRCA cohort to delineate the enriched pathways. **(B)** Differences of ESTIMATE score, immune score, stromal score, and tumor purity. **(C)** Expression levels of immune checkpoints. **(D)** Violin plots to display the proportions of 22 immune infiltrating cells in total BC patients. *p < 0.05; **p < 0.01; ***p < 0.001; ****p < 0.0001.

survival status, T stage or tumor size, N stage or positive nodes, AJCC stage, PAM50 subtypes, and LMI levels of various subgroups were then compared. In general, increasing LMI value was associated with larger tumors, more metastasis lymph nodes, and a more severe AJCC stage. Nevertheless, the results of the three different cohorts were not in complete agreement with each other, and naturally, a much larger cohort should be required to confirm these findings in

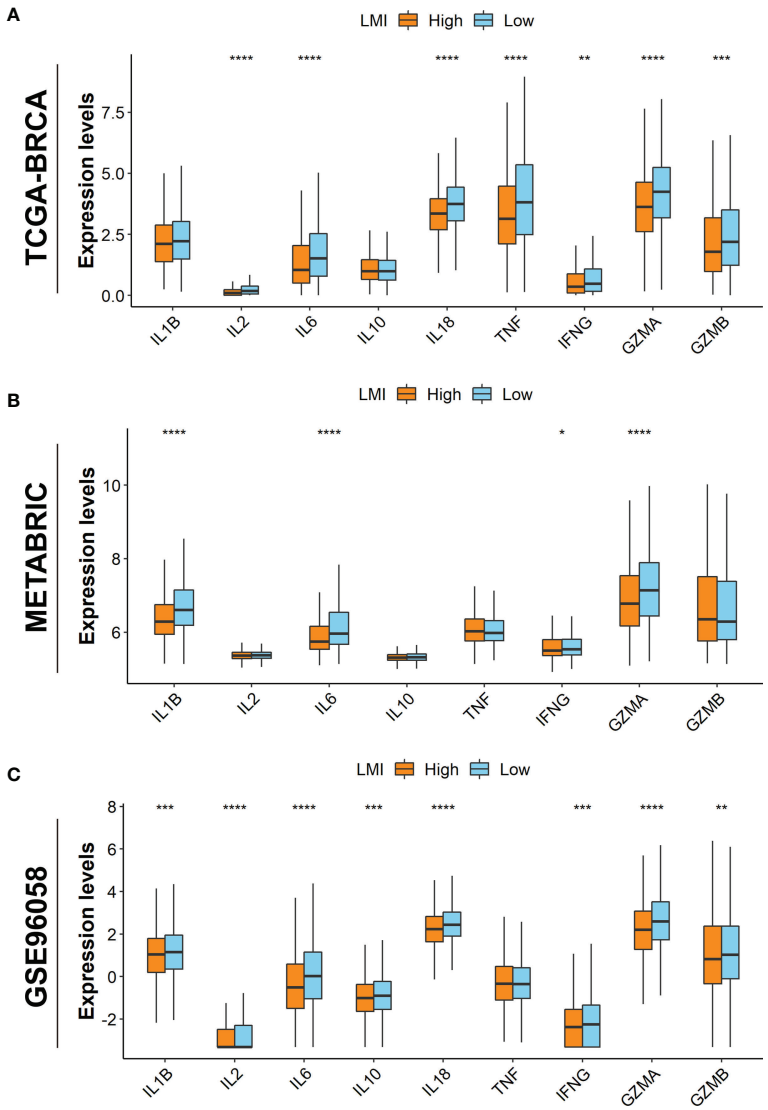

FIGURE 7 | Investigations of TME cytokines. Expression levels of IL-1B, IL-2, IL-6, IL-10, IL-18, TNF, IFNG, GZMA, and GZMB in TCGA-BRCA **(A)**, METABRIC **(B)**, and GSE96058 **(C)** datasets. *p < 0.05; **p < 0.01; ***p < 0.001; ****p < 0.0001.

prospective studies. Furthermore, the LMI signature was identified as an independent prognostic indicator when adjusted for several vital clinical variables, such as age, T stage, N stage, AJCC stage, and PAM50 subtypes in the training set, through univariate and multivariate Cox regression analyses. Finally, a prognostic nomogram, which incorporated LMI value, age, and AJCC stage, was developed for predicting the OS rate of breast cancer patients in TCGA-BRCA. Calibration plots and DCA plots were also applied to assess the practicability of the prognostic nomogram, which exhibited good fitness and the potential clinical feasibility. Moreover, to investigate LMI-related molecular functions, GSVA results revealed that tumor metabolism-related signaling pathways were highly enriched in the high-LMI group, such as ether lipid metabolism, cytokine cytokine-receptor interaction, and arachidonic acid metabolism pathways, while immune-related functions were highly enriched in the low-LMI group, like B-cell receptor signaling pathway, T-cell receptor signaling pathway, and natural killer cell-mediated cytotoxicity pathways. Certainly, further studies should be warranted to elucidate clearly the complete and detailed mechanisms involved in this process.

As lactate metabolism has become a hotspot in cancer research due to its important role in TME (12), we further explored the TME landscape estimation based on LMI. Above all, ESTIMATE results presented that LMI was negatively correlated with estimate score, immune score, and stromal score but positively with tumor purity, suggesting that LMI signature could serve as a novel and potential immune indicator in breast cancer. Meanwhile, cancer

immunotherapy has now become one of the pillars in the treatment of various cancer, including breast cancer (39). However, tumor-induced immune suppression, to which lactate metabolism has contributed to some extent, has been a major barrier to the effective responses of immune therapy until the present time (40). Thus, it remains especially important to find reliable biomarkers that could be used to precisely identify breast cancer patients for immunotherapy. After comparing the expression levels of common immune checkpoints between high- and low-LMI groups in breast cancer, we found that expressions of PD-1, CTLA4, CD96, VSIR, and TIGIT except PD-L1 were significantly upregulated in the low-LMI group, which hinted that breast cancer patients with lower LMI value might have had a better immunotherapy response. To some extent, the results were consistent that high lactate has contributed to immune invasion and suppressed antitumor immune responses. Subsequently, the landscape of tumor-infiltrating immune cells between high- and low-LMI groups was estimated and the result disclosed that CD8+ T cells, gamma delta T cells, resting NK cells, resting dendritic cells, and neutrophils were notably enriched in the TME of the low-LMI group while macrophages M0 and M2 were markedly strengthened in the high-LMI group. Increased lactate has been confirmed as a major contributor to acidosis in the TME, and accordingly decreased extracellular pH has been verified to weaken functions of CD8+ and CD4+ lymphocytes, including activation, cytotoxicity, chemotaxis, motility, and proliferation (41). As well as inhibiting effector T cell function, lactate concentrations in the TME favor immunosuppressive Treg development (42). As will be discussed, lactate can directly suppress the cytotoxic functions of DCs, natural killer (NK), and natural killer T (NKT) cells (12, 14). For tumor-associated macrophages (TAMs), lactate-driven TAM polarization is a vital mechanism of immune escape for cancer cells (40). Taken together, breast cancer patients with high-LMI value have unfavorable immunotherapy responses due to the deficiency of effective antitumor immune cells and the enrichment of immunosuppressive cells. In addition, cytokines, which are present in the TME, have an essential role in cancer pathogenesis and cancer therapy (43). Generally, host-derived cytokines can suppress tumor progression and tumor cells can exploit host-derived cytokines to promote development (44). Through evaluating the expression levels of several cytokines in three datasets, we concluded that IL-6, IFNG, and GZMA were highly expressed in the low-LMI group.

Strikingly, the present study provided a comprehensive analysis of LMGs in breast cancer and constructed an effective LMI signature which has implications for future studies of breast cancer immune treatment. Nevertheless, there remain some limitations that should be contemplated. All the conclusions should be further supported by experimental data.

CONCLUSION

To conclude, our research established a reliable clinical signature of LMI rooted in lactate metabolism-related genes for BC patients. Additionally, the signature was unraveled as an independent prognostic factor, and a nomogram with high usability embodying LMI was generated. The latent connotations between LMI and tumor immune microenvironment were unveiled. In a nutshell, our study might support crucial preclinical significance in cancer research about lactate metabolism and immunotherapy.

DATA AVAILABILITY STATEMENT

The original contributions presented in the study are included in the article/**Supplementary Material**. Further inquiries can be directed to the corresponding authors.

AUTHOR CONTRIBUTIONS

All authors participated in the present study, including conception and design (ZZ and YP), data collection, data analysis, drafting or critically revising the article (LY, PT, and HS), as well as study supervision (ZZ and YP). All authors have read and approved the final version submitted.

FUNDING

This study was supported by the Guangzhou Municipal Science and Technology Project (201804010132 to HS) and the National Natural Science Foundation of Guangdong Province, China (2022A1515012536 to LY).

ACKNOWLEDGMENTS

We are also grateful to the contributors to the public databases used in this study and the reviewers for their constructive and helpful comments.

SUPPLEMENTARY MATERIAL

The Supplementary Material for this article can be found online at: https://www.frontiersin.org/articles/10.3389/fonc.2022.874731/full#supplementary-material

REFERENCES

1. Sung H, Ferlay J, Siegel RL, Laversanne M, Soerjomataram I, Jemal A, et al. Global Cancer Statistics 2020: GLOBOCAN Estimates of Incidence and Mortality Worldwide for 36 Cancers in 185 Countries. *CA Cancer J Clin* (2021) 71(3):209–49. doi: 10.3322/caac.21660

2. Early Breast Cancer Trialists' Collaborative G, Darby S, McGale P, Correa C, Taylor C, Arriagada R, et al. Effect of Radiotherapy After Breast-Conserving Surgery on 10-Year Recurrence and 15-Year Breast Cancer Death: Meta-Analysis of Individual Patient Data for 10,801 Women in 17 Randomised Trials. *Lancet* (2011) 378(9804):1707–16. doi: 10.1016/S0140-6736(11)61629-2

3. Hirschhaeuser F, Sattler UG, Mueller-Klieser W. Lactate: A Metabolic Key Player in Cancer. *Cancer Res* (2011) 71(22):6921–5. doi: 10.1158/0008-5472.CAN-11-1457
4. Walenta S, Wetterling M, Lehrke M, Schwickert G, Sundfor K, Rofstad EK, et al. High Lactate Levels Predict Likelihood of Metastases, Tumor Recurrence, and Restricted Patient Survival in Human Cervical Cancers. *Cancer Res* (2000) 60(4):916–21.
5. Ziebart T, Walenta S, Kunkel M, Reichert TE, Wagner W, Mueller-Klieser W. Metabolic and Proteomic Differentials in Head and Neck Squamous Cell Carcinomas and Normal Gingival Tissue. *J Cancer Res Clin Oncol* (2011) 137 (2):193–9. doi: 10.1007/s00432-010-0875-y
6. Sattler UG, Meyer SS, Quennet V, Hoerner C, Knoerzer H, Fabian C, et al. Glycolytic Metabolism and Tumour Response to Fractionated Irradiation. *Radiother Oncol* (2010) 94(1):102–9. doi: 10.1016/j.radonc.2009.11.007
7. Cheung SM, Husain E, Masannat Y, Miller ID, Wahle K, Heys SD, et al. Lactate Concentration in Breast Cancer Using Advanced Magnetic Resonance Spectroscopy. *Br J Cancer* (2020) 123(2):261–7. doi: 10.1038/s41416-020-0886-7
8. Castagnoli L, Iorio E, Dugo M, Koschorke A, Faraci S, Canese R, et al. Intratumor Lactate Levels Reflect HER2 Addiction Status in HER2-Positive Breast Cancer. *J Cell Physiol* (2019) 234(2):1768–79. doi: 10.1002/jcp.27049
9. Hinshaw DC, Shevde LA. The Tumor Microenvironment Innately Modulates Cancer Progression. *Cancer Res* (2019) 79(18):4557–66. doi: 10.1158/0008-5472.CAN-18-3962
10. Certo M, Tsai CH, Pucino V, Ho PC, Mauro C. Lactate Modulation of Immune Responses in Inflammatory Versus Tumour Microenvironments. *Nat Rev Immunol* (2021) 21(3):151–61. doi: 10.1038/s41577-020-0406-2
11. Comito G, Iscaro A, Bacci M, Morandi A, Ippolito L, Parri M, et al. Lactate Modulates CD4(+) T-Cell Polarization and Induces an Immunosuppressive Environment, Which Sustains Prostate Carcinoma Progression *via* TLR8/miR21 Axis. *Oncogene* (2019) 38(19):3681–95. doi: 10.1038/s41388-019-0688-7
12. Husain Z, Huang Y, Seth P, Sukhatme VP. Tumor-Derived Lactate Modifies Antitumor Immune Response: Effect on Myeloid-Derived Suppressor Cells and NK Cells. *J Immunol* (2013) 191(3):1486–95. doi: 10.4049/jimmunol.1202702
13. Xie D, Zhu S, Bai L. Lactic Acid in Tumor Microenvironments Causes Dysfunction of NKT Cells by Interfering With mTOR Signaling. *Sci China Life Sci* (2016) 59(12):1290–6. doi: 10.1007/s11427-016-0348-7
14. Gottfried E, Kunz-Schughart LA, Ebner S, Mueller-Klieser W, Hoves S, Andreesen R, et al. Tumor-Derived Lactic Acid Modulates Dendritic Cell Activation and Antigen Expression. *Blood* (2006) 107(5):2013–21. doi: 10.1182/blood-2005-05-1795
15. Chen P, Zuo H, Xiong H, Kolar MJ, Chu Q, Saghatelian A, et al. Gpr132 Sensing of Lactate Mediates Tumor-Macrophage Interplay to Promote Breast Cancer Metastasis. *Proc Natl Acad Sci USA* (2017) 114(3):580–5. doi: 10.1073/pnas.1614035114
16. Schouwenburg MG, Suijkerbuijk KPM, Koornstra RHT, Jochems A, van Zeijl MCT, van den Eertwegh AJM, et al. Switching to Immune Checkpoint Inhibitors Upon Response to Targeted Therapy; The Road to Long-Term Survival in Advanced Melanoma Patients With Highly Elevated Serum LDH? *Cancers (Basel)* (2019) 11(12). doi: 10.3390/cancers11121940
17. Zhang Z, Li Y, Yan X, Song Q, Wang G, Hu Y, et al. Pretreatment Lactate Dehydrogenase may Predict Outcome of Advanced non Small-Cell Lung Cancer Patients Treated With Immune Checkpoint Inhibitors: A Meta-Analysis. *Cancer Med* (2019) 8(4):1467–73. doi: 10.1002/cam4.2024
18. Wang X, Zhang B, Chen X, Mo H, Wu D, Lan B, et al. Lactate Dehydrogenase and Baseline Markers Associated With Clinical Outcomes of Advanced Esophageal Squamous Cell Carcinoma Patients Treated With Camrelizumab (SHR-1210), a Novel Anti-PD-1 Antibody. *Thorac Cancer* (2019) 10(6):1395–401. doi: 10.1111/1759-7714.13083
19. Zou Y, Zou X, Zheng S, Tang H, Zhang L, Liu P, et al. Efficacy and Predictive Factors of Immune Checkpoint Inhibitors in Metastatic Breast Cancer: A Systematic Review and Meta-Analysis. *Ther Adv Med Oncol* (2020) 12:1758835920940928. doi: 10.1177/1758835920940928
20. Mayakonda A, Lin DC, Assenov Y, Plass C, Koeffler HP. Maftools: Efficient and Comprehensive Analysis of Somatic Variants in Cancer. *Genome Res* (2018) 28(11):1747–56. doi: 10.1101/gr.239244.118
21. McCarthy DJ, Chen Y, Smyth GK. Differential Expression Analysis of Multifactor RNA-Seq Experiments With Respect to Biological Variation. *Nucleic Acids Res* (2012) 40(10):4288–97. doi: 10.1093/nar/gks042
22. Zhang H, Meltzer P, Davis S. RCircos: An R Package for Circos 2D Track Plots. *BMC Bioinf* (2013) 14:244. doi: 10.1186/1471-2105-14-244
23. Zhang Z, Kattan MW. Drawing Nomograms With R: Applications to Categorical Outcome and Survival Data. *Ann Transl Med* (2017) 5(10):211. doi: 10.21037/atm.2017.04.01
24. Alba AC, Agoritsas T, Walsh M, Hanna S, Iorio A, Devereaux PJ, et al. Discrimination and Calibration of Clinical Prediction Models: Users' Guides to the Medical Literature. *JAMA* (2017) 318(14):1377–84. doi: 10.1001/jama.2017.12126
25. Hanzelmann S, Castelo R, Guinney J. GSVA: Gene Set Variation Analysis for Microarray and RNA-Seq Data. *BMC Bioinf* (2013) 14:7. doi: 10.1186/1471-2105-14-7
26. Yoshihara K, Shahmoradgoli M, Martinez E, Vegesna R, Kim H, Torres-Garcia W, et al. Inferring Tumour Purity and Stromal and Immune Cell Admixture From Expression Data. *Nat Commun* (2013) 4:2612. doi: 10.1038/ncomms3612
27. Newman AM, Liu CL, Green MR, Gentles AJ, Feng W, Xu Y, et al. Robust Enumeration of Cell Subsets From Tissue Expression Profiles. *Nat Methods* (2015) 12(5):453–7. doi: 10.1038/nmeth.3337
28. Zhou X, Hao Q, Liao JM, Liao P, Lu H. Ribosomal Protein S14 Negatively Regulates C-Myc Activity. *J Biol Chem* (2013) 288(30):21793–801. doi: 10.1074/jbc.M112.445122
29. Wang X, Yao S, Luo G, Zhou Y, Fang Q. Downregulation of RPS14 Inhibits the Proliferation and Metastasis of Estrogen Receptor-Positive Breast Cancer Cells. *Anticancer Drugs* (2021) 32(10):1019–28. doi: 10.1097/CAD.0000000000001112
30. Ritchie C, Cordova AF, Hess GT, Bassik MC, Li L. SLC19A1 Is an Importer of the Immunotransmitter cGAMP. *Mol Cell* (2019) 75(2):372–81.e5. doi: 10.1016/j.molcel.2019.05.006
31. Luteijn RD, Zaver SA, Gowen BG, Wyman SK, Garelis NE, Onia L, et al. SLC19A1 Transports Immunoreactive Cyclic Dinucleotides. *Nature* (2019) 573(7774):434–8. doi: 10.1038/s41586-019-1553-0
32. Han Y, Sun S, Zhao M, Zhang Z, Gong S, Gao P, et al. CYC1 Predicts Poor Prognosis in Patients With Breast Cancer. *Dis Markers* (2016) 2016:3528064. doi: 10.1155/2016/3528064
33. Chishiki M, Takagi K, Sato A, Miki Y, Yamamoto Y, Ebata A, et al. Cytochrome C1 in Ductal Carcinoma *In Situ* of Breast Associated With Proliferation and Comedo Necrosis. *Cancer Sci* (2017) 108(7):1510–9. doi: 10.1111/cas.13251
34. Wang X, Zhenchuk A, Wiman KG, Albertioni F. Regulation of P53r2 and its Role as Potential Target for Cancer Therapy. *Cancer Lett* (2009) 276(1):1–7. doi: 10.1016/j.canlet.2008.07.019
35. Liu X, Lai L, Wang X, Xue L, Leora S, Wu J, et al. Ribonucleotide Reductase Small Subunit M2B Prognoses Better Survival in Colorectal Cancer. *Cancer Res* (2011) 71(9):3202–13. doi: 10.1158/0008-5472.CAN-11-0054
36. Tian H, Ge C, Li H, Zhao F, Hou H, Chen T, et al. Ribonucleotide Reductase M2B Inhibits Cell Migration and Spreading by Early Growth Response Protein 1-Mediated Phosphatase and Tensin Homolog/Akt1 Pathway in Hepatocellular Carcinoma. *Hepatology* (2014) 59(4):1459–70. doi: 10.1002/hep.26929
37. Okumura H, Natsugoe S, Yokomakura N, Kita Y, Matsumoto M, Uchikado Y, et al. Expression of P53r2 is Related to Prognosis in Patients With Esophageal Squamous Cell Carcinoma. *Clin Cancer Res* (2006) 12(12):3740–5. doi: 10.1158/1078-0432.CCR-05-2416
38. Xue L, Liu X, Wang Q, Liu CQ, Chen Y, Jia W, et al. Ribonucleotide Reductase Subunit M2B Deficiency Leads to Mitochondrial Permeability Transition Pore Opening and is Associated With Aggressive Clinicopathologic Manifestations of Breast Cancer. *Am J Transl Res* (2018) 10(11):3635–49.
39. Emens LA. Breast Cancer Immunotherapy: Facts and Hopes. *Clin Cancer Res* (2018) 24(3):511–20. doi: 10.1158/1078-0432.CCR-16-3001
40. Hayes C, Donohoe CL, Davern M, Donlon NE. The Oncogenic and Clinical Implications of Lactate Induced Immunosuppression in the Tumour Microenvironment. *Cancer Lett* (2021) 500:75–86. doi: 10.1016/j.canlet.2020.12.021
41. Erra Diaz F, Dantas E, Geffner J. Unravelling the Interplay Between Extracellular Acidosis and Immune Cells. *Mediators Inflamm* (2018) 2018:1218297.

42. Angelin A, Gil-de-Gomez L, Dahiya S, Jiao J, Guo L, Levine MH, et al. Foxp3 Reprograms T Cell Metabolism to Function in Low-Glucose, High-Lactate Environments. *Cell Metab* (2017) 25(6):1282–93.e7. doi: 10.1016/j.cmet.2016.12.018
43. Ozer H. Cytokines in Oncology. *Curr Opin Oncol* (1989) 1(2):241–8.
44. Dranoff G. Cytokines in Cancer Pathogenesis and Cancer Therapy. *Nat Rev Cancer* (2004) 4(1):11–22. doi: 10.1038/nrc1252

Conflict of Interest: The authors declare that the research was conducted in the absence of any commercial or financial relationships that could be construed as a potential conflict of interest.

Publisher's Note: All claims expressed in this article are solely those of the authors and do not necessarily represent those of their affiliated organizations, or those of the publisher, the editors and the reviewers. Any product that may be evaluated in this article, or claim that may be made by its manufacturer, is not guaranteed or endorsed by the publisher.

Copyright © 2022 Yang, Tan, Sun, Zeng and Pan. This is an open-access article distributed under the terms of the Creative Commons Attribution License (CC BY). The use, distribution or reproduction in other forums is permitted, provided the original author(s) and the copyright owner(s) are credited and that the original publication in this journal is cited, in accordance with accepted academic practice. No use, distribution or reproduction is permitted which does not comply with these terms.

frontiers | Frontiers in Cell and Developmental Biology

ORIGINAL RESEARCH
published: 03 May 2022
doi: 10.3389/fcell.2022.815480

OAS3 is a Co-Immune Biomarker Associated With Tumour Microenvironment, Disease Staging, Prognosis, and Treatment Response in Multiple Cancer Types

*Xin-yu Li[1,2†], Lei Hou[3†], Lu-yu Zhang[4†], Liming Zhang[1†], Deming Wang[1], Zhenfeng Wang[1], Ming-Zhe Wen[1] and Xi-tao Yang[1]**

[1]Department of Interventional Therapy, Shanghai Ninth People's Hospital, Shanghai Jiao Tong University School of Medicine, Shanghai, China, [2]Department of Neurosurgery, Shanghai Ninth People's Hospital, Shanghai JiaoTong University School of Medicine, Shanghai, China, [3]Jiading District Central Hospital Affiliated Shanghai University of Medicine and Health Sciences, Shanghai, China, [4]Department of Urologic Surgery, The First Affiliated Hospital of Zhengzhou University, Zhengzhou, China

OPEN ACCESS

Edited by:
Pranav Gupta,
Albert Einstein College of Medicine,
United States

Reviewed by:
Chengdong Liu,
Southern Medical University, China
Bienyameen Baker,
Stellenbosch University, South Africa

***Correspondence:**
Xi-tao Yang
xitao123456@126.com

†These authors share first authorship

Specialty section:
This article was submitted to Molecular and Cellular Oncology, a section of the journal Frontiers in Cell and Developmental Biology

Received: 15 November 2021
Accepted: 28 March 2022
Published: 03 May 2022

Citation:
Li X-y Hou L, Zhang L-y Zhang L, Wang D, Wang Z, Wen M-Z and Yang X-t (2022) OAS3 is a Co-Immune Biomarker Associated With Tumour Microenvironment, Disease Staging, Prognosis, and Treatment Response in Multiple Cancer Types. Front. Cell Dev. Biol. 10:815480. doi: 10.3389/fcell.2022.815480

2′,5′-oligoadenylate synthase (OAS) is a class of enzymes induced by interferons and mainly encoded by the OAS1, OAS2, and OAS3 genes, which activate the potential RNA enzymes to degrade viral mRNA, inhibit viral protein synthesis and promote apoptosis in virus-infected cells. *OAS3* is associated with breast cancer prognosis. However, the expression and prognosis of *OAS3* and tumour-infiltrating lymphocytes in pan-cancer remain unknown. In the present study, we have systematically investigated and confirmed the role of *OAS3* in tumour immune infiltration, immune escape, tumour progression, response to treatment, and prognosis of different cancer types using various bioinformatics methods. The findings suggest that *OAS3* is aberrantly expressed in almost all TCGA cancer types and subtypes and is associated with tumour staging, metastasis, and prognostic deterioration in different tumours. In addition, *OAS3* expression is associated with the prognosis and chemotherapeutic outcomes of various cancers. In terms of immune-infiltrating levels, *OAS3* expression is positively associated with the infiltration of immunosuppressive cells. These findings suggest that *OAS3* is correlated with prognosis and immune-infiltrating levels.

Keywords: OAS3, pancancer analysis, biomarker, tumour microenvironment, prognosis carcinoma

INTRODUCTION

The development and progression of malignancy is a complex process involving several stages (Yang et al., 2019). Malignant tumours are heterogeneous and result from an accumulation of distinct genetic and epigenetic alterations (Lin et al., 2015). Several studies have suggested that genetic and epigenetic alterations can be functionally associated with carcinogenesis (Toyota and Suzuki, 2010; Coppedè et al., 2014; Grady et al., 2021). The tumor microenvironment (TME) is a complex cellular ecosystem in which tumor, stroma, and immune cells interact dynamically through secreted factors and physical interactions in a dynamic extracellular matrix (Grauel et al., 2020). The complexity of TME results in an interplay of various cellular signalling systems in which tumour cells infiltrate immune cells, making them dysfunctional, and hence unable to initiate any anti-tumour immune

TABLE 1 | Basic clinical characteristics of LIHC patients in validation cohort.

Characteristic	Levels	Overall
n		36
T stage, n (%)	T1	18 (50%)
	T2	7 (20%)
	T3	7 (20%)
	T4	4 (10%)
N stage, n (%)	N0	32 (90%)
	N1	4 (10%)
M stage, n (%)	M0	32 (90%)
	M1	4 (10%)
Pathologic stage, n (%)	Stage I	18 (50%)
	Stage II	9 (25%)
	Stage III	4(10%)
	Stage IV	9 (13%)
Age, n (%)	<=60	18 (50%)
	>60	
Gender, n (%)	Female	15 (40%)
	Male	21(60%)
Age, median (IQR)		55 (50, 61)

TABLE 2 | Basic clinical characteristics of LUAD patients in validation cohort.

Characteristic	Levels	Overall
n		30
T stage, n (%)	T1	9 (30%)
	T2	15(50%)
	T3	3(10%)
	T4	3(10%)
N stage, n (%)	N0	21(70%)
	N1	5 (16%)
	N2	3 (10%)
	N3	1 (4%)
M stage, n (%)	M0	27(90%)
	M1	3 (10%)
Pathologic stage, n (%)	Stage I	15(50%)
	Stage II	6 (20%)
	Stage III	5 (16%)
	Stage IV	4 (14%)
Gender, n (%)	Female	15(50%)
	Male	15(50%)
Age, n (%)	<=65	15(50%)
	>65	15(50%)
Age, median (IQR)		60 (53, 71)

TABLE 3 | Basic clinical characteristics of KIRP patients in validation cohort.

Characteristic	Levels	Overall
n		30
Pathologic T stage, n (%)	T1	21 (70%)
	T2	3 (10%)
	T3	3 (10%)
	T4	3 (10%)
Pathologic N stage, n (%)	N0	18 (60%)
	N1	9 (30%)
	N2	3 (10%)
Pathologic M stage, n (%)	M0	27 (90%)
	M1	3 (10%)
Pathologic stage, n (%)	Stage I	18 (60%)
	Stage II	3 (10%)
	Stage III	6 (20%)
	Stage IV	3 (10%)
Gender, n (%)	Female	9 (30%)
	Male	21 (70%)
Age, n (%)	<=60	15 (50%)
	>60	15 (50%)
Age, median (IQR)		62 (55, 70)

action (Jiang et al., 2015; Thommen and Schumacher, 2018). In addition, the immunosuppressive cellular component of TME may inhibit T-cell responses, antibody production and the induction of cytotoxic T lymphocytes, promoting tumour growth, impairing the immune response, and leading to treatment resistance (Liu and Cao, 2016; Monteran and Erez, 2019). Bioinformatics can accurately capture cell-type-specific profiles and cell–cell interactions at the tissue level, resulting in relevant genomic differences in the diagnosis, staging, prognosis, and therapeutic responses among various tumours.

2′-5′-oligoadenylate synthetase (OAS), an interferon-induced antiviral enzyme, is composed of OAS1, OAS2, OAS3, and OASL. OAS3 plays a critical role in antiviral action and signal transduction, and high OAS3 expression is associated with the poor prognosis of patients with breast cancer (Zhang and Yu, 2020). Owing to the complexity of tumorigenesis, pan-cancer analysis of the expression patterns of target genes and assessment of their correlation with clinical prognosis and potential molecular mechanisms are of great importance. In this study, we performed a pan-cancer analysis to examine the expression profiles of OAS3 in different cancer tissues and identify its underlying molecular mechanisms in the clinical prognosis of tumours.

MATERIALS AND METHODS

Data Collection and Evaluation of OAS3 Expression in Pan-Cancer

RNA sequence data, survival data, and clinicopathologic characteristics of the 33 cancers were obtained from the UCEC online database (https://xena.ucsc.edu/), which was obtained from the TCGA database (Tomczak et al., 2015). Using the rma function in the R package, the whole dataset was filtered, and missing and duplicate results were removed and converted to log2 (TPM + 1). OAS3 sequencing data were obtained from the GTEx Project and Broad Institute CCLE database to analyse differences between tumours and adjacent normal tissues. In addition, 36 patients with liver hepatocellular carcinoma (LIHC), 30 patients with lung adenocarcinoma (LUAD), and 30 patients with kidney renal papillary cell carcinoma (KIRP) were recruited from the First Affiliated Hospital of Zhengzhou University and Jiading District Central Hospital Affiliated Shanghai University of Medicine as the validation cohort. The basic clinical characteristics of patients are shown in **Table 1**, **Table 2**, and **Table 3**. All patients provided written informed consent for the data to be included in the study. The study flowchart is presented in **Figure 1**.

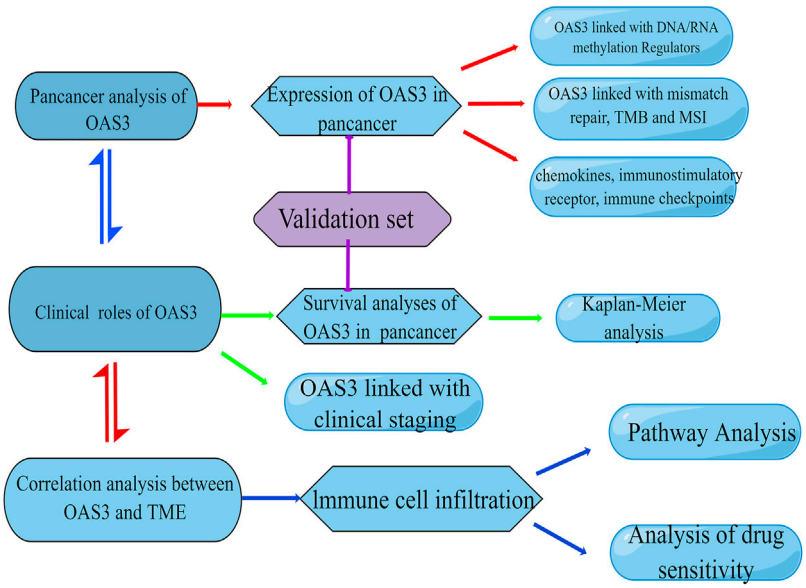

FIGURE 1 | Flowchart of the study. This image was drawn by Figdraw (www.figdraw.com).

Prognostic Significance of OAS3

We used four prognostic indicators (including overall survival [OS], disease-specific survival [DSS], disease-free survival [DFS], and disease progression-free survival [PFS]) and investigated the relationship between *OAS3* expression and the prognosis of patients with 33 cancers using forest plots. Survival results were summarised using "forestplot" (R package). Patients were divided into high and low *OAS3* expression groups based on the median *OAS3* expression. Kaplan–Meier survival analysis was conducted using the R packages "survminer" and "survival" to examine differential survival outcomes between the two groups.

Correlation Analysis of OAS3 Expression With Microsatellite Instability and Tumour Mutational Burden

Tumour mutational burden (TMB) is defined as the total number of mutations per million bases in the coding region of the exons of genes encoding specific tumour cell proteins, including insertions, substitutions, deletions, and other forms of mutations (Alexandrov et al., 2013). It is also an emerging biomarker for tumour immunotherapy prediction and may help to predict the benefits of immunotherapy in certain tumours. Microsatellite instability (MSI) is characterised by a genetic change. During the proliferation of normal cells, an intact DNA mismatch repair (MMR) system detects replication errors in microsatellite sequences in a timely manner and corrects them quickly so that the sequences are replicated with high fidelity, thus maintaining microsatellite stability. Owing to defective DNA MMR during tumorigenesis in certain tumours, errors in microsatellite sequence replication cannot be detected promptly, leading to the insertion or deletion of repetitive units and changes in microsatellite sequence length, eventually leading to MSI (Ellegren, 2004). Several clinical trials, retrospective studies and meta-analyses have confirmed that MSI is strongly associated with tumour prognosis (Petrelli et al., 2019). In this study, gene mutation data of 33 cancer types were obtained from TCGA database of UCSC Xena. TMB was calculated for each sample using R. The correlation of OAS3 expression with TMB and MSI was analysed via Spearman's correlation test, and the R package "fmsb" was used to visualise the results.

Correlation Analysis of OAS3 Expression With TME

TME is critical for the regulation of cancer development and therapy (Zhou et al., 2019). It contains stromal, tumour, and immune cells (Luo and Vögeli, 2020). The number of stromal and immune cells in TME affects many aspects of cancer growth and development. The "ESTIMATE" R package was used to assess immune infiltration (based on the ImmuneScore, StromalScore, and ESTIMATEScore) using the transcriptome data (Chen et al., 2021a). Subsequently, we analysed the association between OAS3 and TME using R.

Analysis of Tumour Immune Cell Infiltration

We used TIMER2, Xcell, CIBERSORT, and ImmuCellAI to analyse the correlation between OAS3 expression and infiltration of various immune cell types. The TIMER2 database contains information on 32 cancers and 10,897 tissues from TCGA database, which allows systematic analysis of the correlation between one or more tumours and immune cell infiltration as well as the correlation between the expression of relevant genes in tumour tissues and the prognosis, mutation and copy number of patients (Ju et al., 2020). ImmuCellAI (http://

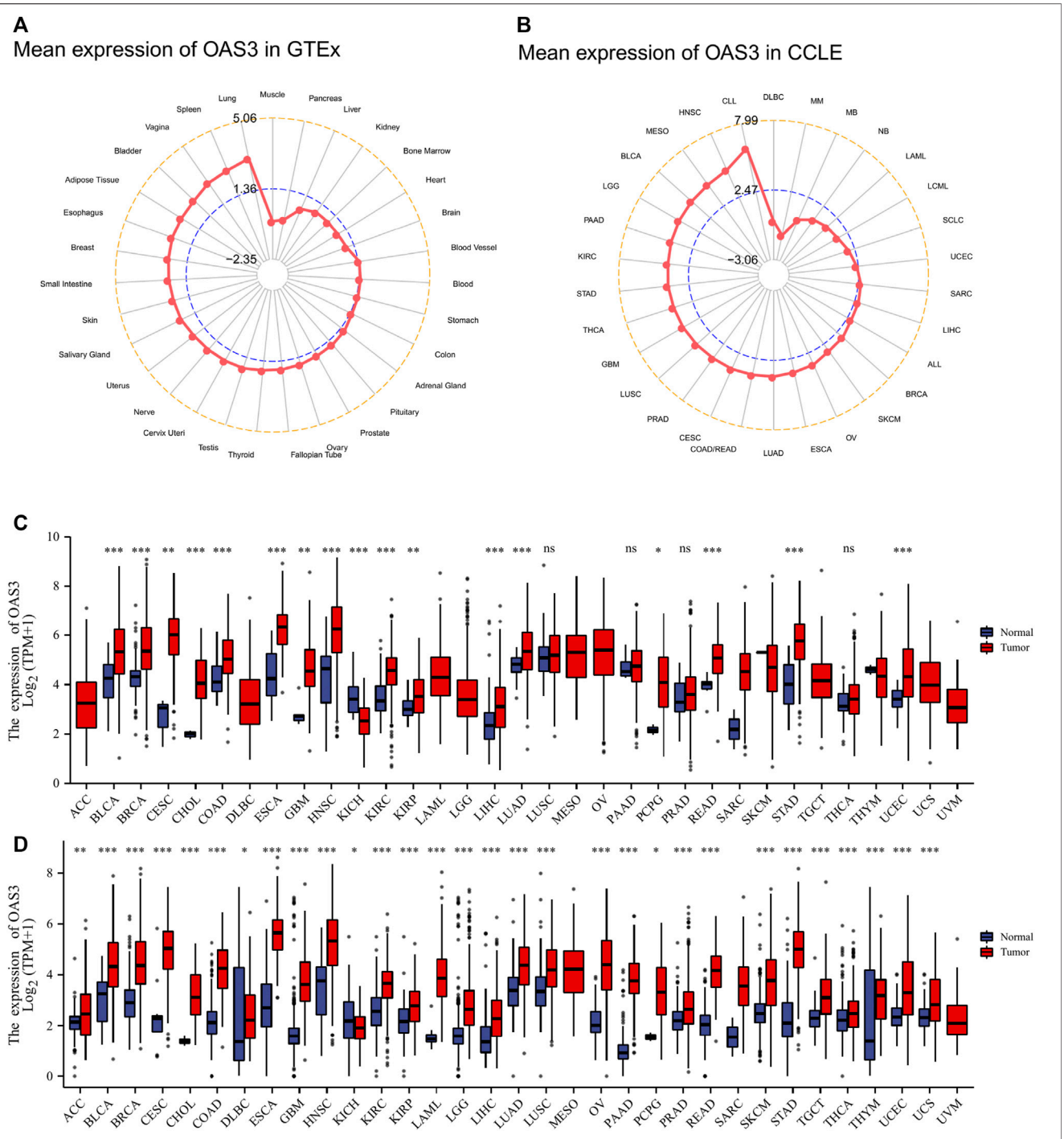

FIGURE 2 | (A): OAS3 mRNA expressions in various normal human tissues from the GTEx database. OAS3 is most highly expressed in lung and least expressed in muscle. **(B)**: OAS3 mRNA expressions from the CCLE database. The results showed that OAS3 was highly expressed in most tumors. **(C)**: Boxplots showing differential OAS3 expression levels (log2TPM + 1) between tumor and adjacent normal tissues across TCGA database. *$p < 0.05$; **$p < 0.01$; ***$p < 0.001$. **(D)**: Boxplots showing differential OAS3 expression levels (log2TPM + 1) between tumor and adjacent normal tissues across TCGA and GTEx database. *$p < 0.05$; **$p < 0.01$; ***$p < 0.001$.

bioinfo.life.hust.edu.cn/web/ImmuCellAI/) is a powerful and unique method for accurately screening tumour immune function using 24 different types of immune cells, including T cells (Huang et al., 2021). Furthermore, the XCell algorithm was used to examine several features of tumours, including the composition of infiltrating immune cells, based on the gene expression data (Schulze et al., 2020). In addition, the CIBERSORT algorithm was used to identify immune cell infiltration signatures using the R package "cibersort" (Wu et al., 2020).

Correlation of OAS3 Expression With Immune Checkpoint-Related Genes and Immune Neoantigens

Immune checkpoints refer to a subset of inhibitory signalling pathways involved in the immune response (Yuan et al., 2020). Abnormal expression of immune checkpoint-related genes is associated with tumorigenesis (Liu et al., 2021a). We examined the association of OAS3 with 47 immune checkpoint-associated genes in 33 cancers using Pearson correlation analysis. Neoantigens are abnormal proteins derived from "nonsynonymous mutations" from biological events such as point mutations, deletion mutations, and gene fusions and are specific to tumour cells (Liao and Zhang, 2021; Xu et al., 2021). The immune activity of tumour neoantigens can be used to design and synthesise neoantigen vaccines according to the conditions of the bulge of the swollen cell; these vaccines can be used to immunise patients to achieve therapeutic effects (Chen et al., 2021b). We counted the number of neoantigens in each tumour sample and used Spearman's correlation test to investigate the relationship between OAS3 and the number of antigens.

Correlation of OAS3 Expression With the Expression of DNA MMR Genes, RNA Methylation-Related Genes and DNA Methyltransferase

MMR is a critical post-replicative DNA repair process, which is essential for maintaining genomic integrity (Popp and Bohlander, 2010). Defects in the MMR system lead to genetic instability referred to as MSI (Alhopuro et al., 2012). DNA methylation is a chemical modification of DNA that can change genetic performance without changing the DNA sequence (Alhopuro et al., 2012). RNA methylation is one of the most important post-transcriptional epigenetic RNA modifications (Tian et al., 2021). The most commonly used RNA modifications are m6A, m1A, and m5C, which play a key role in the progression of cancers, including growth and invasion (Mcelhinney et al., 2020). In this study, we examined the relationship between OAS3 expression and the abovementioned genes using the R package "RColorBrewer".

Correlation of OAS3 Expression With Drug Sensitivity

The relationship between OAS3 and IC50 of drugs was analysed based on the GDSC2 data. In addition, we compared the drug sensitivity of the OAS family using the Cancer Therapeutics Response Portal 21 (CTRP, http://portals.broadinstitute.org/ctrp/). The likelihood of an immunotherapy response was estimated using the TIDE algorithm (Khanna et al., 2019; Yang et al., 2020).

Quantitative Real-Time PCR

Total RNA was extracted from the target tissue samples and thoroughly ground in a mortar under liquid nitrogen. To lyse the cells, 1 ml of Trizol reagent (Life Technology, Grand Island, NY, United States) was added and the sample was incubated for 15 min at room temperature on a shaker. To assess the mRNA expression level, the RevertAid First Strand cDNA Synthesis Kit (Thermo Scientific, Lithuania) was used to synthesis the first-strand cDNA. Quantitative PCR was performed using Roche LightCycler® 480 Real-Time PCR System with SYBR® Green qPCR mix 2.0 kit. The primers used in this study were obtained from TsingKe biological technology (Nanjing, China), including *OAS3* (forward 5′- CAC CGGCGATGCCCGCATCTCACTG -3′, reverse 5′- AAACCA GTGAGATGCGGGCATCGCC-3′). The relative mRNA levels were calculated by the 2-ΔΔCt method.

Western Blot

Western blot was performed to determine the protein expression level. The protein samples were denatured for 5 min at 95°C in a sample buffer and separated by SDS–PAGE. Western blot analysis was performed using antibodies against mouse monoclonal antibody-anti-human OAS3, and mouse monoclonal antibody-anti-human β-actin (Santa Cruz Biotechnology), followed by incubation with horseradish peroxidase (HRP)-coupled mouse secondary antibody (1: 10,000). The blots were re-probed with a β-actin antibody (BD Bioscience, United States), and the signals were quantified using an image analyzer (UVtec, United Kingdom). The data were shown as percentages of the normalized control signal.

RESULTS

Expression Levels of OAS3 in Various Normal and Cancerous Tissues

Data from the GTEx database showed that *OAS3* was abundantly expressed in various normal tissues, with the highest and lowest expression observed in the lung and muscle, respectively (**Figure 2A**). In addition, the expression of *OAS3* was higher in various cancer cell lines in the Cancer Cell Line Encyclopedia (CCLE) database than in normal tissue (**Figure 2B**). In TCGA data, differences in *OAS3* expression were significant among 17 of the 33 cancer types analysed (except for KICH, in which *OAS3* expression was lower than that in most tumour tissues) (**Figure 2C**). However, when the GTEx and TCGA data were combined, the difference was significant among 29 of the 33 cancers, and *OAS3* expression was lower in KICH than in normal tissues (**Figure 2D**). To investigate the intracellular localisation of *OAS3*, we assessed the distribution of *OAS3* in the endoplasmic reticulum (ER) and microtubules of A431, A549, and U-2 osteosarcoma (OS) cells using an indirect immunofluorescence assay. We observed that *OAS3* colocalised with ER and microtubule markers in A431, A549 and U-2 OS cells, suggesting the subcellular localisation of *OAS3* in ER and microtubules. However, *OAS3* exhibited no overlap with the nucleus of A431, A549, and U-2 OS cells (**Supplementary Figure S1**).

Relationship of OAS3 With Clinical Staging and Prognosis

We examined the relationship between *OAS3* expression and different tumour stages and found that DLBC, HNSC, KIRC, LIHC, LUSC, MESO, OV, PAAD, LUAD, SKCM, and UCS were

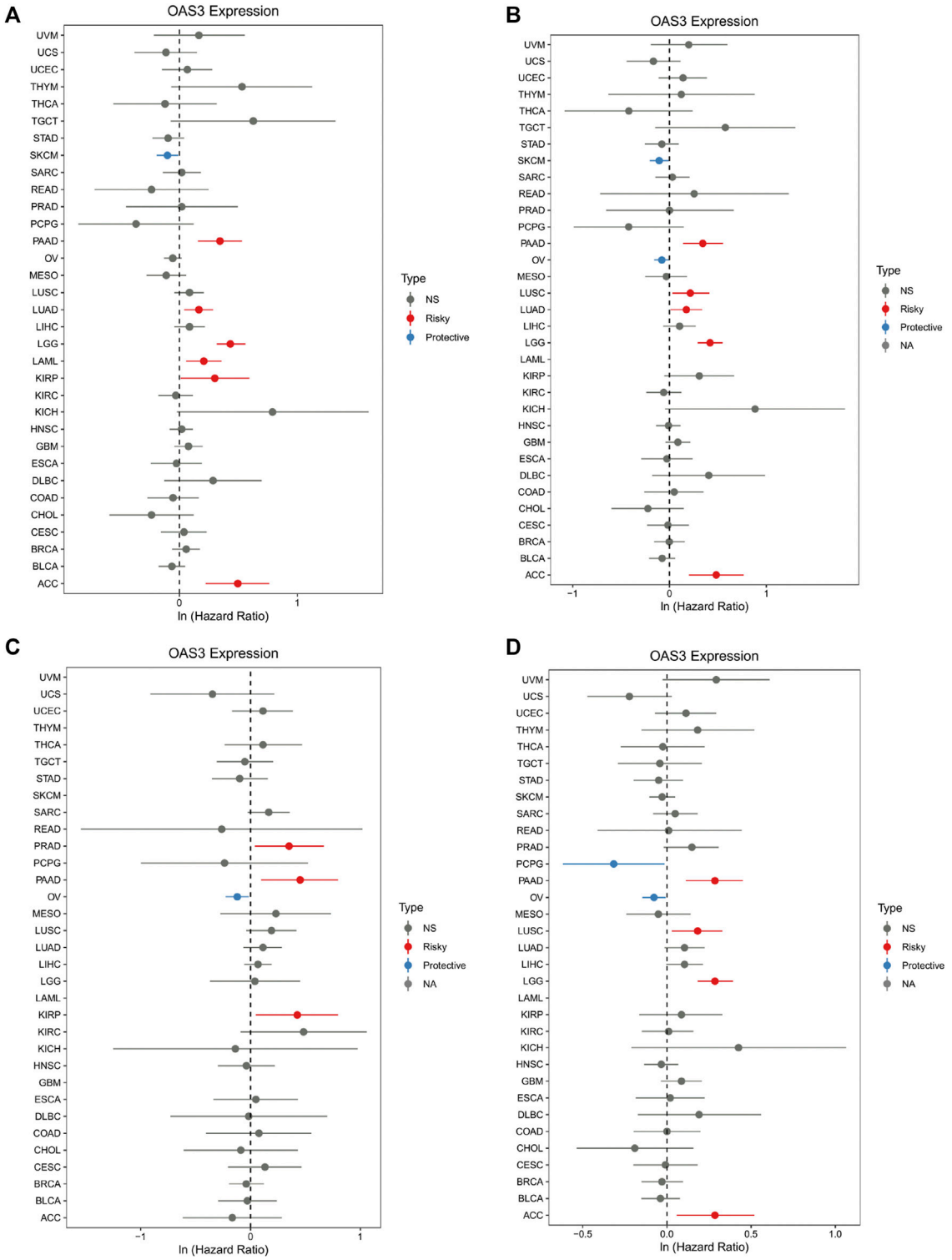

FIGURE 3 | Forest plot of the association of OAS3 expression with OS **(A)**, DSS **(B)**, DFS **(C)**, and PFS **(D)**. **(A)**: OAS3 is highly expressed in patients with PAAD, LUAD, LGG, LAML, KIRP, ASS with poor OS. In SKCM, high expression of OAS3 is a protective factor for OS. **(B)**: In PAAD, LUSC, LUAD, LGG, ACC, patients with high OAS3 expression showed shorter DSS than those with low expression. in SKCM, OV, the opposite effect of OAS3 was observed. **(C)**: OAS3 was highly expressed in PAAD, PRAD, and KIRP patients with poor DFS. In contrast, in OV, high OAS3 expression was associated with longer DFS. **(D)**: Patients with high OAS3 expression in PAAD, LUSC, LGG, and ACC had shorter DFS than those with low expression. In PCPG, the opposite role of OAS3 was observed.

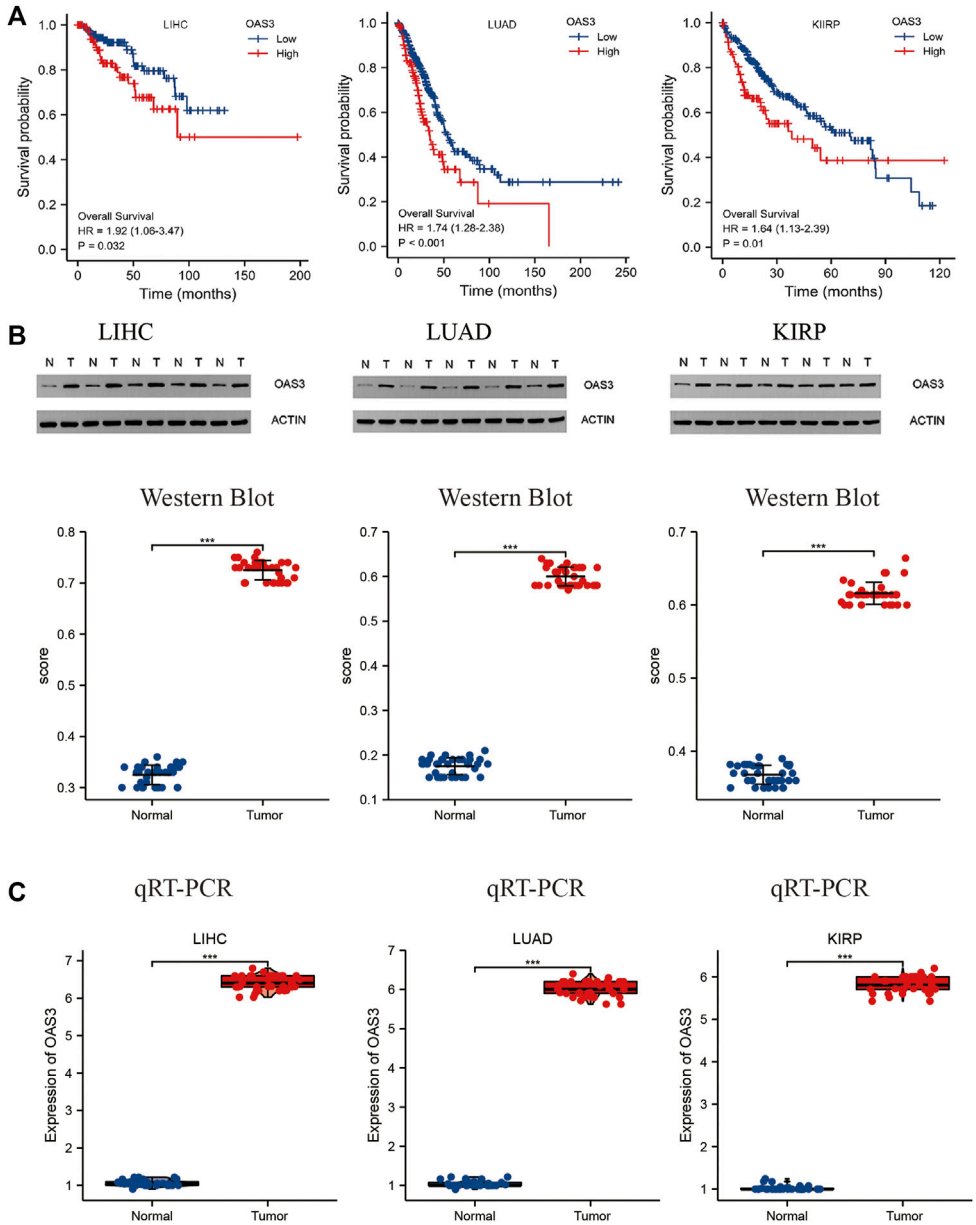

FIGURE 4 | (A) Relationship between OAS3 and OS of LIHC, LUAD, KIRP in validation cohort. The results showed that patients with high OAS3 expression had a poor prognosis in the three tumors mentioned above. **(B,C)**: Results of Western Blot **(B)** and qRT-PCR **(C)** showed a clear overexpression in protein expression levels of OAS3 in validation cohort.

positively correlated with the expression of *OAS3*. This finding suggests that *OAS3* plays an important role in tumorigenesis (**Supplementary Figure S2**). Furthermore, we investigated the relationship between *OAS3* expression and the prognosis of 33 cancers. According to the Cox proportional hazards model, *OAS3* expression was positively correlated with OS in patients with PAAD, LUAD, LGG, LAML, KIRP, and ACC and negatively correlated with OS in patients with SKCM (**Figure 3A**). In addition, we analysed the DSS data and found a positive correlation between *OAS3* expression and prognosis in patients with PAAD, LUSC, LUAD, LGG, and ACC. However, *OAS3* expression was negatively correlated with the prognosis of SKCM and OV (**Figure 3B**). Based on the correlation between *OAS3* expression and DFS, we identified *OAS3* as a prognostic risk factor for PRAD, PAAD, and KIRP but as a protective factor for OV (**Figure 3C**). Similarly, high *OAS3* expression was associated with worse PFS in PAAD, LUSC, LGG, and ACC (**Figure 3D**). Furthermore, Kaplan–Meier analysis showed that high *OAS3* expression was associated with worse OS in ACC, DLBC, KICH, KIRP, LAML, LGG, LUAD, and PAAD but with better OS in MESO (**Supplementary Figure S3**). High *OAS3* expression was correlated with worse DFS in four types of

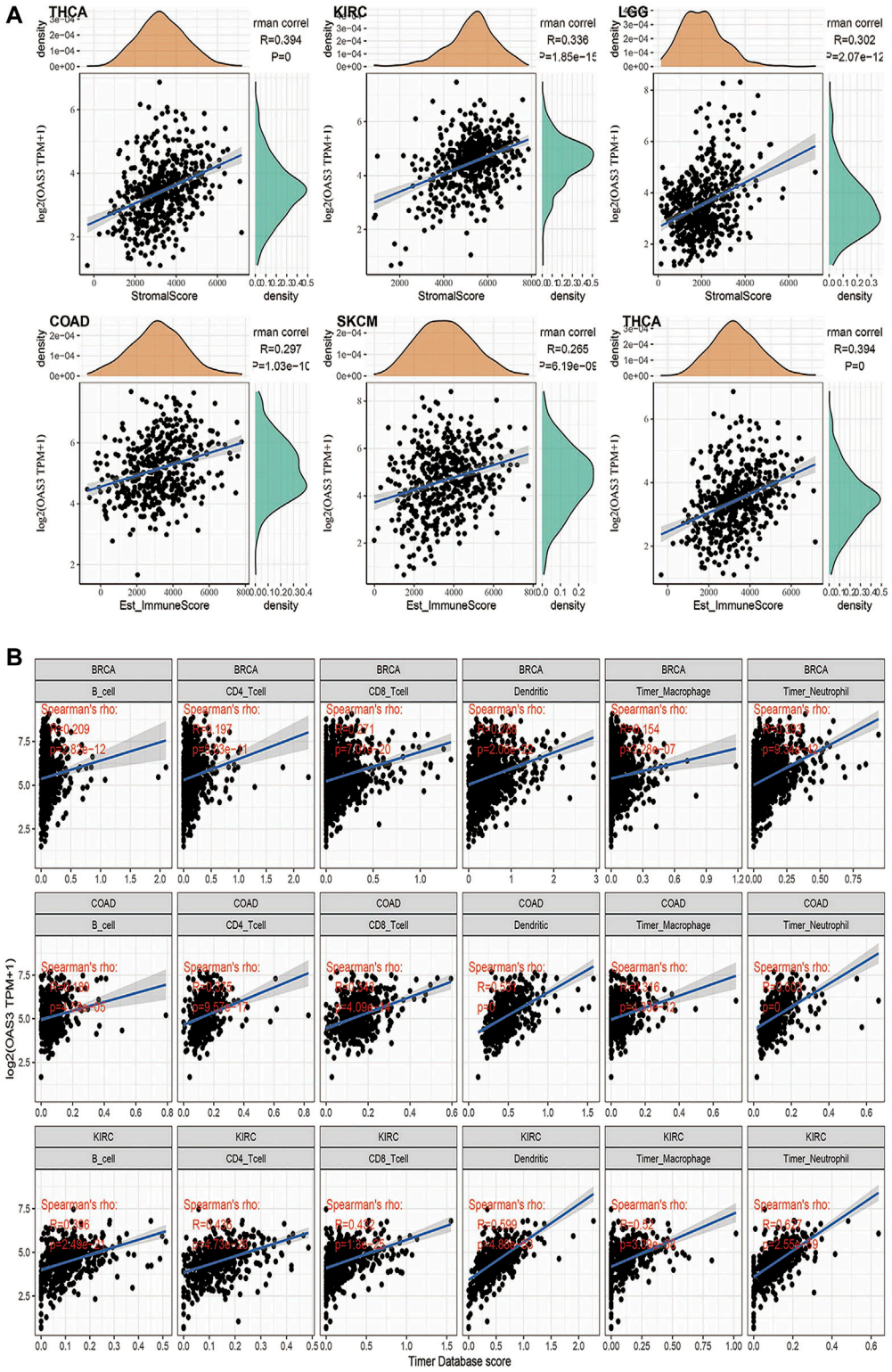

FIGURE 5 | (A) Among the 33 tumors, the top 3 tumors with the highest stromal scores were THCA, KIRC, LGG; the highest immune scores were COAD, SKCM, THCA; the highest ESTIMATEScore was COAD, SKCM,THCA. **(B)** TIMER analyzed relationship between OAS3 expression and the abundance of tumor-infiltrating immune cells in BRCA, COAD, KIRC. The results showed a positive correlation between OAS3 expression and immune cell infiltration.

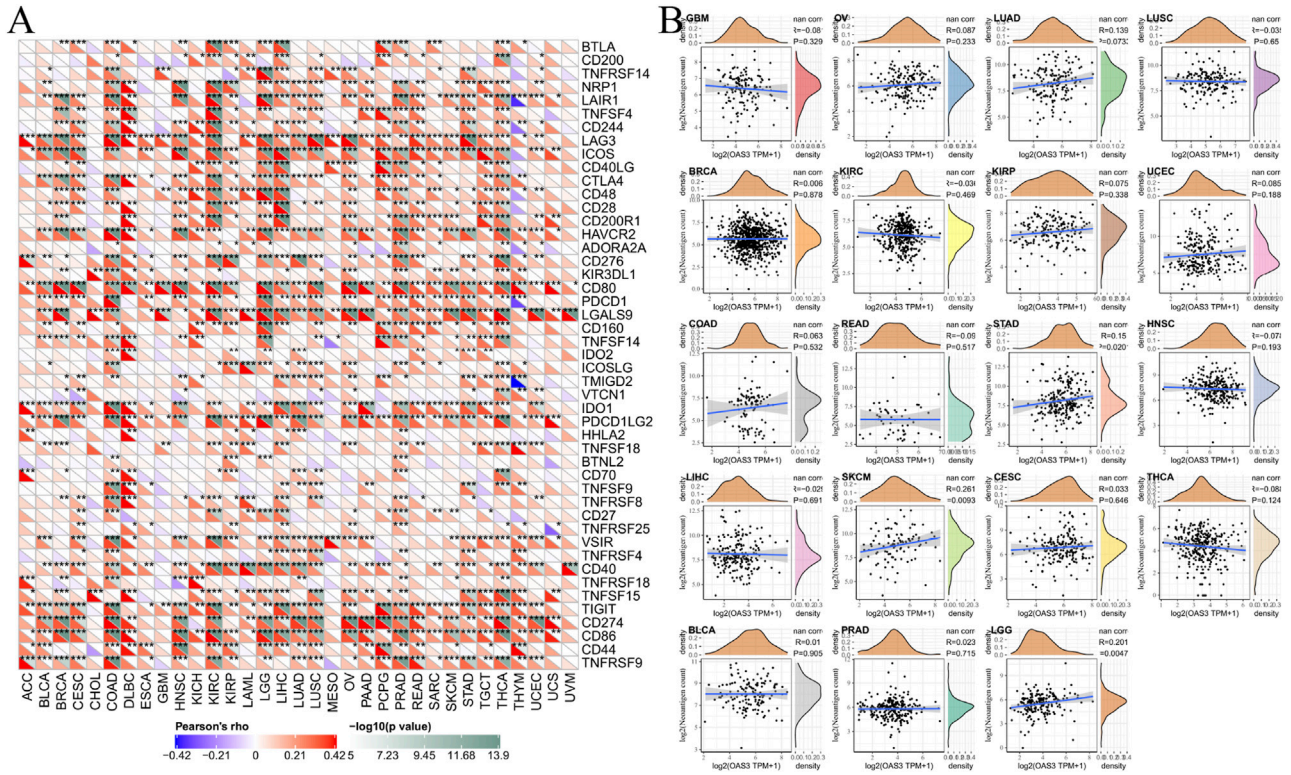

FIGURE 6 | (A) The correlation between OAS3 expression and immune checkpoint genes in pan-cancer. Each square corresponded to the correlation between OAS3 expression and the expression of one immune checkpoint gene in a particular tumor. The upper triangle of each square represented the magnitude of the *p* value of the correlation test, and the lower triangle represented the correlation coefficient (**p* < 0.05, ***p* < 0.01, ****p* < 0.001). **(B)** The correlation between OAS3 expression and neoantigens.

tumours, including KIRP and PAAD (**Supplementary Figure S4**). In seven types of tumours, including ACC and DLBC, patients with high *OAS3* expression had worse DSS (**Supplementary Figure S5**). These findings suggest that *OAS3* is an oncogene that is associated with tumour progression, can help to predict survival in patients with various tumours and is a potential biomarker for tumour prognosis, especially for the prognosis of PAAD, LUAD, KIRP, and UVM.

Validation of the Expression and Prognostic Role of OAS3

To substantiate the conclusion of the data analysis, we validated *OAS3* expression in 36 patients with LIHC, 30 patients with LUAD and 30 patients with KIRP and performed survival analysis in conjunction with clinical trials. As shown in **Figure 4A**, patients with high *OAS3* expression in the validation group had a poorer prognosis in patients with LUAD, KIRP; this is consistent with our findings in the TCGA cohort. Also, we found a poorer prognosis for patients with high *OAS3* expression in LIHC in the validation group. Meanwhile, OAS3 was detected using qRT-PCR and western blotting. The results of western blotting was consistent with those of qRT-PCR: *OAS3* was highly expressed in tumor tissues in LIHC, LUAD, KIRP, and low in normal tissues (**Figures 4B, C**). TCGA cohort results are mostly consistent with our findings. This ensured breadth and thereby enhanced credibility in the data.

Correlation of OAS3 With TME and Immune-Infiltrating Cells

We evaluated the correlation between OAS3 and immune and stromal scores. As shown in **Supplementary Figure S6**, immune scores, ESTIMATEScore and stromal scores were significantly correlated with OAS3 expression in 20, 25, and 20 of the 33 cancers, respectively. **Figure 5A** shows the top three significant genes in each score, with COAD having the highest immune score and ESTIMATEScore and THCA having the highest substrate score. The results showed that *OAS3* expression strongly correlates with the degree of immune infiltration in different cancer types. Therefore, we investigated the relationship between *OAS3* and immune infiltrating cells in 33 cancer types using the TIMER database. The top three significant cell types are shown in **Figure 5B**, demonstrating that *OAS3* correlates significantly with tumor purity and with six types of immunoinfiltrated cells, including $CD8^+$ T cells, $CD4^+$ T cells, B cells, dendritic cells, and macrophages in KIRC, COAD and BRCA. Based on the

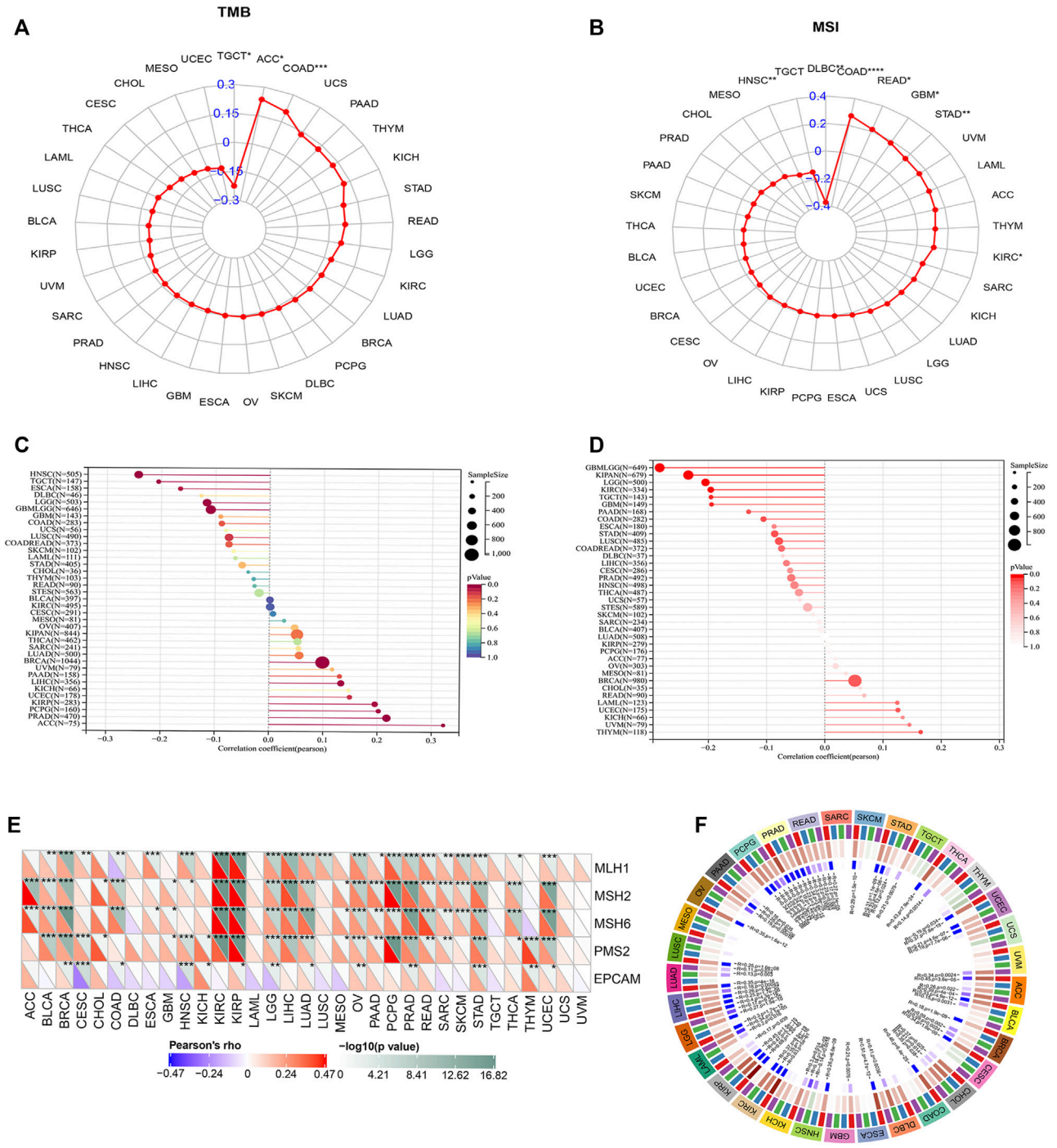

FIGURE 7 | (A) Radar plot showing the correlation between OAS3 expression and TMB in pan-cancer. The blue number represents Spearman's correlation coefficient. $*p < 0.05$, $**p < 0.01$, $***p < 0.001$. **(B)** Radar plot showing the correlation between OAS3 expression and MSI in pan-cancer. The blue number represents Spearman's correlation coefficient. $*p < 0.05$, $**p < 0.01$, $***p < 0.001$. **(C)** The correlation between OAS3 expression and HBD in pan-cancer. The size of the circle represents the number of samples. The colors represent significant *p*-values ($p < 0.05$) for each section; red low *p*-value, blue high *p*-value. **(D)** Relationship between OAS3 and heterogeneity. The size of the circle represents the number of samples. Color represents *p*-value, the darker the color the more significant the result. **(E)** OAS3 was closely associated with DNA MMR genes. The upper triangle of each square represented the magnitude of the *p* value of the correlation test, and the lower triangle represented the correlation coefficient. $*p < 0.05$; $**p < 0.01$; $***p < 0.001$. **(F)** OAS3 was positively correlated with four major DNA methyltransferases including DNMT1, DNMT2, DNMT3A, and DNMT3B in most cancer types.

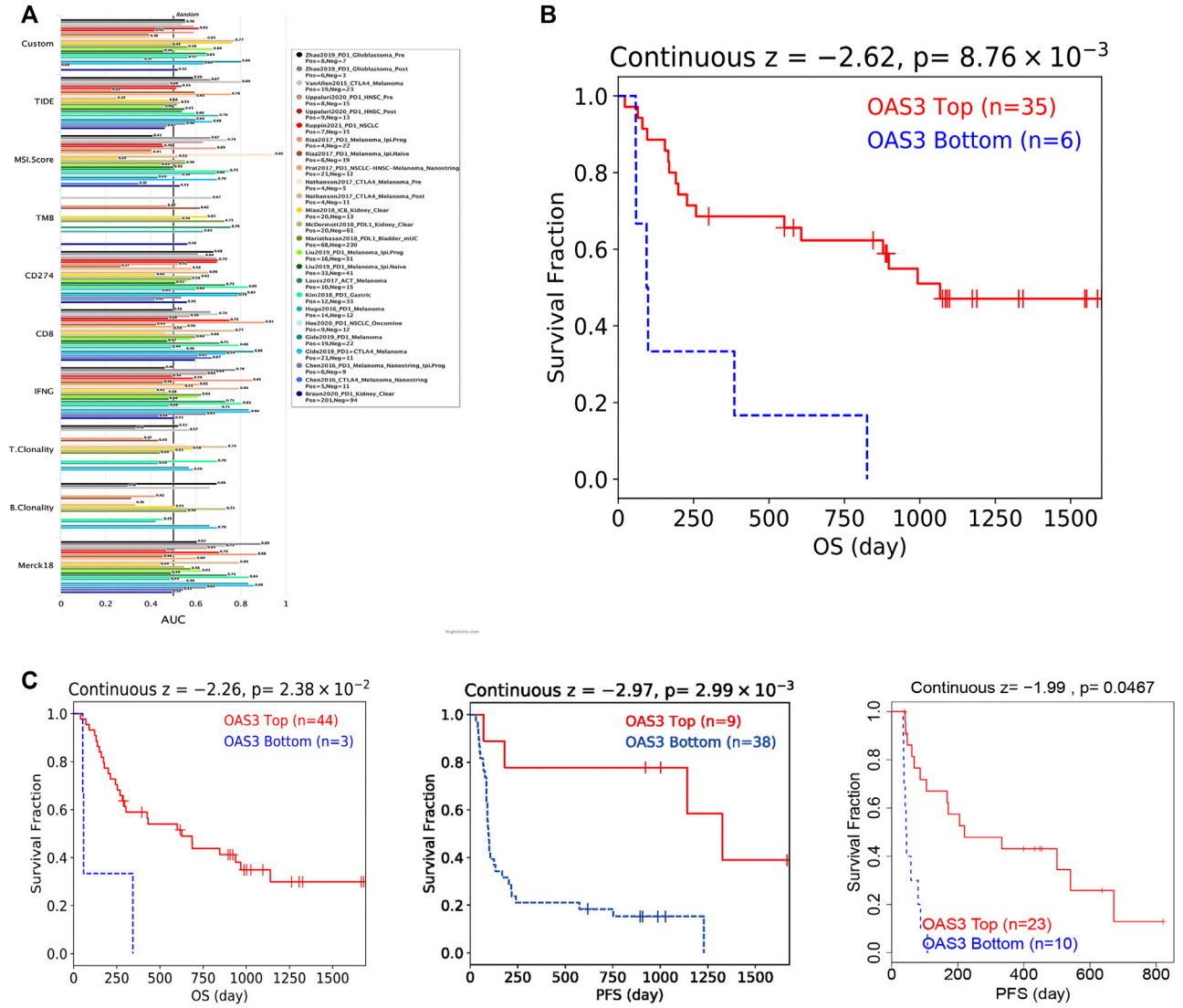

FIGURE 8 | (A) Bar plot showing the biomarker relevance of OAS3 compared to standardized cancer immune evasion biomarkers in immune checkpoint blockade (ICB) sub-cohorts. The area under the receiver operating characteristic curve (AUC) was used to assess the predictive efficacy of test biomarkers for determining IBC response to TCGA for different cancer types. **(B,C)** Kaplan-Meier curves of survival ratios as a measure of the immunotherapeutic response (immune checkpoint blockade) between cancer cohorts with high and those with low expression levels of OAS3.

results of immune analysis, *OAS3* was related to poor prognosis in some tumours and might affect immune activities. Therefore, we examined the correlation between *OAS3* and immune-related cells using Xcell, TIMER2, CIBERSORT and ImmuCellAI to validate the results and found that *OAS3* was significantly correlated with neutrophils and macrophages (**Supplementary Figures S7A–C**). In addition, cancer-associated fibroblasts, a type of immunosuppressive cells, had a strong positive correlation with *OAS3* expression. The data from the ImmuCellAI database further suggested a significant positive correlation between *OAS3*and the immunosuppressive cells iTregs and nTregs (**Supplementary Figure S7D**). Therefore, *OAS3* may affect tumour progression through macrophages, iTregs, CAFs, and other immune cells.

Correlation of OAS3 Expression With Immune Checkpoint Genes and the Number of Immune Neoantigens Implicates OAS3 in the Tumour Immune Response

The correlation between *OAS3* expression and 47 immune checkpoint genes in pan-cancer is shown in **Figure 6A**. In diverse cancer types, the correlation between *OAS3* and the expression of checkpoint genes indicated a high correlation with TNF-related immune genes including TNFRSF14, TNFRSF8, TNFRSF25, TNFRSF4, TNFRSF18, TNFSF15, and TNFRSF9. The expression of *OAS3* was positively correlated with that of immune checkpoint-related genes in most tumours, suggesting that *OAS3* is involved in the

regulation of tumour immune response through the regulation of immune checkpoint activity. Therefore, *OAS3* may provide some help for tumour immunotherapy, thus facilitating the spread of tumours. The correlation between *OAS3* expression and neoantigens is shown in **Figure 6B**. A significant positive correlation was found between *OAS3* expression and the number of neoantigens in LGG, SKCM, and STAD.

OAS3 Expression Was Significantly Correlated With TMB and MSI

We obtained *OAS3* mutation data of various tumours from the UCSC Xena database. *OAS3* mRNA was found to be significantly mutated in TGCT, ACC, COAD, and other tumours (**Figure 7A**), suggesting that mutated *OAS3* plays a key role in promoting the development of these tumours (**Figure 7B**). HRD produces specific, quantifiable, and stable genomic alterations, and the HRD status is a key indicator of treatment choice and prognosis in various tumours. Clinical studies have confirmed that the HRD status is highly correlated with sensitivity to platinum-based chemotherapeutic agents and PARP inhibitors (Min et al., 2020). We found that *OAS3* was positively correlated with HRD in ACC, PRAD, and KIRP (**Figure 7C**), and the heterogeneity of THYM, UVM, and KICH increases with an increase in OAS3 expression (**Figure 7D**).

Coexpression of OAS3 With Some Specific Genes

Based on the association between *OAS3* expression and the mutational markers TMB and MSI, the relationship between *OAS3* expression and oncogenic processes was further investigated. We found that *OAS3* was closely associated with DNA MMR genes, showing a positive correlation with MLH1, MSH2, MSH6, and PMS2 and a negative correlation with EPCAM in most tumours (**Figure 7E**). In addition, *OAS3* was positively correlated with four major DNA methyltransferases including DNMT1, DNMT2, DNMT3A, and DNMT3B in most cancer types (**Figure 7F**). RNA methylation is a post-transcriptional modification that widely exists in eukaryotes and prokaryotes. We found that *OAS3* had a significant positive correlation with RNA methylation-related genes (m1A, m5C, and m6A) in most tumours (**Supplementary Figure S8A**). In addition, a positive correlation was found between *OAS3* and four immune pathway-related genes [receptor (Chen et al., 2021a), MHC (Schulze et al., 2020), immunoinhibitors (Liu et al., 2021a) and immunostimulators [46]] in many tumour types (**Supplementary Figure S8B**).

Analysis of Drug Sensitivity

We analysed 198 drugs and found that *OAS3* shared the most evident positive correlation with BI-2536, GSK269962A, vorinostat, sorafenib, BMS-754807, and nutlin-3a (−), indicating that high *OAS3* expression may lead to drug resistance. *OAS3* had the strongest negative correlation with trametinib, sapitinib, SCH772984, selumetinib, and dasatinib (**Supplementary Figure S9A**). A bubble plot demonstrating the correlation between the sensitivity of drugs in the CTRP database and mRNA expression of *OAS3* is shown in **Supplementary Figure S9B**.

OAS3 Was Correlated With Immunotherapeutic Responses

We assessed the reliability of *OAS3* as a biomarker by comparing it with standardised biomarkers for predicting response and OS in the IBC subpopulation. We found that the area under the receiver operating characteristic curve (AUC) of *OAS3* alone was greater than 0.5 in 16 of 23 IBC subgroups (**Figure 8A**), and that the predictive value of *OAS3* alone was higher than that of TMB, T. clonalum, and B. clonalum. However, the predictive ability of OAS3 was similar to that of IFGN (AUC>0.5 for 17 ICD subgroups), but lower than that of CD274, TIDE and Merk18. In addition, the results demonstrated that high expression levels of *OAS3* were associated with better PD1 OS in melanoma (Gide2019_PD1, Liu2019_PD1) and better PFS in kidney renal clear cell carcinoma and melanoma (Miao2018_ICB, Liu2019_PD1) (**Figures 8B, C**).

Pathway Analysis

We performed Spearman correlation analysis on *OAS3* and pathway scores. A close association was observed between *OAS3* and pathways including tumour inflammation signature, cellular response to hypoxia, tumour proliferation signature, angiogenesis, and apoptosis. The higher the expression of *OAS3*, the stronger the activity of the related pathway (**Supplementary Figure S10**).

DISCUSSION

The molecular mechanisms underlying the role of *OAS3* in the immune microenvironment and pathogenesis of different tumours remain unknown. In this study, we performed an integrative analysis of molecular characteristics, oncogenic roles and relevant immune and pharmacogenomic features of *OAS3* in pan-cancer. The findings suggest that *OAS3* is closely associated with the development of various systemic diseases and cancers. In addition, a functional association was observed between *OAS3* and TME, especially immunosuppressive cells.

We compared the expression of *OAS3* in normal and tumour tissues of 33 cancers and found that *OAS3* was dysregulated and highly expressed in almost all TCGA tumour types and was associated with the staging or metastasis of DLBC, HNSC, KIRC, LIHC, LUSC, MESO, OV, PAAD, LUAD, SKCM, and UCS. These findings suggest that OAS3 is an important regulator of carcinogenesis, progression, invasion and metastasis in various cancers. Regarding the prognostic value of *OAS3* in pan-cancer, we observed that *OAS3* was closely associated with survival indicators such as OS, DSS, DFS, and PFS, and high *OAS3* expression was associated with poorer survival rates in CESC, GBM, KICH, KIRP, LAML, LGG, LIHC, LUAD, LUSC, PAAD, TGCT, and ACC. In previous studies, *OAS3* has been reported as a risk factor for different cancers, which is consistent with the

results of this study (Piera-Velazquez et al., 2021; Calvet et al., 2022; Shi et al., 2022).

TME is closely associated with tumour growth, progression and prognosis and immune cells play an important role in tumour growth and progression (Lei et al., 2021). Previous studies have found that cytokines in TME regulate immune function and eventually suppress the immune response, leading to tumour progression (Hinshaw and Shevde, 2019). Therefore, analysing the components of TME can help to develop drugs for targeted tumour immunotherapy. In this study, a significant positive correlation was observed between *OAS3* and the immunosuppressive cells iTregs and nTregs. Immune checkpoint inhibitors are effective anti-cancer immunotherapeutic approaches (Li et al., 2019). In this study, *OAS3* expression was positively correlated with 47 immune checkpoint genes in most cancer types. Therefore, *OAS3* can be used as a novel drug target for anti-cancer immunotherapy.

Furthermore, we analysed the correlation between the expression of *OAS3* and MMR-related genes, RNA methylation genes and four DNA methyltransferases. MMR can repair errors that occur during DNA replication (Vilar and Gruber, 2010) and is known to repair microsatellite replication errors. However, defects in MMR (dMMR) can lead to MSI (Jiricny, 2006). RNA methylation plays a crucial role in the tumorigenesis and progression of tumours (Chen et al., 2020). Altered DNA methylation is also associated with tumorigenesis (Kulis and Esteller, 2010). Based on the findings of this study, *OAS3* expression is positively correlated with MMR-related genes, RNA methylation and four DNA methyltransferases in most cancers. Altogether, the findings demonstrate that *OAS3* mediates tumorigenesis by regulating DNA damage and DNA and RNA methylation.

Based on the abovementioned results, *OAS3* may serve as a very important biomarker for tumour immunotherapy. Monoclonal antibodies-targeting CTLA-4, PD-1 or PDL-1 have shown clinical potential for effectively controlling and treating human cancers (Liu et al., 2021b). This study showed that patients with melanoma and kidney renal clear cell carcinoma with high *OAS3* expression had a higher clinical benefit from ICB treatment (PD-1 or PD-L1). On analysing the relationship between *OAS3* and the IC50 of drugs using the GDSC2 database, we found that high *OAS3* expression might lead to resistance to BI-2536, GSK269962A, vorinostat, sorafenib, and BMS-754807. However, high *OAS3* expression was negatively correlated with trametinib, sapitinib, SCH772984, selumetinib, and dasatinib. This finding provides a basis for selecting anti-tumour agents for patients in the future.

CONCLUSION

This study showed that *OAS3* is highly expressed in various tumours, and high *OAS3* expression is associated with poor survival outcomes. In addition, we demonstrated the association between *OAS3* and the expression of immune-infiltrating cells, immune checkpoint genes, TMB, and MSI. *OAS3* may influence tumour progression through immunosuppression. The evidence for the significant immunological utility of *OAS3* as a prognostic and immunotherapeutic biomarker for pan-cancer provides compelling new insights into the potential development of future immunotherapeutic and diagnostic trials. Therefore, the findings of this study will contribute to the development of new therapeutic approaches for patients with cancer, improving their treatment and prognosis.

DATA AVAILABILITY STATEMENT

The datasets presented in this study can be found in online repositories. The names of the repository/repositories and accession number(s) can be found in the article/ **Supplementary Material**.

ETHICS STATEMENT

The studies involving human participants were reviewed and approved by the Committees for Ethical Review of Research of The First Affiliated Hospital of Zhengzhou University and Jiading District Central Hospital Affiliated Shanghai University of Medicine. Written informed consent to participate in this study was provided by the participants or their legal guardian/ next of kin.

AUTHOR CONTRIBUTIONS

Xi-tao Yang, Xin-yu Li, Lei Hou, Lu-yu Zhang carried out experiments; Xin-yu Li, Lei Hou, Lu-yu Zhang, Liming Zhang, Deming Wang, Zhenfeng Wang, Ming-Zhe Wen wrote the manuscript, Xi-tao Yang performed manuscript review.

FUNDING

This study received Fundamental research program funding of Ninth People's Hospital affiliated to Shanghai Jiao Tong university School of Medicine (No. JYZZ076), Clinical Research Program of Ninth People's Hospital, Shanghai Jiao Tong University School of Medicine (No. JYLJ201801, JYLJ201911), the China Postdoctoral Science Foundation (No. 2017M611585), and the National Natural Science Foundation of China (No. 81871458).

ACKNOWLEDGMENTS

We gratefully acknowledge the Home for Researchers editorial team (www.home-for-researchers.com). Thanks to Figdraw (www.figdraw) for technical support. We thank Dr. Jianxiong You, Department of Interventional Therapy, Ninth People's

Hospital, Shanghai Jiao Tong University Medical College, for providing the samples.

SUPPLEMENTARY MATERIAL

The Supplementary Material for this article can be found online at: https://www.frontiersin.org/articles/10.3389/fcell.2022.815480/full#supplementary-material

Supplementary Figure 1 | Immunofluorescence staining of the subcellular distribution of OAS3 from the HPA database. We observed that OAS3 colocalised with ER and microtubule markers in A431, A549, and U-2 OS cells, suggesting the subcellular localisation of OAS3 in ER and microtubules.

Supplementary Figure 2 | Boxplots showing differential OAS3 expression levels (log2 TPM + 1) between pathological stages and DLBC, HNSC, KIRC, LIHC, LUSC, MESO, OV, PAAD, LUAD, SKCM, and UCS were positively correlated with the expression of OAS3. This finding suggests that OAS3 plays an important role in tumorigenesis. Only TCGA cancers with statistically significant differences between the pathological stages are presented.

Supplementary Figure 3 | Kaplan-Meier analysis for OS according to OAS3 expression. Only statistically significant cancers (p-value < 0.05) are listed.

Supplementary Figure 4 | Kaplan-Meier analysis for DFS according to OAS3 expression. Only statistically significant cancers (p-value < 0.05) are listed.

Supplementary Figure 5 | Kaplan-Meier analysis for DSS according to OAS3 expression. Only statistically significant cancers (p-value < 0.05) are listed.

Supplementary Figure 6 | The correlation between OAS3 and immune scores **(A)**, ESTIMATEScore **(B)**, and stromal scores **(C)** in pancancer.

Supplementary Figure 7 | Four methods were used to calculate the correlation between OAS3 and immune-related cells. Xcell **(A)**, TIMER2 **(B)**, CIBERSORT **(C)**, and ImmuCellAI **(D)**. The lower upper triangle of each square represented the magnitude of the p value of the correlation test, and the upper triangle represented the correlation coefficient (*p < 0.05, **p < 0.01, ***p < 0.001).

Supplementary Figure 8 | (A) OAS3 had a significant positive correlation with RNA methylation-related genes (m1A, m5C, and m6A) in most tumours. The lower upper triangle of each square represented the magnitude of the p value of the correlation test, and the upper triangle represented the correlation coefficient (*p < 0.05, **p < 0.01, ***p < 0.001). **(B)** A positive correlation was found between OAS3 and four immune pathway-related genes (receptor, MHC, immunoinhibitors, and immunostimulators) in many tumour types. The lower upper triangle of each square represented the magnitude of the p value of the correlation test, and the upper triangle represented the correlation coefficient (*p < 0.05, **p < 0.01, ***p < 0.001).

Supplementary Figure 9 | The correlation between the sensitivity of drugs in the Genomic of Drug Sensitivity in Cancer (GDSC) database **(A)**, CTRP database **(B)**, and mRNA expression of OAS3. The Pearson's correlation indicates the correlation between gene expression and drugs sensitivity. Blue bubbles represented negative correlations, and red bubbles represented positive correlations; the deeper the color, the higher the correlation. The bubble size was positively correlated with the FDR significance.

Supplementary Figure 10 | Pathway analysis. The abscissa represents the distribution of the gene expression, and the ordinate represents the distribution of the pathway score. The density curve on the right represents the trend in distribution of pathway immune score, the upper density curve represents the trend in distribution of the gene expression. The value on the top represents the correlation p value, correlation coefficient and correlation calculation method.

REFERENCES

Alexandrov, L. B., Nik-Zainal, S., Wedge, D. C., Aparicio, S. A., Behjati, S., Biankin, A. V., et al. (2013). Signatures of Mutational Processes in Human Cancer. *Nature* 500 (7463), 415–421. doi:10.1038/nature12477

Alhopuro, P., Sammalkorpi, H., Niittymäki, I., Biström, M., Raitila, A., Saharinen, J., et al. (2012). Candidate Driver Genes in Microsatellite-Unstable Colorectal Cancer. *Int. J. Cancer* 130 (7), 1558–1566. doi:10.1002/ijc.26167

Calvet, J., Berenguer-Llergo, A., Gay, M., Massanella, M., Domingo, P., Llop, M., et al. (2022). Biomarker Candidates for Progression and Clinical Management of COVID-19 Associated Pneumonia at Time of Admission. *Sci. Rep.* 12 (1), 640. doi:10.1038/s41598-021-04683-w

Chen, J., Yu, K., Zhong, G., and Shen, W. (2020). Identification of a m6A RNA Methylation Regulators-Based Signature for Predicting the Prognosis of clear Cell Renal Carcinoma. *Cancer Cel Int* 20, 157. doi:10.1186/s12935-020-01238-3

Chen, Y.-J., Liao, W.-X., Huang, S.-Z., Yu, Y.-F., Wen, J.-Y., Chen, J., et al. (2021). Prognostic and Immunological Role of CD36: A Pan-Cancer Analysis. *J. Cancer* 12 (16), 4762–4773. doi:10.7150/jca.50502

Chen, Y., Meng, Z., Zhang, L., and Liu, F. (2021). CD2 Is a Novel Immune-Related Prognostic Biomarker of Invasive Breast Carcinoma that Modulates the Tumor Microenvironment. *Front. Immunol.* 12, 664845. doi:10.3389/fimmu.2021.664845

Coppedè, F., Lopomo, A., Spisni, R., and Migliore, L. (2014). Genetic and Epigenetic Biomarkers for Diagnosis, Prognosis and Treatment of Colorectal Cancer. *Wjg* 20 (4), 943–956. doi:10.3748/wjg.v20.i4.943

Ellegren, H. (2004). Microsatellites: Simple Sequences with Complex Evolution. *Nat. Rev. Genet.* 5 (6), 435–445. doi:10.1038/nrg1348

Grady, W. M., Yu, M., and Markowitz, S. D. (2021). Epigenetic Alterations in the Gastrointestinal Tract: Current and Emerging Use for Biomarkers of Cancer. *Gastroenterology* 160 (3), 690–709. doi:10.1053/j.gastro.2020.09.058

Grauel, A. L., Nguyen, B., Ruddy, D., Laszewski, T., Schwartz, S., Chang, J., et al. (2020). Tgfβ-Blockade Uncovers Stromal Plasticity in Tumors by Revealing the Existence of a Subset of Interferon-Licensed Fibroblasts. *Nat. Commun.* 11 (1), 6315. doi:10.1038/s41467-020-19920-5

Hinshaw, D. C., and Shevde, L. A. (2019). The Tumor Microenvironment Innately Modulates Cancer Progression. *Cancer Res.* 79 (18), 4557–4566. doi:10.1158/0008-5472.CAN-18-3962

Huang, C., Jiang, X., Huang, Y., Zhao, L., Li, P., and Liu, F. (2021). Identifying Dendritic Cell-Related Genes through a Co-expression Network to Construct a 12-Gene Risk-Scoring Model for Predicting Hepatocellular Carcinoma Prognosis. *Front. Mol. Biosci.* 8, 636991. doi:10.3389/fmolb.2021.636991

Jiang, Y., Li, Y., and Zhu, B. (2015). T-cell Exhaustion in the Tumor Microenvironment. *Cell Death Dis* 6, e1792. doi:10.1038/cddis.2015.162

Jiricny, J. (2006). The Multifaceted Mismatch-Repair System. *Nat. Rev. Mol. Cel Biol* 7 (5), 335–346. doi:10.1038/nrm1907

Ju, Q., Li, X., Zhang, H., Yan, S., Li, Y., and Zhao, Y. (2020). NFE2L2 Is a Potential Prognostic Biomarker and Is Correlated with Immune Infiltration in Brain Lower Grade Glioma: A Pan-Cancer Analysis. *Oxidative Med. Cell. longevity* 2020, 1–26. doi:10.1155/2020/3580719

Khanna, K., Jamwal, V. L., Kohli, S. K., Gandhi, S. G., Ohri, P., Bhardwaj, R., et al. (2019). Plant Growth Promoting Rhizobacteria Induced Cd Tolerance in Lycopersicon esculentum through Altered Antioxidative Defense Expression. *Chemosphere* 217, 463–474. doi:10.1016/j.chemosphere.2018.11.005

Kulis, M., and Esteller, M. (2010). DNA Methylation and Cancer. *Adv. Genet.* 70, 27–56. doi:10.1016/B978-0-12-380866-0.60002-2

Lei, K., Li, J., Tu, Z., Liu, F., Ye, M., Wu, M., et al. (2021). Prognostic and Predictive Value of Immune-Related Gene Pair Signature in Primary Lower-Grade Glioma Patients. *Front. Oncol.* 11, 665870. doi:10.3389/fonc.2021.665870

Li, B., Chan, H. L., and Chen, P. (2019). Immune Checkpoint Inhibitors: Basics and Challenges. *Cmc* 26 (17), 3009–3025. doi:10.2174/0929867324666170804143706

Liao, J.-Y., and Zhang, S. (2021). Safety and Efficacy of Personalized Cancer Vaccines in Combination with Immune Checkpoint Inhibitors in Cancer Treatment. *Front. Oncol.* 11, 663264. doi:10.3389/fonc.2021.663264

Lin, Q. H., Zhang, K. D., Duan, H. X., Liu, M. X., Wei, W. L., and Cao, Y. (2015). ERGIC 3, Which Is Regulated by miR-203a, Is a Potential Biomarker for Non-small Cell Lung Cancer. *Cancer Sci.* 106 (10), 1463–1473. doi:10.1111/cas.12741

Liu, C., Zhang, G., Xiang, K., Kim, Y., Lavoie, R. R., Lucien, F., et al. (2021). Targeting the Immune Checkpoint B7-H3 for Next-Generation Cancer

Immunotherapy. *Cancer Immunol Immunother* 11, 654684. doi:10.1007/s00262-021-03097-x

Liu, S., Liang, J., Liu, Z., Zhang, C., Wang, Y., Watson, A. H., et al. (2021). The Role of CD276 in Cancers. *Front. Oncol.* 11, 654684. doi:10.3389/fonc.2021.654684

Liu, Y., and Cao, X. (2016). Immunosuppressive Cells in Tumor Immune Escape and Metastasis. *J. Mol. Med.* 94 (5), 509–522. doi:10.1007/s00109-015-1376-x

Luo, Q., and Vögeli, T.-A. (2020). A Methylation-Based Reclassification of Bladder Cancer Based on Immune Cell Genes. *Cancers* 12 (10), 3054. doi:10.3390/cancers12103054

Mcelhinney, J. M. W. R., Hasan, A., and Sajini, A. A. (2020). The Epitranscriptome Landscape of Small Noncoding RNAs in Stem Cells. *Stem cells (Dayton, Ohio)* 38 (10), 1216–1228. doi:10.1002/stem.3233

Min, A., Kim, K., Jeong, K., Choi, S., Kim, S., Suh, K. J., et al. (2020). Homologous Repair Deficiency Score for Identifying Breast Cancers with Defective DNA Damage Response. *Sci. Rep.* 10 (1), 12506. doi:10.1038/s41598-020-68176-y

Monteran, L., and Erez, N. (2019). The Dark Side of Fibroblasts: Cancer-Associated Fibroblasts as Mediators of Immunosuppression in the Tumor Microenvironment. *Front. Immunol.* 10, 1835. doi:10.3389/fimmu.2019.01835

Petrelli, F., Ghidini, M., Cabiddu, M., Pezzica, E., Corti, D., Turati, L., et al. (2019). Microsatellite Instability and Survival in Stage II Colorectal Cancer: A Systematic Review and Meta-Analysis. *Anticancer Res.* 39 (12), 6431–6441. doi:10.21873/anticanres.13857

Piera-Velazquez, S., Mendoza, F. A., Addya, S., Pomante, D., and Jimenez, S. A. (2021). Increased Expression of Interferon Regulated and Antiviral Response Genes in CD31+/CD102+ Lung Microvascular Endothelial Cells from Systemic Sclerosis Patients with End-Stage Interstitial Lung Disease. *Clin. Exp. Rheumatol.* 39 (6), 1298–1306.

Popp, H. D., and Bohlander, S. K. (2010). Genetic Instability in Inherited and Sporadic Leukemias. *Genes Chromosom. Cancer* 49 (12), 1071–1081. doi:10.1002/gcc.20823

Schulze, A., Oshi, M., Endo, I., and Takabe, K. (2020). MYC Targets Scores Are Associated with Cancer Aggressiveness and Poor Survival in ER-Positive Primary and Metastatic Breast Cancer. *Ijms* 21 (21), 8127. doi:10.3390/ijms21218127

Shi, Y., Xu, Y., Xu, Z., Wang, H., Zhang, J., Wu, Y., et al. (2022). TKI Resistant-Based Prognostic Immune Related Gene Signature in LUAD, in Which FSCN1 Contributes to Tumor Progression. *Cancer Lett.* 532, 215583. doi:10.1016/j.canlet.2022.215583

Thommen, D. S., and Schumacher, T. N. (2018). T Cell Dysfunction in Cancer. *Cancer cell* 33 (4), 547–562. doi:10.1016/j.ccell.2018.03.012

Tian, S., Lai, J., Yu, T., Li, Q., and Chen, Q. (2021). Regulation of Gene Expression Associated with the N6-Methyladenosine (m6A) Enzyme System and its Significance in Cancer. *Front. Oncol.* 10, 623634. doi:10.3389/fonc.2020.623634

Tomczak, K., Czerwińska, P., and Wiznerowicz, M. (2015). Review the Cancer Genome Atlas (TCGA): an Immeasurable Source of Knowledge. *wo* 1A (1A), 68–77. doi:10.5114/wo.2014.47136

Toyota, M., and Suzuki, H. (2010). Epigenetic Drivers of Genetic Alterations. *Adv. Genet.* 70, 309–323. doi:10.1016/B978-0-12-380866-0.60011-3

Vilar, E., and Gruber, S. B. (2010). Microsatellite Instability in Colorectal Cancer-The Stable Evidence. *Nat. Rev. Clin. Oncol.* 7 (3), 153–162. doi:10.1038/nrclinonc.2009.237

Wu, Z., Zhu, K., Liu, Q., Liu, Y., Chen, L., Cui, J., et al. (2020). Profiles of Immune Infiltration in Bladder Cancer and its Clinical Significance: an Integrative Genomic Analysis. *Int. J. Med. Sci.* 17 (6), 762–772. doi:10.7150/ijms.42151

Xu, C., Zang, Y., Zhao, Y., Cui, W., Zhang, H., Zhu, Y., et al. (2021). Comprehensive Pan-Cancer Analysis Confirmed that ATG5 Promoted the Maintenance of Tumor Metabolism and the Occurrence of Tumor Immune Escape. *Front. Oncol.* 11, 652211. doi:10.3389/fonc.2021.652211

Yang, M., Huang, W., Sun, Y., Liang, H., Chen, M., Wu, X., et al. (2019). Prognosis and Modulation Mechanisms of COMMD6 in Human Tumours Based on Expression Profiling and Comprehensive Bioinformatics Analysis. *Br. J. Cancer* 121 (8), 699–709. doi:10.1038/s41416-019-0571-x

Yang, Y., Deng, X., Chen, X., Chen, S., Song, L., Meng, M., et al. (2020). Landscape of Active Enhancers Developed De Novo in Cirrhosis and Conserved in Hepatocellular Carcinoma. *Am. J. Cancer Res.* 10 (10), 3157–3178.

Yuan, F., Ming, H., Wang, Y., Yang, Y., Yi, L., Li, T., et al. (2020). Molecular and Clinical Characterization of Galectin-9 in Glioma through 1,027 Samples. *J. Cel Physiol* 235 (5), 4326–4334. doi:10.1002/jcp.29309

Zhang, Y., and Yu, C. (2020). Prognostic Characterization of OAS1/OAS2/OAS3/OASL in Breast Cancer. *BMC cancer* 20 (1), 575. doi:10.1186/s12885-020-07034-6

Zhou, R., Zeng, D., Zhang, J., Sun, H., Wu, J., Li, N., et al. (2019). A Robust Panel Based on Tumour Microenvironment Genes for Prognostic Prediction and Tailoring Therapies in Stage I-III colon Cancer. *EBioMedicine* 42, 420–430. doi:10.1016/j.ebiom.2019.03.043

Conflict of Interest: The authors declare that the research was conducted in the absence of any commercial or financial relationships that could be construed as a potential conflict of interest.

Publisher's Note: All claims expressed in this article are solely those of the authors and do not necessarily represent those of their affiliated organizations, or those of the publisher, the editors and the reviewers. Any product that may be evaluated in this article, or claim that may be made by its manufacturer, is not guaranteed or endorsed by the publisher.

Copyright © 2022 Li, Hou, Zhang, Zhang, Wang, Wang, Wen and Yang. This is an open-access article distributed under the terms of the Creative Commons Attribution License (CC BY). The use, distribution or reproduction in other forums is permitted, provided the original author(s) and the copyright owner(s) are credited and that the original publication in this journal is cited, in accordance with accepted academic practice. No use, distribution or reproduction is permitted which does not comply with these terms.

frontiers | Frontiers in Oncology

ORIGINAL RESEARCH
published: 06 May 2022
doi: 10.3389/fonc.2022.882328

Low CRIM1 Levels Predict Poor Prognosis in Breast Cancer Patients

Wei Wen[1†], *Baohong Jiang*[2†], *Xi Cao*[1], *Liming Xie*[3], *Xiaoli Zhang*[1], *Yuehua Li*[3*] *and Rongfang He*[1*]

[1] Department of Pathology, The First Affiliated Hospital, Hengyang Medical School, University of South China, Hengyang, China, [2] Department of Pharmacy, The First Affiliated Hospital, Hengyang Medical School, University of South China, Hengyang, China, [3] Department of Medical Oncology, The First Affiliated Hospital, Hengyang Medical School, University of South China, Hengyang, China

OPEN ACCESS

Edited by:
Shaoquan Zheng,
Sun Yat-sen University Cancer Center (SYSUCC), China

Reviewed by:
Guopei Zheng,
Guangzhou Medical University Cancer Hospital, China
Jianming Tang,
First Hospital of Lanzhou University, China
Guixiong Zhang,
The First Affiliated Hospital of Sun Yat-sen University, China

***Correspondence:**
Rongfang He
herongfang2019@fsyy.usc.edu.cn
Yuehua Li
liyuehua2020@stu.usc.edu.cn

[†]These authors have contributed equally to this work

Specialty section:
This article was submitted to Molecular and Cellular Oncology, a section of the journal Frontiers in Oncology

Received: 23 February 2022
Accepted: 12 April 2022
Published: 06 May 2022

Citation:
Wen W, Jiang B, Cao X, Xie L, Zhang X, Li Y and He R (2022) Low CRIM1 Levels Predict Poor Prognosis in Breast Cancer Patients. Front. Oncol. 12:882328. doi: 10.3389/fonc.2022.882328

Background: CRIM1 is involved in the development and preservation of the nervous system, capillary development, and vascular maintenance. Although CRIM1 was reported to involve in multiple cancers, its role in breast cancer is unclear.

Methods: We investigated CRIM1 expression levels using Oncomine, HPA, and immunohistochemistry analyses. BC-GenExMiner was employed to evaluate the relationship of CRIM1 expression with the clinicopathological characteristics of breast cancer. Its association with breast cancer prognosis was assessed by Kaplan-Meier analysis and PrognoScan. The correlation of the expression of CRIM1 with tumor immune infiltration was explored *via* TIMER. Gene set enrichment analysis (GSEA) was utilized to determine the cascades that are linked to CRIM1 in breast cancer. Finally, we explored CRIM1 and its co-expressed genes using R (3.6.3).

Results: Here, we find that CRIM1 expression was downregulated in various subtypes of breast cancer, and it was lowest in triple-negative breast cancers. ER and PR status were positively correlated with CRIM1 expression, while HER-2 expression was negatively correlated with CRIM1 expression. But in our immunohistochemical results in breast cancer specimens collected from our laboratory, HER-2 expression was positively correlated with CRIM1 expression. The expression of CRIM1 was correlated with menopause status, T stage, pathologic stage, histological type, and P53 status but not with age, N-stage, M-stage, Radiation therapy, and BRCA1/2 status. Survival analysis found that low CRIM1 expression was correlated with poorer DMFS, RFS and OS. Notably, CRIM1 expression was positively linked to the level of infiltration by $CD8^+$ T-cells, endothelial cells, and neutrophils, and negatively linked to NK, B-cells, $CD4^+$ T-cells, tumor purity, macrophage M1, and Tregs. Besides, DIXDC1 and PFDN6 were correlated to CRIM1 possibly.

Conclusion: Our findings demonstrated that low CRIM1 expression predict poor prognosis of breast cancer and CRIM1 might be used as a possible treatment target or prognostic marker in breast cancer. More researches are needed to better understand the prognostic value of CRIM1 in breast cancer.

Keywords: breast cancer, CRIM1, poor prognosis, bioinformatics analysis, biomarker

INTRODUCTION

Breast cancer is one of the commonest cancers (1) and a leading cause of cancer-linked deaths, globally (2). Early diagnosis of breast cancer is crucial for successful treatment (3, 4). Clinical and pathological features, such as the size of the tumor, tumor grade, rate of lymph node metastasis, patient age, patient morbidity (5), and various biomarkers (e.g., ER, Ki-67, PR, as well as HER-2) (6, 7) are used to predict breast cancer prognosis. However, these methods have many limitations. Thus, novel, effective prognostic biomarkers for breast cancer are urgently needed.

CRIM1 (cysteine-rich transmembrane bone morphogenetic protein regulator 1) is a Type I transmembrane protein. Past studies had shown that CRIM1 regulated the development and preservation of the nervous system and that it influenced capillary generation and vascular maintenance. CRIM1 was suggested to function as a BMP antagonist (8). CRIM1 was also reported to regulate the adhesion and migration of lung cancer cells (9). Its downregulation reduced the expression of E-cadherin, indicating that CRIM1 may inhibit EMT by suppressing cell migration and invasion (10). CRIM1 also promoted the expression of leukemia suppressor receptors by regulating miR-93 and miR-182 *via* circCRIM1 (11). Thus, CRIM1 may have therapeutic or biomarker potential against cancer.

In this study, we used bioinformatics analysis of data from several large online databases to examine gene expression differences in tumors vs normal samples, and to determine the relationship of its expression with clinicopathological features. Besides, we examined the expression of CRIM1 in breast cancer tissues by immunohistochemistry. And then, the prognostic significance of CRIM1 and its co-expressed genes in breast cancer were assessed.

MATERIALS AND METHODS

Oncomine Analysis

Oncomine data resource (http://www.oncomine.org) is a cancer microarray repository and comprehensive data mining platform. Differential expression analysis of most cancers and their subtypes versus their normal tissues was performed (12). We used p=1e-4, fold change=2, and gene rank=top10% as significance thresholds for determining differences between CRIM1 levels in breast cancer vs normal tissues, as well as to identify genes that are co-expressed with CRIM1.

Human Protein Atlas

The Human Protein Atlas is an online tool (www.proteatlas.org) on which immunohistochemistry-centered protein expression patterns of normal tissues, cancers along with cell lines are freely available (13). Currently Survival data are available for >900,000 patients (14). Imaging data on differences in CRIM1 expression in non-malignant breast tissues versus breast cancer tissues were obtained from HPA.

Immunohistochemistry

This study involved 265 cases of invasive breast cancer patients diagnosed at the First Affiliated Hospital, Hengyang Medical School, the University of South China from 2010 to 2012. Patients underwent curative surgical treatment (mastectomy or breast-conserving surgery with axillary evaluation) and did not receive any chemotherapy or radiation therapy before surgery. We used IHC to examine CRIM1 expression levels in breast cancer tissues vs non-malignant breast tissues. Tissues were fixed using 4% formaldehyde, dehydrated in ethanol, paraffin-embedded, then sectioned continuously at 5μm thickness. The concentration of the antibody was 1:50. Antigen retrieval was done by autoclaving the sections in LBP buffer pH 6.0. They were then inoculated with H_2O_2 for 10 minutes for blocking the activity of endogenous peroxidase, followed by overnight inoculation with a primary antibody (1:50) at 4°C. Afterwards, we rinsed the sections with TBS and inoculated with a secondary antibody. They were next rinsed in TBS, and counter-staining using hematoxylin was done. Signal was then developed using DBA, followed by sample dehydration with ethanol, and mounting using neutral resin. They were then examined microscopically and CRIM1 expression scored as negative (-), weak (+), moderate (++), or strong (+++) staining. All statistical data analyses were done on SPSS 25.0 and data between groups were compared using the chi-square test, with p=<0.05 signifying statistical significance. This study was approved by the hospital ethics committee.

Breast Cancer Gene-Expression Miner

Breast cancer gene-expression miner v4.6 (bc-GenExMiner v4.6, http://bcgenex.ico.unicancer.fr/) is a breast cancer gene expression mining program. Bc-GenExMiner is employed to examine the relationship of molecular subtypes or gene expression patterns, with disease prognosis (15–17). Here, we used bc-GenExMiner to determine the relationship of different clinical features with CRIM1 expression.

TIMER 2.0 Database

TIMER 2.0 data resource (http://timer.cistrome.org/) is a platform for comprehensive assessment of invading immune cells in various cancers. Timer offers 6 primary analysis modules, which allow users to interactively assess the association of immune invasion with somatic copy number alterations, gene expression, clinical outcomes, as well as somatic mutations (18). Timer 2.0 uses six advanced algorithms to analyze data from more than 10,000 samples from TCGA, providing users with more reliable estimates of immune invasion levels (19, 20). Here, we analyzed CRIM1 expression in breast cancer and its correlation with the abundance of B-cells, neutrophils, $CD4^+$ T-cells, NK cells, endothelial cells, $CD8^+$ T-cells, macrophages, Tregs, and tumor purity.

Kaplan-Meier Survival Analysis

The Kaplan-Meier Plotter data tool (http://kmplot.com/analysis/) is an online resource for plotting survival maps that can be utilized to

Abbreviations: CRIM1, cysteine-rich transmembrane bone morphogenetic protein regulator 1; BC, breast cancer; DIX, Dishevelled-Axin; GSEA, Gene set enrichment analysis; ER, estrogen receptor; PR, progesterone receptor; HER-2, human epidermal growth factor receptor 2; DMFS, distant metastasis-free surviva l; RFS, relapse-free survival; OS, overall survival; IHC, Immunohistochemistry; BMP, bone morphogenetic protein; VEGF, vascular endothelial growth factor; TGF-b, transforming growth factor-beta.

explore the relationship of diverse gene expression levels of various with the clinical outcomes of individuals with breast cancer. RNA-seq, survival data, along with HTSeq counts for 26 diverse tumor types are obtained from the TCGA data resource (21, 22). Here, we assessed the association of CRIM1 expression with DMFS (distant metastasis-free survival), OS (overall survival), and RFS (relapse-free survival) in breast cancer cohorts. Hazard ratios along with log P values with 95% confidence intervals were calculated and displayed.

PrognoScan

Prognoscan (http://www.prognoscan.org/), a large collection of cancer microarray datasets with clinical annotation, is a tool for assessing biological relationships between gene expression and prognosis. Here, we used Prognoscan to determine the relationship between CRIM1 levels and prognosis (23). Automatic calculation of COX P-values and hazard ratios (HR) with 95% confidence intervals was done based on mRNA levels.

Gene Set Enrichment Analysis

Gene set enrichment analysis (GSEA), which is utilized in interpreting gene expression data, reveals many common biological pathways (24). Here, GSEA was done using the R package, clusterProfiler (25). Ggplot2 (3.6.3) (26) was employed to determine the biological cascades linked to CRIM1 and the rate of breast cancer in 'CRIM1 low' vs 'CRIM1 high' groups using FDR = <0.25 and adjusted p=<0.05 as significance thresholds.

RESULTS

Expression of CRIM1 is Downregulated in Breast Cancer

Oncomine assessment exhibited that CRIM1 was remarkably downregulated in breast cancer compared with normal tissue, including in infiltrative ductal carcinoma, infiltrative lobular carcinoma, and medullary carcinoma (**Figure 1**; **Table 1**).

Analysis of CRIM1 protein levels in breast cancer on human protein atlas exhibited that CRIM1 protein was not expressed in cancer cells (**Figures 2B, D**), although it was modestly and moderately expressed in myoepithelial cells and glandular cells, respectively (**Figures 2A, C**).

In addition, we performed immunohistochemistry on breast cancer and normal tissues using anti-CRIM1 antibody (ab272542) and analyzed the results. This analysis revealed that relative to normal tissues, CRIM1 levels were remarkably lower in breast cancer tissues (**Figures 3A, B**, $\chi 2$=10.444, p=0.001). The rate of CRIM1 positivity in normal breast tissues was 58.42%, relative to 39.62% in carcinoma. Overall,

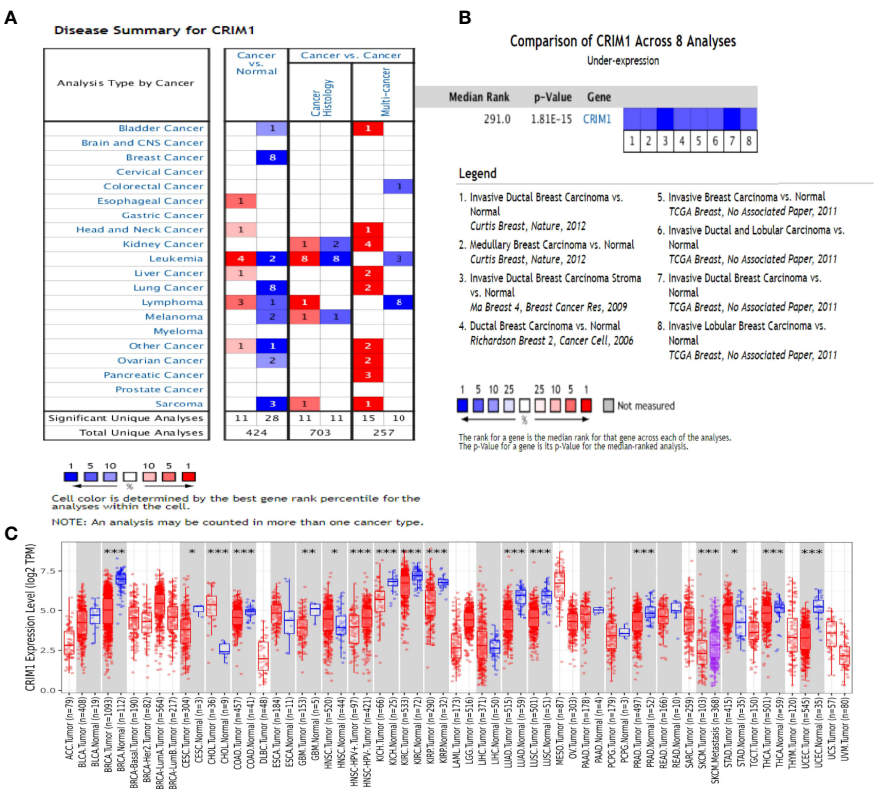

FIGURE 1 | The expression of CRIM1 in various human cancers (ONCOMINE data resource). **(A)** Increased or decreased CRIM1 levels in different cancer datasets in contrast with non-malignant tissues. Red = upregulation, blue = downregulation. The lighter the color, the more meaningful it is. **(B)** Eight analyses show low levels of CRIM1 in breast cancer. **(C)** Expression of CRIM1 in distinct types of human tumors in the TIMER database. *p<0.05, **p<0.01, ***p<0.001.

TABLE 1 | CRIM1 expression in different subtypes of breast cancer and normal tissues using the Oncomine database.

Breast cancer subtype	P-value*	t test	Fold change	Patient number	Reference
Invasive Ductal Breast Carcinoma	3.28E-42	-21.901	-4.038	389	TCGA
Invasive Lobular Breast Carcinoma	3.63E-15	-10.071	-2.722	36	TCGA
Invasive Breast Carcinoma	8.33E-21	-11.021	-2.583	76	TCGA
Invasive Ductal and Lobular Carcinoma	9.81E-05	-6.407	-2.026	3	TCGA
Ductal Breast Carcinoma	4.41E-10	-7.754	-2.93	40	PMID: 16473279
Medullary Breast Carcinoma	4.51E-20	-16.058	-3.276	32	PMID: 22522925
Invasive Ductal Breast Carcinoma	2.48E-67	-26.654	-2.306	1556	PMID: 22522925
Invasive Ductal Breast Carcinoma	2.38E-05	-5.235	-2.312	9	PMID:19187537

Statistical significance was determined by the Student's t test.

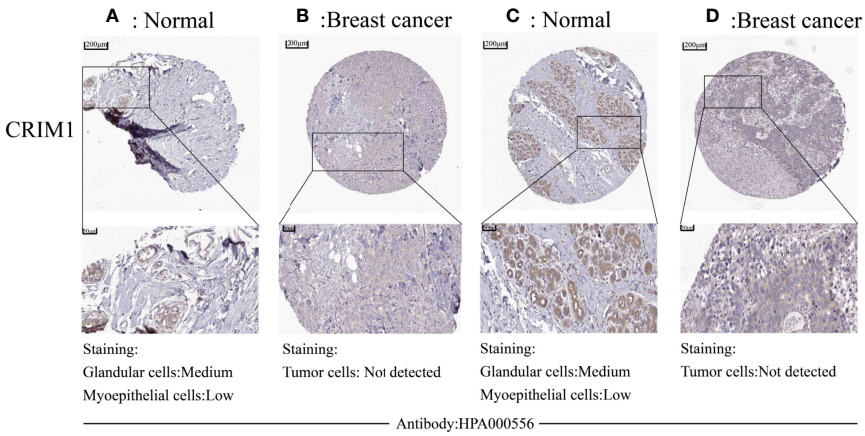

FIGURE 2 | Downregulation of protein levels in breast cancer tissues was observed in human protein atlas. CRIM1 protein levels were medium in glandular cells and low in myoepithelial cells **(A, C)**, and were negative in tumor cells **(B, D)**.

whether the protein expression or mRNA expression of CRIM1 were lower in breast cancer than in normal breast tissues.

Relationship Between CRIM1 Expression and Breast Cancer Clinicopathologic Features

CRIM1 expression in luminal A, luminal B, HER-2-positive, and triple-negative breast cancer tissues collected in our laboratory is shown in **Table 2**. By chi-square test, the difference regarding the expression of CRIM1 in the above four groups was statistically significant ($\chi2$ = 16.377, P=0.001). The expression of CRIM1 in triple-negative group was lowest, but in HER-2-positive group was highest. We compared these four sets of data in pairs. It showed significant difference in CRIM1 expression between the HER-2-positive group with the Luminal A, Luminal B, and triple-negative groups ($\chi2$ = 7.402, p=0.007; $\chi2$ = 13.516, p=0.000; $\chi2$ = 13.650, p=0.000). However, there was no significant difference between Luminal A group with Luminal B and TNBC groups ($\chi2$ = 0.408, p=0.523; $\chi2$ = 1.334, p=0.248), nor between Luminal B and TNBC groups ($\chi2$ = 0.579, p=0.447).

Next, we divided breast cancer patients into various groups according to various clinical characteristics and compared differences in CRIM1 mRNA levels using bc-GenExMiner. The groups did not differ remarkably with regards to age and nodal status (**Figures 4A, E**). ER and PR status were positively correlated with CRIM1 expression (**Figures 4B, C**), while HER-2 expression was negatively correlated with CRIM1 expression (**Figure 4D**). That was somewhat different from our immunohistochemical results in breast cancer specimens collected in our laboratory. We also found that CRIM1 was remarkably downregulated in the basal-like subtype when compared to the non-basal-like subtype. Similar observations were made for triple-negative breast cancer (TNBC, **Figures 4F, G, I**). P53 is one of the most commonly mutated oncogenes (27). Our analysis found that CRIM1 was remarkably downregulated in the p53 mutant group than the p53 wild-type group (**Figure 4H**). We further found that the expression of CRIM1 had a correlation with the pathological tumor stage of breast cancer, and it was obvious to observe that its expression was highest in stage I (**Figure 4J**). And there was no relevance between CRIM1 expression and BRCA1/2 status (**Figures 4K, L**). Next, we evaluated CRIM1 expression in clinical specimens in relation to breast cancer clinicopathological parameters. Breast cancer patients were then grouped into the high- and low-CRIM1 expression groups and their correlation with age, menopause, TNM stage, histological type, pathologic stage, HER2 status, and radiotherapy were investigated. CRIM1 expression correlated with menopause status(p=0.005), T stage(p=0.002), pathologic stage(p=0.040),

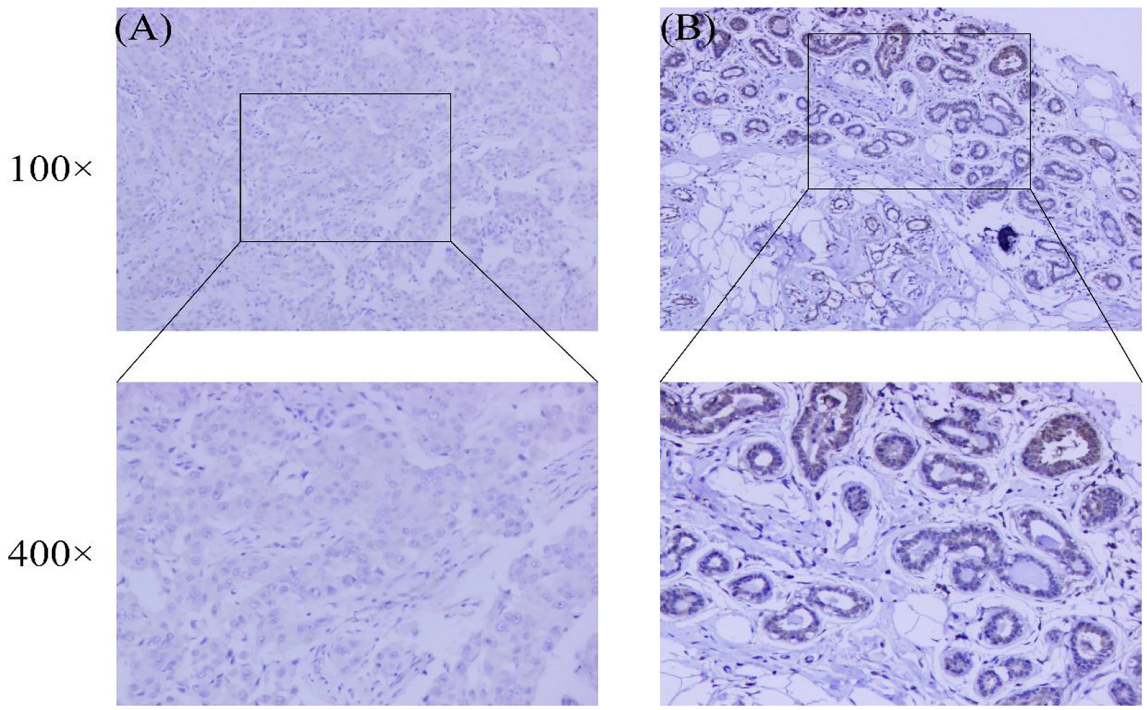

FIGURE 3 | Expression of CRIM1 in 265 breast cancer patient samples and 101 normal breast tissues were examined by immunohistochemistry. **(A)** CRIM1 expression is negative (-) in breast cancer; **(B)** CRIM1 expression is moderate (++) in normal breast tissues.

TABLE 2 | CRIM1 expression in different subtypes of breast cancer and normal tissues using Immunohistochemistry [n(%)].

clinicopathological features	number	CRIM1 expression		χ2	*P*-value
		negative	positive		
group					
breast cancer tissues	265	160 (60.4)	105 (39.6)		
normal breast tissues	101	42 (41.6)	59 (58.4)	10.444	0.001
pathological type					
Luminal A	36	22 (61.1)	14 (38.9)		
Luminal B	103	69 (67.0)	34 (33.0)		
HER2	21	5 (23.8)	16 (76.2)		
TNBC	38	38 (73.7)	10 (26.3)	16.377	0.001

histological type(p=0.011), and HER2 status(p<0.001) but not with age(p=0.411), N-stage(p=0.372), M-stage(p=0.219), and Radiation therapy (p=0.435) (**Table 3**).

Decreased CRIM1 Expression Impacted the Prognosis of Breast Cancer Patients

Kaplan-Meier and log-rank test analyses of the significance of CRIM1 expression on breast prognosis revealed that higher CRIM1 levels correlated with better DMFS (HR=0.7, *p*=4.4e-06), OS (HR=0.78, *p*=0.009), and RFS (HR=0.85, *p*=0.002). However, low CRIM1 levels were correlated with worse survival (**Figures 5A–C**). Similar observations were made using PrognoScan analysis which exhibited that low CRIM1 expression remarkably linked to poorer RFS, OS, DSS, DFS, and DMFS (**Table 4**). Receiver operating characteristic (ROC) curve analysis of the relationship of CRIM1 with survival time of breast cancer patients revealed an AUC of 0.891 (**Figure 5D**), indicating good performance for CRIM1 in predicting survival.

CRIM1 Expression Levels Correlated With Immune Cells Invasion Levels in Breast Cancer

Further, we adopted TIMER to examine the relationship of CRIM1 with invading immune cells in breast cancer, consisting of $CD4^+$ T-cells, neutrophils, $CD8^+$ T-cells, macrophage M1, B-cells, NK, endothelial cells, and Tregs. This analysis illustrated that CRIM1 expression was positively linked to $CD8^+$ T-cells (r=0.297, *p*=9.47e-22), endothelial cells (r=0.392, *p*=8.87e-38) and neutrophils (r=0.498, *p*=2.31e-63), and negatively linked to NK (r=-0.204, *p*=8.50e-11), B-cells (r=-0.3, *p*=3.70e-22), $CD4^+$ T-cells (r=-0.574,

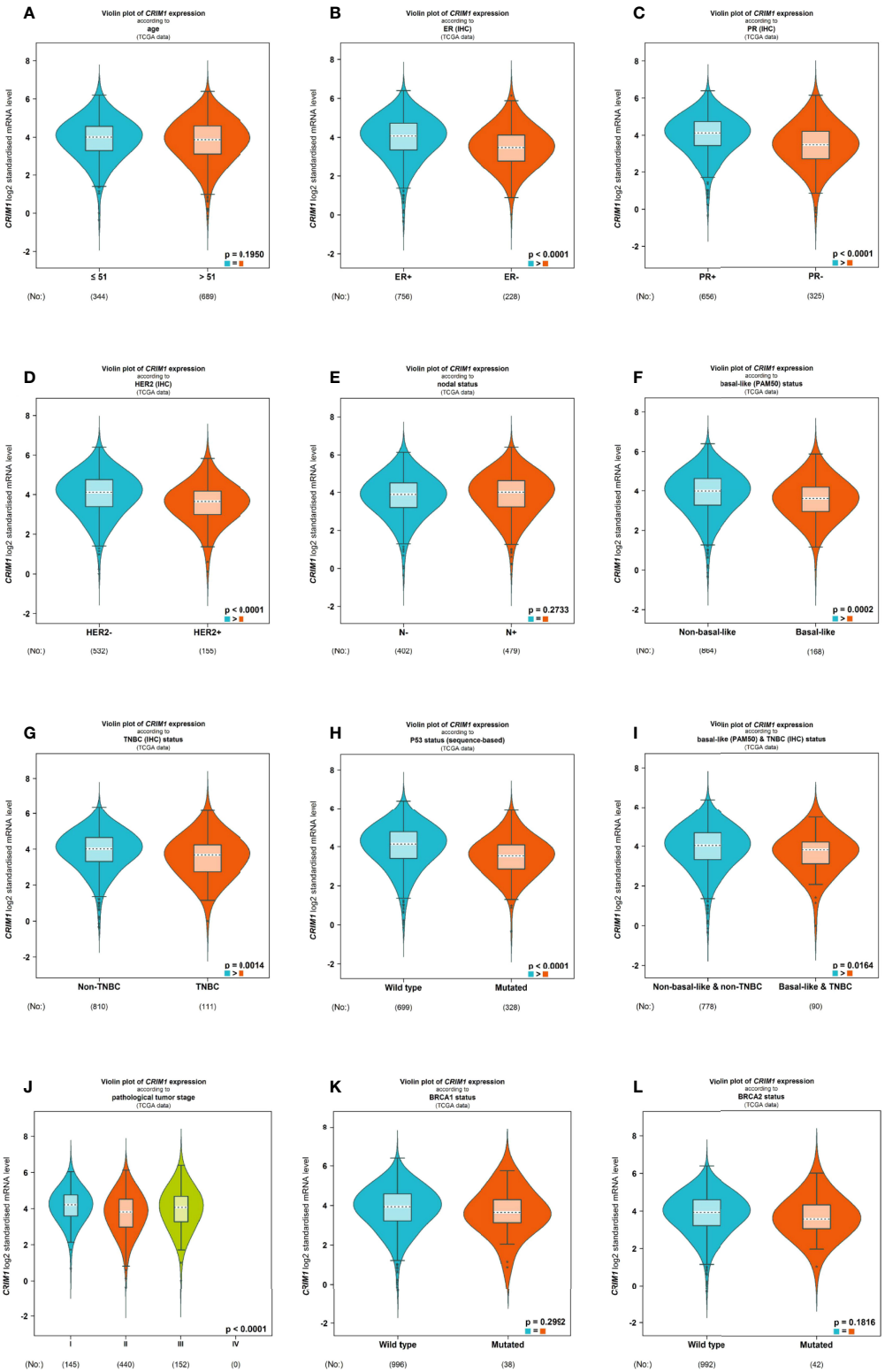

FIGURE 4 | Violin plot illustrated the relationship of CRIM1 expression with clinical indicators using bc-GenExMiner. Data include age **(A)**, ER **(B)**, PR **(C)**, HER-2 **(D)**, nodal status **(E)**, basal-like status **(F)**, TNBC status **(G)**, P53 status **(H)**, basal-like & TNBC status **(I)**, pathological tumor stage **(J)**, BRCA1 status **(K)** and BRCA2 status **(L)**.

TABLE 3 | Relationship between CRIM1 expression and clinicopathologic parameters of breast cancer patients.

Characteristic	Low expression of CRIM1	High expression of CRIM1	p
n	541	542	
Age, n (%)			0.411
<=60	293 (27.1%)	308 (28.4%)	
>60	248 (22.9%)	234 (21.6%)	
Menopause status, n (%)			**0.005**
Pre	92 (9.5%)	137 (14.1%)	
Peri	20 (2.1%)	20 (2.1%)	
Post	370 (38.1%)	333 (34.3%)	
T stage, n (%)			**0.002**
T1	112 (10.4%)	165 (15.3%)	
T2	338 (31.3%)	291 (26.9%)	
T3	69 (6.4%)	70 (6.5%)	
T4	20 (1.9%)	15 (1.4%)	
N stage, n (%)			0.372
N0	255 (24%)	259 (24.3%)	
N1	182 (17.1%)	176 (16.5%)	
N2	51 (4.8%)	65 (6.1%)	
N3	43 (4%)	33 (3.1%)	
M stage, n (%)			0.219
M0	438 (47.5%)	464 (50.3%)	
M1	13 (1.4%)	7 (0.8%)	
Pathologic stage, n (%)			**0.040**
Stage I	74 (7%)	107 (10.1%)	
Stage II	324 (30.6%)	295 (27.8%)	
Stage III	123 (11.6%)	119 (11.2%)	
Stage IV	11 (1%)	7 (0.7%)	
Histological type, n (%)			**0.011**
Infiltrating Ductal Carcinoma	407 (41.7%)	365 (37.4%)	
Infiltrating Lobular Carcinoma	87 (8.9%)	118 (12.1%)	
HER2 status, n (%)			**< 0.001**
Negative	239 (32.9%)	319 (43.9%)	
Indeterminate	7 (1%)	5 (0.7%)	
Positive	99 (13.6%)	58 (8%)	
Radiation therapy, n (%)			0.435
No	226 (22.9%)	208 (21.1%)	
Yes	273 (27.7%)	280 (28.4%)	

Values in bold indicate that the results are statistically significant.

p=4.08e-88), tumor purity (r=-0.177, *p*=1.98e-08), macrophage M1 (r=-0.318, p=8.21e-25), and Tregs (r=-0.266, *p*=1.53e-17) (**Figure 6**). These findings indicated that CRIM1 levels may regulate immune cells infiltration in breast cancer.

GSEA Identified CRIM1-Associated Pathways in Breast Cancer

To evaluate the possible mechanisms accounting for the effects of CRIM1 on breast cancer, we performed GSEA analysis on samples with low CRIM1 levels relative to those with high CRIM1 levels. This analysis revealed significant differences in the abundance of MSigDB collections (c2.cp.v7.2.symbols.gmt) and that M phase, metabolism of amino acids and derivatives were remarkably differentially enriched in samples with low CRIM1 levels (**Figures 7A, B**), indicating that low CRIM1 levels may influence breast cancer development *via* these pathways.

CRIM1, PFDN6, and DIXDC1 Were Co-Expressed in Breast Cancer Patients

Finally, we analyzed TCGA data resources (https://portal.gdc.cancer.gov/) BRCA RNAseq (data in level 3 HTSeq-FPKM format) for genes that are co-expressed with CRIM1 using the R packages, stat (28) and ggplot2 (26) (3.6.3). This analysis identified 5254 IDs that met the cutoff threshold of |cor|>0.3, *p*=<0.05. Results showed that 5091 genes were positively correlated with CRIM1 levels, while 163 genes were negatively correlated with CRIM1. Notably, DIXDC1 had a strong positive correlation with CRIM1, while PFDN6 had a strong negative association with CRIM1 (**Figures 8A, B**). It was reported that DIXDC1 deletion enhances SNAIL-dependent gene expression, which enhances invasion and remodeling of the tumor microenvironment (29). PFDN6 (Prefoldin 6) is a β-like subunit of hetero-hexameric chaperone proteins (30). Prefoldins are highly specialized co-chaperones of actin and microtubule protein folding (31).

DISCUSSION

Despite advances in chemotherapy, radiotherapy, and surgical treatment of breast cancer, its survival rate remains low (32). Breast cancer is the primary cause of mortality along with

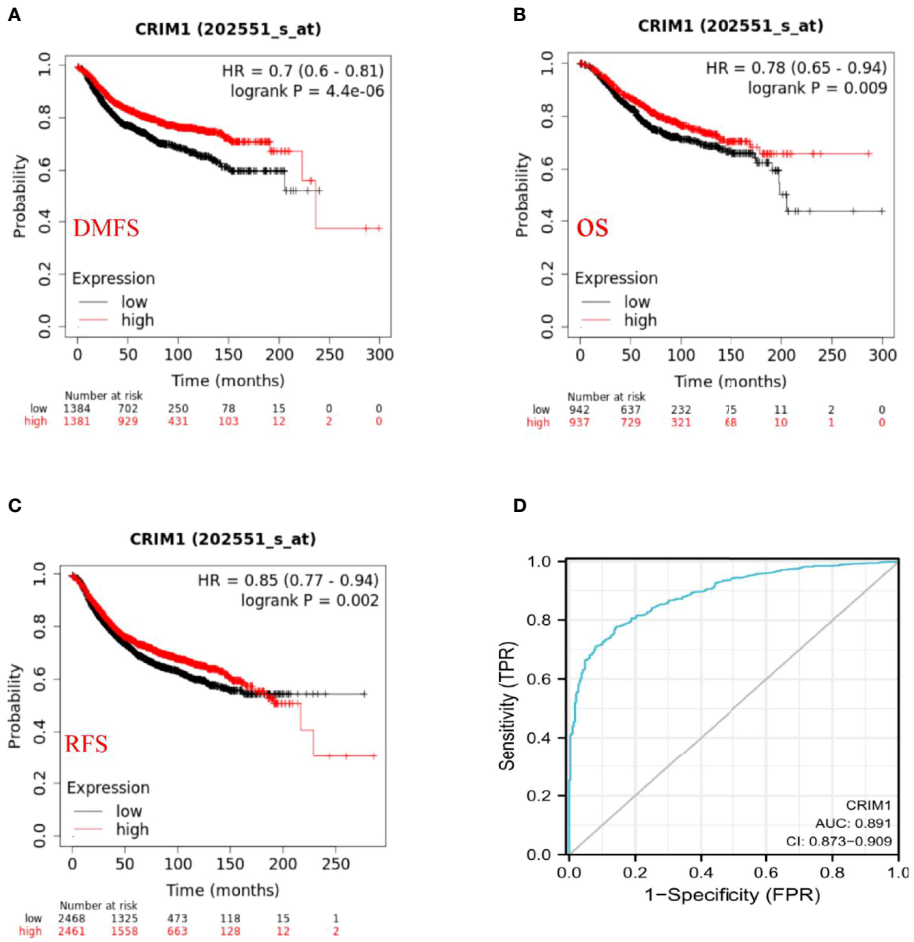

FIGURE 5 | Prognostic significance of CRIM1 expression in breast cancer **(A–D)**. **(A–C)** Kaplan-Meier analysis revealed that high CRIM1 levels were correlated with better DMFS (distant metastasis-free survival), OS (overall survival), and RFS (relapse-free survival). **(D)** Receiver operating characteristic (ROC) curve analysis of the correlation between CRIM1 and survival in breast cancer patients showed that CRIM1 had good performance in predicting breast cancer survival.

TABLE 4 | CRIM1 expression and survival data of breast cancer patients through the PrognoScan database.

DATASET	ENDPOINT	PROBE ID	N	COX P-VALUE	HR [95% CI-low- CI-up]
GSE1456-GPL96	Relapse Free Survival	202552_s_at	159	2.71452E-05	0.35 [0.21 - 0.57]
GSE1456-GPL96	Disease Specific Survival	202552_s_at	159	0.000165802	0.32 [0.18 - 0.58]
GSE1456-GPL96	Overall Survival	202552_s_at	159	0.0277991	0.55 [0.33 - 0.94]
GSE1456-GPL97	Overall Survival	228496_s_at	159	0.0436275	0.64 [0.41 - 0.99]
GSE1456-GPL97	Relapse Free Survival	228496_s_at	159	0.000131085	0.47 [0.32 - 0.69]
GSE1456-GPL97	Disease Specific Survival	228496_s_at	159	9.81953E-05	0.42 [0.27 - 0.65]
GSE7378	Disease Free Survival	202552_s_at	54	0.0470036	0.47 [0.23 - 0.99]
GSE3494-GPL96	Disease Specific Survival	202552_s_at	236	0.00154078	0.39 [0.22 - 0.70]
GSE3494-GPL97	Disease Specific Survival	228496_s_at	236	0.0100557	0.56 [0.36 - 0.87]
GSE4922-GPL96	Disease Free Survival	202552_s_at	249	0.00532698	0.55 [0.36 - 0.84]
GSE4922-GPL97	Disease Free Survival	228496_s_at	249	0.00296997	0.62 [0.45 - 0.85]
GSE2990	Relapse Free Survival	202552_s_at	62	0.0181867	0.49 [0.27 - 0.88]
GSE2990	Distant Metastasis Free Survival	202552_s_at	54	0.0170378	0.38 [0.17 - 0.84]

morbidity in women (33). Thus, new breast cancer biomarkers are urgently needed for better outcomes.

CRIM1 is involved in histogenesis *via* its interaction with growth factors, including bone morphogenetic protein (BMP), vascular endothelial growth factor (VEGF), as well as transforming growth factor-beta (TGF-β) (34). Reduced CRIM1 expression is associated with reduced E-cadherin levels. CRIM1 suppresses cell migration and invasion by

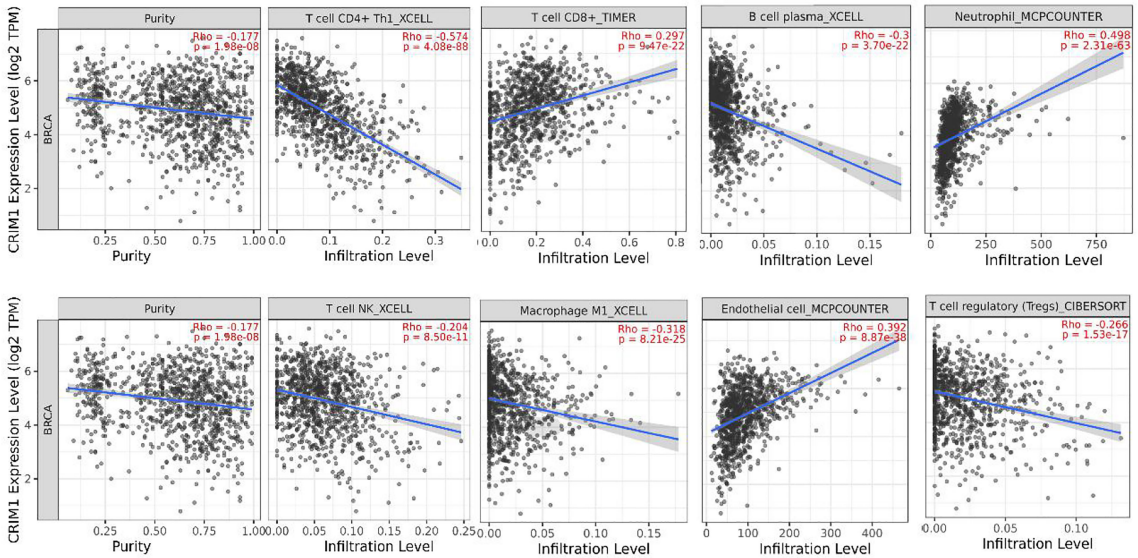

FIGURE 6 | TIMER analysis of the relationship of CRIM1 expression with immune cells invasion levels in breast cancer. CRIM1 expression in breast cancer tissues were negatively correlated with tumor purity, Tregs, NK, B-cells, and $CD4^+$ T-cells, macrophage M1, and positively correlated with $CD8^+$ T-cells, endothelial cells, and neutrophils (n=1100).

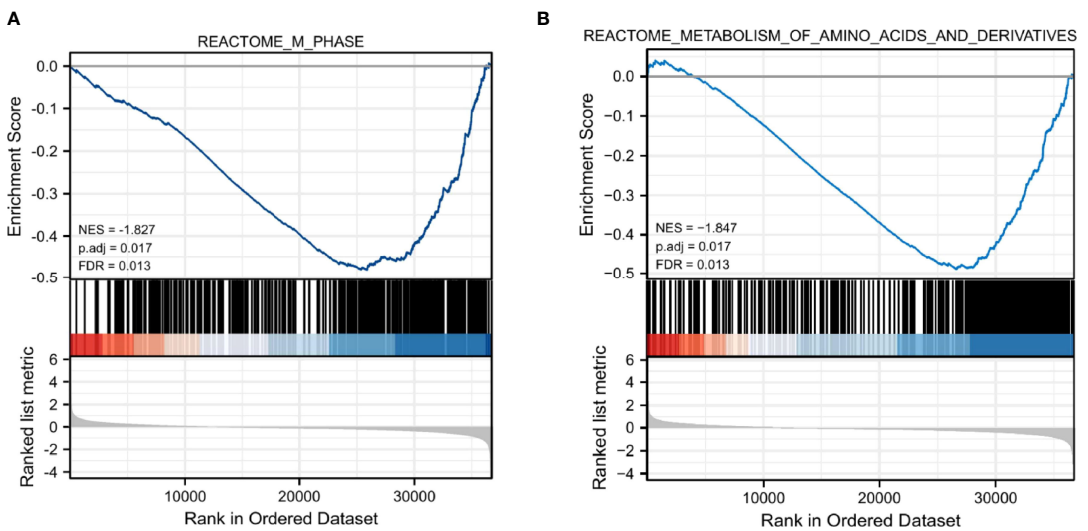

FIGURE 7 | GSEA revealed that M phase **(A)** and metabolism of amino acids and derivatives **(B)** were enriched in the low CRIM1 expression group. NES, normalized ES; FDR, false discovery rate.

regulating the expression of various EMT-related factors (10). However, the significance of CRIM1 expression in breast cancer is unclear.

Oncomine analysis of CRIM1 expression in breast cancer revealed decreased CRIM1 levels in many kinds of breast carcinoma, such as infiltrative ductal breast carcinoma, infiltrative lobular breast carcinoma, and medullary breast carcinoma. Analysis using bc-GenExMiner revealed that ER and PR status were positively associated with CRIM1 expression, while HER-2, basal-like status, triple-negative status along with p53 status were negatively correlated with CRIM1 expression in breast cancer tissues. That was somewhat different from our immunohistochemical results in breast cancer specimens collected in our laboratory. In our immunohistochemical results, HER-2 expression was positively correlated with CRIM1

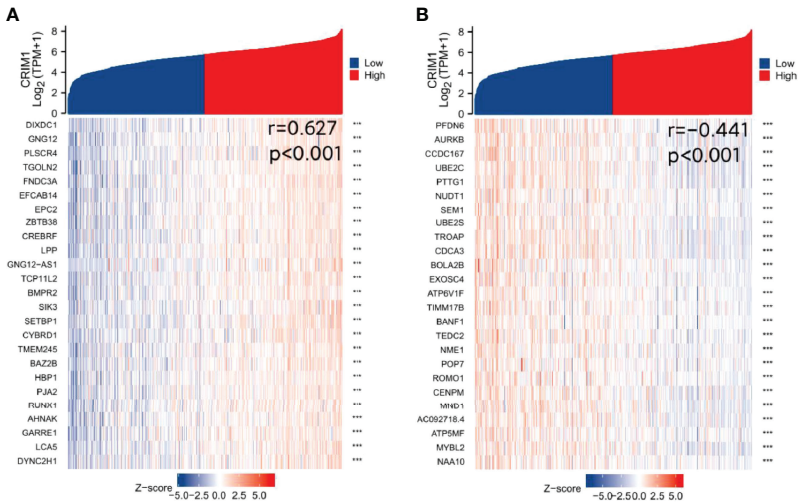

FIGURE 8 | Identification of genes that are co-expressed with CRIM1. **(A)** DIXDC1 was positively correlated with CRIM1. **(B)** PFDN6 was negatively correlated with CRIM1. ***p=<0.001.

expression. More experimental evidence is needed to verify. Human Protein Atlas results showed that CRIM1 expression was lower than normal in breast cancer and IHC analyses revealed the expression of CRIM1 was lowest in triple-negative breast cancer. The pathological tumor stage of breast cancer was in connection with CRIM1 expression, with the highest expression in stage I. Expression of CRIM1 was correlated with menopause status, T stage, pathologic stage, histological type, and P53 status but not with age, N-stage, M-stage, and Radiation therapy.

Investigation of the impact of CRIM1 on breast cancer prognosis using Kaplan-Meier and PrognoScan analyses revealed that reduced CRIM1 levels correlated with poorer RFS, OS, DSS, DFS, and DMFS. These findings indicated that low CRIM1 expression may effectively predict breast cancer prognosis.

TIMER analysis of the mechanisms underlying CRIM1 effects on breast cancer revealed that CRIM1 levels were negatively linked to tumor purity, macrophage M1, Tregs, NK cells, B-cells, and $CD4^+$ T-cells, but were positively correlated with $CD8^+$ T-cells, endothelial cells, macrophage M1 as well as neutrophils.

Using co-expression along with correlation analyses, we found that DIXDC1 was positively correlated with CRIM1 expression, while PFDN6 expression was negatively related to CRIM1 levels. DIXDC1 is a scaffolding protein consisting of 3 protein-interacting structural domains (an actin-binding calponin homology (CH) domain, a coiled-coil (CC) domain, and a Dishevelled-Axin (DIX) oligomerization domain). Numerous studies have reported its positive regulation of the DIX structural domain in Wnt signaling. Reduced DIXDC1 expression promotes malignant behavior and is associated with the survival in cancer (29, 35).

In conclusion, our findings indicated that CRIM1 was downregulated in breast cancer in contrast with non-malignant tissues and that reduced CRIM1 expression was correlated with poor prognosis. Our studies were mainly based on bioinformatics analysis and lacked systematic experimental validation. Further researches are needed to better characterize the prognostic value of CRIM1 in breast cancer.

DATA AVAILABILITY STATEMENT

Publicly available datasets were analyzed in this study. This data can be found here: TCGA (https://portal.gdc.cancer.gov/) RNAseq data in level 3 HTSeq - Counts format from the BRCA (Breast Invasive Cancer) project.

ETHICS STATEMENT

This study was approved by the Ethics Committee of the First Affiliated Hospital of University of South China (Approval number:2020ll1010014). The patients/participants provided their written informed consent to participate in this study.

AUTHOR CONTRIBUTIONS

RH and YL participated in the designing of experiments. Experiments were conducted with WW, BJ, XC, LX, and XZ participated in analyzing and interpreting data. WW, YL and RH were the main writers of the manuscript. All authors contributed to the article and approved the submitted version.

FUNDING

This work was funded by the Natural Science Foundation of Hunan Province (2019JJ80036) and the funds from the Health Committee of Hunan Province (20201974, B20180052).

REFERENCES

1. Harbeck N, Gnant M. Breast Cancer. *Lancet* (2017) 389(10074):1134–50. doi: 10.1016/S0140-6736(16)31891-8
2. Akram M, Iqbal M, Daniyal M. Awareness and Current Knowledge of Breast Cancer. *Biol Res* (2017) 50(1):33. doi: 10.1186/s40659-017-0140-9
3. Jafari SH, Saadatpour Z, Salmaninejad A. Breast Cancer Diagnosis: Imaging Techniques and Biochemical Markers. *J Cell Physiol* (2018) 233(7):5200–13. doi: 10.1002/jcp.26379
4. Rossi S, Cinini C, Di Pietro C. Diagnostic Delay in Breast Cancer: Correlation With Disease Stage and Prognosis. *Tumori* (1990) 76(6):559–62. doi: 10.1177/030089169007600609
5. Duffy MJ, Walsh S, McDermott EW. Biomarkers in Breast Cancer: Where Are We and Where Are We Going? *Adv Clin Chem* (2015) 71:1–23. doi: 10.1016/bs.acc.2015.05.001
6. Duffy MJ, Harbeck N, Nap M. Clinical Use of Biomarkers in Breast Cancer: Updated Guidelines From the European Group on Tumor Markers (EGTM). *Eur J Cancer* (2017) 75:284–98. doi: 10.1016/j.ejca.2017.01.017
7. Li G, Hu J, Hu G. Biomarker Studies in Early Detection and Prognosis of Breast Cancer. *Adv Exp Med Biol* (2017) 1026:27–39. doi: 10.1007/978-981-10-6020-5_2
8. Zeng H, Tang L. CRIM1, the Antagonist of BMPs, is a Potential Risk Factor of Cancer. *Curr Cancer Drug Targets* (2014) 14(7):652–8. doi: 10.2174/1568009614666140725094125
9. Zeng H, Zhang Y, Yi Q. CRIM1, A Newfound Cancer-Related Player, Regulates the Adhesion and Migration of Lung Cancer Cells. *Growth Factors* (2015) 33(5-6):384–92. doi: 10.3109/08977194.2015.1119132
10. Ogasawara N, Kudo T, Sato M. Reduction of Membrane Protein CRIM1 Decreases E-Cadherin and Increases Claudin-1 and MMPs, Enhancing the Migration and Invasion of Renal Carcinoma Cells. *Biol Pharm Bull* (2018) 41(4):604–11. doi: 10.1248/bpb.b17-00990
11. Hong X, Liu N, Liang Y. Circular RNA CRIM1 Functions as a ceRNA to Promote Nasopharyngeal Carcinoma Metastasis and Docetaxel Chemoresistance Through Upregulating FOXQ1. *Mol Cancer* (2020) 19(1):33–48. doi: 10.1186/s12943-020-01149-x
12. Rhodes DR, Yu J, Shanker K. ONCOMINE: A Cancer Microarray Database and Integrated Data-Mining Platform1. *Neoplasia (New York NY)* (2004) 6(1):1–6. doi: 10.1016/s1476-5586(04)80047-2
13. Pontén F, Jirström K, Uhlen M. The Human Protein Atlas-A Tool for Pathology. *J Pathol* (2008) 216(4):387–93. doi: 10.1002/path.2440
14. Uhlen M, Zhang C, Lee S. A Pathology Atlas of the Human Cancer Transcriptome. *Science* (2017) 357(6352):n2507. doi: 10.1126/science.aan2507
15. Jézéquel P, Gouraud W, Ben Azzouz F. Bc-GenExMiner 4.5: New Mining Module Computes Breast Cancer Differential Gene Expression Analyses. *Database* (2021) 00:1–10. doi: 10.1093/database/baab007
16. Jézéquel P, Campone M, Gouraud W. Bc-GenExMiner: An Easy-to-Use Online Platform for Gene Prognostic Analyses in Breast Cancer. *Breast Cancer Res Treat* (2012) 131(3):765–75. doi: 10.1007/s10549-011-1457-7
17. Jezequel P, Frenel JS, Campion L. Bc-GenExMiner 3.0: New Mining Module Computes Breast Cancer Gene Expression Correlation Analyses. *Database* (2013) 2013:s60. doi: 10.1093/database/bas060
18. Li B, Severson E, Pignon J. Comprehensive Analyses of Tumor Immunity: Implications for Cancer Immunotherapy. *Genome Biol* (2016) 17(1):174–88. doi: 10.1186/s13059-016-1028-7
19. Li T, Fan J, Wang B. TIMER: A Web Server for Comprehensive Analysis of Tumor-Infiltrating Immune Cells. *Cancer Res* (2017) 77(21):e108–10. doi: 10.1158/0008-5472.CAN-17-0307
20. Li T, Fu J, Zeng Z. TIMER2.0 for Analysis of Tumor-Infiltrating Immune Cells. *Nucleic Acids Res* (2020) 48(W1):W509–14. doi: 10.1093/nar/gkaa407
21. Győrffy B, Lanczky A, Eklund AC. An Online Survival Analysis Tool to Rapidly Assess the Effect of 22,277 Genes on Breast Cancer Prognosis Using Microarray Data of 1,809 Patients. *Breast Cancer Res Treat* (2010) 123(3):725–31. doi: 10.1007/s10549-009-0674-9
22. Nagy Á, Munkácsy G, Győrffy B. Pancancer Survival Analysis of Cancer Hallmark Genes. *Sci Rep* (2021) 11(1):6047–56. doi: 10.1038/s41598-021-84787-5
23. Mizuno H, Kitada K, Nakai K. PrognoScan: A New Database for Meta-Analysis of the Prognostic Value of Genes. *BMC Med Genomics* (2009) 2(1):18. doi: 10.1186/1755-8794-2-18
24. Subramanian A, Tamayo P, Mootha VK. Gene Set Enrichment Analysis: A Knowledge-Based Approach for Interpreting Genome-Wide Expression Profiles. *Proc Natl Acad Sci - PNAS* (2005) 102(43):15545–50. doi: 10.1073/pnas.0506580102
25. Yu G, Wang LG, Han Y. Clusterprofiler: An R Package for Comparing Biological Themes Among Gene Clusters. *OMICS* (2012) 16(5):284–7. doi: 10.1089/omi.2011.0118
26. Wickham H. *Ggplot2 :Elegant Graphics for Data Analysis1*. New York: Springer (2016).
27. Chen M-S, Yuan J, Cheng H. Expression of P53 in Breast Cancer and its Clinical Significance. *Chongqing Med* (2014) 43(09):1069–71.
28. Bolar K. *STAT: Interactive Document for Working With Basic Statistical Analysis*. (2019). Available at: https://CRAN.R-project.org/package=STAT.
29. Goodwin JM, Svensson RU, Lou HJ. An AMPK-Independent Signaling Pathway Downstream of the LKB1 Tumor Suppressor Controls Snail1 and Metastatic Potential. *Mol Cell* (2014) 55(3):436–50. doi: 10.1016/j.molcel.2014.06.021
30. Vainberg IE, Lewis SA, Rommelaere H. Prefoldin, A Chaperone That Delivers Unfolded Proteins to Cytosolic Chaperonin. *Cell* (1998) 93(5):863–73. doi: 10.1016/S0092-8674(00)81446-4
31. Millan-Zambrano G, Chavez S. Nuclear Functions of Prefoldin. *Open Biol* (2014) 4(7):140085–93. doi: 10.1098/rsob.140085
32. Fredholm H, Eaker S, Frisell J. Breast Cancer in Young Women: Poor Survival Despite Intensive Treatment. *PloS One* (2009) 4(11):e7695. doi: 10.1371/journal.pone.0007695
33. Anastasiadi Z, Lianos GD, Ignatiadou E. Breast Cancer in Young Women: An Overview. *Updates Surg* (2017) 69(3):313–7. doi: 10.1007/s13304-017-0424-1
34. Furuichi T, Tsukamoto M, Saito M. Crim1C140S Mutant Mice Reveal the Importance of Cysteine 140 in the Internal Region 1 of CRIM1 for its Physiological Functions. *Mamm Genome* (2019) 30(11-12):329–38. doi: 10.1007/s00335-019-09822-3
35. Zhou S, Shen J, Lin S. Downregulated Expression of DIXDC1 in Hepatocellular Carcinoma and Its Correlation With Prognosis. *Tumor Biol* (2016) 37(10):13607–16. doi: 10.1007/s13277-016-5213-9

Conflict of Interest: The authors declare that the research was conducted in the absence of any commercial or financial relationships that could be construed as a potential conflict of interest.

Publisher's Note: All claims expressed in this article are solely those of the authors and do not necessarily represent those of their affiliated organizations, or those of the publisher, the editors and the reviewers. Any product that may be evaluated in this article, or claim that may be made by its manufacturer, is not guaranteed or endorsed by the publisher.

Copyright © 2022 Wen, Jiang, Cao, Xie, Zhang, Li and He. This is an open-access article distributed under the terms of the Creative Commons Attribution License (CC BY). The use, distribution or reproduction in other forums is permitted, provided the original author(s) and the copyright owner(s) are credited and that the original publication in this journal is cited, in accordance with accepted academic practice. No use, distribution or reproduction is permitted which does not comply with these terms.

frontiers | Frontiers in Oncology

ORIGINAL RESEARCH
published: 10 May 2022
doi: 10.3389/fonc.2022.879563

Development and Validation of a Risk Prediction Model for Breast Cancer Prognosis Based on Depression-Related Genes

Xuan Wang[1,2†], Neng Wang[1,3,4†], Linda L. D. Zhong[4,5], Kexin Su[6], Shengqi Wang[1,2,4,7], Yifeng Zheng[1,2], Bowen Yang[1,2], Juping Zhang[1,2], Bo Pan[1,2], Wei Yang[8] and Zhiyu Wang[1,2,4,7]*

[1] State Key Laboratory of Dampness Syndrome of Chinese Medicine, The Second Affiliated Hospital of Guangzhou University of Chinese Medicine, Guangzhou, China, [2] The Research Center of Integrative Cancer Medicine, Discipline of Integrated Chinese and Western Medicine, the Second Clinical College of Guangzhou University of Chinese Medicine, Guangzhou, China, [3] The Research Center for Integrative Medicine, School of Basic Medical Sciences, Guangzhou University of Chinese Medicine, Guangzhou, China, [4] Guangdong-Hong Kong-Macau Joint Lab on Chinese Medicine and Immune Disease Research, Guangzhou University of Chinese Medicine, Guangzhou, China, [5] School of Chinese Medicine, Hong Kong Baptist University, Hong Kong, Hong Kong SAR, China, [6] School of Pharmaceutical Sciences, Guangzhou University of Chinese Medicine, Guangzhou, China, [7] Guangdong Provincial Key Laboratory of Clinical Research on Traditional Chinese Medicine Syndrome, Guangdong Provincial Academy of Chinese Medical Sciences, Guangdong Provincial Hospital of Chinese Medicine, Guangzhou, China, [8] Atrius Health, Harvard Vanguard Medical Associates, Burlington, MA, United States

OPEN ACCESS

Edited by:
Shaoquan Zheng, Sun Yat-sen University Cancer Center (SYSUCC), China

Reviewed by:
Sen Li, Beijing University of Chinese Medicine, China
Weihuan Huang, Jinan University, China

***Correspondence:**
Zhiyu Wang
wangzhiyu976@126.com

†These authors have contributed equally to this work

Specialty section:
This article was submitted to Molecular and Cellular Oncology, a section of the journal Frontiers in Oncology

Received: *19 February 2022*
Accepted: *01 April 2022*
Published: *10 May 2022*

Citation:
Wang X, Wang N, Zhong LLD, Su K, Wang S, Zheng Y, Yang B, Zhang J, Pan B, Yang W and Wang Z (2022) Development and Validation of a Risk Prediction Model for Breast Cancer Prognosis Based on Depression-Related Genes. Front. Oncol. 12:879563. doi: 10.3389/fonc.2022.879563

Background: Depression plays a significant role in mediating breast cancer recurrence and metastasis. However, a precise risk model is lacking to evaluate the potential impact of depression on breast cancer prognosis. In this study, we established a depression-related gene (DRG) signature that can predict overall survival (OS) and elucidate its correlation with pathological parameters and sensitivity to therapy in breast cancer.

Methods: The model training and validation assays were based on the analyses of 1,096 patients from The Cancer Genome Atlas (TCGA) database and 2,969 patients from GSE96058. A risk signature was established through univariate and multivariate Cox regression analyses.

Results: Ten DRGs were determined to construct the risk signature. Multivariate analysis revealed that the signature was an independent prognostic factor for OS. Receiver operating characteristic (ROC) curves indicated good performance of the model in predicting 1-, 3-, and 5-year OS, particularly for patients with triple-negative breast cancer (TNBC). In the high-risk group, the proportion of immunosuppressive cells, including M0 macrophages, M2 macrophages, and neutrophils, was higher than that in the low-risk group. Furthermore, low-risk patients responded better to chemotherapy and endocrine therapy. Finally, a nomogram integrating risk score, age, tumor-node-metastasis (TNM) stage, and molecular subtypes were established, and it showed good agreement between the predicted and observed OS.

Conclusion: The 10-gene risk model not only highlights the significance of depression in breast cancer prognosis but also provides a novel gene-testing tool to better prevent the potential adverse impact of depression on breast cancer prognosis.

Keywords: breast cancer, depression, predictive model, overall survival, nomogram

INTRODUCTION

As a formidable health problem for women worldwide, breast cancer ranks first in incidence and mortality among women's malignancies. According to the World Health Statistics 2020, breast cancer incidence accounted for 11.7% of new cases in 2020 and 6.9% of mortalities worldwide (1). Despite advances in early detection and drug development, significant barriers remain in the prediction of metastasis or recurrence risk (2). Given the long latent period and relatively young age of breast cancer, the development of prognosis-risk prediction models is of great value to improve treatment strategies and overall survival (OS).

Prognostic risk factors of breast cancer have attracted increasing interest for more than a decade. In 2007, the St. Gallen Expert Consensus considered that the risk of breast cancer recurrence was mainly related to age, tumor size, histological grade, peritumor intravascular cancer emboli, and expression of the estrogen receptor (ER)/progesterone receptor (PR) and human epidermal growth factor receptor 2 (HER2) (3). In St. Gallen 2011, breast cancer was divided into four types, namely, luminal A, luminal B, HER2+, and triple-negative breast cancer (TNBC) (4), of which TNBC was considered to have a poor prognosis. In fact, only 77% of TNBC patients survive 5 years after diagnosis, while the survival rate of other subtypes reached 93% (5). The 5-year survival rate in the metastatic TNBC is less than 30% and almost all patients will ultimately die of their disease (6). However, breast cancer is a highly heterogenous disease (7), and some TNBC patients have a low recurrence risk and relatively long survival period. It is believed that more genes are involved in determining breast cancer prognosis in addition to ER, PR and HER2. For example, the luminal A type was further classified into low-, intermediate-, and high-risk recurrence subgroups by a 21-gene recurrence score system (8). In addition, risk prediction tools, such as MammaPrint, Breast Cancer Index, PAM50 and EPclin, have also been developed to address the needs for precise diagnosis and treatment (9–12). Nevertheless, these tools are greatly limited by specific platforms and pathological subtype. Thus, it is significant and urgent to establish novel gene panels to assist with risk prediction and anti-cancer drug development.

Numerous studies have emphasized the close correlation between depression and breast cancer (13–16). The meta-analysis showed that 32.3% of breast cancer patients suffer from depression (17). Nearly half of breast cancer patients at early stage would have depression, anxiety, or both after diagnosis (18). Depression is related to a 24% increased risk of breast cancer recurrence, 30% increased risk of all-cause mortality, as well as 29% increased risk of cancer-specific mortality (19). Animal studies have demonstrated that psychological stress could accelerate tumor growth and promote lung metastasis (20–22). Thus, it is crucial to explore the role of depression-related gene (DRGs) for the prognosis of breast cancer.

Herein, a 10-DRG risk signature was determined and it presented a positive prediction with OS in The Cancer Genome Atlas (TCGA) and GSE96058 cohorts, particularly for TNBC patients. A high-risk score was related to age, tumor size, tumor stage, metastasis, and immunosuppressive cells. Moreover, low-risk patients might be highly sensitive to chemotherapy and endocrine therapy. Finally, a nomogram was successfully established by integrating the risk score and other clinical parameters. Taken together, our study not only provides a novel risk prediction model for evaluating breast cancer prognosis based on DRGs analysis but also highlights the clinical significance of depression evaluation in breast cancer treatment.

MATERIALS AND METHODS

Data Source and Collection

Breast cancer related clinical information and the gene expression profiles were collected from TCGA database, which was chosen as testing dataset containing 1,096 patient samples and 113 non-tumor tissues. For further verification, the dataset GSE96058 (n=2969) downloaded from the GEO database was selected for validation.

Selection of DEGs in Breast Cancer

A total of 8,479 DRGs were acquired from the Genecard database, which supplies a comprehensive, up-to-date list of human genes. We obtained the expression values of 8,479 DRGs from TCGA. Based on TCGA dataset, DEGs were identified *via* Wilcoxon test after averaging replicate probes. Those genes with |log2-fold change (FC)| > 2 and adjusted *P* value (FDR) < 0.05 were considered DEGs.

Subsequently, PPIs of the DEGs were constructed based on the STRING (The Search Tool for the Retrieval of Interacting Genes) online tool. Then Cytoscape software 3.6.1 was applied to visualized the network. Additionally, the key modules in network were analyzed by MCODE in Cytoscape software. The options were set as degree cutoff = 2, K-Core = 4, and Node Score Cutoff = 0.3.

Identification of Prognostic Genes and Construction of a Risk Model

The univariate Cox regression analysis was performed to explore the correlation between genes and OS in the testing dataset. DEGs with p <0.05 were considered as candidate genes. Then LASSO regression was applied to shrink scope of gene screening.

Finally, a multivariate Cox analysis was constructed to screen highly prognosis-associated genes and generate the prognostic risk model.

The risk score was calculated as follows:

$$\text{Risk Score (patient)} = \sum_{i=1}^{n} \beta i Exp i .$$

(where "*Exp*" represents gene expression level and "β" represents the regression coefficient from the multivariate Cox analysis).

According to the risk score, the optimal cut-off value obtained by Receiver operating characteristic (ROC) analysis was performed for patient risk stratification.

Validation of the Constructed Model

To validate this model, Kaplan-Meier survival analysis along with log-rank test was employed to analyze survival difference between patients with different scores. To confirm whether the signature can be applied as an independent factor predictive of survival, univariate and multivariate Cox regression analyses were carried out.

GSEA

To explore the potential biological pathways, GSEA was carried out during the enrichment of the MSigDB Collection (c2.cp.kegg.v7.1.symbols.gmt). Pathways with |NES| > 1 and $p < 0.05$ were considered significantly enriched.

Exploration of Tumor-Infiltrating Immune Cells

As the most frequently cited tool for analyzing immune cells infiltration, CIBERSORT was used to quantify the immune cell proportion based on their RNA sequencing data (23). In the study, the tool was used to estimate the proportion of immune cell fractions in each breast patients in TCGA cohort.

Investigation of the Significance of Risk Signature for Drug Treatment

Genomics of Drug Sensitivity in Cancer website (24) was employed to discuss differences between patients with low and high score in response to chemotherapy, endocrine therapy, and targeted therapy. The IC_{50} of common therapeutic drugs in the TCGA breast cancer cohort was calculated.

Identification of Potential Small Molecule Drugs Targeting High Risk Patients

CMap is an online pharmacogenomic database based on gene expression data of cultured human cells treated with bioactive substance. Those up- and down-regulated target genes were uploaded to CMap. The connectivity score ranges from -1 to 1, which was used to reveal the closeness between expression profiles. The drugs with negative scores were generally considered as potential therapeutic molecules.

Construction and Evaluation of the Nomogram

The rms R package was performed to build a nomogram containing the model and clinicopathological features. The C-index and calibration plot were applied to assess predicted probabilities.

Statistical Analysis

The R software (version 3.6.3) was used to analyze the statistical data. Kaplan-Meier survival curves at 1-, 3-, and 5-years were illustrated with the survminer package. The prognostic effect of the risk model and clinicopathological features were assessed through univariate Cox analysis and multivariate Cox analysis. A two-sided $p < 0.05$ was considered statistically significant.

RESULTS

Identification of DRGs and Establishment of a 10-Gene Risk Model for Predicting Breast Cancer Prognosis

To construct a risk model based on DRGs, TCGA-BC cohort and GSE96058 cohort were selected as testing and validation datasets, respectively. The flow chart of bioinformatic analysis is illustrated in **Figure 1**. This study included 1,027 cases from TCGA cohort in which primary breast cancer had been followed up for more than 1 month. Clinical characteristics are summarized in **Table S1**. In total, 358 upregulated and 400 downregulated DRGs were finally identified (**Figures 2A, B**). To narrow the gene set and determine the hub genes, a protein–protein interaction (PPI) network based on the differentially expressed genes (DEGs) was built. Subsequently, module analyses of the network were conducted using Molecular Complex Detection (MCODE) to obtain hub genes (**Figure 2C**). Five significant modules were screened out and genes identified as hub genes were further analyzed.

In univariate Cox analysis, 34 DRGs were found significantly related to OS (**Figure 2D**). Through lasso regression analyses, 15 genes were further identified as prognosis-related genes (**Figure 2E**). Multivariate Cox analysis confirmed the following 10 DRGs for constructing the risk model: *MT3*, *SORBS1*, *IGFALS*, *AMH*, *IL12B*, *TP53AIP1*, *PXDNL*, *MC5R*, *FOXD1* and *LHX1* (**Table S2**). The formula was developed as below:

$$\begin{aligned}\text{Risk score} = {} & (-0.160) \times \text{Exp}_{(MT3)} + (-0.129) \\ & \times \text{Exp}_{(SORBS1)} + (-0.084) \times \text{Exp}_{(IGFALS)} + 0.089 \\ & \times \text{Exp}_{(AMH)} + (-0.137) \times \text{Exp}_{(IL1\ 2B)} \\ & + (-0.164) \times \text{Exp}_{(TP5\ 3AIP1)} + 0.137 \times \text{Exp}_{(PXDNL)} \\ & + 0.120 \times \text{Exp}_{(MC5R)} + 0.073 \times \text{Exp}_{(FOXD1)} \\ & + 0.055 \times \text{Exp}_{(LHX1)} .\end{aligned}$$

Prognostic Effect of the Model on Predicting OS of Breast Cancer

To explore the predictive effect of the model, risk scores in TCGA-Breast cancer and GSE96058 cohorts were calculated according to the formula. Subsequently, patients were divided into either low- or high-risk group based on the cut-off point of −1.281, as determined by MedCalc version 15.2.2 (MedCalc Software bvba, Ostend, Belgium). Survival analysis demonstrated a shorter

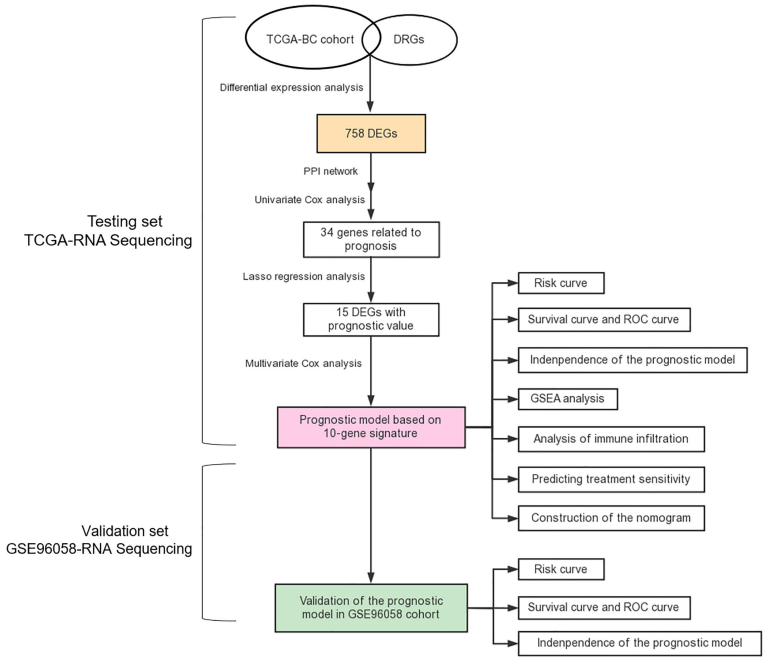

FIGURE 1 | Flow chart of this study.

survival time in high-risk patients ($p < 0.001$), which was verified by the GSE96058 dataset ($p < 0.001$) (**Figure 3A**). As illustrated in the **Figures 3B, C**, the higher the score, the higher proportion of patients dying in TCGA and GSE96058 datasets. Heatmap analysis showed that *MT3*, *SORBS1*, *IGFALS*, *IL12B* and *TP53AIP1* in the low-risk group were overexpressed, whereas *AMH*, *PXDNL*, *MC5R*, *FOXD1* and *LHX1* in the high-risk group were overexpressed. The outcomes in GSE96058 dataset were in line with those in TCGA (**Figure 3D**). As displayed in **Figure 3E**, the maximum area under the ROC curve (AUC) values reached 0.789, indicating the good sensitivity and specificity of the model. Consistently, in GSE96058 cohort the model achieved the maximum AUC of 0.725. These results revealed that the model was effective in predicting the survival probability.

Considering tumor heterogeneity, survival and ROC analyses of different molecular subtypes of breast cancer were carried out, respectively. The risk model had good prognostic performance, particularly for TNBC. As shown in **Figure S1**, the survival analyses proved the prognostic value for TNBC in both TCGA and GSE96058 cohorts ($p < 0.001$). ROC analyses further revealed that in the TCGA cohort, the AUC of TNBC was 0.709, 0.732, and 0.730 at 1, 3 and 5 years, respectively. The results were validated in the GSE96058 dataset in which AUC at 1, 3, and 5 years reached 0.747, 0.657, and 0.609 for TNBC, respectively (**Figure S2**).

Correlation Analysis Between the Model and Pathological Parameters

The relationship between the risk model and pathological parameters was further investigated. As displayed in **Figures 4A, B**, the risk model in the TCGA testing cohort was closely associated with age, molecular subtypes, clinical stage, T stage, and M stage, whereas N stage was not. Similarly, significant differences were also observed in GSE96058 cohorts, including age, molecular subtypes, tumor size, and positive nodes (**Figure S3A, B**). The risk score was significant for prognosis prediction when evaluated by univariate Cox analysis (HR = 2.926, 95% CI: 2.306–3.711) (**Figure 4C**). Furthermore, multivariable Cox analysis revealed that the model remained statistically significant (HR = 1.075, 95% CI:1.058–1.092), indicating that the model is an independent prognostic factor (**Figure 4D**). Likewise, in GSE96058 cohort, the univariate Cox regression analysis demonstrated that risk score (HR=2.329, 95% CI:1.879–2.887) is significantly related to survival (**Figure S3C**). The multivariate Cox regression analysis indicated that risk score (HR=1.648, 95% CI:1.324–2.049) is still an independent prognostic factor for breast cancer (**Figure S3D**).

Molecular Mechanism Analysis of the Model in Predicting Prognosis

We continued to explore the potential biological mechanisms of the risk model. GSEA revealed that group at high-risk was enriched in terpenoid backbone biosynthesis, cell cycle, pentose, and glucuronate interconversions, DNA replication, steroid biosynthesis, fructose, and mannose metabolism as well as mismatch repair. By contrast, the group at low-risk was enriched in pathways such as cell adhesion molecules, intestinal immune network for IgA production, cytokine-cytokine receptor interaction, JAK-STAT signaling pathway, chemokine signaling pathway, T cell receptor signaling pathway, and leukocyte transendothelial migration (**Figure 5A**).

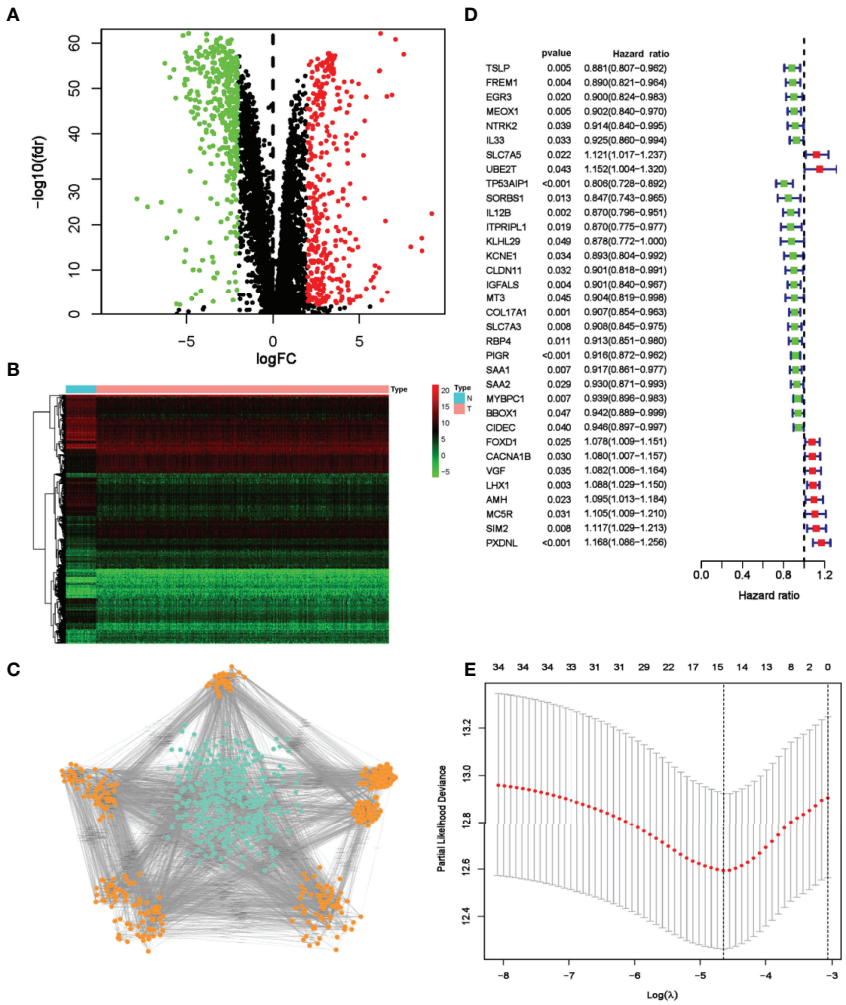

FIGURE 2 | Screening and identification of prognostic DRGs of TCGA breast cancer patients. **(A)** Volcano map visualizes DEGs between breast cancer and normal tissues. Red dots indicate upregulated genes, green dots indicate downregulated genes, and black dots indicate no differences gene; **(B)** Heatmap analysis of differential DRGs; **(C)** MCODE analysis from the PPI network. The orange nodes represent genes in significant module, while the blue nodes represent genes in insignificant module. **(D)** Forest plot of 34 genes identified by the univariate Cox regression analysis. **(E)** LASSO coefficient profiles of 15 prognosis-related genes. The red dots represent the partial likelihood values. The optimal parameter (λ) was calculated by ten-fold cross-validation.

Growing evidence shows that depression could inhibit the immune effector cells and facilitate immune escape, thus protecting cancer cells from immunological killing (14, 25). Moreover, the preliminary GSEA analyses in this study illustrated that the signature is closely associated with immune pathways. Herein, the abundance of 22 immune cells in low-risk and high-risk cases was analyzed *via* the CIBERSORT method (**Figure 5B**). The results revealed that high-risk patients had higher abundances of immunosuppressive cells including M0 macrophages, M2 macrophages, and neutrophils, but significantly lower abundances of M1 macrophages, naive B cells, CD8 T cells, resting memory CD4 T cells, regulatory T cells, resting dendritic cells, and resting mast cells (**Figure 5C**). In summary, the immunosuppressive microenvironment might be responsible for worse prognosis in high-risk cases.

Then the expression of the immune checkpoint regulators was analyzed in patients with different risk score. As shown in **Figure 5D**, the expressions of PD-1, PD-L1, and CTLA-4 increased significantly in patients with low-scores ($p < 0.05$), whereas LAG3 showed no statistical difference. These results implied that low-risk patients might be sensitive to immune checkpoint blockade therapies.

Additionally, it is well established that cytokines play a crucial role in the tumor immune microenvironment. Therefore, the results in TCGA cohort demonstrated that GZMA, GZMB, and IFNG in the low-risk group were highly expressed, while TGFB1 was elevated in high-risk breast cancer patients ($p < 0.001$) (**Figure 5E**).

Clinical Effects of the Model in Predicting Treatment Sensitivity

We further identified associations between the model and treatment effect of chemotherapeutics, endocrine drugs, and

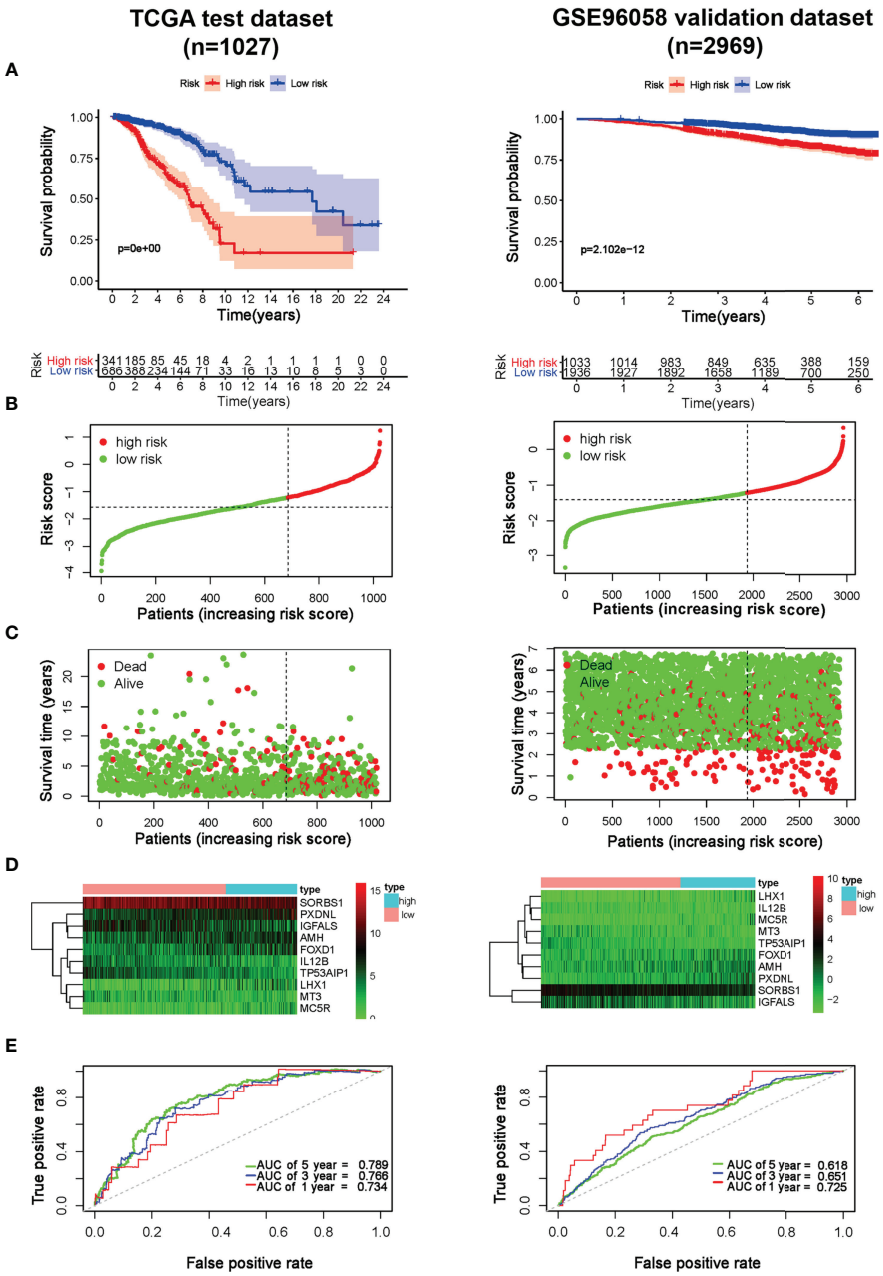

FIGURE 3 | Prognostic effect of the model in breast cancer. **(A)** Kaplan-Meier OS curves of breast cancer patients in TCGA and GSE96058 cohorts; **(B)** The distribution of risk score of breast cancer patients in TCGA and GSE96058 cohorts. X-axis here is patient number and Y-axis is risk score; **(C)** Survival status of the patients with different risk score in TCGA and GSE96058 cohorts. X-axis here is patient number and Y-axis is survival time; **(D)** A heatmap showing 10 gene expression profiles in TCGA and GSE96058 cohorts; **(E)** ROC Analysis of the risk model in TCGA and GSE96058 cohorts.

targeted agents. Low-risk patients had lower half-maximal inhibitory concentration (IC_{50}) of chemotherapeutics such as cisplatin, doxorubicin, cytoxan, methotrexate, and vinorelbine except for paclitaxel, indicating the predictive potential of the model for chemosensitivity (**Figure 6A**). Regarding endocrine therapy, low-risk patients had lower IC_{50} of endocrine therapies, such as tamoxifen, fulvestrant, and letrozole (**Figure 6B**). Low-risk patients had lower IC_{50} of targeted therapies, such as trastuzumab, olaparib, and temsirolimus, whereas high-risk patients had lower IC_{50} for targeted therapies such as palbociclib and sorafenib. The two groups showed no statistical differences for lapatinib (**Figure 6C**). Moreover, the DEGs were subjected to Connectivity Map (CMap) analysis and a total of six drugs, including pronetalol, puromycin, chlorphenamine, megestrol, semustine, and acacetin, were indicated for high-risk breast patients (**Figure 6D**).

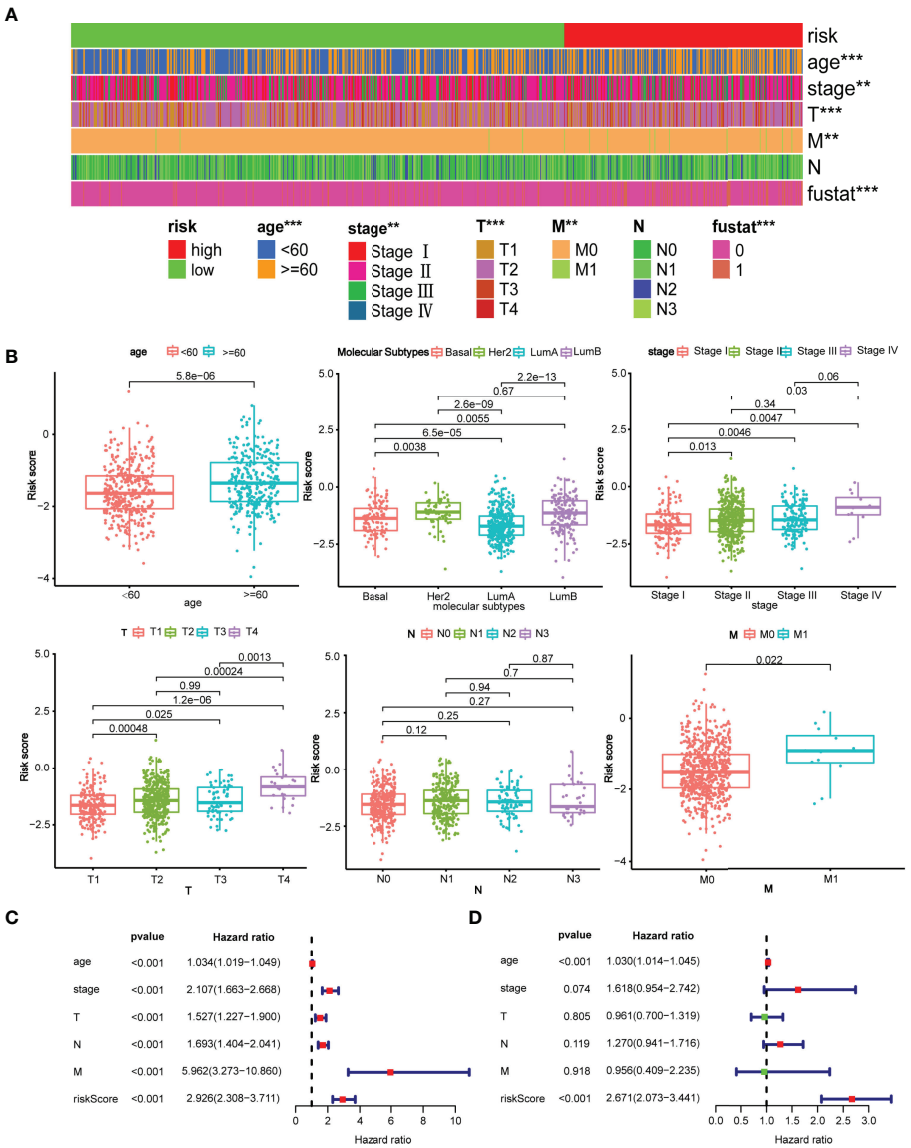

FIGURE 4 | Clinical evaluation of the risk model with pathological parameters. **(A)** The distribution of the model with the clinicopathological features including age, stage, TNM stage, survival state; **p < 0.01 and ***p < 0.001. **(B)** Comparison of risk score between patients with different pathological parameters. Age, molecular subtype, clinical stage, T stage, M stage were significantly associated with the risk score, while N stage was not; **(C)** Forrest plot of univariate Cox regression analysis. The result revealed that age, clinical stage, T stage, N stage, M stage, and risk score were statistically different. **(D)** Forrest plot of multivariate Cox regression analysis. Either age or risk score acted as an independent prognostic factor.

Nomogram Construction Based on the 10-Gene Risk Model

To create a quantitative method to predict OS, the nomogram for predicting 1-year, 3-year and 5-year OS was developed. Four risk factors, including age, stage, molecular subtypes, and risk score, were included in the nomogram (**Figure 7A**). The C-index reached 0.782 (95%CI: 0.733–0.831). As shown by the calibration curves, the actual and predicted OS matched well (**Figures 7B–D**).

DISCUSSION

In this study, a novel prognostic model consisting of 10-DRGs was established to enhance predictive capability of OS in breast cancer. The findings demonstrated that the model can effectively distinguish high-risk from low-risk patients and the model was effective in predicting OS in both the testing and validation sets, particularly for TNBC patients. Additionally, when pathological factors were included in multivariate Cox analysis, the model

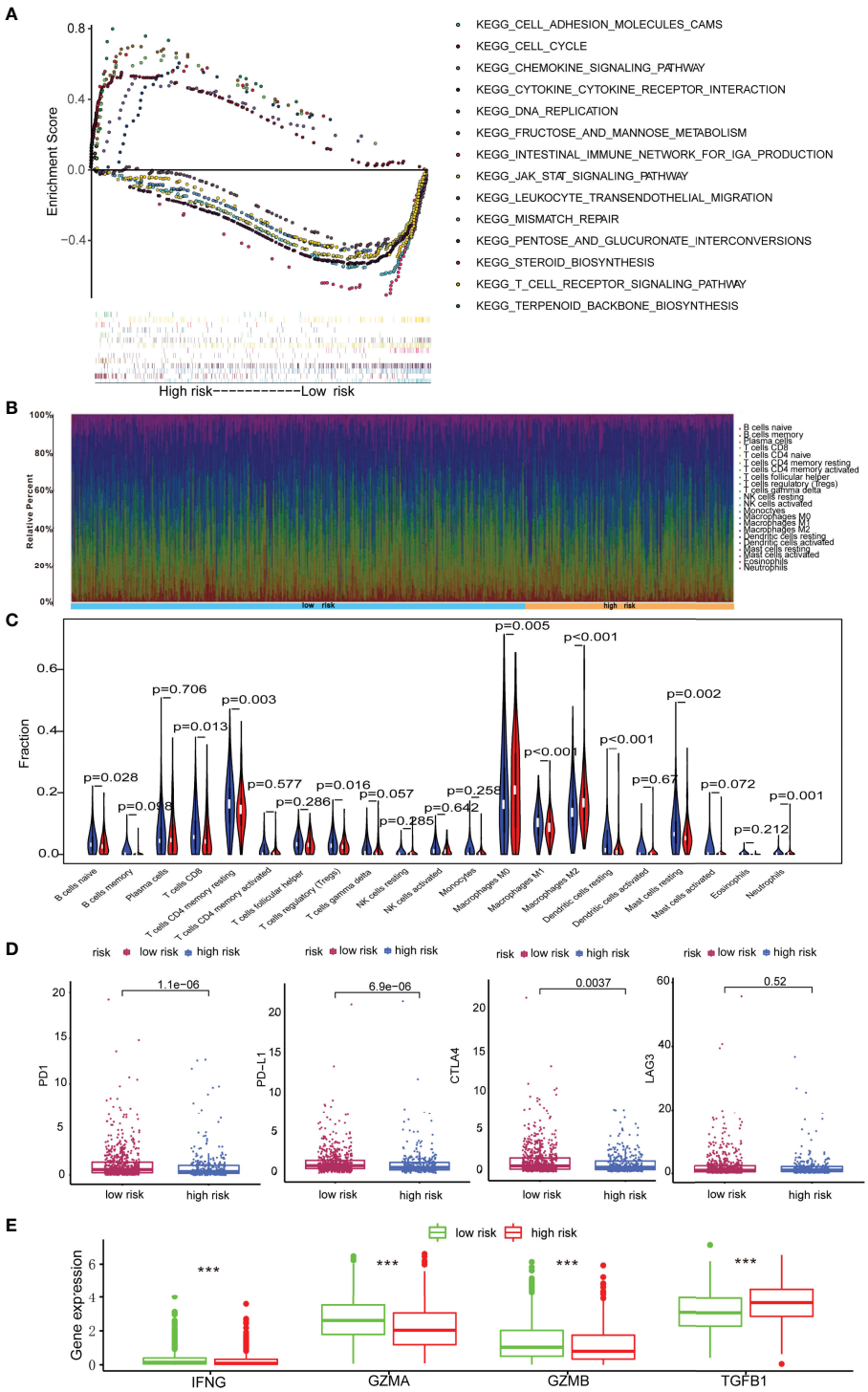

FIGURE 5 | Immune landscape in breast cancer patients with low- and high-score. **(A)** GSEA revealing biological processes correlated with risk model; **(B)** The abundances of immune cells in tumor microenvironment; **(C)** Comparison of proportion of immune cells types in patients with low- and high-score; **(D)** Immune checkpoints including PD1, PD-L1, CTLA4, and LAG3 expression in patients with low-score and high-score. **(E)** Expression levels of IFNG, GZMA, GZMB and TGFB1 in patients with low-score and high-score. ***p < 0.001.

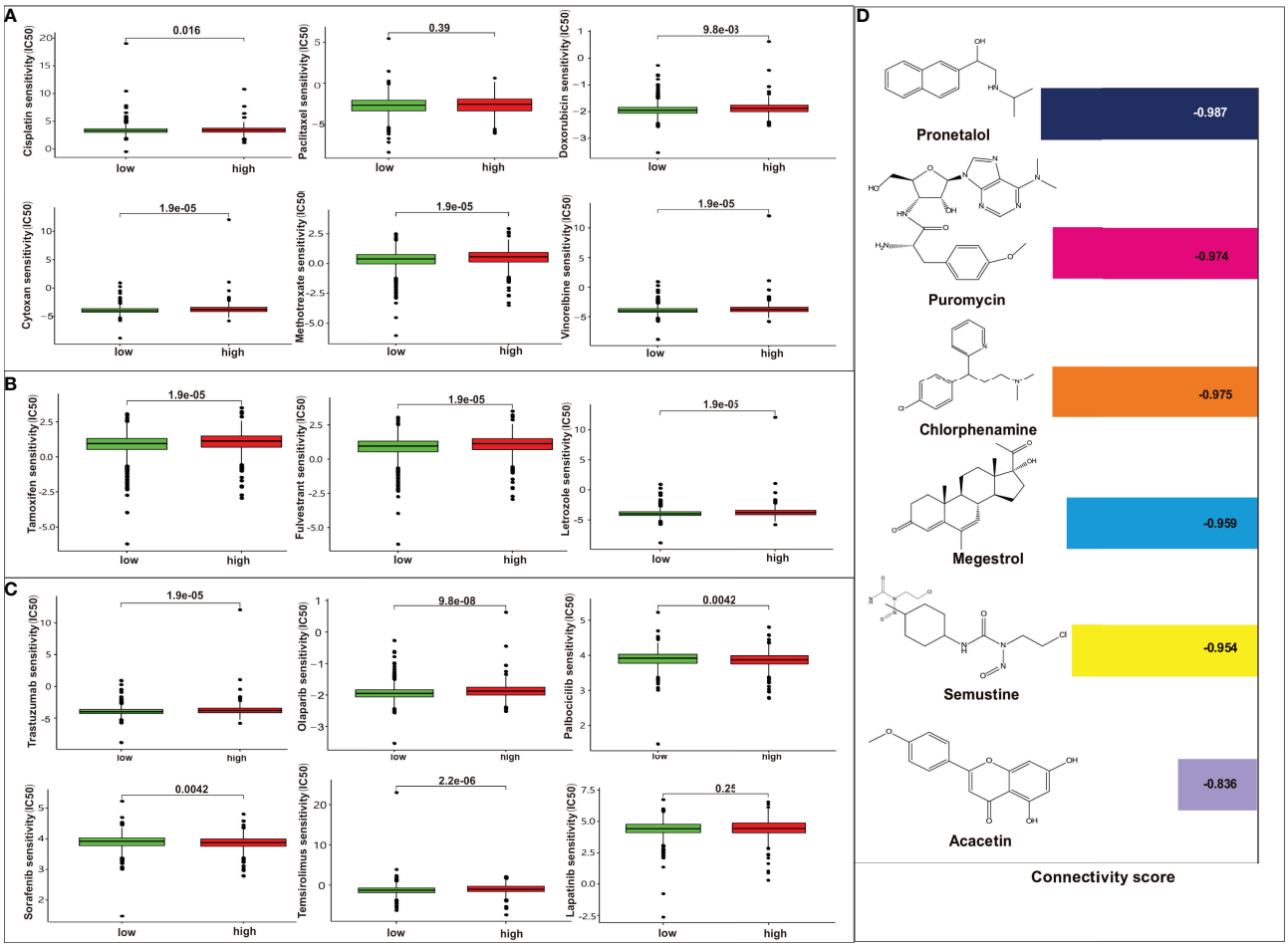

FIGURE 6 | Analysis of the association between the risk model and chemotherapeutics, endocrine therapy, and targeted therapy. **(A)** The model predicting the sensitivity to chemosensitivity. It was estimated that low-risk patients had lower IC_{50} for chemotherapeutics such as paclitaxel, cisplatin, and doxorubicin, cytoxan, methotrexate, vinorelbine, except for paclitaxel; **(B)** The model predicting the sensitivity to endocrine therapy. It was estimated that low-risk patients had lower IC_{50} such as tamoxifen, fulvestrant, and letrozole. **(C)** The model predicting the sensitivity to targeted therapy. It was estimated that low-risk patients had lower IC_{50} such as trastuzumab, olaparib, temsirolimus, whereas high-risk patients had lower IC_{50} for targeted therapy such as palbociclib, sorafenib. There are no differences between high risk or low risk patient for lapatinib; **(D)** CMap analysis for high-risk score patients. Six targeted drugs such as pronetalol, puromycin, chlorphenamine, megestrol, semustine, and acacetin are predicted therapy for this risk score in breast cancer.

remained as an independent prognostic factor. These results implied that the risk model is a robust prognostic tool. Moreover, it presented that a high score was related to poor survival in TNBC patients. Given that TNBC is the most challenging subtype of breast cancer, predicting prognosis of TNBC by this risk model is of great significance.

Among the 10 genes, five (*PXDNL*, *MC5R*, *AMH*, *FOXD1*, and *LHX1*) were high-risk genes and five (*IGFALS*, *SORBS1*, *IL12B*, *MT3*, and *TP53AIP1*) were protective factors. *PXDNL* is reported as a susceptibility gene in patients with depression (26). *MC5R*, a melanocortin receptor, could mediate the axis responsiveness to integrated signals from diurnal rhythms and cortisol negative feedback. It was reported that MC5R antagonist could treat the depressive or generalized anxiety disorder (27). *MT3* may be related to the antidepressant-like activity of eugenol, resulting in increased expression of the brain-derived neurotrophic factor (28). Furthermore, compared with those of the wild-type mice, Koumura et al. (29) found that *MT3* KO mice had shorter social interactions duration as well as diminished prepulse inhibition for the acoustic startle response, indicating abnormal psychological behavior in schizophrenia, anxiety, autism, and phencyclidine-induced psychosis. In general, the 10 genes are related to depression but are not solely related to depression. The mental diseases including depression, anxiety, and panic are usually interrelated. Patients with depression, anxiety, or panic experienced declines in quality of life and showed poor treatment adherence as compared with patients without mental disorders (30). Our previous meta-analysis indicated that depression and anxiety would increase the risk of breast cancer recurrence and mortality (19). Likewise, the 10 genes included in this study are not only depression-related but also related to breast cancer progression. Gomulkiewicz et al. (31) demonstrated that patients

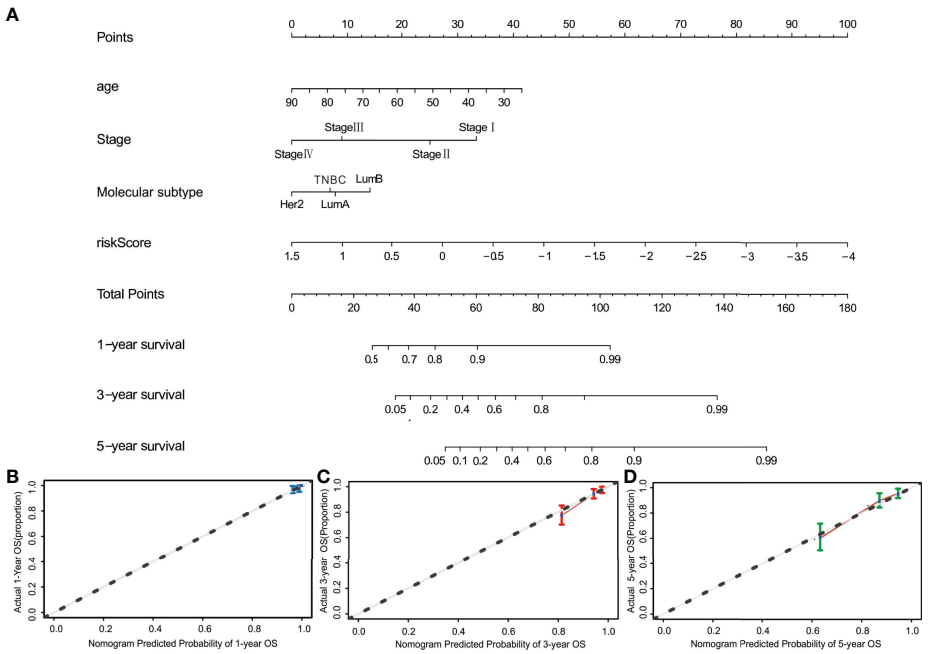

FIGURE 7 | Construction of the nomogram. **(A)** The nomogram for predicting 1-, 3-, and 5-year OS was constructed by combining risk score, age, stage, and molecular subtype. **(B–D)** The calibration curves of nomograms between predicted and observed 1-, 3- and 5-year OS. The dashed line of 45° indicates the perfect prediction.

with ductal breast cancer had lower expression of *MT3* than that in non-malignant breast tissue and the level of *MT3* in breast cancer patients with lymph node metastasis decreased compared to patients without metastasis. Moreover, the expression of *MT3* in breast cancer cell lines was lower than that in the normal human breast epithelial cell lines. These findings indicated that *MT3* might be correlated with the malignant transformation of breast epithelial cells and tumor progression. In addition, *PXDNL* and *FOXD1* were reportedly involved in breast cancer pathogenesis and were significant in predicting prognosis. FOXD1 was found to be significantly related to the prognosis of basal-like breast cancer (32). Zhao et al. (33) demonstrated that *FOXD1* could increase cell proliferation and enhance chemoresistance of cancer cells by targeting p27. It was demonstrated that decreased levels of *SORBS1* have significant correlation with worse survival, distant metastasis, and more malignant phenotype. *SORBS1* could inhibit tumorigenesis and metastasis through preventing JNK activation and attenuate cisplatin chemotherapy through p53 accumulation in breast cancer (34). *TP53AIP1* inhibits proliferation and growth of breast cancer cells through cell-cycle arrest, apoptosis induction, elevation of the expression of cleaved-caspase-3, cleaved-caspase-9, Bax, p53, and the inhibition of Bcl-2, Ki67, and PI3K/Akt pathways (35). Although reports on the prognostic effect of the remaining genes in breast cancer are limited, it is worth further evaluating their potential as biomarkers of breast cancer progression.

Furthermore, the model was associated with tumor-infiltrating immune cells, as the abundance of M2 macrophages and neutrophils in high-risk patients significantly increased. The abundance of M1 macrophages, naive B cells, CD8 T cells, resting memory CD4 T cells, resting dendritic cells, and resting mast cells was lower in the high-risk group and was related to better OS. It is well established that cytokines play a crucial role in the tumor immune microenvironment. As high-risk patients in our study had higher abundances of immunosuppressive cells, but significantly lower proportions of M1 macrophages, naive B cells, CD8 T cells, resting memory CD4 T cells, resting dendritic cells, resting mast cells, and immune inhibitory cytokines such as *TGFB1* and biomarkers of T cell activation such as *GZMA*, *GZMB*, and *IFNG* are selected to explore the differences between high-risk and low-risk groups. Notably, the results in TCGA cohort demonstrated that *GZMA*, *GZMB*, and *IFNG* in the low-risk cases were highly expressed, while *TGFB1* was elevated in the high-risk group. Future research should be conducted on the mechanisms of this model in influencing immune cells in tumor microenvironment. Accumulating evidence also demonstrated the potential of immune checkpoint inhibitors (ICIs) in breast cancer treatment (36); however, only a few patients obtained therapeutic benefit from ICIs. It was found that low-risk patients had increased expression of PD-1, PD-L1, as well as CTLA-4, suggesting that low-risk patients are promising candidates for ICIs. In addition, the model provided an opportunity to choose the optimal therapy for breast cancer patients. Our study revealed that low-risk patients seem to be more sensitive to chemotherapy and endocrine therapy, which is in line with better OS of the low-risk patients. These results indicate the potential effect of the model in predicting therapy sensitivity, which is also beneficial for selecting optimal therapeutic strategies and improving breast cancer patients' prognosis.

Furthermore, our study provides potential therapeutic options for high-risk patients. Among them, pronethalol, a β-adrenoceptor antagonist, is used to treat coronary heart disease and arrhythmias. Clinical studies have demonstrated that the application of β-blocker could improve the prognosis of patients with lung cancer, ovarian cancer, and melanoma (37–39). Although the use of pronethalol in clinical practice was restricted because it proved to be a carcinogen in mice (40), other β-blocker agents, such as propranolol, may be a valid approach for patients at high risk. It was reported that propranolol inhibits metastasis, reduces recurrence, and cancer-specific mortality in several clinical studies (41, 42). In addition, the safety of propranolol in breast cancer patients has been proven in a phase II pilot study (43). Chlorpheniramine, an alkylamine antihistamine, is used to prevent allergic symptoms. Although not generally recognized as an antidepressant or anxiolytic drug, chlorphenamine seems to have these properties as well. Shoko et al. (44) found that chlorpheniramine exerted antidepressant-like effects by activating dopamine D1 and α1-adrenoceptors. This result indicates that antidepressants may be another choice for breast cancer patients. It was proved that application of antidepressants for breast cancer may reduce mortality risk (45). However, antidepressants, such as selective serotonin re-uptake inhibitor, can reduce tamoxifen's effectiveness and increase death risk (46). Thus, further studies are warranted for validation. Acacetin is a natural flavonoid, which can inhibit the secretion of carcinogenic estrogen metabolites, as well as tumor cell proliferation, invasion, and migration (47, 48). It is worth exploring its potential application in regulating DRGs during breast cancer treatment.

CONCLUSION

This study provides a novel 10-DRGs risk model to predict breast cancer survival. The model is particularly significant for TNBC and is promising for predicting drug sensitivity and is thus helpful for designing optimal therapeutic strategies to improve clinical prognosis. Our findings further highlight the significance of monitoring and treating psychological stress in preventing recurrence and metastasis of breast cancer. Further experimental validation and prospective clinical trials are worth conducting.

DATA AVAILABILITY STATEMENT

The original contributions presented in the study are included in the article/**Supplementary Material**. Further inquiries can be directed to the corresponding author.

AUTHOR CONTRIBUTIONS

ZW and XW conceived and designed the study. XW and NW conducted the bioinformatic analysis and wrote the manuscript. LZ, WY, and KS participated in data interpretation and revised the manuscript. SW, YZ, BY, JZ, and BP contributed to data collection and discussion.

FUNDING

This work was supported by the National Natural Science Foundation of China [81873306, 81973526, 82004373, 82104869]; the State Key Laboratory of Dampness Syndrome of Chinese Medicine [SZ2021ZZ19]; Science and Technology Planning Project of Guangdong Province [2021A0505030059, 2017B030314166]; Department of Education of Guangdong Province [2018KZDXM022, A1-2606-19-111-009, 2019KQNCX019]; The 2020 Guangdong Provincial Science and Technology Innovation Strategy Special Fund (Guangdong-Hong Kong-Macau Joint Lab) [2020B1212030006]; Guangdong traditional Chinese medicine bureau project [20201132, 20211114]; Guangzhou science and technology project [202102010316, 202102010241, 201904010407]; The Specific Research Fund for TCM Science and Technology of Guangdong provincial Hospital of Chinese Medicine [YN2018MJ07, YN2018QJ08], and the Foundation for Young Scholars of Guangzhou University of Chinese Medicine [QNYC20190101].

SUPPLEMENTARY MATERIAL

The Supplementary Material for this article can be found online at: https://www.frontiersin.org/articles/10.3389/fonc.2022.879563/full#supplementary-material

REFERENCES

1. Sung H, Ferlay J, Siegel RL, Laversanne M, Soerjomataram I, Jemal A, et al. Global Cancer Statistics 2020: GLOBOCAN Estimates of Incidence and Mortality Worldwide for 36 Cancers in 185 Countries. *CA Cancer J Clin* (2021) 71:209–49. doi: 10.3322/caac.21660
2. Kimbung S, Loman N, Hedenfalk I. Clinical and Molecular Complexity of Breast Cancer Metastases. *Semin Cancer Biol* (2015) 35:85–95. doi: 10.1016/j.semcancer.2015.08.009
3. Goldhirsch A, Wood WC, Gelber RD, Coates AS, Thürlimann B, Senn HJ. Progress and Promise: Highlights of the International Expert Consensus on the Primary Therapy of Early Breast Cancer 2007. *Ann Oncol* (2007) 18:1133–44. doi: 10.1093/annonc/mdm271
4. Goldhirsch A, Wood WC, Coates AS, Gelber RD, Rlimann BT, Senn H-J. Strategies for Subtypes—Dealing With the Diversity of Breast Cancer: Highlights of the St Gallen International Expert Consensus on the Primary Therapy of Early Breast Cancer. *Ann Oncol* (2011) 22:1736–47. doi: 10.1093/annonc/mdr304
5. Bauer KR, Brown M, Cress RD, Parise CA, Caggiano V. Descriptive Analysis of Estrogen Receptor (ER)-Negative, Progesterone Receptor (PR)-Negative, and HER2-Negative Invasive Breast Cancer, the So-Called Triple-Negative Phenotype: A Population-Based Study From the California Cancer Registry. *Cancer* (2010) 109:1721–8. doi: 10.1002/cncr.22618
6. Liedtke C, Mazouni C, Hess KR, André F, Tordai A, Mejia JA, et al. Response to Neoadjuvant Therapy and Long-Term Survival in Patients With Triple-Negative Breast Cancer. *J Clin Oncol* (2008) 26:1275–81. doi: 10.1200/jco.2007.14.4147
7. Zardavas D, Irrthum A, Swanton C, Piccart M. Clinical Management of Breast Cancer Heterogeneity. *Nat Rev Clin Oncol* (2015) 12:381–94. doi: 10.1038/nrclinonc.2015.73

8. Sparano JA, Gray RJ, Ravdin PM, Makower DF, Pritchard KI, Albain KS, et al. Clinical and Genomic Risk to Guide the Use of Adjuvant Therapy for Breast Cancer. *N Engl J Med* (2019) 380:2395–405. doi: 10.1056/NEJMoa1904819
9. Cardoso F, van't Veer LJ, Bogaerts J, Slaets L, Viale G, Delaloge S, et al. 70-Gene Signature as an Aid to Treatment Decisions in Early-Stage Breast Cancer. *N Engl J Med* (2016) 375:717–29. doi: 10.1056/NEJMoa1602253
10. Filipits M, Rudas M, Jakesz R, Dubsky P, Fitzal F, Singer CF, et al. A New Molecular Predictor of Distant Recurrence in ER-Positive, HER2-Negative Breast Cancer Adds Independent Information to Conventional Clinical Risk Factors. *Clin Cancer Res* (2011) 17:6012–20. doi: 10.1158/1078-0432.Ccr-11-0926
11. Sestak I, Buus R, Cuzick J, Dubsky P, Kronenwett R, Denkert C, et al. Comparison of the Performance of 6 Prognostic Signatures for Estrogen Receptor-Positive Breast Cancer: A Secondary Analysis of a Randomized Clinical Trial. *JAMA Oncol* (2018) 4:545–53. doi: 10.1001/jamaoncol.2017.5524
12. Pu M, Messer K, Davies SR, Vickery TL, Pittman E, Parker BA, et al. Research-Based PAM50 Signature and Long-Term Breast Cancer Survival. *Breast Cancer Res Treat* (2020) 179:197–206. doi: 10.1007/s10549-019-05446-y
13. Reich M, Lesur A, Perdrizet-Chevallier C. Depression, Quality of Life and Breast Cancer: A Review of the Literature. *Breast Cancer Res Treat* (2008) 110:9–17. doi: 10.1007/s10549-007-9706-5
14. Borgi M, Collacchi B, Ortona E, Cirulli F. Stress and Coping in Women With Breast Cancer:Unravelling the Mechanisms to Improve Resilience. *Neurosci Biobehav Rev* (2020) 119:406–21. doi: 10.1016/j.neubiorev.2020.10.011
15. Carreira H, Williams R, Müller M, Harewood R, Stanway S, Bhaskaran K. Associations Between Breast Cancer Survivorship and Adverse Mental Health Outcomes: A Systematic Review. *J Natl Cancer Inst* (2018) 110:1311–27. doi: 10.1093/jnci/djy177
16. Johns SA, Stutz PV, Talib TL, Cohee AA, Beck-Coon KA, Brown LF, et al. Acceptance and Commitment Therapy for Breast Cancer Survivors With Fear of Cancer Recurrence: A 3-Arm Pilot Randomized Controlled Trial. *Cancer* (2020) 126:211–8. doi: 10.1002/cncr.32518
17. Pilevarzadeh M, Amirshahi M, Afsargharehbagh R, Rafiemanesh H, Hashemi SM, Balouchi A. Global Prevalence of Depression Among Breast Cancer Patients: A Systematic Review and Meta-Analysis. *Breast Cancer Res Treat* (2019) 176:519–33. doi: 10.1007/s10549-019-05271-3
18. Burgess C, Cornelius V, Love S, Graham J, Ramirez AJB. Depression and Anxiety in Women With Early Breast Cancer: Five Year Observational Cohort Study. *BMJ* (2005) 330:702. doi: 10.1136/bmj.38343.670868.D3
19. Wang X, Wang N, Zhong L, Wang S, Zheng Y, Yang B, et al. Prognostic Value of Depression and Anxiety on Breast Cancer Recurrence and Mortality: A Systematic Review and Meta-Analysis of 282,203 Patients. *Mol Psychiatry* (2020) 25:3186–97. doi: 10.1038/s41380-020-00865-6
20. Chen H, Liu D, Guo L, Cheng X, Guo N, Shi M. Chronic Psychological Stress Promotes Lung Metastatic Colonization of Circulating Breast Cancer Cells by Decorating a Pre-Metastatic Niche Through Activating β-Adrenergic Signaling. *J Pathol* (2018) 244:49–60. doi: 10.1002/path.4988
21. Flaherty RL, Intabli H, Falcinelli M, Bucca G, Hesketh A, Patel BA, et al. Stress Hormone-Mediated Acceleration of Breast Cancer Metastasis is Halted by Inhibition of Nitric Oxide Synthase. *Cancer Lett* (2019) 459:59–71. doi: 10.1016/j.canlet.2019.05.027
22. Cui B, Luo Y, Tian P, Peng F, Lu J, Yang Y, et al. Stress-Induced Epinephrine Enhances Lactate Dehydrogenase A and Promotes Breast Cancer Stem-Like Cells. *J Clin Invest* (2019) 129:1030–46. doi: 10.1172/jci121685
23. Newman AM, Liu CL, Green MR, Gentles AJ, Feng W, Xu Y, et al. Robust Enumeration of Cell Subsets From Tissue Expression Profiles. *Nat Methods* (2015) 12:453–7. doi: 10.1038/nmeth.3337
24. Yang W, Soares J, Greninger P, Edelman EJ, Lightfoot H, Forbes S, et al. Genomics of Drug Sensitivity in Cancer (GDSC): A Resource for Therapeutic Biomarker Discovery in Cancer Cells. *Nucleic Acids Res* (2013) 41:D955–961. doi: 10.1093/nar/gks1111
25. Blume J, Douglas SD, Evans DL. Immune Suppression and Immune Activation in Depression. *Brain Behav Immun* (2011) 25:221–9. doi: 10.1016/j.bbi.2010.10.008
26. Chen X, Long F, Cai B, Chen X, Qin L, Chen G. A Novel Relationship for Schizophrenia, Bipolar, and Major Depressive DisorderPart 8: A Hint From Chromosome 8 High Density Association Screen. *Mol Neurobiol* (2016) 16:5868–82. doi: 10.1007/s12035-016-0102-1
27. Hruby VJ, Cai M, Morgan C. Methods for the Treatment of Depression and Anxiety by a Melanocortin 5 Receptor Antagonist, PG-20n. *United States Patent US 10653743* (2020).
28. Irie Y, Itokazu N, Anjiki N, Ishige A, Watanabe K, Keung WM. Eugenol Exhibits Antidepressant-Like Activity in Mice and Induces Expression of Metallothionein-III in the Hippocampus. *Brain Res* (2004) 1011:243–6. doi: 10.1016/j.brainres.2004.03.040
29. Koumura A, Kakefuda K, Honda A, Ito Y, Hara HJNL. Metallothionein-3 Deficient Mice Exhibit Abnormalities of Psychological Behaviors. *Neurosci Lett* (2009) 467:11–4. doi: 10.1016/j.neulet.2009.09.051
30. Lawrence WR, Kuliszewski MG, Hosler AS, Leinung MC, Zhang X, Zhang W, et al. Association Between Preexisting Mental Illnesses and Mortality Among Medicaid-Insured Women Diagnosed With Breast Cancer. *Soc Sci Med* (2021) 270:113643. doi: 10.1016/j.socscimed.2020.113643
31. Gomulkiewicz A, Jablonska K, Pula B, Grzegrzolka J, Borska S, Podhorska-Okolow M, et al. Expression of Metallothionein3 in Ductal Breast Cancer. *Int J Oncol* (2016) 49:2487–97. doi: 10.3892/ijo.2016.3759
32. Liu Q, Song X, Liu Z, Yu Z. Investigation of Candidate Genes and Pathways in Basal/TNBC Patients by Integrated Analysis. *Technol Cancer Res Treat* (2021) 20:15330338211019506. doi: 10.1177/15330338211019506
33. Zhao YF, Zhao JY, Yue H, Hu KS, Shen H, Guo ZG, et al. FOXD1 Promotes Breast Cancer Proliferation and Chemotherapeutic Drug Resistance by Targeting P27. *Biochem Biophys Res Commun* (2015) 456:232–7. doi: 10.1016/j.bbrc.2014.11.064
34. Song L, Chang R, Dai C, Wu Y, Guo J, Qi M, et al. SORBS1 Suppresses Tumor Metastasis and Improves the Sensitivity of Cancer to Chemotherapy Drug. *Oncotarget* (2017) 8:9108–22. doi: 10.18632/oncotarget.12851
35. Liang Y, Wang S, Liu J. Overexpression of Tumor Protein P53-Regulated Apoptosis-Inducing Protein 1 Regulates Proliferation and Apoptosis of Breast Cancer Cells Through the PI3K/Akt Pathway. *J Breast Cancer* (2019) 22:172–84. doi: 10.4048/jbc.2019.22.e21
36. Gaynor N, Crown J, Collins DM. Immune Checkpoint Inhibitors: Key Trials and an Emerging Role in Breast Cancer. *Semin Cancer Biol* (2020) 79:44–57. doi: 10.1016/j.semcancer.2020.06.016
37. De Giorgi V, Grazzini M, Gandini S, Benemei S, Lotti T, Marchionni N, et al. Treatment With β-Blockers and Reduced Disease Progression in Patients With Thick Melanoma. *Arch Intern Med* (2011) 171:779–81. doi: 10.1001/archinternmed.2011.131
38. Diaz ES, Karlan BY, Li AJ. Impact of Beta Blockers on Epithelial Ovarian Cancer Survival. *Gynecol Oncol* (2012) 127:375–8. doi: 10.1016/j.ygyno.2012.07.102
39. Wang HM, Liao ZX, Komaki R, Welsh JW, O'Reilly MS, Chang JY, et al. Improved Survival Outcomes With the Incidental Use of Beta-Blockers Among Patients With Non-Small-Cell Lung Cancer Treated With Definitive Radiation Therapy. *Ann Oncol* (2013) 24:1312–9. doi: 10.1093/annonc/mds616
40. Shanks RG, Wood TM, Dornhorst AC, Clark ML. Some Pharmacological Properties of a New Adrenergic Beta-Receptor Antagonist. *Nature* (1966) 212:88–90. doi: 10.1038/212088a0
41. Barron TI, Connolly RM, Sharp L, Bennett K, Visvanathan K. Beta Blockers and Breast Cancer Mortality: A Population- Based Study. *J Clin Oncol* (2011) 29:2635–44. doi: 10.1200/jco.2010.33.5422
42. Melhem-Bertrandt A, Chavez-Macgregor M, Lei X, Brown EN, Lee RT, Meric-Bernstam F, et al. Beta-Blocker Use is Associated With Improved Relapse-Free Survival in Patients With Triple-Negative Breast Cancer. *J Clin Oncol* (2011) 29:2645–52. doi: 10.1200/jco.2010.33.4441
43. Shaashua L, Shabat-Simon M, Haldar R, Matzner P, Zmora O, Shabtai M, et al. Perioperative COX-2 and β-Adrenergic Blockade Improves Metastatic Biomarkers in Breast Cancer Patients in a Phase-II Randomized Trial. *Clin Cancer Res* (2017) 23:4651–61. doi: 10.1158/1078-0432.Ccr-17-0152
44. Shoko H, Miyata S, Onodera K, Kamei J. Involvement of Dopamine D1 Receptors and Alpha1-Adrenoceptors in the Antidepressant-Like Effect of Chlorpheniramine in the Mouse Tail Suspension Test. *Eur J Pharmacol* (2007) 562:72–6. doi: 10.1016/j.ejphar.2007.01.063
45. Shim EJ, Lee JW, Cho J, Jung HK, Kim NH, Lee JE, et al. Association of Depression and Anxiety Disorder With the Risk of Mortality in Breast Cancer: A National Health Insurance Service Study in Korea. *Breast Cancer Res Treat* (2020) 179:491–8. doi: 10.1007/s10549-019-05479-3
46. Kelly CM, Juurlink DN, Gomes T, Duong-Hua M, Pritchard KI, Austin PC, et al. Selective Serotonin Reuptake Inhibitors and Breast Cancer Mortality in

Women Receiving Tamoxifen: A Population Based Cohort Study. *Bmj* (2010) 340:c693. doi: 10.1136/bmj.c693
47. Ren H, Ma J, Si L, Ren B, Chen X, Wang D, et al. Low Dose of Acacetin Promotes Breast Cancer MCF-7 Cells Proliferation Through the Activation of ERK/ PI3K /AKT and Cyclin Signaling Pathway. *Recent Pat Anticancer Drug Discov* (2018) 13:368–77. doi: 10.2174/1574892813666180420154012
48. Jones AA, Gehler S. Acacetin and Pinostrobin Inhibit Malignant Breast Epithelial Cell Adhesion and Focal Adhesion Formation to Attenuate Cell Migration. *Integr Cancer Ther* (2020) 19:1534735420918945. doi: 10.1177/1534735420918945

Conflict of Interest: The authors declare that the research was conducted in the absence of any commercial or financial relationships that could be construed as a potential conflict of interest.

Publisher's Note: All claims expressed in this article are solely those of the authors and do not necessarily represent those of their affiliated organizations, or those of the publisher, the editors and the reviewers. Any product that may be evaluated in this article, or claim that may be made by its manufacturer, is not guaranteed or endorsed by the publisher.

Copyright © 2022 Wang, Wang, Zhong, Su, Wang, Zheng, Yang, Zhang, Pan, Yang and Wang. This is an open-access article distributed under the terms of the Creative Commons Attribution License (CC BY). The use, distribution or reproduction in other forums is permitted, provided the original author(s) and the copyright owner(s) are credited and that the original publication in this journal is cited, in accordance with accepted academic practice. No use, distribution or reproduction is permitted which does not comply with these terms.

frontiers | Frontiers in Oncology

ORIGINAL RESEARCH
published: 12 May 2022
doi: 10.3389/fonc.2022.871771

Identification of LSM Family Members as Novel Unfavorable Biomarkers in Hepatocellular Carcinoma

Hongkai Zhuang[1,2†], Bo Chen[3†], Chenwei Tang[1,2†], Xinming Chen[4†], Wenliang Tan[1,2], Lei Yang[1,2], Zhiqin Xie[1,2], Xiaowu Ma[1,2], Qingbin Wang[1,2], Chuanzhao Zhang[5], Changzhen Shang[1,2*] and Yajin Chen[1,2*]*

[1] Department of Hepatobiliary Surgery, Sun Yat-sen Memorial Hospital, Sun Yat-sen University, Guangzhou, China, [2] Guangdong Provincial Key Laboratory of Malignant Tumor Epigenetics and Gene Regulation, Sun Yat-sen Memorial Hospital, Sun Yat-Sen University, Guangzhou, China, [3] Department of Breast Cancer, Cancer Center, Guangdong Provincial People's Hospital, Guangdong Academy of Medical Sciences, Guangzhou, China, [4] Department of Hepatobiliary Surgery, Shenshan Medical Hospital, Sun Yat-Sen Memorial Hospital, Sun Yat-Sen University, Shanwei, China, [5] Department of General Surgery, Guangdong Provincial People's Hospital, Guangdong Academy of Medical Sciences, Guangzhou, China

OPEN ACCESS

Edited by:
Pranav Gupta, Albert Einstein College of Medicine, United States

Reviewed by:
Yunqiang Tang, Guangzhou Medical University Cancer Hospital, China
Xing Wang, Chongqing Medical University, China

***Correspondence:**
Chuanzhao Zhang
zhangchuanzhao@gdph.org.cn
Changzhen Shang
shangcz_sysu@163.com
Yajin Chen
cyj0509@126.com

[†]*These authors have contributed equally to this manuscript*

Specialty section:
This article was submitted to Molecular and Cellular Oncology, a section of the journal Frontiers in Oncology

Received: *08 February 2022*
Accepted: *13 April 2022*
Published: *12 May 2022*

Citation:
Zhuang H, Chen B, Tang C, Chen X, Tan W, Yang L, Xie Z, Ma X, Wang Q, Zhang C, Shang C and Chen Y (2022) Identification of LSM Family Members as Novel Unfavorable Biomarkers in Hepatocellular Carcinoma. Front. Oncol. 12:871771. doi: 10.3389/fonc.2022.871771

Background: Smith-like (LSM) family members play critical roles in multiple oncologic processes in several types of malignancies. The study on LSM family members of HCC might provide new insights into the tumorigenesis and therapeutic strategies of HCC.

Methods: The clinical significance and oncologic biological functions of LSM family members were assessed through multiple bioinformatics methods and *in vitro* studies. The potential correlation between LSM family members and tumor immunity was also investigated using single sample gene set enrichment analysis (ssGSEA) and the ESTIMATE algorithm.

Results: LSM family member overexpression in HCC was significantly correlated with poor clinical outcomes such as higher TNM stage, advanced histologic grade, and worse prognosis. A risk score system based on LSM5, LSM10, LSM12, and LSM14B showed a reliable predictive ability for OS of HCC patients. Functional enrichment analysis demonstrated that LSM family members overexpressed were all involved in cell cycle related biological processes. Besides, LSM12, LSM14A, and LSM14B were found to be significantly associated with PI3K-Akt-mTOR and T cell receptor signaling pathways. Tumors with LSM12, LSM14A, and LSM14B overexpression exhibited lower infiltration of activated $CD8^+$ T cells with declined cytolytic activity and immune score, but increased infiltration of Th2 cells and Th2/Th1. LSM12, LSM14A, and LSM14B overexpression is also associated with higher tumor-related immune checkpoints (e.g., PD-L1, B7-H3, and PVR) expression and increased therapeutic insensitivity to immune checkpoint blockade

(ICB). Moreover, the knockdown of LSM12, LSM14A, and LSM14B significantly inhibited the proliferation and invasion of HCC cells.

Conclusion: This study systematically investigated the expression pattern and biological values of LSM family members in HCC and identified LSM family members as novel therapeutic targets in HCC.

Keywords: HCC, LSM, prognosis, ICB, immunosuppression, $CD8^+$ T cell

INTRODUCTION

Hepatocellular carcinoma (HCC), one of the most prevalent malignancies, ranks as the third leading cause of tumor-related death worldwide, with an overall 5-year survival rate of less than 20% (1, 2). Despite numerous efforts for early diagnosis and novel therapeutic strategies, the survival of HCC patients remains unsatisfactory, due to the specific tumor microenvironment (TME) and tumor heterogeneity in HCC (3–6). Therefore, it is urgent to investigate the molecular mechanisms underlying hepatocarcinogenesis and TME development to design more effective precision treatments for HCC.

The Smith-like (LSM) family consists of 13 members (e.g., LSM1, LSM2, LSM3, LSM4, LSM5, LSM6, LSM7, LSM8, LSM10, LSM11, LSM12, LSM14A, and LSM14B), which are widely known as the RNA-binding protein family, and are generally involved in various cellular biological processes (e.g., RNA-processing tasks and ion mobilizations) (7, 8). For example, the LSM1-7 complex functions in cytoplasmic mRNA decay through interaction with mRNA degradative factors (9). Furthermore, the LSM2-8 complex in the nucleus functions in pre-mRNA splicing by interacting with the U6 snRNA (10). Additionally, a previous study by Zhang et al. also identified LSM12 as an NAADP receptor essential for NAADP-evoked TPC activation and $Ca2^+$ transportation from intracellular acidic stores (11). The oncologic roles of LSM family members have also been identified in several tumor types (12–14). LSM1 overexpression contributes to a more advanced malignant phenotype in pancreatic cancer (12). Moreover, Watson et al. also identified the essential role of LSM1 overexpression in tumor progression in lung cancer and mesothelioma (13). Besides, it is also reported that LSM4 knockdown inhibits tumor proliferation, invasion, and glycolysis metabolism in ovarian cancer (14). However, the underlying mechanism of LSM family members in carcinogenesis still remains poorly understood, especially for HCC. Therefore, it is of great significance to explore the potential biological roles of LSM family members in tumorigenesis and TME development in HCC.

Through public databases and multiple bioinformatics analyses, we comprehensively investigated the expression patterns and clinical significance of LSM family members in HCC. Additionally, with the help of gene set variation analysis, we are also the first to investigate the underlying biological functions of LSM family members in hepatocarcinogenesis and tumor immunity.

MATERIALS AND METHODS

RNA Information Acquisition

Publicly available mRNA data and corresponding clinical information of HCC patients were downloaded from the Cancer Genome Atlas (TCGA, https://cancergenome.nih.gov/). Of the 371 HCC cases in the TCGA HCC cohort, 343 had an OS of >1 month. Besides, the HCC cohort from the International Cancer Genome Consortium (ICGC, https://icgc.org/) database was also used for expression pattern and prognostic value validation for LSM family members. The TCGA and ICGC HCC cohorts are both available freely as public databases, for which local ethics approval was not needed.

LSM Family Member Expression Analysis

First, the expression differences of LSM family members between HCC tissues (n = 50) and the corresponding adjacent normal tissues (n = 50) were evaluated using the TCGA HCC cohort. Then, the ICGC HCC cohort was also used to evaluate the expression differences of LSM family members between HCC tissues (n = 231) and adjacent normal tissues (n = 201). Furthermore, LSM family member expression in various TNM stages and histologic grades was evaluated using the Kruskal–Wallis test or Wilcoxon test.

Prognostic Values of LSM Family Members

A Kaplan–Meier survival analysis was conducted to investigate the prognostic value [e.g., overall survival (OS) and disease-free survival (DFS)] of LSM family members in HCC. Additionally, using the R package 'glmnet', the critical prognosis-associated LSM family members were further determined through the least absolute shrinkage and selection operator (Lasso) regression analysis. Then, a risk score system for OS was established as the following formula: risk score = $\sum$coef (LSM_i) × expr (LSM_i). For external validation, using the same multivariable Cox regression coefficients obtained in the TCGA HCC cohort, the risk score was further calculated for HCC cases in the ICGC HCC cohort. Using the R package 'survminer', KM survival analysis was also performed according to the optimal cutoff point from X-tile (version 3.6.1) (15). The predictive performance of the risk score system was evaluated using the AUC values of the ROC curves and C-index. To verify whether the risk score system could be used as an independent prognostic factor, we conducted univariate and multivariate Cox regression analyses for clinicopathological

characteristics (e.g., TNM stage and histologic grade) and the risk score system.

Functional Enrichment Analysis

A gene set variation analysis (GSVA) was used to calculate the enrichment scores of specific gene sets for each sample based on RNA-seq (16). Using the R package 'gsva', we performed GSVA to estimate the enrichment level of 13 critical ontology gene sets obtained from the Molecular Signatures Database (MSigDB, http://software.broadinstitute.org/gsea/msigdb) in the TCGA HCC cohort, namely, DNA repair, G2M checkpoint, E2F targets, mitotic spindle, glycolysis, hedgehog signaling, mTORC1 signaling, MYC targets V1, MYC targets V2, Notch signaling, PI3K-AKT-mTOR signaling, TGF-β signaling, and WNT β-catenin signaling. Then, the correlation between the expression of LSM family members and these critical oncogenic biological processes was assessed by the Pearson correlation analysis (|Cor| >0.3, P-value <0.05). Additionally, significant co-expressed genes of LSM family members were figured out by the Pearson correlation analysis (|Cor| ≥0.55 and P-value <0.05). Then, these co-expressed genes of LSM family members were imported into ConsensusPathDB (http://cpdb.molgen.mpg.de/) for Kyoto Encyclopedia of Genes and Genomes (KEGG) analysis; P <0.05 was considered statistically significant.

T-Cell Infiltration in HCC

GSVA was also performed to quantify the enrichment levels of T cell-related terms extracted from previous studies, namely, activated CD8+ T cell, regulatory T cell (Treg cell), type 1 T helper cell (Th1 cell), type 2 T helper cell (Th2), Th2/Th1, T follicular helper cell, and cytolytic activity (17, 18). Then, correlation analysis between LSM family members and these T cell-related terms in HCC was assessed with |Pearson correlated coefficient| >0.2 and a P-value of <0.05. We also evaluated the differences in these T cell-related terms between high- and low-LSM family member expression groups. Additionally, using the R package 'ESTIMATE', we performed the ESTIMATE algorithm to generate an immune score, the higher of which suggested a higher level of anti-tumor immunity in tumor tissues (19). Then, we investigated the difference in immune scores between low- and high-LSM family member expression groups.

Cell Cultural and Transfection

Human SNU-387 cells, purchased from the Cell Bank of the Chinese Academy of Sciences (Shanghai, China), were cultured with Dulbecco's Modified Eagle Medium (DMEM; Gibco BRL, USA), and supplied with 10% fetal bovine serum (FBS; Procell Life Science & Technology Co., Ltd., Wuhan, China) in an incubator with 5% CO2 at 37 °C. The small interfering RNAs (si-RNA) of LSM12, LSM14A, and LSM14B (si-LSM12#1/2; si-LSM14A#1/2; si-LSM14B#1/2) were obtained from RiboBio (Guangzhou, China). In short, cells were seeded in 6-well plates and cultured to an appropriate confluence, then transfected with different si-RNAs by Lipofectamine 3000 (Thermo Fisher Scientific, USA) according to its protocol. After 48 h incubation, the transfected cells were collected for further analysis. The efficacy of si-LSM12/14A/14B RNAs in SNU-387 cells was assessed using qRT-PCR. The target sequences of LSM12, LSM14A, and LSM14B siRNAs were as follows: si-LSM12#1: 5`-GCAGACATCTTGCTCATAA-3`; si-LSM12#2: 5`-GAGCCATGTACGCAAAATA-3`; si-LSM14A#1: 5`-GAGCAACTCAGAAATGATA-3`; si-LSM14A#2: 5`-GGAGAAGCCTGTAAATGGT-3`; si-LSM14B#1: 5`-GAAGACCGTCCCACAGATA-3`; si-LSM14B#2: 5`-CGACAACATCTCTTCTGAA-3`. Furthermore, the PCR primers were as follows: LSM12, 5`-TCTTCCAGTGGAAAGCCCAAC-3` (forward), 5`-GCTTTGCTGGCAAGCTTACT-3` (reverse); LSM14A, 5`-TGTGATGACAATAGAGAACGGAGA-3` (forward), 5`-AAGGTACCACCTCTGCCAC-3` (reverse); LSM 14B, 5`-CTGAACTCAAGACCAGCTCCAG-3` (forward), 5`-GAACTGCGGCCACGAAGAA-3` (reverse); GAPDH forward, 5`-TGACTTCAACAGCGACACCCA-3`; GAPDH reverse, and 5`-CACCCTGTTGCTGTAGCCAAA-3`.

Cell Counting Kit-8 (CCK-8) Assay

Cell viability was examined using the Cell Counting Kit-8 (APExBIO, USA). In short, SNU-387 cells transfected with different small interfering RNAs for LSM12, LSM14A, and LSM14B (LSM12: si-NC, si-LSM12#1, si-LSM12#2; LSM14A: si-NC, si-LSM14A#1, LSM14A#2; LSM14B: si-NC, si-LSM14B#1, si-LSM14B#2) were seeded into 96-well plates at a density of 2×10^3. At 1, 2, 3, 4, 5, and 6 days, the mix solution with 10 μl CCK-8 reagent and 100 μl DMEM was added to each well and re-incubated for 3 h, followed by the absorbance at 450 nm measured by a microplate reader (Thermo MK3, Thermo Fisher Scientific, USA).

Transwell Invasion Assays

Transfected cells suspended in serum-free medium were seeded in triplicate into each of the upper transwell chambers (Corning, USA) with Matrigel (Corning, USA) at a density of 1×10^4 and incubated in 200 μl DMEM with free serum. Furthermore, the lower chambers contained 500 μl DMEM supplemented with 100 μl FBS. Then cells from the upper compartments were wiped out after 24 h, and the invaded cells were fixed with paraformaldehyde for 15 min, followed by staining with 0.3% crystal violet for 15 min at room temperature. Cell counting was conducted using microscopy.

Statistical Analysis

All statistical analyses were conducted using the R software 4.0.5 (http://r-project.org/) and GraphPad Prism 8.0 software (GraphPad Software, Inc.). Group difference analyses were conducted using the Kruskal–Wallis test or Wilcoxon test and expressed as mean ± standard deviation (SD). Correlation analyses were performed using the Pearson correlation coefficient. Moreover, a P-value of < 0.05 was considered statistically significant.

RESULTS

Overexpression of LSM Family Members in HCC

Firstly, the paired differential expression analysis based on the TCGA HCC cohort demonstrated that LSM family members

were all notably overexpressed in HCC tissues compared to adjacent normal tissues (**Figure 1A**). Additionally, the ICGC HCC cohort also revealed that all LSM family members were significantly upregulated in HCC tissues compared with adjacent normal tissues (**Figure 1B**). Taken together, these results suggest the overexpression of LSM family members in HCC.

LSM Family Members in Various TNM Stage and Histologic Grade

Twelve LSM family members (e.g., LSM1, LSM2, LSM4, LSM5, LSM6, LSM7, LSM8, LSM10, LSM11, LSM12, LSM14A, and LSM14B) were significantly associated with advanced TNM stage (**Figure 2A**). Besides, higher expressions of ten LSM family members (e.g., LSM1, LSM2, LSM3, LSM4, LSM7, LSM8, LSM11, LSM12, LSM14A, and LSM14B) were also observed in tumors with higher histological grade, though not statistically significant for LSM5, LSM6, and LSM10 (**Figure 2B**). Taken together, these findings suggest that LSM family member overexpression may be associated with tumor progression in HCC.

The Prognostic Value of LSM Family Members in HCC

To determine the prognostic values of LSM family members in patients with HCC, we assessed the associations between the mRNA expression of LSM family members and OS or DFS using KM survival analysis. KM survival analysis demonstrated that LSM family members were all notably associated with shorter OS or DFS of HCC patients (**Figures 3**, **4**). Additionally, four critical prognosis-associated LSM family members, namely, LSM5, LSM10, LSM12, and LSM14B, were identified using Lasso regression analysis (**Figures 5A, B**). Then, a risk score system based on these four critical prognosis-associated LSM family members was established using multivariate correlation analysis. Risk score = 0.1435 × LSM5 expression + 06358 × LSM10 expression + 0.2092 × LSM12 expression + 0.1019 × LSM14B expression. The KM survival curves for OS demonstrated that patients with low-risk scores had superior OS compared with those with high-risk scores (**Figure 5C**). For validation, risk scores were also calculated for 229 patients with HCC in the ICGC HCC cohort. Furthermore, similar results of KM survival analysis were also observed in the ICGC HCC cohort (**Figure 5D**). The C-indexes of the risk score system for OS prediction in the TCGA and ICGC cohorts were 0.676 (95% CI, 0.621–0.731) and 0.658 (95% CI, 0.571–0.744), respectively, suggesting a reliable predictive capability of the risk score system. Additionally, in the TCGA HCC cohort, the AUC values of the risk score system for 1-, 2-, 3-, and 4-year OS prediction were 0.733, 0.711, 0.705, and 0.697, respectively

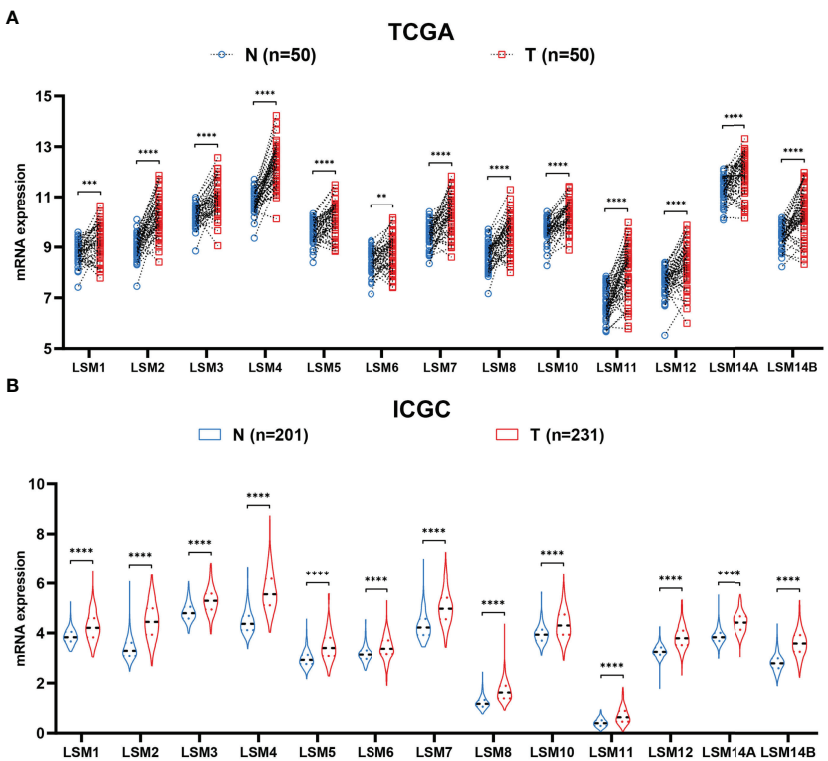

FIGURE 1 | Differential expression analysis of LSM family members. **(A)** LSM family members were significantly upregulated in HCC tissues compared with that in the adjacent non-tumor tissues in the TCGA HCC cohort. **(B)** LSM family members were significantly up-regulated in HCC tissues compared with that in the adjacent non-tumor tissues in the ICGC HCC cohort. LSM, Smith-like (LSM) family members; HCC, hepatocellular carcinoma; TCGA, the Cancer Genome Atlas; ICGC, the International Cancer Genome Consortium. **P-value <0.01; ***P-value <0.001; ****P-value <0.0001.

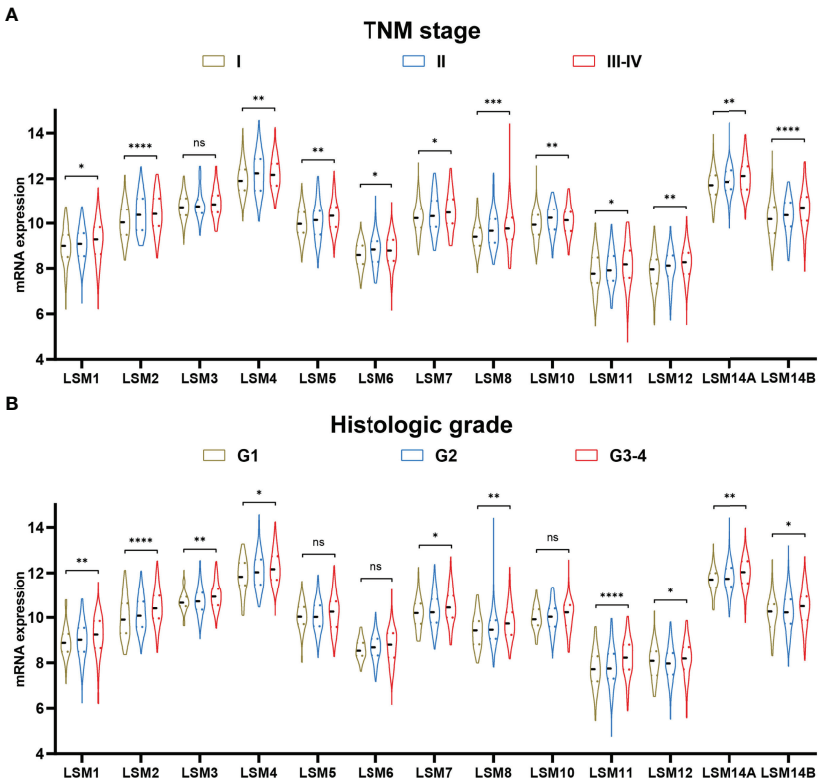

FIGURE 2 | LSM family member expression in TNM stage and histologic grade. **(A)** Higher expression of LSM1, LSM2, LSM4, LSM5, LSM6, LSM7, LSM8, LSM10, LSM11, LSM12, LSM14A, and LSM14B were observed in tumors with advanced TNM stage. **(B)** Higher expression of LSM1, LSM2, LSM3, LSM4, LSM7, LSM8, LSM11, LSM12, LSM14A, and LSM14B were also observed in tumors with higher histologic grade. LSM, Smith-like (LSM) family members. ns >0.05; *P-value <0.05; **P-value <0.01; ***P-value <0.001; ****P-value <0.0001.

(**Figure 5E**). Consistently, the AUC values of the risk score system for 1-, 2-, 3-, and 4-year OS predictions were 0.683, 0.682, 0.702, and 0.683 in the ICGC HCC cohort (**Figure 5F**). Moreover, univariate and multivariate Cox analyses identified the risk score system as an independent unfavorable prognostic parameter in HCC (**Figures 5G, H**). These results proved the significant prognostic value of LSM family members in HCC.

Analysis of Biological Pathways in LSM Family Members

Correlation analyses between LSM family members and thirteen critical biological pathways are shown in **Figure 6A**. Interestingly, all LSM family members but LSM10 were significantly associated with cell cycle related biological processes, such as the G2M checkpoint, E2F targets, and mitotic spindle. Nine LSM family members, including LSM2-8, LSM10, and LSM11, were notably associated with MYC signaling pathways. Then, six LSM family members may play crucial roles in PI3K-Akt-mTRO signaling in HCC, namely, LSM1, LSM8, LSM11, LSM12, LSM14A, and LSM14B. Besides, four LSM family members (e.g., LSM8, LSM11, LSM14A, and LSM14B) were significantly associated with WNT β-catenin signaling in HCC. Additionally, co-expression genes of LSM family members (|Pearson correlated coefficient| ≥0.55 and P-value <0.05) were imported into ConsensusPathDB for KEGG analysis, which is shown in **Table S1**. Interestingly, LSM12, LSM14A, and LSM14B were observed to play critical roles in the T-cell receptor signaling pathway, suggesting their potential effects on tumor immunity in HCC (**Figure 6B**). Of note, KEGG analysis also consistently identified the underlying interactions between the mTOR signaling pathway and LSM12, LSM14A, and LSM14B (**Figure 6C**). Then, the overlapped co-expressed genes involved in the mTOR signaling pathway and the T-cell receptor signaling pathway were also presented in heat maps for LSM12, LSM14A, and LSM14B, respectively (**Figures 6D–F**).

LSM12, LSM14A, and LSM14B Overexpression Correlated With Immune Suppression in HCC

Considering that the T-cell receptor signaling pathway was significantly enriched for LSM12, LSM14A, and LSM14B, we further investigated the association between T-cell-related terms and LSM12, LSM14A, and LSM14B expressions. The LSM12, LSM14A, and LSM14B expressions were negatively correlated with the enrichment levels of activated $CD8^+$ T cell and cytolytic activity, but positively correlated with the enrichment

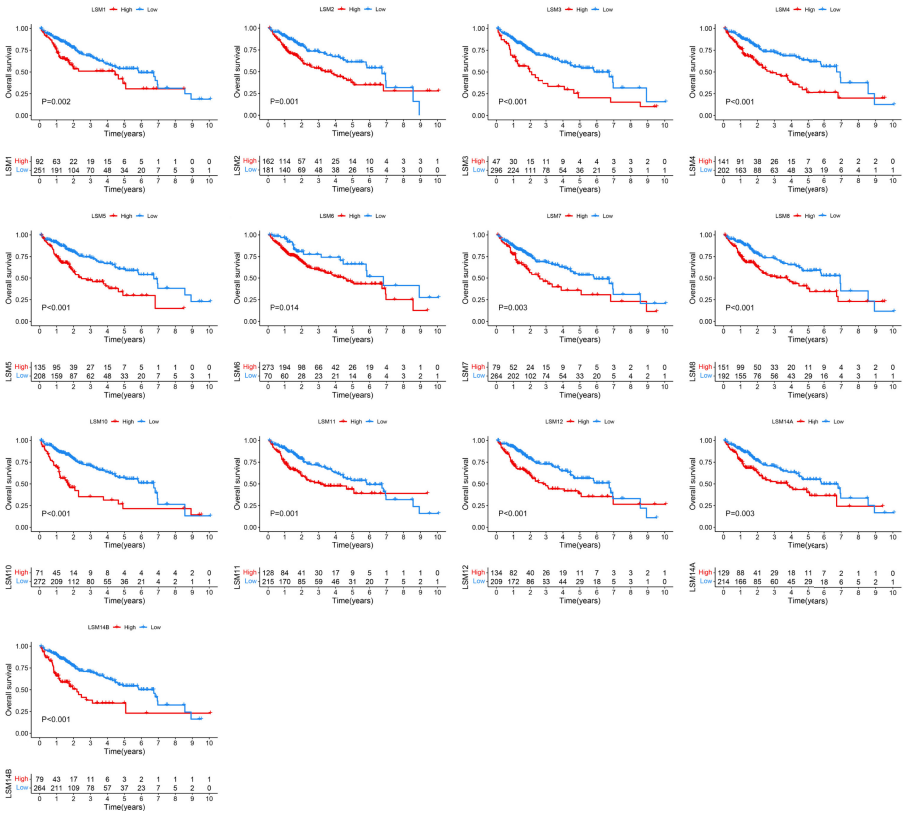

FIGURE 3 | KM survival curves for OS of LSM family members in HCC. KM, Kaplan–Meier; OS, overall survival; LSM, Smith-like (LSM) family members.

levels of Th2 cell and Th2/Th1 (**Figure 7A**). Furthermore, tumors with higher expression of LSM12, LSM14A, or LSM14B had lower infiltration of activated $CD8^+$ T cell and impaired cytolytic activity, but increased infiltration of Th2 cell and higher Th2/Th1 (**Figures 7B–F**). Of note, through the ESTIMATE algorithm, a lower immune score was observed in tumors with higher expression of LSM12, LSM14A, and LSM14B (**Figure 7G**).

We also found that tumors with higher expression of LSM12, LSM14A, and LSM14B had higher expression of tumor-related immune checkpoints (e.g., PD-L1, B7-H3, and PVR), which are important for the immunosuppressive phenotype in malignancies (**Figures 8A–C**) (20–24). Furthermore, ImmuneCellAI (http://bioinfo.life.hust.edu.cn/ImmuCellAI/#!/) was used to predict the therapeutic response to immune checkpoint blockade (ICB). Then, higher expression of LSM12, LSM14A, and LSM14B were observed in ICB-non-response tumors (**Figures 8D–F**). To further verify the association between the response of patients to ICB and the expressions of LSM12, LSM14A, and LSM14B, we evaluated the differences in immunophenoscore (IPS) between different LSM12, LSM14A, and LSM14B expression levels, which were obtained from the Cancer Immunome Atlas (https://tcia.at/) (25). Three subtypes of IPS values (IPS-CTLA4, IPS-PD-1/PD-L1/PD-L2, and IPS-CTLA4/PD-1/PD-L1/PD-L2) were selected to assess the response of HCC patients to anti-PD-1/PD-L1/PD-L2 therapy, anti-CTLA4 therapy, or anti- PD-1/PD-L1/PD-L2 and anti-CTLA4 combination therapy. The IPS-PD-1/PD-L1/PD-L2 was notably higher in tumors with lower expression of LSM14A and LSM14B, but not significantly for LSM12 (**Figure 8G**). Moreover, tumors with lower expression of LSM12, LSM14A, and LSM14B all exhibited increased IPS-CTLA and IPS-CTLA4/PD-1/PD-L1/PD-L2 (**Figures 8H, I**). These results indicate that overexpression of LSM12, LSM14A, and LSM14B might be correlated with immunotolerance and evasion and therapeutic resistance to ICB in HCC.

LSM12, LSM14A, and LSM14B Knockdown Inhibits the Proliferation and Invasion of HCC Cells

To further investigate the underlying role of LSM12, LSM14A, and LSM14B in tumor cell proliferation and invasion, we transfected SNU-387 cells with si-LSM12, si-LSM14A, and si-LSM14B RNAs. Moreover, LSM12, LSM14A, and LSM14B expressions were significantly downregulated in the si-RNA groups ($P < 0.0001$) (**Figures 9A–C**). The CCK-8 assay demonstrated that tumor cell proliferation was notably inhibited in LSM12, LSM14A, and LSM14B depleted SNU-387 cells ($P < 0.0001$) (**Figures 9D–F**). Furthermore, the transwell

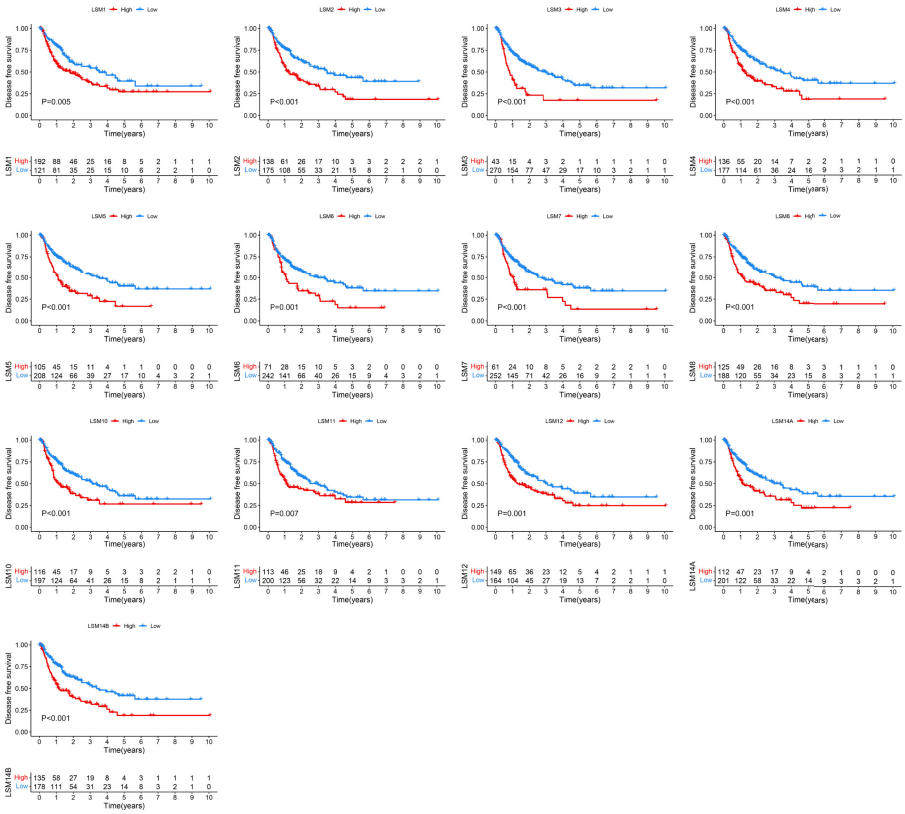

FIGURE 4 | KM survival curves for DFS of LSM family members in HCC. KM, Kaplan–Meier; DFS, disease-free survival; LSM, Smith-like (LSM) family members; HCC, hepatocellular carcinoma.

invasion assay demonstrated that the number of invading cells was significantly decreased in the si-RNAs groups compared with those in the NC group (P <0.0001) (**Figures 9G–I**).

DISCUSSION

These studies showed that overexpression of LSM family members was significantly correlated with advanced TNM stage, histological grade, and worse survival. Additionally, we also constructed a risk score system based on LSM5, LSM10, LSM12, and lsm14B, which was also identified as an independent prognostic factor with optimal predictive ability with reliable C-indexes [0.676 (95% CI, 0.621–0.731) in the TCGA HCC cohort and 0.658 (95% CI, 0.571–0.744) in the ICGC HCC cohort]. These results suggest that LSM family members could serve as novel unfavorable prognostic biomarkers for patients with HCC.

Functional enrichment analysis demonstrated that all LSM family members might take part in the regulation of the cell cycle in HCC. Consistently, suppression of LSM1 expression results in tumor cell proliferation block with decreased G1-phase (26). Fraser et al. also reported that LSM1 knockdown leads to a cytostatic block of the cell cycle (27). Besides, Mili et al. reported that LSM14A interacts directly with tubulin, which is implicated in the stabilization of the mitotic spindle (28). Therefore, it is quite likely that targeting LSM family members may block tumor proliferation through cell cycle arrest in HCC, which deserves further experimental studies.

KEGG analysis revealed that LSM12, LSM14A, and LSM14B were associated with the T-cell receptor signaling pathway, indicating their possible biological roles in T-cell infiltration into the TME of HCC. Additionally, ssGSEA demonstrated that LSM12, LSM14A, and LSM14B overexpression significantly correlated with declined activated $CD8^+$ T-cell infiltration and impaired cytolytic activity, but increased infiltration of Th2 cells and higher Th2/Th1. Previous studies have demonstrated that Th2 cells have been widely considered tumor-promoting immune cells, leading to unfavorable clinical outcomes for HCC (29, 30). Besides, a higher level of Th2 cytokines (e.g., IL4 and IL10) are observed in metastatic HCC, whereas Th1 cytokines (e.g., IFN-γ and IL1) are notably decreased (31). Furthermore, IL-4 and IL-10 restrain IFN-γ production and impair cytotoxic cell-mediated anti-tumor immunity, suggesting that an increased shift from Th1 cells to Th2 cells promotes tumor progression and immunosuppression (31–34). Of note, higher expression of tumor-related immune

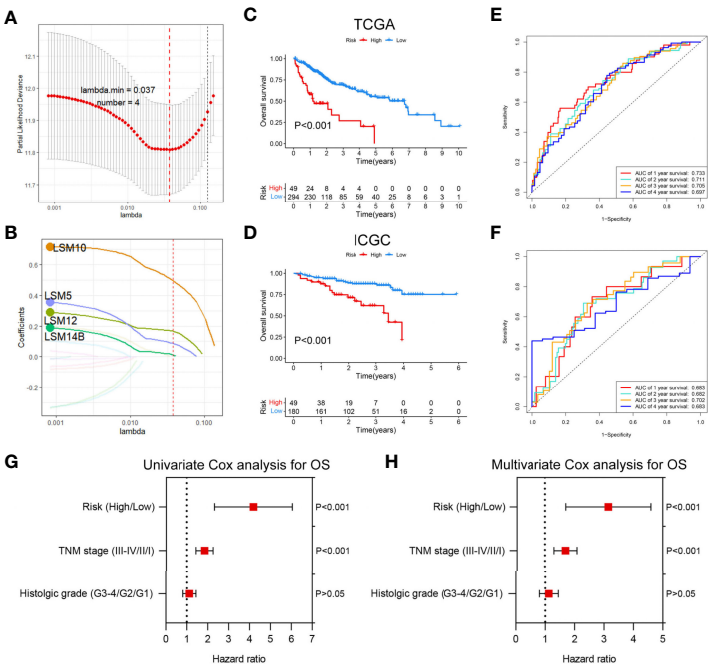

FIGURE 5 | Development and validation of a risk score system for OS based on LSM family members. **(A, B)** Lasso regression analysis identified five critical prognosis-associated LSM family members (e.g., LSM5, LSM10, LSM12, and LSM14B) for HCC. **(C, D)** KM survival curves for OS of patients with HCC according to the risk scores in the TCGA HCC and ICGC HCC cohorts. **(E, F)** ROC curve analysis of the risk score system for 1-, 2-, 3-, and 4-year OS prediction in the TCGA HCC and ICGC HCC cohorts. **(G)** Univariate Cox regression analysis demonstrated that the risk score system and TNM stage were prognostic factor for OS of patients with HCC. **(H)** Multivariate Cox regression analysis demonstrated that the risk score system was an independent unfavorable prognostic factor for OS of patients with HCC. OS, overall survival; LSM, Smith-like (LSM) family members; Lasso, least absolute shrinkage and selection operator regression analysis; HCC, hepatocellular carcinoma; KM, Kaplan–Meier; TCGA, the Cancer Genome Atlas; ICGC, the International Cancer Genome Consortium; ROC, the receiver operating characteristic curve.

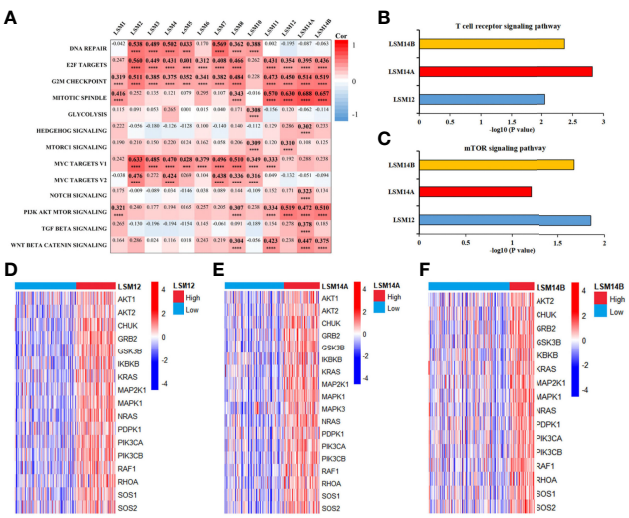

FIGURE 6 | Functional enrichment analysis for LSM family members in HCC. **(A)** Heat map to show the correlation between LSM family and critical biological pathway. **(B)** KEGG analysis demonstrated that LSM12, LSM14A, and LSM14B may play important role in T cell receptor signaling pathway in HCC. **(C)** KEGG analysis also identified the underlying interactions between the mTOR signaling pathway and LSM12, LSM14A, and LSM14B. **(D–F)** Heat maps to show the overlapped co-expressed genes involved in T-cell receptor signaling pathway and mTOR signaling pathway for LSM12, LSM14A, and LSM14B, respectively. LSM, Smith-like (LSM) family members; KEGG, Kyoto Encyclopedia of Genes and Genomes analysis; HCC, hepatocellular carcinoma. ****P-value <0.0001.

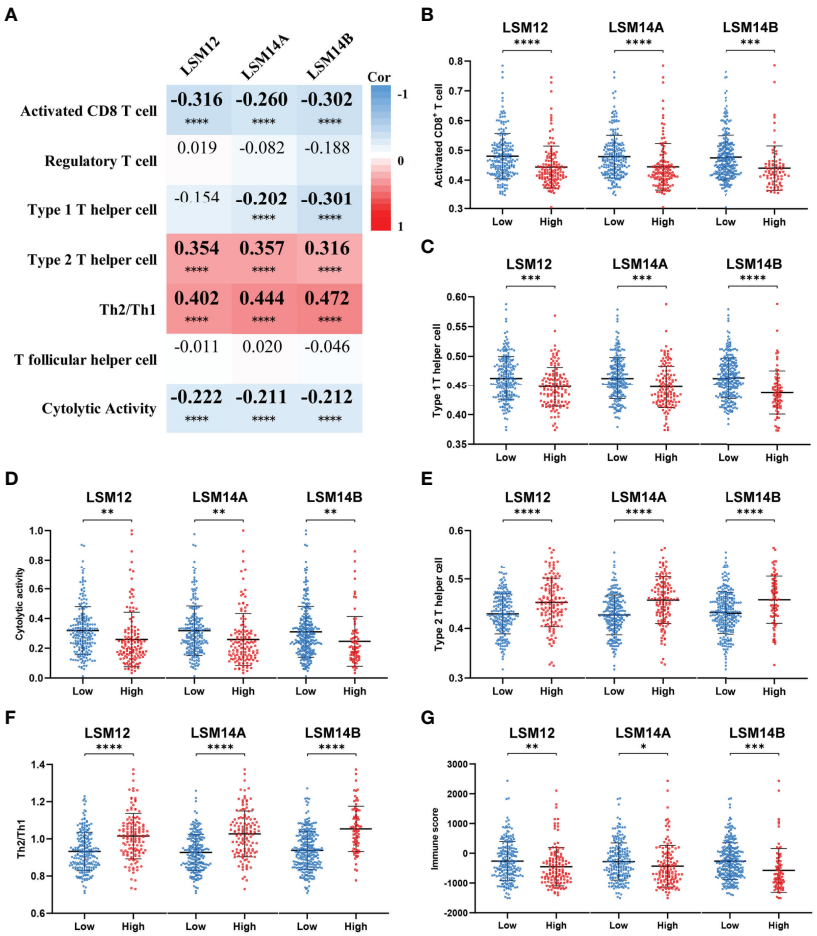

FIGURE 7 | Tumors with LSM12, LSM14A, and LSM14B overexpression were associated with an immunosuppressive phenotype. **(A)** Heat map to show the association between LSM12, LSM14A, and LSM14B expression and T-cell-related terms. **(B)** Tumors with higher LSM12, LSM14A, and LSM14B expression exhibited decreased activated $CD8^+$ T-cell infiltration compared with those with lower LSM12, LSM14A, and LSM14B expression. **(C)** Tumors with higher LSM12, LSM14A, and LSM14B expression exhibited decreased Th1 cell infiltration compared with those with lower LSM12, LSM14A, and LSM14B expression. **(D)** Tumors with higher LSM12, LSM14A, and LSM14B expression exhibited decreased cytolytic activity compared with those with lower LSM12, LSM14A, and LSM14B expression. **(E)** Tumors with higher LSM12, LSM14A, and LSM14B expression exhibited increased Th2 cell infiltration compared with those with lower LSM12, LSM14A, and LSM14B expression. **(F)** Tumors with higher LSM12, LSM14A, and LSM14B expression exhibited increased Th2/Th1 compared with those with lower LSM12, LSM14A, and LSM14B expression. **(G)** Tumors with higher LSM12, LSM14A, and LSM14B expression exhibited decreased immune score compared with those with lower LSM12, LSM14A, and LSM14B expression. Th1, type 1 T helper cell; Th2 cell, type 2 T helper cell. *P-value <0.05; **P-value <0.01; ***P-value <0.001; ****P-value <0.0001.

checkpoints (e.g., PD-L1, B7-H3, and PVR) was also observed in tumors with LSM12, LSM14A, and LSM14B overexpression. Of note, LSM12, LSM14A, and LSM14B overexpression was observed in patients non-responsive to ICB. Moreover, tumors with LSM12, LSM14A, and LSM14B overexpression exhibited decreased IPS to ICB. These results further suggested the potential functions of LSM12, LSM14A, and LSM14B in promoting immunotolerance and evasion in HCC.

This study also found that LSM12, LSM14A, and LSM14B overexpression significantly correlated with higher enriched level of the PI3K-Akt-mTOR signaling pathway. Tumors with LSM12, LSM14A, and LSM14B overexpression also exhibited notably higher expression of critical molecules overlapped between the mTOR signaling pathway and T-cell receptor signaling pathway, namely, AKT2, CHUK, GRB2, GSK3B, IKBKB, KRAS, MAP2K1, MAPK1, NRAS, PDPK1, PIK3CA, PIK3CB, RAF1, RHOA, SOS1, and SOS2, which may be the potential targets of LSM12, LSM14A, and LSM14B for tumor immunity in HCC. It has been shown that the activation of the mTOR signaling pathway is associated with PD-L1 overexpression at both levels of mRNA expression and protein translation in multiple malignancies (35). Suppression of the PI3K-Akt-mTOR signaling pathway cannot only restrain tumor growth itself, but also modulates anti-tumor cytokine production and increase-activated $CD8^+$ T-cell infiltration (35, 36). Besides, Liu et al. also reported that the inhibition of mTOR signaling by tubermoside-1 decreases PD-L1

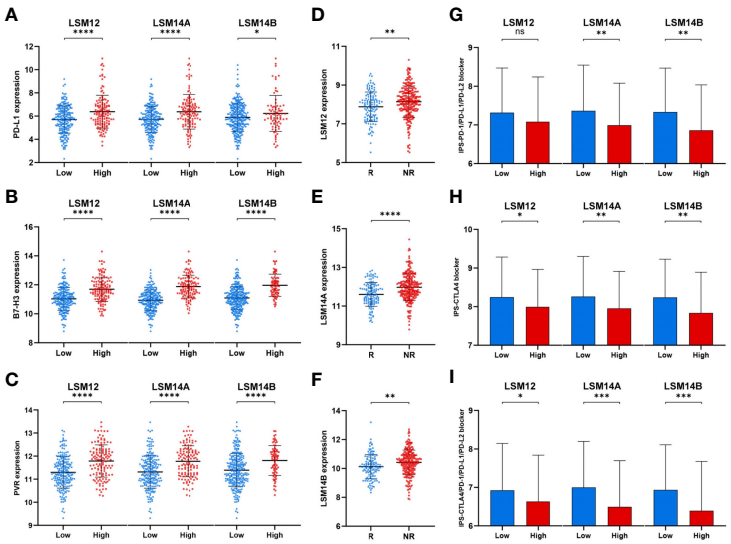

FIGURE 8 | Tumors with higher LSM12, LSM14A, and LSM14B expression exhibited higher expression of tumor-related immune checkpoints and increased therapeutic insensitivity to immune checkpoint blockade. **(A–C)** Differential expression analysis of tumor-related immune checkpoints (e.g., PD-L1, B7-H3, and PVR) between high- and low-expression groups of LSM12, LSM14A, and LSM14B, respectively. **(D–F)** Higher expression of LSM12, LSM14A, and LSM14B were observed in ICB-non-response tumors. **(G)** Tumors with higher LSM14A and LSM14B expression exhibited lower IPS-PD-1/PD-L1/PD-L2. **(H)** Tumors with higher LSM12, LSM14A, and LSM14B expression exhibited lower IPS-CTLA. (**I**) Tumors with higher LSM12, LSM14A, and LSM14B expression exhibited lower IPS-CTLA4/PD-1/PD-L1/PD-L2. ICB, immune checkpoint blockade; NR, non-response; R, response. *P-value <0.05; **P-value <0.01; ***P-value <0.001; ****P-value <0.0001.

expression and enhances anti-tumor immunity (37). Additionally, we preliminarily demonstrated knockdown of LSM12, LSM14A, and LSM14B significantly inhibited tumor cell proliferation and invasion. Taken together, these findings suggest the critical pro-tumor effects of LSM12, LSM14A, and LSM14B overexpression on HCC tumor cell proliferation and metastasis. But in depth experimental works are supposed to be done to demonstrate the underlying mechanisms of LSM12,

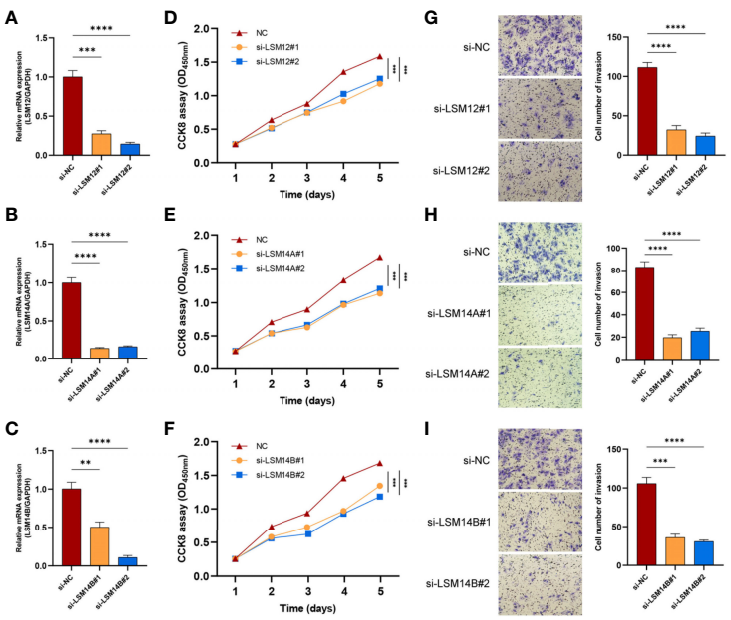

FIGURE 9 | The knockdowns of LSM12, LSM14A, and LSM14B suppress the proliferation and invasion of HCC cells. **(A–C)** qRT-PCR analysis evaluated the efficacies of si-LSM12/14A/14B RNAs in SNU-387 cell. **(D–F)** Assessment of tumor cell proliferation using the CCK8 assay. **(G–I)** Assessment of the invasive capacity of SNU-387 cells using transwell invasion assay. **P-value <0.01; ***P-value <0.001; ****P-value <0.0001.

LSM14A, and LSM14B in hepatocellular carcinogenesis and immunosuppression.

As far as we are aware, this study is the first to systematically describe the expression patterns, clinical significance, and underlying biological functions of LSM family members in HCC. Additionally, for the first time, we proposed that LSM12, LSM14A, and LSM14B overexpression may promote immunotolerance and evasion in HCC. However, several limitations should be acknowledged in this study. First, the prognostic prediction capability of the risk score system should be evaluated in a multi-centered and large cohort. Second, further *in vivo* studies should be performed to investigate the underlying mechanisms by which LSM family members promote tumor progression and immune suppression in HCC.

In summary, our study demonstrated the overexpressed patterns and unfavorable prognostic values of LSM family members in HCC. Of note, we identified the potential inhibition effects of LSM12, LSM14A, and LSM14B on tumor immunity, which laid a novel foundation to further explore the role of LSM family members as novel potential therapeutic targets in HCC.

DATA AVAILABILITY STATEMENT

The raw data supporting the conclusions of this article will be made available by the authors, without undue reservation.

AUTHOR CONTRIBUTIONS

Conceptualization: HZ, YC, CS, and CZ. Methodology: HZ, BC, CT, and XC. Investigation: HZ, BC, CT, and XC. Writing—Original Draft: HZ. Writing—Review and Editing: HZ, BC, CT, XC, WT, LY, ZX, XM, and QW. Visualization: HZ and BC. Supervision: HZ, YC, CS, and CZ. Funding Acquisition: YC, CS, and LW. All authors listed have made a substantial, direct, and intellectual contribution to the work and approved it for publication.

FUNDING

This work was supported by grants from the National Natural Science Foundation of China (Nos. 81972263, 82103221, 82072714), the program of Guangdong Provincial Clinical Research Center for Digestive Diseases (2020B1111170004), and the China Postdoctoral Science Foundation (2020M683094).

SUPPLEMENTARY MATERIAL

The Supplementary Material for this article can be found online at: https://www.frontiersin.org/articles/10.3389/fonc.2022.871771/full#supplementary-material

REFERENCES

1. Villanueva A. Hepatocellular Carcinoma. *N Engl J Med* (2019) 380:1450–62. doi: 10.1056/NEJMra1713263
2. Nault JC, Villanueva A. Biomarkers for Hepatobiliary Cancers. *Hepatology* (2021) 73 Suppl 1:115–27. doi: 10.1002/hep.31175
3. Bruix J, da Fonseca LG, Reig M. Insights Into the Success and Failure of Systemic Therapy for Hepatocellular Carcinoma. *Nat Rev Gastroenterol Hepatol* (2019) 16:617–30. doi: 10.1038/s41575-019-0179-x
4. Farzaneh Z, Vosough M, Agarwal T, Farzaneh M. Critical Signaling Pathways Governing Hepatocellular Carcinoma Behavior; Small Molecule-Based Approaches. *Cancer Cell Int* (2021) 21:208. doi: 10.1186/s12935-021-01924-w
5. Gao Q, Wang XY, Zhou J, Fan J. Heterogeneity of Intermediate-Stage HCC Necessitates Personalized Management Including Surgery. *Nat Rev Clin Oncol* (2015) 12:10. doi: 10.1038/nrclinonc.2014.122-c1
6. Gao Q, Wang XY, Zhou J, Fan J. Multiple Carcinogenesis Contributes to the Heterogeneity of HCC. *Nat Rev Gastroenterol Hepatol* (2015) 12:13. doi: 10.1038/nrgastro.2014.6-c1
7. Mura C, Phillips M, Kozhukhovsky A, Eisenberg D. Structure and Assembly of an Augmented Sm-Like Archaeal Protein 14-Mer. *Proc Natl Acad Sci U S A* (2003) 100:4539–44. doi: 10.1073/pnas.0538042100
8. Fischer S, Benz J, Spath B, Maier LK, Straub J, Granzow M, et al. The Archaeal Lsm Protein Binds to Small RNAs. *J Biol Chem* (2010) 285:34429–38. doi: 10.1074/jbc.M110.118950
9. Tharun S, He W, Mayes AE, Lennertz P, Beggs JD, Parker R. Yeast Sm-Like Proteins Function in mRNA Decapping and Decay. *Nature* (2000) 404:515–8. doi: 10.1038/35006676
10. Achsel T, Brahms H, Kastner B, Bachi A, Wilm M, Luhrmann R. A Doughnut-Shaped Heteromer of Human Sm-Like Proteins Binds to the 3'-End of U6 snRNA, Thereby Facilitating U4/U6 Duplex Formation *In Vitro*. *EMBO J* (1999) 18:5789–802. doi: 10.1093/emboj/18.20.5789
11. Zhang J, Guan X, Shah K, Yan J. Lsm12 is an NAADP Receptor and a Two-Pore Channel Regulatory Protein Required for Calcium Mobilization From Acidic Organelles. *Nat Commun* (2021) 12:4739. doi: 10.1038/s41467-021-24735-z
12. Little EC, Camp ER, Wang C, Watson PM, Watson DK, Cole DJ. The CaSm (LSm1) Oncogene Promotes Transformation, Chemoresistance and Metastasis of Pancreatic Cancer Cells. *Oncogenesis* (2016) 5:e182. doi: 10.1038/oncsis.2015.45
13. Watson PM, Miller SW, Fraig M, Cole DJ, Watson DK, Boylan AM. CaSm (LSm-1) Overexpression in Lung Cancer and Mesothelioma is Required for Transformed Phenotypes. *Am J Respir Cell Mol Biol* (2008) 38:671–8. doi: 10.1165/rcmb.2007-0205OC
14. Hou W, Zhang Y. Circ_0025033 Promotes the Progression of Ovarian Cancer by Activating the Expression of LSM4 *via* Targeting miR-184. *Pathol Res Pract* (2021) 217:153275. doi: 10.1016/j.prp.2020.153275
15. Camp RL, Dolled-Filhart M, Rimm DL. X-Tile: A New Bio-Informatics Tool for Biomarker Assessment and Outcome-Based Cut-Point Optimization. *Clin Cancer Res* (2004) 10:7252–9. doi: 10.1158/1078-0432.CCR-04-0713
16. Hanzelmann S, Castelo R, Guinney J. GSVA: Gene Set Variation Analysis for Microarray and RNA-Seq Data. *BMC Bioinf* (2013) 14:7. doi: 10.1186/1471-2105-14-7
17. Bindea G, Mlecnik B, Tosolini M, Kirilovsky A, Waldner M, Obenauf AC, et al. Spatiotemporal Dynamics of Intratumoral Immune Cells Reveal the Immune Landscape in Human Cancer. *Immunity* (2013) 39:782–95. doi: 10.1016/j.immuni.2013.10.003
18. Rooney MS, Shukla SA, Wu CJ, Getz G, Hacohen N. Molecular and Genetic Properties of Tumors Associated With Local Immune Cytolytic Activity. *Cell* (2015) 160:48–61. doi: 10.1016/j.cell.2014.12.033
19. Yoshihara K, Shahmoradgoli M, Martinez E, Vegesna R, Kim H, Torres-Garcia W, et al. Inferring Tumour Purity and Stromal and Immune Cell Admixture From Expression Data. *Nat Commun* (2013) 4:2612. doi: 10.1038/ncomms3612
20. Fang H, Guo Z, Chen J, Lin L, Hu Y, Li Y, et al. Combination of Epigenetic Regulation With Gene Therapy-Mediated Immune Checkpoint Blockade Induces Anti-Tumour Effects and Immune Response *In Vivo*. *Nat Commun* (2021) 12:6742. doi: 10.1038/s41467-021-27078-x
21. Kontos F, Michelakos T, Kurokawa T, Sadagopan A, Schwab JH, Ferrone CR, et al. B7-H3: An Attractive Target for Antibody-Based Immunotherapy. *Clin Cancer Res* (2021) 27:1227–35. doi: 10.1158/1078-0432.CCR-20-2584

22. Marin-Acevedo JA, Dholaria B, Soyano AE, Knutson KL, Chumsri S, Lou Y. Next Generation of Immune Checkpoint Therapy in Cancer: New Developments and Challenges. *J Hematol Oncol* (2018) 11:39. doi: 10.1186/s13045-018-0582-8
23. Qin S, Xu L, Yi M, Yu S, Wu K, Luo S. Novel Immune Checkpoint Targets: Moving Beyond PD-1 and CTLA-4. *Mol Cancer* (2019) 18:155. doi: 10.1186/s12943-019-1091-2
24. Peng H, Fu YX. The Inhibitory PVRL1/PVR/TIGIT Axis in Immune Therapy for Hepatocellular Carcinoma. *Gastroenterology* (2020) 159:434–6. doi: 10.1053/j.gastro.2020.06.024
25. Charoentong P, Finotello F, Angelova M, Mayer C, Efremova M, Rieder D, et al. Pan-Cancer Immunogenomic Analyses Reveal Genotype-Immunophenotype Relationships and Predictors of Response to Checkpoint Blockade. *Cell Rep* (2017) 18:248–62. doi: 10.1016/j.celrep.2016.12.019
26. Kelley JR, Fraser MM, Hubbard JM, Watson DK, Cole DJ. CaSm Antisense Gene Therapy: A Novel Approach for the Treatment of Pancreatic Cancer. *Anticancer Res* (2003) 23:2007–13.
27. Fraser MM, Watson PM, Fraig MM, Kelley JR, Nelson PS, Boylan AM, et al. CaSm-Mediated Cellular Transformation is Associated With Altered Gene Expression and Messenger RNA Stability. *Cancer Res* (2005) 65:6228–36. doi: 10.1158/0008-5472.CAN-05-0650
28. Mili D, Georgesse D, Kenani A. Localization and Role of RAP55/LSM14 in HeLa Cells: A New Finding on the Mitotic Spindle Assembly. *Acta Biochim Pol* (2015) 62:613–9. doi: 10.18388/abp.2015_1107
29. Lee HL, Jang JW, Lee SW, Yoo SH, Kwon JH, Nam SW, et al. Inflammatory Cytokines and Change of Th1/Th2 Balance as Prognostic Indicators for Hepatocellular Carcinoma in Patients Treated With Transarterial Chemoembolization. *Sci Rep* (2019) 9:3260. doi: 10.1038/s41598-019-40078-8
30. Kogame M, Nagai H, Shinohara M, Igarashi Y, Sumino Y, Ishii K. Th2 Dominance Might Induce Carcinogenesis in Patients With HCV-Related Liver Cirrhosis. *Anticancer Res* (2016) 36:4529–36. doi: 10.21873/anticanres.11000
31. Hattori E, Okumoto K, Adachi T, Takeda T, Ito J, Sugahara K, et al. Possible Contribution of Circulating Interleukin-10 (IL-10) to Anti-Tumor Immunity and Prognosis in Patients With Unresectable Hepatocellular Carcinoma. *Hepatol Res* (2003) 27:309–14. doi: 10.1016/j.hepres.2003.07.002
32. Mao JX, Guo WY, Guo M, Liu C, Teng F, Ding GS. Acute Rejection After Liver Transplantation Is Less Common, But Predicts Better Prognosis in HBV-Related Hepatocellular Carcinoma Patients. *Hepatol Int* (2020) 14:347–61. doi: 10.1007/s12072-020-10022-4
33. DeNardo DG, Coussens LM. Inflammation and Breast Cancer. Balancing Immune Response: Crosstalk Between Adaptive and Innate Immune Cells During Breast Cancer Progression. *Breast Cancer Res* (2007) 9:212. doi: 10.1186/bcr1746
34. Zhuang H, Zhou Z, Zhang Z, Chen X, Ma Z, Huang S, et al. B3GNT3 Overexpression Promotes Tumor Progression and Inhibits Infiltration of CD8 (+) T Cells in Pancreatic Cancer. *Aging (Albany NY)* (2020) 13:2310–29. doi: 10.18632/aging.202255
35. Kobayashi Y, Lim SO, Yamaguchi H. Oncogenic Signaling Pathways Associated With Immune Evasion and Resistance to Immune Checkpoint Inhibitors in Cancer. *Semin Cancer Biol* (2020) 65:51–64. doi: 10.1016/j.semcancer.2019.11.011
36. Zhu S, Ma AH, Zhu Z, Adib E, Rao T, Li N, et al. Synergistic Antitumor Activity of Pan-PI3K Inhibition and Immune Checkpoint Blockade in Bladder Cancer. *J Immunother Cancer* (2021) 9:e002917. doi: 10.1136/jitc-2021-002917
37. Liu X, Yin M, Dong J, Mao G, Min W, Kuang Z, et al. Tubeimoside-1 Induces TFEB-Dependent Lysosomal Degradation of PD-L1 and Promotes Antitumor Immunity by Targeting mTOR. *Acta Pharm Sin B* (2021) 11:3134–49. doi: 10.1016/j.apsb.2021.03.039

Conflict of Interest: The authors declare that the research was conducted in the absence of any commercial or financial relationships that could be construed as a potential conflict of interest.

Publisher's Note: All claims expressed in this article are solely those of the authors and do not necessarily represent those of their affiliated organizations, or those of the publisher, the editors and the reviewers. Any product that may be evaluated in this article, or claim that may be made by its manufacturer, is not guaranteed or endorsed by the publisher.

Copyright © 2022 Zhuang, Chen, Tang, Chen, Tan, Yang, Xie, Ma, Wang, Zhang, Shang and Chen. This is an open-access article distributed under the terms of the Creative Commons Attribution License (CC BY). The use, distribution or reproduction in other forums is permitted, provided the original author(s) and the copyright owner(s) are credited and that the original publication in this journal is cited, in accordance with accepted academic practice. No use, distribution or reproduction is permitted which does not comply with these terms.

frontiers | Frontiers in Oncology

SYSTEMATIC REVIEW
published: 12 May 2022
doi: 10.3389/fonc.2022.899145

The Role of miRNAs in the Resistance of Anthracyclines in Breast Cancer: A Systematic Review

Zihan Si[1,4*], *Yan Zhong*[3*], *Sixian Lao*[1,4], *Yufeng Wu*[1,4], *Guoping Zhong*[1,4†] *and Weiwei Zeng*[2,3†]

[1] Institute of Clinical Pharmacology, School of Pharmaceutical Sciences, Sun Yat-sen University, Guangzhou, China, [2] The Second People's Hospital of Longgang District, Shenzhen, China, [3] Shenzhen Baoan Women's and Children's Hospital, Jinan University, Shenzhen, China, [4] Guangdong Provincial Key Laboratory of New Drug Design and Evaluation, Guangzhou, China

OPEN ACCESS

Edited by:
Zhe-Sheng Chen,
St. John's University, United States

Reviewed by:
Yuying Zhang,
Shenzhen Longhua Maternity and Child Healthcare Hospital, China
Dinglan Wu,
Southern Medical University, China

***Correspondence:**
Weiwei Zeng
zwwspring@126.com
Guoping Zhong
zhonggp@mail.sysu.edu.cn

†These authors have contributed equally to this work and share first authorship

Specialty section:
This article was submitted to Molecular and Cellular Oncology, a section of the journal Frontiers in Oncology

Received: 18 March 2022
Accepted: 13 April 2022
Published: 12 May 2022

Citation:
Si Z, Zhong Y, Lao S, Wu Y, Zhong G and Zeng W (2022) The Role of miRNAs in the Resistance of Anthracyclines in Breast Cancer: A Systematic Review. Front. Oncol. 12:899145. doi: 10.3389/fonc.2022.899145

Breast cancer has been reported as the most common cancer in women globally, with 2.26 million new cases in 2020. While anthracyclines are the first-line drug for breast cancer, they cause a variety of adverse reactions and drug resistance, especially for triple-negative breast cancer, which can lead to poor prognosis, high relapse, and mortality rate. MicroRNAs (miRNAs) have been shown to be important in the initiation, development and metastasis of malignancies and their abnormal transcription levels may influence the efficacy of anthracyclines by participating in the pathologic mechanisms of breast cancer. Therefore, it is essential to understand the exact role of miRNAs in the treatment of breast cancer with anthracyclines. In this review, we outline the mechanisms and signaling pathways involved in miRNAs in the treatment of breast cancer using anthracyclines. The role of miRNA in the diagnosis, prognosis and treatment of breast cancer patients is discussed, along with the involvement of miRNAs in chemotherapy for breast cancer.

Keywords: breast cancer, miRNAs, anthracyclines, drug resistance, efficacy

INTRODUCTION

Different kinds of treatments are applied to different immunohistological types of breast cancer. Triple-negative breast cancer (TNBC), which is not sensitive to endocrine and targeted therapies, is treated with a combination of anthracyclines in the clinical. As the first-line drug class for TNBC, anthracyclines can influence the development of tumors by inhibiting the synthesis of biological DeoxyriboNucleic Acid(DNA). Studies have shown that anthracyclines can affect the activity of DNA topoisomerase to stabilize the DNA double-strand and prevent DNA replication (1, 2). Since daunorubicin, the first anthracycline drug, was discovered, many other anthracycline drugs have been developed one after another, including adriamycin, epirubicin, clarithromycin, and so on. They have been widely used in the treatment of hematological malignancies and solid tumors. However, the frequent use of anthracyclines can cause drug resistance to develop gradually. As a result, cancer will continue to develop, proliferate, invade and metastasize, and eventually lead to patient death. Meanwhile, many adverse reactions caused by anthracyclines, in particular,

cardiotoxicity, also affect the prognosis of patients. Clinical studies have shown that this adverse reaction is often irreversible and fatal to patients. Even the first use of anthracyclines may cause heart damage (3). In addition, it can also induce liver damage (4) and promote breast cancer metastasis to the lungs (5). Therefore, many researchers are now working on the mechanisms of breast cancer cell resistance to anthracyclines and the mechanisms of anthracycline adverse reactions.

As a non-coding Ribonucleic Acid(RNA), miRNA is composed of approximately 20 nucleotides, and participates in the regulation of RNA transcription by activating or blocking the translation of mRNA targets. More and more studies have found that miRNA plays a significant role in biological processes, such as embryonic development, cell proliferation, differentiation, migration, apoptosis, and signal transduction (6). Therefore, the abnormal expression of miRNA is closely related to the development of tumor cells (7). In recent years, many studies have shown that miRNA is involved in the regulation of the efficacy of anthracyclines in the treatment of breast cancer, and may be used as a specific biomarker for diagnosis, control and prediction of adverse reactions. Through reviewing past research, this article summarizes the effects of various miRNAs in breast cancer treated by anthracyclines, and provides certain guidance for future research. At the same time, we prove the clinical application potential of various miRNAs in risk prediction, diagnosis and treatment.

MIRNAS AND ANTHRACYCLINES RESISTANCE

An important problem to overcome in the application of anthracyclines is drug resistance. The emergence of drug resistance makes tumor cells more aggressive and metastatic and leads to failure in clinical treatments, eventually leading to patient death (8). Therefore, in hopes of overcoming the resistance of anthracyclines through miRNA regulation, scientists have been studying the mechanism of drug resistance. To modify sensitization, transformation, and metastasis, miRNAs regulate their downstream signaling pathways or associated proteins by modulating their target genes. Increased drug efflux *via* altering cell membrane transporters is one of the mechanisms of drug resistance generated by anthracyclines, according to Li, X.J. et al.The key factor is the ATP-bindingcassette transporter (ABC) family and its derivatives, P-glycoprotein (P-gp), Multidrug Resistance-associated Protein (MRP) and topoisomerase II. The other potential mechanism of drug resistance is the inhibition of tumor cell apoptosis. Anthracycline reduces tumor cell apoptosis and increases cell survival and causes cell cycle arrest, then activates the epithelial-mesenchymal transition (EMT) by activating or inhibiting cell signaling transduction pathways (9). In addition, the drug resistance of tumors depends on some tumor proteins, which can affect the metabolic function of tumor cells and control their microenvironment.

Wang, Y.D. et al. reported that the target genes of miRNAs can be divided into four types: oncogenes, tumor suppressor genes, signaling pathway genes, and cell cycle regulatory genes (10). The upstream or downstream of these pathways are also interspersed with various apoptotic proteins, oncogenes, and tumor suppressor genes to affect cell apoptosis, changes in EMT processes, and cell cycle arrest. Accumulating studies have found that one miRNA may be able to regulate multiple genes, and these genes can cooperate to influence each other, and even produce feedback loops.

MIRNAS AND MEMBRANE TRANSPORT

The factors that cause changes in cell membrane transport mainly include the ABC family, P-gp protein, MRP protein, topoisomerase, etc. MiRNAs participate in their regulation cells to anthracycline drugs. Xie, M.X. et al. demonstrated that the expression of miR-132 and miR-212 inhibits the expression of nuclear factor kappa-β (NF-κβ), which leads to an increase in the expression of breast cancer resistance protein (BCRP), a member of ABC family, and reduces the sensitivity of tumor cells to anthracyclines (11). Some studies have reported that miR-128 exerts its function of reducing drug resistance of tumor cells by inhibiting the B-cell- specific Moloney murine leukemia virusintegration site-1 (Bmi-1) and ABCC5 (9, 12, 13). The relationship between miR-760 and ABCA1 has also been studied. The high expression of miR-760 can mediate the decline of tumor cell resistance to drugs by reducing the expression of ABCA1 (13). There was a negative correlation between miR-134 and ABCC1, the high expression of miR-134 resulting in reduced tumor cell proliferation and increased apoptosis, which reflects its potential to reduce drug resistance (14). miR-145, miR-451, miR-326, and miR-199a are also implicated in MRP1 (ABCC1) (15–18). Di, H. et al. reported that miR-124-3p enhanced the sensitivity of tumor cells to drugs by reducing the expression of ABCC4 (19).

P-gp is a molecular pump located on the cell membrane to protect cells from harmful exogenous molecules (20). However, this protective mechanism on tumor cells can hinder the entry of anticancer drugs, thereby inducing drug resistance. P-gp genes can be downstream targets of many oncogenes and tumor suppressor genes. MiRNAs affect the number of transcription and synthesis of P-gp through modulating related signaling pathways. Research showed that miR-302s can cause cancer cells susceptible to anthracyclines by down-regulating the expression of P-gp through the MAP/ERK kinase 1 (MAKK1) pathway (21). The overexpression of miR-195 can inhibit the expression of P-gp through the Raf-1 signaling pathway, making more breast cancer cells susceptible to apoptosis and increasing their sensitivity to anthracyclines (22).

MiRNAs and Cell Apoptosis

Most of the miRNAs achieve their aims by regulating signaling pathways. The most important and widely studied pathways are the Phosphatase and tensin homolog deleted on chromosome

ten- phosphatidylinositol 3 kinase- AKT (PTEN-PI3K-AKT) signaling pathway, Notch signaling pathway, Ras signaling p–athway, etc (23). The antiapoptotic protein, B cell leukemia oncogene (Bcl) protein family is the most important link in cell apoptosis, including Bcl-2, Bcl-Xl, Mcl-1, Bcl-w, and so on (24). Many studies have shown that various signaling pathways related to apoptosis have a common junction, which is regulated by the Bcl family. Therefore, Bcl family proteins can inhibit cell death caused by a variety of cytotoxic factors. This phenomenon is even more prominent in tumor cells. Many researchers are trying to link miRNAs with the expression of Bcl family proteins to find a therapeutic strategy to reduce the resistance of tumor cells to anthracyclines. miR-181a is a well recognized miRNA at present. Ying, Z. et al. found that Bcl-2 was decreased by increasing the expression of miR-181a and induced the apoptosis of mitochondria, thereby increasing the apoptosis induced by doxorubicin drugs (25). There is evidence that the overexpression of miR-192-5p will also reduce the expression of Bcl-2, which makes the Bcl-2-Asociated Agonist of Cell Death (BAD) gene competitively increases. As a result, the expression of Peptidylprolyl Isomerase A (PPIA) is inhibited and the resistance of tumor cells to anthracyclines reduced (26). Furthermore, miR-122-5p, miR-195, miR-125b, miR-193b, miR-34a, and miR-200c are negatively related to the regulation of Bcl-2 or Myeloid cell leukemia sequence (Mcl) family and other Bcl family proteins (24, 27–31). Other studies showed that some miRNAs, such as miR-222, miR-19a, and miR-21, are positively correlated with the expression of the Bcl family (32, 33).

The Bcl activating gene proteins are tumor suppressors. Their mutations can affect the process of cell proliferation, transcription and apoptosis. The relationship between the mutation of P53 and miRNA is attractive to researchers. miR-214 has been shown to down-regulate RFWD2-p53 cascade, causing tumor cells sensitive to anthracyclines (34). Yuan, Y. et al. identified that miR-133a improves sensitization of tumor cells by suppressing the expression of the uncoupling protein-2 (UCP-2) (35). This mechanism is considered to be related to P53 mutation (36). Furthermore, it is interesting to note that miR-191-5p declines the expression of P53, which binds to the promoter of miR-191-5p, forming a negative feedback regulation chain by downregulating the expression of SOX4 (37). Not only can miRNAs change drug resistance by regulating the mutation of P53, recent studies demonstrated that some miRNAs can also be regulated by P53. Lin, S. et al. found that the expression level of miR-30c is controlled by P53 mutation, which could contribute to tumor cell sensitivity to doxorubicin by regulating the Fanconi anemia complementation group F protein (FANCY) and REV1 protein (38). In addition, miR-127, miR-34a, and miR-542-3p are all mentioned to be related to P53 network in other studies (16, 39).

PI3K-AKT is also a classic signaling pathway that can induce the apoptosis of cells. The abnormal expression of PTEN protein is enough to antagonize PI3K-AKT *via* dephosphorylating the Phosphatidylinositol (3–5) Trisphosphate (PIP3) on the cell membrane to produce phosphati-dylinositol-4,5-bisphosphate (PIP2), which plays a role in the growth, apoptosis, adhesion (40), infiltration and migration of cancer cells (41). Once the PI3K-AKT signaling pathway is inhibited or damaged, it will promote the activation of tumor cell apoptosis and reduce the occurrence of drug resistance. It was reported that the expression of miR-222 (42, 43) and miR-29a (44) were decreased after treatment with anthracyclines. As a result, it led to anthracycline resistance because of the decreased of PTEN. In addition, miR-221 has been shown to make the PI3K-AKT pathway more active by targeting the PTEN protein, which strengthens the tolerance of tumor cells to anthracyclines. Many miRNAs, such as miR-21 (45, 46), miR-19a (47), miR-132 (11), and miR-212 (11), are negatively correlated with PTEN expression to promote anthracycline resistance in breast cancer. In contrast, miR-200c raised the expression of PTEN, contributing to reverse drug resistance (48). Not only can the PTEN protein affect the PI3K-AKT pathway, but this pathway also accepts other regulations. For example, insulin-like growth factor-1 receptor (IGF-1R) is a tyrosine kinase receptor that can activate the expression of PI3K-AKT and prevent cell apoptosis. Zhang, H. et al. found that the downregulation of miR-520b expression can increase the expression of PI3K-AKT by activating IGF-1R so that tumor cells can acquire drug resistance (49). Similarly, the downregulation of miR-452 can also induce drug resistance through the IGF-1 signaling pathway (50). Other studies have shown that miR-7 can restrain the expression of epidermal growth factor receptor (EGFR), thereby regulating the PI3K-AKT pathway to enhance the sensitivity of cells to anthracycline drugs (51). miR-200c can enhance tumor cell resistance to anthracyclines by decreasing the expression of Friend of GATA2 (FOG2) protein (52). In addition to the above pathways, vascular endothelial growth factor A (VEGFA) and fibroblast growth factor 2 (FGF2) also target the PI3K-AKT pathway. miR-205 has also been shown to inhibit the synthesis of VEGFA and FGF2, causing damage to the pathway and tumor cell apoptosis (53).

The Notch gene, as a highly conserved gene, regulates cell proliferation, differentiation, and apoptosis (54, 55). It also plays an important role in the interaction of adjacent cells, which makes the Notch pathway a possible target for tumor treatment. Among published studies, miR-34a is closely related to the Notch pathway (56). The expression of homolog 1 declined after downregulating miR-34a. Cell drug resistance is reduced because of the inhibition of the Notch pathway, after upregulating miR-34a (57). Moreover, it has been reported that miR-34a can suppress tumor cell migration effectively through the Notch pathway (28).

Beyond the above pathways, the mitogen-activated protein kinase/the extracellular signal-related kinases (MAPK/ERK) pathway is also a potential direction that countributes to regulate the resistance to anthracyclines (58). The MAPK family are highly conserved serine/threonine protein kinases, a group of major signaling molecules in the process of signal transduction. Thus, it plays an important role in cancer development and disease occurrence (59). It has been reported that miR-302s inhibited the transcription of P-gp glycoprotein and resensitized the resistance of breast cancer cells to

Adriamycin (ADR) to death by reducing the expression of mitogen-activated protein kinase/ERK kinase 1 (MEKK1) (21). Furthermore, P38 is an another important member of the MAPK family. miR-381 executes its function by inhibiting the expression of Fyn, a Src-family kinase (60) and cutting down the synthesis of P38 (61). This means that it may become a potential target for overcoming the resistance of anthracyclines in the future. Tyrosine 3-monooxygenase/tryptophan 5-monooxygenase activation protein zeta (YWHAZ), an antiapoptotic gene located downstream of miR-30c, can inhibit the expression of the P38 pathway (62). Other pathways have also been mentioned. For example, miR-140-5p was found to suppress the Wnt1 pathway, resulting in decline of anthracyclines resistance (63). Another miRNA, miR-148a, plays a role in tumor migration and erosion by inhibiting the expression of the Wnt-1 pathway (64). Lastly, miR-129-5p induced apoptosis of cancer cells by disrupting SOX2 expression (65).

MiRNAs and the Cell Cycle

In addition to the function of apoptosis and the EMT process in the formation of drug resistance, abnormal cell cycle is also an important factor to consider. As we all know, cancer cells can produce infinite proliferation, so uncontrollable proliferation is a manifestation of cancer drug resistance. The cell cycle includes the division phase and the interphase. When the cell cycle is in the G0 phase, the cells stop dividing. Therefore, restraining the cancer cell cycle in the G0 phase is a potential way to overcome cancer drug resistance. Cyclin-dependent kinase (CDK), a regulator of the cell cycle, are divided into two categories based on their positive and negative effects (66). The positive regulation is *via* cyclin and the negative regulation is *via* cyclin-dependent protein kinase inhibitor (CKI) (67). The reduced expression of p27kip, a CKI regulated by miR-222, causing proliferation of tumor cells and reducing apoptosis. Based on the view of Wang, D.D. et al., the IC50 of tumor cells was increased after upregulating miR-222, which indicated that the increased resistance to anthracyclines (68). Additionly, miR-24 inhibited expression of p27kip (69, 70). It changed the chemosensitivity by regulating autophagy and tumor vascular survival. miR-574 has also been found to inhibit the expression of Smad4. It accelerates the G1-S phase of the cell cycle through regulating the Transforming Growth Factor-β (TGF-β), inducing cell growth and reducing the sensitivity of cells to anthracyclines (71). Other studies have discovered a negative feedback regulation of CDKs. miR-449 could inhibit cell cycle gene expression against drug resistance by reducing the synthesis of CDK2, E2F transcription factor 1 (E2F1), E2F transcription factor 3 (E2F3). Surprisingly, E2F1 regulates the expression of miR-449, forming a negative feedback loop (72). Furthermore, the aforementioned miR-122-5p can reduce the expression of drug resistance by targeting CDKs (27). A mircoRNA targeting cyclin was rarely discovered. The downregulation of miR-135b-5p was confirmed to promote the synthesis of Anterior Gradient 2 (AGR2), an enzyme that functions as a folding protein on the endoplasmic reticulum of tumor cells. It can mediate the expression of cyclin D1 and make cells sensitive to anthracyclines (73).

MiRNAs and Epithelial-Mesenchymal Transition

EMT ensures the cells with the ability of transformation and invasion, therefore against cell senescence and apoptosis (74). EMT regulates the process of cell development, as well as participates in the process of tissue healing, cancer occurrence, and metastasis. So EMT is critical to the development of drug resistance in the treatment of breast cancer with anthracyclines (75). miR-93 was found to strengthen cell proliferation and reduce the sensitivity of tumor cells to the drug by inhibiting the PTEN pathway and promoting the occurrence of EMT (76). Du, F.Y. and his colleagues showed that the overexpression of miR-137 would be detrimental to the synthesis of dual-specifificity phosphatase 4 (DUSP4), which blocked the EMT process. Therefore, it implied that miR-137 has a great potential for sensitivity enhancement against anthracyclines resistance (77). In addition, studies have validated that miR-124 targets the expression of t signal transducer and activator of transcription 3 (STAT3), suppressing the activity of the hypoxia-inducible factor-1(HIF-1) pathway, resulting in the reversal of drug resistance (78). An intriguing discovery is the miR-448 positive feedback. It has been reported that the downregulation of miR-448 can promote the high expression of special AT-rich sequence-binding protein-1 (SATB1) sequence binding protein, sequentially activating the EMT process and the nuclear factor NF-κβ (79). Moreover, NF-κβ, when bonded to miR-448, inhibits the transcription of miR-448. This positive feedback phenomenon enhances the drug resistance of tumor cells. Vimentin and cadherin are important protein targets in the EMT process and are closely related to miRNAs. Zhou, Y. et al. found that miR-25 played a major role in the miR106b-25 cluster, which can reduce the expression of EP300, a transcriptional activator of E-cadherin. This change obstructed the occurrence of EMT and restored the chemosensitivity of tumor cells (80). Similarly, miR-181c renders tumor cells to regain sensitivity to anthracyclines by suppressing vimentin and N-cadherin (81). miR-489 performed its function of improving drug resistance of tumor cells by losing vimentin, but increasing the synthesis of E-cadherin, through reducing the synthesis of Smad3 (82, 83). Because there are many potential targets for a miRNA, a miRNA can also be regulated in many ways. As previously mentioned, it affects drug resistance through the PTEN-PI3K-AKT pathway and also can inhibit the EMT process by reducing the synthesis of E-calcein (48).

MiRNAs and Other Mechanisms of Resistance

In addition to the above-mentioned key factors, exosomes have been discovered as having an emerging role. Exosomes encapsulates specific signaling molecules or biologically active molecules and can transmit from one cell to another, ventually, changing the biological activity of recipient cells (84). Tumor cells with anthracyclines resistance can deliver miRNA to sensitive tumor cells through exosomes so that sensitive cells can be transformed into resistant cells. Therefore, the emergence of drug resistance is also closely related to exosomes (85). From the prespective of Chen, W.X. et al., miR-222 and miR-100 are

potential biomarkers that can be used to predic 4t drug resistance and prognosis. Moreover, upregulated miR-222 and miR-29 can be secreted from drug-resistant cells through exosomes and enter sensitive cells to infect them to endure anthracyclines (86). Among them, miR-222 was further studied to show that it can be transported from drug-resistant tumor cells to macrophages through exosomes. Finally, research showed its overall tumor cell resistance by causing inhibition of the PTEN pathway and remodeling of macrophages. Conversely, this mechanism can be used to improve medicinal properties to overcome drug resistance after anthracycline treatment of breast cancer. For example, drug-resistant cells combined with integrin and dvβ3 can deliver miR-159 through exosomes to inhibit tumor cell proliferation (87).

In addition, some miRNAs are associated with the anthracycline resistance of breast cancer cells through their unique effects. For example, miR-548p can elevate the synthesis of phenazine biosynthesis-like domain-containing protein (PBLD),which was identified as a tumor suppressor. Therefore, the overexpression of miR-548p expression restricted tumor growth and proliferation (88). miR-770 proomotes the polarization of macrophages by inhibiting the Stathmin1 (STMN1) protein, indicating that miR-770 controls the tumor microenvironment, which is conducive to reducing the drug resistance of tumor cells (89). miR-548c-3p and miR-1236-3p moderated drug resistance by inhibiting DNA damage and repair (52, 90). The downregulation of miR-149 contributes to the activation of heparinase by increasing the expression of GlcNAc N-deacetylase/N-sulfotransferase-1 (NDST1) and inducing drug resistance (91). In addition, miR-3609 causes tumor cells to become sensitive to anthracyclines through promoting the synthesis of Programmed death-ligand 1 (PDL1) (92). Meanwhile, Drug metabolizing enzymes and transporters can be inhibited by miR-148 and miR-152 to reduce the drug resistance of tumor cells (64). miR-133a plays its role in enhancing cell drug sensitivity by targeting ferritin light chain (FTL) protein (93). It has been shown that the decreasing expression of FBXW7, a tumor suppressor gene regulated by miR-188-5p, leads to the emergence of drug resistance (94).

MiRNAs and Adverse Effects

In the process of applying anthracyclines to treat breast cancer patients, many adverse reactions often emerge. Among them, cardiovascular adverse reactions are the most prominent (95). Studies have shown that when using anthracycline chemotherapy regimens, the occurrence of cardiovascular events increases the risk of patient death (96). Therefore, urgent attention is needed on the occurrence of cardiovascular adverse events clinically. Appropriate stratification of risk factors and early detection is extremely meaningful for the survival and prognosis of breast cancer patients. Thus, a large number of miRNA related research is ongoing. miRNAs clearly show an objective quantitative or expression-intensity correlation with the occurrence of adverse reactions, which may help avoid or reduce the harm caused by adverse reactions to patients. It has guiding significance in improving the prognosis. Furthermore, X-ray photography, a commonly used method in clinical diagnosis, has the unavoidable disadvantage of discomfort, overdiagnosis, and false positives. **Figure 1** shows that the different roles of above mentioned miRNAs plays in anthracyclines resistance. As a detection method of peripheral blood indicators, miRNA is more nontoxic, convenient (97).

Qin, X. et al. (98). showed that anthracyclines induce myocardium damage in three possible ways: Firstly, it increased free radicals can cause tissue lipid oxidation leading to destruction of sarcomeres and causing autophagy and

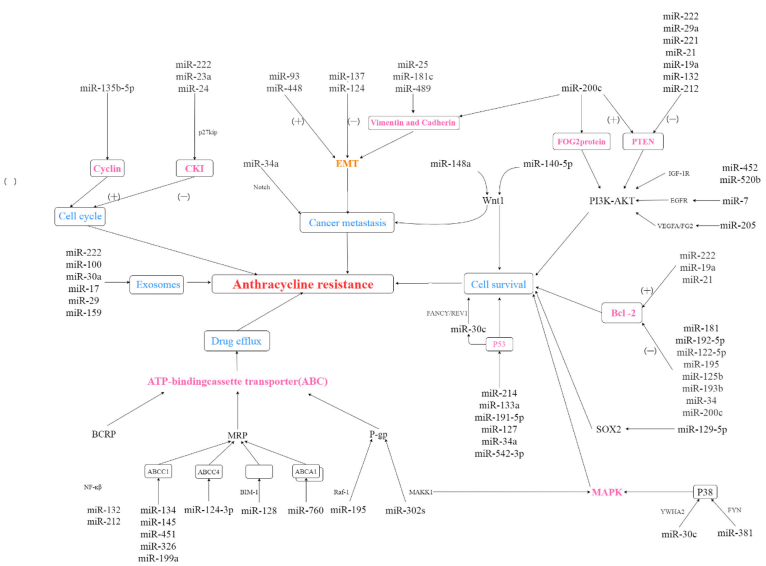

FIGURE 1 | The role of miRNAs in anthracyclines resistance. (+): microRNA promotes expression of dowmstream protein; (-): microRNA suppresses expression of dowmstream protein.

apoptosis of cardiomyocytes. The second mechanism is that it renders the death of cardiomyocytes by influencing topoisomerase II and opening the double strands of DNA of cardiomyocytes. Lastly, anthracyclines can damage myocardial fibers by inhibiting the ErbB-2 pathway (99). Anthacyclines induce early toxicity particularly in the left ventricle. The process of reconstruction is closely related to the reactivation of embryonic genes (100). miRNA can contribute to the cardiotoxicity occurrence (101).

The lethal-7 (let-7) family, a member of miRNAs, is mentioned extensivly. Upregulation of let-7a can predict the occurrence of cardiotoxicity (102). The downregulation of the expression of let-7f, a family member of let-7, signified the appearance of cardiac dysfunction because of its good correlation with N-terminal pro-B type natriuretic peptide (NT-proBNP) (98, 103). In addition to the let-7 family, miR-1 is another important biomarker, and has also been used as a clinical indicator. Expression of miR-1 implies the occurrence of arrhythmia to heart failure through a good response with left ventricular ejection fraction (LVEF) (98). Rigaud. et al. further explored its mechanism by demonstrating that miR-1 has a direct connection with the inhibition of antioxidant genes, leading to oxidative stress, promoting cardiomyocyte apoptosis, and myocardial damage (104). In another study, it was also found that miR-1 expression was increased in patients with adverse cardiotoxic reactions, possibly indicating that miR-1 was released by necrotic cardiomyocytes. miR-20a, miR-210, miR-34a, miR-126, and miR-130a are also have great potential. There is evidence that miR-20a is a dependable predictor of the occurrence of cardiotoxicity *via* the mechanism of activating angiogenesis and abnormal tumor vascular development. Another miRNA that plays a role in the development of chemoresistance, metastasis, proliferation, and self-renewal of tumor cells from hypoxic conditions is miR-210 (103). miR-34a-5p was also significantly increased after treatment with anthracyclines, which induces DNA breakage and P53 activation (105). MiR-126 also has the potential to be used to predict cardiotoxicity because it was validated to protect cardiomyocyte from apoptosis with its elevated expression (106–108). Recent findings have suggested that β-adrenergic pathway can modulate the contractile function in the heart by stimulating guanylyl nucleotide binding proteins, including adenylyl cyclase,cyclic adenosine monophosphate (cAMP), and so on (109–111). miR-30 affects the activation of the elements of the contraction coupling system by targeting the expression of β-adrenergic receptors. It was also concluded that miR-30 is a cardioprotective biomarker to monitor calcium overload and myocardial damage (112, 113).

In addition, another common adverse effect is liver metastasis. Studies have shown that miR-1-3p can mediate the occurrence of liver injury during the application of anthracyclines (4). Meanwhile, miRNA also plays a role in regulating the metastasis of breast cancer. miR-222 can promote the EMT process through the the mitogen-activated protein kinase (RAS-RAF-MEK-ERK) pathway, inducing breast cancer to be more aggressive and metastatic (68). Moreover, Deng, Z. et al. found that myelosuppressive cells (MDSC) can release miR-126a through exosomes to generate T helper 2 (Th2) cells with Interleukin-13 (IL-13) positive after Dox treatment. It promoted tumor angiogenesis, and ultimately led to breast cancer metastasis to the lungs (5). This also shows that miR-126a has the potential to predict breast cancer metastasis. **Table 1** presents the link of several miRNAs involved in response to adverse effects of anthracyclines treatment in breast cancer.

CONCLUSIONS AND OUTLOOK

There are many mechanisms and signaling pathways involved in the miRNA implications in breast cancer patients being treated with anthracyclines, and there is an abundance of possible miRNAs involved in the diagnosis, prognosis, and treatment of breast cancer patients. The study of microRNAs in regulating the resistance of anthracyclines in the treatment of breast cancer signifies that people may be able to control various types of microRNAs to overcome the shortcomings of anthracyclines application. MicroRNAs may be the key to the selection and development of personalized and safe anticancer drugs in the future. Moreover, as mentioned above, microRNAs can be used as a more accurate and safe early prediction tool, and has the potential as prognostic markers to be used in the clinic. Therefore, to overcome the challenge of providing individualized medicine in a complex disease, especially breast cancer, it is essential that more understanding of the biological effects of the various miRNAs will guide the possible direction of future academic interests.

TABLE 1 | MicroRNAs involved in response to adverse effects linked to anthracyclines treatment in breast cancer.

microRNA expression	Adverse effect	Reference
let-7a(↑)	cardiotoxicity	(102)
let-7f(↓)	cardiac dysfunction	(98, 103)
miR-1(↑)	Arrhythmia, heart failure	(98, 103, 104)
miR-20a(↑)	cardiotoxicity	(103)
miR-210(↑)	tumor metastasis	(98, 103)
miR-34a-5p(↑)	P53 activation,	(105)
	cardiotoxicity	(98)
miR-130a(↓)	myocardial damage	(98)
miR-1-3p(↑)	liver injury	(4)
miR-222(↑)	tumor metastasis	(117)
miR-126a(↑)	lung metastasis	(5)

↑, *microRNA expression increasing;* ↓, *microRNA expression decline.*

Moreover, there are many challenges in current researches. Firstly, many groups of miRNAs involving breast cancer were found by metabonomics methods (9, 114, 115). To a certain extent, these results only found a simple quantitative relationship between them. But do not provide adequate epidemiological information, such as age, the course of disease, the breast cancer type and stage, complications, the dosage and dosing interval of anthracyclines administration and so on. More importantly, most studies do not consider whether drug interactions, especially some cardioprotective drugs, have influence on the outcomes. Whether this relationship could be used as a reliable early detection indicator for the clinic is doubtful. Therefore, more effort should be invested into a more deeper study. Lastly, not only are the traditional techniques of miRNA detection complex and require special laboratory skills, but they can also generate false-positives during the amplification process (116). The optimization of methods for quantification and visualization of abnormal miRNA expression are needed for early clinical diagnosis. A more accurate and economical detection method is an absolutely need in the future.

DATA AVAILABILITY STATEMENT

The original contributions presented in the study are included in the article/supplementary material. Further inquiries can be directed to the corresponding authors.

AUTHOR CONTRIBUTIONS

ZS and WZ: conceptualization, interpretation of data, and writing original draft. SL and YW: review, interpretation of data, and editing. WZ, GZ and YZ: conceptualization, writing original draft, review, editing, and supervision. All authors contributed to the article and approved the submitted version.

FUNDING

This study was supported by the Baoan District Medical and Health Basic Research Project (2021JD054).

REFERENCES

1. Momparler RL, Karon M, Siegel SE, Avila F. Effect of Adriamycin on DNA, RNA, and Protein Synthesis in Cell-Free Systems and Lntactcells1. *Cancer Res* (1976) 36(8):2891–5.
2. Pommier Y, Leo E, Zhang H, Marchand C. DNA Topoisomerases and Their Poisoning by Anticancer and Antibacterial Drugs. *Chem Biol* (2010) 17 (5):421–33. doi: 10.1016/j.chembiol.2010.04.012
3. Vejpongsa P, Yeh ET. Prevention of Anthracycline-Induced Cardiotoxicity: Challenges and Opportunities. *J Am Coll Cardiol* (2014) 64(9):938–45. doi: 10.1016/j.jacc.2014.06.1167
4. Zhang Y, Wang D, Shen D, Luo Y, Che YQ. Identification of Exosomal miRNAs Associated With the Anthracycline-Induced Liver Injury in Postoperative Breast Cancer Patients by Small RNA Sequencing. *PeerJ* (2020) 8:e9021. doi: 10.7717/peerj.9021
5. Deng Z, Rong Y, Teng Y, Zhuang X, Samykutty A, Mu J, et al. Exosomes miR-126a Released From MDSC Induced by DOX Treatment Promotes Lung Metastasis. *Oncogene* (2017) 36(5):639–51. doi: 10.1038/onc.2016.229
6. Anglicheau D, Muthukumar T, Suthanthiran M. MicroRNAs: Small RNAs With Big Effects. *Transplantation* (2010) 90(2):105–12. doi: 10.1097/TP.0b013e3181e913c2
7. McManus MT. MicroRNAs and Cancer. *Semin Cancer Biol* (2003) 13 (4):253–8. doi: 10.1016/s1044-579x(03)00038-5
8. Holohan C, Van Schaeybroeck S, Longley DB, Johnston PG. Cancer Drug Resistance: An Evolving Paradigm. *Nat Rev Cancer* (2013) 13(10):714–26. doi: 10.1038/nrc3599
9. Li XJ, Zha QB, Ren ZJ, Tang JH, Yao YF. Mechanisms of Breast Cancer Resistance to Anthracyclines or Taxanes: An Overview of the Proposed Roles of Noncoding RNA. *Curr Opin Oncol* (2015) 27(6):457–65. doi: 10.1097/CCO.0000000000000235
10. Yadi W, Shurui C, Tong Z, Suxian C, Qing T, Dongning H. Bioinformatic Analysis of Peripheral Blood miRNA of Breast Cancer Patients in Relation With Anthracycline Cardiotoxicity. *BMC Cardiovasc Disord* (2020) 20(1):43. doi: 10.1186/s12872-020-01346-y
11. Xie M, Fu Z, Cao J, Liu Y, Wu J, Li Q, et al. MicroRNA-132 and microRNA-212 Mediate Doxorubicin Resistance by Down-Regulating the PTEN-AKT/NF-κB Signaling Pathway in Breast Cancer. *Biomed Pharmacother* (2018) 102:286–94. doi: 10.1016/j.biopha.2018.03.088
12. Turashvili G, Lightbody ED, Tyryshkin K, SenGupta SK, Elliott BE, Madarnas Y, et al. Novel Prognostic and Predictive microRNA Targets for Triple-Negative Breast Cancer. *FASEB J* (2018) 32(11):5937–54. doi: 10.1096/fj.201800120R
13. Lv J, Fu Z, Shi M, Xia K, Ji C, Xu P, et al. Systematic Analysis of Gene Expression Pattern in has-miR-760 Overexpressed Resistance of the MCF-7 Human Breast Cancer Cell to Doxorubicin. *Biomed Pharmacother* (2015) 69:162–9. doi: 10.1016/j.biopha.2014.11.028
14. Lu L, Ju F, Zhao H, Ma X. MicroRNA-134 Modulates Resistance to Doxorubicin in Human Breast Cancer Cells by Downregulating ABCC1. *Biotechnol Lett* (2015) 37(12):2387–94. doi: 10.1007/s10529-015-1941-y
15. Gao M, Miao L, Liu M, Li C, Yu C, Yan H, et al. miR-145 Sensitizes Breast Cancer to Doxorubicin by Targeting Multidrug Resistance-Associated Protein-1. *Oncotarget* (2016) 7(37):59714–26. doi: 10.18632/oncotarget.10845
16. Kovalchuk O, Filkowski J, Meservy J, Ilnytskyy Y, Tryndyak VP, Chekhun VF, et al. Involvement of microRNA-451 in Resistance of the MCF-7 Breast Cancer Cells to Chemotherapeutic Drug Doxorubicin. *Mol Cancer Ther* (2008) 7(7):2152–9. doi: 10.1158/1535-7163.Mct-08-0021
17. Liang Z, Wu H, Xia J, Li Y, Zhang Y, Huang K, et al. Involvement of miR-326 in Chemotherapy Resistance of Breast Cancer Through Modulating Expression of Multidrug Resistance-Associated Protein 1. *Biochem Pharmacol* (2010) 79(6):817–24. doi: 10.1016/j.bcp.2009.10.017
18. Chang L, Hu Z, Zhou Z, Zhang H. Linc00518 Contributes to Multidrug Resistance Through Regulating the MiR-199a/MRP1 Axis in Breast Cancer. *Cell Physiol Biochem* (2018) 48(1):16–28. doi: 10.1159/000491659
19. Hu D, Li M, Su J, Miao K, Qiu X. Dual-Targeting of miR-124-3p and ABCC4 Promotes Sensitivity to Adriamycin in Breast Cancer Cells. *Genet Test Mol Biomarkers* (2019) 23(3):156–65. doi: 10.1089/gtmb.2018.0259
20. Pearce HL, Winter MA, Beck WT. Structural Characteristics of Compounds That Modulate P-Glycoprotein-Associated Multidrug Resistance. *Adv Enzyme Regul* (1990) 30:357–73. doi: 10.1016/0065-2571(90)90026-x
21. Zhao L, Wang Y, Jiang L, He M, Bai X, Yu L, et al. MiR-302a/B/C/D Cooperatively Sensitizes Breast Cancer Cells to Adriamycin *via* Suppressing P-Glycoprotein(P-Gp) by Targeting MAP/ERK Kinase Kinase 1 (MEKK1). *J Exp Clin Cancer Res* (2016) 35:25. doi: 10.1186/s13046-016-0300-8
22. Yang G, Wu D, Zhu J, Jiang O, Shi Q, Tian J, et al. Upregulation of miR-195 Increases the Sensitivity of Breast Cancer Cells to Adriamycin Treatment Through Inhibition of Raf-1. *Oncol Rep* (2013) 30(2):877–89. doi: 10.3892/or.2013.2532
23. He H, Shao X, Li Y, Gihu R, Xie H, Zhou J, et al. Targeting Signaling Pathway Networks in Several Malignant Tumors: Progresses and Challenges. *Front Pharmacol* (2021) 12:675675. doi: 10.3389/fphar.2021.675675
24. Xie X, Hu Y, Xu L, Fu Y, Tu J, Zhao H, et al. The Role of miR-125b-Mitochondria-Caspase-3 Pathway in Doxorubicin Resistance and Therapy in Human Breast Cancer. *Tumour Biol* (2015) 36(9):7185–94. doi: 10.1007/s13277-015-3438-7

25. Zhu Y, Wu J, Li S, Ma R, Cao H, Ji M, et al. The Function Role of miR-181a in Chemosensitivity to Adriamycin by Targeting Bcl-2 in Low-Invasive Breast Cancer Cells. *Cell Physiol* (2013) 32(5):1225–37. doi: 10.1159/000354521
26. Zhang Y, He Y, Lu LL, Zhou ZY, Wan NB, Li GP, et al. miRNA-192-5p Impacts the Sensitivity of Breast Cancer Cells to Doxorubicin *via* Targeting Peptidylprolyl Isomerase a. *Kaohsiung J Med Sci* (2019) 35(1):17–23. doi: 10.1002/kjm2.12004
27. Zhang W, Jiang H, Chen Y, Ren F. Resveratrol Chemosensitizes Adriamycin-Resistant Breast Cancer Cells by Modulating miR-122-5p. *J Cell Biochem* (2019) 120(9):16283–92. doi: 10.1002/jcb.28910
28. Deng X, Cao M, Zhang J, Hu K, Yin Z, Zhou Z, et al. Hyaluronic Acid-Chitosan Nanoparticles for Co-Delivery of MiR-34a and Doxorubicin in Therapy Against Triple Negative Breast Cancer. *Biomaterials* (2014) 35(14):4333–44. doi: 10.1016/j.biomaterials.2014.02.006
29. Gioffré S, Chiesa M, Cardinale DM, Ricci V, Vavassori C, Cipolla CM, et al. Circulating MicroRNAs as Potential Predictors of Anthracycline-Induced Troponin Elevation in Breast Cancer Patients: Diverging Effects of Doxorubicin and Epirubicin. *J Clin Med* (2020) 9(5):1418. doi: 10.3390/jcm9051418
30. Long J, Ji Z, Jiang K, Wang Z, Meng G. miR-193b Modulates Resistance to Doxorubicin in Human Breast Cancer Cells by Downregulating MCL-1. *BioMed Res Int* (2015) 2015:373574. doi: 10.1155/2015/373574
31. Kopp F, Oak PS, Wagner E, Roidl A. miR-200c Sensitizes Breast Cancer Cells to Doxorubicin Treatment by Decreasing TrkB and Bmi1 Expression. *PloS One* (2012) 7(11):e50469. doi: 10.1371/journal.pone.0050469
32. Dai H, Xu LY, Qian Q, Zhu QW, Chen WX. MicroRNA-222 Promotes Drug Resistance to Doxorubicin in Breast Cancer *via* Regulation of miR-222/Bim Pathway. *Biosci Rep* (2019) 39(7):BSR20190650. doi: 10.1042/BSR20190650
33. Chen GQ, Zhao ZW, Zhou HY, Liu YJ, Yang HJ. Systematic Analysis of microRNA Involved in Resistance of the MCF-7 Human Breast Cancer Cell to Doxorubicin. *Med Oncol (Northwood London England)* (2010) 27(2):406–15. doi: 10.1007/s12032-009-9225-9
34. Zhang J, Su B, Gong C, Xi Q, Chao T. miR-214 Promotes Apoptosis and Sensitizes Breast Cancer Cells to Doxorubicin by Targeting the RFWD2-P53 Cascade. *Biochem Biophys Res Commun* (2016) 478(1):337–42. doi: 10.1016/j.bbrc.2016.07.054
35. Yuan Y, Yao YF, Hu SN, Gao J, Zhang LL. MiR-133a Is Functionally Involved in Doxorubicin-Resistance in Breast Cancer Cells MCF-7 *via* Its Regulation of the Expression of Uncoupling Protein 2. *PloS One* (2015) 10(6):e0129843. doi: 10.1371/journal.pone.0129843
36. Baffy G, Derdak Z, Robson SC. Mitochondrial Recoupling: A Novel Therapeutic Strategy for Cancer? *Br J Cancer* (2011) 105(4):469–74. doi: 10.1038/bjc.2011.245
37. Sharma S, Nagpal N, Ghosh PC, Kulshreshtha R. P53-miR-191-SOX4 Regulatory Loop Affects Apoptosis in Breast Cancer. *RNA (New York NY)* (2017) 23(8):1237–46. doi: 10.1261/rna.060657.117
38. Lin S, Yu L, Song X, Bi J, Jiang L, Wang Y, et al. Intrinsic Adriamycin Resistance in P53-Mutated Breast Cancer is Related to the miR-30c/FANCF/REV1-Mediated DNA Damage Response. *Cell Death Dis* (2019) 10(9):666. doi: 10.1038/s41419-019-1871-z
39. Wang S, Zhang J, Wang Y, Chen M. Hyaluronic Acid-Coated PEI-PLGA Nanoparticles Mediated Co-Delivery of Doxorubicin and miR-542-3p for Triple Negative Breast Cancer Therapy. *Nanomed Nanotechnol Biol Med* (2016) 12(2):411–20. doi: 10.1016/j.nano.2015.09.014
40. Gu F, Ma Y, Zhang J, Qin F, Fu L. Function of Slit/Robo Signaling in Breast Cancer. *Front Med* (2015) 9(4):431–6. doi: 10.1007/s11684-015-0416-9
41. Goncalves MD, Hopkins BD, Cantley LC. Phosphatidylinositol 3-Kinase, Growth Disorders, and Cancer. *N Engl J Med* (2018) 379(21):2052–62. doi: 10.1056/NEJMra1704560
42. Wang DD, Yang SJ, Chen X, Shen HY, Luo LJ, Zhang XH, et al. miR-222 Induces Adriamycin Resistance in Breast Cancer Through PTEN/Akt/p27 (kip1) Pathway. *Tumour Biol* (2016) 37(11):15315–24. doi: 10.1007/s13277-016-5341-2
43. Shen H, Wang D, Li L, Yang S, Chen X, Zhou S, et al. MiR-222 Promotes Drug-Resistance of Breast Cancer Cells to Adriamycin *via* Modulation of PTEN/Akt/FOXO1 Pathway. *Gene* (2017) 596:110–8. doi: 10.1016/j.gene.2016.10.016
44. Zhong S, Li W, Chen Z, Xu J, Zhao J. MiR-222 and miR-29a Contribute to the Drug-Resistance of Breast Cancer Cells. *Gene* (2013) 531(1):8–14. doi: 10.1016/j.gene.2013.08.062
45. Wang ZX, Lu BB, Wang H, Cheng ZX, Yin YM. MicroRNA-21 Modulates Chemosensitivity of Breast Cancer Cells to Doxorubicin by Targeting PTEN. *Arch Med Res* (2011) 42(4):281–90. doi: 10.1016/j.arcmed.2011.06.008
46. Rui M, Qu Y, Gao T, Ge Y, Feng C, Xu X. Simultaneous Delivery of Anti-Mir21 With Doxorubicin Prodrug by Mimetic Lipoprotein Nanoparticles for Synergistic Effect Against Drug Resistance in Cancer Cells. *Int J Nanomedicine* (2017) 12:217–37. doi: 10.2147/ijn.S122171
47. Li Q, Liu M, Ma F, Luo Y, Cai R, Wang L, et al. Circulating miR-19a and miR-205 in Serum may Predict the Sensitivity of Luminal A Subtype of Breast Cancer Patients to Neoadjuvant Chemotherapy With Epirubicin Plus Paclitaxel. *PloS One* (2014) 9(8):e104870. doi: 10.1371/journal.pone.0104870
48. Chen Y, Sun Y, Chen L, Xu X, Zhang X, Wang B, et al. miRNA-200c Increases the Sensitivity of Breast Cancer Cells to Doxorubicin Through the Suppression of E-Cadherin-Mediated PTEN/Akt Signaling. *Mol Med Rep* (2013) 7(5):1579–84. doi: 10.3892/mmr.2013.1403
49. Zhang H, Zheng XD, Zeng XH, Li L, Zhou Q. miR-520b Inhibits IGF-1R to Increase Doxorubicin Sensitivity and Promote Cell Apoptosis in Breast Cancer. *Yakugaku Zasshi* (2021) 141(3):415–26. doi: 10.1248/yakushi.20-00160
50. Hu Q, Gong JP, Li J, Zhong SL, Chen WX, Zhang JY, et al. Down-Regulation of miRNA-452 is Associated With Adriamycin-Resistance in Breast Cancer Cells. *Asian Pac J Cancer Prev* (2014) 15(13):5137–42. doi: 10.7314/apjcp.2014.15.13.5137
51. Huang Q, Wu YY, Xing SJ, Yu ZW. Effect of miR-7 on Resistance of Breast Cancer Cells to Adriamycin *via* Regulating EGFR/PI3K Signaling Pathway. *Eur Rev Med Pharmacol Sci* (2019) 23(12):5285–92. doi: 10.26355/eurrev_201906_18195
52. Tormo E, Pineda B, Serna E, Guijarro A, Ribas G, Fores J, et al. MicroRNA Profile in Response to Doxorubicin Treatment in Breast Cancer. *J Cell Biochem* (2015) 116(9):2061–73. doi: 10.1002/jcb.25162
53. Hu Y, Qiu Y, Yagüe E, Ji W, Liu J, Zhang J. miRNA-205 Targets VEGFA and FGF2 and Regulates Resistance to Chemotherapeutics in Breast Cancer. *Cell Death Dis* (2016) 7(6):e2291. doi: 10.1038/cddis.2016.194
54. Zhou B, Lin W, Long Y, Yang Y, Zhang H, Wu K, et al. Notch Signaling Pathway: Architecture, Disease, and Therapeutics. *Signal Transduct Target Ther* (2022) 7(1):95. doi: 10.1038/s41392-022-00934-y
55. Andersson ER, Sandberg R, Lendahl U. Notch Signaling: Simplicity in Design, Versatility in Function. *Development* (2011) 138(17):3593–612. doi: 10.1242/dev.063610
56. Li WJ, Wang Y, Liu R, Kasinski AL, Shen H, Slack FJ, et al. MicroRNA-34a: Potent Tumor Suppressor, Cancer Stem Cell Inhibitor, and Potential Anticancer Therapeutic. *Front Cell Dev Biol* (2021) 9:640587. doi: 10.3389/fcell.2021.640587
57. Li XJ, Ji MH, Zhong SL, Zha QB, Xu JJ, Zhao JH, et al. MicroRNA-34a Modulates Chemosensitivity of Breast Cancer Cells to Adriamycin by Targeting Notch1. *Arch Med Res* (2012) 43(7):514–21. doi: 10.1016/j.arcmed.2012.09.007
58. Salaroglio IC, Mungo E, Gazzano E, Kopecka J, Riganti C. ERK is a Pivotal Player of Chemo-Immune-Resistance in Cancer. *Int J Mol Sci* (2019) 20(10):2505. doi: 10.3390/ijms20102505
59. Sun Y, Liu WZ, Liu T, Feng X, Yang N, Zhou HF. Signaling Pathway of MAPK/ERK in Cell Proliferation, Differentiation, Migration, Senescence and Apoptosis. *J Recept Signal Transduct Res* (2015) 35(6):600–4. doi: 10.3109/10799893.2015.1030412
60. Kefalas P, Brown TR, Brickell PM. Signalling by the P60c-Src Family of Protein-Tyrosine Kinases. *Int J Biochem Cell Biol* (1995) 27(6):551–63. doi: 10.1016/1357-2725(95)00024-J
61. Mi H, Wang X, Wang F, Li L, Zhu M, Wang N, et al. miR-381 Induces Sensitivity of Breast Cancer Cells to Doxorubicin by Inactivation of MAPK Signaling *via* FYN. *Eur J Pharmacol* (2018) 839:66–75. doi: 10.1016/j.ejphar.2018.09.024
62. Fang Y, Shen H, Cao Y, Li H, Qin R, Chen Q, et al. Involvement of miR-30c in Resistance to Doxorubicin by Regulating YWHAZ in Breast Cancer Cells. *Braz J Med Biol Res* (2014) 47(1):60–9. doi: 10.1590/1414-431x20133324

63. Wu D, Zhang J, Lu Y, Bo S, Li L, Wang L, et al. miR-140-5p Inhibits the Proliferation and Enhances the Efficacy of Doxorubicin to Breast Cancer Stem Cells by Targeting Wnt1. *Cancer Gene Ther* (2019) 26(3-4):74–82. doi: 10.1038/s41417-018-0035-0
64. Chen X, Wang YW, Gao P. SPIN1, Negatively Regulated by miR-148/152, Enhances Adriamycin Resistance *via* Upregulating Drug Metabolizing Enzymes and Transporter in Breast Cancer. *J Exp Clin Cancer Res* (2018) 37(1):100. doi: 10.1186/s13046-018-0748-9
65. Zeng H, Wang L, Wang J, Chen T, Li H, Zhang K, et al. microRNA-129-5p Suppresses Adriamycin Resistance in Breast Cancer by Targeting SOX2. *Arch Biochem Biophys* (2018) 651:52–60. doi: 10.1016/j.abb.2018.05.018
66. Malumbres M, Barbacid M. Cell Cycle, CDKs and Cancer: A Changing Paradigm. *Nat Rev Cancer* (2009) 9(3):153–66. doi: 10.1038/nrc2602
67. Vermeulen K, Berneman ZN, Bockstaele DRV. Cell Cycle and Apoptosis. *Cell Prolif* (2003) 36(3):165–75. doi: 10.1046/j.1365-2184.2003.00267.x
68. Wang DD, Li J, Sha HH, Chen X, Yang SJ, Shen HY, et al. miR-222 Confers the Resistance of Breast Cancer Cells to Adriamycin Through Suppression of P27(Kip1) Expression. *Gene* (2016) 590(1):44–50. doi: 10.1016/j.gene.2016.06.013
69. Mao L, Li J, Chen WX, Cai YQ, Yu DD, Zhong SL, et al. Exosomes Decrease Sensitivity of Breast Cancer Cells to Adriamycin by Delivering microRNAs. *Tumour* (2016) 37(4):5247–56. doi: 10.1007/s13277-015-4402-2
70. Giglio S, Cirombella R, Amodeo R, Portaro L, Lavra L, Vecchione A. MicroRNA miR-24 Promotes Cell Proliferation by Targeting the CDKs Inhibitors p27Kip1 and P16ink4a. *J Cell Physiol* (2013) 228(10):2015–23. doi: 10.1002/jcp.24368
71. Sun FD, Wang PC, Luan RL, Zou SH, Du X. MicroRNA-574 Enhances Doxorubicin Resistance Through Down-Regulating SMAD4 in Breast Cancer Cells. *Eur Rev Med Pharmacol Sci* (2018) 22(5):1342–50. doi: 10.26355/eurrev_201803_14476
72. Tormo E, Ballester S, Adam-Artigues A, Burgués O, Alonso E, Bermejo B, et al. The miRNA-449 Family Mediates Doxorubicin Resistance in Triple-Negative Breast Cancer by Regulating Cell Cycle Factors. *Sci Rep* (2019) 9 (1):5316. doi: 10.1038/s41598-019-41472-y
73. Zhang Y, Xia F, Zhang F, Cui Y, Wang Q, Liu H, et al. miR-135b-5p Enhances Doxorubicin-Sensitivity of Breast Cancer Cells Through Targeting Anterior Gradient 2. *J Exp Clin Cancer Res* (2019) 38(1):26. doi: 10.1186/s13046-019-1024-3
74. Pastushenko I, Blanpain C. EMT Transition States During Tumor Progression and Metastasis. *Trends Cell Biol* (2019) 29(3):212–26. doi: 10.1016/j.tcb.2018.12.001
75. Du B, Shim JS. Targeting Epithelial-Mesenchymal Transition (EMT) to Overcome Drug Resistance in Cancer. *Molecules* (2016) 21(7):965. doi: 10.3390/molecules21070965
76. Chu S, Liu G, Xia P, Chen G, Shi F, Yi T, et al. miR-93 and PTEN: Key Regulators of Doxorubicin-Resistance and EMT in Breast Cancer. *Oncol Rep* (2017) 38(4):2401–7. doi: 10.3892/or.2017.5859
77. Du F, Yu L, Wu Y, Wang S, Yao J, Zheng X, et al. miR-137 Alleviates Doxorubicin Resistance in Breast Cancer Through Inhibition of Epithelial-Mesenchymal Transition by Targeting DUSP4. *Cell Death Dis* (2019) 10 (12):922. doi: 10.1038/s41419-019-2164-2
78. Liu C, Xing H, Guo C, Yang Z, Wang Y, Wang Y. MiR-124 Reversed the Doxorubicin Resistance of Breast Cancer Stem Cells Through STAT3/HIF-1 Signaling Pathways. *Cell Cycle (Georgetown Tex)* (2019) 18(18):2215–27. doi: 10.1080/15384101.2019.1638182
79. Li QQ, Chen ZQ, Cao XX, Xu JD, Xu JW, Chen YY, et al. Involvement of NF-κb/miR-448 Regulatory Feedback Loop in Chemotherapy-Induced Epithelial-Mesenchymal Transition of Breast Cancer Cells. *Cell Death Differ* (2011) 18(1):16–25. doi: 10.1038/cdd.2010.103
80. Zhou Y, Hu Y, Yang M, Jat P, Li K, Lombardo Y, et al. The miR-106b~25 Cluster Promotes Bypass of Doxorubicin-Induced Senescence and Increase in Motility and Invasion by Targeting the E-Cadherin Transcriptional Activator EP300. *Cell Death Differ* (2014) 21(3):462–74. doi: 10.1038/cdd.2013.167
81. Han B, Huang J, Han Y, Hao J, Wu X, Song H, et al. The microRNA miR-181c Enhances Chemosensitivity and Reduces Chemoresistance in Breast Cancer Cells *via* Down-Regulating Osteopontin. *Int J Biol Macromol* (2019) 125:544–56. doi: 10.1016/j.ijbiomac.2018.12.075
82. He DX, Gu F, Gao F, Hao JJ, Gong D, Gu XT, et al. Genome-Wide Profiles of Methylation, microRNAs, and Gene Expression in Chemoresistant Breast Cancer. *Sci Rep* (2016) 6:24706. doi: 10.1038/srep24706
83. Jiang L, He D, Yang D, Chen Z, Pan Q, Mao A, et al. MiR-489 Regulates Chemoresistance in Breast Cancer *via* Epithelial Mesenchymal Transition Pathway. *FEBS Lett* (2014) 588(11):2009–15. doi: 10.1016/j.febslet.2014.04.024
84. Kalluri R, LeBleu VS. The Biology, Function, and Biomedical Applications of Exosomes. *Science* (2020) 367(6478):3. doi: 10.1126/science.aau6977
85. Chen WX, Liu XM, Lv MM, Chen L, Zhao JH, Zhong SL, et al. Exosomes From Drug-Resistant Breast Cancer Cells Transmit Chemoresistance by a Horizontal Transfer of microRNAs. *PloS One* (2014) 9(4):e95240. doi: 10.1371/journal.pone.0095240
86. Zhong S, Chen X, Wang D, Zhang X, Shen H, Yang S, et al. MicroRNA Expression Profiles of Drug-Resistance Breast Cancer Cells and Their Exosomes. *Oncotarget* (2016) 7(15):19601–9. doi: 10.18632/oncotarget.7481
87. Gong C, Tian J, Wang Z, Gao Y, Wu X, Ding X, et al. Functional Exosome-Mediated Co-Delivery of Doxorubicin and Hydrophobically Modified microRNA 159 for Triple-Negative Breast Cancer Therapy. *J Nanobiotechnology* (2019) 17(1):93. doi: 10.1186/s12951-019-0526-7
88. Liang Y, Song X, Li Y, Su P, Han D, Ma T, et al. cirCKDM4C Suppresses Tumor Progression and Attenuates Doxorubicin Resistance by Regulating miR-548p/PBLD Axis in Breast Cancer. *Oncogene* (2019) 38(42):6850–66. doi: 10.1038/s41388-019-0926-z
89. Li Y, Liang Y, Sang Y, Song X, Zhang H, Liu Y, et al. MiR-770 Suppresses the Chemo-Resistance and Metastasis of Triple Negative Breast Cancer *via* Direct Targeting of STMN1. *Cell Death Dis* (2018) 9(1):14. doi: 10.1038/s41419-017-0030-7
90. Hao J, Du X, Lv F, Shi Q. Knockdown of Circ_0006528 Suppresses Cell Proliferation, Migration, Invasion, and Adriamycin Chemoresistance *via* Regulating the miR-1236-3p/CHD4 Axis in Breast Cancer. *J Surg Res* (2021) 260:104–15. doi: 10.1016/j.jss.2020.10.031
91. He DX, Gu XT, Li YR, Jiang L, Jin J, Ma X. Methylation-Regulated miR-149 Modulates Chemoresistance by Targeting GlcNAc N-Deacetylase/N-Sulfotransferase-1 in Human Breast Cancer. *FEBS J* (2014) 281(20):4718–30. doi: 10.1111/febs.13012
92. Li D, Wang X, Yang M, Kan Q, Duan Z. Mir3609 Sensitizes Breast Cancer Cells to Adriamycin by Blocking the Programmed Death-Ligand 1 Immune Checkpoint. *Exp Cell Res* (2019) 380(1):20–8. doi: 10.1016/j.yexcr.2019.03.025
93. Chekhun VF, Lukyanova NY, Burlaka CA, Bezdenezhnykh NA, Shpyleva SI, Tryndyak VP, et al. Iron Metabolism Disturbances in the MCF-7 Human Breast Cancer Cells With Acquired Resistance to Doxorubicin and Cisplatin. *Int J Oncol* (2013) 43(5):1481–6. doi: 10.3892/ijo.2013.2063
94. Yi X, Lou L, Wang J, Xiong J, Zhou S. Honokiol Antagonizes Doxorubicin Resistance in Human Breast Cancer *via* miR-188-5p/FBXW7/c-Myc Pathway. *Cancer Chemother Pharmacol* (2021) 87(5):647–56. doi: 10.1007/s00280-021-04238-w
95. Gianni L, Herman EH, Lipshultz SE, Minotti G, Sarvazyan N, Sawyer DB. Anthracycline Cardiotoxicity: From Bench to Bedside. *J Clin Oncol* (2008) 26 (22):3777–84. doi: 10.1200/JCO.2007.14.9401
96. Cardinale D, Colombo A, Bacchiani G, Tedeschi I, Meroni CA, Veglia F, et al. Early Detection of Anthracycline Cardiotoxicity and Improvement With Heart Failure Therapy. *Circulation* (2015) 131(22):1981–8. doi: 10.1161/CIRCULATIONAHA.114.013777
97. Nassar FJ, Chamandi G, Tfaily MA, Zgheib NK, Nasr R. Peripheral Blood-Based Biopsy for Breast Cancer Risk Prediction and Early Detection. *Front Med (Lausanne)* (2020) 7:28. doi: 10.3389/fmed.2020.00028
98. Qin X, Chang F, Wang Z, Jiang W. Correlation of Circulating Pro-Angiogenic miRNAs With Cardiotoxicity Induced by Epirubicin/Cyclophosphamide Followed by Docetaxel in Patients With Breast Cancer. *Cancer Biomarkers section A Dis markers.* (2018) 23(4):473–84. doi: 10.3233/cbm-181301
99. Sawyer DB, Peng X, Chen B, Pentassuglia L, Lim CC. Mechanisms of Anthracycline Cardiac Injury: Can We Identify Strategies for Cardioprotection? *Prog Cardiovasc Dis* (2010) 53(2):105–13. doi: 10.1016/j.pcad.2010.06.007

100. Roca-Alonso L, Pellegrino L, Castellano L, Stebbing J. Breast Cancer Treatment and Adverse Cardiac Events: What are the Molecular Mechanisms? *Cardiology* (2012) 122(4):253–9. doi: 10.1159/000339858
101. Fa HG, Chang WG, Zhang XJ, Xiao DD, Wang JX. Noncoding RNAs in Doxorubicin-Induced Cardiotoxicity and Their Potential as Biomarkers and Therapeutic Targets. *Acta Pharmacol Sin* (2021) 42(4):499–507. doi: 10.1038/s41401-020-0471-x
102. Todorova VK, Makhoul I, Wei J, Klimberg VS. Circulating miRNA Profiles of Doxorubicin-Induced Cardiotoxicity in Breast Cancer Patients. *Ann Clin Lab Sci* (2017) 47(2):115–9.
103. Pereira JD, Tosatti JAG, Simões R, Luizon MR, Gomes KB, Alves MT. microRNAs Associated to Anthracycline-Induced Cardiotoxicity in Women With Breast Cancer: A Systematic Review and Pathway Analysis. *Biomed Pharmacother* (2020) 131:110709. doi: 10.1016/j.biopha.2020.110709
104. Rigaud VO, Ferreira LR, Ayub-Ferreira SM, Ávila MS, Brandão SM, Cruz FD, et al. Circulating miR-1 as a Potential Biomarker of Doxorubicin-Induced Cardiotoxicity in Breast Cancer Patients. *Oncotarget* (2017) 8 (4):6994–7002. doi: 10.18632/oncotarget.14355
105. Frères P, Bouznad N, Servais L, Josse C, Wenric S, Poncin A, et al. Variations of Circulating Cardiac Biomarkers During and After Anthracycline-Containing Chemotherapy in Breast Cancer Patients. *BMC Cancer* (2018) 18(1):102. doi: 10.1186/s12885-018-4015-4
106. An Q, Han C, Zhou Y, Li F, Li D, Zhang X, et al. Matrine Induces Cell Cycle Arrest and Apoptosis With Recovery of the Expression of miR-126 in the A549 non-Small Cell Lung Cancer Cell Line. *Mol Med Rep* (2016) 14 (5):4042–8. doi: 10.3892/mmr.2016.5753
107. Zhu Z, Li X, Dong H, Ke S, Zheng WH. Let-7f and miRNA-126 Correlate With Reduced Cardiotoxicity Risk in Triple-Negative Breast Cancer Patients Who Underwent Neoadjuvant Chemotherapy. *Int J Clin Exp Pathol* (2018) 11(10):4987–95.
108. Luo Q, Guo D, Liu G, Chen G, Hang M, Jin M. Exosomes From MiR-126-Overexpressing Adscs Are Therapeutic in Relieving Acute Myocardial Ischaemic Injury. *Cell Physiol Biochem* (2017) 44(6):2105–16. doi: 10.1159/000485949
109. Xiao RP. β-Adrenergic Signaling in the Heart: Dual Coupling of the β2-Adrenergic Receptor to Gs and Gi Proteins. *Sci STKE* (2001) 104:re15. doi: 10.1126/stke.2001.104.re15
110. Yang J, Liu Y, Fan X, Li Z, Cheng Y. A Pathway and Network Review on Beta-Adrenoceptor Signaling and Beta Blockers in Cardiac Remodeling. *Heart Fail Rev* (2014) 19(6):799–814. doi: 10.1007/s10741-013-9417-4
111. Najafi A, Sequeira V, Kuster DW, van der Velden J. Beta-Adrenergic Receptor Signalling and its Functional Consequences in the Diseased Heart. *Eur J Clin Invest* (2016) 46(4):362–74. doi: 10.1111/eci.12598
112. Saddic LA, Muehlschlegel JD. Sarco"MiR" Friend or Foe: A Perspective on the Mechanisms of Doxorubicin-Induced Cardiomyopathy. *Ann Trans Med* (2016) 4(10):203. doi: 10.21037/atm.2016.05.30
113. Roca-Alonso L, Castellano L, Mills A, Dabrowska AF, Sikkel MB, Pellegrino L, et al. Myocardial MiR-30 Downregulation Triggered by Doxorubicin Drives Alterations in Beta-Adrenergic Signaling and Enhances Apoptosis. *Cell Death Dis* (2015) 6:e1754. doi: 10.1038/cddis.2015.89
114. Bertoli G, Cava C, Castiglioni I. MicroRNAs: New Biomarkers for Diagnosis, Prognosis, Therapy Prediction and Therapeutic Tools for Breast Cancer. *Theranostics* (2015) 5(10):1122–43. doi: 10.7150/thno.11543
115. Kahraman M, Roske A, Laufer T, Fehlmann T, Backes C, Kern F, et al. MicroRNA in Diagnosis and Therapy Monitoring of Early-Stage Triple-Negative Breast Cancer. *Sci Rep* (2018) 8(1):11584. doi: 10.1038/s41598-018-29917-2
116. Ye J, Xu M, Tian X, Cai S, Zeng S. Research Advances in the Detection of miRNA. *J Pharm Anal* (2019) 9(4):217–26. doi: 10.1016/j.jpha.2019.05.004
117. Chen WX, Wang DD, Zhu B, Zhu YZ, Zheng L, Feng ZQ, et al. Exosomal miR-222 From Adriamycin-Resistant MCF-7 Breast Cancer Cells Promote Macrophages M2 Polarization *via* PTEN/Akt to Induce Tumor Progression. *Aging* (2021) 13(7):10415–30. doi: 10.18632/aging.202802

Conflict of Interest: The authors declare that the research was conducted in the absence of any commercial or financial relationships that could be construed as a potential conflict of interest.

Publisher's Note: All claims expressed in this article are solely those of the authors and do not necessarily represent those of their affiliated organizations, or those of the publisher, the editors and the reviewers. Any product that may be evaluated in this article, or claim that may be made by its manufacturer, is not guaranteed or endorsed by the publisher.

Copyright © 2022 Si, Zhong, Lao, Wu, Zhong and Zeng. This is an open-access article distributed under the terms of the Creative Commons Attribution License (CC BY). The use, distribution or reproduction in other forums is permitted, provided the original author(s) and the copyright owner(s) are credited and that the original publication in this journal is cited, in accordance with accepted academic practice. No use, distribution or reproduction is permitted which does not comply with these terms.

frontiers | Frontiers in Oncology

ORIGINAL RESEARCH
published: 19 May 2022
doi: 10.3389/fonc.2022.870840

Characterization of the Estrogen Response Helps to Predict Prognosis and Identify Potential Therapeutic Targets in Cholangiocarcinoma

Chenglin Lu[1†], Ji Miao[1†], Minhuan Li[2†], Qisi Zheng[3†], Feng Xu[6], Yiming Pan[1], Yizhou Wang[1], Zhi Yang[1], Xuefeng Xia[1], Hao Zhu[5], Jie Chen[4*] and Shanhua Bao[1*]*

[1] Department of General Surgery, Nanjing Drum Tower Hospital, The Affiliated Hospital of Nanjing University Medical School, Nanjing, China, [2] Department of Andrology, Nanjing Drum Tower Hospital, The Affiliated Hospital of Nanjing University Medical School, Nanjing, China, [3] Department of Laboratory Medicine, Nanjing Drum Tower Hospital, The Affiliated Hospital of Nanjing University Medical School, Nanjing, China, [4] Department of Anesthesiology, Nanjing Drum Tower Hospital, The Affiliated Hospital of Nanjing University Medical School, Nanjing, China, [5] Department of Gastroenterology, Nanjing Drum Tower Hospital, The Affiliated Hospital of Nanjing University Medical School, Nanjing, China, [6] Department of General Surgery, Changshu NO.1 People's Hospital, The Affiliated Hospital of Soochow University, Changshu, China

Cholangiocarcinoma (CCA) is an aggressive malignancy originating from the epithelium of the bile duct. The prognosis of patients is poor regardless of radical resection and chemoradiotherapy. The current classification and prognostic model of CCA are unable to satisfy the requirements for predicting the clinical outcome and exploring therapeutic targets. Estrogen signaling is involved in diverse cancer types, and it has long been established that CCA could be regulated by estrogen. In our study, estrogen response was identified to be significantly and stably correlated with poor prognosis in CCA. Employing several algorithms, CCA was classified into ES cluster A and B. ES cluster B was mainly composed of patients with fluke infection and overlapped with CCA cluster 1/2, and ES cluster A was mainly composed of patients without fluke infection and overlapped with CCA cluster 3/4. COMT and HSD17B1 were identified to be responsible for the differential estrogen response between ES clusters A and B, and the estrogen response may be correlated with the differentiation and cancer stemness of CCA at the single-cell level. Complement activation and the expression of C3 and C5, which are mainly expressed by CCA cells, were significantly downregulated in ES cluster B. An estrogen response risk score (ESRS) model was constructed to predict the prognosis of CCA, followed by a nomogram integrating ESRS and clinical features. Finally, altered pathways, applicable drugs and sensitivity to chemical drugs were analyzed specific to the estrogen response. In summary, our results provide insights into the role of the estrogen response in CCA progression as well as applicable drugs and potential therapeutic targets in estrogen metabolism, the complement system and ESRS-related pathways.

Keywords: Cholangiocarcinoma, estrogen response, estrogen metabolism, complement activation, chemotherapeutic targets

OPEN ACCESS

Edited by:
Shaoquan Zheng, Sun Yat-sen University Cancer Center (SYSUCC), China

Reviewed by:
Wei Chen, Zhejiang Academy of Traditional Chinese Medicine, China
Xing Huang, Zhejiang University, China
Longyun Ye, Fudan University, China
Wanxiang Wang, Inner Mongolia International Hospital, China

***Correspondence:**
Shanhua Bao
shanhua_bao@126.com
Jie Chen
jiechen028@163.com
Hao Zhu
zhuhao0918@126.com

†These authors contributed equally to this work and share first authorship

Specialty section:
This article was submitted to Molecular and Cellular Oncology, a section of the journal Frontiers in Oncology

Received: *07 February 2022*
Accepted: *19 April 2022*
Published: *19 May 2022*

Citation:
Lu C, Miao J, Li M, Zheng Q, Xu F, Pan Y, Wang Y, Yang Z, Xia X, Zhu H, Chen J and Bao S (2022) Characterization of the Estrogen Response Helps to Predict Prognosis and Identify Potential Therapeutic Targets in Cholangiocarcinoma. Front. Oncol. 12:870840. doi: 10.3389/fonc.2022.870840

INTRODUCTION

Cholangiocarcinoma (CCA) is one of the most malignant cancers derived from cholangiocytes of the bile duct (1, 2). The epidemiology of CCA varies around the world. Fluke infection is the leading cause of CCA in some regions, such as Thailand (3). In the Western world, primary sclerosing cholangitis (PSC) is the only identifiable risk factor (4). CCA can be subdivided into intrahepatic (iCCA), perihilar (pCCA), and distal CCA (dCCA) according to anatomic location and differential treatment (5). Surgery is the preferred treatment for early resectable CCA. Most patients with CCA are diagnosed at late stages due to a lack of obvious symptoms (~70%), and only 25% of them are recommended for surgery (6, 7). Unfortunately, patients with unresectable CCA share a median overall survival time of less than 1 year (8). For patients after radical resection of CCA, the 5-year overall survival is lower than 30% (9). In addition, current radiotherapy and chemotherapy show limited effects on patients with CCA (8). Existing CCA classification is mainly based on anatomic location or pathologic features. Until recently, the International Cancer Genome Consortium classified CCA into CCA clusters 1-4 based on integrated analysis of genomic, epigenomic, and transcriptomic information of nearly 500 CCAs from 10 countries, which provided insights into the mechanisms of tumorigenesis of CCA as well as potential therapeutic targets (10). Further studies in the classification and characterization of CCA are necessary and instrumental in breaking the predicament of the poor prognosis of patients with CCA.

Beyond physiological functions in regulating the menstrual cycle, reproduction, bone density, brain function and cholesterol mobilization, estrogen is associated with the development and progression of various types of cancer, such as cancers in the breast, ovary, endometrium, colon, prostate and lung (11). The role of estrogen also varies among different cancer types, which are mediated by the activation of the different estrogen receptor (ER) subtypes: ERα and ERβ. Generally, ERα is involved in proliferation, inflammation and tumorigenesis and is responsible for the adverse effect of estrogen. ERβ is involved in the suppression of proliferation, differentiation and apoptosis and is responsible for the beneficial effect of estrogen (12). Estrogen also plays an important role in the tumor immune microenvironment (TIME). For instance, estrogen may promote the accumulation of myeloid-derived suppressor cells (MDSCs) and impair the antitumor effect of $CD8^+$ T cells (13). In addition, the aberrant estrogen effect could also arise from the fluctuation of estrogen concentration by change of endogenous or exogenous estrogen or the disorder of estrogen metabolism. For example, under chronic inflammatory conditions, steroid sulfatase (STS), which can catalyze inactive estrogen sulfates to active estrogen, is upregulated, thus increasing the concentration of active estrogen in chronic liver disease (12).

Both ERα and ERβ are expressed in cholangiocytes (14, 15). Substantial evidence shows that estrogen promotes carcinogenesis and the development of CCA, and selective modulation of estrogen receptors could inhibit the growth of CCA (16–19). In addition, a meta-analysis enrolling 1,107,498 women of 12 North American-based cohort studies suggested that long-term use of oral contraceptives with only estrogen may be associated with an increased iCCA risk (20).

Until recently, however, the whole picture of the complexity of the estrogen response in CCA has remained obscure and largely incomplete. To what extent the estrogen response could influence CCA progression has not been determined. With the development of high-throughput sequencing and bioinformatic technologies, we are equipped to evaluate the level of estrogen response of CCA samples and even single cells. In this study, we systematically characterized the estrogen response in CCA. Furthermore, we will explore the mechanism of the differential estrogen response, the role of the estrogen response in the TIME and potential targets specific to the estrogen response (**Supplementary Figure 1**).

MATERIALS AND METHODS

Data Gathering and Preprocessing

In our investigation, four microarray datasets from the GEO database (https://www.ncbi.nlm.nih.gov/gds/), including GSE26566, GSE33327, GSE76297 and GSE89749, a microarray dataset from the ArrayExpress database (https://www.ebi.ac.uk/arrayexpress/) named E-MTAB-6389, and an RNA-sequencing dataset from The Cancer Genome Atlas (TCGA, https://portal.gdc.cancer.gov/) named TCGA-CHOL, were downloaded. In brief, primary microarray data sets were preprocessed with background adjustment and normalization employing the R package for microarray data processing (21). Probe IDs or ensembl gene IDs were transferred into gene symbols according to the corresponding annotation file, and the median value was selected to represent the expression value for gene symbols with multiple probes. All the expression data enrolled in this study were log2 transformed. Only the survival information of the GSE89749 cohort, E-MTAB-6389 cohort and TCGA-CHOL cohort was publicly accessible. In addition, a single-cell sequencing dataset for 5 iCCA samples was also retrieved from the GEO database, named GSE138709 (22). Basic information on the datasets used in this study is summarized in **Supplementary Table S1**.

Weighted Gene Coexpression Network Analysis

All microarray datasets of CCA samples, including GSE26566 (n = 104), GSE33327 (n = 149), GSE76297 (n = 91), GSE89749 (n = 118) and E-MTAB-6389 (n = 78), were merged and followed with bath correction. The expression of the top 30% genes with the highest variance in the merged dataset was performed with WGCNA utilizing the R package WGCNA 1.70.3. First, the optimal soft thresholding power β of five was selected to construct a scale-free network topology. Then, a topological overlap matrix (TOM) was generated out of the adjacency matrix to calculate the corresponding dissimilarity. Genes were hierarchically clustered to produce a dendrogram that was divided into different gene modules using the dynamic tree cut method. The eigengene was calculated to represent each module,

and the most relevant gene module for specific traits was evaluated by Spearman correlation analysis.

Gene Set Enrichment Analysis and Gene Set Variation Analysis

The hallmark gene sets, biological processes and canonical pathways were downloaded from the Molecular Signatures Database (MSigDB, http://www.gsea-msigdb.org/gsea/index.jsp). GSEA was performed to demonstrate the altered biological processes or canonical pathways between different patient groups. The R package fgsea 1.18.0 was employed to carry out the GSEA and plot the results. GSVA was performed to evaluate the relative level of specific biological processes for a single sample. The R package GSVA 1.40.1 was employed to evaluate the GSVA score for each sample with the "ssgsea" method.

Single Cell Data Processing

For the analysis of single-cell sequencing data, the R package Seurat 4.0.5 was used to process the raw data of GSE138709 (23). Only CCA samples of GSE138709 were loaded followed by filtration with the criteria of >20% mitochondria-related genes and more than 1,000 genes.

Expressed per cell. A total of 17,090 cells were selected for subsequent analysis. After data normalization, identification of variable features and principal component analysis (PCA) dimensional reduction, the dataset was batch corrected by the "RunHarmony" function of the R package 0.1.0 All the cells were clustered into 16 cell populations using the "FindClusters" function of Seurat (resolution = 0.5). TSNE dimensionality reduction was performed to generate the TSNE plot. The annotation of the cell clusters was fulfilled by the R package singleR 1.6.1 and adjusted by signatures from the original publication (22). EPCAM, KRT7, KRT19, ANXA4 and TM4SF4 were chosen as markers for CCA cells. The AUCell score of specific gene sets for single cells was calculated using the R package irGSEA 1.0.0. Monocle 2.30.0 was employed to perform the cell trajectory analysis.

Survival Analyses

The survival curves were plotted with the R package survminer 0.4.9. In brief, the Kaplan–Meier method was employed for the drawing, and the log-rank test was used for evaluation of differences in survival. The best cutoff value of parameters was calculated by the 'surv_cutpoint' function. The R package survivalROC 1.0.3 was used to plot the time-dependent receiver operating characteristic curve (ROC) for prognostic factors.

Establishment of the Estrogen Response-Related Score

First, the GSE89749 cohort and E-MTAB-6389 cohort were merged and followed with batch correction. Samples without valid survival information were removed. Then, the merged dataset was randomly divided into a training cohort (n = 128) and a testing cohort (n = 55) at a ratio of 7:3 *via* the "sample" function in R. Subsequently, we performed univariate Cox regression for genes in the gene set "Estrogen response late" using the "coxph" function of the R package survival 3.2.13, and 65 genes with a p value less than 0.1 were included in the least absolute shrinkage and selection operator (LASSO) regression by the R package glmnet 4.1.2. In our model, 11 genes maintained their Cox coefficients under a tuned penalty parameter (λ). The ESRS was established based on multivariate regression of the selected genes. The stability of the model was further tested in the testing cohort. We also integrated the ESRS with the clinical information of CCA patients to construct a nomogram with the R package regplot 1.1. A calibration curve was plotted to check the veracity of the nomogram using the R package rms 6.2.0.

Additional Bioinformatics and Statistical Analyses

The differential expression of genes between patient groups was calculated using the R package limma 3.48.3. Correlation analysis was performed using the R package Hmisc 4.6.0. The immune infiltration of 22 types of immune cells was estimated by the R package Cibersort at 1,000 permutations. Unsupervised clustering analysis was carried out to define the optimal clustering of CCA samples based on the expression of genes related to the estrogen response by the R package ConsensusClusterPlus 1.56.0 at 1,000 permutations, and the R package Rtsne 0.15 was employed to visualize the clustering. The protein–protein interaction (PPI) networks were constructed by the STRING database (https://cn.string-db.org/) and visualized by Cytoscape 3.8.2 software. The network of biological processes based on genes in estrogen response-related genes was generated by ClueGO, a plug-in of Cytoscape. A connectivity map (CMap) was employed to identify potential targets and drugs for the ESRS_high group. The IC50 of each chemical compound of each cancer cell line along with the RNA sequencing data of all the cancer cell lines were downloaded from the Genomics of Drug Sensitivity in Cancer database (GDSC, https://www.cancerrxgene.org/) To which drugs the CCA patients with high estrogen response are sensitive or resistant is evaluated by Spearman correlation analysis between the GSVA score of "Estrogen response late" and IC50 of the drugs in all cancer cell lines.

For comparison of two groups, Student's t test and Wilcoxon rank-sum tests were employed to estimate the statistical significance of normally distributed and nonnormally distributed variables, respectively. For comparisons of more than two groups, Kruskal–Wallis tests were used. Differences with $p < 0.05$ were considered statistically significant. Statistical p value (*, $P < 0.05$; **, $P < 0.01$; ***, $P < 0.001$; ****, $P<0.0001$; ns, not significant).

RESULTS

Identification of an Estrogen Response-Related Gene Set

First, the GSE89749 cohort containing 118 CCA samples was chosen as the discovery cohort due to the appropriate sample size and clinical information. Then, we scored the active level of all the

hallmark gene sets utilizing the GSVA algorithm, and the result was further subjected to univariate Cox regression. It showed that "Estrogen response late" along with "Estrogen response early" were significantly correlated with poor prognosis (**Figure 1A**). These two gene sets were curated by MSigDB according to transcriptomic alterations in early (within 6 hours) or late (over 12 hours) stage of cellular response to estrogen. The Kaplan–Meier curves for the GSVA score of these two gene sets in the GSE89749 cohort, E-MTAB-6389 cohort and TCGA-CHOL cohort were plotted, and only "Estrogen response late" showed stable predictive capability for prognosis (**Figure 1B**, HR=4.02, log-rank test p value= 1.7×10^{-5}; **Supplementary Figures 2A–E**). Through dimensionality reduction of 200 genes in "Estrogen response late" for 32 types of cancer in TCGA cohort, we found that the response to estrogen differs in almost all cancer types (**Supplementary Figure 2F**). Additionally, the prognostic value of the GSVA score of "Estrogen response late" varies among different solid cancer types, and the hazard ratio of which in CCA was highest of all the solid cancer types. Meanwhile, we investigated the difference in estrogen response score between non-tumoral and tumoral tissues in those cohorts with considerable sample size of normal bile duct tissues. Surprisingly, the estrogen response was stably upregulated in CCA tumor tissues, which further indicates the role of estrogen response in CCA progression (**Figures 1C, D**).

Subsequently, a scale-free coexpression network was established from the expression matrix of the GSE89749 cohort with the WGCNA algorithm. Genes were divided into 11 gene modules according to a similar expression pattern, and the green module was significantly correlated with the GSVA score of "Estrogen response late" (r=0.66, $p=2\times10^{-58}$) and "Estrogen response early" (r=0.61, $p=8\times10^{-49}$) (**Figures 1E–G**). Therefore, genes in the green module were identified as estrogen response-related genes (ESRGs). To determine the molecular function of ESRGs, gene enrichment analysis was performed and the results demonstrated that digestion, neutrophil activation and epithelial cell differentiation were among the top enriched biological processes (**Figure 1H**).

Clinical and Transcriptomic Characteristics of Estrogen Response in the GSE89749 Cohort

Then, to investigate the clinical features of estrogen response, we attempted to cluster the CCA samples into different clusters on the basis of the expression of ESRGs in 118 CCA samples in the GSE89749 cohort. These samples were divided into two clusters (ES cluster A, n = 52; ES cluster B, n = 66) according to the optimal clustering chosen by delta area (**Figure 2A**, **Supplementary Figure 3A**). The UMAP plot based on dimensionality reduction of ESRGs indicated that these two clusters exhibited great transcriptome heterogeneity (**Figure 2B**). These two clusters showed significant differences in response to estrogen (**Figure 2C**) and overall survival probability (**Figure 2D**, HR = 2.99, log-rank p value = 5.8×10^{-5}). Furthermore, the expression of genes in "Estrogen response late" also differed between the two clusters (**Figure 2E**).

The different clinical classification constitutions of the two ES clusters and the GSVA score of "Estrogen response late" in different clinical classifications were analysed (**Figure 2E**, **Supplementary Figure 3B**, **Supplementary Table S2**). ES cluster B contained the majority of people with fluke infection. Fluke infection is supposed to be a major cause of CCA in some regions, such as Thailand (3). Fluke infection could cause mechanical damage to cholangiocytes as well as chronic inflammation (24). Abnormal estrogen metabolism has long been detected in chronic liver disease (25). It has been reported that estrogen can act as an anti-inflammatory hormone and that STS chronic inflammation induced by chronic inflammation can increase the level of estrogen, which in turn alleviates the inflammatory response (26). Therefore, we hypothesized that the chronic inflammation caused by fluke infection may be responsible for the higher estrogen response in ES cluster B. In addition, ES cluster B was mainly composed of eCCA, which is mostly caused by fluke infection, and well-differentiated CCA (**Figure 2F**). The GSE89749 cohort was classified into 4 distinct CCA subtypes based on multiomics data (10). Our results indicated that CCA cluster 1 and 2 had higher GSVA scores for "Estrogen response late" than CCA cluster 3 and 4 (**Figure 2G**). Meanwhile, ES cluster A was mainly composed of CCA clusters 3 and 4, and ES cluster B was mainly composed of CCA clusters 1 and 2 (**Figure 2H**). As reported, CCA cluster 1/2 was enriched in ERBB2 amplifications and TP53 mutations. In addition, CCA cluster 3/4 are characterized by high copy number alterations and expression of PD-1/PD-L2 or epigenetic changes (IDH1/2, BAP1) along with FGFR/PRKA-related gene rearrangements. The overlaps of ES clusters and CCA subtypes indicated the potential of ES clusters in selecting personalized treatment, for example, promising IDH inhibitors (ClinicalTrials.gov identifier: NCT02073994). In addition, CCA had also been classified into "Inflammation" and "Proliferation" subtypes based on multiomics data (27). The inflammation-related class shows enrichment of inflammation and cytokine pathway, like overexpression of IL-6, IL-10, IL-17, and STAT3 constitutive activation, while the proliferation-related class shows more aggressive behavior, reflected by earlier recurrence and an enrichment of several oncogenic pathways, such as RTK signaling and angiogenesis-related pathways, and gene signatures of poor prognosis. Our results showed that the proliferation-related class showed significantly higher estrogen response than that in inflammation-related class (**Supplementary Figure 3C**).

We also analyzed the difference in biological processes between ES cluster A and ES cluster B (**Supplementary Figure 3D**). O-GlcNAcylation and glycosylation were significantly enriched in ES cluster B, which have been shown to mediate invasiveness and metastasis of CCA (28). The activation of complement was significantly suppressed in ES cluster B, indicating that the humoral immune response against CCA was compromised. Considering that a few metabolism-related processes were enriched, we analyzed several metabolism-specific gene sets between ES cluster A and B, including "Amino acid", "Carbohydrate", "Energy", "Lipid", "Nucleotide", "TCA cycle", and "Vitamin cofactor" (29). Among them, "TCA cycle" and "amino acid" were significantly

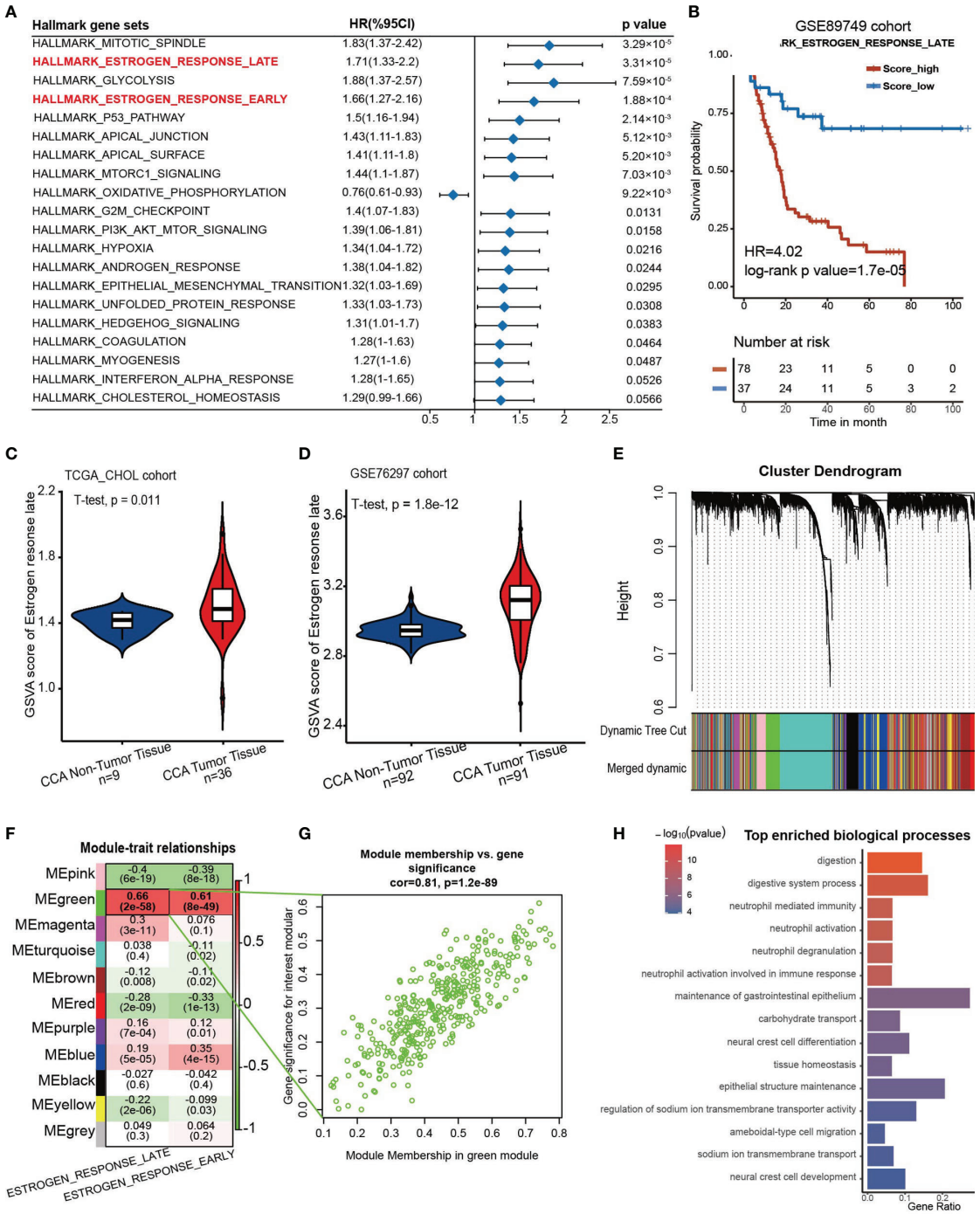

FIGURE 1 | An estrogen response-related gene set was identified. **(A)** Forest plot showing the prognostic value of the GSVA score of the top 20 hallmark gene sets in the GSE89749 cohort. The horizontal coordinates represent the univariate regression coefficient of the normalized GSVA score of each hallmark of cancer, and the horizontal line represents the 95% confidence interval of the univariate regression coefficient. **(B)** Kaplan–Meier curves for overall survival of the patients with high or low GSVA scores of "Estrogen response late" in the GSE89749 cohort. Score_low, n = 37; Score_high, n = 78. HR=4.02, Log-rank test, p value = 1.7×10^{-5}. **(C, D)** Violin plots showing the GSVA score of " HALLLMARK_ESTROGEN_RESPONSE_LATE" in CCA tumoral and non-tumoral tissues in TCGA_CHOL cohort and GSE76297 cohort. **(E)** Weighted gene coexpression network analysis (WGCNA) was performed with an expression matrix of 462 samples in the meta cohort to construct a scale-free coexpression network. The cluster dendrogram shows the clustering of genes into gene modules. **(F)** Eleven gene modules were generated, and a green module exhibited the highest correlation with the GSVA score of "Estrogen response late" (Spearman correlation test, r= 0.9, P = 2e-58) and was considered an "ES-specific module". **(G)** Scatter plot showing the Spearman correlation coefficient between the expression of genes in the green module and the eigengene of the green module or the GSVA score of "Estrogen response late". **(H)** Bar plot showing the top 15 enriched biological processes in the green module.

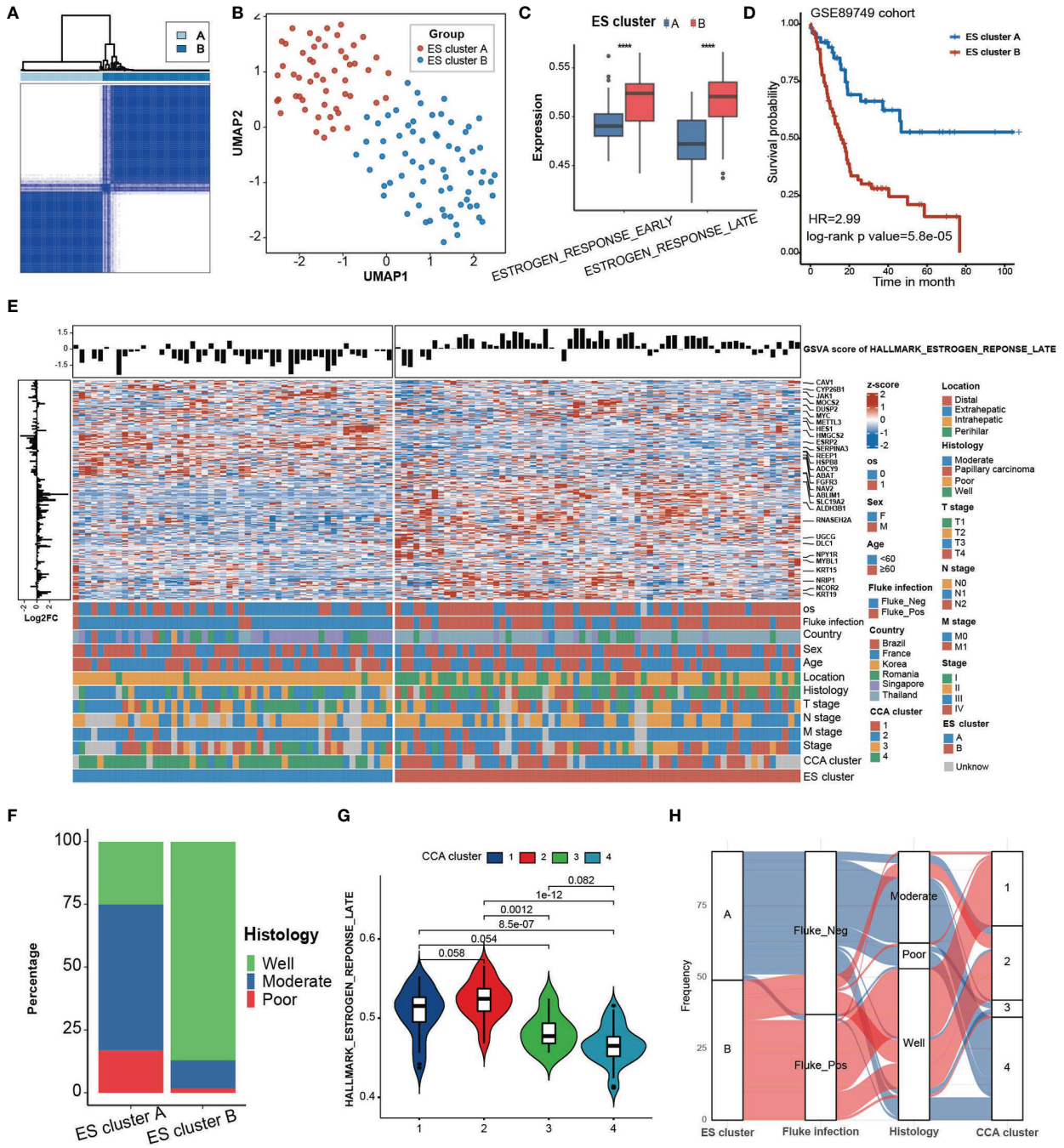

FIGURE 2 | Clinical characteristics of ES clusters in the GSE89749 cohort. **(A)** Consensus matrixes of the GSE89749 cohort based on the expression of genes in the green module. K=2 was chosen as optimal clustering by delta area. **(B)** A UMAP plot of 118 patients by dimensionality reduction of genes in the blue module showing 2 distinct ES clusters. **(C)** ES cluster B exhibited significantly higher GSVA scores for "estrogen response late" and "estrogen response early" than ES cluster **(A, D)** Kaplan–Meier curves for overall survival of the patients in ES cluster A and ES cluster B in the GSE89749 cohort. ES cluster A, n = 51; Score_high, n = 64. HR = 2.99, Log-rank test, p value = 5.8×10^{-5}. **(E)** Heatmap showing the expression of 198 genes involved in "estrogen response late" in 118 CCA patients in the GSE89749 cohort. Clinical information, including overall survival status, sex, age, fluke infection status, country, CCA clusters, location, histology, T stage, N stage, M stage, clinical stage, and ES clusters, is shown as patient annotation. The GSVA score of "Estrogen response early" of each patient was annotated on the top of the heatmap. The log2FoldChange of each gene between ES cluster A and ES cluster B is annotated on the left of the heatmap. **(F)** Stacked bar chart showing the proportion of different histological classifications in the ES cluster A and B groups in the GSE89749 cohort. **(G)** Violin plot showing the GSVA score of "Estrogen response early" in four subtypes of CCA clusters. **(H)** Alluvial diagram showing the relation among different ES clusters, fluke infection status, histology and CCA clusters. Statistical p-value (****,P < 0.0001).

downregulated in ES cluster B, and no difference was detected in other gene sets, indicating a role of the estrogen response in CCA metabolism (**Supplementary Figures S3E, F**).

Potential Cause and Spatiotemporal Specificity of Differential Estrogen Response

To explore the potential mechanism of the differential estrogen response in ES cluster A and B, we compared the expression of estrogen receptors and genes related to estrogen metabolism (**Figure 3A**). There was no difference in the expression of ESR1 (estrogen receptor alpha) and ESR2 (estrogen receptor beta) between the two ES clusters, while genes related to estrogen metabolism differed, especially catechol-O-methyltransferase (COMT) and hydroxysteroid (17beta) dehydrogenase 1 (HSD17B1). COMT could catalyze O-methylation of catechol estrogens and significantly compromise its estrogen receptor binding affinities (30). HSD17B1 efficiently catalyzes the conversion from estrone (E1) to the highly active estrogen estradiol (E2) (31). Coincidentally, COMT was significantly downregulated in ES cluster B, and HSD17B1 was significantly upregulated in ES cluster B. Then, we performed Spearman correlation analysis between the GSVA score of "Estrogen response late" and the expression of COMT and HSD17B1. As expected, the expression of COMT negatively correlated with the estrogen response (**Figure 3B**, Spearman correlation test, r = -0.28, p=0.002), and the expression of HSD17B1 positively correlated with the estrogen response (**Figure 3C**, Spearman correlation test, $r = 0.43$, $p = 1.3\times10^{-6}$). Furthermore, the expression of COMT was a favorable factor for CCA patients (**Figure 3D**, HR = 0.453, log-rank p value = 0.0023), and HSD17B1 was a risk factor for CCA patients (**Figure 3E**, HR = 0.453, log-rank p value = 0.00023).

Subsequently, we attempted to investigate the heterogeneity of the estrogen response within CCA tissues at the single-cell level. A total of 17,090 qualified single cells from cancer tissues of 5 CCA samples in the GSE138709 cohort were clustered after batch correction. Seven types of cells were identified according to the annotation of the R package singleR along with the cell markers from the literature (22), including CCA cells, macrophages, CD8+ T cells, endothelial cells, fibroblasts, B cells and monocytes (**Figure 3F**). The estimation of the score of "Estrogen response late" for single cells *via* the AUCell method showed that the CCA cells exhibited the strongest estrogen response (**Figure 3G**, **Supplementary Figure 4A**). Then, we figured the expression of COMT and HSD17B1 in different cell types within CCA tissues to confirm the responsible cell types. It was shown that COMT was highly expressed in almost all cell types except for $CD8^+$ T cells and HSD17B1 was mainly expressed in part of CCA cells, indicating CCA cells may directly regulate the estrogen response (**Supplementary Figures 4C, D**). Then, the CCA cells were further divided into 6 subgroups (**Figure 3H**). The estrogen response score also differed among the 6 subgroups (**Supplementary Figure 4B**). Transient cell states often followed with dynamic regulation of gene expression. Single cell RNA-seq helps in placing the cells on a hypothetical time trajectory that reflects gradual transition of their transcriptomes and also called pseudotime (32). The cell trajectory of CCA cells was plotted and annotated by cell clusters and pseudotim (**Figures 3I, J**). Interestingly, the estrogen response score significantly correlated with pseudotime (**Figure 3K**, Spearman correlation test $r = 0.72$, $p < 2.2\times10^{-16}$), indicating the potential links between the estrogen response and differentiation of CCA cells. KRT19 is considered to be a cholangiocyte/stem-cell marker (33, 34). Annexin A4 (ANXA4) is a marker of epithelial cell polarity (35). It seems that the expression of KRT19 was positively correlated and the expression of ANXA4 was negatively correlated with the estrogen response (**Supplementary Figure 4E–H**). Moreover, KRT19 increased and ANXA4 decreased following pseudotime (**Supplementary Figures 4I, J**). In summary, we hypothesized that the estrogen response is higher in cancer stem cells (CSCs) and may also be involved in cancer stemness acquisition. In addition, we found that the expression of COMT and HSD17B was also increased following pseudotime (**Figure 3L**).

The Immune Microenvironment Differs Between Different ES Clusters

The functional analysis of ESRGs and GSEA results between ES clusters indicated that the immune microenvironment might be different between ES cluster A and B. Therefore, first, we established the landscape of immune cells in CCA. The immune filtration of 22 immune cells in 118 CCA samples of the GSE89749 cohort was estimated utilizing the cibersort algorithm. The hazard ratio of each cell type and the correlation between different cell types were calculated (**Figure 4A**). M2 macrophages, $CD8^+$ T cells, $CD4^+$ memory T cells, $CD4^+$ naïve T cells, eosinophils, activated mast cells, and naïve B cells were favorable prognostic factors, and plasma cells, resting mast cells, activated NK cells, $CD4^+$ activated memory T cells, M1 macrophages, activated dendritic cells, memory B cells and resting dendritic cells were risk prognostic factors. Then, we compared the abundance of these cells between ES cluster A and B. M2 macrophages and M1 macrophages decreased in ES cluster B, and $CD4^+$ activated memory T cells, plasma cells and activated dendritic cells increased in ES cluster B (**Supplementary Figure 5A**). However, the immune score evaluated by the estimation algorithm between these two clusters showed no significant difference. (Data not shown) Among these differential immune cells, M2 macrophages were the top favorable factors, and plasma cells were the top risk factors, with the most significant difference between ES cluster A and B. Spearman correlation analysis also showed that the estrogen response was positively correlated with the abundance of plasma cells and negatively correlated with the abundance of M2 macrophages or M1 macrophages (**Figure 4B**). Interestingly, both plasma cells and macrophages are major components of humoral immunity, and aberrant humoral immunity is associated with tumor development (36). Several biological processes concerning humoral immunity were significantly downregulated in ES cluster B, such as "complement activation", "regulation of humoral immune response" and "humoral immune response mediated by circulating

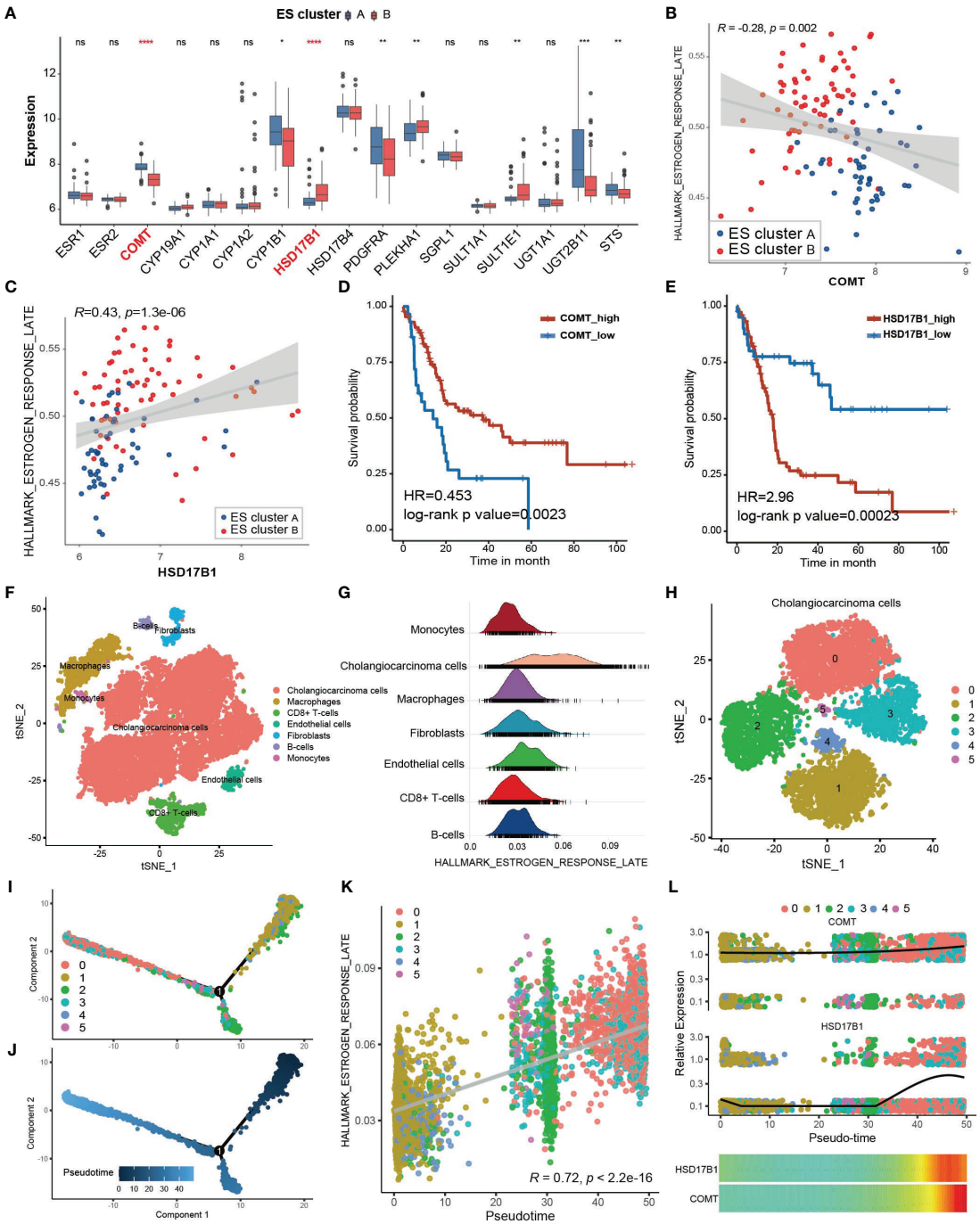

FIGURE 3 | Potential cause and spatiotemporal specificity of the differential estrogen response. **(A)** Differential expression of estrogen receptors and estrogen metabolism-related genes. The top and bottom of the boxes represent the interquartile range of the values. The thick lines in the middle of the boxes represent the median values. The black dots show the outliers. The significant differences among different ECM clusters were evaluated using Student's t test. **(B, C)** Scatter plot depicting the correlation between the GSVA score of "Estrogen response late" and the expression of COMT (Spearman correlation test, R = -0.28, p value =0.002) or HSD17B1 (Spearman correlation test, R = 0.43, p value =1.3×10^{-6}). The color of the dots represents the ES clusters annotated by the legend. **(D, E)** Kaplan–Meier curves for overall survival of the patients with low or high expression of COMT or HSD17B1 in the GSE89749 cohort. **(F)** Single cell clusters for tumor tissues from five CCA samples. **(G)** Ridge plot showing the AUCell score of "Estrogen response late" in different cell types. **(H)** CCA cells were further divided into six subgroups exhibited by the TSNE plot. **(I, J)** Cell trajectory plot of cholangiocarcinoma cells annotated by subgroups of CCA cells and pseudotime. **(K)** Scatter plot showing the correlation between the AUCell score of "Estrogen response late" and the pseudotime of CCA cells. Spearman correlation test, r = 0.72, p <2.2×10^{-16}. **(L)** The combined scatter plot and heatmap plot exhibiting the change in expression of COMT and HSD17B1 following pseudotime in CCA cells. Statistical p-value (*,P < 0.05; **,P < 0.01; ***,P < 0.001, ****,P < 0.0001). ns, not significant.

immunoglobulin" (**Figures 4C–E**). It is well known that complement activation is an important part of antibody opsonization, and in terms of that the core enrichment of humoral immunity processes were mainly complement components, we supposed that the complement activation is the main difference between ES cluster A and B.

The role of the complement system in tumor progression is sophisticated. It may directly eliminate antibody-coated tumor cells or mediate an immunosuppressive environment supporting tumor development. The activation of complement consists of three pathways, including the classical pathway, lectin pathway and alternative pathway, which could further initiate the terminal

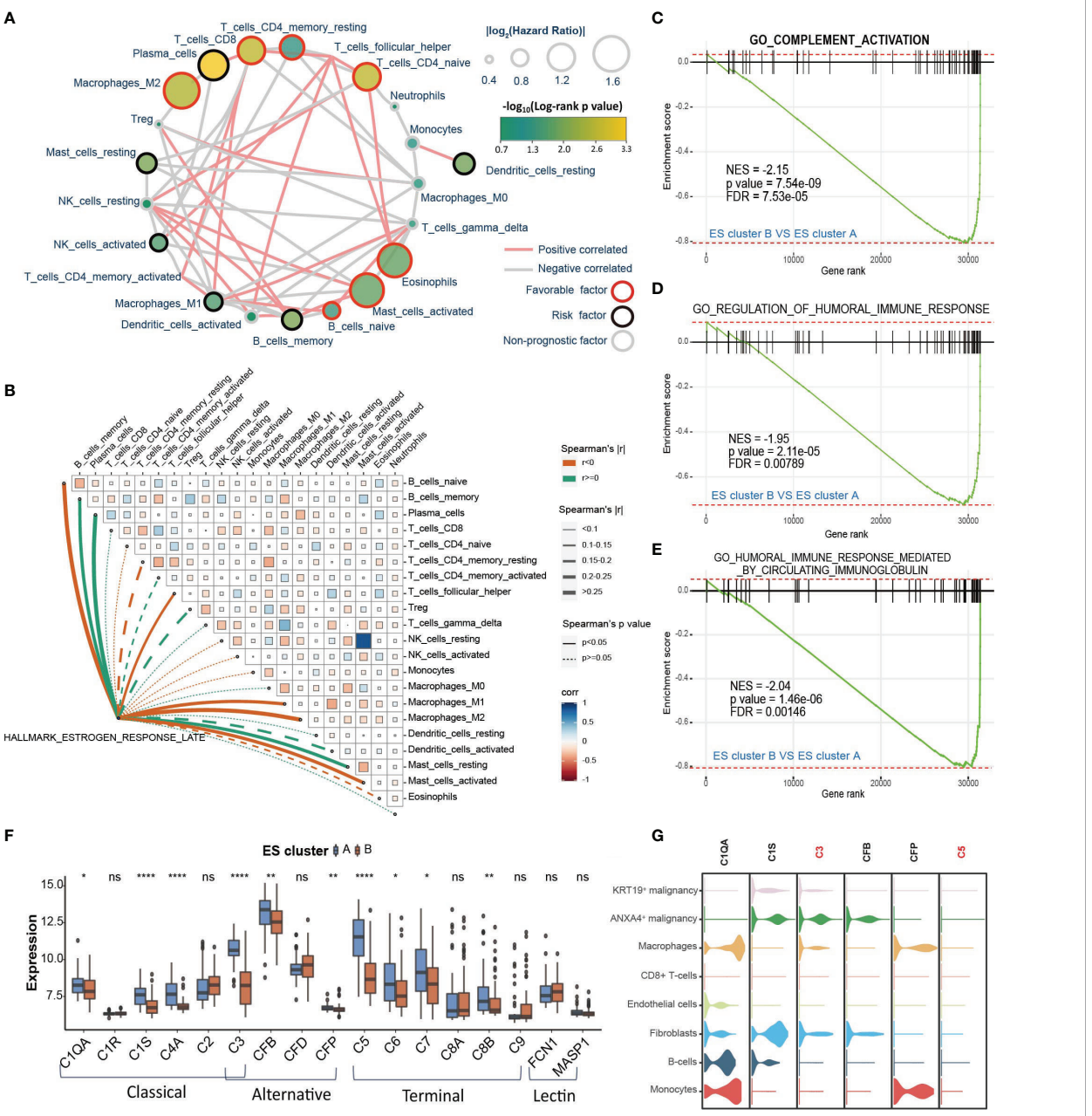

FIGURE 4 | The immune microenvironment differs between different ES clusters. **(A)** Landscape of immune cells in CCA. The size of the circle represents the |log2HazardRatio| of each immune cell. The color filling the circle represents the -$\log_{10}$(log-rank p value). The color of the border represents the prognostic value of the immune cells, and the color of the line between two immune cells represents the cell interaction estimated by Spearman correlation analysis. **(B)** Correlation analysis among the GSVA score of "Estrogen response late" and infiltration of different immune cells. **(C–E)** GSEA plot showing that complement activation and humoral immune response are downregulated in ES cluster B versus ES cluster A **(F)** The expression of complement of different complement activation pathways in ES clusters A and B. **(G)** The expression of specific complements in different cell types of CCA tissues. Statistical p-value (*,P < 0.05; **,P < 0.01; ****,P < 0.0001). ns, not significant.

pathway and the formation of the membrane attack complex (MAC) (37). Then, we analyzed the differential expression of the key genes in these four pathways between ES cluster A and B. The expression of C1QA, C1S, C4A, C3, CFB, CFP, C5, C6, C7 and C8B was downregulated, and no gene was upregulated in ES cluster B (**Figure 4F**). The genes in the classical pathway shared the greatest difference, and C3 and C5 were the top differentially expressed genes between the two groups. Then, we attempted to examine complement activation at the single-cell level. Considering the distinction between $KRT19^+$ and $ANXA4^+$ CCA cells were then subdivided into $KRT19^+$ and $ANXA4^+$ subtypes (**Supplementary Figure 5B**). We scored the complement activation process with the AUCell method and found that complement activation was most significant in macrophages and monocytes (**Supplementary Figures 5C, D**). Therefore, we supposed that the decrease in macrophages may partially account for the downregulation of complement activation in ES cluster B. In addition, it was surprising that the level of complement activation in $ANXA4^+$ CCA cells ranked second only to macrophages and monocytes. Then, we checked the expression of these differentially expressed genes at the single-cell level (**Figure 4G**). The expression of C3 and C5 was highest in $ANXA4^+$ CCA cells and hardly expressed in $KRT19^+$ CCA cells. Moreover, C1S was mainly expressed in $ANXA4^+$ CCA cells, and C1QA and CFP were mainly expressed in macrophages and monocytes. Meanwhile, we investigated the difference in activity of complement activation between CCA tumor and non-tumor tissues. Surprisingly, "GO_COMPLEMENT_ACTIVATION" was significantly downregulated in CCA tissues, and all the key genes in the four complement activation pathways were significantly declined (**Supplementary Figures 5E, F**). Finally, the results showed that both the expression of C3 and C5 could predict good prognosis (**Supplementary Figures 5G, H**, C3: HR = 0.442, log-rank p value = 0.0036; C5: HR = 0.338, log-rank p value = 0.00011).

Establishment and Validation of the Estrogen Response-Related Score in CCA Patients

Because the estrogen response varies among different clinicopathological features and stably correlates with poor prognosis, we attempted to construct a prognostic model based on genes in "Estrogen response late" to predict overall survival probability in CCA. First, the GSE89749 cohort and E-MTAB-6389 cohort were merged into meta-data, followed by batch correction. The TCGA-CHOL cohort was dismissed due to incompatible RNA sequencing data and a small sample size. The merged data set was further randomly divided into a training cohort (n = 128) and a testing cohort (n=55). Then, univariate Cox regression analysis was performed for each gene in "Estrogen response late" (**Figure 5A**). Sixty-five genes with univariate Cox regression p values less than 0.1 were subsequently entered into the LASSO Cox regression model (**Figure 5B**). Tenfold cross-validation was then employed to tune parameter selection in the LASSO model, and 11 genes, including ANXA9, NRIP1, FKBP5, PDLIM3, GJB3, MYOF, PTGES, ID2, CDC20, MDK and SNX10, were filtered to construct the ESRS *via* multivariate Cox regression analysis (**Figure 5C**). The best cutoff value, used to divide the training cohort into ESRS_high and ESRS_low groups, was chosen by maximally selected rank statistics (**Figure 5D**). It was shown that the ESRS did an excellent job in predicting prognosis in the training cohort (**Figure 5E**, HR = 5.68, log-rank p value= 7×10^{-15}). To test the stability of the ESRS model, the computational formula along with the best cutoff value was applied in the testing cohort. The ESRS also performed well in predicting overall survival probability in the testing cohort (**Figure 5F**, HR = 6.78, log-rank p value= 2×10^{-7}).

To improve the risk stratification and personalized assessment of the prognostic model, we integrated the ESRS with the clinical information of CCA patients. In total, 98 samples with full clinical information on age, sex, fluke infection status, anatomy and clinical stage in the GSE89749 cohort were selected for the construction of the integrated prognostic model. Next, a nomogram was established based on the selected clinical information and ESRS, which could provide personalized and convenient assessment of 3-year and 5-year survival probability. The red arrow is an example (**Figure 5G**). As shown in the nomogram, ESRS and the clinical stage of CCA patients were independent and stable prognostic factors in CCA patients. Time-dependent ROC curves indicated that combining clinical stage could improve the predictive ability of ESRS for OS (**Figure 5H**). Finally, to check the validity of the nomogram, we drew calibration curves for the prediction of 1-year and 3-year OS, which were closely correlated with the ideal performance, indicating the accuracy of the prediction of the nomogram (**Figure 5I**). Altogether, the integrated prognostic model could accurately and effectively predict the OS of CCA patients.

Potential Therapeutic Targets and Applicable Drugs According to ESRS or Estrogen Response

Since the estrogen response and the established ESRS are closely correlated with CCA progression, we attempted to explore personalized chemotherapeutic agents or molecular targeted therapeutic drugs for individuals, taking the estrogen response as a clue. First, we performed GSEA for the differentially expressed genes between the ESRS_high and ESRS_low groups to identify the potential pathways involved in CCA progression. The top enriched pathway in the ESRS_high group was "keratinization" (**Figure 6A**; **Supplementary Figure 6A**). A protein–protein interaction network (PPI) was constructed based on the differentially expressed genes in the gene set "Keratinization" utilizing the STRING database (**Supplementary Figure 6B**). Desmoglein 3 (DSG3) was identified as the core gene of the network to the highest degree. Similarly, "drug metabolism cytochrome P450" was the top enriched pathway in the ESRS_low group (**Figure 6B**; **Supplementary Figure 6C**). Cytochrome P450 Family 2 Subfamily C Member 9 (CYP2C9) and Cytochrome P450 Family 3 Subfamily A Member 7 (CYP3A7) were identified as core genes in the PPI network of "Drug metabolism cytochrome P450" (**Supplementary Figure 6D**). These identified pathways and core genes could be potential targets for drug development.

Thanks to previous efforts, CMap, a map of disease-gene-drug connections, has been constructed, which takes differential gene

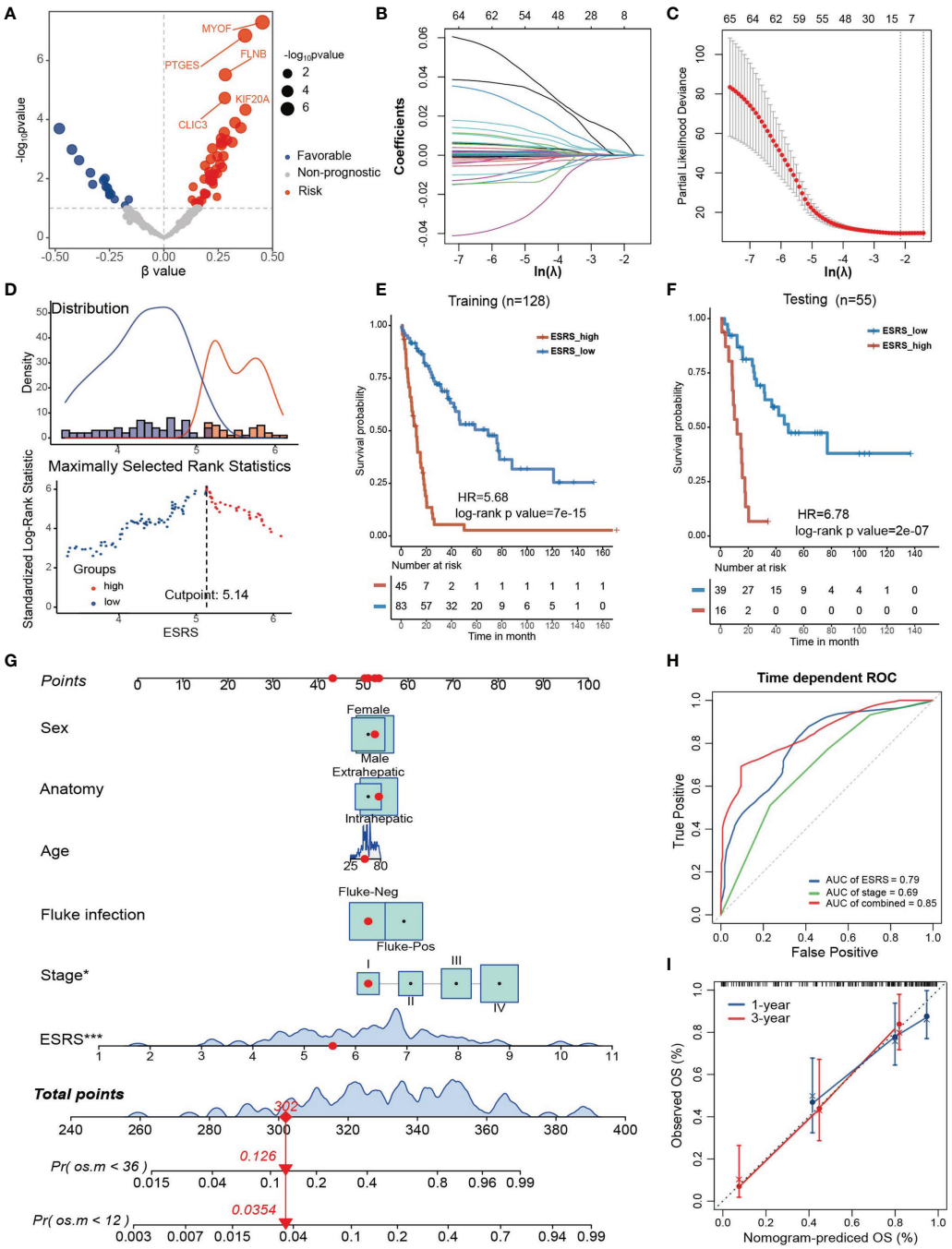

FIGURE 5 | Establishment and validation of the estrogen response-related score (ESRS) in CCA patients. **(A)** Volcano plot showing the univariate Cox regression results of the estrogen response-related genes in the meta-cohort. The horizontal coordinate represents the coefficient of univariate Cox regression, and the vertical coordinate represents the -log10p value of univariate Cox regression. **(B)** With a filtering threshold of a P value less than 0.1, 65 candidates remained and were entered into the LASSO Cox regression model. **(C)** Tenfold cross-validation for tuning parameter selection in the LASSO model. The dotted vertical lines are drawn at the optimal values by minimum criteria (lambda.min, left vertical dotted line) and 1-SE criteria (lambda.1 se, right vertical dotted line). **(D)** The best cutoff value of ESRS was chosen by maximally selected rank statistics. **(E)** Kaplan–Meier analysis demonstrated that patients with higher ESRS exhibited worse prognosis in the training cohort (HR = 5.68, log-rank p value = 7×10^{-15}). **(F)** In the testing cohort, Kaplan–Meier analysis showed that patients with higher IRS exhibited worse prognosis (HR = 6.78, log-rank p value = 2×10^{-7}). **(G)** A personalized scoring nomogram was generated to predict 3- and 5-year OS probability with the seven parameters, and the red arrow shows an example. **(H)** Time-dependent ROC analysis demonstrated that combining ESRS and stage information could better predict the 5-year OS probability. **(I)** Calibration curves of 1-year and 3-year OS prediction were close to the ideal performance (45-degree line). Statistical p-value (*,P < 0.05; ***,P < 0.001).

expression as a common language of disease and chemical compounds (38, 39). We submitted a list of 150 upregulated and 150 downregulated genes between the ESRS_high and ESRS_low groups to the mode-of-action (MoA) analysis of CMap to search for chemical compounds that could lead to similar or reverse genomic fluctuations (**Supplementary Table S3**). 39 mechanisms of action were shared by the top 50 compounds potentially applicable for ESRS_high patients, which could cause reverse changes between the ESRS_high and ESRS_low groups (**Figure 6C**). In particular, SB-202190, a p38 MAPK inhibitor, ranked first among all the potential compounds, and 7 potential compounds, namely, apicidin, panobinostat, ISOX, scriptaid, HC-toxin, vorinostat and THM-I-

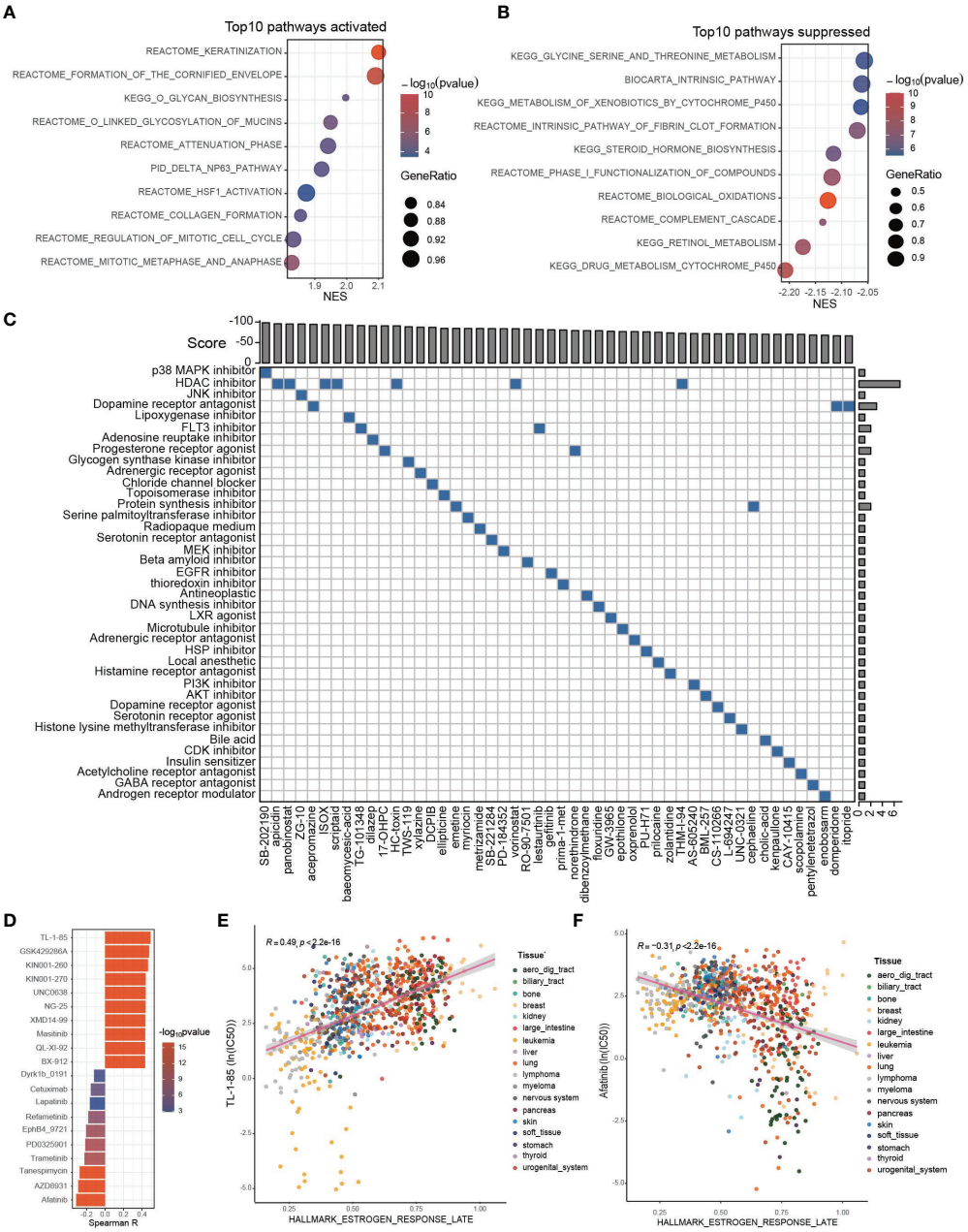

FIGURE 6 | Potential therapeutic targets and applicable drugs according to ESRS or estrogen response. **(A, B)** GSEA was performed between the ESRS_high and ESRS_low groups. The bar plots show the top 10 upregulated or downregulated pathways in the ESRS_high group. **(C)** The differentially expressed genes were submitted to CMap mode-of-action (MoA) analysis, and the results showed 39 mechanisms of action shared by the top 50 compounds potentially applicable for ESRS_high patients. **(D)** The correlation between GSVA score of "Estrogen response late" and ln(IC50) of drugs in cancer cell lines. **(E, F)** Scatter plots showing the correlation between the GSVA score of "Estrogen response late" and the ln(IC50) of TL-1-85 or afatinib in cancer cell lines. The color of the dot represents the histologic origin of the cancer cell lines.

94, were all histone deacetylase (HDAC) inhibitors. In addition, we also showed 42 mechanisms of action shared by the top 50 compounds that show similar impacts on cancer cells to ESRS, which should be dismissed for ESRS_high patients (**Supplementary Figure 6E**).

Drug resistance has always been the principal factor impeding satisfactory cures for patients with cancer, for which tumor heterogeneity may be partially blamed (40, 41). To optimize drug selection, we correlated the IC50 of chemical drugs with the GSVA score of "Estrogen response late" in all cancer cell lines from GDSC (**Figure 6D**; **Supplementary Table S4**). Patients with a high estrogen response may be more likely to acquire resistance to drugs with a positive correlation with the estrogen response and more sensitive to drugs with a negative correlation with the estrogen response. Among them, the IC50 of TL-1-85 was the top drug positively correlated with the estrogen response (**Figure 6E**, Spearman correlation test, $r = 0.49$, $p < 2.2\times10^{-16}$). The IC50 of afatinib was the top drug negatively correlated with the estrogen response (**Figure 6F**, Spearman correlation test, $r = -0.31$, $p < 2.2\times10^{-16}$).

DISCUSSION

Estrogen has been proven to be involved in cancer progression by modulating proliferation, apoptosis, epithelial-to-mesenchymal transition (EMT), angiogenesis, tumor metabolism and the immunosuppressive microenvironment (42–47). Therapeutics targeting selective estrogen receptor or estrogen signaling have been developed and have achieved satisfactory clinical outcomes, especially in breast cancer (48, 49). While it has long been established that CCA could be regulated by estrogen, current knowledge about the mechanism of estrogen signaling regulating CCA progression is still in its infancy. Let alone exploration for potential therapeutic targets specific to the heterogeneity of estrogen response.

We were the first to characterize the clinical and transcriptomic landscape of the estrogen response in CCA. In our study, it was shown that the estrogen response differs among different cancer types and that the estrogen response predicted the worst prognosis in patients with CCA. WGCNA was conducted to identify the ESRGs, based on which patients with CCA were clustered into ES cluster A and B. The clinical features, biological characteristics and estrogen metabolism were significantly different between the two clusters. Single-cell level analysis indicated that the estrogen response was strongest in CCA cells and possibly correlated with cancer stemness acquisition. The immune landscape in CCA was constructed, and it was shown that the estrogen response was positively correlated with the infiltration of plasma cells and negatively correlated with that of macrophages. The activation of complement was significantly downregulated in ES cluster B, and the decrease in C3, C5 and C1S in CCA cells may be a potential cause. We also established an ESRS prognostic model based on the expression of estrogen response-related genes and integrated the ESRS with clinical features to construct a nomogram. Finally, we constructed a pharmacological landscape specific to the estrogen response in patients with CCA, taking advantage of CMap and the GDSC database.

In the GSE89749 cohort, ES cluster B with an intense estrogen response was mainly composed of patients with fluke infection. Estrogen is well known for its anti-inflammatory effect (26, 50). Meanwhile, the main risk factors to date are fluke infection and primary sclerosing cholangitis, both of which could give rise to a chronic inflammatory environment (2). In addition, the liver is the primary site for estrogen metabolism (30, 51), and substantial evidence has indicated that chronic liver inflammation is accompanied by elevated estrogen levels and endocrine disturbance, potentially on account of the impaired function of liver cells to inactivate estrogen (25, 52, 53). Therefore, we hypothesized that chronic inflammation and elevated estrogen response accompany each other and are involved in the tumorigenesis and progression of CCA. The ES clusters also overlapped with the classification of the International Cancer Genome Consortium (10). ES cluster A was mainly composed of CCA cluster 3/4 characterized by high copy number alterations and expression of PD-1/PD-L2 or epigenetic changes (IDH1/2, BAP1) along with FGFR/PRKA-related gene rearrangements. ES cluster B was composed of CCA cluster 1/2, characterized by ERBB2 amplifications and TP53 mutations. Therefore, ES clusters may provide a reference in the development and selection of specific chemotherapeutic targets in CCA, such as therapies targeting ERBB2/HER2 signaling (54), IDH inhibitors (ClinicalTrials.gov identifier: NCT02073994) and RGFR-targeting agents (55).

The differential estrogen response could be derived either from the different expression of estrogen receptors or the disturbance in estrogen metabolism. For example, genetic variations in COMT may influence the risk of breast cancer as a result of significant changes in catechol estrogen and methoxyestrogen levels (56). Studies have shown that five cytochrome P450 1B1 (CYP1B1) variants, which could change the hydroxylation activity of estrogen, have greater than twofold higher activity than the wild-type enzyme, thereby increasing the risk for cancers (57). The expression of HSD17B2, which catalyzes estradiol (E2) to E1 in human CRC tissue, was also proven to be downregulated in colon cancers and predicts poor prognosis, suggesting an important role of estrogen metabolism in CRC progression (58). In our study, we found that COMT, which is responsible for the inactivation of estrogen, was negatively correlated with the estrogen response and HSD17B1, which catalyzes E1 to more active E2, was positively correlated with the estrogen response. Meanwhile, COMT correlates with good prognosis, and HSD17B1 predicts poor prognosis. These findings strongly suggest the important role of these two genes in estrogen metabolism in CCA and provide potential targets for CCA treatment. In addition, we also found that the estrogen response was correlated with cancer cell differentiation and cancer stemness, marked by KRT19, in CCA, which deserves further investigation.

Complement plays a key role in the innate immune system and defense against pathogens and is also a neglected component

of the TME derived from tumor cells, infiltrated cells or the circulation (37). The role of the complement system in cancer progression is crucial and complex. For example, C1q can also exert antitumoural effects by induction of apoptosis in breast or prostate cancer cell lines (59, 60). While C5a exerts immunosuppression effect by recruiting MDSCs to the TME, which in turn suppress effector T cells (61). In our study, we found that downregulation of complement activation was a representative feature of ES cluster B. Further investigation indicated that most of the complement components were decreased in ES cluster B, including C1QA, C1S, C4A, C3, CFB, CFP, C5, C6, C7 and C8B. Single-cell level analysis revealed that the expression of C3 and C5 was highest in $ANXA4^+$ CCA cells and hardly expressed in $KRT19^+$ CCA cells, both of which were correlated with good prognosis in patients with CCA. Interestingly, the downregulation of complement activation in CCA tumor tissues compared with CCA non-tumor tissues was even more significant. Our findings suggested that complement activation may play a protective role in patients with CCA, and the downregulation of complement activation may be attributed to an upregulated estrogen response, which needs further investigation. Many agents targeting complement are in the pipeline for various diseases, including cancer therapy (62–64). For example, IgG hexamerization was designed to promote C1q binding and complement activation and enhance the anticancer effect (65). Our findings of complement in CCA may provide insights into the exploration of relevant chemotherapeutic agents.

Several prognostic models have been established in CCA based on signatures of mRNA, DNA methylation or alternative splicing (66–68). These prognostic models could help predict overall or disease-free survival and are beneficial to the individual management of CCA patients. In our study, we constructed an ESRS model based on the expression of estrogen response-related genes, which performed well in predicting the prognosis of patients with CCA and performed well in both the training and testing cohorts. PPI networks concerning "keratinization" and "drug metabolism cytochrome P450" were constructed to find potential gene targets for the ESRS_high group. Then, the CMap database was employed to identify potential chemotherapeutic agents for the ESRS_high group. Among them, SB-202190, a p38 MAPK inhibitor, ranked at the top of recommended drugs, and p38 MAPK signaling has been reported to be a downstream signal of estrogen (69). In addition, 7 HDAC inhibitors were on the recommended list. It was reported that the addition of the HDAC inhibitor vorinostat (VPA), which is also in the recommended list, to ER-positive breast cancer cells could significantly increase the efficacy of tamoxifen treatment (70). Thus, we supposed that the drug list for the ESRS_high group was trustworthy. Furthermore, we also scanned all the chemotherapy drugs to make a list of drugs sensitive or resistant to CCA with a high estrogen response employing the data from the GDSC database.

Despite comprehensive characterization of the estrogen response, the preliminary research basis is insufficient. We obtained thrilling results, while the explanation for the findings was mainly based on speculation. Further clinical trials and experiments are needed to illuminate our findings. In addition, the size of the samples with available clinical information was limited, and the source of the datasets was diverse, which may cause bias of the results. Finally, further multiomics analyses, such as copy number variation, DNA methylation, and gene mutation, may promote an in-depth understanding of the role of estrogen in CCA progression and broaden the range of potential molecular targets.

In summary, our study characterized the landscape of the estrogen response in the clinical features, transcriptome and TIME of CCA. Estrogen response-based classification and risk models were established to predict prognosis and optimize individual management for patients with CCA. In addition, our results also provide applicable drugs and potential therapeutic targets in estrogen metabolism, the complement system and ESRS-related pathways for CCA.

DATA AVAILABILITY STATEMENT

The authors declare that the original contributions presented in the study are included in the article/**Supplementary Materials**, and further inquiries can be directed to the corresponding authors.

AUTHOR CONTRIBUTIONS

Conception and design of the study: SB, JC and HZ. Data collection and preprocessing: ML, QZ. Analysis and interpretation of data: CL, JM and QZ. Manuscript writing: CL, JM and ML. Visualization, statistical expertise: FX, YP, YW, ZY, XX. All authors contributed to the article and approved the submitted version.

FUNDING

The Nanjing Health Science and Technology Development Special Fund for Distinguished Young Scholar [No. JQX19001], the National Science Foundation for Young Scholars of China [No. 81501380] and the Suzhou Science and Education Guardian Youth Science and Technology Project [No. KJXW2017065].

SUPPLEMENTARY MATERIAL

The Supplementary Material for this article can be found online at: https://www.frontiersin.org/articles/10.3389/fonc.2022.870840/full#supplementary-material

REFERENCES

1. Banales JM, Marin JJ, Lamarca A, Rodrigues PM, Khan SA, Roberts LR, et al. Cholangiocarcinoma 2020: The Next Horizon in Mechanisms and Management. *Nat Rev Gastroenterol Hepatol* (2020) 17:557–88. doi: 10.1038/s41575-020-0310-z
2. Brindley PJ, Bachini M, Ilyas SI, Khan SA, Loukas A, Sirica AE, et al. Cholangiocarcinoma. *Nat Rev Dis Primers* (2021) 7:65. doi: 10.1038/s41572-021-00300-2
3. Sripa B, Tangkawattana S, Brindley PJ. "Update on Pathogenesis of Opisthorchiasis and Cholangiocarcinoma,". In: *Asiatic Liver Fluke - From Basic Science to Public Health, Part B*. Khon Kaen, Thailand: Elsevier (2018). p. 97–113.
4. Khan SA, Tavolari S, Brandi G. Cholangiocarcinoma: Epidemiology and Risk Factors. *Liver Int* (2019) 39:19–31. doi: 10.1111/liv.14095
5. Rizvi S, Khan SA, Hallemeier CL, Kelley RK, Gores GJ. Cholangiocarcinoma - Evolving Concepts and Therapeutic Strategies. *Nat Rev Clin Oncol* (2018) 15:95–111. doi: 10.1038/nrclinonc.2017.157
6. Forner A, Vidili G, Rengo M, Bujanda L, Ponz-Sarvisé M, Lamarca A. Clinical Presentation, Diagnosis and Staging of Cholangiocarcinoma. *Liver Int* (2019) 39:98–107. doi: 10.1111/liv.14086
7. van Vugt JLA, Gaspersz MP, Coelen RJS, Vugts J, Labeur TA, de Jonge J, et al. The Prognostic Value of Portal Vein and Hepatic Artery Involvement in Patients With Perihilar Cholangiocarcinoma. *HPB* (2018) 20:83–92. doi: 10.1016/j.hpb.2017.08.025
8. Valle J, Wasan H, Palmer DH, Cunningham D, Anthoney A, Maraveyas A, et al. Cisplatin Plus Gemcitabine Versus Gemcitabine for Biliary Tract Cancer. *N Engl J Med* (2010) 362:1273–81. doi: 10.1056/NEJMoa0908721
9. Groot Koerkamp B, Wiggers JK, Gonen M, Doussot A, Allen PJ, Besselink MG, et al. Survival After Resection of Perihilar Cholangiocarcinoma-Development and External Validation of a Prognostic Nomogram. *Ann Oncol* (2016) 27:753. doi: 10.1093/annonc/mdw063
10. Jusakul A, Cutcutache I, Yong CH, Lim JQ, Huang MN, Padmanabhan N, et al. Whole-Genome and Epigenomic Landscapes of Etiologically Distinct Subtypes of Cholangiocarcinoma. *Cancer Discov* (2017) 7:1116–35. doi: 10.1158/2159-8290.CD-17-0368
11. Liang J, Shang Y. Estrogen and Cancer. *Annu Rev Physiol* (2013) 75:225–40. doi: 10.1146/annurev-physiol-030212-183708
12. Nilsson S, Koehler KF, Gustafsson J-Å. Development of Subtype-Selective Oestrogen Receptor-Based Therapeutics. *Nat Rev Drug Discov* (2011) 10:778–92. doi: 10.1038/nrd3551
13. Milette S, Hashimoto M, Perrino S, Qi S, Chen M, Ham B, et al. Sexual Dimorphism and the Role of Estrogen in the Immune Microenvironment of Liver Metastases. *Nat Commun* (2019) 10:5745. doi: 10.1038/s41467-019-13571-x
14. Alvaro D, Alpini G, Onori P, Franchitto A, Glaser SS, Le Sage G, et al. Alfa and Beta Estrogen Receptors and the Biliary Tree. *Mol Cell Endocrinol* (2002) 193:105–8. doi: 10.1016/s0303-7207(02)00103-x
15. Alvaro D, Barbaro B, Franchitto A, Onori P, Glaser SS, Alpini G, et al. Estrogens and Insulin-Like Growth Factor 1 Modulate Neoplastic Cell Growth in Human Cholangiocarcinoma. *Am J Pathol* (2006) 169:877–88. doi: 10.2353/ajpath.2006.050464
16. Isse K, Specht SM, Lunz JG, Kang L-I, Mizuguchi Y, Demetris AJ. Estrogen Stimulates Female Biliary Epithelial Cell Interleukin-6 Expression in Mice and Humans. *Hepatology* (2010) 51:869–80. doi: 10.1002/hep.23386
17. Mancino A, Mancino MG, Glaser SS, Alpini G, Bolognese A, Izzo L, et al. Estrogens Stimulate the Proliferation of Human Cholangiocarcinoma by Inducing the Expression and Secretion of Vascular Endothelial Growth Factor. *Digestive Liver Dis* (2009) 41:156–63. doi: 10.1016/j.dld.2008.02.015
18. Sampson LK, Vickers SM, Ying W, Phillips JO. Tamoxifen-Mediated Growth Inhibition of Human Cholangiocarcinoma. *Cancer Res* (1997) 57:1743–9.
19. Tanjak P, Thiantanawat A, Watcharasit P, Satayavivad J. Genistein Reduces the Activation of AKT and EGFR, and the Production of IL6 in Cholangiocarcinoma Cells Involving Estrogen and Estrogen Receptors. *Int J Oncol* (2018) 53:177–88. doi: 10.3892/ijo.2018.4375
20. Petrick JL, McMenamin ÚC, Zhang X, Zeleniuch-Jacquotte A, Wactawski-Wende J, Simon TG, et al. Exogenous Hormone Use, Reproductive Factors and Risk of Intrahepatic Cholangiocarcinoma Among Women: Results From Cohort Studies in the Liver Cancer Pooling Project and the UK Biobank. *Br J Cancer* (2020) 123:316–24. doi: 10.1038/s41416-020-0835-5
21. Bolstad BM, Irizarry RA, Astrand M, Speed TP. A Comparison of Normalization Methods for High Density Oligonucleotide Array Data Based on Variance and Bias. *Bioinformatics* (2003) 19:185–93. doi: 10.1093/bioinformatics/19.2.185
22. Zhang M, Yang H, Wan L, Wang Z, Wang H, Ge C, et al. Single-Cell Transcriptomic Architecture and Intercellular Crosstalk of Human Intrahepatic Cholangiocarcinoma. *J Hepatol* (2020) 73:1118–30. doi: 10.1016/j.jhep.2020.05.039
23. Stuart T, Butler A, Hoffman P, Hafemeister C, Papalexi E, Mauck WM, et al. Comprehensive Integration of Single-Cell Data. *Cell* (2019) 177:1888–1902.e21. doi: 10.1016/j.cell.2019.05.031
24. Suttiprapa S, Sotillo J, Smout M, Suyapoh W, Chaiyadet S, Tripathi T, et al. Opisthorchis Viverrini Proteome and Host-Parasite Interactions. *Adv Parasitol* (2018) 102:45–72. doi: 10.1016/bs.apar.2018.06.002
25. Adlercreutz H. Oestrogen Metabolism in Liver Disease. *J Endocrinol* (1970) 46:129–63. doi: 10.1677/joe.0.0460129
26. Jiang M, Klein M, Zanger UM, Mohammad MK, Cave MC, Gaikwad NW, et al. Inflammatory Regulation of Steroid Sulfatase: A Novel Mechanism to Control Estrogen Homeostasis and Inflammation in Chronic Liver Disease. *J Hepatol* (2016) 64:44–52. doi: 10.1016/j.jhep.2015.07.022
27. Sia D, Hoshida Y, Villanueva A, Roayaie S, Ferrer J, Tabak B, et al. Integrative Molecular Analysis of Intrahepatic Cholangiocarcinoma Reveals 2 Classes That Have Different Outcomes. *Gastroenterology* (2013) 144:829–40. doi: 10.1053/j.gastro.2013.01.001
28. Phoomak C, Silsirivanit A, Park D, Sawanyawisuth K, Vaeteewoottacharn K, Wongkham C, et al. O-GlcNAcylation Mediates Metastasis of Cholangiocarcinoma Through FOXO3 and MAN1A1. *Oncogene* (2018) 37:5648–65. doi: 10.1038/s41388-018-0366-1
29. Peng X, Chen Z, Farshidfar F, Xu X, Lorenzi PL, Wang Y, et al. Molecular Characterization and Clinical Relevance of Metabolic Expression Subtypes in Human Cancers. *Cell Rep* (2018) 23:255–269.e4. doi: 10.1016/j.celrep.2018.03.077
30. Zhu B. Functional Role of Estrogen Metabolism in Target Cells: Review and Perspectives. *Carcinogenesis* (1998) 19:1–27. doi: 10.1093/carcin/19.1.1
31. Zhang C-Y, Chen J, Yin D-C, Lin S-X. The Contribution of 17beta-Hydroxysteroid Dehydrogenase Type 1 to the Estradiol-Estrone Ratio in Estrogen-Sensitive Breast Cancer Cells. *PLoS One* (2012) 7:e29835. doi: 10.1371/journal.pone.0029835
32. Mondal PK, Saha US, Mukhopadhyay I. PseudoGA: Cell Pseudotime Reconstruction Based on Genetic Algorithm. *Nucleic Acids Res* (2021) 49:7909–24. doi: 10.1093/nar/gkab457
33. Kim H, Choi GH, Na DC, Ahn EY, Kim GI, Lee JE, et al. Human Hepatocellular Carcinomas With "Stemness"-Related Marker Expression: Keratin 19 Expression and a Poor Prognosis. *Hepatology* (2011) 54:1707–17. doi: 10.1002/hep.24559
34. Lee K, Lee K-B, Jung HY, Yi N-J, Lee K-W, Suh K-S, et al. The Correlation Between Poor Prognosis and Increased Yes-Associated Protein 1 Expression in Keratin 19 Expressing Hepatocellular Carcinomas and Cholangiocarcinomas. *BMC Cancer* (2017) 17:441. doi: 10.1186/s12885-017-3431-1
35. Gerke V, Moss SE. Annexins: From Structure to Function. *Physiol Rev* (2002) 82:331–71. doi: 10.1152/physrev.00030.2001
36. Tan T-T, Coussens LM. Humoral Immunity, Inflammation and Cancer. *Curr Opin Immunol* (2007) 19:209–16. doi: 10.1016/j.coi.2007.01.001
37. Roumenina LT, Daugan MV, Petitprez F, Sautès-Fridman C, Fridman WH. Context-Dependent Roles of Complement in Cancer. *Nat Rev Cancer* (2019) 19:698–715. doi: 10.1038/s41568-019-0210-0
38. Lamb J, Crawford ED, Peck D, Modell JW, Blat IC, Wrobel MJ, et al. The Connectivity Map: Using Gene-Expression Signatures to Connect Small Molecules, Genes, and Disease. *Science* (2006) 313:1929–35. doi: 10.1126/science.1132939
39. Subramanian A, Narayan R, Corsello SM, Peck DD, Natoli TE, Lu X, et al. A Next Generation Connectivity Map: L1000 Platform and the First 1,000,000 Profiles. *Cell* (2017) 171:1437–52.e17. doi: 10.1016/j.cell.2017.10.049
40. Holohan C, van Schaeybroeck S, Longley DB, Johnston PG. Cancer Drug Resistance: An Evolving Paradigm. *Nat Rev Cancer* (2013) 13:714–26. doi: 10.1038/nrc3599

41. Vasan N, Baselga J, Hyman DM. A View on Drug Resistance in Cancer. *Nature* (2019) 575:299–309. doi: 10.1038/s41586-019-1730-1
42. Andruska N, Zheng X, Yang X, Helferich WG, Shapiro DJ. Anticipatory Estrogen Activation of the Unfolded Protein Response Is Linked to Cell Proliferation and Poor Survival in Estrogen Receptor α-Positive Breast Cancer. *Oncogene* (2015) 34:3760–9. doi: 10.1038/onc.2014.292
43. Huang Z-X, Mao X-M, Wu R-F, Huang S-M, Ding X-Y, Chen Q-H, et al. RhoA/ROCK Pathway Mediates the Effect of Oestrogen on Regulating Epithelial-Mesenchymal Transition and Proliferation in Endometriosis. *J Cell Mol Med* (2020) 24:10693–704. doi: 10.1111/jcmm.15689
44. Kulkoyluoglu-Cotul E, Arca A, Madak-Erdogan Z. Crosstalk Between Estrogen Signaling and Breast Cancer Metabolism. *Trends Endocrinol Metab* (2019) 30:25–38. doi: 10.1016/j.tem.2018.10.006
45. Muhammad JS, Guimei M, Jayakumar MN, Shafarin J, Janeeh AS, AbuJabal R, et al. Estrogen-Induced Hypomethylation and Overexpression of YAP1 Facilitate Breast Cancer Cell Growth and Survival. *Neoplasia* (2021) 23:68–79. doi: 10.1016/j.neo.2020.11.002
46. Smida T, Bruno TC, Stabile LP. Influence of Estrogen on the NSCLC Microenvironment: A Comprehensive Picture and Clinical Implications. *Front Oncol* (2020) 10:137. doi: 10.3389/fonc.2020.00137
47. Wu J, Miao C, Lv X, Zhang Y, Li Y, Wang Di. Estrogen Regulates Forkhead Transcription Factor 2 to Promote Apoptosis of Human Ovarian Granulosa-Like Tumor Cells. *J Steroid Biochem Mol Biol* (2019) 194:105418. doi: 10.1016/j.jsbmb.2019.105418
48. Patel HK, Bihani T. Selective Estrogen Receptor Modulators (SERMs) and Selective Estrogen Receptor Degraders (SERDs) in Cancer Treatment. *Pharmacol Ther* (2018) 186:1–24. doi: 10.1016/j.pharmthera.2017.12.012
49. Saha T, Makar S, Swetha R, Gutti G, Singh SK. Estrogen Signaling: An Emanating Therapeutic Target for Breast Cancer Treatment. *Eur J Med Chem* (2019) 177:116–43. doi: 10.1016/j.ejmech.2019.05.023
50. Straub RH. The Complex Role of Estrogens in Inflammation. *Endocr Rev* (2007) 28:521–74. doi: 10.1210/er.2007-0001
51. Falany CN. Enzymology of Human Cytosolic Sulfotransferases. *FASEB J* (1997) 11:206–16. doi: 10.1096/fasebj.11.4.9068609
52. Gavaler JS. Alcohol Effects on Hormone Levels in Normal Postmenopausal Women and in Postmenopausal Women With Alcohol-Induced Cirrhosis. *Recent Dev Alcohol* (1995) 12:199–208. doi: 10.1007/0-306-47138-8_11
53. Long RS, Simmons EE. The Liver and Estrogen Metabolism; Report of Cases. *AMA Arch Intern Med* (1951) 88:762–9. doi: 10.1001/archinte.1951.03810120063006
54. Law LY. Dramatic Response to Trastuzumab and Paclitaxel in a Patient With Human Epidermal Growth Factor Receptor 2-Positive Metastatic Cholangiocarcinoma. *J Clin Oncol* (2012) 30:e271–3. doi: 10.1200/JCO.2012.42.3061
55. Goyal L, Kongpetch S, Crolley VE, Bridgewater J. Targeting FGFR Inhibition in Cholangiocarcinoma. *Cancer Treat Rev* (2021) 95:102170. doi: 10.1016/j.ctrv.2021.102170
56. Yim D-S, Park SK, Yoo K-Y, Yoon K-S, Chung HH, Kang HJ, et al. Relationship Between the Val158Met Polymorphism of Catechol O-Methyl Transferase and Breast Cancer. *Pharmacogenetics* (2001) 11:279–86. doi: 10.1097/00008571-200106000-00001
57. Hanna IH, Dawling S, Roodi N, Guengerich FP, Parl FF. Cytochrome P450 1b1 (CYP1B1) Pharmacogenetics: Association of Polymorphisms With Functional Differences in Estrogen Hydroxylation Activity. *Cancer Res* (2000) 60:3440–4.
58. Oduwole OO, Isomaa VV, Nokelainen PA, Stenbäck F, Vihko PT. Downregulation of Estrogen-Metabolizing 17 Beta-Hydroxysteroid Dehydrogenase Type 2 Expression Correlates Inversely With Ki67 Proliferation Marker in Colon-Cancer Development. *Int J Cancer* (2002) 97:1–6. doi: 10.1002/ijc.1567
59. Bandini S, Macagno M, Hysi A, Lanzardo S, Conti L, Bello A, et al. The non-Inflammatory Role of C1q During Her2/neu-Driven Mammary Carcinogenesis. *Oncoimmunology* (2016) 5:e1253653. doi: 10.1080/2162402X.2016.1253653
60. Hong Q, Sze C-I, Lin S-R, Lee M-H, He R-Y, Schultz L, et al. Complement C1q Activates Tumor Suppressor WWOX to Induce Apoptosis in Prostate Cancer Cells. *PLoS One* (2009) 4:e5755. doi: 10.1371/journal.pone.0005755
61. Markiewski MM, DeAngelis RA, Benencia F, Ricklin-Lichtsteiner SK, Koutoulaki A, Gerard C, et al. Modulation of the Antitumor Immune Response by Complement. *Nat Immunol* (2008) 9:1225–35. doi: 10.1038/ni.1655
62. Ricklin D, Mastellos DC, Reis ES, Lambris JD. The Renaissance of Complement Therapeutics. *Nat Rev Nephrol* (2018) 14:26–47. doi: 10.1038/nrneph.2017.156
63. Pio R, Ajona D, Ortiz-Espinosa S, Mantovani A, Lambris JD. Complementing the Cancer-Immunity Cycle. *Front Immunol* (2019) 10:774. doi: 10.3389/fimmu.2019.00774
64. Mastellos DC, Ricklin D, Lambris JD. Clinical Promise of Next-Generation Complement Therapeutics. *Nat Rev Drug Discov* (2019) 18:707–29. doi: 10.1038/s41573-019-0031-6
65. Diebolder CA, Beurskens FJ, de Jong RN, Koning RI, Strumane K, Lindorfer MA, et al. Complement Is Activated by IgG Hexamers Assembled at the Cell Surface. *Science* (2014) 343:1260–3. doi: 10.1126/science.1248943
66. Guo H, Cai J, Wang X, Wang B, Wang F, Li X, et al. Prognostic Values of a Novel multi-mRNA Signature for Predicting Relapse of Cholangiocarcinoma. *Int J Biol Sci* (2020) 16:869–81. doi: 10.7150/ijbs.38846
67. Liang J, Liu T, Liao J, Zhang L, Zhou M, Xu W, et al. Development and Validation of a CpG Island Methylator Phenotype-Related Prognostic Signature for Cholangiocarcinoma. *J Cell Physiol* (2021) 236:3143–56. doi: 10.1002/jcp.30082
68. Lin Z, Gong J, Zhong G, Hu J, Cai D, Zhao L, et al. Identification of Mutator-Derived Alternative Splicing Signatures of Genomic Instability for Improving the Clinical Outcome of Cholangiocarcinoma. *Front Oncol* (2021) 11:666847. doi: 10.3389/fonc.2021.666847
69. Sprague R, Kim JW, Kirimlioglu E, Guo X, Günay N, Guzeloglu-Kayisli O, et al. Catecholestradiol Activation of Adrenergic Receptors Induces Endometrial Cell Survival *via* P38 MAPK Signaling. *J Clin Endocrinol Metab* (2021) 106:337–50. doi: 10.1210/clinem/dgaa866
70. Thomas S, Thurn KT, Biçaku E, Marchion DC, Münster PN. Addition of a Histone Deacetylase Inhibitor Redirects Tamoxifen-Treated Breast Cancer Cells Into Apoptosis, Which is Opposed by the Induction of Autophagy. *Breast Cancer Res Treat* (2011) 130:437–47. doi: 10.1007/s10549-011-1364-y

Conflict of Interest: The authors declare that the research was conducted in the absence of any commercial or financial relationships that could be construed as a potential conflict of interest.

Publisher's Note: All claims expressed in this article are solely those of the authors and do not necessarily represent those of their affiliated organizations, or those of the publisher, the editors and the reviewers. Any product that may be evaluated in this article, or claim that may be made by its manufacturer, is not guaranteed or endorsed by the publisher.

Copyright © 2022 Lu, Miao, Li, Zheng, Xu, Pan, Wang, Yang, Xia, Zhu, Chen and Bao. This is an open-access article distributed under the terms of the Creative Commons Attribution License (CC BY). The use, distribution or reproduction in other forums is permitted, provided the original author(s) and the copyright owner(s) are credited and that the original publication in this journal is cited, in accordance with accepted academic practice. No use, distribution or reproduction is permitted which does not comply with these terms.

frontiers | Frontiers in Oncology

ORIGINAL RESEARCH
published: 24 May 2022
doi: 10.3389/fonc.2022.887318

Necroptosis-Related LncRNAs Signature and Subtypes for Predicting Prognosis and Revealing the Immune Microenvironment in Breast Cancer

Yuhao Xu[1], Qinghui Zheng[2], Tao Zhou[3], Buyun Ye[1], Qiuran Xu[4] and Xuli Meng[2]**

[1] The Second Clinical Medical College, Zhejiang Chinese Medical University, Hangzhou, China, [2] General Surgery, Cancer Center, Department of Breast Surgery, Zhejiang Provincial People's Hospital (Affiliated People's Hospital, Hangzhou Medical College), Hangzhou, China, [3] Hangzhou Medical College, Hangzhou, China, [4] Laboratory of Tumor Molecular Diagnosis and Individualized Medicine of Zhejiang Province, Zhejiang Provincial People's Hospital (Affiliated People's Hospital, Hangzhou Medical College), Hangzhou, China

OPEN ACCESS

Edited by:
Shaoquan Zheng, Sun Yat-sen University Cancer Center (SYSUCC), China

Reviewed by:
Chang Gong, Sun Yat-sen University, China
Jiong Wu, Fudan University, China

***Correspondence:**
Xuli Meng
mxlmail@126.com
Qiuran Xu
windway626@sina.com

Specialty section:
This article was submitted to Molecular and Cellular Oncology, a section of the journal Frontiers in Oncology

Received: *01 March 2022*
Accepted: *15 April 2022*
Published: *24 May 2022*

Citation:
Xu Y, Zheng Q, Zhou T, Ye B, Xu Q and Meng X (2022) Necroptosis-Related LncRNAs Signature and Subtypes for Predicting Prognosis and Revealing the Immune Microenvironment in Breast Cancer. Front. Oncol. 12:887318. doi: 10.3389/fonc.2022.887318

Purpose: Necroptosis is a mode of programmed cell death that overcomes apoptotic resistance. We aimed to construct a steady necroptosis-related signature and identify subtypes for prognostic and immunotherapy sensitivity prediction.

Methods: Necroptosis-related prognostic lncRNAs were selected by co-expression analysis, and were used to construct a linear stepwise regression model *via* univariate and multivariate Cox regression, along with least absolute shrinkage and selection operator (LASSO). Quantitative reverse transcription polymerase chain reaction (RT-PCR) was used to measure the gene expression levels of lncRNAs included in the model. Based on the riskScore calculated, we separated patients into high- and low-risk groups. Afterwards, we performed CIBERSORT and the single-sample gene set enrichment analysis (ssGSEA) method to explore immune infiltration status. Furthermore, we investigated the relationships between the signature and immune landscape, genomic integrity, clinical characteristics, drug sensitivity, and immunotherapy efficacy.

Results: We constructed a robust necroptosis-related 22-lncRNA model, serving as an independent prognostic factor for breast cancer (BRCA). The low-risk group seemed to be the immune-activated type. Meanwhile, it showed that the higher the tumor mutation burden (TMB), the higher the riskScore. PD-L1-CTLA4 combined immunotherapy seemed to be a promising treatment strategy. Lastly, patients were assigned to 4 clusters to better discern the heterogeneity among patients.

Conclusions: The necroptosis-related lncRNA signature and molecular clusters indicated superior predictive performance in prognosis and the immune microenvironment, which may also provide guidance to drug regimens for immunotherapy and provide novel insights into precision medicine.

Keywords: breast cancer, necroptosis, immune infiltration, immunotherapy, long non-coding RNAs

INTRODUCTION

Among the causes of global cancer incidence, breast cancer (BRCA) ranked the first in 2020 and was the fifth leading cause of cancer-related mortalities worldwide. According to the data reported, approximately 2.3 million new cases of BRCA were recorded in 2020 (1, 2). As a highly complex and heterogeneous disease with different molecular profiles, the decision-making of BRCA diagnostic and treatment were difficult, as well as the prediction of the clinical responses to therapeutic agents and prognoses (3). Thus, new effective targeted-therapeutic precision strategies are necessary.

The dynamic change in tumor microenvironment (TME) heterogeneity is considered to be the most important aspect of tumor heterogeneity, which depends on the tumor cells themselves in the microenvironment where the infiltrating immune cells and matrix together form an antitumor and/or pro-tumor network (4). The TME, a complex ecosystem composed of stromal cells, cancer cells, fibroblasts, chemokines, and immune cells (5), serves as a site of tumor cell growth and metastasis for promoting tumor immune escape, tumor growth, and metastasis (6–8), further influencing prognosis and prediction of response to specific treatments (9).

Necroptosis, seen as a novel form of programmed necrotic cell death, plays an important part in overcoming apoptosis resistance, triggering and amplifying antitumor immunity in cancer therapy (10, 11), similar to apoptosis in mechanism and necrosis in morphology (12).

LncRNAs are involved in regulating gene expression and transcription and post-transcription processes through chromatin modification (13) and then play an important role in dysregulation of gene expression and signaling pathways that are closely related to tumorigenesis, progression, and distant metastasis (14). According to recent research results, by participating in immune gene expression (TIM) and regulating inflammation, lncRNAs could influence the malignant phenotype of cancer by changing the tumor immune microenvironment (15–17).

Nevertheless, the prognostic value of necroptosis-related lncRNAs in BRCA has not been systematically demonstrated yet, and we still lack direct evidence about the predictive power of necroptosis-related genes (NRGs) in the prognosis and immunotherapy of BRCA. In this study, we identified a novel 22-prognostic-NRlncRNA signature and four NRLClusters to characterize the molecular features of BRCA using The Cancer Genome Atlas (TCGA) database. Subsequently, we further validated that the signature could serve as a robust independent predictor of prognosis and immunosensitivity response.

Abbreviations: TCGA, The Cancer Genome Atlas; Lasso, least absolute shrinkage and selection operator; TME, tumor microenvironment; UCSC, University of California, Santa Cruz; TCIA, The Cancer Immunome Atlas; IC_{50}, half-maximum inhibitory concentration; ROC, receiver operating characteristic; NRG, necroptosis-related gene; NRlncRNA, necroptosis-related lncRNA; NRCluster, necroptosis-related cluster; NRLScore, necroptosis-related lncRNA score; CNV, copy number variation; GSVA, the gene set variation analysis; ssGSEA, single-sample gene set enrichment analysis; TMB, tumor mutation burden; PCA, principal component analysis; ICI, immune checkpoint inhibitor; TIC, tumor-infiltrating immune cell; IPS, immunophenoscore.

METHODS

Data Acquisition and Processing

Primary expression data, corresponding clinical characteristics, and mutation data for 1,078 BRCA samples were extracted from the TCGA database. A total of 1,078 patients were assigned to train and test cohorts randomly with the ratio of 1:1 using the "createDataPartition" function in the "caret" package. Copy number variation (CNV) data were collected from the University of California, Santa Cruz (UCSC) website, and the immunology treatment response data were from The Cancer Immunome Atlas (TCIA) (18–20). Based on the expression files of 67 genes associated with necroptosis sorted out from the previous literature, 1,520 necroptosis-related lncRNAs were acquired by correlation analysis using the "cor" function in the "limma" R package (21).

Construction and Validation of the Necroptosis-Related LncRNA Signature

Univariate Cox regression analysis was performed to screen out prognostic necroptosis-related lncRNAs in the train cohort using the "coxph" function in the "survival" R package. Then, the least absolute shrinkage and selection operator (LASSO) was used for the dimension reduction and K-fold cross-validation using the "cv.glmnet" function, which was multiplied by ten, and the optimal parameter was the λ value that corresponded to the lowest deviation. Subsequently, the riskScore of each patient was calculated based on each selected gene expression value multiplied by their coefficients, which were derived from the coefficient of multivariate Cox regression in the train cohort. The LASSO regression model was as follows:

$$\textit{the riskScore formula} = \textit{coefficients} * \textit{expressing values of A IncRNA} + \textit{coefficients} * \textit{expressing values of B IncRNA}$$

We divided patients into a high-risk and low-risk group with the median value of riskScore in the train cohort, and applied the value in the test and the entire cohort. The time-dependent receiver operating characteristic (ROC) curve using the "timeROC" R package and Kaplan–Meier (K-M) survival curves using the "survival" package were used to assess the signature's predictive accuracy in the train, test, and entire cohort. Based on the value of riskScore, the K-M method was used to plot survival curves with log-rank p-value < 0.05 considered statistically significant. Moreover, we paid attention to the association between clinicopathological parameters and riskScore.

Cell Culture

We purchased the normal breast epithelial cell line MCF-10A, and the epithelial BRCA cell lines MCF-7, T47D, MDA-MB-231, MDA-MB-468, and BT-549 from the American Type and Culture Collection (ATCC; Manassas, VA, USA). MDA-MB-231 and BT-549 cells were cultured in Dulbecco's Modified Eagle's Medium (DMEM) (ATCC; Manassas, VA, USA) supplemented with 10% fetal bovine serum (HyClone; Logan, UT, USA) and 1% antibiotic (100 IU/ml of penicillin and 100 μg/

ml of streptomycin; HyClone; Logan, UT, USA). MCF-10A cells were cultured in DMEM/F12 medium supplemented with 20 ng/μl EGF, insulin, hydrocortisone, NEAA, 5% HS, and 1% P/S Solution (Procell; Wuhan, China). MCF-7 and MDA-MB-468 were cultured in Minimum Essential Medium (MEM) (Gibco BRL, USA) supplemented with 10% fetal bovine serum (HyClone; Logan, UT, USA) and 1% antibiotic (100 IU/ml of penicillin and 100 μg/ml of streptomycin; HyClone; Logan, UT, USA). T-47D cells were cultured in RPMI 1640 (HyClone, Logan, UT, USA) with 10% fetal bovine serum (HyClone; Logan, UT, USA). All the cell lines were incubated at 37°C, with a humidified atmosphere of 5% CO_2.

RNA Isolation and Real-Time PCR of LncRNAs in the Signature

Total RNAs were isolated from cells using the Trizol reagent (Invitrogen). The PrimeScript™ RT reagent Kit (Takara, Japan) was employed to perform reverse transcription to synthesize cDNA following the manufacturer's protocol. Then, SYBR Green PCRMaster Mix (Applied TaKaRa, Otsu, Shiga, Japan) was used to conduct real-time PCR on Applied Biosystems 7500 Fast Real-Time RCR System (Applied Biosystems, Foster City, CA, USA). The primers of NRlncRNAs for qRT-PCR used in this research are shown as follows, which could also be seen in **Table 1**.

Construction and Validation of a Prognostic Nomogram

To improve the accuracy of predicting the prognosis of BRCA patients, we further built a prognostic nomogram based on the NRL signature and other clinicopathologic features FOR forecast the 1-, 2-, and 3-year OS using the "rms" R package (22, 23), with corresponding calibration plots reflecting the predictive accuracy of the nomogram *via* the "calibrate" function (24).

Prediction of Chemotherapy and Target Agent Response

Via the "pRRophetic" package, we calculated the half-maximum inhibitory concentration (IC_{50}) to evaluate the difference in drug response between different groups in the Genomics of Drug Sensitivity in Cancer (GDSC) database (25, 26) using Ridge's regression, along with 10-fold cross-validation for the purpose of improving the accuracy of the prediction (27, 28).

TABLE 1 | The primers of NRlncRNAs for qRT-PCR used in this research.

Primer name	Primer sequence (5' to 3')
LINC00377 Forward	5′-GGAAAAGTGCATTTGCTTCGG-3′
LINC00377 Reverse	5′-TGACCTTGATGGCTTTTGATCC-3′
MEF2C-AS1 Forward	5′-ACTTGTTGCCTACTATCATACCTG-3′
MEF2C-AS1 Reverse	5′-ATAGCCATACAATAAGTTGCTCT-3′
LMNTD2-AS1 Forward	5′-AGTGACAGGCACTCACCTAC-3′
LMNTD2-AS1 Reverse	5′-TCTCCTGGAGCAGAGGGAATA-3′
LINC02446 Forward	5′-ATAGAGGCAAAGCAAGCCACT-3′
LINC02446 Reverse	5′-GTCACATCGTAGGAGGTGCTG-3′
GAPDH Forward	5′-CTGGGCTACACTGAGCACC-3′
GAPDH Reverse	5′-AAGTGGTCGTTGAGGGCAATG-3′

Assessment of Immune Cell Infiltration, Immune Checkpoint, and Immunotherapy

We calculated immune cell infiltration in each sample using the single-sample gene set enrichment analysis (ssGSEA) algorithm and found out the significantly differential pathways between the two groups with gene set variation analysis, using the "GSEABase" and "GSVA" packages. Furthermore, we further performed CIBERSORT algorithm, which used expression data to assess the stromal and immune cells using the "e1071", "parallel", and "preprocessCore" packages, and Spearman rank correlation analysis for analyzing the correlation between the riskScore and the relative expression level of the 22 tumor-infiltrating leukocytes using the "limma" package. We also probed into the expression levels of known immune checkpoint genes in high- and low-risk groups. Furthermore, we discussed the relationship between the NRLscore and clinical PD-L1 and CTLA-4 subtypes in the TCIA database using Student's *t*-test.

Tumor Mutation Burden Analyses

Using mutation data of BRCA patients, the waterfall plot was generated with Maftools R-package to compare the differences in gene mutation frequency between high- and low-risk BRCA patients. We analyzed the correlation between TMB and riskScore using Student's *t*-test and Spearman rank correlation analysis.

Profiles of Necroptosis-Related LncRNAs Identified Four Distinct Molecular Phenotypes of BRCA

By using hierarchical agglomerative clustering on the basis of Euclidean distance and Ward's linkage (29), BRCAs with qualitatively varying necroptosis-related lncRNA expressions were clustered. The K-means method was applied to classify patients for further study using the "ConsensusClusterPlus" package (30).

Statistical Analysis

All statistical data analyses were performed in GraphPad Prism (version 7) and R software (version 4.1.1). Wilcoxon test (for comparison between two groups) and Kruskal–Wallis test (for comparison among more than two groups) were applied to discuss the statistically significant differences. Log-rank test was used to determine the differences in overall survival between different risk groups and molecular clusters. The correlations between the two were evaluated *via* Spearman's correlation analysis. $p < 0.05$ was considered to be the threshold for statistical significance, and all the *p*-values mentioned in the paper were two-tailed.

RESULTS

Genetic Variation Landscape of Necroptosis-Related Genes in BRCA

According to the previous literature, we confirmed 67 NRGs (22). Genomic mutations were common in these genes, with genetic changes occurring in 145 (14.75%) of 983 patients, in which ATRX (2%) had the most genetic alteration, and a

mutation frequency of 1% was observed in CASP8, GATA3, BACH2, EGFR, STAT3, TLR3, DNMT1, BRAF, RIPK1, TSC1, AXL, HSPA4, FLT3, ALK, RNF31, and IDH1 (**Figure 1A**). The location of the 67 NRGs in human chromosomes can be seen in **Figure 1B**. Meanwhile, we found that most genetic variations had CNV amplification (**Figure 1C**). In order to discover the interaction of the 67 NRGs directly, we constructed a network to show the connection between each other (**Figure 1D**). The differential analysis in normal breast tissue and tumor tissue revealed that, except for RIPK1, RIPK3, TNF, MAP3K7, and STAT3, all the other genes showed significantly differential expression in BRCA (**Figure 1E**). PLK1, CDKN2A, TERT, LEF1, MYCN, GATA3, ZBP1, TRIM11, IDH2, FLT3, TRAF2, and FADD were seen as upregulated genes in BRCA, with the value of log FC of TERT being the highest (log FC = 2.627). ALK, ID1, BACH2, EGFR, and KLF9 were seen as downregulated genes in BRCA, with the value of log FC of KLF9 being the highest (log FC = −1.601) (**Figure 1F**). The alteration and genetic variation of NRGs acted as an important part in regulating the happening, aggravation, and prognosis of BRCA.

Identification of Prognostic Necroptosis-Related LncRNAs

The clinical data and transcriptome data were retrieved from the TCGA database, including 1,096 BRCA specimens and 112 normal specimens. We performed Spearman correlation analysis between the lncRNAs and NRGs, and 1,520 necroptosis-related lncRNAs (NRlncRNAs) were sorted out with the filter criteria of correlation coefficients >0.4 and $p < 0.001$ (21, 22, 31, 32) (**Table S1** and **Figure 2A**). Forty-six

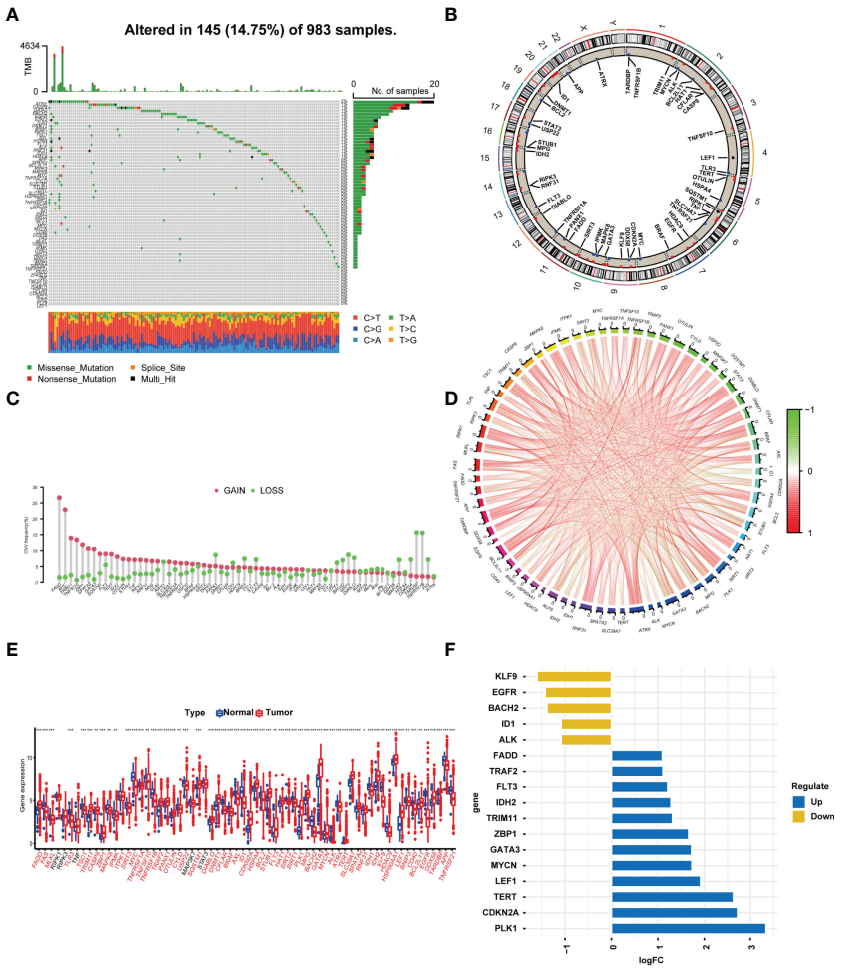

FIGURE 1 | Profile of the 67 necroptosis-related genes in BRCA. **(A)** In all, 145 of 983 (14.75%) BC patients experienced 67 necroptosis-related gene alterations. **(B)** The location of the 67 necroptosis-related genes in chromosomes. Blue points represented that the gene mainly had CNV deletion, red points represented that the gene mainly had CNV amplification. **(C)** CNV mutation frequency of the 67 necroptosis-related genes. This column represents the frequency of change. Deletion frequency is represented by green dots, while amplification frequency is represented by pink dots. **(D)** Expression interaction of the 67 necroptosis-related genes in BRCA. The lines connecting the necroptosis-related genes show how they are correlated with each other, with positive associations in red and negative associations in green. **(E)** Expression of the necroptosis-related genes in normal tissues and BRCA tissues. Genes with red color represented the differentially expressed genes. **(F)**. The value of logFC of the genes. *P<0.05; **P<0.01; ***P<0.001.

prognostic NRlncRNAs in BRCA were extracted by univariate analysis, of which the significant filtering condition was $p < 0.05$ (**Table S2** and **Figures 2B, C**).

Establishment and Validation of Prognostic Signature for NRlncRNAs in BRCA

LASSO-penalized Cox regression was used to establish the following equation based on the expression of 22 NRlncRNAs in the train cohort (**Figures 2D, E**):

$$riskScore = [(0.0314 \times AC125807.2) + (0.3155 \times ZBTB40 - IT1) + (-0.0010 \times AC124319.2) + (-0.0086 \times LMNTD2AS1) + (0.0394 \times AC079298.3) + (0.0044 \times AP001505.1) + (-0.2655 \times NDUFA6 - DT) + (-0.9949 \times AL450322.1) + (0.0230 \times AC009237.14) + (-0.0061 \times LINC02446) + (0.3555 \times AC007608.3) + (0.0979 \times MIR600HG) + (0.1248 \times LINC00900) + (-0.0385 \times LINC01871) + (0.6195 \times MFF - DT) + (0.0054 \times AL078581.2) + (-0.7159 \times LINC00377) + (-0.0019 \times AL133467.1) + (-0.6298 \times MEF2C - AS1) + (-0.1186 \times AP001107.9) + (-0.0838 \times AC010201.2) + (-0.1161 \times AL451085.3)$$

Compared with the normal breast tissue, the expression levels of LMNTD2-AS1, AC007608.3, and LINC02446 were significantly higher in the BRCA group, while the expression levels of LINC00377, AL450322.1, MEF2C-AS1, and AC079298.3 were lower with the filter criteria of $p < 0.05$ and |log FC| > 1 (**Figures 2F–H**). qRT-PCR analyses verified the results of bioinformatics analysis, revealing that expression levels of LncRNA LINC00377 MEF2C-AS1 were significantly downregulated in BRCA cell lines compared with the normal breast cell line ($p < 0.05$, **Figures 2I–L**).

Combining the coefficients and expression of the above NRlncRNAs, we computed the riskScore for each BRCA patient. The entire cohort included 1,078 samples, which were randomly divided into a train cohort (540 samples) (**Table S3**, Sheet train) and a test cohort (538 samples) (**Table S3**, Sheet test) according to the ratio of 1:1. Based on the value of the median riskScore in the train cohort, we divided patients into high- and low-risk groups in the train and test cohort, respectively. A total of 270 patients were categorized into the high-risk group, and 270 patients were categorized into the low-risk group in the train cohort while 258 patients were categorized into the high-risk group and 280 patients were categorized into the low-risk group in the test cohort (**Figures 3A, G, M**).

We performed principal component analyses (PCAs), and the result indicated good discriminative performance of the NRlncRNA model in the train, test, and entire cohort (**Figures 3B, H, N**). The K-M survival curve displayed that compared with the high-risk group, the OS of patients in the low-risk group was significantly longer$p < 0.001$ in three cohorts) (**Figures 3E, K, Q**). The area under curve (AUC) values for the 1-year (0.812), 2-year (0.801), and 3-year (0.776) survival rates in

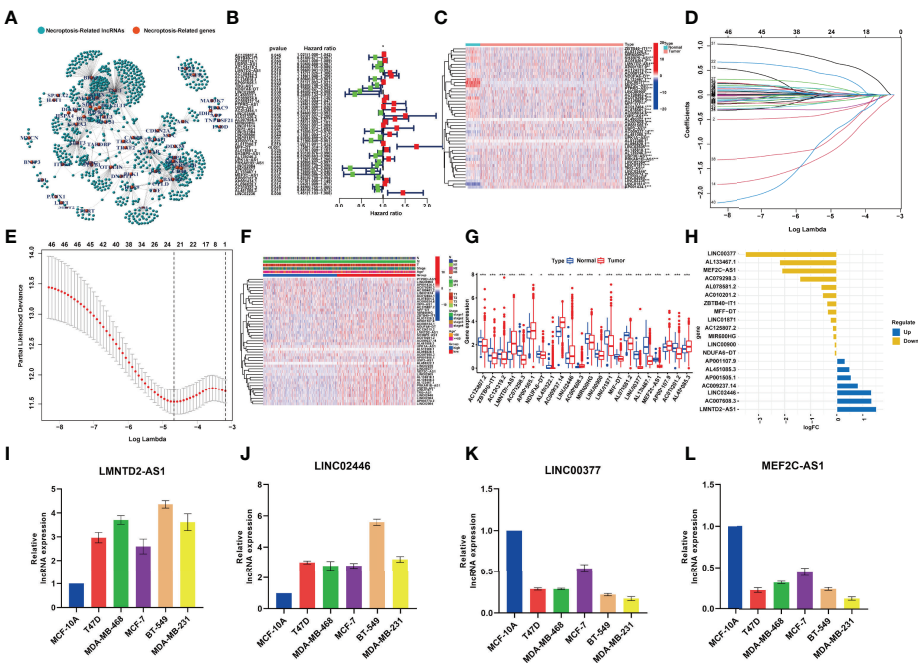

FIGURE 2 | **(A)** The network between necroptosis-related genes and lncRNAs (correlation coeffcients >0.4 and $p < 0.001$). **(B)** The prognostic necroptosis-related lncRNAs extracted by univariate Cox regression analysis. **(C)**. The heatmap that showed the expression profiles of 46 prognostic lncRNAs, which showed significant difference between normal and cancer tissues. **(D)** The 10-fold cross-validation for variable selection in the LASSO model. **(E)** The LASSO coeffcient profile of 22 necroptosis-related lncRNAs. **(F)** Correlation analysis between risk groups and clinical features. **(G)** Expression of the 22 NRlncRNAs in the model between normal tissues and BRCA tissues. **(H)** The value of logFC of the 22 NRlncRNAs. **(I–L)** qRT-PCR results showing the expression of lncRNAs in the normal breast and five breast cancer cell lines. *P<0.05; **P<0.01; ***P<0.001.

the train cohort, 1-year (0.720), 2-year (0.696), and 3-year (0.682) survival rates in the test cohort, and 1-year (0.765), 2-year (0.745), and 3-year (0.732) survival rates in the entire cohort showed favorable specificity and sensitivity of the signature in predicting OS (**Figures 3F, L, R**). Lastly, we performed univariate and multivariate Cox regression analyses internally and externally, implying that age and riskScore, which served as high-risk factors, were significantly correlated with OS ($p < 0.05$, HR > 1) (**Figures 3C, D, I, J, O, P**). These results revealed that the NRlncRNA signature could efficiently and independently identify the risk of BRCA prognosis.

Stratified Prognostic Analysis and Association of NRlncRNA Signature With Clinical Logical Features

To further demonstrate the predictive power of the prognostic model, we performed the K-M analysis by log-rank test for the purpose of assessing the prediction capacity of multiple clinical characteristics on BRCA patients after stratifying the patients into subgroups of age (≥55 and <55), AJCC stage (I + II and III + IV), T stage (T1-2 and T3-4), N stage (N0-1 and N2-3), and M stage (M0 and M1). The results revealed that the NRlncRNA signature had good prognostic ability in each clinical subgroup (**Figures 4A–J**).

We also focused our attention to the association of NRlncRNA signature with age, T stage, M stage, N stage, and AJCC stage in BRCA patients. The riskScore was significantly higher in the T4, M1, and stage IV groups compared with the other corresponding groups (**Figures 4K–O**). However, we also observed that HER-2-positive BRCA indicated a higher riskScore, while Luminal BRCA indicated a lower riskScore (**Figure 4P**).

Development of the Nomogram for Prognostic Prediction

To further enhance the prognostic prediction power, we developed a nomogram that integrated age, TNM stage, and riskScore (**Figure 4P**). Then, we built calibration curves, of which the *y*- and *x*-axis represent the actual and predicted survival rate from the nomogram to assess the predictive accuracy and clinical practicability of this nomogram. The calibration plot for OS probability at 1, 2, and 3 years suggested satisfactory consistency between the actual and predicted survival probabilities (**Figures 4Q–T**).

Prediction of Chemotherapy or Target Agent Response

The IC_{50} values of several chemotherapeutic agents were used to evaluate chemotherapeutic response to BRCA patients. We observed that low-risk patients had dramatically reduced IC_{50} values of bleomycin, bortezomib, cisplatin, dasatinib, doxorubicin, gefitinib, and paclitaxel compared to those with high risk, suggesting

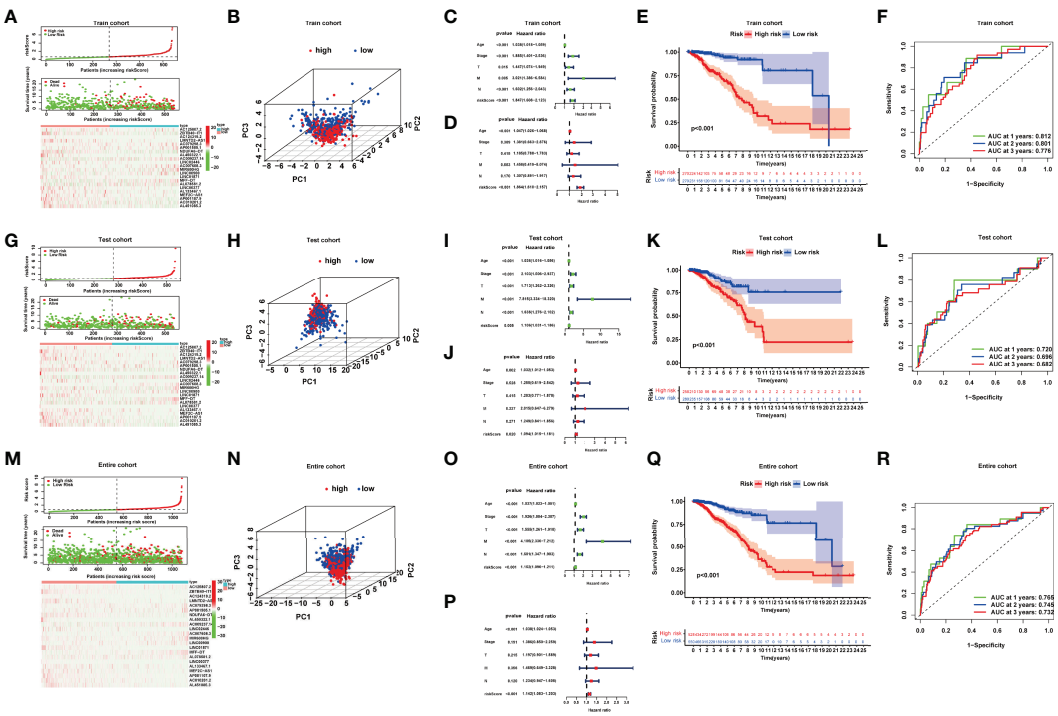

FIGURE 3 | **(A, G, M)** Risk curve; scatter plot of vital status by risk score; heatmap of the 22 lncRNAs' expression in the train, test, and entire cohort. **(B, H, N)** Principal component analysis (PCA) of BRCAs based on the riskScore in the train, test, and entire cohort. **(C, D, I, J, O, P)** Univariate and multivariate Cox regression analyses in the train, test, and entire cohort. **(E, K, Q)** Kaplan–Meier curves of the high- and low-risk patients in the train, test, and entire cohort. **(F, L, R)** Time-dependent ROC curves for predicting 1-, 2-, and 3-year OS in the train, test, and entire cohort.

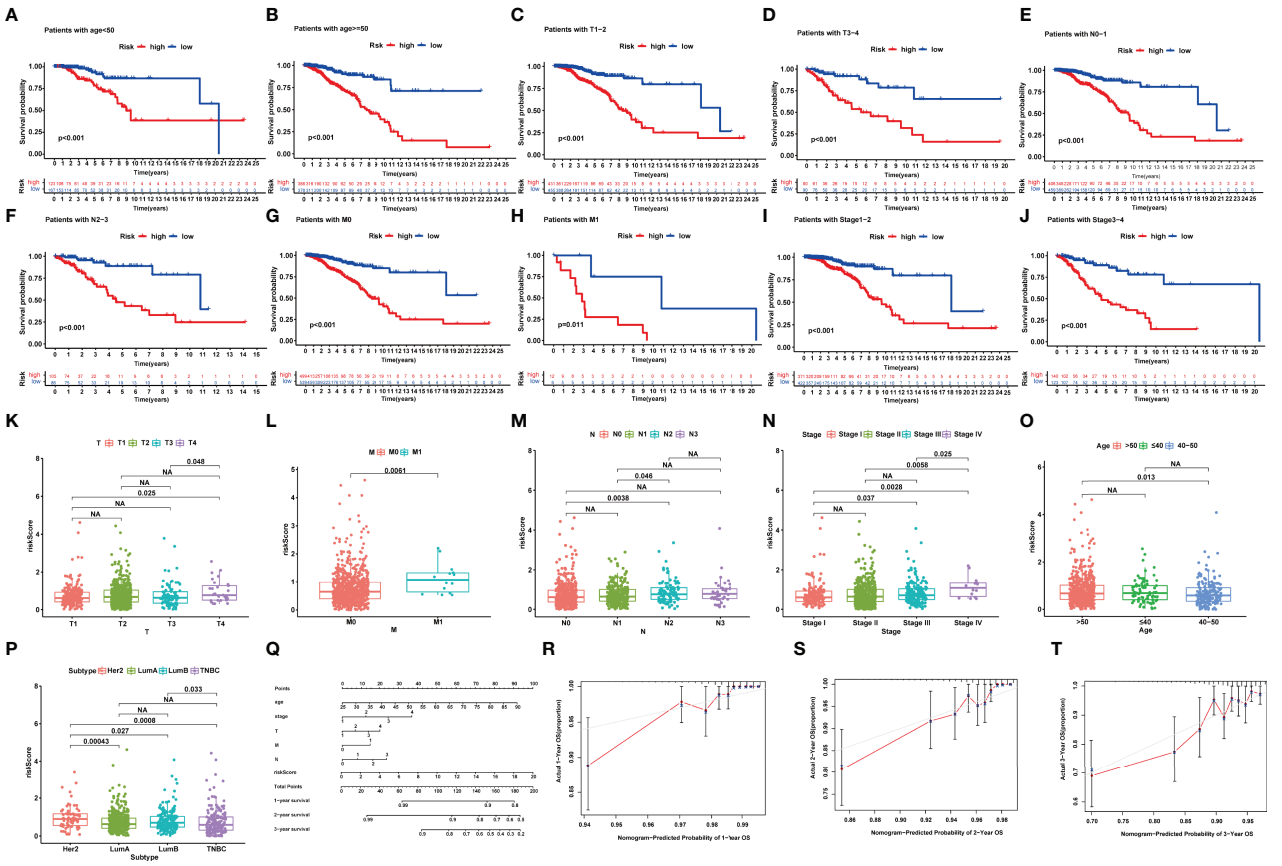

FIGURE 4 | **(A–J)** Kaplan–Meier survival analysis for BRCA patients with diverse clinical characteristics of **(A, B)** age, **(C, D)** T-Stage, **(E, F)** N-stage, **(G, H)** M-stage, and **(I, J)** AJCC stage. **(K–P)** Correlation between signature and clinical characteristics. **(Q)** The nomogram plot integrating NRlncRNA riskScore, age, T-, N-, and M-classification. **(R–T)** The calibration plot for the probability of 1-, 2-, and 3-year OS. NA, P>0.05.

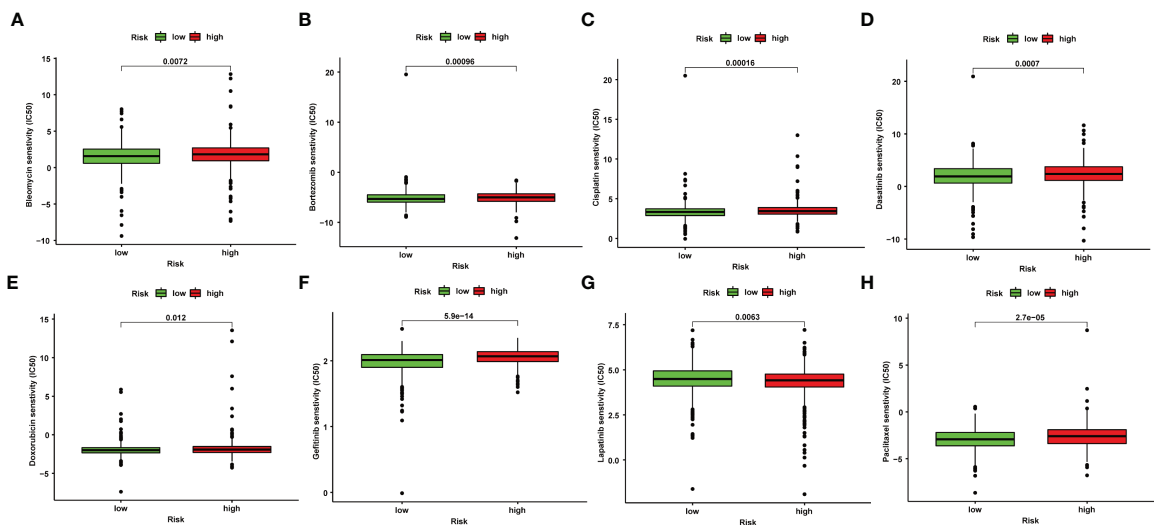

FIGURE 5 | Correlation between NRlncRNA signature and drug sensitivity. Box plots for the estimated IC_{50} of drugs between high- and low-risk BRCA patients. Bleomycin **(A)**, Bortezomib **(B)**, Cisplatin **(C)**, Dasatinib **(D)**, Doxorubicin **(E)**, Gefitinib **(F)**, Lapatinib **(G)**, Paclitaxel **(H)**.

that low risk was indicative of increased sensitivity to the above drugs (**Figures 5A–H**). Therefore, the NRlncRNA signature could act as a potential chemotherapy predictor.

Mutation Analysis and Tumor Mutation Burden Calculation

We observed a broader TMB in the high-risk group with 365 (76.2%) of 479 patients compared to the low-risk group. PIK3CA, TP53, and TTN had the most genetic alteration, of which mutation frequency was all over 10%. The results revealed a potential interaction between individual somatic mutations and riskScore (**Figures 6A, B**). The K-M curves showed a significantly better OS in the low-TMB group compared with the high-TMB group (**Figure 6C**). Moreover, we noticed that the tumor mutation load (TMB) was closely related to the riskScore with $R = 0.18$, $p < 4e\text{-}08$ (**Figure 6F**); the higher the riskScore, the higher the TMB (**Figure 6E**). Then, the two factors were taken into account together; the patients with a low riskScore and low TMB had the best prognosis; meanwhile, the patients with a high riskScore and high TMB had the worst prognosis (**Figure 6D**).

Gene Set Enrichment Analysis and Gene Set Variation Analysis Between the High- and Low-Risk Groups

After GSEA was performed, we observed that several pathways with enrichment in the high-risk group were related to immunity with the filter criteria of FDR q-value<0.05 (**Table S4**), including "ECM_RECEPTOR_INTERACTION", "FOCAL_ADHESION", and "GAP_JUNCTION" (**Figure 7A**). Based on the calculated enrichment score of each sample, we identified enriched-pathway variation between the low-risk and high-risk group using the GSVA method (FDR < 0.05). We observed that from the low-risk to the high-risk group, the enrichment score was obviously increased in "HALLMARK_PROTEIN_SECRETION", "MTORC1_SIGNALING", "MYC_TARGETS_V1", "OXIDATIVE_PHOSPHORYLATION", "UNFOLDED_PROTEIN_RESPONSE","G2M_CHECKPOINT", and "E2F_TARGETS". The above results indicating the NRlncRNAs may affect immune-related mechanisms (**Figure 7B**).

Potential Application of Necroptosis LncRNA Signature for Predicting Tumor Immune Microenvironment and Immunotherapy Responses

Subsequently, we used the "CIBERSORT" algorithm to investigate the correlation between riskScore and tumor-infiltrating immune cell (TIC) infiltration (**Table S5**). The relative proportion of immune cells in the BRCA samples by the "CIBERSORT" algorithm can be seen in **Figure S1**. The scatter plots showed the association between riskScore and the proportion of related TIC species ($p < 0.05$) in BRCA samples. We observed that the value of riskScore was positively correlated with the infiltrating levels of M2 macrophages and M0 macrophages, while the value of riskScore was negatively associated with the infiltrating levels of naive B cell, resting dendritic cells, activated NK cells, plasma cells, CD4+ T cells, CD8+ T cells, CD4+ memory T cells, follicular helper CD4 T cells, and regulatory T cells (**Figures 7D–M**).

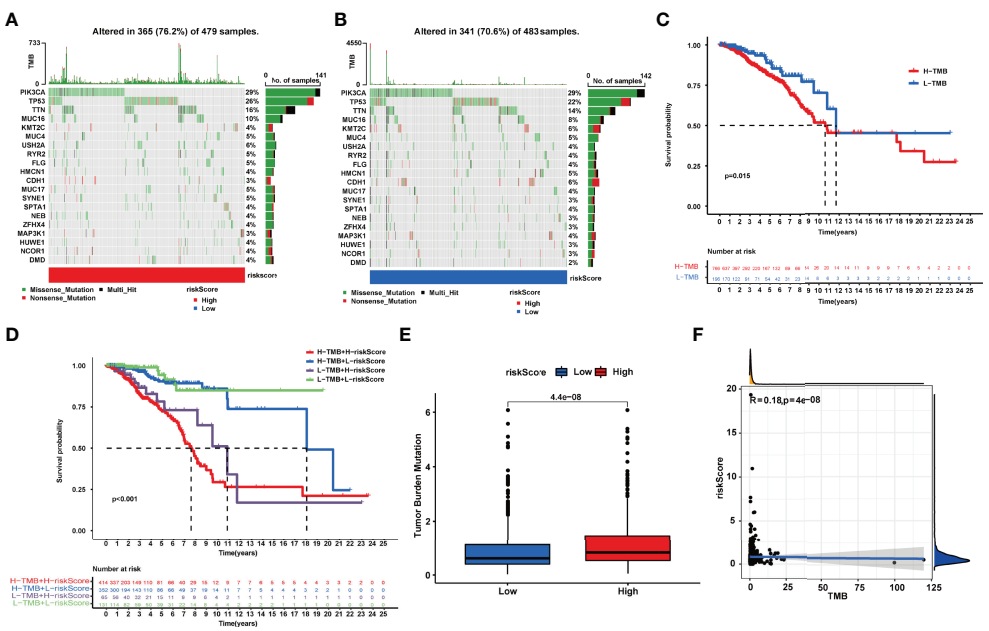

FIGURE 6 | **(A, B)**. Tumor somatic mutation waterfall chart established from patients with high and low riskScores: **(A)** High-riskScore group and **(B)** low-riskScore group. **(C)** Kaplan–Meier survival analyses of TMB in BRCA patients on overall survival. **(D)** Kaplan–Meier survival analyses of TMB and riskScore on overall survival. **(E)** The relationship between TMB and riskScore groups. **(F)** Correlation analysis of the riskScore and tumor mutation load.

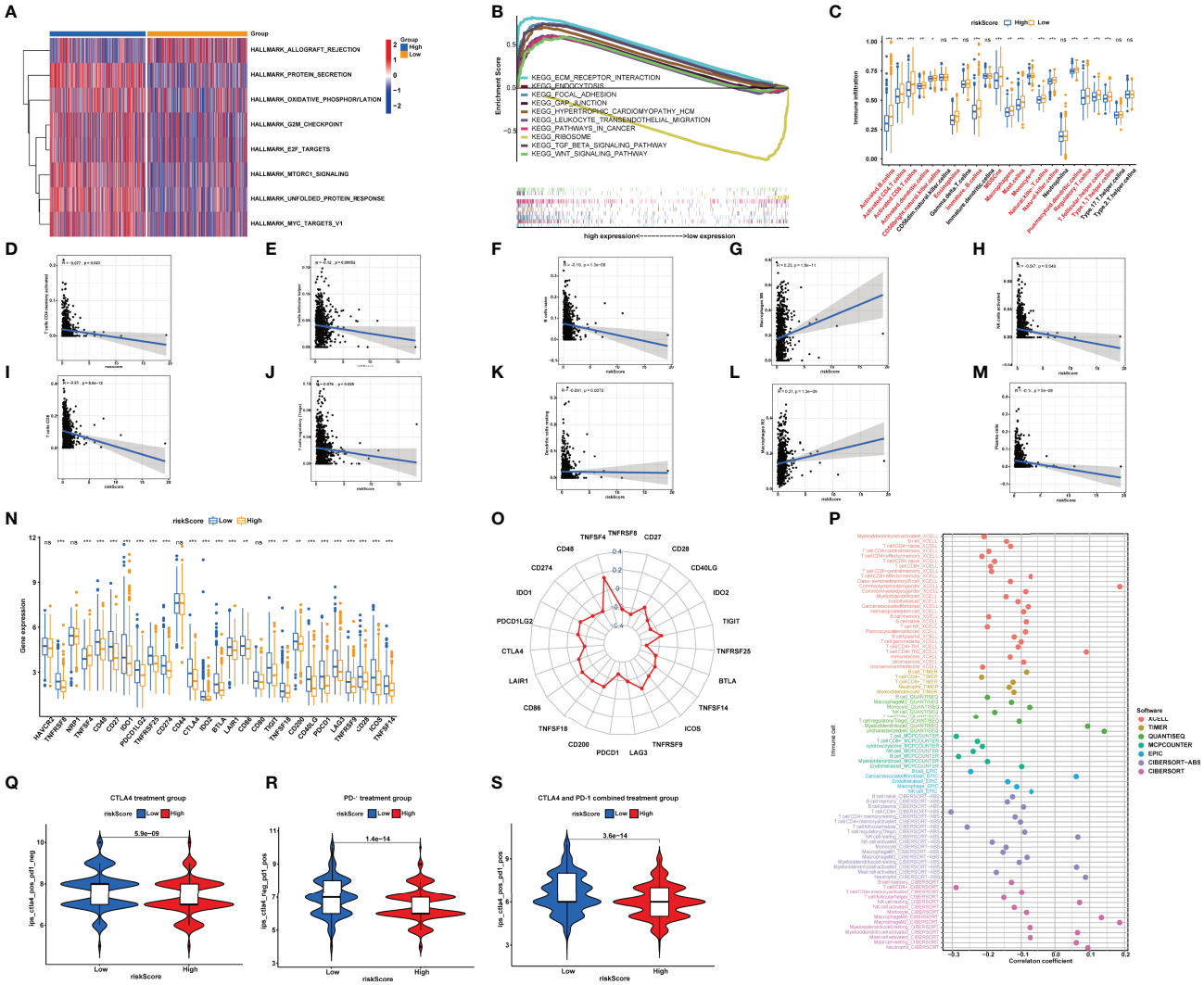

FIGURE 7 | **(A)** Different pathways between the high-risk and low-risk groups. **(B)** Enrichment analyses of biological functions and pathways in the high- and low-risk group. **(C)** Single-sample gene set enrichment analysis of immune status between low- and high-risk subgroups. **(D–M)** Correlation between the distribution of tumor immune cells and value of NRlncRNA riskScore. **(N, O)** Comparisons of the expression levels of immune checkpoints between two groups. **(P)** The immune cell bubble of risk groups. **(Q–S)**. Treatment effects of CTLA-4 or PD-1 and combined CTLA-4 and PD-1 were evaluated in patients with high and low riskScores. **(Q)** CTLA-4 treatment group, **(R)** PD-1 treatment group, and **(S)** CTLA-4 and PD-1 combined treatment group. *P<0.05; **P<0.01; ***P<0.001. ns, P>0.05.

We furthermore aimed to explore the relationship between the risk groups and immune cell infiltration by calculating the number of immune cells in BRCA using ssGSEA (**Table S6** and **Figure 7C**). The results demonstrated that the contents of CD56+ NK cells, γδ-T cells, immature dendritic cells, neutrophils, and type 17 T-helper cells did not show a significant difference among the 28 types of immune cells between two groups. The other 22 types of immune cells were decreased in the high-risk group (**Figure 7C**). Thus, it was concluded that low risk is a type of immune activation, while high risk is a type of immune failure. The above results were validated based on XCELL, CIBERSORT-ABS, TIMER, QUANTISEQ, MCPCOUNTER, EPIC, and CIBERSORT-ABS algorithms (**Figure 7P**). According to the conclusion, we speculated that the riskScore may be significantly correlated with regulating immunity and then affecting the prognosis of BRCA patients.

Synthesizing the results of ssGSEA and CIBERSORT, we came to a conclusion: the riskScore was negatively correlated with the infiltrating levels of naive B cells, resting dendritic cells, activated NK cells, plasma cells, CD4+ memory T cells, CD8+ T cells, follicular helper T cells, and regulatory T cells, indicating that the riskScore may affect tumor-infiltrating immune cell (TIC) infiltration.

Immune Checkpoint and Immunotherapy

Immune checkpoint inhibitors (ICIs) were a rising and valid treatment strategy targeting numerous species of cancers; filtrating patients sensitive to ICIs will be beneficial to precise and

effective medicine. As previous results showed that riskScore was a dependable prognostic factor, and was associated with TMB and tumor infiltration, we then aimed to verify the ability of riskScores in predicting immunotherapeutic benefits. We observed that a lower riskScore indicated a higher expression level of the other immune checkpoints except for TNFSF4 (**Figures 7N, O**).

In TCIA, the IPS (immunophenoscore), which was based on immunogenicity, could achieve a high accuracy on predicting the immunotherapy response of patients. Therefore, we analyzed the relationship of IPS between high- and low-riskScore groups. We perceived that in the CTLA-4 and PD-1 groups, patients in the low-riskScore group both showed better treatment effects (CTLA-4: 5.9e−09; PD-1: 1.4e-14) (**Figures 7Q, R**). In the CTLA-4 and PD-1 combined treatment group, patients in the high-m6A score group still indicated better treatment effects (p = 3.6e−14) (**Figure 7S**), which meant that patients accepting the treatment of both PD-L1 and CTLA4 showed superior reactivity of immune response. The result provided us advice in clinical practice on whether to use and what to use for immunotherapy. Overall, the riskScore established by us had great potential in predicting prognosis and immunotherapeutic benefits, which may provide sally ports for us to provide individualized and precise treatment.

Identification of Necroptosis-Related Molecular Phenotypes

Based on the expression profiles of the 22 NRlncRNAs in the signature, we performed consensus clustering. k = 4 was identified with optimal clustering stability from k = 2 to 9, which showed the greatest correlation within the group and a low correlation among groups (**Figure 8B**), suggesting the practicability of dividing the patients into four clusters based on 22 NRlncRNAs. A consensus cumulative distribution function (CDF) diagram showed that when k = 4, CDF reached an approximate maximum (**Figure 8C**), and classification was robust (**Figures 8A, D**). The K-M curve revealed that patients in NRLCluster 4 had the best OS, while those in NRLCluster 3 had the worst OS (**Figure 8E**).

Development of NRLScore to Quantify Individual Necroptosis Pattern

In view of the individual heterogeneity and complexity of BRCA patients, we calculated NRLScore based on the PCA on the 22 NRlncRNAs in the model. We defined NRLScore = PC1+PC2 to quantify the individual necroptosis pattern of BRCA patients and further to facilitate precise treatment. As indicated from the K-M curve, patients with a higher NRLScore had a better OS (**Figure 8F**). We also observed that NRLScores of patients in ferrCluster 4 were significantly higher than NRLClusters 1, 2, and 3 (**Figure 8G**). The Sankey diagram shows the attribute changes in riskScore, NRLCluster, NRLScore, and survival status, indicating that the higher the riskScore and the lower the NRLScore, the higher the risk of death (**Figure 8H**). The above results enriched treatment strategies for BRCA patients not only in targeted therapy and chemotherapy but also in immunotherapy.

DISCUSSION

Immunotherapy is a rapidly evolving concept that has been given the tag “fifth pillar” of cancer therapy (33), which has shown clinical efficacy in a variety of cancers (34), and has become an

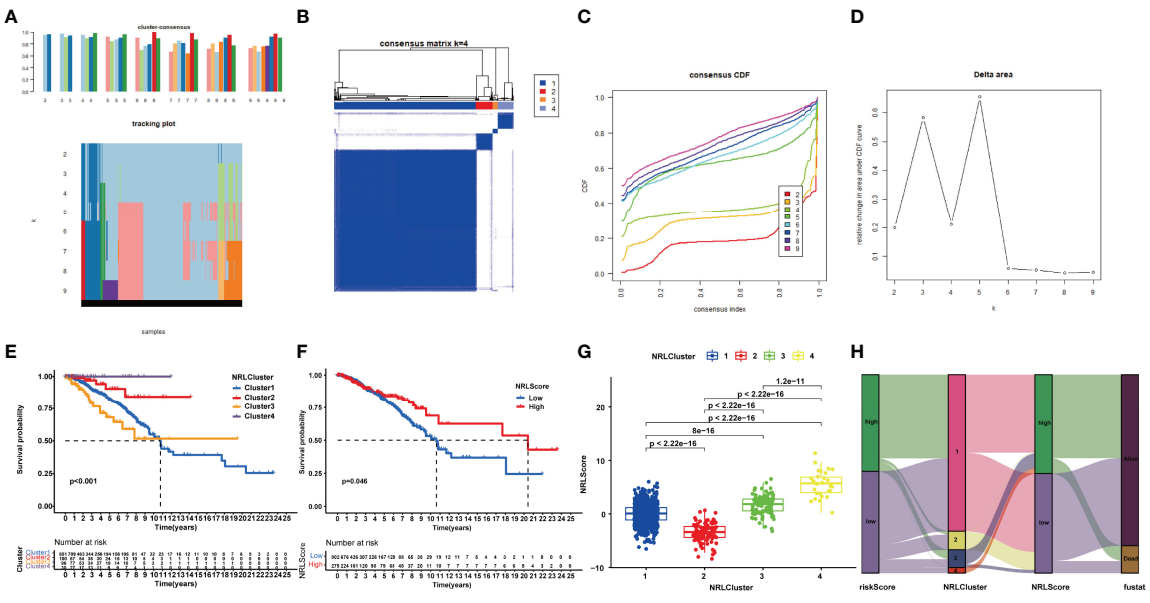

FIGURE 8 | Consensus clustering of 22 NRlncRNAs identified four clusters of patients. **(A)** The tracking plot for k = 2 to k = 9. **(B)** The heatmap for k = 4. **(C)** Consensus clustering CDF with k = 2 to k = 9. **(D)** Relative change in area under the CDF curve for k = 2–9. **(E)** KM curve of the survival difference among clusters 1–4. **(F)** KM curve of the survival difference between high- and low-risk groups. **(G)** Correlation between NRLCusters and NRLScore. **(H)** Sankey diagram showing the co-expression of riskScores, NRLClusters, and NRLScores.

established form of cancer treatment (35). Historically, BRCA has been considered to be an immunogenic "cold" tumor. However, the appearance of ICIs resulted in immunotherapy becoming an emerging new treatment modality for BRCA (36). BRCA subtypes are both genetically and phenotypically distinct, and response rates to immunotherapy in BRCA vary among the different clinical subtypes of BRCA, which may not be the optimal classification to assess immunotherapy sensitivity (37).

Necroptosis plays an integral part in the induction and amplification of cancer immunity (10). RIPK3 is required to regulate cytokine expression in DCs, which is a key sentinel in regulating immune homeostasis (38). As is reported, necroptosis occurs during the late stage of T-cell proliferation and necroptotic signaling is markedly intensified in T cells absent in FADD, suggesting that FADD may negatively regulate necroptosis mediated by T-cell receptors (39). Furthermore, necroptosis initiates adaptive immune responses by releasing DAMPs into the tissue microenvironment (40). The TME status is the leading cause of the differential responses and outcomes in cancer patients receiving the same treatment, especially for multiple immunotherapies (41, 42). Therefore, explaining the diversity and complexity of TME is an indispensable step to enhance the predictive power and clinical guidance of immunotherapy.

Extensive interest in cancer immunotherapy is reported according to the clinical importance of CTLA-4 and PD-1/PD-L1 [programmed death (PD) and programmed death-ligand (PD-L1)] in immune checkpoint therapies (43). The main immune checkpoints for BRCA include cytotoxic T-lymphocyte-associated protein-4 (CTLA-4), programmed death receptor 1/programmed cell death ligand 1 (PD-1/L1), lymphocyte activation gene 3 (LAG-3), T-cell immunoglobulin domain and mucin 3 (TIM-3), and other molecules (44). Clinical trials like SOLTI-1503 PROMETEO TRIAL (45), KEYNOTE-086 (46), NIMBUS (47), KEYNOTE-173 (48), KEYNOTE-522 (49), and KEYNOTE-355 (50) showed that ICIs have made significant progress in BRCA immunotherapy, which is expected to become a new treatment for BRCA.

In this study, 46 NRlncRNAs were obtained by using the univariate Cox regression analysis. To prevent model overfitting, we performed LASSO regression analysis to identify 22 key NRlncRNAs, and multivariate Cox regression analysis was applied to calculate coefficients and construct the risk model. The K-M curves showed that patients in the low-risk group had longer survival than those in the high-risk group. Afterwards, we established forest plots and ROC plots including age, sex, T-stage, N-stage, M-stage, AJCC stage, and risk scores. By plotting a risk heatmap, a risk curve, an ROC curve, and a survival curve, we drew a conclusion that the risk model indeed had a good predictive effect. Meanwhile, we obtained similar results in the test cohort. According to the results of GSEA and GSVA, it was concluded that these two groups were associated with immunity. Then, ssGSEA and CIBERSORT algorithms were used to assess the status of the immune cell infiltration of each patient, and we found out that the low-risk group could be described as the immune-activated type, while the high-risk group could be described as the immune failure type. Meanwhile, the riskScore has a positive correlation with TMB; the higher the TMB, the worse the prognosis. The PD-L1 combined CTLA4 immunotherapy seemed suitable for patients who had a lower riskScore. Finally, we identified three necroptosis-related molecular patterns using consensus clustering analysis.

Compared with existing signature makers, Xu et al. provided an RNA binding protein-related lncRNA prognostic signature for prognosis (51), Yan et al. built a signature for CRISPR-Cas9-Based Cancer Dependency Map Genes (52), and Zou et al. identified glycolysis-related lncRNAs (53); the NRlncRNA signature showed higher values of AUCs and performed better prediction of prognosis in stratified risk analysis of survival. However, we also noticed TNBC patients with a lower riskScore, which seemed not so rational. We thought that based on our small sample size (we chose the BRCA patients whose clinicopathological parameters were complete), a certain degree of deviation rather than the NRlncRNAs signature itself might contribute to this strange phenomenon. Nonetheless, there are certain limitations to our study. First, our conclusions were only based on the datasets from TCGA. In other words, only retrospective datasets were used to identify our conclusion. Thus, a large, prospective, and multicenter clinical cohort is needed to confirm and improve the accuracy of the model. Moreover, the range of studies included all subtypes of BRCA. However, anti-PD-1/PD-L1 or anti-CTLA4 was mainly used in triple-negative breast cancer (TNBC) (54–56); thus, we would choose TNBC patients in further studies. Finally, the specific mechanism of necroptosis-related lncRNAs in BRCA and their interconnection with immunity are not yet fully understood; we will verify the expression levels of LINC00377, MEF2C-AS1, LMNTD2-AS1, and LINC02446 in patients in Zhejiang Provincial People's Hospital rather than only in BRCA cells, and more experimental studies are needed to reveal the detailed molecular mechanisms in BRCA of the NRlncRNAs in the signature.

CONCLUSIONS

Our research constructed a novel NRlncRNA signature that is useful for predicting the survival outcome of patients with BRCA to evaluate the TME immune cell infiltration characteristics of a single patient with BRCA. Furthermore, it also showed superior predictive power in clinical response to immunotherapy. In short, our results provide insights to improve personalized cancer immunotherapy and to distinguish the drug response of patients with BRCA well.

DATA AVAILABILITY STATEMENT

The original contributions presented in the study are included in the article/**Supplementary Material**. Further inquiries can be directed to the corresponding authors.

AUTHOR CONTRIBUTIONS

XM and QX substantially contributed to the conception of the work. YX, TZ, and BY contributed to the data collection. YX and

QZ performed the nomogram model analyses and wrote the manuscript. YX, BY, and TZ helped to perform the enrichment and network analysis. YX, QZ, XM and QX drafted and revised the manuscript. All authors contributed to the article and approved the submitted version.

FUNDING

This research was supported by grants from the National Natural Science Foundation of China (81973861) and the Zhejiang Provincial Ministry Medical and Health Co-construction Major Project (20214355173).

SUPPLEMENTARY MATERIAL

The Supplementary Material for this article can be found online at: https://www.frontiersin.org/articles/10.3389/fonc.2022.887318/full#supplementary-material

Supplementary Figure 1 | The relative proportion of immune cells in the BRCA samples.

Supplementary Table 1 | 1520 necroptosis-related lncRNAs (NRlncRNAs) (correlation coefficients >0.4 and $p < 0.001$).

Supplementary Table 2 | 46 prognostic NRlncRNAs ($p < 0.05$).

Supplementary Table 3 | riskScores of patients in train and test cohorts.

Supplementary Table 4 | Gene set enrichment analysis between the high-risk and low-risk groups.

Supplementary Table 5 | "CIBERSORT" algorithm to investigate the correlation between riskScore and tumor-infiltrating immune cells (TIC) infiltration.

Supplementary Table 6 | The relationship between the risk groups and immune cells infiltration *via* calculating the number of immune cells in BRCA using single-sample gene set enrichment analysis.

REFERENCES

1. Sung H, Ferlay J, Siegel RL, Laversanne M, Soerjomataram I, Jemal A, et al. Global Cancer Statistics 2020: GLOBOCAN Estimates of Incidence and Mortality Worldwide for 36 Cancers in 185 Countries. *CA Cancer J Clin* (2021) 71 (3):209–49. doi: 10.3322/caac.21660
2. Siegel RL, Miller KD, Fuchs HE, Jemal A. Cancer Statistics, 2021. *CA Cancer J Clin* (2021) 71(1):7–33. doi: 10.3322/caac.21654
3. Perou CM, Sorlie T, Eisen MB, van de Rijn M, Jeffrey SS, Rees CA, et al. Molecular Portraits of Human Breast Tumours. *Nature* (2000) 406(6797):747–52. doi: 10.1038/35021093
4. Li W, Li F, Zhang X, Lin H, Xu C. Insights Into the Post-Translational Modification and its Emerging Role in Shaping the Tumor Microenvironment. *Signal Transduct Tar Ther* (2021) 6(1):422. doi: 10.1038/s41392-021-00825-8
5. Liu J, Wang X, Deng Y, Yu X, Wang H, Li Z. Research Progress on the Role of Regulatory T Cell in Tumor Microenvironment in the Treatment of Breast Cancer. *Front Oncol* (2021) 11:766248. doi: 10.3389/fonc.2021.766248
6. Shi R, Wang Z, Zhang J, Yu Z, An L, Wei S, et al. N6-Methyladenosine-Related Long Noncoding RNAs as Potential Prognosis Biomarkers for Endometrial Cancer. *Int J Gen Med* (2021) 14:8249–62. doi: 10.2147/IJGM.S336403
7. Balkwill FR, Capasso M, Hagemann T. The Tumor Microenvironment at a Glance. *J Cell Sci* (2012) 125(Pt 23):5591–6. doi: 10.1242/jcs.116392
8. Miao D, Margolis CA, Gao W, Voss MH, Li W, Martini DJ, et al. Genomic Correlates of Response to Immune Checkpoint Therapies in Clear Cell Renal Cell Carcinoma. *Science* (2018) 359(6377):801–6. doi: 10.1126/science.aan5951
9. D'Andrea MR, Cereda V, Coppola L, Giordano G, Remo A, De Santis E. Propensity for Early Metastatic Spread in Breast Cancer: Role of Tumor Vascularization Features and Tumor Immune Infiltrate. *Cancers (Basel)* (2021) 13(23). doi: 10.3390/cancers13235917
10. Gong Y, Fan Z, Luo G, Yang C, Huang Q, Fan K, et al. The Role of Necroptosis in Cancer Biology and Therapy. *Mol Cancer* (2019) 18(1):100. doi: 10.1186/s12943-019-1029-8
11. Rosenbaum SR, Wilski NA, Aplin AE. Fueling the Fire: Inflammatory Forms of Cell Death and Implications for Cancer Immunotherapy. *Cancer Discovery* (2021) 11(2):266–81. doi: 10.1158/2159-8290.CD-20-0805
12. Christofferson DE, Yuan J. Necroptosis as an Alternative Form of Programmed Cell Death. *Curr Opin Cell Biol* (2010) 22(2):263–8. doi: 10.1016/j.ceb.2009.12.003
13. Liz J, Esteller M. lncRNAs and microRNAs With a Role in Cancer Development. *Biochim Biophys Acta* (2016) 1859(1):169–76. doi: 10.1016/j.bbagrm.2015.06.015
14. Slack FJ, Chinnaiyan AM. The Role of Non-Coding RNAs in Oncology. *Cell* (2019) 179(5):1033–55. doi: 10.1016/j.cell.2019.10.017
15. Mathy NW, Chen XM. Long non-Coding RNAs (lncRNAs) and Their Transcriptional Control of Inflammatory Responses. *J Biol Chem* (2017) 292(30):12375–82. doi: 10.1074/jbc.R116.760884
16. Ulitsky I, Bartel DP. lincRNAs: Genomics, Evolution, and Mechanisms. *Cell* (2013) 154(1):26–46. doi: 10.1016/j.cell.2013.06.020
17. Chen YG, Satpathy AT, Chang HY. Gene Regulation in the Immune System by Long Noncoding RNAs. *Nat Immunol* (2017) 18(9):962–72. doi: 10.1038/ni.3771
18. Xu B, Peng Z, Yan G, Wang N, Chen M, Yao X, et al. Establishment and Validation of a Genetic Label Associated With M2 Macrophage Infiltration to Predict Survival in Patients With Colon Cancer and to Assist in Immunotherapy. *Front Genet* (2021) 12:726387. doi: 10.3389/fgene.2021.726387
19. Xu Y, Wang Z, Li F. Survival Prediction and Response to Immune Checkpoint Inhibitors: A Prognostic Immune Signature for Hepatocellular Carcinoma. *Transl Oncol* (2021) 14(1):100957. doi: 10.1016/j.tranon.2020.100957
20. Liu J, Wang J, Wu M, Zhang W, Meng L, Wang J, et al. Comprehensive Analysis of N6-Methyladenosine Modification Patterns Associated With Multiomic Characteristics of Bladder Cancer. *Front Med (Lausanne)* (2021) 8:757432. doi: 10.3389/fmed.2021.757432
21. Xiao S, Liu X, Yuan L, Wang F. A Ferroptosis-Related lncRNAs Signature Predicts Prognosis and Therapeutic Response of Gastric Cancer. *Front Cell Dev Biol* (2021) 9:736682. doi: 10.3389/fcell.2021.736682
22. Zhao Z, Liu H, Zhou X, Fang D, Ou X, Ye J, et al. Necroptosis-Related lncRNAs: Predicting Prognosis and the Distinction Between the Cold and Hot Tumors in Gastric Cancer. *J Oncol* (2021) 2021:6718443. doi: 10.1155/2021/6718443
23. Zhang X, Li X, Xie J, Zhu Q, Yuan Y. A Novel Immune-Related Prognostic Signature Predicting Survival in Patients With Pancreatic Adenocarcinoma. *J Oncol* (2022) 2022:8909631. doi: 10.1155/2022/8909631
24. Wang W, Xiang M, Liu H, Chu X, Sun Z, Feng L, et al. A Prognostic Risk Model Based on DNA Methylation Levels of Genes and lncRNAs in Lung Squamous Cell Carcinoma. *PeerJ* (2022) 10:e13057. doi: 10.7717/peerj.13057
25. Yang J, Hong S, Zhang X, Liu J, Wang Y, Wang Z, et al. Tumor Immune Microenvironment Related Gene-Based Model to Predict Prognosis and Response to Compounds in Ovarian Cancer. *Front Oncol* (2021) 11:807410. doi: 10.3389/fonc.2021.807410
26. Su P, Peng Z, Xu B, Yang B, Jin F. Establishment and Validation of an Individualized Macrophage-Related Gene Signature to Predict Overall Survival in Patients With Triple Negative Breast Cancer. *PeerJ* (2021) 9: e12383. doi: 10.7717/peerj.12383
27. Zhu K, Deng W, Deng H, Liu X, Wang G, Fu B, et al. Identification of a Novel PPAR Signature for Predicting Prognosis, Immune Microenvironment, and

Chemotherapy Response in Bladder Cancer. *PPAR Res* (2021) 2021:7056506. doi: 10.1155/2021/7056506
28. Wang Y, Wang Z, Sun J, Qian Y. Identification of HCC Subtypes With Different Prognosis and Metabolic Patterns Based on Mitophagy. *Front Cell Dev Biol* (2021) 9:799507. doi: 10.3389/fcell.2021.799507
29. Wilkerson MD, Hayes DN. ConsensusClusterPlus: A Class Discovery Tool With Confidence Assessments and Item Tracking. *Bioinformatics* (2010) 26 (12):1572–3. doi: 10.1093/bioinformatics/btq170
30. Grotkjaer T, Winther O, Regenberg B, Nielsen J, Hansen LK. Robust Multi-Scale Clustering of Large DNA Microarray Datasets With the Consensus Algorithm. *Bioinformatics* (2006) 22(1):58–67. doi: 10.1093/bioinformatics/bti746
31. Sun X, Li S, Lv X, Yan Y, Wei M, He M, et al. Immune-Related Long Non-Coding RNA Constructs a Prognostic Signature of Ovarian Cancer. *Biol Proc Online* (2021) 23(1):24. doi: 10.1186/s12575-021-00161-9
32. Yu W, Ma Y, Hou W, Wang F, Cheng W, Qiu F, et al. Identification of Immune-Related lncRNA Prognostic Signature and Molecular Subtypes for Glioblastoma. *Front Immunol* (2021) 12:706936. doi: 10.3389/fimmu.2021.706936
33. Kumar AR, Devan AR, Nair B, Vinod BS, Nath LR. Harnessing the Immune System Against Cancer: Current Immunotherapy Approaches and Therapeutic Targets. *Mol Biol Rep* (2021) 48(12):8075–95. doi: 10.1007/s11033-021-06752-9
34. Zhan L, Zhang J, Zhu S, Liu X, Zhang J, Wang W, et al. N(6)-Methyladenosine RNA Modification: An Emerging Immunotherapeutic Approach to Turning Up Cold Tumors. *Front Cell Dev Biol* (2021) 9:736298. doi: 10.3389/fcell.2021.736298
35. Talty R, Olino K. Metabolism of Innate Immune Cells in Cancer. *Cancers (Basel)* (2021) 13(4). doi: 10.3390/cancers13040904
36. Zhao J, Huang J. Breast Cancer Immunology and Immunotherapy: Targeting the Programmed Cell Death Protein-1/Programmed Cell Death Protein Ligand-1. *Chin Med J (Engl)* (2020) 133(7):853–62. doi: 10.1097/CM9.0000000000000710
37. Santa-Maria CA, Nanda R. Immune Checkpoint Inhibitor Therapy in Breast Cancer. *J Natl Compr Canc Netw* (2018) 16(10):1259–68. doi: 10.6004/jnccn.2018.7046
38. Moriwaki K, Balaji S, McQuade T, Malhotra N, Kang J, Chan FK. The Necroptosis Adaptor RIPK3 Promotes Injury-Induced Cytokine Expression and Tissue Repair. *Immunity* (2014) 41(4):567–78. doi: 10.1016/j.immuni.2014.09.016
39. Seyfried TN, Huysentruyt LC. On the Origin of Cancer Metastasis. *Crit Rev Oncog* (2013) 18(1-2):43–73. doi: 10.1615/CritRevOncog.v18.i1-2.40
40. Pasparakis M, Vandenabeele P. Necroptosis and its Role in Inflammation. *Nature* (2015) 517(7534):311–20. doi: 10.1038/nature14191
41. Binnewies M, Roberts EW, Kersten K, Chan V, Fearon DF, Merad M, et al. Understanding the Tumor Immune Microenvironment (TIME) for Effective Therapy. *Nat Med* (2018) 24(5):541–50. doi: 10.1038/s41591-018-0014-x
42. Zhang C, Zhang G, Sun N, Zhang Z, Xue L, Zhang Z, et al. An Individualized Immune Signature of Pretreatment Biopsies Predicts Pathological Complete Response to Neoadjuvant Chemoradiotherapy and Outcomes in Patients With Esophageal Squamous Cell Carcinoma. *Signal Transduct Tar Ther* (2020) 5(1):182. doi: 10.1038/s41392-020-00221-8
43. Son HY, Jeong HK. Immune Evasion Mechanism and AXL. *Front Oncol* (2021) 11:756225. doi: 10.3389/fonc.2021.756225
44. Zhang W, Kong X, Ai B, Wang Z, Wang X, Wang N, et al. Research Progresses in Immunological Checkpoint Inhibitors for Breast Cancer Immunotherapy. *Front Oncol* (2021) 11:582664. doi: 10.3389/fonc.2021.582664
45. Pascual T, Cejalvo JM, Oliveira M, Vidal M, Vega E, Ganau S, et al. SOLTI-1503 PROMETEO TRIAL: Combination of Talimogene Laherparepvec With Atezolizumab in Early Breast Cancer. *Future Oncol* (2020) 16(24):1801–13. doi: 10.2217/fon-2020-0246
46. Adams S, Loi S, Toppmeyer D, Cescon DW, De Laurentiis M, Nanda R, et al. Pembrolizumab Monotherapy for Previously Untreated, PD-L1-Positive, Metastatic Triple-Negative Breast Cancer: Cohort B of the Phase II KEYNOTE-086 Study. *Ann Oncol* (2019) 30(3):405–11. doi: 10.1093/annonc/mdy518
47. Harris KM, Smilek DE, Byron M, Lim N, Barry WT, McNamara J, et al. Effect of Costimulatory Blockade With Abatacept After Ustekinumab Withdrawal in Patients With Moderate to Severe Plaque Psoriasis: The PAUSE Randomized Clinical Trial. *JAMA Dermatol* (2021) 157(11):1306–15. doi: 10.1001/jamadermatol.2021.3492
48. Schmid P, Salgado R, Park YH, Munoz-Couselo E, Kim SB, Sohn J, et al. Pembrolizumab Plus Chemotherapy as Neoadjuvant Treatment of High-Risk, Early-Stage Triple-Negative Breast Cancer: Results From the Phase 1b Open-Label, Multicohort KEYNOTE-173 Study. *Ann Oncol* (2020) 31(5):569–81. doi: 10.1016/j.annonc.2020.01.072
49. Cetin B, Gumusay O. Pembrolizumab for Early Triple-Negative Breast Cancer. *N Engl J Med* (2020) 382(26):e108. doi: 10.1056/NEJMc2006684
50. Cortes J, Cescon DW, Rugo HS, Nowecki Z, Im SA, Yusof MM, et al. Pembrolizumab Plus Chemotherapy Versus Placebo Plus Chemotherapy for Previously Untreated Locally Recurrent Inoperable or Metastatic Triple-Negative Breast Cancer (KEYNOTE-355): A Randomised, Placebo-Controlled, Double-Blind, Phase 3 Clinical Trial. *Lancet* (2020) 396 (10265):1817–28. doi: 10.1016/S0140-6736(20)32531-9
51. Xu S, Xie J, Zhou Y, Liu H, Wang Y, Li Z. Integrated Analysis of RNA Binding Protein-Related lncRNA Prognostic Signature for Breast Cancer Patients. *Genes (Basel)* (2022) 13(2). doi: 10.3390/genes13020345
52. Yan X, You SN, Chen Y, Qian K. Construction and Validation of a Newly Prognostic Signature for CRISPR-Cas9-Based Cancer Dependency Map Genes in Breast Cancer. *J Oncol* (2022) 2022:4566577. doi: 10.1155/2022/4566577
53. Zou J, Gu Y, Zhu Q, Li X, Qin L. Identifying Glycolysis-Related LncRNAs for Predicting Prognosis in Breast Cancer Patients. *Cancer biomark* (2022). doi: 10.3233/CBM-210446
54. Segovia-Mendoza M, Romero-Garcia S, Lemini C, Prado-Garcia H. Determining Factors in the Therapeutic Success of Checkpoint Immunotherapies Against PD-L1 in Breast Cancer: A Focus on Epithelial-Mesenchymal Transition Activation. *J Immunol Res* (2021) 2021:6668573. doi: 10.1155/2021/6668573
55. Li CJ, Lin LT, Hou MF, Chu PY. PDL1/PD1 Blockade in Breast Cancer: The Immunotherapy Era (Review). *Oncol Rep* (2021) 45(1):5–12. doi: 10.3892/or.2020.7831
56. Lotfinejad P, Kazemi T, Mokhtarzadeh A, Shanehbandi D, Jadidi Niaragh F, Safaei S, et al. PD-1/PD-L1 Axis Importance and Tumor Microenvironment Immune Cells. *Life Sci* (2020) 259:118297. doi: 10.1016/j.lfs.2020.118297

Conflict of Interest: The authors declare that the research was conducted in the absence of any commercial or financial relationships that could be construed as a potential conflict of interest.

Publisher's Note: All claims expressed in this article are solely those of the authors and do not necessarily represent those of their affiliated organizations, or those of the publisher, the editors and the reviewers. Any product that may be evaluated in this article, or claim that may be made by its manufacturer, is not guaranteed or endorsed by the publisher.

Copyright © 2022 Xu, Zheng, Zhou, Ye, Xu and Meng. This is an open-access article distributed under the terms of the Creative Commons Attribution License (CC BY). The use, distribution or reproduction in other forums is permitted, provided the original author(s) and the copyright owner(s) are credited and that the original publication in this journal is cited, in accordance with accepted academic practice. No use, distribution or reproduction is permitted which does not comply with these terms.

frontiers | Frontiers in Cell and Developmental Biology

ORIGINAL RESEARCH
published: 27 May 2022
doi: 10.3389/fcell.2022.824938

Comprehensive Analyses of MELK-Associated ceRNA Networks Reveal a Potential Biomarker for Predicting Poor Prognosis and Immunotherapy Efficacy in Hepatocellular Carcinoma

*Yu Liu[1†], Rongkuan Li[1†], Xiaobo Wang[2], Zuguang Xue[2], Xiaozhou Yang[1] and Bo Tang[2]**

[1]Department of Infectious Disease, The Second Affiliated Hospital of Dalian Medical University, Dalian, China, [2]Department of Hematology, The Second Affiliated Hospital of Dalian Medical University, Dalian, China

OPEN ACCESS

Edited by:
Pranav Gupta,
Albert Einstein College of Medicine,
United States

Reviewed by:
Nissar Ahmad Wani,
Central University of Kashmir, India
Lei Lyu,
Wuhan No.1 Hospital, China

***Correspondence:**
Bo Tang
bo_tang@126.com

[†]These authors have contributed equally to this work

Specialty section:
This article was submitted to Molecular and Cellular Oncology, a section of the journal Frontiers in Cell and Developmental Biology

Received: 29 November 2021
Accepted: 13 April 2022
Published: 27 May 2022

Citation:
Liu Y, Li R, Wang X, Xue Z, Yang X and Tang B (2022) Comprehensive Analyses of MELK-Associated ceRNA Networks Reveal a Potential Biomarker for Predicting Poor Prognosis and Immunotherapy Efficacy in Hepatocellular Carcinoma. Front. Cell Dev. Biol. 10:824938. doi: 10.3389/fcell.2022.824938

Background: Hepatocellular carcinoma (HCC) is one of the most common malignant tumors in the world with high morbidity and mortality. Identifying specific molecular markers that can predict HCC prognosis is extremely important. MELK has been reported to play key roles in several types of human cancers and predict poor prognosis. This study was aimed to explore the impact of MELK on HCC.

Methods: A pan-cancer analysis of MELK was conducted by The Cancer Genome Atlas (TCGA) and the Genotype-Tissue Expression (GTEx) data. The prognosis of MELK in various cancers was analyzed in GEPIA. Then, a ceRNA network of MELK was constructed based on the comprehensive consideration of the expression analysis, the correlation analysis, and the survival analysis by R software. The correlation of MELK and immune cell infiltration was analyzed by TIMER and CIBERSORT. Then, the overall survival of differentially expressed immune cells was conducted. The correlation of MELK and immune checkpoints expression was analyzed by GEPIA.

Results: MELK was overexpressed in 14 types of human cancers, and its expression was significantly higher than that in both unmatched and paired normal samples in HCC. Higher MELK expression was correlated with poorer survival and advanced clinical stage, topography (T) stage, and histological grade. The univariate and multivariate Cox regression analyses showed that MELK was an independent risk factor for poor prognosis in HCC. Then, we constructed a ceRNA network consisting of MELK, miR-101-3p, and two lncRNAs (SNHG1 and SNHG6) after evaluating the expression and impact on prognosis in HCC of these RNAs. TIMER and CIBERSORT databases indicated that MELK was correlated with various immune cells including B cells, $CD8^+$ T cells, $CD4^+$ T cells, macrophage, neutrophil, and dendritic cells in HCC. Of them, B cells, $CD4^+$ T cells, macrophage, and neutrophil were related to the prognosis of HCC. In addition, MELK was significantly positively correlated with the immune checkpoint genes.

Conclusions: MELK may be a novel potential biomarker for predicting prognosis and immunotherapy efficacy in patients with HCC. Our study may provide new molecular and therapeutic strategies for the treatment of HCC patients.

Keywords: MELK, ceRNA network, immune cell infiltration, biomarker, immunotherapy, hepatocellular carcinoma

INTRODUCTION

Primary liver cancer is the sixth most commonly diagnosed cancer and the third leading cause of cancer death worldwide in 2020, with approximately 906,000 new cases and 830,000 deaths (Sung et al., 2021). HCC is the main type of primary liver cancer, comprising 75–85% of cases (Llovet et al., 2012). In contrast to the decreasing disease burden and impact of many other major cancers, the overall burden of HCC is increasing worldwide over time (Yang et al., 2019). Due to lack of specific clinical manifestations in the early stage, many HCC patients are diagnosed at advanced stages when they suffer from an aggravated condition and miss the best timing of treatment. Although the diagnostic and therapeutic approaches of HCC have gradually improved, the overall survival of the patients with HCC remains very low. The recurrence is still common and elusive, even for the patients who received successful surgical excision or liver transplantation. Given the lack of early diagnostic methods, it is often difficult to detect the early recurrence and metastasis. Immune checkpoint inhibitors (ICIs) have already shown systemic and durable anti-tumor responses in many types of cancers including HCC (Federico et al., 2020). However, the immune-related adverse events during the ICI therapy can affect any organ system and in some cases can be lethal (Postow et al., 2018). Therefore, early prediction for the HCC progression as well as the immunotherapy efficacy is of great importance to improve the prognosis of HCC patients.

Maternal embryonic leucine zipper kinase (MELK) was a member of the snfl/AMPK kinase family, encoding a serine/threonine kinase that is highly conserved across a variety of mammalian and non-mammalian species. Unlike most members of this family, only functioning in cell survival under metabolically challenging conditions, MELK participates in diverse processes, including cell cycle, cell proliferation, apoptosis, RNA processing, and embryonic development (Davezac et al., 2002; Vulsteke et al., 2004; Jung et al., 2008). Furthermore, MELK is involved in multiple protein interactions that affect many stages of tumorigenesis (Chung et al., 2012). Recent studies indicated that MELK was highly expressed in several human cancers, including breast cancer, prostate cancer, gastric cancer, liver cancer, glioblastoma multiforme, and lung cancer (Gray et al., 2005; Xia et al., 2015). Furthermore, overexpression of MELK has been markedly associated with decreased survival and poor prognosis for some tumors (Gray et al., 2005; Sun et al., 2021). However, a comprehensive study to identify the role and mechanism of MELK in HCC is still absent. Also, the impact of MELK on the tumor immune infiltration in HCC is still not evaluated.

The competitive endogenous RNA (ceRNA) hypothesis was first proposed in 2011 and suggested that the long non-coding RNAs (lncRNAs) could act as ceRNAs to bind to microRNAs (miRNAs) and affect the regulation of miRNAs on target mRNAs, thus regulating the expression of related target genes (Cao et al., 2018). In this study, we performed expression analysis, correlation analysis, and survival analysis for MELK in HCC using TCGA database. Then, a ceRNA network consisting of MELK, lncRNAs, and miRNAs was established. Finally, we explored the association of MELK with the immune cell infiltration, markers of immune cells, and immune checkpoints expression in HCC. In summary, our work suggested that ncRNA-mediated overexpression of MELK was correlated with poor prognosis, tumor immune infiltration, and immunotherapy efficacy of patients in HCC. Our study may provide new molecular and therapeutic strategies for the treatment and prognosis of HCC patients.

MATERIALS AND METHODS

The Cancer Genome Atlas Data Download and Analysis

The RNA-seq data and clinical data of 33 types of cancer were downloaded from TCGA database (https://portal.gdc.cancer.gov/). The RNA expression data from different patients were integrated separately into files. Duplicated samples were removed from the RNA expression matrix, and the expression data of duplicated genes were averaged. The expression analysis of MELK was performed in pan-cancer using the R package *limma*, and $p < 0.05$ was considered statistically significant. Then, the RNA expression data and the clinical characteristics of 421 samples, including 371 tumor samples and 50 adjacent non-tumor samples, were obtained from TCGA-LIHC dataset.

GEPIA Database Analysis

GEPIA (http://gepia.cancer-pku.cn/) is a public data platform containing gene expression data and patient characteristics for the majority of human tumors based on TCGA and GTEx data (Tang et al., 2017). We used this web tool to perform the comparison of the MELK expression between tumor and normal groups. p value < 0.05 and $\log_2FC > 1$ were considered statistically significant. GEPIA was also employed to conduct the overall survival (OS) and disease-free survival (DFS) analysis for MELK in various human cancers. In addition, the correlation of MELK and markers of various immune cells in HCC was also evaluated using the GEPIA database. $|R| > 0.1$ and p value < 0.05 were considered statistically significant.

Survival Analysis

The OS time and OS status in the clinical phenotype data from TCGA were used to perform survival analysis. The Cox proportional hazard model was performed to estimate whether

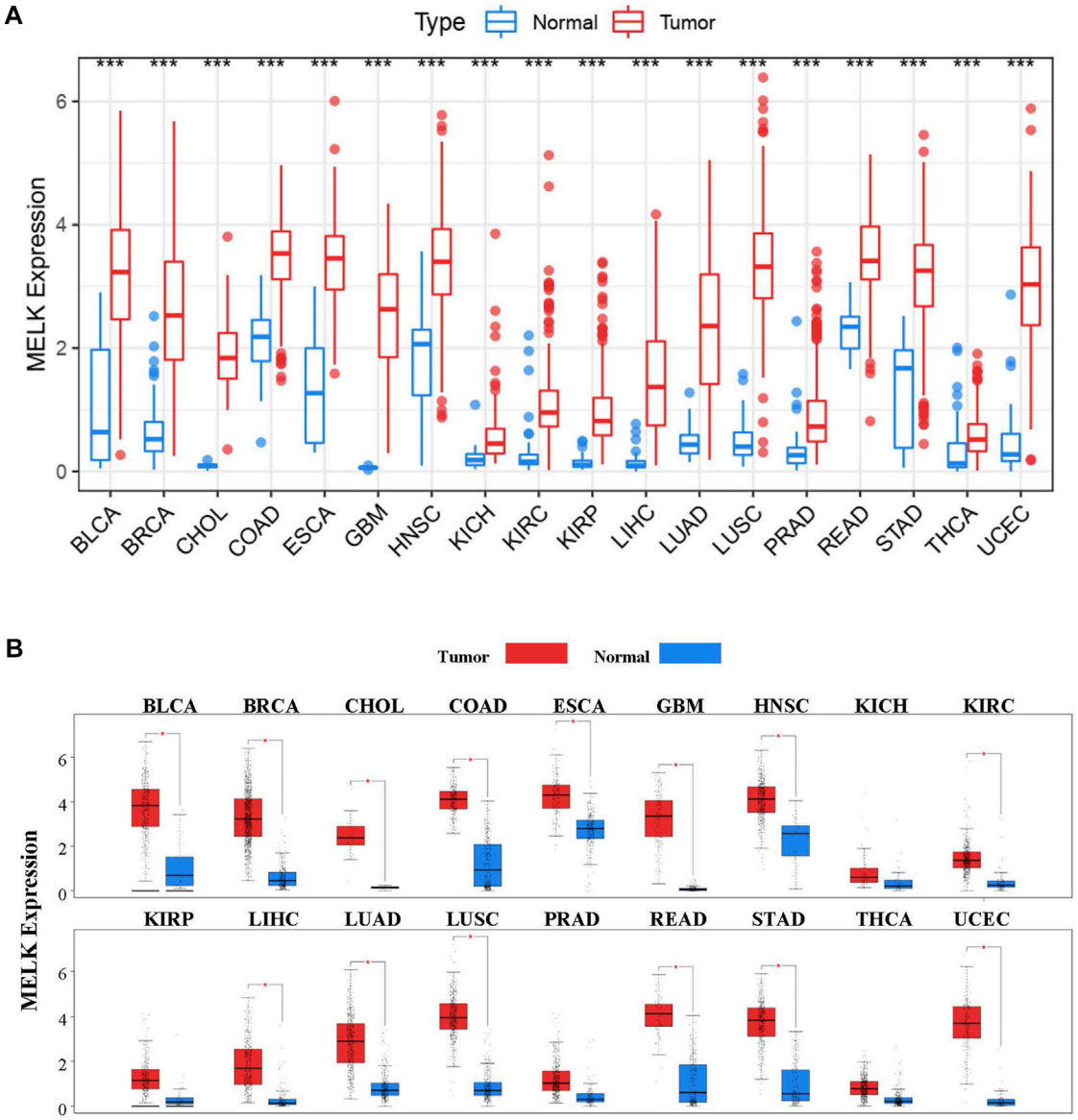

FIGURE 1 | Pan-cancer analysis of MELK expression in TCGA database. **(A)** Expression of MELK in diverse cancers compared with the corresponding normal samples in TCGA database. **(B)** Expression of MELK in 18 types of human cancer based on TCGA and GTEx normal tissues. **p* value < 0.05; ***p* value < 0.01; ****p* value < 0.001.

the expression of MELK was related to patient prognosis. Hazard ratios (HR) > 1 and $p < 0.05$ indicated a significant relationship between MELK and increased risk of death. Kaplan–Meier (KM) analysis based on the log-rank test was conducted using R software (version 4.1.1). The plotted curves were visualized using a ggsurvplot R package. A *p*-value < 0.05 was considered to represent a significant difference in survival.

Constructing the ceRNA Network

A co-expressed regulatory network comprised MELK, miRNA, and lncRNA was constructed to explore the potential functions of MELK in HCC. Based on the hypothesis, the candidate lncRNA and mRNA expression must have the same expression variation trend in HCC, while miRNA and mRNA expression should have the opposite trend. We predicted the miRNA–lncRNA interactions and MELK–miRNA interactions based on starBase 3.0 (http://starbase.sysu.edu.cn/). The differentially expressed miRNAs and lncRNAs between HCC samples and normal liver samples in TCGA-LIHC were identified using the *limma* package in R with a $|\log_2 FC| > 1$ and adjusted *p*-value < 0.05 threshold. To improve the reliability, the Spearman's correlation analysis was conducted between the expression of MELK–miRNA and miRNA–lncRNA individually. The criteria were set at $r < -0.2$ and FDR < 0.05. Finally, we established a ceRNA network by matching lncRNA–miRNA and miRNA–MELK pairs.

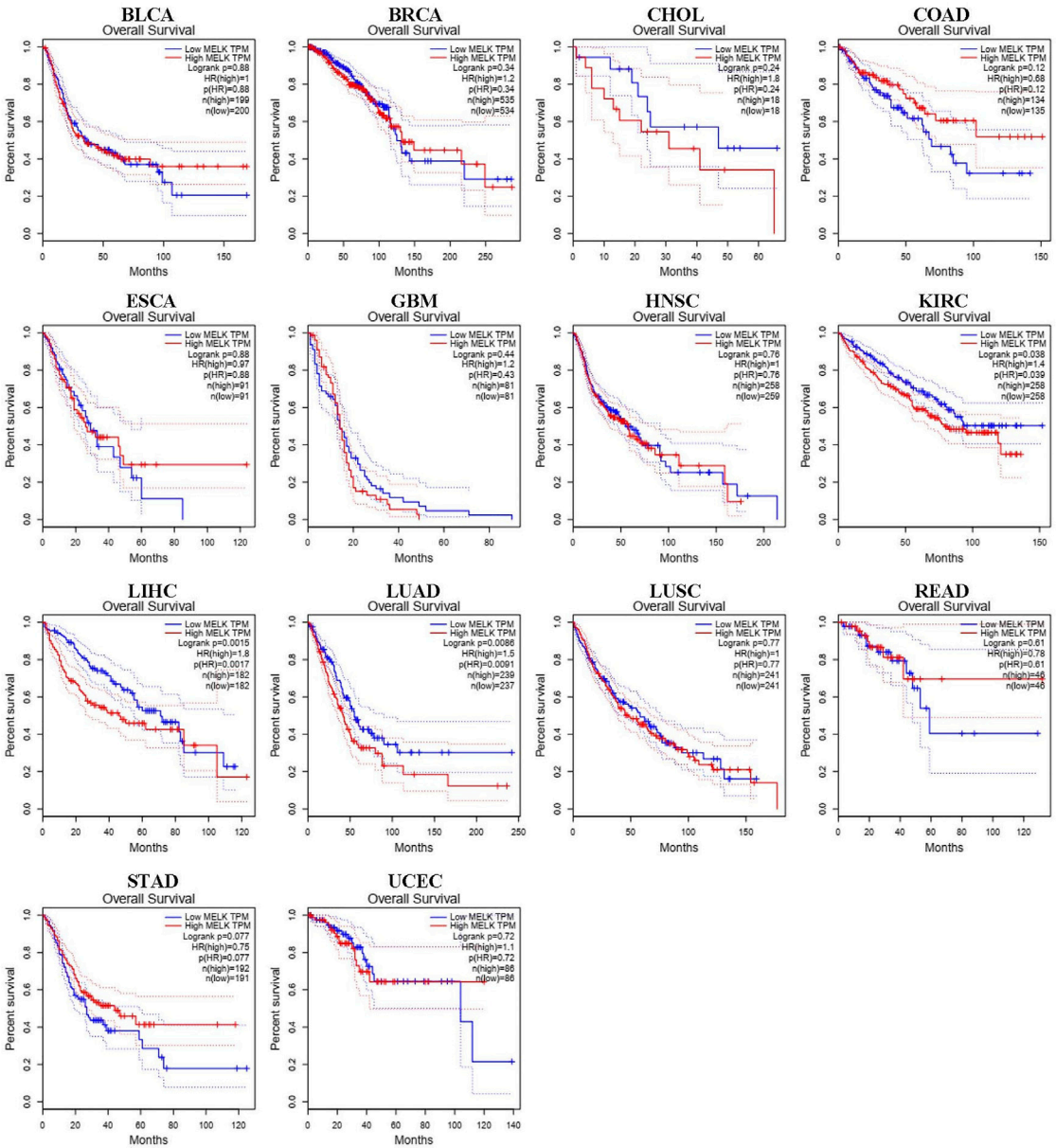

FIGURE 2 | Overall survival (OS) analysis of MELK in various human cancers determined by GEPIA database.

Then, we conducted OS analysis to assess the prognostic value of miRNA and lncRNA in the constructed ceRNA network. The surv_cutpoint function of the *survminer* package in R was used to determine the optimal cutoff value of the candidate miRNA and lncRNA. The KM survival curve was plotted to analyze the difference in survival between patients in high- and low-expression groups.

Evaluation of Tumor Immune Cell Infiltration

The TIMER database (https://cistrome.shinyapps.io/timer/) is a web database for comprehensive analysis of tumor-infiltrating immune cells (Uhlen et al., 2017). Correlations between the MELK expression and various immune cell types, including B cells, neutrophils, $CD4^+$ T cells, macrophages, $CD8^+$ T cells, and dendritic cells, were estimated using TIMER. Then, we analyzed the correlation of MELK expression and the immune checkpoints expression in HCC. In addition, we estimated the proportion of 22 kinds of immune cell types in HCC patients by CIBERSORT. The p value and root mean-squared error were calculated for each sample. Samples with $p < 0.05$ were selected for further analysis. The immune cell abundance in different MELK expression groups was compared using the Wilcoxon rank-sum test. A KM survival curve analysis was performed to evaluate the OS of different immune cells in HCC patients.

Statistical Analysis

Data were processed and analyzed by Perl and R software. The MELK expression in unmatched HCC samples and normal

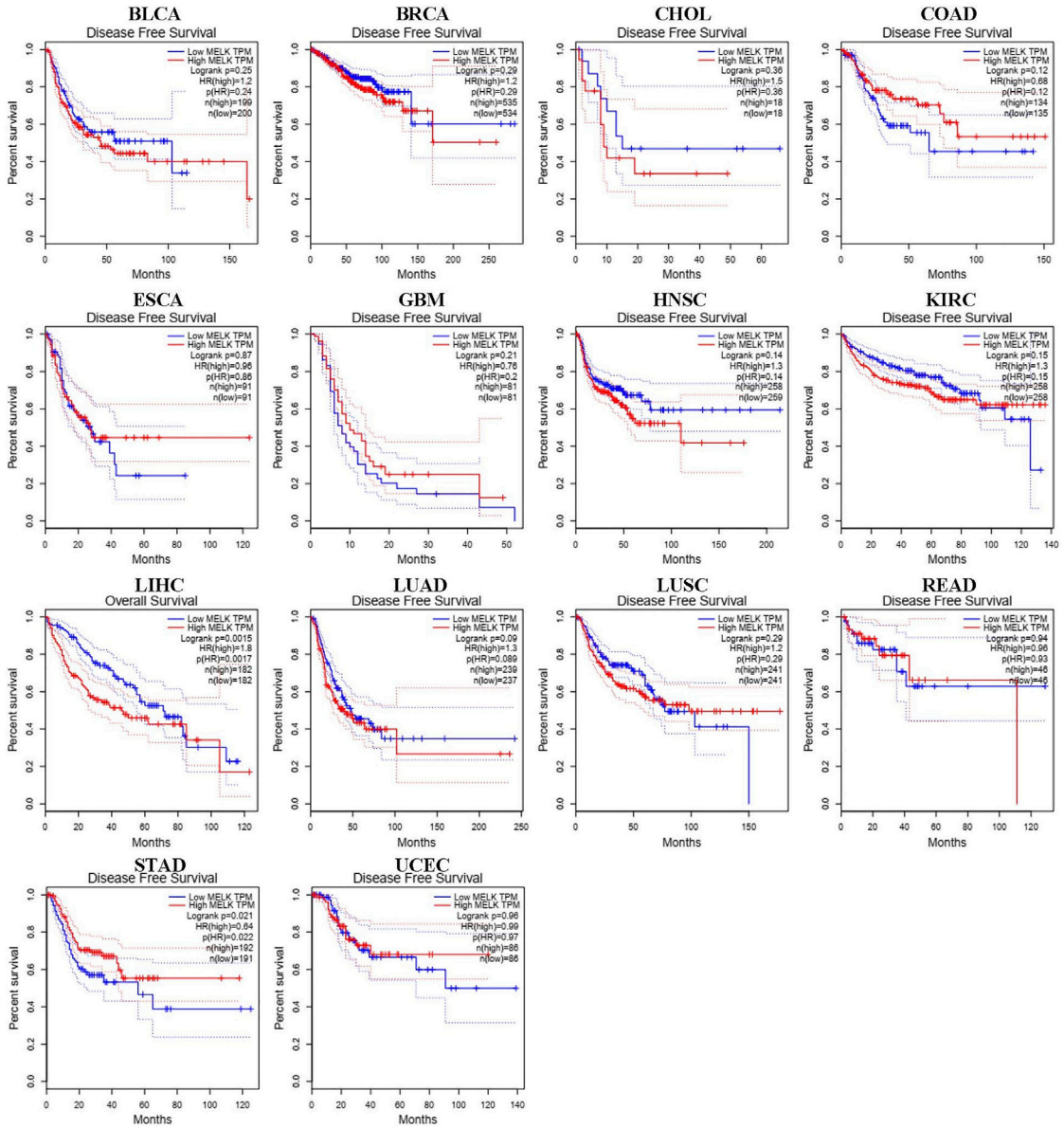

FIGURE 3 | Disease-free survival (DFS) analysis of MELK in various human cancers determined by the GEPIA database.

samples and matched HCC samples and adjacent normal samples were analyzed by Wilcoxon rank-sum tests and Wilcoxon signed-rank tests, individually. Comparisons of clinicopathological characteristics were performed *via* Wilcoxon rank-sum tests for quantitative variables and chi-square or Fisher's exact tests for categorical variables. Differences among multiple groups were analyzed by the Kruskal–Wallis test. The correlation analysis was conducted by the Spearman's correlation. Univariate and multivariate Cox regression analyses were performed to find independent variables related to prognosis.

RESULTS

Pan-Cancer Analysis of MELK Expression in The Cancer Genome Atlas Database

To explore the possible roles of MELK in carcinogenesis, we compared its expression between tumor and normal tissues in 33 types of human cancer in TCGA database. As shown in **Figure 1A**, the MELK has a significant higher expression in 18 human cancers including BLCA, BRCA, CHOL, COAD, ESCA, GBM, HNSC, KICH, KIRC, KIRP, LIHC, LUAD, LUSC, PRAD, READ, STAD, THCA, and UCEC. To further validate the expression of MELK in 18 types of human cancer,

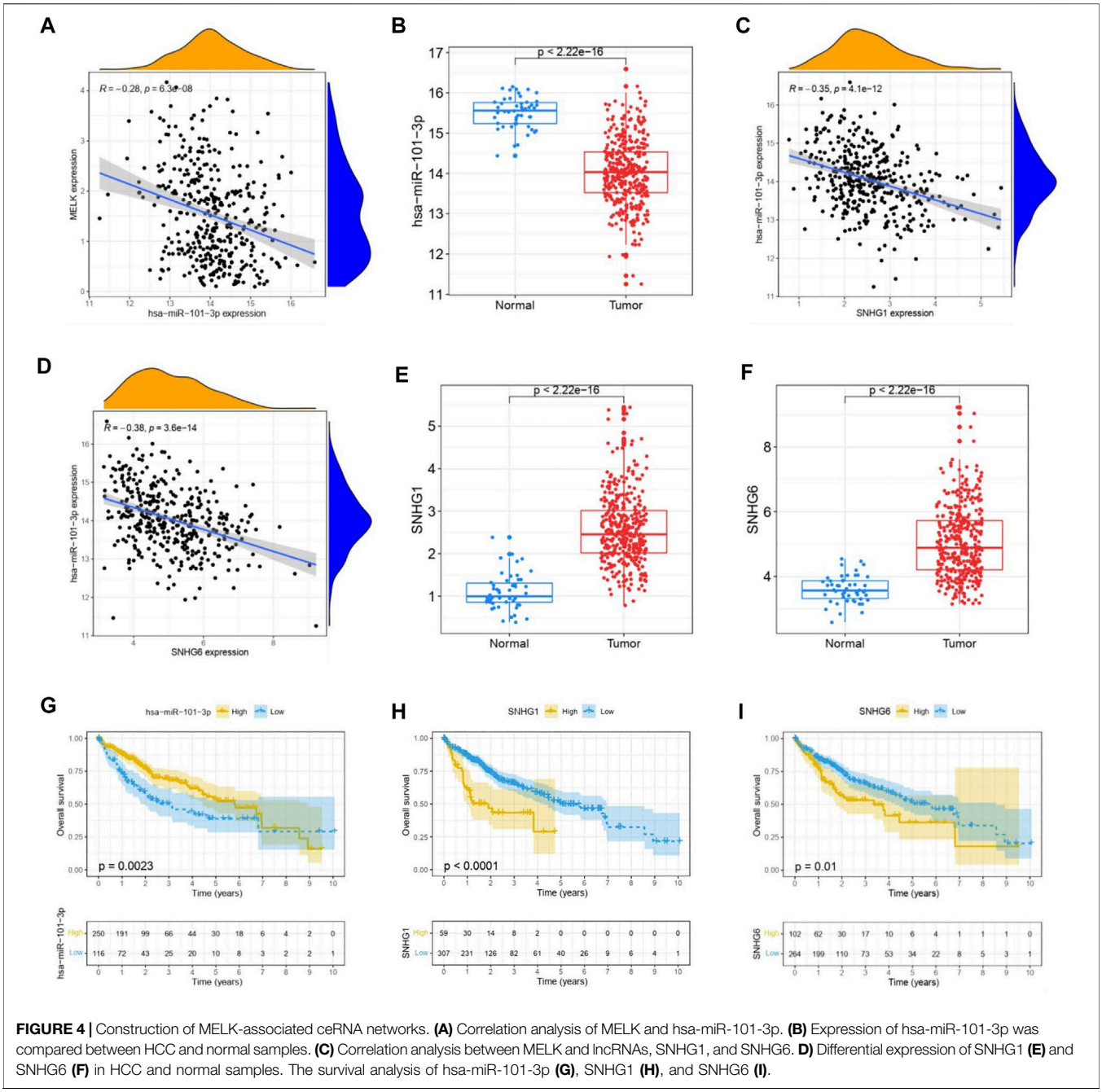

FIGURE 4 | Construction of MELK-associated ceRNA networks. **(A)** Correlation analysis of MELK and hsa-miR-101-3p. **(B)** Expression of hsa-miR-101-3p was compared between HCC and normal samples. **(C)** Correlation analysis between MELK and lncRNAs, SNHG1, and SNHG6. **D)** Differential expression of SNHG1 **(E)** and SNHG6 **(F)** in HCC and normal samples. The survival analysis of hsa-miR-101-3p **(G)**, SNHG1 **(H)**, and SNHG6 **(I)**.

the GEPIA database consisting of TCGA data and the GTEx data was employed. As shown in **Figure 1B**, the MELK expression was significantly increased in BLCA, BRCA, CHOL, COAD, ESCA, GBM, HNSC, KIRC, LIHC, LUAD, LUSC, READ, STAD, and UCEC compared with the normal group.

The Impact on Prognosis of MELK in Pan-Cancer

We used different methods to investigate the prognostic effect of MELK in the 14 types of cancer. The Cox analysis showed that higher expression of MELK was significantly correlated with OS of HCC (HR = 1.79, 95%CI: 1.26~2.53, $p = 0.001$), LUAD (HR = 1.41, 95%CI: 1.06~1.89, $p = 0.02$), and KIRC (HR = 1.43, 95%CI: 1.05~1.94, $p = 0.022$). Then, KM analysis based on the log-rank test was accordingly employed indicating that the higher expression of MELK in LIHC, LUAD, and KIRC predicted a poor prognosis (**Figure 2**). Then, the DFS was further analyzed and higher expression of MELK indicated poor prognosis in HCC (**Figure 3**), while no statistical significance of MELK for predicting prognosis of patients in other cancer types was observed. Therefore, MELK may be utilized as a prognostic biomarker in patients with HCC based on the OS and DFS results.

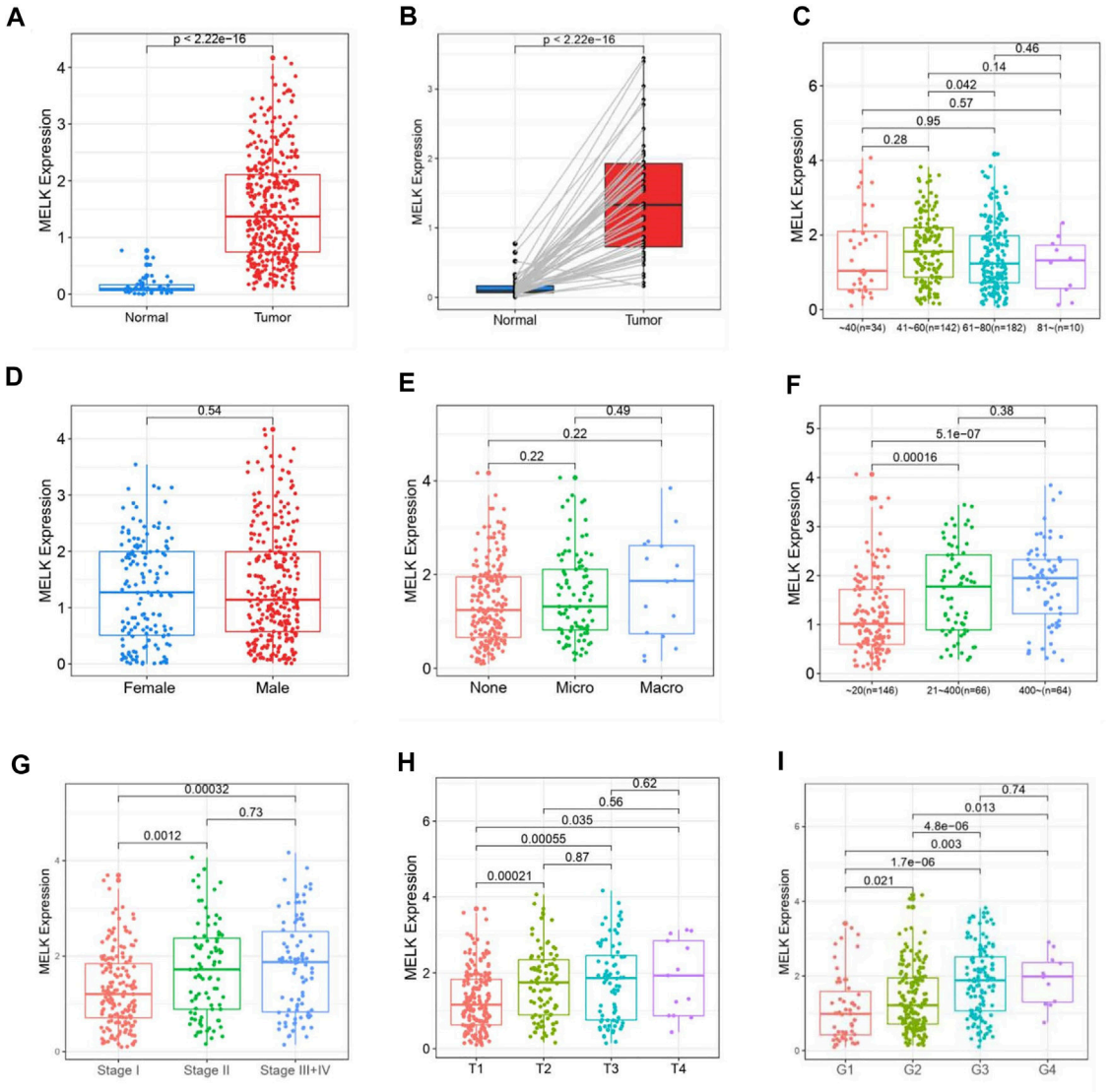

FIGURE 5 | Association of MELK expression and clinicopathological features in HCC. The expression of MELK in HCC was upregulated in both unmatched **(A)** and paired **(B)** normal samples in HCC. Relationship of MELK with age, gender, vascular invasion, clinical stage, T stage, and histological grade **(C–I)**.

MELK-Related ceRNA Network Construction in Hepatocellular Carcinoma

The ceRNA hypothesis suggests that some RNAs possessing miRNA-binding sites can competitively bind to target miRNAs as molecular sponges and subsequently alter the expression of genes encoding proteins (Salmena et al., 2011). It has been widely acknowledged that lncRNAs are responsible for the regulation of gene expression. To ascertain whether MELK was regulated by some lncRNAs, the miRNAs that could potentially bind to MELK were predicted by starBase, and we finally identified 35 miRNAs (**Supplementary Table S1**). Based on the principle of negative correlation between miRNA and its regulating target gene expression, the correlation between the 35 screened miRNAs and MELK was analyzed. As shown in the **Supplementary Tables S1, S7**, miRNAs were negatively correlated with MELK in HCC but only hsa-miR-101-3p met the criteria of $r < -0.2$ and FDR < 0.05 (**Figure 4A**). Then, the differential expression of hsa-miR-101-3p between HCC samples and normal samples was confirmed (**Figure 4B**). Taken together, the hsa-miR-101-3p was identified as the most potential regulatory miRNA of MELK in HCC. Also, the binding site between MELK and miR-101-3p is chr9:36677537-36677542 [+].

Next, we used starBase to further predict the lncRNAs that may bind to the hsa-miR-101-3p, and a total of 25 lncRNAs were forecasted. According to the ceRNA hypothesis, lncRNA could upregulate mRNA expression by competitively binding to shared miRNA. Therefore, there should be negative correlation between lncRNA and miRNA or positive correlation between lncRNA and

TABLE 1 | Univariate and multivariate Cox regression analyses of OS/DFS and clinicopathological features in HCC patients.

Overall survival	Univariate analysis		Multivariate analysis	
	HR (95%CI)	*p*-value	HR (95%CI)	*p*-value
Age (≥60 vs. < 60)	1.27 (0.9–1.8)	0.181		
Gender (male vs. female)	1.21 (0.85–1.73)	0.282		
MELK (high vs. low)	1.66 (1.17–2.37)	0.005	1.54 (1.05–2.24)	0.026*
T stage (T3–T4 vs. T1–T2)	2.5 (1.76–3.56)	<0.001	2.3 (1.58–3.35)	<0.001*
Pathologic stage (III–IV vs. I–II)	2.41 (1.66–3.49)	<0.001	1.21 (0.17–8.82)	0.849
Histologic grade (III–IV vs. I–II)	1.14 (0.8–1.63)	0.47		
Child–Pugh grade (B–C vs. A)	1.62 (0.8–3.28)	0.183		
Vascular invasion (positive vs. negative)	1.32 (0.87–2)	0.188		
Family history (yes vs. no)	1.16 (0.81–1.68)	0.415		
Disease-free survival	**Univariate analysis**		**Multivariate analysis**	
	HR (95%CI)	***p*-value**	**HR (95%CI)**	***p*-value**
Age (≥60 vs. < 60)	1.04 (0.77–1.4)	0.817		
Gender (male vs. female))	0.97 (0.7–1.33)	0.828		
MELK (high vs. low)	1.53 (1.13–2.08)	0.006	1.51 (1.05–2.16)	0.026*
T stage (T3–T4 vs. T1–T2)	2.15 (1.55–2.97)	<0.001	0.33 (0.08–1.4)	0.131
Pathologic stage (III–IV vs. I–II)	2.18 (1.56–3.05)	<0.001	5.82 (1.4–24.16)	0.015*
Histologic grade (III–IV vs. I–II)	1.19 (0.87–1.62)	0.273		
Child–Pugh grade (B-C vs. A)	1.42 (0.78–2.6)	0.253		
Vascular invasion (positive vs. negative)	1.64 (1.16–2.32)	0.005	1.33 (0.91–1.93)	0.141
Family history (yes vs. no)	1 (0.72–1.39)	0.991		

mRNA. As shown in **Supplementary Table S2**, correlation analysis proved that there are six lncRNAs significantly negatively correlating with hsa-miR-101-3p, namely, SNHG1(**Figure 4C**), LINC00265, MIR3142HG, GSEC, SNHG6 (**Figure 4D**), and SNHG14. Of them, SNHG1 (**Figure 4E**) and SNHG6 (**Figure 4F**) were differentially expressed between the HCC samples and the normal samples with a $\log_2FC > 1$ and $p < 0.05$ threshold. The binding site between SNHG1 and miR-101-3p is chr11:62622753-62622772 [-], and the binding site of SNHG6 targeting miR-101-3p is chr8:67834696-67834716 [-]. Then, the correlation of the two lncRNAs and MELK expression was also conducted. As shown in FigureS1A, they both positively correlated with the MELK.

Finally, combining the lncRNA–miRNA pairs and miRNA–mRNA pairs, a lncRNA–miRNA–mRNA network was constructed, including MELK, hsa-miR-101-3p, and two lncRNAs, SNHG1 and SNHG6. The survival analysis of these RNAs grouping by the calculated optimal cutoff was conducted by the KM curve. The results showed that hsa-miR-101-3p (**Figure 4G**), SNHG1 (**Figure 4H**), and SNHG6 (**Figure 4I**) were significantly correlated with OS in HCC. Taking expression analysis and correlation analysis together, SNHG1 and SNHG6 might be the two most potential upstream lncRNAs of the hsa-miR-101-3p/MELK axis in HCC.

Relationship of MELK Expression and Clinicopathological Features of Hepatocellular Carcinoma Patients

The clinicopathological features of HCC patients were obtained from TCGA-LIHC database. Then, we investigated the relationship between the expression of MELK and the clinical features. The expression of MELK in the HCC samples was significantly higher than that in both unmatched (**Figure 5A**) and paired (**Figure 5B**) normal samples based on TCGA database. The MELK expression was positively correlated with the AFP level (**Figure 5F**). The higher level of MELK tended to be correlated with advanced HCC. The Kruskal–Wallis tests revealed that the MELK expression was higher in the advanced clinical stage (**Figure 5G**), topography (T) stage (**Figure 5H**), and histological grade (**Figure 5I**). The univariate and multivariate Cox regression analyses showed that MELK was an independent risk factor for poor prognosis in HCC (**Table1**). However, the MELK expression was not associated with age, gender, and vascular invasion (**Figures 5C–E**). The chi-square test was also performed with other clinical information (**Supplementary Table S3**).

Characteristics of MELK Immune Cell Infiltration

Immune cells in the tumor microenvironment (TME) largely influence the biological behavior of the tumor (Xiong et al., 2018). Previous studies have confirmed that tumor infiltration is associated with the recurrence of HCC (Shi et al., 2011; Gabrielson et al., 2016). Therefore, the correlation of the MELK expression with immune cell infiltration was evaluated using TIMER. As presented in **Figure 6A**, the MELK expression was significantly positively correlated with all analyzed immune cells, including B cells, $CD8^+$ T cells, $CD4^+$ T cells, macrophage, neutrophil, and dendritic cell, in HCC. However, the immune cell infiltration level did not alter by various copy numbers of MELK in HCC (**Figure 6B**). The KM analysis showed that the higher B cells and $CD8^+$ T cells were correlated to a better prognosis, while the higher macrophage and neutrophil indicated poor prognosis in

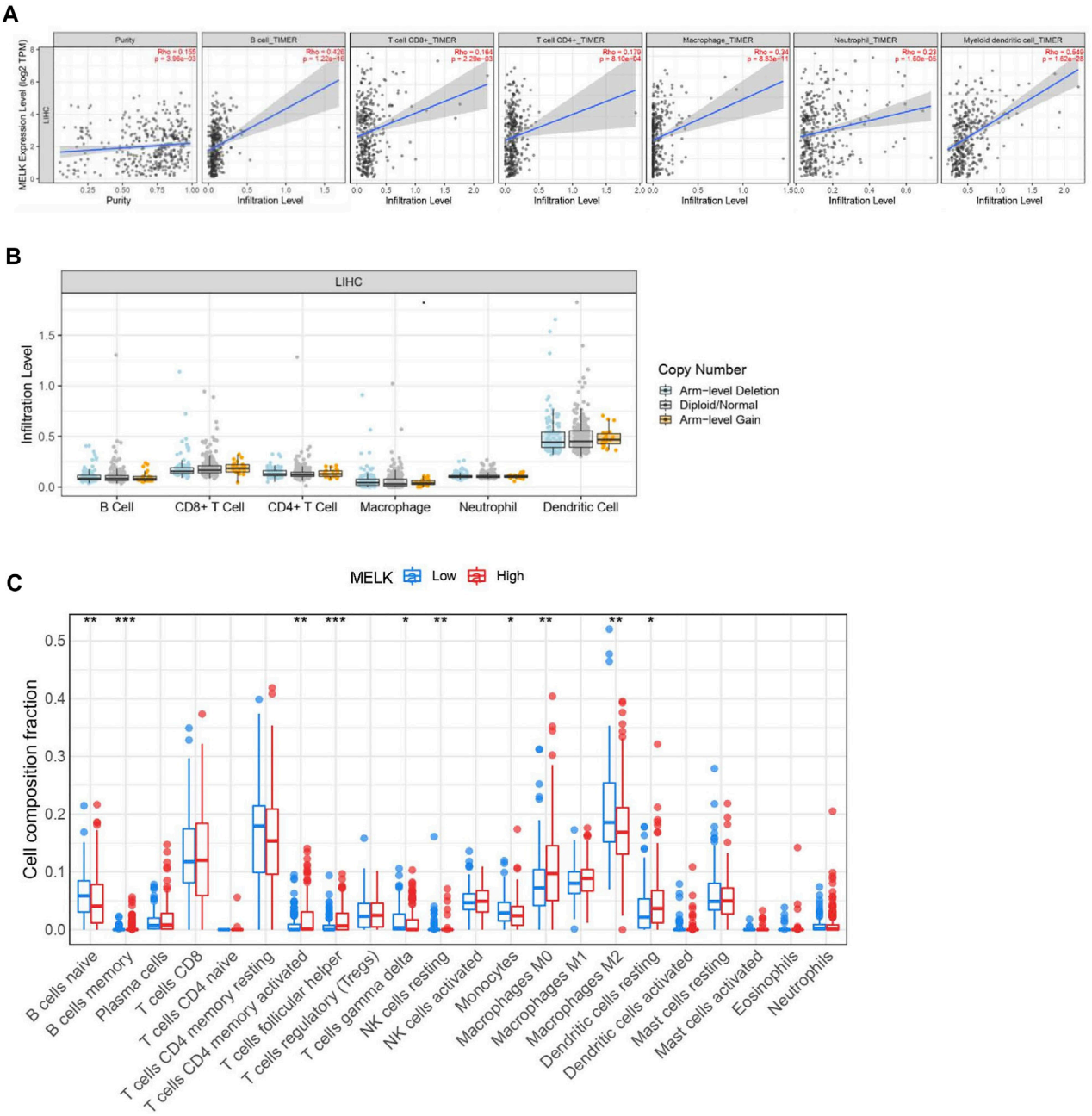

FIGURE 6 | . Relationship of immune cell infiltration with the MELK level in HCC. **(A)** Correlation of the MELK expression level with B cell, $CD8^+$ T cell, $CD4^+$ T cell, macrophage, neutrophil, and dendritic cell in HCC. **(B)** Infiltration level of various immune cells under different copy numbers of MELK in HCC. **(C)** 22 immune cell subtypes in the high- and low-MELK expression groups in HCC by CIBERSORT. *$p < 0.05$; **$p < 0.01$; ***$p < 0.001$; ****$p < 0.0001$. ns, not significant.

HCC (**Figures 7A–F**). Then, we determined the correlation of MELK and the markers of immune cells using the GEPIA database. The MELK expression was significantly positively correlated with the markers of B cells, M1 macrophage, M2 macrophage, natural killer cell, neutrophil, dendritic cell, and T cells including Treg, Th1, Th2, Tfh, and $CD8^+$ T cell (**Table2**).

In addition, 22 types of immune-infiltrating cells were calculated by CIBERSORT. After removing samples that might be computationally inaccurate, the HCC samples were divided into two groups according to the median of MELK expression, the high group and the low group. As shown in the **Figure 6C**, the naïve B cell, the gamma delta T cell, the resting NK cell, the monocytes, and the M2 macrophage were significantly higher in the low-expression group of MELK, while the memory B cell, the activated CD4 + T cell, the follicular T helper cell, the M0 macrophage, and the resting DC cell were higher in the high-expression group of

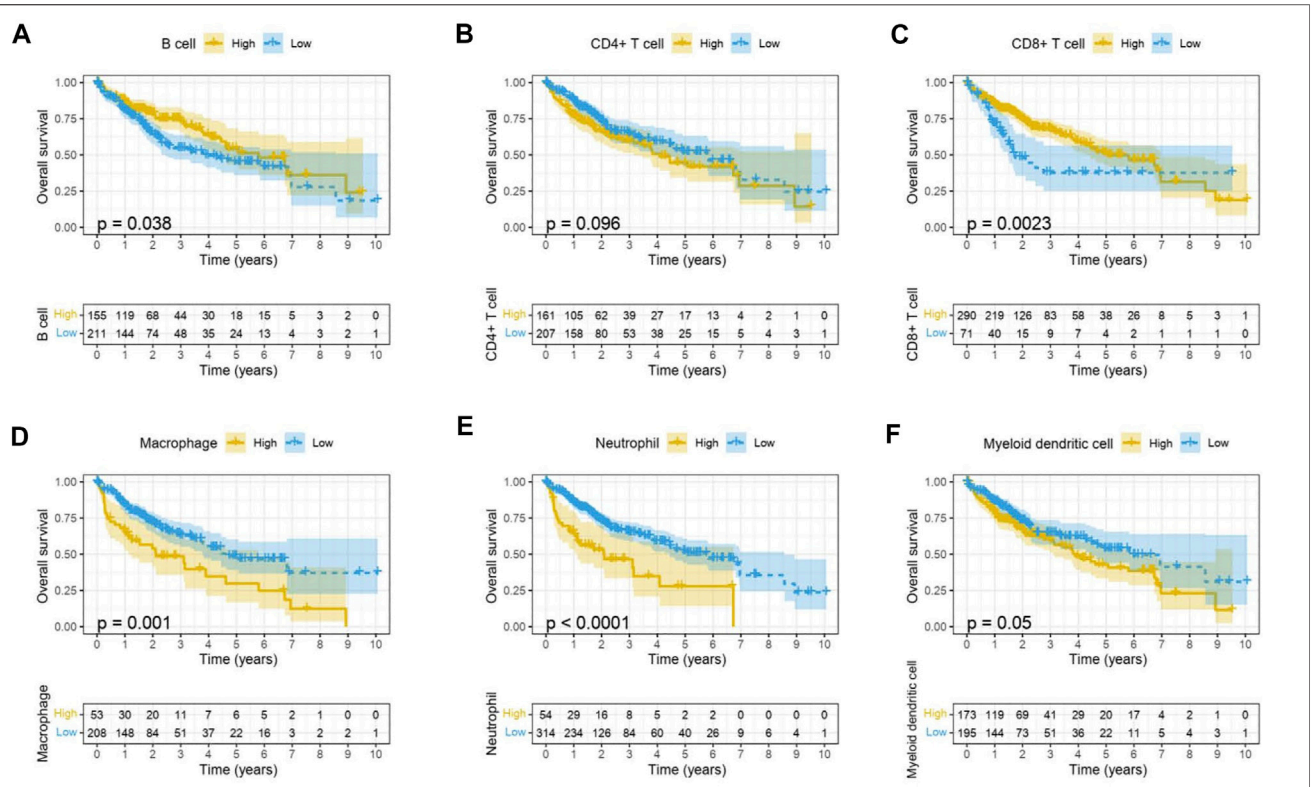

FIGURE 7 | Prognostic value of immune cell infiltration in HCC. B cell **(A)**, $CD8^+$ T cell **(B)**, $CD4^+$ T cell **(C)**, macrophage **(D)**, neutrophil, **(E)** and dendritic cell **(F)**.

MELK. The OS analysis of the differential expression of immune cells is shown in **Supplementary Figure S2**. Altogether, it suggested that MELK may participate in immune response in the tumor microenvironment through affecting immune cells.

Relationship Between MELK and Immune Checkpoints in Hepatocellular Carcinoma

Immune checkpoints are inhibitory immunoreceptors expressed by effector immune cells that prevent them from becoming overactivated (Liu et al., 2021). ICIs increase anti-tumor immunity by blocking intrinsic downregulators of immunity, such as cytotoxic T lymphocyte antigen 4 (CTLA-4), programmed cell death protein-1 (PD-1), and its ligand programmed cell death-ligand 1 (PD-L1) (Postow et al., 2018). In our study, the correlation between the MELK expression and the immune checkpoint genes was conducted by TIMER. MELK was significantly positively correlated with PD1, PD-L1, and CTLA-4 in HCC (**Figure 8**). These results provide further evidence that MELK is associated with immunotherapy prognosis.

DISCUSSION

HCC is one of the most common malignant tumors with high mortality worldwide. The main treatments for HCC include radiofrequency ablation, surgical resection, immunotherapy, and liver implantation. Due to the lack of early clinical symptoms, most HCC patients are generally diagnosed at an advanced stage and lose the timing of better or thorough treatments. They are also at high risk of recurrence and metastasis. Therefore, it is crucial to find effective biomarkers for early diagnosis and prognostic prediction.

It has been reported that MELK is highly upregulated in various types of human cancer according to TCGA dataset and that elevated MELK expression is correlated with poor prognosis of cancer patients (Inoue et al., 2016; Xia et al., 2016). Silencing MELK inhibited the cell growth, invasion, stemness, and tumorigenicity of HCC cells by inducing apoptosis and mitosis (Xia et al., 2016). An orally available MELK inhibitor, OTSSP167, could suppress the growth of GBM (Zhang et al., 2021). This indicated that, especially inhibiting the MELK could be a potential treatment for not only GBM but also other tumors. Nevertheless, the underlying molecular mechanism of MELK affecting HCC is not defined and needs to be further investigated.

We first conducted pan-cancer analysis of the expression of MELK by analyzing RNA-seq data from TCGA database and GEPIA database. MELK was highly expressed in 14 types of tumors including the BLCA, BRCA, CHOL, COAD, ESCA, GBM, HNSC, KIRC, LIHC, LUAD, LUSC, READ, STAD, and UCEC. This suggested that MELK may have a potential promoting role in tumor development. We observed that MELK overexpression significantly indicated the advancement of clinical stages, histological grades, and T stages in HCC patients, and MELK was positively correlated with AFP, the specific HCC marker. For OS and RFS, increased expression

TABLE 2 | Correlation analysis between MELK and biomarkers of immune cells in HCC by the GEPIA database.

Immune cell	Marker	R value	*p*-value
B cell	CD19	0.25	9.8E–07
	CD79A	0.11	3.2E-02
	CD70	0.22	3.0E–05
	CD86	0.3	4.1E–09
$CD8^+$ T cell	CD8A	0.17	8.6E-04
	CD8B	0.15	4.0E-03
Treg cells	FOXP3	0.16	1.5E-03
	CCR8	0.38	8.2E–14
	STAT5B	0.33	1.1E–10
	TGFB1	0.21	5.2E–05
Th1	TNF	0.24	4.2E–06
	STAT1	0.38	3.6E–14
	STAT4	0.22	1.4E–05
Th2	IL13	0.12	1.9E-02
	GATA3	0.16	1.5E-03
	STAT5A	0.32	4.9E–10
	STAT6	0.22	2.8E–05
Tfh	CD183	0.22	2.4e–05
	CD185	0.23	5.3e–06
	CD278	0.28	5e–08
Th17	CD360	0.31	1.6e–09
	IL23R	0.18	0.00053
	CD196	0.16	0.0025
M1 macrophage	NOS2	0.032	5.4E-01
	IRF5	0.38	7.4E–14
	PTGS2	0.094	7.2E-02
M2 macrophage	CD163	0.051	3.3E-01
	VSIG4	0.13	1.0E-02
	MS4A4A	0.14	7.4E-03
Neutrophil	CEACAM8	0.12	2.7E-02
	ITGAM	0.35	7.2E–12
	CCR7	0.065	2.1E-01
Dendritic cell	HLA-DPB1	0.18	5.6E-04
	HLA-DRA	0.22	3.0E–05
	HLA-DPA1	0.18	4.7E-04
	CD1C	0.068	1.9E-01
	NRP1	0.26	2.6E–07
	ITGAX	0.33	1.3E–10
Monocyte	CSF1R	0.18	5.9E-04
	CCL2	0.059	2.6E-01
	CD68	0.24	3.4E–06
Natural killer cells	KIR3DL3	0.15	4.9E-03
	KIR2DS4	0.072	1.7E-01
	XCL1	0.31	9.1E–10
	XCL2	0.13	1.3E-02

of MELK indicated poor prognosis in HCC among all cancer types. Based on the expression analysis and survival analysis, MELK may be utilized as an unfavorable prognostic biomarker for HCC patients.

The ncRNAs, including miRNAs, lncRNAs, and circular RNAs (circRNAs), participated in regulation of gene expression by communicating with each other through the ceRNA mechanism. In this study, we combined the analyses of multiple databases to construct a ceRNA network consisting of lncRNA–miRNA–MELK. A total of thirty five miRNAs that could potentially bind to MELK were predicted by the starBase database. According to our strict screening criteria, hsa-miR-101-3p was chosen as the upstream miRNA. Numerous studies have revealed that miR-101-3p emerges as an essential modulator in the development of human cancers (Ramírez-Salazar et al., 2014; Floor et al., 2015). miR-101-3p has been shown to be downregulated in HCC tissues and cells and could be a potential diagnostic marker of HCC (Yang et al., 2018). In addition, miR-101-3p is responsible for the sensitivity of HCC cells to oxaliplatin by inhibiting Beclin-1-mediated autophagy (Sun et al., 2019). In our study, we found that miR-101-3p was downregulated in HCC patients, and the survival analysis showed a poor prognosis of HCC. Then, we further predicted the upstream lncRNAs of miR-101-3p. A total of twenty five lncRNAs were forecasted. By combining the expression analysis and correlation analysis, two potential upregulated lncRNAs, SNHG1 and SNHG6, were identified. The two lncRNAs have been reported to function as oncogenes in multiple malignancies, including HCC. SNHG1 is upregulated in HCC (Gao et al., 2018), and the knockdown contributed to suppression of HCC cell viability, invasion, and migration properties and promotion of apoptosis, exerting anti-tumor activity in HCC (Meng et al., 2021). SNHG6 is reported to be remarkably increased in HCC tissues and functioned in the proliferation, migration, and invasion abilities of HCC (Fan et al., 2021). The results of the two lncRNAs in our study were consistent with the previous reports. We also found that the higher expression of SNHG1 and SNHG6 was related to poor prognosis and indicated advanced HCC progression (**Supplementary Figure S3**). Synthetically considering, we suggested that the SNHG1 or SNHG6/miR-101-3p/MELK axis functioned in the HCC progression and could be a potential treatment target in HCC.

In recent decades, convincing evidence has shown that the TME plays an important part in the development of many malignant tumors (Lu J. et al., 2019). The TME of HCC is a complex mixture of hepatic non-parenchymal resident cells, tumor cells, immune cells, and tumor-associated fibroblasts (Sangro et al., 2021). Many types of immune cells are abundant in HCC tumors cooperating in the generation of an immunosuppressive TME, and their presence generally correlates with a worse prognosis (Sangro et al., 2021). Intratumor infiltration of B cells is significantly impaired during HCC progression. The densities of B-cell subsets significantly decreased in the tumor, and high densities of tumor-infiltrating B cells imply a better clinical outcome (Zhang et al., 2019). MELK was significantly positively correlated with the B cells and the markers of B cells. Also, the lower density of B cells predicted a poor prognosis in HCC. Tumor-infiltrating T lymphocytes, especially $CD4^+$ and $CD8^+$ T cells, play an adaptive immune role in HCC progression. $CD8^+$ T cells could recognize tumor-associated antigens and kill tumor cells. The presence of tumor-infiltrating $CD8^+$ T cells was significantly correlated with longer OS (Itoh et al., 2020). $CD4^+$ T cells could differentiate into Th1, Th2, Th17, Treg cells, and Tfh cells. Treg cells increase in HCC and promote tumor evasion by impairing the function of $CD8^+$ T cells and lead to disease progression (Fu et al., 2007). In our study, MELK was positively correlated with the $CD8^+$ T cells, $CD4^+$ T cells, and the markers of these cells including the subsets of $CD4^+$ T cells, Th1, Th2, Th17, Tfh cells, and Tregs. The accumulation of $CD8^+$ T cells showed a better prognosis in HCC patients. In the TME, some immune cells could help tumor cells to proliferate, invade, and metastasize. The immunosuppressive features are not only participating in the tumor progression but also a big challenge for effective immunotherapy. The immunosuppressive cells mainly include tumor-associated macrophages (TAMs), tumor-

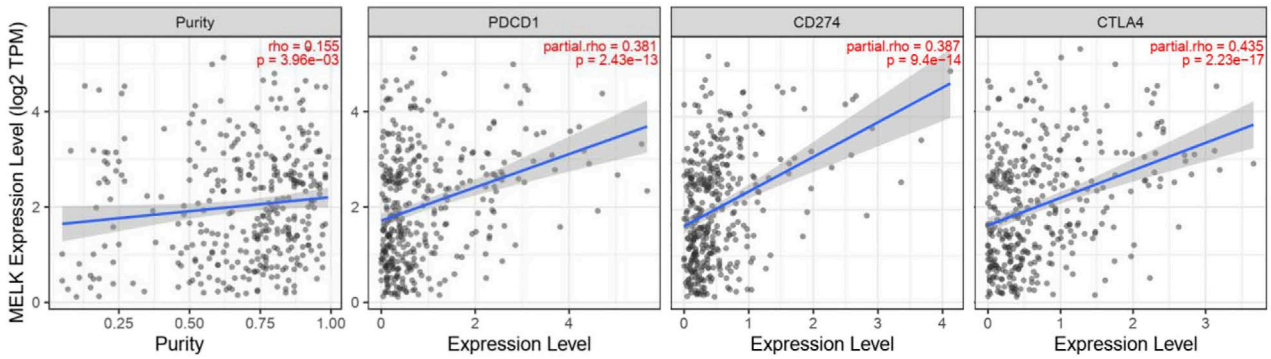

FIGURE 8 | Correlation between MELK and immune checkpoint genes, PD1, PD-L1, and CTLA4.

associated neutrophils (TANs), DCs, and Treg cells (Lu C. et al., 2019). MELK was positively correlated with TAMs, TANs, and DCs and the markers of these immune cells. Also, the abundance of TAMs, TANs, and DCs in tumor showed a poor clinical outcome in the HCC patients. This indicated that MELK may involve in the immunosuppression with these immunosuppressive cells.

However, in the CIBERSORT analysis, decreased M2 macrophages were detected in HCC samples (**Supplementary Figure S1C**) and higher MELK group. Also, better prognosis was found in the group with lower M2 macrophages. Traditionally, macrophages are classified into a classical M1 pro-inflammatory phenotype and a dichotomic M2 anti-inflammatory phenotype (Tacke and Zimmermann, 2014). TAMs are mostly polarized into the M2 phenotype and promote HCC growth, angiogenesis, invasion, and metastasis (Qian and Pollard, 2010). In our work, the analysis of macrophage subsets showed a complicated result remaining to be investigated in further research studies. In addition, CIBERSORT is a convenient and widely used method to determine the composition of immune-infiltrating cells; it is still inaccurate compared with immunohistochemistry and flow cytometry. Overall, the MELK overexpression was significantly correlated with various immune cells, which might indicate its contributions to the immune regulation leading to HCC development.

With the improving understanding of the TME of HCC, the immunotherapy that enhanced tumor immune response and blocked tumor immunosuppression has become a new direction for the treatment of HCC. ICIs targeting PD1, PD-L2, or CTLA-4 are most widely used in the field of advanced HCC (El-Khoueiry et al., 2017; Zhu et al., 2018). PD-1 could transmit inhibitory signals to T cells after binding with PD-L1 or PD-L2 resulting in an immunosuppression and immune tolerance environment and induce the immune escape of tumor cells (Okazaki and Honjo, 2007). CTLA-4 is mainly expressed in activated T cells and dendritic cells and inhibits the activation of T cells, leading to immune escape of HCC cells (Liu and Zheng, 2020). ICIs can cause immune-related adverse events, such as pneumonitis, myocarditis, hypophysitis, and diabetes. It is an important reason preventing the extensive application of ICIs although many patients benefit from the therapy. Therefore, it is of great importance to monitor the treatment efficacy and balance the benefits and side effects for patients receiving ICI therapy. In our study, MELK expression is significantly positively correlated with the immune checkpoint expression, CD274, CTLA4, and PDCD1. This indicated that MELK could predict the efficacy of immunotherapies and provided a direction for new immunotherapy methods.

CONCLUSION

In summary, we constructed the MELK–ceRNA network by various bioinformatic analyses which was related to HCC and impacted the prognosis. MELK may also play a vital role in the microenvironment of HCC by regulating various tumor-infiltrating immune cells. In addition, the MELK expression was positively correlated with the immune checkpoint expression. MELK may be a suitable biomarker for HCC patients receiving immunotherapy and can be used as a monitor method to evaluate benefits of patients undergoing ICIs.

DATA AVAILABILITY STATEMENT

The datasets presented in this study can be found in online repositories. The names of the repository/repositories and accession number(s) can be found in the article/**Supplementary Material**.

ETHICS STATEMENT

This study did not require ethical approval as publicly available data were analyzed.

AUTHOR CONTRIBUTIONS

BT and YL developed the idea and designed the research. YL and RL contributed to the writing of the manuscript. YL and XW performed the data analyses. ZX and XY contributed to the language modification, reference search, and manuscript review. BT guided the manuscript writing, assigned work tasks, and provided funding support. All authors contributed to the article and approved the submitted version.

FUNDING

The study was supported by the National Natural Science Foundation of China (81800203) and Doctoral Scientific Research Foundation of Liaoning Province (20180540088).

SUPPLEMENTARY MATERIAL

The Supplementary Material for this article can be found online at: https://www.frontiersin.org/articles/10.3389/fcell.2022.824938/full#supplementary-material

REFERENCES

Cao, Z., Pan, X., Yang, Y., Huang, Y., and Shen, H.-B. (2018). The lncLocator: A Subcellular Localization Predictor for Long Non-coding RNAs Based on a Stacked Ensemble Classifier. *Bioinformatics* 34, 2185–2194. doi:10.1093/bioinformatics/bty085

Chung, S., Suzuki, H., Miyamoto, T., Takamatsu, N., Tatsuguchi, A., Ueda, K., et al. (2012). Development of an Orally-Administrative MELK-Targeting Inhibitor that Suppresses the Growth of Various Types of Human Cancer. *Oncotarget* 3, 1629–1640. doi:10.18632/oncotarget.790

Davezac, N., Baldin, V., Blot, J., Ducommun, B., and Tassan, J.-P. (2002). Human pEg3 Kinase Associates with and Phosphorylates CDC25B Phosphatase: A Potential Role for pEg3 in Cell Cycle Regulation. *Oncogene* 21, 7630–7641. doi:10.1038/sj.onc.1205870

El-Khoueiry, A. B., Sangro, B., Yau, T., Crocenzi, T. S., Kudo, M., Hsu, C., et al. (2017). Nivolumab in Patients with Advanced Hepatocellular Carcinoma (CheckMate 040): an Open-Label, Non-comparative, Phase 1/2 Dose Escalation and Expansion Trial. *The Lancet*. 389. 2492-2502. doi:10.1016/S0140-6736(17)31046-2

Fan, X., Zhao, Z., Song, J., Zhang, D., Wu, F., Tu, J., et al. (2021). LncRNA-SNHG6 Promotes the Progression of Hepatocellular Carcinoma by Targeting miR-6509-5p and HIF1A. *Cancer Cel Int* 21, 150. doi:10.1186/s12935-021-01835-w

Federico, P., Petrillo, A., Giordano, P., Bosso, D., Fabbrocini, A., Ottaviano, M., et al. (2020). Immune Checkpoint Inhibitors in Hepatocellular Carcinoma: Current Status and Novel Perspectives. *Cancers* 12, 3025. doi:10.3390/cancers12103025

Floor, S. L., Trésallet, C., Hébrant, A., Desbuleux, A., Libert, F., Hoang, C., et al. (2015). MicroRNA Expression in Autonomous Thyroid Adenomas: Correlation with mRNA Regulation. *Mol. Cell Endocrinol.* 411, 1–10. doi:10.1016/j.mce.2015.04.001

Fu, J., Xu, D., Liu, Z., Shi, M., Zhao, P., Fu, B., et al. (2007). Increased Regulatory T Cells Correlate With CD8 T-Cell Impairment and Poor Survival in Hepatocellular Carcinoma Patients. *Gastroenterology* 132, 2328–2339. doi:10.1053/j.gastro.2007.03.102

Gabrielson, A., Wu, Y., Wang, H., Jiang, J., Kallakury, B., Gatalica, Z., et al. (2016). Intratumoral CD3 and CD8 T-Cell Densities Associated with Relapse-free Survival in HCC. *Cancer Immunol. Res.* 4, 419–430. doi:10.1158/2326-6066.CIR-15-0110

Gao, S., Xu, X., Wang, Y., Zhang, W., and Wang, X. (2018). Diagnostic Utility of Plasma lncRNA Small Nucleolar RNA Host Gene 1 in Patients with Hepatocellular Carcinoma. *Mol. Med. Rep.* 18, 3305. doi:10.3892/mmr.2018.9336

Gray, D., Jubb, A. M., Hogue, D., Dowd, P., Kljavin, N., Yi, S., et al. (2005). Maternal Embryonic Leucine Zipper Kinase/murine Protein Serine-Threonine Kinase 38 Is a Promising Therapeutic Target for Multiple Cancers. *Cancer Res.* 65, 9751–9761. doi:10.1158/0008-5472.CAN-04-4531

Inoue, H., Kato, T., Olugbile, S., Tamura, K., Chung, S., Miyamoto, T., et al. (2016). Effective Growth-Suppressive Activity of Maternal Embryonic Leucine-Zipper Kinase (MELK) Inhibitor against Small Cell Lung Cancer. *Oncotarget* 7, 13621–13633. doi:10.18632/oncotarget.7297

Itoh, S., Yoshizumi, T., Yugawa, K., Imai, D., Yoshiya, S., Takeishi, K., et al. (2020). Impact of Immune Response on Outcomes in Hepatocellular Carcinoma: Association with Vascular Formation. *Hepatology* 72, 1987–1999. doi:10.1002/hep.31206

Jung, H., Seong, H.-A., and Ha, H. (2008). Murine Protein Serine/threonine Kinase 38 Activates Apoptosis Signal-Regulating Kinase 1 via Thr838 Phosphorylation. *J. Biol. Chem.* 283, 34541–34553. doi:10.1074/jbc.M807219200

Liu, Y., and Zheng, P. (2020). Preserving the CTLA-4 Checkpoint for Safer and More Effective Cancer Immunotherapy. *Trends Pharmacol. Sci.* 41, 4–12. doi:10.1016/j.tips.2019.11.003

Liu, Z., Liu, X., Liang, J., Liu, Y., Hou, X., Zhang, M., et al. (2021). Immunotherapy for Hepatocellular Carcinoma: Current Status and Future Prospects. *Front. Immunol.* 12, 765101. doi:10.3389/fimmu.2021.765101

Llovet, J. M., Ducreux, M., Lencioni, R., Di Bisceglie, A. M., Galle, P. R., Dufour, J. F., et al. (2012). EASL-EORTC Clinical Practice Guidelines: Management of Hepatocellular Carcinoma. *J. Hepatol.* 56, 908–943. doi:10.1016/j.jhep.2011.12.001

Lu, C., Rong, D., Zhang, B., Zheng, W., Wang, X., Chen, Z., et al. (2019). Current Perspectives on the Immunosuppressive Tumor Microenvironment in Hepatocellular Carcinoma: Challenges and Opportunities. *Mol. Cancer* 18, 130. doi:10.1186/s12943-019-1047-6

Lu, J., Xu, Y., Wu, Y., Huang, X.-y., Xie, J.-w., Wang, J.-b., et al. (2019). Tumor-infiltrating CD8+ T Cells Combined with Tumor-Associated CD68+ Macrophages Predict Postoperative Prognosis and Adjuvant Chemotherapy Benefit in Resected Gastric Cancer. *BMC Cancer* 19, 920. doi:10.1186/s12885-019-6089-z

Meng, F., Liu, J., Lu, T., Zang, L., Wang, J., He, Q., et al. (2021). SNHG1 Knockdown Upregulates miR-376a and Downregulates FOXK1/Snail axis to Prevent Tumor Growth and Metastasis in HCC. *Mol. Ther. - Oncolytics* 21, 264–277. doi:10.1016/j.omto.2021.02.002

Okazaki, T., and Honjo, T. (2007). PD-1 and PD-1 Ligands: From Discovery to Clinical Application. *Int. Immunol.* 19, 813–824. doi:10.1093/intimm/dxm057

Postow, M. A., Sidlow, R., and Hellmann, M. D. (2018). Immune-Related Adverse Events Associated with Immune Checkpoint Blockade. *N. Engl. J. Med.* 378, 158–168. doi:10.1056/NEJMra1703481

Qian, B.-Z., and Pollard, J. W. (2010). Macrophage Diversity Enhances Tumor Progression and Metastasis. *Cell* 141, 39–51. doi:10.1016/j.cell.2010.03.014

Ramírez-Salazar, E. G., Salinas-Silva, L. C., Vázquez-Manríquez, M. E., Gayosso-Gómez, L. V., Negrete-Garcia, M. C., Ramírez-Rodriguez, S. L., et al. (2014). Analysis of microRNA Expression Signatures in Malignant Pleural Mesothelioma, Pleural Inflammation, and Atypical Mesothelial Hyperplasia Reveals Common Predictive Tumorigenesis-Related Targets. *Exp. Mol. Pathol.* 97, 375–385. doi:10.1016/j.yexmp.2014.09.016

Salmena, L., Poliseno, L., Tay, Y., Kats, L., and Pandolfi, P. P. (2011). A ceRNA Hypothesis: The Rosetta Stone of a Hidden RNA Language? *Cell* 146, 353–358. doi:10.1016/j.cell.2011.07.014

Sangro, B., Sarobe, P., Hervás-Stubbs, S., and Melero, I. (2021). Advances in Immunotherapy for Hepatocellular Carcinoma. *Nat. Rev. Gastroenterol. Hepatol.* 18, 525–543. doi:10.1038/s41575-021-00438-0

Shi, F., Shi, M., Zeng, Z., Qi, R.-Z., Liu, Z.-W., Zhang, J.-Y., et al. (2011). PD-1 and PD-L1 Upregulation Promotes CD8+ T-Cell Apoptosis and Postoperative Recurrence in Hepatocellular Carcinoma Patients. *Int. J. Cancer* 128, 887–896. doi:10.1002/ijc.25397

Sun, H., Ma, H., Zhang, H., and Ji, M. (2021). Up-regulation of melk by e2f1 promotes the proliferation in cervical cancer cells. *Int. J. Biol. Sci.* 17, 3875–3888. doi:10.7150/ijbs.62517

Sun, W., Zhang, Q., Wu, Z., and Xue, N. (2019). miR-101-3p Sensitizes Hepatocellular Carcinoma Cells to Oxaliplatin by Inhibiting Beclin-1-Mediated Autophagy. *Int. J. Clin. Exp. Pathol.* 12, 2056–2065.

Sung, H., Ferlay, J., Siegel, R. L., Laversanne, M., Soerjomataram, I., Jemal, A., et al. (2021). Global Cancer Statistics 2020: GLOBOCAN Estimates of Incidence and Mortality Worldwide for 36 Cancers in 185 Countries. *CA A. Cancer J. Clin.* 71, 209–249. doi:10.3322/caac.21660

Tacke, F., and Zimmermann, H. W. (2014). Macrophage Heterogeneity in Liver Injury and Fibrosis. *J. Hepatol.* 60, 1090–1096. doi:10.1016/j.jhep.2013.12.025

Tang, Z., Li, C., Kang, B., Gao, G., Li, C., and Zhang, Z. (2017). GEPIA: A Web Server for Cancer and normal Gene Expression Profiling and Interactive Analyses. *Nucleic Acids Res.* 45, W98–W102. doi:10.1093/nar/gkx247

Uhlen, M., Zhang, C., Lee, S., Sjöstedt, E., Fagerberg, L., Bidkhori, G., et al. (2017). A Pathology Atlas of the Human Cancer Transcriptome. *Science* 357, eaan2507. doi:10.1126/science.aan2507

Vulsteke, V., Beullens, M., Boudrez, A., Keppens, S., Van Eynde, A., Rider, M. H., et al. (2004). Inhibition of Spliceosome Assembly by the Cell Cycle-Regulated Protein Kinase MELK and Involvement of Splicing Factor NIPP1. *J. Biol. Chem.* 279, 8642–8647. doi:10.1074/jbc.M311466200

Xia, H., Chen, J., Shi, M., Gao, H., Sekar, K., Seshachalam, V. P., et al. (2015). EDIL3 Is a Novel Regulator of Epithelial-Mesenchymal Transition Controlling Early Recurrence of Hepatocellular Carcinoma. *J. Hepatol.* 63, 863–873. doi:10.1016/j.jhep.2015.05.005

Xia, H., Kong, S. N., Chen, J., Shi, M., Sekar, K., Seshachalam, V. P., et al. (2016). MELK Is an Oncogenic Kinase Essential for Early Hepatocellular Carcinoma Recurrence. *Cancer Lett.* 383, 85–93. doi:10.1016/j.canlet.2016.09.017

Xiong, Y., Wang, K., Zhou, H., Peng, L., You, W., and Fu, Z. (2018). Profiles of Immune Infiltration in Colorectal Cancer and Their Clinical Significant: A Gene Expression-based Study. *Cancer Med.* 7, 4496–4508. doi:10.1002/cam4.1745

Yang, J. D., Hainaut, P., Gores, G. J., Amadou, A., Plymoth, A., and Roberts, L. R. (2019). A Global View of Hepatocellular Carcinoma: Trends, Risk, Prevention and Management. *Nat. Rev. Gastroenterol. Hepatol.* 16, 589–604. doi:10.1038/s41575-019-0186-y

Yang, X., Pang, Y.-Y., He, R.-Q., Lin, P., Cen, J.-M., Yang, H., et al. (2018). Diagnostic Value of Strand-specific miRNA-101-3p and miRNA-101-5p for Hepatocellular Carcinoma and a Bioinformatic Analysis of Their Possible Mechanism of Action. *FEBS Open Bio* 8, 64–84. doi:10.1002/2211-5463.12349

Zhang, X., Wang, J., Wang, Y., Liu, G., Li, H., Yu, J., et al. (2021). MELK Inhibition Effectively Suppresses Growth of Glioblastoma and Cancer Stem-like Cells by Blocking AKT and FOXM1 Pathways. *Front. Oncol.* 10, 608082. doi:10.3389/fonc.2020.608082

Zhang, Z., Ma, L., Goswami, S., Ma, J., Zheng, B., Duan, M., et al. (2019). Landscape of Infiltrating B Cells and Their Clinical Significance in Human Hepatocellular Carcinoma. *OncoImmunology* 8, e1571388. doi:10.1080/2162402X.2019.1571388

Zhu, A. X., Finn, R. S., Edeline, J., Cattan, S., Ogasawara, S., Palmer, D., et al. (2018). Pembrolizumab in Patients with Advanced Hepatocellular Carcinoma Previously Treated with Sorafenib (KEYNOTE-224): a Non-randomised, Open-Label Phase 2 Trial. *Lancet Oncol.* 19, 940. doi:10.1016/S1470-2045(18)30351-6

Conflict of Interest: The authors declare that the research was conducted in the absence of any commercial or financial relationships that could be construed as a potential conflict of interest.

Publisher's Note: All claims expressed in this article are solely those of the authors and do not necessarily represent those of their affiliated organizations, or those of the publisher, the editors, and the reviewers. Any product that may be evaluated in this article, or claim that may be made by its manufacturer, is not guaranteed or endorsed by the publisher.

Copyright © 2022 Liu, Li, Wang, Xue, Yang and Tang. This is an open-access article distributed under the terms of the Creative Commons Attribution License (CC BY). The use, distribution or reproduction in other forums is permitted, provided the original author(s) and the copyright owner(s) are credited and that the original publication in this journal is cited, in accordance with accepted academic practice. No use, distribution or reproduction is permitted which does not comply with these terms.

frontiers | Frontiers in Cell and Developmental Biology

ORIGINAL RESEARCH
published: 13 June 2022
doi: 10.3389/fcell.2022.874588

Analysis of Omics Data Reveals Nucleotide Excision Repair-Related Genes Signature in Highly-Grade Serous Ovarian Cancer to Predict Prognosis

Danian Dai[1†], Qiang Li[2†], Pengfei Zhou[3†], Jianjiang Huang[4], Hongkai Zhuang[5], Hongmei Wu[4]* and Bo Chen[6]**

[1]Department of Vascular and Plastic Surgery, Guangdong Provincial People's Hospital and Guangdong Academy of Medical Sciences, Guangzhou, China, [2]Department of Cardiology, Guangdong Cardiovascular Institute, Guangdong Provincial People's Hospital, Guangdong Academy of Medical Sciences, Guangzhou, China, [3]Chongqing Key Laboratory of Oral Diseases and Biomedical Sciences, Stomatological Hospital of Chongqing Medical University, Chongqing, China, [4]Department of Pathology, Guangdong Provincial People's Hospital and Guangdong Academy of Medical Sciences, Guangzhou, China, [5]Department of General Surgery, Guangdong Provincial People's Hospital and Guangdong Academy of Medical Sciences, Guangzhou, China, [6]Department of Breast Cancer, Guangdong Provincial People's Hospital and Guangdong Academy of Medical Sciences, Guangzhou, China

Most of the high-grade serous ovarian cancers (HGSOC) are accompanied by P53 mutations, which are related to the nucleotide excision repair (NER) pathway. This study aims to construct a risk signature based on NER-related genes that could effectively predict the prognosis for advanced patients with HGSOC. In our study, we found that two clusters of HGSOC with significantly different overall survival (OS) were identified by consensus clustering and principal component analysis (PCA). Then, a 7-gene risk signature (DDB2, POLR2D, CCNH, XPC, ERCC2, ERCC4, and RPA2) for OS prediction was developed subsequently based on TCGA cohort, and the risk score-based signature was identified as an independent prognostic indicator for HGSOC. According to the risk score, HGSOC patients were divided into high-risk group and low-risk group, in which the distinct OS and the predictive power were also successfully verified in the GEO validation sets. Then we constructed a nomogram, including the risk signature and clinical-related risk factors (age and treatment response) that predicted an individual's risk of OS, which can be validated by assessing calibration curves. Furthermore, GSEA showed that the genes in the high-risk group were significantly enriched in cancer-related pathways, such as "MAPK signaling pathway", "mTOR signaling pathway", "VEGF signaling pathway" and so on. In conclusion, our study has developed a robust NER-related genes-based molecular signature for prognosis prediction, and the nomogram could be used as a convenient tool for OS evaluation and guidance of therapeutic strategies in advanced patients with HGSOC.

Keywords: high-grade serous ovarian cancers, nucleotide excision repair, prognosis, nomogram, gene signature predicting prognosis of NER genes

OPEN ACCESS

Edited by:
Shaoquan Zheng,
Sun Yat-sen University Cancer Center (SYSUCC), China

Reviewed by:
Shanshan Jiang,
Fudan University, China
Jiangping Li,
Sichuan University, China
Shi-Tong Yu,
Southern Medical University, China

****Correspondence:***
Hongkai Zhuang
799002305@qq.com
Hongmei Wu
whm-happy@163.com
Bo Chen
chenbo@gdph.org.cn

[†]These authors have contributed equally to this work and share first authorship

Specialty section:
This article was submitted to Cancer Cell Biology, a section of the journal Frontiers in Cell and Developmental Biology

Received: *12 February 2022*
Accepted: *02 May 2022*
Published: *13 June 2022*

Citation:
Dai D, Li Q, Zhou P, Huang J, Zhuang H, Wu H and Chen B (2022) Analysis of Omics Data Reveals Nucleotide Excision Repair-Related Genes Signature in Highly-Grade Serous Ovarian Cancer to Predict Prognosis. Front. Cell Dev. Biol. 10:874588. doi: 10.3389/fcell.2022.874588

INTRODUCTION

High-grade serous ovarian cancer (HGSOC) is of great concern to the researchers among all ovarian cancers, as it accounts for 70%–80% of deaths from ovarian cancer. The modes of carcinogenesis, molecular-genetic characteristics, and the origin are distinctive from low-grade serous ovarian cancer (Kurman et al., 2014; Bowtell et al., 2015). Due to the lack of effective early screening methods for ovarian cancer, almost 90% of serous ovarian cancer patients are diagnosed as stage III–IV at first diagnosis, while the 10-year survival rate of advanced patients with HGSOC is only 15% (Narod, 2016). So far, surgery remains the most important treatment approach and the subsequent chemotherapy, targeted therapy, radiation, and immunotherapy are used to enhance the curative effect according to the International Federation of Gynecology and Obstetrics (FIGO) staging system (González-Martín et al., 2010; Jessmon et al., 2017). However, for advanced patients, the current FIGO classification method failed to provide accurate information to predict prognosis, nor guide physicians' treatment decisions (Llueca et al., 2018; Tajik et al., 2018). It is a widespread phenomenon for advanced patients with HGSOC at the same FIGO stage to have completely different prognostic outcomes due to complex biological processes and unintelligible molecular mechanisms. Therefore, it is necessary and urgent to prompt a search for novel and reliable prognostic molecular signatures for predicting prognosis and guiding appropriate therapeutic strategies.

In recent years, genome-wide expression profiling detection can effectively provide detailed information for the prognosis assessment of cancer patients (Anurag et al., 2018; Zhu et al., 2018). In breast cancer, the genomic panel detection methods, which included 21-gene recurrent score and 70-gene MammaPrint assay, could provide some valuable information for the prognosis evaluation and treatment selection of patients (Cardoso et al., 2016; Sparano et al., 2018). Notably, although HGSOC shares high molecular similarity with basal-like breast cancer, there is no molecular evaluation system available for clinical use in HGSOC (Cancer Genome Atlas Network, 2012).

DNA damage response and repair pathways play an essential regulatory role in the occurrence and development of ovarian cancer (Majidinia et al., 2017). DNA repair mechanisms mainly contain various pathways, such as mismatch repair, base excision repair, nucleotide excision repair (NER), homologous recombination, and non-homologous end joining (Mirza-Aghazadeh-Attari et al., 2019). Importantly, HGSOC is mostly accompanied by mutations of P53 that are near related to the NER pathway (Williams and Schumacher, 2016). The NER pathway is composed of various proteins acting in concert and is the main pathway to remove large DNA lesions caused by ionizing radiation and other mutagens (Shuck et al., 2008). In addition, the NER pathway also can repair the damage caused by platinum drugs (such as cisplatin and carboplatin), which are most widely used in the treatment of ovarian cancer. In recent years, a large number of studies have reported that NER-related genes, such as ERCC1, XPC, and GTF2H5, could be used as biomarkers of treatment response or prognosis for tumor patients (Lin et al., 2010; Fleming et al., 2012; Gayarre et al., 2015). Besides, other studies have found that subtle changes of NER function may greatly increase the susceptibility of healthy individuals to lung cancer and head and neck squamous cell cancer (Wei et al., 1996; Cheng et al., 1998). However, despite the increased concern of NER in the field of ovarian cancer, there is still a lack of comprehensive analysis of NER-related genes in advanced patients with HGSOC to assess prognosis and guide therapy strategies effectively.

In the present study, we comprehensively explored the roles of 31 NER-related genes in HGSOC based on multiple transcriptome datasets, such as The Cancer Genome Atlas (TCGA), the Genotype-Tissue Expression (GTEx) Project, and the Gene Expression Omnibus (GEO) database. We evaluated the interaction and correlation among the 31 NER-related genes and employed the consensus cluster analysis to identify two HGSOC clusters with different clinical outcomes based on their expression patterns of these genes. Then we conducted the least absolute shrinkage and selection operator (LASSO) Cox regression to obtain a 7-gene signature on TCGA HGSOC cohort. This robust risk signature was successfully confirmed in two GEO validation sets and showed an excellent predictive effect on prognosis. Moreover, the risk signature and clinical characteristics were used to construct a nomogram to predict the prognosis of advanced patients with HGSOC. Finally, we also used the gene set enrichment analysis (GSEA) to explore the differences in the signaling pathways between subgroups classified by risk signature. Our results indicated that the risk signature derived from seven NER-related genes could serve as novel prognostic biomarkers for advanced patients with HGSOC.

MATERIALS AND METHODS

Public Data Collection and Processing

The study design flowchart is presented in **Supplementary Figure S1**. The Fragments per Kilobase of transcript per Million mapped reads (FPKM) for RNA-seq data of 378 ovarian cancer tissues and 88 normal ovarian tissues were respectively extracted from two datasets, including the Cancer Genome Atlas (TCGA) and the Genotype-Tissue Expression (GTEx), which were downloaded from UCSC Xena (https://xenabrowser.net/datapages) (Goldman et al., 2018). According to patients' clinicopathological information of TCGA, RNA-seq data and clinical data of 326 advanced HGSOC samples were eventually enrolled in our analysis. The exclusive criteria were as follows: 1) patients with stage I–II or unclear stage; 2) patients with neoadjuvant chemotherapy; 3) patients with well differentiation or unspecified defined; 4) patients with non-ovarian primary tumor or other histological types; 5) patients with survival less than 30 days. We re-annotated the gene symbols based on the information recorded in the HUGO Gene Nomenclature Committee (HGNC; http://www.genenames.org) (Eyre et al., 2006), and the gene expression of both datasets was unified as log2 (x + 1) to increase comparability. Then, the "*limma*" package was used to average the repeated data of each expression and merge the two datasets with

normalization in programming language R (version 4.0.1; https://cran.r-project.org) (Ritchie et al., 2015).

Four independent expression data of advanced patients with HGSOC (GSE13876, GSE49997, GSE17260, and GSE63885) were downloaded from Gene Expression Omnibus (GEO) database (https://www.ncbi.nlm.nih.gov/geo). Gene expression in GSE13876 was performed using Operon human v3 ~35 K 70-mer two-color oligonucleotide microarrays (GPL7759; N = 415); Gene expression in GSE49997 was performed using ABI Human Genome Survey Microarray Version 2 (GPL2986; N = 204); Gene expression in GSE17260 was performed using Agilent-014850 Whole Human Genome Microarray 4 × 44K G4112F (Probe Name version) (GPL6480; N = 110); Gene expression in GSE63885 was performed using Affymetrix Human Genome U133 Plus 2.0 Array (GPL570; N = 101). Then, we integrated 346 standards-compliant samples from three datasets [GSE49997 (N = 166), GSE17260 (N = 110) and GSE63885 (N = 70)] as a combined validation set based on the exclusive criteria to improve the sample size, and we executed batch normalization between these three platforms using the "*sav*" and "*limma*" packages in R to avoid generating unreliable results (Johnson et al., 2007; Leek et al., 2012). Gene expression values of all GEO datasets were converted by log2 and for genes with multiple probes, and we used average values to represent the performance of specific genes.

The 31 Candidate Genes

We used the database (TCGA, GTEx, and four GEO databases) for gene screening. A total of 8,466 common genes were selected. According to previous studies (Friedberg, 2001; Marteijn et al., 2014), 31 shared genes among TCGA-GTEx and four GEO datasets related to nucleotide excision repair (NER) were used for our analysis, including RAD23A, RAD23B, RPA2, RPA3, ERCC8, POLR2A, POLR2B, POLR2C, POLR2D, POLR2F, POLR2G, POLR2K, POLR2L, DDB1, DDB2, LIG1, GTF2H1, GTF2H3, GTF2H5, CUL3, CUL4A, CUL5, RBX1, CCNH, CDK7, XPA, XPC, ERCC2, ERCC3, ERCC4, and MNAT1.

mRNA Expression Analysis of 31 NER-Related Genes

We first analyzed the mRNA expression levels between HGSOC tissues and normal tissues by using the "limma" package with cut-off criteria of $p < 0.05$. The mRNA expression profiles of 31 NER-related genes were obtained. The heatmap and violin plots were presented by "*pheatmap*" and "*ggplot2*" packages in R.

Protein-Protein Interaction Network Analysis and Correlation Analysis

All 31 NER-related genes were used for the protein-protein interaction (PPI) analysis with a combined confidence score ≥ 0.9 *via* the Search Tool for the Retrieval of Interacting Genes (STRING) (https://string-db.org/) (Szklarczyk et al., 2015). Pearson correlation analysis was utilized to present the collinearity among different NER-related genes.

Consensus Clustering Analysis and Principal Component Analysis

The "*ConsensusClusterPlus*" package in R (50 iterations, resample rate of 80%) was applied to explore the clinical implications of the 31 NER-related genes in the TCGA HGSOC cohort. The number of clusters and their stability were determined by the consensus clustering algorithm (Kanungo et al., 2002). Then, the TCGA HGSOC cohort was clustered into different two clusters. To further confirm the rationality of clustering, principal component analysis (PCA) was carried out in R to observe the distribution of gene expression in two clusters. The Kaplan-Meier method and log-rank test were used to present the difference of overall survival (OS) between two clusters. The associations between the clinical characteristics and two different clusters were analyzed by Chi-square test.

Construction of Gene Signature

Seven candidate genes associated with OS ($p < 0.1$) were determined by the univariate Cox regression analysis of 31 NER-related genes; the hazard ratios (HRs) of genes <1 or >1 were regarded as protective or risk genes, respectively. To prevent over-fitting in our analysis, the least absolute shrinkage and selection operator (LASSO) regression analysis was used to identify the optimal prognostic model out of the selected seven candidate genes (Goeman, 2010), and genes' coefficients were determined based on the best penalty parameter λ. The risk score for the signature was estimated accurately using the following formula:

$$\text{Risk Score} = \sum_{i=1}^{n} \text{Coefi} * \text{Expi}$$

N is the number of selected genes, Coefi is the regression coefficient generated by the LASSO regression and Expi is the expression value of each selected gene. TCGA HGSOC patients were divided into low- and high-risk groups according to the median risk score. Kaplan-Meier (K-M) survival was used to estimate the OS between two risk groups. In addition, the receiver operating characteristic (ROC) curves and area under the ROC curves (AUC) were also performed to estimate sensitivity and specificity. Chi-square test was used to assess the association between the clinical characteristics and two risk groups.

Validation of the Prognostic Signature

Similarly, the risk score of each advanced patient with HGSOC from the GSE13876 and the merged GEO datasets was calculated based on the formula above. Taking the median risk score in the TCGA cohort as the cut-off value, HGSOC patients in both validation sets were divided into high- or low-groups. The K-M method and log-rank test were employed to calculate OS with an overall significance level of $p < 0.05$. The risk score was identified as an independent prognostic factor by the method of the univariate and multivariate Cox regression analyses. Moreover, the prognostic nomogram based on the risk score of NER-related signature and clinical-related variables was constructed. The performance of the prediction model developed was validated by assessing

TABLE 1 | The clinical characteristics of the HGSOV cohort in the TCGA database.

Variable	Number
Age	
Mean (SD)	59.29 (11.30)
Pathological diagnosis	
Serous	326
Grade	
G2	34 (10.4%)
G3	292 (89.6%)
FIGO stage	
IIIA	6 (1.8%)
IIIB	13 (4.0%)
IIIC	256 (78.5%)
IV	51 (15.6%)
Treatment response	
CR	183 (56.1)
PR	42 (12.9%)
SD	20 (6.1%)
PD	24 (7.4%)
Unknown	57 (17.5%)
Residual tumor (post-operation)	
<1 cm	211 (64.7%)
≥1 cm	87 (26.7%)
Unknown	28 (8.6%)

Abbreviation: HGSOV, High-grade serous ovarian cancers; TCGA, The Cancer Genome Atlas; SD, Standard deviation; G2, Moderately differentiated; G3, Poorly differentiated; FIGO, International Federation of Gynecology and Obstetrics; CR, Complete remission; PR, Partial remission; SD, Stable disease; PD, Progressive disease

the internal calibration curves of the TCGA cohort. To further confirm the expression of seven selected genes, we analyzed normal ovarian tissues and serous ovarian cancer tissues obtained from the Human Protein Atlas (HPA) database.

Gene Set Enrichment Analysis

Gene set enrichment analysis (GSEA) was used in the TCGA cohort to investigate the potential biological pathways underlying the different risk groups defined by the 7-gene expression signature. Kyoto Encyclopedia of Genes and Genomes (KEGG) gene sets (v7.1) and phenotype label (high risk vs. low risk) files were generated and loaded into the GSEA software (v4.0.3; Broad Institute, Cambridge, MA). The permutation test run 1,000 times. The pathways with normalized enrichment score (NSE) absolute value >1, normalized p-value < 0.05, and false discovery rate (FDR) q-value < 0.25 were significantly enriched.

Statistical Analysis

Unless otherwise specified, all statistics analyses were performed with R software. The differences between groups for the continuous and categorical variables were respectively assessed by student's t-test or one-way ANOVA and the Chi-square test. The "*limma*", "*sva*", "*ConsensusClusterPlus*", "*pheatmap*", "*ggplot2*", "corrplot", "*pROC*", "*rms*", "*survival*" packages were used for analysis or visualization in R. All statistical tests were two-sided and $p < 0.05$ was considered statistically significant.

RESULTS

The Expression of 31 NER-Related Genes Between Tumor Samples and Normal Control Samples

To better understand the importance of the NER-related genes in tumor initiation and progression, we firstly investigated expression levels of NER-related genes in different tissue samples of the merged TCGA-GTEx dataset. The TCGA-GTEx cohort comprised 326 advanced patients with HGSOC and 88 ovaries of healthy donors. The clinicopathological characteristics of the TCGA HGSOC cohort were listed in **Table 1**. We selected 31 NER-related candidate genes among 8,466 shared genes in all datasets for further analysis (**Figure 1A**). Then, mRNA expression levels of the 31 genes were presented for HGSOC along with corresponding normal controls by the heatmap (**Figure 1B**). Overall, the expression levels of 13 NER-related genes were significantly increased, and 15 genes were significantly downregulated in HGSOC tissues when compared to those with normal controls (**Figure 1C**). However, the expression levels of three genes (including POLR2B, ERCC4, and POLR2A) had no significant difference.

The Interaction and Correlation Among the NER-Related Genes

The interaction relationships among the 31 NER-related genes were shown by the PPI network, and the number of interactions for each gene was counted in **Figure 2**. Our results showed that the interrelationships among 31 genes were of high closeness and great complexity (**Figure 2A**). Except CUL3 and CUL5, the other 29 genes seemed to be the hub genes of the interaction network, because they had interactions with more than half of the genes (**Figure 2B**). We also conducted correlation analysis and observed that there were various degrees of positive and negative collinearity among some NER-related genes in HGSOC (**Figure 2C**). We believe that the changes in the correlation of 31 NER-related genes may reflect the inherent characteristics of antagonistic or synergistic effects between the corresponding transcribed functional proteins.

Consensus Clustering of NER-Related Genes Identified Two Clusters of HGSOC With Different Prognostic Outcomes

Next, TCGA HGSOC samples were selected for the subsequent consensus clustering analysis. According to the expression similarity of the 31 NER-related genes, k = 2 could be the optimal choice when clustering stability datasets increased from k = 2–9 (**Figures 3A–C**). We noticed that the distribution of sample numbers in each group was roughly balanced, and the interference between groups was minimal in the two groups when k = 2 (**Figure 3C**). Hence, TCGA HGSOC samples were correspondingly classified as two groups (184 samples in cluster1 and 142 samples in cluster2) through

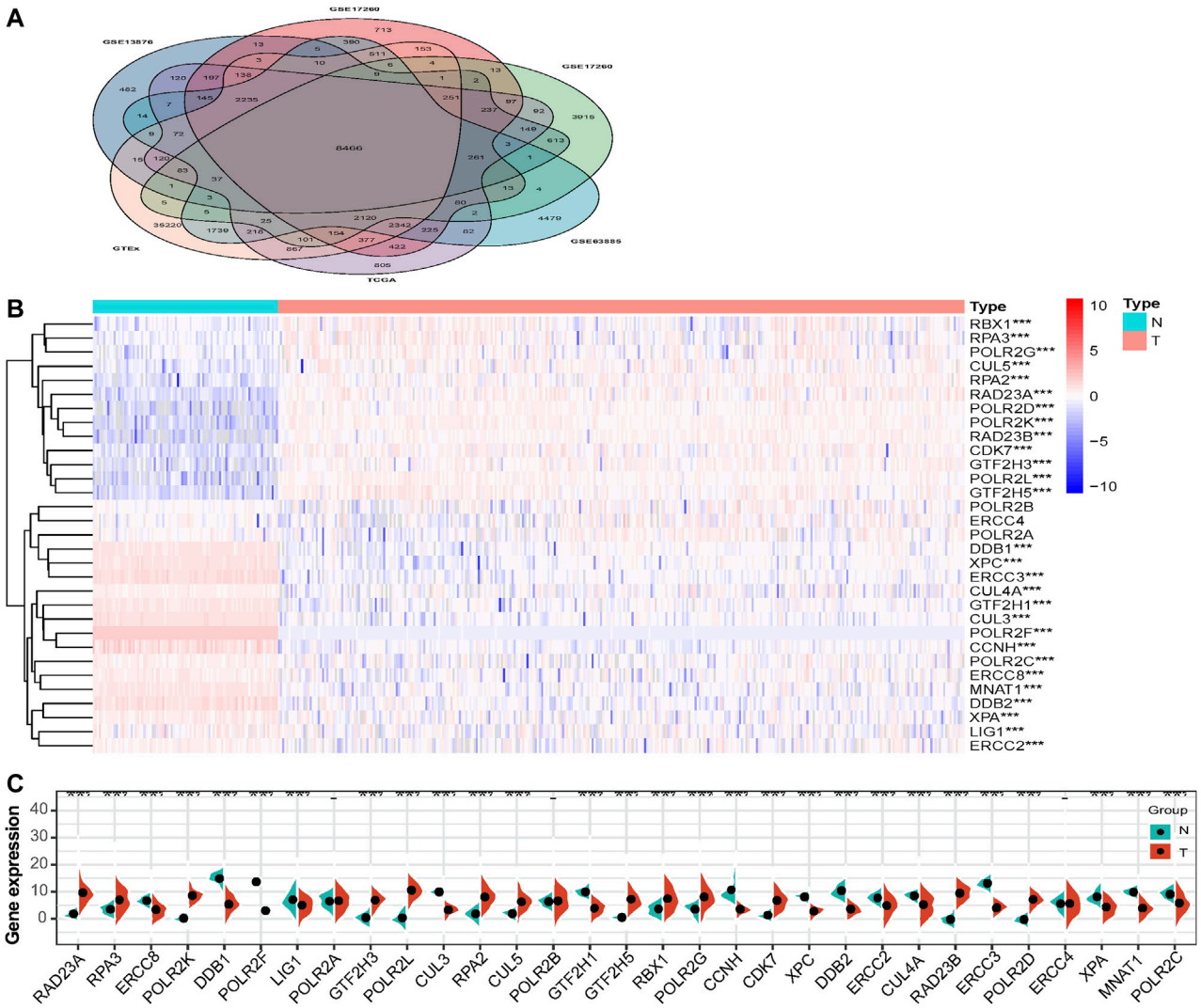

FIGURE 1 | The expression levels of NER-related genes between tumor samples and normal samples in TCGA HGSOC cohort and GTEx normal ovary cohort. **(A)** Venn diagram displays that 8,466 shared genes were contained in the TCGA, GTEx, and four GEO datasets. **(B)** The TCGA and GTEx databases were used to jointly analyze 31 NER-related genes and the heatmap was used to visualize the expression levels of these genes in each clinical sample. **(C)** The violin-plot shows the expression of 31 NER-related genes between tumor tissues and the normal tissues. $*p < 0.05$, $**p < 0.01$, and $***p < 0.001$. Abbreviation: HGSOC: high-grade serous ovarian cancer; TCGA: The Cancer Genome Atlas; GTEx: the Genotype-Tissue Expression project; GEO: Gene Expression Omnibus; NER: Nucleotide excision repair.

consensus cluster analysis. The clinical characteristics of the two clusters were shown in **Supplementary Table S1**. Moreover, Principal component analysis (PCA) was used to compare the difference of transcriptional profiles between the two clusters, and the results exhibited a significant distinction (**Figure 3D**). Besides, advanced patients with HGSOC were found to have the significantly lower OS in the cluster1 than those in the cluster2 ($p = 0.021$), which suggested that the 31 NER-related genes could classify the advanced patients with HGSOC at the prognostic level (**Figure 3E**). We then analyzed the associations between the clusters and clinicopathological characteristics. However, no significant difference was found between two clusters in the age, grade, stage, treatment response, and residual tumor (all $p > 0.05$).

Identification of Prognostic Value and a Risk Signature Based on NER-Related Genes

To further explore the prognostic value of 31 NER-related genes, univariate Cox regression analysis was performed based on the mRNA expression levels of genes from TCGA. The results demonstrated that seven out of the 13 NER-related genes were potentially associated with the OS ($p < 0.1$). Among these seven genes, only DDB2 and POLR2D were considered as protective

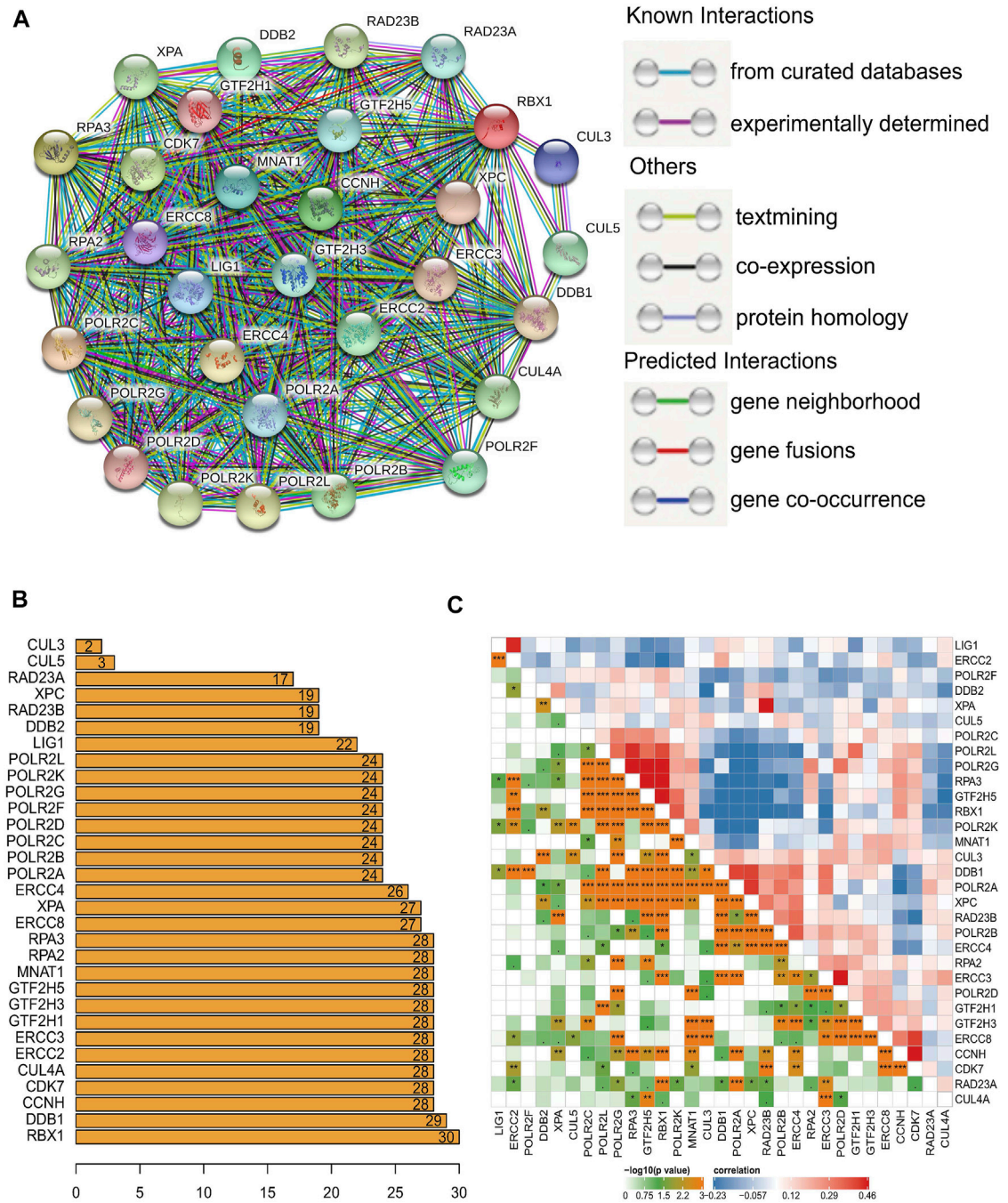

FIGURE 2 | The interaction and correlation among 31 NER-related genes. **(A)** The PPI network of the 31 NER-related genes was constructed by STRING database and each line represents a reported physical protein–protein interaction between nodes. **(B)** The number of bar graphs represents the total connections of each node to other nodes frequency. **(C)** The Pearson correlation analysis shows the collinearity among 31 NER-related genes. Abbreviation: NER: Nucleotide excision repair; PPI: Protein-protein interaction; STRING: the Search Tool for the Retrieval of Interacting Genes.

genes with HR <1, while RPA2, CCNH, XPC, ERCC2, and ERCC4 were considered as risky genes with HR >1 (**Figure 4A**).

According to our previous results, the collinearity between these genes may affect the accuracy of traditional Cox regression analysis (**Figure 2C**). Therefore, the LASSO Cox regression method to the seven potentially prognosis-related genes was performed to identify the most powerfully prognostic NER-related genes finally. The LASSO results demonstrated that all seven genes were chosen to construct the prognostic risk signature (**Figures 4B,C**), and the coefficients of selected genes were shown in **Figure 4D**. Then, the risk scores were calculated according to the coefficients, and the median risk score was the

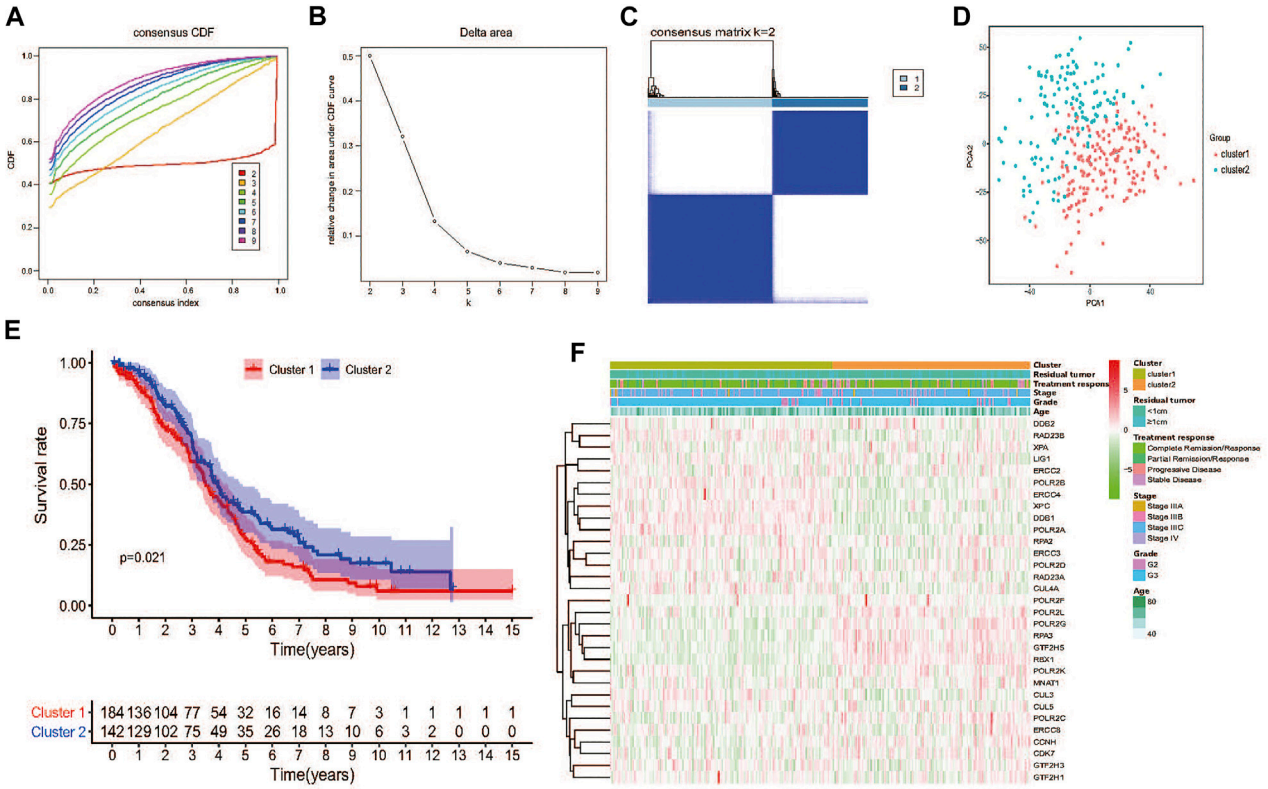

FIGURE 3 | Consensus clustering and overall survival of TCGA HGSOC patients in the different two clusters. **(A)** Consensus clustering CDF for k = 2 to 9. **(B)** Relative change in area under CDF curve for k = 2 to 9. **(C)** The TCGA HGSOC patients was divided into two distinct clusters when k = 2. Consensus clusteringmatrix for k = 2. **(D)** PCA of the total mRNA expression profile in the TCGA dataset. HGSOC patients in the cluster1 subgroup are marked with red, HGSOC patients in cluster2 are marked with green. **(E)** Kaplan–Meier OS curves for different clusters. **(F)** No significant difference was found for the clinicopathologic features between cluster1 and cluster2.

cut-off value. A total of 326 HGSOC patients were divided evenly into the high- and low-risk groups. The distributions of the 7-gene signature-based risk scores, OS status, and mRNA expression profiles were displayed in **Figures 4E–G**. The K-M survival plot showed that the OS of the advanced patients with HGSOC was significantly worse in the high-risk group than that in the low-risk group (p = 5.707e-05) (**Figure 4H**). The 5-year OS was 14.1% in high-risk group and 27.0% in low-risk group. The predicting power of the risk signature showed well-prediction efficiency with the AUC value equal to 0.693 (**Figure 4I**). Next, the associations between the risk groups and clinicopathological characteristics were also investigated in the present study (**Figure 4J** and **Supplementary Table S2**). The results showed that except treatment response (p = 0.049), there were no significant differences between the high- and low-risk groups in the age, grade, stage, and residual tumor (all $p > 0.05$).

Moreover, the Human Protein Atlas (HPA) database was used to validate the cellular sub-localization and expression patterns of the seven selected genes in serous ovarian cancer tissues and normal ovarian tissues at the protein levels (**Figures 5A–G**). HPA analysis showed that at protein levels, the expressions of DDB2, POLR2D, CCNH, and RPA2 in HGSOC tissues and normal controls were similar to the mRNA level changes and were mainly located in the nucleus (**Figures 1C**, **5**). However, XPC and ERCC2 did not show significant distinctions at the protein levels between serous ovarian tissues and normal ovarian tissues (**Figures 5C,E**). The heterogeneity between the HPA data and TCGA RNA-seq data may be ascribed to the differences in post-transcriptional regulation. Altogether, the results further verified that the regulation of NER-related genes was highly disordered in serous ovarian cancer.

Validation of the Risk Signature to Predict OS of Advanced Patients With HGSOC

To confirm that the NER-related genes based on classifier had similar prognostic value in different cohorts, we assessed the samples in GSE13876 (n = 415) and the merged GEO dataset (n = 346), respectively. According to the median risk score as the cut-off value in the TCGA HGSOC cohort, 192 (46.3%) patients were classified as low-risk, and 223 (53.7%) as high-risk in GSE13876;

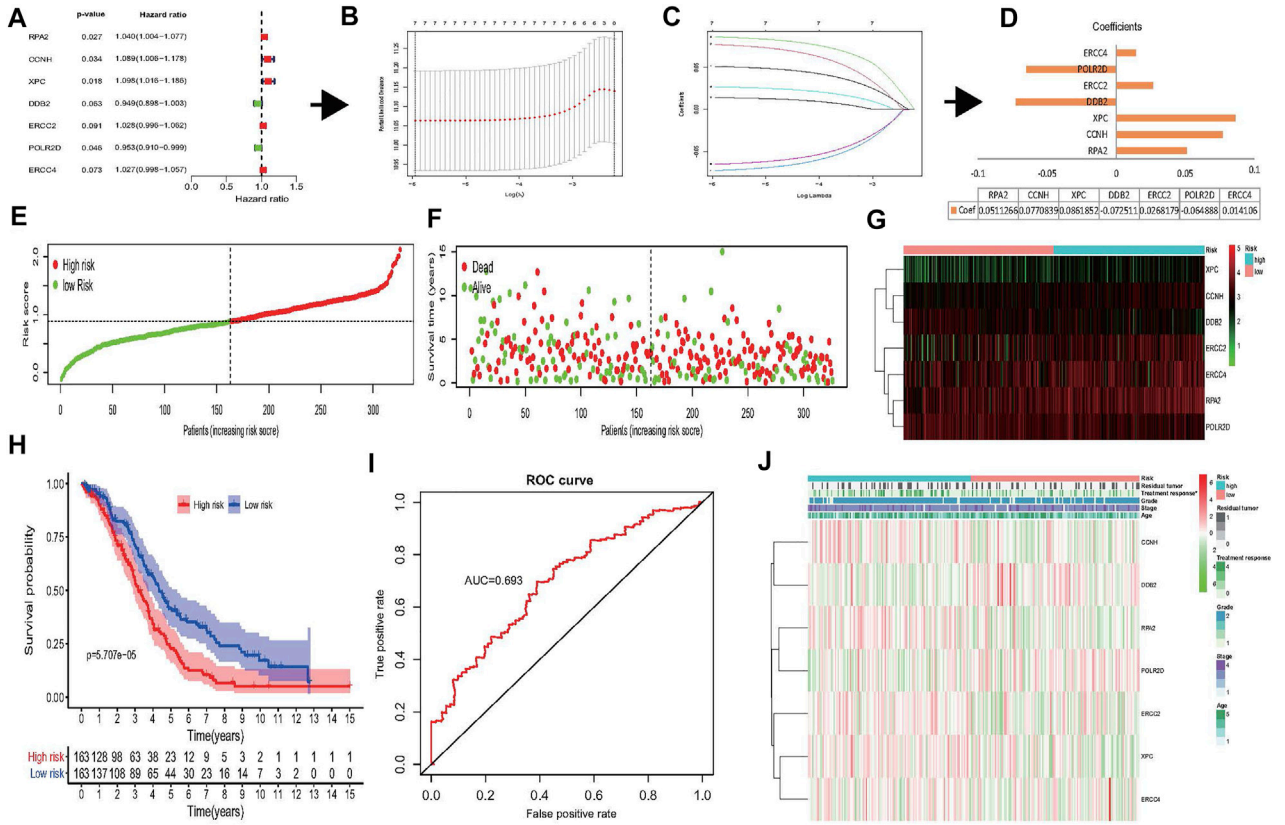

FIGURE 4 | Construction of risk signature based on seven NER-related genes. **(A–D)** The process of constructing the signature based on seven NER-related genes. **(A)** Univariate Cox regression analysis of the NER-related genes was identified seven genes that potentially correlated with OS ($p < 0.1$). **(B)** LASSO algorithms was used to identify and evaluate the 7-gene signature in the TCGA HGSOC cohort and seven genes were finally selected and used to develop a risk signature to predict patients prognosis. **(C)** LASSO coefficient profiles of the seven genes based on the TCGA HGSOC cohort. **(D)** The coefficients estimated by multivariate Cox regression via LASSO are presented. **(E–G)** Visualization of the association of the risk scores with survival status and gene expression profiles in HGSOC. **(H)** The OS was remarkably worse in the high-risk group than that of low-risk group. **(I)** ROC curve was used to evaluate the prediction efficiency of the risk signature. **(J)** Significant differences were found for the treatment response between high- and low-risk groups. Abbreviation: NER: Nucleotide excision repair; OS: Overall survival; LASSO: Least absolute shrinkage and selection operator; TCGA: The Cancer Genome Atlas; HGSOC: Highly-grade serous ovarian cancer; ROC: Receiver operating characteristic.

255 (73.7%) patients were classified as low-risk, and 91 (26.3%) as high-risk in the merged GEO datasets. The corresponding 5-year OS was 24.1% for the high-risk group and 35.0% for the low-risk group in GSE13876 (HR: 1.394, 95% CI: 1.107–1.754; p = 3.901e-03; **Figure 5H**). Similarly, in the merged GEO validation set, the 5-year OS was 35.3% for the high-risk group and 67.8% for the low-risk group (HR: 2.300, 95%CI: 1.663–3.181; p = 2.035e-07; **Figure 5I**). The distributions of the risk scores, OS status, and mRNA expression profiles of the two validation sets were respectively conducted (**Figures 5J,K**). As shown in **Figures 6A–F**, the worse OS rate was observed in the high-risk group compared to that in the low-risk group for patients with FIGO stage IIIC (p = 6.78e-04), or patients with CR/PR (p = 1.214e-03), or patients with optimal cytoreductive surgery (p = 2.263e-03), or those with non-optimal cytoreductive surgery (p = 0.025). However, no significant difference was observed for OS between high- and low-risk groups for patients with FIGO stage IV (p = 0.116), or patients with SD/PD (p = 0.245) due to sample size limitation.

Nomogram Combined NER-Related Risk Signature and Clinical-Related Features to Predict Patients' OS

To investigate whether the prediction was better by the risk signature constructed from mRNA expression than from any other clinical-related features, various variables, such as age, stage, grade, treatment response, and residual tumor were included as the potential prognostic factors. In the TCGA HGSOC cohort, the results of both univariate and multivariate analysis revealed that treatment response and risk signature were significantly associated with OS (**Figures 7A,B**). Due to the potential impact of age on OS (p = 0.077), a nomogram that combined the age, treatment response, and risk signature was developed to predict 3- or 5-year survival of advanced patients with HGSOC (**Figure 7C**). The calibration plots for the nomogram presented the acceptability and conformance in the original cohort between the nomogram forecast and actual observation for the 3- or 5-year OS (**Figure 7D**). Conclusively, we constructed a nomogram combining various clinical-related

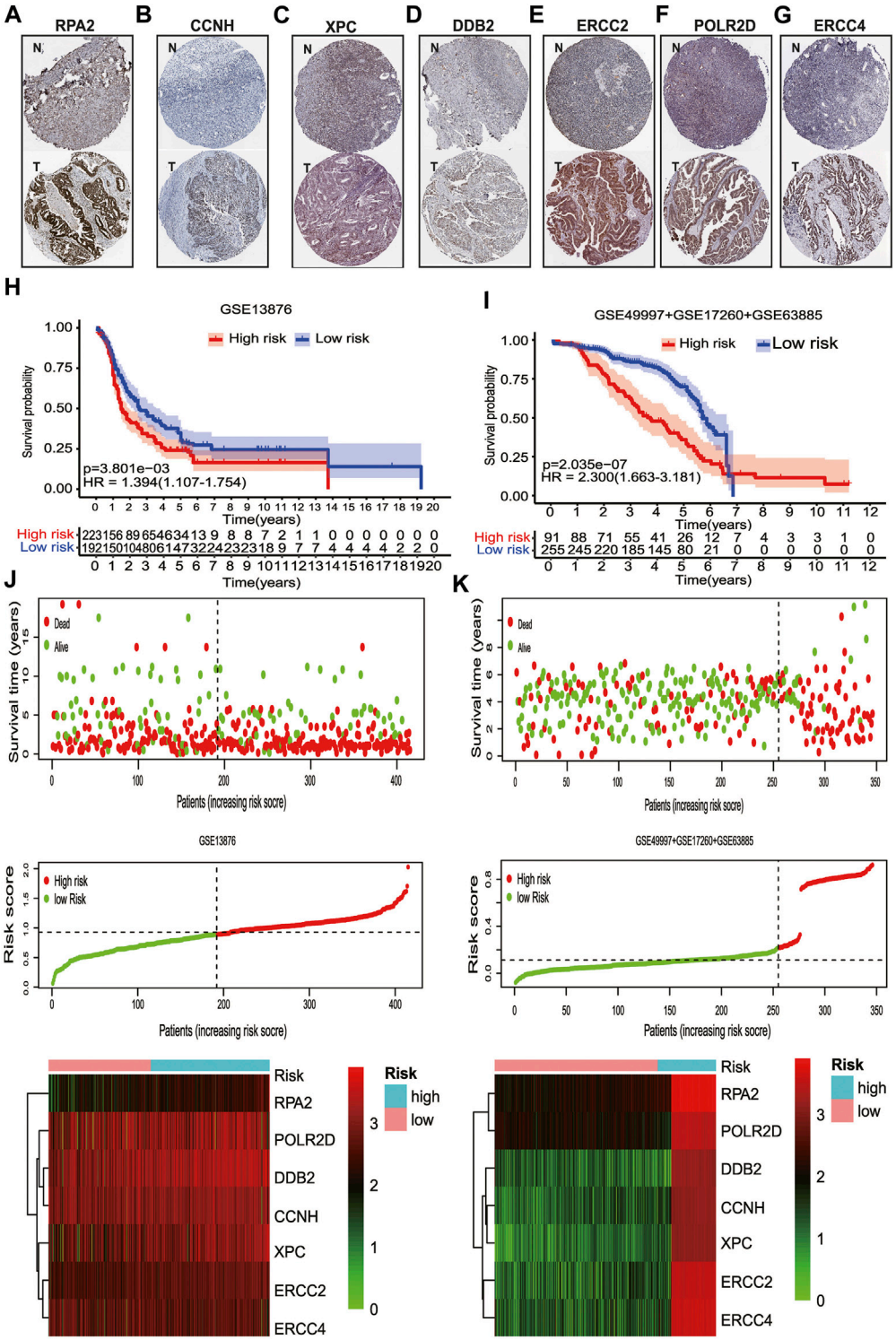

FIGURE 5 | The protein expression levels of seven NER-related genes by IHC staining and the validation of the prognostic signature. **(A)** Representative IHC staining of RPA2 in serous ovarian cancer and normal ovarian tissues. **(B)** Representative IHC staining of CCNH in serous ovarian cancer and normal ovarian tissues. **(C)** Representative IHC staining of XPC in serous ovarian cancer and normal ovarian tissues. **(D)** Representative IHC staining of DDB2 in serous ovarian cancer and normal ovarian tissues. **(E)** Representative IHC staining of ERCC2 in serous ovarian cancer and normal ovarian tissues. **(F)** Representative IHC staining of POLR2D in serous ovarian cancer and normal ovarian tissues. **(G)** Representative IHC staining of ERCC4 in serous ovarian cancer and normal ovarian tissues. **(H)** For advanced patients with HGSOC, the high-risk group had a significantly worse OS than that in the low-risk group in GSE13876. **(I)** For advanced patients with HGSOC, the high-risk

(*Continued*)

FIGURE 5 | group had a significantly worse OS than that in the low-risk group for the combined GEO datasets. **(J)** Visualization of the association of the risk scores with survival status and gene expression profiles in GSE13876. **(K)** Visualization of the association of the risk scores with survival status and gene expression profiles in the combined GEO datasets. Abbreviation: T: Serous ovarian cancer; N: Normal ovarian tissue; NER: Nucleotide excision repair; HPA: The human protein atlas; IHC: Immunohistochemistry. GEO: Gene Expression Omnibus; HGSOC: Highly-grade serous ovarian cancer; OS: Overall survival.

factors. NER-related risk signature could provide the most useful and accurate information for the prognosis of these advanced patients with HGSOC.

Gene Set Enrichment Analysis of High-Risk and Low-Risk Groups

To better understand the significance of risk signature based NER-related genes, GSEA analysis was performed to scrutinize the signaling pathways between the high-risk group and low-risk group from the TCGA cohort. Intriguingly, genes involved in the following biological processes/signaling pathways showed active expression in the high-risk group: mTOR signaling pathway (NSE = 2.15, normalized $p < 0.0001$, FDR q = 0.009), inositol phosphate metabolism (NSE = 2.14, normalized $p < 0.0001$, FDR q = 0.007), phosphatidylinositol signaling system (NSE = 2.13, normalized $p < 0.0001$, FDR q = 0.006), MAPK signaling pathway (NSE = 1.97, normalized $p < 0.0001$, FDR q = 0.014), and VEGF signaling pathway (NSE = 1.94, normalized $p < 0.0001$, FDR q = 0.018). In contrast, two downregulated biological processes/signaling pathways were observed in the high-risk group: DNA replication (NSE = -1.82, normalized $p = 0.024$, FDR q = 0.144) and spliceosome (NSE = -1.80, normalized $p = 0.037$, FDR q = 0.112) (**Supplementary Figure S2**). These results above showed the risk signature identified based on the seven NER-related genes were closely associated with the malignancy of HGSOC.

DISCUSSION

Serous ovarian cancer was divided into low-grade serous ovarian cancer and HGSOC, and they had significantly different features in genomics, clinical manifestations, origin, and prognosis (Schmeler and Gershenson, 2008). The previous study initially explored the value of a single NER-related gene in HGSOC (Gayarre et al., 2015), but we considered that it failed to provide a robust predictive efficacy due to the expression of a single gene restricted by multiple factors. Therefore, we comprehensively analyzed the specific value of 31 NER-related genes in HGSOC. Our results demonstrated that the expression levels of NER-related genes were closely associated with the prognostic outcomes of advanced patients with HGSOC. Firstly, we compared the expression levels of 31 NER-related genes using the merged TCGA-GTEx dataset and found that most genes were abnormally expressed in HGSOC. Then, two clusters (cluster1 and cluster2) of HGSOC with completely different prognosis were identified through consensus clustering. Also, based on the data of TCGA HGSOC, a prognostic risk signature of seven NER-related genes was retrieved through the LASSO algorithm. Advanced patients with HGSOC were assigned into two risk subgroups with significant differences for OS according to the risk signature. More importantly, in the external validation datasets, the risk signature was further successfully confirmed as a highly robust prognostic indicator. In addition, a stratified analysis based on clinical factors demonstrated the robustness of the risk signature in prognostic evaluation, and it also implied that the difference in survival based on the risk signature was more likely to be associated with the tumor inherent biological characteristics. Taking advantage of the risk signature, we constructed a nomogram including 7-gene signature and clinical-related factors (age and treatment response) to predict OS of advanced HGSOC patients. Finally, the GSEA analysis explored the differences in oncology-related pathways and key biological processes between the two risk subgroups classified based on the risk signature. Overall, our nomogram could be used as a prognostic classification tool and help clinicians make individualized therapeutic strategies for advanced patients with HGSOC.

NER is a complex biochemical process that requires multiple proteins assemble in an ordered at base damaged sites and then function as a multi-protein complex (De Boer and Hoeijmakers, 2000; Hoeijmakers, 2001). In our research, we also noticed the complex association between various genes expression levels and protein interactions in the NER pathway of HGSOC patients (**Figure 2**). Surprisingly, two clusters with distinctive OS were identified based on 31 NER-related genes consensus clustering analysis (**Figure 3**), which indicated the practical possibility of further distinguishing the HGSOC patients at the molecular level.

We also identified a risk signature of seven genes consisting of ERCC2, ERCC4, POLR2D, DDB2, XPC, CCNH, and RPA2 that predicts OS in the TCGA and GEO datasets. ERCC2 single nucleotide polymorphisms (SNPs) were found to be associated with an increased risk of ovarian cancer (Bernard-Gallon et al., 2008; Bicher et al., 1997). The same is applied for ERCC4 (Osorio et al., 2013). POLR2D is also known as DNA-directed RNA polymerase II, which was associated with shorter disease-free survival in prostate cancer (Yamada et al., 2018). In contrast, our results showed that POLR2D was a protective factor for the OS in HGSOC patients (**Figure 4A**), and this difference may attribute to the fact that the same gene may play different roles in the occurrence and development of different cancers. The other protective factor discovered in our study was DDB2 (**Figure 4A**), and it was reported that DDB2 could repress ovarian cancer stem cell properties (Cui et al., 2018). In addition, the highly expressed DDB2 could enhance the sensitivity of ovarian cancer cells to cisplatin by increasing cell apoptosis (Barakat et al., 2010). Moreover, downregulation

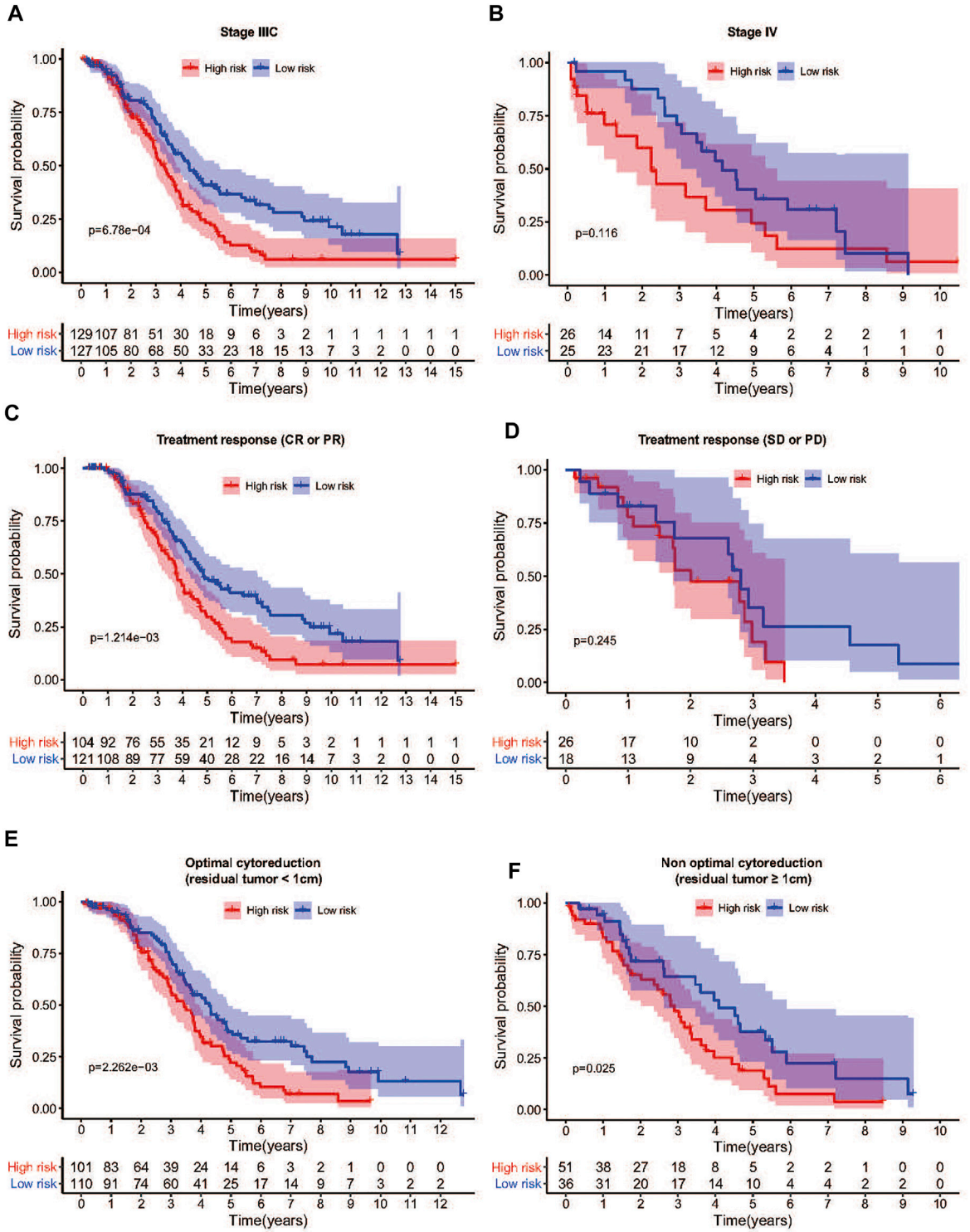

FIGURE 6 | Differences in survival between high- and low-risk groups stratified by clinicopathological factors in TCGA cohort. **(A)** The OS was remarkably worse in the high-risk group than that of low-risk group in FIGO stage IIIC patients. **(B)** The low-risk group showed a better prognosis trend than the high-risk group in FIGO stage IV patients. **(C)** Among patients who achieved CR or PR after treatment, the OS of the high-risk group was also shorter than that of the low-risk group. **(D)** Among patients who achieved SD or PD after treatment, there was no significant difference in OS between the high-risk group and the low-risk group. **(E)** The OS was remarkably worse in the high-risk group than that of low-risk group among patients with optimal cytoreductive surgery. **(F)** The OS was remarkably worse in the high-risk group than that of low-risk group among patients with non-optimal cytoreductive surgery. Abbreviation: OS: Overall survival; CR: Complete remission; PR: Partial remission; SD: Stable disease; PD: Progressive disease.

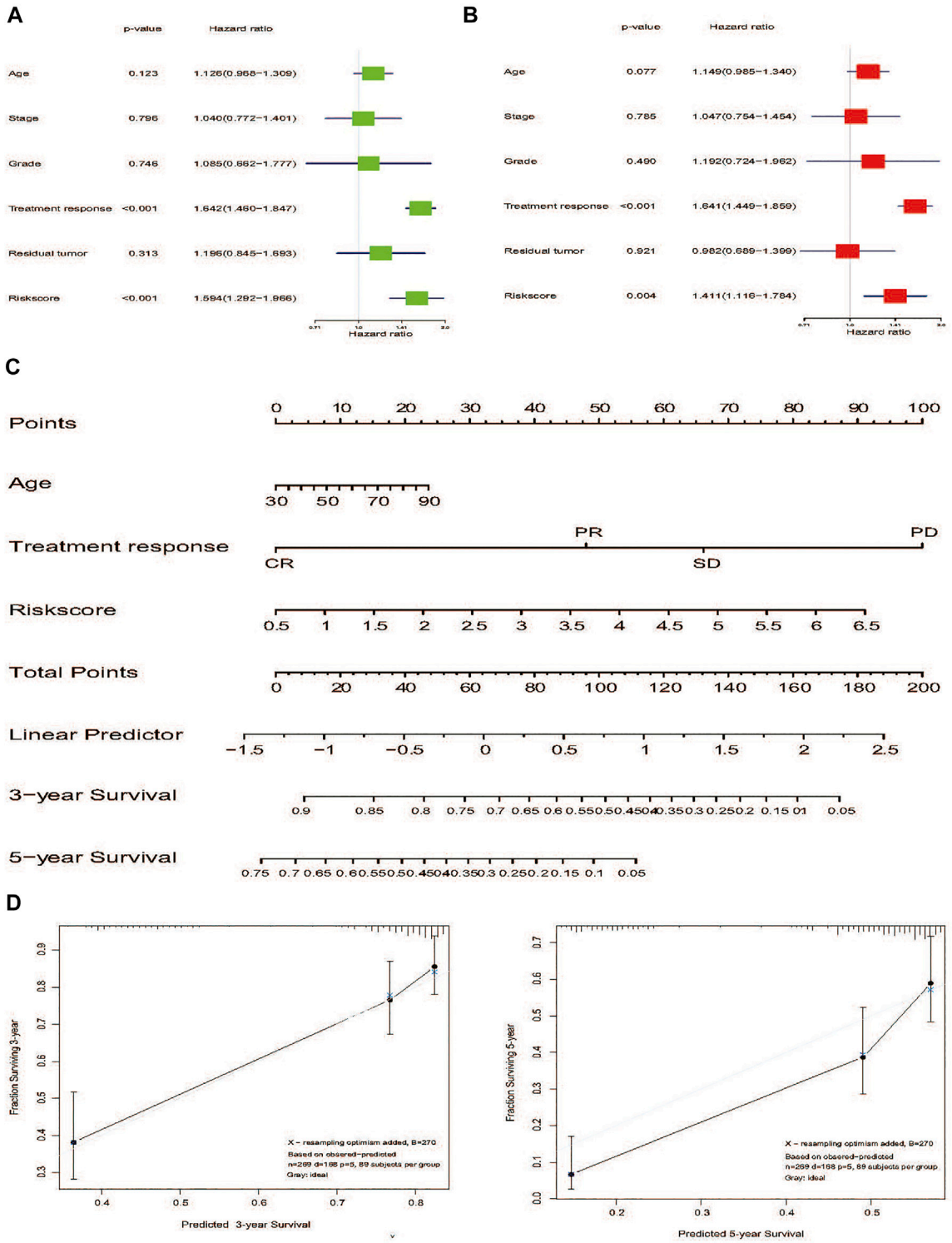

FIGURE 7 | Nomogram development of 7-gene signature to predict the risk of survial in advanced patients with HGSOC. **(A)** Univariate Cox regression analysis of the risk score and clinicopathological factors to identify the indicators that were significantly associated with OS. **(B)** Multivariate Cox regression analysis of the risk score and clinicopathological parameters to reveal the independent prognostic factors. **(C)** A nomogram was constructed to predict three- or 5-year survival. **(D)** Calibration curves of the nomogram to predict 3-or 5-year OS in TCGA internal validation. The actual OS is plotted on the y-axis; nomogram predicted probability is plotted on the x-axis. Abbreviation: NER: Nucleotide excision repair; HGSOC: Highly-grade serous ovarian cancer; OS: Overall survival.

of XPC could also enhance the sensitivity of ovarian cancer to cisplatin (Zhang et al., 2015), and XPC SNPs were correlated with survival outcomes of ovarian cancer treated with platinum-based chemotherapy (Kang et al., 2013). Our results also demonstrated that the low-risk group was associated with better treatment response, which meant that these patients had upregulated DDB2 and downregulated XPC expression and were more sensitive to chemotherapy (**Figure 4J**). In addition, CCNH was related to the promotion of cancer cell migration (Wang et al., 2013), and RPA2 expression was an independent predictor of adverse outcome in ovarian cancer (Levidou et al., 2012). Taken together, these findings revealed the universal importance of NER-related genes, and indicated that these inhibitor or promotor genes in cancer development were interdependent.

The mechanisms were further investigated to reveal the causes of the different prognosis of the two HGSOC risk subgroups stratified by the 7-gene signature. GSEA demonstrated that some pivotal signaling pathways and biological processes were significantly enriched in the high-risk group with poor survival, including inositol phosphate metabolism, MAPK signaling pathway, mTOR signaling pathway, phosphatidylinositol signaling system, and VEGF signaling pathway. It was reported that inositol phosphate recycling regulated glycolytic and lipid metabolism that drove cancer aggressiveness (Benjamin et al., 2014). It was known that MAPK signaling pathway, mTOR signaling pathway, and VEGF signaling pathway were crucial in tumorigenesis, progression, and drug therapy (Pópulo et al., 2012; Santarpia et al., 2012; Apte et al., 2019). In the low-risk group, GSEA enriched two significant biological processes related to cancer, including DNA replication and splicesome (Herrick and Bensimon, 2009; Ladd et al., 2013). In the current study, the cellular process of NER-related DNA repair was consistent with the biological function of these identified signal pathways. DNA damage and repair processes affect most of all aspects of biological processes, including RNA metabolism, protein translation, and modification. Therefore, the different clinical phenotypes (high-risk group and low-risk group) were further supported by the difference in signal pathways and biological processes.

Despite encouraging findings in the present study, several limitations still exist. First of all, our results are mainly based on bioinformatics analysis. Although there are multiple datasets for mutual verification, experimental and clinical data will be needed to verify our results in the future. Secondly, although the risk signature and nomogram showed good prediction accuracy in the internal verification, their performance is still warranted validation in different HGSOC populations. Finally, our study did not contain clinicopathological information such as the scope of surgical resection and specific chemotherapy drugs, since TCGA did not cover such information, and the treatment standard for advanced patients with HGSOC has been controversial.

CONCLUSION

Taken together, we profiled the sharply altered NER-related genes between HGSOC and normal samples, which may play a vital role in the progression of HGSOC. More importantly, a robust risk signature that was significantly associated with the clinical outcome of HGSOC was constructed and validated in two different GEO validation sets. In addition, we also developed a 7-gene nomogram containing the risk signature and clinical-related risk factors, which may aid the individualized prediction of the prognosis of advanced patients with HGSOC. Finally, further research on these genes may provide new insights into the potential relationship between the NER repair pathway and HGSOC prognosis.

DATA AVAILABILITY STATEMENT

The datasets presented in this study can be found in online repositories. The names of the repository/repositories and accession number(s) can be found in the article/**Supplementary Material**.

AUTHOR CONTRIBUTIONS

DD, QL, PZ, and BC contributed to the conception and design of the study. DD, QL, and PZ contributed to data collection. DD, JH, HZ, and HW analysed and interpreted the data. DD, QL, and PZ drafted the report which was critically revised for important intellectual content by HZ, HW, and BC. All authors approved the final version of the report.

FUNDING

This work was supported by funds from the Guangdong Basic and Applied Basic Research Foundation (2022A1515011599, BC), the High-level Hospital Construction Project (DFJH201921, BC), the Excellent Young Talent Program of Guangdong Provincial People's Hospital (KY012021190, BC), the National Natural Science Foundation of China (81902828, BC). The funding agencies had no role in the design of the study; the collection, analysis, and interpretation of data; or the writing of the manuscript.

SUPPLEMENTARY MATERIAL

The Supplementary Material for this article can be found online at: https://www.frontiersin.org/articles/10.3389/fcell.2022.874588/full#supplementary-material

Supplementary Figure S1 | The flow chart of the study design and analysis.

Supplementary Figure S2 | Differential signaling pathways and cellular processes between risk subgroups defined by 7 NER-related gene signatures.

REFERENCES

Anurag, M., Punturi, N., Hoog, J., Bainbridge, M. N., Ellis, M. J., and Haricharan, S. (2018). Comprehensive Profiling of DNA Repair Defects in Breast Cancer Identifies a Novel Class of Endocrine Therapy Resistance Drivers. *Clin. Cancer Res.* 24 (19), 4887–4899. doi:10.1158/1078-0432.ccr-17-3702

Apte, R. S., Chen, D. S., and Ferrara, N. (2019). VEGF in Signaling and Disease: Beyond Discovery and Development. *Cell* 176 (6), 1248–1264. doi:10.1016/j.cell.2019.01.021

Barakat, B. M., Wang, Q. E., Han, C., Milum, K., Yin, D. T., Zhao, Q., et al. (2010). Overexpression of DDB2 Enhances the Sensitivity of Human Ovarian Cancer Cells to Cisplatin by Augmenting Cellular Apoptosis. *Int. J. Cancer* 127 (4), 977–988. doi:10.1002/ijc.25112

Benjamin, D. I., Louie, S. M., Mulvihill, M. M., Kohnz, R. A., Li, D. S., Chan, L. G., et al. (2014). Inositol Phosphate Recycling Regulates Glycolytic and Lipid Metabolism that Drives Cancer Aggressiveness. *ACS Chem. Biol.* 9 (6), 1340–1350. doi:10.1021/cb5001907

Bernard-Gallon, D., Bosviel, R., Delort, L., Fontana, L., Chamoux, A., Rabiau, N., et al. (2008). DNA Repair Gene ERCC2 Polymorphisms and Associations with Breast and Ovarian Cancer Risk. *Mol. Cancer* 7 (1), 36. doi:10.1186/1476-4598-7-36

Bicher, A., Ault, K., Kimmelman, A., Gershenson, D., Reed, E., and Liang, B. (1997). Loss of Heterozygosity in Human Ovarian Cancer on Chromosome 19q. *Gynecol. Oncol.* 66 (1), 36–40. doi:10.1006/gyno.1997.4709

Bowtell, D. D., Böhm, S., Ahmed, A. A., Aspuria, P.-J., Bast, R. C., Jr, Beral, V., et al. (2015). Rethinking Ovarian Cancer II: Reducing Mortality from High-Grade Serous Ovarian Cancer. *Nat. Rev. Cancer* 15 (11), 668–679. doi:10.1038/nrc4019

Cancer Genome Atlas Network (2012). Comprehensive Molecular Portraits of Human Breast Tumours. *Nature* 490 (7418), 61–70. doi:10.1038/nature11412

Cardoso, F., van't Veer, L. J., Bogaerts, J., Slaets, L., Viale, G., Delaloge, S., et al. (2016). 70-Gene Signature as an Aid to Treatment Decisions in Early-Stage Breast Cancer. *N. Engl. J. Med.* 375 (8), 717–729. doi:10.1056/nejmoa1602253

Cheng, L., Eicher, S. A., Guo, Z., Hong, W. K., Spitz, M. R., and Wei, Q. (1998). Reduced DNA Repair Capacity in Head and Neck Cancer Patients. *Cancer Epidemiol. Biomarkers Prev.* 7 (6), 465–468.

Cui, T., Srivastava, A. K., Han, C., Wu, D., Wani, N., Liu, L., et al. (2018). DDB2 Represses Ovarian Cancer Cell Dedifferentiation by Suppressing ALDH1A1. *Cell Death Dis.* 9 (5), 561–615. doi:10.1038/s41419-018-0585-y

De Boer, J., and Hoeijmakers, J. H. J. (2000). Nucleotide Excision Repair and Human Syndromes. *Carcinogenesis* 21 (3), 453–460. doi:10.1093/carcin/21.3.453

Eyre, T. A., Ducluzeau, F., Sneddon, T. P., Povey, S., Bruford, E. A., and Lush, M. J. (2006). The HUGO Gene Nomenclature Database, 2006 Updates. *Nucleic Acids Res.* 34 (Suppl. l_1), D319–D321. doi:10.1093/nar/gkj147

Fleming, N. D., Agadjanian, H., Nassanian, H., Miller, C. W., Orsulic, S., Karlan, B. Y., et al. (2012). Xeroderma Pigmentosum Complementation Group C Single-Nucleotide Polymorphisms in the Nucleotide Excision Repair Pathway Correlate with Prolonged Progression-Free Survival in Advanced Ovarian Cancer. *Cancer* 118 (3), 689–697. doi:10.1002/cncr.26329

Friedberg, E. C. (2001). How Nucleotide Excision Repair Protects Against Cancer. *Nat. Rev. Cancer* 1 (1), 22–33. doi:10.1038/35094000

Gayarre, J., Kamieniak, M. M., Cazorla-Jiménez, A., Muñoz-Repeto, I., Borrego, S., García-Donas, J., et al. (2015). The NER-Related Gene GTF2H5 Predicts Survival in High-Grade Serous Ovarian Cancer Patients. *J. Gynecol. Oncol.* 27 (1), e7. doi:10.3802/jgo.2016.27.e7

Goeman, J. J. (2010). L1 Penalized Estimation in the Cox Proportional Hazards Model. *BIOM J.* 52 (1), 70–84. doi:10.1002/bimj.200900028

Goldman, M., Craft, B., Brooks, A., Zhu, J., and Haussler, D. (2018). The UCSC Xena Platform for Cancer Genomics Data Visualization and Interpretation. *BioRxiv*, 326470. doi:10.1101/326470

González-Martín, A., Toledo, G., and Chiva, L. (2010). Epithelial Ovarian Carcinoma: Current Evidences and Future Perspectives in the First-Line Setting. *Clin. Transl. Oncol.* 12 (6), 418–430. doi:10.1007/s12094-010-0529-1

Herrick, J., and Bensimon, A. (2009). Introduction to Molecular Combing: Genomics, DNA Replication, and Cancer. *Methods Mol. Biol.* 521, 71–101. doi:10.1007/978-1-60327-815-7_5

Hoeijmakers, J. H. J. (2001). Genome Maintenance Mechanisms for Preventing Cancer. *Nature* 411 (6835), 366–374. doi:10.1038/35077232

Jessmon, P., Boulanger, T., Zhou, W., and Patwardhan, P. (2017). Epidemiology and Treatment Patterns of Epithelial Ovarian Cancer. *Expert Rev. Anticancer Ther.* 17 (5), 427–437. doi:10.1080/14737140.2017.1299575

Johnson, W. E., Li, C., and Rabinovic, A. (2007). Adjusting Batch Effects in Microarray Expression Data Using Empirical Bayes Methods. *Biostatistics* 8 (1), 118–127. doi:10.1093/biostatistics/kxj037

Kang, S., Sun, H.-Y., Zhou, R.-M., Wang, N., Hu, P., and Li, Y. (2013). DNA Repair Gene Associated with Clinical Outcome of Epithelial Ovarian Cancer Treated with Platinum-Based Chemotherapy. *Asian Pac. J. Cancer Prev.* 14 (2), 941–946. doi:10.7314/apjcp.2013.14.2.941

Kanungo, T., Mount, D. M., Netanyahu, N. S., Piatko, C. D., Silverman, R., and Wu, A. Y. (2002). An Efficient K-Means Clustering Algorithm: Analysis and Implementation. *IEEE Trans. Pattern Anal. Mach. Intell.* 24 (7), 881–892. doi:10.1109/tpami.2002.1017616

Kurman, R. J., Carcangiu, M. L., and Herrington, C. S. (2014). "*World Health Organisation Classification of Tumours of the Female Reproductive Organs*," in International Agency for Research on Cancer. 4th Revised ed. (Edinburgh).

Ladd, J. J., Chao, T., Johnson, M. M., Qiu, J., Chin, A., Israel, R., et al. (2013). Autoantibody Signatures Involving Glycolysis and Splicesome Proteins Precede a Diagnosis of Breast Cancer Among Postmenopausal Women. *Cancer Res.* 73 (5), 1502–1513. doi:10.1158/0008-5472.can-12-2560

Leek, J. T., Johnson, W. E., Parker, H. S., Jaffe, A. E., and Storey, J. D. (2012). The Sva Package for Removing Batch Effects and Other Unwanted Variation in High-Throughput Experiments. *Bioinformatics* 28 (6), 882–883. doi:10.1093/bioinformatics/bts034

Levidou, G., Ventouri, K., Nonni, A., Gakiopoulou, H., Bamias, A., Sotiropoulou, M., et al. (2012). Replication Protein A in Nonearly Ovarian Adenocarcinomas: Correlation with MCM-2, MCM-5, Ki-67 Index and Prognostic Significance. *Int. J. Gynecol. Pathol.* 31 (4), 319–327. doi:10.1097/pgp.0b013e31823ef92e

Lin, F., Lin, K., Xie, X., and Zhou, C. (2010). Increased ERCC1 Protein Expression Is Associated with Suboptimal Debulking in Advanced Epithelial Ovarian Cancer. *Anticancer Res.* 30 (6), 2447–2452.

Llueca, A., Escrig, J., Serra-Rubert, A., Gomez-Quiles, L., Rivadulla, I., Játiva-Porcar, R., et al. (2018). Prognostic Value of Peritoneal Cancer Index in Primary Advanced Ovarian Cancer. *Eur. J. Surg. Oncol.* 44 (1), 163–169. doi:10.1016/j.ejso.2017.11.003

Majidinia, M., Sadeghpour, A., Mehrzadi, S., Reiter, R. J., Khatami, N., and Yousefi, B. (2017). Melatonin: A Pleiotropic Molecule that Modulates DNA Damage Response and Repair Pathways. *J. Pineal Res.* 63 (1), e12416. doi:10.1111/jpi.12416

Marteijn, J. A., Lans, H., Vermeulen, W., and Hoeijmakers, J. H. J. (2014). Understanding Nucleotide Excision Repair and its Roles in Cancer and Ageing. *Nat. Rev. Mol. Cell Biol.* 15 (7), 465–481. doi:10.1038/nrm3822

Mirza-Aghazadeh-Attari, M., Ostadian, C., Saei, A. A., Mihanfar, A., Darband, S. G., Sadighparvar, S., et al. (2019). DNA Damage Response and Repair in Ovarian Cancer: Potential Targets for Therapeutic Strategies. *DNA Repair* 80, 59–84. doi:10.1016/j.dnarep.2019.06.005

Narod, S. (2016). Can Advanced-Stage Ovarian Cancer Be Cured? *Nat. Rev. Clin. Oncol.* 13 (4), 255–261. doi:10.1038/nrclinonc.2015.224

Osorio, A., Bogliolo, M., Fernández, V., Barroso, A., De la Hoya, M., Caldés, T., et al. (2013). Evaluation of Rare Variants in the New Fanconi Anemia Gene ERCC4 (FANCQ) as Familial Breast/Ovarian Cancer Susceptibility Alleles. *Hum. Mutat.* 34 (12), 1615–1618. doi:10.1002/humu.22438

Pópulo, H., Lopes, J. M., and Soares, P. (2012). The mTOR Signalling Pathway in Human Cancer. *Int. J. Mol. Sci.* 13 (2), 1886–1918. doi:10.3390/ijms13021886

Ritchie, M. E., Phipson, B., Wu, D., Hu, Y., Law, C. W., Shi, W., et al. (2015). Limma Powers Differential Expression Analyses for RNA-Sequencing and Microarray Studies. *Nucleic Acids Res.* 43 (7), e47. doi:10.1093/nar/gkv007

Santarpia, L., Lippman, S. M., and El-Naggar, A. K. (2012). Targeting the MAPK-RAS-RAF Signaling Pathway in Cancer Therapy. *Expert Opin. Ther. Targets* 16 (1), 103–119. doi:10.1517/14728222.2011.645805

Schmeler, K. M., and Gershenson, D. M. (2008). Low-Grade Serous Ovarian Cancer: A Unique Disease. *Curr. Oncol. Rep.* 10 (6), 519–523. doi:10.1007/s11912-008-0078-8

Shuck, S. C., Short, E. A., and Turchi, J. J. (2008). Eukaryotic Nucleotide Excision Repair: From Understanding Mechanisms to Influencing Biology. *Cell Res.* 18 (1), 64–72. doi:10.1038/cr.2008.2

Sparano, J. A., Gray, R. J., Makower, D. F., Pritchard, K. I., Albain, K. S., Hayes, D. F., et al. (2018). Adjuvant Chemotherapy Guided by a 21-Gene Expression Assay in Breast Cancer. *N. Engl. J. Med.* 379 (2), 111–121. doi:10.1056/nejmoa1804710

Szklarczyk, D., Franceschini, A., Wyder, S., Forslund, K., Heller, D., Huerta-Cepas, J., et al. (2015). STRING V10: Protein-Protein Interaction Networks, Integrated Over the Tree of Life. *Nucleic Acids Res.* 43 (D1), D447–D452. doi:10.1093/nar/gku1003

Tajik, P., van de Vrie, R., Zafarmand, M. H., Coens, C., Buist, M. R., Vergote, I., et al. (2018). The FIGO Stage IVA versus IVB of Ovarian Cancer: Prognostic Value and Predictive Value for Neoadjuvant Chemotherapy. *Int. J. Gynecol. Cancer* 28 (3), 453–458. doi:10.1097/igc.0000000000001186

Wang, Y., Liu, F., Mao, F., Hang, Q., Huang, X., He, S., et al. (2013). Interaction with Cyclin H/Cyclin-Dependent Kinase 7 (CCNH/CDK7) Stabilizes C-Terminal Binding Protein 2 (CtBP2) and Promotes Cancer Cell Migration. *J. Biol. Chem.* 288 (13), 9028–9034. doi:10.1074/jbc.m112.432005

Wei, Q., Cheng, L., Hong, W. K., and Spitz, M. R. (1996). Reduced DNA Repair Capacity in Lung Cancer Patients. *Cancer Res.* 56 (18), 4103–4107.

Williams, A. B., and Schumacher, B. (2016). p53 in the DNA-Damage-Repair Process. *Cold Spring Harb. Perspect. Med.* 6 (5), a026070. doi:10.1101/cshperspect.a026070

Yamada, Y., Nishikawa, R., Kato, M., Okato, A., Arai, T., Kojima, S., et al. (2018). Regulation of HMGB3 by Antitumor miR-205-5p Inhibits Cancer Cell Aggressiveness and is Involved in Prostate Cancer Pathogenesis. *J. Hum. Genet.* 63 (2), 195–205. doi:10.1038/s10038-017-0371-1

Zhang, Y., Yu, J.-J., Tian, Y., Li, Z.-Z., Zhang, C.-Y., Zhang, S.-F., et al. (2015). eIF3a Improve Cisplatin Sensitivity in Ovarian Cancer by Regulating XPC and p27Kip1 Translation. *Oncotarget* 6 (28), 25441–25451. doi:10.18632/oncotarget.4555

Zhu, J., Chen, Z., and Yong, L. (2018). Systematic Profiling of Alternative Splicing Signature Reveals Prognostic Predictor for Ovarian Cancer. *Gynecol. Oncol.* 148 (2), 368–374. doi:10.1016/j.ygyno.2017.11.028

Conflict of Interest: The authors declare that the research was conducted in the absence of any commercial or financial relationships that could be construed as a potential conflict of interest.

Publisher's Note: All claims expressed in this article are solely those of the authors and do not necessarily represent those of their affiliated organizations, or those of the publisher, the editors and the reviewers. Any product that may be evaluated in this article, or claim that may be made by its manufacturer, is not guaranteed or endorsed by the publisher.

Copyright © 2022 Dai, Li, Zhou, Huang, Zhuang, Wu and Chen. This is an open-access article distributed under the terms of the Creative Commons Attribution License (CC BY). The use, distribution or reproduction in other forums is permitted, provided the original author(s) and the copyright owner(s) are credited and that the original publication in this journal is cited, in accordance with accepted academic practice. No use, distribution or reproduction is permitted which does not comply with these terms.

frontiers | Frontiers in Oncology

ORIGINAL RESEARCH
published: 27 June 2022
doi: 10.3389/fonc.2022.844082

Tumor Microenvironment Characterization in Breast Cancer and an Immune Cell Infiltration Score Development, Validation, and Application

*Lang Li**

Department of Hematology, Jinhua Hospital of Traditional Chinese Medicine, Jinhua, China

OPEN ACCESS

Edited by:
Shaoquan Zheng,
Sun Yat-sen University Cancer Center (SYSUCC), China

Reviewed by:
Ann Hanna,
Vanderbilt University Medical Center, United States
Suzanne Marie Ponik,
University of Wisconsin-Madison, United States
Haidong Gao,
Shandong University, China

***Correspondence:**
Lang Li
20181111511167@zcmu.edu.cn

Specialty section:
This article was submitted to Molecular and Cellular Oncology, a section of the journal Frontiers in Oncology

Received: *12 January 2022*
Accepted: *19 May 2022*
Published: *27 June 2022*

Citation:
Li L (2022) Tumor Microenvironment Characterization in Breast Cancer and an Immune Cell Infiltration Score Development, Validation, and Application. Front. Oncol. 12:844082. doi: 10.3389/fonc.2022.844082

The tumor microenvironment (TME) refers to the cellular environment in which tumors exist. An increasing number of reports have emphasized its role in tumor progression, prognosis, relapse, metastasis, and therapeutic response with breast cancer (BRCA). Few studies have revealed a systematic landscape of immune cell infiltration (ICI) in BRCA. In this study, we comprehensively analyzed the immune cells infiltrating TME in BRCA. Three ICI patterns were identified through an unsupervised clustering method and an ICI score was developed by a principal component analysis (PCA). A Kaplan-Meier survival with log-rank test revealed a significant overall survival (OS) difference of BRCA patients with these three ICI patterns. We also found that a high ICI score was characterized by an elevated tumor mutation burden (TMB), effector T-cell infiltration, INF-γ-related cytotoxicity, and cytolytic activity score. An independent cohort validated that this ICI score could be a prognostic indicator for BRCA. Two immunotherapeutic cohorts and two chemotherapeutic cohorts confirmed that patients with higher ICI scores showed significant chemotherapeutic and immunotherapeutic advantages. In summary, these results suggest that the ICI patterns could act as a prognostic indicator and that the ICI score could precisely predict the clinical outcome for BRCA patients.

Keywords: breast cancer, tumor microenvironment, immune cellular infiltration, tumor mutation burden, immunotherapy, chemotherapy

Abbreviations: BRCA, Breast Cancer; TME, Tumor microenvironment; ICI, Immune cells infiltration; ssGSEA, single sample gene set enrichment analysis; OS, overall survival; PFS, free progress survival; PCA, principal component analysis; CDF, cumulative distribution function; TMB, tumor mutation burden; DEGs, differential expressed genes; MRDEGs, the most representative differential expressed genes; TCGA, The Cancer Genome Atlas; GEO, Gene Expression Omnibus; AUC, Area under curve; ROC, receiver operating characteristic; PD1, Programmed cell death-1; PD-L1, Programmed cell death-ligand-1; MAGE-A3, Melanoma-associated antigen 3; METABRIC, Molecular Taxonomy of Breast Cancer International Consortium; RR, Responder rate; HR, Hazard ratio; CI, Confidence interval; GO, Gene Ontology; CC, Cellular components; BP, Biological processes; MF, Molecular functions; TILs, Tumor-infiltrating lymphocytes.

INTRODUCTION

Breast cancer (BRCA) is one of the most common malignancies worldwide with more than 2.2 million newly diagnosed and 680 thousand deaths per year (1). Current therapies have greatly improved the survival rate of early-stage patients. However, the 5-year survival rate remains less than 28% in terminal BRCA patients. To date, the prediction of BRCA prognosis and therapeutic responses mainly depends on the tumour-node-metastasis (TNM) stage. However, BRCA patients in the same TNM stage show different prognoses and therapeutic responses because of tumor heterogeneity. Thus, it is of great importance to incorporate other valuable indicators to predict prognosis and therapeutic responses.

The tumor microenvironment (TME) refers to a cellular environment in which tumors exist, including the surrounding immune cells, stromal cells, and signaling molecules (2–5). Extensive studies have reported a critical role of tumor infiltrating immune components in cancer progression, prognosis, relapse, metastasis, and therapeutic response. For instance, Erdag et al. (6) found that TME differences in immune homing receptors and ligands that influence prognosis in melanoma patients by affecting immune cell recruitment. Kulasinghe et al. (7) reported that tumor-infiltrating lymphocyte-associated biomarkers in the triple-negative breast cancer TME affect chemotherapeutic response and survival. Hu et al. (8) revealed that distinct immune phenotypes have different prognoses, gene mutations, immune infiltrations, and drug sensitivities in TNBC. Risom et al. (9) revealed that myoepithelial disruption in the TME protects BRCA against recurrence *via* multiplexed ion beam imaging by time of flight. Medrek et at. (10) reported that the M2 phenotype tumor-associated macrophages is related to immunosuppressive TME that is permissive to tumor growth and spread. However, one or two single immune components of BRCA are not sufficient to characterize a complex TME. Hence, it is of great significance to investigate the expansive landscape of immune cells infiltrating TME in BRCA.

To date, quantitating the immune cell abundances of tumor tissues in the lab has been a challenge to researchers. A newly issued computational algorithm, single sample gene set enrichment analysis (ssGSEA), can estimate the relative immune cell abundances of bulk RNA-seq samples through a given immune cell gene set (11). This algorithm enables researchers to depict the immune cell infiltration (ICI) landscape. Through this algorithm, previous studies had comprehensively sketched the ICI landscape to predict prognoses and therapeutic benefits in other types of cancers, such as lung adenocarcinoma, gastric cancer, and head and neck squamous cell carcinoma (5, 12, 13). However, a comprehensive ICI landscape in the TME with BRCA has not yet been fully elucidated.

In this study, we compared immune cell abundances and stromal cells contents in TME among tumor with normal tissues. Additionally, we systematically characterized ICI patterns in the TME with tumor tissues using the TCGA-BRCA cohort. Through principal component analysis (PCA), we defined an ICI score to quantify the ICI status for each sample. An independent cohort, METABRIC, confirmed that the ICI score was a robust prognostic tool for BRCA patients. We found that a high ICI score was related to upregulated tumor mutation burden (TMB), effector T-cell infiltration, INF-γ-related cytotoxicity, and cytolytic activity. Two chemotherapeutic cohorts confirmed that patients with high ICI scores had a higher responder rate to chemotherapy (GSE5462 cohort: responder rate [RR], 35.71% in the high ICI group versus 20.83% in the low ICI group; chi-square test, $P < 0.001$; GSE20181 cohort: [RR], 71% in the high ICI group versus 50% in the low ICI group; chi-square test, $P < 0.05$). Two immunotherapeutic cohorts confirmed that patients with the high ICI score had a higher responder rate to immunotherapy (GSE35640 cohort: [RR], 42.9% in the high ICI group versus 21.4% in the low ICI group; chi-square test, $P < 0.0001$; GSE91061 cohort: [RR], 30.7% in the high ICI group versus 13.2% in the low ICI group; chi-square test, $P < 0.0001$). In conclusion, in this study, we developed an ICI score to characterize the extensive immune cell infiltrating TME for BRCA, which could precisely predict the prognoses and response to chemotherapy and immunotherapy.

METHODS

Data Accession

Discovery cohort: The RNA-seq data, clinical information, and somatic structural variation data of BRCA patients, were downloaded from The Cancer Genome Atlas (TCGA) (https://portal.gdc.cancer.gov) database. We enrolled 967 tumor samples and 112 adjacent normal samples with complete information including survival time, vital status, treatment strategies, RNA-seq data, and somatic variation data.

Validation cohort: We downloaded the RNA-seq data and clinical information of the Molecular Taxonomy of Breast Cancer International Consortium (METABRIC) cohort (14) from the cBio Cancer Genomics Portal website (www.cbioportal.org). A total of 1424 samples were enrolled to validation cohort with complete information including RNA-seq data, overall survival (OS), progression-free survival (PFS), and survival status.

Application cohorts: In total, we gathered 2 chemotherapeutic cohorts (GSE5462 and GSE20181) and 2 immunotherapeutic cohorts (GSE35640 and GSE91061). We downloaded the RNA-seq data and clinical data with these datasets from the Gene Expression Omnibus (GEO, https://www.ncbi.nlm.nih.gov/geo) database by the GEOquery R package (15). We removed these samples with absent or vague therapeutic responses.

Evaluation of Immune Cell Abundances in the Discovery Cohort

To evaluate specific immune cell subsets, we systematically retrieved the issued studies and adopted an immune cell gene set that was proposed by Beibei Ru et al (16). This gene set was consisted of 742 gene signatures representing 28 immune cell subtypes including activated CD8 T cells, central memory CD8 T

cells, effector memory CD8 T cells, activated CD4 T cells, central memory CD4 T cells, effector memory CD4 T cells, T follicular helper cells, gamma delta T cells, type 1 T helper cells, type 17 T helper cells, type 2 T helper cells, regulatory T cells, activated B cells, immature B cells, memory B cells, natural killer cells, CD56 bright natural killer cells, CD56 dim natural killer cells, myeloid derived suppressor cells, natural killer T cells, activated dendritic cells, plasmacytoid dendritic cells, immature dendritic cells, macrophages, eosinophils, mast cells, monocytes, and neutrophils (**Supplementary File 1**). The ssGSEA algorithm of the GSVA R package (17) was used to evaluate the relative immune cell abundances in each patients based on bulk RNA-seq data. The estimate R package (2) was used to asses immune and stromal cell contents for each sample. To comprehensively analyze the ICI status, we merged the immune cell abundance matrix and stromal cell content matrix for subsequent analyses. (**Supplementary File 2**).

Comparison of the TME Between Normal and Tumor Tissues in the Discovery Cohort

To investigate TME differences between normal and tumor tissues, we compared the immune cell abundances and stromal cell contents of 112 normal tissues and their matched tumor tissues. We visualized the landscape of immune cell abundances and stromal cell contents through a heatmap by the pheatmap R package (18). The Wilcoxon test was used to compare the significant differences, and a two-tailed P <0.05 was considered to indicate a significant difference. Paired Student's t test was used to compare the significant differences in PD1 and PD-L1 expression. The box plot drawn by the ggplot 2 R package (19) was used to show these data.

Clustering for ICI Phenotypes With the Discovery Cohort

Based on the immune cell abundances and stromal cell contents of 967 tumor tissues, we performed unsupervised clustering by the consensusClusterPlus R package (20) to identify the ICI phenotypes. Unsupervised clustering depended on Euclidean distance and Ward's linkage, and was repeated 1000 times to ensure the classification stability. The optimal number of clusters was determined by consensus matrix and relative change of area under a cumulative distribution function (CDF) curve. Finally, we obtained three distinct ICI phenotypes termed ICI Cluster ABC that divided the discovery cohort into three groups.

Differentially Expressed Gene Analysis and Genotype Identification in the Discovery Cohort

To reveal the internal molecular characterizations with these three distinct ICI phenotypes, we performed pairwise comparisons to identify differentially expressed genes (DEGs) by the edgeR R package (21). Genes with a false discovery rate (FDR) adjusted P *value* < 0.05 and absolute value of $|\log_2 FC|$ (fold change) >1.3 were considered to statistically significant. To identify ICI genotypes, each Fragments Per Kilobase Million (FPKM) normalized DEGs expression value was standardized through $\log_2$ (expression value +1) formula across 967 BRCA samples. Additionally, the unsupervised clustering method proposed above was applied to identify ICI genotypes. A relative change in the area under the CDF curve and a consensus matrix were used to determine the optimal number of clusters. We obtained three ICI genotypes termed Gene Cluster ABC that classified the discovery cohort into three distinct groups.

Gene Ontology Functional Annotations and ICI Score Development

The steps with ICI score development were processed as follows. First, we utilized a random forest algorithm to screen the most representative differentially expressed genes (MRDEGs) for these three distinct ICI genotypes by the randomForest R package (22). The random forest algorithm performed classifications and predictions to DEGs through multidecision trees. This algorithm ranked these DEGs by scoring their representativeness according to an accuracy or a Gini value. Here, the top one-third DEGs ranked by accuracy value were recognized as MRDEGs. Furthermore, GO functional annotations were used to investigate the functions of these MRDEGs by the clusterProfiler R package (23), and a P < 0.05 was considered to statistically significant. GO functional annotations included biological processes (BP), molecular functions (MF), and cellular components (CC). Next, we performed PCA using R software (version 4.0.2) to compute signature scores for each BRCA patient based on MRDEGs expression levels. Component 1 was extracted as signature scores according to a pervious study (13). Finally, we applied a method similar to gene expression grade index (24) to define the ICI scores for each patient as follows:

$$\text{ICI score} = \sum \text{PC1}i - \sum \text{PC1}_j$$

Where i is the signature score whose Cox efficiency is positive, and j is the signature score whose Cox efficiency is negative. Additionally, we calculated the ICI score of validation cohort based on the above steps using MRDEGs expression value. To investigate the prognostic value of the ICI score, we grouped the BRCA patients in the discovery cohort and validation cohort by an optimal cutoff area under the curve (AUC) of time-dependent receiver operating characteristic (ROC) analysis (25).

Somatic Genetic Variation Data Analysis With the Discovery Cohort

The maftools R package (26) was used to count the total number of non-synonymous mutations to determine the TMB. To further investigate the prognostic value of TMB, we classified 967 tumor samples in the discovery cohort into high and low TMB subgroups based on an optimal cutoff AUC of ROC analysis. The maftools R package was used to visualize the landscape of the top 30 highest frequent alteration genes among the high and low ICI score subgroups. The chi-square test was used to detect the mutated genetic differences between high and low ICI score subgroups by the maftools R package, and a P <0.05 was regarded as statistically significance.

Genomic and Clinical Dataset Analysis With Application Cohorts

To investigate the predictive role of the ICI score for therapeutic benefits, we filtered these MRDEGs expression value of the application cohorts. Next, we developed the ICI scores with application cohorts through the methodology proposed above. Finally, we grouped the patients who received corresponding therapies into high and low ICI score subgroups according to a median cutoff of the ICI score for further analysis.

Statistical Analysis

All statistical analyses were conducted by R software (Version 4.0.2), and a $P < 0.05$ was considered to statistically significant. Univariate Cox regression analysis was performed to evaluate relationships between immune cells abundances and OS by survival R package (27). The comparisons of OS with specific groups were performed by the log-rank test of the survminer R package (28). The Kruskal–Wallis test and Wilcoxon test were utilized to examine the non-normalized distribution data. Student's t test was used to compare normalized distribution data. The chi-square test was used to compare the categorical data.

RESULTS

The TME Difference Between Tumor and Normal Tissues

We compared the relative immune cell abundances and stromal cell contents of 112 normal tissues and their matched tumor tissues. Firstly, we visualized the relative immune cell abundances and stromal cell contents with tumor and normal tissues by a heatmap. Next, the Wilcoxon test was utilized to compare these immune cell abundances and stromal cell contents. We found that tumor tissues were remarkably characterized by high densities of central memory CD8 T cells, activated CD4 T cells, immature B cells, CD56 dim natural killer cells, myeloid-derived suppressor cells, and activated dendritic cells, but normal tissues were significantly characterized by high densities of effector memory CD8 T cells, T follicular helper cells, type 1 T helper cells, activated B cells, natural killer cells, CD56 bright natural killer cells, plasmacytoid dendritic cells, immature dendritic cells, mast cells, stromal score, and immune score (**Figures 1A, B**). In addition, we observed a significantly upregulated PD1 (paired Student's t test; $P < 0.0001$, **Figure 1C**) and an undifferentiated PDL1 (paired Student's t test; $P > 0.05$, **Figure 1D**) expression level in tumor tissues.

Landscape of ICI Phenotypes With BRCA

We performed an unsupervised clustering to systematically characterize the ICI patterns for BRCA using the relative immune cell abundances and stromal cell contents of tumor tissues. According to a consensus matrix and a relative change in area under the CDF curve, three divisions for TCGA-BRCA cohort was the best segregation that divided 967 BRCA patients into three heterogeneous phenotypes termed ICI Cluster A (464 patients), ICI Cluster B (425 patients), and ICI Cluster C (78 patients) (**Figure S1B–F**). **Figure 2A** sketched a landscape of BRCA clinical information and immune cellular distributions with these three ICI phenotypes. Prognostic analysis revealed a significant survival difference in these three ICI phenotypes (log-rank test; $P = 0.00019$, **Figure 2B**). Almost all immune cell types were remarkably different except for activated CD8 T cells, effector memory CD4 T cells, T follicular cells, type 17 T helper cells, type 2 T helper cells, regulatory T cells, immature B cells, natural killer T cells, activated dendritic cells, immature dendritic cells, macrophages, and eosinophils (Kruskal–Wallis test; $P > 0.05$, **Figure 2C**) in these ICI phenotypes. Among these distinct ICI phenotypes, ICI Cluster A patients, characterized by the lowest densities of almost all immune cell types except for activated CD4 T cells, CD56 dim natural killer cells, and monocytes, were associated with a favorable prognosis (median survival of 6472 days). The ICI Cluster B patients with a median survival time of 3842 days, were significantly marked by high densities of all immune cell types. Conversely, ICI Cluster C patients were witnessed the shortest OS (median survival of 2464 days) and were characterized by the lowest densities of activated CD4 T cells, CD56 dim natural killer cells, and monocytes. (**Figures 2B, C**).

We also performed univariate Cox regression analysis to reveal the prognostic roles of 28 immune cell abundances and stromal cell contents. As depicted in a forest plot, the abundances of activated CD4 T cells (hazard ratio [HR], 0.68; 95% confidence interval [CI], 0.58-0.8; $P < 0.0001$), CD56 dim natural killer cells (HR, 0.4; 95% CI, 0.26-0.62; $P < 0.0001$), activated CD8 T cells (HR, 0.75; 95% CI, 0.63-0.9; $P < 0.01$), immature B cells (HR, 0.76; 95% CI, 0.63-0.93; $P < 0.01$), myeloid derived suppressor cells (HR, 0.82; 95% CI, 0.7-0.96; $P < 0.05$), activated B cells (HR, 0.84; 95% CI, 0.72-0.97; $P<0.05$), activated dendritic cells (HR, 0.63; 95% CI, 0.42-0.95; $P < 0.01$), monocytes (HR, 0.49; 95% CI, 0.25-0.94; $P < 0.05$), and memory B cells (HR, 0.64; 95% CI, 0.42-0.98; $P < 0.05$) could serve as protective factors for BRCA patients. Conversely, the abundances of plasmacytoid dendritic cells (HR, 1.93; 95% CI, 1.19-3.13; $P < 0.01$) and mast cells (HR, 1.32; 95% CI, 1.07-1.62; $P < 0.05$) were the hazard factors for BRCA patients (**Figure 2D**). These findings were consistent with the worse OS with ICI Cluster C patients and the favorable OS with ICI Cluster A patients. Moreover, we compared the mRNA expression levels of two vital immune checkpoints (PD1 and PD-L1) in each ICI phenotypes by Wilcoxon test. We found that ICI Cluster A was remarkably characterized by the lowest PD1 (Wilcoxon test, $P < 0.0001$) and PD-L1 expression (Wilcoxon test, $P < 0.0001$). Conversely, ICI Cluster B was observed to have the highest PD1 (Wilcoxon test, $P < 0.0001$) and PD-L1 (Wilcoxon test, $P < 0.0001$) expression. Compared with ICI Cluster A, ICI Cluster C was observed to have the same PD1 (Wilcoxon test, $P > 0.05$) but significantly higher expression of PD-L1 (Wilcoxon test, $P < 0.0001$) (**Figure 2E, F**).

Differentially Expressed Gene Analysis and Genotype Clustering

To investigate the intrinsic biological differences that led to distinct ICI phenotypes, we performed pairwise comparisons to identify the DEGs among these three ICI phenotypes. In total, 1183 DEGs

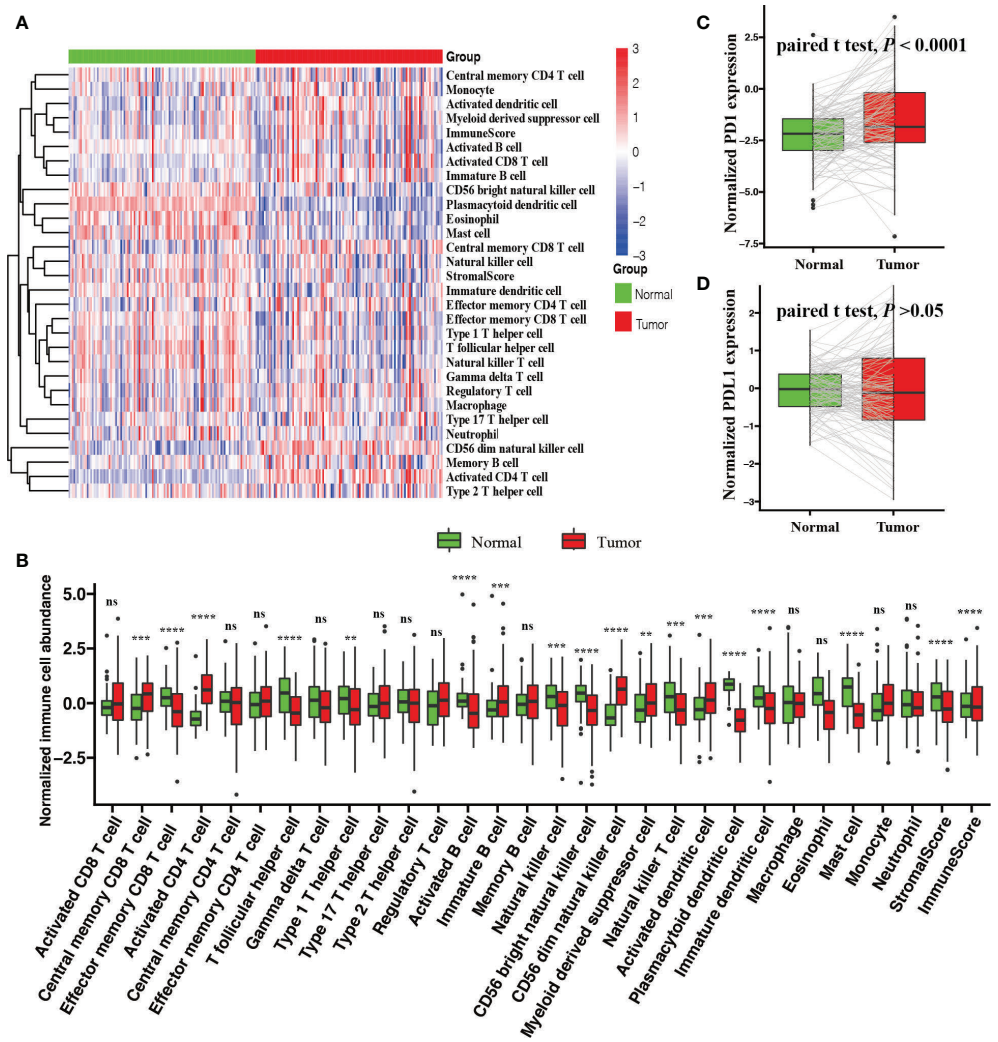

FIGURE 1 | Comparison of the TME between tumor and normal tissues with BRCA. **(A)** Heatmap of the ICI landscape between tumor and normal tissues. **(B)** Box plot of normalized immune cell abundances (Kruskal–Wallis test, ns, no significance $P > 0.05$; $^{**}P < 0.01$; $^{***}P < 0.001$; $^{****}P < 0.0001$). Comparison of the expression levels of two vital immune checkpoint molecules; **(C)** PD-1 and **(D)** PD-L1 (paired Student's t test).

were observed among these three ICI phenotypes (**Supplementary File 3**). As depicted in **Figure S2**, compared with ICI Cluster A, 265 upregulated and 94 downregulated mRNAs were identified in ICI Cluster B (**Figure S2A**). Compared with ICI Cluster B, 456 downregulated and 138 upregulated mRNAs were identified in ICI Cluster C (**Figure S2B**). Compared with ICI Cluster A, 49 upregulated and 605 downregulated mRNAs were observed in ICI Cluster C (**Figure S2C**). **Figure S2D** shows the gene relationships among these three ICI phenotypes. **Figure S2E** depicts a whole landscape of these 1183 DEGs expression levels. Next, an unsupervised clustering using these 1183 DEGs was performed to identify genotypes for BRCA patients. Three classifications dividing the discovery cohort into Gene Cluster A (437 patients), Gene Cluster B (342 patients), and Gene Cluster C (189 patients) were the best optimal according to the consensus matrix and relative change in the area under the CDF curve (**Figures S3A–E**).

Figure 3A delineates a landscape of these 1183 DEGs and the clinical feature distributions with these 967 BRCA patients among distinct ICI genotypes. A significant difference in OS was observed among these three ICI genotypes (log-rank test; $P = 0.0061$, **Figure 3B**). Gene Cluster A patients characterized by the highest densities of neutrophils (Kruskal–Wallis test; $P < 0.0001$), suffered from the shortest median OS time with 3682 days. Gene Cluster B patients had a median OS time (4326 days), characterized by high densities of activated CD8 T cells, central memory CD8 T cells, effector memory CD8 T cells, central memory CD4 T cells, T follicular helper cells, type 1 T helper cells, immature B cells, memory B cells, natural killer cells, CD56 bright natural killer T cells, CD 56 dim natural killer T cells,

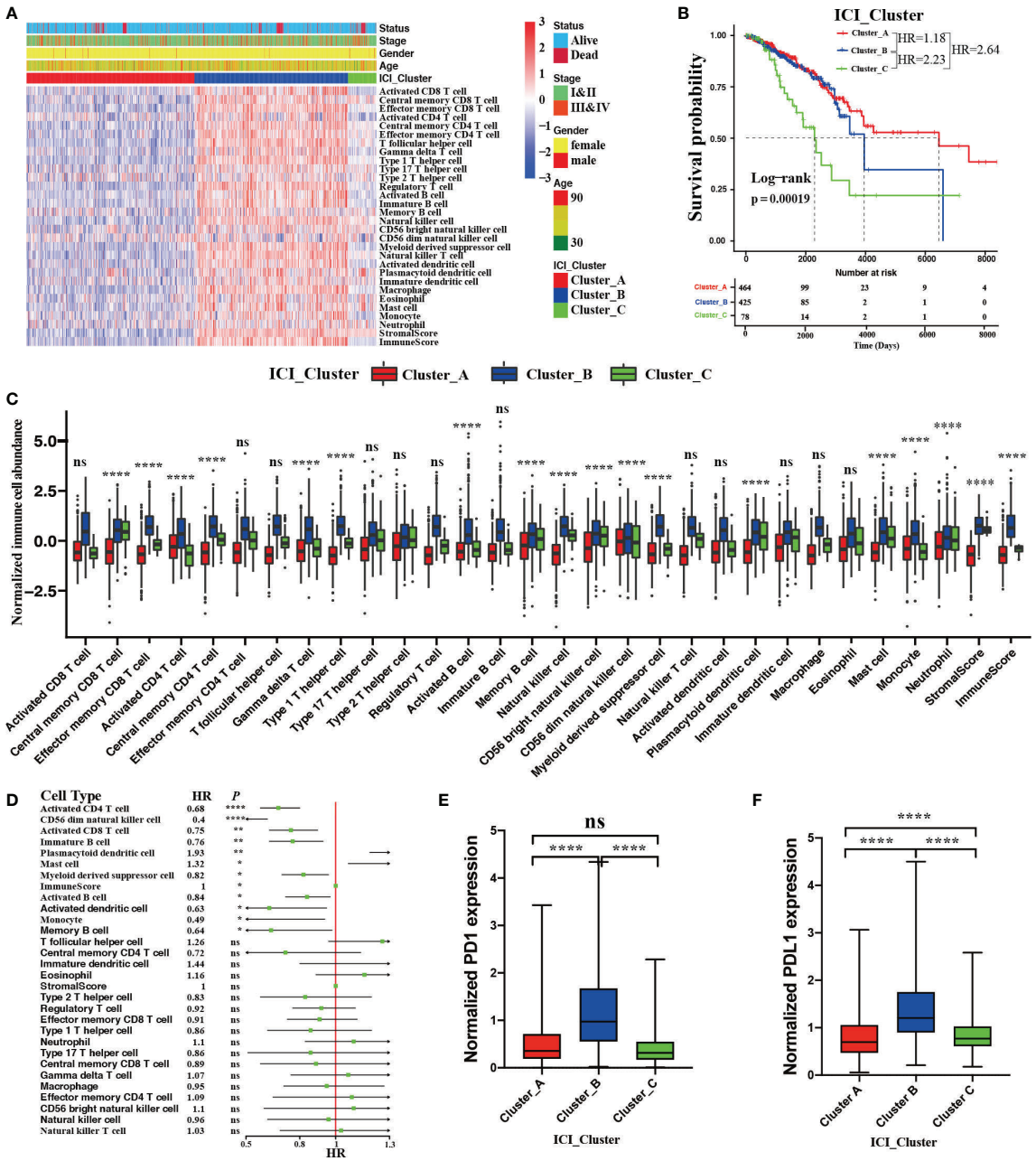

FIGURE 2 | The ICI landscape in the TME of BRCA. **(A)** Unsupervised clustering for ICI phenotypes in the TME. The rows represent immune cells, and the columns represent BRCA samples. **(B)** The Kaplan–Meier curves showing OS (overall survival) outcomes in BRCA patients among these distinct ICI clusters. Log-rank test showing P = 0.00019. **(C)** The normalized immune cell abundances and stromal cell contents with distinct ICI clusters. (Kruskal–Wallis test, ns, no significance $P > 0.05$; ****$P < 0.0001$). **(D)** The prognostic role of immune cell abundance and stromal cell content. (Univariate Cox regression model, ns $P > 0.05$; *$P < 0.05$; **$P < 0.01$; ****$P < 0.0001$). Comparison of the expression level of two vital immune checkpoint molecules with these distinct ICI clusters; PD1 **(E)** and PD-L1 **(F)**. (Wilcoxon test, ns $P > 0.05$; ****$P < 0.0001$).

plasmacytoid dendritic cells, immature dendritic cells, macrophages, eosinophils, mast cells, stromal score, and immune score. Conversely, Gene Cluster C patients enjoyed the longest median OS time (7345 days), characterized by high densities of activated CD4 T cells, effector memory CD4 T cells, gamma delta T cells, type 2 T helper cells, regulatory T cells, activated B cells, myeloid derived suppressor cells, natural killer T cells, activated dendritic cells, and monocytes (Kruskal–Wallis test; $P < 0.0001$, **Figures 3B, C**). Significantly upregulated PD1 and PD-L1 expression was observed in Gene Cluster B and Cluster C compared with Gene Cluster A (Kruskal–Wallis test; $P < 0.0001$, **Figures 3D, E**).

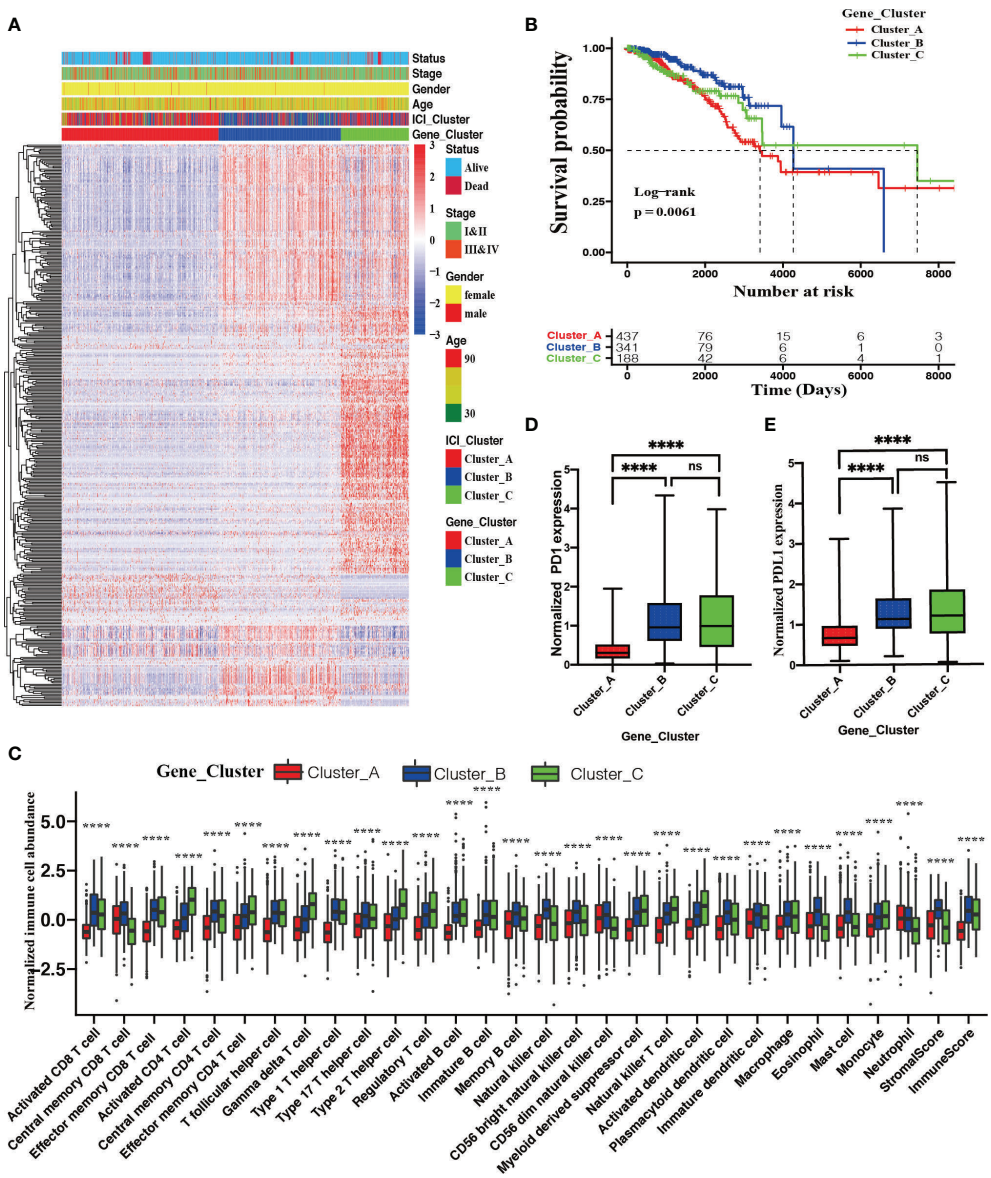

FIGURE 3 | Identification of ICI genotypes. **(A)** Unsupervised clustering for DEGs among these distinct ICI clusters, which grouped BRCA patients into three Gene Clusters **(A–C)**. **(B)** The Kaplan–Meier curves showing OS outcomes in BRCA patients among these distinct gene clusters. Log-rank test showing P = 0.0061. **(C)** Normalized immune cell abundances and stromal cell contents in distinct gene clusters. (Kruskal–Wallis test, ****$P < 0.0001$). Comparison of the expression levels of two vital immune checkpoints **(D)** and PD-L1 **(E)** among these distinct ICI clusters; (Wilcoxon test, ns, no significance $P > 0.05$; ****$P < 0.0001$).

Immune Cell Infiltration Score Development and Validation

First, we extracted 398 MRDEGs *via* a random forest algorithm (**Supplementary File 4**; **Figures S4A, B**). **Figure S4C** shows the whole landscape of these MRDEG expression levels with distinct ICI genotypes. To further validate the functions of these MRDEGs, we performed GO functional annotations. GO BP analysis showed that these MRDEGs were significantly enriched in the terms T-cell selection, lymphocyte costimulation, and positive regulation of T-cell proliferation. GO CC analysis showed that these MRDEGs were significantly enriched in the terms immunological synapse and alpha-beta T-cell receptor complex. GO MF analysis showed that these MRDEGs were significantly enriched in the terms T-cell receptor binding and cytokine receptor activity (**Figure S4D**, **Supplementary File 5**). Next, we utilized PCA to calculate the signature scores using these 398 MRDEG expression levels. Then, the patients were divided into two groups as high or low ICI scores basing on an

optimal AUC cutoff value with ROC analysis. We also developed an ICI score and grouped the validation cohort using the methodology proposed above (**Supplementary File 6**).

Figure 4A depicts the distribution of BRCA patients among these three genotypes. In addition, we assessed the level of effector T-cell infiltration (CD8A and CXCL10) and INF-γ-related cytotoxicity (IFNG, GZMA, GZMB, EOMES, and TBX21) for each ICI group based on a seven-gene panel designed in the POPLAR trial (29). Moreover, a cytolytic activity score calculated by the geometrical mean of PRF1 and GZMA mRNA expression levels was used to reflect the magnitude of the antitumor response (30). All of these eight parameters in the high ICI score group were remarkably higher than those in low ICI score group (Wilcoxon test; $P < 0.0001$, **Figure 4B**; Student's t test; $P < 0.0001$, **Figure 4C**).

Kaplan–Meier survival with log-rank test was used to assess the relationships between OS and ICI score. We observed that BRCA patients with high ICI scores (median survival time: 6632

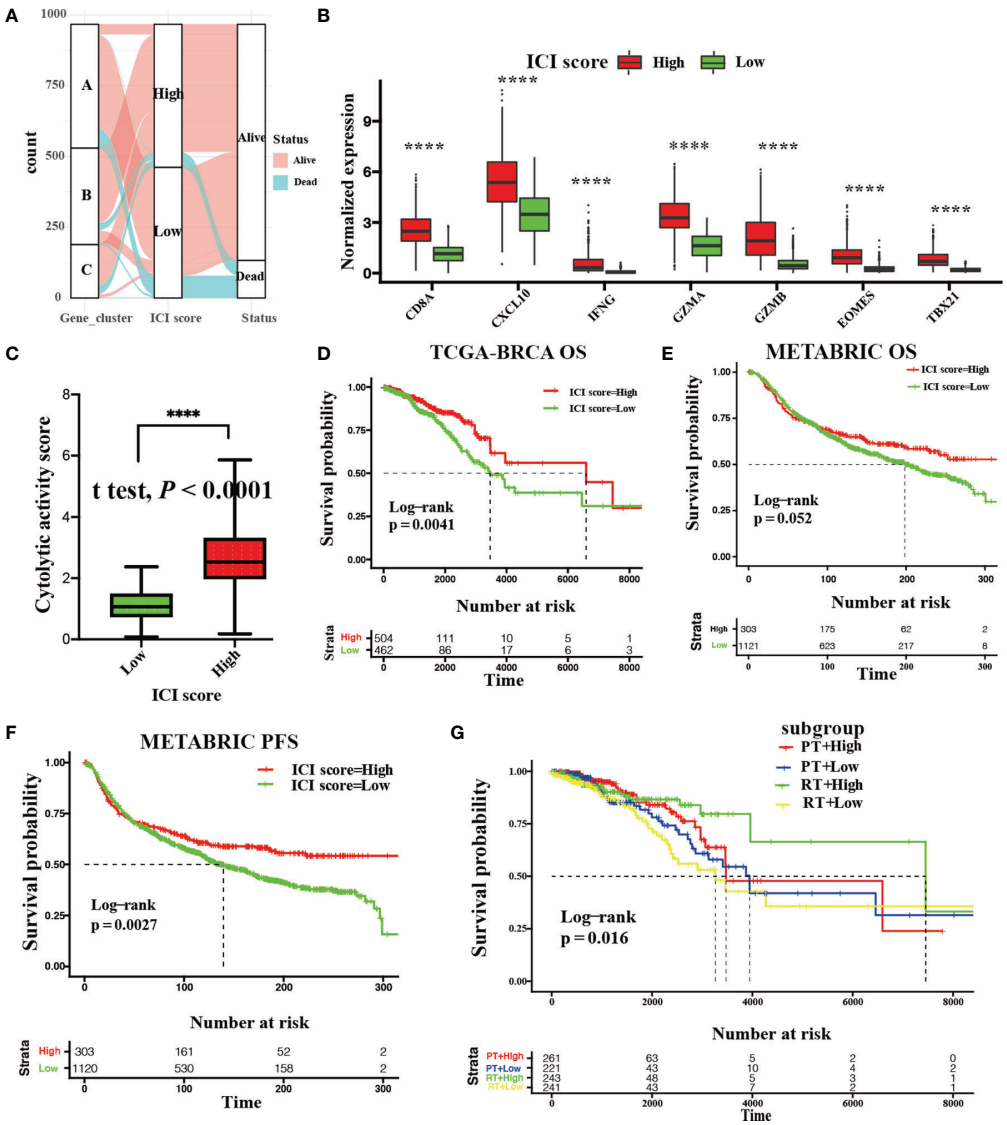

FIGURE 4 | Development and validation with the ICI score. **(A)** Gene phenotype distribution of the ICI score and clinical outcomes. **(B)** Gene expression levels of effector T-cell infiltration (CD8A and CXCL10) and INF-γ-related cytotoxicity (IFNG, GZMA, GZMB, EOMES, and TBX21) between the high and low ICI score group. (Wilcoxon test ****$P < 0.0001$). **(C)** The cytolytic activity score between the high and low ICI score groups. (Student's t test, ****$P < 0.0001$). **(D)** Kaplan–Meier curve showing OS outcomes between the high and low ICI score groups in the TCGA-BRCA cohort. Log-rank test showing $P = 0.0041$. **(E, F)** Kaplan–Meier curve showing OS outcomes (**E**; log-rank test, $P = 0.052$) and PFS outcomes (**F**; log-rank test, $P = 0.0027$.) with BRCA patients between the high and low ICI score groups in METABRIC cohort. **(G)** Kaplan–Meier curve showing OS outcomes of BRCA patients between the high and low ICI score groups treated with radiotherapy (RT) or chemotherapy (CT) in the TCGA-BRCA cohort (log-rank test, $P = 0.016$).

days) had significantly favorable OS versus patients with low ICI scores (median survival time: 3564 days) in the discovery cohort (log-rank test: $P = 0.0041$, **Figure 4D**). Additionally, a significant survival advantage of BRCA patients with high ICI scores was observed in PFS (log-rank test; $P = 0.0027$, **Figure 4F**) rather than OS (log-rank test; $P = 0.052$, **Figure 4E**) in the validation cohort. We also found that BRCA patients with high ICI scores who received radiotherapy or chemotherapy retained a significant survival advantage in discovery cohort (log-rank test; $P = 0.016$, **Figure 4G**).

The Relationships Between the ICI Score and Somatic Genetic Variation

Previous studies have reported that tumor somatic genetic variation is related to cancer prognoses and determines therapeutic responses (31, 32). Inspired by these studies, we investigated the relationships between TMB and ICI score. First, a significantly elevated TMB was observed in BRCA patients with high ICI scores (Wilcoxon test; $P < 0.05$, **Figure 5A**). We also found that TMB was remarkably and positively correlated with ICI score (Spearman coefficient: R = 0.093, $P = 0.0039$,

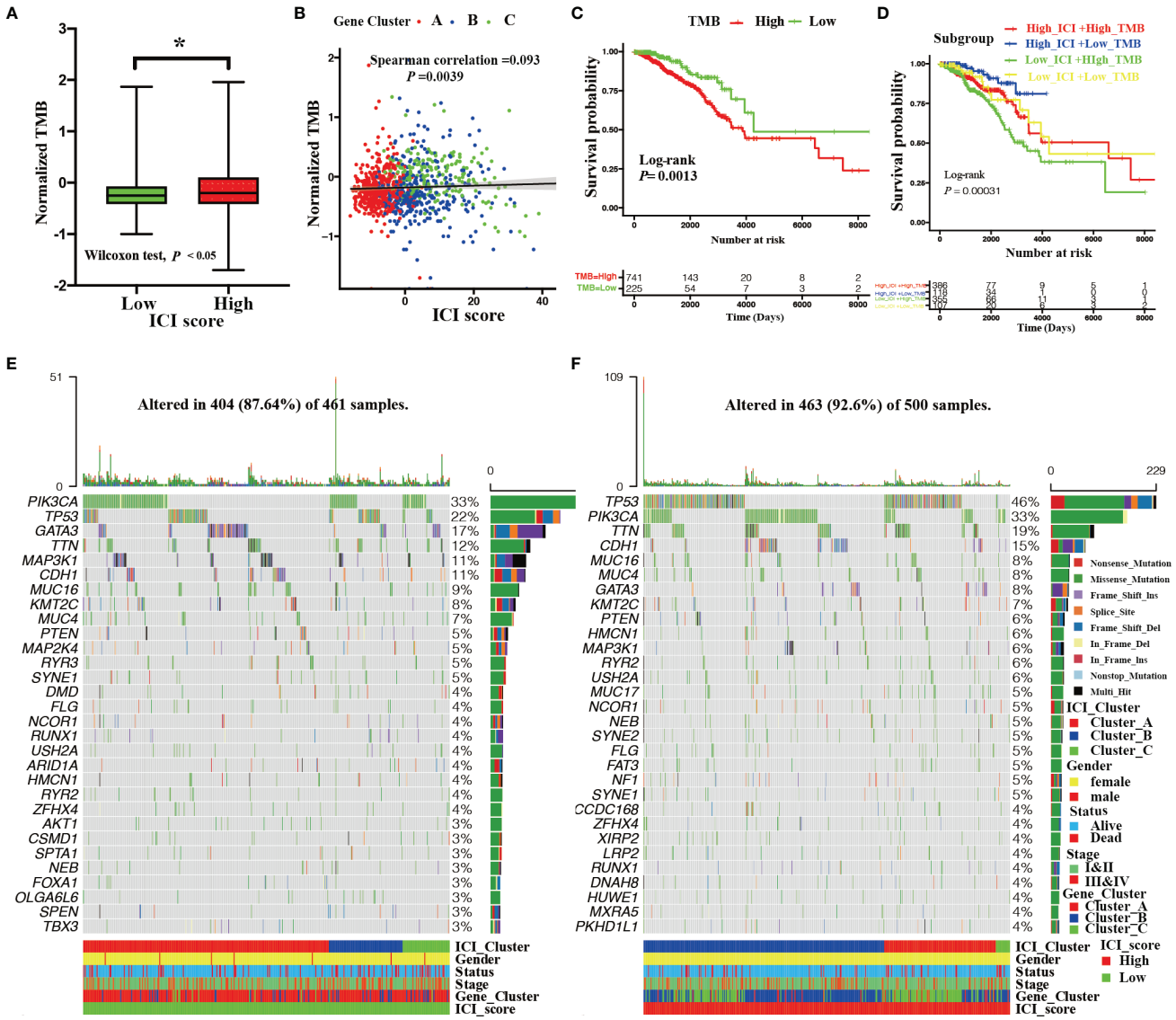

FIGURE 5 | Correlation between ICI score and somatic mutation. **(A)** The TMB among the high and low ICI score groups (Wilcoxon test, $^*P < 0.05$). **(B)** Correlation between the ICI score and TMB with distinct gene clusters (Spearman correlation test, $P = 0.0039$; spearman correlation coefficient = 0.093). **(C)** Kaplan–Meier curves showing OS outcomes of BRCA patients between high and low TMB group. Log-rank test showing $P = 0.0013$. **(D)** Kaplan–Meier curves for BRCA patients stratified by both TMB and ICI scores. Log-rank test showing $P = 0.00031$. **(E, F)** Landscape of the top 30 drive mutated genes for the low ICI score **(E)** and high ICI score groups **(F)**. Each column represents the individual patients and each row represents a drive mutated gene.

Figure 5B). To further study the prognostic value of TMB, we categorized BRCA patients into high TMB or low TMB subgroups based on an optimal cutoff of TMB value (0.37) with ROC analysis. As shown in **Figure 5C**, BRCA patients with low TMB had statistical survival advantage over those with high TMB (log-rank test; $P = 0.0013$). Additionally, hierarchical survival analysis revealed that this survival advantage was independent of TMB (log-rank test; $P = 0.00031$, **Figure 5D**).

The subsequent analyses assessed the distribution of driver somatic variant genes between the high and low ICI score subgroups. **Figure 5** shows the top 30 most frequently mutated genes with high (**Figure 5E**) and low (**Figure 5F**) ICI score groups. A total of 124 statistically different somatic variant genes were detected between high and low ICI score groups through the chi-square test conducted by the maftools R package (**Supplementary File 7**).

The Role of the ICI Score in the Prediction of Therapeutic Benefits

We assessed the role of ICI score in predicting chemotherapeutic benefits using the GSE5462 and GSE20181 datasets. The GSE5462 and GSE20181 datasets recorded microarray and clinical data from BRCA patients before and after letrozole treatment. As depicted in **Figure 6**, letrozole did not elevate the ICI score of BRCA patients (paired Wilcoxon test; $P > 0.05$, **Figures 6A, C**) but patients with high ICI scores had higher responder rate (GSE5462 cohort: responder rate [RR], 35.71% in the high ICI group versus 20.83% in the low ICI group; chi-square test, $P < 0.001$, **Figure 6B**; GSE20181 cohort: [RR], 71% in the high ICI group versus 50% in the low ICI group; chi-square test, $P < 0.05$, **Figure 6D**). We also investigated the immunotherapeutic benefit prediction role of the ICI score using GSE35640 and GSE91061 datasets. The GSE35640 and

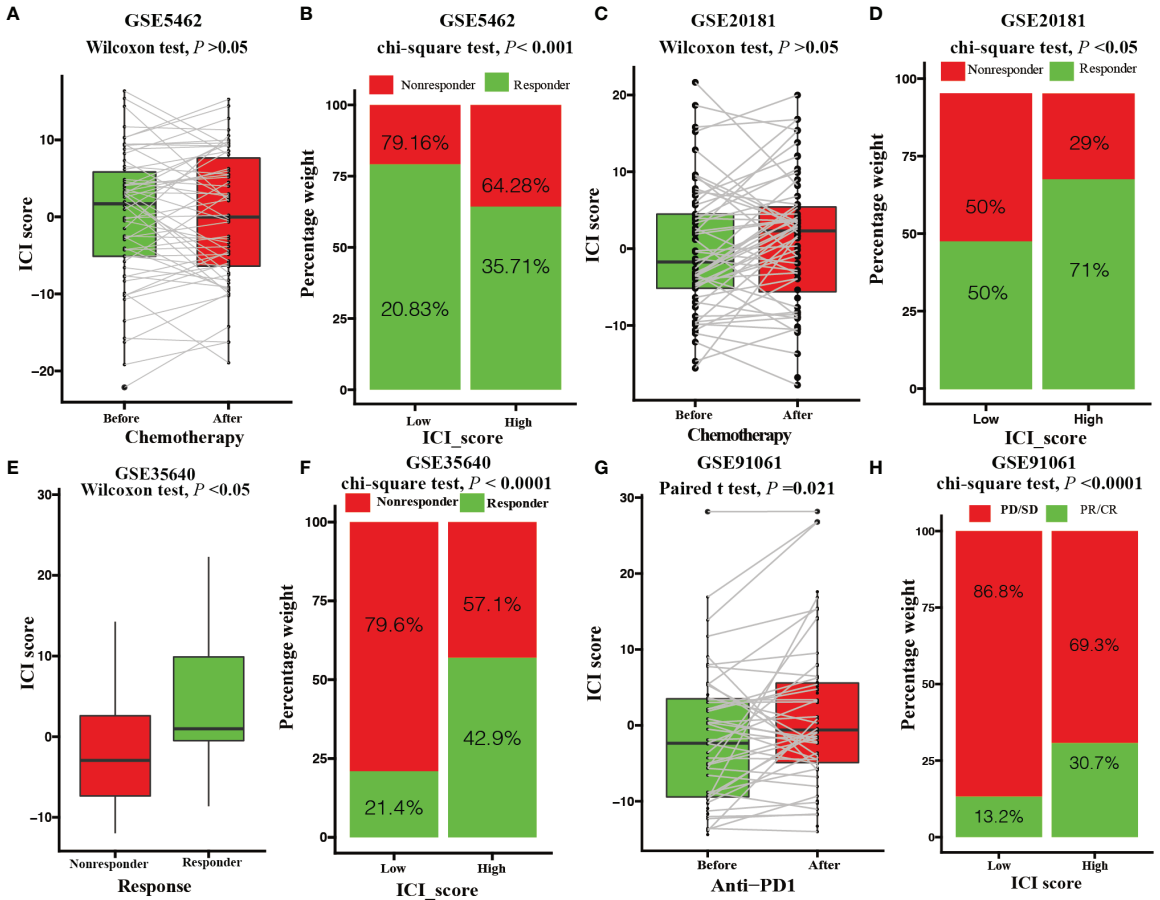

FIGURE 6 | Value of the ICI score in predicting chemotherapeutic and immunotherapeutic benefits. **(A)** ICI score of patients with letrozole treatment before and after 10-14 days. (Paired Wilcoxon test; $P > 0.05$). **(B)** Rate of clinical response to letrozole among the low and high ICI score group after 10-14 days (chi-square test; $P < 0.001$). **(C)** ICI score of patients with letrozole treatment before and after 90 days. (paired Wilcoxon test; $P > 0.05$). **(D)** Rate of clinical response to letrozole in the low and high ICI score groups after 90 days (chi-square test; $P < 0.05$). **(E)** ICI score of melanoma patients with MAGE-A3 antigen treatment between responder and nonresponder groups (Wilcoxon test; $P < 0.05$). **(F)** Rate of clinical response to MAGE-A3 antigen treatment among the low and high ICI score groups (chi-square test; $P < 0.0001$). **(G)** ICI score of melanoma patients before and after PD-L1 antigen treatment (paired Student's t test; $P = 0.021$). **(H)** Rate of clinical response to PD-L1 antigen among the low and high ICI score groups (chi-square test; $P < 0.0001$).

GSE91061 datasets recorded microarray and clinical data of melanoma patients with anti-MAGE-A3 and anti-PD1 treatments, respectively. We found that melanoma patients in the anti-MAGE-A3 responder group had higher ICI scores (GSE35640 cohort: paired Wilcoxon test; $P < 0.05$, **Figure 6E**). In contrast to chemotherapy, anti-PD1 treatment was found to elevate the ICI score of melanoma patients (GSE91061 cohort: paired Student's t test; $P < 0.0001$, **Figure 6G**). Moreover, higher responder rates were observed in the high ICI score group with both anti-MAGE-A3 and anti-PD1 treatments (GSE35640 cohort: [RR], 42.9% in the high ICI group versus 21.4% in the low ICI group; chi-square test; $P < 0.0001$, **Figure 6F**; GSE91061 cohort: [RR], 30.7% in the high ICI group versus 13.2% in the low ICI group; chi-square test; $P < 0.0001$, **Figure 6H**).

DISCUSSION

An increasing number of studies have reported that the TME plays an indispensable role in tumor progression, prognosis, relapse, metastasis, and therapeutic response in BRCA. However, most studies have focused on a single TME component or regulator. A comprehensive TME characterization has not yet been recognized. Identifying distinct ICI patterns will promote our understanding of the TME and guide precise individual therapies.

In this study, based on the TCGA-BRCA cohort, we first investigated the difference in the TME between normal and tumor tissues. Our results revealed relatively sparse immune cells and an upregulated PD1 and an undifferentiated PDL1 expression level in BRCA tissues, which indicated that immune cell dysfunction and immune escape in the tumorous TME plays critical roles in tumorigenesis. The PD1/PDL1 pathway is regarded as a brake of immune system which attenuates the tumor-infiltrating lymphocytes (TILs) activation through increasing PDL1 expression on tumor cell surface (33). In line with our study, Uhercik et al. (34) also revealed an upregulated PD1 and an undifferentiated PDL1 expression level in BRCA tissues. However, Jun fang et al. (35) reported that mRNA expression level of PD1 was up-regulated but the PDL1 was down-regulated in BRCA tissues.

Our primary concerns were the TME with BRCA tissues, so we focused on an ICI with tumor tissues. Based on immune cell abundances and stromal cell contents with each tumor sample, we identified three ICI phenotypes for BRCA termed ICI cluster ABC. ICI Cluster A was characterized by sparse immune cells and stromal cell contents that corresponded to the immune-desert phenotype; ICI Cluster B was characterized by an activation of innate immunity and adaptive immunity that corresponded to the immune-inflamed phenotype; and ICI Cluster C was characterized by an activation of innate immunity and upregulated PD1 expression that corresponded to the immune-exclude phenotype. So far, few studies have reported the PD1 and PDL1 expression levels among those three ICI phenotypes in BRCA. But, in the Head and Neck Squamous Cell Carcinoma, Xinhai Zhang et al. (13) revealed a consistent PD1 and PDL1 expression levels with our study. In addition, we observed that the abundances of activated CD4 T cells, CD56 dim natural killer cells, activated CD8 T cells, immature B cells, myeloid-derived suppressor cells, monocytes, and memory B cells were associated with a better OS, but the abundances of plasmacytoid dendritic cells and mast cells were related with a worse OS, which was consistent with previous studies (30, 36–38). However, the prognostic analysis showed a mismatching OS order with these three ICI phenotypes. Although the immune-exclude phenotype was also characterized by high immune cell densities compared with immune-inflame phenotype, the abundant surrounding stromal cells protected these immune cells against penetrating the parenchyma, which suppressed their antitumor effects (39). Compared with the immune-desert phenotype, the OS disadvantage of the immune-inflame phenotype should be attributed to upregulated PD1 and PD-L1 expression, which inhibits immune cellular activation and increases the developmental T-cell exhaustion (40, 41). The mismatching OS orders with these three ICI phenotypes also implied that the ICI phenotypes cannot absolutely predict the prognosis. The extensive genetic alterations of these three ICI phenotypes might affect tumor prognosis.

These genetic alterations in tumor tissues changed the original patterns of intercellular interactions of infiltrating immune cells, which disturbed the balance of immunity tolerance and activity (42). Therefore, we hypothesized that ICI phenotype-associated genes could be novel biomarkers to determine suitable therapeutic strategies for BRCA patients, so we performed DEGs analysis and consensus clustering for genotypes. We found that Gene Clusters B and C had favorable OS with intact antigen presenting cells, CD8 T cells, and CD4 T cells indicating an immune-hot phenotype (43, 44). In contrast, the sparse immune and stromal cell distributions in Gene Cluster A imply an immune-cold phenotype. In addition, we observed that a survival advantage with Gene Cluster C might be associated with its high immune score and low density of neutrophils, eosinophils, and mast cells. In line with previous studies, we found that immune-hot phenotypic patients with a survival advantage had upregulated PD1 and PD-L1 expression, implying that immune-hot phenotypic BRCA patients might benefit more from immunotherapy (34, 45). In the clinical practice, the immune cell abundances of each sample can be detected by the Flow cytometry directly or the methodology proposed at present study. Basing on the immune cell abundances detected in the clinical practice and the characterizations of each ICI phenotype or genotype we identified, the doctors could group the patients in the matched ICI phenotype or genotype we proposed.

Through a random forest algorithm, we identified 394 MRDEGs for these ICI genotypes. As expected, a survival advantage of BRCA patients with high ICI score was observed in the discovery cohort and validation cohort. This survival advantage profited from its high level of effector T-cell infiltration, INF-γ-related cytotoxicity, and cytokine activity. Importantly, a hierarchical survival analysis of the discovery cohort revealed that the prognostic role of ICI score was

independent of therapy strategies. Recent studies have explored a correlation between gene mutation and response or tolerance to therapies (46–49). We also investigated the correlation between the ICI score and variant frequency in multiple genes. Consistent with previous studies, therapy-sensitive somatic mutation genes were remarkably reduced in BRCA patients with low ICI scores (13). The correlation between the ICI score and TMB was 0.0093. A hierarchical analysis revealed that the prognostic value of the ICI score was independent of TMB. A low correlation coefficient and different predictive values implied that the ICI score and TMB were two distinct aspects of tumor biology.

Currently, chemotherapy remains a primary strategy for BRCA. Thus, it is necessary to assess the predictive value of the ICI score for chemotherapeutic benefits in BRCA patients. Our data indicated that chemotherapeutic agents could not elevate the ICI score, but patients with high ICI scores benefited more from chemotherapies. This phenomenon should be attributed to immunosuppression of chemotherapeutic agents. For a long time, immunotherapies have not been considered to a suitable strategy for BRCA due to low immunogenic peptide presentation (50). The phase III Impassion 130 trial reported that immune checkpoint block gained promising clinical efficacy in extending survival time with BRCA patients, which news recaptured researchers' attention (51). Despite a successful application of immunotherapies across a broad range of cancers, only a few patients could benefit from it. Even the issued guidelines with Society for Immunotherapy of Cancer had emphasized that a population suitable for immunotherapies should be further identified (52). Here, our data revealed that patients with high ICI scores benefited more from immunotherapies, which indicated that ICI scores could guide immunotherapies. Generally, the ICI score we developed could be a robust tool to guide individual treatments for cancer.

Our study also has several limitations. First, a PFS not OS confirmed the prognostic value of the ICI score in the validation cohort. Second, due to the absent of public BRCA immunotherapeutic cohorts, we validated the prognostic value with ICI score for immunotherapies using two melanoma cohorts. Third, a comprehensive study integrating ICI patterns, clinical information, and somatic mutation information was solely performed in the TCGA-BRCA cohort. However, the accessibility of these data to BRCA patients is insufficient in the validation cohort, thus, we failed to validate all of our findings in multiomics. Considering that these 967 TCGA-BRCA tumor samples could sufficiently contain all ICI patterns in the TME, we did not merge the RNA-seq datasets from different sequencing platforms to avoid batch effects. Last, we failed to perform RNA sequencing with an internal validation cohort for research funding limitations. Therefore, we included 1424 samples with complete information in the validation cohort to overcome this shortcoming. Further comprehensive studies integrating multiomics data are still prospective in this field.

In conclusion, by applying bioinformatics and multiomics analyses, we identified there ICI patterns and developed an ICI score to characterize the extensive immune cell-infiltrating TME for BRCA, which could precisely predict the clinical outcome and response to chemotherapy and immunotherapy.

DATA AVAILABILITY STATEMENT

The datasets presented in this study can be found in online repositories. The names of the repository/repositories and accession number(s) can be found in the article/**Supplementary Material**.

ETHICS STATEMENT

Ethical review and approval was not required for the study of human participants in accordance with the local legislation and institutional requirements. Written informed consent from the participants was not required to participate in this study in accordance with the national legislation and the institutional requirements.

AUTHOR CONTRIBUTIONS

LL designed this study, performed the statistical analysis, and prepared the manuscript; The author approved the final version for submission.

ACKNOWLEDGMENTS

We thank those researchers who shared their data and R packages for this study.

SUPPLEMENTARY MATERIAL

The Supplementary Material for this article can be found online at: https://www.frontiersin.org/articles/10.3389/fonc.2022.844082/full#supplementary-material

Supplementary Figure 1 | The workflow of study design and clustering for ICI phenotypes. The workflow diagram of study design **(A)**. Consensus matrix with 2 **(B)**, 3 **(C)**, 4 **(D)**, and 5 **(E)** divisions for BRCA samples. **(F)** Scree plot of relative change in area under cumulative distribution function (CDF) curve.

Supplementary Figure 2 | Differentially expressed genes (DEGs) identification with these distinct ICI phenotypes. The volcano plot of DEGs with ICI Cluster A versus Cluster B **(A)**, ICI Cluster B versus Cluster C **(B)**, and ICI Cluster A versus Cluster C **(C)**. The red dots represent upregulated genes, while the green dots represent downregulated genes. **(D)** The relationships between the DEGs among distinct ICI phenotypes. **(E)** The expressional landscape with DEGs.

Supplementary Figure 3 | Clustering for ICI genotypes. Consensus matrix with 2 **(A)**, 3 **(B)**, 4 **(C)**, 5 **(D)**, and 6 **(E)** divisions for the TCGA-BRCA cohorts. **(E)** Scree plot with relative change in area under cumulative distribution function (CDF) curves. The elbow indicates that three divisions for the TCGA-BRCA cohorts were the best optimal.

Supplementary Figure 4 | Screening of MRDEGs. **(A)** The relationships between the predictive error rate and the number of trees with random forest. The three lines in different colors represent three distinct ICI genotypes. **(B)** The top 30 MRDEGs according to mean decreasing accuracy and decreasing Gini. **(C)** The landscape of these top 398 MRDEGs. The rows represent MRDEGs and the columns represent BRCA samples. **(D)** The bubble plot of GO functional annotations with MRDEGs.

Supplementary File 1 | The immune cells gene set.

Supplementary File 2 | Relative Fractions of tumor-infiltrating immune cells of 112 normal tissues and 968 tumor tissues with TCGA-BRCA patients.

Supplementary File 3 | Different expressional genes of these distinct ICI phenotypes.

Supplementary File 4 | The representativeness of DEGs with descending order by random forest algorithm and top 398 most representative DEGs expression level.

Supplementary File 5 | GO functional annotations with these top 398 most representative DEGs.

Supplementary File 6 | ICI score of TCGA-BRCA cohort, METABRIC cohort, immunotherapeutic cohorts, and chemotherapeutic cohorts.

Supplementary File 7 | The somatic gene mutations between high and low ICI groups with TCGA-BRCA cohort.

REFERENCES

1. Sung H, Ferlay J, Siegel RL, Laversanne M, Soerjomataram I, Jemal A, et al. Global Cancer Statistics 2020: GLOBOCAN Estimates of Incidence and Mortality Worldwide for 36 Cancers in 185 Countries. *CA Cancer J Clin* (2021) 71(3):209–49. doi: 10.3322/caac.21660
2. Becht E, Giraldo NA, Lacroix L, Buttard B, Elarouci N, Petitprez F, et al. Estimating the Population Abundance of Tissue-Infiltrating Immune and Stromal Cell Populations Using Gene Expression. *Genome Biol* (2016) 17 (1):218. doi: 10.1186/s13059-016-1070-5
3. Spill F, Reynolds DS, Kamm RD, Zaman MH. Impact of the Physical Microenvironment on Tumor Progression and Metastasis. *Curr Opin Biotechnol* (2016) 40:41–8. doi: 10.1016/j.copbio.2016.02.007
4. Del Prete A, Schioppa T, Tiberio L, Stabile H, Sozzani S. Leukocyte Trafficking in Tumor Microenvironment. *Curr Opin Pharmacol* (2017) 35:40–7. doi: 10.1016/j.coph.2017.05.004
5. Bi G, Chen Z, Yang X, Liang J, Hu Z, Bian Y, et al. Identification and Validation of Tumor Environment Phenotypes in Lung Adenocarcinoma by Integrative Genome-Scale Analysis. *Cancer Immunol Immunother* (2020) 69 (7):1293–305. doi: 10.1007/s00262-020-02546-3
6. Erdag G, Schaefer JT, Smolkin ME, Deacon DH, Shea SM, Dengel LT, et al. Immunotype and Immunohistologic Characteristics of Tumor-Infiltrating Immune Cells are Associated With Clinical Outcome in Metastatic Melanoma. *Cancer Res* (2012) 72(5):1070–80. doi: 10.1158/0008-5472.Can-11-3218
7. Kulasinghe A, Monkman J, Shah ET, Matigian N, Adams MN, O'Byrne K. Spatial Profiling Identifies Prognostic Features of Response to Adjuvant Therapy in Triple Negative Breast Cancer (TNBC). *Front Oncol* (2021) 11:798296. doi: 10.3389/fonc.2021.798296
8. Hu S, Qu X, Jiao Y, Hu J, Wang B. Immune Classification and Immune Landscape Analysis of Triple-Negative Breast Cancer. *Front Genet* (2021) 12:710534. doi: 10.3389/fgene.2021.710534
9. Risom T, Glass DR, Averbukh I, Liu CC, Baranski A, Kagel A, et al. Transition to Invasive Breast Cancer is Associated With Progressive Changes in the Structure and Composition of Tumor Stroma. *Cell* (2022) 185(2):299–310.e218. doi: 10.1016/j.cell.2021.12.023
10. Medrek C, Pontén F, Jirström K, Leandersson K. The Presence of Tumor Associated Macrophages in Tumor Stroma as a Prognostic Marker for Breast Cancer Patients. *BMC Cancer* (2012) 12:306. doi: 10.1186/1471-2407-12-306
11. Barbie DA, Tamayo P, Boehm JS, Kim SY, Moody SE, Dunn IF, et al. Systematic RNA Interference Reveals That Oncogenic KRAS-Driven Cancers Require TBK1. *Nature* (2009) 462(7269):108–12. doi: 10.1038/nature08460
12. Zeng D, Li M, Zhou R, Zhang J, Sun H, Shi M, et al. Tumor Microenvironment Characterization in Gastric Cancer Identifies Prognostic and Immunotherapeutically Relevant Gene Signatures. *Cancer Immunol Res* (2019) 7(5):737–50. doi: 10.1158/2326-6066.Cir-18-0436
13. Zhang X, Shi M, Chen T, Zhang B. Characterization of the Immune Cell Infiltration Landscape in Head and Neck Squamous Cell Carcinoma to Aid Immunotherapy. *Mol Ther Nucleic Acids* (2020) 22:298–309. doi: 10.1016/j.omtn.2020.08.030
14. Pereira B, Chin SF, Rueda OM, Vollan HK, Provenzano E, Bardwell HA, et al. The Somatic Mutation Profiles of 2,433 Breast Cancers Refines Their Genomic and Transcriptomic Landscapes. *Nat Commun* (2016) 7:11479. doi: 10.1038/ncomms11479
15. Davis S, Meltzer PS. GEOquery: A Bridge Between the Gene Expression Omnibus (GEO) and BioConductor. *Bioinformatics* (2007) 23(14):1846–7. doi: 10.1093/bioinformatics/btm254
16. Ru B, Wong CN, Tong Y, Zhong JY, Zhong SSW, Wu WC, et al. TISIDB: An Integrated Repository Portal for Tumor-Immune System Interactions. *Bioinformatics* (2019) 35(20):4200–2. doi: 10.1093/bioinformatics/btz210
17. Hänzelmann S, Castelo R, Guinney J. GSVA: Gene Set Variation Analysis for Microarray and RNA-Seq Data. *BMC Bioinf* (2013) 14:7. doi: 10.1186/1471-2105-14-7
18. Kolde R. *Pheatmap: Pretty Heatmaps*. (2019).
19. Wickham H. *Ggplot2: Elegant Graphics for Data Analysis*. New York: Springer-Verlag (2016).
20. Wilkerson MD, Hayes DN. ConsensusClusterPlus: A Class Discovery Tool With Confidence Assessments and Item Tracking. *Bioinformatics* (2010) 26 (12):1572–3. doi: 10.1093/bioinformatics/btq170
21. Robinson MD, McCarthy DJ, Smyth GK. Edger: A Bioconductor Package for Differential Expression Analysis of Digital Gene Expression Data. *Bioinformatics* (2010) 26(1):139–40. doi: 10.1093/bioinformatics/btp616
22. Andy Liaw MW. Classification and Regression by Randomforest. *R News* (2002) 2:18–22.
23. Yu G, Wang LG, Han Y, He QY. Clusterprofiler: An R Package for Comparing Biological Themes Among Gene Clusters. *Omics* (2012) 16(5):284–7. doi: 10.1089/omi.2011.0118
24. Sotiriou C, Wirapati P, Loi S, Harris A, Fox S, Smeds J, et al. Gene Expression Profiling in Breast Cancer: Understanding the Molecular Basis of Histologic Grade to Improve Prognosis. *J Natl Cancer Inst* (2006) 98(4):262–72. doi: 10.1093/jnci/djj052
25. Obuchowski NA, Bullen JA. Receiver Operating Characteristic (ROC) Curves: Review of Methods With Applications in Diagnostic Medicine. *Phys Med Biol* (2018) 63(7):07tr01. doi: 10.1088/1361-6560/aab4b1
26. Mayakonda A, Lin DC, Assenov Y, Plass C, Koeffler HP. Maftools: Efficient and Comprehensive Analysis of Somatic Variants in Cancer. *Genome Res* (2018) 28(11):1747–56. doi: 10.1101/gr.239244.118
27. Therneau TM. *A Package for Survival Analysis in R*. (2021).
28. Kassambara A, Kosinski M, Biecek P. Survminer: Drawing Survival Curves Using 'Ggplot2'. (2021).
29. Fehrenbacher L, Spira A, Ballinger M, Kowanetz M, Vansteenkiste J, Mazieres J, et al. Atezolizumab Versus Docetaxel for Patients With Previously Treated non-Small-Cell Lung Cancer (POPLAR): A Multicentre, Open-Label, Phase 2 Randomised Controlled Trial. *Lancet* (2016) 387(10030):1837–46. doi: 10.1016/s0140-6736(16)00587-0
30. Rooney MS, Shukla SA, Wu CJ, Getz G, Hacohen N. Molecular and Genetic Properties of Tumors Associated With Local Immune Cytolytic Activity. *Cell* (2015) 160(1-2):48–61. doi: 10.1016/j.cell.2014.12.033
31. Rizvi NA, Hellmann MD, Snyder A, Kvistborg P, Makarov V, Havel JJ, et al. Cancer Immunology. Mutational Landscape Determines Sensitivity to PD-1 Blockade in non-Small Cell Lung Cancer. *Science* (2015) 348(6230):124–8. doi: 10.1126/science.aaa1348

32. McGranahan N, Furness AJ, Rosenthal R, Ramskov S, Lyngaa R, Saini SK, et al. Clonal Neoantigens Elicit T Cell Immunoreactivity and Sensitivity to Immune Checkpoint Blockade. *Science* (2016) 351(6280):1463–9. doi: 10.1126/science.aaf1490
33. Zielinski C, Knapp S, Mascaux C, Hirsch F. Rationale for Targeting the Immune System Through Checkpoint Molecule Blockade in the Treatment of non-Small-Cell Lung Cancer. *Ann Oncol* (2013) 24(5):1170–9. doi: 10.1093/annonc/mds647
34. Uhercik M, Sanders AJ, Owen S, Davies EL, Sharma AK, Jiang WG, et al. Clinical Significance of PD1 and PDL1 in Human Breast Cancer. *Anticancer Res* (2017) 37(8):4249–54. doi: 10.21873/anticanres.11817
35. Fang J, Chen F, Liu D, Gu F, Chen Z, Wang Y. Prognostic Value of Immune Checkpoint Molecules in Breast Cancer. *Biosci Rep* (2020) 40(7):45–58. doi: 10.1042/bsr20201054
36. He Y, Jiang Z, Chen C, Wang X. Classification of Triple-Negative Breast Cancers Based on Immunogenomic Profiling. *J Exp Clin Cancer Res* (2018) 37 (1):327. doi: 10.1186/s13046-018-1002-1
37. Ge P, Wang W, Li L, Zhang G, Gao Z, Tang Z, et al. Profiles of Immune Cell Infiltration and Immune-Related Genes in the Tumor Microenvironment of Colorectal Cancer. *BioMed Pharmacother* (2019) 118:109228. doi: 10.1016/j.biopha.2019.109228
38. Zeng D, Ye Z, Wu J, Zhou R, Fan X, Wang G, et al. Macrophage Correlates With Immunophenotype and Predicts Anti-PD-L1 Response of Urothelial Cancer. *Theranostics* (2020) 10(15):7002–14. doi: 10.7150/thno.46176
39. Joyce JA, Fearon DT. T Cell Exclusion, Immune Privilege, and the Tumor Microenvironment. *Science* (2015) 348(6230):74–80. doi: 10.1126/science.aaa6204
40. Han Y, Liu D, Li L. PD-1/PD-L1 Pathway: Current Researches in Cancer. *Am J Cancer Res* (2020) 10(3):727–42.
41. Dolina JS, Van Braeckel-Budimir N, Thomas GD, Salek-Ardakani S. CD8(+) T Cell Exhaustion in Cancer. *Front Immunol* (2021) 12:715234. doi: 10.3389/fimmu.2021.715234
42. Chen DS, Mellman I. Elements of Cancer Immunity and the Cancer-Immune Set Point. *Nature* (2017) 541(7637):321–30. doi: 10.1038/nature21349
43. Hamanishi J, Mandai M, Iwasaki M, Okazaki T, Tanaka Y, Yamaguchi K, et al. Programmed Cell Death 1 Ligand 1 and Tumor-Infiltrating CD8+ T Lymphocytes are Prognostic Factors of Human Ovarian Cancer. *Proc Natl Acad Sci U S A* (2007) 104(9):3360–5. doi: 10.1073/pnas.0611533104
44. Hwang ML, Lukens JR, Bullock TN. Cognate Memory CD4+ T Cells Generated With Dendritic Cell Priming Influence the Expansion, Trafficking, and Differentiation of Secondary CD8+ T Cells and Enhance Tumor Control. *J Immunol* (2007) 179(9):5829–38. doi: 10.4049/jimmunol.179.9.5829
45. Sabatier R, Finetti P, Mamessier E, Adelaide J, Chaffanet M, Ali HR, et al. Prognostic and Predictive Value of PDL1 Expression in Breast Cancer. *Oncotarget* (2015) 6(7):5449–64. doi: 10.18632/oncotarget.3216
46. Burr ML, Sparbier CE, Chan YC, Williamson JC, Woods K, Beavis PA, et al. CMTM6 Maintains the Expression of PD-L1 and Regulates Anti-Tumour Immunity. *Nature* (2017) 549(7670):101–5. doi: 10.1038/nature23643
47. George S, Miao D, Demetri GD, Adeegbe D, Rodig SJ, Shukla S, et al. Loss of PTEN Is Associated With Resistance to Anti-PD-1 Checkpoint Blockade Therapy in Metastatic Uterine Leiomyosarcoma. *Immunity* (2017) 46(2):197–204. doi: 10.1016/j.immuni.2017.02.001
48. Kaur RP, Vasudeva K, Kumar R, Munshi A. Role of P53 Gene in Breast Cancer: Focus on Mutation Spectrum and Therapeutic Strategies. *Curr Pharm Des* (2018) 24(30):3566–75. doi: 10.2174/1381612824666180926095709
49. Penson RT, Valencia RV, Cibula D, Colombo N, Leath CA, Bidziński M, et al. Olaparib Versus Nonplatinum Chemotherapy in Patients With Platinum-Sensitive Relapsed Ovarian Cancer and a Germline BRCA1/2 Mutation (SOLO3): A Randomized Phase III Trial. *J Clin Oncol* (2020) 38(11):1164–74. doi: 10.1200/jco.19.02745
50. Li Z, Qiu Y, Lu W, Jiang Y, Wang J. Immunotherapeutic Interventions of Triple Negative Breast Cancer. *J Transl Med* (2018) 16(1):147. doi: 10.1186/s12967-018-1514-7
51. Schmid P, Rugo HS, Adams S, Schneeweiss A, Barrios CH, Iwata H, et al. Atezolizumab Plus Nab-Paclitaxel as First-Line Treatment for Unresectable, Locally Advanced or Metastatic Triple-Negative Breast Cancer (IMpassion130): Updated Efficacy Results From a Randomised, Double-Blind, Placebo-Controlled, Phase 3 Trial. *Lancet Oncol* (2020) 21(1):44–59. doi: 10.1016/s1470-2045(19)30689-8
52. Cohen EEW, Bell RB, Bifulco CB, Burtness B, Gillison ML, Harrington KJ, et al. The Society for Immunotherapy of Cancer Consensus Statement on Immunotherapy for the Treatment of Squamous Cell Carcinoma of the Head and Neck (HNSCC). *J Immunother Cancer* (2019) 7(1):184. doi: 10.1186/s40425-019-0662-5

Conflict of Interest: The author declares that the research was conducted in the absence of any commercial or financial relationships that could be construed as a potential conflict of interest.

Publisher's Note: All claims expressed in this article are solely those of the authors and do not necessarily represent those of their affiliated organizations, or those of the publisher, the editors and the reviewers. Any product that may be evaluated in this article, or claim that may be made by its manufacturer, is not guaranteed or endorsed by the publisher.

Copyright © 2022 Li. This is an open-access article distributed under the terms of the Creative Commons Attribution License (CC BY). The use, distribution or reproduction in other forums is permitted, provided the original author(s) and the copyright owner(s) are credited and that the original publication in this journal is cited, in accordance with accepted academic practice. No use, distribution or reproduction is permitted which does not comply with these terms.

frontiers | Frontiers in Oncology

ORIGINAL RESEARCH
published: 04 July 2022
doi: 10.3389/fonc.2022.880100

Glia Maturation Factor β as a Novel Independent Prognostic Biomarker and Potential Therapeutic Target of Kidney Renal Clear Cell Carcinoma

Tong Zhu[1,2†], Tianyu Wang[1,3†], Zijun Feng[2], Furong Gao[1,2], Jieping Zhang[1,4], Caixia Jin[1,2], Haibin Tian[1,2], Jingying Xu[1,2], Hao Chen[3], Qingjian Ou[1], Juan Wang[1,5‡], Guotong Xu[1,4*‡] and Lixia Lu[1,2*‡]*

[1] Department of Ophthalmology of Shanghai Tongji Hospital, Laboratory of Clinical Visual Science of Tongji Eye Institute, School of Medicine, Tongji University, Shanghai, China, [2] Department of Biochemistry and Molecular Biology, Tongji University School of Medicine, Shanghai, China, [3] Department of Ophthalmology of Shanghai Tenth People's Hospital, Tongji University School of Medicine, Shanghai, China, [4] Department of Pharmacology, Tongji University School of Medicine, Shanghai, China, [5] Department of Human Genetics, Tongji University School of Medicine, Shanghai, China

OPEN ACCESS

Edited by:
Zhe-Sheng Chen,
St. John's University, United States

Reviewed by:
Jean Paul Thiery,
Institute of Molecular and Cell Biology (A*STAR), Singapore
Yuchen Liu,
Shenzhen University, China

***Correspondence:**
Lixia Lu
98738@tongji.edu.cn
Guotong Xu
gtxu@tongji.edu.cn
Juan Wang
juanwang@tongji.edu.cn

†These authors have contributed equally to this work and share first authorship

‡These authors have contributed equally to this work and share last authorship

Specialty section:
This article was submitted to Molecular and Cellular Oncology, a section of the journal Frontiers in Oncology

Received: 21 February 2022
Accepted: 30 May 2022
Published: 04 July 2022

Citation:
Zhu T, Wang T, Feng Z, Gao F, Zhang J, Jin C, Tian H, Xu J, Chen H, Ou Q, Wang J, Xu G and Lu L (2022) Glia Maturation Factor β as a Novel Independent Prognostic Biomarker and Potential Therapeutic Target of Kidney Renal Clear Cell Carcinoma. Front. Oncol. 12:880100. doi: 10.3389/fonc.2022.880100

Kidney renal clear cell carcinoma (KIRC) has the highest mortality rate and potential for invasion among renal cancers. The diagnosis and treatment of KIRC are becoming challenging because of its diverse pathogenic mechanisms. Glia (GMFB) is a highly conserved growth and differentiation factor for glia cells and neurons, and it is closely associated with neurodegenerative diseases. However, its role in KIRC remains unknown. The present study integrated bioinformatics approaches with suitable meta-analyses to determine the position of GMFB in KIRC. There was a significant decrease in *Gmfb* expression in KIRC kidneys compared with normal controls. *Gmfb* expression was negatively associated with pathologic stage, T and M stages, and histologic grade. Univariate and multivariate analyses showed that elevated *Gmfb* expression was an independent factor for a favorable prognosis. Furthermore, the nomogram verified that *Gmfb* is a low-risk factor for KIRC. Knockdown of *Gmfb* in Caki-2 cells increased viability and decreased p21 and p27 levels. Overexpression of *Gmfb* inhibited Caki-2 cell proliferation, migration, and invasion and decreased mitochondrial membrane potential. Gene ontology and Kyoto Encyclopedia of Genes and Genomes pathway enrichment analyses considering *Gmfb* co-expressed differentially expressed genes (DEGs) showed that collecting duct acid secretion and mineral absorption ranked were the most important upregulated and downregulated DEGs, respectively. The upregulated hub genes for DEGs were mainly involved in nucleosome assembly, nucleosome organization, and chromatin assembly, and the downregulated hub genes were primarily associated with keratinization. The ratio of tumor-infiltrating immune cells in KIRC tissues was evaluated using CIBERSORTx. The results showed that the *Gmfb* expression was significantly positively correlated with macrophage M2 cells and mast resting cell infiltration levels and negatively correlated with T follicular helper, T regulatory, and B plasma cell infiltration levels. The former cell types were associated with a beneficial outcome, while the latter

had a worse outcome in patients with KIRC. In summary, this study identified GMFB as a novel independent biomarker and therapeutic target for KIRC, and it provides a helpful and distinct individualized treatment strategy for KIRC with a combination of molecular targets and tumor microenvironment.

Keywords: kidney renal clear cell carcinoma, Glia maturation factor-beta, biomarker, prognosis, immune infiltration

INTRODUCTION

Kidney cancer is one of the ten most common types of cancer worldwide (1, 2). It is estimated that 300,000 people worldwide develop kidney cancer each year, and approximately half of them die from this disease (3). Kidney renal clear cell carcinoma (KIRC), which originates from the epithelial cells of the proximal convoluted tubule of the nephron, has become one of the most rapidly evolving areas of oncology, accounting for approximately 75% of kidney cancers (3–5). In addition to being the most common subtype, KIRC has the highest aggressiveness and metastasis and the highest mortality rate (4), as well as the highest immunity and vascular infiltration of cancer types (6, 7).

The molecular mechanisms involved in KIRC pathogenesis are diverse (8), including direct chromatin configuration alteration, vasculogenesis, and glucose metabolism (8, 9). Over the past few years, many studies have focused on the oncogenes of renal cell carcinoma, resulting in the discovery of a repetitive mutation in KIRC (10). However, oncogenes and suppressors such as RAS genes, TP53, Rb, CDKN2A, BRAF, PIK3CA, PTEN, EGFR, and ERBB2, which are highly mutated in other adult epithelial cancers, play only a minor role in KIRC (10). The diagnosis and treatment of KIRC are becoming a challenge for the oncology community. Currently, the most reliable prognostic predictors for KIRC are T, N, and M stages (11). However, in these indicators, survival rates may vary considerably, even among patients with the same set of illnesses (11, 12). Therefore, there is an urgent need to identify novel, reliable prognostic biomarkers and therapeutic targets for patients with KIRC.

Recently, bioinformatics techniques have become crucial for deciphering the molecular mechanisms underlying KIRC. A considerable number of KIRC-related high-throughput microarray datasets and sequencing datasets have been accumulated, resulting in groundbreaking changes in KIRC research. Multi-omics have identified some genes, such as CHAC1 (13), METTL14 (14), P4HB (15), and FOXM1 (16), as novel prognostic indicators for KIRC. However, the analysis of the tumor microenvironment (TME) linked to the specific targets of KIRC is lacking.

It is well known that heterogeneity, an essential feature of tumors, may contribute to the distinct responses of cancer patients to the same treatment. Single-cell sequencing technology allows for dissecting tumor heterogeneity at the molecular and cellular levels. The TME is increasingly considered a target for drug treatment strategies (17). Recently, Hu et al. revealed intratumoral heterogeneity in KIRC, resulting in different clinical outcomes in single-cell transcriptomes (18).

Glia maturation factor-beta (GMFB), a highly conserved brain-specific protein, is a 17-kDa brain protein recognized as a growth and differentiation factor acting on neurons and glia (19, 20). It is essential for brain growth and development, and it is widely expressed in mammalian neuronal, glia, and parenchymal cells (21). GMFB is phosphorylated by protein kinase A (PKA) (19). Furthermore, PKA-phosphorylated GMFB inhibits extracellular signal-regulated kinase (ERK) and enhances p38 (22). It has been shown that the upregulation of GMFB is closely related to neurodegenerative disorders such as Parkinson's disease (23). Our previous work revealed that GMFB functions as a novel independent prognostic biomarker and therapeutic target for liver hepatocellular carcinoma (LIHC) (24). However, the role of GMFB in KIRC remains unclear.

The present study employed The Cancer Genome Atlas (TCGA) database and the CIBERSORTx tool (https://cibersortx.stanford.edu) to explore the potential effects of GMFB and GMFB-related TME, and the significant findings of molecular signatures were confirmed by quantitative real-time PCR (qRT-PCR), Western blotting, and immunostaining in human renal clear cell carcinoma cell line Caki-2. The obtained results allow further understanding of the interaction between GMFB and the TME in KIRC and thus provide a novel strategy for GMFB-based KIRC immunotherapies.

METHODS

Data Collection and Differential Expression Analysis

RNA sequencing (RNA-seq), somatic mutations, and related clinical data were downloaded from TCGA (https://portal.gdc.cancer.gov/), containing 11,069 samples from 33 types of cancer (25). RNA sequence data from 539 patients with KIRC and 72 normal tissues were also downloaded from TCGA database. RNA-seq data and patient clinical information (Workflow Type: HTSeq-FPKM) were acquired using UCSC Xena (https://xena.ucsc.edu/), an online tool for the exploration of gene expression and clinical and phenotypic data. UALCAN (http://ualcan.path.uab.edu) (26) and the Human Protein Atlas (HPA) (https://www.Proteinatlas.org/) (27) were used to analyze GMFB protein expression patterns and immunohistochemical results in normal kidney tissue and KIRC samples.

Survival Analysis and the Relationship Between *Gmfb* Expression and Prognosis

Survival and clinical phenotype data were extracted for each sample downloaded from TCGA database. Overall survival (OS)

and disease-free survival (DFS) were evaluated to determine the relationship between *Gmfb* expression and patient prognosis. The Kaplan–Meier curve and Cox regression analyses were performed to assess the association between *Gmfb* expression and OS in KIRC patients. Subsequently, multivariate analysis was employed to estimate whether *Gmfb* expression was an independent prognostic factor for survival in patients with KIRC.

Gene expression profiling interactive analysis (GEPIA) (http://gepia2.cancer-pku.cn/#index) was used to confirm the correlation between *Gmfb* expression and clinicopathological information in multiple cancer types (28).

Enrichment Analysis

The top 2,000 upregulated and downregulated differentially expressed genes (DEGs) between the high and low *Gmfb* expression groups, defined by Spearman's rho above 0.30, were used for enrichment analyses. Pathways within the Kyoto Encyclopedia of Genes and Genomes (KEGG) and Gene Ontology (GO) terms were assessed for enrichment using the KEGG Orthology-Based Annotation System (KOBAS) platform (http://kobas.cbi.pku.edu.cn/) (29–32) and Metascape (https://metascape.org/gp/index.html#/main/step1) (33, 34).

Assessment of Immune Infiltration

CIBERSORTx (http://cibersort.stanford.edu/) is a deconvolution algorithm that predicts the cell type components of intricate tissues based on normalized gene expression profiles; its results are usually in agreement with true estimates for many types of cancer (35). As so, CIBERSORTx was used to evaluate the relative proportions of 22 infiltrating immune cell subtypes in KIRC and LIHC (35). The percentages of the 22 immune cell subtypes derived from CIBERSORTx were regarded as a correction at $p < 0.05$ (36). The relationship between the expression of 22 subtypes of tumor-infiltrating immune cells (TIICs) and the survival of KIRC and LIHC patients was conducted using GEPIA2021 (http://gepia2021.cancer-pku.cns/) (37). The results of the survival analysis were considered statistically significant at $p < 0.05$.

Protein–Protein Interaction Network Construction and Hub Gene Screening

Protein–protein interaction (PPI) networks were constructed using the Search Tool for the Retrieval of Interacting Genes (STRING; http://string-db.org/) database (38) (version 11.5) and Metascape (http://metascape.org). Hub genes were identified using the CytoHubba plugin (39) in the Cytoscape software (40) (version 3.7.7). The maximal clique centrality (MCC) algorithm was employed to identify hub genes.

Cell Lines

The human embryonic kidney cell line 293T purchased from American Type Culture Collection (ATCC) and Caki-2 purchased from the Fenghui Institute of Biotechnology were used in this study. The HEK293T and Caki-2 cells were separately maintained in Dulbecco's modified Eagle's medium (DMEM)/high glucose and DMEM/nutrient mixture F12, respectively, supplemented with 10% fetal bovine serum (FBS) (Cat. No. 10091148, Gibco, Waltham, MA, USA) and 1% penicillin/streptomycin (Cat. No. 60162ES76, Yeasen, Shanghai, China) at 37°C and 5% CO_2.

Cell Transfection

The three pairs of small interfering RNA (siRNA) sequences of human *Gmfb* are shown in **Supplementary Table 1A**. A scrambled sequence was used as a siRNA control. The pcDNA-GMFB plasmid and pcDNA3.1 were kindly provided by Wan Sun. Caki-2 cells were transfected using Lipofectamine 2000 (Cat. No. T101, Vazyme, Nanjing, China), according to the manufacturer's instructions. After transfection for 12, 24, and 48 h, cells were collected for subsequent experiments.

Western Blotting

Caki-2 cells were lysed in radioimmunoprecipitation assay buffer (Cat. No. P0013B, Beyotime, Jiangsu, China) with protease inhibitors (Thermo Fisher Scientific, Waltham, MA, USA) to extract whole-cell proteins. Protein concentration was quantified using a bicinchoninic acid (BCA) kit (Cat. No. 20201ES76, Yeasen, Shanghai, China). A sample (30 μg) of each protein was then separated by sodium dodecyl sulfate–polyacrylamide gel electrophoresis, transferred to a polyvinylidene fluoride membrane (Millipore, Burlington, MA, USA), and blocked with 5% bovine serum albumin (BSA) at room temperature for 1 h. After incubation overnight at 4°C with primary antibodies against GMFB (1:1,000; Cat. No. 10690-1-AP, ProteinTech, Rosemont, IL, USA), GMFG (1:1,000; Cat. No. D121824, Sangon Biotech, Shanghai, China), p21 (1:1,000; Cat. No. 10355-1-AP, ProteinTech, Rosemont, IL, USA), p27 (1:1,000; Cat. No. #3686, CST, Danvers, MA, USA), and actin (1:10,000; Cat. No. 20536-1-AP, ProteinTech, Rosemont, IL, USA), membranes were incubated with a secondary antibody for 2 h. The secondary antibody used was horseradish peroxidase (HRP)-conjugated goat anti-rabbit IgG (1:10,000; Cat. No. SA00001-2, ProteinTech, Rosemont, IL, USA). The proteins were visualized using enhanced chemiluminescence (ECL) (Cat. No. E412-02, Vazyme, Jiangsu, China). Tanon 5200S (Tanon Science & Technology, Shanghai, China) was used to evaluate the density of protein bands, and relative protein levels were quantified using ImageJ software (https://imagej.nih.gov/ij/).

Quantitative Real-Time PCR

Total RNA was extracted with TRIzol reagent (Cat. No. R401-01, Vazyme) and reverse transcribed into cDNA using the Revert Aid Reverse Transcription System (Takara, Dalian, China) according to the manufacturer's protocol. PrimeScript RT polymerase (Cat. No. RR036A, Takara, Dalian, China) and SYBR Green Master Mix (Cat. No. FP205-02, Tiangen Biotech, Beijing, China) were used for conducting qRT-PCR on a LightCycler 96 Detection System (Bio-Rad Laboratories, Hercules, CA, USA). Data were analyzed using the $2^{-\Delta\Delta Ct}$ method (24). Oligos were synthesized by Sangon Biotech. The oligo sequences are shown in **Supplementary Table 1B**.

Immunofluorescence

Immunofluorescence analysis was performed to detect the colocalization of GMFB and Arp2/3 complex. 293T and Caki-2 cells were fixed with 4% paraformaldehyde for 15 min,

permeabilized with 0.3% Triton X-100 in phosphate-buffered saline (PBS) for 30 min, blocked with 3% BSA for 1 h, and incubated with primary antibodies against GMFB (1:200 Cat. No. 10690-1-AP, 60062-1-Ig, ProteinTech, Rosemont, IL, USA), Arp2 (1:50; Cat. No. D260865, Sangon Biotech, Shanghai, China), and Arp3 (1:50; Cat. No. sc-48344, Santa Cruz, Dallas, TX, USA) overnight with immunofluorescence buffer at 4°C. Cells were then incubated with secondary antibodies (Invitrogen, Waltham, MA, USA), goat anti-mouse IgG(H+L) cross-adsorbed secondary antibody, Alexa Fluor 488 (Cat. No. A-11001); goat anti-mouse IgG(H+L) cross-adsorbed secondary antibody, Alexa Fluor 555 (Cat. No. A-21422); goat anti-rabbit IgG(H+L) cross-adsorbed secondary antibody, Alexa Fluor 488 (Cat. No. A-11008); and goat anti-rabbit IgG(H+L) cross-adsorbed secondary antibody, Alexa Fluor 555 (Cat. No. A-21428) for 1 h at room temperature. After three washes for 10 min each with 1× PBS, cell sections were counterstained and mounted with DAPI Fluoromount-G (Cat. No. D9542, Sigma-Aldrich, St. Louis, MO, USA) and examined under a confocal microscope (Leica, Wetzlar, Germany).

Determination of Cell Viability

Caki-2 cells were transfected with siRNA and pcDNA-GMFB using Lipo2000 (Cat. No. T101-01, Vazyme, Jiangsu, China). At 12, 24, and 48 h post-transfection, cell viability was tested using a Cell Counting Kit-8 (Cat. No. C0037, Beyotime, Jiangsu, China), according to the manufacturer's instructions. This experiment was repeated four times.

Measurement of Mitochondrial Membrane Potential

Caki-2 cells were transfected with an empty vector or *Gmfb* overexpression (OE) plasmid. JC-1 staining (Cat. No. C2003S, Beyotime, Jiangsu, China) was performed to determine mitochondrial membrane potential (MMP), according to the manufacturer's instructions. Cell visualization was performed using fluorescence microscopy (Leica, Wetzlar, Germany).

Wound Healing Assay

Caki-2 cells were seeded in six-well plates and grown to 80%–90% confluence. Confluent cell monolayers were scratched using a sterile 200-µl pipette tip and rinsed with PBS to remove scratched cells according to our previous work (24). Wound closure was observed after 24 h. The wound closure rate was calculated as follows: wound closure (%) = (the area of initial wound − the area of the final wound)/area of initial wound × 100.

Transwell Migration and Invasion Assays

The migration and invasion abilities of cells were assessed using transwell migration (without Matrigel) and invasion (with Matrigel) assays in 24 wells according to our previous work (24). Cell suspensions in an FBS-free medium were added to the upper transwell chambers (24-well, 8-µm pores; BD, Franklin Lakes, NJ, USA), whereas 600 µl of the medium was supplemented with 10% FBS and added to the lower transwell chambers. The cell count after positive staining with crystal violet indicated migration or invasion.

RESULTS

Clinical Characteristics of Kidney Renal Clear Cell Carcinoma Patients

Detailed information on the clinical and gene expression data of the downloaded 539 samples is presented in **Table 1**. The median age of participants was 61 years. Among the 539 patients, 353 were male (65.5%) and 186 were female (34.5%). The 269 samples of participants under the age of 60 accounted for 49.9% of all samples. The topographic distribution included 51.6% T1 (n = 278), 13.2% T2 (n = 71), 33.2% T3 (n = 179), and 2% T4 (n = 11) cases. Only 16 patients (6.2%) showed lymph node involvement, while 78 cases (15.4%) had distant metastases. Most patients (467, 87.8%) were white.

Survival Atlas of *Gmfb* in Multiple Cancer Types and Differential Expression of GMFB Between Tumor and Normal Tissue Samples

The contribution of *Gmfb* to pan-cancer OS and DFS in the GEPIA2 database was compared using the Mantel–Cox test. The criterion for significant differences was a false discovery rate (FDR) <0.05, also known as p-value adjustment. OS analysis showed that *Gmfb* expression was negatively correlated with the hazard ratio (HR) of KIRC but positively correlated with the HR of LIHC in pan-cancers (**Figure 1A**). This was consistent with a previous report (24), in which *Gmfb* expression was negatively correlated with the HR of KIRC but positively correlated with the HR of adrenocortical carcinoma (ACC) (**Figure 1A**). Based on the correlation of *Gmfb* with OS and DFS in pan-cancer analysis, GMFB may be a promising novel prognostic factor for KIRC.

Gmfb expression levels were analyzed in pan-cancer tissues using TCGA dataset. Analysis of unpaired samples of 63 types of cancer tissues showed that *Gmfb* expression differed in 15 types of cancer tissues (**Figure 1B**), and it was downregulated in KIRC ($p < 0.001$) (**Figure 1B**). In the paired KIRC samples, the expression of *Gmfb* was also downregulated ($p < 0.001$) (**Figure 1C**). Protein expression analysis indicated that GMFB was weakly expressed in KIRC ($p < 0.001$) (**Figure 1E**). To verify GMFB expression at the protein level, we used the immunohistochemical results of KIRC provided by the HPA database (**Figure 1F**), which were consistent with those obtained from TCGA database. *Gmfb* was generally downregulated in renal cancer tissues.

In vitro, we confirmed that the *Gmfb* mRNA (**Figure 1D**) and protein (**Figure 1G**) levels were significantly decreased in Caki-2 cells when compared with HEK293T cells, which was consistent with the results of immunostaining of GMFB in HEK293T and Caki-2 cells (**Figures 1H–I**). We also detected the colocalization of GMFB and Arp2/3, which were known interaction partners of GMFB (**Figures 1H,I**), supporting that GMFB was an intracellular protein.

Correlation of *Gmfb* Expression With Clinical Characteristics of Kidney Renal Clear Cell Carcinoma

The association between *Gmfb* expression and clinical features of KIRC patients is summarized in **Table 2**. T stage ($p < 0.001$), M

TABLE 1 | Clinical characteristics of the kidney renal clear cell carcinoma patients.

Characteristic	Levels	Overall
n		539
T stage, n (%)	T1	278 (51.6%)
	T2	71 (13.2%)
	T3	179 (33.2%)
	T4	11 (2%)
N stage, n (%)	N0	241 (93.8%)
	N1	16 (6.2%)
M stage, n (%)	M0	428 (84.6%)
	M1	78 (15.4%)
Pathologic stage, n (%)	Stage I	272 (50.7%)
	Stage II	59 (11%)
	Stage III	123 (22.9%)
	Stage IV	82 (15.3%)
Gender, n (%)	Female	186 (34.5%)
	Male	353 (65.5%)
Race, n (%)	Asian	8 (1.5%)
	Black or African American	57 (10.7%)
	White	467 (87.8%)
Age, n (%)	≤60	269 (49.9%)
	>60	270 (50.1%)
Histologic grade, n (%)	G1	14 (2.6%)
	G2	235 (44.3%)
	G3	207 (39%)
	G4	75 (14.1%)
OS event, n (%)	Alive	366 (67.9%)
	Dead	173 (32.1%)
Age, median (IQR)		61 (52, 70)

OS, overall survival; IQR, interquartile range.

stage ($p < 0.004$), primary therapy outcome ($p = 0.016$), pathologic stage ($p < 0.001$), gender ($p = 0.002$), histological grade ($p < 0.001$), and OS events ($p < 0.001$) were all significantly associated with *Gmfb* expression.

The differential expression of *Gmfb* was examined according to age, gender, pathologic stage, T classification, N classification, M classification, and histological grade (G) of KIRC patients (**Figure 2**). Expression of *Gmfb* was significantly downregulated in men compared to women ($p = 0.004$) (**Figure 2A**); it was also significantly associated with pathologic stage (stage IV compared to stage I, $p = 0.002$; stage III compared to stage I, $p < 0.001$) (**Figure 2B**), T stage (T3 compared to T1, $p < 0.001$) (**Figure 2C**), M stage (M1 compared to M0, $p = 0.007$) (**Figure 2D**), and histological grade (G4 compared to G2, $p < 0.001$; G3 compared to G2, $p = 0.003$) (**Figure 2E**). There was no significant relationship between *Gmfb* expression and age (**Figure 2F**) or N classification (**Figure 2G**).

Prognostic Value of *Gmfb* Across Kidney Renal Clear Cell Carcinoma

OS analysis showed that *Gmfb* was a low-risk gene in kidney tissue ($p = 0.00018$) (**Figure 3A**). The Kaplan–Meier DFS analysis also demonstrated that patients with high *Gmfb* expression levels survived longer than patients with low *Gmfb* expression ($p = 0.00013$) (**Figure 3B**). Cox OS analysis demonstrated that a significant prognostic difference existed between the high and low *Gmfb* expression groups in both univariate (HR 0.541, 95% CI, 0.397–0.736, $p < 0.001$) and multivariate (HR 0.578, 95% CI, 0.374–0.892; $p = 0.013$) analyses (**Table 3**). A receiver operating characteristic (ROC) curve was used to evaluate the prediction accuracy of intensity. The *Gmfb* score, in terms of the ROC curve, was 0.905 (**Figure 3C**), indicating that *Gmfb* was a very sensitive biomarker for KIRC.

The Sankey diagram further demonstrated the association between age, gender, *Gmfb* expression, and clinical status (**Figure 3D**). Each column represents a characteristic (gender; T, N, and M stages; and expression of *Gmfb*; different colors represent the various states of these characteristics, and lines represent the distribution of the same sample in other characteristic variables). As shown in the diagram, most female and male patients progressed to stage I. Most patients with stage I disease had high *Gmfb* expression and a high survival rate. Conversely, patients with more severe diseases tended to have lower *Gmfb* expression and lower survival rates. A nomogram of OS was constructed to integrate *Gmfb* expression and some prognostic factors, including T, N, and M classifications and age (**Figure 3E**). A higher nomogram score represented worse predictive probability. The calibration curve assessed the performance of the nomogram for *Gmfb*, and the C-index for OS was 0.755 (**Figure 3F**). In conclusion, this nomogram is a good model for predicting the survival of patients with KIRC.

The Effects of Overexpression of *Gmfb* in Caki-2 Cells on Viability, Proliferation, Invasion, and Mitochondrial Membrane Potential

To clarify the association between *Gmfb* expression and cell viability in KIRC, the effects of *Gmfb* OE and knockdown (KD) on the viability of Caki-2 cells were examined. First, we designed three siRNA sequences for *Gmfb*, and KD efficiency was determined in HEK293T by Western blotting. As shown in **Figure 4A**, the siRNA1 with the highest KD efficiency in HEK 293T cells was used for the subsequent experiment (**Figure 4A**). Then, *Gmfb* KD and OE in Caki-2 cells were confirmed by Western blotting (**Figures 4B, C**) and qRT-PCR (**Figures 4D, E**). In parallel, the expression of GMFG protein, a homolog of GMFB, remained unchanged after transfection with *siGmfb* or Gmfb OE plasmid, indicating that *Gmfb* KD specificity was reasonable (**Figures 4F, G**). After transfection with siRNA and OE plasmids at 12, 24, and 48 h, a significant increase in viability after *Gmfb* KD was obtained at 24 h ($p < 0.05$) and 48 h ($p < 0.01$) (**Figure 4H**), while a significant decrease in viability after *Gmfb* OE was observed at 24 h ($p < 0.01$) and 48 h ($p < 0.001$) (**Figure 4I**). These results indicated that GMFB expression level was negatively correlated with tumor cell viability. Moreover, we investigate the effect of altered *Gmfb* expression on the Caki-2 cell cycle. At 48 h post-transfection of *siGmfb* in Caki-2 cells, the expression levels of p21 (CDKN1A) and p27 (CDKN1B) significantly decreased when compared with those in the scramble group (**Figures 4J, K**). The downregulation of p21 and p27 was required for the cellular transition from quiescence to the proliferative state (41). *Gmfb* OE in Caki-2 cells led to a lower number of migrated cells than in the empty vector group

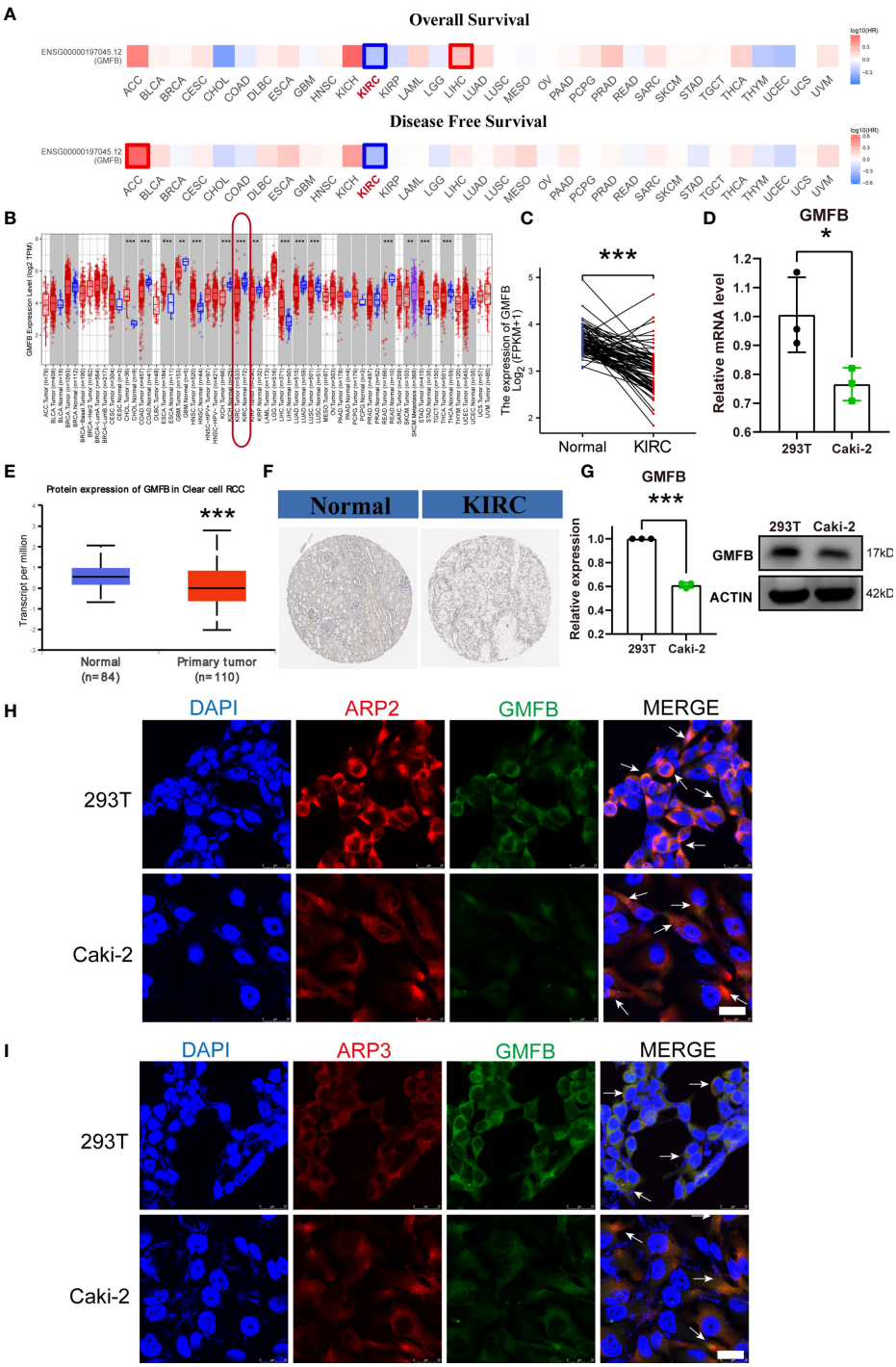

FIGURE 1 | Survival map and differential expression of the mRNA and protein level of GMFB in pan-cancer and KIRC. **(A)** Comparing the survival contribution of GMFB in pan-cancer, estimated using Mantel–Cox test, including overall survival (OS) and disease-free survival (DFS). Tumor types with significant differences (p-value adjustment <0.05) were highlighted. HR, hazard ratio. **(B)** Comparison expression of *Gmfb* mRNA level between tumor and normal tissues (pair samples). **(C)** Comparison expression of *Gmfb* mRNA level between tumor and normal tissues (unpaired samples). **(D)** Comparison expression of *Gmfb* mRNA level between HEK293T and Caki-2 cells tested by RT-qPCR. **(E)** Comparison of GMFB protein level expression between normal and KIRC tumor tissues (unpaired samples). **(F)** Immunohistochemistry images in normal and KIRC tumor tissues. **(G)** Comparison expression of GMFB protein level between 293T and Caki-2 cells tested by Western blotting. **(H)** Colocalization of GMFB with Arp2 in 293T and Caki-2 cells. **(I)** Colocalization of GMFB co-localized with Arp3 in 293T and Caki-2 cells. Scale bar = 25 μm. White arrows indicate co-location. KIRC, kidney renal clear cell carcinoma. Error bars represent SD. *p < 0.05, **p < 0.01, ***p < 0.001.

TABLE 2 | Logistic analysis of the association between *Gmfb* expression and clinical characteristics.

Characteristics	Total (N)	Odds ratio (OR)	p-Value
T stage (T2 and T3 and T4 vs. T1)	530	0.503 (0.356–0.710)	<0.001
Pathologic stage (stage II and stage III and stage IV vs. stage I)	527	0.490 (0.346–0.692)	<0.001
N stage (N1 vs. N0)	255	0.299 (0.082–0.886)	0.041
M stage (M1 vs. M0)	498	0.468 (0.279–0.768)	0.003
Gender (male vs. female)	530	0.511 (0.355–0.734)	<0.001
Age (>60 vs. ≤60)	530	0.941 (0.669–1.323)	0.728
Hemoglobin (low and elevated vs. normal)	450	0.815 (0.559–1.188)	0.287

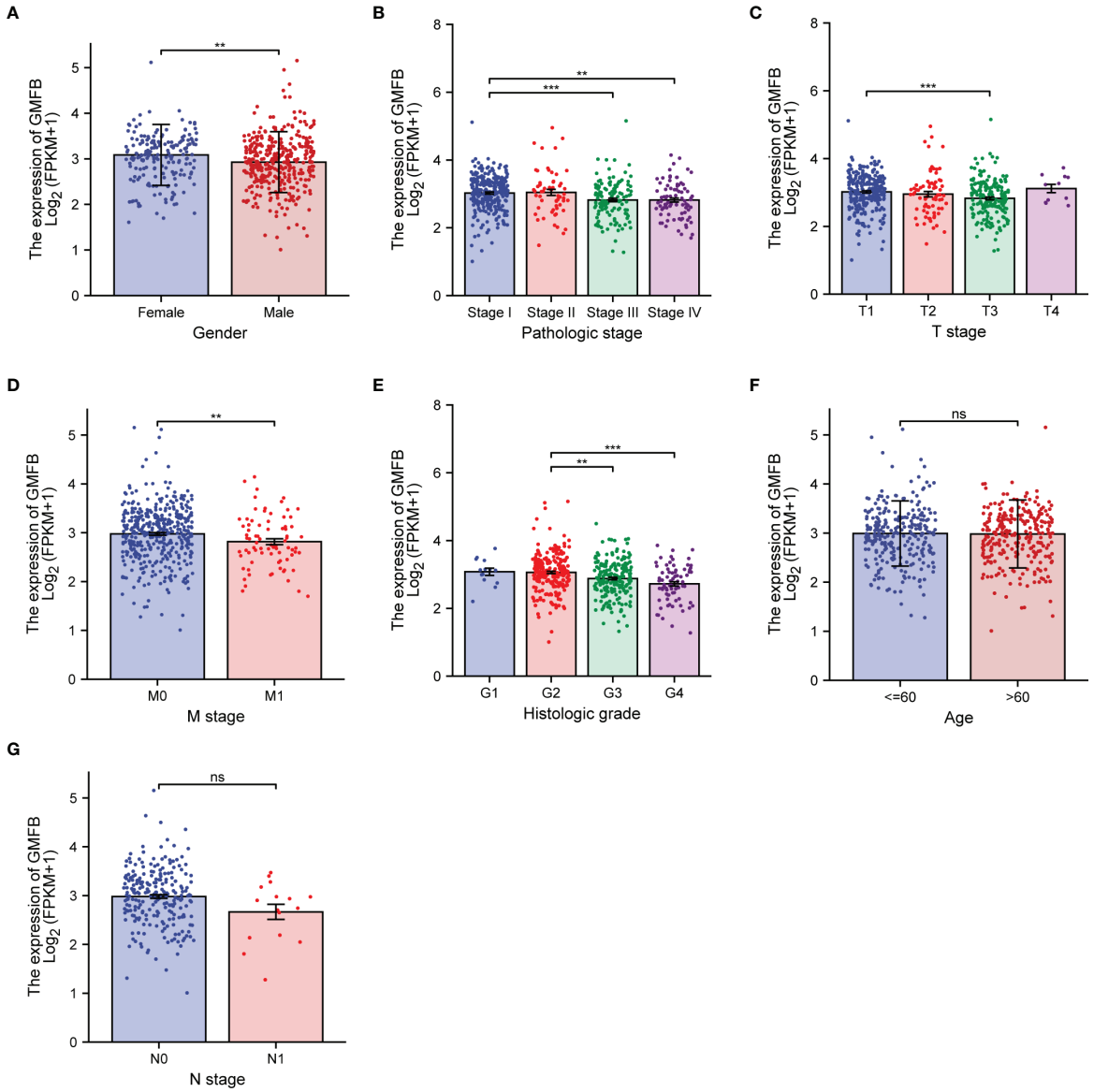

FIGURE 2 | Association between the expression of *Gmfb* and the key clinicopathological characteristics of kidney renal clear cell carcinoma (KIRC). **(A)** Gender. **(B)** Pathologic grade. **(C)** T stage. **(D)** M stage. **(E)** Histologic grade. **(F)** Age. **(G)** N stage. **p < 0.01, ***p < 0.001, ns not significant.

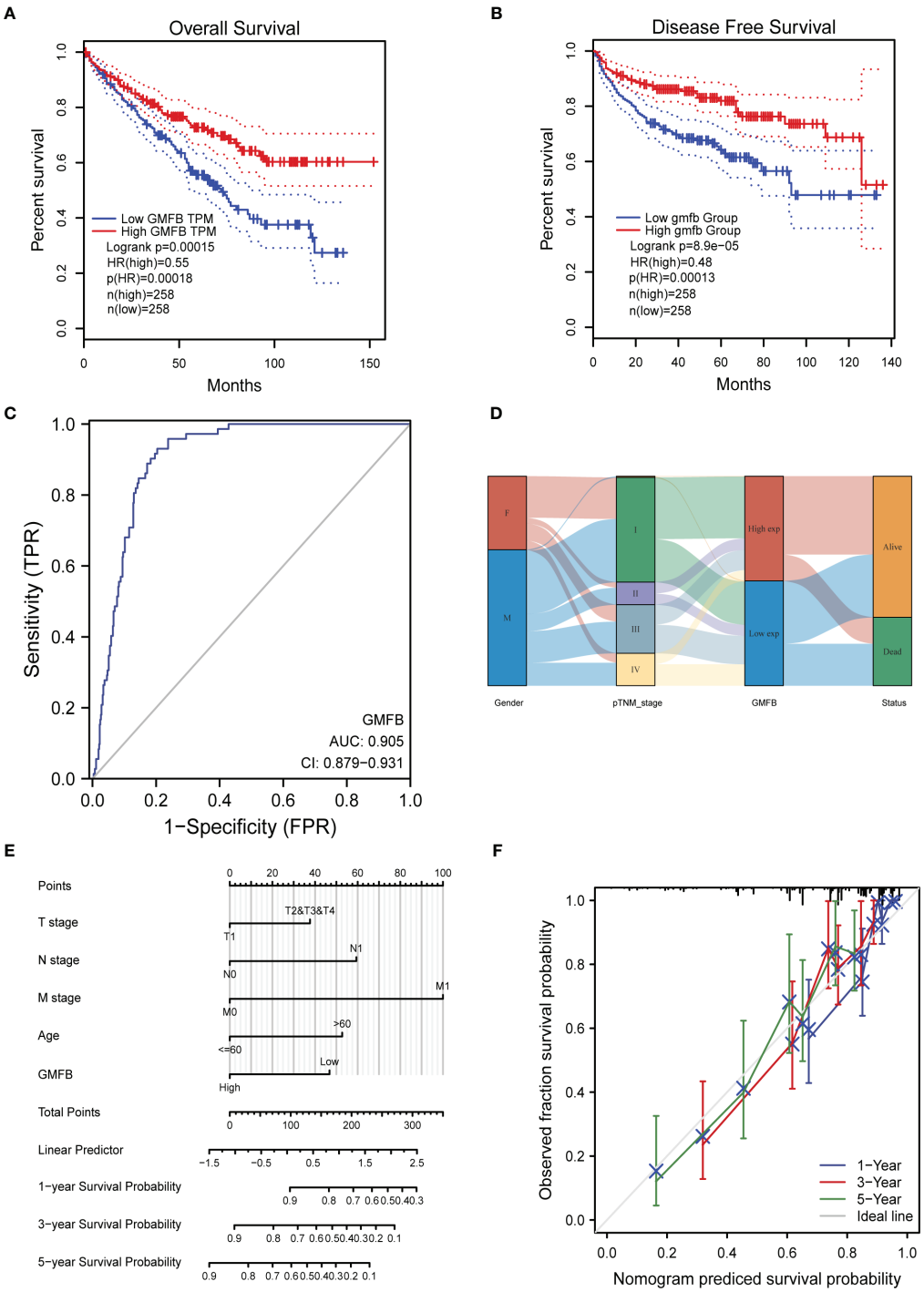

FIGURE 3 | The prognostic value of *GMFB* expression in kidney renal clear cell carcinoma (KIRC). **(A)** Kaplan–Meier survival curves for the effect of *Gmfb* expression on overall survival. **(B)** Kaplan–Meier survival curves for the outcome of GMFB expression on disease-free survival. **(C)** Receiver operating characteristic analysis (ROC) curve of GMFB in KIRC. **(D)** *Gmfb* expression association with different clinical characteristics shown on the Sankey diagram. **(E)** The integrated *Gmfb* and other prognostic factors in KIRC from The Cancer Genome Atlas (TCGA) data by nomogram. **(F)** The calibration curve of the nomogram.

TABLE 3 | Univariate and multivariate Cox proportional hazard analyses of *Gmfb* expression and overall survival (OS) for patients with KIRC.

Characteristics	Total (N)	Univariate analysis		Multivariate analysis	
		Hazard ratio (95% CI)	p-Value	Hazard ratio (95% CI)	p-Value
T stage (T2 and T3 and T4 vs. T1)	530	2.872 (2.063–3.998)	**<0.001**	1.555 (0.936–2.584)	0.088
N stage (N1 vs. N0)	255	3.426 (1.818–6.456)	**<0.001**	2.006 (1.037–3.879)	**0.039**
M stage (M1 vs. M0)	498	4.333 (3.170–5.922)	**<0.001**	3.230 (1.994–5.232)	**<0.001**
Age (>60 vs. ≤60)	530	1.753 (1.290–2.383)	**<0.001**	1.856 (1.211–2.844)	**0.005**
Gender (male vs. female)	530	0.951 (0.697–1.296)	0.750		
GMFB (high vs. low)	530	0.541 (0.397–0.736)	**<0.001**	0.578 (0.374–0.892)	**0.013**

KIRC, kidney renal clear cell carcinoma. Bold values, p < 0,05

(**Figures 4L, M**). Invasion assays showed that *Gmfb* OE inhibited Caki-2 cell invasion (**Figures 4L, N**) and significantly reduced wound closure (**Figures 4O, P**). Detection of MMP using the JC-1 assay revealed a shift from red to green fluorescence in *Gmfb* OE Caki-2 cells (**Figure 4Q**), indicating that a high level of GMFB led to MMP loss. Taken together, we proposed that *Gmfb* was a suppressor gene in KIRC.

Functional Enrichment Analysis of *Gmfb* in Kidney Renal Clear Cell Carcinoma Patients

To elucidate the molecular mechanism of GMFB in KIRC, *Gmfb* co-expressed DEGs were used for functional enrichment analysis. The 3493 DEGs identified based on |log2 fold-change| > 1 (adjusted $p < 0.05$) corresponded to 912 upregulated genes and 2,581 downregulated genes. Detailed information on the DEGs is presented in **Supplementary Table 2**. DEG expression is shown in the volcano plot (**Figure 5A**), and the heatmap exhibits a corresponding hierarchical clustering analysis (**Figure 5B**). The details of the top 10 DEGs with upregulation and downregulation are listed in **Table 4** and **Supplementary Table 3**, respectively. Most of these DEGs have not been reported in previous KIRC studies, except for ALDH6A1 and NCR3LG1. Six DEGs with unknown biological functions and three non-coding RNAs were not identified, including AC003072.1, AC073896.4, AC108673.3, AP001505.1, AC012510.1, AC084036.1, PWAR5, SCARNA10, and SNORA53. Among these, the mRNA levels of seven upregulated and four downregulated DEGs with known functions were further validated by qRT-PCR. Due to the very high cycle threshold values for ZNF196 and SELENOP (38 to 39), we did not redesign the primer for the validation experiment. Consistent with the results of the meta-analysis, INAFM1, HCFC1R1, and METTL26 were downregulated, and ATP6V0D2, TBC1D14, OXCT1, ALDH6A1, FAM160A1, and NCR3LG1 were upregulated in *Gmfb* OE Caki-2 cells (**Figures 5C, D**). The details of the nine validated DEGs are listed in **Table 4**, and the remaining 11 DEGs that were not validated are provided in **Supplementary Table 3**.

The KEGG pathway and GO enrichment analyses using KOBAS are shown in **Figure 6**. The neuroactive ligand–receptor interaction ranked 1 in the top 10 DEGs enriched KEGG pathways, followed by collecting duct acid secretion, linoleic acid metabolism, alpha-linolenic acid metabolism, and mineral absorption (**Supplementary Figure 1A**). GO enrichment analysis showed that cornification, extracellular region, and serine-type endopeptidase activity were the most enriched terms in biological process (BP), cellular compartment (CC), and molecular function (MF) categories, respectively (**Supplementary Figure 1B** and **Supplementary Table 4**). The top ten enriched KEGG pathways, GO terms, and the heatmap of associated DEGs are shown in **Figures 6A–D** (upregulated DEGs) and **Figures 6E–H** (downregulated DEGs). Upregulated DEGs were most enriched in collecting duct acid secretion (KEGG pathway), cellular protein metabolic process (BP category of GO), an integral component of the plasma membrane (CC of GO), and serine-type endopeptidase activity (MF of GO) (**Figures 6A–D**). Downregulated DEGs were most enriched in mineral absorption (KEGG pathway), cornification (BP of GO), extracellular region (CC of GO), and antigen-binding (MF of GO) (**Figures 6E–H**). There was more overlap in the KEGG pathway and GO analyses between total DEGs and downregulated DEGs than between upregulated DEGs, indicating that the downregulated DEGs may play a more critical and dominant role in KIRC. To this end, we selected five genes involved in the mineral absorption pathway (MT2A, 1G, 1F, TF, and S100G) for qRT-PCR validation of the RNA-seq results. The qRT-PCR revealed that MT2A, MT1G, and MT1F were downregulated, whereas S100G and TF did not show a significant change in *Gmfb* OE Caki-2 cells (**Figures 6I, J**).

To clarify the links between terms, PPI network and MCODE component analyses of the top 2,000 DEGs (**Supplementary Figure 1C**), upregulated (**Figure 7A**) and downregulated (**Figure 7B**), were performed using Metascape. **Supplementary Table 5** provides detailed data. The PPI network showed that the predominant GO annotations of MCODE1 were cornified envelopes and keratinization in the total DEGs. Among the DEGs associated with upregulated *Gmfb*, GO annotations of MCODE1 were mainly linked with nucleosome assembly, nucleosome organization, and chromatin assembly. Among the DEGs related to downregulated *Gmfb*, GO annotations of MCODE1 were specifically associated with G-protein-coupled receptor (GPCR) downstream signaling, GPCR signaling, and GPCR ligand binding (**Supplementary Table 5**).

Identification of Hub Genes Using STRING and Cytoscape

Upregulated DEGs were projected separately into the human PPI network in the STRING database, and the hub genes were filtered

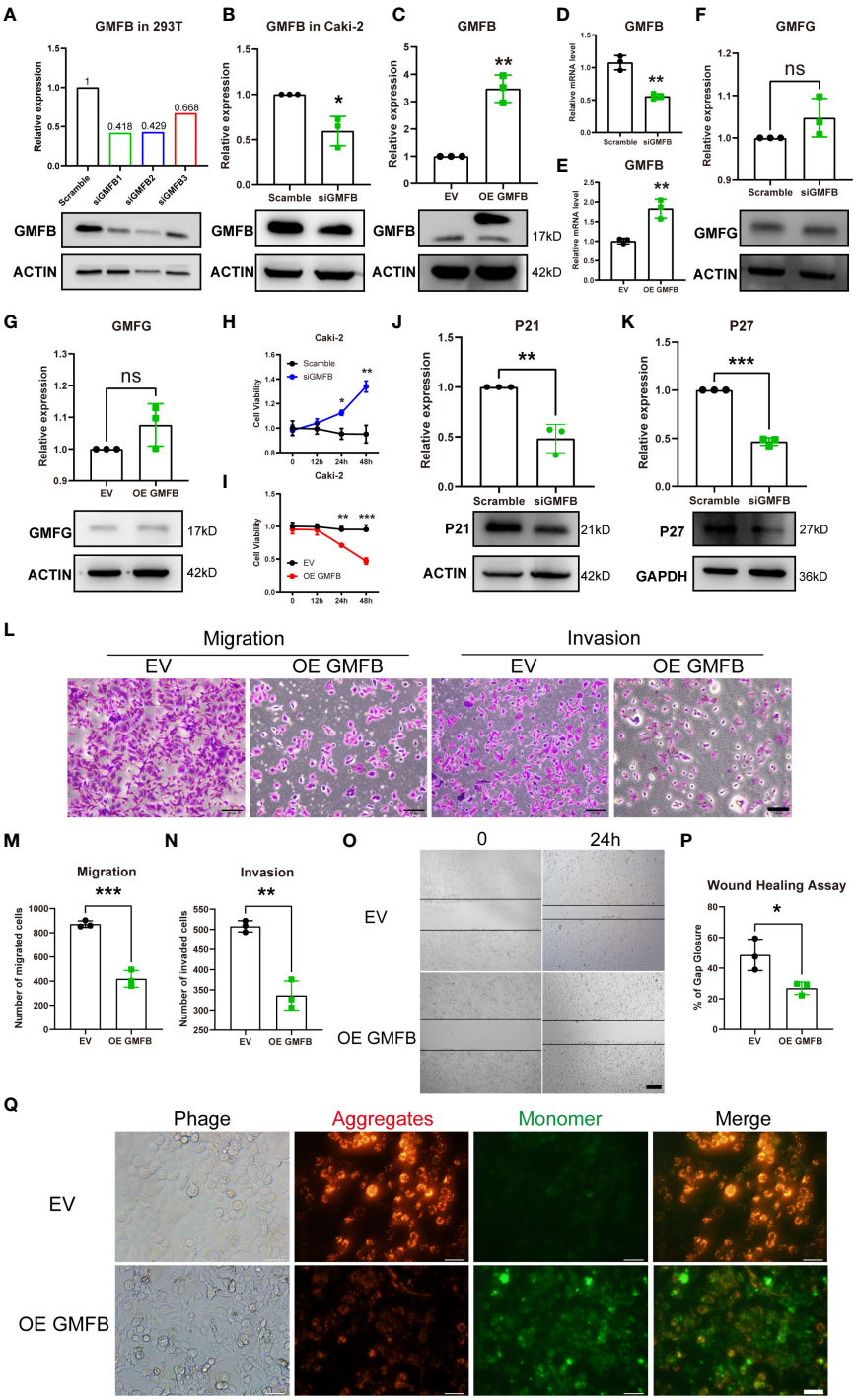

FIGURE 4 | The effects of *Gmfb* knockdown and *Gmfb* overexpression on proliferation, migration, and invasion in Caki-2 cells. **(A)** The knockdown efficiency of three pairs of *siGmfb* was tested by Western blotting in HEK 293T cells. **(B–E)** GMFB silencing RNA and overexpression *Gmfb* plasmid efficiency were tested by Western blotting and RT-qPCR in Caki-2 cells. **(F, G)** GMFG protein level was tested by Western blotting after Caki-2 cells were transferred with siRNA and overexpression plasmid of GMFB. **(H, I)** Cell viabilities were determined after Caki-2 cells were transferred with siRNA and overexpression plasmid of *Gmfb* by CCK8 assay at 12, 24, and 48(h) **(J, K)** The extent of the cell cycle was further determined by CDKN1A (p21) and CDKN1B (p27) using Western blotting. **(L)** Transwell migration and invasion assays were used to examine the migration and invasion ability of Caki-2 cells. Scale bar = 50 μm. **(M, N)** Quantification of migration and invasion assays. **(O)** Image of the scratch assay. Scale bar = 100 μm. **(P)** Quantification of the scratch assay. **(Q)** Fluorescence microscopy imaging of Caki-2 cells stained with JC-1. Scale bar = 50 μm. Error bars represent SD. *p < 0.05, **p < 0.01, ***p < 0.001.

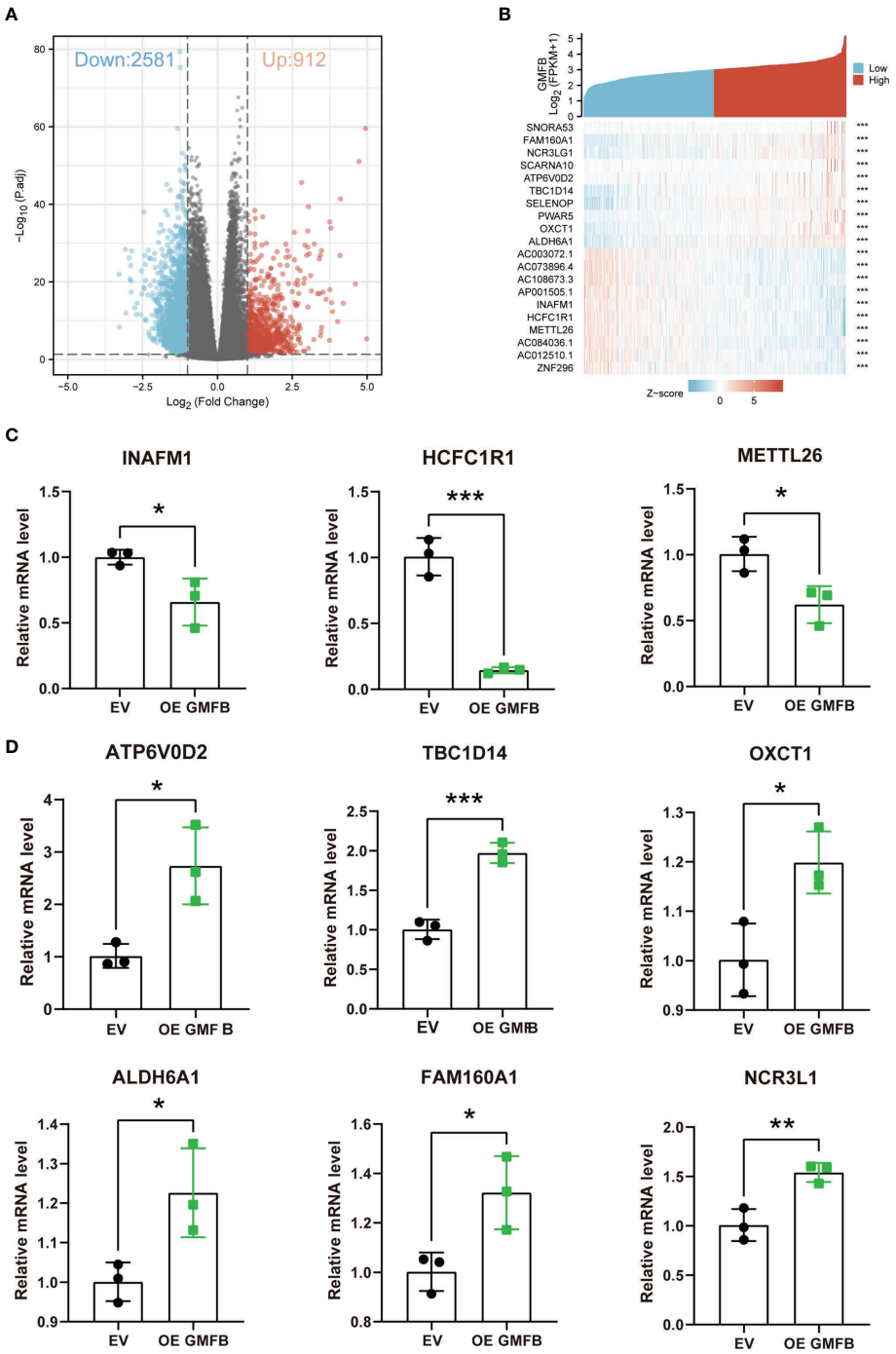

FIGURE 5 | The identification of DEGs. **(A)** Volcano plot of differentially expressed genes (DEGs). **(B)** Heatmap of DEGs. **(C)** Downregulated DEGs (INAFM1, HCFC1R1, and METTL26) were determined by RT-qPCR. **(D)** Upregulated DEGs (ATP6V0D2, TBC1D14, OXCT1, ALDH6A1, FAM160A1, and NCR3LG1) were determined by RT-qPCR. Error bars represent SD. *p < 0.05, **p < 0.01, ***p < 0.001.

using the MCC algorithm (**Figure 8**). The details of the top ten hub genes are shown in **Supplementary Table 6**. The top six upregulated hub genes (HIST1H2BB, HIST1H1A, HIST1H4F, HIST1H3J, HIST2H2AB, and HIST1H1B) (**Figure 8B**) belong to the histone cluster family and are mainly involved in nucleosome assembly, nucleosome organization, and chromatin assembly. The top ten downregulated hub genes included SPRR1B, SPRR1A, IVL, SPRR3, SPRR2A, TGM1, SPRR2D, SPRR2E,

TABLE 4 | The significant DEGs with validation.

Gene symbol	p adj	Gene ID	Published role in KIRC	Function	Correlation with GMFB in meta-analysis	Validation in Caki-2
INAFM1	6.27E−53	255783	NOT	Predicted to be an integral component of membrane	Negative	Negative
HCFC1R1	8.32E−51	54985	NOT	Regulating HCFC1 activity by modulating its subcellular localization	Negative	Negative
METTL26	3.24E−50	84326	NOT	Diseases associated with METTL26 include anauxetic dysplasia 1	Negative	Negative
ATP6V0D2	4.02E−40	245972	NOT	Predicted to be involved in vacuolar acidification and vacuolar transport. Located in the apical plasma membrane. Part of vacuolar proton-transporting V-type ATPase complex	Positive	Positive
TBC1D14	3.95E−39	57533	NOT	Enabling protein kinase binding activity. Involved in negative regulation of autophagy, recycling endosome to Golgi transport, and regulation of autophagosome assembly	Positive	Positive
OXCT1	4.44E−37	5019	NOT	Key enzyme for ketone body catabolism. Transfers the CoA moiety from succinate to acetoacetate	Positive	Positive
ALDH6A1	2.68E−36	4329	PMID:33686951 PMID:32737333 PMID:30793530	Playing a role in valine and pyrimidine metabolism. Binds fatty acyl-CoA	Positive	Positive
FAM160A1	3.20E−33	729830	NOT	Involved in protein localization to perinuclear region of cytoplasm	Positive	Positive
NCR3LG1	4.93E−33	374383	PMID:31921143	Interaction of B7H6 with NK p30 results in natural killer (NK) cell activation and cytotoxicity	Positive	Positive
ZNF296	1.04E−46	162979	NOT	Enabling sequence-specific double-stranded DNA binding activity	Negative	NA
SELENOP	5.77E−38	6414	NOT	Might be responsible for some of the extracellular antioxidant defense properties of selenium or might be involved in the transport of selenium	Positive	NA

DEGs, differentially expressed genes; KIRC, kidney renal clear cell carcinoma. NA, Not Available

PI3, and CASP14 (**Figure 8D**). Except for CASP14 and TGM1, these genes were mainly associated with keratinization, and none has been reported in KIRC. These results suggest that GMFB may play a vital role in modulating nucleosome structure, cellular senescence, mitotic prophase, and keratinization in KIRC.

Correlation Between *Gmfb* Expression, Immune Cell Infiltration, and Prognostic Value of Tumor-Infiltrating Immune Cells in Kidney Renal Clear Cell Carcinoma

Based on the importance of TME, the relationship between immunity and *Gmfb* expression was further explored. Tumor RNA-seq data (retrieved from TCGA) of 33 different tumor patients and matched normal tissue samples from the Genomic Data Commons (GDC) website were downloaded to analyze the relationship between *Gmfb* expression and 22 types of TIICs. The heatmap of KIRC and LIHC analysis indicated *Gmfb* mRNA expression significantly correlated with TIICs (**Figure 9A**). The analysis by CIBERSORTx showed that the *Gmfb* mRNA expression positively correlated with the infiltration of T CD4+ memory resting cells (p = 0.00007, R = 0.172), monocytes (p = 5.68E−06, R = 0.196), mast resting cells (p = 0.047, R = 0.086), mast activated cells (p = 0.0017, R = 0.136), macrophage M2 cells (p = 1.81E−09, R = 0.257), macrophage M1 T cells (p = 0.0028, R = 0.13), eosinophil (p = 7.74E−11, R = 0.278), and B naïve cells (p = 9.95E−08, R = 0.229) but negatively correlated with the infiltration of regulatory T cells (Tregs) (p = 1.09E−31, R = −0.479), T follicular helper cells (TFH) (p = 1.43E−15, R = −0.337), T CD8+ cells (p = 4.97E−14, R = −0.319), natural killer activated cells (p = 7.42E−13, R = −0.305), B plasma cells (p = 0.0058, R = −0.12), and B memory cells (p = 0.00001, R = −0.185) (**Figure 9A**). However, our previous work showed that higher expression levels of *Gmfb* predicted poor prognostic outcomes in LIHC (26). To explore the possible mechanism underlying the differential effects of *Gmfb* on LIHC and KIRC, the correlation between *Gmfb* expression and TIIC in LIHC was analyzed. As shown in **Supplementary Figure 2**, the infiltration of B memory cells, mast activated cells, and neutrophils was significantly increased in LIHC (**Supplementary Figures 2A–B**) and was uniformly correlated with worse OS (**Supplementary Figures 2C–E**). None of these three immune cell types affected the OS of KIRC patients (**Supplementary Figure 3**). Moreover, the levels of B memory cells, mast activated cells, and neutrophils did not correlate significantly with *Gmfb* expression in the LIHC group (**Figure 9A**).

The association between TIICs and KIRC tumor tissues was examined. The relationship between the 22 TIICs and KIRC prognosis was investigated using GEPIA2021. The Kaplan–Meier survival curves ($p < 0.05$) are shown in **Figures 9B–F**, and further results are summarized in **Supplementary Figure 3**. The fractions of macrophages M2 cells (p = 0.05) and resting mast cells (p = 0.000403) were associated with improved survival (**Figures 9B, C**), but high levels of TFH cells (p = 0.05), Tregs (p = 0.00138), and B plasma cells (p = 0.00844) were associated with worse outcomes (**Figures 9D–F**).

Taken together, the higher expression of *Gmfb* in KIRC predicted a better prognosis, partially due to the optimal TME.

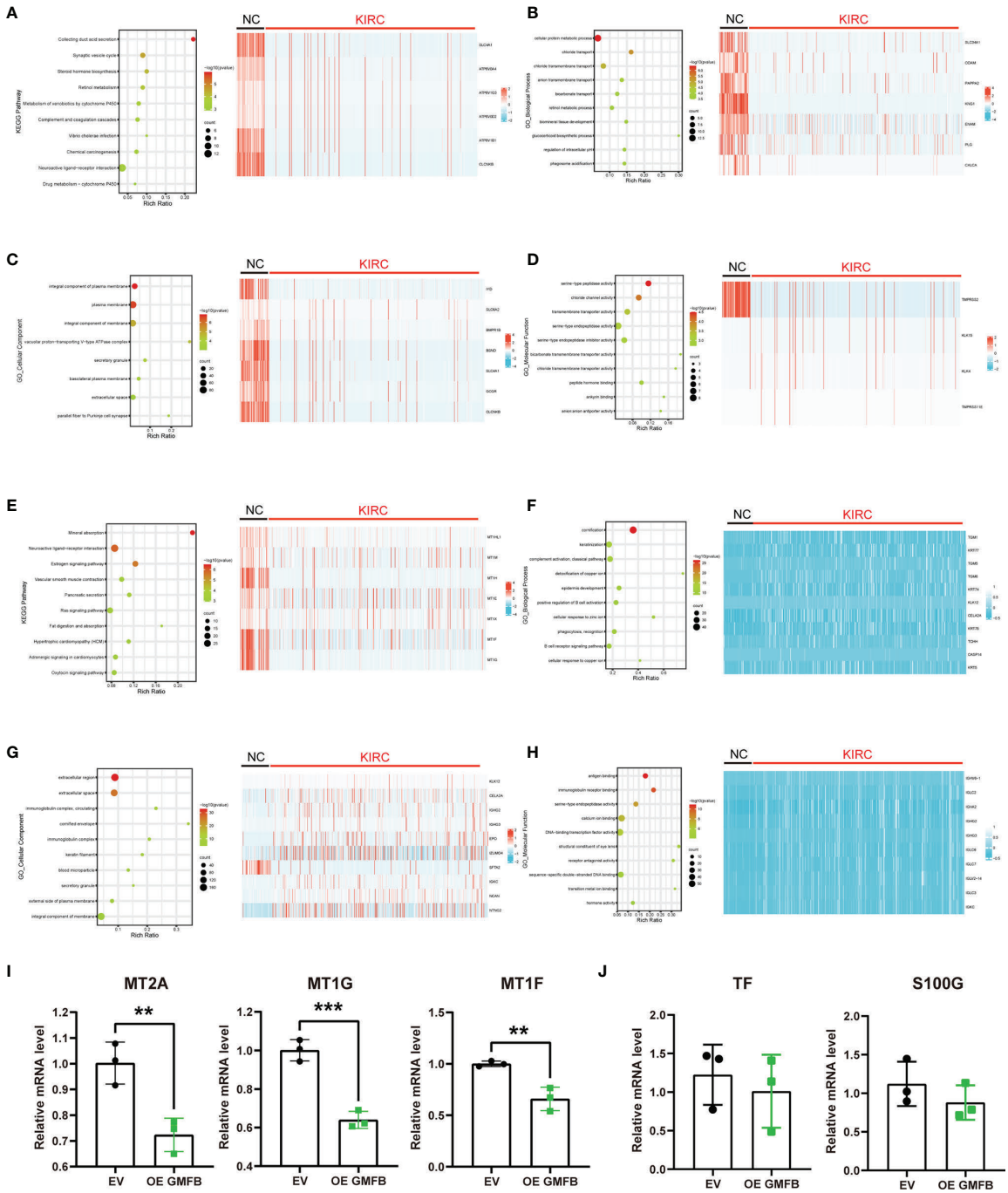

FIGURE 6 | Differentially expressed genes with *Gmfb* in significant Kyoto Encyclopedia of Genes and Genomes (KEGG) pathway and Gene Ontology (GO) term analyses in kidney renal clear cell carcinoma (KIRC). **(A)** Significant KEGG pathways of 958 upregulated differentially expressed genes (DEGs) and the heatmap of genes in the first pathway collecting duct acid secretion. **(B)** Enriched GO-BP terms in 958 upregulated DEGs and the heatmap of genes in the first term cellular protein metabolic process. **(C)** Enriched GO-CC terms in 958 upregulated DEGs and the heatmap of genes in the first term integral component of the plasma membrane. **(D)** Enriched GO-MF terms in 958 upregulated DEGs and the heatmap of genes in the first term serine-type peptidase activity of **(G, E)** Significant KEGG pathways of 2,581 downregulated DEGs and the heatmap of genes in the first pathway mineral absorption. **(F)** Enriched GO-BP terms in 2,581 downregulated DEGs and the heatmap of genes in the first term cornification. **(G)** Enriched GO-CC terms in 2581 downregulated DEGs and the heatmap of genes in the first term extracellular region. **(H)** Enriched GO-MF terms in 2,581 downregulated DEGs and the heatmap of genes in the first term antigen binding. **(I, J)** The downregulated DEGs of mineral absorption were determined by RT-qPCR. **(I)** MT2A, MT1G, and MT1F had a significant difference. **(J)** TF and S100G had no significant difference. Error bars represent SD. $^{**}p < 0.01$, $^{***}p < 0.001$.

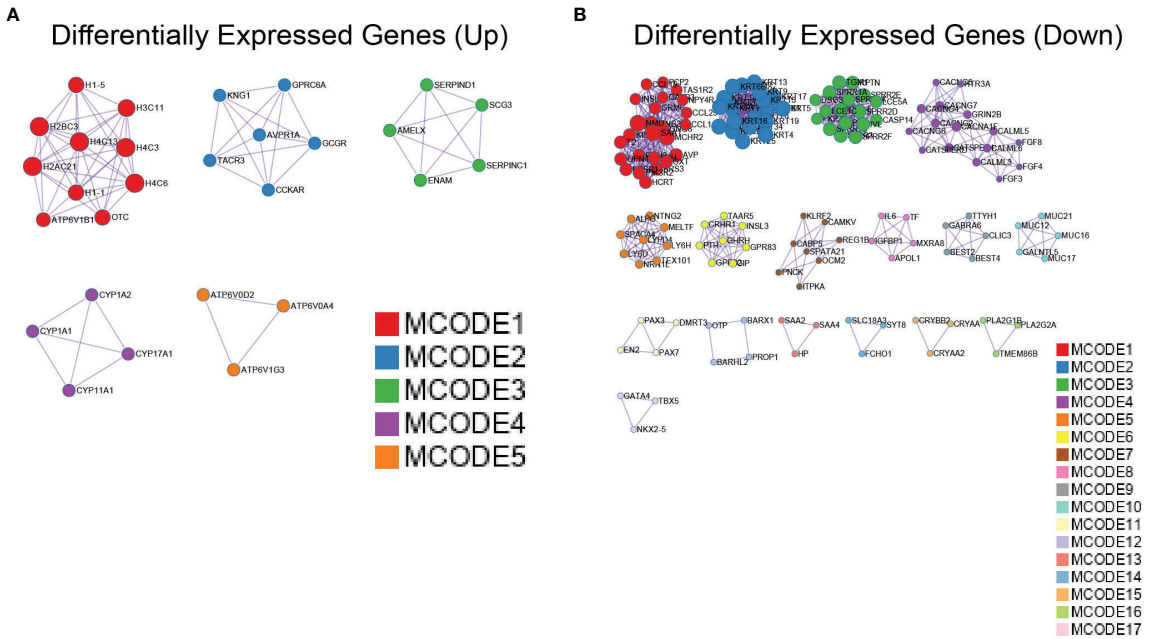

FIGURE 7 | Protein–protein interaction (PPI) network of differentially expressed genes (DEGs) with *Gmfb* in kidney renal clear cell carcinoma (KIRC) by Metascape. **(A)** Upregulated DEGs. **(B)** Downregulated DEGs.

DISCUSSION

KIRC is a cancer with high prevalence and mortality (3). However, it can be diagnosed early and successfully treated with surgical or ablative strategies; up to a third of cases present with or develop metastases (42). Thus, a deeper understanding of the molecular mechanisms underlying KIRC is needed. The present study integrated different KIRC databases with suitable meta-analysis approaches, identified GMFB as a novel independent prognostic biomarker, positively correlated with OS and DFS in KIRC patients, and further dissected the possible contribution of GMFB-relevant TME to good clinical outcomes in KIRC patients.

Two studies have shown that GMFB is a prognostic biomarker for astrocytomas (43) and serous ovarian cancers (44). However, using GEPIA2.0 and TCGA in pan-cancer analysis, we failed to obtain consistent results with previous reports (data not shown), possibly due to dynamic updates of the cancer database with increasing sample data deposition. We previously found that *Gmfb* KD significantly inhibited the proliferation, migration, and invasion of Hep3B cells, and higher *Gmfb* expression predicted a poor prognosis in LIHC (24). In the present study, a completely distinct relationship between *Gmfb* and OS/DFS in KIRC was obtained; namely, higher expression of GMFB was associated with a better prognosis for KIRC patients (**Figure 3**). To confirm the meta-analysis results, *Gmfb* KD and OE were performed in Caki-2 cells. We found that *Gmfb* KD promoted cell viability partly due to the downregulation of p21 and p27 protein levels in Caki-2 cells (**Figures 4J, K**). The downregulation of p21 and p27 protein levels indicated the transition of the cell cycle from quiescent to proliferation (41). Moreover, *Gmfb* OE inhibited the proliferation, migration, and decreased MMP in Caki-2 cells, and when MMP was disturbed, reactive oxygen species caused the oxidation of mitochondrial pores (45). Taken together, the *in vitro* results support that high expression of GMFB is beneficial for KIRC patients' survival. The distinct molecular mechanisms underlying GMFB in LIHC and KIRC merit further investigation.

To reveal the molecular mechanism underlying *Gmfb* effects in KIRC, we enriched the DEGs with *Gmfb* co-expression for bioinformatics analysis. KEGG pathway and GO analyses were performed for the top 2,000 downregulated and upregulated DEGs. We validated nine significant DEGs. Consistent with the results from the meta-analysis, INAFM1, HCFC1R1, and METTL26 were downregulated, and ATP6V0D2, TBC1D14, OXCT1, ALDH6A1, FAM160A1, and NCR3LG1 were upregulated in GMFB overexpressed Caki-2 cells (**Figures 5C, D**). The validated DEGs with GMFB co-expression may participate in multiple pathways in KIRC biology, including enhancing response in KIRC cell to NK cell (NCR3LG1) (46), negatively regulating autophagy (TBC1D14) (47), and being regulated by lactate (ATP6V0D2) (48) in TMEs.

In the upregulated pathways, collecting duct acid secretion was the most enriched, containing DEGs ATP6V0A4, ATP6V1G3, ATP6V0D2, ATP6V1B1 (vacuolar proton pump subunit), SLC4A1 (chloride/bicarbonate exchanger), and CLCNKB (voltage-gated chloride channels). Lower CLCNKB expression has been reported in renal cancer (49). We hypothesized that the upregulated collecting duct acid secretion might play a role in maintaining acid–base homeostasis in the renal tubule.

Mineral absorption, neuroactive ligand–receptor interaction, and estrogen signaling in the downregulated panel were the three most enriched pathways (**Figure 6E**). Metallothionein (MT)

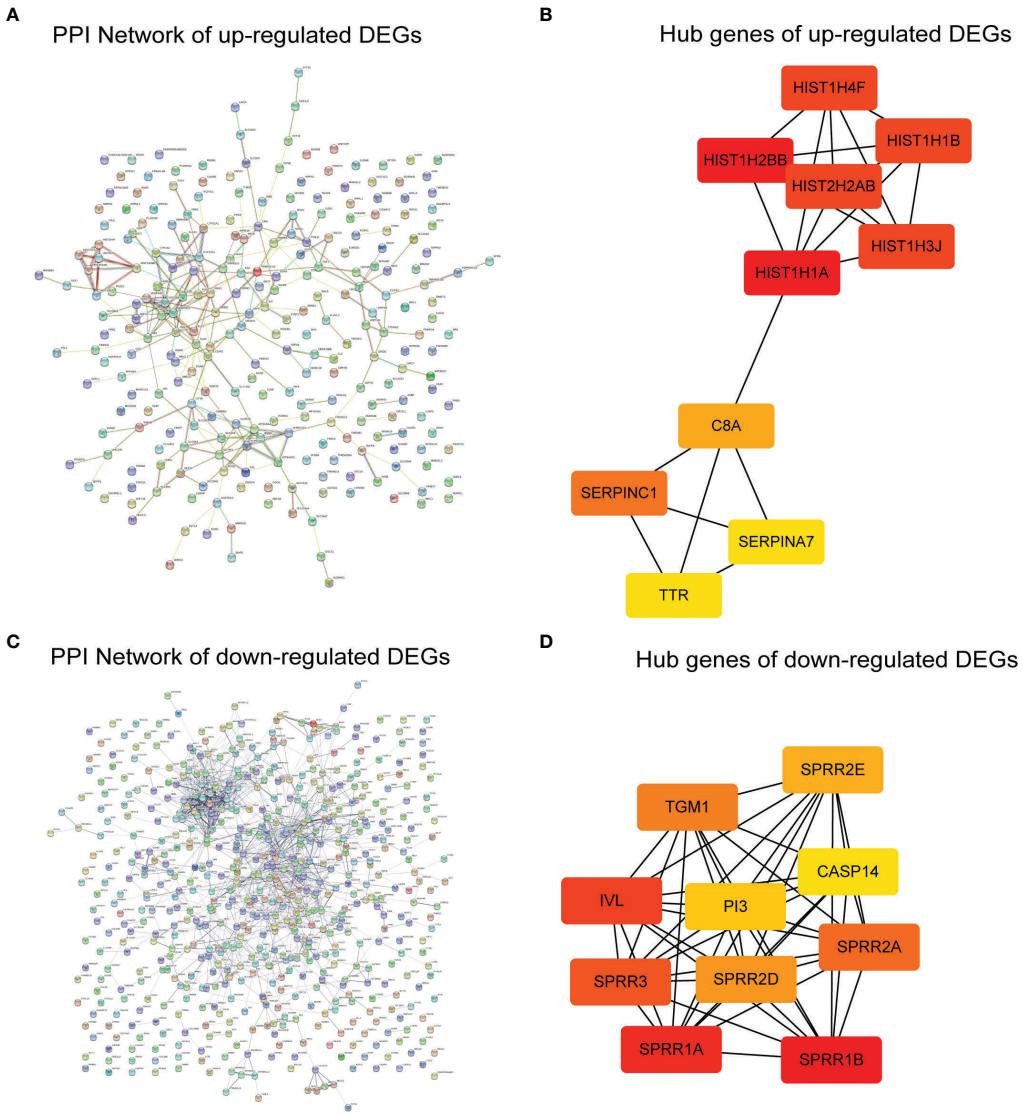

FIGURE 8 | Identification of hub genes. **(A)** The protein–protein interaction (PPI) network was constructed with upregulated differentially expressed genes (DEGs). **(B)** The hub genes identified with Cytoscape for upregulated DEGs. **(C)** The PPI network was constructed with downregulated DEGs. **(D)** The hub genes identified with Cytoscape for downregulated DEGs.

proteins, such as MT1A, B, E, G, F, H, 349 HL1, X, M, MT2A, TF, and S100G, were enriched in the mineral absorption pathway. MTs have a high content of cysteine residues that bind various heavy metals. In this family, MT1A, B, E, G, F, H, HL1, X, M, MT2A, TF, and S100G (vitamin D-dependent calcium-binding protein) are enriched in the mineral absorption pathway. The dysregulation of MTs in renal cell cancer has also been reported. The toxic metals cadmium and lead are associated with renal cell cancer progression (50). A decrease in MT levels in renal cell cancer has also been reported (51). In the present study, we conducted qRT-PCR to validate some of the mRNA levels of several MTs in Caki-2 cells. The results showed that MT2A, MT1G, and MT1F were downregulated, but S100G and TF did not show a significant change in *Gmfb* OE Caki-2 cells (**Figure 6I**). This indicates that low expression of *Gmfb* may lead to increased circulating levels of toxic heavy metals, thus contributing to the progression of KIRC. Currently, there are no relevant reports on S100G and TF in KIRC, and their role, therefore, remains unclear. Cornification, keratinization, and the classical complement activation pathway were significantly enriched in the BP category of GO. There were 23 shared genes between the BP terms cornification and keratinization (**Supplementary Table 7**). Only CK7 (52, 53) and AE1AE3 (54) cytokeratins have been examined in KIRC. The fundamental functions of other cornification-related genes remain elusive, probably implicating

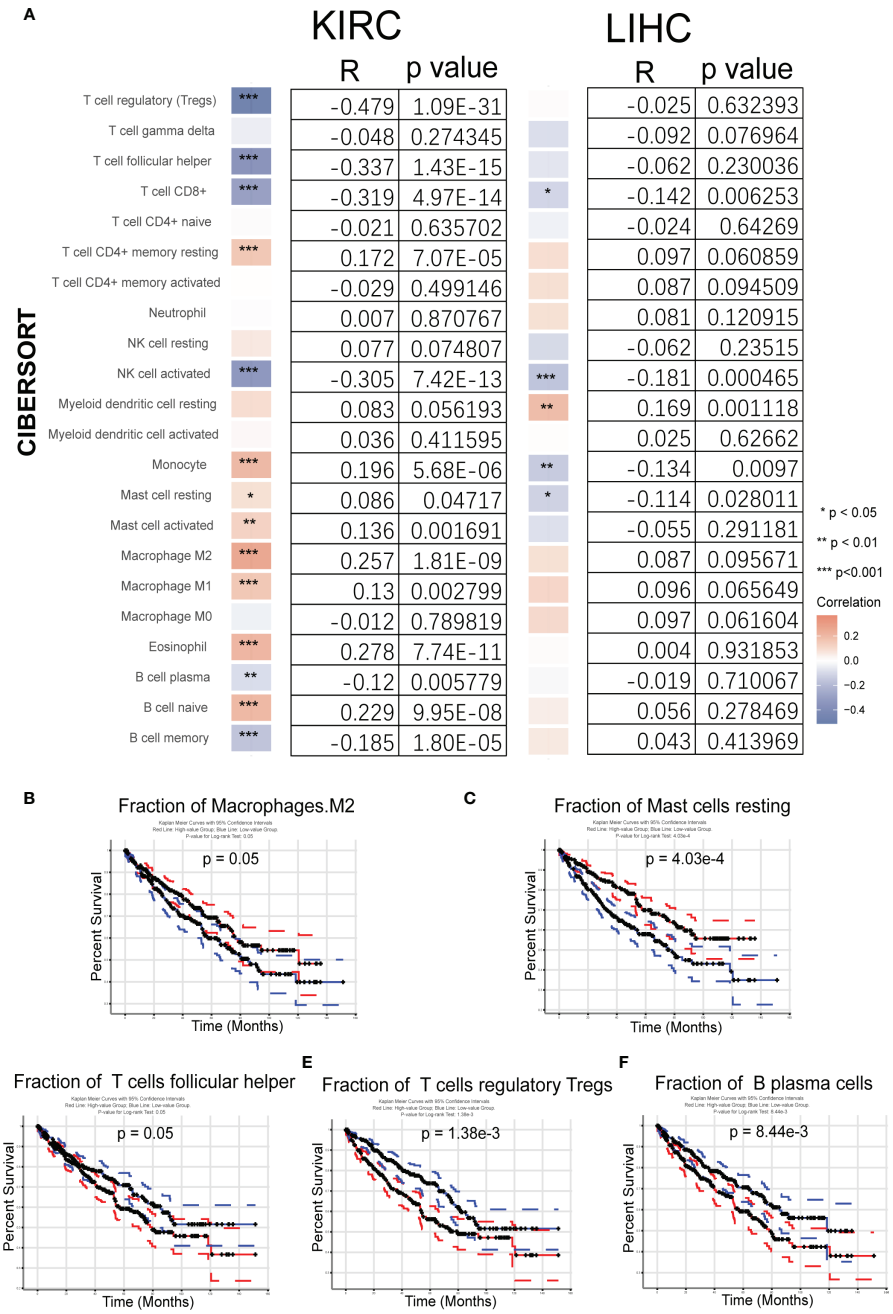

FIGURE 9 | Analysis of the fraction of tumor-infiltrating immune cells (TIICs) in kidney renal clear cell carcinoma (KIRC) and liver hepatocellular carcinoma (LIHC). **(A)** Correlation between 22 tumor-infiltrating immune cells and *Gmfb* expression in KIRC and LIHC samples from The Cancer Genome Atlas (TCGA). **(B–F)** Kaplan–Meier survival curves for TIICs on overall survival. **(B)** Macrophages M2, **(C)** resting mast cells, **(D)** T help cells, **(E)** regulatory T cells (Tregs), and **(F)** plasma cells. *p < 0.05, **p < 0.01, ***p < 0.001

an alteration of epithelial and mesenchymal immunophenotypes for KIRC, which requires further investigation. KOBAS-based GO enrichment analysis revealed downregulated DEGs in the extracellular region, extracellular space, and Ig complex circulating GO-CC category (**Figure 6G**). Most genes in the extracellular region (**Supplementary Table 4**) encode MMPs, cytokines, chemokines, growth factors, and others. These results, combined with the DEGs enriched in GO-MF (antigen binding, Ig receptor binding, and serine-type endopeptidase activity) (**Figure 6H**), suggest cell–cell interactions.

Analyzing PPI networks is increasingly recognized as meaningful to characterize the underlying biology of genes associated with complex diseases (55). As shown in **Figure 8**, histone cluster family members were enriched in CytoHubba with

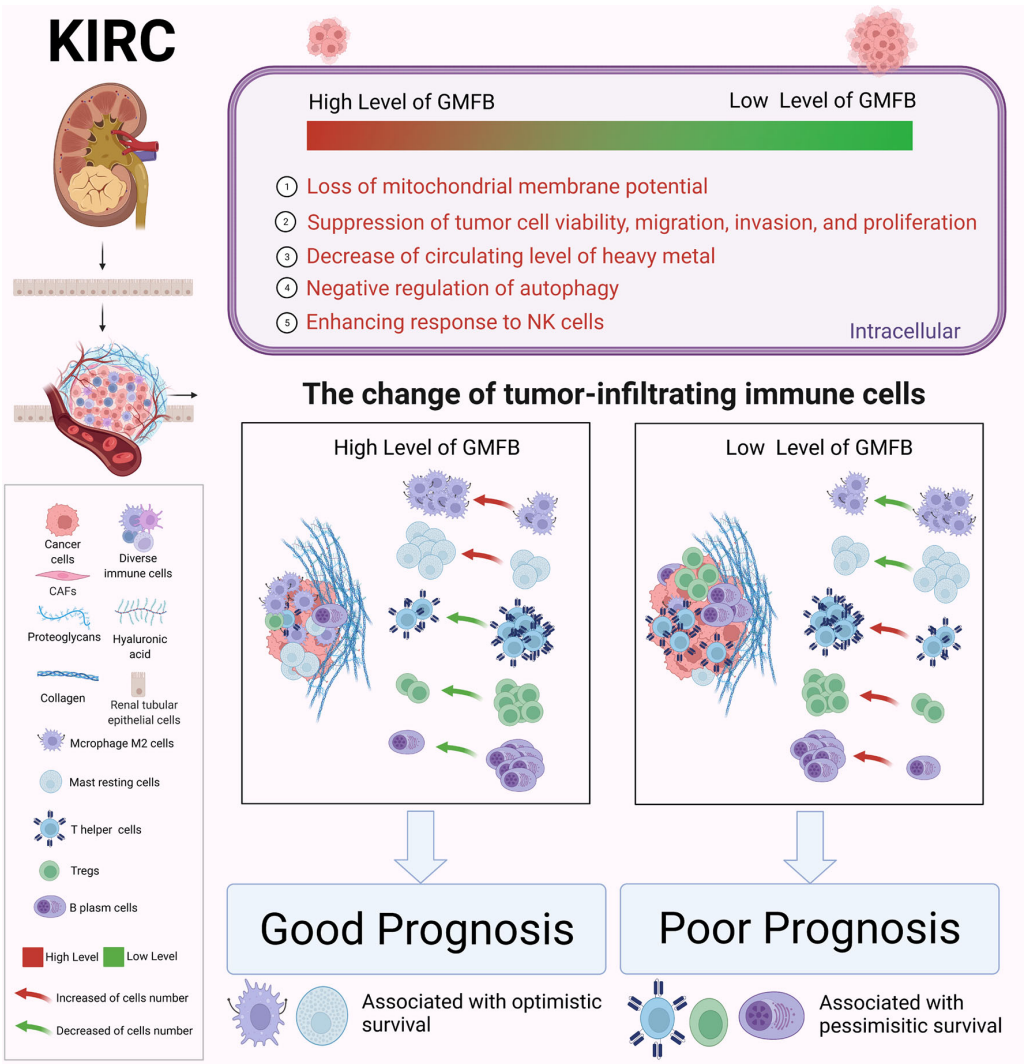

FIGURE 10 | Schematic molecular mechanism of GMFB in the development of kidney renal clear cell carcinoma (KIRC). Created with BioRender.com.

upregulated DEGs (**Figure 8B**), and the formation of the cornified envelope was enriched in CytoHubba with downregulated DEGs (**Figure 8D**). The former is possibly linked to epigenetic regulation in KIRC. In contrast, the latter may contribute to metastasis by disrupting the formation of the cornified envelope, which requires further validation.

The actual context of KIRC is quite diverse due to intratumoral or intertumoral TME heterogeneity. The enriched pathways and GO terms, including extracellular region and neuroactive ligand–receptor binding, encouraged us to analyze the *Gmfb*-relevant TME.

TME is a complex ecosystem, and it plays a crucial function in cancer progression and response to immunotherapy (7, 56). The TME is composed of adaptive immune cells (T and B lymphocytes) and innate immune response cells (including dendritic cells, mast cells, macrophages, neutrophils, myeloid-derived suppressor cells, and natural killer cells) as well as cancer cells and stroma (i.e., endothelial cells, fibroblasts, pericytes, and mesenchymal cells) (56). Immune and inflammatory responses are strongly associated with survival outcomes in patients with KIRC. Zhang et al. recently revealed insights into the TME in KIRC using single-cell sequencing technology (57) and elucidated an active role for tumor epithelia in promoting immune cell infiltration. In contrast, the immune cell composition in the TME may impact clinical outcomes. Infiltration by CD8+ T cells is associated with a worse prognosis in KIRC (58). CCR4 has been identified as a TME target for renal cancer (59). In the present study, we further integrated the OS data obtained from GEPIA2021 with the results of CIBERSORTx. We found a significant association between GMFB-associated immune cells and OS in patients with KIRC. A significant correlation between GMFB expression and KIRC is shown in **Figure 9A**. GMFB expression was positively correlated with macrophage M2 cells and resting mast cells but negatively associated with T follicular

helper cells, Tregs, and plasma cells (**Figure 9A**). In addition, high levels of M2 macrophages (p = 0.05) and resting mast cells (p = 0.000403) favored a better prognosis (**Figures 9B, C**), while high levels of TFH cells (p = 0.05), Tregs (p = 0.00138), and plasma cells (p = 0.00844) caused deleterious clinical outcomes in patients with KIRC (**Figures 9D–F**). We summarized the role of *Gmfb* and *Gmfb*-related TME in KIRC in **Figure 10**.

The *Gmfb*-related TME in LICH was analyzed. Unexpectedly, the *Gmfb*-related TME in LIHC was quite different from that in KIRC (**Supplementary Figure 2**). Thus, we speculated that the distinct effects of *Gmfb* expression on the OS of LIHC and KIRC patients might be due to different immune cell infiltration.

This study had several limitations. The first one was mainly based on bioinformatics analysis, especially datasets from bulk RNA-seq, and lacked validation experiments with human KIRC samples. Secondly, the *Gmfb*-related TME also needed to be validated with human KIRC samples. The critical molecular signatures identified in KIRC merit further clinical investigation.

In conclusion, our study demonstrated that GMFB could be considered a novel independent prognostic biomarker for KIRC. Modulation of the TME in KIRC by GMFB intervention may represent a novel immunotherapeutic strategy for KIRC and probably improve clinical outcomes.

DATA AVAILABILITY STATEMENT

The datasets presented in this study can be found in online repositories. The names of the repository/repositories and accession number(s) can be found in the article/**Supplementary Material**.

AUTHOR CONTRIBUTIONS

LL, GX, and JW conceived, developed, and mentored the project. TZ designed the study, performed the experiments, and wrote the manuscript. TW performed part of the data analysis and interpreted the experimental data. ZF performed part of the data analysis. FG, JZ, CJ, HT, JX, HC, and QO provided technical support and analyzed the data. All authors read and approved the final manuscript.

FUNDING

This paper was supported by the Ministry of Science and Technology of China (2020YFA0113101), the National Natural Science Foundation of China (32070719, 81770942), and the Fundamental Research Funds for the Central Universities (22120220009).

ACKNOWLEDGMENTS

We thank all members of our laboratory for many helpful discussions.

SUPPLEMENTARY MATERIAL

The Supplementary Material for this article can be found online at: https://www.frontiersin.org/articles/10.3389/fonc.2022.880100/full#supplementary-material

REFERENCES

1. Siegel RL, Miller KD, Jemal A. Cancer Statistics, 2019. *CA Cancer J Clin* (2019) 69(1):7–34. doi: 10.3322/caac.21551
2. Jiang H, Chen H, Wan P, Chen N. Decreased Expression of HADH is Related to Poor Prognosis and Immune Infiltration in Kidney Renal Clear Cell Carcinoma. *Genomics* (2021) 113(6):3556–64. doi: 10.1016/j.ygeno.2021.08.008
3. Mitchell TJ, Turajlic S, Rowan A, Nicol D, Farmery JHR, O'Brien T, et al. Timing the Landmark Events in the Evolution of Clear Cell Renal Cell Cancer: TRACERx Renal. *Cell* (2018) 173(3):611–23.e17. doi: 10.1016/j.cell.2018.02.020
4. Shuch B, Amin A, Armstrong AJ, Eble JN, Ficarra V, Lopez-Beltran A, et al. Understanding Pathologic Variants of Renal Cell Carcinoma: Distilling Therapeutic Opportunities From Biologic Complexity. *Eur Urol* (2015) 67 (1):85–97. doi: 10.1016/j.eururo.2014.04.029
5. Pena-Llopis S, Vega-Rubín-de-Celis S, Liao A, Leng N, Pavía-Jiménez A, Wang S, et al. BAP1 Loss Defines a New Class of Renal Cell Carcinoma. *Nat Genet* (2012) 44(7):751–9. doi: 10.1038/ng.2323
6. Koh MY, Sayegh N, Agarwal N. Seeing the Forest for the Trees-Single-Cell Atlases Link CD8(+) T Cells and Macrophages to Disease Progression and Treatment Response in Kidney Cancer. *Cancer Cell* (2021) 39(5):594–6. doi: 10.1016/j.ccell.2021.03.008
7. Braun DA, Street K, Burke KP, Cookmeyer DL, Denize T, Pedersen CB, et al. Progressive Immune Dysfunction With Advancing Disease Stage in Renal Cell Carcinoma. *Cancer Cell* (2021) 39(5):632–48.e8. doi: 10.1016/j.ccell.2021.02.013
8. Hakimi AA, Ostrovnaya I, Jacobsen A, Susztak K, Coleman JA, Russo P, et al. Validation and Genomic Interrogation of the MET Variant Rs11762213 as a Predictor of Adverse Outcomes in Clear Cell Renal Cell Carcinoma. *Cancer* (2016) 122(3):402–10. doi: 10.1002/cncr.29765
9. Singer EA, Bratslavsky G, Middelton L, Srinivasan R, Linehan WM. Impact of Genetics on the Diagnosis and Treatment of Renal Cancer. *Curr Urol Rep* (2011) 12(1):47–55. doi: 10.1007/s11934-010-0156-y
10. Dalgliesh GL, Furge K, Greenman C, Chen L, Bignell G, Butler A, et al. Systematic Sequencing of Renal Carcinoma Reveals Inactivation of Histone Modifying Genes. *Nature* (2010) 463(7279):360–3. doi: 10.1038/nature08672
11. Martinez-Salamanca JI, Huang WC, Millán I, Bertini R, Bianco FJ, Carballido JA, et al. Prognostic Impact of the 2009 UICC/AJCC TNM Staging System for Renal Cell Carcinoma With Venous Extension. *Eur Urol* (2011) 59(1):120–7. doi: 10.1016/j.eururo.2010.10.001
12. Delahunt B, Dagher J, Egevad L, Yaxley J, Varma M, Samaratunga H, et al. Is the UICC/AJCC Pt2 Staging Category for Clear Cell Renal Cell Carcinoma Meaningful? *Am J Surg Pathol* (2019) 43(9):1249–52. doi: 10.1097/PAS.0000000000001308
13. Li D, Liu S, Xu J, Chen L, Xu C, Chen F, et al. Ferroptosis-Related Gene CHAC1 is a Valid Indicator for the Poor Prognosis of Kidney Renal Clear Cell Carcinoma. *J Cell Mol Med* (2021) 25(7):3610–21. doi: 10.1111/jcmm.16458
14. Wang Q, Zhang H, Chen Q, Wan Z, Gao X, Qian W, et al. Identification of METTL14 in Kidney Renal Clear Cell Carcinoma Using Bioinformatics Analysis. *Dis Markers* (2019) 2019:5648783. doi: 10.1155/2019/5648783
15. Xie L, Li H, Zhang L, Ma X, Dang Y, Guo J, et al. Autophagy-Related Gene P4HB: A Novel Diagnosis and Prognosis Marker for Kidney Renal Clear Cell Carcinoma. *Aging (Albany NY)* (2020) 12(2):1828–42. doi: 10.18632/aging.102715
16. Song J, Song F, Liu K, Zhang W, Luo R, Tang Y, et al. Multi-Omics Analysis Reveals Epithelial-Mesenchymal Transition-Related Gene FOXM1 as a Novel Prognostic Biomarker in Clear Cell Renal Carcinoma. *Aging (Albany NY)* (2019) 11(22):10316–37. doi: 10.18632/aging.102459
17. Albini A, Sporn MB. The Tumor Microenvironment as a Target for Chemoprevention. *Nat Rev Cancer* (2007) 7(2):139–47. doi: 10.1038/nrc2067

18. Hu J, Chen Z, Bao L, Zhou L, Hou Y, Liu L, et al. Single-Cell Transcriptome Analysis Reveals Intratumoral Heterogeneity in ccRCC, Which Results in Different Clinical Outcomes. *Mol Ther* (2020) 28(7):1658–72. doi: 10.1016/j.ymthe.2020.04.023
19. Inagaki M, Aoyama M, Sobue K, Yamamoto N, Morishima T, Moriyama A, et al. Sensitive Immunoassays for Human and Rat GMFB and GMFG, Tissue Distribution and Age-Related Changes. *Biochim Biophys Acta* (2004) 1670 (3):208–16. doi: 10.1016/j.bbagen.2003.12.006
20. Zuo P, Fu Z, Tao T, Ye F, Chen L, Wang X, et al. The Expression of Glia Maturation Factors and the Effect of Glia Maturation Factor-Gamma on Angiogenic Sprouting in Zebrafish. *Exp Cell Res* (2013) 319(5):707–17. doi: 10.1016/j.yexcr.2013.01.004
21. Yin G, Du M, Li R, Li K, Huang X, Duan D, et al. Glia Maturation Factor Beta is Required for Reactive Gliosis After Traumatic Brain Injury in Zebrafish. *Exp Neurol* (2018) 305:129–38. doi: 10.1016/j.expneurol.2018.04.008
22. Zaheer A, Lim R. Protein Kinase A (PKA)- and Protein Kinase C-Phosphorylated Glia Maturation Factor Promotes the Catalytic Activity of PKA. *J Biol Chem* (1997) 272(8):5183–6. doi: 10.1074/jbc.272.8.5183
23. Werner CJ, Heyny-von Haussen R, Mall G, Wolf S. Proteome Analysis of Human Substantia Nigra in Parkinson's Disease. *Proteome Sci* (2008) 6:8. doi: 10.1186/1477-5956-6-8
24. Sun W, Hu C, Wang T, Wang J, Zhang J, Gao F, et al. Glia Maturation Factor Beta as a Novel Biomarker and Therapeutic Target for Hepatocellular Carcinoma. *Front Oncol* (2021) 11:744331. doi: 10.3389/fonc.2021.744331
25. Hutter C, Zenklusen JC. The Cancer Genome Atlas: Creating Lasting Value Beyond Its Data. *Cell* (2018) 173(2):283–5. doi: 10.1016/j.cell.2018.03.042
26. Chandrashekar DS, Bashel B, Balasubramanya SAH, Creighton CJ, Ponce-Rodriguez I, Chakravarthi BVSK, et al. UALCAN: A Portal for Facilitating Tumor Subgroup Gene Expression and Survival Analyses. *Neoplasia* (2017) 19 (8):649–58. doi: 10.1016/j.neo.2017.05.002
27. Thul PJ, Lindskog C. The Human Protein Atlas: A Spatial Map of the Human Proteome. *Protein Sci* (2018) 27(1):233–44. doi: 10.1002/pro.3307
28. Tang Z, Kang B, Li C, Chen T, Zhang Z. GEPIA2: An Enhanced Web Server for Large-Scale Expression Profiling and Interactive Analysis. *Nucleic Acids Res* (2019) 47(W1):W556–60. doi: 10.1093/nar/gkz430
29. Bu D, Luo H, Huo P, Wang Z, Zhang S, He Z, et al. KOBAS-I: Intelligent Prioritization and Exploratory Visualization of Biological Functions for Gene Enrichment Analysis. *Nucleic Acids Res* (2021) 49(W1):W317–25. doi: 10.1093/nar/gkab447
30. Ai C, Kong L. CGPS: A Machine Learning-Based Approach Integrating Multiple Gene Set Analysis Tools for Better Prioritization of Biologically Relevant Pathways. *J Genet Genomics* (2018) 45(9):489–504. doi: 10.1016/j.jgg.2018.08.002
31. Wu J, Mao X, Cai T, Luo J, Wei L. KOBAS Server: A Web-Based Platform for Automated Annotation and Pathway Identification. *Nucleic Acids Res* (2006) 34(Web Server issue):W720–4. doi: 10.1093/nar/gkl167
32. Xie C, Mao X, Huang J, Ding Y, Wu J, Dong S, et al. KOBAS 2.0: A Web Server for Annotation and Identification of Enriched Pathways and Diseases. *Nucleic Acids Res* (2011) 39(Web Server issue):W316–22. doi: 10.1093/nar/gkr483
33. Yuan S, Xu Y, Yi T, Wang H. The Anti-Tumor Effect of OP-B on Ovarian Cancer *In Vitro* and *In Vivo*, and its Mechanism: An Investigation Using Network Pharmacology-Based Analysis. *J Ethnopharmacol* (2021) p:114706. doi: 10.1016/j.jep.2021.114706
34. Zhou Y, Zhou B, Pache L, Chang M, Khodabakhshi AH, Tanaseichuk O, et al. Metascape Provides a Biologist-Oriented Resource for the Analysis of Systems-Level Datasets. *Nat Commun* (2019) 10(1):1523. doi: 10.1038/s41467-019-09234-6
35. Chen B, Khodadoust MS, Liu CL, Newman AM, Alizadeh AA. Profiling Tumor Infiltrating Immune Cells With CIBERSORT. *Methods Mol Biol* (2018) 1711:243–59. doi: 10.1007/978-1-4939-7493-1_12
36. Newman AM, Liu CL, Green MR, Gentles AJ, Feng W, Xu Y, et al. Robust Enumeration of Cell Subsets From Tissue Expression Profiles. *Nat Methods* (2015) 12(5):453–7. doi: 10.1038/nmeth.3337
37. Li C, Tang Z, Zhang W, Ye Z, Liu F. GEPIA2021: Integrating Multiple Deconvolution-Based Analysis Into GEPIA. *Nucleic Acids Res* (2021) 49(W1): W242–6. doi: 10.1093/nar/gkab418
38. Szklarczyk D, Gable AL, Lyon D, Junge A, Wyder S, Huerta-Cepas J, et al. STRING V11: Protein-Protein Association Networks With Increased Coverage, Supporting Functional Discovery in Genome-Wide Experimental Datasets. *Nucleic Acids Res* (2019) 47(D1):D607–13. doi: 10.1093/nar/gky1131
39. Chin CH, Chen SH, Wu HH, Ho CW, Ko MT, Lin CY. Cytohubba: Identifying Hub Objects and Sub-Networks From Complex Interactome. *BMC Syst Biol* (2014) 8 Suppl 4:S11. doi: 10.1186/1752-0509-8-S4-S11
40. Shannon P, Markiel A, Ozier O, Baliga NS, Wang JT, Ramage D, et al. Cytoscape: A Software Environment for Integrated Models of Biomolecular Interaction Networks. *Genome Res* (2003) 13(11):2498–504. doi: 10.1101/gr.1239303
41. Kaji N, Ohashi K, Shuin M, Niwa R, Uemura T, Mizuno K, et al. Cell Cycle-Associated Changes in Slingshot Phosphatase Activity and Roles in Cytokinesis in Animal Cells. *J Biol Chem* (2003) 278(35):33450–5. doi: 10.1074/jbc.M305802200
42. Jonasch E, Gao J, Rathmell WK. Renal Cell Carcinoma. *BMJ* (2014) 349: g4797. doi: 10.1136/bmj.g4797
43. Kuang XY, Xu SL, Cui W, Jiang XF. Association of GMF-Beta Expression With Ki-67 and its Significance in the Prognostic Evaluation of Astrocytoma. *Zhonghua Bing Li Xue Za Zhi* (2021) 50(11):1252–6. doi: 10.3760/cma.j.cn112151-20210627-00459
44. Li YL, Ye F, Cheng XD, Hu Y, Zhou CY, Lü WG, et al. Identification of Glia Maturation Factor Beta as an Independent Prognostic Predictor for Serous Ovarian Cancer. *Eur J Cancer* (2010) 46(11):2104–18. doi: 10.1016/j.ejca.2010.04.015
45. Garcia-Martinez T, Vendrell-Flotats M, Martínez-Rodero I, Ordóñez-León EA, Álvarez-Rodríguez M, López-Béjar M, et al. Glutathione Ethyl Ester Protects *In Vitro*-Maturing Bovine Oocytes Against Oxidative Stress Induced by Subsequent Vitrification/Warming. *Int J Mol Sci* (2020) 21(20):7547. doi: 10.3390/ijms21207547
46. Sheffer M, Lowry E, Beelen N, Borah M, Amara SN, Mader CC, et al. Genome-Scale Screens Identify Factors Regulating Tumor Cell Responses to Natural Killer Cells. *Nat Genet* (2021) 53(8):1196–206. doi: 10.1038/s41588-021-00889-w
47. Lu T, Li Y, Pan M, Yu D, Wang Z, Liu C, et al. TBC1D14 Inhibits Autophagy to Suppress Lymph Node Metastasis in Head and Neck Squamous Cell Carcinoma by Downregulating Macrophage Erythroblast Attacher. *Int J Biol Sci* (2022) 18(5):1795–812. doi: 10.7150/ijbs.68992
48. Liu N, Luo J, Kuang D, Xu S, Duan Y, Xia Y, et al. Lactate Inhibits ATP6V0d2 Expression in Tumor-Associated Macrophages to Promote HIF-2alpha-Mediated Tumor Progression. *J Clin Invest* (2019) 129(2):631–46. doi: 10.1172/JCI123027
49. Murakami T, Sano F, Huang Y, Komiya A, Baba M, Osada Y, et al. Identification and Characterization of Birt-Hogg-Dube Associated Renal Carcinoma. *J Pathol* (2007) 211(5):524–31. doi: 10.1002/path.2139
50. Tarabay HH, Abol-Enein H, Awadalla A, Mortada WI, Abdel-Aziz AF. Gene Expression and Oxidative Stress Markers Profile Associated With Toxic Metals in Patients With Renal Cell Carcinoma. *Mol Biol Rep* (2022) 49 (2):1161–9. doi: 10.1007/s11033-021-06944-3
51. Ishii K, Usui S, Yamamoto H, Sugimura Y, Tatematsu M, Hirano K, et al. Decreases of Metallothionein and Aminopeptidase N in Renal Cancer Tissues. *J Biochem* (2001) 129(2):253–8. doi: 10.1093/oxfordjournals.jbchem.a002852
52. Truong LD, Shen SS. Immunohistochemical Diagnosis of Renal Neoplasms. *Arch Pathol Lab Med* (2011) 135(1):92–109. doi: 10.5858/2010-0478-RAR.1
53. Williamson SR, Gadde R, Trpkov K, Hirsch MS, Srigley JR, Reuter VE, et al. Diagnostic Criteria for Oncocytic Renal Neoplasms: A Survey of Urologic Pathologists. *Hum Pathol* (2017) 63:149–56. doi: 10.1016/j.humpath.2017.03.004
54. Stepan AE, Mărgăritescu C, Stoica LE, Stepan MD, Simionescu CE. Clear Cell Renal Cell Carcinomas - Epithelial and Mesenchymal Immunophenotype. *Rom J Morphol Embryol* (2018) 59(4):1189–94.
55. Goni J, Esteban FJ, de Mendizábal NV, Sepulcre J, Ardanza-Trevijano S, Agirrezabal I, et al. A Computational Analysis of Protein-Protein Interaction Networks in Neurodegenerative Diseases. *BMC Syst Biol* (2008) 2:52. doi: 10.1186/1752-0509-2-52
56. Grivennikov SI, Greten FR, Karin M. Immunity, Inflammation, and Cancer. *Cell* (2010) 140(6):883–99. doi: 10.1016/j.cell.2010.01.025
57. Zhang Y, Narayanan SP, Mannan R, Raskind G, Wang X, Vats P, et al. Single-Cell Analyses of Renal Cell Cancers Reveal Insights Into Tumor

Microenvironment, Cell of Origin, and Therapy Response. *Proc Natl Acad Sci U S A* (2021) 118(24):e2103240118. doi: 10.1073/pnas.2103240118
58. Giraldo NA, Becht E, Vano Y, Petitprez F, Lacroix L, Validire P, et al. Tumor-Infiltrating and Peripheral Blood T-Cell Immunophenotypes Predict Early Relapse in Localized Clear Cell Renal Cell Carcinoma. *Clin Cancer Res* (2017) 23(15):4416–28. doi: 10.1158/1078-0432.CCR-16-2848
59. Berlato C, Khan MN, Schioppa T, Thompson R, Maniati E, Montfort A, et al. A CCR4 Antagonist Reverses the Tumor-Promoting Microenvironment of Renal Cancer. *J Clin Invest* (2017) 127(3):801–13. doi: 10.1172/JCI82976

Conflict of Interest: The authors declare that the research was conducted in the absence of any commercial or financial relationships that could be construed as a potential conflict of interest.

Publisher's Note: All claims expressed in this article are solely those of the authors and do not necessarily represent those of their affiliated organizations, or those of the publisher, the editors and the reviewers. Any product that may be evaluated in this article, or claim that may be made by its manufacturer, is not guaranteed or endorsed by the publisher.

Copyright © 2022 Zhu, Wang, Feng, Gao, Zhang, Jin, Tian, Xu, Chen, Ou, Wang, Xu and Lu. This is an open-access article distributed under the terms of the Creative Commons Attribution License (CC BY). The use, distribution or reproduction in other forums is permitted, provided the original author(s) and the copyright owner(s) are credited and that the original publication in this journal is cited, in accordance with accepted academic practice. No use, distribution or reproduction is permitted which does not comply with these terms.

frontiers | Frontiers in Oncology

ORIGINAL RESEARCH
published: 19 July 2022
doi: 10.3389/fonc.2022.875131

Immune Characteristics and Prognosis Analysis of the Proteasome 20S Subunit Beta 9 in Lower-Grade Gliomas

Junzhe Liu[1,2,3†], *Xinyu Yang*[1,2,3†], *Qiankun Ji*[1,2,3†], *Lufei Yang*[1,2,3], *Jingying Li*[4], *Xiaoyan Long*[5], *Minhua Ye*[1,2,3*], *Kai Huang*[1,2,3*] *and Xingen Zhu*[1,2,3*]

[1] *Department of Neurosurgery, The Second Affiliated Hospital of Nanchang University, Nanchang, China,* [2] *Institute of Neuroscience, Nanchang University, Nanchang, China,* [3] *Jiangxi Key Laboratory of Neurological Tumors and Cerebrovascular Diseases, Nanchang, China,* [4] *Department of Comprehensive Intensive Care Unit, Second Affiliated Hospital of Nanchang University, Nanchang, China,* [5] *East China Institute of Digital Medical Engineering, Shangrao, China*

OPEN ACCESS

Edited by:
Shaoquan Zheng, Sun Yat-sen University Cancer Center (SYSUCC), China

Reviewed by:
Bo Wang, Nankai university, China
Pengjie Hong, Fudan University, China

***Correspondence:**
Minhua Ye
yeminhua2007@126.com
Kai Huang
kaihuang@ncu.edu.cn
Xingen Zhu
ndefy89006@ncu.edu.cn

[†]*These authors have contributed equally to this work*

Specialty section:
This article was submitted to Molecular and Cellular Oncology, a section of the journal Frontiers in Oncology

Received: *13 February 2022*
Accepted: *21 June 2022*
Published: *19 July 2022*

Citation:
Liu J, Yang X, Ji Q, Yang L, Li J, Long X, Ye M, Huang K and Zhu X (2022) Immune Characteristics and Prognosis Analysis of the Proteasome 20S Subunit Beta 9 in Lower-Grade Gliomas. Front. Oncol. 12:875131. doi: 10.3389/fonc.2022.875131

Glioma is a common intracranial malignancy in adults and has a high mortality due to its poor prognosis and high recurrence rate. Dysregulation of protein degradation is one of the main promoting factors in glioma development. As an indispensable unit of the proteasome, Proteasome 20S Subunit Beta 9 (PSMB9) is one of the major enzymes in ubiquitin-dependent protein degradation in cells. In addition, proteasomes also participate in a series of cellular processing, like immune regulation, nerve signal transduction, material transport through channels, cell adhesion, and various signaling pathways. However, the relationship between the PSMB9 expression and the occurrence of lower-grade glioma (LGG) is still unknown. First, we collected the RNA-seq and clinical information about LGG clinical samples from The Cancer Genome Atlas (TCGA) cohort, Chinese Glioma Genome Atlas (CGGA; including CGGAseq1 and CGGAseq2) cohort, and Gene Expression Omnibus (GEO; GSE16011, GSE61374, and Rembrandt) cohort. Then, these data were used for differential analysis, survival analysis, enrichment analysis, clinical model construction, etc. In addition, we combine immune-related data for immune-related analysis, including immune infiltration and immunotherapy. Through the above research, we have provided a new biomarker for LGG prognosis prediction and more comprehensively explained the role of PSMB9 in the development of LGG. This study determined that PSMB9 can be used as an immunotherapy target through the analysis of immune data, providing new ideas for the clinical treatment of LGG.

Keywords: lower-grade glioma (LGG), prognostic biomarker, immunotherapy, clinical prognosis prediction, overall survival, proteasome, PSMB9

INTRODUCTION

Gliomas are the major cause of central nervous system tumors that cause death in patients, which occupy half of the primary intracranial tumors and always occur in adults (1). According to the different degrees of tumor malignancy, the WHO system divides gliomas into four grades (2, 3). Because of the good prognosis of grade 1 gliomas, we regard them as benign tumors and usually do

not include them when conducting glioma research. Recent evidence has shown that grades 2 and 3 gliomas have similar molecular features and fewer prognostic differences, so The Cancer Genome Atlas (TCGA) database classifies grades 2 and 3 gliomas as lower-grade gliomas (LGGs) (4); glioblastoma (GBM) has been studied alone due to its high degree of malignancy and poor prognosis (5). During the analysis, we found that there is a very large heterogeneity between LGG and GBM, so we consider that it is unreasonable to perform an integrated analysis (6, 7). Therefore, we separately conducted our study in LGG cohorts. Due to GBM's high degree of malignancy, the common clinical treatments are surgical resection supplemented by radiotherapy and chemotherapy, but these strategies have failed to achieve the desired results (8, 9). Given the fact that clinical treatments of gliomas are not satisfactory, we have come up with novel immunotherapies that garnered positive responses, so it is urgently needed to seek new therapeutic targets and prognostic biomarkers (10, 11). As an indispensable component of the proteasome, PSMB9 is closely related to a variety of biological behaviors by participating in the protein degradation process. Our survey provided conclusive evidence for the potential of PSMB9 to act as a robust biomarker to predict the prognosis for patients in LGG.

PSMB9 is an integral member of the proteasome B-type family, involved in the composition of the proteasome. Proteasomes widely exist in the cytoplasm of eukaryotic cells and are involved in protein degradation through the non-lysosomal pathway supplemented by ATP/ubiquitin cleavage (12, 13). PSMB9 is particularly significant for the inactivation and degradation of various proteins in cells. The PSMB9 expression level in tumor tissues is much higher than in para-carcinoma tissue, suggesting that the expression of PSMB9 is highly correlated with LGG and affects various pathways in a subtle and complex way. Through subsequent analysis, we found a high correlation between PSMB9 and immunity in tumors. PSMB9 participates in a variety of biological processes and accelerates the progression of cancer. In view of its versatility, no studies have shown its mechanism of action in the pathogenesis of LGG and its potential application as a clinical immunotherapy target. By examining several databases, we have revealed its role in tumors and potential as an immunotherapy target, demonstrating a stable prognostic marker that can be used as a therapeutic target to alter the course of LGG.

Our research mainly analyzed the relationship between PSMB9 gene expression and characteristics among tumor samples through bioinformatics. We used the TCGA database as the training set and made a preliminary conclusion. Then Chinese Glioma Genome Atlas (CGGA) and Gene Expression Omnibus (GEO) databases were analyzed as the validation set to prove the universality and accuracy of the above conclusions again. We performed a correlation analysis by matching the clinical information and PSMB9 expression levels, and nomograms were constructed to predict the overall survival (OS) of patients. Through the analysis of the RNA-seq data in the low-high expression group of PSMB9, differentially expressed genes (DEGs) were screened out for functional and pathway analysis. Function annotation was conducted through Gene Ontology (GO) analysis and Kyoto Encyclopedia of Genes and Genomes (KEGG) analysis. Gene set enrichment analysis (GSEA) was performed to identify the hallmark gene sets and reveal their enrichment pathways, which can roughly predict gene functions and their roles in tumor progression (14–16). By examining the expression relationships between PSMB9 and several well-known immune checkpoints in different expression groups, we further identified a robust association between the expression of PSMB9 and the immune system. Finally, we explored the relationship between PSMB9 expression in the immunotherapy cohort and sample response in two immunotherapy databases, providing effective guidance for the application of PSMB9 as an effective prognostic marker in LGG immunotherapy. Through the above analysis, we identified that PSMB9 can be used as the prognostic marker; immune analysis was also implemented to confirm the relationship with tumor immune environment and its prospect in tumor immunotherapy application in patients with LGG.

MATERIALS AND METHODS

Acquisition and Preprocessing of Lower-Grade Glioma Datasets

The LGG data were mainly downloaded from three public datasets for the analysis of the whole article, including TCGA, CGGA, and GEO databases. The mRNA sequencing and clinical information of the LGG samples were downloaded from the Genomic Data Commons Data Portal website (https://portal.gdc.cancer.gov/). Analogously, the data of the CGGA and GEO databases can be downloaded from the CGGA website (http://www.cgga.org.cn/) and GEO website (https://www.ncbi.nlm.nih.gov/gds/). In the GEO dataset, GSE16011, GSE61374, and Rembrandt cohorts were selected for this research. After the original data were obtained, the samples were screened according to the predesigned inclusion criteria to pick the meaningful samples. The specific inclusion criteria are as follows: 1) patients with primary glioma were chosen for the analysis; 2) grade 2 and 3 glioma patients according to the WHO classification; 3) the mRNA expression of each gene in this sample was clear without deletion value; 4) the minimum follow-up time of patients was more than 30 days, and there were no missing values of basic information such as age and sex; and 5) there is no missing value of each gene information, such as 1p19q co-deletion, IDH status (17), MGMT promoter methylation (18). The summary of the proportion of clinical features is shown in **Table 1**. A total of 473 LGG samples out of 529 remained after TCGA dataset was filtered. The original RNA-seq data were fragments per kilobase of transcript per million fragments mapped (FPKM) data, and a calculation formula that was previously publicly available was used to convert them into transcripts per kilobase million (TPM) data for bioinformatics analysis to make the obtained results more convincing (19–21). In addition, the RNA-seq data and clinical

TABLE 1 | Summary of clinical information of LGG patients included in this study.

Characteristics	TCGA dataset (n = 473)		Meta-CGGA dataset (n = 413)		GEO dataset (n = 379)	
Age						
≥40	254	53.70%	218	52.78%	313	82.59%
<40	219	46.30%	195	47.22%	65	17.15%
PSMB9						
High	131	27.70%	91	22.03%	111	29.29%
Low	342	72.30%	322	77.97%	268	70.71%
Grade						
WHO II	229	48.41%	183	44.31%	159	41.95%
WHO III	244	51.59%	230	55.69%	220	58.05%
Gender						
Male	258	54.55%	238	57.63%	245	64.64%
Female	215	45.45%	175	42.37%	134	35.36%
IDH						
Wild type	85	17.97%	102	24.70%	58	15.30%
Mutant	388	82.03%	311	75.30%	159	41.95%
N/A	N/A	N/A	N/A	N/A	162	42.74%
1p19q						
Coded	156	32.98%	126	30.51%	74	19.53%
Non-coded	317	67.02%	287	69.49%	139	36.68%
N/A	N/A	N/A	N/A	N/A	166	43.80%
MGMT						
Unmethylated	82	17.34%	169	40.92%	N/A	N/A
Methylated	391	82.66%	244	59.08%	N/A	N/A

LGG, lower-grade glioma; TCGA, The Cancer Genome Atlas; CGGA, Chinese Glioma Genome Atlas; GEO, Gene Expression Omnibus.

information of IMvigor210 (n = 398) and Gide2019 (n = 41) were downloaded from the GEO dataset to verify the prognostic role of PSMB9 in immunotherapy (22, 23).

Potential of PSMB9 as a Prognostic Biomarker

TCGA, CGGA, and GEO cohorts were divided into two subgroups artificially. The optimal cutoff value was calculated using the R package "survival" and "survminer" in the cohort, and the subsequent studies used this criterion to group the low and high PSMB9 expression groups. The survplots were drawn from the data in three databases. Furthermore, the area under the curve (AUC) was performed to identify the prognostic accuracy of PSMB9 in three cohorts. Multivariate Cox regression analyses were also conducted to ascertain the independent prognostic ability.

Enrichment Analysis of PSMB9

The RNA-seq data of TCGA cohort were obtained, the samples were grouped into two according to the previous grouping criteria, and 1,288 DEGs were screened out. GO and KEGG enrichment analyses were carried out through the R package "clusterProfiler" to obtain the cell functions and pathways in which DEG participated (24). At last, the tumor hallmarks enriched in LGG were sorted out by the GSEA software, and pathways with higher enrichment scores (ESs) were singled out for multi-GSEA.

Prediction Model Construction and Accuracy Verification

Univariate and multivariate Cox regression analyses were conducted to determine the independent prognostic effect of PSMB9. Relevant clinical information was included, such as age, gender, WHO grade, IDH mutation, 1p19q co-deletion, and MGMT promoter mutation. The nomogram model was constructed based on the multivariate Cox regression analysis results using the R package "rms." TCGA calibration curves were constructed by the "calibrate" function in the "rms" packages, and the results above were verified in the CGGA and GEO cohorts. Decision curve analysis (DCA) curves were built to better illustrate the clinical utility of the nomogram model by comparing the benefits of different variables in the model.

Analysis of Immune Cell Infiltration in Lower-Grade Glioma

Infiltrating cell types in glioma samples were analyzed through single-sample GSEA (ssGSEA), CIBERSORT, and ESTIMATE methods and obtained the scores of corresponding immune signatures. The rank of gene expression values was standardized in a single sample, and the ES was calculated using an empirical cumulative distribution function, which is called ssGSEA (25). The r package "GSVA" was applied to evaluate the microenvironment of immune cell infiltration in LGG tumor samples (26). The median PSMB9 expression level was used as the grouping basis to divide LGG samples into high and low expression groups for ssGSEA. Tumor purity, estimated score, immune score, and interstitial score of LGG samples can be obtained through the calculation of the ESTIMATE package. In addition, the relative abundance of each type of immune cell in tumors can be obtained by ssGSEA calculation. CIBERSORT online tool (http://cibersort.stanford.edu/) was used to analyze the proportion of 22 human hematopoietic cell types cells in TCGA cohort (27). The difference analysis of the immune cell types in the PSMB9 high and low expression groups was carried out through the "vioplot" packages. In addition, a single-cell analysis of PSMB9 was also performed in the existing single-cell

cohort on the Tumor Immune Single-cell Hub website (TISCH: http://tisch.comp-genomics.org/).

Prediction of Tumor Immunotherapy

Immunotherapy is the latest progress in tumor therapy, among which antagonistic antibodies are one of the important therapeutic methods, like cytotoxic T-cell lymphocyte antigen 4 (CTLA-4) and programmed death 1 (PD-1) (28). In the IMvigor210 cohort (29), patients who received atezolizumab, an anti-PD-L1 drug, were divided into four groups based on their treatment response: complete response (CR), partial response (PR), stable disease (SD), and progressive disease (PD). By analyzing the gene expression in the cohort and its influence on the immunotherapy effect, the difference in PSMB9 expression level in LGG patients against the PD-L1 immunotherapy effect can be predicted. To further access the potential of PSMB9 as an immunotherapy target, PSMB9 expression and acceptance were also validated in another cohort (Gide2019) that was treated with nivolumab, pembrolizumab, and ipilimumab.

Acquisition of Clinical Samples

Twelve clinical samples were collected from inpatients in the Nanchang University Second Affiliated Hospital to conduct our survey, including six clinical normal brain tissues (NBTs), three grade 2 samples, and three grade 3 samples according to WHO classification. All of the samples were stored at a temperature of −196°C immediately after surgical excision. The study has been approved by the Medical Ethics Committee of the Second Affiliated Hospital of Nanchang University. The collection and utilization of clinical samples are strictly in compliance with the established guidelines, and informed consent of patients was obtained.

Cell Culture

SW-1088 and SW-1783 LGG cell lines used in this study were purchased from American Type Culture Collection (ATCC; Manassas, VA, USA). SW-1088 and SW-1783 were cultured with Leibovitz's L-15 Medium (Gibco, Grand Island, NY, USA) mixed with 10% fetal bovine serum (FBS; Gibco) and 1% Pen Strep (Gibco) and at a temperature of 37°C under normoxic conditions. All the cell samples were obtained during the logarithmic growth period to ensure that the cell morphology and cell function are in the best condition for observation and processing.

Immunofluorescence Protein Localization

To determine the functional pathway of PSMB9, the intracellular localization of PSMB9 was detected by immunofluorescence assay. SW1088 and SW1783 cells were planted on slides, immobilized with 4% paraformaldehyde for 60 min until the cells grew into a suitable density, washed with PBS several times to remove the residual paraformaldehyde, and then incubated in 0.3% Triton X-100 (dissolve in PBS) for 15 min. The cells were washed with PBS another three times, and the antigen was blocked with 5% goat serum for 1 h. Then a rabbit anti-PSMB9 antibody (14544-1-AP; 1:50; proteintech, Wuhan, China) was used to especially bind the PSMB9 protein in the cells at 4°C for no less than 12 h. Alexa Fluor 488-conjugated AffiniPure Goat Anti-Rabbit IgG was used as the secondary antibody to conjugate with the primary antibody after the primary antibody incubation is complete. Next, the sample needs to be incubated with 10 μg/ml of DAPI for 20 s in the dark. Finally, the sample was washed three times with PBS, and anti-quench sealing tablets were used for anti-quench treatment (Fluorescent Mounting Media; Bioss, Woburn, M, USA; Cat. C02-04003) if necessary, followed by confocal microscopy (Leica, Wetzlar, Germany).

Western Blotting of Clinical Samples

The tissue samples were ground and crushed after being cleaned with PBS and then digested and lysed with radioimmunoprecipitation assay (RIPA) lysate dissolved with 1% phenylmethylsulfonyl fluoride (PMSF) on ice for 30 min. After the samples were completely lysed, they were centrifuged in a high-speed refrigerated centrifuge at 12,000 rpm for 15 min, and the tissue protein was obtained. The concentration of the tissue protein was measured with the bicinchoninic acid (BCA) kit (Beyotime, Shanghai, China). Then 10% sodium dodecyl sulfate–polyacrylamide gel electrophoresis (SDS-PAGE) was applied to separate the protein lysates, and 20 ng of total proteins was added to each lane. The protein in the SDS-PAGE glue is transferred to the polyvinylidene difluoride (PVDF) membranes by membrane transfer operation. A 5% bovine serum albumin (BSA) solution was used to block the antigen epitope on the membrane for 2 h at room temperature. Then, the membrane was treated with the primary antibody (PSMB9, 1:2,000, proteintech, Cat. 14544-1-AP; Tubulin, 1:5,000, proteintech Cat. 11224-1-AP) and secondary antibody (horseradish peroxidase (HRP)-conjugated anti-rabbit secondary antibody, 1:5,000, proteintech, Cat. 15001). Enhanced chemiluminescence (ECL; UE; Cat. S6009M) kit was used to visualize the position and abundance of PSMB9 protein. Tanon-5200 Multi was used to visualize the protein brand. The final image was read with ImageJ software (version 1.52a) for gray value, and Tubulin was used as an internal reference control for semi-quantitative statistical analysis of the expression of the target protein.

Fluorescence Immunohistochemistry of Clinical Samples

Previous studies have shown that there is a significant relationship between PSMB9 protein and CD8+ T cells. In order to further detect the relationship between PSMB9 and CD8+ T cell infiltration in tumor tissues, fluorescence immunohistochemistry (FIHC) was performed on tumor samples. The effect of PSMB9 on the infiltration of CD8+ T cells in tumor tissues was revealed by detecting the CD8 and PSMB9 proteins. Five tumor tissue samples were obtained from the biological sample bank of the Second Affiliated Hospital of Nanchang University. First, the tumor tissue was embedded in paraffin, and the sample was cut into 4–6 μm thick slices with a microtome. The samples were placed on glass slides and incubated in xylene solution for 15 min twice, 100% ethanol for 10 min, 85% and 75% ethanol for 5 min for deparaffinization, and antigen was recovered in EDTA buffer (PH 8.0). A 3% BSA

solution was used to incubate the slices for 0.5 h to block the antigen, and then anti-CD8 (1:100) and anti PSMB9 (1:100) antibodies were used as the primary antibody to incubate the slices overnight. The residual primary antibody was cleaned with PBS solution, and Cy3 (1:300) and AF 488 (1:400) were used as secondary antibodies for fluorescent labeling and incubated in the dark for 1 h. Finally, the nuclei were stained using DAPI dye for localization. The slides were observed and photographed with a fluorescence microscope.

Statistical Analysis

An OS analysis was conducted by the Kaplan–Meier method (two-sided log-rank test) to analyze the clinical characteristics of two LGG subgroups with high and low PSMB9 expressions. The optical cutoff value was sorted out so that the samples can be divided into two subgroups at that point, and the p-value was the lowest when the "survminer" package was used (30). The optical cutoff value was used as the basis for grouping the dataset into two subgroups in the following study. The predictive potential of PSMB9 mRNA can be accessed by time-dependent receiver operating characteristic (ROC) curves, and the ability was compared by calculating the AUC values. A Students' t-test was performed to calculate the value of immune-related factors including immune score, stromal score, and tumor mutational burden (TMB) between the low and high PSMB9 expression subgroups, which were artificially divided. Moreover, univariate and multivariate Cox regression analyses were performed through the R package "rms" to evaluate the effectiveness of PSMB9 as an independent prognostic factor, and the nomogram model was constructed based on the above results. The C-index and calibration plot were used to consolidate the above results. All the statistics and methods mentioned above were processed with R software (version 4.0.4, http://www.r-project.org/), Perl (version 5.24.3), and SPSS 22.0 for windows (SPSS, Chicago, IL, USA). The flow chart of this study for performing the data analysis is shown in **Figure 1**.

RESULT

The Difference in PSMB9 Expression in Tumor Tissues

We explored the expression of PSMB9 in pan-cancer using TCGA and GTEx datasets, and the results show that PSMB9 was upregulated in most tumors, including LGG (**Figure 2A**). We performed the protein–protein interaction (PPI) network through the data from the comPPI website (http://comppi.linkgroup.hu/), and each kind of PPI can be traced back to PubMed. The results show that there are many kinds of proteins that interact with PSMB9 at different subcellular locations in the cell, such as the cytosol extracellular, membrane, and nucleus (**Figure 2B**). We downloaded the gene expression and DNA methylation data of TCGA database from UCSC Xena (http://xena.ucsc.edu), and the "DESeq2" package was employed to normalize and visually analyze the raw data. We realized that the higher the methylation level of the PSMB9 promoter, the harder it is for transcription factors to bind the PSMB9 promoter region, and the expression will decrease (**Figure 2C**). To observe the abundance and distribution of PSMB9 protein in LGG cells, we performed the immunofluorescence assays in SW-1088 and SW-1783 LGG cell lines. We found that the protein is distributed in the nucleus and cytoplasm, which can preliminarily prove that the protein can play a role in both the nucleus and cytoplasm (**Figure 2D**). In order to further verify the differential expression of PSMB9 protein in normal and tumor tissues, we downloaded immunohistochemical pictures of LGG samples from the

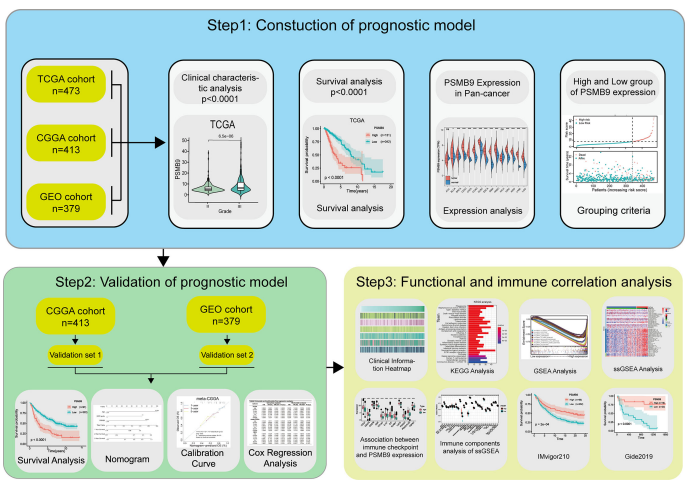

FIGURE 1 | Flow chart of this study. Step1: The sequencing data and clinical information data of LGG patients were downloaded from the TCGA, CGGA and GEO databases respectively, and the PSMB9 gene expression was extracted and matched with the clinical information for analysis of survival and expression differences. Step2: Nomogram model was constructed and its predictive stability was tested for the prognose in LGG patients. Step3: GO, KEGG, and GSEA analysis were performed to predict the function of PSMB9. Immune-related analyses including ssGSEA, CIBERSORT and ESTIMATE were performed to verify the correlation of PSMB9 with the immune environment and its potential in immunotherapy was identified in two independent immunotherapy cohorts(IMvigor210 and Gide2019).

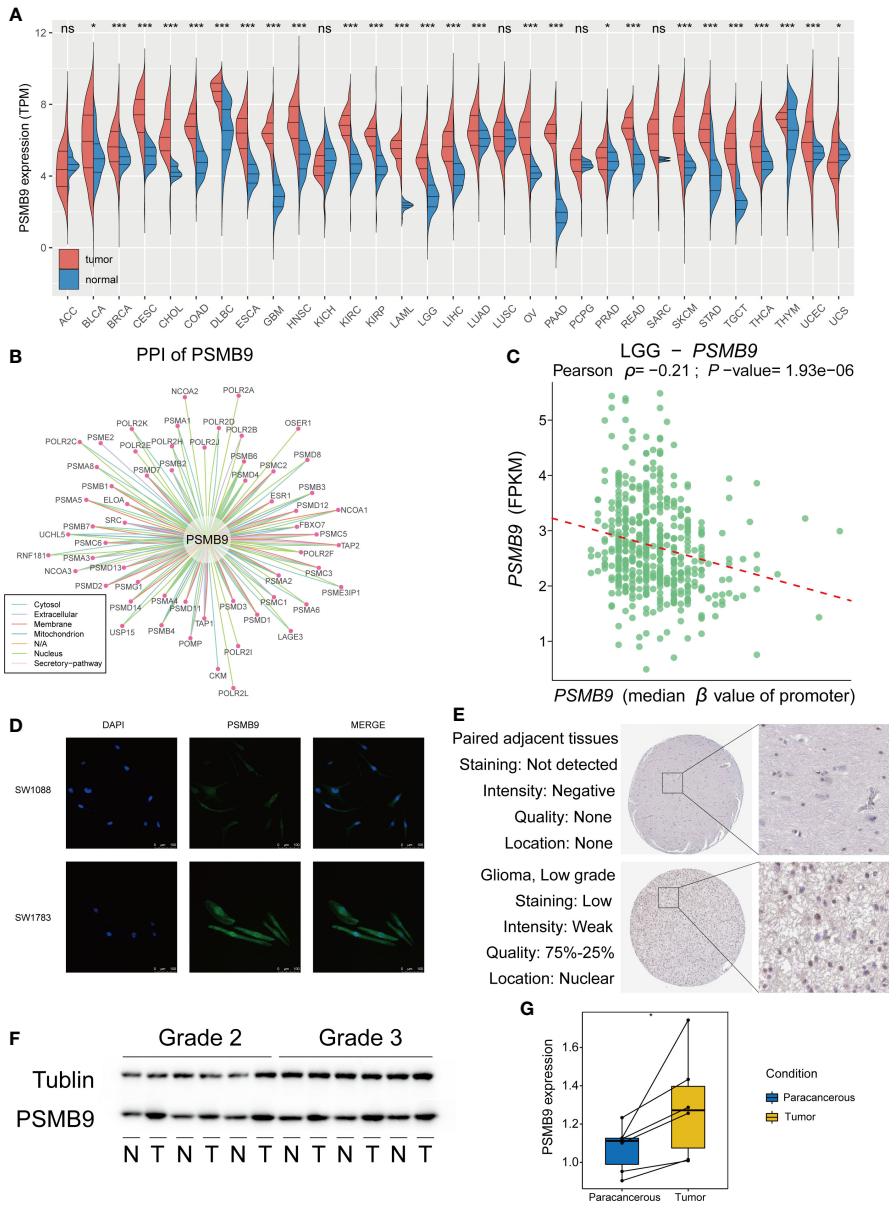

FIGURE 2 | Overview of PSMB9 protein in tumor samples. Basic expression, characteristics and distribution of PSMB9. **(A)** PSMB9 protein is differentially expressed in most tumors and is usually highly expressed in tumor tissues. **(B)** The PPI network of PSMB9. (Data derived from Pubmed). **(C)** The relationship between the level of promoter methylation and PSMB9 expression shows a higher PSMB9 expression correlated with a lower promoter methylation level. **(D)** Confocal images verify the distribution of PSMB9 in SW-1088 and SW-1783 cells and indicate that PSMB9 protein was expressed in both nucleus and cytoplasm. **(E)** The difference of PSMB9 protein expression and location between normal and tumor tissues were detected by immunohistochemistry which suggested that the expression level of PSMB9 was significantly increased in tumor tissues (Images were downloaded from Human Protein Altas). **(F)** WB verifies PSMB9 protein expression differences in clinical tissue samples. Tumor tissues have a higher PSMB9 expression than normal tissue. **(G)** ImageJ detects protein gray values for paired tests to determine protein expression differences.

Human Protein Atlas (HPA; https://www.proteinatlas.org/). The results show that the expression of PSMB9 is much more than that in NBTs (**Figure 2E**). Finally, we performed Western blotting (WB) with 12 clinical samples to identify the expression of PSMB9. It was proven that the higher the WHO grade, the higher the protein expression of PSMB9 (**Figure 2F**), which is in accordance with the conclusions we have drawn from the statistical analysis of the database. According to the WB results, we used ImageJ to calculate the corresponding gray value to represent the expression level (**Figure 2G**). All the evidence mentioned above proves that the expression of PSMB9 in tumor tissues is higher than that in normal tissues.

Clinical Features of PSMB9 Expression

We downloaded the clinical characteristic data of each sample from TCGA database and analyzed their differences through the grouping obtained previously. We sorted the samples according to the expression level of PSMB9; however, some values are so high that it is difficult to distinguish the expression differences in other samples with smaller expression levels. Therefore, we use $\log_2(\text{TPM} + 1)$ transformation to logarithmically process them to reduce the disparity in expression levels between samples. As for clinical information, we made a heatmap of the correlation between expression level and clinical features (**Figure 3A**). We can observe the different expressions between the status of clinical features and judge if there is a significant statistical difference based on the p-value. The results show that there are statistical differences in the expression of PSMB9 in different WHO classifications and IDH statuses. However, there is no clear difference between the 1p19q co-deletion in TCGA database and the methylation of the MGMT promoter in the GEO database (**Figures 3B–E**).

Survival Analysis Based on the PSMB9 Expression

After screening according to the aforementioned screening criteria, we retained 473, 413, and 379 samples in TCGA, CGGA, and GEO databases, respectively. By analyzing the mRNA-seq data of TCGA dataset, the expression level of PSMB9 gene was extracted and analyzed as well as the survival time and survival state of patients. After statistical analysis, we sorted the optimal cutoff value and drew the relevant survplot. The figures indicated that among the groups of different PSMB9 expression levels, there were significant differences in patient survival, and samples with high PSMB9 expression tended to have poor prognoses (**Figure 4A**). The same conclusion is also confirmed in the validation set of the CGGA and GEO databases (**Figures 4B, C**). However, the situation is not the same in other tumors. For example, the patients with higher PSMB9 expression tend to have better prognoses in BCLA, BRCA, OV, SARC, SKCM, and THCA (**Supplementary Figures 1**, **2**), which is contrary to the conclusion in LGG. This indicates that different types of tumors contain different tumor environments, resulting in different functions of PSMB9 involved. In addition, we verify the accuracy of the PSMB9 prognostic model in the three datasets of TCGA, CGGA, and GEO. The results show that it is robust and convincing in the analysis of 1-, 3-, and 5-year survival rates. The AUC values were totally beyond 0.6, which proves the accuracy of the clinical prognosis model (**Figure 4D**). The above prognostic-related analysis results indicate the feasibility of PSMB9 as a prognostic-related marker in LGG patients.

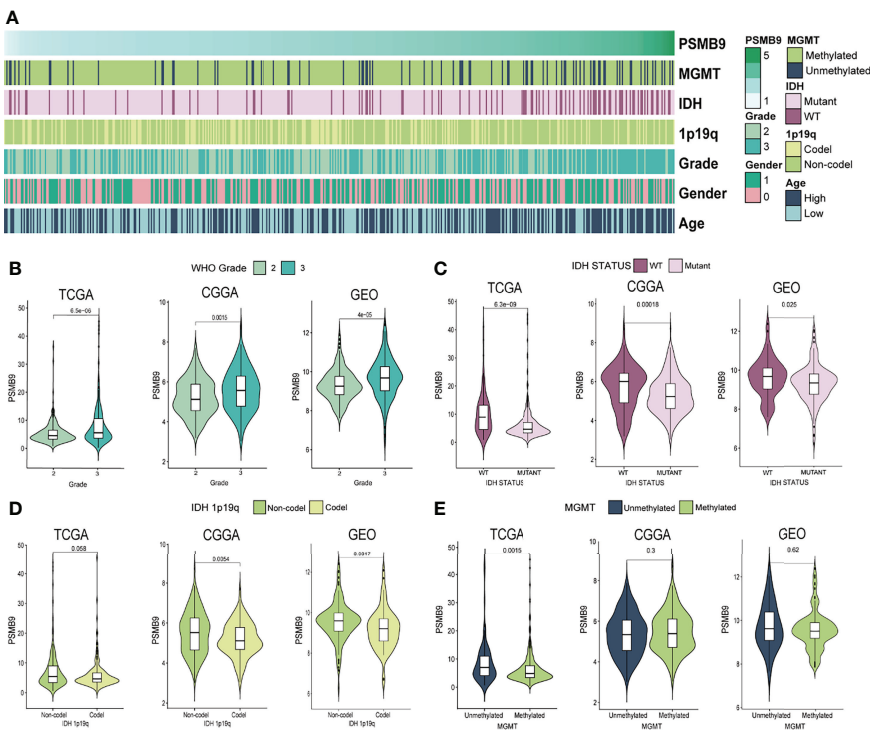

FIGURE 3 | PSMB9 correlated with the clinical and molecular characteristics of gliomas. **(A)** Heatmap reveals the relationship between various clinical features in each sample of different PSMB9 expressions. **(B–E)** The violin plot shows the significant difference in WHO Grade **(B)**, IDH status **(C)**, IDH 1p19q **(D)** and MGMT **(E)** in different PSMB9 expression subgroups.

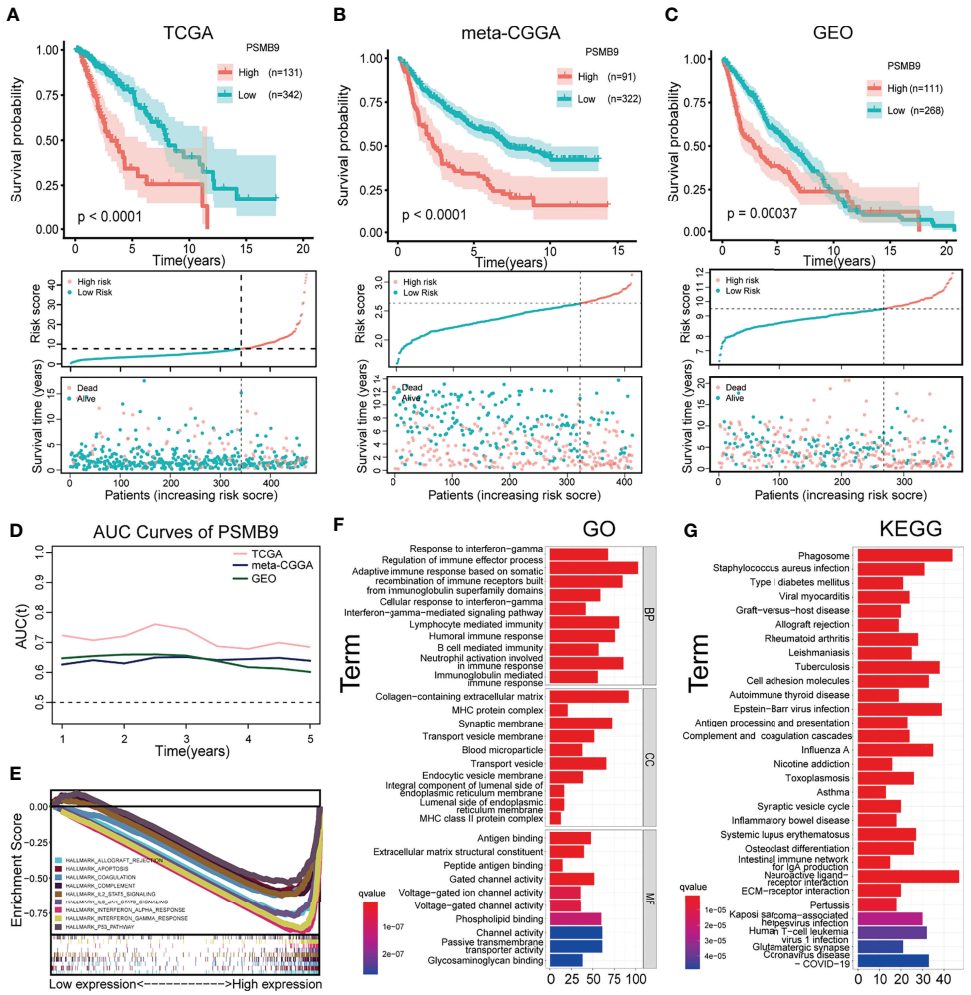

FIGURE 4 | Survival analysis and enrichment analysis. **(A–C)** K-M survival analysis was performed to validate that shorter survival and poorer prognosis in LGG patients with high PSMB9 expression in three databases (TCGA **(A)**, CGGA **(B)** and GEO **(C)**). **(D)** AUC curve values were all above 0.6, indicating that the predictive power of PSMB9 was stable **(E)** Multi-enrichment analysis of PSMB9 related DEGs. **(F)** Gene Ontology analysis of PSMB9-related DEGs. **(G)** Kyoto Encyclopedia of Genes and Genomes pathway analysis of PSMB9 related DEGs.

Differentially Expressed Gene Enrichment Analysis of PSMB9

We obtained the DEGs between the high and low PSMB9 groups through the website Morpheus (https://software.broadinstitute.org/morpheus/), and the enrichment analysis was conducted based on the above results. GO analysis proved that the close connection between DEGs and immune-related biological behavior and the DEGs of PSMB9 were enriched in the regulation of the immune effector process and neutrophil activation involved in immune response (**Figure 4F**). KEGG analysis identified that DEGs of PSMB9 were highly related to the phagosome and neuroactive ligand–receptor interaction and many other enrichment analysis results (**Figure 4G**). The above enrichment analysis results prove the function of PSMB9 in the nervous system and its connection with immunity, which further verifies its role in the occurrence of brain tumors and also reveals that there must be some relationship between PSMB9 and tumor immunity. These inevitable connections provide guidance for our subsequent immune-related analysis of PSMB9. GSEA was performed to reveal detailed information on enrichment results such as "interferon gamma response" and "IL6 JAK STAT3 signaling" in the whole LGG samples in TCGA dataset. A multi-GSEA was conducted to compare the DEGs in different pathways clearly (**Figure 4E**).

Construction of Nomogram Model and Clinical Prediction Model

We collected the mRNA sequencing data of LGG patients downloaded from TCGA dataset and performed screening according to the aforementioned criteria. TCGA dataset (n = 473) was regarded as the training dataset, and the CGGA (n = 413) and GEO (n = 379) datasets were used as the validation dataset. We conducted univariate and multivariate Cox regression analyses to verify the robustness of the PSMB9

expression as an independent prognostic biomarker (**Table 2**). The results show that higher age, PSMB9 expression, and WHO grade were risk factors and that IDH status, 1p19q co-deletion, and MGMT were protective factors in the three LGG cohorts. Furthermore, the nomogram model was constructed to evaluate the clinical application of PSMB9 as a prognostic biomarker with three risk factors (age, WHO grade, and PSMB9 expression level) confirmed in the multivariate model (**Figure 5A**). Moreover, we identified the accuracy of the nomogram by calculating the C-index of each cohort (TCGA:0.762; CGGA:0.678; GEO:0.671), and calibration curves indicated that the nomogram based on PSMB9 expression has a robust prediction ability in 1/3/5-year prognosis (**Figures 5B–D**). The DCA curves showed that in several datasets, the predictive ability of the nomogram model for 3/5-year survival was significantly higher than that of other prognostic factors. In addition, at a higher threshold, the prediction ability of the nomogram model is better than that of other factors (**Figures 5E–J**).

Relationship Between PSMB9 and Immune Checkpoint Expression

KEGG and GO enrichment revealed the robust linkage between the expression of PSMB9 and the immune microenvironment, especially in the B cell-mediated immunity and interferon-gamma-associated pathways. To further our research, we shifted the focus of our research to the analysis of immune infiltration. The first thing we did is identify the relationship between the expression of immune checkpoints and PSMB9, and we extracted the mRNA-seq data of different immune checkpoints and conducted the differential analysis in the high and low PSMB9 expression subgroup of LGG samples in TCGA dataset. We concluded that the expression of 12 kinds of the immune checkpoint is usually elevated in the high expression group compared with the low expression subgroup, and all the results were statistically different ($p < 0.05$) (**Figure 6A**). These results suggest that PSMB9 may be involved in the regulation of immune checkpoint expression, which may promote the effective response of immunotherapy drugs to tumor cells by increasing its expression and thus improving the efficacy. However, there is still insufficient evidence to show the exact relationship between PSMB9 and immune checkpoint expression, and the regulation mechanism of PSMB9 on immune checkpoint expression needs to be further explored.

Analysis of Tumor Immune Infiltration

Since we identified the fact that the expression of immune checkpoints in the PSMB9-high group is higher than that in the PSMB9-low group, we made a further study to show the connection between PSMB9 expression and other immune items. To understand the infiltration of various subtypes of immune cells and molecules in tumors, we calculated the enrichment degree of 29 immune-related molecules and processes by the ssGSEA algorithm and conducted a correlation analysis by separating them into two subgroups according to the previous expression criteria (**Figure 6B**). We found that all immune-related signature indexes were upregulated in the PSMB9 high expression group, and the immune-related scores of most items were significantly increased in the high expression group ($p <$

TABLE 2 | Univariate and multivariate Cox regression analyses.

Cohort	Univariate analysis				Multivariate analysis			
	HR	HR.95L	HR.95H	p-Value	HR	HR.95L	HR.95H	p-Value
TCGA								
Age	1.0669	1.0501	1.0841	0.0000	1.0578	1.0390	1.0768	0.0000
Gender	1.0069	0.6854	1.4791	0.9721	1.1295	0.7565	1.6866	0.5515
Grade	3.0486	2.0002	4.6465	0.0000	1.6487	1.0436	2.6047	0.0321
1p/19q	0.4080	0.2455	0.6782	0.0005	0.4632	0.2621	0.8187	0.0081
IDH	0.1509	0.1008	0.2260	0.0000	0.3803	0.1995	0.7248	0.0033
MGMT	0.3525	0.2327	0.5341	0.0000	0.9495	0.5383	1.6748	0.8579
PSMB9	1.0596	1.0377	1.0821	0.0000	1.0276	1.0019	1.0539	0.0348
Meta-CGGA								
Age	1.0146	1.0011	1.0283	0.0338	1.3702	0.9696	1.9364	0.0743
Gender	1.0599	0.8093	1.3881	0.6725	1.0659	0.8091	1.4041	0.6502
Grade	3.0521	2.2666	4.1097	0.0000	2.8738	2.1190	3.8976	0.0000
1p/19q	0.2603	0.1799	0.3764	0.0000	0.3018	0.2039	0.4465	0.0000
IDH	0.4180	0.3142	0.5560	0.0000	0.7180	0.5201	0.9911	0.0440
MGMT	0.8416	0.6442	1.0995	0.2061	0.9061	0.6814	1.2050	0.4978
PSMB9	1.4398	1.2633	1.6411	0.0000	1.2232	1.0772	1.3890	0.0019
GEO								
Age	1.0559	1.0324	1.0799	0.0000	1.0645	1.0377	1.0919	0.0000
Gender	1.6641	0.8945	3.0956	0.1078	0.9962	0.4986	1.9905	0.9914
Grade	1.1546	0.6252	2.1325	0.6460	1.1989	0.6036	2.3814	0.6045
1p/19q	0.2991	0.1177	0.7598	0.0112	0.2632	0.0973	0.7122	0.0086
IDH	0.2522	0.1342	0.4742	0.0000	0.3551	0.1495	0.8434	0.0190
MGMT	0.4929	0.2575	0.9434	0.0327	1.3304	0.5858	3.0217	0.4952
PSMB9	1.4267	1.0683	1.9053	0.0161	1.2770	0.9517	1.7136	0.1031

TCGA, The Cancer Genome Atlas; CGGA, Chinese Glioma Genome Atlas; GEO, Gene Expression Omnibus.

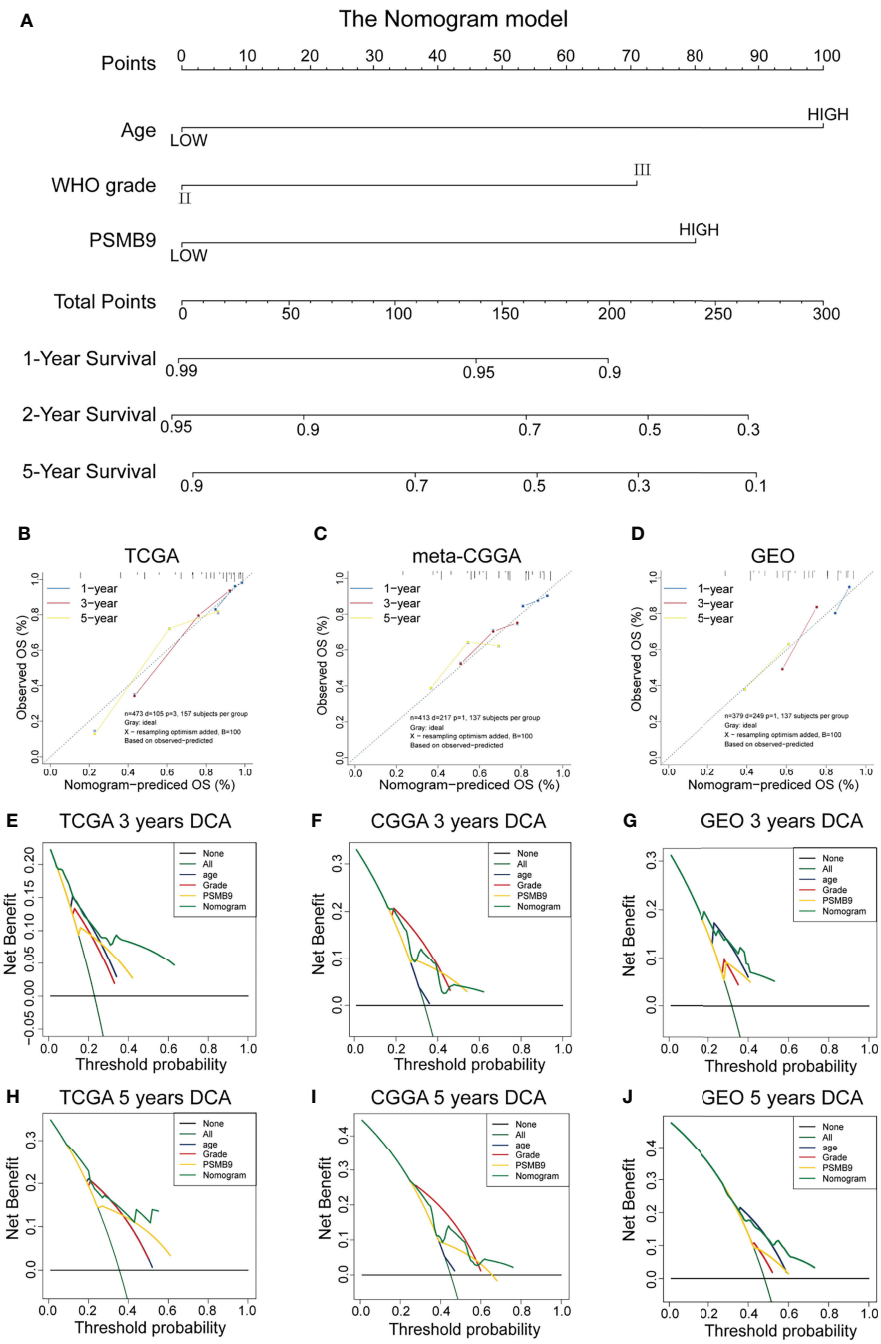

FIGURE 5 | Construction and validation of the nomogram model. **(A)** Construction of Nomogram Model about clinical features (including WHO Grade, IDH Status, IDH 1p19q and MGMT) in patients with low-grade glioma. **(B–D)** The 1/3/5-year OS calibration curves verify the prediction accuracy of the PSMB9-based nomogram model in the TCGA(B), meta-CGGA **(C)** and GEO **(D)** LGG cohorts. **(E–J)** Decision Curves Analysis (DCA) construction in TCGA **(E, H)**, meta-CGGA **(F, I)** and GEO **(G, J)**.

0.05). The above results indicate that PSMB9 expression is significantly correlated with most tumor immune characteristics and also demonstrates the great potential and role of PSMB9 in the tumor immune system. Apart from ssGSEA, CIBERSORT and ESTIMATE algorithms were applied to acquire other hallmarks of immunity and tumor, like stromal score and tumor purity (**Figure 7A**). TISCH website analysis showed that PSMB9 showed high infiltration in CD8+ T cells in the glioma single-cell cohort (**Supplementary Figure 3**), indicating that PSMB9 may be helpful for CD8+ T-cell activation and chemotaxis. Then, we conducted a difference test and linear regression analysis and found that there were significant

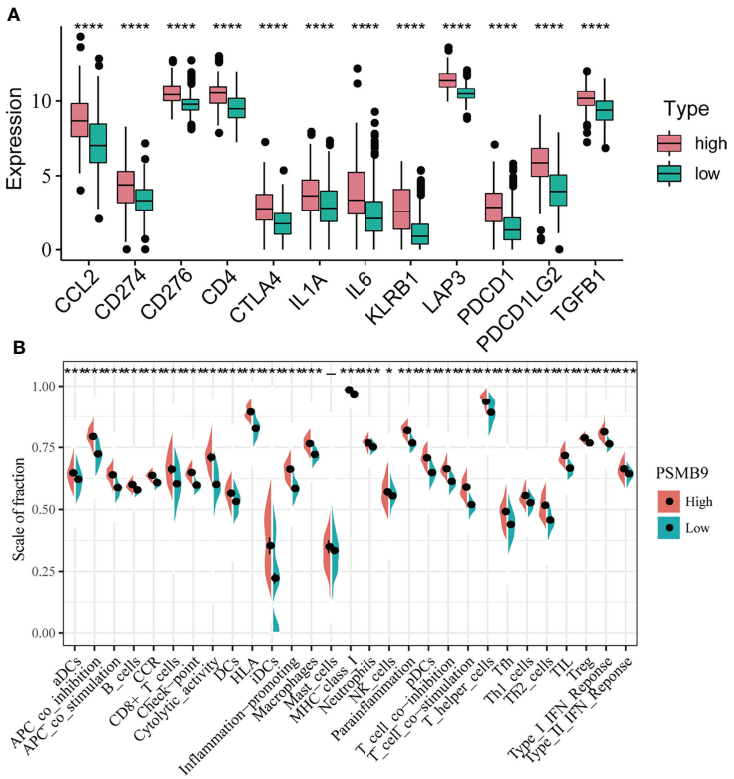

FIGURE 6 | Differential analysis of immune characteristics between high and low PSMB9 expression groups. **(A)** In the high-PSMB9 expression group, the expression of 12 common immune checkpoints is up-regulated, and there was significant statistical significance in the high and low expression groups of PSMB9. **(B)** In the high-PSMB9 expression group, the infiltration scale of immune cells and abundance of immune-related molecules based on the results of ssGSEA were significantly up-regulated. (ns P>0.05; *P<0.05; **P<0.01; ***P<0.001; ****P<0.0001).

differences in each indicator between the high and low expression groups, indicating that PSMB9 plays a role in tumor immunity and has stable prognostic ability in LGG patients (**Figures 7B–E, K–N**). FIHC revealed the relationship between PSMB9 expression and CD8+ T-cell infiltration in LGG (**Figure 8**). The results showed that PSMB9 was significantly expressed in LGG tissues, and CD8+ T cells infiltrated LGG tissues with high PSMB9 expression. This is consistent with our bioinformatics conclusion. Moreover, PSMB9 is also related to other immune cell infiltrations, such as macrophages, CD4+ T cells, and B cells, which need to be verified by further experiments. These results show that PSMB9 has a great impact on the tumor immune microenvironment.

Prediction of the Effect of Immunotherapy in Patients With Glioma

Due to the lack of immune response cohorts for patients with LGG, we use the anti-PD-L1 cohort (IMvigor210) and a combined anti-PD-L1 and anti-CTLA-4 cohort (Gide2019) for further identification of the prognostic value of PSMB9. We divided the cohort into two subgroups according to the expression of PSMB9, and we performed the survival curves that identified that the higher expression of PSMB9 predicts a better prognosis in patients with melanoma (**Figure 7F**). The results of anti-PD-L1 clinical immunotherapy can be divided into 4 groups, which are described previously. According to whether there is a therapeutic effect, we divided the 4 groups into two subgroups, namely, the effective group (PR/CR) and the ineffective group (PD/SD). The immune response of patients' anti-PD-L1 was better in the PSMB9 high expression group than in the lower expression group. We divided the different treatment responses into two groups and found that the expression of PSMB9 gene was statistically different between the two groups. In the subgroups with effects on the treatment, the expression of PSMB9 was significantly increased (**Figure 7G**). In addition, in the PSMB9 high expression group, the proportions of effective and ineffective treatment were 39.8% and 60.2%, respectively, compared with 16.3% in the PSMB9 low expression group. Additionally, 83.7% form a clear contrast (**Figure 7H**). It shows that PSMB9 has the potential to be used as an immunotherapy target for tumor treatment. The above results show that compared with the low PSMB9 expression group, the anti-PD-L1 treatment effect in the high PSMB9 expression group was more robust, indicating that PSMB9 can assist immunotherapy to a certain extent. It is deduced that PSMB9 protein may participate in the presentation of antigen proteins to reduce the immune escape of tumor cells, so it has great potential for immunotherapy. The survival analysis was performed in the Gide2019 cohort to identify the prognostic role of PSMB9 in

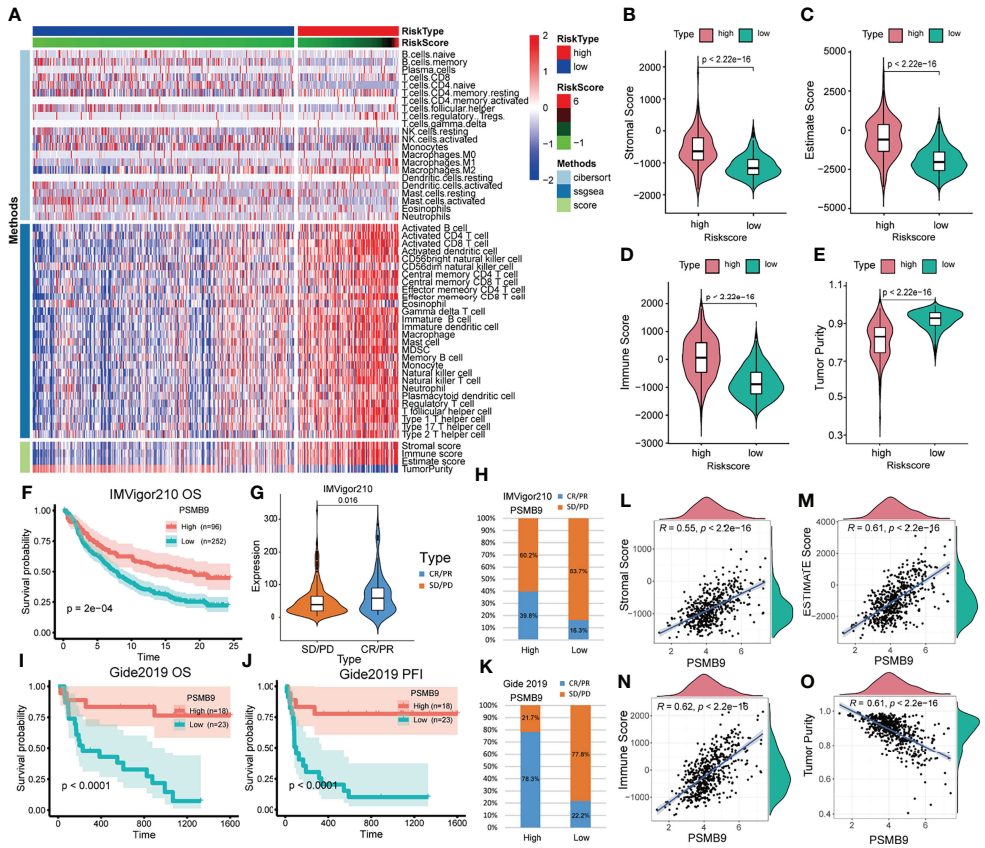

FIGURE 7 | Analysis of immune-related differences and treatment prediction. **(A)** Heatmap revealed the immune infiltration in the LGG cohort through CIBERSORT, ssGSEA and ESTIMATE algorithm. **(B–E)** The relevance between PSMB9 expression and immune-related score (including Stromal score, Estimate score, Immune score and Tumor purity). **(F)** Kaplan–Meier overall survival (OS) analysis in anti-PD-L1 (IMvigor210) cohorts in PSMB9 expression high and low group. **(G)** Expression of PSMB9 in different treatment response groups. **(H)** The proportion of the difference in response to anti-PD-L1 immunotherapy in PSMB9 high and low expression group. **(I)** Kaplan–Meier overall survival (OS) analysis in Gide2019. **(J)** Kaplan–Meier progression-free interval (PFI) analysis in Gide2019 cohort. **(K)** The proportion of the difference in response to anti-CTLA4 and anti-PD1 immunotherapy in PSMB9 high and low expression group. (L-O) The scatter plot confirmed the relationship between PSMB9 expression and immune-related score.

immunotherapy, and analogous results were concluded (**Figures 7I, J**). Therefore, based on the response of the two abovementioned treatment cohorts, PSMB9 can be basically concluded as an effective and stable positive prognostic factor for tumor immunotherapy. The proportions of effective and ineffective treatment in the two subgroups also enhanced the conclusion that patients with higher PSMB9 expression receive better curative effects through immunotherapy (**Figure 7K**).

DISCUSSION

Clinical treatment for glioma is relatively lacking, and with the existence of the blood–brain barrier (BBB), conventional treatment programs are difficult to work in patients with glioma, and conventional surgical treatment has difficulty achieving satisfactory results. The therapeutic effect achieved by various chemotherapy drugs is also very limited (31, 32). Therefore, patients with glioma have a high mortality rate and a very poor prognosis. New tumor prognostic markers and treatment options are in urgent need of development. Therefore, we conducted this study to explore the feasibility of PSMB9 as a clinical prognostic marker for analysis.

In this study, a total of 1,265 samples from three databases were included to confirm the possibility of PSMB9 as a prognostic marker. First, we performed survival analysis and molecular characteristic relevant analysis in three independent cohorts to test the association between PSMB9 expression and the prognosis of patients. We realized that the patients with higher PSMB9 expression have a poorer prognosis. Then we carried out the multivariate Cox regression to ascertain the independent prognostic value of PSMB9. The outcome of AUC curves made further consolidation of PSMB9 as a prognostic factor; calibration curves and DCA curves were conducted to validate the nomogram model, and the results seem to be strongly stable. Next, we focused on the function of PSMB9; thus GO, KEGG, and GSEA were carried out, and evidence showed that PSMB9 participates in a series of immune-related

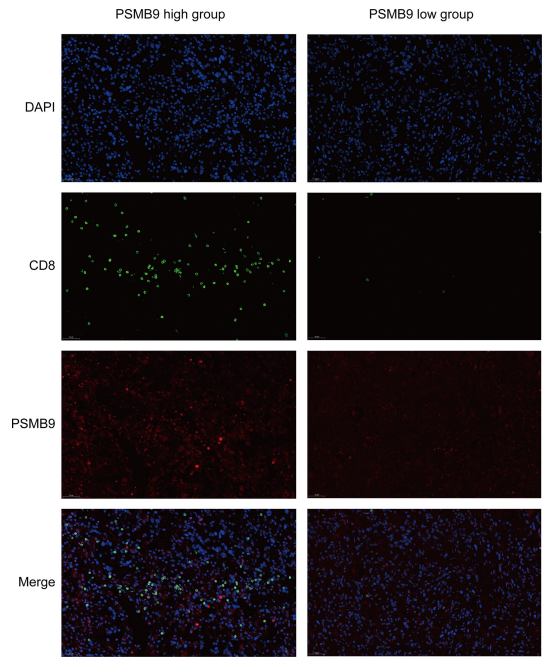

FIGURE 8 | Fluorescent Immunohistochemistry of LGG tumor tissue. DAPI is used to display the localization of nucleus, green represents CD8 protein, red represents PSMB9 protein, and Merge is the overlapping of three pictures.

activities. Therefore, ssGSEA, CIBERSORT, ESTIMATE, and immune checkpoint expression analyses were applied to reveal the immune characteristics, which are described in the previous text. At last, we investigated the relationship between PSMB9 expression and the prognosis of patients who received immunotherapy in two immunotherapy cohorts; surprisingly, after immunotherapy, the patients with higher PSMB9 expression have better prognoses, which is opposite to the result in TCGA dataset. This fact shows that PSMB9 functions differently in the different tumors, which matched the previous conclusion, and the consequence is the result of co-regulation by various components of the tumor microenvironment, but its ability as a prognostic marker in tumors is well established.

As one of the important components of proteasome, PSMB9 mainly plays a role in protein degradation. In addition to ubiquitin–proteasome degradation of abnormal or redundant proteins, the proteasome can also participate in a variety of cell biological processes, like cell cycle, apoptosis, and oxidative stress (33). Here we mainly discuss its role in the development of tumors. In the progression of cancer, the proteasome is highly expressed to specifically degrade tumor suppressor factors and block cell apoptosis, thus playing a protective role in tumor cells and promoting tumor progression (34). Therefore, the expression level of PSMB9 was increased in almost tumor tissues, and the higher the level, the more the expression.

Solid tumors consist mainly of tumor cells, with stromal cells and immune cells infiltrating, which constitute the tumor microenvironment (35, 36). The tumor microenvironment is the surrounding environment of tumor cell growth, including not only tumor cells but also surrounding neovascularization, immune cells, and various cell signaling molecules. The complex and diverse biological composition of the tumor microenvironment leads to the complexity of its function, and different tumor cells exist in different tumor microenvironments (37). Researchers have compared the effect of the tumor microenvironment to the relationship between soil and seed (38). Generally speaking, tumor cells are highly amplified, and the blood supply of cells is greatly reduced so that tumor cells can carry out anaerobic glycolysis (39). This effect can act on the immune microenvironment, which can make surrounding cells release a large number of cytokines and chemokines, affecting the tumor microenvironment (40). Chemotactic immune cells acting on tumor cells can affect the growth and development of cancer cells and mediate immune tolerance (41). Many cancer treatment options require a good grasp of the tumor microenvironment. For example, immunotherapy represented by the latest immune checkpoint blockade therapy must be adapted to the tumor microenvironment to function well (42). The study of tumor microenvironment enables us to have a better understanding of tumor cell growth and provides us with research on tumor treatment strategies.

In summary, we constructed a risk model based on the expression level of PSMB9. Based on relevant clinical information, we conducted univariate and multivariate regression analyses to find out if PSMB9 is a possible independent prognostic factor of LGG, and we constructed a nomogram of the prognosis of LGG patients to verify its credibility as a prognostic factor. The results of the enrichment analysis make us focus on its role in tumor immunity. For this reason, we conducted an immune infiltration analysis and proved that the distribution of immune cells in the PSMB9 high and low expression groups is different and the expression of common immune checkpoints is also significantly statistical differences. By verifying the immunotherapy effect of PSMB9 in the melanoma cohort, we proved its promising prospect as a tumor immunotherapy target. Therefore, PSMB9 protein may have great potential for the prognosis of LGG.

DATA AVAILABILITY STATEMENT

The original contributions presented in the study are included in the article/**Supplementary Material**. Further inquiries can be directed to the corresponding authors.

ETHICS STATEMENT

The studies involving human participants were reviewed and approved by the Medical Ethics Committee of the Second Affiliated Hospital of Nanchang University. The patients/participants provided their written informed consent to participate in this study. Written informed consent was obtained from the individual(s) for the publication of any potentially identifiable images or data included in this article.

AUTHOR CONTRIBUTIONS

XZ, KH, and MY designed the study. JZL and LY conducted the data analysis, image stitching, and manuscript writing. JYL and XL collected the clinical samples and revised the manuscript. XY performed the Western blotting and immunofluorescence experiments. QJ conducted the immunofluorescence staining of tumor pathological sections. All authors contributed to the manuscript and approved it for submission.

FUNDING

Our research is supported by the National Natural Science Foundation (grant nos. 82002660, 82172989, and 81760445), the Jiangxi Key research and development projects-Key Project (20212BBG71012), Jiangxi Provincial Science and Technology Innovation Base Plan-Provincial Key Laboratory (20212BCD42008), and Province-Youth Talent Project (20212BCJ23023).

ACKNOWLEDGMENTS

We sincerely appreciated the data provided by TCGA, CGGA, and GEO databases and their contributions to this research.

SUPPLEMENTARY MATERIAL

The Supplementary Material for this article can be found online at: https://www.frontiersin.org/articles/10.3389/fonc.2022.875131/full#supplementary-material

REFERENCES

1. Ostrom QT, Bauchet L, Davis FG, Deltour I, Fisher JL, Langer CE, et al. Response to "The Epidemiology of Glioma in Adults: A 'State of the Science' Review". *Neuro Oncol* (2015) 17(4):624–6. doi: 10.1093/neuonc/nov022
2. Wesseling P, Capper D. WHO 2016 Classification of Gliomas. *Neuropathol Appl Neurobiol* (2018) 44(2):139–50. doi: 10.1111/nan.12432
3. Lapointe S, Perry A, Butowski NA. Primary Brain Tumours in Adults. *Lancet (London Engl)* (2018) 392(10145):432–46. doi: 10.1016/S0140-6736(18)30990-5
4. Suzuki H, Aoki K, Chiba K, Sato Y, Shiozawa Y, Shiraishi Y, et al. Mutational Landscape and Clonal Architecture in Grade II and III Gliomas. *Nat Genet* (2015) 47(5):458–68. doi: 10.1038/ng.3273
5. Cahill DP, Sloan AE, Nahed BV, Aldape KD, Louis DN, Ryken TC, et al. The Role of Neuropathology in the Management of Patients With Diffuse Low Grade Glioma: A Systematic Review and Evidence-Based Clinical Practice Guideline. *J Neurooncol* (2015) 125(3):531–49. doi: 10.1007/s11060-015-1909-8
6. van den Bent MJ. : Interobserver Variation of the Histopathological Diagnosis in Clinical Trials on Glioma: A Clinician's Perspective. *Acta Neuropathol* (2010) 120(3):297–304. doi: 10.1007/s00401-010-0725-7
7. Molinaro AM, Taylor JW, Wiencke JK, Wrensch MR. Genetic and Molecular Epidemiology of Adult Diffuse Glioma. *Nat Rev Neurol* (2019) 15(7):405–17. doi: 10.1038/s41582-019-0220-2
8. Hervey-Jumper SL, Berger MS. Maximizing Safe Resection of Low- and High-Grade Glioma. *J Neurooncol* (2016) 130(2):269–82. doi: 10.1007/s11060-016-2110-4
9. Tomiyama A, Ichimura K. Signal Transduction Pathways and Resistance to Targeted Therapies in Glioma. *Semin Cancer Biol* (2019) 58:118–29. doi: 10.1016/j.semcancer.2019.01.004
10. Xu S, Tang L, Li X, Fan F, Liu Z. Immunotherapy for Glioma: Current Management and Future Application. *Cancer Lett* (2020) 476:1–12. doi: 10.1016/j.canlet.2020.02.002
11. Tivnan A, Heilinger T, Lavelle EC, Prehn JH. Advances in Immunotherapy for the Treatment of Glioblastoma. *J Neurooncol* (2017) 131(1):1–9. doi: 10.1007/s11060-016-2299-2
12. Bard JAM, Goodall EA, Greene ER, Jonsson E, Dong KC, Martin A. Structure and Function of the 26S Proteasome. *Annu Rev Biochem* (2018) 87:697–724. doi: 10.1146/annurev-biochem-062917-011931
13. Mishra R, Upadhyay A, Prajapati VK, Mishra A. Proteasome-Mediated Proteostasis: Novel Medicinal and Pharmacological Strategies for Diseases. *Med Res Rev* (2018) 38(6):1916–73. doi: 10.1002/med.21502
14. Subramanian A, Tamayo P, Mootha VK, Mukherjee S, Ebert BL, Gillette MA, et al. Gene Set Enrichment Analysis: A Knowledge-Based Approach for Interpreting Genome-Wide Expression Profiles. *Proc Natl Acad Sci U S A* (2005) 102(43):15545–50. doi: 10.1073/pnas.0506580102
15. The Gene Ontology Consortium. The Gene Ontology Resource: 20 Years and Still GOing Strong. *Nucleic Acids Res* (2019) 47(D1):D330–8. doi: 10.1093/nar/gky1055
16. Kanehisa M, Furumichi M, Tanabe M, Sato Y, Morishima K. KEGG: New Perspectives on Genomes, Pathways, Diseases and Drugs. *Nucleic Acids Res* (2017) 45(D1):D353–61. doi: 10.1093/nar/gkw1092
17. Dang L, Jin S, Su SM. IDH Mutations in Glioma and Acute Myeloid Leukemia. *Trends Mol Med* (2010) 16(9):387–97. doi: 10.1016/j.molmed.2010.07.002
18. Huse JT, Aldape KD. The Evolving Role of Molecular Markers in the Diagnosis and Management of Diffuse Glioma. *Clin Cancer Res* (2014) 20(22):5601–11. doi: 10.1158/1078-0432.CCR-14-0831
19. Zhao Y, Li MC, Konate MM, Chen L, Das B, Karlovich C, et al. TPM, FPKM, or Normalized Counts? A Comparative Study of Quantification Measures for the Analysis of RNA-Seq Data From the NCI Patient-Derived Models Repository. *J Transl Med* (2021) 19(1):269. doi: 10.1186/s12967-021-02936-w
20. Li B, Ruotti V, Stewart RM, Thomson JA, Dewey CN. RNA-Seq Gene Expression Estimation With Read Mapping Uncertainty. *Bioinformatics* (2010) 26(4):493–500. doi: 10.1093/bioinformatics/btp692
21. Wagner GP, Kin K, Lynch VJ. Measurement of mRNA Abundance Using RNA-Seq Data: RPKM Measure is Inconsistent Among Samples. *Theory Biosci* (2012) 131(4):281–5. doi: 10.1007/s12064-012-0162-3
22. Gide TN, Quek C, Menzies AM, Tasker AT, Shang P, Holst J, et al. Distinct Immune Cell Populations Define Response to Anti-PD-1 Monotherapy and Anti-PD-1/Anti-CTLA-4 Combined Therapy. *Cancer Cell* (2019) 35(2):238–255 e236. doi: 10.1016/j.ccell.2019.01.003
23. Mariathasan S, Turley SJ, Nickles D, Castiglioni A, Yuen K, Wang Y, et al. TGFbeta Attenuates Tumour Response to PD-L1 Blockade by Contributing to Exclusion of T Cells. *Nature* (2018) 554(7693):544–8. doi: 10.1038/nature25501
24. Yu G, Wang LG, Han Y, He QY. Clusterprofiler: An R Package for Comparing Biological Themes Among Gene Clusters. *OMICS* (2012) 16(5):284–7. doi: 10.1089/omi.2011.0118
25. Reimand J, Isserlin R, Voisin V, Kucera M, Tannus-Lopes C, Rostamianfar A, et al. Pathway Enrichment Analysis and Visualization of Omics Data Using G: Profiler, GSEA, Cytoscape and EnrichmentMap. *Nat Protoc* (2019) 14(2):482–517. doi: 10.1038/s41596-018-0103-9
26. Hanzelmann S, Castelo R, Guinney J. GSVA: Gene Set Variation Analysis for Microarray and RNA-Seq Data. *BMC Bioinformatics* (2013) 14:7. doi: 10.1186/1471-2105-14-7
27. Newman AM, Liu CL, Green MR, Gentles AJ, Feng W, Xu Y, et al. Robust Enumeration of Cell Subsets From Tissue Expression Profiles. *Nat Methods* (2015) 12(5):453–7. doi: 10.1038/nmeth.3337
28. Sampson JH, Maus MV, June CH. Immunotherapy for Brain Tumors. *J Clin Oncol* (2017) 35(21):2450–6. doi: 10.1200/JCO.2017.72.8089
29. Rosenberg JE, Hoffman-Censits J, Powles T, van der Heijden MS, Balar AV, Necchi A, et al. Atezolizumab in Patients With Locally Advanced and

Metastatic Urothelial Carcinoma Who Have Progressed Following Treatment With Platinum-Based Chemotherapy: A Single-Arm, Multicentre, Phase 2 Trial. *Lancet (London Engl)* (2016) 387(10031):1909–20. doi: 10.1016/S0140-6736(16)00561-4
30. Wu W, Xu W, Sun W, Zhang D, Zhao J, Luo Q, et al. Forced Vital Capacity Predicts the Survival of Interstitial Lung Disease in Anti-MDA5 Positive Dermatomyositis: A Multi-Centre Cohort Study. *Rheumatology (Oxford Engl)* (2021) 61(1):230–9. doi: 10.1093/rheumatology/keab305
31. Carlsson SK, Brothers SP, Wahlestedt C. Emerging Treatment Strategies for Glioblastoma Multiforme. *EMBO Mol Med* (2014) 6(11):1359–70. doi: 10.15252/emmm.201302627
32. Sampson JH, Gunn MD, Fecci PE, Ashley DM. Brain Immunology and Immunotherapy in Brain Tumours. *Nat Rev Cancer* (2020) 20(1):12–25. doi: 10.1038/s41568-019-0224-7
33. Zhao J, Zhai B, Gygi SP, Goldberg AL. mTOR Inhibition Activates Overall Protein Degradation by the Ubiquitin Proteasome System as Well as by Autophagy. *Proc Natl Acad Sci U S A* (2015) 112(52):15790–7. doi: 10.1073/pnas.1521919112
34. Budenholzer L, Cheng CL, Li Y, Hochstrasser M. Proteasome Structure and Assembly. *J Mol Biol* (2017) 429(22):3500–24. doi: 10.1016/j.jmb.2017.05.027
35. Hinshaw DC, Shevde LA. The Tumor Microenvironment Innately Modulates Cancer Progression. *Cancer Res* (2019) 79(18):4557–66. doi: 10.1158/0008-5472.CAN-18-3962
36. DeBerardinis RJ. Tumor Microenvironment, Metabolism, and Immunotherapy. *N Engl J Med* (2020) 382(9):869–71. doi: 10.1056/NEJMcibr1914890
37. Anderson NM, Simon MC. The Tumor Microenvironment. *Curr Biol* (2020) 30(16):R921–5. doi: 10.1016/j.cub.2020.06.081
38. Langley RR, Fidler IJ. The Seed and Soil Hypothesis Revisited–the Role of Tumor-Stroma Interactions in Metastasis to Different Organs. *Int J Cancer* (2011) 128(11):2527–35. doi: 10.1002/ijc.26031
39. Gatenby RA, Gillies RJ. Why do Cancers Have High Aerobic Glycolysis? *Nat Rev Cancer* (2004) 4(11):891–9. doi: 10.1038/nrc1478
40. Nagarsheth N, Wicha MS, Zou W. Chemokines in the Cancer Microenvironment and Their Relevance in Cancer Immunotherapy. *Nat Rev Immunol* (2017) 17(9):559–72. doi: 10.1038/nri.2017.49
41. Lim AR, Rathmell WK, Rathmell JC. The Tumor Microenvironment as a Metabolic Barrier to Effector T Cells and Immunotherapy. *Elife* (2020) 9: e55185. doi: 10.7554/eLife.55185
42. Bader JE, Voss K, Rathmell JC. Targeting Metabolism to Improve the Tumor Microenvironment for Cancer Immunotherapy. *Mol Cell* (2020) 78(6):1019–33. doi: 10.1016/j.molcel.2020.05.034

Conflict of Interest: The authors declare that the research was conducted in the absence of any commercial or financial relationships that could be construed as a potential conflict of interest.

Publisher's Note: All claims expressed in this article are solely those of the authors and do not necessarily represent those of their affiliated organizations, or those of the publisher, the editors and the reviewers. Any product that may be evaluated in this article, or claim that may be made by its manufacturer, is not guaranteed or endorsed by the publisher.

Copyright © 2022 Liu, Yang, Ji, Yang, Li, Long, Ye, Huang and Zhu. This is an open-access article distributed under the terms of the Creative Commons Attribution License (CC BY). The use, distribution or reproduction in other forums is permitted, provided the original author(s) and the copyright owner(s) are credited and that the original publication in this journal is cited, in accordance with accepted academic practice. No use, distribution or reproduction is permitted which does not comply with these terms.

frontiers | Frontiers in Oncology

ORIGINAL RESEARCH
published: 25 July 2022
doi: 10.3389/fonc.2022.948169

Effect of Pyroptosis-Related Genes on the Prognosis of Breast Cancer

Ying Zhou[1,2], *Jianfeng Zheng*[3], *Mengru Bai*[1,2], *Yuzhen Gao*[4] *and Nengming Lin*[1,5*]

[1] Department of Clinical Pharmacology, Key Laboratory of Clinical Cancer Pharmacology and Toxicology Research of Zhejiang Province, Affiliated Hangzhou First People's Hospital, Cancer Center, Zhejiang University School of Medicine, Hangzhou, China, [2] Department of Clinical Pharmacy, Affiliated Hangzhou First People's Hospital, Zhejiang University School of Medicine, Hangzhou, China, [3] Department of Obstetrics and Gynecology, Affiliated Hangzhou Hospital, Nanjing Medical University, Hangzhou, China, [4] Department of Clinical Laboratory, Sir Run Run Shaw Hospital of Zhejiang University School of Medicine, Hangzhou, Zhejiang, China, [5] Translational Medicine Research Center, Affiliated Hangzhou First People's Hospital, Zhejiang University School of Medicine, Hangzhou, China

Backgrounds: Pyroptosis, a newly pattern of specific programmed cell death, has been reported to participate in several cancers. However, the value of pyroptosis in breast cancer (BRCA) is still not clear.

Methods: Herein, we analyzed the data of BRCA from both The Cancer Genome Atlas (TCGA) and GSEA MSigDB database. Based on the obtained pyroptosis-related genes (PRGs), we searched the interactions by STRING. After that, we performed clustering analysis by ConsensusClusterPlus. The PRGs with significant prognostic value were then screened through univariate cox regression and further evaluate by constructing a risk model by least absolute shrinkage and selection operator (LASSO) Cox regression. The immune and sensitivity to drugs were also predicted by comprehensive algorithms. Finally, real-time quantitative PCR (qPCR) was performed on two of the screened signature PRGs.

Results: A total of 49 PRGs were obtained from public database and 35 of them were significantly differentially expressed genes (DEGs). Cluster analysis was then performed to explore the relationship between DEGs with overall survival. After that, 6 optimal PRGs (GSDMC, IL-18, CHMP3, TP63, GZMB and CHMP6) were screened out to construct a prognostic signature, which divide BRCA patients into two risk groups. Risk scores were then confirmed to be independent prognostic factors in BRCA. Functional enrichment analyses showed that the signature were obviously associated with tumor-related and immune-associated pathways. 79 microenvironmental cells and 11 immune checkpoint genes were found disparate in two groups. Besides, tumor immune dysfunction and exclusion (TIDE) scores revealed that patients with higher risk scores are more sensitive to immune checkpoint blockade treatment. Patients in the low-risk group were more sensitive to Cytarabine, Docetaxel, Gefitinib, Paclitaxel, and Vinblastine. Inversely, patients in the high-risk group were more sensitive to Lapatinib. Finally, we found that,

OPEN ACCESS

Edited by:
Shaoquan Zheng,
Sun Yat-sen University Cancer Center (SYSUCC), China

Reviewed by:
Sun Zhaoyang,
Fudan University, China
Guixiong Zhang,
The First Affiliated Hospital of Sun Yat-sen University, China

****Correspondence:***
Nengming Lin
lnm1013@zju.edu.cn

Specialty section:
This article was submitted to Molecular and Cellular Oncology, a section of the journal Frontiers in Oncology

Received: *19 May 2022*
Accepted: *20 June 2022*
Published: *25 July 2022*

Citation:
Zhou Y, Zheng J, Bai M, Gao Y and Lin N (2022) Effect of Pyroptosis-Related Genes on the Prognosis of Breast Cancer. Front. Oncol. 12:948169. doi: 10.3389/fonc.2022.948169

CHMP3 were down-regulated in both BRCA tissues and cell lines, while IL-18 were up-regulated.

Conclusion: PRGs play important roles in BRCA. Our study fills the gaps of 6 selected PRGs in BRCA, which were worthy for the further study as predict potential biomarkers and therapeutic targets.

Keywords: breast cancer, algorithm, programmed cell death, bioinformatic analyses, PRGs

INTRODUCTION

Breast cancer (BRCA) remains the most common and leading deadliest malignancy of women worldwide, despite huge advances in epidemiological, laboratory and clinical research (1). 70–80% of BRCA patients with early-stage and non-metastatic could be cured (2). Early diagnosis has been proved to effectively improve the cure rate of BRCA, about 30% of early-stage patients developed into advanced malignant BRCA with distant organ metastases. The advanced BRCA is considered incurable, in which the median overall survival time was only 2-3 years and the 5-years survival rate was only 20% (3, 4). Therefore, there is an urgent need to understand the molecular mechanism underlying of BRCA, and then identify and characterize specificity and sensitivity biomarkers for BRCA diagnosis, treatment and prognosis.

Pyroptosis was firstly found in 1986 (5), and defined as a new pattern of specifically programmed cell death in 2001 (6). It could be characterized by continuous cell swelling, bubble-like protrusions formation on the cell membrane surface before its rupture and release of cell contents which could trigger a strong inflammatory response (7). Similar to apoptosis, chromatin condensation and DNA damage also appear in the progress of pyroptosis (8, 9). As we all know, tumors are skilled at escaping the cell death pathways including apoptosis, autophagy, necrosis and pyroptosis (10, 11). All these death pathways are fully studied for their roles in anticancer defense mechanisms except for pyroptosis. Pyroptosis was reported to participate in various pathogenesis of nervous system diseases (12), autoimmune diseases (13), and cardiovascular diseases (14). In recent years, more and more researches have been performed to focus on the relationship between cancers and pyroptosis. Studies suggested that pyroptosis might be involved in the early diagnosis and treatment of cancers. In addition, it was also reported to relate to the progress of drug resistance (15). However, the role of pyroptosis in BRCA remains unclear.

In our study, we found six prognostic pyroptosis-relate genes (PRGs) from a public database for BRCA. The PRG-signature based on the six PRGs was developed. In addition, we also found differences in enrichment pathways, immune checkpoints, immune microenvironment, and sensitivity to several chemotherapeutic agents between risk groups.

Abbreviations: BRCA, Breast cancer; TCGA, The Cancer Genome Atlas; PRG, Pryroptosis-relate gene; LASSO, Least absolute shrinkage and selection operator; Quantitative PCR, qPCR; DEG, Differentially expressed gene; TIDE, Tumor immune dysfunction and exclusion; PCC, Pearson correlation coefficient; DEPG, Differentially expressed PRG; RS, risk score; ssGSEA, Single-sample gene set enrichment analysis; ICB, Immune checkpoint blockade; IHC, immunohistochemical; RS, Risk score; PPI, protein-protein interaction; OS, Overall survival.

MATERIALS AND METHODS

Data Collection

We obtained processed RNA sequencing and clinicopathological data from TCGA including 1075 BRCA samples and 113 normal ones. GSE20685 (16) including 327 BRCA samples with clinical prognostic information, and GSE42568 (17) including 17 normal samples and 104 BRCA samples with clinical prognostic information were downloaded from GEO database (18). PRGs were screened from GSEA-MSigDB database (19). We used t-test of R3.6.1 (http://127.0.0.1:15190/library/stats/html/t.test.html) to analyze PRGs expression differences in tumor and normal samples ($p < 0.05$). The expression values are hierarchically clustered using pheatmap (https://cran.r-project.org/web/packages/pheatmap/index.html) (20).

Interactive Network Construction

Based on the PRGs obtained, the interactions among proteins were searched by STRING 11.0 (http://string-db.org/) (21). The interaction scores higher than 0.4 were selected as the screening threshold to construct the interaction network, which was visualized by Cytoscape 3.6.1 (http://www.cytoscape.org/) (22). The pearson correlation coefficients (PCCs) among the targeted PRGs were also calculated by cor function of R3.6.1 (http://77.66.12.57/R-help/cor.test.html). $|PCC|>0.3$ and $P<0.05$ was selected as the screening threshold to construct the co-expression network, which was also visualized by Cytoscape 3.6.1.

Subtype Analysis

Based on significantly differentially expressed PRGs (DEPGs) selected above, ConsensusClusterPlus1.54.0 (23)(http://www.bioconductor.org/packages/release/bioc/html/ConsensusClusterPlus.html) was then applied to analyze subtypes of BRCA. Survival and prognosis of different BRCA subtypes were then assessed (24). Then, based on the obtained cancer subtypes, the R3.6.1 language survival pack version 2.41-1 was applied to evaluate the correlation between prognosis and different subtypes. The clinical information of different subtypes was then statistically plotted, and chi-square test was used to compare the distribution among different subtypes.

Signature Development Based on PRGs With Significant Prognosis

After screening the prognostic PRGs by Univariate Cox regression (P<0.05) (24), the LASSO Cox regression model (25) in the R penalty package (26) and 1000 cross-validation analysis were used to screen out the best combination of PRG markers. In addition, a risk model for BRCA patients was constructed based on the following formula:

$$\text{Risk score(RS)} = \sum \beta_{PRG} \times Exp_{PRG}$$

In the formula, β_{PRG} represented the LASSO for optimized PRGs and Exp_{PRG} means the expression level of homologous PRGs in the TCGA-BRCA dataset. Calculate the RS of each BRCA patient, and use the calculated median RS as the cutoff value, and further divide the BRCA patients into high-risk groups and low-risk groups. In the TCGA-BRCA training set and GSE42568, GSE20685 validation data sets, the same method was applied to build the risk model. Subsequently, the Kaplan-Meier analysis (24) was used to evaluate the prognostic value between the two risk subgroups.

Immunity Analysis and Sensitivity of Chemotherapy Drugs

The immune microenvironment is also closely related to the occurrence and development of BRCA. Based on single-sample gene set enrichment analysis (ssGSEA) (27), the enrichment fraction of 28 immune cells (28) was calculated to represent the relative abundance of each TME-infiltrated cell in BRCA samples using GSVA (29). In addition, three arithmetics, CIBERSORT (30, 31), xCELL (32), MCPcounter (33), were wielded to compare the difference in the proportion of various immune cells in different risk groups. Further, according to the expression data of the BRCA samples, the immune and stromal scores were estimated from R3.6.1 through ESTIMATE to represent the presence of matrix and immune cells (34). The expression levels of 13 immune checkpoint genes (BTLA, TNFRSF9, ICOS, PDCD1, TIGIT, CTLA4, LAG3, CD274, TNFRSF4, HAVCR2, SIRPA, CD47, and VTCN1) were extracted, and their expression differences in the risk group were compared by the intergroup t-test.

The potential response to immune checkpoint blockade (ICB) was predicted using the TIDE algorithm (35). We extracted chemotherapy drugs from the Genomics of Drug Sensitivity in Cancer database (https://www.cancerrxgene.org/) (36) and used R3.6.1 pRRophetic (37) to assess IC50 levels.

HPA Analysis

Expression of PRGs showed by immunohistochemical (IHC) staining in both normal and BRCA tissuses were searched by the resource of the HPA database (https://www.proteinatlas.org/). For IL-18, normal tissue, NOS(M-00100), patient id (2773); breast lobular carcinoma (M-85203), patient id (2199). For CHMP3, normal tissue, NOS(M-00100), patient id (3856); Breast lobular carcinoma (M-85203), patient id (4229).

Real-Time qPCR Analysis

MDA-MB-123 and MDA-MB-453 cells were purchased from the National Collection of Authenticated Cell Cultures (Shanghai, China) and incubated in the L-15 culture medium (Gibco, 41300039) with 10% fetal bovine serum. MCF-7 cells was culture in the MEM culture medium (Gibco, 41500034) with 1.5 g/L NaHCO3, 0.11 g/L sodium pyruvate (Invitrogen, 11360070) and 0.01 mg/mL bovine insulin (Sigma, 91077c-1G). MCF-10A purchased from American Type Culture Collection (ATCC, CRL-10317) was cultured in special culture medium (Procell, China) containing DMEM/F12, 5% HS, 20ng/mL EGF, 0.5μg/mL Hydrocortisone, 10μg/mL Insulin, 1% NEAA and 1% P/S. Real-time qPCR was performed by ABI7500 (Thermo Fisher, Singapore) after RNA extraction and reversed transcription from all these four cell lines. The primers we used for qPCR were listed in the **Additional file 1 Table S1.**

Statistical Analysis

We used R package (v4.0.2), TBtools and GraphPad Prism (v8.0) to perform and visualize statistical analysis. Kaplan-Meier survival analysis was performed on the risk group by log-rank test to draw a survival curve. Wilcoxon test is used to compare the difference between two groups.

RESULTS

Figure 1 showed the flowchart we created for the entire study.

Differentially Expressed PRGs (DEPGs)

Combining the GSEA MSigDB and the attached documents of literature, we obtained a total of 49 PRGs. By comparing the expression differences of the above genes in BRCA and normal tissues, a total of 35 significantly DEPGs were screened. **Figure 2A** showed the clustering heat map of significantly DEPGs. Among them, 16 PRGs (ELANE, TP63, IL6, NLRP1, NLRP3, NOD1, CASP1, IL1B, CASP4, GSDMB, CHMP3, SCAF11, GPX4, TIRAP, IRF2, and PLCG1) were down-expressed in the tumor samples while 19 PRGs (CASP8, CHMP6, GZMB, CHMP2A, IRF1, CHMP4B, CYCS, CASP3, CASP6, CHMP4C, NLRP6, GSDMD, BAK1, IL-18, BAX, AIM2, GSDMC, PYCARD, and NOD2.) were over-expressed in the tumor samples. Then, we conducted a protein-protein interactions (PPIs) analysis by using the STRING database to explore further the interactions of these PRGs, 310 pairs of PPIs were obtained to construct the interaction network (**Figure 2B** and **Additional file 2 Table S2**). A total of 300 co-expression connection pairs were obtained to construct the co-expression network (**Figure 2C** and **Additional file 3 Table S3**).

Subtype Analysis

Based on 35 significantly DEPGs screened out above, subtype analysis of BRCA was performed. When k=3 (k: clustering variable), the correlation within the group was the highest, and

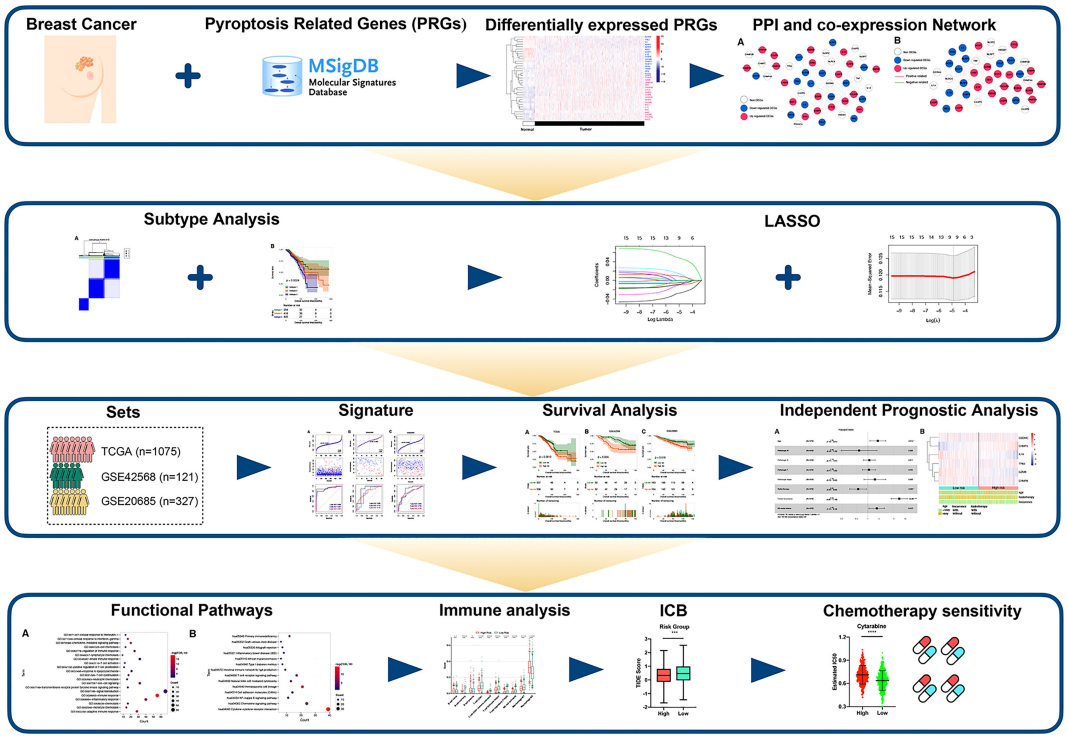

FIGURE 1 | Flow diagram of our study.

the correlation between the groups was low, a total of three different subtypes were obtained therewith (**Figure 3A**). Subtype1, 2, and 3 contained 254, 416, and 405 tumor samples, respectively. We then assessed the survival outcomes of patients with BRCA in the three subtypes. The Kaplan-Meier analysis illustrated that survival prognosis was significantly different among the three subtypes, and subtype 1 had the best prognosis, however, subtype 3 had the worst prognosis (**Figure 3B**). The expression level of PRGs and the clinical information are presented in a heatmap to display their distribution difference (**Figure 3C**). The distribution number and comparison of clinical characteristics in different subtypes are shown in **Table 1**.

Construction and Validation of a Prognostic Signature

Univariate cox regression and K–M survival analysis were performed on the 35 significantly DEPGs acquired to find out PRGs with significant prognosis. a total of 15 significant prognostic PRGs (IRF2, TP63, IRF1, CHMP6, GZMB, NLRP6, CHMP3, IL-18, TIRAP, GPX4, GSDMD, PYCARD, CASP4, GSDMC, CHMP2A) were screened (**Additional file 4 Table S4**). Six optimal DEPGs (GSDMC, CHMP3, IL-18, TP63, GZMB and CHMP6) with significant prognostic value were screened out through the least absolute contraction and selection operator LASSO cox analysis (**Additional file 5 Figure S1**) to construct the prognostic signature based on the following formula:

$$\begin{aligned} RS = {} & (-0.000377234) * Exp_{TP63} + (0.03382393) * Exp_{CHMP3} \\ & + (-0.01643936) * Exp_{CHMP6} + (-0.005408124) * Exp_{GZMB} \\ & + (-0.00004699097) * Exp_{IL\text{-}18} + (0.001271756) * Exp_{GSDMC} \end{aligned}$$

BRCA patients from the TCGA-BRCA, GSE42568, and GSE20685 databases were then divided into low-risk or high-risk subgroups based on the average RS. The distribution of RS value and survival status of each risk group in the three databases is shown in **Figures 4A–C**. In addition, the time-dependent ROC curve proves that the risk assessment model is relatively stable in predicting the 1-year, 3-year, and 5-year survival rates of BRCA patients (survival AUC exceeds 0.7, **Figures 4A–C**). The Kaplan-Meier survival curve shows that the overall survival (OS) rate of the high-risk group in the three databases is significantly lower than that of the low-risk group, indicating the accuracy of the risk model in predicting survival status (**Figures 5A–C**). The univariate and multivariate cox regression analysis of clinical characteristics and RS model showed that age, radiotherapy, recurrence and RS model are independent prognostic factors for BRCA patients (**Figure 6A** and **Table 2**). The expression levels of six optimal PRGs and the distribution of the independent prognostic factors were shown in **Figure 6B**.

Functional Pathways

A total of 525 DEGs between the two risk groups were screened out by the limma of R (**Additional file 6 Table S5**). After that,

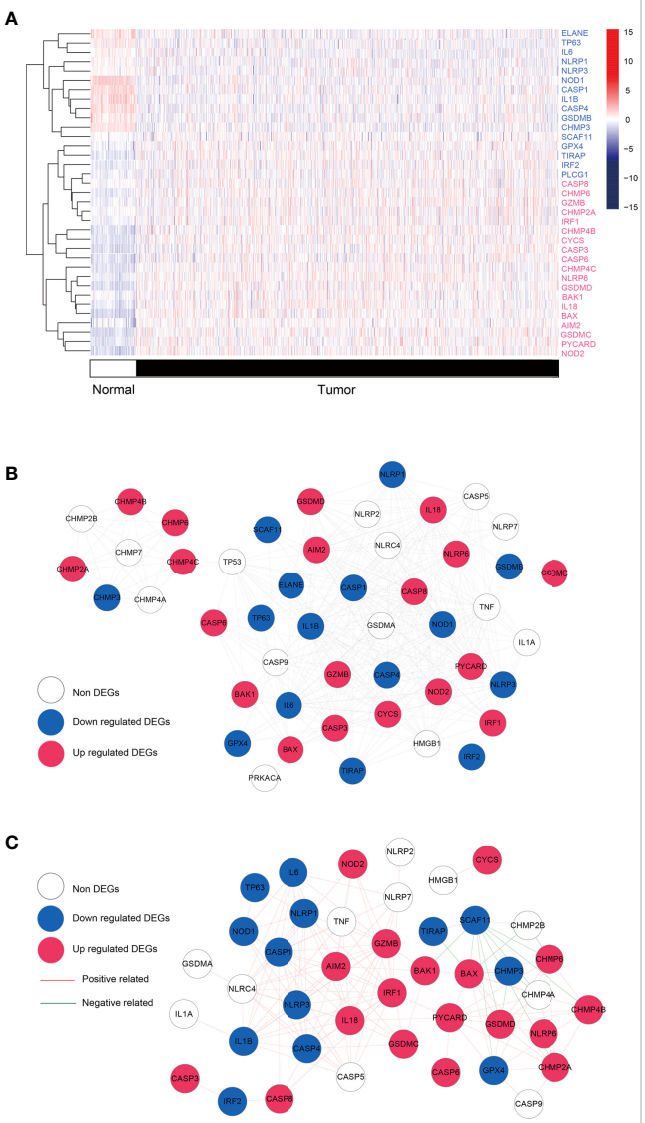

FIGURE 2 | Differential analysis and network. **(A)** Heatmap showing the expression levels of pyroptosis-related genes with significant expression levels in breast cancer tumors and control samples. Red: up regulated; blue: down regulated. **(B)** Protei-protein interaction. Blue, red, and white nodes represent genes that are significantly down-regulated, up-regulated, and insignificantly differentially expressed in tumor tissue, respectively. **(C)** co-expression network based on pyroptosis-related genes. Blue, red, and white nodes represent significantly down-regulated, up-regulated, and insignificantly differentially expressed genes in tumor tissues, respectively. Red and green junctions represent significantly positive and negative correlations.

functional enrichment analysis were performed by DAVID. 41 significantly correlated biological processes and 14 KEGG signaling pathways were enriched and top 20 of them were selected for display (**Figures 7A, B**). The results suggested that those DEGs were obviously related to several biological processes in immunity and tumor development.

Immunity Analysis

According to five algorithms (ssGSEA, Estimate, MCPcounter, xCELL and Cibersort), immune score, estimate score, the stromal score and the relative infiltration abundance of stromal cells and immune cells are estimated for each sample (**Additional file 7 Table S6**). The results of our analysis showed that immune score and Estimate score were higher in the low-risk group (**Figure 8A**). Based on the remaining 4 algorithms, we found that a total of 79 microenvironmental cells appeared, with significant differences. The first 10 are selected for display (**Figures 8B–E**). In view of the importance of immune checkpoints in cancer treatment, the expression of 13 checkpoint genes (BTLA, TNFRSF9, ICOS, PDCD1, TIGIT, CTLA4, LAG3, CD274, TNFRSF4, HAVCR2, SIRPA, CD47 and VTCN1) were compared. The box plot of the expression distribution of 13 immune checkpoint genes between the two risk groups is shown in **Figure 8F**. The results showed that, except for CD47 and VTCN1, there were significant differences in the other 11 genes ($P<0.05$). The expression of 11 genes in the high-risk group was low. The TIDE score is closely related to the response to ICB. In **Figure 8G**, the TIDE score of BRCA patients in the high-risk group is lower than that in the low-risk group, indicating that BRCA patients with higher RS are more sensitive to ICB treatment.

Sensitivity of Chemotherapy Drugs

In view of the significance of chemotherapy in BRCA treatment, we quantified the response ability of BRCA patients with different risk scores to 21 chemotherapy drugs. **Figure 9** showed the results of six commonly used BRCA chemotherapy drugs. Our data showed that the IC50 level of Lapatinib was significantly higher in the low-risk group than in the high-risk group (**Figure 9A**). In contrast, the IC50 levels of Cytarabine (**Figure 9B**), Docetaxel (**Figure 9C**), Gefitinib (**Figure 9D**), Paclitaxel (**Figure 9E**), and Vinblastine (**Figure 9F**) in the low-risk group were significantly lower than the high-risk group, indicating that BRCA patients in the low-risk group are more sensitive to these drugs.

Expression of the Signature PRGs

To explore the expression level of the signature PRGs, we performed real-time qPCR analysis on three PRGs in different cell lines. Results suggested that CHMP3 were down-regulated in the BRCA cell lines including MDA-MB-231, MDA-MB-453 and MCF-7 compared with in the normal breast MCF-10A cell line. While IL-18 were up-regulated (**Figures 10A, B**). We also checked the IHC staining data from both normal and BRCA tissues in the HPA database. As shown in **Figures 10C, D**, expression of IL-18 was higher in BRCA tissues than normal ones, while expression of CHMP3 was lower in BRCA tissues.

DISCUSSION

Pyrolysis is a kind of programmed cell death accompanied by the inflammatory response, mainly triggered by activating

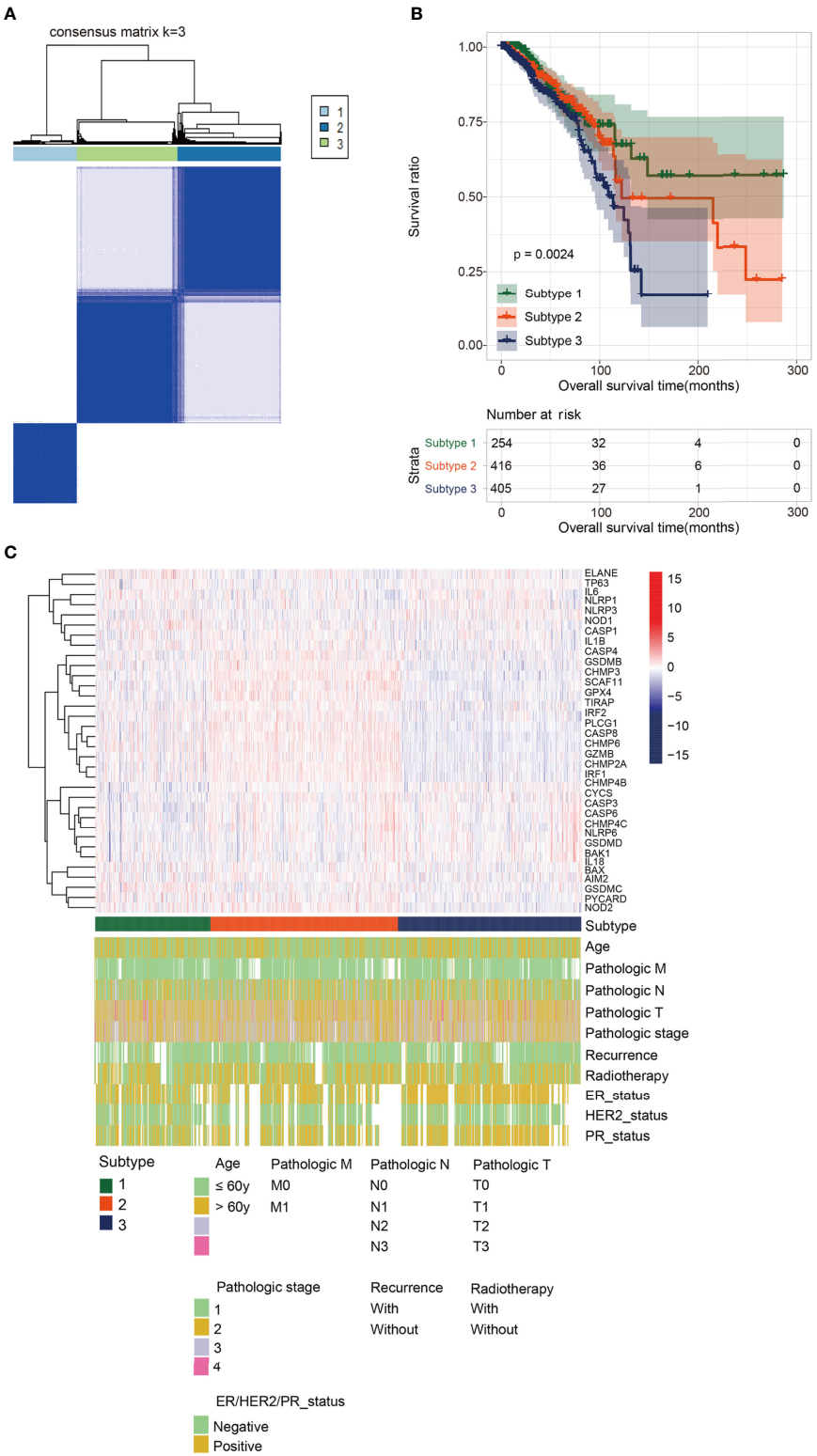

FIGURE 3 | Subtype analysis. **(A)** Cluster diagram for subtype analysis of breast cancer samples. The intragroup correlations were the highest and the inter-group correlations were low when k=2. **(B)** The Kaplan-Meier analysis for the three different subtypes. Subtype 1 had the best prognosis, while Subtype 3 had the worst prognosis. **(C)** The distribution map of pyroptosis- related genes and clinicopathologic characters in the three subtypes.

TABLE 1 | Distribution of clinical information among different subtypes.

Characteristics total cases	N of case 1075	Subtype			P value
		Subtype 1 (N=254)	Subtype 2 (N=416)	Subtype 3 (N=405)	
Age(years)					
≤60	596	140	257	199	1.28E-03
>60	479	114	159	206	
ER status					
Positive	584	132	179	273	2.20E-16
Negative	178	79	78	21	
HER2 status					
Positive	111	43	35	33	2.38E-02
Negative	635	169	210	256	
PR status					
Positive	509	109	164	236	8.64E-12
Negative	249	102	92	55	
Pathologic M					
M0	892	226	331	335	5.38E-01
M1	22	4	7	11	
Pathologic N					
N0	504	129	181	194	2.27E-01
N1	356	79	142	135	
N2	120	27	49	44	
N3	75	14	39	22	
Pathologic T					
T1	279	60	123	96	1.86E-02
T2	622	164	227	231	
T3	133	21	56	56	
T4	38	9	9	20	
Pathologic stage					
Stage I	181	41	76	64	4.54E-01
Stage II	609	154	222	233	
Stage III	244	50	104	90	
Stage IV	20	4	6	10	
Radiation therapy					
Yes	550	115	233	202	7.44E-02
No	441	111	157	173	
Recurrence					
Yes	96	20	37	39	8.09E-01
No	808	177	331	300	

inflammatory cysteine protease caspase-1/4/5/11 to cleave GSDMD or apoptotic cysteine protease Caspase-3 to cleave GSDME (11). Pyroptosis is involved in the occurrence and development of various diseases (38, 39). In recent years, the significance of pyroptosis in cancer has received extensive attention, accumulated many new achievements, and formed some new insights (40, 41). Chemotherapeutic agents activate Caspases to induce tumor cell death in either apoptosis or pyroptosis, depending on the expression level of GSDME in the cells. In lung cancer cells, loss of GSDME expression promotes resistance to chemotherapy, while overexpression of GSDME enhances the sensitivity of cells to chemotherapy drugs (42, 43). In HPV-infected cervical cancer cells, AIM2 plays a cancer-suppressive role by promoting pyroptosis (44). Studies have shown that the combination of low-dose PLK1 inhibitor BI2536 can enhance the sensitivity of esophageal squamous cancer cells to cisplatin. The mechanism lies in that BI2536 can inhibit the DNA damage repair pathway and promote cell pyroptosis mediated by the Caspase-3-GSDME pathway in coordination with cisplatin (45).

In order to verify the importance of pyrolysis in BRCA progression, we developed the prognostic and diagnostic models related to pyrolysis. The gene expression levels of 49 PRGs were studied in BRCA and normal tissues, and 35 PRGs were found to be differentially expressed. Then we studied the importance of these PRGs related to survival. Several PRGs that are highly expressed in BRCA tissues also predicted a poor prognosis, such as GSDMC. GSDMC has also been proved to be over-expressed in lung adenocarcinoma and function as a predictive factor for poor prognosis (46), which inspired us to put much more effort into exploring the function of GSDMC as a prognostic biomarker in BRCA. To further prove the PRGs expression signature has significant prognostic value in BRCA, we constructed a prognostic risk model through univariate and multivariate Cox regression analysis. Our research generated a signature characteristic of 6 PRGs, which could predict prognosis in BRCA patients. Among them, GSDMC firstly caught our attention. As we introduced above, Caspase-1/4/5/11 cleavage of GSDMD or cleavage of GSDME by caspase-3 has defined the canonical pyroptosis pathways. However,

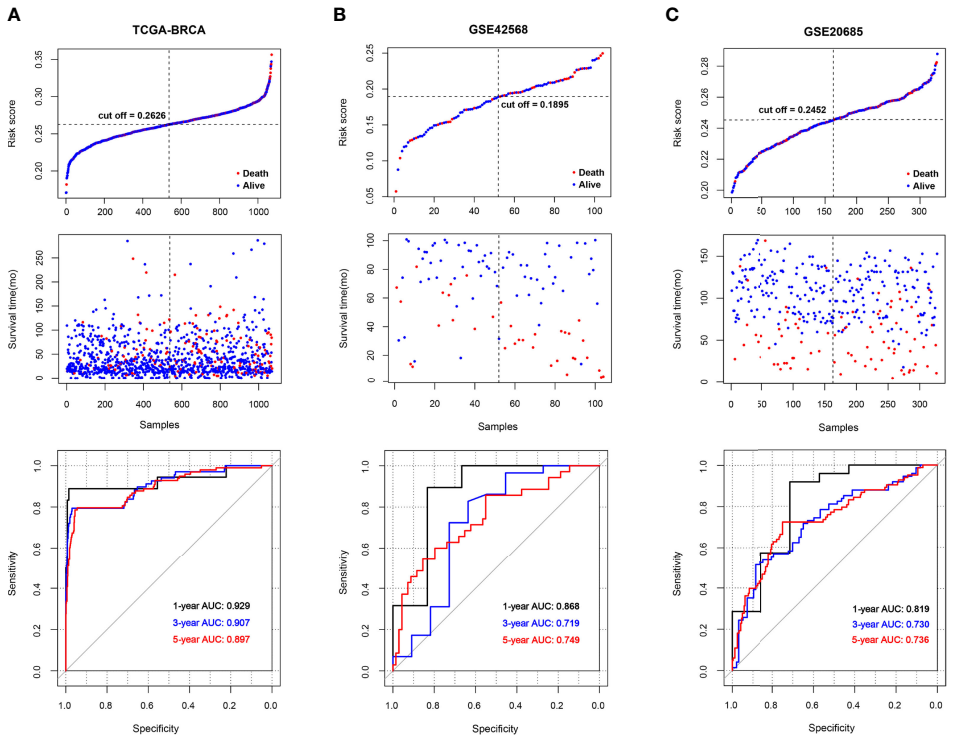

FIGURE 4 | The survival status and ROC curves. **(A-C)** The survival status for each patient and the time-dependent ROC curve in TCGA **(A)**, GSE42568 **(B)**, and GSE20685 **(C)**.

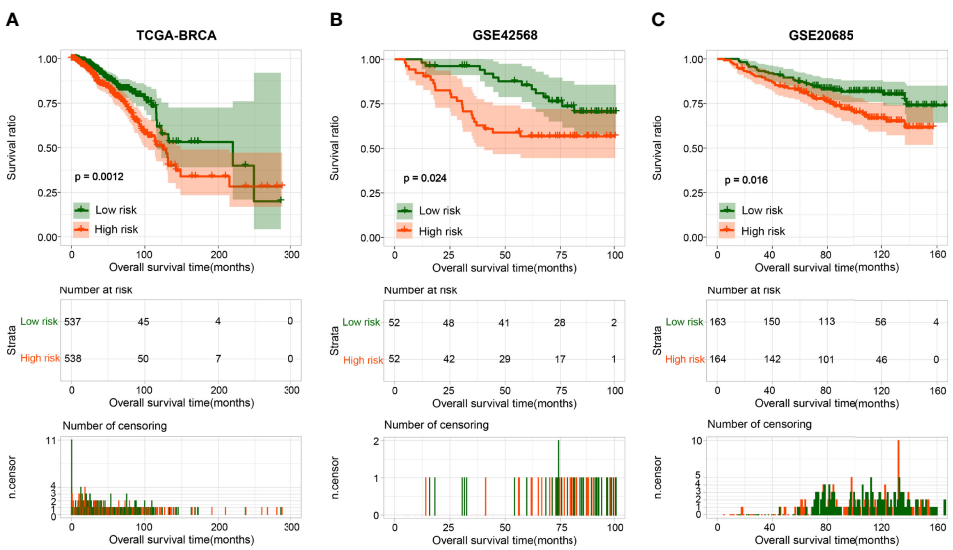

FIGURE 5 | The Kaplan-Meier analysis based on the prognostic signature. The Kaplan-Meier analysis for TCGA **(A)**, GSE42568 **(B)**, and GSE20685 **(C)**. The blue and red curves represent low- or high-risk samples, respectively.

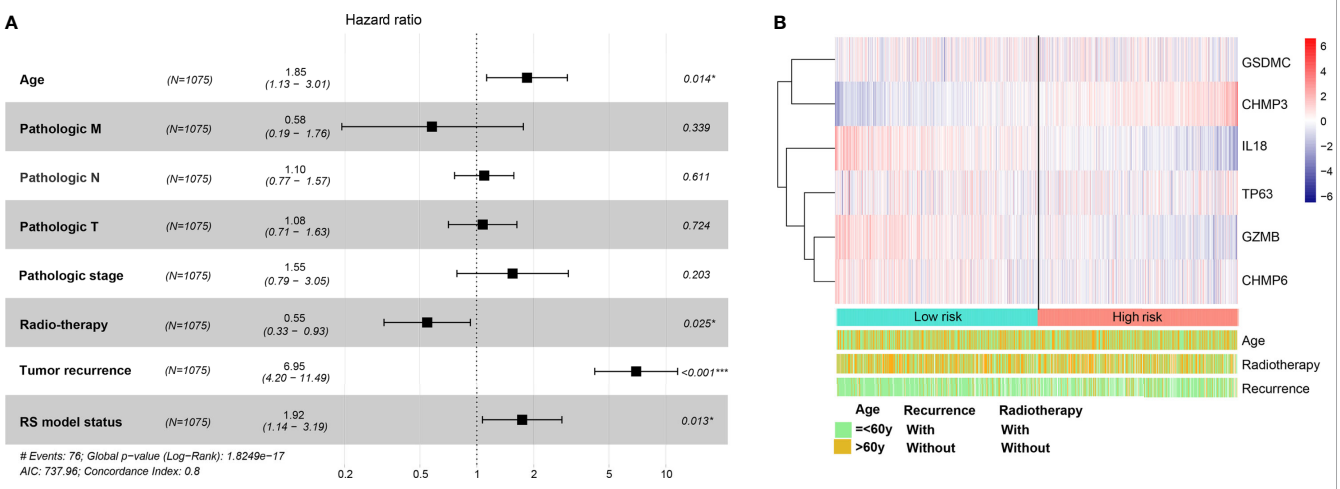

FIGURE 6 | The univariate and multivariate Cox regression analysis for prognostic signature. **(A)** Forest plot for the prognosis of clinicopathologic characters. **(B)** Heatmap for the connections between the expression levels of six optimal PRGs and the distribution of the independent prognostic factors. Red: up regulated; blue: down regulated. *p < 0.05, ***p < 0.001.

few studies have been focused on the GSDMC. GSDMC, also known as gasdermin C, was one member of the six human gasdermin family, of which five were reported to relate with significant biological functions, while the function of GSDMC has not been identified clearly (47). GSDMC is expressed mainly in the trachea and spleen (48). In recent reports, it also detected in the gastric epithelium (49). The full length of GSDMC before cleavage is inactive. The released N-terminal moiety binds to membranes and forms pores upon cleavage, triggering cell death (50). The most recent study of GSDMC proposed that under the condition of hypoxia and TNF-α treatment, GSDMC gene transcription was enhanced by PD-L1 and cleaved by activated caspase-8. Generated GSDMC N-terminal domain induced tumor necrosis by switch apoptosis to pyroptosis (51). This GSDMC/caspase-8-mediated cell death provides new and valuable insights into the pathway of cancer cell pyrolysis. Interestingly, in our research, caspase-8 (CASP8) also appears to be up-regulated in BRCA organizations (**Figure 2A**). A wonder whether GSDMC/caspase-8-mediated pyrolysis can be a potential therapeutic target for BRCA. It is also valuable to study whether GSDMC/caspase-8-mediated pyrolysis has a role in other types of cancer. GZMB, also named Granzyme B, take participate in the classical pyroptosis pathway. It was reported that GZMB from killer cells could cleave the GSDME directly and promote the occurrence of pyroptosis, which could further activate the anti-tumor immune response and inhibit tumor growth (52). However, the function of GZMB-related pyroptosis in BRCA remains unclear. Our results suggested that GZMB was highly expressed in BRCA tissues. In addition, the highly GZMB expression was connected with a good survival outcome, which is consistent with the conclusion proved in other cancers. Our study indicated that GZMB should also function as a promising target for BRCA prognosis. IL-18 is a chemokine that attracts basophils, neutrophils and T cells. It is released from several cell types in response to inflammatory stimuli (53, 54). When caspase-1 mediated cell pyroptosis occurred, the activated caspase-1 would cleave the precursor of IL-18 and IL-1β and release these two factors into cells. The release of IL-18 is regarded as the key signal of cell pyroptosis. We found that the IL-18 expression was up-regulated in

TABLE 2 | The univariate and multivariate Cox regression analysis.

Clinical characteristics	Uni-variables cox			Multi-variables cox		
	HR	95%CI	P	HR	95%CI	P
Age (=<60/>60y)	1.964	1.423-2.710	2.88E-05	1.846	1.131-3.013	1.42E-02
Pathologic_M (M0/M1/-)	1.731	1.236-2.422	4.23E-11	0.582	0.192-1.764	3.39E-01
Pathologic_N (N0/N1/N2/N3)	1.611	1.356-1.912	2.91E-08	1.098	0.766-1.574	6.11E-01
Pathologic_T (T1/T2/T3/T4)	1.461	1.199-1.780	1.63E-04	1.078	0.711-1.634	7.24E-01
Pathologic_stage (I/II/III/IV)	2.204	1.761-2.759	3.67E-12	1.551	0.789-3.046	2.03E-01
ER status (Positive/Negative)	0.991	0.641-1.532	9.69E-01	–	–	–
HER2 status (Positive/Negative)	1.031	0.585-1.811	9.20E-01	–	–	–
PR status (Positive/Negative)	0.922	0.627-1.356	6.80E-01	–	–	–
Radio-therapy (Yes/No)	0.585	0.402-0.852	4.62E-03	0.549	0.325-0.929	2.54E-02
Recurrence (Yes/No)	7.679	5.069-11.63	2.00E-16	6.951	4.202-11.49	4.15E-14
RS model status (High/Low)	1.731	1.236-2.422	1.08E-03	1.912	1.142-3.191	1.30E-02

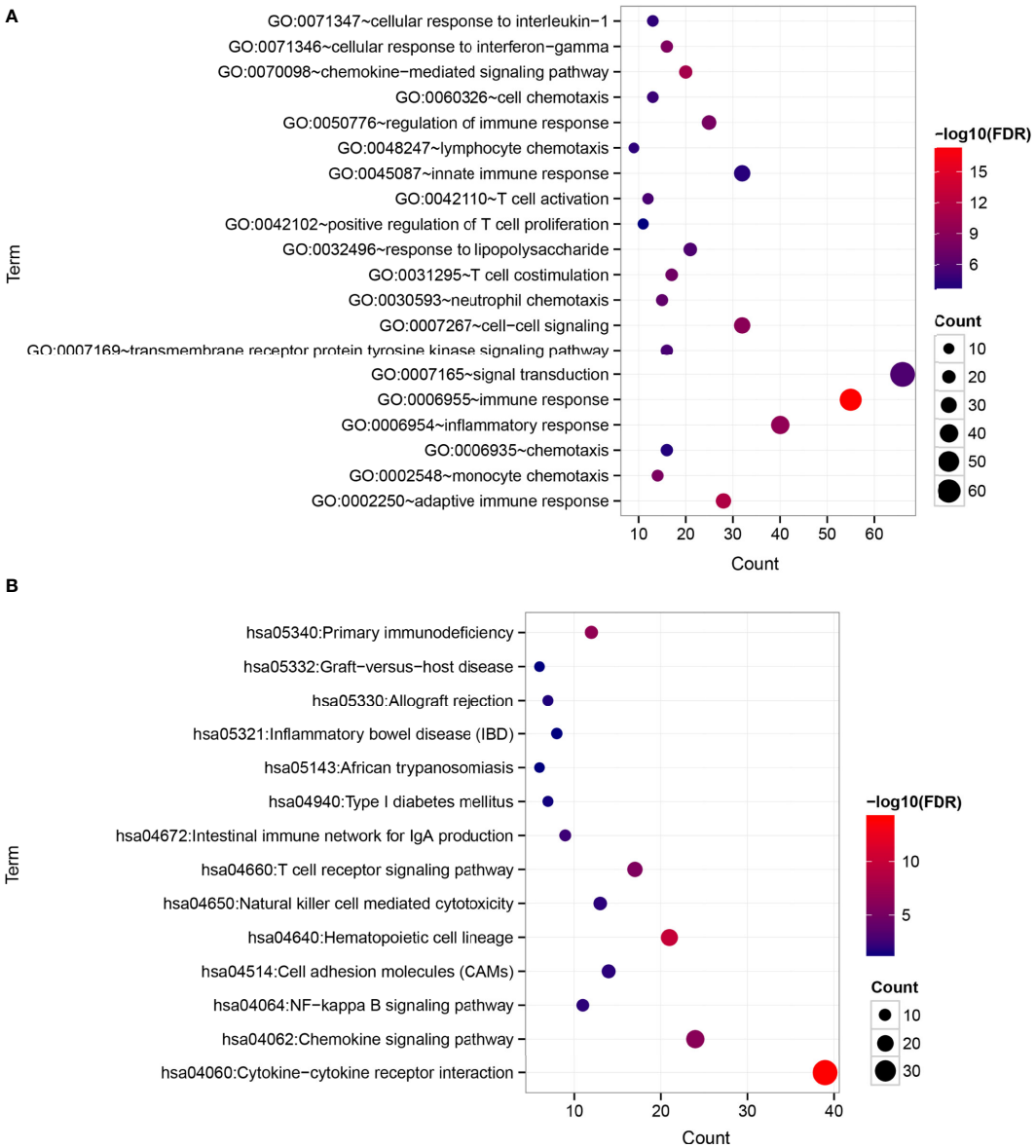

FIGURE 7 | Differences in functional pathways between the risk groups. **(A)** Biological processes (BP). **(B)** KEGG signaling pathways. The horizontal axis represents the number of significantly differentially expressed genes, the vertical axis represents the item name, the size of the dots represents the number of DEGs, the color of the dots represents the enrichment significance, and the closer the color is to red, the higher the significance.

BRCA tissues and predicted a good survival rate in BRCA. This result differs from its expression related to prognosis in other cancers. We speculate that it might be due to the inflammatory microenvironment induced by IL-18 and other inflammatory factors. Inflammasome plays a "double-edged sword" role in tumor progress. On the one hand, inflammasome, such as IL-18, could induce pyroptosis and inhibit tumor cell proliferation; On the other hand, the cumulative effect of inflammatory bodies could also build a suitable microenvironment for tumor growth. Thus, the precise condition that IL-18 participates in pyropyosis and its related prognosis in BRCA is worth discussing further issues. The relationship between CHMP6,CHMP3 and TP63 with cell pyrophosis has rarely been mentioned. Previous studies reported that CHMP6 was significantly down-regulated across several kinds of cancers including BRCA, especially in triple-negative breast cancer. Increasing understanding of these PRGs will provide a new insight into the therapeutic strategies for BRCA.

We further explored the differences in responding to ICB therapy, chemotherapy drug sensitivity between the two risk groups. Our data showed that BRCA patients with higher RS are more sensitive to ICB treatment and lapatinib, while patients in the low-risk group are more sensitive to Cytarabine, Docetaxel, Gefitinib, Paclitaxel, and Vinblastine. Our findings reveal the potential biomarkers and therapeutic targets of PRG-based risk models.

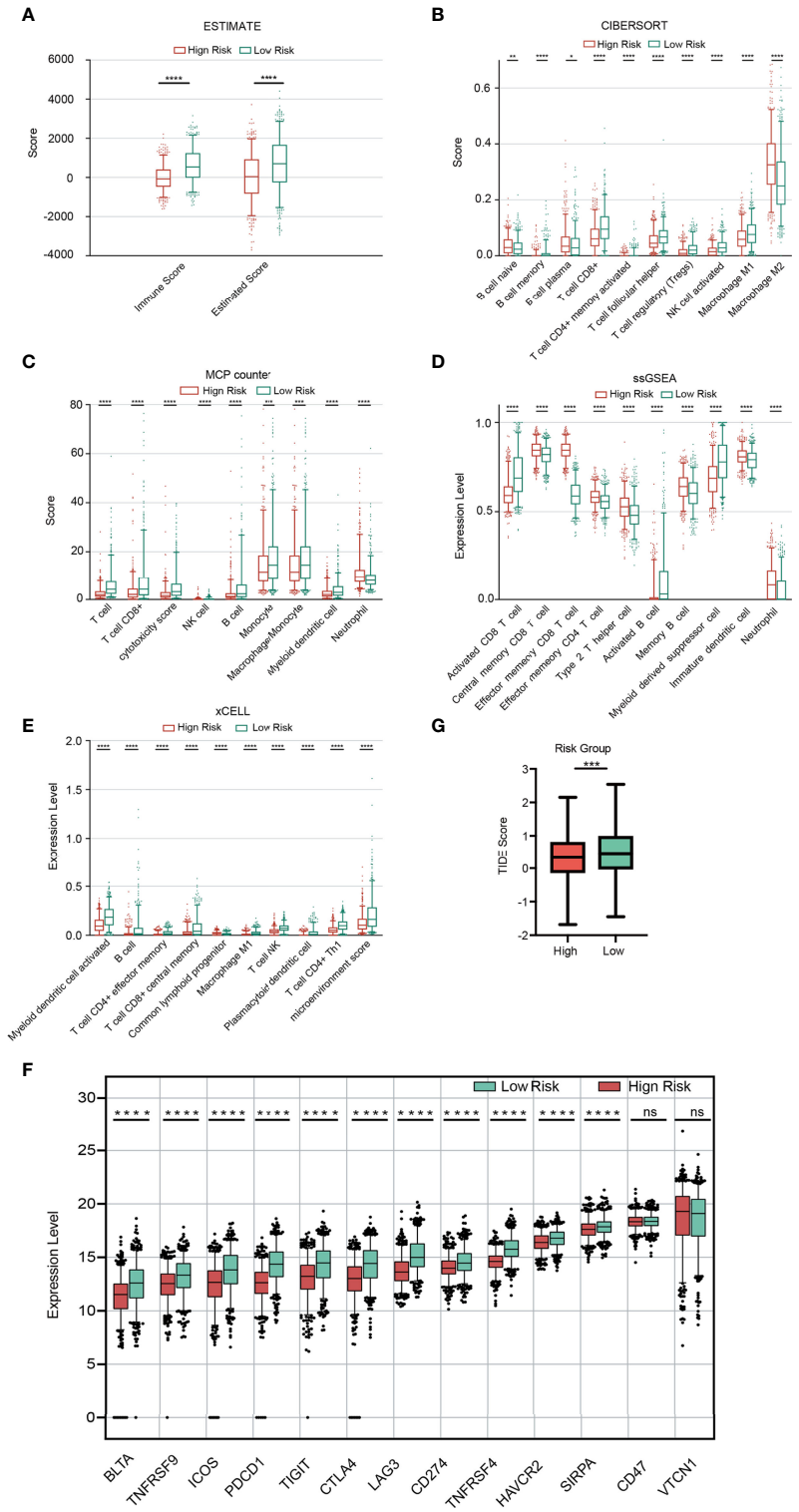

FIGURE 8 | Immune analysis. **(A)** Comparison of the immune score and ESTIMATE score between the two risk groups. **(B-E)** Comparison of immune cells between the two risk groups based on Cibersort **(B)**, MCPcount **(C)**, ssGSEA **(D)** and xCELL **(E)**. Expression distribution of 13 immune checkpoint genes between the two risk groups **(F)**. TIDE score between the two risk groups **(G)**.

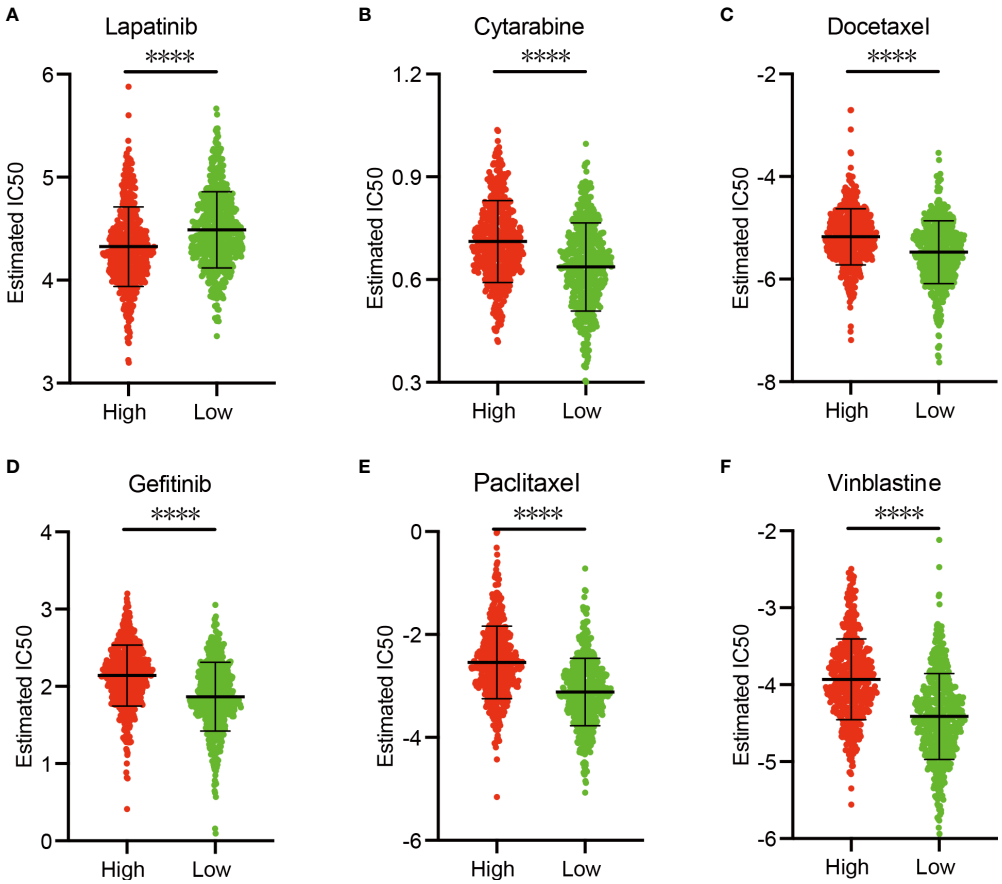

FIGURE 9 | Sensitivity of chemotherapy drugs. **(A–F)** Difference in the estimated IC50 levels of Lapatinib **(A)**, Cytarabine **(B)**, Docetaxel **(C)**, Gefitinib **(D)**, Paclitaxel **(E)**, and Vinblastine **(F)**. Data are shown as means ± S.D. ns: not significant, *p < 0.05, **p < 0.01, ***p < 0.001, ****p < 0.0001.

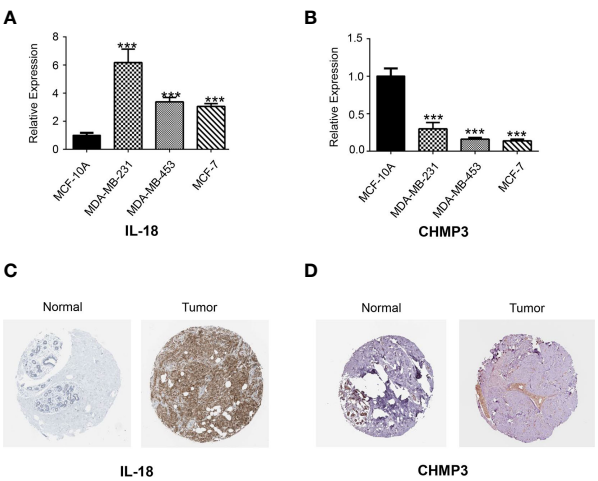

FIGURE 10 | Real-time qPCR and HPA analysis. The expression of two candidate PRGs including IL-18 **(A)** and CHMP3 **(B)** in both normal breast cell line (MCF-10A) and breast cancer cell lines (MDA-MB-231, MDA-MB-453 and MCF-7) were checked by qPCR analysis. IHC staining for IL-18 **(C)** and CHMP3 **(D)** from HPA database.

Our research still has limitations. For example, we mainly explore the functions of these PRGs through bioinformatics analysis. Therefore, further experimental data is needed to support these conclusions. Despite these limitations, our study used two validation sets to prove the effectiveness of the risk model for predicting prognosis.

CONCLUSIONS

In conclusion, our risk model based on six PRGs identified and validated is an independent prognostic factor for BRCA patients. Through comprehensive analysis, our research results reveal the potential biomarkers and treatment targets of PRG-based risk models.

DATA AVAILABILITY STATEMENT

The original contributions presented in the study are included in the article/**Supplementary Material**. Further inquiries can be directed to the corresponding author.

AUTHOR CONTRIBUTIONS

NL conceived, designed, and supervised the study. YZ drafted the manuscript. JZ performed the data analysis. MB arranged the figures. YG performed the HPA analysis and *in vitro* assay. All authors contributed to the article and approved the submitted version.

FUNDING

This work was supported by the National Natural Science Foundation of China (Grant No. 31900922), the Beijing Zhongwei Joint Funds of the Zhejiang Provincial Natural Science Foundation of China (Grant No. LBY22H200007) and the National Natural Science Foundation of China (Grant No. 82003838).

ACKNOWLEDGMENTS

We are grateful for the data from The Cancer Genome Atlas.

SUPPLEMENTARY MATERIAL

The Supplementary Material for this article can be found online at: https://www.frontiersin.org/articles/10.3389/fonc.2022.948169/full#supplementary-material

Additional file 1 Table S1 | The primer sequences in PCR analysis.

Additional file 2 Table S2 | Protein–protein interactions.

Additional file 3 Table S3 | Co-expression network.

Additional file 4 Table S4 | 15 significant prognostic PRGs.

Additional file 5 Figure S1 | λ selection diagram.

Additional file 6 Table S5 | DEGs of the two risk groups.

Additional file 7 Table S6 | Immunity analysis.

REFERENCES

1. Lotter W, Diab AR, Haslam B, Kim JG, Grisot G, Wu E, et al. Robust Breast Cancer Detection in Mammography and Digital Breast Tomosynthesis Using an Annotation-Efficient Deep Learning Approach. *Nat Med* (2021) 27 (2):244–9. doi: 10.1038/s41591-020-01174-9
2. Harbeck N, Penault-Llorca F, Cortes J, Gnant M, Houssami N, Poortmans P, et al. Breast Cancer. *Nat Rev Dis Primers* (2019) 5(1):66. doi: 10.1038/s41572-019-0111-2
3. [Guidelines for Clinical Diagnosis and Treatment of Advanced Breast Cancer in China (2020 Edition)]. *Zhonghua Zhong Liu Za Zhi [Chinese J Oncology]* (2020) 42(10):781–97. doi: 10.3760/cma.j.cn112152-20200817-00747
4. Rossi L, Mazzara C, Pagani O. Diagnosis and Treatment of Breast Cancer in Young Women. *Curr Treat Options Oncol* (2019) 20(12):86. doi: 10.1007/s11864-019-0685-7
5. Friedlander AM: Macrophages are Sensitive to Anthrax Lethal Toxin Through an Acid-Dependent Process. *J Biol Chem* (1986) 261(16):7123–6.
6. D'Souza CA, Heitman J. Dismantling the Cryptococcus Coat. *Trends Microbiol* (2001) 9(3):112–3. doi: 10.1016/S0966-842X(00)01945-4
7. Yu P, Zhang X, Liu N, Tang L, Peng C, Chen X. Pyroptosis: Mechanisms and Diseases. *Signal Transduction Targeted Ther* (2021) 6(1):128. doi: 10.1038/s41392-021-00507-5
8. Chen X, He WT, Hu L, Li J, Fang Y, Wang X, et al. Pyroptosis is Driven by non-Selective Gasdermin-D Pore and Its Morphology is Different From MLKL Channel-Mediated Necroptosis. *Cell Res* (2016) 26(9):1007–20. doi: 10.1038/cr.2016.100
9. Rudel T, Bokoch GM. Membrane and Morphological Changes in Apoptotic Cells Regulated by Caspase-Mediated Activation of PAK2. *Sci (New York NY)* (1997) 276(5318):1571–4. doi: 10.1126/science.276.5318.1571
10. Cerella C, Teiten MH, Radogna F, Dicato M, Diederich M. From Nature to Bedside: Pro-Survival and Cell Death Mechanisms as Therapeutic Targets in Cancer Treatment. *Biotechnol Adv* (2014) 32(6):1111–22. doi: 10.1016/j.biotechadv.2014.03.006
11. Shi J, Gao W, Shao F. Pyroptosis: Gasdermin-Mediated Programmed Necrotic Cell Death. *Trends Biochem Sci* (2017) 42(4):245–54. doi: 10.1016/j.tibs.2016.10.004
12. Zhang X, Zhang Y, Li R, Zhu L, Fu B, Yan T. Salidroside Ameliorates Parkinson's Disease by Inhibiting NLRP3-Dependent Pyroptosis. *Aging* (2020) 12(10):9405–26. doi: 10.18632/aging.103215
13. Wu J, Sun J, Meng X. Pyroptosis by Caspase-11 Inflammasome-Gasdermin D Pathway in Autoimmune Diseases. *Pharmacol Res* (2021) 165:105408. doi: 10.1016/j.phrs.2020.105408
14. Wang Q, Wu J, Zeng Y, Chen K, Wang C, Yang S, et al. Pyroptosis: A Pro-Inflammatory Type of Cell Death in Cardiovascular Disease. *Clinica Chimica Acta; Int J Clin Chem* (2020) 510:62–72. doi: 10.1016/j.cca.2020.06.044
15. Ruan J, Wang S, Wang J. Mechanism and Regulation of Pyroptosis-Mediated in Cancer Cell Death. *Chem Biol Interact* (2020) 323:109052. doi: 10.1016/j.cbi.2020.109052
16. Kao KJ, Chang KM, Hsu HC, Huang AT. Correlation of Microarray-Based Breast Cancer Molecular Subtypes and Clinical Outcomes: Implications for Treatment Optimization. *BMC Cancer* (2011) 11:143. doi: 10.1186/1471-2407-11-143
17. Clarke C, Madden SF, Doolan P, Aherne ST, Joyce H, O'Driscoll L, et al. *Et Al*: Correlating Transcriptional Networks to Breast Cancer Survival: A Large-Scale Coexpression Analysis. *Carcinogenesis* (2013) 34(10):2300–8. doi: 10.1093/carcin/bgt208

18. Hendrick RE. Radiation Doses and Cancer Risks From Breast Imaging Studies. *Radiology* (2010) 257(1):246–53. doi: 10.1148/radiol.10100570
19. Ye Y, Dai Q, Qi H. A Novel Defined Pyroptosis-Related Gene Signature for Predicting the Prognosis of Ovarian Cancer. *Cell Death Discovery* (2021) 7 (1):71. doi: 10.1038/s41420-021-00451-x
20. Wang L, Cao C, Ma Q, Zeng Q, Wang H, Cheng Z, et al. : RNA-Seq Analyses of Multiple Meristems of Soybean: Novel and Alternative Transcripts, Evolutionary and Functional Implications. *BMC Plant Biol* (2014) 14:169. doi: 10.1186/1471-2229-14-169
21. Szklarczyk D, Morris JH, Cook H, Kuhn M, Wyder S, Simonovic M, et al. The STRING Database in 2017: Quality-Controlled Protein-Protein Association Networks, Made Broadly Accessible. *Nucleic Acids Res* (2017) 45(D1):D362–d368. doi: 10.1093/nar/gkw937
22. Shannon P, Markiel A, Ozier O, Baliga NS, Wang JT, Ramage D, et al. Cytoscape: A Software Environment for Integrated Models of Biomolecular Interaction Networks. *Genome Res* (2003) 13(11):2498–504. doi: 10.1101/gr.1239303
23. Zhang X, Ren L, Yan X, Shan Y, Liu L, Zhou J, et al. Identification of Immune-Related lncRNAs in Periodontitis Reveals Regulation Network of gene-lncRNA-Pathway-Immunocyte. *Int Immunopharmacol* (2020) 84:106600. doi: 10.1016/j.intimp.2020.106600
24. Wang P, Wang Y, Hang B, Zou X, Mao JH. A Novel Gene Expression-Based Prognostic Scoring System to Predict Survival in Gastric Cancer. *Oncotarget* (2016) 7(34):55343–51. doi: 10.18632/oncotarget.10533
25. Tibshirani R. The Lasso Method for Variable Selection in the Cox Model. *Stat Med* (1997) 16(4):385–95. doi: 10.1002/(SICI)1097-0258(19970228)16:4<385::AID-SIM380>3.0.CO;2-3
26. Goeman JJ. L1 Penalized Estimation in the Cox Proportional Hazards Model. *Biomet J Biometris Z* (2010) 52(1):70–84. doi: 10.1002/bimj.200900028
27. Shi J, Jiang D, Yang S, Zhang X, Wang J, Liu Y, et al. LPAR1, Correlated With Immune Infiltrates, Is a Potential Prognostic Biomarker in Prostate Cancer. *Front Oncol* (2020) 10:846. doi: 10.3389/fonc.2020.00846
28. Jia Q, Wu W, Wang Y, Alexander PB, Sun C, Gong Z, et al. Local Mutational Diversity Drives Intratumoral Immune Heterogeneity in non-Small Cell Lung Cancer. *Nat Commun* (2018) 9(1):5361. doi: 10.1038/s41467-018-07767-w
29. Hänzelmann S, Castelo R, Guinney J. GSVA: Gene Set Variation Analysis for Microarray and RNA-Seq Data. *BMC Bioinf* (2013) 14:7. doi: 10.1186/1471-2105-14-7
30. Chen B, Khodadoust MS, Liu CL, Newman AM, Alizadeh AA. Profiling Tumor Infiltrating Immune Cells With CIBERSORT. *Methods Mol Biol (Clifton NJ)* (2018) 1711:243–59. doi: 10.1007/978-1-4939-7493-1_12
31. Newman AM, Liu CL, Green MR, Gentles AJ, Feng W, Xu Y, et al. Robust Enumeration of Cell Subsets From Tissue Expression Profiles. *Nat Methods* (2015) 12(5):453–7. doi: 10.1038/nmeth.3337
32. Aran D, Hu Z, Butte AJ. Xcell: Digitally Portraying the Tissue Cellular Heterogeneity Landscape. *Genome Biol* (2017) 18(1):220. doi: 10.1186/s13059-017-1349-1
33. Xu Q, Xu H, Deng R, Wang Z, Li N, Qi Z, et al. Multi-Omics Analysis Reveals Prognostic Value of Tumor Mutation Burden in Hepatocellular Carcinoma. *Cancer Cell Int* (2021) 21(1):342. doi: 10.1186/s12935-021-02049-w
34. Hu D, Zhou M, Zhu X. Deciphering Immune-Associated Genes to Predict Survival in Clear Cell Renal Cell Cancer. *BioMed Res Int* (2019) 2019:2506843. doi: 10.1155/2019/2506843
35. Fu J, Li K, Zhang W, Wan C, Zhang J, Jiang P, et al. Large-Scale Public Data Reuse to Model Immunotherapy Response and Resistance. *Genome Med* (2020) 12(1):21. doi: 10.1186/s13073-020-0721-z
36. Yang W, Soares J, Greninger P, Edelman EJ, Lightfoot H, Forbes S, et al. Genomics of Drug Sensitivity in Cancer (GDSC): A Resource for Therapeutic Biomarker Discovery in Cancer Cells. *Nucleic Acids Res* (2013) 41(Database issue):D955–961. doi: 10.1093/nar/gks1111
37. Geeleher P, Cox N, Huang RS. Prrophetic: An R Package for Prediction of Clinical Chemotherapeutic Response From Tumor Gene Expression Levels. *PLoS One* (2014) 9(9):e107468. doi: 10.1371/journal.pone.0107468
38. Jia C, Chen H, Zhang J, Zhou K, Zhuge Y, Niu C, et al. Role of Pyroptosis in Cardiovascular Diseases. *Int Immunopharmacol* (2019) 67:311–8. doi: 10.1016/j.intimp.2018.12.028
39. Man SM, Karki R, Kanneganti TD. Molecular Mechanisms and Functions of Pyroptosis, Inflammatory Caspases and Inflammasomes in Infectious Diseases. *Immunol Rev* (2017) 277(1):61–75. doi: 10.1111/imr.12534
40. Fang Y, Tian S, Pan Y, Li W, Wang Q, Tang Y, et al. Pyroptosis: A New Frontier in Cancer. *Biomed Parmacot = Biomed Pharmacoth* (2020) 121:109595. doi: 10.1016/j.biopha.2019.109595
41. Xia X, Wang X, Cheng Z, Qin W, Lei L, Jiang J, et al. The Role of Pyroptosis in Cancer: Pro-Cancer or Pro-"Host"? *Cell Death Dis* (2019) 10(9):650. doi: 10.1038/s41419-019-1883-8
42. Lu H, Zhang S, Wu J, Chen M, Cai MC, Fu Y, et al. Molecular Targeted Therapies Elicit Concurrent Apoptotic and GSDME-Dependent Pyroptotic Tumor Cell Death. *Clin Cancer Res* (2018) 24(23):6066–77. doi: 10.1158/1078-0432.CCR-18-1478
43. Zhang CC, Li CG, Wang YF, Xu LH, He XH, Zeng QZ, et al. Chemotherapeutic Paclitaxel and Cisplatin Differentially Induce Pyroptosis in A549 Lung Cancer Cells via Caspase-3/GSDME Activation. *Apoptos An Int J Progr Cell Death* (2019) 24(3-4):312–25. doi: 10.1007/s10495-019-01515-1
44. So D, Shin HW, Kim J, Lee M, Myeong J, Chun YS, et al. Cervical Cancer is Addicted to SIRT1 Disarming the AIM2 Antiviral Defense. *Oncogene* (2018) 37(38):5191–204. doi: 10.1038/s41388-018-0339-4
45. Wu M, Wang Y, Yang D, Gong Y, Rao F, Liu R, et al. A PLK1 Kinase Inhibitor Enhances the Chemosensitivity of Cisplatin by Inducing Pyroptosis in Oesophageal Squamous Cell Carcinoma. *EBioMedicine* (2019) 41:244–55. doi: 10.1016/j.ebiom.2019.02.012
46. Wei J, Xu Z, Chen X, Wang X, Zeng S, Qian L, et al. Overexpression of GSDMC is a Prognostic Factor for Predicting a Poor Outcome in Lung Adenocarcinoma. *Mol Med Rep* (2020) 21(1):360–70. doi: 10.3892/mmr.2019.10837
47. Kovacs SB, Miao EA. Gasdermins: Effectors of Pyroptosis. *Trends Cell Biol* (2017) 27(9):673–84. doi: 10.1016/j.tcb.2017.05.005
48. Watabe K, Ito A, Asada H, Endo Y, Kobayashi T, Nakamoto K, et al. Structure, Expression and Chromosome Mapping of MLZE, a Novel Gene Which is Preferentially Expressed in Metastatic Melanoma Cells. *Jpn J Cancer Res* (2001) 92(2):140–51. doi: 10.1111/j.1349-7006.2001.tb01076.x
49. Saeki N, Usui T, Aoyagi K, Kim DH, Sato M, Mabuchi T, et al. Distinctive Expression and Function of Four GSDM Family Genes (GSDMA-D) in Normal and Malignant Upper Gastrointestinal Epithelium. *Genes Chromosomes Cancer* (2009) 48(3):261–71. doi: 10.1002/gcc.20636
50. Ding J, Wang K, Liu W, She Y, Sun Q, Shi J, et al. Pore-Forming Activity and Structural Autoinhibition of the Gasdermin Family. *Nature* (2016) 535 (7610):111–6. doi: 10.1038/nature18590
51. Hou J, Zhao R, Xia W, Chang CW, You Y, Hsu JM, et al. PD-L1-Mediated Gasdermin C Expression Switches Apoptosis to Pyroptosis in Cancer Cells and Facilitates Tumour Necrosis. *Nat Cell Biol* (2020) 22(10):1264–75. doi: 10.1038/s41556-020-0575-z
52. Zhang Z, Zhang Y, Xia S, Kong Q, Li S, Liu X, et al. Gasdermin E Suppresses Tumour Growth by Activating Anti-Tumour Immunity. *Nature* (2020) 579 (7799):415–20. doi: 10.1038/s41586-020-2071-9
53. Van Damme J, Rampart M, Conings R, Decock B, Van Osselaer N, Willems J, et al. The Neutrophil-Activating Proteins Interleukin 8 and Beta-Thromboglobulin: *In Vitro* and *In Vivo* Comparison of NH2-Terminally Processed Forms. *Eur J Immunol* (1990) 20(9):2113–8. doi: 10.1002/eji.1830200933
54. Hébert CA, Luscinskas FW, Kiely JM, Luis EA, Darbonne WC, Bennett GL, et al. Endothelial and Leukocyte Forms of IL-8. Conversion by Thrombin and Interactions With Neutrophils. *J Immunol* (1990) 145(9):3033–40.

Conflict of Interest: The authors declare that the research was conducted in the absence of any commercial or financial relationships that could be construed as a potential conflict of interest.

Publisher's Note: All claims expressed in this article are solely those of the authors and do not necessarily represent those of their affiliated organizations, or those of the publisher, the editors and the reviewers. Any product that may be evaluated in this article, or claim that may be made by its manufacturer, is not guaranteed or endorsed by the publisher.

Copyright © 2022 Zhou, Zheng, Bai, Gao and Lin. This is an open-access article distributed under the terms of the Creative Commons Attribution License (CC BY). The use, distribution or reproduction in other forums is permitted, provided the original author(s) and the copyright owner(s) are credited and that the original publication in this journal is cited, in accordance with accepted academic practice. No use, distribution or reproduction is permitted which does not comply with these terms.

frontiers | Frontiers in Oncology

TYPE Original Research
PUBLISHED 04 August 2022
DOI 10.3389/fonc.2022.951631

Check for updates

OPEN ACCESS

EDITED BY
Shaoquan Zheng,
Sun Yat-sen University Cancer Center (SYSUCC), China

REVIEWED BY
Xiayao Diao,
Peking Union Medical College Hospital (CAMS), China
Boyang Wu,
Tsinghua University, China

*CORRESPONDENCE
Wenfeng Xu
foxwf@sina.com
Zhe Lin
lzmedic@sina.cn

†These authors have contributed equally to this work

SPECIALTY SECTION
This article was submitted to Molecular and Cellular Oncology, a section of the journal Frontiers in Oncology

RECEIVED 24 May 2022
ACCEPTED 11 July 2022
PUBLISHED 04 August 2022

CITATION
Wu Z, Wang Y, Yan M, Liang Q, Li B, Hou G, Xia T, Lin Z and Xu W (2022) Comprehensive analysis of the endoplasmic reticulum stress-related long non-coding RNA in bladder cancer.
Front. Oncol. 12:951631.
doi: 10.3389/fonc.2022.951631

COPYRIGHT
© 2022 Wu, Wang, Yan, Liang, Li, Hou, Xia, Lin and Xu. This is an open-access article distributed under the terms of the Creative Commons Attribution License (CC BY). The use, distribution or reproduction in other forums is permitted, provided the original author(s) and the copyright owner(s) are credited and that the original publication in this journal is cited, in accordance with accepted academic practice. No use, distribution or reproduction is permitted which does not comply with these terms.

Comprehensive analysis of the endoplasmic reticulum stress-related long non-coding RNA in bladder cancer

Zhenyu Wu[1†], Yue Wang[2†], Mengxin Yan[2], Quan Liang[1], Bin Li[1], Guoliang Hou[1], Taolin Xia[1], Zhe Lin[1*] and Wenfeng Xu[1*]

[1]Department of Urology, The First People's Hospital of Foshan, Foshan, China, [2]The First Clinical Medical College, GuangDong Medical University, ZhanJiang, China

Background: Bladder cancer is ranked the second most frequent tumor among urological malignancies. The research strived to establish a prognostic model based on endoplasmic reticulum stress (ERS)-related long non-coding RNA (lncRNA) in bladder cancer.

Methods: We extracted the ERS-related genes from the published research and bladder cancer data from the Cancer Genome Atlas database. ERS-related lncRNAs with prognostic significance were screened by univariate Cox regression, least absolute shrinkage and selection operator regression analysis and Kaplan-Meier method. Multivariate Cox analysis was leveraged to establish the risk score model. Moreover, an independent dataset, GSE31684, was used to validate the model's efficacy. The nomogram was constructed based on the risk score and clinical variables. Furthermore, the biological functions, gene mutations, and immune landscape were investigated to uncover the underlying mechanisms of the ERS-related signature. Finally, we employed external datasets (GSE55433 and GSE89006) and qRT-PCR to investigate the expression profile of these lncRNAs in bladder cancer tissues and cells.

Results: Six ERS-related lncRNAs were identified to be closely coupled with patients' prognosis. On this foundation, a risk score model was created to generate the risk score for each patient. The ERS-related risk score was shown to be an independent prognostic factor. And the results of GSE31684 dataset also supported this conclusion. Then, a nomogram was constructed based on risk scores and clinical characteristics, and proven to have excellent predictive value. Moreover, the gene function analysis demonstrated that ERS-related lncRNAs were closely linked to fatty extracellular matrix, cytokines, cell adhesion, and tumor pathways. Further analysis revealed the association of the 6-lncRNAs signature with gene mutations and immunity in bladder cancer. Finally, the external datasets and qRT-PCR verified high expressions of the ERS-related lncRNAs in bladder cancer tissues and cells.

Conclusions: Overall, our findings indicated that ERS-related lncRNAs, which may affect tumor pathogenesis in a number of ways, might be exploited to assess the prognosis of bladder cancer patients.

KEYWORDS

bladder cancer, TCGA, lncRNA, prognostic model, ERS

Introduction

As the world's number ten most frequent malignant tumor and number two most prevalent urological malignancy, bladder cancer has caused a total of 213,000 deaths and 573,000 new cases in 2020 (1). Patients with bladder cancer receive a prognosis that is closely linked to the pathological diagnosis, comprising non-muscle invasive bladder cancer (NMIBC) as well as muscle invasive bladder cancer (MIBC). Most patients with NMIBC eventually progress to MIBC, whose 5-year overall survival (OS) was less than 50% (2, 3). Even with proper treatment, approximately half of bladder cancer patients suffer from recurrence or distant metastasis after radical surgery (4, 5). However, prognosis prediction and individualized treatment of bladder cancer still remain a challenge as it may be relevant to the biological heterogeneity of tumor (6). Because current approaches are insufficient for reliably assessing the prognosis of bladder cancer, a more trustworthy method must be investigated.

Endoplasmic reticulum stress (ERS) is defined as an imbalance in endoplasmic reticulum homeostasis, which includes the unfolded protein response (UPR) and perturbation in calcium (7). Relevant studies have demonstrated that ERS has a major part in the genesis and progression of a variety of human malignancies (8). Sustained mobilization of ERS endows malignant cells with greater tumorigenic, metastatic and drug resistant capacities (9). However, ERS overactivation may disrupt cellular homeostasis and leads to tumor cell death (10). On account for this, ERS and their downstream signaling pathways have emerged as a key regulator of tumor progression and response to chemotherapy and immunotherapy (11).

Recently, emerging studies have indicated that long non-coding RNA (lncRNA) plays a significant role in the regulation of gene expression and contributes to the development of numerous human diseases (12). Abnormalities of lncRNAs have been verified to be tumor-suppressive or tumor-oncogenic and to play a key role in tumor development (13). LncRNAs are important in multi-gene regulatory networks, and they can be utilized to diagnose and predict survival in a variety of cancers (14). Multiple lncRNAs signature have been researched in bladder cancer (15–17). However, the role of ERS-related lncRNA in bladder cancer remains to be studied.

In this research, we extracted the sequencing data and corresponding clinical data from the Cancer Genome Atlas (TCGA) and ERS-related genes from published research. We strived to establish a prognostic model based on ERS-related lncRNA, which can evaluate the prognosis of bladder cancer patients, and to explore its function in the occurrence and development of bladder cancer.

Materials and methods

Identification of ERS-related LncRNAs

We downloaded the RNA sequencing data, gene mutation data and corresponding clinical information of bladder cancer from TCGA database[1], and extracted an ERS-related genes from published literature (18). On the premise that correlation coefficient $|R^2| > 0.3$ and $p < 0.05$ were considered to be statistically significant, we identified ERS-related lncRNAs through Pearson correlation analysis. In the condition of $|\log_2$ (Fold Change)$| > 1$ and False Discovery Rate < 0.05, we obtained the ERS-related lncRNAs differentially expressed between tumor and normal adjacent tissues (NATs).

Screening of prognosis-related LncRNAs

Patients with follow-up of more than one month were included in the following study. Univariate Cox regression was performed to identify prognosis-associated lncRNAs with a criteria of $p < 0.05$. Least absolute shrinkage and selection operator (LASSO) regression analysis and Kaplan-Meier analysis were used to further screened lncRNAs tightly related to OS.

Building a risk score model

Patients were randomly classified into the training and testing sets in a 2:1 ratio. In the training set, we executed multivariate stepwise Cox regression on the above lncRNA to compute their

[1] https://cancergenome.nih.gov/

respective coefficients (βi). Then, a risk score model was constructed from βi and gene expression levels (Expi). According to the formula, the risk score for each patient is calculated. In addition, we used the median risk score as a cutoff to classify all eligible patients into high- and low-risk teams. Prognostic differences between high- and low-risk patients were revealed using Kaplan-Meier survival curves, and we applied the testing group to validate the above findings. Meanwhile, we collected the GSE31684 dataset (n = 93) from the Gene Expression Omnibus (GEO) database[2] to verify the model's efficacy.

Constructing and evaluating nomogram

In the training set, we used univariate and multivariate Cox regression analyses to estimate the prognostic significance of risk scores and clinical factors, including gender, age, and TMN stage. In order to predict OS of each patient, risk scores and clinical characteristics were incorporated to establish a nomogram. Next, the area under the curve (AUC) values were acquired by receiver operating characteristic (ROC) curves to evaluate the nomogram's predictive efficacy. Subsequently, the predictability of this nomogram was verified by concordance index (C-index) method, calibration plots, and testing cohort.

Functional analysis

We performed gene set enrichment analysis (GSEA) on the gene expression profile between the high- and low-risk cohorts using the gene Ontology (GO) and Kyoto Encyclopedia of Genes and Genomics (KEGG) gene sets. The molecular mechanism and biological functions of risk score may provide insights into the underlying mechanisms of ERS-related lncRNAs. Besides, we analyzed the gene mutation status between two groups to explore possible links between ERS-related lncRNAs and mutations. To explore the relationship between these lncRNAs and immunity, the immune cell abundance, immune function, and immune checkpoints were compared between two cohorts. Furthermore, the immunophenoscore was used to predict response to immunotherapy between two groups, which were acquired from the Cancer Immunome Atlas[3] (19).

External datasets and qRT-PCR validation

GSE89006 dataset (4 pairs of bladder cancer and NATs) and GSE55433 dataset (tumor = 57, normal = 26) were collected in the GEO database to verify the expression of target lncRNAs.

Next, bladder cancer cells (EJ-1, U3, and 5637) and normal bladder epithelium cells (SV-HUC-1) were purchased from Cell Bank, Institute of Life Sciences, Chinese Academy of Sciences Cell Bank (Shanghai, China). Total RNA was isolated using TRIzol reagent (Bioteke, Beijing, China). Then, reverse transcription was conducted utilizing the HiScript II Q RT SuperMix reagent (Vazyme, Nanjing, China). Subsequently, qRT-PCR was performed by the Hieff TMqPCR SYBR® Green Master Mix (Yeasen, Shanghai, China) with the primers provided in the Supplementary Table S1. We executed qRT-PCR with the Bio-Rad CFX96 Real-time Quantitative PCR System (Bio-Rad, California, USA).

Statistical analysis

Statistical analyses of this research were entirely conducted in the R software[4]. To identify the relationships between ERS-related genes and lncRNAs, Pearson correlation analysis was carried out. For comparison of the differences of categorical and continuous variables, the Chi-square test as well as the t-test was used, respectively. Univariate Cox regression, multivariate Cox regression, LASSO regression analysis, and Kaplan-Meier method were conducted to identify the optimal prognostic factors. In evaluating the OS of patients in various groups, the Kaplan-Meier method was utilized, and differences between groups were assessed utilizing log-rank test. At a two-tailed $p < 0.05$, the results were regarded statistically significant.

Results

Identification of ERS-related LncRNAs

Figure 1 presented the flowchart of our investigation. We obtained data of 411 tumor tissues and 19 NATs from 411 patients in TCGA database, and 252 ERS-related genes from the published research (Supplementary Table S2). A total of 263 ERS-related lncRNAs were identified with Pearson correlation analysis. Then, we screened out 53 ERS-related lncRNAs that were differentially expressed in bladder cancer and NATs, including 18 upregulated and 35 downregulated in tumors (Figure 2).

Screening of prognosis-associated LncRNAs

We performed univariate Cox regression on the above ERS-related lncRNAs and recognized 13 lncRNAs associated with

[2] https://www.ncbi.nlm.nih.gov/gds/

[3] https://tcia.at/

[4] https://www.r-project.org, version 4.0.2

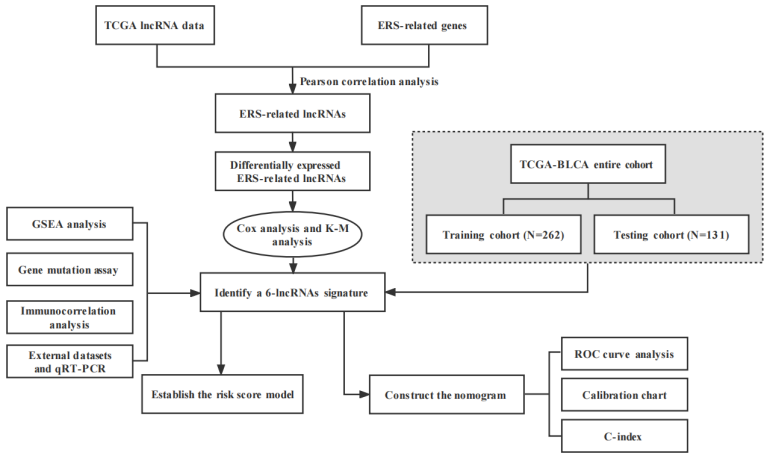

FIGURE 1
This study's design and flowchart.

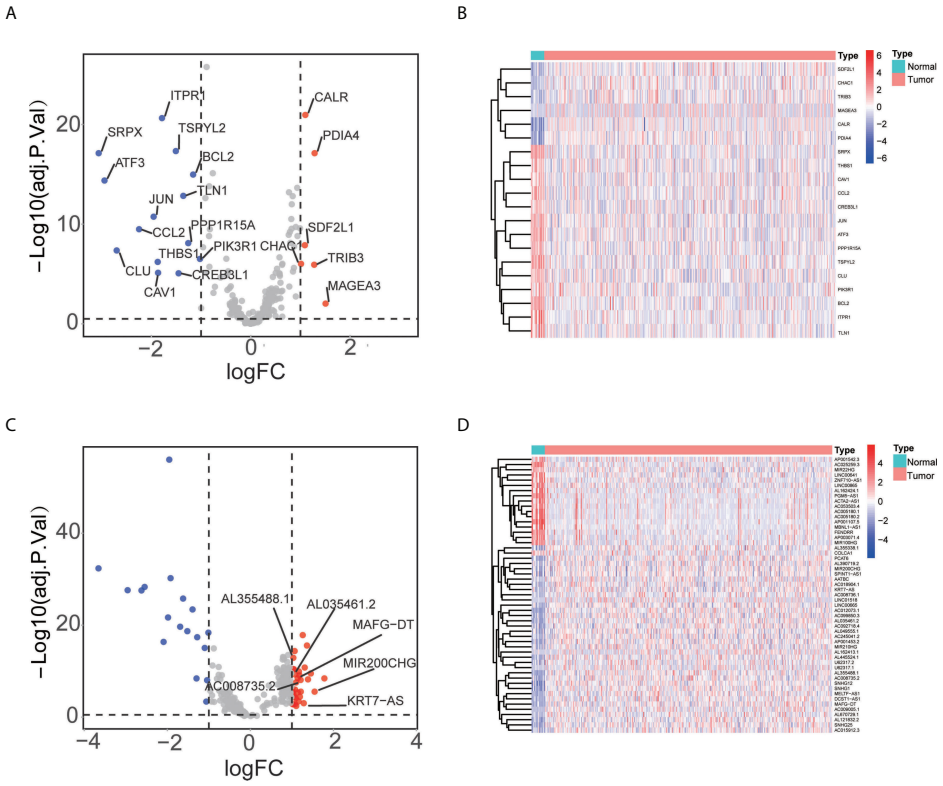

FIGURE 2
Identifying ERS-related lncRNA in tumor. **(A)** The volcano plot revealed that in tumors, 6 ERS-related genes were up-regulated whereas 14 were down-regulated. **(B)** The heatmap showed expression profile of ERS-related genes. **(C)** The volcano plot visualized that in tumors, 35 ERS-related lncRNAs were up-regulated and 18 were down-regulated. **(D)** The heatmap illustrated expression profile of ERS-related lncRNAs.

prognosis (Figure 3A). Six key lncRNAs were further screened by LASSO analysis (Figure 3B, C) and Kaplan-Meier analysis (Supplementary Figure S1), namely AL355488.1, AL035461.2, MAFG-DT, AC008735.2, MIR200CHG, and KRT7-AS.

Establishing a risk scoring model

In the training set, we constructed a risk score model including Expi and βi: Risk score = $\sum_{i=1}^{5}(Exp_i * \beta_i)$ (Table 1). Patients were split into two groups, a high-risk group and a low-risk group, according to the median risk score. The high-risk group's OS was considerably shorter in comparison to the low-risk group (Figure 4). Comparing to the risk coefficient and the mortality of patients of the low-risk group, those of the high-risk group were higher (Figure 4D). Similar findings were revealed using the same method on the testing group (Figure 4E, F). Meanwhile, the results of GSE31684 dataset also verified the model's efficacy (Figure 4G, H).

Constructing and evaluating nomogram

In the training set, it was observed that the clinical variables and risk score were closely associated to OS in the univariate Cox regression. Further multivariate Cox analysis indicated that risk score was an independent prognostic factor (Figure 5A, B). In addition, the ROC curve illustrated that the 6-lncRNAs signature was a remarkable prognostic predictor (Figure 5C). Then, using the multivariate Cox regression results, including clinical factors and risk scores, we constructed a nomogram (Figure 6A). Then we analyzed the 3- and 5-year OS of this prognostic model using ROC curves and obtained AUCs of 0.782 and 0.781, respectively (Figure 6B). The C-index of the model was 0.742. The established calibration plots demonstrated that the model had a favorable predictive effect (Figure 6C, D). We obtained similar outcomes with the same technique on the testing cohort (Figure 5D–F, 6E–G). The C-index of testing cohort was 0.717.

Functional analysis

ERS-related lncRNAs may be involved in fatty acid metabolism, peroxidation, extracellular matrix, endoplasmic reticulum, and cytokines (Figure 7A), which were demonstrated by GO analysis. KEGG analysis indicated that these lncRNAs may be associated with functions such as cell adhesion, cytokines, drug metabolism, tumor pathways, and oxidative phosphorylation (Figure 7B). Gene mutations between the high-risk patients and the low-risk patients were displayed in waterfall plots (Figures 7C, D). The top five genes with the highest mutation frequency in the high-risk team were TP53, TTN, MUC16, ARID1A, and KMT2D, while the top five genes in the low-risk team were TTN, TP53, KMT2D, MUC16, and KDM6A, revealing ERS-related lncRNAs may be associated with gene mutations. As it was shown in Figure 8A, the abundances of CD4+ T cells, CD8+ T cells, neutrophils, and macrophages were markedly enriched in the high-risk team compared to the low-risk team. Immune functions including cytolytic activity, HLA function, IFN response, and T cell stimulation were relatively active in the high-risk group (Figure 8B). In addition, the study of immune checkpoints uncovered a high expression of immunosuppressive receptors (CTLA4, PD-1, LAG3, BTLA, and TIGIT) and immunosuppressive ligands (PD-L2 and TNFSF14) in high-risk cohort (Figure 8C). Further analysis showed that the response to immunotherapy in the high-risk set was better than that in the low-risk set, suggesting that risk scores can predict the efficacy of immunotherapy (Figure 8D, E). Overall, the association between the risk score and tumor immune landscape were assessed, and the outcomes demonstrated that the risk score was related to different immune landscape.

External datasets and qRT-PCR validation

Next, we validated the expression level of target lncRNAs using the GSE55433 and GSE89006 datasets. The GSE55433 dataset discovered that KRT7-AS and AL355488.1 were

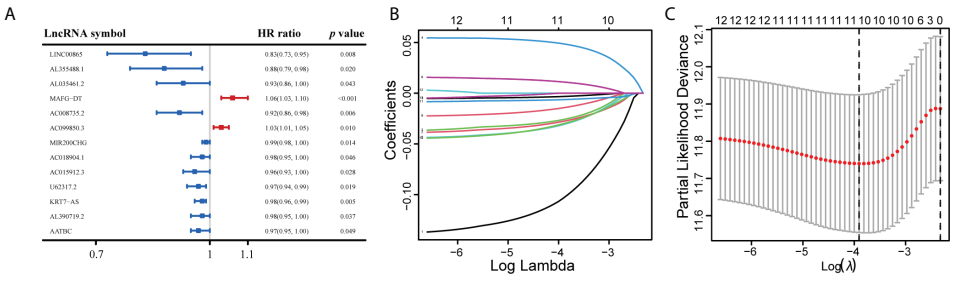

FIGURE 3
Identifying ERS-related lncRNAs associated to OS. **(A)** The forest plot recognized 13 ERS-related lncRNAs substantially associated with OS. **(B)** Lasso regression analysis. **(C)** The LASSO coefficient spectrum for lncRNA associated with OS was presented.

TABLE 1 The prognostic significance of the 6-lncRNAs signature.

ERS-related lncRNAs	Coef	HR
AL355488.1	-0.024623135	0.881333378
AL035461.2	-0.018783391	0.926879906
MAFG-DT	0.044346228	1.062089764
AC008735.2	-0.017581442	0.917739074
MIR200CHG	-0.002668355	0.987752228
KRT7-AS	-0.003720336	0.976742661

significantly overexpressed in tumor compared with NATs (Figure 9A). Furthermore, GSE89006 dataset showed a high expression of AL035461, AC008735.2, and MIR200CHG in bladder cancer compared with NATs (Figure 9B).

Moreover, qRT-PCR showed that the expression of AL355488.1, AL035461.2, MAFG-DT, and AC008735.2 was significantly upregulated in EJ-1 and U3 cells compared with SV-HUC-1 cells (Figure 9C). In 5637 cell line, MIR200CHG and KRT7-AS were considerably upregulated (Figure 9D). The results of external datasets and qRT-PCR were consistent with the findings of TCGA analysis.

Discussion

Bladder cancer is one of the most common malignancies of the genitourinary system, with approximately 550,000 new cases each year (20). The high incidence, malignant behavior, and drug resistance of bladder cancer have made the therapy and prognostic management an increasing challenge (21). The search for a novel molecular marker to assess the prognosis and guide the treatment of patients with bladder cancer is therefore of great importance.

Accumulated studies have developed multiple signatures to predict prognosis of patients with tumors. Huang et al. (18) uncovered a ERS-related signature which may serve as a marker for prognosis prediction and individualized therapy of glioma. Zhou et al. (22) revealed that the immune-related lncRNAs signature had prognostic value for glioblastoma patients. Zheng et al. (23) have developed a hypoxia-immune signature to predict the prognosis and immune status for triple-negative breast cancer. Xie et al. (24) constructed a necroptosis signature to predict prognosis and drug sensitivity of triple-negative breast cancer. Meanwhile, a ferroptosis-based signature has been established, which may serve as a novel therapy biomarker for lung squamous cell carcinoma (25). However, the role of ERS-related lncRNA in bladder cancer remains to be studied.

In this study, we extracted ERS-related genes and sequencing data of bladder cancer from online database, and obtained ERS-related lncRNAs differentially expressed between tumor and NATs. Next, we further screened prognosis-associated lncRNAs by univariate Cox regression, LASSO regression and Kaplan-Meier analyses. The 6-lncRNAs signature was utilized to develop a risk model that separated patients of bladder cancer into a high-risk group and a low-risk group. Prognosis analysis revealed that the

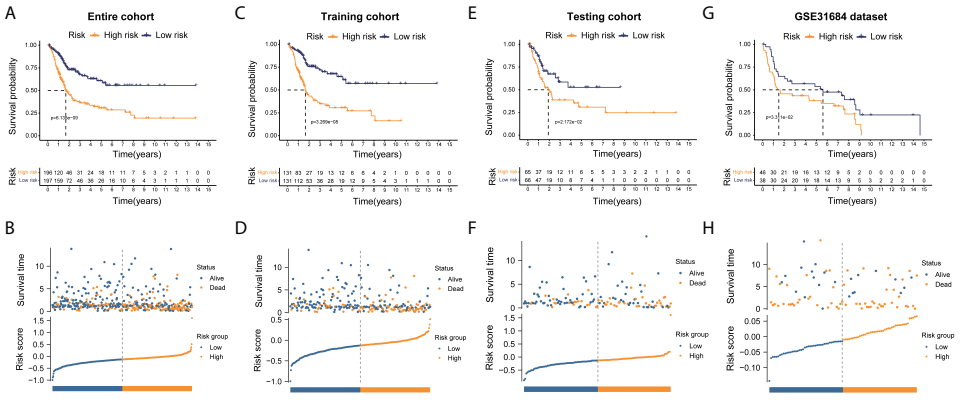

FIGURE 4
Risk score model establishment utilizing ERS-related lncRNAs. **(A, C, E, G)** The Kaplan-Meier analysis unveiled a significantly shorter OS of the high-risk group than that of the low-risk group in entire, training, testing cohorts, and GSE31684 dataset, respectively. **(B, D, F, H)** The overview of each patient's survival status and risk rating distributions in entire, training, testing cohorts, and GSE31684 dataset, respectively.

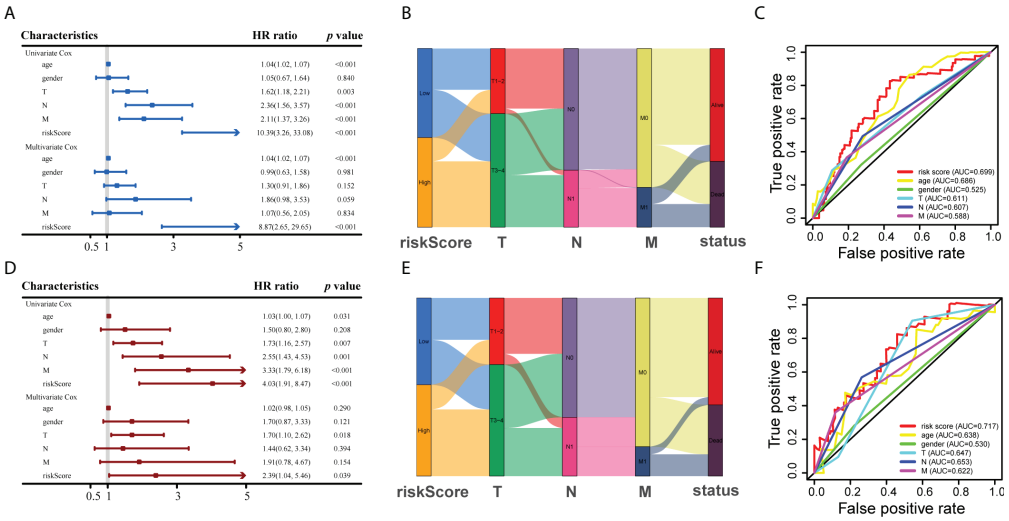

FIGURE 5
Analyses of prognostic values using the risk score and clinical variables. **(A, D)** Risk score was revealed to be strongly associated to OS in the univariate Cox analysis and multivariate Cox analysis in training and testing cohort, respectively. **(B, E)** Alluvial diagrams showing the associations between risk scores and clinical variables in training and testing groups, respectively. **(C, F)** ROC curve analyses of the risk scores and clinical variables in training and testing sets, respectively.

low-risk group patients presented favorable OS. Additionally, a nomogram was established and demonstrated to have a strong prognostic effect.

Through our study, 6 lncRNAs were identified to be associated with bladder cancer prognosis. Among them, AL355488.1, AL035461.2, MIR200CHG, AC008735.2, and KRT7-AS had a protective effect for prognosis, while MAFG-DT presented the opposite effect. AL355488.1 has previously been shown to be a potential biomarker for targeted therapy and prognosis in hepatocellular liver cancer (26). And MIR200CHG was found to be a protective indicator for bladder cancer patients (27). AC008735.2 was significantly associated with targeted therapy and prognosis in patients with clear cell renal cell carcinoma (28). KRT7-AS played an important role in cancer

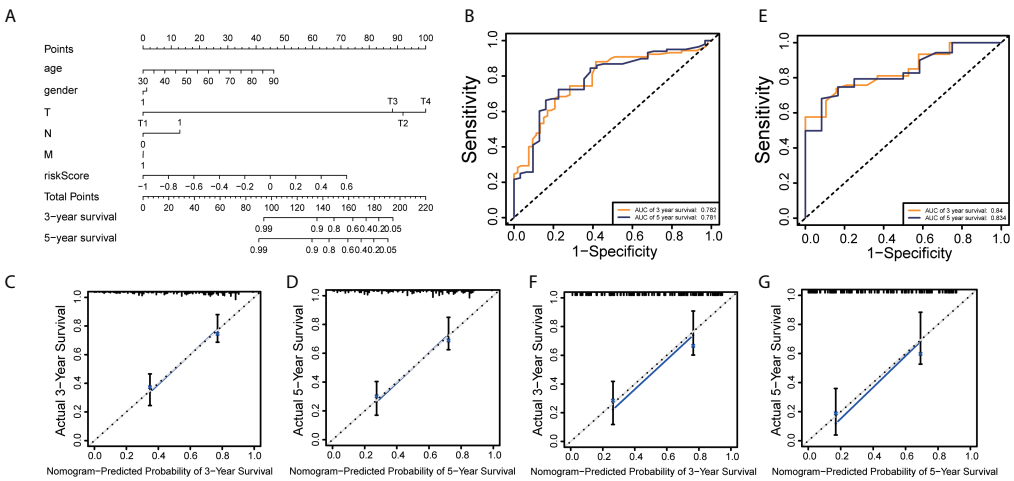

FIGURE 6
Establishment and interpretation of the nomogram for clinical variables and ERS-related lncRNAs. **(A)** Establishment of the nomogram. **(B, E)** ROC curve analyses of the nomogram in training and testing sets, respectively. **(C, F)** The nomogram's 3-year OS calibration curve in training and testing groups, respectively. **(D, G)** The nomogram's calibration curve for a 5-year OS in training and testing sets, respectively.

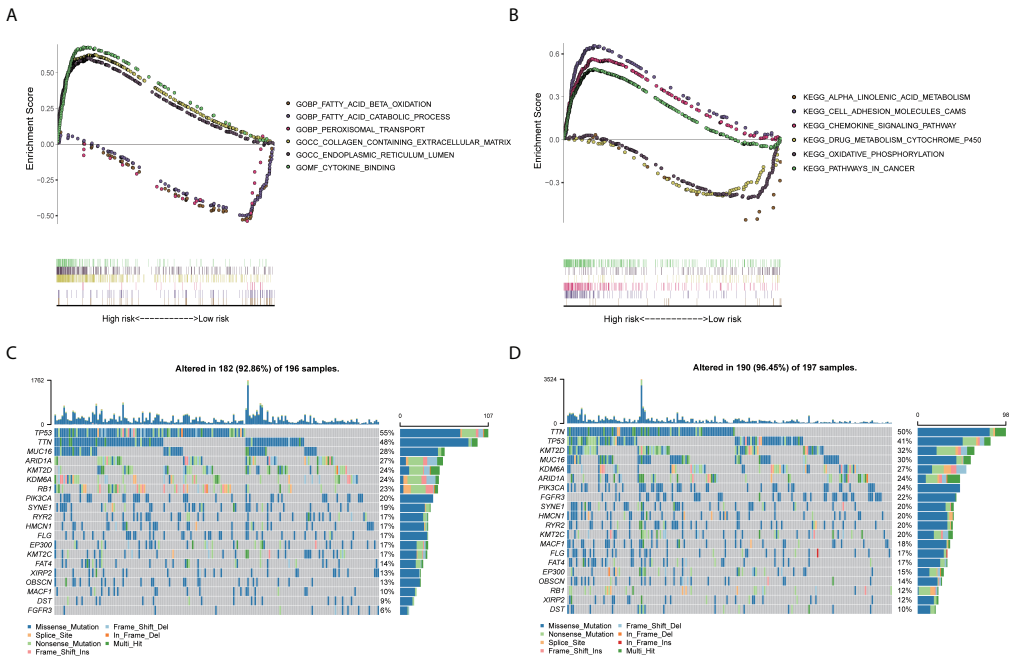

FIGURE 7
The results of GSEA and gene mutation analyses. **(A)** According to GO enrichment analysis, ERS-related lncRNAs were may be involved in fatty acid metabolism, peroxidation, extracellular matrix, endoplasmic reticulum, and cytokines. **(B)** KEGG pathway analysis showed that these lncRNAs may be associated with functions such as cell adhesion, cytokines, drug metabolism, tumor pathways, and oxidative phosphorylation. **(C, D)** Waterfall plots of gene somatic mutations in high- and low-risk patients, respectively.

regulation and was superior to other clinicopathological features in predicting survival (29). In addition, the expression of MAFG-DT in bladder cancer was higher than that in NATs and can promote tumor growth and progression, which can be served as a predictor of patient prognosis (30).

In GSEA analysis, these ERS-related lncRNAs were associated with functions of fatty acid metabolism, peroxidation, extracellular matrix, cytokines, cell adhesion, tumor pathways, and oxidative phosphorylation. It has been shown that fatty acid metabolism may be associated with the production and stemness-maintenance of cancer stem cell, thereby affecting the prognosis of tumors (31, 32). Besides, extracellular matrix regulation could not only facilitate tumor cells invasion but also contribute to the generation and maintenance of cancer stem cell niche (33). Moreover, the regulation of cell adhesion alters the ability of tumor cells to interact with extracellular matrix and adjacent cells, thereby affecting the biological behavior of tumors (34). It was generally known that the endoplasmic reticulum was the origin of ERS, and the degradation of stress proteins helped restore cellular homeostasis (35, 36). Taken together, these findings may inspire scholars to further explore the molecular mechanism of ERS-related lncRNAs in bladder cancer.

In addition, we analyzed the mutations between the high- and low-risk patients. The top five mutated genes in the high-risk cohort were TP53, TTN, MUC16, ARID1A, and KMT2D, while those in the low-risk cohort were TTN, TP53, KMT2D, MUC16, and KDM6A. It was reported that TP53 mutation can increase cancer cells' resistance to ERS through maintaining the activation of UPR regulator ATF6 and inhibition of pro-apoptotic factors JNK and CHOP (37). This led us to speculate that increased TP53 mutations in high-risk team may inhibit the ERS damage in tumor cells, resulting in a poorer prognosis of patients. Similarly, ARID1A mutation was demonstrated to protect cancer cells from changes in tumor microenvironment by upregulating ERS (38). It made us hypothesize that elevated ARID1A mutations in the high-risk team might promote tumor progression and bring about poor prognosis. Furthermore, the investigation of immune landscape showed that the infiltration of immune cell and immune functions in the high-risk team were relatively active compared to those in the low-risk team. Notably, the infiltration of CD8+ T cells was significantly higher in the high-risk group than in the low-risk group, which contradicted the antitumor effect of these cells. On this basis, we further explored the immune checkpoints and uncovered a high expression of immunosuppressive receptors (CTLA4, PD-1, LAG3, BTLA, and TIGIT) and immunosuppressive ligands (PD-L2 and TNFSF14) in high-risk cohort. Overexpression of these molecules might promote immune tolerance in bladder cancer, thereby affecting the prognosis of patients. The elucidation of immune

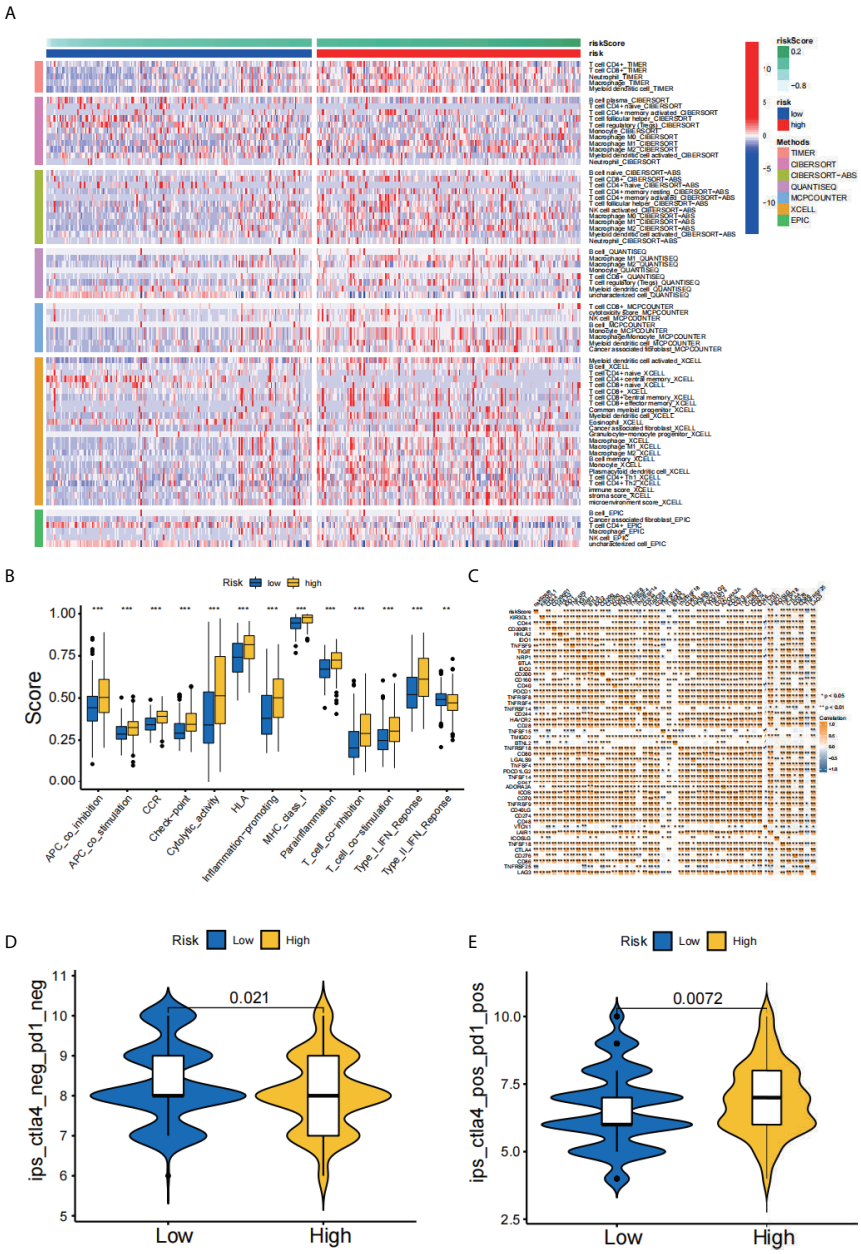

FIGURE 8
Analysis of immune landscape. **(A)** A heatmap for immunological responses between high- and low-risk groups. **(B)** Immune cell subpopulations and associated functions. **(C)** Expression of immune checkpoints in high- and low-risk cohorts. **(D, E)** Relative response of anti-PD-1 and anti-CTLA4 therapy between two groups. **p < 0.01; ***p < 0.001.

checkpoints could also help identify potential target patients and contribute to the development of immunotherapy.

Our research has a few limitations. For starters, it is just a retrospective research based on lncRNA data and few clinical variables from TCGA database, which is lacking in some detailed clinical information. Second, the prognostic value and the biological functions of ERS-related lncRNAs are not yet fully elucidated. Finally, although the validation was performed in the cell lines through qRT-PCR, further *in vivo* or *in vitro* experiments were needed to investigate the concrete mechanisms of the lncRNAs.

Conclusion

We constructed a prognostic model in the basis of ERS-related lncRNA, which had a superior effect on predicting the

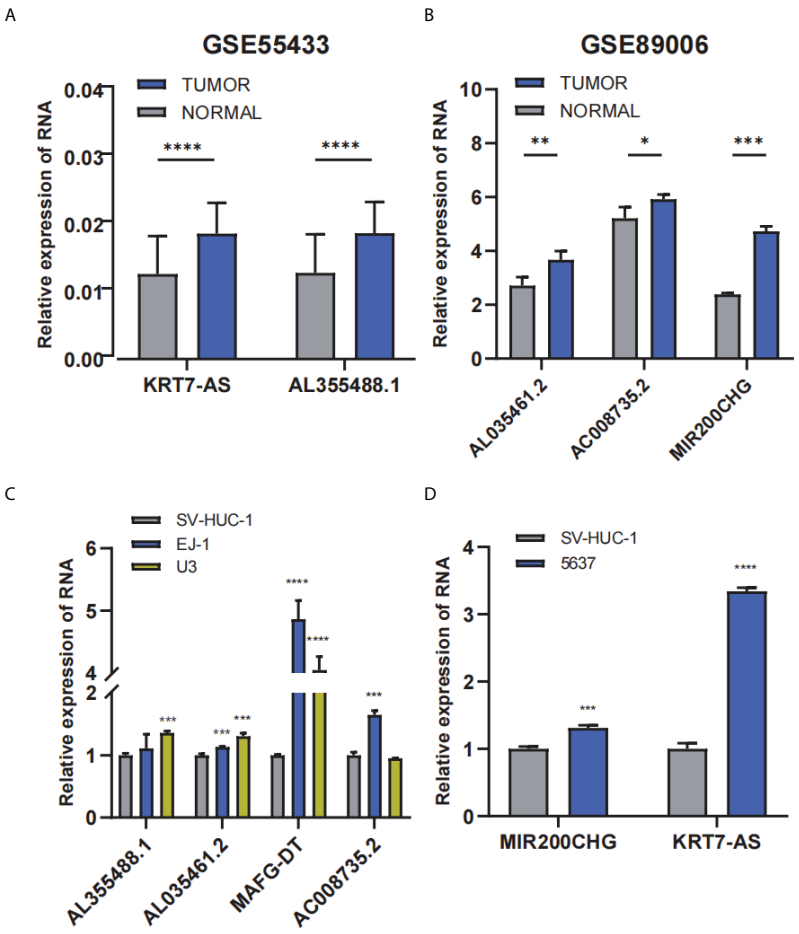

FIGURE 9
The expression profile of the 6-lncRNAs signature with external validation. **(A, B)** The lncRNA expression profile in GSE55433 and GSE89006 datasets, respectively. **(C, D)** The lncRNA expression level in bladder cancer cells and normal cells. *p < 0.05; **p < 0.01; ***p < 0.001; ****p < 0.0001.

survival rate of patients with bladder cancer. Therefore, this indicated that ERS-related lncRNAs can be a reliable predictor of the prognosis for bladder cancer patients and may be closely related to the occurrence and development of bladder cancer.

Data availability statement

The original contributions presented in the study are included in the article/Supplementary Material. Further inquiries can be directed to the corresponding authors.

Ethics statement

All data of our research were derived from TCGA and GEO database and required no ethical approval.

Author contributions

WX and ZL designed and facilitated the study. ZW and YW analyzed the data and completed the draft. MY and QL participated in the revision of the manuscript. BL, GH, and TX collected the data. All authors read the manuscript and concur with its submission.

Funding

This work was funded by the Foshan Ascending Peak Plan Project (grant no. 2020A012), Guangdong Basic and Applied Basic Research Foundation (grant no. 2021A1515111197), and Guangdong Medical Scientific Research Foundation (grant no. A2022222).

Acknowledgments

We thank the researchers and patients who contributed data to TCGA and GEO database.

Conflict of interest

The authors declare that the research was conducted in the absence of any commercial or financial relationships that could be construed as a potential conflict of interest.

Publisher's note

All claims expressed in this article are solely those of the authors and do not necessarily represent those of their affiliated organizations, or those of the publisher, the editors and the reviewers. Any product that may be evaluated in this article, or claim that may be made by its manufacturer, is not guaranteed or endorsed by the publisher.

Supplementary material

The Supplementary Material for this article can be found online at: https://www.frontiersin.org/articles/10.3389/fonc.2022.951631/full#supplementary-material

References

1. Sung H, Ferlay J, Siegel RL, Laversanne M, Soerjomataram I, Jemal A, et al. Global cancer statistics 2020: Globocan estimates of incidence and mortality worldwide for 36 cancers in 185 countries. *CA: Cancer J Clin* (2021) 71(3):209–49. doi: 10.3322/caac.21660

2. Ghandour R, Singla N, Lotan Y. Treatment options and outcomes in nonmetastatic muscle invasive bladder cancer. *Trends Cancer* (2019) 5(7):426–39. doi: 10.1016/j.trecan.2019.05.011

3. Patel VG, Oh WK, Galsky MD. Treatment of muscle-invasive and advanced bladder cancer in 2020. *CA: Cancer J Clin* (2020) 70(5):404–23. doi: 10.3322/caac.21631

4. Alfred Witjes J, Lebret T, Compérat EM, Cowan NC, De Santis M, Bruins HM, et al. Updated 2016 eau guidelines on muscle-invasive and metastatic bladder cancer. *Eur Urol* (2017) 71(3):462–75. doi: 10.1016/j.eururo.2016.06.020

5. Wu Y, Zhang L, He S, Guan B, He A, Yang K, et al. Identification of immune-related lncrna for predicting prognosis and immunotherapeutic response in bladder cancer. *Aging* (2020) 12(22):23306–25. doi: 10.18632/aging.104115

6. Lenis AT, Lec PM, Chamie K, Mshs MD. Bladder cancer: A review. *Jama* (2020) 324(19):1980–91. doi: 10.1001/jama.2020.17598

7. Hetz C. The unfolded protein response: Controlling cell fate decisions under er stress and beyond. *Nat Rev Mol Cell Biol* (2012) 13(2):89–102. doi: 10.1038/nrm3270

8. da Silva DC, Valentão P, Andrade PB, Pereira DM. Endoplasmic reticulum stress signaling in cancer and neurodegenerative disorders: Tools and strategies to understand its complexity. *Pharmacol Res* (2020) 155:104702. doi: 10.1016/j.phrs.2020.104702

9. Cubillos-Ruiz JR, Bettigole SE, Glimcher LH. Tumorigenic and immunosuppressive effects of endoplasmic reticulum stress in cancer. *Cell* (2017) 168(4):692–706. doi: 10.1016/j.cell.2016.12.004

10. Oakes SA, Papa FR. The role of endoplasmic reticulum stress in human pathology. *Annu Rev Pathol* (2015) 10:173–94. doi: 10.1146/annurev-pathol-012513-104649

11. Chen X, Cubillos-Ruiz JR. Endoplasmic reticulum stress signals in the tumour and its microenvironment. *Nat Rev Cancer* (2021) 21(2):71–88. doi: 10.1038/s41568-020-00312-2

12. Esteller M. Non-coding rnas in human disease. *Nat Rev Genet* (2011) 12 (12):861–74. doi: 10.1038/nrg3074

13. Wang J, Su Z, Lu S, Fu W, Liu Z, Jiang X, et al. Lncrna hoxa-As2 and its molecular mechanisms in human cancer. *Clinica chimica acta; Int J Clin Chem* (2018) 485:229–33. doi: 10.1016/j.cca.2018.07.004

14. Jiang C, Li X, Zhao H, Liu H. Long non-coding rnas: Potential new biomarkers for predicting tumor invasion and metastasis. *Mol Cancer* (2016) 15 (1):62. doi: 10.1186/s12943-016-0545-z

15. Lai C, Wu Z, Li Z, Yu H, Li K, Tang Z, et al. A robust signature of immune-related long non-coding rna to predict the prognosis of bladder cancer. *Cancer Med* (2021) 10(18):6534–45. doi: 10.1002/cam4.4167

16. Chen K, Zhu S, Yu W, Xia Y, Xing J, Geng J, et al. Comprehensive analysis of N6-Methylandenosine-Related long non-coding rnas signature in prognosis and tumor microenvironment of bladder cancer. *Front Oncol* (2022) 12:774307. doi: 10.3389/fonc.2022.774307

17. Lai C, Wu Z, Shi J, Li K, Zhu J, Chen Z, et al. Autophagy-related long noncoding rnas can predict prognosis in patients with bladder cancer. *Aging* (2020) 12(21):21582–96. doi: 10.18632/aging.103947

18. Huang R, Li G, Wang K, Wang Z, Zeng F, Hu H, et al. Comprehensive analysis of the clinical and biological significances of endoplasmic reticulum stress in diffuse gliomas. *Front Cell Dev Biol* (2021) 9:619396. doi: 10.3389/fcell.2021.619396

19. Charoentong P, Finotello F, Angelova M, Mayer C, Efremova M, Rieder D, et al. Pan-cancer immunogenomic analyses reveal genotype-immunophenotype relationships and predictors of response to checkpoint blockade. *Cell Rep* (2017) 18 (1):248–62. doi: 10.1016/j.celrep.2016.12.019

20. Richters A, Aben KKH, Kiemeney L. The global burden of urinary bladder cancer: An update. *World J Urol* (2020) 38(8):1895–904. doi: 10.1007/s00345-019-02984-4

21. Mirzaei S, Paskeh MDA, Hashemi F, Zabolian A, Hashemi M, Entezari M, et al. Long non-coding rnas as new players in bladder cancer: Lessons from pre-clinical and clinical studies. *Life Sci* (2022) 288:119948. doi: 10.1016/j.lfs.2021.119948

22. Zhou M, Zhang Z, Zhao H, Bao S, Cheng L, Sun J. An immune-related six-lncrna signature to improve prognosis prediction of glioblastoma multiforme. *Mol Neurobiol* (2018) 55(5):3684–97. doi: 10.1007/s12035-017-0572-9

23. Zheng S, Zou Y, Liang JY, Xiao W, Yang A, Meng T, et al. Identification and validation of a combined hypoxia and immune index for triple-negative breast cancer. *Mol Oncol* (2020) 14(11):2814–33. doi: 10.1002/1878-0261.12747

24. Xie J, Tian W, Tang Y, Zou Y, Zheng S, Wu L, et al. Establishment of a cell necroptosis index to predict prognosis and drug sensitivity for patients with triple-negative breast cancer. *Front Mol Biosci* (2022) 9:834593. doi: 10.3389/fmolb.2022.834593

25. Diao X, Guo C, Liu L, Wang G, Li S. Identification and validation of an individualized prognostic signature of lung squamous cell carcinoma based on ferroptosis-related genes. *Thorac Cancer* (2021) 12(23):3236–47. doi: 10.1111/1759-7714.14195

26. Huang K, Lu Z, Li L, Peng G, Zhou W, Ye Q. Construction of a cerna network and a genomic-clinicopathologic nomogram to predict survival for hbv-related hcc. *Hum Cell* (2021) 34(6):1830–42. doi: 10.1007/s13577-021-00607-y

27. He RQ, Huang ZG, Li TY, Wei YP, Chen G, Lin XG, et al. Rna-sequencing data reveal a prognostic four-Lncrna-Based risk score for bladder urothelial carcinoma: An in silico update. *Cell Physiol Biochem* (2018) 50(4):1474–95. doi: 10.1159/000494647

28. Li X, Yu H, Wei Z, Gou X, Liang S, Liu F. A novel prognostic model based on autophagy-related long non-coding rnas for clear cell renal cell carcinoma. *Front Oncol* (2021) 11:711736. doi: 10.3389/fonc.2021.711736

29. Peng Y, Wang H, Huang Q, Wu J, Zhang M. A prognostic model based on immune-related long noncoding rnas for patients with epithelial ovarian cancer. *J Ovarian Res* (2022) 15(1):8. doi: 10.1186/s13048-021-00930-w

30. Cui Y, Zhou Z, Chai Y, Che X, Zhang Y. Identification of a nomogram from ferroptosis-related long noncoding rnas signature to analyze overall survival in patients with bladder cancer. *J Oncol* (2021) 2021:8533464. doi: 10.1155/2021/8533464

31. Yi M, Li J, Chen S, Cai J, Ban Y, Peng Q, et al. Emerging role of lipid metabolism alterations in cancer stem cells. *J Exp Clin Cancer Res CR* (2018) 37 (1):118. doi: 10.1186/s13046-018-0784-5

32. Tang Y, Tian W, Xie J, Zou Y, Wang Z, Li N, et al. Prognosis and dissection of immunosuppressive microenvironment in breast cancer based on fatty acid metabolism-related signature. *Front Immunol* (2022) 13:843515. doi: 10.3389/fimmu.2022.843515

33. Walker C, Mojares E, Del Río Hernández A. Role of extracellular matrix in development and cancer progression. *Int J Mol Sci* (2018) 19(10):3028. doi: 10.3390/ijms19103028

34. Läubli H, Borsig L. Altered cell adhesion and glycosylation promote cancer immune suppression and metastasis. *Front Immunol* (2019) 10:2120. doi: 10.3389/fimmu.2019.02120

35. Mohamed E, Cao Y, Rodriguez PC. Endoplasmic reticulum stress regulates tumor growth and anti-tumor immunity: A promising opportunity for cancer immunotherapy. *Cancer immunol immunother CII* (2017) 66(8):1069–78. doi: 10.1007/s00262-017-2019-6

36. Yoo YS, Han HG, Jeon YJ. Unfolded protein response of the endoplasmic reticulum in tumor progression and immunogenicity. *Oxid Med Cell Longevity* (2017) 2017:2969271. doi: 10.1155/2017/2969271

37. Sicari D, Fantuz M, Bellazzo A, Valentino E, Apollonio M, Pontisso I, et al. Mutant P53 improves cancer cells' resistance to endoplasmic reticulum stress by sustaining activation of the upr regulator Atf6. *Oncogene* (2019) 38(34):6184–95. doi: 10.1038/s41388-019-0878-3

38. Zundell JA, Fukumoto T, Lin J, Fatkhudinov N, Nacarelli T, Kossenkov AV, et al. Targeting the Ire1α/Xbp1 endoplasmic reticulum stress response pathway in Arid1a-mutant ovarian cancers. *Cancer Res* (2021) 81(20):5325–35. doi: 10.1158/0008-5472.Can-21-1545

frontiers | Frontiers in Cell and Developmental Biology

TYPE Review
PUBLISHED 10 August 2022
DOI 10.3389/fcell.2022.942828

Check for updates

OPEN ACCESS

EDITED BY
Shaoquan Zheng,
Sun Yat-sen University Cancer Center (SYSUCC), China

REVIEWED BY
Kuo-Hui Su,
University of Toledo, United States
Miodrag Guzvic,
University Medical Center Regensburg, Germany

*CORRESPONDENCE
Shuai Wang,
sdwftcmws@163.com
Yuhua Chi,
chiyuhuading@163.com

†These authors share first authorship

SPECIALTY SECTION
This article was submitted to Cancer Cell Biology, a section of the journal Frontiers in Cell and Developmental Biology

RECEIVED 13 May 2022
ACCEPTED 18 July 2022
PUBLISHED 10 August 2022

CITATION
Du S, Liu Y, Yuan Y, Wang Y, Chen Y, Wang S and Chi Y (2022), Advances in the study of HSP70 inhibitors to enhance the sensitivity of tumor cells to radiotherapy.
Front. Cell Dev. Biol. 10:942828.
doi: 10.3389/fcell.2022.942828

COPYRIGHT
© 2022 Du, Liu, Yuan, Wang, Chen, Wang and Chi. This is an open-access article distributed under the terms of the Creative Commons Attribution License (CC BY). The use, distribution or reproduction in other forums is permitted, provided the original author(s) and the copyright owner(s) are credited and that the original publication in this journal is cited, in accordance with accepted academic practice. No use, distribution or reproduction is permitted which does not comply with these terms.

Advances in the study of HSP70 inhibitors to enhance the sensitivity of tumor cells to radiotherapy

Sihan Du[1†], Ying Liu[1], Yuan Yuan[2], Yuran Wang[2], Yanfang Chen[2], Shuai Wang[2*] and Yuhua Chi[3*]

[1]School of Medical Imaging, Weifang Medical University, Weifang, Shandong, China, [2]Department of Radiotherapy, Affiliated Hospital of Weifang Medical University, Weifang, Shandong, China, [3]Department of General Medicine, Affiliated Hospital of Weifang Medical University, Weifang, Shandong, China

The 70 kDa heat shock protein (HSP70) is one of the most conserved proteins and a ubiquitous molecular chaperone that plays a role in the folding, remodeling, and degradation of various proteins to maintain proteostasis. It has been shown that HSP70 is abundantly expressed in cancer and enhances tumor resistance to radiotherapy by inhibiting multiple apoptotic pathways, such as interfering with the cellular senescence program, promoting angiogenesis, and supporting metastasis. Thus, HSP70 provides an effective target for enhancing the effects of radiation therapy in the clinical management of cancer patients. Inhibition of HSP70 enhances the radiation-induced tumor-killing effect and thus improves the efficacy of radiotherapy. This article reviews the sensitivity of Hsp70 and its related inhibitors to radiotherapy of tumor cells.

KEYWORDS

HSP70, HSP70 inhibitor, radiotherapy, sensitivity, tumour

Introduction

The Heat shock proteins (HSPs) family, highly conserved, are present in all organisms and play a vital role in protein folding, translocation and degradation, hence their name molecular chaperones, a concept first used by Laskey et al. (1978). They were first discovered in 1962, when Ritossa and colleagues observed that the giant chromosomes contained heat-inducible genes and heat-inducible proteins in the gland cells of Drosophila larvae exposed to high temperatures, opening a new field of study of heat shock responses (Ritossa, 1962). HSPs are classified into several families such as HSPH (HSP110), HSPC (HSP90), HSPA (HSP70), HSPD (HSP60), DNAJ (HSP40), and HSPB (small HSPs) (Kampinga et al., 2009). Among them, Hsp70 is the most conserved protein in evolution, which can stabilize proteins against denaturation, help nascent proteins to fold, and dissolve damaged or abnormal proteins. Hsp70 is not only produced under heat stress but also expressed under stress conditions such as heavy metals, small molecule chemical toxins, infection, oxidative stress, inflammation, ischemia, cancer, and neurodegenerative diseases, among other stress conditions (Westerheide and

TABLE 1 The role of HSP70 in resistance to radiotherapy.

Cancer type	Findings	References
Lung cancer	Induction of HSP70 expression and AKT phosphorylation by Redd1 to acquire resistance to radiotherapy	Jin et al. (2019)
Nasopharyngeal carcinoma	TPL (HSP70 inhibitor) enhances cellular radiosensitivity by inhibiting GRP78 to trigger apoptosis and induce G2/M phase arrest	Li et al. (2016)
Endometrial cancer	Silencing of HSP70 expression enhances radiotherapy efficacy	Du et al. (2009)
Oropharyngeal cancer	GRP78 (HSP70) confers radioresistance by increasing radiation-induced DNA double-strand break repair and cell autophagy and the subsequent inhibition of apoptosis	Sun et al. (2017)
Glioblastoma and lung cancer	Antibodies targeting GRP78 exhibit antitumor activity and enhance the efficacy of radiotherapy on tumors	Dadey et al. (2017)

TPL, triptolide.

Morimoto, 2005). Notably, tumors frequently overexpress HSP70 in the cytoplasm, present HSP70 on their plasma membrane, and actively release HSP70 compared to normal cells (Multhoff et al., 2015). And it has been demonstrated that HSP70 is associated with early tumor recurrence, poor prognosis, and resistance to radiotherapy (Brondani Da Rocha et al., 2004; Yang et al., 2015; Jin et al., 2016).

Hsp70 is closely related to tumor therapy such as tumor radiotherapy and chemotherapy, among which radiotherapy is a commonly used tumor treatment method. After prolonged radiation exposure of tumor cells in radiotherapy, some genes and proteins are expressed abnormally so that tumor cells acquire a radiation-resistant phenotype and become less radiosensitive, leading to increased invasion, metastasis, and recurrence of certain tumors (Kim et al., 2015). Therefore, many researchers have worked to discover a radiosensitizer with good pharmacological properties to enhance the sensitivity of tumor cells to radiotherapy and thus improve the efficacy of radiotherapy. Studies have shown that HSP70 plays an essential role in tumor transformation and tumor development, as they are both necessary for tumor cell survival and growth and are closely related to tumor radioresistance (Table 1). Moreover, malignant cells express higher levels of HSP70 than normal cells, and high expression of HSP70 induces resistance to radiotherapy (Xu et al., 2010; Kumar et al., 2016). Inhibition of HSP70 inhibits the growth of many tumor cells and significantly promotes radiation-induced apoptosis, increasing the sensitivity of tumors to radiotherapy. Thus, HSP70 inhibitors can be used as radiosensitizers to enhance the efficacy of radiotherapy (Wen et al., 2014). HSP70 inhibitors can be classified as small molecules or compounds. Common small molecule-like inhibitors include 2-phenylethynesulfonamide (PES) and Apoptozole (Az), a small molecule inhibitor of HSP70 ATPase activity (Leu et al., 2011; Yang et al., 2020a), and common compound-like inhibitors such as the naturally occurring flavonoids -Epigallocatechin gallate (EGCG) and quercetin (Li et al., 2009).

Studies have found that inhibiting HSP70 (GRP78) can induce endoplasmic reticulum (ER) stress and trigger unfolded protein response (UPR), thereby inducing cancer cell apoptosis and slowing tumor growth (Jiang et al., 2007; Samanta et al., 2021). Jäättelä et al. (Nylandsted et al., 2000) first showed that silencing HSP70 by antisense RNA induced massive cell death in breast cancer cell lines but was not toxic to non-tumorigenic breast epithelial cells or normal human fibroblasts (Nylandsted et al., 2000), suggesting that targets HSP70 selectively induces tumor cell death. In addition, it has been shown that silencing HSP70 alone in the absence of HSC70 is toxic to some cancer cell lines (human cervical cancer, human breast cancer, human prostate cancer, and human liver cancer) but has no effect on normal cells (Rohde et al., 2005). Interestingly, however, in prostate cancer cells, only simultaneous silencing of HSP70 and HSC70 was accompanied by an increase in the rate of apoptosis (Wang et al., 2014). Workman et al. (Powers et al., 2008) reported a similar finding that only simultaneous silencing of HSP70 and HSC70 reduced cell survival in HCT116 colorectal cancer cells and A2780 ovarian cancer cells. Therefore, there may be cell-specific differences in sensitivity to HSP70 inhibition.

HSP70 as a target for cancer therapy

Hsp70 is an important molecular chaperone and is abundantly expressed in malignancies of many different origins. Hsp70 not only inhibits apoptosis by reducing cytoplasmic Ca2+, stabilizing lysosomes, and inhibiting cellular protein aggregation but also forms stable complexes with tumor antigens in the cytoplasm, which can escape from dying cells intact and interact with antigen presenting cells (APCs) to suppress tumor immunity (Calderwood et al., 2005; Dudeja et al., 2009). In addition, overexpression of HSP70 induces the expression of MMP-9, which increases the invasiveness of tumor cells (Du et al., 2009). It is not surprising that HSP70 interacts with a variety of tumor-related proteins, as its binding sites are present in almost all protein sequences in the cell (Rüdiger et al., 1997). HSP70 is important as a molecular chaperone for protein

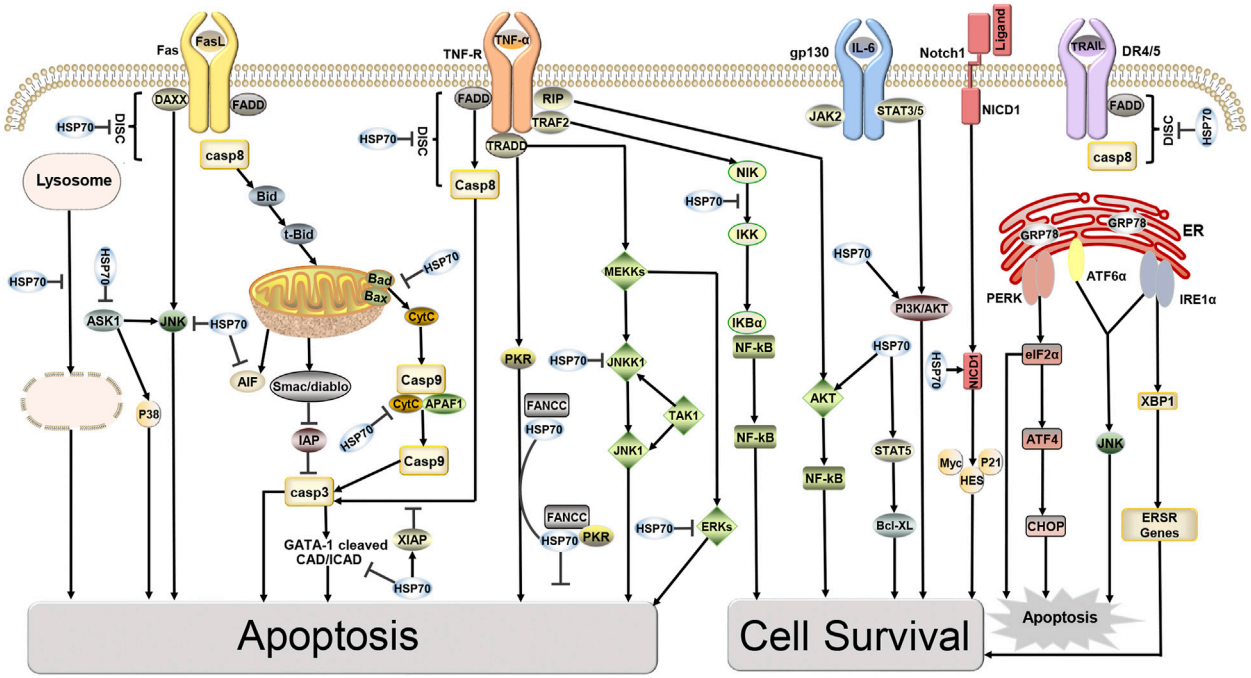

FIGURE 1
Targets of HSP70 in Apoptosis and Survival Pathways. HSP70 inhibits apoptosis, induces cell survival, and increases tumor resistance to radiotherapy through various pathways, including the mitochondrial pathway, death receptor pathway, DNA degradation pathway, and endoplasmic reticulum stress pathway.

folding, however, this is likely not its direct role in the cell death pathway. Beere et al. (2000) first suggested in 2000 that HSP70 could inhibit apoptosis by directly binding specifically to Apaf-1 to block the assembly of the apoptotic complex, but it could not block Fas-induced apoptosis. A subsequent study by Clemons overturned this conclusion that HSP72 acts upstream of mitochondria to inhibit Fas-mediated apoptosis and provide long-term cytoprotection in type II CCRF-CEM cells (Clemons et al., 2005). Furthermore, the discovery that HSP70 inhibits cell senescence establishes a clear link with cancer, and HSP70 controls the expression of major regulators of oncogene induced senescence (OIS). Knockdown of HSP70 in certain tumor epithelial cell lines leads to senescence, which provides a defense against cancer (Colvin et al., 2014; Sherman and Gabai, 2015). More importantly, overexpression of HSP70 provides a survival advantage for cancer cells as it can interact with multiple components of the caspase dependent and non-caspase-independent apoptotic pathway to inhibit cancer cell apoptosis (Figure 1). Mitochondrial pathway: In the pre-mitochondrial phase HSP70 reduces the permeability of the outer mitochondrial membrane by blocking the migration of Bax and Bad, thereby inhibiting the release of apoptotic factors such as cytochrome C (Cytc), apoptosis Inducing Factor (AIF), and SMAC/Diablo from the mitochondria (Vostakolaei et al., 2021). In late mitochondrial stages, HSP70 binds directly to apoptotic protease activating factor-1 (Apaf-1), blocking the aggregation of procaspase-9 so that the apoptotic complex cannot form and downstream caspase-3 cannot be activated (Saleh et al., 2000). An ultimate target of caspase-3 is the transcription factor GATA-1, however, HSP70 protects GATA-1 from cleavage by caspase-3, thereby increasing erythroid differentiation and survival (Dong et al., 2020). Death receptor pathway: HSP70 interacts with death receptors (TNFR, FasR, DR4/5) to prevent the formation of the death inducing signaling complex (DISC) and inhibits receptor-mediated stress kinases such as apoptosis signal-regulating kinase 1 (ASK1) and C-Jun amino acid terminal kinase 1 (JNK1) activation (Vostakolaei et al., 2021). The role of HSP70 in regulating Nuclear factor kappa B (NF-κB) function is controversial. It is hypothesized that HSP70 in the cytoplasm can repress NF-κB expression, whereas membrane-bound HSP70 can induce this transcription factor (Boudesco et al., 2018). HSP70 in the cytoplasm blocks NF-κB activation by inhibiting I-kB-α kinase (IKK) and degrading I-kB-α (Sheppard et al., 2014). In addition, in hematopoietic cells, TNFα activates pro-apoptotic double-stranded RNA-dependent protein kinase

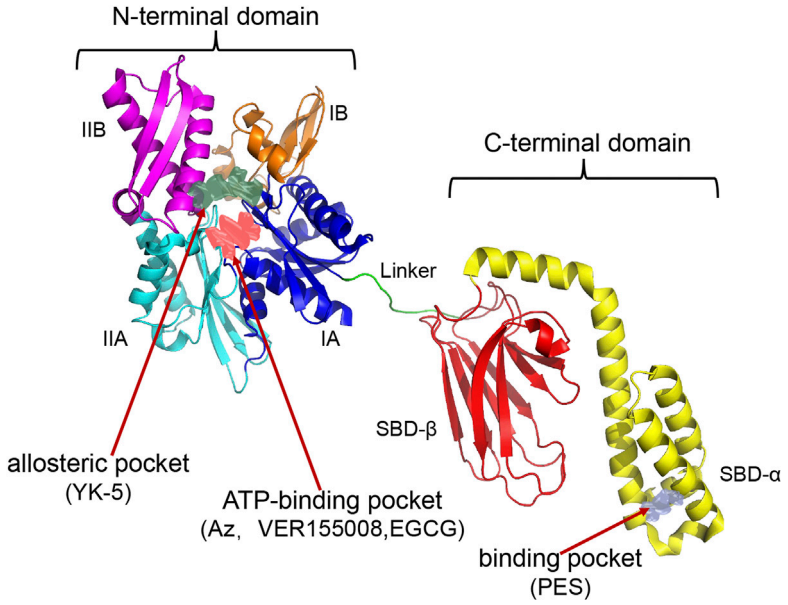

FIGURE 2
Establishment of HSP70 Homology Model and Potential Drug Sites. The following HSP70 inhibitors bind in separate pockets of HSP70: Az, VER155008, EGCG binds in the N-terminal ATP-binding pocket; YK5 binds in the N-terminal allosteric pocket (the allosteric pocket shown at the N-terminus in the figure is the binding site for YK-5); PES binds in the binding pocket of the C-terminal helical domain. The PDB code used to construct the homology model crystal structure is 1S3X, 2KHO.

(PKR). One inhibitor of PKR is the Fanconi Anemia Complementation group C gene product (FANCC), in which HSP70 interacts with FANCC proteins through its ATPase structural domain to form the ternary complex HSP70, FANCC, and PKR to inhibit TNF-induced apoptosis (Pang et al., 2002). DNA degradation pathway: The HSP70, HSP40,and ICAD complex inhibit the activity and folding effect of Caspase Activated DNAse (CAD), preventing the degradation of chromosomal DNA at late stages of apoptosis, thus achieving an anti-apoptotic effect (Kumar et al., 2016). Endoplasmic reticulum stress pathway: The multiple environmental stresses experienced by tumor cells during growth, infiltration, and metastasis, such as ischemia and hypoxia, can cause endoplasmic reticulum stress to tumor cells. Endoplasmic reticulum stress initiates the unfolded protein response (UPR) to restore cellular homeostasis but mediates apoptosis when endoplasmic reticulum stress exceeds the cell's ability to survive (Gong et al., 2017). When cells are exposed to endoplasmic reticulum stress, GRP78 (HSP70) binds to unfolded proteins and dissociates from protein kinase RNA-like ER kinase (PERK), inositol-requiring enzyme 1α (IRE1α) and activating transcription factor 6 (ATF6), and three signaling pathways are activated. Among them, IRE1 is activated by autophosphorylation, and activated IRE1 has RNase activity, which in turn shears 26 introns from XBP1 mRNA to generate active transcription factors XBP1s that promote tumorigenesis, cancer cell survival, and regulate tumor invasion (Nath et al., 2021). Other pathways: HSP70 promotes cell survival by activating PI3K/AKT, a downstream target of JAK2/STAT5 (De Almeida et al., 2020). Overexpression of HSP70 can upregulate the level and activity of STAT5, and phosphorylated STAT5 binds DNA and increases the expression of the anti-apoptotic protein Bcl-xL (Guo et al., 2005). HSP70 promotes tumor cell survival by inhibiting lysosomal membrane permeability (Nylandsted et al., 2004). In addition, HSP70 interacts with the Notch1 intracellular domain (NICD) and contributes to the activity of the cellular Notch signaling pathway (Juryńczyk et al., 2015). The above data suggest that HSP70 promotes tumor cell survival and inhibits tumor cell apoptosis in several ways. Inhibition of HSP70 can induce tumor apoptosis and increase radiosensitivity, providing evidence for Hsp70 as an anticancer target (Du et al., 2009).

HSP70 consists of an N-terminal nucleotide binding domain (NBD), a C-terminal substrate binding domain (SBD), and a linker connecting the N-terminal to the C-terminal. The N terminus comprises two adjacent lobes (lobe I and lobe II), each of which is further divided into two structural subregions (IA, IIA, IB, and IIB). The C-terminus consists of a twisted β-sandwich domain (SBDβ) that binds to the substrate and an α-helical lid domain (SBDα) that

TABLE 2 Demonstrates Hsp70 inhibitors including their sites of action and applications in preclinical studies and clinical trials.

Hsp70 inhibitors	Site of interaction	Preclinical studies	Clinical trials	Mechanism
MKT-077 (Rousaki et al., 2011; Wadhwa et al., 2000; Deocaris et al., 2007)	NBD	*In vitro* and *in vivo*	Phase I failed	Induces tumor growth arrest; induces senescence in human tumor cell lines
VER-155008 (Wen et al., 2014; Williamson et al., 2009; Sakai et al., 2021; Schlecht et al., 2013)	NBD	*In vitro* and *in vivo*		Inhibits tumour cell proliferation; inhibits cell cycle progression; promotes radiation-induced cancer cell death; disrupts signalling pathways
EGCG (Tran et al., 2010; Khan and Mukhtar, 2010; Ermakova et al., 2006)	NBD	*In vitro* and *in vivo*		Inhibits tumour cell proliferation; induces apoptosis; induces cell cycle arrest; inhibits tumour angiogenesis
Apoptozole (Cho et al., 2011; Ko et al., 2015; Park et al., 2017; Park et al., 2018)	NBD	*In vitro* and *in vivo*		Promotes lysosome-mediated apoptosis in tumour cells; impairs autophagy in cancer cells; inhibits tumour growth
YK-5 (Rodina et al., 2013)	NBD	*In vitro*		interferes with the formation of a competent chaperone/onco-client complex; induces cancer cell growth arrest; induces tumour apoptosis
JG-98 (Li et al., 2015; Yaglom et al., 2018)	NBD HSP70-BAG3 interaction	*In vitro* and *in vivo*		Affects cell signaling pathways; inhibits tumor growth; anti-proliferative; increases cell cycle-dependent kinase inhibitor P27, P21 levels; upregulates DNA damage response and UPR in tumor cells
S1g-2 (Song et al., 2021; Zhang et al., 2022)	NBD HSP70-Bim PPI	*In vitro* and *in vivo*		Interferes with signalling pathways; induces apoptosis in cancer cells
PES (Kumar et al., 2016; Jiang and Xiao, 2020; Leu et al., 2009)	SBD	*In vitro* and *in vivo*		Interferes with cell survival and signaling pathways; causes dysfunctional autophagy and altered lysosomal function; disrupts HSP70-associate chaperone interactions; induces cell cycle arrest; reduces HSP70 client protein levels; induces apoptosis in cancer cells
15-DSG (Nadler et al., 1998; Kawada et al., 2000; Kawada et al., 2002; Ramya et al., 2006)	C-terminal EEVD motif D	*In vitro* and *in vivo*	Phase II failed	Inhibits protein synthesis; induces apoptosis; inhibits tumor cell growth; inhibits tumor-forming angiogenesis; induces cell cycle arrest

EGCG, epigallocatechin-3-gallate; PES, 2-phenylethynesulfonamide; 15-DSG, 15-deoxyspergualin; UPR, unfolded protein response.

closes the substrate. HSP70 inhibitors can inhibit HSP70 activity by different mechanisms (Figure 2; Table 2), most known HSP70 inhibitors bind to the NBD, such as Az, VER155008, and EGCG which usually bind to the N-terminal ATP-binding pocket of HSP70 to inhibit HSP70 activity (Williamson et al., 2009; Tran et al., 2010; Cho et al., 2011). YK-5 interacts with the allosteric pocket of HSP70, a site located in the cleft region outside the ATP/ADP binding domain, flanked by subregions IB and IIB (Rodina et al., 2013); MKT-077 binds to an allosteric site within the nucleotide-binding domain (Rousaki et al., 2011); the HSP70 inhibitors 2,5′-thiodipyrimidine and 5-(phenylthio)-pyrimidine acrylamides designed by G. Chisosis et al. bound to a novel variant pocket of the NBD of HSP70 (Kang et al., 2014); HSP70-Bim protein-protein interaction (PPI) inhibitor, S1g-2, which is located in the hydrophobic cleft between the IA and IIA substructural domains of the Hsc70 NBD, induces cell-specific apoptosis in chronic myeloid leukemia (CML) cells by selectively disrupting HSP70-Bim PPI (Song et al., 2021). Some HSP70 inhibitors act by different mechanisms: 15-deoxyspergualin (DSG) inhibits HSP70 ATPase activity by interacting with the C-terminal EEVD motif (Nadler et al., 1998), and 2-phenylethynesulfonamide (PES) acts on the binding pocket in the C-terminal helical domain of HSP70 to inhibit its activity (Balaburski et al., 2013). A number of new HSP70 inhibitors have now been tested in preclinical models and they have been shown to increase the sensitivity of tumors to chemotherapy and radiotherapy (Multhoff et al., 2015). Here we mainly summarise the studies related to HSP70 inhibitors increasing tumor radiosensitivity.

Mechanisms of radiosensitization by HSP70 inhibitors

The protective effect of HSP70 against radiation-induced apoptosis may underlie resistance to tumor radiotherapy. During ionizing radiation-induced cell damage HSP70 is released into the tumor microenvironment, triggering the immune system to activate dendritic cell maturation and cytotoxic T cell recruitment, thereby inhibiting tumor cell apoptosis, increasing cancer cell resistance to ionizing radiation-induced oxidative stress, and inducing resistance to radiotherapy (Ashrafizadeh et al., 2020). HSP70 knockout

mice exhibit not only increased susceptibility to necrosis and inflammation, but also genomic instability and enhanced radiosensitivity (Hunt et al., 2004). Therefore, Hsp70 inhibitors could be a promising candidate for cancer therapy to enhance the effects of clinical radiosensitization. The mechanism of radiosensitization by Hsp70 inhibitors is described here.

Disruption of the activity of HSP70 chaperone clients

At the molecular level, the increased radiosensitivity of tumor cells induced by inhibition of HSP70 activity is closely associated with the down-regulation of protein expression of bcl-2, bcl-xl, mdr1, chk-1, and mcl-1 and the up-regulation of protein expression of bax, p53, fax and bad (Kim et al., 2013; Meng et al., 2014; Wang et al., 2020a; Tang et al., 2020). HSP70 inhibitors have been found to inhibit HSP70 activity in certain tumors by disrupting the activity of client proteins associated with HSP70, thereby inhibiting cell proliferation, inducing apoptosis and increasing tumor radiosensitivity (Li et al., 2013; Jiang and Xiao, 2020). Li et al. (2013) treated MDA-MB-231 and MCF-7 breast cancer cells with the HSP70 inhibitor MKT-077 analogue (JG-83) for 24 h and then assayed Akt1 and Raf1 by Western blot and found that the levels of Akt1 and Raf1 were reduced by approximately 25% in MDA-MB-231 and MCF-7 cells. This reflects the fact that HSP70 inhibitors modestly destabilize the chaperone clients Akt1 and Raf1 and induce apoptosis in these cells. Another study reached similar conclusions in oral squamous carcinoma cells, the HSP70 inhibitor PES reduced its client protein X-linked inhibitor of apoptosis protein (XIAP) and cellular inhibitors of apoptosis proteins 1 (c-IAP1) levels and significantly blocked the association of HSP70 with XIAP, suggesting that PES inhibited the function of HSP70 in oral squamous cell carcinoma cells by destroying HSP70 client proteins, and ultimately inhibiting the growth of oral squamous cell carcinoma cells (Jiang and Xiao, 2020).

In addition, inhibitors can target not only HSP70 but also the dimeric structure of HSP70 to promote apoptosis in tumor cells. Dimerization of HSP70 is essential for regulating HSP70 activity (Takakuwa et al., 2019; Pan et al., 2021), and common co-chaperone proteins of HSP70 such as Bim and JDP can combine with HSP70 as a dimer structure to regulate HSP70 activity and substrate specificity (Pan et al., 2021; Wyszkowski et al., 2021). In contrast, the HSP70-Bim PPI inhibitor S1g induces apoptosis in tumor cells by dissociating the HSP70/Bim dimer (Song et al., 2021; Wang et al., 2021). Among them, the co-chaperone Bim helps HSP70 recognize some cancer-associated clients, making some cancer cells such as T47D cells, BV173 cells, KCL-22 cells, etc. dependent on HSP70-Bim function (Guo et al., 2020). HSP70-bim PPI inhibits apoptosis by regulating the folding of oncogenic clients AKT and Raf-1 in cancer cells (Guo et al., 2020), whereas S1g-6, an HSP70 inhibitor targeting the tumor-associated HSP70-Bim PPI, significantly decreased the expression and phosphorylation levels of AKT and Raf-1 proteins when BV173 and KCL22 cells in CML cell lines were treated with S1g-6 (Wang et al., 2021). This data suggests that S1g-6 can disrupt HSP70-Bim function in living cells and has an anti-tumor effect. Several other studies have supported the idea that HSP70 inhibitors can increase the sensitivity of tumors to radiotherapy by modulating client proteins (Kim et al., 2014; Meng et al., 2014).

Blocking the HSP70-dependent signalling pathway

Several studies have demonstrated that HSP70 inhibitors can promote apoptosis and increase tumor sensitivity to radiotherapy by blocking HSP70-dependent signaling pathways. For example, quercetin enhances the radiosensitivity of colon cancer cells *in vivo* by targeting Notch-1 signaling and colonic CSCs (Li et al., 2020). These authors found that quercetin combined with IR eliminated CRC stem cells (CRC-SCs) by inhibiting Notch1 signaling and that the expression of biomarkers in CSCs was significantly reduced in both *in vitro* and *in vivo* studies. Quercetin and IR inhibited the growth of primary and secondary colonosphere and suppressed the Notch-1 signaling pathway by downregulating γ-secretase complex proteins, Jagged-1, HES1, and HEY1. The above results suggest that the combination of quercetin and IR may be a promising strategy for tumor sensitization by radiotherapy. The PI3K/Akt signaling pathway plays a key role in the development of many tumors, and the activation of the PI3K/Akt pathway is closely associated with the chemoresistance and radioresistance of tumor cells (Fresno Vara et al., 2004). The PI3K/Akt signaling pathway is aberrantly activated in most malignancies and activated AKT phosphorylates downstream target proteins, including FOXO1, WEE1, GSK3b, and mTORC1, which lead to tumor cell survival, promote cell cycle progression, ribosome biogenesis or protein synthesis (Song et al., 2019). Therefore, the topic of whether HSP70 inhibitors can improve the radiosensitivity of tumor cells by inhibiting the PI3K/Akt signaling pathway is worthy of further investigation. Shu et al. (2021) demonstrated the possibility that TPL could radiosensitize U251 cells by inhibiting the PI3K/Akt signaling pathway. When the 10nmol/L HSP70 inhibitor triptolide (TPL) was combined with 4GyX-rays, the expression levels of p-PI3K and p-Akt in human glioma U251 cells decreased more significantly than with TPL or X-rays alone. In addition, CHOP is a transcription factor that promotes apoptosis by regulating apoptosis-related genes such as down-regulation of bcl2, bcl-xl, and mcl-1 expression and up-regulation of BIM, BAK, and Bax expression (Hu et al., 2018). Using a human ovarian cancer xenograft model, one study showed that

quercetin induced CHOP via the PERK/ATF4/eIF2α pathway, thereby enhancing ionizing radiation-induced apoptosis (Gong et al., 2018). AKT, MAPK, and ERK signaling pathways are also important pathways that regulate cell cycle progression and apoptosis. PES inhibited the activation of Akt and ERK pathways to promote apoptosis in NSCLC cells (Zhou et al., 2017a) or induced apoptosis in oral squamous cell carcinoma cells by reducing the expression and phosphorylation levels of AKT and ERK (Jiang and Xiao, 2020), these data reflect the positive effects of PES in inhibiting tumor development. NF-κB is an important transcriptional activator involved in various physiological and pathological processes such as inflammatory response, immune response, and cell proliferation and apoptosis. NF-κB not only promotes cell proliferation and inhibits apoptosis, but upregulation of NF-κB in tumor cells also promotes upregulation of tumor metastasis factors and lymphatic barrier breach, which plays an important role in the development of tumorigenesis (Nguyen et al., 2015). Upregulation of NF-κB leads to inflammatory responses and oxidative stress, and it can lead to tumor resistance to radiotherapy and chemotherapy by regulating angiogenesis and inhibiting apoptosis (Mortezaee et al., 2019). Zhang et al. (2012) found that EGCG significantly enhanced radiation-induced apoptosis and was accompanied by a decrease in NF-κB protein levels, suggesting that HSP70 inhibitors may reduce tumor resistance to radiotherapy by inhibiting the NF-κB signaling pathway. In addition, Meng et al. (2014) reported a similar finding that the HSP70 inhibitor TPL could inhibit NF-κB activity not only directly by inhibiting the trans-activation of the p65 subunit of NF-κB but also indirectly through the AKT/GSK3β/mTOR pathway to inhibit NF-κB signaling and promote apoptosis. In summary, HSP70 inhibitors increase radiation-induced apoptosis in tumor cells by blocking a variety of HSP70-dependent signaling pathways.

Inhibition of repair of radiation-induced DNA damage

DNA is the main target of ionizing radiation, which has cytotoxic effects on DNA, mainly resulting in single-strand breaks (SSBs) and double-strand breaks (DSBs) (Goldstein and Kastan, 2015). The efficacy of radiotherapy depends on its ability to induce lethal DNA damage in cancer cells and the ability of cells to repair radiation-induced DNA damage (Schaue and McBride, 2005; Buckley et al., 2020). Unrepaired and inaccurately repaired DNA double-strand breaks are the main cause of radiation-induced cell death (Morgan and Lawrence, 2015). There are two main pathways for DSB repair, nonhomologous end-joining (NHEJ) and homologous recombination (HR) (Scully et al., 2019). NHEJ occurs throughout the cell cycle and is the main repair pathway for G1 phase DSBs (Takata et al., 1998; Zhao et al., 2017). HR uses sister chromatids as a template for repair and is therefore restricted to the S/G2 phase (Takata et al., 1998; Orthwein et al., 2015).

Ionizing radiation increased γ-H2AX levels in a dose-dependent manner, with the abundance of γ-H2AX lesions peaking 30 min after IR and returning to baseline levels approximately 24 h after IR (Yang et al., 2020b). γ-H2AX is one of the earliest DSB-induced DNA damage repair (DDR) events (Willers et al., 2015). Several preclinical studies have shown that the combination of IR and HSP70 inhibitors exacerbates γ-H2AX lesions, increases unrepaired DSB and induces delayed DSB repair, and increases the radiosensitivity of tumor cells (van Rijn and van den Berg, 1997; Lin et al., 2012; Gong et al., 2018). Furthermore, the combination of IR and HSP70 inhibitors leads to HR defects by reducing RAD51 expression. The DNA recombinase RAD51 is the most critical component of the HR pathway, catalyzing the typical key responses of HR. In contrast, the ataxia telangiectasia mutated (ATM) kinase is an upstream regulator of RAD51 and is activated to enhance the HR response to DSB (Li and Heyer, 2008; Yang et al., 2020b). Within minutes of DSB formation, different proteins are phosphorylated by active ATM, which are required for the DNA damage response and repair (Hakem, 2008). HSP70 inhibitors can impede DNA damage repair in irradiated tumor cells, so ionizing radiation combined with HSP70 inhibitor treatment can exacerbate DNA damage and enhance radiation-induced cell death (Figure 3). *In vitro* and *in vivo* studies have confirmed that quercetin can specifically inhibit ATM activation and ATM-mediated phosphorylation of downstream targets, leading to tumor radiosensitization (Lin et al., 2012). In support of this finding, the radiosensitizing effect of quercetin was lost in ATM-deficient cells (Lin et al., 2012). Although no interaction between HSP70 and ATM was detected, HSP70 was found to interact with its downstream factor RAD51 and to be associated with radiosensitivity (Tambini et al., 2010). Gong et al. (2018) showed that quercetin reduced RAD51 expression via the p53-mediated endoplasmic reticulum stress pathway and that cells lacking RAD51 function had a defect in HR repair leading to reduced DSB repair and increased ionizing radiation-induced apoptosis. The above results highlight the potential of quercetin as a novel radiosensitizer. In addition, TPL and its derivatives exhibit cytotoxicity by inducing DNA damage, thus increasing the sensitivity of different cell types to DNA damage-based chemotherapy or radiotherapy. TPL impairs NHEJ repair by directly interacting with and inhibiting the autophosphorylation of DNA-PKcs (Cai et al., 2020). TPL can also reduce the expression of HSP70 by downregulating Sp1, thereby promoting the apoptosis of tumor cells (Arora et al., 2017). Moreover, Sp1 interacted with DNA-PKcs in several types of tumor tissues (gastric, colon, and pancreatic cancer) to participate in DNA damage repair (Odegaard et al., 1998; Hosoi et al., 2004). In conclusion, TPL can not only impair

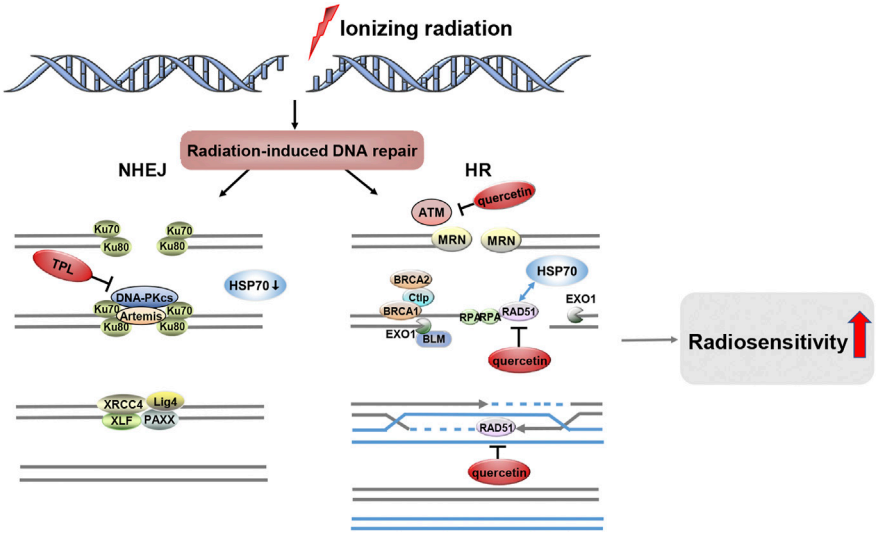

FIGURE 3
HSP70 Inhibitors Inhibit the Repair of Radiation-induced DNA Damage. After ionizing radiation-induced DSBs, two distinct DNA repair systems emerged, namely NHEJ and HR. HSP70 inhibitors such as quercetin and TPL can be involved in the DNA damage repair pathway, and they increase the radiosensitivity of tumors by inhibiting radiation-induced DNA damage repair.

DNA repair by directly inhibiting DNA-PKcs, but may also affect the interaction between sp1 and DNA-PKcs by inhibiting DNA-PKcs, and ultimately downregulate the expression level of HSP70 to promote tumor cell apoptosis. However, the current data do not demonstrate that HSP70 inhibitors in combination with IR inhibit NHEJ activity while attenuating HR efficiency.

Cell cycle blockade

Disturbances in cell cycle regulation play an important role in the development of tumors. The operation of the cell cycle is largely dependent on cyclin dependent kinase (CDK), which relies on the binding of cyclin to perform key functions in the orderly progression of the cell cycle. Different CDK-Cyclin complexes phosphorylate specific target proteins to stimulate cell cycle phases, facilitating the G1/S and G2/M transitions. Cell cycle arrest is a key determinant of radiosensitivity, and HSP70 causes a delay in cell growth that reduces G2/M phase arrest (Lee et al., 2001). Notably, G2/M phase cells are the most sensitive to radiation (Terasima and Tolmach, 1961; Sinclair and Morton, 1966). Lee et al. (Lee et al., 2001) examined the G2/M phase arrest in two cell lines, the vector control and HSP70-transfected cell group, by measuring the accumulation of G2/M phase cells at approximately 3, 6, 12, and 24 h after 4 Gy irradiation using flow cytometry. The cell cycle arrest was significantly reduced in HSP70 overexpressing cells at 6 and 12 h after irradiation, with a 20% and 24% reduction in G2/M phase block, respectively. These data indicate that HSP70 causes a reduction in radiation-induced G2/M phase block, resulting in reduced radiosensitivity.

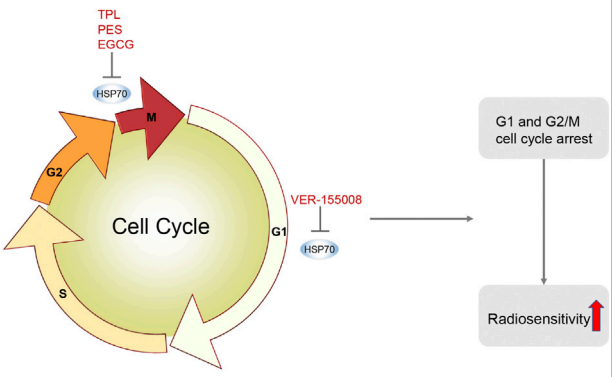

FIGURE 4
HSP70 Inhibitors Induce Cell Cycle Arrest. HSP70 inhibitors induce cell cycle arrest by inhibiting HSP70. For example, TPL induces G2/M phase arrest in nasopharyngeal carcinoma; VER-155008 induces G1 phase arrest in pleural mesothelioma; PES induces G2/M phase arrest in oral squamous cell carcinoma; EGCG induces G2/M phase arrest in MCF-7 cells in breast cancer. HSP70 inhibitors induce cell cycle arrest, make tumor cells more sensitive to radiotherapy, and increase radiotherapy-induced apoptosis.

In addition, inhibition of HSP70 expression significantly inhibits tumor cell growth and induces cell cycle arrest (Lin

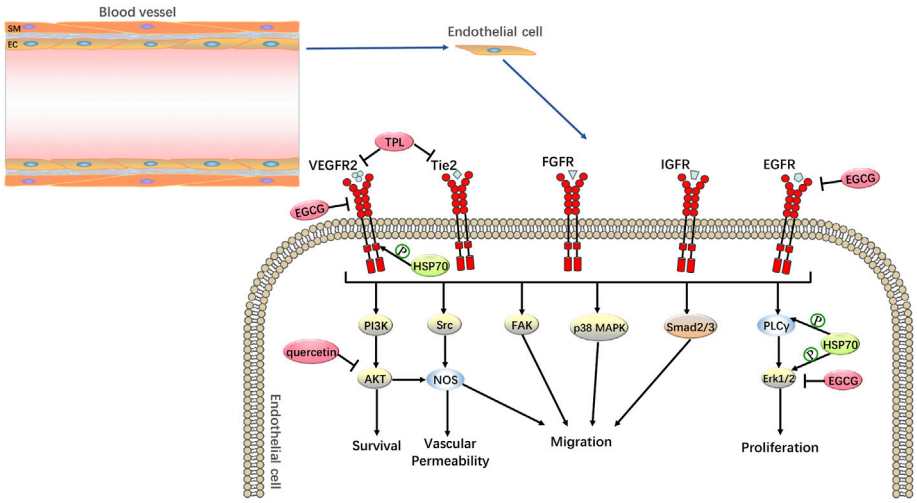

FIGURE 5
Anti-tumor Angiogenesis by HSP70 Inhibitors. HSP70 inhibitors can increase the radiosensitivity of tumor cells through anti-tumor angiogenesis. For example, in pancreatic cancer, TPL inhibits tumor angiogenesis by inhibiting Tie2 and VEGFR-2; in acute myeloid leukemia and breast cancer, quercetin targets the VEGFR-2-mediated angiogenic pathway and inhibits the expression of the downstream regulator AKT; in breast cancer, EGCG is anti-tumor angiogenic by inhibiting the expression of VEGF and suppressing the phosphorylation levels of EGFR and ERK1/2.

et al., 2014), so Hsp70 inhibitors could be considered to counteract the effects of Hsp70 on the cell cycle.

The DNA damage caused by radiotherapy leads to the activation of cell cycle regulatory mechanisms by the relevant genes, causing cell cycle arrest at two checkpoints, the G1/S phase and the G2/M phase, and the blockage of cell cycle checkpoints is an important determinant of the radiosensitivity of tumor cells (Figure 4). HSP70 inhibitors can radiosensitize tumors by inhibiting HSP70-induced cell cycle checkpoint arrest, as in nasopharyngeal carcinoma TPL can trigger apoptosis and induce G2/M phase arrest by inhibiting GRP78, thus TPL can be used as a new radiosensitizer for the treatment of nasopharyngeal carcinoma (Li et al., 2016).

Furthermore, in pleural mesothelioma, VER-155008 inhibits HSP70 by inducing G1 cell cycle arrest and disrupting the PI3K/AKT/mTOR pathway, thereby suppressing tumor proliferation (Sakai et al., 2021). In oral squamous cell carcinoma, PES blocked the cell cycle in the G2/M phase and induced apoptosis (Jiang and Xiao, 2020). In breast cancer, EGCG induced a G2/M phase cell cycle arrest in MCF-7 cells and enhanced the radiosensitivity of breast cancer (Tran et al., 2010). In summary, HSP70 inhibitors can make tumor cells more sensitive to radiotherapy by inducing cell cycle arrest.

Anti-tumor angiogenesis

Solid tumors are associated with significant tumor neovascularization during their development. Angiogenesis refers to the development of new blood vessels from existing capillaries or post-capillary veins. Due to the increasing demand for oxygen and nutrients by the expanding tumor, tumor cells induce angiogenesis by secreting a variety of growth factors (Kleibeuker et al., 2012). Among them, vascular endothelial growth factor (VEGF) is an important angiogenic factor that induces endothelial cell proliferation and migration and promotes angiogenesis. VEGF not only causes reoxygenation of tumor cells, leading to excessive DNA replication and increased synthesis of radioresistant genes but also enhances tumor radioresistance by promoting the development of autophagy (Meng et al., 2014; Chen et al., 2020). Anti-VEGF can increase tumor radiosensitivity by blocking angiogenesis, inducing apoptosis in vascular endothelial cells, and activating the mTOR pathway to inhibit radiation-induced autophagy (Chen et al., 2020). Furthermore, both preclinical and clinical studies have shown that radiotherapy can affect tumour angiogenesis and that inhibition of angiogenesis can enhance the effects of radiotherapy (Kleibeuker et al., 2012). Meanwhile, Colvin et al. (2014) found that HSP70 could affect VEGF production in human breast cancer MCF-7 cells. Further studies also showed that GRP78 (HSP70) knockdown significantly inhibited VEGF-induced endothelial cell proliferation and VEGF-induced extracellular regulated protein kinase 1/2 (ERK1/2), phospholipase C-γ (PLC-γ), and VEGFR-2 phosphorylation, thereby suppressing tumour angiogenesis (Katanasaka et al., 2010). Therefore, HSP70 inhibitors can act as inhibitors of tumor-induced angiogenesis and radiosensitizers of tumor vasculature (Figure 5). One study showed that HSP70 inhibitors inhibited tumor angiogenesis and tumor metastasis (He et al., 2010). TPL inhibits pancreatic cancer tumor

angiogenesis and tumor metastasis by inhibiting Tie2 and VEGFR-2 and down-regulating VEGF expression. This was confirmed by another study with quercetin, which targeted the VEGFR-2-mediated angiogenic pathway, inhibited the expression of the downstream regulator AKT, and suppressed tumor growth in acute myeloid leukemia and breast cancer (Balakrishnan et al., 2016; Shi et al., 2020). Furthermore, in breast cancer, EGCG inhibits tumor invasion and angiogenesis by suppressing VEGF expression, as well as inhibiting epidermal growth factor receptor (EGFR) and ERK1/2 phosphorylation levels, which also supports the use of HSP70 inhibitors as radiosensitizers for tumors (Khan and Mukhtar, 2010).

Other mechanisms

The transcription factor HSF1 drives tumor development by regulating the expression of heat shock proteins, inhibiting apoptosis, promoting cancer cell proliferation and metastasis, and facilitating DNA repair (Wang et al., 2020b). HSF1 is highly expressed in a variety of tumors (Mendillo et al., 2012) and high HSF1 expression in tumor tissues is negatively correlated with the prognosis of cancer patients (Zhou et al., 2017b). For example, higher levels of HSF1 expression in breast, oral cavity, myeloma, and endometrial cancers are associated with poor prognosis and increased metastasis in patients (Santagata et al., 2011; Ishiwata et al., 2012; Engerud et al., 2014; Fok et al., 2018). In addition, gene transcription of HSP70 is also regulated by HSF1, which is activated in response to stress stimuli. Since activated HSF1 induces the expression of HSP70 and enhances cellular radioresistance (Kabakov et al., 2006), inhibition of HSF1 may be an effective way to block HSP70 expression and increase radiosensitivity (Kumar et al., 2016). Considering the role of HSF1 in tumor development, HSF1 could be a potential therapeutic target. Activation of HSF1 is a rather complex process: HSF1 binds to molecular chaperones (e.g., HSP70) to form a complex and remains free in the cytoplasm as an inactive monomer, gradually acquiring transcriptional activity in response to heat shock. First HSF1 is depolymerized from the complex and then oligomerized into a DNA-bound trimer that translocates to the nucleus. The trimeric HSF1 that enters the nucleus then binds to the heat shock element (HSE) in the promoter of the target gene. HSF1 is subsequently activated by casein kinase 2 (CK2) and calcium/calmodulin-dependent protein kinase II (CaMKII) phosphorylation, and hyperphosphorylated HSF1 acquires full transcriptional activity, thereby inducing transcription of heat shock genes (Westerheide et al., 2006; Wang et al., 2009). HSP70 inhibitors can block HSP70 expression by inhibiting HSF1, thereby reducing tumor radioresistance. Inhibition of HSF1 activation can be achieved by HSP70 inhibitors TPL and quercetin (Dai and Sampson, 2016). TPL has been found to block HSF1 activation and transcription during steps such as trimerization, phosphorylation, and DNA binding, while quercetin may inhibit HSP70 by blocking phosphorylation of HSF1 by CK2 and CaMKII (Wang et al., 2009). Tran et al. (2010) demonstrated for the first time that EGCG significantly reduced HSF1 levels in a dose-dependent manner, suggesting that EGCG can suppress the expression of HSP70 by inhibiting the expression of the HSP70 transcription factor HSF1. Furthermore, KRIBB11 was the first reported direct inhibitor of HSF1, when cells were exposed to heat shock in the presence of KRIBB11, the induction of HSF1 downstream target proteins such as HSP27 and HSP70 was blocked, inducing tumour growth arrest and apoptosis (Yoon et al., 2011). The above studies suggest that HSP70 inhibitors may also block HSP70 expression by inhibiting HSF1 to radiosensitize tumors. However, inhibition of HSF-1 not only affects the expression of heat shock proteins but also other regulatory factors involved in various cellular pathways (Fok et al., 2018). Therefore, the complex mechanisms affected by inhibition of HSF-1 should be taken into account.

HSP70 inhibitors can also induce other biological phenotypes, providing a mechanistic basis for the use of HSP70 inhibitors in combination with radiation therapy. For example, the induction of senescence, i.e., irreversible growth arrest, is considered in cancer cells as a means of stopping tumor initiation and progression (Zamin et al., 2009). Firstly, long-term exposure to HSP70 inhibitors induces a cellular senescence phenotype in many cancer cell lines, such as quercetin-mediated senescence in human colon cancer cells (Özsoy et al., 2020); TPL promotes heterochromatin formation and thus represses gene transcription by inhibiting histone H3 methylation levels and upregulating H3K9me3 and H3K27me3, ultimately inducing a senescence-like phenotype in prostate cancer cells (Tamgue and Lei, 2017); and resveratrol and quercetin significantly increase the proportion of senescence-associated β-galactosidase (SA-β-GAL)-positive cells in C6 rat gliomas (Zamin et al., 2009). All of the above studies can confirm that HSP70 inhibitors can induce events of tumor cell senescence. On the other hand, radiation therapy also triggers premature senescence in solid tumor cell lines (Mirzayans et al., 2005). This finding is attributed to the fact that IR causes massive DNA damage and activates two major DNA damage-induced signaling pathways, namely the p53/p21waf1 pathway and the P16INK4a/Rb pathway, leading to sustained cell cycle arrest and cellular senescence (Panganiban et al., 2013). In addition, it has been shown that the radiosensitivity of many cancer cells can be enhanced by promoting senescence (Nam et al., 2013). Therefore, radiotherapy and HSP70 inhibitors can combine to induce tumor cell senescence and enhance the radiosensitivity of multiple tumors, thereby inhibiting tumor progression.

In addition to the classical radiosensitization mechanisms described above, HSP70 inhibitors can also inhibit tumor growth by modulating the tumor immune response (Bandyopadhyay et al., 2008; Liang and Fu, 2008; Liu et al., 2013; Chan et al., 2017). In tumor cells, regulatory T cells (Treg) play a key role in the regulation of the tumor immune response, leading to immune tolerance through direct killer cell activity, secretion of immunosuppressive molecules, and suppression of B cells, macrophages, dendritic cells (DCs), etc (Liu et al., 2013;

Tanaka and Sakaguchi, 2017). Therefore, reducing the number of Treg cells or inhibiting their function could be considered as new immunotherapeutic targets for tumor therapy. Among them, IL-10 and TGF-β, two important immunosuppressive factors produced by Treg cells, can directly kill T cells or antigen-presenting cells by secreting granzymes (Tanaka and Sakaguchi, 2017). Thus, Treg cells play a key role in tumor immune tolerance, and the HSP70 inhibitor TPL significantly reduced the proportion of Treg cells in the spleen and axillary lymph nodes of tumor-bearing mice and decreased Foxp3 levels and secretion of IL-10 and TGF-β in peripheral blood (Liu et al., 2013), these data reflect the possibility that TPL may counteract tumor immune responses and inhibit tumor growth by suppressing Treg cells and immunosuppressive factors. On the other hand, radiation therapy is an ideal tool to enhance tumor MHC-I expression, which would continuously allow a cytotoxic $CD8^+$ T-cell (CTL)-mediated response to specifically kill tumor cells (Frey et al., 2017). The initiation of an immune response after radiation therapy has been demonstrated in several preclinical studies, not only because of the induction of different forms of tumor cell death, but also because the interferon-gene stimulated protein signaling pathway (STING), which senses DNA, is activated (Frey et al., 2017). Although ionizing radiation recruited Treg cells and other immunosuppressive cells into the tumor microenvironment, TPL significantly reduced the proliferation of Treg (Liu et al., 2013). Interestingly, other researchers have reported that TPL can amplify Treg cells in non-tumor cells (Zhang et al., 2009; Xu et al., 2016). These varied results suggest that the effects of natural compounds in different disease states may be complex. In addition, radiation therapy sensitizes refractory "cold" tumors to immune checkpoint inhibitors by promoting the recruitment of anti-tumor T cells (Demaria et al., 2016). In conclusion, the above data suggest that both HSP70 inhibitors and radiotherapy can improve local tumor control through an anti-tumor immune response. These potential mechanisms provide new perspectives for future exploration and offer the possibility of combining HSP70 inhibitors, radiotherapy, and immunotherapy.

Tumor cell resistance to HSP70 inhibitor radiosensitization

With the application of HSP70 inhibitors, it is found that tumor has drug resistance to HSP70 inhibitors, which reduces their radiosensitization effect. For example, the radiosensitizing effect of the HSP70 inhibitor MAL3-101 is achieved by inhibiting HSP70ATPase activity, yet tumor cells can overcome MAL3-101-induced apoptosis through endoplasmic reticulum-associated degradation and autophagy and become resistant to HSP70 inhibitors (Moradi-Marjaneh et al., 2019).

One study found that quercetin enhanced the phosphorylation of HSP27 upon down-regulation of HSP70, and that phosphorylated HSP27 had anti-apoptotic activity, reducing the radiosensitizing effect of quercetin due to inhibition of HSP70 (Wang et al., 2009). The data reflect that inhibition of HSP70 without enhanced phosphorylation of HSP27 is beneficial in reducing the resistance of tumor cells to radiosensitization by HSP70 inhibitors, and therefore HSP70 inhibitors may be considered in combination with HSP27 inhibitors. In addition, the combination use of HSP70 inhibitors may also be an effective strategy to reduce tumor resistance to HSP70 inhibitor radiosensitization (Li et al., 2009). Quercetin down-regulated the expression of HSP70 but up-regulated the expression of GRP78 in human breast cancer cells in a dose-dependent manner. Whereas EGCG promoted quercetin-induced cell death by binding to the ATP-binding domain of GRP78 and blocking its protective function, the combined application of EGCG and quercetin inhibited both HSP70 and GRP78. The authors demonstrated a way to increase the sensitivity of breast cancer cells to a single HSP70 inhibitor by using a combination of HSP70 inhibitors (Li et al., 2009). Another study also supported the above notion that TPL enhanced kahweol-induced cytotoxicity by inhibiting Hsp70 activity and synergistically promoted colon cancer cell apoptosis (Choi et al., 2015). In summary, when heat shock protein inhibitors are used in combination, they may reduce the resistance of tumor cells to radiosensitization by HSP70 inhibitors. However, considering that toxicity to normal cells/tissues should be evaluated, their combined use still needs further study.

Effect of dual targeting of HSP70 and HSP90 on sensitivity to radiotherapy

Many HSP90 client proteins are components of cancer cell-associated signaling pathways that ensure unlimited tumor growth and their resistance to radiotherapy. Following Hsp90 inhibition, these client proteins are degraded, disrupting multiple pathways critical for tumor cell survival. Thus, HSP90 inhibitors may also be used as agents to sensitize human tumors to radiotherapy (Kabakov et al., 2010). The majority of tumors and cancer cell lines are radioresistant to HSP90 inhibitors, therefore, there is an urgent need for a biomarker to predict the response of target cells to inhibitory therapy. HSP70 is a co-chaperone protein whose upregulation serves as a biomarker for HSP90 inhibition (Spiegelberg et al., 2020; Naz et al., 2021). In their study of the effect of HSP90 inhibitors on cellular radiation response, Kudryavtsev et al. (Kudryavtsev et al., 2017) found that radiosensitizing effects were present only in cell cultures with early and significant induction of HSP70 after treatment with HSP90 inhibitors, and that the level of HSP70 induction was positively correlated with the degree of radiosensitization. This study supports the idea that HSP70 induction can be a valid marker for predicting the effects of HSP90-inhibited

radiosensitizers on tumor and normal tissue ionizing radiation. HSP70 can be used as a biomarker to quantify the inhibitory effect of low concentrations of HSP90 inhibitors on HSP90 (Mehta et al., 2020). The authors demonstrate that the inhibition of Hsp90 by even low-dose Hsp90 inhibitors can be monitored by measuring HSP70 expression in peripheral blood individual nucleated cells, which also suggests the potential use of HSP70 from blood cells as a clinical biomarker in future studies. In addition, Hsp70 as a biomarker has the advantage of being easily detected by Western blot (Kudryavtsev et al., 2017) and consistent in clinical trials (Zhang et al., 2006).

More importantly, HSP90 inhibitors have been shown to increase the radiosensitivity of tumor cells, but at the same time they also strongly enhance the expression of cytoprotective HSP70 (Ambati et al., 2014). This result is thought to reduce the overall anti-tumor effect of these compounds, and therefore dual targeting of HSP90 and HSP70 is an emerging concept for making tumor cells more sensitive to radiotherapy. Several preclinical studies have investigated the radiosensitivity of tumor cells in combined HSP90 and HSP70 therapy. Schilling et al. (2017) found that HSP70 inhibition peptide aptamer A17 inhibition of HSP70 by itself did not significantly increase the radiosensitization of lung and breast cancer cells, but it could enhance the radiosensitization of tumors by the Hsp90 inhibitor NVP-AUY922. In previous work, the research group has reported similar findings that NZ28 in combination with NVP-AUY922 achieved the same radiosensitization as high-concentration NZ28 monotherapy even when the NZ28 concentration was reduced to 1/10-1/20 (Schilling et al., 2015). Another study supports the idea that HSP90 inhibitors and HSP70 inhibitors in combination can help overcome the high radiation resistance of some tumors and sensitize them to radiation therapy (Kudryavtsev et al., 2017).

Conclusion

HSP70 inhibitors play an important role in increasing the sensitivity of tumor radiotherapy. Important data suggest that HSP70 inhibitors have radiosensitizing effects by disrupting the activity of HSP70 client proteins, blocking multiple HSP70-dependent signaling pathways, inhibiting the repair of radiation-induced DNA damage, inhibiting cell cycle checkpoint activation, and inhibiting tumor angiogenesis. Furthermore, HSP70 inhibitors prevent HSF1 activation and transcription, induce cellular senescence and promote antitumor immunity, which may be a potential mechanism for clinical radiosensitization. As tumors are drug-resistant to HSP70 inhibitors, this can reduce the radiosensitizing effect of the inhibitor. Although several preclinical studies have demonstrated that combinations between heat shock protein inhibitors can reduce tumor resistance to HSP70 inhibitor radiosensitization, the feasibility of such regimens needs to be further investigated in the future. Currently, drugs that have been studied using heat shock proteins as targets are mainly HSP90 inhibitors, but HSP70 is a more suitable drug target than HSP90 in terms of therapeutic efficacy (Balaburski et al., 2013). However, the research on HSP70 is still inadequate and the experimental data is insufficient. Moreover, most of the experiments had a limitation, that is, they did not knock out the endpoints affected by HSP70 and then tested whether HSP70 inhibitors had the same effect on the intrinsic radiosensitivity under the same conditions, thus providing a clearer illustration of the interaction between radiosensitization and Hsp70 inhibition.

In conclusion, our data provide a strong rationale for the use of HSP70 inhibitors as radiosensitizers. It is hoped that in the near future clinically available HSP70 inhibitors, either as monoclonal antibodies or in combination with radiotherapy, will be developed as an effective route of anti-tumor therapy.

Author contributions

SD was responsible for the conception and writing of the paper, YL and YY for the design of the paper, YW and YC for the analysis of the data and the production of the figures, YC for the selection of references for the paper and SW for the overall ideas.

Funding

General project of Shandong Natural Science Foundation, project number: ZR2020MH242.

Conflict of interest

The authors declare that the research was conducted in the absence of any commercial or financial relationships that could be construed as a potential conflict of interest.

Publisher's note

All claims expressed in this article are solely those of the authors and do not necessarily represent those of their affiliated organizations, or those of the publisher, the editors and the reviewers. Any product that may be evaluated in this article, or claim that may be made by its manufacturer, is not guaranteed or endorsed by the publisher.

References

Ambati, S. R., Lopes, E. C., Kosugi, K., Mony, U., Zehir, A., Shah, S. K., et al. (2014). Pre-clinical Efficacy of PU-H71, a Novel HSP90 Inhibitor, Alone and in Combination with Bortezomib in Ewing Sarcoma. *Mol. Oncol.* 8 (2), 323–336. doi:10.1016/j.molonc.2013.12.005

Arora, N., Alsaied, O., Dauer, P., Majumder, K., Modi, S., Giri, B., et al. (2017). Downregulation of Sp1 by Minnelide Leads to Decrease in HSP70 and Decrease in Tumor Burden of Gastric Cancer. *PLoS One* 12 (2), e0171827. doi:10.1371/journal.pone.0171827

Ashrafizadeh, M., Farhood, B., Eleojo Musa, A., Taeb, S., and Najafi, M. (2020). Damage-associated Molecular Patterns in Tumor Radiotherapy. *Int. Immunopharmacol.* 86, 106761. doi:10.1016/j.intimp.2020.106761

Balaburski, G. M., Leu, J. I., Beeharry, N., Hayik, S., Andrake, M. D., Zhang, G., et al. (2013). A Modified HSP70 Inhibitor Shows Broad Activity as an Anticancer Agent. *Mol. Cancer Res.* 11 (3), 219–229. doi:10.1158/1541-7786.MCR-12-0547-T

Balakrishnan, S., Bhat, F. A., Raja Singh, P., Mukherjee, S., Elumalai, P., Das, S., et al. (2016). Gold Nanoparticle-Conjugated Quercetin Inhibits Epithelial-Mesenchymal Transition, Angiogenesis and Invasiveness via EGFR/VEGFR-2-mediated Pathway in Breast Cancer. *Cell. Prolif.* 49 (6), 678–697. doi:10.1111/cpr.12296

Bandyopadhyay, S., Romero, J. R., and Chattopadhyay, N. (2008). Kaempferol and Quercetin Stimulate Granulocyte-Macrophage Colony-Stimulating Factor Secretion in Human Prostate Cancer Cells. *Mol. Cell. Endocrinol.* 287 (1-2), 57–64. doi:10.1016/j.mce.2008.01.015

Beere, H. M., Wolf, B. B., Cain, K., Mosser, D. D., Mahboubi, A., Kuwana, T., et al. (2000). Heat-shock Protein 70 Inhibits Apoptosis by Preventing Recruitment of Procaspase-9 to the Apaf-1 Apoptosome. *Nat. Cell. Biol.* 2 (8), 469–475. doi:10.1038/35019501

Boudesco, C., Cause, S., Jego, G., and Garrido, C. (2018). Hsp70: A Cancer Target inside and outside the Cell. *Methods Mol. Biol.* 1709, 371–396. doi:10.1007/978-1-4939-7477-1_27

Brondani Da Rocha, A., Regner, A., Grivicich, I., Pretto Schunemann, D., Diel, C., Kovaleski, G., et al. (2004). Radioresistance Is Associated to Increased Hsp70 Content in Human Glioblastoma Cell Lines. *Int. J. Oncol.* 25, 777–785. doi:10.3892/ijo.25.3.777

Buckley, A. M., Lynam-Lennon, N., O'Neill, H., and O'Sullivan, J. (2020). Targeting Hallmarks of Cancer to Enhance Radiosensitivity in Gastrointestinal Cancers. *Nat. Rev. Gastroenterol. Hepatol.* 17 (5), 298–313. doi:10.1038/s41575-019-0247-2

Cai, B., Hu, Z., Tang, H., Hu, Z., Mao, Z., Liu, B., et al. (2020). Triptolide Impairs Genome Integrity by Directly Blocking the Enzymatic Activity of DNA-PKcs in Human Cells. *Biomed. Pharmacother.* 129, 110427. doi:10.1016/j.biopha.2020.110427

Calderwood, S. K., Theriault, J. R., and Gong, J. (2005). Message in a Bottle: Role of the 70-kDa Heat Shock Protein Family in Anti-tumor Immunity. *Eur. J. Immunol.* 35 (9), 2518–2527. doi:10.1002/eji.200535002

Chan, S. F., Chen, Y. Y., Lin, J. J., Liao, C. L., Ko, Y. C., Tang, N. Y., et al. (2017). Triptolide Induced Cell Death through Apoptosis and Autophagy in Murine Leukemia WEHI-3 Cells *In Vitro* and Promoting Immune Responses in WEHI-3 Generated Leukemia Mice *In Vivo*. *Environ. Toxicol.* 32 (2), 550–568. doi:10.1002/tox.22259

Chen, L., Lin, G., Chen, K., Wan, F., Liang, R., Sun, Y., et al. (2020). VEGF Knockdown Enhances Radiosensitivity of Nasopharyngeal Carcinoma by Inhibiting Autophagy through the Activation of mTOR Pathway. *Sci. Rep.* 10 (1), 16328. doi:10.1038/s41598-020-73310-x

Cho, H. J., Gee, H. Y., Baek, K. H., Ko, S. K., Park, J. M., Lee, H., et al. (2011). A Small Molecule that Binds to an ATPase Domain of Hsc70 Promotes Membrane Trafficking of Mutant Cystic Fibrosis Transmembrane Conductance Regulator. *J. Am. Chem. Soc.* 133 (50), 20267–20276. doi:10.1021/ja206762p

Choi, D. W., Lim, M. S., Lee, J. W., Chun, W., Lee, S. H., Nam, Y. H., et al. (2015). The Cytotoxicity of Kahweol in HT-29 Human Colorectal Cancer Cells Is Mediated by Apoptosis and Suppression of Heat Shock Protein 70 Expression. *Biomol. Ther.* 23 (2), 128–133. doi:10.4062/biomolther.2014.133

Clemons, N. J., Buzzard, K., Steel, R., and Anderson, R. L. (2005). Hsp72 Inhibits Fas-Mediated Apoptosis Upstream of the Mitochondria in Type II Cells. *J. Biol. Chem.* 280 (10), 9005–9012. doi:10.1074/jbc.M414165200

Colvin, T. A., Gabai, V. L., Gong, J., Calderwood, S. K., Li, H., Gummuluru, S., et al. (2014). Hsp70-Bag3 Interactions Regulate Cancer-Related Signaling Networks. *Cancer Res.* 74 (17), 4731–4740. doi:10.1158/0008-5472.CAN-14-0747

Dadey, D. Y. A., Kapoor, V., Hoye, K., Khudanyan, A., Collins, A., Thotala, D., et al. (2017). Antibody Targeting GRP78 Enhances the Efficacy of Radiation Therapy in Human Glioblastoma and Non-small Cell Lung Cancer Cell Lines and Tumor Models. *Clin. Cancer Res.* 23 (10), 2556–2564. doi:10.1158/1078-0432.Ccr-16-1935

Dai, C., and Sampson, S. B. (2016). HSF1: Guardian of Proteostasis in Cancer. *Trends Cell. Biol.* 26 (1), 17–28. doi:10.1016/j.tcb.2015.10.011

De Almeida, S., Regimbeau, M., Jego, G., Garrido, C., Girodon, F., and Hermetet, F. (2020). Heat Shock Proteins and PD-1/pd-L1 as Potential Therapeutic Targets in Myeloproliferative Neoplasms. *Cancers (Basel)* 12 (9), E2592. doi:10.3390/cancers12092592)

Demaria, S., Coleman, C. N., and Formenti, S. C. (2016). Radiotherapy: Changing the Game in Immunotherapy. *Trends Cancer* 2 (6), 286–294. doi:10.1016/j.trecan.2016.05.002

Deocaris, C. C., Widodo, N., Shrestha, B. G., Kaur, K., Ohtaka, M., Yamasaki, K., et al. (2007). Mortalin Sensitizes Human Cancer Cells to MKT-077-Induced Senescence. *Cancer Lett.* 252 (2), 259–269. doi:10.1016/j.canlet.2006.12.038

Dong, X. M., Zhao, K., Zheng, W. W., Xu, C. W., Zhang, M. J., Yin, R. H., et al. (2020). EDAG Mediates Hsp70 Nuclear Localization in Erythroblasts and Rescues Dyserythropoiesis in Myelodysplastic Syndrome. *Faseb J.* 34 (6), 8416–8427. doi:10.1096/fj.201902946R

Du, X. L., Jiang, T., Wen, Z. Q., Gao, R., Cui, M., and Wang, F. (2009). Silencing of Heat Shock Protein 70 Expression Enhances Radiotherapy Efficacy and Inhibits Cell Invasion in Endometrial Cancer Cell Line. *Croat. Med. J.* 50 (2), 143–150. doi:10.3325/cmj.2009.50.143

Dudeja, V., Mujumdar, N., Phillips, P., Chugh, R., Borja-Cacho, D., Dawra, R. K., et al. (2009). Heat Shock Protein 70 Inhibits Apoptosis in Cancer Cells through Simultaneous and Independent Mechanisms. *Gastroenterology* 136 (5), 1772–1782. doi:10.1053/j.gastro.2009.01.070

Engerud, H., Tangen, I. L., Berg, A., Kusonmano, K., Halle, M. K., Oyan, A. M., et al. (2014). High Level of HSF1 Associates with Aggressive Endometrial Carcinoma and Suggests Potential for HSP90 Inhibitors. *Br. J. Cancer* 111 (1), 78–84. doi:10.1038/bjc.2014.262

Ermakova, S. P., Kang, B. S., Choi, B. Y., Choi, H. S., Schuster, T. F., Ma, W. Y., et al. (2006). (-)-Epigallocatechin Gallate Overcomes Resistance to Etoposide-Induced Cell Death by Targeting the Molecular Chaperone Glucose-Regulated Protein 78. *Cancer Res.* 66 (18), 9260–9269. doi:10.1158/0008-5472.Can-06-1586

Fok, J. H. L., Hedayat, S., Zhang, L., Aronson, L. I., Mirabella, F., Pawlyn, C., et al. (2018). HSF1 Is Essential for Myeloma Cell Survival and A Promising Therapeutic Target. *Clin. Cancer Res.* 24 (10), 2395–2407. doi:10.1158/1078-0432.Ccr-17-1594

Fresno Vara, J. A., Casado, E., de Castro, J., Cejas, P., Belda-Iniesta, C., and González-Barón, M. (2004). PI3K/Akt Signalling Pathway and Cancer. *Cancer Treat. Rev.* 30 (2), 193–204. doi:10.1016/j.ctrv.2003.07.007

Frey, B., Rückert, M., Deloch, L., Rühle, P. F., Derer, A., Fietkau, R., et al. (2017). Immunomodulation by Ionizing Radiation-Impact for Design of Radio-Immunotherapies and for Treatment of Inflammatory Diseases. *Immunol. Rev.* 280 (1), 231–248. doi:10.1111/imr.12572

Goldstein, M., and Kastan, M. B. (2015). The DNA Damage Response: Implications for Tumor Responses to Radiation and Chemotherapy. *Annu. Rev. Med.* 66, 129–143. doi:10.1146/annurev-med-081313-121208

Gong, C., Yang, Z., Zhang, L., Wang, Y., Gong, W., and Liu, Y. (2018). Quercetin Suppresses DNA Double-Strand Break Repair and Enhances the Radiosensitivity of Human Ovarian Cancer Cells via P53-dependent Endoplasmic Reticulum Stress Pathway. *Onco. Targets. Ther.* 11, 17–27. doi:10.2147/OTT.S147316

Gong, J., Wang, X. Z., Wang, T., Chen, J. J., Xie, X. Y., Hu, H., et al. (2017). Molecular Signal Networks and Regulating Mechanisms of the Unfolded Protein Response. *J. Zhejiang Univ. Sci. B* 18 (1), 1–14. doi:10.1631/jzus.B1600043

Guo, F., Sigua, C., Bali, P., George, P., Fiskus, W., Scuto, A., et al. (2005). Mechanistic Role of Heat Shock Protein 70 in Bcr-Abl-Mediated Resistance to Apoptosis in Human Acute Leukemia Cells. *Blood* 105 (3), 1246–1255. doi:10.1182/blood-2004-05-2041

Guo, Z., Song, T., Wang, Z., Lin, D., Cao, K., Liu, P., et al. (2020). The Chaperone Hsp70 Is a BH3 Receptor Activated by the Pro-apoptotic Bim to Stabilize Anti-apoptotic Clients. *J. Biol. Chem.* 295 (37), 12900–12909. doi:10.1074/jbc.RA120.013364

Hakem, R. (2008). DNA-Damage Repair; the Good, the Bad, and the Ugly. *Embo J.* 27 (4), 589–605. doi:10.1038/emboj.2008.15

He, M. F., Huang, Y. H., Wu, L. W., Ge, W., Shaw, P. C., and But, P. P. (2010). Triptolide Functions as a Potent Angiogenesis Inhibitor. *Int. J. Cancer* 126 (1), 266–278. doi:10.1002/ijc.24694

Hosoi, Y., Watanabe, T., Nakagawa, K., Matsumoto, Y., Enomoto, A., Morita, A., et al. (2004). Up-regulation of DNA-dependent Protein Kinase Activity and Sp1 in Colorectal Cancer. *Int. J. Oncol.* 25 (2), 461–468. doi:10.3892/ijo.25.2.461

Hu, H., Tian, M., Ding, C., and Yu, S. (2018). The C/EBP Homologous Protein (CHOP) Transcription Factor Functions in Endoplasmic Reticulum Stress-Induced Apoptosis and Microbial Infection. *Front. Immunol.* 9, 3083. doi:10.3389/fimmu.2018.03083

Hunt, C. R., Dix, D. J., Sharma, G. G., Pandita, R. K., Gupta, A., Funk, M., et al. (2004). Genomic Instability and Enhanced Radiosensitivity in Hsp70.1- and Hsp70.3-deficient Mice. *Mol. Cell. Biol.* 24 (2), 899–911. doi:10.1128/mcb.24.2.899-911.2004

Ishiwata, J., Kasamatsu, A., Sakuma, K., Iyoda, M., Yamatoji, M., Usukura, K., et al. (2012). State of Heat Shock Factor 1 Expression as a Putative Diagnostic Marker for Oral Squamous Cell Carcinoma. *Int. J. Oncol.* 40 (1), 47–52. doi:10.3892/ijo.2011.1178

Jiang, C. C., Chen, L. H., Gillespie, S., Wang, Y. F., Kiejda, K. A., Zhang, X. D., et al. (2007). Inhibition of MEK Sensitizes Human Melanoma Cells to Endoplasmic Reticulum Stress-Induced Apoptosis. *Cancer Res.* 67 (20), 9750–9761. doi:10.1158/0008-5472.Can-07-2047

Jiang, L., and Xiao, J. (2020). 2-phenylethynesulfonamide Inhibits Growth of Oral Squamous Cell Carcinoma Cells by Blocking the Function of Heat Shock Protein 70. *Biosci. Rep.* 40 (3), BSR20200079. doi:10.1042/BSR20200079

Jin, H., Ji, M., Chen, L., Liu, Q., Che, S., Xu, M., et al. (2016). The Clinicopathological Significance of Mortalin Overexpression in Invasive Ductal Carcinoma of Breast. *J. Exp. Clin. Cancer Res.*, 35–42. doi:10.1186/s13046-016-0316-0

Jin, H. O., Hong, S. E., Kim, J. Y., Kim, M. R., Chang, Y. H., Hong, Y. J., et al. (2019). Induction of HSP27 and HSP70 by Constitutive Overexpression of Redd1 Confers Resistance of Lung Cancer Cells to Ionizing Radiation. *Oncol. Rep.* 41 (5), 3119–3126. doi:10.3892/or.2019.7036

Juryńczyk, M., Lewkowicz, P., Domowicz, M., Mycko, M. P., and Selmaj, K. W. (2015). Heat Shock Protein 70 (Hsp70) Interacts with the Notch1 Intracellular Domain and Contributes to the Activity of Notch Signaling in Myelin-Reactive CD4 T Cells. *J. Neuroimmunol.* 287, 19–26. doi:10.1016/j.jneuroim.2015.08.007

Kabakov, A. E., Kudryavtsev, V. A., and Gabai, V. L. (2010). Hsp90 Inhibitors as Promising Agents for Radiotherapy. *J. Mol. Med.* 88 (3), 241–247. doi:10.1007/s00109-009-0562-0

Kabakov, A. E., Malyutina, Y. V., and Latchman, D. S. (2006). Hsf1-mediated Stress Response Can Transiently Enhance Cellular Radioresistance. *Radiat. Res.* 165 (4), 410–423. doi:10.1667/rr3514.1

Kampinga, H. H., Hageman, J., Vos, M. J., Kubota, H., Tanguay, R. M., Bruford, E. A., et al. (2009). Guidelines for the Nomenclature of the Human Heat Shock Proteins. *Cell. Stress Chaperones* 14 (1), 105–111. doi:10.1007/s12192-008-0068-7

Kang, Y., Taldone, T., Patel, H. J., Patel, P. D., Rodina, A., Gozman, A., et al. (2014). Heat Shock Protein 70 Inhibitors. 1. 2, 5'-thiodipyrimidine and 5-(phenylthio)pyrimidine Acrylamides as Irreversible Binders to an Allosteric Site on Heat Shock Protein 70. *J. Med. Chem.* 57 (4), 1188–1207. doi:10.1021/jm401551n

Katanasaka, Y., Ishii, T., Asai, T., Naitou, H., Maeda, N., Koizumi, F., et al. (2010). Cancer Antineovascular Therapy with Liposome Drug Delivery Systems Targeted to BiP/GRP78. *Int. J. Cancer* 127 (11), 2685–2698. doi:10.1002/ijc.25276

Kawada, M., Masuda, T., Ishizuka, M., and Takeuchi, T. (2002). 15-Deoxyspergualin Inhibits Akt Kinase Activation and Phosphatidylcholine Synthesis. *J. Biol. Chem.* 277 (31), 27765–27771. doi:10.1074/jbc.M200318200

Kawada, M., Someno, T., Inuma, H., Masuda, T., Ishizuka, M., and Takeuchi, T. (2000). The Long-Lasting Antiproliferative Effect of 15-deoxyspergualin through its Spermidine Moiety. *J. Antibiot.* 53 (7), 705–710. doi:10.7164/antibiotics.53.705

Khan, N., and Mukhtar, H. (2010). Cancer and Metastasis: Prevention and Treatment by Green Tea. *Cancer Metastasis Rev.* 29 (3), 435–445. doi:10.1007/s10555-010-9236-1

Kim, B. M., Hong, Y., Lee, S., Liu, P., Lim, J. H., Lee, Y. H., et al. (2015). Therapeutic Implications for Overcoming Radiation Resistance in Cancer Therapy. *Int. J. Mol. Sci.* 16 (11), 26880–26913. doi:10.3390/ijms161125991

Kim, J. A., Kim, Y., Kwon, B. M., and Han, D. C. (2013). The Natural Compound Cantharidin Induces Cancer Cell Death through Inhibition of Heat Shock Protein 70 (HSP70) and Bcl-2-Associated Athanogene Domain 3 (BAG3) Expression by Blocking Heat Shock Factor 1 (HSF1) Binding to Promoters. *J. Biol. Chem.* 288 (40), 28713–28726. doi:10.1074/jbc.M113.488346

Kim, S. H., Kang, J. G., Kim, C. S., Ihm, S. H., Choi, M. G., Yoo, H. J., et al. (2014). The Hsp70 Inhibitor VER155008 Induces Paraptosis Requiring De Novo Protein Synthesis in Anaplastic Thyroid Carcinoma Cells. *Biochem. Biophys. Res. Commun.* 454 (1), 36–41. doi:10.1016/j.bbrc.2014.10.060

Kleibeuker, E. A., Griffioen, A. W., Verheul, H. M., Slotman, B. J., and Thijssen, V. L. (2012). Combining Angiogenesis Inhibition and Radiotherapy: a Double-Edged Sword. *Drug resist. updat.* 15 (3), 173–182. doi:10.1016/j.drup.2012.04.002

Ko, S. K., Kim, J., Na, D. C., Park, S., Park, S. H., Hyun, J. Y., et al. (2015). A Small Molecule Inhibitor of ATPase Activity of HSP70 Induces Apoptosis and Has Antitumor Activities. *Chem. Biol.* 22 (3), 391–403. doi:10.1016/j.chembiol.2015.02.004

Kudryavtsev, V. A., Khokhlova, A. V., Mosina, V. A., Selivanova, E. I., and Kabakov, A. E. (2017). Induction of Hsp70 in Tumor Cells Treated with Inhibitors of the Hsp90 Activity: A Predictive Marker and Promising Target for Radiosensitization. *Plos One*, e0173640. doi:10.1371/journal.pone.0173640

Kumar, S., Stokes, J., 3rd, Singh, U. P., Scissum Gunn, K., Acharya, A., Manne, U., et al. (2016). Targeting Hsp70: A Possible Therapy for Cancer. *Cancer Lett.* 374 (1), 156–166. doi:10.1016/j.canlet.2016.01.056

Laskey, R. A., Honda, B. M., Mills, A. D., and Finch, J. T. (1978). Nucleosomes Are Assembled by an Acidic Protein Which Binds Histones and Transfers Them to DNA. *Nature* 275 (5679), 416–420. doi:10.1038/275416a0

Lee, S. J., Choi, S. A., Lee, K. H., Chung, H. Y., Kim, T. H., Cho, C. K., et al. (2001). Role of Inducible Heat Shock Protein 70 in Radiation-Induced Cell Death. *Cell. Stress Chaperones* 6 (3), 273–281. doi:10.1379/1466-1268(2001)006<0273:roihsp>2.0.co;2

Leu, J. I., Pimkina, J., Frank, A., Murphy, M. E., and George, D. L. (2009). A Small Molecule Inhibitor of Inducible Heat Shock Protein 70. *Mol. Cell.* 36 (1), 15–27. doi:10.1016/j.molcel.2009.09.023

Leu, J. I., Pimkina, J., Pandey, P., Murphy, M. E., and George, D. L. (2011). HSP70 Inhibition by the Small-Molecule 2-phenylethynesulfonamide Impairs Protein Clearance Pathways in Tumor Cells. *Mol. Cancer Res.* 9 (7), 936–947. doi:10.1158/1541-7786.MCR-11-0019

Li, C., Zhang, B., Lv, W., Lai, C., Chen, Z., Wang, R., et al. (2016). Triptolide Inhibits Cell Growth and GRP78 Protein Expression but Induces Cell Apoptosis in Original and Radioresistant NPC Cells. *Oncotarget* 7 (31), 49588–49596. doi:10.18632/oncotarget.10412

Li, M., Wang, J., Jing, J., Hua, H., Luo, T., Xu, L., et al. (2009). Synergistic Promotion of Breast Cancer Cells Death by Targeting Molecular Chaperone GRP78 and Heat Shock Protein 70. *J. Cell. Mol. Med.* 13 (11-12), 4540–4550. doi:10.1111/j.1582-4934.2008.00575.x

Li, X., Colvin, T., Rauch, J. N., Acosta-Alvear, D., Kampmann, M., Dunyak, B., et al. (2015). Validation of the Hsp70-Bag3 Protein-Protein Interaction as a Potential Therapeutic Target in Cancer. *Mol. Cancer Ther.* 14 (3), 642–648. doi:10.1158/1535-7163.Mct-14-0650

Li, X., and Heyer, W. D. (2008). Homologous Recombination in DNA Repair and DNA Damage Tolerance. *Cell. Res.* 18 (1), 99–113. doi:10.1038/cr.2008.1

Li, X., Srinivasan, S. R., Connarn, J., Ahmad, A., Young, Z. T., Kabza, A. M., et al. (2013). Analogues of the Allosteric Heat Shock Protein 70 (Hsp70) Inhibitor, MKT-077, as Anti-cancer Agents. *ACS Med. Chem. Lett.* 4 (11), 1042–1047. doi:10.1021/ml400204n

Li, Y., Wang, Z., Jin, J., Zhu, S. X., He, G. Q., Li, S. H., et al. (2020). Quercetin Pretreatment Enhances the Radiosensitivity of Colon Cancer Cells by Targeting Notch-1 Pathway. *Biochem. Biophys. Res. Commun.* 523 (4), 947–953. doi:10.1016/j.bbrc.2020.01.048

Liang, M., and Fu, J. (2008). Triptolide Inhibits Interferon-Gamma-Induced Programmed Death-1-Ligand 1 Surface Expression in Breast Cancer Cells. *Cancer Lett.* 270 (2), 337–341. doi:10.1016/j.canlet.2008.05.025

Lin, C., Yu, Y., Zhao, H. G., Yang, A., Yan, H., and Cui, Y. (2012). Combination of Quercetin with Radiotherapy Enhances Tumor Radiosensitivity *In Vitro* and *In Vivo*. *Radiother. Oncol.* 104 (3), 395–400. doi:10.1016/j.radonc.2011.10.023

Lin, J. A., Fang, S. U., Su, C. L., Hsiao, C. J., Chang, C. C., Lin, Y. F., et al. (2014). Silencing Glucose-Regulated Protein 78 Induced Renal Cell Carcinoma Cell Line G1 Cell-Cycle Arrest and Resistance to Conventional Chemotherapy. *Urol. Oncol.* 32 (1), e1–11. doi:10.1016/j.urolonc.2012.10.006

Liu, B., Zhang, H., Li, J., Lu, C., Chen, G., Zhang, G., et al. (2013). Triptolide Downregulates Treg Cells and the Level of IL-10, TGF-β, and VEGF in Melanoma-Bearing Mice. *Planta Med.* 79 (15), 1401–1407. doi:10.1055/s-0033-1350708

Mehta, R. K., Pal, S., Kondapi, K., Sitto, M., Dewar, C., Devasia, T., et al. (2020). Low-Dose Hsp90 Inhibitor Selectively Radiosensitizes HNSCC and Pancreatic Xenografts. *Clin. Cancer Res.* 26 (19), 5246–5257. doi:10.1158/1078-0432.Ccr-19-3102

Mendillo, M. L., Santagata, S., Koeva, M., Bell, G. W., Hu, R., Tamimi, R. M., et al. (2012). HSF1 Drives a Transcriptional Program Distinct from Heat Shock to Support Highly Malignant Human Cancers. *Cell.* 150 (3), 549–562. doi:10.1016/j.cell.2012.06.031

Meng, C., Zhu, H., Song, H., Wang, Z., Huang, G., Li, D., et al. (2014). Targets and Molecular Mechanisms of Triptolide in Cancer Therapy. *Chin. J. Cancer Res.* 26 (5), 622–626. doi:10.3978/j.issn.1000-9604.2014.09.01

Mirzayans, R., Scott, A., Cameron, M., and Murray, D. (2005). Induction of Accelerated Senescence by Gamma Radiation in Human Solid Tumor-Derived Cell Lines Expressing Wild-type TP53. *Radiat. Res.* 163 (1), 53–62. doi:10.1667/rr3280

Moradi-Marjaneh, R., Paseban, M., and Moradi Marjaneh, M. (2019). Hsp70 Inhibitors: Implications for the Treatment of Colorectal Cancer. *IUBMB Life* 71 (12), 1834–1845. doi:10.1002/iub.2157

Morgan, M. A., and Lawrence, T. S. (2015). Molecular Pathways: Overcoming Radiation Resistance by Targeting DNA Damage Response Pathways. *Clin. Cancer Res.* 21 (13), 2898–2904. doi:10.1158/1078-0432.Ccr-13-3229

Mortezaee, K., Najafi, M., Farhood, B., Ahmadi, A., Shabeeb, D., and Musa, A. E. (2019). NF-κB Targeting for Overcoming Tumor Resistance and Normal Tissues Toxicity. *J. Cell. Physiol.* 234 (10), 17187–17204. doi:10.1002/jcp.28504

Multhoff, G., Pockley, A. G., Schmid, T. E., and Schilling, D. (2015). The Role of Heat Shock Protein 70 (Hsp70) in Radiation-Induced Immunomodulation. *Cancer Lett.* 368 (2), 179–184. doi:10.1016/j.canlet.2015.02.013

Nadler, S. G., Dischino, D. D., Malacko, A. R., Cleaveland, J. S., Fujihara, S. M., and Marquardt, H. (1998). Identification of a Binding Site on Hsc70 for the Immunosuppressant 15-deoxyspergualin. *Biochem. Biophys. Res. Commun.* 253 (1), 176–180. doi:10.1006/bbrc.1998.9775

Nam, H. Y., Han, M. W., Chang, H. W., Kim, S. Y., and Kim, S. W. (2013). Prolonged Autophagy by MTOR Inhibitor Leads Radioresistant Cancer Cells into Senescence. *Autophagy* 9 (10), 1631–1632. doi:10.4161/auto.25879

Nath, A., Oak, A., Chen, K. Y., Li, I., Splichal, R. C., Portis, J., et al. (2021). Palmitate-Induced IRE1-XBP1-ZEB Signaling Represses Desmoplakin Expression and Promotes Cancer Cell Migration. *Mol. Cancer Res.* 19 (2), 240–248. doi:10.1158/1541-7786.Mcr-19-0480

Naz, S., Leiker, A. J., Choudhuri, R., Preston, O., Sowers, A. L., Gohain, S., et al. (2021). Pharmacological Inhibition of HSP90 Radiosensitizes Head and Neck Squamous Cell Carcinoma Xenograft by Inhibition of DNA Damage Repair, Nucleotide Metabolism, and Radiation-Induced Tumor Vasculogenesis. *Int. J. Radiat. Oncol. Biol. Phys.* 110 (5), 1295–1305. doi:10.1016/j.ijrobp.2021.03.048

Nguyen, C. H., Senfter, D., Basilio, J., Holzner, S., Stadler, S., Krieger, S., et al. (2015). NF-κB Contributes to MMP1 Expression in Breast Cancer Spheroids Causing Paracrine PAR1 Activation and Disintegrations in the Lymph Endothelial Barrier *In Vitro*. *Oncotarget* 6 (36), 39262–39275. doi:10.18632/oncotarget.5741

Nylandsted, J., Gyrd-Hansen, M., Danielewicz, A., Fehrenbacher, N., Lademann, U., Høyer-Hansen, M., et al. (2004). Heat Shock Protein 70 Promotes Cell Survival by Inhibiting Lysosomal Membrane Permeabilization. *J. Exp. Med.* 200 (4), 425–435. doi:10.1084/jem.20040531

Nylandsted, J., Rohde, M., Brand, K., Bastholm, L., Elling, F., and Jäättelä, M. (2000). Selective Depletion of Heat Shock Protein 70 (Hsp70) Activates a Tumor-specific Death Program that Is Independent of Caspases and Bypasses Bcl-2. *Proc. Natl. Acad. Sci. U. S. A.* 97 (14), 7871–7876. doi:10.1073/pnas.97.14.7871

Odegaard, E., Yang, C. R., and Boothman, D. A. (1998). DNA-Dependent Protein Kinase Does Not Play a Role in Adaptive Survival Responses to Ionizing Radiation. *Environ. Health Perspect.* 106, 301–305. doi:10.1289/ehp.98106s1301

Orthwein, A., Noordermeer, S. M., Wilson, M. D., Landry, S., Enchev, R. I., Sherker, A., et al. (2015). A Mechanism for the Suppression of Homologous Recombination in G1 Cells. *Nature* 528 (7582), 422–426. doi:10.1038/nature16142

Özsoy, S., Becer, E., Kabadayı, H., Vatansever, H. S., and Yücecan, S. (2020). Quercetin-Mediated Apoptosis and Cellular Senescence in Human Colon Cancer. *Anticancer. Agents Med. Chem.* 20 (11), 1387–1396. doi:10.2174/1871520620666200408082026

Pan, H., Song, T., Wang, Z. Q., Guo, Y. F., Zhang, H., Ji, T., et al. (2021). Ectopic BH3-Only Protein Bim Acts as a Cochaperone to Positively Regulate Hsp70 in Yeast. *J. Biochem.* 170 (4), 539–545. doi:10.1093/jb/mvab073

Pang, Q., Christianson, T. A., Keeble, W., Koretsky, T., and Bagby, G. C. (2002). The Anti-apoptotic Function of Hsp70 in the Interferon-Inducible Double-Stranded RNA-dependent Protein Kinase-Mediated Death Signaling Pathway Requires the Fanconi Anemia Protein, FANCC. *J. Biol. Chem.* 277 (51), 49638–49643. doi:10.1074/jbc.M209386200

Panganiban, R. A., Snow, A. L., and Day, R. M. (2013). Mechanisms of Radiation Toxicity in Transformed and Non-transformed Cells. *Int. J. Mol. Sci.* 14 (8), 15931–15958. doi:10.3390/ijms140815931

Park, S. H., Baek, K. H., Shin, I., and Shin, I. (2018). Subcellular Hsp70 Inhibitors Promote Cancer Cell Death via Different Mechanisms. *Cell. Chem. Biol.* 25 (10), 1242–1254. doi:10.1016/j.chembiol.2018.06.010

Park, S. H., Kim, W. J., Li, H., Seo, W., Park, S. H., Kim, H., et al. (2017). Anti-leukemia Activity of a Hsp70 Inhibitor and its Hybrid Molecules. *Sci. Rep.* 7 (1), 3537. doi:10.1038/s41598-017-03814-6

Powers, M. V., Clarke, P. A., and Workman, P. (2008). Dual Targeting of HSC70 and HSP72 Inhibits HSP90 Function and Induces Tumor-specific Apoptosis. *Cancer Cell.* 14 (3), 250–262. doi:10.1016/j.ccr.2008.08.002

Ramya, T. N., Surolia, N., and Surolia, A. (2006). 15-Deoxyspergualin Modulates Plasmodium Falciparum Heat Shock Protein Function. *Biochem. Biophys. Res. Commun.* 348 (2), 585–592. doi:10.1016/j.bbrc.2006.07.082

Ritossa, F. (1962). A New Puffing Pattern Induced by Temperature Shock and DNP in drosophila. *Experientia* 18 (12), 571–573. doi:10.1007/BF02172188

Rodina, A., Patel, P. D., Kang, Y., Patel, Y., Baaklini, I., Wong, M. J., et al. (2013). Identification of an Allosteric Pocket on Human Hsp70 Reveals a Mode of Inhibition of This Therapeutically Important Protein. *Chem. Biol.* 20 (12), 1469–1480. doi:10.1016/j.chembiol.2013.10.008

Rohde, M., Daugaard, M., Jensen, M. H., Helin, K., Nylandsted, J., and Jäättelä, M. (2005). Members of the Heat-Shock Protein 70 Family Promote Cancer Cell Growth by Distinct Mechanisms. *Genes. Dev.* 19 (5), 570–582. doi:10.1101/gad.305405

Rousaki, A., Miyata, Y., Jinwal, U. K., Dickey, C. A., Gestwicki, J. E., and Zuiderweg, E. R. (2011). Allosteric Drugs: the Interaction of Antitumor Compound MKT-077 with Human Hsp70 Chaperones. *J. Mol. Biol.* 411 (3), 614–632. doi:10.1016/j.jmb.2011.06.003

Rüdiger, S., Germeroth, L., Schneider-Mergener, J., and Bukau, B. (1997). Substrate Specificity of the DnaK Chaperone Determined by Screening Cellulose-Bound Peptide Libraries. *Embo J.* 16 (7), 1501–1507. doi:10.1093/emboj/16.7.1501

Sakai, K., Inoue, M., Mikami, S., Nishimura, H., Kuwabara, Y., Kojima, A., et al. (2021). Functional Inhibition of Heat Shock Protein 70 by VER-155008 Suppresses Pleural Mesothelioma Cell Proliferation via an Autophagy Mechanism. *Thorac. Cancer* 12 (4), 491–503. doi:10.1111/1759-7714.13784

Saleh, A., Srinivasula, S. M., Balkir, L., Robbins, P. D., and Alnemri, E. S. (2000). Negative Regulation of the Apaf-1 Apoptosome by Hsp70. *Nat. Cell. Biol.* 2 (8), 476–483. doi:10.1038/35019510

Samanta, S., Yang, S., Debnath, B., Xue, D., Kuang, Y., Ramkumar, K., et al. (2021). The Hydroxyquinoline Analogue YUM70 Inhibits GRP78 to Induce ER Stress-Mediated Apoptosis in Pancreatic Cancer. *Cancer Res.* 81 (7), 1883–1895. doi:10.1158/0008-5472.Can-20-1540

Santagata, S., Hu, R., Lin, N. U., Mendillo, M. L., Collins, L. C., Hankinson, S. E., et al. (2011). High Levels of Nuclear Heat-Shock Factor 1 (HSF1) Are Associated with Poor Prognosis in Breast Cancer. *Proc. Natl. Acad. Sci. U. S. A.* 108 (45), 18378–18383. doi:10.1073/pnas.1115031108

Schaue, D., and McBride, W. H. (2005). Counteracting Tumor Radioresistance by Targeting DNA Repair. *Mol. Cancer Ther.* 4 (10), 1548–1550. doi:10.1158/1535-7163.Mct-05-co1

Schilling, D., Garrido, C., Combs, S. E., and Multhoff, G. (2017). The Hsp70 Inhibiting Peptide Aptamer A17 Potentiates Radiosensitization of Tumor Cells by Hsp90 Inhibition. *Cancer Lett.* 390, 146–152. doi:10.1016/j.canlet.2017.01.015

Schilling, D., Kuhnel, A., Konrad, S., Tetzlaff, F., Bayer, C., Yaglom, J., et al. (2015). Sensitizing Tumor Cells to Radiation by Targeting the Heat Shock Response. *Cancer Lett.* 360 (2), 294–301. doi:10.1016/j.canlet.2015.02.033

Schlecht, R., Scholz, S. R., Dahmen, H., Wegener, A., Sirrenberg, C., Musil, D., et al. (2013). Functional Analysis of Hsp70 Inhibitors. *PLoS One* 8 (11), e78443. doi:10.1371/journal.pone.0078443

Scully, R., Panday, A., Elango, R., and Willis, N. A. (2019). DNA Double-Strand Break Repair-Pathway Choice in Somatic Mammalian Cells. *Nat. Rev. Mol. Cell. Biol.* 20 (11), 698–714. doi:10.1038/s41580-019-0152-0

Sheppard, P. W., Sun, X., Khammash, M., and Giffard, R. G. (2014). Overexpression of Heat Shock Protein 72 Attenuates NF-Kb Activation Using a Combination of Regulatory Mechanisms in Microglia. *PLoS Comput. Biol.* 10 (2), e1003471. doi:10.1371/journal.pcbi.1003471

Sherman, M. Y., and Gabai, V. L. (2015). Hsp70 in Cancer: Back to the Future. *Oncogene* 34 (32), 4153–4161. doi:10.1038/onc.2014.349

Shi, H., Li, X. Y., Chen, Y., Zhang, X., Wu, Y., Wang, Z. X., et al. (2020). Quercetin Induces Apoptosis via Downregulation of Vascular Endothelial Growth Factor/Akt Signaling Pathway in Acute Myeloid Leukemia Cells. *Front. Pharmacol.* 11, 534171. doi:10.3389/fphar.2020.534171

Shu, M., Li, C., Zhong, C., Huang, T., Wang, X., Tan, Y., et al. (2021). Effects of Triptolide on Radiosensitivity of Human Glioma Cells and its Mechanism. *J. buon* 26 (4), 1549–1555.

Sinclair, W. K., and Morton, R. A. (1966). X-Ray Sensitivity during the Cell Generation Cycle of Cultured Chinese Hamster Cells. *Radiat. Res.* 29 (3), 450–474. doi:10.2307/3572025

Song, M., Bode, A. M., Dong, Z., and Lee, M. H. (2019). AKT as a Therapeutic Target for Cancer. *Cancer Res.* 79 (6), 1019–1031. doi:10.1158/0008-5472.Can-18-2738

Song, T., Guo, Y., Xue, Z., Guo, Z., Wang, Z., Lin, D., et al. (2021). Small-molecule Inhibitor Targeting the Hsp70-Bim Protein-Protein Interaction in CML Cells Overcomes BCR-ABL-independent TKI Resistance. *Leukemia* 35 (10), 2862–2874. doi:10.1038/s41375-021-01283-5

Spiegelberg, D., Abramenkovs, A., Mortensen, A. C. L., Lundsten, S., Nestor, M., and Stenerlow, B. (2020). The HSP90 Inhibitor Onalespib Exerts Synergistic Anti-cancer Effects when Combined with Radiotherapy: an *In Vitro* and *In Vivo* Approach. *Sci. Rep.*, 5923. doi:10.1038/s41598-020-62293-4

Sun, C., Han, C., Jiang, Y., Han, N., Zhang, M., Li, G., et al. (2017). Inhibition of GRP78 Abrogates Radioresistance in Oropharyngeal Carcinoma Cells after EGFR Inhibition by Cetuximab. *PLoS One* 12 (12), e0188932. doi:10.1371/journal.pone.0188932

Takakuwa, J. E., NitikaKnighton, L. E., and Truman, A. W. (2019). Oligomerization of Hsp70: Current Perspectives on Regulation and Function. *Front. Mol. Biosci.*, 81. doi:10.3389/fmolb.2019.00081

Takata, M., Sasaki, M. S., Sonoda, E., Morrison, C., Hashimoto, M., Utsumi, H., et al. (1998). Homologous Recombination and Non-homologous End-Joining Pathways of DNA Double-Strand Break Repair Have Overlapping Roles in the Maintenance of Chromosomal Integrity in Vertebrate Cells. *Embo J.* 17 (18), 5497–5508. doi:10.1093/emboj/17.18.5497

Tambini, C. E., Spink, K. G., Ross, C. J., Hill, M. A., and Thacker, J. (2010). The Importance of XRCC2 in RAD51-Related DNA Damage Repair. *DNA Repair (Amst)* 9 (5), 517–525. doi:10.1016/j.dnarep.2010.01.016

Tamgue, O., and Lei, M. (2017). Triptolide Promotes Senescence of Prostate Cancer Cells through Histone Methylation and Heterochromatin Formation. *Asian pac. J. Cancer Prev.* 18 (9), 2519–2526. doi:10.22034/apjcp.2017.18.9.2519

Tanaka, A., and Sakaguchi, S. (2017). Regulatory T Cells in Cancer Immunotherapy. *Cell. Res.* 27 (1), 109–118. doi:10.1038/cr.2016.151

Tang, S. M., Deng, X. T., Zhou, J., Li, Q. P., Ge, X. X., and Miao, L. (2020). Pharmacological Basis and New Insights of Quercetin Action in Respect to its Anti-cancer Effects. *Biomed. Pharmacother.* 121, 109604. doi:10.1016/j.biopha.2019.109604

Terasima, T., and Tolmach, L. J. (1961). Changes in X-Ray Sensitivity of HeLa Cells during the Division Cycle. *Nature* 190, 1210–1211. doi:10.1038/1901210a0

Tran, P. L., Kim, S. A., Choi, H. S., Yoon, J. H., and Ahn, S. G. (2010). Epigallocatechin-3-gallate Suppresses the Expression of HSP70 and HSP90 and Exhibits Anti-tumor Activity *In Vitro* and *In Vivo*. *BMC Cancer* 10, 276. doi:10.1186/1471-2407-10-276

van Rijn, J., and van den Berg, J. (1997). Flavonoids as Enhancers of X-Ray-Induced Cell Damage in Hepatoma Cells. *Clin. Cancer Res.* 3 (10), 1775–1779.

Vostakolaei, M. A., Hatami-Baroogh, L., Babaei, G., Molavi, O., Kordi, S., and Abdolalizadeh, J. (2021). Hsp70 in Cancer: A Double Agent in the Battle between Survival and Death. *J. Cell.Physiol.* 236 (5), 3420–3444. doi:10.1002/jcp.30132

Wadhwa, R., Sugihara, T., Yoshida, A., Nomura, H., Reddel, R. R., Simpson, R., et al. (2000). Selective Toxicity of MKT-077 to Cancer Cells Is Mediated by its Binding to the Hsp70 Family Protein Mot-2 and Reactivation of P53 Function. *Cancer Res.* 60 (24), 6818–6821.

Wang, G., Cao, P., Fan, Y., and Tan, K. (2020). Emerging Roles of HSF1 in Cancer: Cellular and Molecular Episodes. *Biochim. Biophys. Acta. Rev. Cancer* 1874 (1), 188390. doi:10.1016/j.bbcan.2020.188390

Wang, H., Song, Y., Hao, D., Bai, M., Jin, L., Gu, J., et al. (2014). Ultrasound-targeted Microbubble Destruction Combined with Dual Targeting of HSP72 and HSC70 Inhibits HSP90 Function and Induces Extensive Tumor-Specific Apoptosis. *Int. J. Oncol.* 45 (1), 157–164. doi:10.3892/ijo.2014.2388

Wang, Q., Chen, Y., Lu, H., Wang, H., Feng, H., Xu, J., et al. (2020). Quercetin Radiosensitizes Non-small Cell Lung Cancer Cells through the Regulation of miR-16-5p/WEE1 axis. *IUBMB Life* 72 (5), 1012–1022. doi:10.1002/iub.2242

Wang, R. E., Kao, J. L., Hilliard, C. A., Pandita, R. K., Roti Roti, J. L., Hunt, C. R., et al. (2009). Inhibition of Heat Shock Induction of Heat Shock Protein 70 and Enhancement of Heat Shock Protein 27 Phosphorylation by Quercetin Derivatives. *J. Med. Chem.* 52 (7), 1912–1921. doi:10.1021/jm801445c

Wang, Z., Song, T., Guo, Z., Uwituze, L. B., Guo, Y., Zhang, H., et al. (2021). A Novel Hsp70 Inhibitor Specifically Targeting the Cancer-Related Hsp70-Bim Protein-Protein Interaction. *Eur. J. Med. Chem.* 220, 113452. doi:10.1016/j.ejmech.2021.113452

Wen, W., Liu, W., Shao, Y., and Chen, L. (2014). VER-155008, a Small Molecule Inhibitor of HSP70 with Potent Anti-cancer Activity on Lung Cancer Cell Lines. *Exp. Biol. Med.* 239 (5), 638–645. doi:10.1177/1535370214527899

Westerheide, S. D., Kawahara, T. L., Orton, K., and Morimoto, R. I. (2006). Triptolide, an Inhibitor of the Human Heat Shock Response that Enhances Stress-Induced Cell Death. *J. Biol. Chem.* 281 (14), 9616–9622. doi:10.1074/jbc.M512044200

Westerheide, S. D., and Morimoto, R. I. (2005). Heat Shock Response Modulators as Therapeutic Tools for Diseases of Protein Conformation. *J. Biol. Chem.* 280 (39), 33097–33100. doi:10.1074/jbc.R500010200

Willers, H., Gheorghiu, L., Liu, Q., Efstathiou, J. A., Wirth, L. J., Krause, M., et al. (2015). DNA Damage Response Assessments in Human Tumor Samples Provide Functional Biomarkers of Radiosensitivity. *Semin. Radiat. Oncol.* 25 (4), 237–250. doi:10.1016/j.semradonc.2015.05.007

Williamson, D. S., Borgognoni, J., Clay, A., Daniels, Z., Dokurno, P., Drysdale, M. J., et al. (2009). Novel Adenosine-Derived Inhibitors of 70 kDa Heat Shock Protein, Discovered through Structure-Based Design. *J. Med. Chem.* 52 (6), 1510–1513. doi:10.1021/jm801627a

Wyszkowski, H., Janta, A., Sztangierska, W., Obuchowski, I., Chamera, T., Kłosowska, A., et al. (2021). Class-specific Interactions between Sis1 J-Domain Protein and Hsp70 Chaperone Potentiate Disaggregation of Misfolded Proteins. *Proc. Natl. Acad. Sci. U. S. A.* (49), e2108163118. doi:10.1073/pnas.2108163118

Xu, H., Zhao, H., Lu, C., Qiu, Q., Wang, G., Huang, J., et al. (2016). Triptolide Inhibits Osteoclast Differentiation and Bone Resorption *In Vitro* via Enhancing the Production of IL-10 and TGF-B1 by Regulatory T Cells. *Mediat. Inflamm.* 2016, 8048170. doi:10.1155/2016/8048170

Xu, J., Wang, K., Zhang, X., Qiu, Y., Huang, D., Li, W., et al. (2010). HSP70: a Promising Target for Laryngeal Carcinoma Radiaotherapy by Inhibiting Cleavage and Degradation of Nucleolin. *J. Exp. Clin. Cancer Res.* 29, 106. doi:10.1186/1756-9966-29-106

Yaglom, J. A., Wang, Y., Li, A., Li, Z., Monti, S., Alexandrov, I., et al. (2018). Cancer Cell Responses to Hsp70 Inhibitor JG-98: Comparison with Hsp90 Inhibitors and Finding Synergistic Drug Combinations. *Sci. Rep.* 8 (1), 3010. doi:10.1038/s41598-017-14900-0

Yang, J., Xu, Y., Yan, Y., Li, W., Zhao, L., Dai, Q., et al. (2020). Small Molecule Inhibitor of ATPase Activity of HSP70 as a Broad-Spectrum Inhibitor against Flavivirus Infections. *ACS Infect. Dis.* 6 (5), 832–843. doi:10.1021/acsinfecdis.9b00376

Yang, Y., Luo, J., Chen, X., Yang, Z., Mei, X., Ma, J., et al. (2020). CDK4/6 Inhibitors: a Novel Strategy for Tumor Radiosensitization. *J. Exp. Clin. Cancer Res.* 39 (1), 188. doi:10.1186/s13046-020-01693-w

Yang, Z., Zhuang, L., Szatmary, P., Wen, L., Sun, H., Lu, Y., et al. (2015). Upregulation of Heat Shock Proteins (HSPA12A, HSP90B1, HSPA4, HSPA5 and HSPA6) in Tumour Tissues Is Associated with Poor Outcomes from HBV-Related Early-Stage Hepatocellular Carcinoma. *Int. J. Med. Sci.* 12 (3), 256–263. doi:10.7150/ijms.10735

Yoon, Y. J., Kim, J. A., Shin, K. D., Shin, D. S., Han, Y. M., Lee, Y. J., et al. (2011). KRIBB11 Inhibits HSP70 Synthesis through Inhibition of Heat Shock Factor 1 Function by Impairing the Recruitment of Positive Transcription Elongation Factor B to the Hsp70 Promoter. *J. Biol. Chem.* 286 (3), 1737–1747. doi:10.1074/jbc.M110.179440

Zamin, L. L., Filippi-Chiela, E. C., Dillenburg-Pilla, P., Horn, F., Salbego, C., and Lenz, G. (2009). Resveratrol and Quercetin Cooperate to Induce Senescence-like Growth Arrest in C6 Rat Glioma Cells. *Cancer Sci.* 100 (9), 1655–1662. doi:10.1111/j.1349-7006.2009.01215.x

Zhang, G., Liu, Y., Guo, H., Sun, Z., and Zhou, Y. H. (2009). Triptolide Promotes Generation of FoxP3+ T Regulatory Cells in Rats. *J. Ethnopharmacol.* 125 (1), 41–46. doi:10.1016/j.jep.2009.06.020

Zhang, G., Wang, Y., Zhang, Y., Wan, X., Li, J., Liu, K., et al. (2012). Anti-cancer Activities of Tea Epigallocatechin-3-Gallate in Breast Cancer Patients under Radiotherapy. *Curr. Mol. Med.* 12 (2), 163–176. doi:10.2174/156652412798889063

Zhang, H., Chung, D., Yang, Y. C., Neely, L., Tsurumoto, S., Fan, J., et al. (2006). Identification of New Biomarkers for Clinical Trials of Hsp90 Inhibitors. *Mol. Cancer Ther.* 5 (5), 1256–1264. doi:10.1158/1535-7163.Mct-05-0537

Zhang, H., Song, T., Wang, Z., Laura Bonnette, U., Guo, Y., Wang, H., et al. (2022). Bcr-Abl Drives the Formation of Hsp70/Bim PPI to Stabilize Oncogenic Clients and Prevent Cells from Undergoing Apoptosis. *Biochem. Pharmacol.* 198, 114964. doi:10.1016/j.bcp.2022.114964

Zhao, X., Wei, C., Li, J., Xing, P., Li, J., Zheng, S., et al. (2017). Cell Cycle-dependent Control of Homologous Recombination. *Acta Biochim. Biophys. Sin.* 49 (8), 655–668. doi:10.1093/abbs/gmx055

Zhou, Y., Ma, J., Zhang, J., He, L., Gong, J., and Long, C. (2017). Pifithrin-mu Is Efficacious against Non-small Cell Lung Cancer via Inhibition of Heat Shock Protein 70. *Oncol. Rep.* 37 (1), 313–322. doi:10.3892/or.2016.5286

Zhou, Z., Li, Y., Jia, Q., Wang, Z., Wang, X., Hu, J., et al. (2017). Heat Shock Transcription Factor 1 Promotes the Proliferation, Migration and Invasion of Osteosarcoma Cells. *Cell. Prolif.* 50 (4), e12346. doi:10.1111/cpr.12346

frontiers | Frontiers in Oncology

TYPE Review
PUBLISHED 12 August 2022
DOI 10.3389/fonc.2022.971462

Check for updates

OPEN ACCESS

EDITED BY
Zhe-Sheng Chen,
St. John's University, United States

REVIEWED BY
Bin Huang,
Shandong University, China
Xing Guo,
Shandong University, China

*CORRESPONDENCE
Fuyi Liu,
liufuyi@zju.edu.cn

SPECIALTY SECTION
This article was submitted to Molecular and Cellular Oncology, a section of the journal Frontiers in Oncology

RECEIVED 22 June 2022
ACCEPTED 25 July 2022
PUBLISHED 12 August 2022

CITATION
Fu Z, Zhu G, Luo C, Chen Z, Dou Z, Chen Y, Zhong C, Su S and Liu F (2022) Matricellular protein tenascin C: Implications in glioma progression, gliomagenesis, and treatment. *Front. Oncol.* 12:971462. doi: 10.3389/fonc.2022.971462

COPYRIGHT
© 2022 Fu, Zhu, Luo, Chen, Dou, Chen, Zhong, Su and Liu. This is an open-access article distributed under the terms of the Creative Commons Attribution License (CC BY). The use, distribution or reproduction in other forums is permitted, provided the original author(s) and the copyright owner(s) are credited and that the original publication in this journal is cited, in accordance with accepted academic practice. No use, distribution or reproduction is permitted which does not comply with these terms.

Matricellular protein tenascin C: Implications in glioma progression, gliomagenesis, and treatment

Zaixiang Fu[1], Ganggui Zhu[2], Chao Luo[3], Zihang Chen[1], Zhangqi Dou[1], Yike Chen[1], Chen Zhong[1], Sheng Su[4] and Fuyi Liu[1]*

[1]Department of Neurosurgery, Second Affiliated Hospital, School of Medicine, Zhejiang University, Hangzhou, China, [2]Department of Neurosurgery, Hangzhou First People's Hospital, School of Medicine, Zhejiang University, Hangzhou, China, [3]Department of Neurosurgery, The Affiliated Hospital of Kunming University of Science and Technology, Kunming, China, [4]Department of Neurosurgery, The Fourth Affiliated Hospital, School of Medicine, Zhejiang University, Yiwu, China

Matricellular proteins are nonstructural extracellular matrix components that are expressed at low levels in normal adult tissues and are upregulated during development or under pathological conditions. Tenascin C (TNC), a matricellular protein, is a hexameric and multimodular glycoprotein with different molecular forms that is produced by alternative splicing and post-translational modifications. Malignant gliomas are the most common and aggressive primary brain cancer of the central nervous system. Despite continued advances in multimodal therapy, the prognosis of gliomas remains poor. The main reasons for such poor outcomes are the heterogeneity and adaptability caused by the tumor microenvironment and glioma stem cells. It has been shown that TNC is present in the glioma microenvironment and glioma stem cell niches, and that it promotes malignant properties, such as neovascularization, proliferation, invasiveness, and immunomodulation. TNC is abundantly expressed in neural stem cell niches and plays a role in neurogenesis. Notably, there is increasing evidence showing that neural stem cells in the subventricular zone may be the cells of origin of gliomas. Here, we review the evidence regarding the role of TNC in glioma progression, propose a potential association between TNC and gliomagenesis, and summarize its clinical applications. Collectively, TNC is an appealing focus for advancing our understanding of gliomas.

KEYWORDS

matricellular protein, tenascin C, glioma progression, neurogenesis, gliomagenesis, clinical significance

Introduction

The extracellular matrix (ECM) is a dynamic and complex meshwork consisting of various multidomain macromolecules that are continually synthesized and secreted by surrounding cells. Many ECM molecules, the basic structural proteins, provide a three-dimensional structural framework that ensures cell cohesion and facilitates formation of tissues and organs (1, 2). In addition to structural matrix molecules, such as collagen and laminin, various non-structural proteins are present in the ECM in specific situations. These secreted nonstructural ECM components, called matricellular proteins (MCPs), are rapidly turned over, rather than remaining as stable structural elements (2, 3). MCPs present in the brain ECM include tenascin C (TNC), thrombospondins (TSPs), secreted protein acidic and rich in cysteine family (SPARC) proteins, and periostin (3). They are characterized by low expression levels in healthy adult tissues, but have high expression levels during development and are promptly upregulated under pathological conditions. By binding to other matrix proteins, specific cell surface receptors, such as integrins, and soluble extracellular factors, including cytokines, growth factors, and proteases, MCPs can directly or indirectly modulate cellular morphology, regulate several cellular processes, such as proliferation, differentiation, migration, apoptosis, and survival, and induce tissue remodeling (3–5). TNC, as an MCP, is highly expressed in most solid cancers of the ECM. This has been associated with poor prognosis and is involved in many malignant biological behaviors (6, 7). In addition, TNC is present in several stem cell niches (8, 9), including neural stem cells (NSCs) and glioma stem cells (GSCs) (10–12). Therefore, understanding the role of TNC in cancers and stem cells can contribute to the development of new therapeutic avenues.

Gliomas, the most common primary intracranial tumors in adults, are grouped into four classes (grades I–IV), based on histological characteristics (13). The mean annual incidence is approximately six per 100,000 people worldwide (14). Although some advances in diagnosis and treatment have been made, the prognosis of patients with gliomas remains poor. In particular, for glioblastoma (GBM), the median survival time is approximately 15 months and the 5-year survival rate is only 5.8% (15–17). The standard regimen for primary GBM includes maximal surgical resection, followed by chemotherapy with temozolomide and radiation therapy, which is referred to as the STUPP protocol (18). Recently, many novel therapeutic options, such as immunotherapy (19, 20), targeted therapy (21, 22), and tumor-treating fields (TTFields) (23, 24) have been proposed, but the efficacy of these protocols is unsatisfactory (16). The main reasons for the poor outcomes of GBM patients are the disease's heterogeneity and adaptability, which lead to resistance to treatment and tumor recurrence. The tumor microenvironment (TME) and cancer stem cells (CSCs) may account for the dynamic and heterogeneous characteristics of GBM (25, 26). Recently, substantial evidence has shown pleiotropic and important roles for TNC in the glioma TME (27, 28), as well as in NSC and GSC niches (10–12). Interestingly, many researchers have reported that GSCs may be derived from NSCs in the adult brain subventricular zone (SVZ) (29–31).

Here, in light of its potential significance, we review the matricellular protein TNC in the glioma ECM, and highlight the implications of TNC in glioma progression, tumorigenesis, and treatment.

Structure of tenascin C

TNC, a member of the tenascin family, was first identified in the 1980s. Other members of this family include tenascin-W, tenascin-X, and tenascin-R. Since the discovery of TNC independently and concurrently in several different laboratories, it is known under various names, such as glial/mesenchymal extracellular matrix protein (GMEM) (32), myotendinous antigen (33, 34), cytotactin (35), J1 220/200 (36), neuronectin (37), and hexabrachion (38). The TNC glycoprotein consists of six identical monomers that are disulfide-linked into a hexamer at their N-termini (38, 39). Each subunit is approximately 180–400 kDa in humans and is composed of four different parts (Figure 1): an N-terminal cysteine-rich domain with highly conserved heptad repeats, 14.5 epidermal growth factor (EGF)-like repeats, eight constitutively expressed fibronectin type III (FNIII) domains, and a fibrinogen-like globe (FBG) at the C-terminus (28, 40, 41). Nine

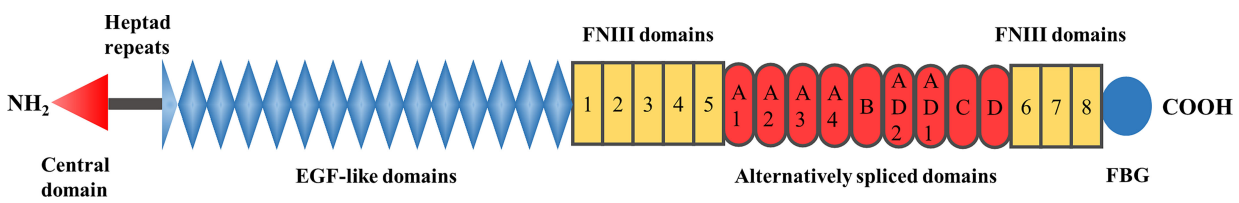

FIGURE 1
Schematic illustration of the domain structure of TNC.

alternatively spliced domains (A1–A4, B, AD2, AD1, C, and D) are inserted between the 5th and 6th FNIII domain in the human gene (42), which can theoretically give rise to 512 possible TNC splice isoforms (43, 44). However, the number of alternatively spliced domains varies among species, with chickens, mice, and rats having six, six, and seven domains, respectively (43, 45, 46). These alternatively spliced repeats with unique interaction sites may not only offer novel binding abilities or susceptibilities to proteolytic cleavage, but may also disrupt the existing binding sites, resulting in the acquisition or loss of certain functions (43). In addition, post-translational modifications, such as glycosylation and citrullination, assembly into a fibrillar matrix, and proteolytic processing, further increase the complexity of the TNC structure and function by exposing hidden binding sites, covering exposed binding sites, or generating smaller soluble fragments (6, 43, 44). For example, glycosylated TNC is likely to regulate proliferation of NSCs (47), and the fragmented EGF-like domain has proapoptotic activity in smooth muscle cells, in contrast to intact TNC (48).

Expression and regulation of tenascin C

TNC is a regulatory glycoprotein that exhibits different spatial and temporal distribution patterns throughout life. In general, during embryogenesis, TNC is highly expressed in neural ectodermal tissues and in some non-neural sites where high cell turnover, tissue remodeling, and epithelial–mesenchymal interactions occur (41, 43). In the embryonic developmental stage and shortly after birth, the expression level of TNC peaks and then decreases significantly with increasing age (49). In fact, this molecule is considered to be mainly secreted by immature and reactive astrocytes, radial glial progenitor cells, and oligodendrocyte precursor cells (OPCs) in the developing central nervous system (CNS) (50–52). In contrast, in the normal adult CNS, it is sparsely expressed and is confined to NSC niches, such as the SVZ and the hippocampus, where it is produced by astrocytes (53) and granule cells (54), respectively, as well as to the cerebellum, where it is produced by Golgi epithelial cells (55). However, TNC is actively re-expressed in the adult CNS in response to pathological conditions, including neuroinflammation (56), neurodegeneration (57, 58), trauma (59, 60), and tumorigenesis (27, 28, 61). For example, many experimental studies have indicated that TNC is expressed in the brain parenchyma (astrocytes, neurons, and brain capillary endothelial cells) and the walls of cerebral arteries (endothelial, smooth muscle, adventitial, and periarterial inflammatory cells) between 24 and 72 h after post-subarachnoid hemorrhage (SAH) (62, 63). As a key regulator of neuroinflammation, TNC is involved in early brain injury, including blood–brain barrier destruction (64), neuronal apoptosis (65), cerebral vasospasm (66), delayed cerebral ischemia (67), and chronic hydrocephalus (56, 62, 68). In addition, Xie et al. (69) reported that TNC plays a role in chronic neuroinflammation in Alzheimer's disease, and that its deficiency could produce an anti-inflammatory pattern and reduce cerebral amyloid β load. More importantly, numerous studies have reported increased levels of TNC in multiple malignant solid tumors, with the highest concentrations found in gliomas (7, 27, 70). TNC expression is correlated with glioma grade, poor patient survival, and disease progression (71, 72).

In humans, *TNC* is located on chromosome 9q32–q34 (73). Upstream of its transcription start site, there is a region with high promoter activity that contains a TATA box (44, 74). Various specific transcription factors, intracellular regulators, and stimuli, including cytokines, growth factors, reactive oxygen species, hypoxia, and mechanical stress, can control *TNC* expression by directly or indirectly regulating the *TNC* promoter (74). For instance, homeobox even-skipped homolog protein-1 (Evx-1) stimulates *TNC* promoter activity by synergizing with transcription factors FOS and/or JUN, which target the AP1 site (75). Another homeobox transcription factor, orthodenticle homolog 2 (OTX2), binds to the *TNC* promoter with high affinity and represses the gene transcription (76). In addition, cyclic tensile strain has been shown to induce mRNA encoding TNC in fibroblasts in β1-integrin-mediated RHO/ROCK signaling (77, 78) and nuclear translocation of the transcriptional regulator megakaryocytic leukemia-1 (MKL-1) (79). After CNS injury, activated microglia and macrophages secrete basic fibroblast growth factor (bFGF) and transforming growth factor-β1 (TGF-β1), which can induce an increase in astrocyte tenascin production (80). Moreover, TNC was also considered a target gene of the transcription factor SOX4, which is overexpressed in many human malignancies, including glioma (81, 82).

Fibroblasts are a major source of the TNC deposited in the solid tumor stroma of the peripheral system, whereas tumor cells themselves rarely express TNC (70). Nevertheless, in gliomas, TNC is expressed by malignant tumor cells (83). The NOTCH signaling pathway plays a critical role in the regulation of TNC expression (Figure 2) (84). NOTCH is a large transmembrane receptor of the cell-binding ligands delta and jagged. After activation, ligand-dependent cleavage allows the release of its intracellular domain, which translocates to the nucleus and affects NOTCH-dependent transcription by binding to RBPJκ/CSL (85). A GBM tissue microarray revealed a significant association between RBPJκ and TNC levels, with the former being a NOTCH2 transcription co-factor (84). Additionally, the human *TNC* promoter contains an RBPJκ-responsive element (84). Sivasankaran et al. (84) proposed a mechanism for NOTCH/RBPJκ-mediated transactivation of *TNC* in GBM, consistent with the report by Ma et al. (86), in which TNC is upregulated in CD47-loss-of-function cells *via* a NOTCH-mediated mechanism. On the other hand, Sarkar et al. (87). found that TNC is a pivotal initiator of enhanced NOTCH signaling and promotes GSC growth through the TNC–α2β1–JAG1–NOTCH signaling axis. In breast cancer cells, Oskarsson

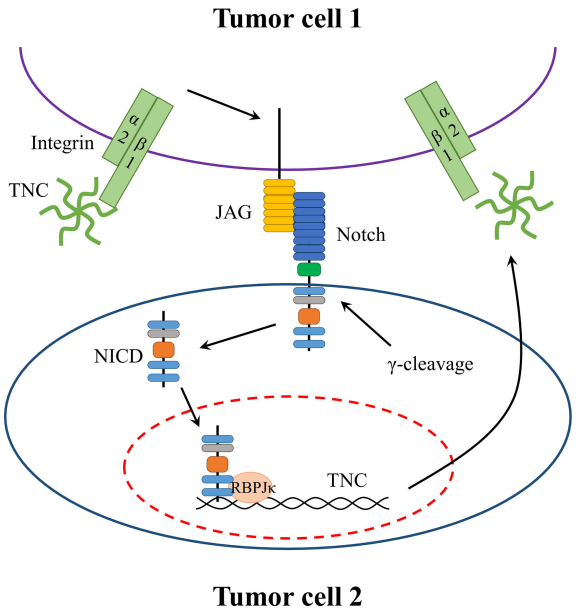

FIGURE 2
Potential positive feedback mechanism in gliomas between TNC expression and NOTCH pathway. TNC binds to integrin α2β1 on the glioma cell and upregulates JAG1 expression which interacts with its receptor NOTCH. The interaction results in the release of intracellular domain that translocates to the nucleus to affect NOTCH-dependent transcription by binding to RBPJκ. Moreover, the human TNC promoter contains an RBPJκ-responsive element. Thus, the activation of NOTCH signaling increases TNC expression.

et al. (88) reported that TNC accumulation enhanced the performance and function of the NOTCH pathway, which is vital for the adaptation of metastasis-initiating breast cancer cells. Taken together, evidence suggests that there may be positive feedback between TNC expression and the NOTCH pathway that ultimately increases the malignant biological behavior of gliomas.

Interaction partners and receptors of tenascin C

As mentioned above, TNC is a hexameric extracellular glycoprotein and each monomer consists of four different domains. This highly complex structure gives TNC the capacity to interact with various binding partners or ligands, such as other ECM components, cell surface receptors, and soluble factors, which affect distinct signaling pathways (28, 44, 70, 89). The first and most studied ECM component that interacts with TNC is fibronectin (89), whose binding sites involve FNIII repeats (90, 91). Additionally, TNC can bind to other ECM proteins, such as periostin (92), perlecan (93), fibrillin-2 (94), aggrecan (95), and SPARC-related modular calcium-binding protein 1 (SMOC1) (96). These complex interactions between TNC and ECM proteins may contribute to changes in the matrix components and the biological properties of the TME. TNC can also bind to proteoglycans (PGs), such as receptor-like protein tyrosine phosphatase beta/zeta (RPTPβ/ζ) (97) and neurocan (98), two nervous tissue-specific chondroitin sulfate proteoglycans: glypican (99), syndecan-4 (100), and two heparan sulfate proteoglycans. These PGs are involved in tumor or stem cell adhesion and proliferation by interacting with multiple domains of TNC or peptides derived from TNC. In addition to PGs, TNC can act directly on cell surface receptors, particularly integrins. Yoshida et al. (70) reported that TNC plays an essential role in cancer cell biology as a ligand for integrins α2/7/8/9β1 and αvβ1/3/6. The EGF-like repeats of TNC are capable of promoting cell proliferation by binding directly to the EGF receptor and activating the ERK/MAPK signaling pathway (101), whereas the FBG domain of TNC is able to maintain the synthesis of proinflammatory cytokines *via* activation of Toll-like receptor 4 (TLR4) in a myeloid differentiation factor-88 (MyD88)-dependent manner (102). Furthermore, a large number of growth factors have been found to bind to the TNC FNIII 1–5 subdomain, including the platelet-derived growth factor (PDGF) family, TGF-β superfamily, FGF family, insulin-like growth factor-binding proteins (IGF-BPs), and neurotrophins (103). More recently, a few studies have suggested that TNC participates in recruiting and concentrating WNT ligands in acute kidney injury and whisker follicle stem cell niches, thereby potentiating WNT/β-catenin signaling, presumably due to the formation of a favorable microenvironment near the cell surface (104, 105). Finally, TNC can even bind to pathogens, such as human immunodeficiency virus, and neutralize viral activity (106). Taken together, the interaction partners of each TNC isoform are thought to be dependent on their domains, thus performing different functions in a context-dependent manner. Notably, TNC harbors some cryptic functional sites within its molecular structure, which are released through proteolytic cleavage by matrix metalloproteinases (MMPs) and a disintegrin and metalloproteinase (ADAM) family. The TNC-derived peptide fragments, such as FNIII A2, contain bioactive sites and may play a different and even opposite role than that of the parental TNC molecule (107).

Tenascin C in glioma

TNC is abundantly expressed in a variety of tumors, including breast cancer, colon adenocarcinoma, prostatic adenocarcinoma, and lung carcinoma, but particularly in gliomas (7, 27, 28, 70). In general, TNC is mainly present in the glioma perivascular and intercellular spaces and less abundantly in the cells (108, 109), and its expression level increases with glioma grade (71, 109). Interestingly, the concentration of TNC in the cerebrospinal fluid and cyst fluid

also seems to reflect the tumor grade (110, 111). Among patients with GBM, those who had TNC immunopositivity survived for a significantly shorter period than those in whom TNC expression was absent (71). Thus, TNC in gliomas can be identified as a predictor of poor prognosis and disease progression (71, 72). Unlike most other tumors, malignant glioma cells are the main source of TNC (112). TNC can also promote many malignant biological behaviors of glioma, such as neovascularization, proliferation, adhesion or migration, and immunomodulation (27, 28).

Tenascin C and neovascularization

Gliomas are characterized by a high degree of vascularization. These blood vessels are necessary for tumor growth, as they are involved in providing nutrients and removing metabolic waste. Over the past few years, some studies have demonstrated that TNC is mainly found in the perivascular niche of gliomas (72, 108), particularly in hyperplastic blood vessels (113, 114). The microvessel endothelial cells (114), pericytes (115) and smooth muscle cells (116) all have the capacity to synthesize and release TN/TNC. In GBM, perivascular TNC is related to microvascular density and vascular endothelial growth factor (VEGF) expression (108). In addition, in melanoma, TNC can regulate the expression of VEGF and affect angiogenesis in tumors (117). Proteome and immunohistochemical comparisons between tissues with physiological angiogenesis and GBM angiogenesis indicated aberrant upregulation of TNC in the latter (118). Therefore, TNC may play an important role in glioma neovascularization (Figure 3).

Recently, Rosińska et al. (119) reported that gliomas deploy diverse neovascularization means to meet a dedicated blood supply, including co-option, angiogenesis, vasculogenesis, vascular mimicry (VM), and transdifferentiation of GSCs. First, TNC is linked to angiogenesis. Zagzag et al. (120) discovered that TNC acts as a permissive substrate that promotes microvascular cell migration *in vitro* by triggering focal adhesion kinase (FAK) phosphorylation in endothelial cells. In *TNC*-knockdown GBM-neurosphere intracranial xenografts, tumor blood vessel density was lower, while the lumen was enlarged as compared to the control (121). It is important to mention that Rupp et al. (122) demonstrated the dual angiogenic effects of TNC in GBM (Figure 3). The direct contact between endothelial cells and TNC represses actin polymerization, impairs YAP signaling, and downregulates pro-angiogenic factors, consequently negatively influencing endothelial cell proliferation, survival, sprouting, and tubulogenesis. TNC also induces GBM cells to secrete pro-angiogenic factors, such as ephrinB2, a soluble molecule released by MMPs and ADAM10/17 and enhances endothelial cell tubulogenesis. These opposing effects are reminiscent of the cell-specific functions of TNC. Another study suggested that direct contact between the TNC-rich glioma matrix and endothelial cells could induce endothelial detachment, anoikis, selection of a highly proliferative phenotype, and defective tubulogenesis *in vitro*, whereas higher FN : TNC ratios reversed these effects (123). In addition to glioma, TNC also promotes cellular processes involved in angiogenesis in fibrovascular membranes in eyes with proliferative diabetic retinopathy (124) and affects colitis-associated cancer angiogenesis through interaction with integrin αvβ3 (125). Second, TNC can also promote vasculogenic mimicry

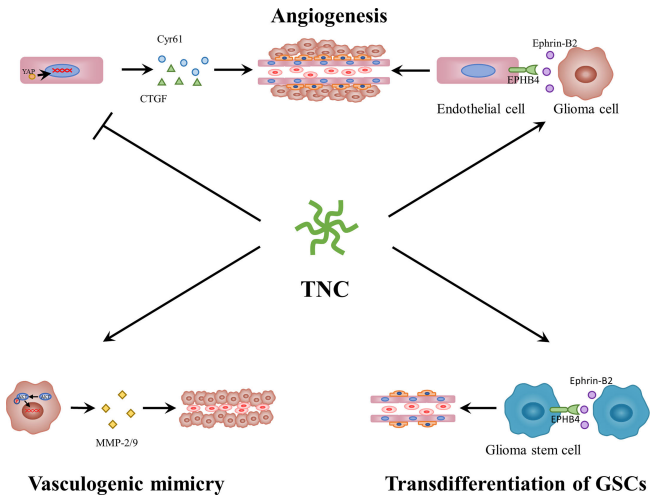

FIGURE 3
The roles of TNC in glioma neovascularization. On the one hand, TNC blocks YAP signaling and endothelial cell behavior through direct contact. On the other hand, TNC induces ephrin-B2 and a pro-angiogenic secretome in glioblastoma cells. In addition, TNC activates AKT/MMP2/MMP9 axis and further promotes vasculogenic mimicry in glioma. Moreover, TNC-ephrinB2-ephB4 signaling pathway supports GSCs differentiation into endothelial cells. YAP, Yes-associated protein; MMP, matrix metalloproteinase.

(Figure 3). Cai et al. (126) showed that TNC activates the AKT/MMP2/MMP9 axis and further promotes VM in glioma, which is similar to the findings of Kang et al. (127), who reported that *TNC*-knockdown suppresses this process in gastric cancer by inhibiting the ERK-mediated epithelial-to-mesenchymal transition (EMT). The third process involves the mechanism of TNC-induced transdifferentiation of GSCs (Figure 3). Angel et al. (128) demonstrated the mechanism by which an autocrine TNC–ephrinB2–ephrinB4 signaling pathway supports GSC differentiation into endothelial cells. Taken together, GBM neovascularization correlates with multiple complex processes, in which TNC plays a vital role. In addition to angiogenesis, VM, and transdifferentiation of GSCs, it is necessary to explore additional functions of TNC in co-option or vasculogenesis in future.

TNC and cell proliferation

The TME is composed of heterogeneous cell types, including endothelial, stromal, multiple immune, and tumor cells (25). As an ECM glycoprotein, TNC has been shown to exert different effects on different cells during tumor proliferation. To date, little information has been available on the TNC-mediated signaling pathways involved in cell proliferation. As mentioned above, TNC appears to play a dual role in endothelial cells in glioma (122, 123). Furthermore, the number of microglia in control and TNC-knockdown tumors was not significantly different in xenografts (121). In contrast to microglia, T-cell proliferation can be suppressed by TNC-containing exosomes produced by GSCs (129). Many studies have reported contradictory results regarding the effects of TNC on glioma cells (Figure 4). Initially, we observed that TNC expression is associated with a high proliferation index (108, 109). Since then, some of the mechanisms underlying the glioma cell proliferation have begun to be revealed. Huang et al. (130) found that TNC was able to bind to FNIII13 in the heparin-binding site II and interfere with cell binding to FN by syndecan-4, thereby leading to human glioma proliferation (Figure 4). Martin et al. (131) proposed that TNC promotes the growth of tumor cells by inducing the expression of 14-3-3 tau. Differential RNA expression analysis has revealed that some TNC-mediated growth-promoting signaling pathways are activated in glioma cells (132). Other *in vivo* and *in vitro* experiments have also reported the proliferative effects of TNC (128, 133, 134). Moreover, the growth of GSCs is related to TNC-activated NOTCH signaling (87). Nevertheless, the opposite phenomenon was described in another study. TNC failed to affect GBM neurosphere cell growth *in vitro*, whereas *TNC*-knockdown enhanced tumor cell proliferation *in vivo* (121). One possible explanation for these different functions is that different domains of TNC have different proliferative properties (27, 61). The EGF-like repeats and FBG region can bind to the EGF receptor and integrinαvβ3, respectively, contributing to growth. Certain alternatively spliced domains, such as AD1, AD2, and C, are also responsible for proliferation (27, 135). However, a fragment composed of all FNIII domains induced a reduction,

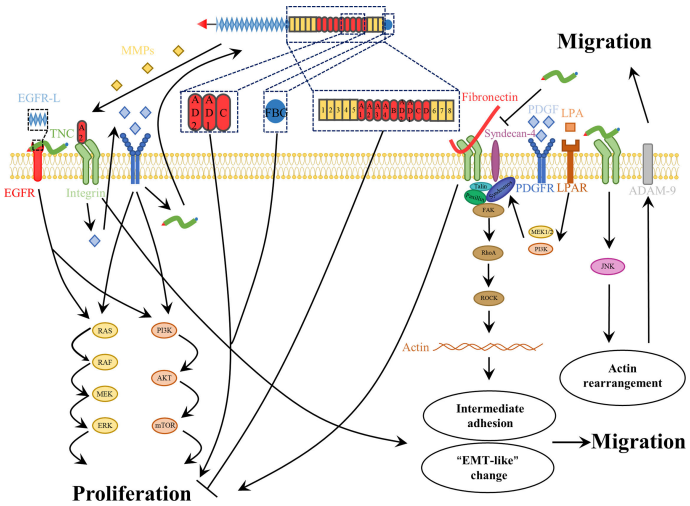

FIGURE 4
The roles of TNC in glioma cell proliferation and migration. For one thing, the role of TNC in glioma cell proliferation is complex. The EGF-like repeats, the FBG region, A2 and some alternatively spliced domains, such as AD1, -AD2 and -C, of TNC as well as integral TNC molecule contribute to the glioma cell proliferation. In contrast, the fragment composed of all FNIII-domains decreases the proliferation of glioma cell. In addition, TNC impairs the adhesive properties of FN, which contributes to glioma cell proliferation. For another thing, TNC promotes glioma cell invasiveness. This molecule not only contributes to the intermediate adhesion that support cell motility, but also promotes "EMT-like" changes. Moreover, TNC also induces matrix destructing enzymes to promote tumor cell migration.

whereas the integral TNC molecule led to an increase in glioma cell proliferation (Figure 4) (61). Another explanation is that the absence or decrease of a specific receptor compromises the proliferative effect. The lack of PDGF-Rβ in the glioma cell lines U87, U251, and GL261 resulted in the attenuation of TNIIIA2-related proliferation (136). Recently, Fujita et al. (136–138) showed that TNIIIA2 derived from TNC plays a vital role in the malignant behavior of glioma cells. They presented a positive spiral loop in which the peptide TNIIIA2 promoted PDGF-dependent proliferation by activating integrin β1 in GBM cells expressing PDGF-receptor β. The consequent upregulation of PDGF stimulated TNC expression, which induced MMP-2-mediated TNIIIA2 liberation (136). Further research is needed to explore the relationship between other domains and cell proliferation.

TNC and cell invasiveness

A major contributor to the poor prognosis of GBM patients is the invasive nature of tumor cells, which readily invade healthy brain tissues. This invasive ability of GBM cells makes maximum safe resection nearly impossible, thereby causing therapy-resistant tumor relapse, even in distant parts of the contralateral hemisphere (139). Generally speaking, glioma cell invasion involves multiple molecular mechanisms, including ECM components, adhesion proteins, proteinases, and cytoskeletal changes (139).

A good balance between assembly and disassembly of cell-matrix adhesion sites is a key determinant of cell adhesion and migration. Appropriate adhesion is essential for migration, yet too strong an adhesion has an adverse effect on cell motility. Hence, intermediate adhesion may be most beneficial for cell migration (140). To date, TNC has been found to play complex modulatory roles in glioma cell adhesion (Figure 4). Briefly, the dual effects of both pro- and anti-adhesion are dependent on the cell type, cellular context, different receptors, and the structure itself (28, 43, 44). On the one hand, TNC is not a good adhesive substrate for glioma cells, and it can impair fibronectin-mediated cell adhesion and spreading (130). However, some studies have found that TNC acts as a surface-coating molecule that supports cell adhesion (141), perhaps in an Arg-Gly-Asp (RGD)-dependent manner (142). Additionally, adhesion of glioma cells to tenascin is mediated by different coating concentrations and integrin receptors (143). Thus, TNC appears to facilitate regulation of glioma cell adhesion turnover.

Furthermore, many reports have demonstrated that TNC expression is related to the infiltrative phenotype of many tumors, including gliomas (43, 44, 89, 144, 145). Hirata et al. (146) revealed that endogenous TNC enhanced glioma invasiveness through compositional changes in the surrounding brain parenchyma. TNC not only directly supports glioma cell migration, but also augments this role, mediated by FN, through interaction with integrin α2β1 (147). In addition, several mechanisms that are involved in the regulation of TNC expression, such as IL-33/NF-κB/TNC (148) and NOTCH/RBPJκ/TNC (84), were found to increase the motility of glioma cells. Some growth factors, including lysophosphatidic acid and PDGF, strongly induce glioma cell migration *via* actin cytoskeleton remodeling in the TNC microenvironment (Figure 4) (149). Remarkably, although TNC can activate high levels of phosphorylated FAK in endothelial cells, leading to microvascular migration (120), it stimulates low levels of FAK phosphorylation in glioma cells (120, 121). Cell migration is a complex and dynamic process, involving the establishment of polar structures, adhesion formation and disassembly, and formation of protrusions at the front, and contractile structures at the rear of the cell (150). FAK phosphorylation is associated with focal adhesion. Therefore, we speculated that the anti-attachment effect of TNC allows glioma cells to detach from ECM molecules and thereby contribute to migration.

Finally, proteolytic degradation of the ECM is another important cause of glioma invasion. Sarkar et al. used a three-dimensional matrix and revealed that some proteinases are associated with TNC-mediated invasiveness, such as MMP-12 in U178 and U251 glioma cell lines (151, 152), as well as ADAM-9 in glioma patient-derived GSC lines (Figure 4) (153). In addition, *in vivo* experiments also demonstrated its influence on invasion. In TNC-knockdown xenografts, gliomas were confined to well-defined tumor boundaries, and decreased TNC led to inhibition of glioma invasion (121). Considering the diverse actions of distinct domains of this protein, some studies have focused on alternatively spliced domains. TNIIIA2 enhances the disseminative migration of GBM (136, 138) and confers anoikis resistance (137), but these activities are both abrogated by peptide FNIII14, which inactivates β1-integrins (136–138, 154).

Thus, TNC is a potential enhancer of glioma invasiveness. It may be responsible for an intermediate cell adhesion state. Moreover, the aggressiveness of gliomas is further enhanced in the presence of TNC. Further studies involving different domains and isoforms of TNC are required.

TNC and immunomodulation

Accumulating evidence has indicated that immune cells fail to function properly in gliomas. By employing immune escape mechanisms, including creating an immunosuppressive microenvironment, gliomas can bypass immunosurveillance and hamper the effect of immunotherapy (155). Recently, it has been proposed that serum TNC could be used as an indicator of the immunosuppressive microenvironment status of low-grade gliomas as well as to predict the efficacy of immunotherapy (156). The effect of TNC on various immune cells has been extensively reviewed elsewhere (28, 157). We have focused on

the main findings. Generally, TNC activates innate immune cells, but exerts immunosuppressive effects on lymphocytes, such as T cells (Figure 5). TNC is regarded as an inducer of the neuroinflammatory response in stroke, particularly SAH (56, 157). By interacting with TLR-4 of microglia or macrophages, the FBG domain of TNC leads to the production and release of pro-inflammatory cytokines, including IL-1β, IL-6, and TNF-α (56, 157). In chronic neuroinflammation in the brains of Alzheimer's disease model mice, TNC deficiency alleviates neuroinflammation and enhances the anti-inflammatory response (69). Hence, it seems reasonable to conclude that TNC has the capacity to induce M1 proinflammatory or anti-tumorigenic phenotypes in macrophages and microglia. However, this phenomenon contrasts with the tumorigenic properties of TNC and its higher expression in high-grade gliomas. One possible explanation is that this dual effect on macrophages is likely to be dependent on the cellular source. In murine models of breast cancer, Deligne et al. (158) found that host-derived TNC enhances antitumor immunity by recruiting proinflammatory macrophages, whereas tumor-derived TNC drives macrophages to produce an immunosuppressive response. Another possibility, proposed by Yalcin et al. (28), is that TNC has different functions in distinct phases of carcinogenesis. TNC plays a pro-inflammatory and anti-tumor role in tumor initiation, and tissue remodeling and tumor-promoting roles during tumor progression. This is similar to the phenomenon in which microglia can inhibit tumor growth and exhibit a tumor-promoting state in the early and late stages of glioma progression, respectively (159). Many studies have illustrated that tumor-associated macrophages (TAMs) are re-educated by glioma cells and show remarkable heterogeneity (160–162). Thus, it is increasingly thought that the M1/M2 dichotomy is an oversimplification and is no longer applicable to gliomas. Due to the complex heterogeneity of TAMs, it is difficult to draw definitive conclusions regarding the role of TNC in TAMs. A study by Ma et al. (86) suggested an intricate relationship between TNC and CD47-mediated macrophage phagocytosis. Decreased CD47, a "don't eat me" signal, not only recruits more M2-like TAMs, but also upregulates TNC expression, which further facilitates phagocytic ability and secretion of proinflammatory factors. Furthermore, TNC-induced cytokines, such as IL-1β and IL-6, and transcription factors, such as NF-κB and signal transducer and activator of transcription 3 (STAT3), have been implicated in cancer-related inflammation (86, 161, 163). These cytokines or transcription factors also induce TNC expression (7). This positive feedback is consistent with the fact that TNC expression increases with an increase in glioma grade. Hence, a more detailed study may be required to clarify the role of TNC in cancer-related inflammation.

Unlike the innate immunity, the immunosuppressive effects of TNC on T cells have been extensively studied in prostate cancer, breast cancer, and GBM. TNC generates barriers and retains CD8 tumor-infiltrating lymphocytes inside the tumor stroma in human breast cancer (164). TNC expressed on GBM cells decreased the T cell amoeba-like shape formation and paralyzed migration, while transmigration of T cells through the monolayer and ECM of glioma cell lines lacking TNC was obviously increased (165). GSC-derived exosomes carrying TNC attenuate T cell activity by interacting with the integrin receptors α5β1 and αvβ6. More importantly, these TNC-containing exosomes pass through the blood–brain barrier and enter into the circulation, suppressing systemic immune responses in patients with GBM (129). In prostate cancer, Jachetti et al. (166). found that CSCs can migrate early to prostate-draining lymph nodes where they overexpress TNC, inhibiting T cell activation, proliferation, and cytokine production, thereby overcoming immune surveillance. In addition, the relationship

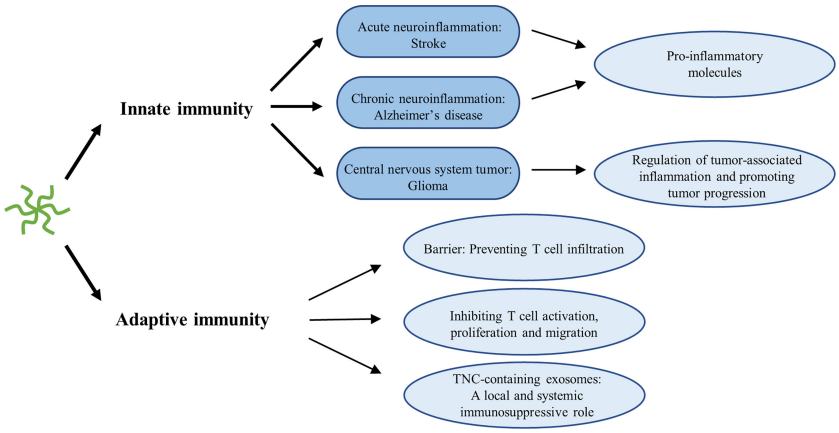

FIGURE 5
Immunomodulatory role of TNC in neuroinflammation.

between TNC and autophagy was uncovered. TNC has been implicated in the suppression of T-cell antitumor responses caused by autophagy defects. Blockade of TNC sensitizes the efficacy of immune checkpoint inhibitors in autophagy-impaired triple-negative breast cancer (167). This finding may present prospects for anti-PD1/PD-L1 treatment of gliomas.

Tenascin C and EMT

EMT is an essential process that confers malignant properties to cancer cells (168). Initially, EMT was defined by changes in cell morphology and behavior, such as repression of the existing epithelial characteristics and gain of mesenchymal properties. In recent years, we have found that activation of EMT programs endows cancer cells with additional properties beyond enhanced motility and invasiveness, such as cancer cell stemness, local immunosuppression, increased drug resistance, changes in genomic stability, and prevention of senescence (168). Accumulating evidence has suggested that TNC can promote "EMT-like" changes in different cancers, including breast cancer (169, 170), gastric cancer (127), colorectal cancer (171), pancreatic ductal adenocarcinoma (172), and nasopharyngeal carcinoma (173). However, the EMT observed in gliomas seems to differ from the classical EMT and therefore the term "glial to mesenchymal transition" has been proposed (174). Notably, mesenchymal GBM shares certain common features with gliomas that undergo "EMT-like" changes. They both exhibit a more aggressive nature and resistance to many treatments, and have the same master regulators, such as STAT3 (175–177). Thus, TNC-induced "EMT-like" changes in gliomas require further exploration.

Tenascin C and mesenchymal GBM

Based on transcriptional signatures, GBMs can be classified into three subtypes: The Cancer Genome Atlas (TCGA) proneural (TCGA-PN), classical (TCGA-CL), and mesenchymal (TCGA-MES) subtypes (178). By applying single-cell RNA-sequencing (scRNA-seq), malignant cells in GBM converge to a limited set of four cellular states: neural-progenitor-like (NPC-like), oligodendrocyte-progenitor-like (OPC-like), astrocyte-like (AC-like), and mesenchymal-like (MES-like) (179). These subtype transitions have become increasingly important, particularly the "proneural-to-mesenchymal transition" (PMT), which is analogous to EMT. This phenomenon is associated with requiring a more aggressive treatment pattern and with resistance to treatment. After reviewing the related literature, we believe that there is an underlying relationship between TNC and MES GBM. Angel et al. (128) found that TNC is overexpressed in MES GBM and that this is positively correlated with the expression of MES markers in TCGA. They further confirmed the role of TNC in regulating glioma cell plasticity in MES GBM. Moreover, Miroshnikova et al. (180) demonstrated that hypoxia-inducible factor 1α (HIF1α) directly regulates TNC expression and that TNC modifies ECM stiffness and mechano-signaling. Interestingly, another study implied that stiff tenascin-rich stroma enhances integrin mechano-signaling to induce PMT in GBMs (181). Additionally, macrophages were found to interact with receptors (OSMR or LIFR) complexed with GP130 on GBM cells *via* macrophage-derived oncostatin M (OSM), thereby activating STAT3 and inducing the transition of GBM cells into MES-like states (182). As mentioned above, TNC is considered an activator of STAT3 (86, 161, 163). Hence, it may be worthwhile to study the significance of TNC in mesenchymal GBM further.

Tenascin C and treatment-related changes

The current treatment of glioma, particularly GBM, remains a challenging problem with poor prognosis. Although many therapeutic options are available, resistance to therapy frequently causes treatment failure and tumor recurrence. Several studies have shown that TNC are likely to be related to this process. Radiation therapy is known to cause tumor cell death triggered by DNA breaks. However, ionizing radiation also induces changes in the TME, leading to an increase in TNC (183). In addition, irradiation-associated inflammation and hypoxia trigger tenascin C expression *via* TGF-β (80) and HIF-1 signaling (180), respectively. Therefore, it is plausible that radiation therapy can kill tumor cells, while simultaneously providing favorable conditions for tumor relapse.

Elevated expression of TNC affects the response of gliomas to chemotherapy with temozolomide (TMZ). In an *in vitro* experiment, *TNC*-knockdown GBM neurospheres were found to be more sensitive to TMZ (121). Another study conducted *in vivo* and *in vitro* showed that peptide FNIII14, which can inhibit the effects of TNIIIA2 through inactivation of β1-integrins, increased the susceptibility of GBM cells to TMZ by suppressing O^6-methylguanine-DNA methyltransferase (MGMT) expression (138). These findings suggest that targeting TNC may augment the anti-tumor efficacy of TMZ.

Immunotherapy is a novel therapeutic strategy that extends beyond radio- and chemotherapy. However, the immunosuppressive microenvironment limits the application of immunotherapy in gliomas. We previously reviewed the immunosuppressive effects of TNC, which further compromise the efficacy of anti-cancer immunotherapy. Recently, TTFields therapy have shown promising prospects. Nothing is currently known about TNC function in TTFields.

Tenascin C in neural stem cell niches: implications for gliomagenesis

Tenascin C and neural stem cells/ oligodendrocyte precursor cells

In the past, neurogenesis was observed to occur mainly during the developmental period. Adult neurogenesis has been widely described. Various newborn neural cells are continuously generated from NSCs located in two canonical regions of the adult CNS: the SVZ of the lateral ventricle and the dentate gyrus of the hippocampus. These stem cells reside in a specialized environment, known as a niche, which is able to maintain the basic properties of stem cells. TNC, secreted by NSCs and OPCs, is considered to be an important component of the stem cell niche and plays a vital role in NSC development (10). The effect of TNC on adult neurogenesis has also been well-characterized (184, 185). Both *in vivo* and *in vitro* assays indicate that *TNC*-knockout reduces OPC proliferation in the mouse CNS, which is associated with a partial loss of response to PDGF (186). In addition, the fact that *TNC*-null OPCs exhibit accelerated maturation rates suggests that this molecule contributes to the maintenance of the immature state (52). The underlying mechanism is gradually being elucidated (187). However, there are distinct perspectives on the role of TNC in OPC migration. Some studies have provided direct evidence for migration-inhibiting effects and mechanisms, including the prevention of WNT signaling (188) and modulation of cell–ECM interactions (189, 190). In contrast, other studies have reported that TNC may be associated with the rostral migratory stream (191), expression of proteinases (151–153) and enhancement of WNT signaling (104, 105). Thus, it is plausible to emphasize the complex migratory role of this molecule. Overall, TNC promotes NSC/OPC proliferation, inhibits differentiation, and regulates migration (Figure 6).

Tenascin C and gliomagenesis

Currently, there is a view that SVZ-derived NSCs or OPCs may have potential glioma cellular origins (Figure 6) (30, 192–195). Lee et al. (29) presented direct molecular genetic confirmation from patients and mouse models, showing that NSCs harboring driver mutations in the SVZ migrate to distant brain regions and lead to GBM development *via* aberrant growth of the OPC lineage. Notably, as shown above, TNC is enriched in the GSC and NSC microenvironments and is responsible for tumor progression and neurogenesis, respectively. Additionally, GSCs share many features and behaviors with NSCs, including common markers (such as nestin and CD133) and self-renewal properties (196). Therefore, it is necessary to explore whether TNC is involved in the malignant transformation of NSCs or OPCs.

Previous studies have indicated that malignant gliomas can arise from neural stem/progenitor cells carrying driver mutations (such as mutations in P53, PTEN, EGFR, and NF1), whereas more differentiated cell types are less likely to undergo malignant transformation (29, 30, 195, 197). However, the causes underlying this phenomenon remain unclear. Interestingly, a relationship between TNC and gene instability has previously been reported (198). One RNA profiling experiment showed that TNC downregulates the expression of cell cycle- and DNA repair-related genes in T98G GBM cells (132). The influence of TNC on cell cycle progression of the SVZ and spinal cord neural stem/progenitor cells has been investigated (199, 200). TNC-mediated enhancement of the proliferative capacity of tumor cells (130) and neural stem/progenitor cells (200) concomitantly increases the

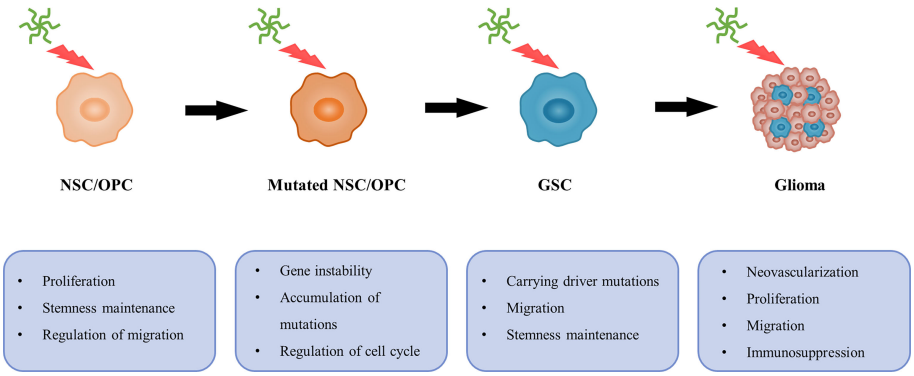

FIGURE 6
A possible relationship between TNC and gliomagenesis. In general, TNC can promote NSC/OPC proliferation, inhibit differentiation and regulate migration. However, TNC is associated with gene instability and cell cycle, and contributes to accumulation of mutations. Then NSC/OPC carrying driver mutations are likely to undergo GSC transformation. Additionally, neovascularization, proliferation, migration and immunosuppressive effects on T cell also provide favorable conditions, which leads to gliomagenesis.

likelihood of accumulation of mutations. Apart from the above, other important factors, such as stemness maintenance and migration of stem cells, as well as immunosuppressive effects on T cells, also provide favorable conditions for the transformation to malignant tumors. These findings suggest a possible relationship between TNC and gliomagenesis (Figure 6).

Clinical significance of tenascin C

The clinical implications of TNC have been extensively recognized (Table 1). TNC could be a potential prognostic marker for gliomas, including GBM (71, 201), diffuse intrinsic pontine glioma (202), and ependymoma (203). In addition, TNC seems to be regarded as a marker for CSCs (201). Another application is as a candidate for targeted therapy, depending on its characteristic expression pattern. Many ligands targeting TNC have been developed, including F16 (204), G11 (205), R6N (206), PL1 (207), PL3 (208), and Ft (209). The new Ft peptide was synthesized to target glioma-associated TNC and neuropilin-1 synergistically in neovasculature for the specific penetration of nanoparticles in anti-GBM therapy (209). Radiolabeled antibodies specific to distinct domains of TNC have been tested for the treatment of malignant gliomas in clinical studies (210–212). In addition, the TNC aptamer GBI-10 was identified (213) and used to modify adenovirus, thereby improving the adenoviral transduction efficiency in glioma cells (214). In a phase I/II trial, a multi-peptide vaccine, IMA950, that targets TNC held good promise for glioma patients (215). RNA interference has been proposed as a novel strategy for treating gliomas to silence TNC expression. One study by Zukiel et al. (216) suggested that, when double-stranded RNA targeting TNC, known as ATN-RNA, was directly injected postoperatively into the region of resection of 10 patients with glioma, almost all treated patients showed a good response. In agreement with this, other studies have also shown a significant improvement in overall survival without loss of quality of life (217, 218). Magnetic resonance imaging and computed tomography showed delayed tumor growth or a lack of tumor recurrence (217, 218). In future, more rigorous trials will be required to support the clinical application of this treatment.

Conclusion

In this review, we focused on the matricellular protein TNC and highlighted its significant implications in gliomas. TNC expression is tightly controlled, with distinct spatial and temporal distribution patterns. Therefore, they are responsible for various physiological and pathophysiological processes. TNC is associated with neurogenesis, as manifested by the promotion

TABLE 1 The clinical applications of TNC in gliomas.

Categories	Compound	Application	Result	Clinical trial	Ref
Marker	TNC	Glioblastoma	Prognosis	—	(71, 201)
	TNC	Diffuse intrinsic pontine glioma	Prognosis	—	(202)
	TNC	Integrated TNC expression and 1q25 status	Prognosis	—	(203)
	TNC	Glioma stem cells	Biomarker	—	(201)
Antibody	IL2-F16 (targeting TNC-A1)	Combined with temozolomide	Complete remission	Preclinical	(204)
	G11 (targeting TNC-C)	—	Tumor targeting	Preclinical	(205)
	IL12-R6N (targeting TNC-D)	—	Cancer regression	Preclinical	(206)
Peptide	PL1 (targeting FN-EDB and TNC-C) + pro-apoptotic payload	Every other day for 10 total injections	Reduced tumor growth and increased survival	Preclinical	(207)
	PL3 (targeting TNC-C and neuropilin-1) + pro-apoptotic payload	Every other day for 10 total injections	Improved survival	Preclinical	(208)
	Ft peptide (targeting TNC and neuropilin-1) + paclitaxel	Intravenously administered every 2 weeks for 3 times	Improved survival	Preclinical	(209)
Radiolabeled antibodies	Radiolabeled anti-TNC monoclonal antibodies such as ^{131}I-81C6	Radiotherapy after resection followed by chemotherapy (temozolomide, lomustine, irinotecan, etoposide)	Low toxicity and prolonged survival	Phase I/II	(210–212)
Aptamer	GBI-10	GBI-10-modified adenovirus	Improved the adenoviral transduction efficiency	Preclinical	(213, 214)
Vaccine	IMA950 (A multi-peptide vaccine IMA950 targeting TNC)	Injections of IMA950/adjuvant poly-ICLC after surgical resection followed by chemoradiotherapy and temozolomide	Improved survival	Phase I/II	(215)
RNA interference	ATN-RNA (anti TNC dsRNA)	Injection into the brain after resection	Improved survival	Patients	(216–218)

TNC, Tenascin C; TNC-A1, Tenascin C with extradomain A1; TNC-C, Tenascin C with extradomain C; TNC-D, Tenascin C with extradomain D; FN-EDB, Fibronectin with extradomain B; ds, double-stranded; IL, Interleukin; Ref, References.

of stem cell proliferation, maintenance of stemness, and regulation of migration. In contrast, TNC is implicated in malignant glioma progression, including neovascularization, proliferation, invasiveness, and immunomodulation. However, because of the complex and various domains and the strong crosstalk between them, it is difficult to allocate diverse roles to specific parts of this molecule. Hence, clarifying the underlying mechanisms is a direction for future research. Additionally, based on the hypothesis that SVZ-derived NSCs are instrumental in glioma development, we proposed a possible link between TNC and gliomagenesis, although direct evidence is currently lacking. Therefore, future studies should be conducted to investigate this relationship specifically. Finally, this molecule has promising potential for application in anti-glioma therapy. Many drugs directed against TNC, such as radiolabeled antibodies and dsRNA, have been proven to be effective in preclinical or clinical studies. The selective targeting of the downstream signaling pathways of TNC warrants further investigation. Thorough research on TNC, particularly on the different domains and critical targets of the signaling pathway, will provide new therapeutic strategies for glioma treatment.

Author contributions

ZF drafted the manuscript and created the figures. GZ, CL, and SS collected the literature. ZD, ZC, YC, and CZ revised the manuscript in English. FL contributed to the correction and final review of this article. All the authors contributed to the study and approved the final version of the manuscript.

Acknowledgments

We thank all those who participated in the preparation of this manuscript. We would like to thank Editage (www.editage.cn) for English language editing.

Conflict of interest

The authors declare that the research was conducted in the absence of any commercial or financial relationships that could be construed as potential conflicts of interest.

Publisher's note

All claims expressed in this article are solely those of the authors and do not necessarily represent those of their affiliated organizations, or those of the publisher, the editors and the reviewers. Any product that may be evaluated in this article, or claim that may be made by its manufacturer, is not guaranteed or endorsed by the publisher.

References

1. Hynes RO. The extracellular matrix: not just pretty fibrils. *Science* (2009) 326 (5957):1216–9. doi: 10.1126/science.1176009

2. Roberts DD. Emerging functions of matricellular proteins. *Cell Mol Life Sci CMLS* (2011) 68(19):3133–6. doi: 10.1007/s00018-011-0779-2

3. Jayakumar AR, Apeksha A, Norenberg MD. Role of matricellular proteins in disorders of the central nervous system. *Neurochem Res* (2017) 42(3):858–75. doi: 10.1007/s11064-016-2088-5

4. Chiodoni C, Colombo MP, Sangaletti S. Matricellular proteins: from homeostasis to inflammation, cancer, and metastasis. *Cancer Metastasis Rev* (2010) 29(2):295–307. doi: 10.1007/s10555-010-9221-8

5. Murphy-Ullrich JE, Sage EH. Revisiting the matricellular concept. *Matrix Biol J Int Soc Matrix Biol* (2014) 37:1–14. doi: 10.1016/j.matbio.2014.07.005

6. Midwood KS, Orend G. The role of tenascin-c in tissue injury and tumorigenesis. *J Cell Commun Signal* (2009) 3(3-4):287–310. doi: 10.1007/s12079-009-0075-1

7. Orend G, Chiquet-Ehrismann R. Tenascin-c induced signaling in cancer. *Cancer Lett* (2006) 244(2):143–63. doi: 10.1016/j.canlet.2006.02.017

8. Chiquet-Ehrismann R, Orend G, Chiquet M, Tucker RP, Midwood KS. Tenascins in stem cell niches. *Matrix Biol J Int Soc Matrix Biol* (2014) 37:112–23. doi: 10.1016/j.matbio.2014.01.007

9. von Holst A. Tenascin C in stem cell niches: Redundant, permissive or instructive?. *Cells Tissues Organs* (2008) 188(1–2):170–7. doi: 10.1159/000112848

10. Garcion E, Halilagic A, Faissner A, ffrench-Constant C. Generation of an environmental niche for neural stem cell development by the extracellular matrix molecule tenascin c. *Dev (Cambridge England)* (2004) 131(14):3423–32. doi: 10.1242/dev.01202

11. Reinhard J, Brösicke N, Theocharidis U, Faissner A. The extracellular matrix niche microenvironment of neural and cancer stem cells in the brain. *Int J Biochem Cell Biol* (2016) 81(Pt A):174–83. doi: 10.1016/j.biocel.2016.05.002

12. Faissner A, Reinhard J. The extracellular matrix compartment of neural stem and glial progenitor cells. *Glia* (2015) 63(8):1330–49. doi: 10.1002/glia.22839

13. Louis DN, Perry A, Reifenberger G, von Deimling A, Figarella-Branger D, Cavenee WK, et al. The 2016 world health organization classification of tumors of the central nervous system: a summary. *Acta neuropathologica* (2016) 131(6):803–20. doi: 10.1007/s00401-016-1545-1

14. Weller M, van den Bent M, Preusser M, Le Rhun E, Tonn JC, Minniti G, et al. EANO guidelines on the diagnosis and treatment of diffuse gliomas of adulthood. *Nat Rev Clin Oncol* (2021) 18(3):170–86. doi: 10.1038/s41571-020-00447-z

15. Ostrom QT, Gittleman H, Truitt G, Boscia A, Kruchko C, Barnholtz-Sloan JS. CBTRUS statistical report: Primary brain and other central nervous system tumors diagnosed in the united states in 2011-2015. *Neuro-oncology* (2018) 20 (suppl_4):iv1–iv86. doi: 10.1093/neuonc/noy131

16. Tan AC, Ashley DM, Lopez GY, Malinzak M, Friedman HS, Khasraw M. Management of glioblastoma: State of the art and future directions. *CA Cancer J Clin* (2020) 70(4):299–312. doi: 10.3322/caac.21613

17. Thakkar JP, Dolecek TA, Horbinski C, Ostrom QT, Lightner DD, Barnholtz-Sloan JS, et al. Epidemiologic and molecular prognostic review of glioblastoma. *Cancer epidemiology Biomarkers Prev Publ Am Assoc Cancer Research cosponsored by Am Soc Prev Oncol* (2014) 23(10):1985–96. doi: 10.1158/1055-9965.Epi-14-0275

18. Stupp R, Mason WP, van den Bent MJ, Weller M, Fisher B, Taphoorn MJ, et al. Radiotherapy plus concomitant and adjuvant temozolomide for glioblastoma. *N Engl J Med* (2005) 352(10):987–96. doi: 10.1056/NEJMoa043330

19. Iorgulescu JB, Reardon DA, Chiocca EA, Wu CJ. Immunotherapy for glioblastoma: going viral. *Nat Med* (2018) 24(8):1094–6. doi: 10.1038/s41591-018-0142-3

20. Jackson CM, Choi J, Lim M. Mechanisms of immunotherapy resistance: lessons from glioblastoma. *Nat Immunol* (2019) 20(9):1100–9. doi: 10.1038/s41590-019-0433-y

21. Gilbert MR, Dignam JJ, Armstrong TS, Wefel JS, Blumenthal DT, Vogelbaum MA, et al. A randomized trial of bevacizumab for newly diagnosed glioblastoma. *N Engl J Med* (2014) 370(8):699–708. doi: 10.1056/NEJMoa1308573

22. Van Den Bent M, Eoli M, Sepulveda JM, Smits M, Walenkamp A, Frenel JS, et al. INTELLANCE 2/EORTC 1410 randomized phase II study of depatux-m alone and with temozolomide vs temozolomide or lomustine in recurrent EGFR amplified glioblastoma. *Neuro-oncology* (2020) 22(5):684–93. doi: 10.1093/neuonc/noz222

23. Stupp R, Wong ET, Kanner AA, Steinberg D, Engelhard H, Heidecke V, et al. NovoTTF-100A versus physician's choice chemotherapy in recurrent glioblastoma: a randomised phase III trial of a novel treatment modality. *Eur J Cancer* (2012) 48(14):2192–202. doi: 10.1016/j.ejca.2012.04.011

24. Hottinger AF, Pacheco P, Stupp R. Tumor treating fields: a novel treatment modality and its use in brain tumors. *Neuro-oncology* (2016) 18(10):1338–49. doi: 10.1093/neuonc/now182

25. Dapash M, Hou D, Castro B, Lee-Chang C, Lesniak MS. The interplay between glioblastoma and its microenvironment. *Cells* (2021) 10(9):2257. doi: 10.3390/cells10092257

26. Lathia JD, Mack SC, Mulkearns-Hubert EE, Valentim CL, Rich JN. Cancer stem cells in glioblastoma. *Genes Dev* (2015) 29(12):1203–17. doi: 10.1101/gad.261982.115

27. Brösicke N, Faissner A. Role of tenascins in the ECM of gliomas. *Cell adhesion migration* (2015) 9(1-2):131–40. doi: 10.1080/19336918.2014.1000071

28. Yalcin F, Dzaye O, Xia S. Tenascin-c function in glioma: Immunomodulation and beyond. *Adv Exp Med Biol* (2020) 1272:149–72. doi: 10.1007/978-3-030-48457-6_9

29. Lee JH, Lee JE, Kahng JY, Kim SH, Park JS, Yoon SJ, et al. Human glioblastoma arises from subventricular zone cells with low-level driver mutations. *Nature* (2018) 560(7717):243–7. doi: 10.1038/s41586-018-0389-3

30. Alcantara Llaguno S, Chen J, Kwon CH, Jackson EL, Li Y, Burns DK, et al. Malignant astrocytomas originate from neural stem/progenitor cells in a somatic tumor suppressor mouse model. *Cancer Cell* (2009) 15(1):45–56. doi: 10.1016/j.ccr.2008.12.006

31. Sanai N, Tramontin AD, Quiñones-Hinojosa A, Barbaro NM, Gupta N, Kunwar S, et al. Unique astrocyte ribbon in adult human brain contains neural stem cells but lacks chain migration. *Nature* (2004) 427(6976):740–4. doi: 10.1038/nature02301

32. Bourdon MA, Wikstrand CJ, Furthmayr H, Matthews TJ, Bigner DD. Human glioma-mesenchymal extracellular matrix antigen defined by monoclonal antibody. *Cancer Res* (1983) 43(6):2796–805.

33. Chiquet M, Fambrough DM. Chick myotendinous antigen. i. a monoclonal antibody as a marker for tendon and muscle morphogenesis. *J Cell Biol* (1984) 98(6):1926–36. doi: 10.1083/jcb.98.6.1926

34. Chiquet M, Fambrough DM. Chick myotendinous antigen. II. a novel extracellular glycoprotein complex consisting of large disulfide-linked subunits. *J Cell Biol* (1984) 98(6):1937–46. doi: 10.1083/jcb.98.6.1937

35. Grumet M, Hoffman S, Crossin KL, Edelman GM. Cytotactin, an extracellular matrix protein of neural and non-neural tissues that mediates glia-neuron interaction. *Proc Natl Acad Sci USA* (1985) 82(23):8075–9. doi: 10.1073/pnas.82.23.8075

36. Kruse J, Keilhauer G, Faissner A, Timpl R, Schachner M. The J1 glycoprotein–a novel nervous system cell adhesion molecule of the L2/HNK-1 family. *Nature* (1985) 316(6024):146–8. doi: 10.1038/316146a0

37. Rettig WJ, Triche TJ, Garin-Chesa P. Stimulation of human neuronectin secretion by brain-derived growth factors. *Brain Res* (1989) 487(1):171–7. doi: 10.1016/0006-8993(89)90954-2

38. Erickson HP, Inglesias JL. A six-armed oligomer isolated from cell surface fibronectin preparations. *Nature* (1984) 311(5983):267–9. doi: 10.1038/311267a0

39. Chiquet M. Tenascin-c: From discovery to structure-function relationships. *Front Immunol* (2020) 11:611789. doi: 10.3389/fimmu.2020.611789

40. Jones PL, Jones FS. Tenascin-c in development and disease: gene regulation and cell function. *Matrix Biol J Int Soc Matrix Biol* (2000) 19(7):581–96. doi: 10.1016/s0945-053x(00)00106-2

41. Jones FS, Jones PL. The tenascin family of ECM glycoproteins: structure, function, and regulation during embryonic development and tissue remodeling. *Dev dynamics an Off Publ Am Assoc Anatomists* (2000) 218(2):235–59. doi: 10.1002/(sici)1097-0177(200006)218:2<235::Aid-dvdy2>3.0.Co;2-g

42. Mighell AJ, Thompson J, Hume WJ, Markham AF, Robinson PA. Human tenascin-c: identification of a novel type III repeat in oral cancer and of novel splice variants in normal, malignant and reactive oral mucosae. *Int J Cancer* (1997) 72(2):236–40. doi: 10.1002/(sici)1097-0215(19970717)72:2<236::aid-ijc6>3.0.co;2-s

43. Giblin SP, Midwood KS. Tenascin-c: Form versus function. *Cell adhesion migration* (2015) 9(1-2):48–82. doi: 10.4161/19336918.2014.987587

44. Midwood KS, Chiquet M, Tucker RP, Orend G. Tenascin-c at a glance. *J Cell Sci* (2016) 129(23):4321–7. doi: 10.1242/jcs.190546

45. Joester A, Faissner A. Evidence for combinatorial variability of tenascin-c isoforms and developmental regulation in the mouse central nervous system. *J Biol Chem* (1999) 274(24):17144–51. doi: 10.1074/jbc.274.24.17144

46. Garwood J, Theocharidis U, Calco V, Dobbertin A, Faissner A. Existence of tenascin-c isoforms in rat that contain the alternatively spliced AD1 domain are developmentally regulated during hippocampal development. *Cell Mol Neurobiol* (2012) 32(2):279–87. doi: 10.1007/s10571-011-9759-1

47. Yagi H, Yanagisawa M, Suzuki Y, Nakatani Y, Ariga T, Kato K, et al. HNK-1 epitope-carrying tenascin-c spliced variant regulates the proliferation of mouse embryonic neural stem cells. *J Biol Chem* (2010) 285(48):37293–301. doi: 10.1074/jbc.M110.157081

48. Wallner K, Li C, Shah PK, Wu KJ, Schwartz SM, Sharifi BG. EGF-like domain of tenascin-c is proapoptotic for cultured smooth muscle cells. *Arteriosclerosis thrombosis Vasc Biol* (2004) 24(8):1416–21. doi: 10.1161/01.Atv.0000134299.89599.53

49. Saga Y, Tsukamoto T, Jing N, Kusakabe M, Sakakura T. Murine tenascin: cDNA cloning, structure and temporal expression of isoforms. *Gene* (1991) 104(2):177–85. doi: 10.1016/0378-1119(91)90248-a

50. Joester A, Faissner A. The structure and function of tenascins in the nervous system. *Matrix Biol J Int Soc Matrix Biol* (2001) 20(1):13–22. doi: 10.1016/s0945-053x(00)00136-0

51. Götz M, Bolz J, Joester A, Faissner A. Tenascin-c synthesis and influence on axonal growth during rat cortical development. *Eur J Neurosci* (1997) 9(3):496–506. doi: 10.1111/j.1460-9568.1997.tb01627.x

52. Garwood J, Garcion E, Dobbertin A, Heck N, Calco V, ffrench-Constant C, et al. The extracellular matrix glycoprotein tenascin-c is expressed by oligodendrocyte precursor cells and required for the regulation of maturation rate, survival and responsiveness to platelet-derived growth factor. *Eur J Neurosci* (2004) 20(10):2524–40. doi: 10.1111/j.1460-9568.2004.03727.x

53. Kazanis I, Belhadi A, Faissner A, Ffrench-Constant C. The adult mouse subependymal zone regenerates efficiently in the absence of tenascin-c. *J Neurosci Off J Soc Neurosci* (2007) 27(51):13991–6. doi: 10.1523/jneurosci.3279-07.2007

54. Niquet J, Jorquera I, Faissner A, Ben-Ari Y, Represa A. Gliosis and axonal sprouting in the hippocampus of epileptic rats are associated with an increase of tenascin-c immunoreactivity. *J neurocytol* (1995) 24(8):611–24. doi: 10.1007/bf01257376

55. Bartsch S, Bartsch U, Dörries U, Faissner A, Weller A, Ekblom P, et al. Expression of tenascin in the developing and adult cerebellar cortex. *J Neurosci Off J Soc Neurosci* (1992) 12(3):736–49. doi: 10.1523/jneurosci.12-03-00736.1992

56. Okada T, Suzuki H. The role of tenascin-c in tissue injury and repair after stroke. *Front Immunol* (2020) 11:607587. doi: 10.3389/fimmu.2020.607587

57. Mi Z, Halfter W, Abrahamson EE, Klunk WE, Mathis CA, Mufson EJ, et al. Tenascin-c is associated with cored amyloid-beta plaques in Alzheimer disease and pathology burdened cognitively normal elderly. *J neuropathol Exp Neurol* (2016) 75(9):868–76. doi: 10.1093/jnen/nlw062

58. Reinhard J, Roll L, Faissner A. Tenascins in retinal and optic nerve neurodegeneration. *Front Integr Neurosci* (2017) 11:30. doi: 10.3389/fnint.2017.00030

59. Hausmann R, Betz P. Course of glial immunoreactivity for vimentin, tenascin and alpha1-antichymotrypsin after traumatic injury to human brain. *Int J legal Med* (2001) 114(6):338–42. doi: 10.1007/s004140000199

60. Brodkey JA, Laywell ED, O'Brien TF, Faissner A, Stefansson K, Dörries HU, et al. Focal brain injury and upregulation of a developmentally regulated extracellular matrix protein. *J Neurosurg* (1995) 82(1):106–12. doi: 10.3171/jns.1995.82.1.0106

61. Brösicke N, van Landeghem FK, Scheffler B, Faissner A. Tenascin-c is expressed by human glioma *in vivo* and shows a strong association with tumor blood vessels. *Cell Tissue Res* (2013) 354(2):409–30. doi: 10.1007/s00441-013-1704-9

62. Suzuki H, Kawakita F. Tenascin-c in aneurysmal subarachnoid hemorrhage: deleterious or protective? *Neural Regener Res* (2016) 11(2):230–1. doi: 10.4103/1673-5374.177721

63. Suzuki H, Kanamaru K, Suzuki Y, Aimi Y, Matsubara N, Araki T, et al. Tenascin-c is induced in cerebral vasospasm after subarachnoid hemorrhage in rats and humans: a pilot study. *Neurol Res* (2010) 32(2):179–84. doi: 10.1179/174313208x355495

64. Fujimoto M, Shiba M, Kawakita F, Liu L, Shimojo N, Imanaka-Yoshida K, et al. Deficiency of tenascin-c and attenuation of blood-brain barrier disruption

following experimental subarachnoid hemorrhage in mice. *J Neurosurg* (2016) 124 (6):1693–702. doi: 10.3171/2015.4.Jns15484

65. Shiba M, Fujimoto M, Imanaka-Yoshida K, Yoshida T, Taki W, Suzuki H. Tenascin-c causes neuronal apoptosis after subarachnoid hemorrhage in rats. *Trans stroke Res* (2014) 5(2):238–47. doi: 10.1007/s12975-014-0333-2

66. Fujimoto M, Shiba M, Kawakita F, Liu L, Shimojo N, Imanaka-Yoshida K, et al. Effects of tenascin-c knockout on cerebral vasospasm after experimental subarachnoid hemorrhage in mice. *Mol Neurobiol* (2018) 55(3):1951–8. doi: 10.1007/s12035-017-0466-x

67. Suzuki H, Kanamaru K, Shiba M, Fujimoto M, Kawakita F, Imanaka-Yoshida K, et al. Tenascin-c is a possible mediator between initial brain injury and vasospasm-related and -unrelated delayed cerebral ischemia after aneurysmal subarachnoid hemorrhage. *Acta neurochirurgica Supplement* (2015) 120:117–21. doi: 10.1007/978-3-319-04981-6_20

68. Suzuki H, Kinoshita N, Imanaka-Yoshida K, Yoshida T, Taki W. Cerebrospinal fluid tenascin-c increases preceding the development of chronic shunt-dependent hydrocephalus after subarachnoid hemorrhage. *Stroke* (2008) 39 (5):1610–2. doi: 10.1161/strokeaha.107.505735

69. Xie K, Liu Y, Hao W, Walter S, Penke B, Hartmann T, et al. Tenascin-c deficiency ameliorates alzheimer's disease-related pathology in mice. *Neurobiol Aging* (2013) 34(10):2389–98. doi: 10.1016/j.neurobiolaging.2013.04.013

70. Yoshida T, Akatsuka T, Imanaka-Yoshida K. Tenascin-c and integrins in cancer. *Cell adhesion migration* (2015) 9(1-2):96–104. doi: 10.1080/19336918.2015.1008332

71. Leins A, Riva P, Lindstedt R, Davidoff MS, Mehraein P, Weis S. Expression of tenascin-c in various human brain tumors and its relevance for survival in patients with astrocytoma. *Cancer* (2003) 98(11):2430–9. doi: 10.1002/cncr.11796

72. Herold-Mende C, Mueller MM, Bonsanto MM, Schmitt HP, Kunze S, Steiner HH. Clinical impact and functional aspects of tenascin-c expression during glioma progression. *Int J Cancer* (2002) 98(3):362–9. doi: 10.1002/ijc.10233

73. Rocchi M, Archidiacono N, Romeo G, Saginati M, Zardi L. Assignment of the gene for human tenascin to the region q32-q34 of chromosome 9. *Hum Genet* (1991) 86(6):621–3. doi: 10.1007/bf00201554

74. Chiovaro F, Chiquet-Ehrismann R, Chiquet M. Transcriptional regulation of tenascin genes. *Cell adhesion migration* (2015) 9(1-2):34–47. doi: 10.1080/19336918.2015.1008333

75. Jones FS, Chalepakis G, Gruss P, Edelman GM. Activation of the cytotactin promoter by the homeobox-containing gene evx-1. *Proc Natl Acad Sci United States America* (1992) 89(6):2091–5. doi: 10.1073/pnas.89.6.2091

76. Gherzi R, Briata P, Boncinelli E, Ponassi M, Querzè G, Viti F, et al. The human homeodomain protein OTX2 binds to the human tenascin-c promoter and trans-represses its activity in transfected cells. *DNA Cell Biol* (1997) 16(5):559–67. doi: 10.1089/dna.1997.16.559

77. Chiquet M, Sarasa-Renedo A, Tunç-Civelek V. Induction of tenascin-c by cyclic tensile strain versus growth factors: distinct contributions by Rho/ROCK and MAPK signaling pathways. *Biochim Biophys Acta* (2004) 1693(3):193–204. doi: 10.1016/j.bbamcr.2004.08.001

78. Maier S, Lutz R, Gelman L, Sarasa-Renedo A, Schenk S, Grashoff C, et al. Tenascin-c induction by cyclic strain requires integrin-linked kinase. *Biochim Biophys Acta* (2008) 1783(6):1150–62. doi: 10.1016/j.bbamcr.2008.01.013

79. Lutz R, Sakai T, Chiquet M. Pericellular fibronectin is required for RhoA-dependent responses to cyclic strain in fibroblasts. *J Cell Sci* (2010) 123(Pt 9):1511–21. doi: 10.1242/jcs.060905

80. Smith GM, Hale JH. Macrophage/Microglia regulation of astrocytic tenascin: synergistic action of transforming growth factor-beta and basic fibroblast growth factor. *J Neurosci Off J Soc Neurosci* (1997) 17(24):9624–33. doi: 10.1523/jneurosci.17-24-09624.1997

81. Scharer CD, McCabe CD, Ali-Seyed M, Berger MF, Bulyk ML, Moreno CS. Genome-wide promoter analysis of the SOX4 transcriptional network in prostate cancer cells. *Cancer Res* (2009) 69(2):709–17. doi: 10.1158/0008-5472.Can-08-3415

82. Li L, Li Q, Chen X, Xu M, Li X, Nie L, et al. SOX4 is overexpressed in diffusely infiltrating astrocytoma and confers poor prognosis. *Neuropathol Off J Japanese Soc Neuropathol* (2015) 35(6):510–7. doi: 10.1111/neup.12212

83. Mahesparan R, Read TA, Lund-Johansen M, Skaftnesmo KO, Bjerkvig R, Engebraaten O. Expression of extracellular matrix components in a highly infiltrative *in vivo* glioma model. *Acta neuropathologica* (2003) 105(1):49–57. doi: 10.1007/s00401-002-0610-0

84. Sivasankaran B, Degen M, Ghaffari A, Hegi ME, Hamou MF, Ionescu MC, et al. Tenascin-c is a novel RBPJkappa-induced target gene for notch signaling in gliomas. *Cancer Res* (2009) 69(2):458–65. doi: 10.1158/0008-5472.Can-08-2610

85. Wang MM. Notch signaling and notch signaling modifiers. *Int J Biochem Cell Biol* (2011) 43(11):1550–62. doi: 10.1016/j.biocel.2011.08.005

86. Ma D, Liu S, Lal B, Wei S, Wang S, Zhan D, et al. Extracellular matrix protein tenascin c increases phagocytosis mediated by CD47 loss of function in glioblastoma. *Cancer Res* (2019) 79(10):2697–708. doi: 10.1158/0008-5472.Can-18-3125

87. Sarkar S, Mirzaei R, Zemp FJ, Wei W, Senger DL, Robbins SM, et al. Activation of NOTCH signaling by tenascin-c promotes growth of human brain tumor-initiating cells. *Cancer Res* (2017) 77(12):3231–43. doi: 10.1158/0008-5472.Can-16-2171

88. Oskarsson T, Acharyya S, Zhang XH, Vanharanta S, Tavazoie SF, Morris PG, et al. Breast cancer cells produce tenascin c as a metastatic niche component to colonize the lungs. *Nat Med* (2011) 17(7):867–74. doi: 10.1038/nm.2379

89. Midwood KS, Hussenet T, Langlois B, Orend G. Advances in tenascin-c biology. *Cell Mol Life Sci CMLS* (2011) 68(19):3175–99. doi: 10.1007/s00018-011-0783-6

90. Chung CY, Zardi L, Erickson HP. Binding of tenascin-c to soluble fibronectin and matrix fibrils. *J Biol Chem* (1995) 270(48):29012–7. doi: 10.1074/jbc.270.48.29012

91. To WS, Midwood KS. Identification of novel and distinct binding sites within tenascin-c for soluble and fibrillar fibronectin. *J Biol Chem* (2011) 286 (17):14881–91. doi: 10.1074/jbc.M110.189019

92. Kii I, Nishiyama T, Li M, Matsumoto K, Saito M, Amizuka N, et al. Incorporation of tenascin-c into the extracellular matrix by periostin underlies an extracellular meshwork architecture. *J Biol Chem* (2010) 285(3):2028–39. doi: 10.1074/jbc.M109.051961

93. Chung CY, Erickson HP. Glycosaminoglycans modulate fibronectin matrix assembly and are essential for matrix incorporation of tenascin-c. *J Cell Sci* (1997) 110(Pt 12):1413–9. doi: 10.1242/jcs.110.12.1413

94. Brinckmann J, Hunzelmann N, Kahle B, Rohwedel J, Kramer J, Gibson MA, et al. Enhanced fibrillin-2 expression is a general feature of wound healing and sclerosis: potential alteration of cell attachment and storage of TGF-beta. *Lab investigation; J Tech Methods Pathol* (2010) 90(5):739–52. doi: 10.1038/labinvest.2010.49

95. Day JM, Olin AI, Murdoch AD, Canfield A, Sasaki T, Timpl R, et al. Alternative splicing in the aggrecan G3 domain influences binding interactions with tenascin-c and other extracellular matrix proteins. *J Biol Chem* (2004) 279 (13):12511–8. doi: 10.1074/jbc.M400242200

96. Brellier F, Ruggiero S, Zwolanek D, Martina E, Hess D, Brown-Luedi M, et al. SMOC1 is a tenascin-c interacting protein over-expressed in brain tumors. *Matrix Biol J Int Soc Matrix Biol* (2011) 30(3):225–33. doi: 10.1016/j.matbio.2011.02.001

97. Adamsky K, Schilling J, Garwood J, Faissner A, Peles E. Glial tumor cell adhesion is mediated by binding of the FNIII domain of receptor protein tyrosine phosphatase beta (RPTPbeta) to tenascin c. *Oncogene* (2001) 20(5):609–18. doi: 10.1038/sj.onc.1204119

98. Milev P, Fischer D, Häring M, Schulthess T, Margolis RK, Chiquet-Ehrismann R, et al. The fibrinogen-like globe of tenascin-c mediates its interactions with neurocan and phosphacan/protein-tyrosine phosphatase-zeta/beta. *J Biol Chem* (1997) 272(24):15501–9. doi: 10.1074/jbc.272.24.15501

99. Abaskharoun M, Bellemare M, Lau E, Margolis RU. Glypican-1, phosphacan/receptor protein-tyrosine phosphatase-ζ/β and its ligand, tenascin-c, are expressed by neural stem cells and neural cells derived from embryonic stem cells. *ASN Neuro* (2010) 2(3):e00039. doi: 10.1042/an20100001

100. Saito Y, Imazeki H, Miura S, Yoshimura T, Okutsu H, Harada Y, et al. A peptide derived from tenascin-c induces beta1 integrin activation through syndecan-4. *J Biol Chem* (2007) 282(48):34929–37. doi: 10.1074/jbc.M705608200

101. Swindle CS, Tran KT, Johnson TD, Banerjee P, Mayes AM, Griffith L, et al. Epidermal growth factor (EGF)-like repeats of human tenascin-c as ligands for EGF receptor. *J Cell Biol* (2001) 154(2):459–68. doi: 10.1083/jcb.200103103

102. Midwood K, Sacre S, Piccinini AM, Inglis J, Trebaul A, Chan E, et al. Tenascin-c is an endogenous activator of toll-like receptor 4 that is essential for maintaining inflammation in arthritic joint disease. *Nat Med* (2009) 15(7):774–80. doi: 10.1038/nm.1987

103. De Laporte L, Rice JJ, Tortelli F, Hubbell JA. Tenascin c promiscuously binds growth factors *via* its fifth fibronectin type III-like domain. *PloS One* (2013) 8 (4):e62076. doi: 10.1371/journal.pone.0062076

104. Chen S, Fu H, Wu S, Zhu W, Liao J, Hong X, et al. Tenascin-c protects against acute kidney injury by recruiting wnt ligands. *Kidney Int* (2019) 95(1):62–74. doi: 10.1016/j.kint.2018.08.029

105. Hendaoui I, Tucker RP, Zingg D, Bichet S, Schittny J, Chiquet-Ehrismann R. Tenascin-c is required for normal wnt/β-catenin signaling in the whisker follicle stem cell niche. *Matrix Biol J Int Soc Matrix Biol* (2014) 40:46–53. doi: 10.1016/j.matbio.2014.08.017

106. Fouda GG, Jaeger FH, Amos JD, Ho C, Kunz EL, Anasti K, et al. Tenascin-c is an innate broad-spectrum, HIV-1-neutralizing protein in breast milk. *Proc Natl Acad Sci USA* (2013) 110(45):18220–5. doi: 10.1073/pnas.1307336110

107. Iyoda T, Fujita M, Fukai F. Biologically active TNIIIA2 region in tenascin-c molecule: A major contributor to elicit aggressive malignant phenotypes from Tumors/Tumor stroma. *Front Immunol* (2020) 11:610096. doi: 10.3389/fimmu.2020.610096

108. Behrem S, Zarković K, Eskinja N, Jonjić N. Distribution pattern of tenascin-c in glioblastoma: correlation with angiogenesis and tumor cell proliferation. *Pathol Oncol Res POR* (2005) 11(4):229–35. doi: 10.1007/bf02893856

109. Kim CH, Bak KH, Kim YS, Kim JM, Ko Y, Oh SJ, et al. Expression of tenascin-c in astrocytic tumors: its relevance to proliferation and angiogenesis. *Surg Neurol* (2000) 54(3):235–40. doi: 10.1016/s0090-3019(00)00307-4

110. Yoshida J, Wakabayashi T, Okamoto S, Kimura S, Washizu K, Kiyosawa K, et al. Tenascin in cerebrospinal fluid is a useful biomarker for the diagnosis of brain tumour. *J neurology neurosurgery Psychiatry* (1994) 57(10):1212–5. doi: 10.1136/jnnp.57.10.1212

111. Jallo GI, Friedlander DR, Kelly PJ, Wisoff JH, Grumet M, Zagzag D. Tenascin-c expression in the cyst wall and fluid of human brain tumors correlates with angiogenesis. *Neurosurgery* (1997) 41(5):1052–9. doi: 10.1097/00006123-199711000-00007

112. Wiese S, Karus M, Faissner A. Astrocytes as a source for extracellular matrix molecules and cytokines. *Front Pharmacol* (2012) 3:120. doi: 10.3389/fphar.2012.00120

113. Zagzag D, Friedlander DR, Miller DC, Dosik J, Cangiarella J, Kostianovsky M, et al. Tenascin expression in astrocytomas correlates with angiogenesis. *Cancer Res* (1995) 55(4):907–14.

114. Zagzag D, Friedlander DR, Dosik J, Chikramane S, Chan W, Greco MA, et al. Tenascin-c expression by angiogenic vessels in human astrocytomas and by human brain endothelial cells in vitro. *Cancer Res* (1996) 56(1):182–9.

115. Schor AM, Canfield AE, Sloan P, Schor SL. Differentiation of pericytes in culture is accompanied by changes in the extracellular matrix. *In Vitro Cell Dev Biol J Tissue Culture Assoc* (1991) 27a(8):651–9. doi: 10.1007/bf02631109

116. Sharifi BG, LaFleur DW, Pirola CJ, Forrester JS, Fagin JA. Angiotensin II regulates tenascin gene expression in vascular smooth muscle cells. *J Biol Chem* (1992) 267(33):23910–5.

117. Tanaka K, Hiraiwa N, Hashimoto H, Yamazaki Y, Kusakabe M. Tenascin-c regulates angiogenesis in tumor through the regulation of vascular endothelial growth factor expression. *Int J Cancer* (2004) 108(1):31–40. doi: 10.1002/ijc.11509

118. Mustafa DA, Dekker LJ, Stingl C, Kremer A, Stoop M, Sillevis Smitt PA, et al. A proteome comparison between physiological angiogenesis and angiogenesis in glioblastoma. *Mol Cell Proteomics MCP* (2012) 11(6):M111.008466. doi: 10.1074/mcp.M111.008466

119. Rosinska S, Gavard J. Tumor vessels fuel the fire in glioblastoma. *Int J Mol Sci* (2021) 22(12):6514. doi: 10.3390/ijms22126514

120. Zagzag D, Shiff B, Jallo GI, Greco MA, Blanco C, Cohen H, et al. Tenascin-c promotes microvascular cell migration and phosphorylation of focal adhesion kinase. *Cancer Res* (2002) 62(9):2660–8.

121. Xia S, Lal B, Tung B, Wang S, Goodwin CR, Laterra J. Tumor microenvironment tenascin-c promotes glioblastoma invasion and negatively regulates tumor proliferation. *Neuro-oncology* (2016) 18(4):507–17. doi: 10.1093/neuonc/nov171

122. Rupp T, Langlois B, Koczorowska MM, Radwanska A, Sun Z, Hussenet T, et al. Tenascin-c orchestrates glioblastoma angiogenesis by modulation of pro- and anti-angiogenic signaling. *Cell Rep* (2016) 17(10):2607–19. doi: 10.1016/j.celrep.2016.11.012

123. Alves TR, da Fonseca AC, Nunes SS, da Silva AO, Dubois LG, Faria J, et al. Tenascin-c in the extracellular matrix promotes the selection of highly proliferative and tubulogenesis-defective endothelial cells. *Exp Cell Res* (2011) 317(15):2073–85. doi: 10.1016/j.yexcr.2011.06.006

124. Kobayashi Y, Yoshida S, Zhou Y, Nakama T, Ishikawa K, Arima M, et al. Tenascin-c promotes angiogenesis in fibrovascular membranes in eyes with proliferative diabetic retinopathy. *Mol Vision* (2016) 22:436–45.

125. Kawamura T, Yamamoto M, Suzuki K, Suzuki Y, Kamishima M, Sakata M, et al. Tenascin-c produced by intestinal myofibroblasts promotes colitis-associated cancer development through angiogenesis. *Inflamm bowel Dis* (2019) 25(4):732–41. doi: 10.1093/ibd/izy368

126. Cai HP, Wang J, Xi SY, Ni XR, Chen YS, Yu YJ, et al. Tenascin-cmediated vasculogenic mimicry formation *via* regulation of MMP2/MMP9 in glioma. *Cell Death Dis* (2019) 10(12):879. doi: 10.1038/s41419-019-2102-3

127. Kang X, Xu E, Wang X, Qian L, Yang Z, Yu H, et al. Tenascin-c knockdown suppresses vasculogenic mimicry of gastric cancer by inhibiting ERK- triggered EMT. *Cell Death Dis* (2021) 12(10):890. doi: 10.1038/s41419-021-04153-1

128. Angel I, Pilo Kerman O, Rousso-Noori L, Friedmann-Morvinski D. Tenascin c promotes cancer cell plasticity in mesenchymal glioblastoma. *Oncogene* (2020) 39(46):6990–7004. doi: 10.1038/s41388-020-01506-6

129. Mirzaei R, Sarkar S, Dzikowski L, Rawji KS, Khan L, Faissner A, et al. Brain tumor-initiating cells export tenascin-c associated with exosomes to suppress T cell activity. *Oncoimmunology* (2018) 7(10):e1478647. doi: 10.1080/2162402x.2018.1478647

130. Huang W, Chiquet-Ehrismann R, Moyano JV, Garcia-Pardo A, Orend G. Interference of tenascin-c with syndecan-4 binding to fibronectin blocks cell adhesion and stimulates tumor cell proliferation. *Cancer Res* (2001) 61(23):8586–94.

131. Martin D, Brown-Luedi M, Chiquet-Ehrismann R. Tenascin-c signaling through induction of 14-3-3 tau. *J Cell Biol* (2003) 160(2):171–5. doi: 10.1083/jcb.200206109

132. Ruiz C, Huang W, Hegi ME, Lange K, Hamou MF, Fluri E, et al. Growth promoting signaling by tenascin-c [corrected]. *Cancer Res* (2004) 64(20):7377–85. doi: 10.1158/0008-5472.Can-04-1234

133. Zhang Q, Xu B, Hu F, Chen X, Liu X, Zhang Q, et al. Tenascin c promotes glioma cell malignant behavior and inhibits chemosensitivity to paclitaxel *via* activation of the PI3K/AKT signaling pathway. *J Mol Neurosci MN* (2021) 71(8):1636–47. doi: 10.1007/s12031-021-01832-8

134. Dang S, Zhang R, Tian S, Hou P, Li G, Ji M. MicroRNA–218 inhibits the malignant phenotypes of glioma by modulating the TNC/AKT/AP–1/TGFβ1 feedback signaling loop. *Int J Mol Med* (2021) 48(5):205. doi: 10.3892/ijmm.2021.5038

135. Hanmin C, Xiangyue Z, Lenahan C, Ling W, Yibo O, Yue H. Pleiotropic role of tenascin-c in central nervous system diseases: From basic to clinical applications. *Front Neurol* (2020) 11:576230. doi: 10.3389/fneur.2020.576230

136. Fujita M, Yamamoto T, Iyoda T, Fujisawa T, Nagai R, Kudo C, et al. Autocrine production of PDGF stimulated by the tenascin-C-Derived peptide TNIIIA2 induces hyper-proliferation in glioblastoma cells. *Int J Mol Sci* (2019) 20(13):3183. doi: 10.3390/ijms20133183

137. Fujita M, Sasada M, Iyoda T, Nagai R, Kudo C, Yamamoto T, et al. Anoikis resistance conferred by tenascin-c-derived peptide TNIIIA2 and its disruption by integrin inactivation. *Biochem Biophys Res Commun* (2021) 536:14–9. doi: 10.1016/j.bbrc.2020.12.050

138. Fujita M, Yamamoto T, Iyoda T, Fujisawa T, Sasada M, Nagai R, et al. Aggressive progression in glioblastoma cells through potentiated activation of integrin α5β1 by the tenascin-C-Derived peptide TNIIIA2. *Mol Cancer Ther* (2019) 18(9):1649–58. doi: 10.1158/1535-7163.Mct-18-1251

139. Seker-Polat F, Pinarbasi Degirmenci N, Solaroglu I, Bagci-Onder T. Tumor cell infiltration into the brain in glioblastoma: From mechanisms to clinical perspectives. *Cancers (Basel)* (2022) 14(2):443. doi: 10.3390/cancers14020443

140. Murphy-Ullrich JE. The de-adhesive activity of matricellular proteins: is intermediate cell adhesion an adaptive state? *J Clin Invest* (2001) 107(7):785–90. doi: 10.1172/jci12609

141. Fiorilli P, Partridge D, Staniszewska I, Wang JY, Grabacka M, So K, et al. Integrins mediate adhesion of medulloblastoma cells to tenascin and activate pathways associated with survival and proliferation. *Lab investigation; J Tech Methods Pathol* (2008) 88(11):1143–56. doi: 10.1038/labinvest.2008.89

142. Bourdon MA, Ruoslahti E. Tenascin mediates cell attachment through an RGD-dependent receptor. *J Cell Biol* (1989) 108(3):1149–55. doi: 10.1083/jcb.108.3.1149

143. Giese A, Loo MA, Norman SA, Treasurywala S, Berens ME. Contrasting migratory response of astrocytoma cells to tenascin mediated by different integrins. *J Cell Sci* (1996) 109(Pt 8):2161–8. doi: 10.1242/jcs.109.8.2161

144. Popova NV, Jucker M. The functional role of extracellular matrix proteins in cancer. *Cancers (Basel)* (2022) 14(1):238. doi: 10.3390/cancers14010238

145. Varga I, Hutóczki G, Szemcsák CD, Zahuczky G, Tóth J, Adamecz Z, et al. Brevican, neurocan, tenascin-c and versican are mainly responsible for the invasiveness of low-grade astrocytoma. *Pathol Oncol Res POR* (2012) 18(2):413–20. doi: 10.1007/s12253-011-9461-0

146. Hirata E, Arakawa Y, Shirahata M, Yamaguchi M, Kishi Y, Okada T, et al. Endogenous tenascin-c enhances glioblastoma invasion with reactive change of surrounding brain tissue. *Cancer Sci* (2009) 100(8):1451–9. doi: 10.1111/j.1349-7006.2009.01189.x

147. Deryugina EI, Bourdon MA. Tenascin mediates human glioma cell migration and modulates cell migration on fibronectin. *J Cell Sci* (1996) 109(Pt 3):643–52. doi: 10.1242/jcs.109.3.643

148. Zhang JF, Tao T, Wang K, Zhang GX, Yan Y, Lin HR, et al. IL-33/ST2 axis promotes glioblastoma cell invasion by accumulating tenascin-c. *Sci Rep* (2019) 9(1):20276. doi: 10.1038/s41598-019-56696-1

149. Lange K, Kammerer M, Saupe F, Hegi ME, Grotegut S, Fluri E, et al. Combined lysophosphatidic acid/platelet-derived growth factor signaling triggers glioma cell migration in a tenascin-c microenvironment. *Cancer Res* (2008) 68(17):6942–52. doi: 10.1158/0008-5472.Can-08-0347

150. Ridley AJ, Schwartz MA, Burridge K, Firtel RA, Ginsberg MH, Borisy G, et al. Cell migration: integrating signals from front to back. *Science* (2003) 302(5651):1704–9. doi: 10.1126/science.1092053

151. Sarkar S, Nuttall RK, Liu S, Edwards DR, Yong VW. Tenascin-c stimulates glioma cell invasion through matrix metalloproteinase-12. *Cancer Res* (2006) 66 (24):11771–80. doi: 10.1158/0008-5472.Can-05-0470

152. Sarkar S, Yong VW. Reduction of protein kinase c delta attenuates tenascin-c stimulated glioma invasion in three-dimensional matrix. *Carcinogenesis* (2010) 31(2):311–7. doi: 10.1093/carcin/bgp297

153. Sarkar S, Zemp FJ, Senger D, Robbins SM, Yong VW. ADAM-9 is a novel mediator of tenascin-c-stimulated invasiveness of brain tumor-initiating cells. *Neuro-oncology* (2015) 17(8):1095–105. doi: 10.1093/neuonc/nou362

154. Fujita M, Sasada M, Iyoda T, Fukai F. Involvement of integrin-activating peptides derived from tenascin-c in cancer aggression and new anticancer strategy using the fibronectin-derived integrin-inactivating peptide. *Molecules (Basel Switzerland)* (2020) 25(14):3239. doi: 10.3390/molecules25143239

155. Ott M, Prins RM, Heimberger AB. The immune landscape of common CNS malignancies: implications for immunotherapy. *Nat Rev Clin Oncol* (2021) 18 (11):729–44. doi: 10.1038/s41571-021-00518-9

156. Zhang P, Liu G, Hu J, Chen S, Wang B, Peng P, et al. Tenascin-c can serve as an indicator for the immunosuppressive microenvironment of diffuse low-grade gliomas. *Front Immunol* (2022) 13:824586. doi: 10.3389/fimmu.2022.824586

157. Wiemann S, Reinhard J, Faissner A. Immunomodulatory role of the extracellular matrix protein tenascin-c in neuroinflammation. *Biochem Soc Trans* (2019) 47(6):1651–60. doi: 10.1042/BST20190081

158. Deligne C, Murdamoothoo D, Gammage AN, Gschwandtner M, Erne W, Loustau T, et al. Matrix-targeting immunotherapy controls tumor growth and spread by switching macrophage phenotype. *Cancer Immunol Res* (2020) 8(3):368–82. doi: 10.1158/2326-6066.CIR-19-0276

159. Gu R, Zhang X, Zhang G, Tao T, Yu H, Liu L, et al. Probing the bi-directional interaction between microglia and gliomas in a tumor microenvironment on a microdevice. *Neurochem Res* (2017) 42(5):1478–87. doi: 10.1007/s11064-017-2204-1

160. Buonfiglioli A, Hambardzumyan D. Macrophages and microglia: the cerberus of glioblastoma. *Acta neuropathologica Commun* (2021) 9(1):54. doi: 10.1186/s40478-021-01156-z

161. Xuan W, Lesniak MS, James CD, Heimberger AB, Chen P. Context-dependent glioblastoma-Macrophage/Microglia symbiosis and associated mechanisms. *Trends Immunol* (2021) 42(4):280–92. doi: 10.1016/j.it.2021.02.004

162. Andersen JK, Miletic H, Hossain JA. Tumor-associated macrophages in gliomas-basic insights and treatment opportunities. *Cancers (Basel)* (2022) 14 (5):1319. doi: 10.3390/cancers14051319

163. Mantovani A, Allavena P, Sica A, Balkwill F. Cancer-related inflammation. *Nature* (2008) 454(7203):436–44. doi: 10.1038/nature07205

164. Murdamoothoo D, Sun Z, Yilmaz A, Riegel G, Abou-Faycal C, Deligne C, et al. Tenascin-c immobilizes infiltrating T lymphocytes through CXCL12 promoting breast cancer progression. *EMBO Mol Med* (2021) 13(6):e13270. doi: 10.15252/emmm.202013270

165. Huang JY, Cheng YJ, Lin YP, Lin HC, Su CC, Juliano R, et al. Extracellular matrix of glioblastoma inhibits polarization and transmigration of T cells: the role of tenascin-c in immune suppression. *J Immunol (Baltimore Md 1950)* (2010) 185 (3):1450–9. doi: 10.4049/jimmunol.0901352

166. Jachetti E, Caputo S, Mazzoleni S, Brambillasca CS, Parigi SM, Grioni M, et al. Tenascin-c protects cancer stem-like cells from immune surveillance by arresting T-cell activation. *Cancer Res* (2015) 75(10):2095–108. doi: 10.1158/0008-5472.Can-14-2346

167. Li ZL, Zhang HL, Huang Y, Huang JH, Sun P, Zhou NN, et al. Autophagy deficiency promotes triple-negative breast cancer resistance to T cell-mediated cytotoxicity by blocking tenascin-c degradation. *Nat Commun* (2020) 11(1):3806. doi: 10.1038/s41467-020-17395-y

168. Derynck R, Weinberg RA. EMT and cancer: More than meets the eye. *Dev Cell* (2019) 49(3):313–6. doi: 10.1016/j.devcel.2019.04.026

169. Nagaharu K, Zhang X, Yoshida T, Katoh D, Hanamura N, Kozuka Y, et al. Tenascin c induces epithelial-mesenchymal transition-like change accompanied by SRC activation and focal adhesion kinase phosphorylation in human breast cancer cells. *Am J Pathol* (2011) 178(2):754–63. doi: 10.1016/j.ajpath.2010.10.015

170. Katoh D, Nagaharu K, Shimojo N, Hanamura N, Yamashita M, Kozuka Y, et al. Binding of αvβ1 and αvβ6 integrins to tenascin-c induces epithelial-mesenchymal transition-like change of breast cancer cells. *Oncogenesis* (2013) 2 (8):e65. doi: 10.1038/oncsis.2013.27

171. Yang Z, Zhang C, Qi W, Cui C, Cui Y, Xuan Y. Tenascin-c as a prognostic determinant of colorectal cancer through induction of epithelial-to-mesenchymal transition and proliferation. *Exp Mol Pathol* (2018) 105(2):216–22. doi: 10.1016/j.yexmp.2018.08.009

172. Yoneura N, Takano S, Yoshitomi H, Nakata Y, Shimazaki R, Kagawa S, et al. Expression of annexin II and stromal tenascin c promotes epithelial to mesenchymal transition and correlates with distant metastasis in pancreatic cancer. *Int J Mol Med* (2018) 42(2):821–30. doi: 10.3892/ijmm.2018.3652

173. Cheng X, Li F, Tao Z. Tenascin-c promotes epithelial-to-mesenchymal transition and the mTOR signaling pathway in nasopharyngeal carcinoma. *Oncol Lett* (2021) 22(1):570. doi: 10.3892/ol.2021.12831

174. Mahabir R, Tanino M, Elmansuri A, Wang L, Kimura T, Itoh T, et al. Sustained elevation of snail promotes glial-mesenchymal transition after irradiation in malignant glioma. *Neuro-oncology* (2014) 16(5):671–85. doi: 10.1093/neuonc/not239

175. Kim Y, Varn FS, Park SH, Yoon BW, Park HR, Lee C, et al. Perspective of mesenchymal transformation in glioblastoma. *Acta neuropathologica Commun* (2021) 9(1):50. doi: 10.1186/s40478-021-01151-4

176. Sadrkhanloo M, Entezari M, Orouei S, Ghollasi M, Fathi N, Rezaei S, et al. STAT3-EMT axis in tumors: Modulation of cancer metastasis, stemness and therapy response. *Pharmacol Res* (2022) 182:106311. doi: 10.1016/j.phrs.2022.106311

177. Carro MS, Lim WK, Alvarez MJ, Bollo RJ, Zhao X, Snyder EY, et al. The transcriptional network for mesenchymal transformation of brain tumours. *Nature* (2010) 463(7279):318–25. doi: 10.1038/nature08712

178. Wang Q, Hu B, Hu X, Kim H, Squatrito M, Scarpace L, et al. Tumor evolution of glioma-intrinsic gene expression subtypes associates with immunological changes in the microenvironment. *Cancer Cell* (2017) 32(1):42–56.e6. doi: 10.1016/j.ccell.2017.06.003

179. Neftel C, Laffy J, Filbin MG, Hara T, Shore ME, Rahme GJ, et al. An integrative model of cellular states, plasticity, and genetics for glioblastoma. *Cell* (2019) 178(4):835–49 e21. doi: 10.1016/j.cell.2019.06.024

180. Miroshnikova YA, Mouw JK, Barnes JM, Pickup MW, Lakins JN, Kim Y, et al. Tissue mechanics promote IDH1-dependent HIF1α-tenascin c feedback to regulate glioblastoma aggression. *Nat Cell Biol* (2016) 18(12):1336–45. doi: 10.1038/ncb3429

181. Barnes JM, Kaushik S, Bainer RO, Sa JK, Woods EC, Kai F, et al. A tension-mediated glycocalyx-integrin feedback loop promotes mesenchymal-like glioblastoma. *Nat Cell Biol* (2018) 20(10):1203–14. doi: 10.1038/s41556-018-0183-3

182. Hara T, Chanoch-Myers R, Mathewson ND, Myskiw C, Atta L, Bussema L, et al. Interactions between cancer cells and immune cells drive transitions to mesenchymal-like states in glioblastoma. *Cancer Cell* (2021) 39(6):779–92.e11. doi: 10.1016/j.ccell.2021.05.002

183. Spenle C, Saupe F, Midwood K, Burckel H, Noel G, Orend G. Tenascin-c: Exploitation and collateral damage in cancer management. *Cell adhesion migration* (2015) 9(1-2):141–53. doi: 10.1080/19336918.2014.1000074

184. Faissner A, Roll L, Theocharidis U. Tenascin-c in the matrisome of neural stem and progenitor cells. *Mol Cell Neurosci* (2017) 81:22–31. doi: 10.1016/j.mcn.2016.11.003

185. Tucic M, Stamenkovic V, Andjus P. The extracellular matrix glycoprotein tenascin c and adult neurogenesis. *Front Cell Dev Biol* (2021) 9:674199. doi: 10.3389/fcell.2021.674199

186. Garcion E, Faissner A, ffrench-Constant C. Knockout mice reveal a contribution of the extracellular matrix molecule tenascin-c to neural precursor proliferation and migration. *Dev (Cambridge England)* (2001) 128(13):2485–96. doi: 10.1242/dev.128.13.2485

187. Czopka T, von Holst A, ffrench-Constant C, Faissner A. Regulatory mechanisms that mediate tenascin c-dependent inhibition of oligodendrocyte precursor differentiation. *J Neurosci Off J Soc Neurosci* (2010) 30(37):12310–22. doi: 10.1523/jneurosci.4957-09.2010

188. Kakinuma Y, Saito F, Osawa S, Miura M. A mechanism of impaired mobility of oligodendrocyte progenitor cells by tenascin c through modification of wnt signaling. *FEBS Lett* (2004) 568(1-3):60–4. doi: 10.1016/j.febslet.2004.05.022

189. Frost E, Kiernan BW, Faissner A, ffrench-Constant C. Regulation of oligodendrocyte precursor migration by extracellular matrix: evidence for substrate-specific inhibition of migration by tenascin-c. *Dev Neurosci* (1996) 18 (4):266–73. doi: 10.1159/000111416

190. Kiernan BW, Götz B, Faissner A, ffrench-Constant C. Tenascin-c inhibits oligodendrocyte precursor cell migration by both adhesion-dependent and adhesion-independent mechanisms. *Mol Cell Neurosci* (1996) 7(4):322–35. doi: 10.1006/mcne.1996.0024

191. Jankovski A, Sotelo C. Subventricular zone-olfactory bulb migratory pathway in the adult mouse: cellular composition and specificity as determined by heterochronic and heterotopic transplantation. *J Comp Neurol* (1996) 371(3):376–96. doi: 10.1002/(sici)1096-9861(19960729)371:3<376::Aid-cne3>3.0.Co;2-

192. Galvao RP, Kasina A, McNeill RS, Harbin JE, Foreman O, Verhaak RG, et al. Transformation of quiescent adult oligodendrocyte precursor cells into malignant glioma through a multistep reactivation process. *Proc Natl Acad Sci USA* (2014) 111(40):E4214–23. doi: 10.1073/pnas.1414389111

193. Shao F, Liu C. Revisit the candidacy of brain cell types as the cell(s) of origin for human high-grade glioma. *Front Mol Neurosci* (2018) 11:48. doi: 10.3389/fnmol.2018.00048

194. Matarredona ER, Pastor AM. Neural stem cells of the subventricular zone as the origin of human glioblastoma stem cells. *Ther Implications. Front Oncol* (2019) 9:779. doi: 10.3389/fonc.2019.00779

195. Chen P, Wang W, Liu R, Lyu J, Zhang L, Li B, et al. Olfactory sensory experience regulates gliomagenesis via neuronal IGF1. *Nature* (2022) 606 (7914):550–6. doi: 10.1038/s41586-022-04719-9

196. Sanai N, Alvarez-Buylla A, Berger MS. Neural stem cells and the origin of gliomas. *N Engl J Med* (2005) 353(8):811–22. doi: 10.1056/NEJMra043666

197. Zheng H, Ying H, Yan H, Kimmelman AC, Hiller DJ, Chen AJ, et al. p53 and pten control neural and glioma stem/progenitor cell renewal and differentiation. *Nature* (2008) 455(7216):1129–33. doi: 10.1038/nature07443

198. Orend G. Potential oncogenic action of tenascin-c in tumorigenesis. *Int J Biochem Cell Biol* (2005) 37(5):1066–83. doi: 10.1016/j.biocel.2004.12.002

199. Schaberg E, Götz M, Faissner A. The extracellular matrix molecule tenascin-c modulates cell cycle progression and motility of adult neural stem/progenitor cells from the subependymal zone. *Cell Mol Life Sci CMLS* (2022) 79 (5):244. doi: 10.1007/s00018-022-04259-5

200. May M, Denecke B, Schroeder T, Götz M, Faissner A. Cell tracking *in vitro* reveals that the extracellular matrix glycoprotein tenascin-c modulates cell cycle length and differentiation in neural stem/progenitor cells of the developing mouse spinal cord. *Biol Open* (2018) 7(7):bio027730. doi: 10.1242/bio.027730

201. Nie S, Gurrea M, Zhu J, Thakolwiboon S, Heth JA, Muraszko KM, et al. Tenascin-c: A novel candidate marker for cancer stem cells in glioblastoma identified by tissue microarrays. *J Proteome Res* (2015) 14(2):814–22. doi: 10.1021/pr5008653

202. Qi J, Esfahani DR, Huang T, Ozark P, Bartom E, Hashizume R, et al. Tenascin-c expression contributes to pediatric brainstem glioma tumor phenotype and represents a novel biomarker of disease. *Acta neuropathologica Commun* (2019) 7(1):75. doi: 10.1186/s40478-019-0727-1

203. Andreiuolo F, Le Teuff G, Bayar MA, Kilday JP, Pietsch T, von Bueren AO, et al. Integrating tenascin-c protein expression and 1q25 copy number status in pediatric intracranial ependymoma prognostication: A new model for risk stratification. *PloS One* (2017) 12(6):e0178351. doi: 10.1371/journal.pone.0178351

204. Pedretti M, Verpelli C, Mårlind J, Bertani G, Sala C, Neri D, et al. Combination of temozolomide with immunocytokine F16-IL2 for the treatment of glioblastoma. *Br J Cancer* (2010) 103(6):827–36. doi: 10.1038/sj.bjc.6605832

205. Silacci M, Brack SS, Späth N, Buck A, Hillinger S, Arni S, et al. Human monoclonal antibodies to domain c of tenascin-c selectively target solid tumors in vivo. *Protein engineering design selection PEDS* (2006) 19(10):471–8. doi: 10.1093/protein/gzl033

206. Nadal L, Corbellari R, Villa A, Weiss T, Weller M, Neri D, et al. Novel human monoclonal antibodies specific to the alternatively spliced domain d of tenascin c efficiently target tumors in vivo. *mAbs* (2020) 12(1):1836713. doi: 10.1080/19420862.2020.1836713

207. Lingasamy P, Tobi A, Haugas M, Hunt H, Paiste P, Asser T, et al. Bi-specific tenascin-c and fibronectin targeted peptide for solid tumor delivery. *Biomaterials* (2019) 219:119373. doi: 10.1016/j.biomaterials.2019.119373

208. Lingasamy P, Tobi A, Kurm K, Kopanchuk S, Sudakov A, Salumäe M, et al. Tumor-penetrating peptide for systemic targeting of tenascin-c. *Sci Rep* (2020) 10 (1):5809. doi: 10.1038/s41598-020-62760-y

209. Kang T, Zhu Q, Jiang D, Feng X, Feng J, Jiang T, et al. Synergistic targeting tenascin c and neuropilin-1 for specific penetration of nanoparticles for anti-glioblastoma treatment. *Biomaterials* (2016) 101:60–75. doi: 10.1016/j.biomaterials.2016.05.037

210. Reardon DA, Zalutsky MR, Akabani G, Coleman RE, Friedman AH, Herndon JE2nd, et al. A pilot study: 131I-antitenascin monoclonal antibody 81c6 to deliver a 44-gy resection cavity boost. *Neuro-oncology* (2008) 10(2):182–9. doi: 10.1215/15228517-2007-053

211. Reulen HJ, Poepperl G, Goetz C, Gildehaus FJ, Schmidt M, Tatsch K, et al. Long-term outcome of patients with WHO grade III and IV gliomas treated by fractionated intracavitary radioimmunotherapy. *J Neurosurg* (2015) 123(3):760–70. doi: 10.3171/2014.12.Jns142168

212. Reardon DA, Zalutsky MR, Bigner DD. Antitenascin-c monoclonal antibody radioimmunotherapy for malignant glioma patients. *Expert Rev Anticancer Ther* (2007) 7(5):675–87. doi: 10.1586/14737140.7.5.675

213. Daniels DA, Chen H, Hicke BJ, Swiderek KM, Gold L. A tenascin-c aptamer identified by tumor cell SELEX: systematic evolution of ligands by exponential enrichment. *Proc Natl Acad Sci United States America* (2003) 100 (26):15416–21. doi: 10.1073/pnas.2136683100

214. Chen H, Zheng X, Di B, Wang D, Zhang Y, Xia H, et al. Aptamer modification improves the adenoviral transduction of malignant glioma cells. *J Biotechnol* (2013) 168(4):362–6.

215. Migliorini D, Dutoit V, Allard M, Grandjean Hallez N, Marinari E, Widmer V, et al. Phase I/II trial testing safety and immunogenicity of the multipeptide IMA950/poly-ICLC vaccine in newly diagnosed adult malignant astrocytoma patients. *Neuro-oncology* (2019) 21(7):923–33. doi: 10.1093/neuonc/noz040

216. Zukiel R, Nowak S, Wyszko E, Rolle K, Gawronska I, Barciszewska MZ, et al. Suppression of human brain tumor with interference RNA specific for tenascin-c. *Cancer Biol Ther* (2006) 5(8):1002–7. doi: 10.4161/cbt.5.8.2886

217. Wyszko E, Rolle K, Nowak S, Zukiel R, Nowak M, Piestrzeniewicz R, et al. A multivariate analysis of patients with brain tumors treated with ATN-RNA. *Acta poloniae Pharm* (2008) 65(6):677–84.

218. Rolle K, Nowak S, Wyszko E, Nowak M, Zukiel R, Piestrzeniewicz R, et al. Promising human brain tumors therapy with interference RNA intervention (iRNAi). *Cancer Biol Ther* (2010) 9(5):396–406. doi: 10.4161/cbt.9.5.10958

frontiers | Frontiers in Oncology

TYPE Original Research
PUBLISHED 12 August 2022
DOI 10.3389/fonc.2022.978006

Check for updates

OPEN ACCESS

EDITED BY
Shaoquan Zheng,
Sun Yat-sen University Cancer Center (SYSUCC), China

REVIEWED BY
Dongfeng Qu,
University of Oklahoma Health Sciences Center, United States
Guopei Zheng,
Guangzhou Medical University Cancer Hospital, China
Xiaofang Guo,
University of South Florida, United States

*CORRESPONDENCE
Anliu Tang
tanganliuxy3@csu.edu.cn

†These authors have contributed equally to this work

SPECIALTY SECTION
This article was submitted to Molecular and Cellular Oncology, a section of the journal Frontiers in Oncology

RECEIVED 25 June 2022
ACCEPTED 25 July 2022
PUBLISHED 12 August 2022

CITATION
Chen B, Zhang L, Zhou H, Ye W, Luo C, Yang L, Fang N and Tang A (2022) HMOX1 promotes lung adenocarcinoma metastasis by affecting macrophages and mitochondrion complexes. *Front. Oncol.* 12:978006. doi: 10.3389/fonc.2022.978006

COPYRIGHT
© 2022 Chen, Zhang, Zhou, Ye, Luo, Yang, Fang and Tang. This is an open-access article distributed under the terms of the Creative Commons Attribution License (CC BY). The use, distribution or reproduction in other forums is permitted, provided the original author(s) and the copyright owner(s) are credited and that the original publication in this journal is cited, in accordance with accepted academic practice. No use, distribution or reproduction is permitted which does not comply with these terms.

HMOX1 promotes lung adenocarcinoma metastasis by affecting macrophages and mitochondrion complexes

Bo Chen[1,2†], Liyang Zhang[1,2†], Hongshu Zhou[1,2], Wenrui Ye[1,2], Cong Luo[2,3], Liting Yang[1,2], Ning Fang[4,5] and Anliu Tang[4,5*]

[1]Department of Neurosurgery, Xiangya Hospital, Central South University, Changsha, China, [2]National Clinical Research Center for Geriatric Disorders, Xiangya Hospital, Central South University, Changsha, China, [3]Department of Urology, Xiangya Hospital, Central South University, Changsha, China, [4]Department of Gastroenterology, The Third Xiangya Hospital of Central South University, Changsha, China, [5]Hunan Key Laboratory of Nonresolving Inflammation and Cancer, Central South University, Changsha, China

Background: Metastasis is the leading cause of lung adenocarcinoma (LUAD) patient death. However, the mechanism of metastasis is unclear. We performed bioinformatic analyses for HMOX1 (Heme oxygenase-1), aiming to explore its role in LUAD metastasis.

Methods: Pan-cancer analysis was first used to identify the metastasis-associated role of HMOX1 in LUAD. HMOX1-related genomic alterations were then investigated. Based on functional enrichment, we systematically correlated HMOX1 with immunological characteristics and mitochondrial activities. Furthermore, weighted gene co-expression network analysis (WGCNA) was applied to construct the HMOX1-mediated metastasis regulatory network, which was then validated at the proteomic level. Finally, we conducted the survival analysis and predicted the potential drugs to target the HMOX1 network.

Results: HMOX1 expression was significantly associated with epithelial-mesenchymal transition (EMT) and lymph and distant metastasis in LUAD. High HMOX1 levels exhibited higher macrophage infiltration and lower mitochondrial complex expression. WGCNA showed a group of module genes co-regulating the traits mentioned above. Subsequently, we constructed an HMOX1-mediated macrophage-mitochondrion-EMT metastasis regulatory network in LUAD. The network had a high inner correlation at the proteomic level and efficiently predicted prognosis. Finally, we predicted 9 potential drugs targeting HMOX1-mediated metastasis in LUAD, like chloroxine and isoliquiritigenin.

Conclusions: Our analysis elaborates on the role of HMOX1 in LUAD metastasis and identified a highly prognostic HMOX1-mediated metastasis regulatory network. Novel potential drugs targeting the HMOX1 network were also

proposed, which should be tested for their activity against LUAD metastasis in future studies.

KEYWORDS

HMOX1, lung adenocarcinoma, metastasis, prognostic model, drug prediction

Introduction

Lung cancer is histologically divided into small cell lung cancer (SCLC, 15% patients) and non-small cell lung cancer (NSCLC, 85% of patients). NSCLC has been classified into three types: adenocarcinoma, squamous cell carcinoma, and large cell. Lung adenocarcinoma (LUAD) is the most common subtype of NSCLC and represents nearly 40% of all lung cancers (1). Frustratingly, only 26% of LUAD and squamous cell carcinoma patients survive 5 years after diagnosis (2). LUAD is often detected at the metastatic stage with prevalence in bone and nervous system (3), and metastasis is the cause of most LUAD patient deaths. Even with therapy, the 5-year relative survival rate for patients suffering metastasis is approximately 6% (2). Unfortunately, the mechanism of LUAD metastasis remains largely unknown, limiting the development of therapeutic drugs.

The process of cancer metastasis mainly consists of 5 essential steps: invasion, intravasation, circulation, extravasation, and colonization (4). At the metastasis initiation stage, epithelial-mesenchymal transition (EMT), a dynamic process where cells abandon their epithelial features and transform into a more mesenchymal phenotype, exerts a vital role (5). EMT is considered as a common characteristic for disseminated tumor cells and circulating tumor cells (6), and EMT cells modulate immune system processes. Cells undergoing EMT can alter the tumor immune microenvironment, which in further induces the EMT process. Many immune cells, like macrophages, neutrophils, T cells, and others, have the potential to promote EMT and further accelerate tumor metastasis (7). In addition, EMT requires a huge energy supply from mitochondria, and inhibition of the mitochondrial complex can hinder tumor growth and metastasis (8).

Heme oxygenase-1 (HMOX1) is an inducible intracellular enzyme to degrade heme, expressed in both malignant tumor cells and tumor-associated macrophages (TAMs) (9). At the level of organelles, HMOX1 mainly localizes to the endoplasmic reticulum, mitochondrion, and others (10, 11). Intrinsically, HMOX1 activity provides cytoprotective effects, including anti-oxidation, anti-apoptosis, and heme clearance. However, HMOX1 has also been demonstrated to promote tumor progression and metastasis in multiple cancers such as glioma, colorectal cancer, melanoma, breast cancer, and others (9). In addition, HMOX1 is functionally associated with TAM polarization and mitochondrial dysfunction (12, 13). Currently, pharmacological inhibition of HMOX1 is considered a promising therapeutic approach to hinder tumor metastasis. However, the role of HMOX1 in metastasis still remains unclear and needs to be fully elucidated (9).

This study aimed to elaborate on the role of HMOX1 in LUAD metastasis through multi-omics analyses including genomics, transcriptomics, and proteomics. The association between HMOX1 and LUAD metastasis was first identified by its relationship to EMT, lymph, and distant metastasis. Next, we investigated associations with the immune microenvironment and mitochondrial pathways and constructed an HMOX1-mediated macrophage-mitochondrion-EMT metastasis regulatory network by weighted gene co-expression network analysis (WGCNA). A prognostic model of the regulatory network was then developed. Potential drugs, like chloroxine and isoliquiritigenin, were also predicted to inhibit the HMOX1-mediated LUAD metastasis.

Methods

Supplemental Figure 1 shows the workflow of this research.

Data collection and preprocessing

The transcriptome data: the Cancer Genome Atlas (TCGA) pan-cancer data and 4 Gene Expression Omnibus (GEO) LUAD cohorts (GSE11969, GSE31210, GSE42127, GSE68465) with their clinical information were separately downloaded from the UCSC Xena and the GEO data portals (https://portal.gdc.cancer.gov/, https://www.ncbi.nlm.nih.gov/geo/). The FPKM value of TCGA sequencing data was transformed into the TPM value. GEO microarray data had 3 different platforms: Illumina, Agilent, and Affymetrix. The normalized microarray data from Illumina maintained the original format. The raw microarray data from Agilent and Affymetrix were processed using the "limma" and "oligo" packages, separately. In addition,

the LUAD genome data, including somatic copy number alternations (CNAs) and mutations, which corresponded to the cases with the transcriptome data, were downloaded from the TCGA database. The proteomic data with paired mRNA datasets were obtained from the National Cancer Institute's Clinical Proteomic Tumor Analysis Consortium (CPTAC) portal (https://proteomics.cancer.gov/data-portal). The detailed information of these datasets was listed in Table 1.

Tumor metastasis

Tumor metastasis potential was evaluated by analysis of EMT, lymph metastasis, and distant metastasis. We collected 77 EMT signatures from a previous study (14). Mesenchymal and epithelial phenotypes were identified by signature gene expression and quantified by Gene Set Variation Analysis scores (GSVA) (15). Furthermore, we identified the lymph and distant metastasis according to pathological TMN staging (N0: no lymph metastasis, N1 – 3: lymph metastasis; M0: no distant metastasis; M1: distant metastasis). To confirm the role of HMOX1 in modulating tumor metastasis, we analyzed the correlation between HMOX1 and metastasis characteristics mentioned above in the terms of pan-cancer and LUAD. In addition, we investigated the HMOX1 expression disparity in primary tumors and multiple metastasis sites in the Human Cancer Metastasis Database (HCMDB, http://hcmdb.i-sanger.com/index).

Genomic alteration

We used cBioPortal (http://www.cbioportal.org/) to identify the CNA and mutation frequency of HOMX1 in the LUAD. Subsequently, we compared the genomic features of LUAD patients with different HMOX1 expression levels in the TCGA database. Arm- and focal-level somatic CNAs were calculated using GISTIC 2.0 (https://cloud.genepattern.org/). Significantly mutated genes and their interaction effect were identified using maftools.

TABLE 1 The datasets used in this study.

Data source	Omics category	Platform	Sample count
TCGA (pan-cancer)	mRNA	Illumina HiSeq 2000	10277
TCGA (LUAD)	mRNA	Illumina HiSeq 2000	515
TCGA (LUAD)	genome	Affymetrix SNP 6.0	516
GSE11969	mRNA	Agilent Homo 2.16 K	90
GSE31210	mRNA	Affymetrix Plus 2.0	226
GSE42127	mRNA	Illumina WG-6 V3.0	133
GSE68465	mRNA	Affymetrix U133A	441
CPTAC	mRNA	Illumina Hiseq 4000	111
CPTAC	protein	Tandem mass tags	111

Functional annotation

To explore other HMOX1-related functional phenotypes, we performed functional annotation for HMOX1. The 33.3th and 66.6th percentiles of HMOX1 expression were set as the cutoffs to divide LUAD patients into low, medium, and high groups. The differentially expressed genes (DEGs) between the low and high groups were screened using the "limma" package ($P < 0.05$). Subsequently, the biological functions of DEGs were annotated by Gene Ontology (GO) and Kyoto Encyclopedia of Genes and Genomes (KEGG).

Immune infiltration

Immune cells can contribute to tumor EMT, invasion, and metastasis. We first investigated 7 cancer immunity cycles in LUAD as previously reported (16). Next, the immunocyte infiltration was estimated at the Cancer Immunome Atlas (TCIA, https://tcia.at/home) and TIMER2.0 (http://timer.cistrome.org/). To reduce the estimation mistakes, we comprehensively applied 9 different algorithms: GSEA (NES>0, FDR<0.1; TCIA website), CIBERSORT, CIBERSORT-ABS, QUANRISEQ, XCELL, TIDE, EPIC, TIMER, MCPCOUNTER (TIMER2.0 website). In addition, we also investigated the expression of immunocyte effector genes and 22 immune checkpoint markers according to the previous work (16). To explore the role of HMOX1 in LUAD immune regulation, we performed the correlation analysis between the HMOX1 and immune characteristics with respect to the above.

Mitochondrion

Mitochondria play a crucial role in tumor cell migration, invasion, and metastasis (17). We downloaded 41 mitochondria-related pathways from the MITOCARTA3.0 database (https://www.broadinstitute.org/mitocarta/mitocarta30-inventory-mammalian-mitochondrial-proteins-and-pathways). The enrichment scores of these pathways were calculated using the "GSVA" package (15). Subsequently, we further analyzed the expression of 5 mitochondrial complexes in LUAD by feature genes and pathway enrichment.

Co-regulatory network construction

To explore the correlation between HMOX1-mediated metastasis and other functional phenotypes, we performed weighted gene co-expression network analysis using the "WGCNA" package. A power of $\beta = 6$ and a scale-free $R^2 = 0.98$ was set to attain a scale-free topology network. We extracted the closest-associated module with HMOX1 expression, EMT

traits, macrophage infiltration, and mitochondrial complex level, which was assumed to be the key module involved in LUAD metastasis. The gene function of the key module was analyzed by GO enrichment.

Next, we intersected the module genes in the key module and phenotype feature genes. The signature genes of EMT and mitochondrial complex have been mentioned above. The macrophage signature genes were derived from the top 5 macrophage terms in the GO enrichment. The intersected genes were then imported into the STRING database with the minimum required interaction score of 0.4 (https://www.string-db.org/). Protein-protein network was further visualized by Cytoscape software (version 3.9.0).

Proteomic analysis

For proteomics, we first performed a differential protein expression analysis between the high and low HMOX1 groups (the student's t-test, $P < 0.05$). GO functional enrichment was then conducted. In terms of the paired sample mRNAs, we estimated the expression level of EMT, mitochondrial complex, and macrophage using the aforementioned methods. After that, we applied the disparity comparison and correlation analysis to the phenotype scores and feature gene expression, to explore the inner correlation of the HMOX1-mediated macrophage-mitochondrion-EMT network at the protein level.

Survival analysis

The TCGA-LUAD cohort was randomly divided into the training set and internal validation set, with a ratio of 7:3. The 4 GEO cohorts were selected as external validation sets. In the training set, we conducted the univariate Cox regression in the HMOX1-mediated metastasis regulatory network and its neighbor genes. Next, the least absolute shrinkage and selection operator (Lasso) algorithm was used to screen genes with optimal prognosis prediction ability. We then developed risk scores using these genes as follows:Σ regression coefficient * gene expression. The optimal cut-off was ascertained to divide the high and low groups by the surv_cutpoint function of the "survminer" packages. Kaplan-Meier curves with the log-rank test were then used to compare survival rates between the two groups. The predictive ability of risk scores was also assessed by the AUC values.

Furthermore, univariate and multivariate Cox regressions were applied to assess the independent prognostic ability of the risk score and other clinical variables. A nomogram consisting of independent prognostic factors was developed using the "rms" package and internally and externally validated by calibration and ROC curves.

Small molecular drug analysis

The Connectivity Map (CMAP) website (https://clue.io/) was applied to explore small molecule drugs with the potential to inhibit HMOX1-mediated LUAD metastasis. The genes in the co-regulatory network were uploaded. The drugs with negative Raw_cs and high fdr_q_nlog10 values were considered as potential therapeutic agents because they could suppress the expression of these genes.

Statistical analysis

For continuous variables, the Wilcoxon test was used to examine the difference between binary groups while the Kruskal-Wallis test was employed for multiple groups. Categorical variables were compared using Fisher's exact test. In addition, the correlation between variables was examined by the Spearman coefficient. All statistical tests were two-sided and $P < 0.05$ was considered statistically significant. Statistical analysis and data visualization was conducted using R version 4.1.2, Matlab version 2021, and Sangerbox version 3.0 (http://vip.sangerbox.com/home.html).

Results

HMOX1 is correlated to metastasis across cancer types and in LUAD

Pan-cancer analyses were performed to investigate the role of HMOX1 in metastasis regulation. Our findings showed that HMOX1 was positively associated with a mesenchymal-like phenotype and was negatively associated with an epithelial phenotype in most tumors, including LUAD (Figures 1A–C). In addition, tumors with lymph node and/or distant metastasis had significantly higher HMOX1 expression than tumors without metastasis, including prostate adenocarcinoma (PRAD) and LUAD (Figures 1D, E). HCMDB data unveiled that HMOX1 was extensively differentially expressed in the multiple types of metastasis comparisons (primary tumors with metastasis *vs.* primary tumors without metastasis; primary tumors *vs.* metastatic tumors; metastatic tumors with different metastasis sites) in the various tumors, including LUAD (Figure 1F).

Next, we focused on LUAD and divided the patients into low, medium, and high groups according to the HMOX1 expression. Heatmap and violin plots showed that the high HMOX1 group had higher expression of the mesenchymal phenotype, followed by the medium and low groups. The opposite trend was observed for the epithelial phenotype (Figures 2A, B). Furthermore, we compared the clinical traits and found that the proportions of patients with squamoid

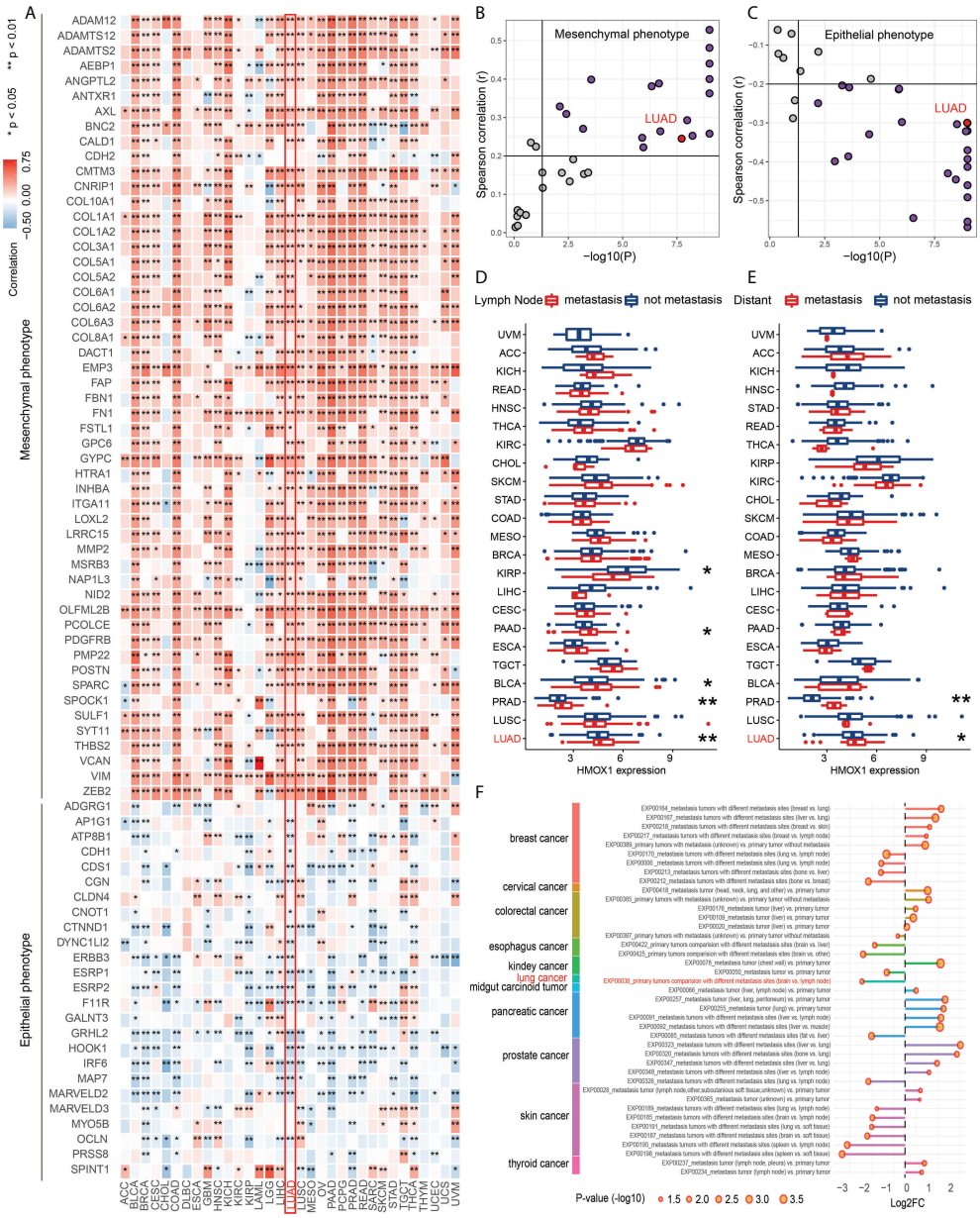

FIGURE 1
The effect of HMOX1 on metastasis across cancer types. **(A)** Correlation between HMOX1 and 77 epithelium-mesenchymal transition (EMT) signature genes. **(B)** Correlation between HMOX1 and mesenchymal phenotype scoring. **(C)** Correlation between HMOX1 and epithelial phenotype scoring. **(D)** Difference in HMOX1 expression between lymph node metastasis and without metastasis groups. **(E)** Difference in HMOX1 expression between distant metastasis and without metastasis groups **(F)** Multiple types of metastasis comparisons for the HMOX1 expression in the HCMDB database. *P < 0.05; **P < 0.01.

subtype, lymph node metastasis, and distant metastasis in the high and medium HMOX1 groups were higher than those in the low group (Figure 2C). Survival analysis suggested that low HMOX1 samples showed a better disease-specific survival (DSS) prognosis than medium and high samples in LUAD. However, we failed to observe the statistical difference among the three groups in overall survival (OS), disease-free interval (DFI), and progress-free interval (PFI) comparisons (Figure 2D).

HMOX1 is associated with novel genomic alterations in LUAD

cBioPortal data showed that the frequency of HMOX1 CNAs and mutations was only 1.5% in the LUAD (Figure 3A). Therefore, we did not focus on self-genomic alterations of HMOX1, and investigated the HMOX1-related alterations in the high, medium, and low HMOX1 groups. A global arm-and focal-level CNA profile was obtained by comparing the three groups (Figures 3B, C). The enriched mutation landscape of the three groups was displayed in waterfall plots. The missense mutation was the predominant mutation type (Figure 3D). Next, we compared the differentially mutated genes between the high and low HMOX1 groups. High HMOX1 groups had significantly higher frequency of mutations to HECW1, THSD7A, TRPM6, FRAS1, PTPRC, and others. Low HMOX1

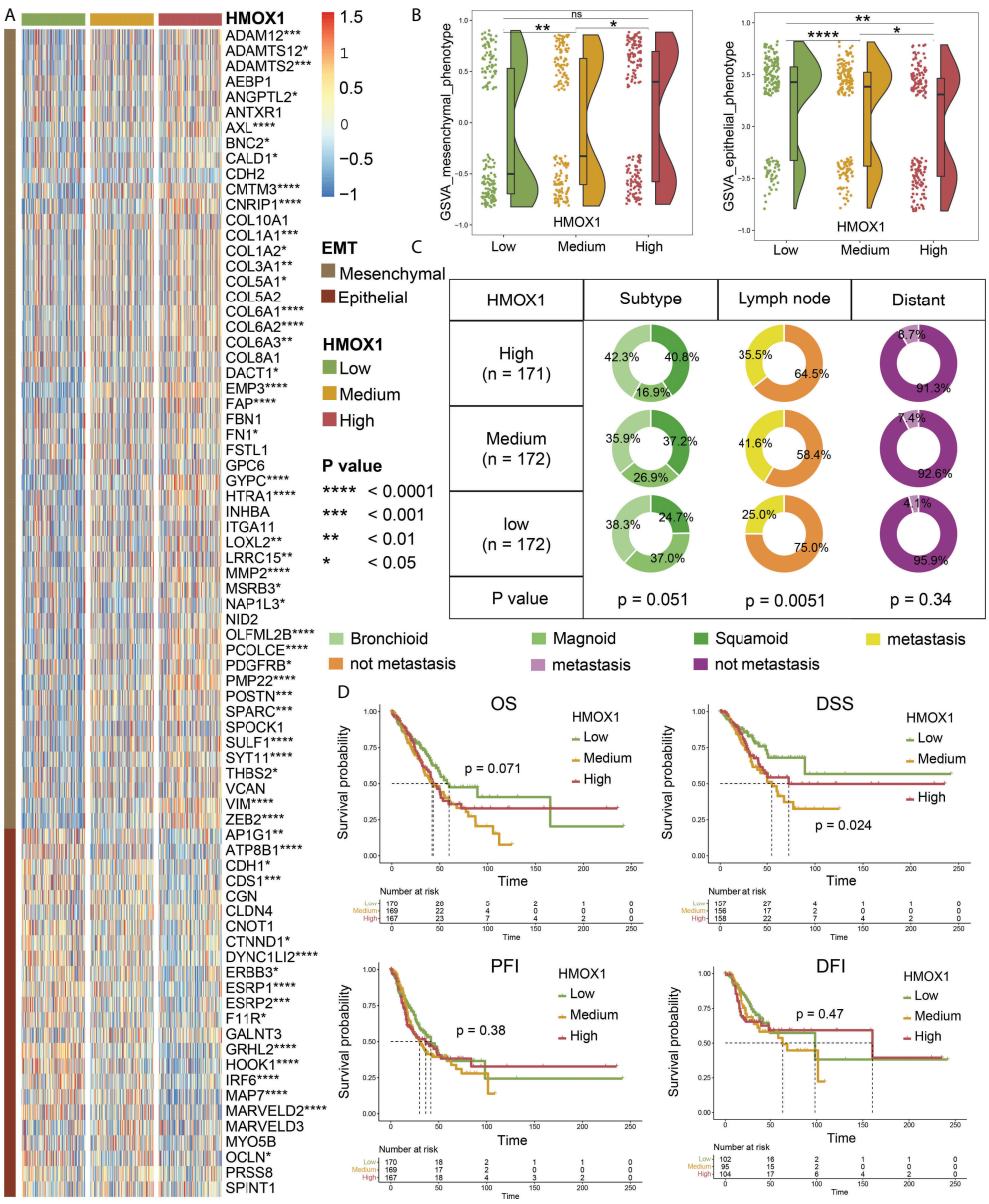

FIGURE 2
The effect of HMOX1 on metastasis in lung adenocarcinoma (LUAD). **(A)** Differences in the expression of EMT signature genes among high, medium, and low HMOX1 groups. **(B)** Differences in the EMT scoring between high, medium, and low HMOX1 groups. **(C)** Differences in the LUAD subtype, lymph node metastasis, and distant metastasis among high, medium, and low HMOX1 groups. **(D)** Survival analyses for the high, medium, and low HMOX1 groups. OS, overall survival; DSS, disease-specific survival; PFI, progress-free interval; DFI, disease-free interval. NS, not significant; *P < 0.05; ** P< 0.01; ***P < 0.001; ****P < 0.0001.

groups had significantly higher frequency of mutations in EGFR, OVCH1, KEAP1, and PTPRT (Figure 3E). The strongest co-occurrent pairs of gene mutation in the high HMOX1 group were PTPRC - TEX15 and PTPRC - SLITRK4 (Figure 3F). In addition, we displayed the mutation frequency distribution of these genes in the three groups (Figure 3G).

HMOX1-high LUAD is functionally enriched in immune and mitochondrial pathways

To explore other HMOX1-related phenotypes that may affect LUAD metastasis, we performed functional enrichment for DEGs between the high- and low-HMOX1 groups. In the GO analysis, DEGs were notably enriched in macrophage activation, macrophage migration, regulation of mitochondrion organization, apoptotic mitochondrial changes, and similar pathways (Supplemental Figure 2A). Among KEGG pathways, the most enriched were phagosome, Th17 cell differentiation, antigen processing and presentation, and others (Supplemental Figure 2B). Therefore, we investigated immune infiltration and mitochondrial processes in LUAD.

HMOX1 is correlated with immune infiltration and immune checkpoint in LUAD

For the high HMOX1 group, activities of the majority of the cancer-immune cycles were found to be up-regulated, including release of cancer antigens (step1), cancer antigen presentation (step 2), priming and activation (step 3), trafficking of immune cells to tumors (step 4, like CD4 T cell, CD8 T cell, macrophage, monocyte, Treg cell), and infiltration of immune cells into tumors (step 5). Interestingly, no statistical difference in the killing of cancer cells (step 7) was observed among the three HMOX1 groups (Figure 4A). Next, we calculated the level of immunocyte infiltration in LUAD by 9 algorithms. GSEA algorithms of TCIA showed that more immune cells, like type 2 T helper cells, regulatory T cells, macrophages, central memory CD8 T cells, activated CD4 T cells, and others were up-regulated in the high HMOX1 group, followed by the medium- and low-groups (Figure 4B). Another 8 algorithms showed that HMOX1 was positively associated with the infiltration level of macrophages, but not CD4 T cells, CD8 T cells, Tregs, or neutrophils (Figure 4C, and Supplemental Figures 3-7). Similarly, HMOX1 was found to be positively correlated to the effector genes of macrophages (Figure 4D). In addition, we found that HMOX1 expression was positively associated with a majority of immune checkpoint inhibitors, including LAIR1, TIM-3, CD86, and PD-L1 (Figure 4E).

Mitochondrional complexes are altered in HMOX1 high LUAD

We then proceeded to investigate the correlation between mitochondrial characteristics and HMOX1 expression in LUAD. Followed by the medium and low HMOX1 groups, the high HMOX1 group had significantly up-regulated expression of cytochrome C and apoptosis, and down-regulated expression of OXPHOS assembly factors, complexV, fission, translation, mtRNA metabolism, carbohydrate metabolism, and others (Figure 5A). Owing to the crucial role of mitochondrial complexes in tumor metastasis (8), we next focused on the analysis of mitochondrial complexes. The heatmap showed the expression disparity of feature genes for five mitochondrial complexes in the three HMOX1 groups (Figure 5B). The radar diagrams display the correlation between the feature gene and HMOX1 expression (Figure 5C). Overall, the high HMOX1 group had significantly less expression of complex I, complex II, and complex IV compared to the medium group, and significantly less expression of complex V compared to the low and medium group (Figure 5D).

Construction of an HMOX1-mediated macrophage-mitochondrion-EMT metastasis regulatory network

Considering that mitochondrion complex, macrophage, and metastasis are all related to HMOX1 expression, we sought to perform the WGCNA co-expression analysis to identify the relationship among these. A power $\beta = 6$ was selected as the software threshold for scale-free network construction (Figure 6A). Twenty-one modules were identified by clustering dendrogram (Figure 6B). HMOX1, EMT, macrophage, and the mitochondrial complex had the same highly correlated module – brown, indicating strong associations among these traits (Figure 6C). The brown module was positively associated with HMOX1, mesenchymal phenotype, and macrophages, and negatively correlated to epithelial phenotype and mitochondrial complex (Figure 6D). GO enrichment indicated that genes in the brown module mainly focused on macrophage activation, macrophage migration, mitochondrial calcium ion homeostasis, mesenchymal cell differentiation, and the like (Figure 6E).

After identifying the correlation, we used the brown module genes to construct a PPI network among these phenotype traits. In the HMOX1-mediated metastasis regulatory network, a total of 8 genes were involved in EMT, 5 were correlated to mitochondrial complex, and 67 were associated with macrophage (Figure 6F). By analyzing the PPI interaction, we found that HMOX1 connected the macrophage and mitochondrial complex, the mitochondrial complex interacted

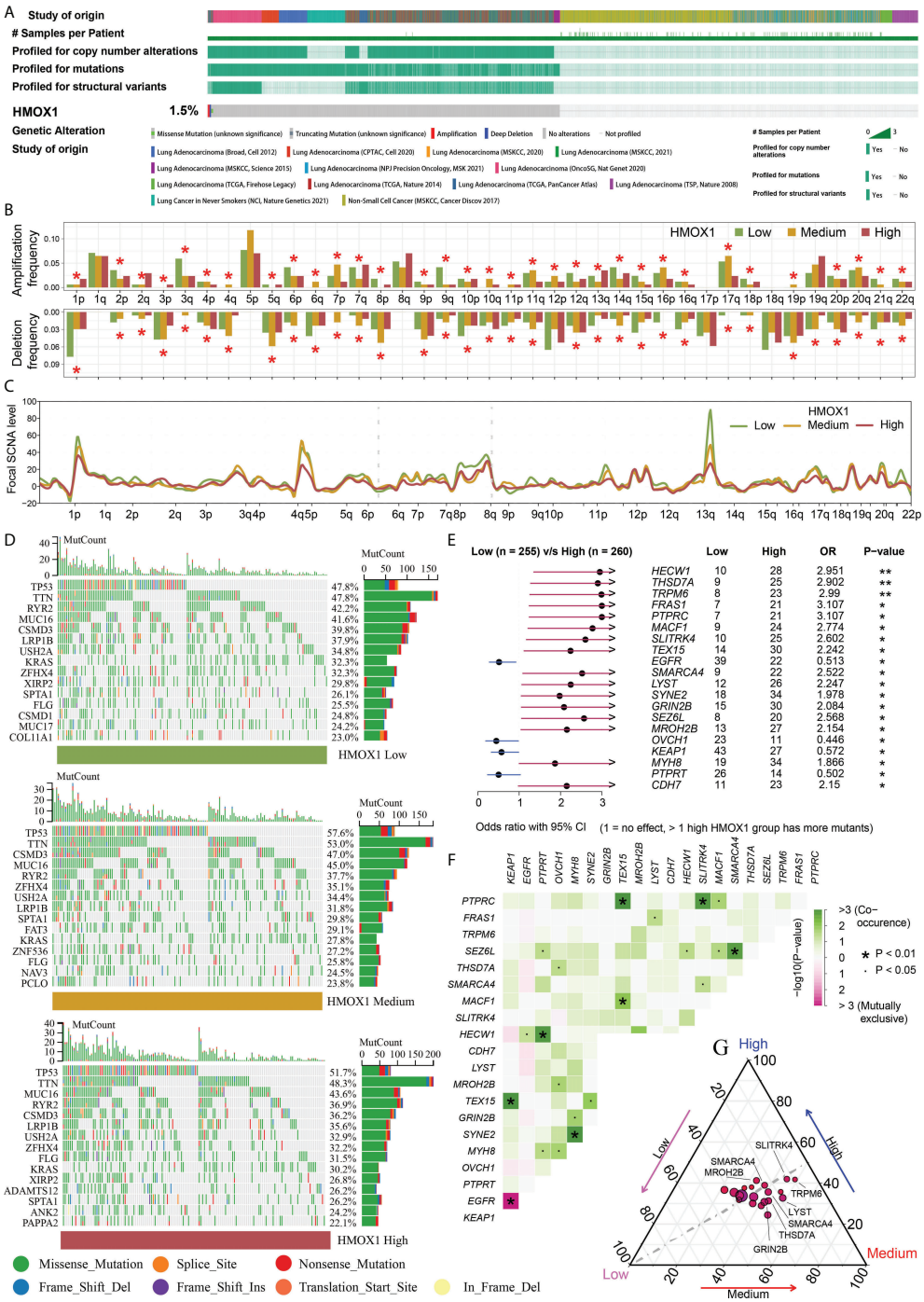

FIGURE 3
Genomic features of different HMOX1 groups. **(A)** The frequency of HMOX1 copy number alterations (CNAs) and mutations in the cBioPortal database. **(B)** Comparison of arm-level amplification and deletion frequencies among the high, medium, and low HMOX1 groups. **(C)** Comparison of focal-level amplification and deletion frequencies among the high, medium, and low HMOX1 groups. **(D)** The waterfall plots showing the mutation landscapes in the high, medium, and low HMOX1 groups. **(E)** The forest plot listing the top 20 most differentially mutated genes between the high and low HMOX1 groups. **(F)** The heatmap showing the concurrence or mutual exclusivity of these 20 mutated genes between the high and low HMOX1 groups. **(G)** The ternary plot showing the mutation frequency distribution of these 20 genes among the high, medium, and low HMOX1 groups. *P < 0.05; **P < 0.01.

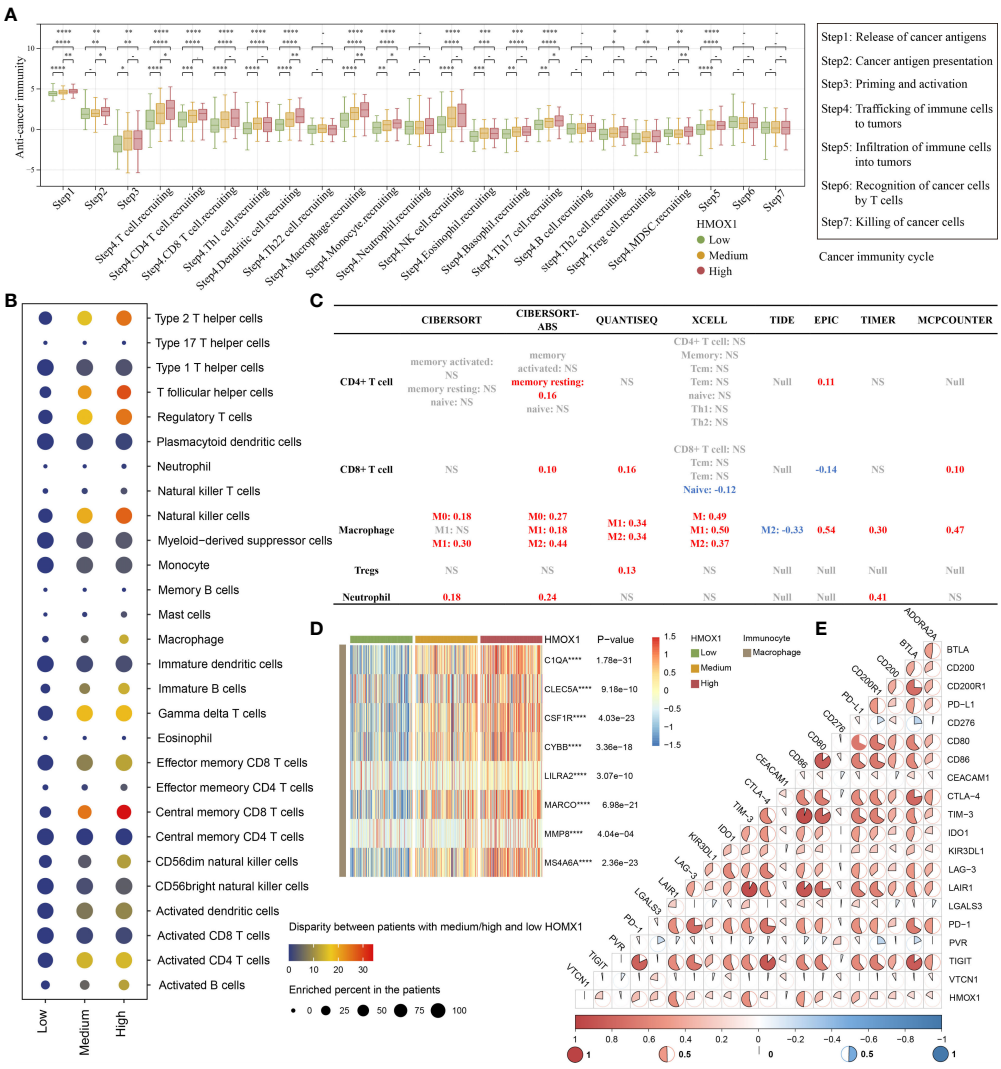

FIGURE 4
The effect of HMOX1 on the immune microenvironment in LUAD. **(A)** Differences in multiple steps of the cancer immunity cycles between the high, medium, and low HMOX1 groups. **(B)** Differences in the infiltration levels of 28 types of immunocytes among the high, medium, and low HMOX1 groups, which were calculated using the GSEA algorithms. **(C)** Correlation between HMOX1 and the infiltration levels of 5 types of immunocytes (CD4+ T cells, CD8+ T cells, macrophages, Tregs, and neutrophils), which were calculated using 8 algorithms. **(D)** Differences in the effector genes of macrophages among the high, medium, and low HMOX1 groups. **(E)** Correlation between HMOX1 and 20 inhibitory immune checkpoints. NS, not significant; *P < 0.05; **P < 0.01; ***P < 0.001; ****P < 0.0001.

with macrophage, and macrophage linked to EMT. However, the interaction between EMT and mitochondrial complex was not observed. (Figure 6G).

Proteomic analysis for the HMOX1-mediated macrophage-mitochondrion-EMT metastasis regulatory network

By comparing the high and low HMOX1 group, 1481 down-regulated proteins and 1559 up-regulated proteins were obtained (Figure 7A). GO analysis showed that these differentially expressed proteins were enriched in the electron transport chain, mitochondrial respiratory chain complex assembly, macrophage activation, epithelial to mesenchymal transition, and similar pathways (Figure 7B). Next, we validated the relationship between HMOX1 and EMT, mitochondrial complex, and macrophage at the protein level. HMOX1 was positively associated with macrophage and mesenchymal phenotype, and negatively correlated to epithelial phenotype and mitochondrial complex III (Figures 7C, D). Furthermore, we analyzed the genes of the regulatory network at the protein level. The high HMOX1 group had higher protein expression of mesenchymal phenotype and macrophage, and lower protein

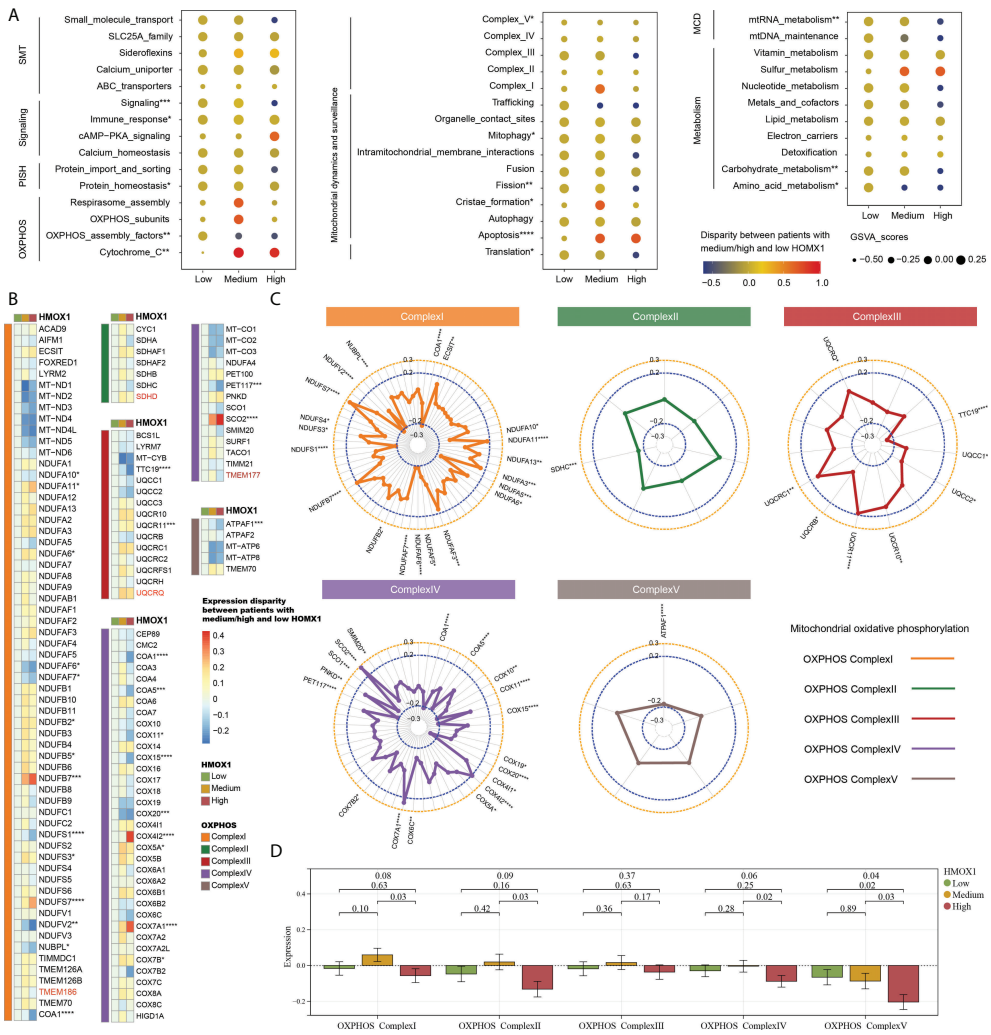

FIGURE 5
The effect of HMOX1 on mitochondrial activities in LUAD. **(A)** Differences in multiple mitochondrial pathways among the high, medium, and low HMOX1 groups. **(B)** Differences in feature genes of mitochondrial complexes among the high, medium, and low HMOX1 groups. **(C)** Correlation between HMOX1 and feature genes of mitochondrial complexes. **(D)** Differences in mitochondrial complex scoring between the high, medium, and low HMOX1 groups. SMT, small molecule transport; PISH, protein import, sorting and homeostasis; OXPHOS, oxidative phosphorylation; MCD, mitochondrial central dogma. *P < 0.05; **P < 0.01; ***P < 0.001; ****P < 0.0001.

expression of mitochondrial complexes, followed by the medium and low HMOX1 group (Figure 7E). Correlation analysis found that mitochondrial complex protein AIFM1 was dramatically negatively correlated to the protein expression of mesenchymal phenotype and macrophage (Figure 7F).

Prognostic significance for the HMOX1-mediated macrophage-mitochondrion-EMT metastasis regulatory network

Using LASSO and Cox algorithms, 26 regulatory-network-related genes were screened to have the best predictive ability for prognosis in LUAD (Figures 8A–C). A risk score was then developed according to the gene expression and Cox regression coefficients of these genes. As shown in Figures 8D, E, the high-risk group had a significantly worse prognosis than the low-risk group in the TCGA training and validating cohorts. External GEO validating cohorts also confirmed this result (Supplemental Figure 8A). The real-time AUC values of our risk score were also generally higher than similar prognostic scoring systems (Dian Guo (18), Jie Ren (19), Jie Zhu (20), Lei Zhang (21), Yingqing Zhang (22)) in LUAD (Figures 8D, E). Next, we identified the independent prognostic factors by Cox analysis, including risk score and pathological stage (Supplemental Figures 8B, C). A nomogram model was

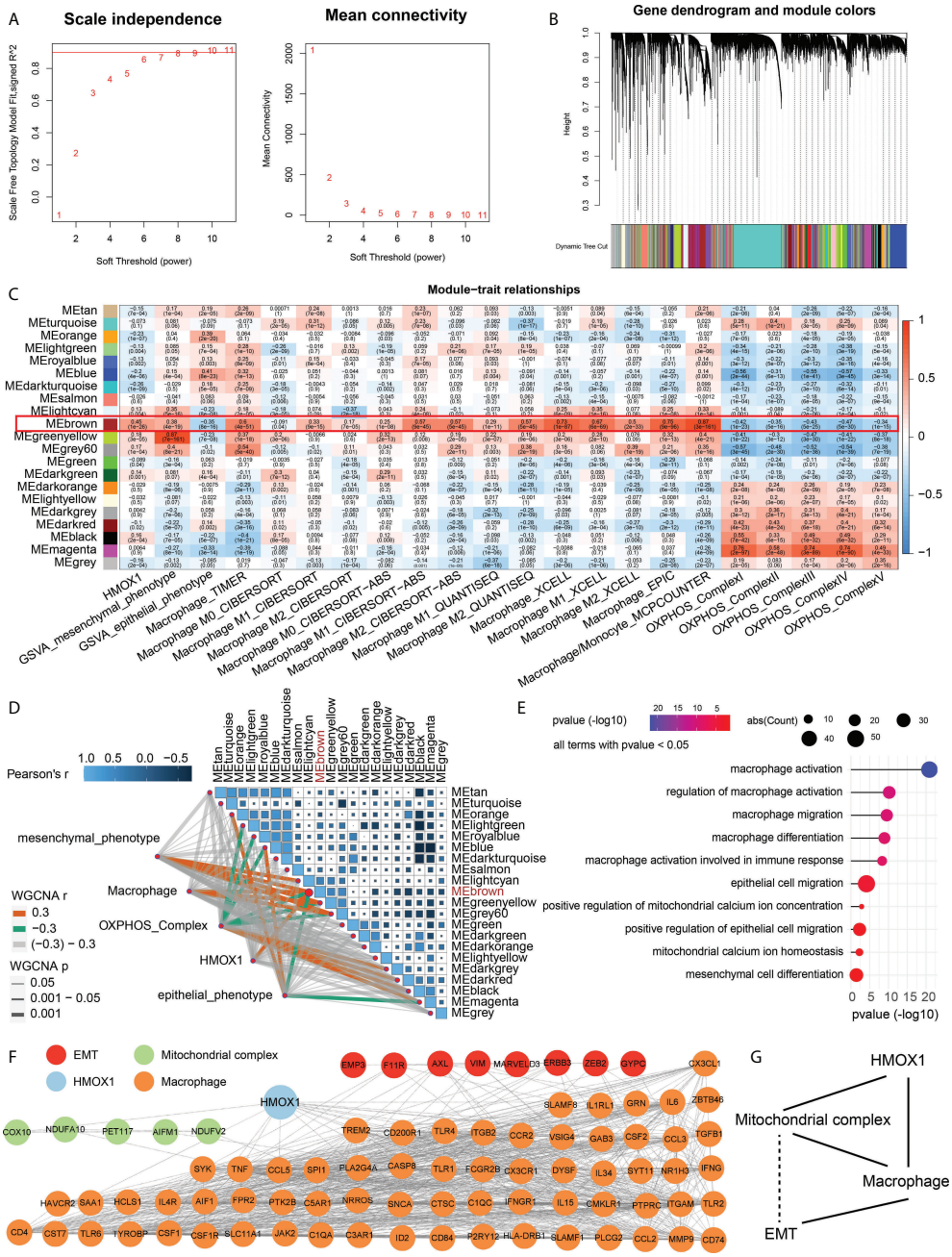

FIGURE 6
Weighted gene coexpression network analysis (WGCNA) for the construction of an HMOX1-mediated metastasis regulatory network in LUAD. **(A)** A scale-free network construction (power threshold β = 6). **(B)** Gene dendrogram generating gene modules. **(C, D)** Correlation analysis between modules and pathophysiological traits. HMOX1, EMT, macrophage, and mitochondrial complex had the same high correlation module (MEbrwon). **(E)** Gene Ontology (GO) enrichment for the MEbrown genes. **(F)** The construction of protein-protein interaction (PPI) network among HMOX1, macrophage, mitochondrial complex, and EMT using the MEbrown module genes. **(G)** The simplified interaction network among HMOX1, macrophage, mitochondrial complex, and EMT. Solid lines indicate interactions. Dashed lines indicate missing interactions.

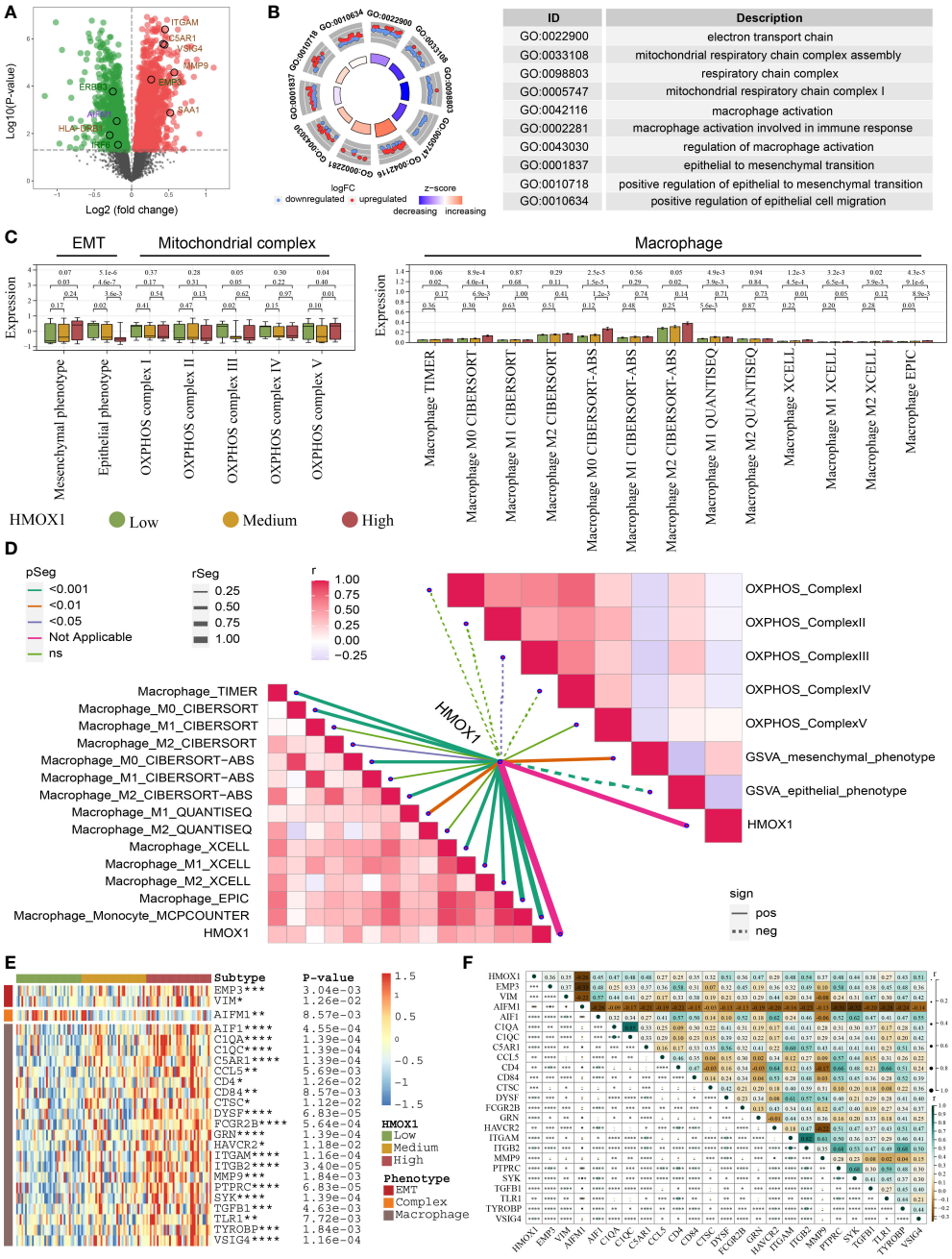

FIGURE 7
Proteomic validation for the HMOX1-mediated metastasis regulatory network in LUAD. **(A)** Volcano plots showing the differentially expressed proteins between the high and low HMOX1 groups. **(B)** GO enrichment for the differentially expressed proteins. **(C)** The difference in EMT, mitochondrial complex, and macrophage between the high, medium, and low HMOX1 groups. **(D)** Correlation between HMOX1 and EMT, mitochondrial complex, macrophage. **(E)** The difference in proteins of the HMOX1 regulatory network among high, medium, and low HMOX1 groups. **(F)** Correlation among proteins of the HMOX1 regulatory network *P < 0.05; **P < 0.01; ***P < 0.001; ****P < 0.0001.

constructed using these factors (Figure 8F). Calibration plots indicated that observed and predicted probabilities for 1-, 3-, and 5-year overall survival (OS) had excellent concordance (Figure 8G and Supplemental Figure 8D). ROC curves further confirmed the excellent predictive power of the nomogram (AUC: 0.789 in training TCGA, 0.854 in validating TCGA 0.765 in GSE11969, 0.877 in GSE31210, 0.639 in GSE42127) in both training and validating cohorts (Figure 8H and

Supplemental Figure 8E). Regrettably, GSE68486 could not be used to validate the nomogram model, owing to a lack of the variable for pathological grade.

Prediction of novel targeting modalities for the HMOX1-mediated macrophage-mitochondrion-EMT metastasis regulatory network

To predict the drugs with the potential to inhibit HMOX1-mediated LUAD metastasis, we uploaded the regulatory network genes to the CMAP online tools. We identified 9 drugs (chloroxine, tetrabenazine, TPCA-1, aminopentamide, coumaric-acid, zosuquidar, lupanine, isoliquiritigenin, pilocarpine) with the negative Raw_cs and the top fdr_q_nlog10 values, which suggested they could inhibit the gene expression in the regulatory network (Table 2 and Supplemental Figure 9).

Discussion

Emerging evidence has indicated the effect of HMOX1 in tumor metastasis, and HMOX1 is attractive as a potential prognostic biomarker and therapeutic target. Since the role of HMOX1 in LUAD metastasis still remains unclear, we performed large-scale and multi-omics bioinformatic analyses to elucidate HMOX1 in LUAD metastasis. In our study, we first demonstrated that HMOX1 contributed to the metastasis of multiple tumors, especially LUAD. Next, we found that HMOX1 was also correlated with the expression of macrophages and the mitochondrial complex. Importantly, by co-expression analysis, we identified a group of genes co-regulating the phenotypes mentioned above, and constructed the HMOX1-mediated macrophage-mitochondrion-EMT metastasis regulatory network. Based on the PPI network and existing studies, we speculated that HMOX1 may mediate the LUAD metastasis by regulating macrophages and the mitochondrial complex. Finally, the survival analysis and drug analysis were performed for HMOX1-mediated metastasis in LUAD.

HMOX1 has been found to be involved in the multiple steps of tumor metastasis including invasion, intravasation, extravasation, and colonization. Previous studies have indicated that the inhibition of HMOX1 reversed tumor EMT and impaired the invasion and migration of tumor cells (23). HMOX1 activity could also facilitate transendothelial migration of tumor cells, which implicates a potential role for HMOX1 in intravasation and extravasation events (24). In addition, myeloid HMOX1 promoted the extravasation and colonization of tumor cells at the metastatic loci (25). Similar to the previous studies, our results demonstrate that HMOX1 expression is positively associated with the EMT and lymph node and distant metastasis in multiple types of tumors, especially LUAD. The high HMOX1 group also had higher proportions of the squamoid subtype, which is a worse LUAD subtype with predilection for brain metastasis in the early stages (26). HMOX1-mediated LUAD metastasis has been preliminarily reported. Tsai *et al.* found that NSCLC patients with high HMOX1 expression had higher metastatic rates and HMOX1 over-overexpression enhanced the migratory ability of LUAD cells (27). However, the detailed mechanism of HMOX1-mediated LUAD metastasis still remains largely unknown.

Genomic alteration drives tumor metastasis (28). HMOX1 self-mutation is rare in LUAD. Therefore, we aimed to understand the HMOX1-related mutational burden and identified 16 differentially mutated genes in patients with high HMOX1 expression. Among these, FRAS1, PTPRC, MACF1 and MYH8 mutations have been found to be more enriched in other metastatic tumors (29–32). SMARCA4 mutation was reported to promote the LUAD early metastasis (33). SMARCA4-deficient LUAD had higher aggressive behavior and metastasis potential to the pleura (34). In addition, Kim *et al.* found that SMARCA4 depletion induced the EMT process in triple-negative breast cancer (35).

Macrophages, as a major immunocyte of the tumor microenvironment, play a vital role in tumor metastasis. The size, shape, metabolism, and M2 polarization of macrophages affect their metastasis (36, 37). At the primary site, macrophages can activate the EMT process and increase tumor cell migration and invasion (7, 38). At the metastatic loci, macrophages can prepare the target tissue for the arrival of tumor cells, and promote tumor cell extravasation, survival, and subsequent growth (38). Our result showed that HMOX1 was positively associated with macrophage recruitment, expression, and activity in LUAD. Similarly, some studies have demonstrated that HMOX1 was critically involved in macrophage polarization (12). In addition, a recent study has identified a novel macrophage subtype, endowed with high heme catabolism by HMOX1, as a pro-metastatic tumor microenvironment remodeling factor favoring EMT (39). Therefore, we retained the macrophage as the candidate constituent for the HMOX1 metastasis regulatory network.

The mitochondria supply the energy for tumor cell migration, invasion, and metastasis (40). Five complexes of the mitochondrial electron transport chain can affect tumor metastasis (8). Emergent evidence indicates that down-modulation of certain complex subunits by genetic or pharmacologic may promote EMT and metastasis (8, 41–43). In our study, we found down-regulated expression of mitochondrial complexes in the high HMOX1 group at the RNA and protein levels. Previous studies have reported the close correlation between HMOX1 and mitochondrion. Bansal *et al.* showed that mitochondria-targeted HMOX1 could induce mitochondrial dysfunction in macrophages (44). Song *et al.* found that HMOX1 up-regulation enhanced the oxidative mitochondrial damage in astroglia (45). Therefore, we speculate that the mitochondrion complex may affect the HMOX1-mediated metastasis in LUAD.

To further identify the correlation between the HMOX1, metastasis, macrophages, and mitochondrion, we performed the

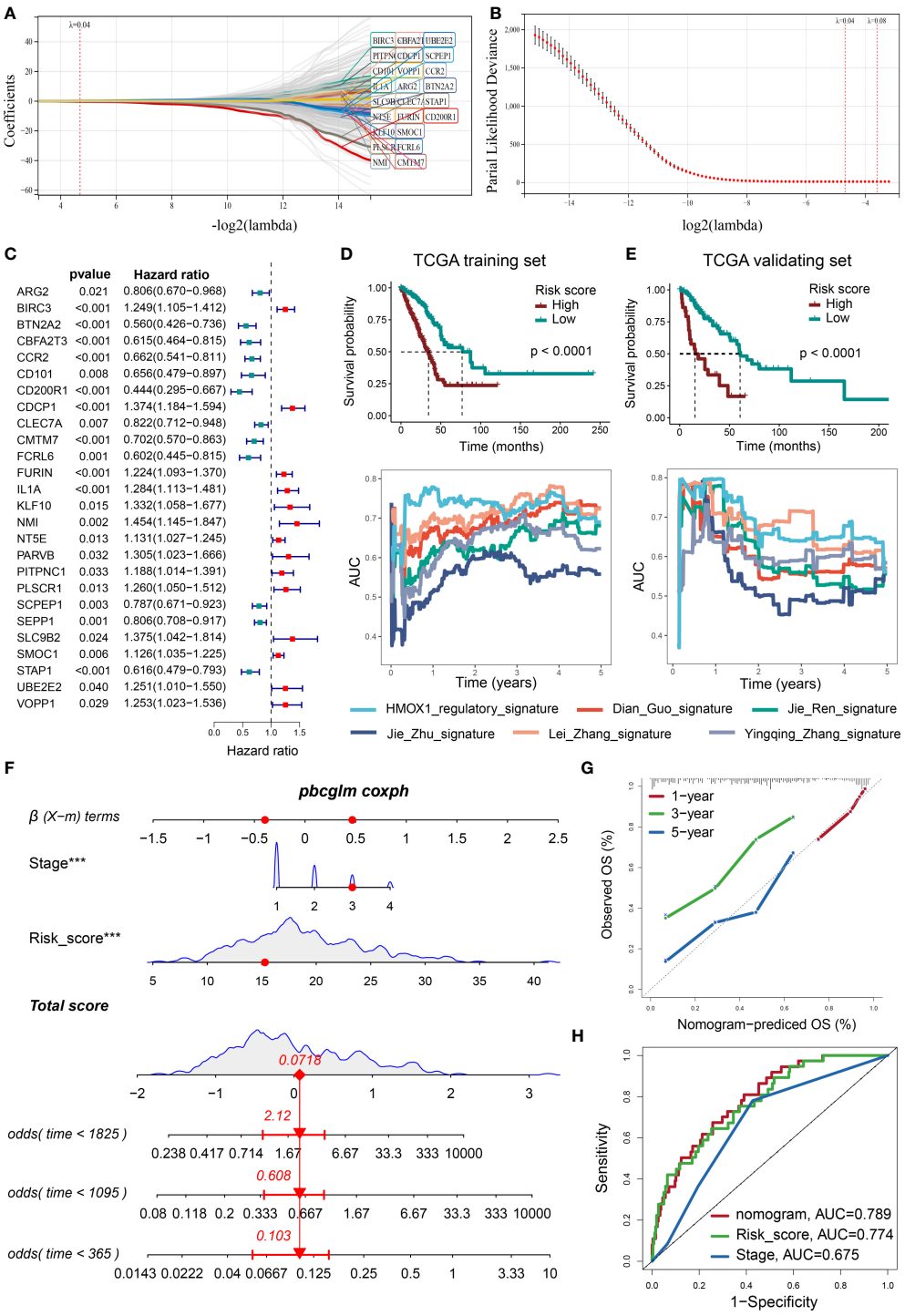

FIGURE 8
Developing a prognosis prediction model using the LASSO COX regression. **(A)** LASSO coefficient profiles of 307 prognosis-related genes, which were selected from the HMOX1-mediated metastasis regulatory network and its neighbor genes. **(B)** Cross-validation for tuning parameter screening in the LASSO regression model. Optimal genes with the best discriminative capability (26 in number) were selected for developing the risk scores. **(C)** Forest plot of the risk score gene-expression profiles in univariate analysis. **(D)** Development of risk score in the TCGA training cohort and its predictive accuracy for survival in comparison to additional 5 signatures. **(E)** validation of risk score in the TCGA validating cohort. **(F)** A nomogram integrating pathological stage, risk score, and OS probability in the TCGA training cohort. **(G)** Calibration plots showing the correlation between actual and predicted OS rates in the TCGA training cohort. **(H)** ROC curve plot evaluating the nomogram model, risk score, and pathological stage in the TCGA training cohort ***P < 0.001.

TABLE 2 Identified 9 small molecular drugs by CMAP.

Rank	CMAP name	MOA	Raw_cs	fdr_q_nlog10
1	chloroxine	Opioid receptor antagonist	-0.6937	15.6536
2	tetrabenazine	Vesicular monoamine transporter inhibitor	-0.6785	15.6536
3	TPCA-1	IKK inhibitor	-0.6768	15.6536
4	aminopentamide	Acetylcholine receptor antagonist	-0.6756	15.6536
5	coumaric-acid	Antioxidant	-0.6734	15.6536
6	zosuquidar	P-glycoprotein inhibitor	-0.673	15.6536
7	lupanine	Sodium channel inhibitor	-0.6646	15.6536
8	isoliquiritigenin	Guanylate cyclase activator	-0.653	15.6536
9	Pilocarpine	Acetylcholine receptor agonist	-0.6476	15.6536

WGCNA analysis and found a group of module genes co-regulating these traits. The module genes had a highly positive correlation with HMOX1, mesenchymal phenotype and macrophages, and a highly negative association with epithelial phenotype, and mitochondrial complexes. Based on the module genes, we constructed an HMOX1-mediated macrophage-mitochondrion-EMT metastasis regulatory network. The network showed a high inner correlation at the proteome level and high predictive ability for survival prognosis in LUAD patients. According to the network and existing studies, we speculate that HMOX1 may mediate the EMT and further LUAD metastasis by regulating mitochondrial complex and macrophage. Interestingly, the network lacks the connection between mitochondrial complex and EMT. Considering the EMT process needs large amounts of energy from the mitochondrion, we speculate that the missing connection may be attributed to the low number of studies on the interaction between mitochondrial complexes and EMT, which deserves further study.

Previous studies have also identified the association between mitochondrion and macrophages. Many mitochondria activities, including tricarboxylic acid cycle, oxidative metabolism, membrane potential, and others, are vital for macrophage activation, differentiation, and survival (46). Among these, mitochondrial fission-induced mtDNA stress could promote tumor-associated macrophage infiltration and ultimately lead to tumor progression (47). Targeting mitochondrial complex I and blocking macrophage-mediated adaptive responses could play a synergistic role to induce cancer indolence (48).

Pharmacological inhibition of HMOX1 is considered a promising therapeutic approach to hinder tumor metastasis. In this research, we predicted nine small molecule drugs targeting the HMOX1-mediated metastasis regulatory network. Among these, chloroxine, belonging to opioid receptor antagonists, has been reported to inhibit tumor metastasis. Chloroxine-inducible Par-4 secretion could induce tumor cell apoptosis and impede tumor metastasis (49). Polymeric chloroquine was also confirmed to suppress the lung metastasis of tumor cells (50). In addition, isoliquiritigenin, a guanylate cyclase activator, has been proven to suppress metastasis in multiple types of tumors, including melanoma (51), breast cancer (52), liver cancer (53), renal cell carcinoma (54), and others. Of note, a previous study showed that isoliquiritigenin reversed the EMT process to inhibit ovarian cancer metastasis (55).

In conclusion, our analyses elaborate on the role of HMOX1 in LUAD metastasis, and identify an HMOX1-mediated macrophage-mitochondrion-EMT metastasis regulatory network. Furthermore, a network-related prognostic model was established, and potential drugs targeting the HMOX1 regulatory network were also proposed, which may inhibit LUAD metastasis. One major limitation was the lack of a single-cell location analysis for HMOX1 expression. Another limitation was the lack of intercellular interaction analysis between macrophage and malignant tumor cells, which we expect to improve in subsequent studies. Additionally, the regulatory network will require further experimental validation.

Data availability statement

The original contributions presented in the study are included in the article/Supplementary Material. Further inquiries can be directed to the corresponding authors.

Ethics statement

This study has been approved by the Medical Ethics committee of the Xiangya Hospital of Central South University (No. 202012388 & No. 2017121019) and the patients/participants have provided their written informed consent.

Author contributions

AT designed the research. AT, BC, and LZ drafted the manuscript. BC, LZ, HZ, AT, WY and CL organized figures and figure legends. WY, CL, NF and AT revised the article. BC,

LZ and HZ conducted data analysis. All authors contributed to the article and approved the submitted version.

Funding

This work was supported by the Nature Science Foundation of China (No. 81402249 to LZ), the Natural Science Foundation of Hunan Province (No. 2019JJ50963 to LZ), and Fundamental Research Funds for the Central Universities of Central South University (No. 160171016 to BC).

Conflict of interest

The authors declare that the research was conducted in the absence of any commercial or financial relationships that could be construed as a potential conflict of interest.

Publisher's note

All claims expressed in this article are solely those of the authors and do not necessarily represent those of their affiliated organizations, or those of the publisher, the editors and the reviewers. Any product that may be evaluated in this article, or claim that may be made by its manufacturer, is not guaranteed or endorsed by the publisher.

Supplementary material

The Supplementary Material for this article can be found online at: https://www.frontiersin.org/articles/10.3389/fonc.2022.978006/full#supplementary-material

SUPPLEMENTARY FIGURE 1
The flow chart of data analysis.

SUPPLEMENTARY FIGURE 2
Function enrichment between the high and low HMOX1 groups. **(A)** Go enrichment for the differentially expressed genes (DEGs) between the high and low HMOX1 groups. **(B)** Kyoto Encyclopedia of Genes and Genomes (KEGG) enrichment for the DEGs between the high and low HMOX1 groups.

SUPPLEMENTARY FIGURE 3
Correlation between HMOX1 and the infiltration levels of immunocytes, including B cell **(A)** and dendritic cell (DC, **B**).

SUPPLEMENTARY FIGURE 4
Correlation between HMOX1 and the infiltration levels of immunocytes, including macrophage **(A)** and T cell CD8+ **(B)**.

SUPPLEMENTARY FIGURE 5
Correlation between HMOX1 and the infiltration levels of immunocytes, including T cell CD4+ **(A)**, Eosinphil **(B)**. and mast cell **(C)**.

SUPPLEMENTARY FIGURE 6
Correlation between HMOX1 and the infiltration levels of immunocytes, including monocyte **(A)**, endothelial cell **(B)**, neutrophil cell **(C)**, T cell gamma delta **(D)**, T cell NK **(E)**, hematopoietic stem cell **(F)**, and myeloid-derived suppressor cell **(**MDCS, **G)**.

SUPPLEMENTARY FIGURE 7
Correlation between HMOX1 and the infiltration levels of immunocytes, including NK cell **(A)**, common myeloid progenitor **(**GMP, **B)**, cancer-associated fibroblast **(C)**, T cell regulatory **(D)**, T cell follicular helper (E), common lymphoid progenitor **(**CLP, **F)**, and common myeloid progenitor **(**CMP, **G)**.

SUPPLEMENTARY FIGURE 8
Validation of the nomogram prognosis model in the TCGA validating and GEO cohorts. **(A)** Comparison of survival curves between the high and low HMOX1 groups in the GSE11969, GSE31210, GSE42127, and GSE68465 cohorts. **(B)** Univariate Cox analysis screened the prognosis variables. **(C)** Multiple Cox analysis screened the prognosis variables. **(D)** Calibration plots showing the correlation between actual and predicted OS rates in the TCGA validating, GSE11969, GSE31210, and GSE42127 cohorts. **(E)** ROC curve plot evaluating the nomogram model in the TCGA, GSE11969, GSE31210, and GSE42127 validating cohort.

SUPPLEMENTARY FIGURE 9
Identifying the molecular structure of 9 small component drugs targeting the HMOX1-mediated LUAD metastasis by CMAP.

References

1. Duma N, Santana-Davila R, Molina JR. Non-small cell lung cancer: Epidemiology, screening, diagnosis, and treatment. *Mayo Clin Proc* (2019) 94 (8):1623–40. doi: 10.1016/j.mayocp.2019.01.013

2. Ettinger DS, Wood DE, Aisner DL, Akerley W, Bauman JR, Bharat A, et al. NCCN guidelines insights: Non-small cell lung cancer, version 2.2021. *J Natl Compr Canc Netw* (2021) 19(3):254–66. doi: 10.6004/jnccn.2021.0013

3. Riihimäki M, Hemminki A, Fallah M, Thomsen H, Sundquist K, Sundquist J, et al. Metastatic sites and survival in lung cancer. *Lung Cancer* (2014) 86(1):78–84. doi: 10.1016/j.lungcan.2014.07.020

4. Fares J, Fares MY, Khachfe HH, Salhab HA, Fares Y. Molecular principles of metastasis: a hallmark of cancer revisited. *Signal Transduct Target Ther* (2020) 5 (1):28. doi: 10.1038/s41392-020-0134-x

5. Kalluri R, Weinberg RA. The basics of epithelial-mesenchymal transition. *J Clin Invest* (2009) 119(6):1420–8. doi: 10.1172/jci39104

6. Wang G, Xu D, Zhang Z, Li X, Shi J, Sun J, et al. The pan-cancer landscape of crosstalk between epithelial-mesenchymal transition and immune evasion relevant to prognosis and immunotherapy response. *NPJ Precis Oncol* (2021) 5(1):56. doi: 10.1038/s41698-021-00200-4

7. El-Kenawi A, Hänggi K, Ruffell B. The immune microenvironment and cancer metastasis. *Cold Spring Harb Perspect Med* (2020) 10(4):a037424. doi: 10.1101/cshperspect.a037424

8. Urra FA, Muñoz F, Lovy A, Cárdenas C. The mitochondrial Complex(I)ty of cancer. *Front Oncol* (2017) 7:118. doi: 10.3389/fonc.2017.00118

9. Luu Hoang KN, Anstee JE, Arnold JN. The diverse roles of heme oxygenase-1 in tumor progression. *Front Immunol* (2021) 12:658315. doi: 10.3389/fimmu.2021.658315

10. Shibahara S, Müller R, Taguchi H, Yoshida T. Cloning and expression of cDNA for rat heme oxygenase. *Proc Natl Acad Sci U.S.A.* (1985) 82(23):7865–9. doi: 10.1073/pnas.82.23.7865

11. Bindu S, Pal C, Dey S, Goyal M, Alam A, Iqbal MS, et al. Translocation of heme oxygenase-1 to mitochondria is a novel cytoprotective mechanism against non-steroidal anti-inflammatory drug-induced mitochondrial oxidative stress, apoptosis, and gastric mucosal injury. *J Biol Chem* (2011) 286(45):39387–402. doi: 10.1074/jbc.M111.279893

12. Weis N, Weigert A, von Knethen A, Brüne B. Heme oxygenase-1 contributes to an alternative macrophage activation profile induced by apoptotic cell supernatants. *Mol Biol Cell* (2009) 20(5):1280–8. doi: 10.1091/mbc.e08-10-1005

13. Higdon AN, Benavides GA, Chacko BK, Ouyang X, Johnson MS, Landar A, et al. Hemin causes mitochondrial dysfunction in endothelial cells through promoting lipid peroxidation: the protective role of autophagy. *Am J Physiol Heart Circ Physiol* (2012) 302(7):H1394–409. doi: 10.1152/ajpheart.00584.2011

14. Mak MP, Tong P, Diao L, Cardnell RJ, Gibbons DL, William WN, et al. A patient-derived, pan-cancer EMT signature identifies global molecular alterations and immune target enrichment following epithelial-to-Mesenchymal transition. *Clin Cancer Res* (2016) 22(3):609–20. doi: 10.1158/1078-0432.Ccr-15-0876

15. Hänzelmann S, Castelo R, Guinney J. GSVA: gene set variation analysis for microarray and RNA-seq data. *BMC Bioinf* (2013) 14:7. doi: 10.1186/1471-2105-14-7

16. Hu J, Yu A, Othmane B, Qiu D, Li H, Li C, et al. Siglec15 shapes a non-inflamed tumor microenvironment and predicts the molecular subtype in bladder cancer. *Theranostics* (2021) 11(7):3089–108. doi: 10.7150/thno.53649

17. Zampieri LX, Silva-Almeida C, Rondeau JD, Sonveaux P. Mitochondrial transfer in cancer: A comprehensive review. *Int J Mol Sci* (2021) 22(6):3245. doi: 10.3390/ijms22063245

18. Guo D, Wang M, Shen Z, Zhu J. A new immune signature for survival prediction and immune checkpoint molecules in lung adenocarcinoma. *J Transl Med* (2020) 18(1):123. doi: 10.1186/s12967-020-02286-z

19. Ren J, Zhang H, Wang J, Xu Y, Zhao L, Yuan Q. Transcriptome analysis of adipocytokines and their-related LncRNAs in lung adenocarcinoma revealing the association with prognosis, immune infiltration, and metabolic characteristics. *Adipocyte* (2022) 11(1):250–65. doi: 10.1080/21623945.2022.2064956

20. Zhu J, Wang M, Hu D. Development of an autophagy-related gene prognostic signature in lung adenocarcinoma and lung squamous cell carcinoma. *Peer J* (2020) 8:e8288. doi: 10.7717/peerj.8288

21. Zhang L, Zhang Z, Yu Z. Identification of a novel glycolysis-related gene signature for predicting metastasis and survival in patients with lung adenocarcinoma. *J Transl Med* (2019) 17(1):423. doi: 10.1186/s12967-019-02173-2

22. Zhang Y, Zhang X, Lv X, Zhang M, Gao X, Liu J, et al. Development and validation of a seven-gene signature for predicting the prognosis of lung adenocarcinoma. *BioMed Res Int* (2020) 2020:1836542. doi: 10.1155/2020/1836542

23. Zhao Z, Zhao J, Xue J, Zhao X, Liu P. Autophagy inhibition promotes epithelial-mesenchymal transition through ROS/HO-1 pathway in ovarian cancer cells. *Am J Cancer Res* (2016) 6(10):2162–77.

24. Muliaditan T, Caron J, Okesola M, Opzoomer JW, Kosti P, Georgouli M, et al. Macrophages are exploited from an innate wound healing response to facilitate cancer metastasis. *Nat Commun* (2018) 9(1):2951. doi: 10.1038/s41467-018-05346-7

25. Lin HH, Chiang MT, Chang PC, Chau LY. Myeloid heme oxygenase-1 promotes metastatic tumor colonization in mice. *Cancer Sci* (2015) 106(3):299–306. doi: 10.1111/cas.12604

26. Hayes DN, Monti S, Parmigiani G, Gilks CB, Naoki K, Bhattacharjee A, et al. Gene expression profiling reveals reproducible human lung adenocarcinoma subtypes in multiple independent patient cohorts. *J Clin Oncol* (2006) 24 (31):5079–90. doi: 10.1200/jco.2005.05.1748

27. Tsai JR, Wang HM, Liu PL, Chen YH, Yang MC, Chou SH, et al. High expression of heme oxygenase-1 is associated with tumor invasiveness and poor clinical outcome in non-small cell lung cancer patients. *Cell Oncol (Dordr)* (2012) 35(6):461–71. doi: 10.1007/s13402-012-0105-5

28. Nguyen B, Fong C, Luthra A, Smith SA, DiNatale RG, Nandakumar S, et al. Genomic characterization of metastatic patterns from prospective clinical sequencing of 25,000 patients. *Cell* (2022) 185(3):563–75.e11. doi: 10.1016/j.cell.2022.01.003

29. Lefebvre C, Bachelot T, Filleron T, Pedrero M, Campone M, Soria JC, et al. Mutational profile of metastatic breast cancers: A retrospective analysis. *PloS Med* (2016) 13(12):e1002201. doi: 10.1371/journal.pmed.1002201

30. Alanazi IO, Alamery SF, Ebrahimie E, Mohammadi-Dehcheshmeh M. Splice-disrupt genomic variants in prostate cancer. *Mol Biol Rep* (2022) 49 (6):4237-46. doi: 10.1007/s11033-022-07257-9

31. Chen C, Shi C, Huang X, Zheng J, Zhu Z, Li Q, et al. Molecular profiles and metastasis markers in Chinese patients with gastric carcinoma. *Sci Rep* (2019) 9 (1):13995. doi: 10.1038/s41598-019-50171-7

32. Park H, Kim D, Kim D, Park J, Koh Y, Yoon SS. Truncation of MYH8 tail in AML: a novel prognostic marker with increase cell migration and epithelial-mesenchymal transition utilizing RAF/MAPK pathway. *Carcinogenesis* (2020) 41 (6):817–27. doi: 10.1093/carcin/bgz146

33. Concepcion CP, Ma S, LaFave LM, Bhutkar A, Liu M, DeAngelo LP, et al. Smarca4 inactivation promotes lineage-specific transformation and early metastatic features in the lung. *Cancer Discovery* (2022) 12(2):562–85. doi: 10.1158/2159-8290.Cd-21-0248

34. Armon S, Hofman P, Ilié M. Perspectives and issues in the assessment of SMARCA4 deficiency in the management of lung cancer patients. *Cells* (2021) 10 (8):1920. doi: 10.3390/cells10081920

35. Kim J, Jang G, Sim SH, Park IH, Kim K, Park C. SMARCA4 depletion induces cisplatin resistance by activating YAP1-mediated epithelial-to-Mesenchymal transition in triple-negative breast cancer. *Cancers (Basel)* (2021) 13(21):5474. doi: 10.3390/cancers13215474

36. Murray PJ. Cancer metastasis linked to macrophage size, shape, and metabolism. *J Exp Med* (2020) 217(11):e20201259. doi: 10.1084/jem.20201259

37. Zhao S, Mi Y, Guan B, Zheng B, Wei P, Gu Y, et al. Tumor-derived exosomal miR-934 induces macrophage M2 polarization to promote liver metastasis of colorectal cancer. *J Hematol Oncol* (2020) 13(1):156. doi: 10.1186/s13045-020-00991-2

38. Qian BZ, Pollard JW. Macrophage diversity enhances tumor progression and metastasis. *Cell* (2010) 141(1):39–51. doi: 10.1016/j.cell.2010.03.014

39. Consonni FM, Bleve A, Totaro MG, Storto M, Kunderfranco P, Termanini A, et al. Heme catabolism by tumor-associated macrophages controls metastasis formation. *Nat Immunol* (2021) 22(5):595–606. doi: 10.1038/s41590-021-00921-5

40. Gundamaraju R, Lu W, Manikam R. Revisiting mitochondria scored cancer progression and metastasis. *Cancers (Basel)* (2021) 13(3):432. doi: 10.3390/cancers13030432

41. Li J, Liang N, Long X, Zhao J, Yang J, Du X, et al. SDHC-related deficiency of SDH complex activity promotes growth and metastasis of hepatocellular carcinoma *via* ROS/NFκB signaling. *Cancer Lett* (2019) 461:44–55. doi: 10.1016/j.canlet.2019.07.001

42. Li LD, Sun HF, Liu XX, Gao SP, Jiang HL, Hu X, et al. Down-regulation of NDUFB9 promotes breast cancer cell proliferation, metastasis by mediating mitochondrial metabolism. *PloS One* (2015) 10(12):e0144441. doi: 10.1371/journal.pone.0144441

43. Yuan Y, Wang W, Li H, Yu Y, Tao J, Huang S, et al. Nonsense and missense mutation of mitochondrial ND6 gene promotes cell migration and invasion in human lung adenocarcinoma. *BMC Cancer* (2015) 15:346. doi: 10.1186/s12885-015-1349-z

44. Bansal S, Biswas G, Avadhani NG. Mitochondria-targeted heme oxygenase-1 induces oxidative stress and mitochondrial dysfunction in macrophages, kidney fibroblasts and in chronic alcohol hepatotoxicity. *Redox Biol* (2014) 2:273–83. doi: 10.1016/j.redox.2013.07.004

45. Song W, Su H, Song S, Paudel HK, Schipper HM. Over-expression of heme oxygenase-1 promotes oxidative mitochondrial damage in rat astroglia. *J Cell Physiol* (2006) 206(3):655–63. doi: 10.1002/jcp.20509

46. Wang Y, Li N, Zhang X, Horng T. Mitochondrial metabolism regulates macrophage biology. *J Biol Chem* (2021) 297(1):100904. doi: 10.1016/j.jbc.2021.100904

47. Bao D, Zhao J, Zhou X, Yang Q, Chen Y, Zhu J, et al. Mitochondrial fission-induced mtDNA stress promotes tumor-associated macrophage infiltration and HCC progression. *Oncogene* (2019) 38(25):5007–20. doi: 10.1038/s41388-019-0772-z

48. Kurelac I, Iommarini L, Vatrinet R, Amato LB, De Luise M, Leone G, et al. Inducing cancer indolence by targeting mitochondrial complex I is potentiated by blocking macrophage-mediated adaptive responses. *Nat Commun* (2019) 10 (1):903. doi: 10.1038/s41467-019-08839-1

49. Burikhanov R, Hebbar N, Noothi SK, Shukla N, Sledziona J, Araujo N, et al. Chloroquine-inducible par-4 secretion is essential for tumor cell apoptosis and inhibition of metastasis. *Cell Rep* (2017) 18(2):508–19. doi: 10.1016/j.celrep.2016.12.051

50. Yu F, Li J, Xie Y, Sleightholm RL, Oupický D. Polymeric chloroquine as an inhibitor of cancer cell migration and experimental lung metastasis. *J Controlled Release* (2016) 244(Pt B):347–56. doi: 10.1016/j.jconrel.2016.07.040

51. Xiang S, Zeng H, Xia F, Ji Q, Xue J, Ren R, et al. The dietary flavonoid isoliquiritigenin induced apoptosis and suppressed metastasis in melanoma cells: An *in vitro* and *in vivo* study. *Life Sci* (2021) 264:118598. doi: 10.1016/j.lfs.2020.118598

52. Peng F, Tang H, Du J, Chen J, Peng C. Isoliquiritigenin suppresses EMT-induced metastasis in triple-negative breast cancer through miR-200c/C-JUN/[Formula: see text]-catenin. *Am J Chin Med* (2021) 49(2):505–23. doi: 10.1142/s0192415x21500233

53. Huang Y, Liu C, Zeng WC, Xu GY, Wu JM, Li ZW, et al. Isoliquiritigenin inhibits the proliferation, migration and metastasis of Hep3B cells *via* suppressing cyclin D1 and PI3K/AKT pathway. *Biosci Rep* (2020) 40(1):BSR20192727. doi: 10.1042/bsr20192727

54. Yamazaki S, Morita T, Endo H, Hamamoto T, Baba M, Joichi Y, et al. Isoliquiritigenin suppresses pulmonary metastasis of mouse renal cell carcinoma. *Cancer Lett* (2002) 183(1):23–30. doi: 10.1016/s0304-3835(02)00113-1

55. Chen C, Huang S, Chen CL, Su SB, Fang DD. Isoliquiritigenin inhibits ovarian cancer metastasis by reversing epithelial-to-Mesenchymal transition. *Molecules* (2019) 24(20):3725. doi: 10.3390/molecules24203725

Glossary

CPTAC	Clinical Proteomic Tumor Analysis Consortium
CMAP	Connectivity Map
CNA	Copy number alternation
DEG	Differentially expressed gene
DFI	Disease-free interval
DSS	Disease-specific survival
EMT	Epithelial-mesenchymal transition
GEO	Gene Expression Omnibus
GO	Gene Ontology
GSVA	Gene Set Variation Analysis
HMOX1	Heme oxygenase-1
HCMDB	Human Cancer Metastasis Database
KEGG	Kyoto Encyclopedia of Genes and Genomes
Lasso	Least absolute shrinkage and selection operator
LUAD	Lung adenocarcinoma
NSCLC	Non-small cell lung cancer
NSCLC	Non-small cell lung cancer
OS	Overall survival
PFI	Progress-free interval
PRAD	Prostate adenocarcinoma
ROC	Receiver operating characteristic
SCLC	Small cell lung cancer
TCGA	The Cancer Genome Atlas
TCIA	The Cancer Immunome Atlas
WGCNA	Weighted gene co-expression network analysis

frontiers | Frontiers in Cell and Developmental Biology

TYPE Review
PUBLISHED 17 August 2022
DOI 10.3389/fcell.2022.938289

Check for updates

OPEN ACCESS

EDITED BY
Pranav Gupta,
Albert Einstein College of Medicine,
United States

REVIEWED BY
Yu-Gang Huang,
Hubei University of Medicine, China
Jing Yang,
University of California, San Diego,
United States

*CORRESPONDENCE
Shiwu Zhang,
zhangshiwu666@aliyun.com

†These authors have contributed equally to this work

SPECIALTY SECTION
This article was submitted to Cancer Cell Biology,
a section of the journal
Frontiers in Cell and Developmental Biology

RECEIVED 07 May 2022
ACCEPTED 19 July 2022
PUBLISHED 17 August 2022

CITATION
Yan M, Zheng M, Niu R, Yang X, Tian S, Fan L, Li Y and Zhang S (2022), Roles of tumor-associated neutrophils in tumor metastasis and its clinical applications. *Front. Cell Dev. Biol.* 10:938289. doi: 10.3389/fcell.2022.938289

COPYRIGHT
© 2022 Yan, Zheng, Niu, Yang, Tian, Fan, Li and Zhang. This is an open-access article distributed under the terms of the Creative Commons Attribution License (CC BY). The use, distribution or reproduction in other forums is permitted, provided the original author(s) and the copyright owner(s) are credited and that the original publication in this journal is cited, in accordance with accepted academic practice. No use, distribution or reproduction is permitted which does not comply with these terms.

Roles of tumor-associated neutrophils in tumor metastasis and its clinical applications

Man Yan[1†], Minying Zheng[2†], Rui Niu[1], Xiaohui Yang[3], Shifeng Tian[4], Linlin Fan[1], Yuwei Li[5] and Shiwu Zhang[2*]

[1]Graduate School, Tianjin University of Traditional Chinese Medicine, Tianjin, China, [2]Department of Pathology, Tianjin Union Medical Center, Tianjin, China, [3]Nankai University School of Medicine, Nankai University, Tianjin, China, [4]Graduate School, Tianjin Medical University, Tianjin, China, [5]Department of Colorectal Surgery, Tianjin Union Medical Center, Tianjin, China

Metastasis, a primary cause of death in patients with malignancies, is promoted by intrinsic changes in both tumor and non-malignant cells in the tumor microenvironment (TME). As major components of the TME, tumor-associated neutrophils (TANs) promote tumor progression and metastasis through communication with multiple growth factors, chemokines, inflammatory factors, and other immune cells, which together establish an immunosuppressive TME. In this review, we describe the potential mechanisms by which TANs participate in tumor metastasis based on recent experimental evidence. We have focused on drugs in chemotherapeutic regimens that target TANs, thereby providing a promising future for cancer immunotherapy.

KEYWORDS

metastasis, neutrophils, tumor-associated neutrophils, tumor microenvironment, prognostic potentials, antitumor immunity

Introduction

In the last few decades, tremendous progress has been made in tumor immunology. Significant advances in immunotherapy, particularly in the use of checkpoint inhibitors, have been successful in targeting metastatic cancers. Although immuno-oncology treatments have gained considerable momentum, most metastatic cancers remain drug-resistant. This resistance is primarily due to innate immune cells such as neutrophils. Increasing evidence indicates that neutrophils increase resistance to clinical checkpoint blockade treatment, which is vital in establishing an immunosuppressive microenvironment and facilitating metastasis (Faget et al., 2021).

Metastasis, a primary characteristic of many malignancies, is associated with more than 90% of cancer-related deaths (Seyfried and Huysentruyt, 2013). Metastasis is the process by which tumor cells break away from their initial locations and are transported through the lymphatic or circulatory systems to form new tumors in other organs. The process involves several steps: 1) invasion of tumor cells into the neighboring parenchyma, 2) intravasation into the blood and/or lymphatic circulation, 3) survival within the circulatory or lymphatic systems, 4) extravasation into the distant parenchyma, and 5) subsequent survival and growth (Kitamura et al., 2015). Metastasis is associated

with differentiation and tumor-associated neutrophils (TANs) that live in the tumor microenvironment (TME) (Lin et al., 2019). TANs constitute a major component of the TME and regulate tumor metastasis in all the five steps mentioned earlier.

TANs impair antitumor immunity and accelerate tumor growth and metastasis through the production of growth factors, chemokines, and inflammatory factors such as matrix metalloproteinase-9 (MMP-9), vascular endothelial growth factor (VEGF), high mobility group box 1 (HMGB1), and interleukin (IL)-17 (Bald et al., 2014; Minder et al., 2015; Li et al., 2019; Shaul and Fridlender, 2019). In recent years, the targeting of TANs has attracted increasing attention from researchers. This review provides an overview of the diversity and heterogeneity of TANs and describes the latest research progress on the potential mechanisms of TAN involvement in tumor metastasis. With a clearer understanding of the relationship between TANs and metastasis, treatment methods targeting TANs may provide a more promising approach to cancer intervention.

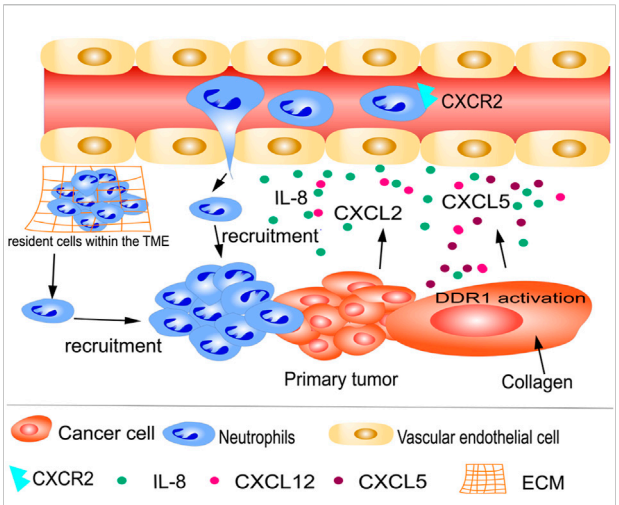

FIGURE 1
Recruitment of tumor-associated neutrophils (TANs) to primary tumors. Neutrophils from circulation and resident cells within the tumor microenvironment (TME) are recruited by cytokines, growth factors, and chemokines, such as IL-8 and CXCL2. Tyrosine kinase discoid domain receptor 1 (DDR1) is a key regulator of tumor cell metastasis. DDR1 activation by collagen in cancer cells is a significant stimulus for the synthesis of CXCL5, leading to the recruitment of TANs to primary tumors.

TANs in tumors

Some studies have indicated that tumorigenesis follows a sequence of inflammatory events that resemble wound healing but without resolution (Hua and Bergers, 2019; Deyell et al., 2021). In response to early signs of inflammation, proinflammatory immune cells are recruited from the bloodstream and local resident cells. Evidence from mouse models and patients indicates that neutrophils are critical components of tumor-promoting inflammation in many tumor types (Galdiero et al., 2018; Shaul and Fridlender, 2019). Inflammation resolution and wound healing are hindered by genomic instability caused by neutrophils. For example, in breast cancer models, TANs produce reactive oxygen species that damage DNA and induce genetic instability, thereby promoting metastasis (Timaxian et al., 2021). Similarly, microparticles equipped with proinflammatory microRNAs (miR-23a and miR-155) are released by tissue-infiltrating neutrophils into intestinal epithelial cells. miRNAs enhance the formation of double-stranded breaks (DSBs) by causing the collapse of the replication fork. Their accumulation in the damaged epithelium hinders colonic repair and increases genomic instability (Butin-Israeli et al., 2019). A transgenic zebrafish tumor model indicated that TANs stimulate the early steps in tumor formation and progression. Direct live imaging revealed an innate inflammatory response at the pre-neoplastic stage. Zebrafish have been established as an indispensable *in vivo* model for cancer research as they can offer dynamic visualization of tumor growth *in vivo*. Their natural transparency combined with fluorescent labeling allows real-time observation of individual cells in a living model. For example, the T-cell leukemia model was the first zebrafish cancer model, allowing the direct monitoring of the initiation and expansion of leukemic cells using fluorescence microscopy (Langenau et al., 2003; Langenau et al., 2005). The rapid development of zebrafish genetic tools and imaging technologies has allowed researchers to better understand the processes that govern leukocyte activity during tumor initiation (Elliot et al., 2020).

Similarly, as tumor cells build their environment to promote survival, they can trigger an inflammatory response, consequently recruiting more neutrophils into the TME (Wei et al., 2021). Neutrophils can infiltrate primary tumors; patients with higher numbers of infiltrating neutrophils have poorer prognoses and are more resistant to drug therapies (Arvanitakis et al., 2021; Kim et al., 2022; Tian et al., 2022). Neutrophil recruitment is triggered by immune mediators, including cytokines, growth factors, and chemokines (Fig. 1). Using immunohistochemistry, Schimek et al. demonstrated that neutrophils preferentially accumulated at locations of apoptotic tumor cells in 35 patients with colorectal cancer (CRC). In another CRC model, interleukin-8 (IL-8) was suggested to be secreted by apoptotic cancer cells, attracting neutrophils into the tumor where they interact with nearby macrophages, thereby establishing an immunologically unfavorable TME (Schimek et al., 2022). Additionally, in neutrophil-specific anterior gradient-2 (AGR2) knockout mice, a recent study reported that CRC cells aggressively attracted $AGR2^{+}$ TANs, which enhanced CRC metastasis, through chemokine (C-X-C motif) ligand 2 (CXCL2) (Tian et al., 2022). Similarly, using co-cultures

of neutrophils and tumors, polymorphonuclear myeloid-derived suppressor cells (PMN-MDSCs) were attracted to brain metastatic variants of breast cancer cells upon upregulation of CXCR2 and CXCL1 (Groth et al., 2021). Furthermore, tyrosine kinase discoid domain receptor 1 (DDR1) is a critical regulator, and its activation by collagen in tumor cells stimulates the synthesis of CXCL5, leading to the recruitment of TANs, invasion, and metastasis (Deng et al., 2021) (Figure 1).

A large body of data suggests that neutrophils recruited to tumor sites secrete cytokines, which induces adaptive immune response and leads to the recruitment of multiple immune cells, including B cells, T cells, and macrophages. Crosstalk between tumor and immune cells likely plays a vital role in maintaining an immunosuppressive TME (Chao et al., 2016; Shaul et al., 2021; Schimek et al., 2022). In another study, TANs with $CD11b^{+}$/$Ly6G^{+}$ cells were hypersegmented, more cytotoxic, and expressed higher levels of proinflammatory cytokines. They were attracted to tumor cells by transforming growth factor-beta (TGF-β) inhibitors through increased levels of neutrophil-attracting chemokines (Fridlender et al., 2009). Therefore, the function of TANs is influenced by the local microenvironment and other immune cells, demonstrating their diversity.

Diversity and plasticity of TAN

Neutrophils have both pro- and anticancer functions. Transcriptomic analysis revealed that TANs have immunosuppressive properties that differ from those of healthy controls in humans and mice with cancer (Shaul and Fridlender, 2019). They can perform various functions related to their metabolic requirements, differentiation stage, and functional state (Shaul and Fridlender, 2019). A consensus has not been reached on the terminology for neutrophil heterogeneity and plasticity in cancer. However, researchers have attempted to distinguish between the subsets of neutrophils. Some molecules are hypothesized to be linked to the antitumor response, such as CD177 and CD101, or the protumor response, such as lectin-like oxidized low-density lipoprotein (LOX1), CD117, and programmed death-ligand 1 (PD-L1) (Noman et al., 2014; Condamine et al., 2016; Cheng et al., 2018; Evrard et al., 2018; Zhou et al., 2018; Zhu et al., 2018).

Neutrophils can also be distinguished based on their densities. Blood samples from patients with cancer contain two distinct populations: low-density neutrophils (LDNs) and high-density neutrophils (HDNs). LDNs exhibit pro-tumorigenic and immunosuppressive properties in cancer (Sagiv et al., 2015) and are composed of a mixture of mature and immature neutrophils. Conversely, HDNs are mature neutrophils with antitumor effects. In healthy controls, HDNs are predominant in circulating neutrophils (Sagiv et al., 2015).

Compared with macrophages, TANs are thought to be polarized into two distinct phenotypes: N1 antitumoral and N2 protumoral, as proposed by Fridlender et al. in 2009 (Fridlender et al., 2009). TGF-β released by the primary tumor can cause neutrophils to develop an N2-type pro-tumor phenotype, characterized by elevated arginase production and immunosuppressive effects on T cells (Fridlender et al., 2009; Eruslanov et al., 2014). Moreover, a recent study indicated that exosomal circPACRGL from CRC induces TGF-β1 production, resulting in neutrophil differentiation from N1 to N2 (Shang et al., 2020). Furthermore, some experiments have demonstrated that type I interferons (IFNs) can transform neutrophils into the N1 antitumor phenotype capable of cytotoxic activity against tumor cells that acquire antigen-presenting cell characteristics (Singhal et al., 2016; Siakaeva et al., 2019). Altering the TME may influence neutrophil plasticity and polarization. Triple-negative breast cancer models have indicated that Lin-28 homolog B (LIN28B) also enables neutrophil N2 conversion, maintaining the immunosuppressive environment by increasing the expression of programmed cell death one ligand 2 (PD-L2) (Qi et al., 2022). Similarly, in a CRC model, the cell migration-inducing protein KIAA1199 was produced by tumor recruitment of neutrophils with pro-tumor activity, indicating that KIAA1199 drives N2 pro-tumor polarization (Wang et al., 2022a). However, the association between N1/N2 neutrophils in mice and HDN and LDN classification in human patients is unclear because classification only considers functional conditions and not neutrophil maturation.

TANs with proven immunosuppressive functions are granulocytic myeloid-derived suppressor cells (G-MDSCs) or PMN-MDSCs, which act as neutrophils during multiple phases of maturation. Biochemical and gene expression profiling helped identify these cells as pathologically active immature myeloid cells that differ from normal myeloid cells (Bronte et al., 2016). The mechanism by which MDSCs differentiate from normal myeloid cells remains unknown, limiting our capacity to target them therapeutically in cancer. However, recent research employing single-cell RNA sequencing (scRNA-seq) has demonstrated that G-MDSCs appear in the spleen via an abnormal and unique neutrophil maturation pathway, contributing to their immunosuppressive features. However, the application of these findings to other tumors remains unexplored, as this study focused only on one type of cancer (Alshetaiwi et al., 2020). G-MDSCs are likely a mixture of immature and mature neutrophils with a low density. Their identification is generally confirmed by the presence of the following surface markers: $CD15^{+}$, $CD11b^{+}$, $CD14^{-}$, $HLA\text{-}DR^{-}$, and CD33; Furthermore, they are capable of inhibiting T cell activities and antitumor immunity (Cassetta et al., 2019). However, whether G-MDSCs should be considered a unique cell type or whether these results shed new light on neutrophil plasticity is debatable.

As shown in Table 1, most surface markers in LDNs, G-MDSCs, TANs immature neutrophil and mature neutrophil

TABLE 1 Main surface markers and function of LDNs, TANs, and G-MDSCs, immature neutrophil and mature neutrophil.

Neutrophil subtype	Function	Surface marker
Immature neutrophil	Pro-tumor	$CD66^+CD15^+CD33^+CD49d^-CD101^+CD10^-CD16^+$ (Evrard et al., 2018; Mukaida et al., 2020)
Mature neutrophil	Anti-tumor	$CD66^+CD15^+CD33^+CD49d^-CD101^+CD10^+CD16^+$ (Evrard et al., 2018; Mukaida et al., 2020)
LDN	Immunosuppressive activities	$CD66b^+$ $CD15^+$ $CD33^+$ $CD11b^+$ HLA-DR^+ $CD16^+$ (Hacbarth and Kajdacsy-Balla, 1986; Fu et al., 2014; Davis et al., 2017; Ui Mhaonaigh et al., 2019)
TAN (N2)	Promote the tumor progression and metastasis	$CD66b^+$ $CD15^+$ $CD33^+$ $CD11b^+$ $CD16^+$ $CD62L^+$ $CD45^+$ (Fortunati et al., 2009; Cui et al., 2013; Eruslanov et al., 2014; Wu et al., 2014; Sionov et al., 2015; Uribe-Querol and Rosales, 2015; Shaul and Fridlender, 2019)
TAN(N1)	Suppress the tumor progression and metastasis	$CD66b^+$ $CD15^+$ $CD33^+$ CD101+ $CD10^+$ $CD16^+$ (Yvan-Charvet and Ng, 2019; Mukaida et al., 2020)
G-MDSC	Suppress immune response and promote tumor progression in mouse model	$CD66b^+$ $CD15^+$ $CD33^+$ $CD11b^+$ $CD14^-$ HLA-DR^- $CD16^+$ (Khaled et al., 2014; Noy and Pollard, 2014; Ding et al., 2016; Cassetta et al., 2019; Shaul and Fridlender, 2019; Mukaida et al., 2020)

are similar. These "subgroups" display similar pro-tumor functions, rendering it challenging to distinguish between these "subgroups." These neutrophil "subgroups" are likely a class of normal neutrophils stimulated by the tumor environment (McKenna et al., 2021). Identifying the cell subtypes within tumors is crucial to remove or repolarize their activity, enabling neutrophils to attack tumor cells rather than promote tumor metastasis.

Mechanisms underlying TAN-facilitated metastasis

TANs promote tumor-cell invasion

Generally, highly invasive tumors lose their intrinsic polarity and become free from surrounding tissues (Savagner, 2010). Epithelial cells lose tight cell junctions and acquire mesenchymal characteristics by downregulating E-cadherin, a process known as the epithelial-mesenchymal transition (EMT). As a result, tumor cells that undergo EMT gain motility and aggressiveness as well as the capacity to rebuild the extracellular matrix (ECM) (Kalluri and Weinberg, 2009). Several studies have revealed that TANs may play a role in controlling EMT. As a natural inhibitor of MMP-9, the tissue inhibitor of metalloproteinase 1 (TIMP-1) exerts antitumor effects. However, recent studies have confirmed that neutrophil-secreted TIMP-1 promotes metastasis by inducing the EMT in breast cancer cells. Owing to the presence of the cluster of differentiation 90 protein (CD90) in these tumor cells, neutrophils produce more TIMPs, thereby promoting tumor development. Therefore, blocking CD90 or TIMP-1 significantly reduces the spread of cancer (Wang et al., 2019a). Similarly, Li et al. demonstrated that gastric cancer tissues exhibit high infiltration of TANs, especially at the invasive edge of the tumor, where IL-17 is expressed via Janus kinase 2 (JAK2)/signal transduction and activator of transcription 3 (STAT3) signaling, allowing them to increase migration, invasion, and EMT. Antibodies that neutralize IL-17a reduce tumor progression in gastric cancer (GC) cells (Li et al., 2019). Moreover, in an oral squamous cell carcinoma (OSCC) model, TANs also promoted EMT in OSCC cells by activating JAK2/STAT3 signaling (Hu et al., 2022).

A recent study found that neutrophil extracellular traps (NETs), the DNA complexes generated by neutrophils to fight bacterial pathogens, may enhance GC growth, invasion, and migration. In patients with GC and postoperative abdominal infectious complications (AIC), NETs were reportedly released by neutrophils within the abdominal fluid (ascites) and omental tissues due to stimulation by postoperative AIC. NETs cause EMT in GC cells through the TGF-β signaling pathway, thereby exacerbating GC metastasis. This also explains the link between postoperative AIC and metastases after radical gastrectomy in patients with advanced GC. Additionally, using a transwell migration assay, AIC-induced NETs captured scattered GC cells to form NET-GC clusters, contributing to metastatic extravasation and implantation (Xia et al., 2022). However, another study showed that TANs inhibited EMT. In tumor-bearing mice, radiotherapy generates persistent DNA damage and subsequently triggers the secretion of the inflammatory chemokines CXCL1, CXCL2, and CCL5. These chemotactic factors recruit neutrophils to tumor sites and generate reactive oxygen species through phosphatidylinositol 3-kinase (PI3K)/protein kinase B (AKT)/zinc finger protein SNAI1 (Snail) signaling, inhibiting EMT and converting neutrophils to an antitumor phenotype (Liu et al., 2021a) (Figure 2A). Therefore, TANs appear to be involved in EMT regulation in cancer, and different types of neutrophils have different effects on EMT. In the future, the physiological polarization of TANs may significantly impact cancer immunotherapy.

Most solid tumors are encapsulated by an ECM composed of collagen, enzymes, and proteins that maintain tissue structure

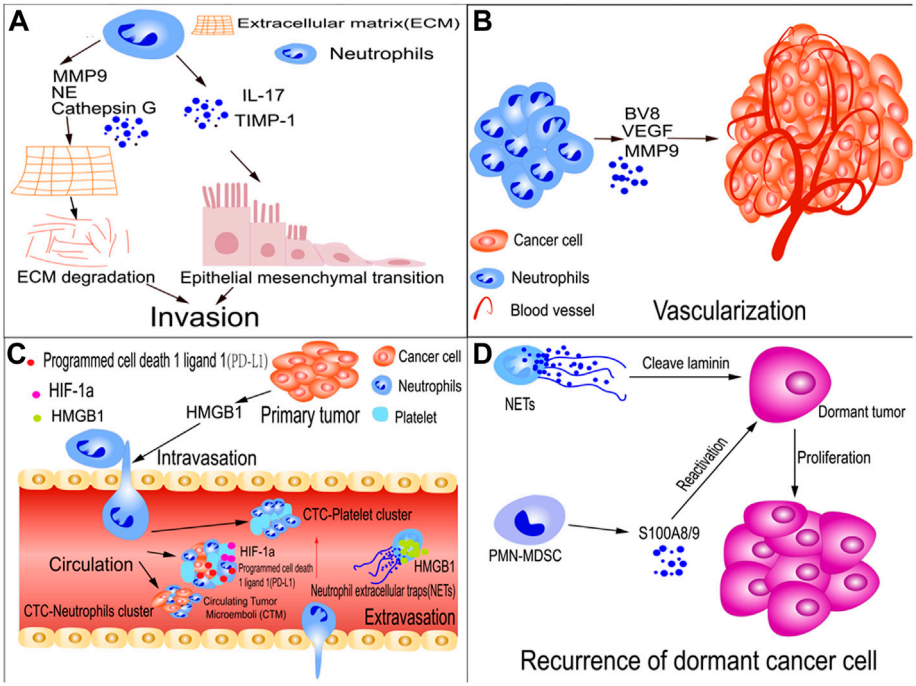

FIGURE 2
TAN roles in tumor metastasis. **(A)** TANs promote tumor-cell invasion; neutrophil-secreted TIMP-1 or IL-17 promote metastasis by inducing the epithelial-mesenchymal transition (EMT). Similarly, TANs cause cancer cells to undergo EMT by activating JAK2/STAT3 signaling. TANs secrete matrix metalloproteinase-9 (MMP-9), cathepsin G, and neutrophil elastase (NE), which degrade the extra-cellular matrix (ECM), thereby allowing tumors to invade adjacent tissues. **(B)** TANs promote tumor cell vascularization; neutrophils encourage tumor metastasis by releasing proteins such as MMP-9, vascular endothelial growth factor (VEGF), and BV8, which promote tumor angiogenesis. **(C)** TANs facilitate intravasation and extravasation of tumor cells and the survival of circulating tumor cells (CTCs); HMGB1 is released by tumor cells to recruit neutrophils, which assist tumor cells in invading blood vessels. CTC, CTC-neutrophil, and CTC-platelet clusters shield tumor cells from shear stress and natural killer (NK) cell assault. Hypoxia-inducible factor-1α (HIF-1α) expression is increased in circulating tumor microemboli (CTM) in the lungs. **(D)** Recurrence of dormant cancer cells; NETs cleave laminin, which results in the generation of an epitope. When a dormant cancer cell recognizes the epitope, signaling encourages tumor cells to awaken and proliferate. Polymorphonuclear myeloid-derived suppressor cells (PMN-MDSCs) awaken dormant tumor cells by S100A8/A9.

and function. However, they also serve as a hurdle for metastasis (Paolillo and Schinelli, 2019). Various proteases secreted by TANs, including cathepsins, MMPs, and neutrophil elastases (NE), are crucial for regulating ECM degradation. They can disrupt the barrier, allowing tumors to invade adjacent tissues (El Rayes et al., 2015; Ci et al., 2018; Wu et al., 2019) (Figure 2A).

TANs promote tumor cell vascularization

When solid tumors reach a size threshold, various factors initiate the development of dense vasculature that provides a constant blood supply to the tumor. This process is called the angiogenic switch (Hanahan and Folkman, 1996). TANs serve as critical regulators of the angiogenic switch by eliciting the release of several proteases. Neutrophils are concentrated near the invasive edge of GC tissues and serve as a primary source of MMP-9, which promotes angiogenesis in GC cells (Li et al., 2017). MMP-9 promotes tumor angiogenesis by activating VEGF and VEGF receptor interactions in endothelial cells (Minder et al., 2015). Furthermore, prokineticin 2 (Bv8) triggers neutrophil-dependent angiogenesis, and inhibition of Bv8 activity limits angiogenesis and tumor development (Shojaei et al., 2007). A recent study showed that the transcription factor forkhead box protein O3a (FOXO3a) regulates the production of pro-angiogenic factors such as VEGF, MMP-9, and BV8 in neutrophils of IFN-deficient mice (Figure 2B). These pro-angiogenic factors play a crucial role in vascularization during tumor growth. Therefore, targeting FOXO3a holds promise as an anti-angiogenic therapy (Bordbari et al., 2021). Similarly, another study showed that nicotinamide phosphoribosyltransferase (NAMPT), a protein implicated in the downstream signaling of the granulocyte colony-stimulating factor receptor (G-CSF-R), is required for vascularization in a transplantable tumor model. Therefore, targeting neutrophils may be therapeutically possible (Pylaeva et al., 2019).

TANs help tumors disseminate distantly through the blood and lymphatic vessels. In the primary tumors of patients with

OSCC, the presence of TAN-cancer cell compounds in areas of lymphangiogenesis indicates that TANs assist in tumor metastasis via lymphatic vessels (Lonardi et al., 2021).

TANs promote tumor-cell intravasation

It is also crucial for cancer cells to gain access to the vasculature through the small holes in the vascular endothelium. In a mouse melanoma model, ultraviolet (UV) irradiation increased the aggregation of tumor cells along the surfaces of the blood vessels. HMGB1 is released by UV-damaged epidermal keratinocytes to recruit neutrophils, which assist tumor cells in invading the blood vessels (Bald et al., 2014) (Figure 2C).

Neutrophils help circulating tumor cells survive in the peripheral circulation

Tumor cells must overcome multiple obstacles, including fluid shear stress, mechanical collisions, and immunosurveillance, to survive in the bloodstream (Lambert et al., 2017). Although several CTCs pass through the bloodstream, only a minimal fraction survive and spread to distant organs (Massagué and Obenauf, 2016). The tumor cells that survive in the bloodstream become more aggressive, and their ability to survive in the blood can be enhanced through various pathways. Numerous studies have demonstrated that the interplay between cancer cells and neutrophils increases tumor metastasis via the blood. Furthermore, neutrophils can communicate with CTCs to survive in the bloodstream. CTCs can form clusters of two to hundreds of cells to overcome the fluidic challenges of the bloodstream. These clusters have a 23–50-fold metastatic capacity compared to that of single CTCs in circulation. In patients with breast cancer, the abundance of CTC clusters was associated with adverse outcomes and metastasis (Aceto et al., 2014) (Figure 2C). CTCs are occasionally associated with leukocytes. Using single-cell RNA sequencing, Szczerba et al. analyzed a 4T1 mammary tumor model and human breast cancer. CTC-associated white blood cells were detected, most of which were $CD11b^{+}$/$Ly\text{-}6G^{+}$ neutrophils. Additionally, CTC neutrophil clusters have a greater tendency for metastatic spread than that of individual CTCs. Therefore, CTC–neutrophil clusters help increase survival and metastatic capacity (Szczerba et al., 2019) (Figure 2C). A recent study using an H22 tumor model reported that multipoint costriking nanodevices are required to kill primary tumors and prevent the dissemination of associated CTCs. Vascular cell adhesion molecule 1 (VCAM1) and glypican-3 are highly expressed on tumor cells and bind to neutrophils. The multipoint costriking nanodevice was developed using an anti-VCAM1 monoclonal antibody (mAb) and anti-Glypican-3 mAb, which can specifically identify and bind to their respective receptors overexpressed on the CTC membrane. Sorafenib and digitoxin located on the multipoint costriking nanodevice dissociated the CTC clusters, blocked the formation of CTC-neutrophil clusters, and destroyed the CTCs, thereby preventing migration (Mu et al., 2022).

Platelets may also protect tumor cells by forming platelet-rich thrombi around them. Platelets attract myeloid cells by secreting chemokines that shield tumor cells from shear stress and natural killer cells (NK), thereby allowing tumor cells to aggregate with platelets on the endothelium and accelerating tumor spread (Schlesinger, 2018). Platelets and neutrophils may also cooperate to shield CTCs from the vasculature via mechanical and immune-mediated destruction. Researchers discovered a pro-metastatic compound in several metastatic tumors consisting of CTC clusters, platelets, and neutrophils, known as circulating tumor microemboli (CTM).

Hypoxia is a vital factor in fostering CTM colonization in the lungs. Hypoxia-inducible factor-1α (HIF-1α) is highly expressed in the CTM, and its downregulation significantly alleviates hypoxia and ultimately inhibits metastasis (Du et al., 2022). Collectively, the presence of platelets and neutrophils in the bloodstream may increase the pro-metastatic activity of single CTCs. However, the mechanisms by which platelets and neutrophils contribute to CTC clusters mediating migration in different tumor types requires further investigation.

TANs help tumor cells colonize and extravasate

In addition to spreading and surviving in blood vessels, CTCs adhere to the endothelium and cross the vascular system into surrounding tissues (Follain et al., 2020). Accumulating evidence indicates that neutrophils regulate tumor cell adhesion to endothelial cells and transmigrate to metastatic sites. Although they are critical for cancer metastasis, the mechanisms underlying extravasation remain poorly understood. In addition, cancer cells recruit TANs to the TME, where they release NETs. Hiroki et al. examined NETs around metastatic tumors using clinical specimens. Through the activation of EMT, high mobility group box protein 1 (HMGB1) derived from NETs enhanced tumor extravasation during metastasis in a murine model of liver metastasis (Kajioka et al., 2021) (Figure 2C).

TANs and persistent growth, dormancy, and recurrence of tumor cells

Tumor cells become dormant upon transmigration to the surrounding tissues. Further, they stop proliferating or growing and evading immunosurveillance until the activation of a trigger mechanism (Vera-Ramirez et al., 2018; Shimizu et al., 2019).

Dormant cancer cells are characterized by increased p38 mitogen-activated protein kinase (p38 MAPK) and decreased extracellular signal-regulated kinase 1/2 (ERK1/2) activity; the p38 $MAPK^{high}/ERK^{low}$ phenotype is commonly used as a marker of dormancy (Recasens and Munoz, 2019). In addition, according to a recent study, some researchers have synthesized the hallmarks of dormant cancer cell states, including niche dependence, cell cycle arrest, drug resistance, immune evasion, metastatic relapse, and reversibility. Dormant cancer cells are partly influenced by the local environment or niche in which they are located (Phan and Croucher, 2020). Overall, targeting dormant tumor cells is contingent on the tumor and its resident TME.

Despite being an essential member of the TME, the involvement of neutrophils in tumor dormancy remains unclear. Studies on animal models have revealed that neutrophils contribute to tumor awakening and recurrence. For example, in a dormant breast cancer metastasis model, sustained smoking or lung infections triggered NET formation at the dormancy site in cancer cells. Neutrophils expelled the extracellular DNA trap net, covered with proteases such as NE and MMP-9s. NETs initiated matrix remodeling through cleavage of laminin, resulting in the generation of an epitope. The recognition of the epitope by the dormant cancer cells activates the signaling pathways that drive the proliferation of tumor cells (Albrengues et al., 2018). Michela et al. demonstrated that PMN-MDSCs awaken dormant tumor cells through stress- and inflammation-dependent mechanisms. Stress hormones cause massive secretion of proinflammatory S100A8/A9 compounds from PMN-MDSCs via β2-adrenergic receptors. Accumulation of oxidized lipids in neutrophils is caused by these proteins, which in turn stimulate an increase in fibroblast growth factors and induce the proliferation of dormant tumor cells (Perego et al., 2020) (Figure 2D). Overall, further research is required to elucidate the mechanisms controlling dormancy in human cancer metastasis.

TANs prepare pre-metastatic niches for tumor cells

Primary tumors can establish favorable locations for metastasis to distant organs, called the pre-metastatic niche (PMN) (Kaplan et al., 2005). Studies have clarified that neutrophils play a crucial role in establishing PMNs. At these sites, neutrophils are recruited by multiple tumor-secreted factors, thereby establishing an immunosuppressive environment that aids the survival and metastasis of tumor cells. The presence of these neutrophils creates a route for recruiting tumor cells from the bloodstream and tissues into the PMN (Seubert et al., 2015; Wculek and Malanchi, 2015; Lee et al., 2019).

Primary tumors secrete multiple cytokines and chemokines to induce PMNs. For example, using a model PMN involving a hyaluronic acid (HA)-based gel loaded with CXCL12 (CLG), the tumors were revealed to induce PMNs in target organs, producing the tumor-derived factor CXCL12, which induces the recruitment of neutrophils and attracts $CXCR4^+$ tumor cells both *in vivo* and *in vitro* (Ieranò et al., 2019). Furthermore, in a mouse metastatic CRC model, KIAA1199 facilitated the infiltration of immunosuppressive neutrophils into the liver. Mechanistically, cell migration-inducing hyaluronidase 1 (KIAA1199) activated the TGFβ signaling pathway by interacting with TGFβ receptor ½ (TGFBR1/2) to stimulate CXCL1 and CXCL3 production, thereby driving neutrophil aggregation in the liver and resulting in the suppression of the antitumor immunity of $CD8^+$ T cells. Therefore, blocking KIAA1199 may hinder the development of tumor metastasis (Wang et al., 2022a).

In addition to cytokines and chemokines, inflammatory factors play a role in establishing PMNs. Lung mesenchymal stromal cells (LMSCs) are triggered by Th2-type cytokines to produce large amounts of complement component 3 (C3) proteins, which increase neutrophil recruitment of highly expressed C3a receptors to the PMN, ultimately promoting metastasis. As the number of NETs increases, more circulating tumor cells may be captured in the lungs and colonize the area. Targeting the Th2-type cytokine–STAT6–C3–NETs axis may offer a promising method for preventing lung metastasis in breast cancer (Zheng et al., 2021). In addition, NETs have been identified in the omenta of mice with ovarian tumors before metastasis and in the omenta of women with early-stage ovarian tumors. In orthotopic ovarian cancer models, tumor-derived factors attract neutrophils to the pre-metastatic omentum, generating NETs and facilitating the capture of ovarian cancer cells (Lee et al., 2019) (Figure 3).

Extracellular vehicles (EVs) are released by tumor cells into the bloodstream. They carry specific molecules, such as DNA and RNA, which contribute to the signaling between cells in the TME. Exosomes are a subset of extracellular vesicles (EVs). Recent studies have shown that tumor cells release exosomes that play a role in PMN formation, thereby promoting metastasis. For example, Meiyan et al. reported that LIN28B secreted by tumor cells attracted neutrophils to the lung and established an immunosuppressive PMN in a triple-negative breast cancer model and patients with breast cancer. LIN28B induced IL-6 and IL-10-mediated neutrophil N2 conversion in the lung PMN, which increased the expression of T cell exhaustion ligands and inhibited the activity of T cells. This promotes the spread of breast cancer to the lungs. Furthermore, they demonstrated that breast cancer-released exosomes with low let-7s are critical for neutrophil recruitment and LIN28B-induced lung PMN formation (Qi et al., 2022). In addition, Maximiliane et al. reported that through genetic ablation of the BAG6 protein and disruption of

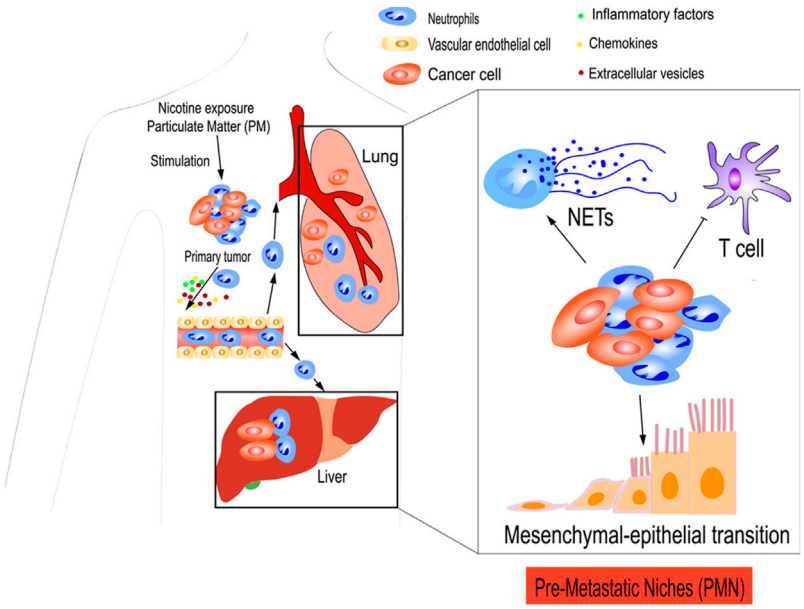

FIGURE 3
TANs prepare pre-metastatic niches (PMNs) for tumor cells. Primary tumors secreted various cytokines, chemokines, and inflammatory factors to establish PMN. CXCL12, CXCL1, and CXCL3 from tumors cause the aggregation of immunosuppressive neutrophils in the PMN, which result in the suppression of antitumor immunity of T cells. Neutrophils recruited to the PMN may release NETs that facilitate the trapping of cancer cells. Extracellular vesicles (EVs) have an important role in the formation of the PMN, which facilitates metastasis. Furthermore, nicotine exposure and particulate matter (PM) can also induce neutrophil recruitment and PMN formation. Nicotine exposure promotes the MET, thereby restoring some epithelial features and contributing to early colonization of the PMN.

p53 acetylation, melanoma cells secrete EVs, which form a PMN in distant tissues that recruit N2 neutrophils and tumors, promoting metastasis and progression (Schuldner et al., 2019). Therefore, EVs play a critical role in the process of PMN, which strengthens the connection between primary tumor cells and distant organs, facilitating the metastasis of tumor cells to secondary organs. A deeper understanding of the mechanism by which tumor-derived exosomes regulate PMN is essential for future research.

In addition, TANs can be used to prepare tumor cell sites using other methods. For example, chronic nicotine exposure plays a critical role in the development of pulmonary PMN. N2-neutrophils stimulate the secretion of the STAT3-activated glycoprotein lipocalin-2 (LCN2) in the PMN, which encourages cancer cells to undergo MET, restore epithelial features, and contribute to early colonization in the PMN (Tyagi et al., 2021). Another study demonstrated that TNF receptor-associated factor 6 (TRAF6) accumulates via autophagic degradation of tripartite motif-containing protein 37 (TRIM37) in lung epithelial cells as a result of particulate matter (PM), which is essential for initiating neutrophil recruitment and PMN formation in the lungs (Liu et al., 2021b) (Figure 3).

Overall, primary tumors can establish PMN for metastatic seeding. However, the cellular mechanisms influenced by TME are complicated. A better understanding of the molecular mechanisms underlying PMN is essential for the development of specific therapeutic strategies targeting TANs.

Prognostic value of TANs

Multiple studies have evaluated the prognostic value of the neutrophil-to-lymphocyte ratio (NLR) in a variety of cancers, including breast cancer (Krenn-Pilko et al., 2014), CRC (Grenader et al., 2016), non-small cell lung cancer (NSCLC) (Wang et al., 2019b), hepatocellular carcinoma (HCC) (Terashima et al., 2015), and melanoma (Cohen et al., 2020). Most studies have correlated a high NLR with poor prognosis. For example, a systematic meta-analysis of 100 studies exploring the prognostic value of NLR in patients with solid tumors emphasized that a high NLR was negatively associated with overall survival (OS) (Templeton et al., 2014). Low NLR is associated with improved survival rates, which was confirmed in 187 metastatic melanoma patients treated with ipilimumab (Ferrucci et al., 2015). Furthermore, in advanced NSCLC patients receiving nivolumab, the NLR has been proven to be a useful predictor of disease progression at 2 and 4 weeks after treatment (Nakaya et al., 2018). Ryoichi et al. indicated that the NLR is a valuable marker for predicting short-term outcomes in gastric

cancer patients (Miyamoto et al., 2018). Neutrophils account for a considerable proportion of immune infiltration in many cancer types; thus, several studies have examined the prognostic value of quantifying tumor-infiltrating neutrophils.

The presence of TANs is associated with poor prognoses in several studies of advanced GC (Kim et al., 2022), early-stage melanoma (Jensen et al., 2012), head and neck cancer (Trellakis et al., 2011), and HCC (Li et al., 2011). However, the prognostic relevance of TANs in some types of cancer, such as CRC, remains controversial. Shaobo et al. reported that TANs promoted the metastasis of CRC cells through an AGR2-CD98hc-xCT-mediated pathway and that patients with CRC with an increased abundance of $AGR2^{+}$ TANs had a poorer prognosis (Tian et al., 2022). In contrast, other studies have indicated that myeloperoxidase $(MPO)^{+}$ neutrophil infiltration is associated with a favorable prognosis in CRC (Berry et al., 2017; Wikberg et al., 2017). Therefore, further research on neutrophil infiltration and its prognostic significance is required. Neutrophils play a vital role in the effectiveness of immune checkpoint inhibitors (ICIs). In one case, neutrophils in NSCLC suppressed T-cell immune function, leading to the failure of ICI therapy and their corresponding efficacy. (Kargl et al., 2019). However, the potential for neutrophil resistance to clinical immune checkpoint blockade treatments has recently been observed. ICIs used in combination with TANs reduce the effectiveness of anti-angiogenic drugs (Faget et al., 2021). Therefore, further exploration of the clinical implications of the role of neutrophils in ICI response may allow researchers to gain a deeper understanding of TAN biology and its effects on patients. Conflicting reports exist on the effects of neutrophils on chemotherapy and radiotherapy. 5-Fluorouracil (5-FU) and gemcitabine eliminate immunosuppressive neutrophils and activate neutrophil inflammasomes and IL-1β secretion, promoting chemotherapy resistance (Bruchard et al., 2013). In contrast, the neutrophil count can also indicate a good prognosis for patients with high-grade ovarian cancer (Posabella et al., 2020). Similar to chemotherapy, neutrophils have paradoxical effects on radiotherapy (Schernberg et al., 2017; Liu et al., 2021a). Therefore, whether the effect of neutrophils in response to chemotherapy and radiotherapy is beneficial or harmful remains controversial and may depend on the type, stage, or nature of cancer treatment.

Strategies for targeting neutrophils

The results of these studies strongly suggest that neutrophils play a significant role in each step of the metastasis cascade. Several preclinical and clinical studies have shown that therapeutic targeting prolongs survival and decreases the risk of metastasis. Therefore, TANs may serve as potential therapeutic targets.

Next, we discuss current agents in terms of various mechanisms, such as inhibition of TAN survival, reprogramming of pre-tumor neutrophils into an antitumoral phenotype, and inhibition of TAN recruitment. The relevant drugs are listed in Table 2.

Agents against TAN survival

DS-8273a, an agonistic death receptor 5 (TRAIL-R2) antibody, can induce apoptosis in various tumor cells while sparing vital normal cells. Two TRAIL receptors, TRAIL-R1 (DR4) and TRAIL-R2 (DR5), induce apoptosis (de Miguel et al., 2016). Researchers have used DS-8273a to selectively target MDSCs in a phase I study of patients with stage III head and neck squamous cell carcinoma. In patients with increased numbers of circulating PMN-MDSCs (CD11b+/CD14+/CD33+/CD15+; low-density fraction cells), treatment with DS8273a decreased their numbers (Dominguez et al., 2017). However, TRAIL receptor agonists are subject to further investigation in terms of their safety and tolerability. Gemcitabine, a nucleoside analog, is an effective antitumor drug. During DNA replication, its incorporation into DNA triggers strand termination leading to cell death. In patients with pancreatic cancer, PMN-MDSCs ($CD11b^{+}/CD14^{-}/CD33^{+}/HLA^{-}/DR^{-}$) were significantly reduced after gemcitabine treatment. However, following the resting phase, the effect of the treatment was attenuated after terminating the administration of gemcitabine. This suggests that continuous administration of gemcitabine is required to achieve a lasting effect on PMN-MDSCs (Eriksson et al., 2016). Similarly, in a phase II clinical trial, gemcitabine increased the efficacy of nivolumab by killing MDSCs to reduce immunosuppression in stage IIIB NSCLC (NCT03302247). Capecitabine, a 5-FU prodrug, selectively induces MDSC death *in vitro* and *in vivo* more strongly than gemcitabine. MDSCs were eliminated by 5-FU, increasing the secretion of IFN-γ by tumor-specific $CD8^{+}$ T cells that infiltrated the tumor and induced an antitumor response *in vivo* (Vincent et al., 2010). In a phase II clinical trial of patients with stage IV CRC, 5-FU plus bevacizumab and anakinra resulted in an approximate doubling of the median progression-free survival and a manageable safety profile (Isambert et al., 2018). However, DS-8273a, capecitabine, and gemcitabine have unavoidable side effects such as unselective neutrophil depletion. Therefore, developing agents that preferentially target N2 neutrophils is essential to minimize toxicity. However, further research is required before substantial clinical applications can be explored.

Agents inhibiting neutrophil recruitment

As mentioned earlier, TME tumors secrete chemokines that attract tumor-associated neutrophils to the tumor sites.

TABLE 2 Clinical trials of agents targeting TANs.

Compound	Target	Combination partner	Tumor type	Phase	Ref. or trial no.
Agents that inhibit TAN survival					
DS-8273a	PMN-MDSCs	Monotherapy	Head and neck tumor	3	Dominguez et al. (2017)
Gemcitabine	PMN-MDSCs	Monotherapy	NSCLC	3	NCT03302247
Fluorouracil (5-FU)	MDSC	Bevacizumab Anakinra	CRC	2	Isambert et al. (2018)
Agents that inhibit TAN recruitment					
SX-682	CXCR2	Pembrolizumab	Melanoma	1	NCT03161431
Reparixin	CXCR1	Paclitaxel	Triple-negative breast cancer	2	NCT02370238
Agents that reprogram pre-tumor neutrophils into an antitumoral phenotype					
Fresolimumab	TGF-β	Monotherapy	Renal cell carcinoma	1	Lacouture et al. (2015)
	TGF-β	Radiation therapy	Metastatic breast cancer	Completed	(Formenti et al., 2018)
	TGF-β	Monotherapy	High-grade gliomas	2	den Hollander et al. (2015)
Galunisertib	TGF-β	Galunisertib	HCC	2	Kelley et al. (2019)
		Sorafenib			
	TGF-β	Durvalumab	Metastatic pancreatic cancer	1	Melisi et al. (2021)

Therefore, a TAN-targeting anticancer therapeutic approach could include disrupting signals that attract neutrophils. The CXCR2 signaling pathway plays a critical role in mediating the movement of neutrophils from the bone marrow into the bloodstream and subsequently into the peripheral tissues. Numerous studies have revealed the efficacy of CXCR2-targeted therapy, which has initiated early-phase clinical trials. This therapy works through the use of SX-682, a small-molecule inhibitor of CXCR1 and CXCR2, which retards tumor development. In tumor-bearing mice, SX-682 reduced the infiltration of MDSCs into tumors and increased activated $CD8^+$ T cells, thereby inhibiting tumor growth (Yang et al., 2021). Moreover, in head and neck cancer models, SX-682 decreased tumor infiltration caused by PMN-MDSCs and increased tumor infiltration and activation of adoptively transferred murine NK cells (Greene et al., 2020). However, further research on SX-682 in clinical trials is required. In stages III and IV melanoma patients, SX-682 was evaluated to determine whether it could block cancer cells from attracting MDSCs (NCT03161431). Identifying and elucidating the mechanism by which blocking CXCR2 may affect tumor growth is of particular interest. Reparixin is a non-competitive allosteric CXCR1/CXCR2 inhibitor. In a mouse cisplatin-induced acute kidney injury (AKI) model, it protected the kidneys by decreasing inflammatory cytokines and neutrophil infiltration (Liu et al., 2020). However, the applications of reparixin have not been extensively studied in the clinical treatment context. Reparixin is currently being evaluated in combination with paclitaxel chemotherapy versus paclitaxel alone in patients with metastatic triple-negative breast cancer for further evaluation of their progression-free survival.

Reprogramming pre-tumor neutrophils into an antitumoral phenotype

Given the critical involvement of neutrophils in the immune system, whether the systemic elimination of neutrophils results in deleterious consequences during long-term treatment remains unknown. Although not studied extensively, pre-tumor neutrophils can reportedly be reprogrammed into antitumor neutrophils. The mechanism underlying this is through TGF-β-blocking antibodies, which enhance the tumor-killing activity of neutrophils. For example, mesoporous silica nanoparticles loaded with SB525334, an inhibitor of the TGF-β1 receptor, were designed in mouse models of pancreatic cancer. Local inhibition of TGF-β increases neutrophil polarization towards an anticancer phenotype in the TME and induces long-term antitumor memory (Peng et al., 2022). Similarly, another study revealed that a novel CRC-derived exosomal circPACRGL facilitated TGF-β1 expression and induced differentiation of N1 to N2 in mouse models (Shang et al., 2020). Moreover, in H22 mice, a novel nanovaccine reportedly changed the protumoral N2 phenotype of neutrophils to the antitumor N1 phenotype in the TME. The effect achieved complete tumor regression (83%) and prolonged survival (Wang et al., 2022b). However, further randomized clinical studies are warranted to validate the potential use of TGF-β in clinical practice. Additionally, fresolimumab was well tolerated and used in participants with osteogenesis imperfecta (OI) type IV, as well as a TGF-β-neutralizing antibody (Song et al., 2022). In phase I/II trials, fresolimumab was shown to have an acceptable safety profile and favorable systemic immune response in patients with melanoma, renal cell carcinoma (Lacouture et al., 2015), and metastatic breast cancer

(Formenti et al., 2018). Zr-fresolimumab penetrated recurrent high-grade gliomas well but did not provide any clinical benefits (den Hollander et al., 2015). Clinical trials of fresolimumab are more commonly associated with TGF-β neutralization. Detailed studies are lacking on the functional reprogramming of neutrophils, which may have significant benefits for future tumor therapy.

Several clinical trials have demonstrated the tolerability and activity of single-agent or combination chemotherapy. Galunisertib is a small-molecule selective inhibitor of TGFβ receptor I. Recently, in a phase II trial with HCC, the combination of galunisertib and sorafenib showed acceptable safety and a longer OS outcome (Kelley et al., 2019). However, galunisertib plus durvalumab provided a disease control rate of 25% in patients with metastatic pancreatic cancer. Median OS and progression-free survival were 5.72 months (95% CI: 4.01–8.38) and 1.87 months (95% CI: 1.58–3.09), respectively. Biomarkers did not correlate with treatment outcomes, and this analysis was limited by the relatively small sample size (Melisi et al., 2021). Expanding the number of clinical samples is required to further evaluate their clinical value.

Conclusion and perspectives

Cancer has a high incidence and mortality rate worldwide and is one of the most significant public health problems. While metastasis is a marker for malignancy, the results achieved with existing treatments are unsatisfactory because most aim to eliminate the tumor cells. However, successful seeding of metastases is greatly dependent on nonmalignant cells within the TME (Güç and Pollard, 2021). As the major components of the TME, TANs promote tumor progression and metastasis through multiple mechanisms. Therapeutic strategies targeting TANs may offer potential therapeutic opportunities contingent on improving our understanding of the relationship between TANs and metastasis. Targeting the pro-metastatic components of the TME to re-establish a healthy environment will undoubtedly offer viable avenues for tumor treatment.

Although these treatments are effective, several fundamental hurdles remain to be overcome. First, TANs exhibit remarkable heterogeneity and plasticity. Although they are usually considered the N2 type, they can display both tumoricidal and protumoral functions. The mechanism by which these phenotypes switch during tumor progression is not entirely understood. There are diverse subsets of neutrophils, including immature, mature, low-density, and high-density. Surface markers on neutrophils constantly change based on the influence of the TME; therefore, they can exhibit pro- or antitumor effects (Hsu et al., 2019). In particular, neutrophil metabolism is regulated by microenvironmental exposures that play different or contrasting roles, varying from killing tumor cells to supporting them. Although the metabolism of tumor cells has been extensively studied, the effect of cancer on neutrophil metabolism remains insufficiently understood. Further experiments are required to determine the mechanism by which TAN metabolism should be targeted to enhance cancer immunotherapy.

Second, the TME is a complex system consisting of several cellular and non-cellular components. Neutrophils, one of the main regulators in the TME, do not function alone but interact with other components. During metastasis, they are intricately linked to the surrounding matrix and to each other (Mao et al., 2021). A recent study reported that IL-8, released by apoptotic tumor cells, recruits neutrophils to the tumor, where they induce macrophages to exhibit an M2-like phenotype in both primary patient-derived and established CRC cells. Crosstalk between TANs and adjacent macrophages creates an immunosuppressive TME (Schimek et al., 2022). Overall, the roles of the components of the TME and the complex interactions between them remain largely unknown but are promising prospects for immunotherapy.

Third, the prediction and detection of micrometastases are major clinical problems. Cancer cells can escape from primary sites and spread to other organs, where they can remain dormant and clinically undetected for a long time. The triggers that cause these largely dormant cells to reawaken, proliferate, and spread are not fully understood. Micrometastases may appear months, years, or even decades before diagnosis in certain cancers (Hu et al., 2020). Understanding the mechanism by which tumors enter and exit dormancy is crucial to providing patients with effective treatment. Neutrophils can activate dormant cells and promote tumor metastasis. For example, in mouse models, a recent study showed that sustained inflammation induces the formation of NETs, which awakens dormant cancer cells by releasing NE and MMP-9. These neutrophil-associated enzymes sequentially cleave laminin, which induces the proliferation of dormant cancer cells by activating integrin α3β1 signaling (Albrengues et al., 2018). However, in most cases, dormant tumor cells can only be investigated through animal studies. Furthermore, detecting individual dormant tumor cells using current techniques is challenging. Further evidence is required to examine the process by which neutrophils awaken dormant tumor cells and disseminate them to secondary organs. A better understanding of this process may pave the way for the clinical exploitation of neutrophils.

In conclusion, this study provides a detailed review of the interactions between TANs and tumor cells during tumor metastasis. TANs are a potential target that could change the future landscape of cancer treatment; however, numerous hurdles remain unexplored. We believe that our review will encourage future research on the development of TAN-targeting drugs for cancer treatment.

Author contributions

Designed the paper; contributed to manuscript writing; and approved the manuscript before submission: SZ, Contributed to manuscript writing; and approved the manuscript before submission: MY, MZ, and RN. Collected literatures and approved the manuscript before submission: XY, LF, ST, and YL. All authors read and approved the final submitted version of the manuscript.

Funding

This work was supported in part by grants from the National Science Foundation of China (#82173283 and #82103088), and Foundation of committee on science and technology of Tianjin (#21JCZDJC00230, #2020036, #20JCYBJC01230). The funders had no roles in the design of the study, data collection, analysis and interpretation, or decision to write and publish the work.

Acknowledgments

We acknowledge Editage service for the manuscript language edit.

Conflict of interest

The authors declare that the research was conducted in the absence of any commercial or financial relationships that could be construed as a potential conflict of interest.

Publisher's note

All claims expressed in this article are solely those of the authors and do not necessarily represent those of their affiliated organizations, or those of the publisher, the editors and the reviewers. Any product that may be evaluated in this article, or claim that may be made by its manufacturer, is not guaranteed or endorsed by the publisher.

References

Aceto, N., Bardia, A., Miyamoto, D. T., Donaldson, M. C., Wittner, B. S., Spencer, J. A., et al. (2014). Circulating tumor cell clusters are oligoclonal precursors of breast cancer metastasis. *Cell* 158, 1110–1122. doi:10.1016/j.cell.2014.07.013

Albrengues, J., Shields, M. A., Ng, D., Park, C. G., Ambrico, A., Poindexter, M. E., et al. (2018). Neutrophil extracellular traps produced during inflammation awaken dormant cancer cells in mice. *Science* 361, eaao4227. doi:10.1126/science.aao4227

Alshetaiwi, H., Pervolarakis, N., McIntyre, L. L., Ma, D., Nguyen, Q., Rath, J. A., et al. (2020). Defining the emergence of myeloid-derived suppressor cells in breast cancer using single-cell transcriptomics. *Sci. Immunol.* 5, eaay6017. doi:10.1126/sciimmunol.aay6017

Arvanitakis, K., Mitroulis, I., and Germanidis, G. (2021). Tumor-associated neutrophils in hepatocellular carcinoma pathogenesis, prognosis, and therapy. *Cancers (Basel)* 13, 2899. doi:10.3390/cancers13122899

Bald, T., Quast, T., Landsberg, J., Rogava, M., Glodde, N., Lopez-Ramos, D., et al. (2014). Ultraviolet-radiation-induced inflammation promotes angiotropism and metastasis in melanoma. *Nature* 507, 109–113. doi:10.1038/nature13111

Berry, R. S., Xiong, M. J., Greenbaum, A., Mortaji, P., Nofchissey, R. A., Schultz, F., et al. (2017). High levels of tumor-associated neutrophils are associated with improved overall survival in patients with stage II colorectal cancer. *PLoS One* 12, e0188799. doi:10.1371/journal.pone.0188799

Bordbari, S., Mörchen, B., Pylaeva, E., Siakaeva, E., Spyra, I., Domnich, M., et al. (2021). SIRT1-mediated deacetylation of FOXO3a transcription factor supports pro-angiogenic activity of interferon-deficient tumor-associated neutrophils. *Int. J. Cancer* 150, 1198–1211. doi:10.1002/ijc.33871

Bronte, V., Brandau, S., Chen, S. H., Colombo, M. P., Frey, A. B., Greten, T. F., et al. (2016). Recommendations for myeloid-derived suppressor cell nomenclature and characterization standards. *Nat. Commun.* 7, 12150. doi:10.1038/ncomms12150

Bruchard, M., Mignot, G., Derangère, V., Chalmin, F., Chevriaux, A., Végran, F., et al. (2013). Chemotherapy-triggered cathepsin B release in myeloid-derived suppressor cells activates the Nlrp3 inflammasome and promotes tumor growth. *Nat. Med.* 19, 57–64. doi:10.1038/nm.2999

Butin-Israeli, V., Bui, T. M., Wiesolek, H. L., Mascarenhas, L., Lee, J. J., Mehl, L. C., et al. (2019). Neutrophil-induced genomic instability impedes resolution of inflammation and wound healing. *J. Clin. Invest.* 129, 712–726. doi:10.1172/JCI122085

Cheng, Y., Li, H., Deng, Y., Tai, Y., Zeng, K., Zhang, Y., et al. (2018). Cancer-associated fibroblasts induce PDL1+ neutrophils through the IL6-STAT3 pathway that foster immune suppression in hepatocellular carcinoma. *Cell Death Dis.* 9, 422. doi:10.1038/s41419-018-0458-4

Cassetta, L., Baekkevold, E. S., Brandau, S., Bujko, A., Cassatella, M. A., Dorhoi, A., et al. (2019). Deciphering myeloid-derived suppressor cells: Isolation and markers in humans, mice and non-human primates. *Cancer Immunol. Immunother.* 68, 687–697. doi:10.1007/s00262-019-02302-2

Chao, T., Furth, E. E., and Vonderheide, R. H. (2016). CXCR2-Dependent accumulation of tumor-associated neutrophils regulates T-cell immunity in pancreatic ductal adenocarcinoma. *Cancer Immunol. Res.* 4, 968–982. doi:10.1158/2326-6066.CIR-16-0188

Ci, Y., Zhang, Y., Liu, Y., Lu, S., Cao, J., Li, H., et al. (2018). Myricetin suppresses breast cancer metastasis through down-regulating the activity of matrix metalloproteinase (MMP)-2/9. *Phytother. Res.* 32, 1373–1381. doi:10.1002/ptr.6071

Cohen, J. T., Miner, T. J., and Vezeridis, M. P. (2020). Is the neutrophil-to-lymphocyte ratio a useful prognostic indicator in melanoma patients? *Melanoma Manag.* 7, Mmt47. doi:10.2217/mmt-2020-0006

Condamine, T., Dominguez, G. A., Youn, J. I., Kossenkov, A. V., Mony, S., Alicea-Torres, K., et al. (2016). Lectin-type oxidized LDL receptor-1 distinguishes population of human polymorphonuclear myeloid-derived suppressor cells in cancer patients. *Sci. Immunol.* 1, aaf8943. doi:10.1126/sciimmunol.aaf8943

Cui, T. X., Kryczek, I., Zhao, L., Zhao, E., Kuick, R., Roh, M. H., et al. (2013). Myeloid-derived suppressor cells enhance stemness of cancer cells by inducing microRNA101 and suppressing the corepressor CtBP2. *Immunity* 39, 611–621. doi:10.1016/j.immuni.2013.08.025

Davis, R. E., Sharma, S., Conceição, J., Carneiro, P., Novais, F., Scott, P., et al. (2017). Phenotypic and functional characteristics of HLA-DR(+) neutrophils in Brazilians with cutaneous leishmaniasis. *J. Leukoc. Biol.* 101, 739–749. doi:10.1189/jlb.4A0915-442RR

de Miguel, D., Lemke, J., Anel, A., Walczak, H., and Martinez-Lostao, L. (2016). Onto better TRAILs for cancer treatment. *Cell Death Differ.* 23, 733–747. doi:10.1038/cdd.2015.174

den Hollander, M. W., Bensch, F., Glaudemans, A. W., Oude Munnink, T. H., Enting, R. H., den Dunnen, W. F., et al. (2015). TGF-B antibody uptake in recurrent high-grade glioma imaged with 89Zr-fresolimumab PET. *J. Nucl. Med.* 56, 1310–1314. doi:10.2967/jnumed.115.154401

Deng, J., Kang, Y., Cheng, C. C., Li, X., Dai, B., Katz, M. H., et al. (2021). DDR1-induced neutrophil extracellular traps drive pancreatic cancer metastasis. *JCI Insight* 6, 146133. doi:10.1172/jci.insight.146133

Deyell, M., Garris, C. S., and Laughney, A. M. (2021). Cancer metastasis as a non-healing wound. *Br. J. Cancer* 124, 1491–1502. doi:10.1038/s41416-021-01309-w

Ding, H., Zhao, L., Dai, S., Li, L., Wang, F., and Shan, B. (2016). CCL5 secreted by tumor associated macrophages may be a new target in treatment of gastric cancer. *Biomed. Pharmacother.* 77, 142–149. doi:10.1016/j.biopha.2015.12.004

Dominguez, G. A., Condamine, T., Mony, S., Hashimoto, A., Wang, F., Liu, Q., et al. (2017). Selective targeting of myeloid-derived suppressor cells in cancer patients using DS-8273a, an agonistic TRAIL-R2 antibody. *Clin. Cancer Res.* 23, 2942–2950. doi:10.1158/1078-0432.CCR-16-1784

Du, J., Wang, C., Chen, Y., Zhong, L., Liu, X., Xue, L., et al. (2022). Targeted downregulation of HIF-1α for restraining circulating tumor microemboli mediated metastasis. *J. Control. Release* 343, 457–468. doi:10.1016/j.jconrel.2022.01.051

El Rayes, T., Catena, R., Lee, S., Stawowczyk, M., Joshi, N., Fischbach, C., et al. (2015). Lung inflammation promotes metastasis through neutrophil protease-mediated degradation of Tsp-1. *Proc. Natl. Acad. Sci. U. S. A.* 112, 16000–16005. doi:10.1073/pnas.1507294112

Elliot, A., Myllymäki, H., and Feng, Y. (2020). Inflammatory responses during tumour initiation: From zebrafish transgenic models of cancer to evidence from mouse and man. *Cells* 9, E1018. doi:10.3390/cells9041018

Eriksson, E., Wenthe, J., Irenaeus, S., Loskog, A., and Ullenhag, G. (2016). Gemcitabine reduces MDSCs, tregs and TGFβ-1 while restoring the teff/treg ratio in patients with pancreatic cancer. *J. Transl. Med.* 14, 282. doi:10.1186/s12967-016-1037-z

Eruslanov, E. B., Bhojnagarwala, P. S., Quatromoni, J. G., Stephen, T. L., Ranganathan, A., Deshpande, C., et al. (2014). Tumor-associated neutrophils stimulate T cell responses in early-stage human lung cancer. *J. Clin. Invest.* 124, 5466–5480. doi:10.1172/JCI77053

Evrard, M., Kwok, I. W. H., Chong, S. Z., Teng, K. W. W., Becht, E., Chen, J., et al. (2018). Developmental analysis of bone marrow neutrophils reveals populations specialized in expansion, trafficking, and effector functions. *Immunity* 48, 364–379. e8. doi:10.1016/j.immuni.2018.02.002

Faget, J., Peters, S., Quantin, X., Meylan, E., and Bonnefoy, N. (2021). Neutrophils in the era of immune checkpoint blockade. *J. Immunother. Cancer* 9, e002242. doi:10.1136/jitc-2020-002242

Ferrucci, P. F., Gandini, S., Battaglia, A., Alfieri, S., Di Giacomo, A. M., Giannarelli, D., et al. (2015). Baseline neutrophil-to-lymphocyte ratio is associated with outcome of ipilimumab-treated metastatic melanoma patients. *Br. J. Cancer* 112, 1904–1910. doi:10.1038/bjc.2015.180

Follain, G., Herrmann, D., Harlepp, S., Hyenne, V., Osmani, N., Warren, S. C., et al. (2020). Fluids and their mechanics in tumour transit: Shaping metastasis. *Nat. Rev. Cancer* 20, 107–124. doi:10.1038/s41568-019-0221-x

Formenti, S. C., Lee, P., Adams, S., Goldberg, J. D., Li, X., Xie, M. W., et al. (2018). Focal irradiation and systemic TGFβ blockade in metastatic breast cancer. *Clin. Cancer Res.* 24, 2493–2504. doi:10.1158/1078-0432.CCR-17-3322

Fortunati, E., Kazemier, K. M., Grutters, J. C., Koenderman, L., and Van den Bosch v, J. (2009). Human neutrophils switch to an activated phenotype after homing to the lung irrespective of inflammatory disease. *Clin. Exp. Immunol.* 155, 559–566. doi:10.1111/j.1365-2249.2008.03791.x

Fridlender, Z. G., Sun, J., Kim, S., Kapoor, V., Cheng, G., Ling, L., et al. (2009). Polarization of tumor-associated neutrophil phenotype by TGF-beta: "N1" versus "N2" TAN. *Cancer Cell* 16, 183–194. doi:10.1016/j.ccr.2009.06.017

Fu, J., Tobin, M. C., and Thomas, L. L. (2014). Neutrophil-like low-density granulocytes are elevated in patients with moderate to severe persistent asthma. *Ann. Allergy Asthma Immunol.* 113, 635–640. doi:10.1016/j.anai.2014.08.024

Galdiero, M. R., Marone, G., and Mantovani, A. (2018). Cancer inflammation and cytokines. *Cold Spring Harb. Perspect. Biol.* 10, a028662. doi:10.1101/cshperspect.a028662

Greene, S., Robbins, Y., Mydlarz, W. K., Huynh, A. P., Schmitt, N. C., Friedman, J., et al. (2020). Inhibition of MDSC trafficking with SX-682, a CXCR1/2 inhibitor, enhances NK-cell immunotherapy in head and neck cancer models. *Clin. Cancer Res.* 26, 1420–1431. doi:10.1158/1078-0432.CCR-19-2625

Grenader, T., Nash, S., Adams, R., Kaplan, R., Fisher, D., Maughan, T., et al. (2016). Derived neutrophil lymphocyte ratio is predictive of survival from intermittent therapy in advanced colorectal cancer: A post hoc analysis of the MRC COIN study. *Br. J. Cancer* 114, 612–615. doi:10.1038/bjc.2016.23

Groth, C., Arpinati, L., Shaul, M. E., Winkler, N., Diester, K., Gengenbacher, N., et al. (2021). Blocking migration of polymorphonuclear myeloid-derived suppressor cells inhibits mouse melanoma progression. *Cancers (Basel)* 13, 726. doi:10.3390/cancers13040726

Güç, E., and Pollard, J. W. (2021). Redefining macrophage and neutrophil biology in the metastatic cascade. *Immunity* 54, 885–902. doi:10.1016/j.immuni.2021.03.022

Hacbarth, E., and Kajdacsy-Balla, A. (1986). Low density neutrophils in patients with systemic lupus erythematosus, rheumatoid arthritis, and acute rheumatic fever. *Arthritis Rheum.* 29, 1334–1342. doi:10.1002/art.1780291105

Hanahan, D., and Folkman, J. (1996). Patterns and emerging mechanisms of the angiogenic switch during tumorigenesis. *Cell* 86, 353–364. doi:10.1016/s0092-8674(00)80108-7

Hsu, B. E., Tabariès, S., Johnson, R. M., Andrzejewski, S., Senecal, J., Lehuédé, C., et al. (2019). Immature low-density neutrophils exhibit metabolic flexibility that facilitates breast cancer liver metastasis. *Cell Rep.* 27, 3902–3915. e6. doi:10.1016/j.celrep.2019.05.091

Hu, X., Xiang, F., Feng, Y., Gao, F., Ge, S., Wang, C., et al. (2022). Neutrophils promote tumor progression in oral squamous cell carcinoma by regulating EMT and JAK2/STAT3 signaling through chemerin. *Front. Oncol.* 12, 812044. doi:10.3389/fonc.2022.812044

Hu, Z., Li, Z., Ma, Z., and Curtis, C. (2020). Multi-cancer analysis of clonality and the timing of systemic spread in paired primary tumors and metastases. *Nat. Genet.* 52, 701–708. doi:10.1038/s41588-020-0628-z

Hua, Y., and Bergers, G. (2019). Tumors vs. Chronic wounds: An immune cell's perspective. *Front. Immunol.* 10, 2178. doi:10.3389/fimmu.2019.02178

Ieranò, C., D'Alterio, C., Giarra, S., Napolitano, M., Rea, G., Portella, L., et al. (2019). CXCL12 loaded-dermal filler captures CXCR4 expressing melanoma circulating tumor cells. *Cell Death Dis.* 10, 562. doi:10.1038/s41419-019-1796-6

Isambert, N., Hervieu, A., Rébé, C., Hennequin, A., Borg, C., Zanetta, S., et al. (2018). Fluorouracil and bevacizumab plus anakinra for patients with metastatic colorectal cancer refractory to standard therapies (IRAFU): A single-arm phase 2 study. *Oncoimmunology* 7, e1474319. doi:10.1080/2162402X.2018.1474319

Jensen, T. O., Schmidt, H., Møller, H. J., Donskov, F., Høyer, M., Sjoegren, P., et al. (2012). Intratumoral neutrophils and plasmacytoid dendritic cells indicate poor prognosis and are associated with pSTAT3 expression in AJCC stage I/II melanoma. *Cancer* 118, 2476–2485. doi:10.1002/cncr.26511

Kajioka, H., Kagawa, S., Ito, A., Yoshimoto, M., Sakamoto, S., Kikuchi, S., et al. (2021). Targeting neutrophil extracellular traps with thrombomodulin prevents pancreatic cancer metastasis. *Cancer Lett.* 497, 1–13. doi:10.1016/j.canlet.2020.10.015

Kalluri, R., and Weinberg, R. A. (2009). The basics of epithelial-mesenchymal transition. *J. Clin. Invest.* 119, 1420–1428. doi:10.1172/JCI39104

Kaplan, R. N., Riba, R. D., Zacharoulis, S., Bramley, A. H., Vincent, L., Costa, C., et al. (2005). VEGFR1-positive haematopoietic bone marrow progenitors initiate the pre-metastatic niche. *Nature* 438, 820–827. doi:10.1038/nature04186

Kargl, J., Zhu, X., Zhang, H., Yang, G. H. Y., Friesen, T. J., Shipley, M., et al. (2019). Neutrophil content predicts lymphocyte depletion and anti-PD1 treatment failure in NSCLC. *JCI Insight* 4, 130850. doi:10.1172/jci.insight.130850

Kelley, R. K., Gane, E., Assenat, E., Siebler, J., Galle, P. R., Merle, P., et al. (2019). A phase 2 study of galunisertib (TGF-β1 receptor type I inhibitor) and sorafenib in patients with advanced hepatocellular carcinoma. *Clin. Transl. Gastroenterol.* 10, e00056. doi:10.14309/ctg.0000000000000056

Khaled, Y. S., Ammori, B. J., and Elkord, E. (2014). Increased levels of granulocytic myeloid-derived suppressor cells in peripheral blood and tumour tissue of pancreatic cancer patients. *J. Immunol. Res.* 2014, 879897. doi:10.1155/2014/879897

Kim, E. Y., Abdul-Ghafar, J., Chong, Y., and Yim, K. (2022). Calculated tumor-associated neutrophils are associated with the tumor-stroma ratio and predict a poor prognosis in advanced gastric cancer. *Biomedicines* 10, 708. doi:10.3390/biomedicines10030708

Kitamura, T., Qian, B. Z., and Pollard, J. W. (2015). Immune cell promotion of metastasis. *Nat. Rev. Immunol.* 15, 73–86. doi:10.1038/nri3789

Krenn-Pilko, S., Langsenlehner, U., Thurner, E. M., Stojakovic, T., Pichler, M., Gerger, A., et al. (2014). The elevated preoperative platelet-to-lymphocyte ratio predicts poor prognosis in breast cancer patients. *Br. J. Cancer* 110, 2524–2530. doi:10.1038/bjc.2014.163

Lacouture, M. E., Morris, J. C., Lawrence, D. P., Tan, A. R., Olencki, T. E., Shapiro, G. I., et al. (2015). Cutaneous keratoacanthomas/squamous cell carcinomas associated with neutralization of transforming growth factor β by the monoclonal antibody fresolimumab (GC1008). *Cancer Immunol. Immunother.* 64, 437–446. doi:10.1007/s00262-015-1653-0

Lambert, A. W., Pattabiraman, D. R., and Weinberg, R. A. (2017). Emerging biological principles of metastasis. *Cell* 168, 670–691. doi:10.1016/j.cell.2016.11.037

Langenau, D. M., Feng, H., Berghmans, S., Kanki, J. P., Kutok, J. L., and Look, A. T. (2005). Cre/lox-regulated transgenic zebrafish model with conditional myc-induced T cell acute lymphoblastic leukemia. *Proc. Natl. Acad. Sci. U. S. A.* 102, 6068–6073. doi:10.1073/pnas.0408708102

Langenau, D. M., Traver, D., Ferrando, A. A., Kutok, J. L., Aster, J. C., Kanki, J. P., et al. (2003). Myc-induced T cell leukemia in transgenic zebrafish. *Science* 299, 887–890. doi:10.1126/science.1080280

Lee, W., Ko, S. Y., Mohamed, M. S., Kenny, H. A., Lengyel, E., and Naora, H. (2019). Neutrophils facilitate ovarian cancer premetastatic niche formation in the omentum. *J. Exp. Med.* 216, 176–194. doi:10.1084/jem.20181170

Li, S., Cong, X., Gao, H., Lan, X., Li, Z., Wang, W., et al. (2019). Tumor-associated neutrophils induce EMT by IL-17a to promote migration and invasion in gastric cancer cells. *J. Exp. Clin. Cancer Res.* 38, 6. doi:10.1186/s13046-018-1003-0

Li, T. J., Jiang, Y. M., Hu, Y. F., Huang, L., Yu, J., Zhao, L. Y., et al. (2017). Interleukin-17-Producing neutrophils link inflammatory stimuli to disease progression by promoting angiogenesis in gastric cancer. *Clin. Cancer Res.* 23, 1575–1585. doi:10.1158/1078-0432.CCR-16-0617

Li, Y. W., Qiu, S. J., Fan, J., Zhou, J., Gao, Q., Xiao, Y. S., et al. (2011). Intratumoral neutrophils: A poor prognostic factor for hepatocellular carcinoma following resection. *J. Hepatol.* 54, 497–505. doi:10.1016/j.jhep.2010.07.044

Lin, Y., Xu, J., and Lan, H. (2019). Tumor-associated macrophages in tumor metastasis: Biological roles and clinical therapeutic applications. *J. Hematol. Oncol.* 12, 76. doi:10.1186/s13045-019-0760-3

Liu, J., Li, S., Fei, X., Nan, X., Shen, Y., Xiu, H., et al. (2021). Increased alveolar epithelial TRAF6 via autophagy-dependent TRIM37 degradation mediates particulate matter-induced lung metastasis. *Autophagy* 18, 971–989. doi:10.1080/15548627.2021.1965421

Liu, P., Li, X., Lv, W., and Xu, Z. (2020). Inhibition of CXCL1-CXCR2 axis ameliorates cisplatin-induced acute kidney injury by mediating inflammatory response. *Biomed. Pharmacother.* 122, 109693. doi:10.1016/j.biopha.2019.109693

Liu, Q., Hao, Y., Du, R., Hu, D., Xie, J., Zhang, J., et al. (2021). Radiotherapy programs neutrophils to an antitumor phenotype by inducing mesenchymal-epithelial transition. *Transl. Lung Cancer Res.* 10, 1424–1443. doi:10.21037/tlcr-21-152

Lonardi, S., Missale, F., Calza, S., Bugatti, M., Vescovi, R., Debora, B., et al. (2021). Tumor-associated neutrophils (TANs) in human carcinoma-draining lymph nodes: A novel TAN compartment. *Clin. Transl. Immunol.* 10, e1252. doi:10.1002/cti2.1252

Mao, X., Xu, J., Wang, W., Liang, C., Hua, J., Liu, J., et al. (2021). Crosstalk between cancer-associated fibroblasts and immune cells in the tumor microenvironment: New findings and future perspectives. *Mol. Cancer* 20, 131. doi:10.1186/s12943-021-01428-1

Massagué, J., and Obenauf, A. C. (2016). Metastatic colonization by circulating tumour cells. *Nature* 529, 298–306. doi:10.1038/nature17038

McKenna, E., Mhaonaigh, A. U., Wubben, R., Dwivedi, A., Hurley, T., Kelly, L. A., et al. (2021). Neutrophils: Need for standardized nomenclature. *Front. Immunol.* 12, 602963. doi:10.3389/fimmu.2021.602963

Melisi, D., Oh, D. Y., Hollebecque, A., Calvo, E., Varghese, A., Borazanci, E., et al. (2021). Safety and activity of the TGFβ receptor I kinase inhibitor galunisertib plus the anti-PD-L1 antibody durvalumab in metastatic pancreatic cancer. *J. Immunother. Cancer* 9, e002068. doi:10.1136/jitc-2020-002068

Minder, P., Zajac, E., Quigley, J. P., and Deryugina, E. I. (2015). EGFR regulates the development and microarchitecture of intratumoral angiogenic vasculature capable of sustaining cancer cell intravasation. *Neoplasia* 17, 634–649. doi:10.1016/j.neo.2015.08.002

Miyamoto, R., Inagawa, S., Sano, N., Tadano, S., Adachi, S., and Yamamoto, M. (2018). The neutrophil-to-lymphocyte ratio (NLR) predicts short-term and long-term outcomes in gastric cancer patients. *Eur. J. Surg. Oncol.* 44, 607–612. doi:10.1016/j.ejso.2018.02.003

Mu, W., Chu, Q., Yang, H., Guan, L., Fu, S., Gao, T., et al. (2022). Multipoint costriking nanodevice eliminates primary tumor cells and associated-circulating tumor cells for enhancing metastasis inhibition and therapeutic effect on HCC. *Adv. Sci.* 9, 2101472. doi:10.1002/advs.202101472

Mukaida, N., Sasaki, S. I., and Baba, T. (2020). Two-faced roles of tumor-associated neutrophils in cancer development and progression. *Int. J. Mol. Sci.* 21, E3457. doi:10.3390/ijms21103457

Nakaya, A., Kurata, T., Yoshioka, H., Takeyasu, Y., Niki, M., Kibata, K., et al. (2018). Neutrophil-to-lymphocyte ratio as an early marker of outcomes in patients with advanced non-small-cell lung cancer treated with nivolumab. *Int. J. Clin. Oncol.* 23, 634–640. doi:10.1007/s10147-018-1250-2

Noman, M. Z., Desantis, G., Janji, B., Hasmim, M., Karray, S., Dessen, P., et al. (2014). PD-L1 is a novel direct target of HIF-1α, and its blockade under hypoxia enhanced MDSC-mediated T cell activation. *J. Exp. Med.* 211, 781–790. doi:10.1084/jem.20131916

Noy, R., and Pollard, J. W. (2014). Tumor-associated macrophages: From mechanisms to therapy. *Immunity* 41, 49–61. doi:10.1016/j.immuni.2014.06.010

Paolillo, M., and Schinelli, S. (2019). Extracellular matrix alterations in metastatic processes. *Int. J. Mol. Sci.* 20, E4947. doi:10.3390/ijms20194947

Peng, H., Shen, J., Long, X., Zhou, X., Zhang, J., Xu, X., et al. (2022). Local release of TGF-β inhibitor modulates tumor-associated neutrophils and enhances pancreatic cancer response to combined irreversible electroporation and immunotherapy. *Adv. Sci.* 9, e2105240. doi:10.1002/advs.202105240

Perego, M., Tyurin, V. A., Tyurina, Y. Y., Yellets, J., Nacarelli, T., Lin, C., et al. (2020). Reactivation of dormant tumor cells by modified lipids derived from stress-activated neutrophils. *Sci. Transl. Med.* 12, eabb5817. doi:10.1126/scitranslmed.abb5817

Phan, T. G., and Croucher, P. I. (2020). The dormant cancer cell life cycle. *Nat. Rev. Cancer* 20, 398–411. doi:10.1038/s41568-020-0263-0

Posabella, A., Köhn, P., Lalos, A., Wilhelm, A., Mechera, R., Soysal, S., et al. (2020). High density of CD66b in primary high-grade ovarian cancer independently predicts response to chemotherapy. *J. Cancer Res. Clin. Oncol.* 146, 127–136. doi:10.1007/s00432-019-03108-6

Pylaeva, E., Harati, M. D., Spyra, I., Bordbari, S., Strachan, S., Thakur, B. K., et al. (2019). NAMPT signaling is critical for the proangiogenic activity of tumor-associated neutrophils. *Int. J. Cancer* 144, 136–149. doi:10.1002/ijc.31808

Qi, M., Xia, Y., Wu, Y., Zhang, Z., Wang, X., Lu, L., et al. (2022). Lin28B-high breast cancer cells promote immune suppression in the lung pre-metastatic niche via exosomes and support cancer progression. *Nat. Commun.* 13, 897. doi:10.1038/s41467-022-28438-x

Recasens, A., and Munoz, L. (2019). Targeting cancer cell dormancy. *Trends Pharmacol. Sci.* 40, 128–141. doi:10.1016/j.tips.2018.12.004

Sagiv, J. Y., Michaeli, J., Assi, S., Mishalian, I., Kisos, H., Levy, L., et al. (2015). Phenotypic diversity and plasticity in circulating neutrophil subpopulations in cancer. *Cell Rep.* 10, 562–573. doi:10.1016/j.celrep.2014.12.039

Savagner, P. (2010). The epithelial-mesenchymal transition (EMT) phenomenon. *Ann. Oncol.* 21 (7), vii89–92. doi:10.1093/annonc/mdq292

Schernberg, A., Blanchard, P., Chargari, C., and Deutsch, E. (2017). Neutrophils, a candidate biomarker and target for radiation therapy? *Acta Oncol.* 56, 1522–1530. doi:10.1080/0284186X.2017.1348623

Schimek, V., Strasser, K., Beer, A., Göber, S., Walterskirchen, N., Brostjan, C., et al. (2022). Tumour cell apoptosis modulates the colorectal cancer immune microenvironment via interleukin-8-dependent neutrophil recruitment. *Cell Death Dis.* 13, 113. doi:10.1038/s41419-022-04585-3

Schlesinger, M. (2018). Role of platelets and platelet receptors in cancer metastasis. *J. Hematol. Oncol.* 11, 125. doi:10.1186/s13045-018-0669-2

Schuldner, M., Dörsam, B., Shatnyeva, O., Reiners, K. S., Kubarenko, A., Hansen, H. P., et al. (2019). Exosome-dependent immune surveillance at the metastatic niche requires BAG6 and CBP/p300-dependent acetylation of p53. *Theranostics* 9, 6047–6062. doi:10.7150/thno.36378

Seubert, B., Grünwald, B., Kobuch, J., Cui, H., Schelter, F., Schaten, S., et al. (2015). Tissue inhibitor of metalloproteinases (TIMP)-1 creates a premetastatic niche in the liver through SDF-1/CXCR4-dependent neutrophil recruitment in mice. *Hepatology* 61, 238–248. doi:10.1002/hep.27378

Seyfried, T. N., and Huysentruyt, L. C. (2013). On the origin of cancer metastasis. *Crit. Rev. Oncog.* 18, 43–73. doi:10.1615/critrevoncog.v18.i1-2.40

Shang, A., Gu, C., Wang, W., Wang, X., Sun, J., Zeng, B., et al. (2020). Exosomal circPACRGL promotes progression of colorectal cancer via the miR-142-3p/miR-506-3p- TGF-β1 axis. *Mol. Cancer* 19, 117. doi:10.1186/s12943-020-01235-0

Shaul, M. E., and Fridlender, Z. G. (2019). Tumour-associated neutrophils in patients with cancer. *Nat. Rev. Clin. Oncol.* 16, 601–620. doi:10.1038/s41571-019-0222-4

Shaul, M. E., Zlotnik, A., Tidhar, E., Schwartz, A., Arpinati, L., Kaisar-Iluz, N., et al. (2021). Tumor-associated neutrophils drive B-cell recruitment and their differentiation to plasma cells. *Cancer Immunol. Res.* 9, 811–824. doi:10.1158/2326-6066.CIR-20-0839

Shimizu, H., Takeishi, S., Nakatsumi, H., and Nakayama, K. I. (2019). Prevention of cancer dormancy by Fbxw7 ablation eradicates disseminated tumor cells. *JCI Insight* 4, 125138. doi:10.1172/jci.insight.125138

Shojaei, F., Wu, X., Zhong, C., Yu, L., Liang, X. H., Yao, J., et al. (2007). Bv8 regulates myeloid-cell-dependent tumour angiogenesis. *Nature* 450, 825–831. doi:10.1038/nature06348

Siakaeva, E., Pylaeva, E., Spyra, I., Bordbari, S., Höing, B., Kürten, C., et al. (2019). Neutrophil maturation and survival is controlled by IFN-dependent regulation of NAMPT signaling. *Int. J. Mol. Sci.* 20, E5584. doi:10.3390/ijms20225584

Singhal, S., Bhojnagarwala, P. S., O'Brien, S., Moon, E. K., Garfall, A. L., Rao, A. S., et al. (2016). Origin and role of a subset of tumor-associated neutrophils with

antigen-presenting cell features in early-stage human lung cancer. *Cancer Cell* 30, 120–135. doi:10.1016/j.ccell.2016.06.001

Sionov, R. V., Fridlender, Z. G., and Granot, Z. (2015). The multifaceted roles neutrophils play in the tumor microenvironment. *Cancer Microenviron.* 8, 125–158. doi:10.1007/s12307-014-0147-5

Song, I. W., Nagamani, S. C., Nguyen, D., Grafe, I., Sutton, V. R., Gannon, F. H., et al. (2022). Targeting TGF-β for treatment of osteogenesis imperfecta. *J. Clin. Invest.* 132, e152571. doi:10.1172/JCI152571

Szczerba, B. M., Castro-Giner, F., Vetter, M., Krol, I., Gkountela, S., Landin, J., et al. (2019). Neutrophils escort circulating tumour cells to enable cell cycle progression. *Nature* 566, 553–557. doi:10.1038/s41586-019-0915-y

Templeton, A. J., McNamara, M. G., Šeruga, B., Vera-Badillo, F. E., Aneja, P., Ocaña, A., et al. (2014). Prognostic role of neutrophil-to-lymphocyte ratio in solid tumors: A systematic review and meta-analysis. *J. Natl. Cancer Inst.* 106, dju124. doi:10.1093/jnci/dju124

Terashima, T., Yamashita, T., Iida, N., Yamashita, T., Nakagawa, H., Arai, K., et al. (2015). Blood neutrophil to lymphocyte ratio as a predictor in patients with advanced hepatocellular carcinoma treated with hepatic arterial infusion chemotherapy. *Hepatol. Res.* 45, 949–959. doi:10.1111/hepr.12436

Tian, S., Chu, Y., Hu, J., Ding, X., Liu, Z., Fu, D., et al. (2022). Tumour-associated neutrophils secrete AGR2 to promote colorectal cancer metastasis via its receptor CD98hc-xCT. *Gut.* 1, 1. doi:10.1136/gutjnl-2021-325137

Timaxian, C., Vogel, C. F. A., Orcel, C., Vetter, D., Durochat, C., Chinal, C., et al. (2021). Pivotal role for Cxcr2 in regulating tumor-associated neutrophil in breast cancer. *Cancers (Basel)* 13, 2584. doi:10.3390/cancers13112584

Trellakis, S., Bruderek, K., Dumitru, C. A., Gholaman, H., Gu, X., Bankfalvi, A., et al. (2011). Polymorphonuclear granulocytes in human head and neck cancer: Enhanced inflammatory activity, modulation by cancer cells and expansion in advanced disease. *Int. J. Cancer* 129, 2183–2193. doi:10.1002/ijc.25892

Tyagi, A., Sharma, S., Wu, K., Wu, S. Y., Xing, F., Liu, Y., et al. (2021). Nicotine promotes breast cancer metastasis by stimulating N2 neutrophils and generating pre-metastatic niche in lung. *Nat. Commun.* 12, 474. doi:10.1038/s41467-020-20733-9

Ui Mhaonaigh, A., Coughlan, A. M., Dwivedi, A., Hartnett, J., Cabral, J., Moran, B., et al. (2019). Low density granulocytes in ANCA vasculitis are heterogenous and hypo-responsive to anti-myeloperoxidase antibodies. *Front. Immunol.* 10, 2603. doi:10.3389/fimmu.2019.02603

Uribe-Querol, E., and Rosales, C. (2015). Neutrophils in cancer: Two sides of the same coin. *J. Immunol. Res.* 2015, 983698. doi:10.1155/2015/983698

Vera-Ramirez, L., Vodnala, S. K., Nini, R., Hunter, K. W., and Green, J. E. (2018). Autophagy promotes the survival of dormant breast cancer cells and metastatic tumour recurrence. *Nat. Commun.* 9, 1944. doi:10.1038/s41467-018-04070-6

Vincent, J., Mignot, G., Chalmin, F., Ladoire, S., Bruchard, M., Chevriaux, A., et al. (2010). 5-Fluorouracil selectively kills tumor-associated myeloid-derived suppressor cells resulting in enhanced T cell-dependent antitumor immunity. *Cancer Res.* 70, 3052–3061. doi:10.1158/0008-5472.CAN-09-3690

Wang, H., Zhang, B., Li, R., Chen, J., Xu, G., Zhu, Y., et al. (2022). KIAA1199 drives immune suppression to promote colorectal cancer liver metastasis by modulating neutrophil infiltration. *Hepatology* 1, 1. doi:10.1002/hep.32383

Wang, Y., Chen, J., Yang, L., Li, J., Wu, W., Huang, M., et al. (2019). Tumor-contacted neutrophils promote metastasis by a CD90-TIMP-1 juxtacrine-paracrine loop. *Clin. Cancer Res.* 25, 1957–1969. doi:10.1158/1078-0432.CCR-18-2544

Wang, Y., Zhao, Q., Zhao, B., Zheng, Y., Zhuang, Q., Liao, N., et al. (2022). Remodeling tumor-associated neutrophils to enhance dendritic cell-based HCC neoantigen nano-vaccine efficiency. *Adv. Sci.* 9, e2105631. doi:10.1002/advs.202105631

Wang, Z., Zhan, P., Lv, Y., Shen, K., Wei, Y., Liu, H., et al. (2019). Prognostic role of pretreatment neutrophil-to-lymphocyte ratio in non-small cell lung cancer patients treated with systemic therapy: A meta-analysis. *Transl. Lung Cancer Res.* 8, 214–226. doi:10.21037/tlcr.2019.06.10

Wculek, S. K., and Malanchi, I. (2015). Neutrophils support lung colonization of metastasis-initiating breast cancer cells. *Nature* 528, 413–417. doi:10.1038/nature16140

Wei, F., Wang, D., Wei, J., Tang, N., Tang, L., Xiong, F., et al. (2021). Metabolic crosstalk in the tumor microenvironment regulates antitumor immunosuppression and immunotherapy resisitance. *Cell. Mol. Life Sci.* 78, 173–193. doi:10.1007/s00018-020-03581-0

Wikberg, M. L., Ling, A., Li, X., Öberg, Å., Edin, S., and Palmqvist, R. (2017). Neutrophil infiltration is a favorable prognostic factor in early stages of colon cancer. *Hum. Pathol.* 68, 193–202. doi:10.1016/j.humpath.2017.08.028

Wu, L., Saxena, S., Awaji, M., and Singh, R. K. (2019). Tumor-associated neutrophils in cancer: Going pro. *Cancers (Basel)* 11, E564. doi:10.3390/cancers11040564

Wu, P., Wu, D., Ni, C., Ye, J., Chen, W., Hu, G., et al. (2014). γδT17 cells promote the accumulation and expansion of myeloid-derived suppressor cells in human colorectal cancer. *Immunity* 40, 785–800. doi:10.1016/j.immuni.2014.03.013

Xia, X., Zhang, Z., Zhu, C., Ni, B., Wang, S., Yang, S., et al. (2022). Neutrophil extracellular traps promote metastasis in gastric cancer patients with postoperative abdominal infectious complications. *Nat. Commun.* 13, 1017. doi:10.1038/s41467-022-28492-5

Yang, J., Yan, C., Vilgelm, A. E., Chen, S. C., Ayers, G. D., Johnson, C. A., et al. (2021). Targeted deletion of CXCR2 in myeloid cells alters the tumor immune environment to improve antitumor immunity. *Cancer Immunol. Res.* 9, 200–213. doi:10.1158/2326-6066.cir-20-0312

Yvan-Charvet, L., and Ng, L. G. (2019). Granulopoiesis and neutrophil homeostasis: A metabolic, daily balancing act. *Trends Immunol.* 40, 598–612. doi:10.1016/j.it.2019.05.004

Zheng, Z., Li, Y. N., Jia, S., Zhu, M., Cao, L., Tao, M., et al. (2021). Lung mesenchymal stromal cells influenced by Th2 cytokines mobilize neutrophils and facilitate metastasis by producing complement C3. *Nat. Commun.* 12, 6202. doi:10.1038/s41467-021-26460-z

Zhou, G., Peng, K., Song, Y., Yang, W., Shu, W., Yu, T., et al. (2018). CD177+ neutrophils suppress epithelial cell tumourigenesis in colitis-associated cancer and predict good prognosis in colorectal cancer. *Carcinogenesis* 39, 272–282. doi:10.1093/carcin/bgx142

Zhu, Y. P., Padgett, L., Dinh, H. Q., Marcovecchio, P., Blatchley, A., Wu, R., et al. (2018). Identification of an early unipotent neutrophil progenitor with pro-tumoral activity in mouse and human bone marrow. *Cell Rep.* 24, 2329–2341. e8. doi:10.1016/j.celrep.2018.07.097

Glossary

AIC abdominal infectious complication
AGR neutrophil-specific anterior gradient
CRC colorectal cancer
CTCs circulating tumor cells
CTM circulating tumor microemboli
DDR1 discoid domain receptor 1
DSBs double-strand breaks
ECM extracellular matrix
EGs empty gels
EMT epithelial-mesenchymal transition
EVs extracellular vesicles
FOXO3a forkhead box protein Oa
GC gastric cancer
G-MDSCs granulocytic myeloid-derived suppressor cells
HA hyaluronic acid
HCC hepatocellular carcinoma
HDNs high-density neutrophils
HIF-1α hypoxia-inducible factor-1α
HMGB1 high mobility group box 1
ICIs immune checkpoint inhibitors
IFN interferon
LDNs low-density neutrophils
LMSCs lung mesenchymal stromal cells
MDSCs myeloid-derived suppressor cells
MET mesenchymal-to-epithelial transition
MMP matrix metalloproteinases
NAMPT nicotinamide phosphoribosyltransferase
NE neutrophils elastases
NETs neutrophil extracellular traps
NSCLC non-small cell lung cancer
OSCC oral squamous cell carcinoma
PMN-MDSCs polymorphonuclear myeloid-derived suppressive cells
PMNs pre-metastatic niche
PM particulate matter
TANs tumor-associated neutrophils
TGF-β transforming growth factor beta
TIMP-1 tissue inhibitor of metalloproteinases 1
TME tumor microenvironment
UV ultraviolet
VCAM1 vascular cell adhesion molecule 1
VEGF vascular endothelial growth factor

frontiers | Frontiers in Oncology

TYPE Original Research
PUBLISHED 18 August 2022
DOI 10.3389/fonc.2022.939994

Check for updates

OPEN ACCESS

EDITED BY
Shaoquan Zheng,
Sun Yat-sen University Cancer Center (SYSUCC), China

REVIEWED BY
Yong Zhang,
Central South University, China
Zhong-Yi Dong,
Nanfang Hospital, Southern Medical University, China
Min Deng,
Guangzhou Medical University, China

*CORRESPONDENCE
Xinyu Tan
tanxy125@126.com
Hongbo Zhu
nhfy_zlnk_zhb_2012@163.com

SPECIALTY SECTION
This article was submitted to Molecular and Cellular Oncology, a section of the journal Frontiers in Oncology

RECEIVED 09 May 2022
ACCEPTED 29 June 2022
PUBLISHED 18 August 2022

CITATION
Tan X, Zeng C, Li H, Tan Y and Zhu H (2022) Circ0038632 modulates MiR-186/DNMT3A axis to promote proliferation and metastasis in osteosarcoma.
Front. Oncol. 12:939994.
doi: 10.3389/fonc.2022.939994

COPYRIGHT
© 2022 Tan, Zeng, Li, Tan and Zhu. This is an open-access article distributed under the terms of the Creative Commons Attribution License (CC BY). The use, distribution or reproduction in other forums is permitted, provided the original author(s) and the copyright owner(s) are credited and that the original publication in this journal is cited, in accordance with accepted academic practice. No use, distribution or reproduction is permitted which does not comply with these terms.

Circ0038632 modulates MiR-186/DNMT3A axis to promote proliferation and metastasis in osteosarcoma

Xinyu Tan[1]*, Canjun Zeng[1], Haomiao Li[1], Yeru Tan[2] and Hongbo Zhu[2]*

[1]The Third Affiliated Hospital of Southern Medical University, Guangzhou, China, [2]Department of Medical Oncology, The First Affiliated Hospital, Hengyang Medical School, University of South China, Hengyang, China

Osteosarcoma is a highly malignant solid tumor with poor prognosis, early metastasis, and rapid progression and has a high mortality rate, in which better therapeutic strategies are needed. Circ0038632, also known as circPLK1, is a tumor promotor in multiple cancers. However, its biological functions and molecular regulatory mechanisms in osteosarcoma remain unclear. To ascertain the function of circ0038632 in osteosarcoma, we checked its expression in cells and in tissues and tested its abilities of proliferation and migration. Expression experiment manifested that circ0038632 showed an enhanced expression in osteosarcoma. Functional studies revealed that circ0038632 inhibition reduced cell proliferation and metastasis abilities of osteosarcoma. Mechanism studies revealed that circ0038632 sponged miR-186 to upregulate the expression of DNA methyltransferase 3A (DNMT3A) to promote osteosarcoma progression. The circ0038632/miR-186/DNMT3A axis was involved in osteosarcoma progression. The results elucidated the potential application of circ0038632 as a novel diagnostic biomarker for progressive process of osteosarcoma.

KEYWORDS

circ0038632, miR-186, DNMT3A, proliferation, metastasis, osteosarcoma

Introduction

Osteosarcoma, one of highly malignant solid tumors, is originated from the bone marrow cavity. It usually occurs in adolescents aged 10–20 years, with a high degree of malignancy, poor prognosis, early metastasis, and rapid progression and a high mortality rate (1). Unfortunately, the cause, progression, and their mechanisms have not been clearly clarified up to now.

Circular RNAs (circRNAs) perform important function in tumor-related gene expression regulating and tumor progression. Recently, increasing studies revealed that circRNAs were deeply involved in malignancy (2). CircRNA_103801 induces osteosarcoma proliferation, migration, and invasion processes by mediating miR-338-3p (3). CircTADA2A accelerates the malignant progression of osteosarcoma *via* modulating miR-203a-3p (4). All these studies reveal that circRNAs exert important functions in osteosarcoma.

Circ0038632, also known as circPLK1, is a tumor promotor in multiple cancers. In breast cancer, circPLK1 has high-level expression and is closely related with poor survival, which may serve as the prognostic biomarker or therapeutic target (5). By mediating miR-1294/HMGA1, circPLK1 promotes the progression of non–small cell lung cancer (6). However, circ0038632 function and its inner regulatory mechanisms in osteosarcoma are still unclear. Therefore, elucidation the role of circ0038632 involving occurrence or progression in osteosarcoma is significant.

Here, we found that circ0038632 showed a boosted expression both in osteosarcoma cells and in tissues. Circ0038632 silencing decreased the proliferation and metastasis abilities of osteosarcoma cells. The process may implement by circ0038632 sponging miR-186, followed by increasing the expression of DNA methyltransferase 3A (DNMT3A), and finally promoting osteosarcoma progression. Aberrant regulation of DNMT3A is important to the tumorigenesis of multiple cancers, which was also confirmed in osteosarcoma (7, 8). Circ0038632 has a potential to function as diagnostic biomarker or therapeutic target in osteosarcoma treatment.

Results

circ0038632 is upregulated in osteosarcoma

Relative mRNA expression of circ0038632 was monitored through quantitative real-time PCR (qRT-PCR), and it was found that it is markedly upregulated in osteosarcoma cell lines in comparison with its control cell (Figure 1A). Next, circ0038632 expression levels were verified in 42 pairs of osteosarcoma tissues and their corresponding paracancerous controls. The results demonstrated that circ0038632 had an enhanced expression in osteosarcoma tissues compared with their control tissues (Figure 1B).

circ0038632 silencing suppresses the function of proliferation and metastasis in osteosarcoma

siRNAs were used to knockdown circ0038632, and si-circ0038632#1 was chosen for the following experiments (Figure 2A). Cell counting kit-8 (CCK-8) and BrdUrd assays were used to find that circ0038632 silencing restrained the proliferation ability of osteosarcoma cells (Figures 2B–D). Moreover, circ0038632 silencing depressed the colony formation capability of osteosarcoma cells (Figures 2E, F). In addition, circ0038632 silencing decreased the cell migration ability in osteosarcoma (Figures 2G, H). Finally, we used mouse xenograft models to investigate circ0038632 function *in vivo*. The results turned out that inhibition of circ0038632 suppressed the capability of growth (Figures 2I, J) and lung metastasis (Figures 2K, L) of osteosarcoma.

circ0038632 serves as miR-186 sponge in osteosarcoma

circRNAs could regulate gene expression by acting as microRNA decoys, also known as the competing endogenous RNA (ceRNA) mechanism. In osteosarcoma cells, cellular location of circ0038632 was inspected and found that circ0038632 mainly localized in cytoplasm (Figure 3A). Next, the prediction of potential binding sites between circ0038632 and

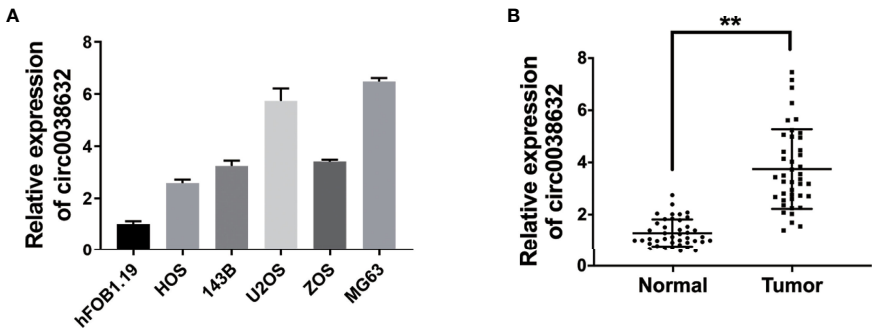

FIGURE 1
circ0038632 is upregulated in osteosarcoma. **(A)** The circ0038632 expression in osteosarcoma cell lines. **(B)** The circ0038632 expression in 42 pairs of osteosarcoma tissues and adjacent normal tissues. $^{**}P < 0.01$.

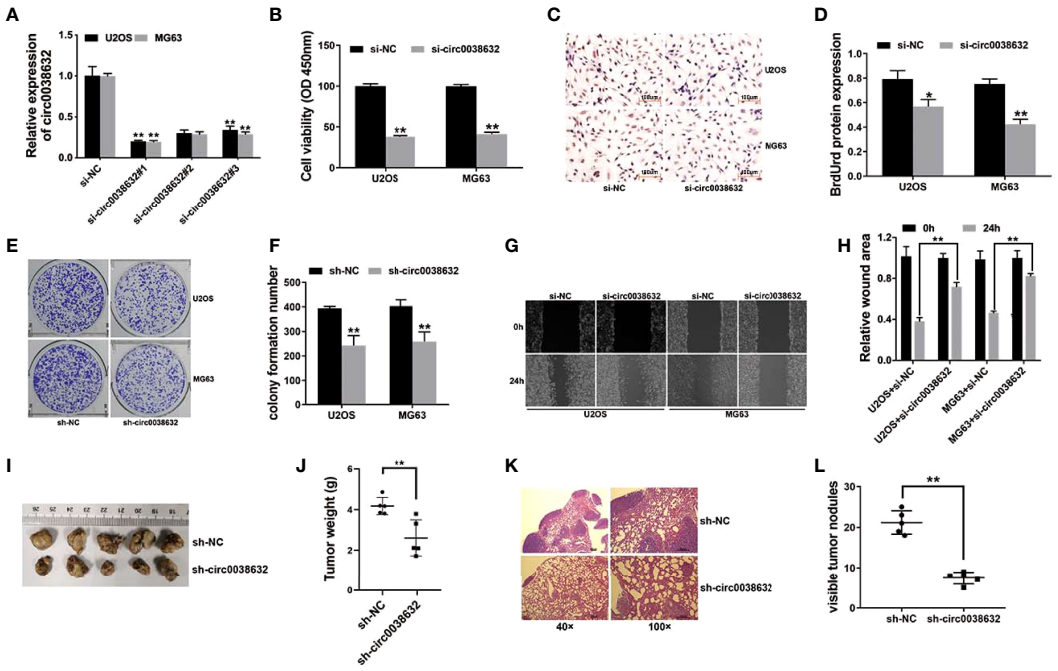

FIGURE 2
circ0038632 silencing suppresses the function of proliferation and metastasis in osteosarcoma. **(A)** siRNAs were used to knockdown circ0038632 expression in osteosarcoma cells. **(B)** Cell proliferation ability was evaluated through CCK-8 assay. **(C)** BrdUrd incorporation was assessed by immunohistochemistry (IHC) to evaluate cell proliferation after transfection. **(D)** Statistical chart of BrdUrd total gray value. **(E)** The pictures of clone formation from osteosarcoma cells were showed. **(F)** Statistical chart of cloning derived from osteosarcoma cells. **(G)** Migration ability was assessed by wound healing assay. **(H)** Statistical chart of wound closure. **(I)** Mouse xenograft models were established to evaluate circ0038632 intravital function. **(J)** Statistical chart of tumor weights. **(K)** The pictures of lung metastatic nodules with HE staining were showed. **(L)** Statistical chart of metastatic nodules. $^{*}P < 0.05$ and $^{**}P < 0.01$.

miR-186 was accomplished adopting the online software Interactom (Figure 3B). Then, wild-type and mutant sequences of the binding sites between miR-186 and circ0038632 were designed, and we found that miR-186 + WT 3′-circ0038632 co-transfection group expressed a strikingly inhibited relative luciferase activity in osteosarcoma cells, when compared with miR-186 + MUT 3′-circ0038632 co-transfection group. In addition, RNA immunoprecipitation (RIP) assay was adopted and the results displayed that miR-186 enrichment was markedly increased in MS2bs-circ0038632 group (Figure 3D), showing that circ0038632 could serve as miR-186 sponge in osteosarcoma. Moreover, miR-186 manifested a tendency of distinct decrease in osteosarcoma cells compared with their control cells (Figure 3E).

circ0038632 functions as a ceRNA by mediating DNMT3A in osteosarcoma

The prediction of potential downstream target genes of miR-186 was performed using the online software TargetScan, and we found that DNMT3A was among them (Figure 4A). Wild-type and mutant sequences were designed for the 3′-UTR of DNMT3A. The results showed that DNMT3A WT 3′-UTR + miR-186 co-transfection group showed a sharp decrease relative luciferase activity in osteosarcoma, and DNMT3A WT 3′-UTR + miR-186 inhibitor co-transfection group showed an apparent increase compared with DNMT3A MUT 3′-UTR + miR-186 co-transfection group (Figure 4B). Moreover, miR-186 was conductive to the inhibition of DNMT3A expression, and miR-186 inhibitor reversed DNMT3A expression (Figure 4C), revealing the expression that its target gene DNMT3A could be regulated by miR-186 in osteosarcoma.

Subsequent RIP assay results demonstrated that circ0038632, DNMT3A, and miR-186 enrichment was majorly raised in anti-AGO2 group in osteosarcoma cells (Figure 4D). Circ0038632 silencing significantly raised the enrichment of DNMT3A to Ago2 (Figure 4E), suggesting that circ0038632 and DNMT3A were rivalrous to binding with miR-186. Moreover, inhibition of circ0038632 decreased the expression of DNMT3A, but miR-186 inhibitor could rescue the decrease (Figure 4F), revealing that circ0038632 could sponge miR-186 and regulate the expression of DNMT3A in osteosarcoma. Next, DNMT3A expression was checked in osteosarcoma cells and tissues, and we found it had a noticeable raised trend (Figures 4G, H). DNMT3A expression in

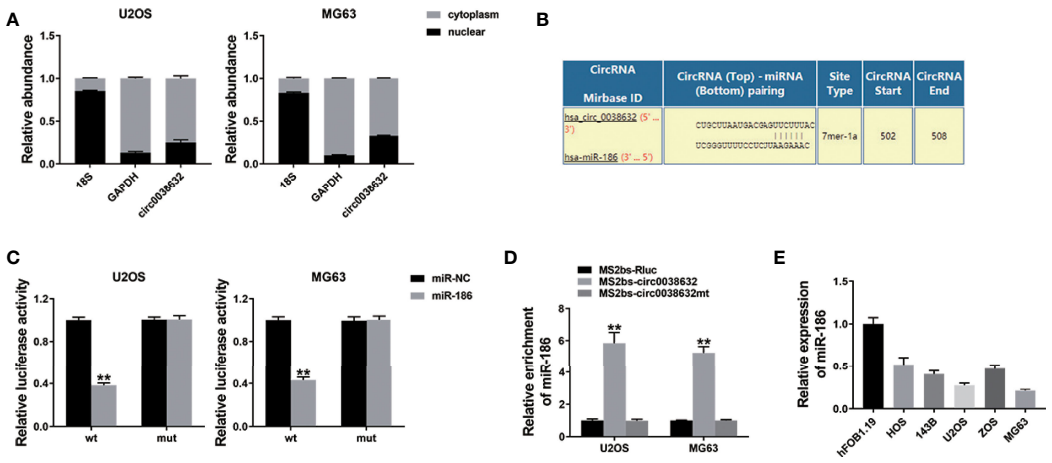

FIGURE 3
circ0038632 serves as miR-186 sponge in osteosarcoma. **(A)** qRT-PCR detected circ0038632, cytoplasmic control (GAPDH), and nuclear control (18S) expression. **(B)** Potential binding sites between miR-186 and circ0038632. **(C)** Relative luciferase activities of different co-transfected groups. **(D)** The enrichment of MS2bs-circ0038632, MS2bs-circ0038632mt, or control group was assessed. **(E)** The expression of miR-186 in osteosarcoma cell lines. $^{**}P < 0.01$.

circ0038632 silencing group from mouse xenograft models showed a markedly reduction (Figure 4I). In addition, circ0038632 knockdown also decreased the expression of Ki-67 in the xenograft tumors (Figure 4I).

Discussion

Although neoadjuvant chemotherapy combined with surgery has improved the survival probability of osteosarcoma in early-stage recently, current reports show that the 5-year patient survival of metastatic osteosarcoma can only reach 30% (9). Moreover, radical surgical treatment of osteosarcoma often leads to severe functional impairment and even disability of the patient's limbs. Therefore, it is urgent to explore new treatment methods for osteosarcoma.

circRNAs play critical roles in cancer progression. Circ0038632 is a progression promotor in multiple malignant tumors. By mediating miR-1294/HMGA1, circPLK1 promoted the abilities of malignant pleural mesothelioma to proliferate, migrate, invade, and keep stemness (10). CircPLK1 silencing inhibited the growth, migration, and invasion of breast cancer (11). However, how circ0038632 functions in osteosarcoma has not yet been revealed. Here, we results revealed that circ0038632 had an enhanced expression in both osteosarcoma cells and tissues (Figure 1). In addition, knockdown of circ0038632 suppressed the capability of proliferation and metastasis of osteosarcoma cells (Figure 2).

Next, we investigated the mechanism of circ0038632 function in osteosarcoma. We explored the potential circRNA/miRNA interaction for circ0038632 and miR-186. MiR-186 is a candidate of tumor suppressors in multiple cancers. In osteosarcoma, miR-186-5p has been proved to downregulate and negatively relate to survival (12). Overexpressed miR-186 restrained the proliferation, invasion, and aerobic glycolysis process in osteosarcoma (13). Moreover, miR-186-5p repressed osteosarcoma migration or invasion through regulating TBL1XR1 expression (14). In this study, miR-186 manifested a tendency of distinct decrease in osteosarcoma cells (Figure 3).

The ceRNA mechanism involved miR-186 was reported in several studies. lncRNA DSCAM-AS1 promotes malignant transformation in osteosarcoma by sponging miR-186-5p (15). lncRNA NEAT1 sponges miR-186-5p and promotes the progression of osteosarcoma invasion and EMT (16). *Via* miR-186-5p, circ_0001174 promotes osteosarcoma progression (17). Our results showed that circ0038632 could regulate the expression of miR-186 by sponging it (Figure 3).

Aberrant regulation of DNMT3A is important to the tumorigenesis of multiple cancers, which has the potential to be a therapeutic target (7). DNMT3A is overexpressed and closely related with worse survival in pancreatic cancer (18). DNMT3A induces promoter methylation and miR-200b silencing to promote tumor progression in breast cancer (19). In osteosarcoma, DNMT3A promotes APCDD1 promoter DNA hyper-methylation, downregulates its expression, and promotes cell invasion and metastasis (8). Here, DNMT3A expression was found to be noticeably increased in osteosarcoma (Figure 4).

The ceRNA mechanisms that involved DNMT3A were also reported in several studies. In breast cancer, circIQCH sponges miR-145 to accelerate proliferation and migration process through upregulating DNMT3A (20). Circ_0084615 could regulate the expression levels of DNMT3A be mediating miR-599 (21). Here, we found that circ0038632 could sponge miR-186

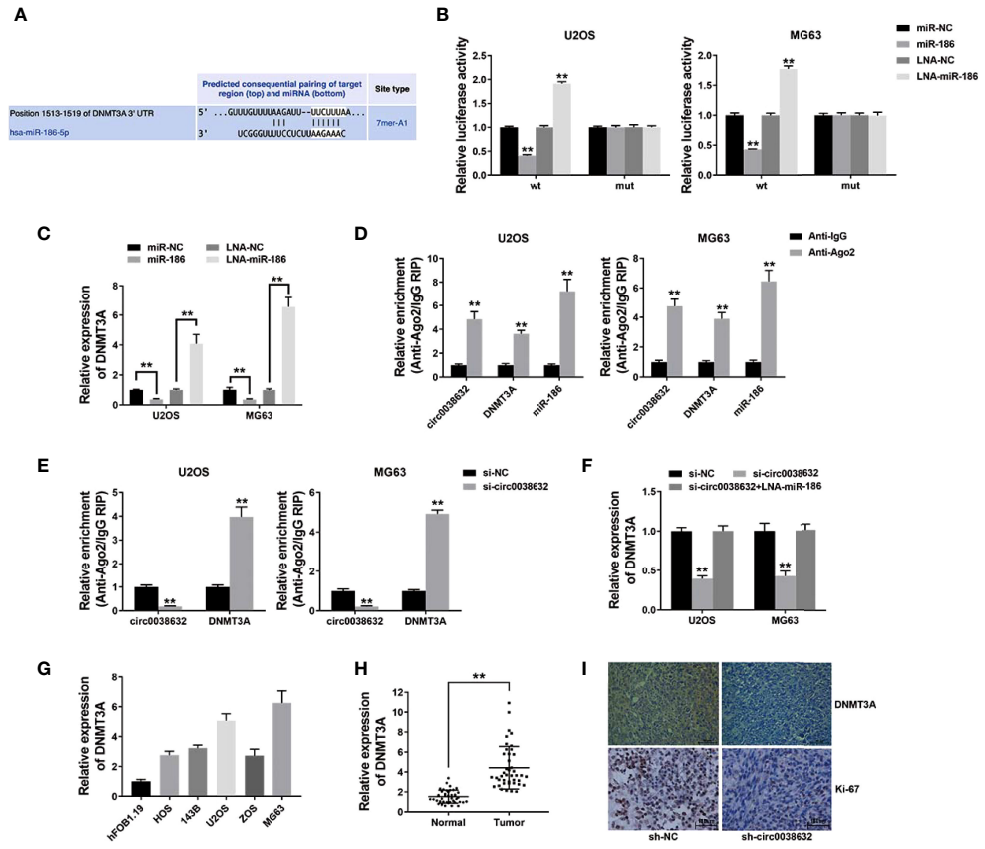

FIGURE 4
circ0038632 functions as a ceRNA by mediating DNMT3A in osteosarcoma. **(A)** Potential binding sites from 3′-UTR of DNMT3A with miR-186. **(B)** Relative luciferase activities of different co-transfected groups. **(C)** DNMT3A expression was tested after transfection by qRT-PCR. **(D)** The degree of circ0038632, DNMT3A, and miR-186 enrichment to Ago2 was examined by RIP assay. **(E)** The enrichment on Ago2 after transfection was tested. **(F)** DNMT3A mRNA expression was examined. **(G)** DNMT3A mRNA expression in osteosarcoma cells was tested. **(H)** DNMT3A mRNA expression in osteosarcoma tissues and its control were detected. **(I)** IHC staining of DNMT3A and Ki-67 were shown. $^{**}P < 0.01$.

followed by regulating its downstream target gene DNMT3A (Figure 4). circRNAs are promising biomarkers for diagnosis and targets for therapeutic management (22). Our study confirmed the cancer-promoting effect of circ0038632 in osteosarcoma, which may lead to the identification as a potential disease biomarker or novel therapeutic target.

In conclusion, we showed that the circ0038632/miR-186/DNMT3A axis was involved in osteosarcoma proliferation and metastasis. Targeting circ0038632 has the potential to be a specific therapeutic strategy for osteosarcoma.

Materials and methods

Cell culture and transfection

Human osteosarcoma cells including U2OS, ZOS, 143B, MG63, HOS, and their control cells, osteoblast hFOB1.19, were obtained from ATCC. DNA fingerprinting was used for cell identification. The detection for mycoplasma infection was performed routinely.

Lipofectamine 3000 was adopted for cell transfection (Invitrogen, USA). siRNAs and shRNAs of circ0038632 and mimics and inhibitors of miR-186 were purchased from GeneCopoeia (USA). The sequences of siRNAs used in this study are as follows: si-NC, UUCUCCGAACGUGUCACGUTT; si-circ0038632#1, ACAGATGTGAATATTCTCTCT; si-circ0038632#2, GATGTGAATATTCTCTCTCCT; and si-circ0038632#3, GTGAATATTCTCTCTCCTGGA. The primer sequences for qRT-PCRs used in this study are as follows: circ0038632: forward (5′- 3′), TACATGTTCGGGTGTGGGTT; reverse (5′- 3′), CTTTCCTCCTCTTGTGCAGC; 18S: forward (5′- 3′), TTAATTCCGATAACGAACGAGA; reverse (5′- 3′), CGCTGAGCCAGTCAGTGTAG; GAPDH: forward (5′- 3′), GGAGCGAGATCCCTCCAAAAT, reverse (5′- 3′), GGCTG TTGTCATACTTCTCATGG; and DNMT3A: forward (5′- 3′), TATGAACAGGCCGTTGGCATC, reverse (5′-3′), AAGAGGTGGCGGATGACTGG.

Quantitative real-time PCR analysis

TRIzol (Invitrogen), NE-PERTM Nuclear, and Cytoplasmic Extraction Reagents (Thermo, USA) were used to extract total RNA or nuclear and cytoplasmic RNA. PrimeScriptTM RT reagent Kit and TB Green Premix Ex TaqTM (RR037A, RR420A, Takara, Japan) were used for qRT-PCR assays. The primers were obtained from GeneCopoeia (Table S2).

Clinical sample collection

Forty-two pairs of primary osteosarcoma samples and their corresponding paracancerous tissue samples were acquired from the Third Affiliated Hospital of Southern Medical University, immediately followed by keeping in liquid nitrogen. qRT-PCR was used to test the expression of circRNA. The research involving human samples and animals was reviewed and approved by the Ethics Committee of the Third Affiliated Hospital of Southern Medical University. All patients provided written informed consents. Declaration of Helsinki revised in 2013 was strictly implemented throughout the research.

Cell counting kit-8 assay

After transfection, 10^3 cells were resuspended and transferred into each well of 96-well plates. After 48 h of incubation at 37°C, 10 µl of CCK-8 solution was added. Then, absorbance of 450 nm was measured 2 h later.

BrdUrd proliferation assay

BrdUrd proliferation assay was applied for cell viability detection. Cells were incubated under BrdUrd at 10 nmol/L for 16 h to test BrdUrd incorporation, followed by 1:1 cold methanol/acetone fixation. Then, immunocytochemistry detection was subsequently performed.

Colony formation assay

After transfection, 10^3 cells were resuspended and transferred into each well of six-well plates. After 14 days of incubation at 37°C. Then, methanol was used to fix the colonies, followed by crystal violet (0.1%) staining. The colonies were counted under the microscopy later.

Wound healing assay

After transfection, 10^3 cells were resuspended and transferred into each well of six-well plates. Pipette tips (10 µl) were used make the linear wound. Migration ability was assessed under microscope.

Mouse xenograft model

The whole process of animal experiments was performed according to the guidelines of Institutional Animal Care and Use Committee of The Third Affiliated Hospital of Southern Medical University. A total of 10^6 U2OS cells stably expressing sh-circ0038632 or its control were subcutaneously injected into each 4-week-old mouse (n = 5, male nude). Tumors were excised for following weights examine 28 days later.

A total of 10^5 U2OS cells stably expressing sh-circ0038632 or its control were injected into each mouse through tail vein (n = 5). Lungs were excised for the following pathological studies 56 days later. The metastatic sites in lungs were counted under microscopy.

Luciferase reporter assay

A total of 10^4 cells were resuspended and transferred into each well of six-well plates. Luciferase-reporting plasmid containing wild or mutant sequences of circ0038632, DNMT3A 3′-UTR, miR-186 mimics, miR-186 inhibitors, and their controls were purchased. The mimics and inhibitors of miR-186 and the wild or mutant reporting vectors were co-transfected. The activities of renilla and firefly luciferase were assessed 48 h after transfection.

RNA immunoprecipitation

MS2bs vector containing wild or mutant sequences of circ0038632 was constructed. The enrichment of circ0038632, miR-186, SLC7A11, and DNMT3A in osteosarcoma cells after transfection of the above vectors was detected by RIP assay using anti-Ago2 antibody, and qRT-PCR detection was completed after RNA purification.

Immunohistochemistry analysis

After deparaffinization and rehydration by xylene, absolute ethanol, and 70% alcohol, slides were drained, citrate buffer was used for antigen retrieval, and PBS was used for washing, followed by 3% H_2O_2 and 5% goat treatment. Anti- DNMT3A (1:200, LSBio, USA) and specific secondary antibodies (1:500, Abcam, USA) were utilized to incubate the slides under the condition of 4°C overnight and room temperature for 2 h, respectively. DAB staining reagent (Beyotime, China) was utilized to stain the slides and then photographed under microscopy.

Statistical analysis

All data were analyzed by SPSS 25.0 software and presented as mean ± SD. T-test was utilized for analyses of between difference groups. Statistical significance was set at $p \leq 0.05$.

Data availability statement

The raw data supporting the conclusions of this article will be made available by the authors, without undue reservation.

Ethics statement

This study was reviewed and approved by Ethics Committee of the Third Affiliated Hospital of Southern Medical University. The patients/participants provided their written informed consent to participate in this study. Written informed consent was obtained from the owners for the participation of their animals in this study.

Author contributions

All experiments were designed by XT and HZ. XT executed the experiments. CZ gathered specimens. HL and YT analysed and demonstrated the data. XT and HZ were the major contributors in writing and revising the manuscript. All authors read and approved the final manuscript. All authors contributed to the article and approved the submitted version.

Funding

This study was supported by the Natural Science Foundation of Guandong (No. 2021A1515012095, Xinyu Tan).

Conflict of interests

The reviewer (ZYD) declared a shared parent affiliation with the authors (XT, CZ, HL) to the handling editor at the time of review.

The authors declare that the research was conducted in the absence of any commercial or financial relationships that could be construed as a potential conflict of interest.

Publisher's note

All claims expressed in this article are solely those of the authors and do not necessarily represent those of their affiliated organizations, or those of the publisher, the editors and the reviewers. Any product that may be evaluated in this article, or claim that may be made by its manufacturer, is not guaranteed or endorsed by the publisher.

References

1. Meltzer PS, Helman LJ. New horizons in the treatment of osteosarcoma. *N Engl J Med* (2021) 385(22):2066–76. doi: 10.1056/NEJMra2103423

2. Li Z, Li X, Xu D, Chen X, Li S, Zh L, et al. An update on the roles of circular RNAs in osteosarcoma. *Cell Prolif* (2021) 54(1):e12936. doi: 10.1111/cpr.12936

3. Kong L, Huang H, Luan S, Liu H, Ye M, Wu F, et al. Inhibition of ASIC1a-mediated ERS improves the activation of HSCs and copper transport under copper load. *Front Pharmacol* (2021) 12:653272. doi: 10.3389/fphar.2021.653272

4. Wu Y, Xie Z, Chen J, Chen J, Ni W, Ma Y, et al. Circular RNA circTADA2A promotes osteosarcoma progression and metastasis by sponging miR-203a-3p and regulating CREB3 expression. *Mol Cancer* (2019) 18(1):73. doi: 10.1186/s12943-019-1007-1

5. Kong Y, Yang L, Wei W, Lyu N, Zou Y, Gao G, et al. CircPLK1 sponges miR-296-5p to facilitate triple-negative breast cancer progression. *Epigenomics* (2019) 11(10):1163–76. doi: 10.2217/epi-2019-0093

6. Li C, Wang G, Ma X, Tao T, Li Q, Yang Y, et al. Upregulation of exosomal circPLK1 promotes the development of non-small cell lung cancer through the miR-1294/ high mobility group protein A1 axis. *Bioengineered* (2022) 13(2):4185–200. doi: 10.1080/21655979.2022.2026727

7. Kataoka I, Funata S, Nagahama K, Kazunobu I, Hirohisa T, Nobutsugu A, et al. DNMT3A overexpression is associated with aggressive behavior and enteroblastic differentiation of gastric adenocarcinoma. *Ann Diagn Pathol* (2020) 44:151456. doi: 10.1016/j.anndiagpath.2019.151456

8. Han W, Liu J. Epigenetic silencing of the wnt antagonist APCDD1 by promoter DNA hyper-methylation contributes to osteosarcoma cell invasion and metastasis. *Biochem Biophys Res Commun* (2017) 491(1):91–7. doi: 10.1016/j.bbrc.2017.07.049

9. Gill J, Gorlick R. Advancing therapy for osteosarcoma. *Nat Rev Clin Oncol* (2021) 18(10):609–24. doi: 10.1038/s41571-021-00519-8

10. Zhang Q, Wang Z, Cai H, Guo D, Xu W, Bu S, et al. CircPLK1 acts as a carcinogenic driver to promote the development of malignant pleural mesothelioma by governing the miR-1294/HMGA1 pathway. *Biochem Genet* (2022). doi: 10.1007/s10528-022-10186-8

11. Lin G, Wang S, Zhang X, Wang D, et al. Circular RNA circPLK1 promotes breast cancer cell proliferation, migration and invasion by regulating miR-4500/IGF1 axis. *Cancer Cell Int* (2020) 20(1):593. doi: 10.1186/s12935-020-01694-x

12. Zhang Z, Zhang W, Mao J, Xu Zh, Fan M, et al. miR-186-5p functions as a tumor suppressor in human osteosarcoma by targeting FOXK1. *Cell Physiol Biochem* (2019) 52(3):553–64. doi: 10.33594/000000039

13. Xiao Q, Wei Z, Li Y, Zhou X, Chen J, Wang T, et al. miR186 functions as a tumor suppressor in osteosarcoma cells by suppressing the malignant phenotype and aerobic glycolysis. *Oncol Rep* (2018) 39(6):2703–10. doi: 10.3892/or.2018.6394

14. Cao Q, Wang Z, Wang Y, Liu F, Dong Y, Zhang W, et al. TBL1XR1 promotes migration and invasion in osteosarcoma cells and is negatively regulated by miR-186-5p. *Am J Cancer Res* (2018) 8(12):2481–93.

15. Ning Y, Bai Z. DSCAM-AS1 accelerates cell proliferation and migration in osteosarcoma through miR-186-5p/GPRC5A signaling. *Cancer Biomark* (2021) 30 (1):29–39. doi: 10.3233/CBM-190703

16. Tan H, Zhao L. lncRNA nuclear-enriched abundant transcript 1 promotes cell proliferation and invasion by targeting miR-186-5p/HIF-1alpha in osteosarcoma. *J Cell Biochem* (2019) 120(4):6502–14. doi: 10.1002/jcb.27941

17. Lin F, Wang X, Zhao X, Ren M, Wang Q, Wang J, et al. Circ_0001174 facilitates osteosarcoma cell proliferation, migration, and invasion by targeting the

miR-186-5p/MACC1 axis. *J Orthop Surg Res* (2022) 17(1):159. doi: 10.1186/s13018-022-03059-8

18. Jing W, Song N, Liu YP, Qu XJ, Qi YF, Li C, et al. DNMT3a promotes proliferation by activating the STAT3 signaling pathway and depressing apoptosis in pancreatic cancer. *Cancer Manag Res* (2019) 11:6379–96. doi: 10.2147/CMAR.S201610

19. Pang Y, Liu J, Li X, Xiao G, Wang H, Yang G, et al. MYC and DNMT3A-mediated DNA methylation represses microRNA-200b in triple negative breast cancer. *J Cell Mol Med* (2018) 22(12):6262–74. doi: 10.1111/jcmm.13916

20. Li Y, Jiang B, He Z, Zhu H, He R, Fan S, et al. circIQCH sponges miR-145 to promote breast cancer progression by upregulating DNMT3A expression. *Aging (Albany NY)* (2020) 12(15):15532–45. doi: 10.18632/aging.103746

21. Zhang B, Yang S, Wang J. Circ_0084615 is an oncogenic circular RNA in colorectal cancer and promotes DNMT3A expression *via* repressing miR-599. *Pathol Res Pract* (2021) 224:153494. doi: 10.1016/j.prp.2021.153494

22. Li D, Li Z, Yang Y, Zeng X, Li Y, Du X, et al. Circular RNAs as biomarkers and therapeutic targets in environmental chemical exposure-related diseases. *Environ Res* (2020) 180:108825. doi: 10.1016/j.envres.2019.108825

frontiers | Frontiers in Cell and Developmental Biology

TYPE Original Research
PUBLISHED 24 August 2022
DOI 10.3389/fcell.2022.957363

Check for updates

OPEN ACCESS

EDITED BY
Pranav Gupta,
Albert Einstein College of Medicine,
United States

REVIEWED BY
Mark Gorrell,
The University of Sydney, Australia
Tomonori Oka,
Massachusetts General Hospital Cancer Center, United States

*CORRESPONDENCE
Kexin Chen,
chenkexin@jlu.edu.cn

†These authors have contributed equally to this work

SPECIALTY SECTION
This article was submitted to Cancer Cell Biology,
a section of the journal
Frontiers in Cell and Developmental Biology

RECEIVED 31 May 2022
ACCEPTED 04 August 2022
PUBLISHED 24 August 2022

CITATION
Gao Y, Hou X, Dai Y, Yang T and Chen K (2022), Radiation-induced FAP + fibroblasts are involved in keloid recurrence after radiotherapy.
Front. Cell Dev. Biol. 10:957363.
doi: 10.3389/fcell.2022.957363

COPYRIGHT
© 2022 Gao, Hou, Dai, Yang and Chen. This is an open-access article distributed under the terms of the Creative Commons Attribution License (CC BY). The use, distribution or reproduction in other forums is permitted, provided the original author(s) and the copyright owner(s) are credited and that the original publication in this journal is cited, in accordance with accepted academic practice. No use, distribution or reproduction is permitted which does not comply with these terms.

Radiation-induced FAP + fibroblasts are involved in keloid recurrence after radiotherapy

Yan Gao[1†], Xue Hou[1†], Yuyin Dai[2], Ting Yang[3] and Kexin Chen[4*]

[1]Department of Radiation Oncology and Therapy, The First Hospital of Jilin University, Changchun, China, [2]Department of Nuclear Medicine, The First Hospital of Jilin University, Changchun, China, [3]Laboratory of Cancer Precision Medicine, The First Hospital of Jilin University, Changchun, China, [4]Institute of Translational Medicine, The First Hospital of Jilin University, Changchun, China

Background: Keloid scars (KSs), which are composed of abnormal hyperplastic scar tissue, form during skin wound healing due to excessive fibroblast activation and collagen secretion. Although surgical resection and radiation therapy are used to prevent recurrence, KS recurrence rates range from 15 to 23%, and the underlying mechanism is unclear.

Methods: To elucidate the mechanism of keloid recurrence, we established a PDX model and the grafts remained for over 20 weeks after transplantation on the bilateral backs of the NCG mice.

Results: RNA-seq revealed that KS tissue gene expression was highly consistent before and after transplantation. Then, one side of the KS graft was irradiated with electron beam therapy (10 Gy), significant increases in vimentin and fibroblast activation protein alpha (FAP) expression were observed after irradiation and were accompanied by severe microvascular destruction. Surprisingly, 4 weeks after irradiation, significantly increased recurrence was observed with increased FAP + tissue and cell cycle regulator expression, resulting in a remarkable altered graft volume. Moreover, irradiation-induced FAP upregulation markedly facilitated radiation resistance and increased cell cycle progression, decreased senescence, and increased energy production.

Conclusion: Our findings revealed that irradiation causes increased abundance of FAP + cells, which was associated with cell proliferation and delayed cellular senescence, accompanied by ATP production.

KEYWORDS

keloid scar, fibroblast activation protein alpha, radiation resistance, recurrence, xenotransplantation

Introduction

Skin wound healing is an extremely complex process that includes the infiltration of inflammatory cells and secretion of growth factors and cytokines (Reinke and Sorg, 2012; Broughton, 2006). Keloid scars (KSs) are produced from a dermal fibroproliferative disorder that develops after burns, deep skin injuries and even

surgical wounds (Ogawa, 2017). Although the mechanism of keloid formation is not fully understood, keloid is characterized by hyperthrophic fibroblast and collagen formation, angiogenesis and the upregulation of pro-inflammatory factors. Radiotherapy is currently recognized as one of the most important strategies for treating KSs (Mankowski et al., 2017). The favorable properties of electron irradiation make it the preferred choice for superficial keloid radiotherapy (Hogstrom and Almond, 2006; Hoppe, 2003; Maarouf et al., 2002). The recurrence rate with surgical resection alone, a traditional treatment for keloids and hypertrophic scars, ranges from 45% to 100% (Lee and Jang, 2018). Radiotherapy is often applied as a postoperative adjuvant therapy for keloids (Mustoe et al., 2002) and might control the rate of keloid recurrence to 15–23% (Mankowski et al., 2017). However, the mechanism remains unknown.

Since KSs occur only in humans, an appropriate animal model is necessary to explore new treatments and therapies. The major barrier to the engraftment of human-derived tissue in immune-competent rodents is robust xenogeneic immune rejection (Yang and Sykes, 2007). Fortunately, several strains of immunodeficient mice have been developed by disrupting relevant genes that are critical to the development, survival and function of immune cells (Marttala et al., 2016). In this study, we attempted to establish a novel PDX transplantation model using unique triple-immunodeficient mice designed using CRISPR-Cas9 technology to alter the *Prkdc* and *IL2rg* genes; the mice are more immunocompromised than commonly used immunodeficient mouse strains, such as SCID and nude mice. To study the mechanism of KS recurrence after surgical resection and electron beam treatment, human KS fragments without epidermal or dermal tissue were implanted into the backs of the NCG mice.

Fibroblast activation protein alpha (FAP) is a plasma membrane serine protease (dipeptidyl peptidase IV) that may play a key role in the invasiveness of keloids (Dienus et al., 2010). Normal adult tissues are generally negative for FAP, which exhibits both protease and collagenase activity and is important for extracellular matrix (ECM) degradation in wound healing and tumor invasion (O'Brien and O'Connor, 2008). These findings suggest that FAP may be a novel target for keloid treatment, but there have been few studies on the relationship between FAP and keloid recurrence after radiation therapy.

In this study, we evaluated the role of FAP in KS recurrence in an NCG xenograft mouse model. Although tissue loss occurred throughout the experiment, our data revealed that the graft was maintained in this new model for at least 20 weeks after implantation at the visible tissue level and that FAP + tissue was restored through radiation resistance, increased levels of cell cycle regulators, and high energy production.

Materials and methods

Ethical approval

Following approval of our protocol, which adhered to the ethical standards formulated in the Declaration of Helsinki, from the Institutional Ethics Committee of The First Hospital of Jilin University and the acquisition of written informed consent from all of the patients, KS tissues were obtained from 8 patients undergoing surgical excision.

Tissue preparation and xenotransplantation

Briefly, immediately after surgical excision, the human KS mass was washed twice with phosphate-buffered saline and cut into 4-mm square pieces under sterile conditions. The mice were anaesthetized by intraperitoneal injection of 5% chloral hydrate with 0.1 ml/10 g body weight, and 1-cm incisions were made on both sides of the dorsal midline above the gluteus maximus. The human keloid tissues were implanted into the subcutaneous pocket between the panniculus carnosus and skin, and the wound was sutured.

Eight-week-old NCG mice were purchased from Charles River (Beijing, China) and bred in the specific pathogen–free (SPF) murine facility. The First Hospital of Jilin University Research Animal Care Committee (Changchun, Jilin) approved the entire process, and all the animals were kept under standard conditions described in the guidelines approved by the institution.

Primary fibroblast isolation

KS tissues were washed twice with phosphate-buffered saline and cut into ~1 mm3 sections under sterile conditions. The washed sections were placed in a culture plate with a distance of 1 cm between each section and incubated at 37°C for 30 min. The sections were then incubated in DMEM containing 10% FBS and antibiotics (penicillin, 100 U/ml; streptomycin, 0.1 mg/ml) at 37°C with 5% CO2. All cell culture reagents were supplied by Gibco (Thermo Fisher Scientific, Inc). The fibroblasts were trypsinized and prepared for subculture when they reached 90% confluency.

TABLE 1 qPCR primers specific for p21, p53, p16, Cyclin D1, CD34, FAP, vimentin and β-actin.

	Sense (5′-3′)	Antisense (5′-3′)
CD34	CCTCAGTGTCTACTGCTGGTCT	GGAATAGCTCTGGTGGCTTGCA
FAP	GGAAGTGCCTGTTCCAGCAATG	TGTCTGCCAGTCTTCCCTGAAG
Vimentin	AGGCAAAGCAGGAGTCCACTGA	ATCTGGCGTTCCAGGGACTCAT
Cyclin D1	GCTGCGAAGTGGAAACCATC	CCTCCTTCTGCACACATTTGAA
p21	AGGTGGACCTGGAGACTCTCAG	TCCTCTTGGAGAAGATCAGCCG
P53	CCTCAGCATCTTATCCGAGTGG	TGGATGGTGGTACAGTCAGAGC
p16	CTCGTGCTGATGCTACTGAGGA	GGTCGGCGCAGTTGGGCTCC
β-Actin	ATTGCCGACAGGATGCAGAAG	CCATGCCAATCTCATCTTGT

Electron beam irradiation

At 4 weeks after implantation, irradiation therapy was performed with an electron beam (Clinac 21ex, Varian Medical System). The irradiation technique was consistent for all radiotherapies: The external beam was administered, with 6 MeV electrons generated by a linear accelerator. A single-fraction dose of 10 Gy (at a dose rate of 600 cGy/min) was delivered to the surgical incision with an electron beam. Nontarget areas were shielded using a 2-cm lead sheet.

RNA preparation and KEGG pathway analysis

Degradation and contamination of the RNA from the samples were monitored on 1% agarose gels. RNA purity was checked by a Nano Photometer® spectrophotometer (IMPLEN, CA, United States). RNA integrity was assessed using the RNA Nano 6000 Assay Kit with the Bioanalyzer 2100 system (Agilent Technologies, CA, United States). The Kyoto Encyclopedia of Genes and Genomes (KEGG) database is a resource used to determine the high-level functions and roles of genes in biological systems. ClusterProfiler R packets were used to detect significant enrichment of differentially expressed genes in the KEGG pathway. Firstly, all significantly enriched terms and then calculated accumulative hypergeometric *p*-values and enrichment factors were identified and used for filtering. The remaining significantly enriched terms then underwent hierarchical clustering into a tree based on kappa-statistical similarities among the gene memberships. Then, a kappa score of 0.3 was applied as the threshold to divide the tree into term clusters.

Quantitative real-time PCR

Total RNA was isolated with Total RNA Miniprep Kit (AP-MN-MS-RNA-250, Axygen), and cDNA was synthesized using 1st Strand cDNA Synthesis kit for qPCR (11123ES60, YEASEN Biotech, Shanghai). Quantitative RT-PCR was performed using Hieff® qPCR SYBR Green Master Mix (11203ES03, YEASEN Biotech, Shanghai) with a QuantStudio 5 RT qPCR system (ABI), and human-specific primer sets (Table 1) were obtained from Sangon Biotech (Shanghai, China). Beta-actin was used for normalization.

Histology and IHC

Tissues were collected, fixed with 4% formalin and embedded in paraffin. The paraffin sections (4 μm) were stained with H&E or subjected to IHC. Briefly, the tissue sections were subjected to antigen retrieval and incubation with primary antibodies against FAP (AF5344, Affinity), vimentin (AF7013, Affinity), or CD34 (AF5149, Affinity), followed by incubation with secondary antibody (KIT-9706, Maixin-Bio), and immunoreactivity was detected using an Peroxidase Kit (KIT-9710, Mai Xin). Quantitative analysis was performed using Image-Pro Plus 6.0 software.

Cell proliferation assay

Cell proliferation was assessed using a Cell Counting Kit-8 (CCK-8) assay kit (C0038, Beyotime) according to the manufacturer's protocol. Briefly, KFs (3×10^3 cells per well) were seeded into a 96-well plate and cultured at 37°C in a 5% CO2 incubator. CCK-8 solution was added for 2 h and the absorbance was measured at 490 nm.

SA-β-gal activity analysis

SA-β-gal active assay was performed as our previous study using an SA-β-gal staining kit (Beyotime, Beijing). Briefly, KFs were plated in 12-well plates (6×10^4/well) and

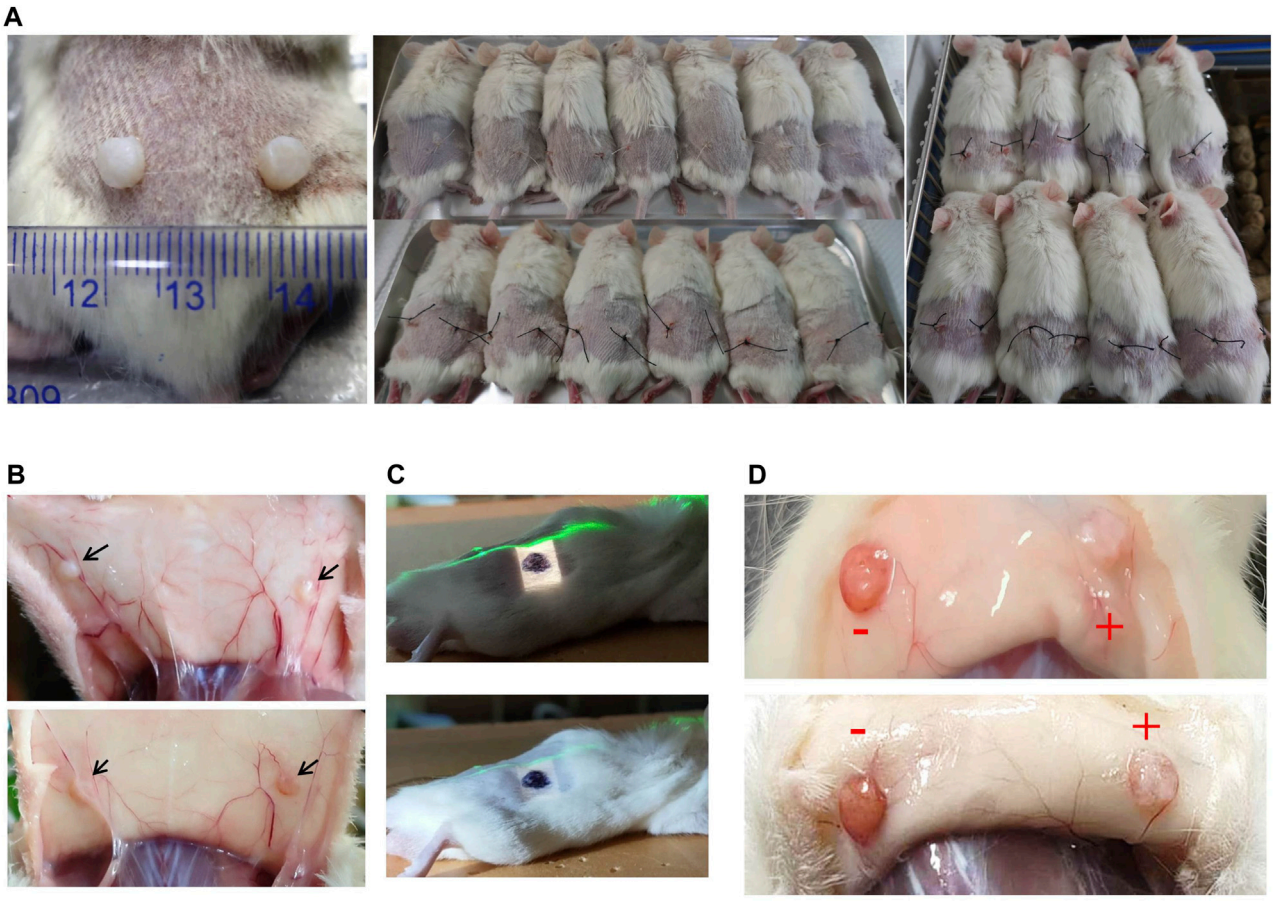

FIGURE 1
Xenotransplantation of patient-derived KS tissue in NCG mice and radiation therapy. **(A)** The grafts and implantation positions of the grafts are shown. **(B)** The grafts were visible at 20 weeks after implantation without irradiation. Representative images are shown. **(C)** Image of the field irradiated with an electron beam. The right side of the graft is marked in black. The green line is the laser alignment line. **(D)** One week after irradiation, graft morphological alterations were observed. Representative images are shown.

were irradiated with 10 Gy and analyzed upon reaching 80–90% confluence. SA-β-gal-positive cells were identified as green-stained cells and the frequency was determined by counting approximately 400 cells in three random fields.

Flow cytometry

To measure radiation-induced cytomembrane expression of FAP or cytoplasmic expression of vimentin, primary KFs were irradiated with a single-fraction dose of 10 Gy (at a dose rate of 600 cGy/min) with an electron beam. The cells were analyzed by staining with an AF488-conjugated anti hFAP antibody (R&D Systems, FAB3715G-100) and a PE-conjugated anti-hVimentin antibody (BD, 562337). FAP+ KFs were sorted according to staining with the AF488-conjugated antihFAP antibody (BD FACSCalibur) at 72 h after irradiation.

Measurement of intracellular ATP levels

Intracellular basal ATP production rates were measured using Seahorse XF Real-Time ATP Rate Assay Kit (Agilent). This assay was performed according to the manufacturer's protocol. Briefly, KF cells were seeded into 24-well plates with 3 × 104 cells per well and incubated at 37°C with 5% CO2 for several days. One hour after medium was replaced by indicated medium without bicarbonate, the OCR and ECAR were measured with XF24 (Seahorse Bioscience, United States) before and after injection of 1.5 μM oligomycin, 0.5 μM rotenone and 0.5 μM antimycin. The basal ATP production rates were compared by mitoATP Production Rate and glycoATP Production Rate.

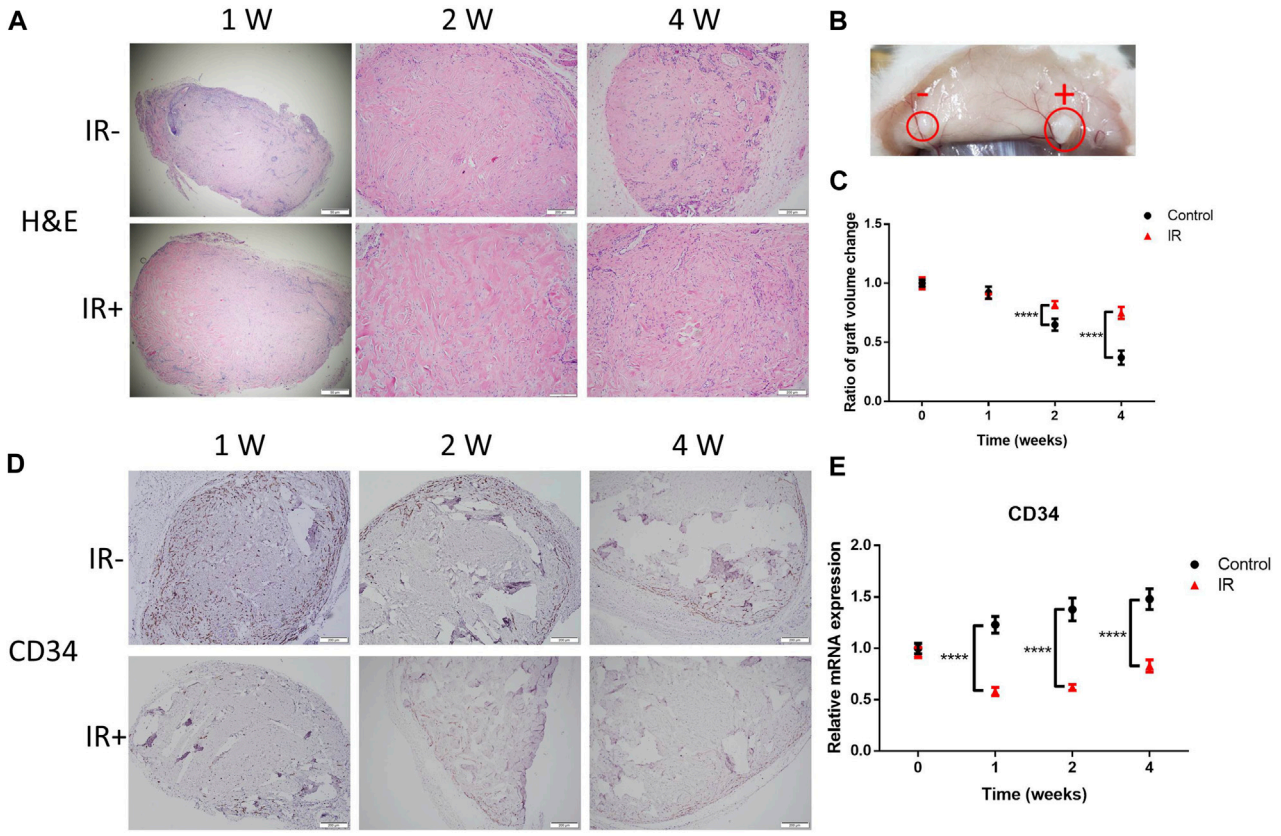

FIGURE 2
Irradiation (IR) induced destruction of the microvasculature and tissue loss. **(A)** Representative images showing H&E staining, **(B)** a morphological comparison at 4 weeks after IR and **(C)** a comparison of the graft volume ratio. Images from 6 representative random fields are shown. The scale bars represent 200 μm except for the scale bar of 1 W in **(A)**, which represents 50 μm. **(D)** Graft sections were stained for CD34 for IHC analysis. Six samples per group were examined, and representative images are shown (scale bar represents 200 μm). **(E)** Comparison of the CD34 levels in the two groups of grafts. Data from 3 experiments were combined and are presented as the mean ± SD; $n = 6$; ****, $p < 0.001$.

Statistical analysis

All studies were repeated at least three times and data are presented as the mean ± SD. Statistical analysis was performed using Prism 6 (GraphPad Software). One-way ANOVA was used for comparison of multiple groups, while the *t* test was used for comparison of two groups. $p < 0.05$ were taken as significant.

Results

Establishment of a patient-derived KS tissue xenotransplantation model using NCG mice and morphological observation

To establish a PDX mouse model to study KSs, human KS tissues (from 8 patients) were cut into 3–4-mm square pieces and implanted into the backs of NCG mice (>60) under sterile conditions (Figure 1A). Previous studies have shown that KS grafts can be maintained in nude mice for at least 4 months after operation, as shown by detection at the cellular level (Park et al., 2016; Shetlar et al., 1985). In this study, the grafts were still visible at 20 weeks after transplantation, although significant tissue loss was observed (Figure 1B). According to our previous work, more than 3 weeks are needed for the graft to establish stable neovascularization. At 4 weeks after implantation, the right sides of the grafts in the KS-bearing mice were irradiated with a single-fraction dose of 10 Gy with an electron beam (Figure 1C). One week after irradiation, morphological alterations in the graft were observed. As shown in Figure 1D, in contrast to nonirradiated grafts (−), the irradiated grafts showed evidence that the electron beam had severely destroyed the neovascularization (+). Taken together, these findings demonstrated that we successfully established a PDX mouse model of KSs using NCG mice and observed severe electron beam-induced damage to the vascular network of the graft.

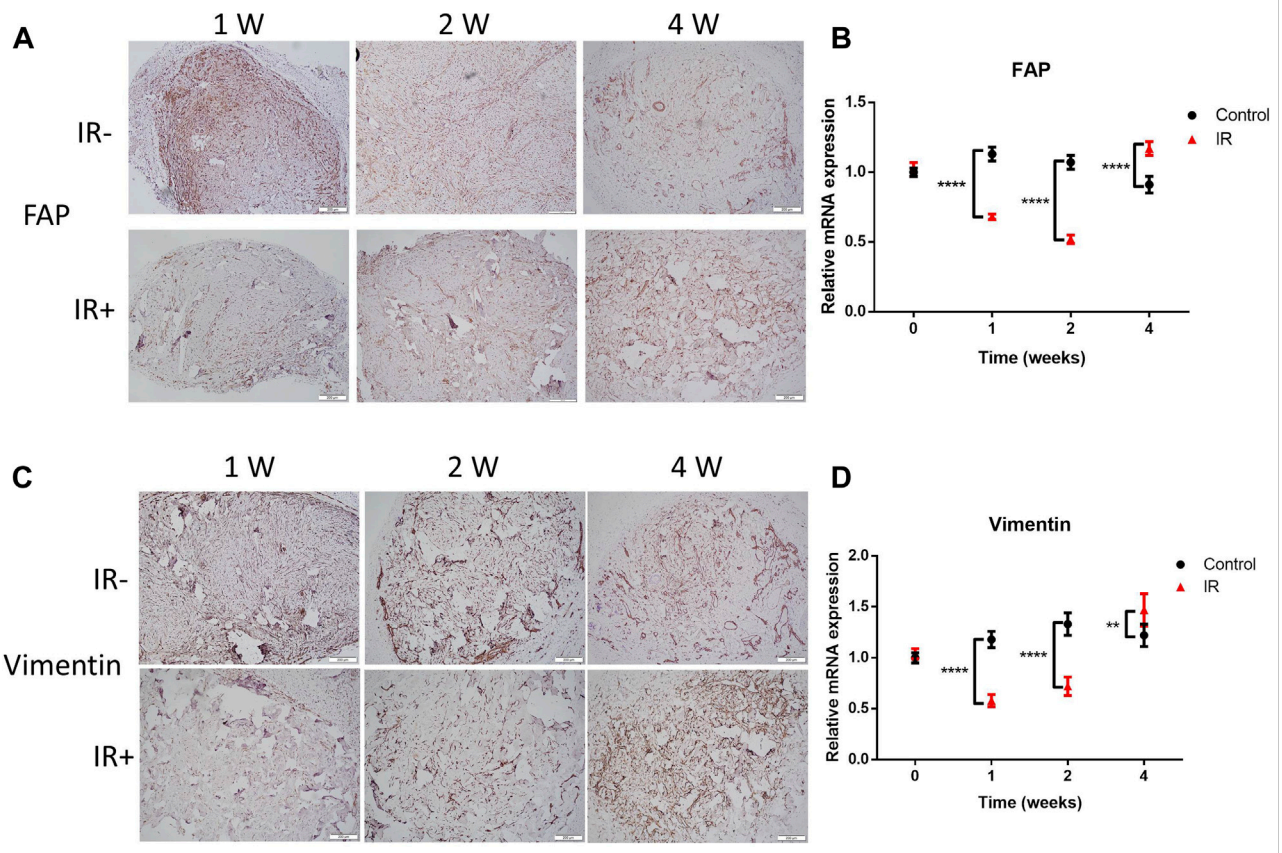

FIGURE 3
Radiation-resistant tissue was quickly restored, with increased FAP and vimentin expression. **(A–C)** Graft sections were stained for FAP and vimentin for IHC analysis. The scale bar represents 200 μm. **(B–D)** Comparison of the mRNA levels of FAP and vimentin between the two groups of grafts. Data from 3 experiments were combined and are presented as the mean ± SD. $n = 6$; **, $p < 0.01$; ****, $p < 0.001$.

Irradiation induced microvascular destruction and tissue loss

To investigate the effect of the electron beam on implanted KS tissue and determine whether irradiation can suppress the development of graft tissue, histological analysis was performed. As shown in Figure 2A, H&E staining of the grafts was performed at 1, 2 and 4 weeks after irradiation. The electron beam induced sharp decreases in the numbers of infiltrating cells in the graft tissues, especially during the first week after irradiation (Figure 2A, left row). Surprisingly, irradiation disrupted the vascular network of the graft but slowed the process of tissue loss (Figures 2A,B). At 4 weeks after irradiation, the volume ratio of the irradiated grafts was significantly larger than that of the control grafts by over twofold (0.75 vs. 0.37). Moreover, histological analysis was performed to determine whether the electron beam would destroy the neovascularization in the graft tissue (Figures 2D,E). Consistent with the results in Figure 1C, our results revealed that irradiation induced a sharp decrease in microvascular density and CD34 mRNA levels.

Irradiation destroyed the internal structure of KS tissues, but FAP+ and vimentin + tissues were quickly restored

Fibroblasts are thought to play a key role in fibrogenesis in KSs. FAP is a plasma membrane-localized protease associated with the development of KSs (Dienus et al., 2010). To determine whether irradiation could promote the expression of FAP in graft tissue, histological analysis was performed. As shown in Figure 3A, the electron beam significantly increased the FAP level compared to that in the control graft after irradiation. This result was consistent with the mRNA level of FAP (Figure 3B). Increased levels of vimentin were reported to serve as a mesenchymal marker, and the frequency of vimentin + epidermal cells was found to be higher in KSs and keloid microvessels than in normal skin (Yan et al., 2015; Hahn et al., 2016). Therefore, we observed changes in vimentin expression in the grafts after irradiation. Surprisingly, the change in vimentin expression beginning in the second week after irradiation was dramatically reversed (Figures 3C,D). These results suggest that irradiation damaged FAP+ and vimentin + tissue in the grafts but

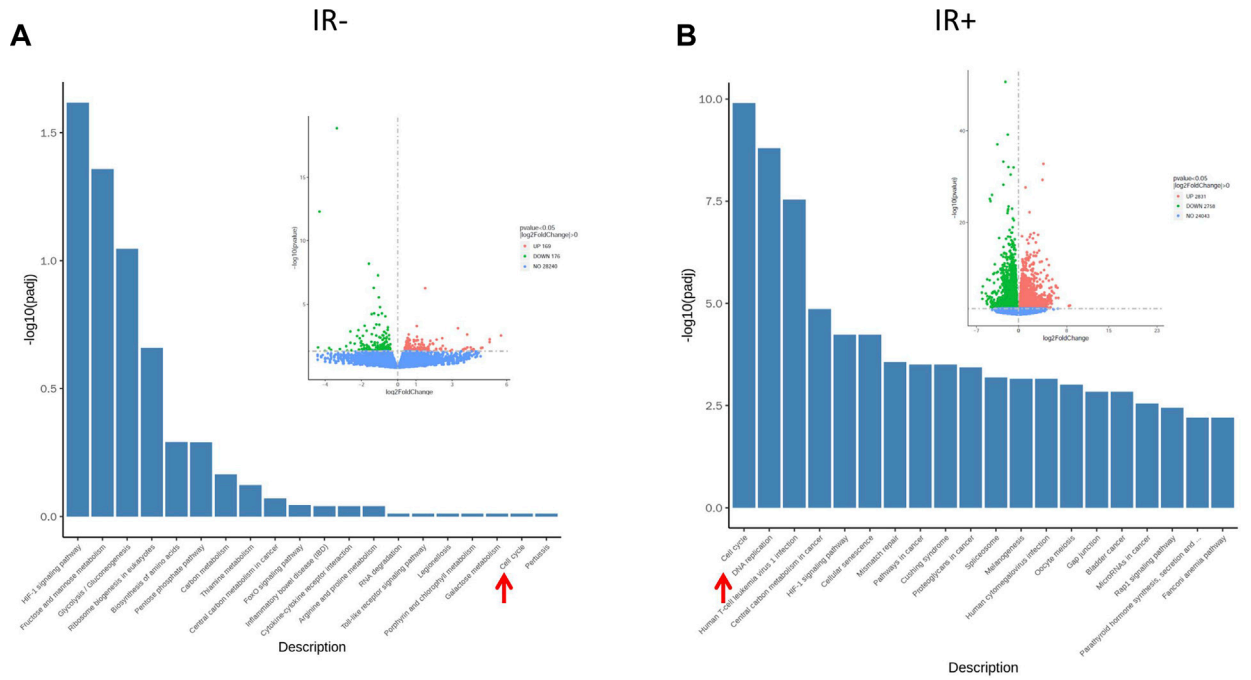

FIGURE 4
Irradiation (IR) promoted cell cycle regulator expression in radiation-resistant tissue. RNA-seq analysis of nonimplanted KS tissue compared with unirradiated tissue at 4 weeks after implantation **(A)** and irradiated tissue at 4 weeks after irradiation **(B)**. The insert from the volcano map indicates the number of gene alterations. The columns are KEGG pathways, and the spots are the number of genes. Green indicates downregulation, and red indicates upregulation. The red arrow indicates the cell cycle pathway. Shown are the mRNA levels (mean ± SD; n = 6) of the CKIs p21/p53/p16 **(C–E)** and the promoter Cyclin D1 **(F)**. Data from three experiments with essentially the same results were combined and are presented as the mean ± SD; $n = 6$; *, $p < 0.05$; ***, $p < 0.005$; ****, $p < 0.001$.

that the levels of both molecules were significantly restored over 3 weeks. This finding is consistent with the observed changes in graft volume after irradiation (Figure 2B).

Irradiation significantly upregulated cell cycle regulators

To clarify the effects of transplantation and irradiation on KSs, we compared the transcriptome activity of nonimplanted KS tissue with that of KS tissue at 4 weeks after transplantation (Figure 4A) and 4 weeks after irradiation (Figure 4B). Compared to the control, in our PDX model, only 169 genes were upregulated, and 176 genes were downregulated, despite the 4-week experimental period (Figure 4A insert). However, irradiation induced a large change in expression, with 2831 genes upregulated and 2758 genes downregulated compared to their expression in the PDX model (Figure 4B, insert). Moreover, KEGG analysis revealed that the expression of cell cycle regulators was significantly increased by irradiation. Furthermore, the mRNA expressions were compared for the key cell cycle inhibitors (cyclin-dependent kinase (CDK) inhibitors, CKIs) p21, p53 and p16, which are known tumor suppressor proteins that are upregulated in irradiated tissue (Aratani et al., 2018). Consistent with the immunohistochemistry (IHC) results (Figure 3), expression of the CKIs p53, p21 and p16 after 4 weeks was significantly reduced by irradiation compared with that in the control (Figures 4C–E). Interestingly, the expression of p53, the primary guardian of the DNA damage response, was significantly upregulated 1 week after irradiation compared with that in the control group but sharply downregulated 1 week later (Figure 3B). On the other hand, irradiation significantly increased the level of Cyclin D1 (Figure 4F), a cell cycle promoter that regulates cell cycle progression by phosphorylating CDK4/6 to inhibit retinoblastoma (Connell-Crowley et al., 1997). Taken together, these results suggested that radiation-resistant tissue (some of which may be positive for FAP) among KS tissue may cause KS recurrence due to irradiation.

FAP + keloid fibroblasts (KFs) promoted cell cycle regulator expression in radiation-resistant tissue with increased energy production

Our data indicated that FAP + tissue could be quickly restored *in vivo*. To investigate whether irradiation could

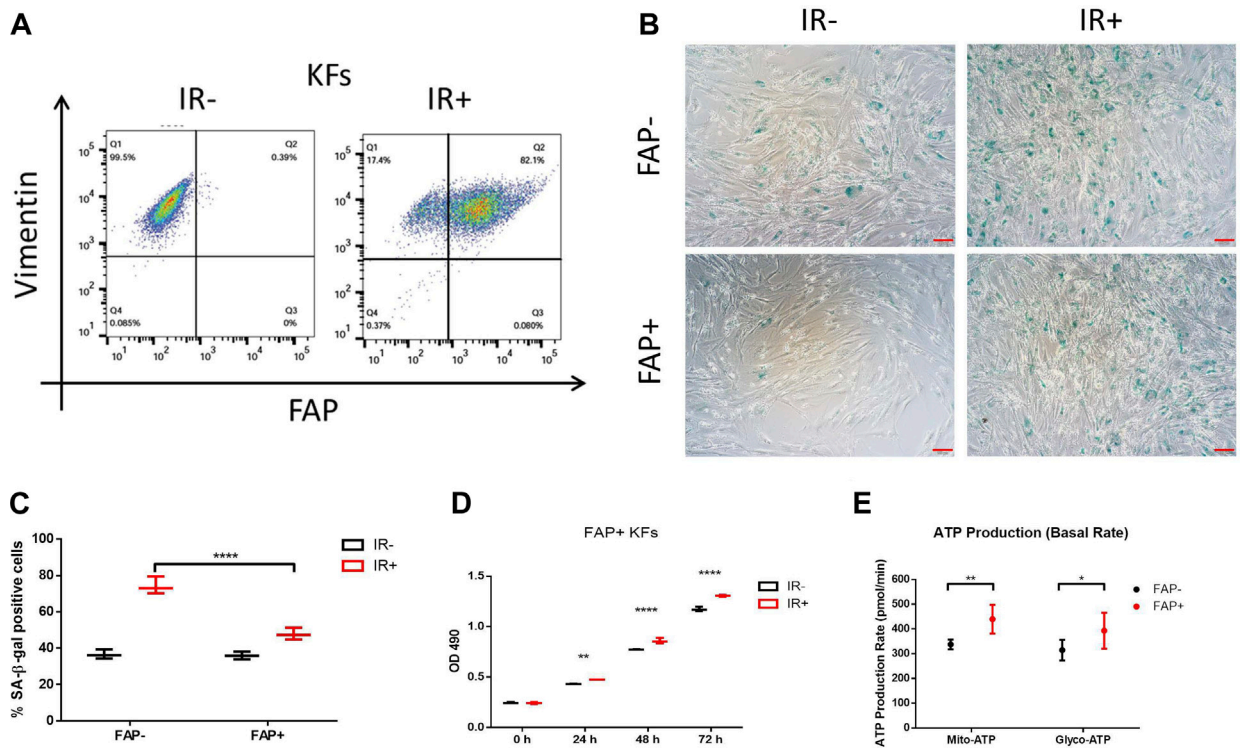

FIGURE 5
Irradiation (IR) promoted FAP + KF proliferation and inhibited senescence, accompanied by high energy production. *In vitro*, primary KFs with or without IR treatment were analyzed by anti-hFAP and anti-hVimentin antibody staining **(A)**. Representative images of SA-β-gal staining **(B)**; senescent cells are stained green, scale bar = 100 μm. The percentage of senescent cells in FAP- versus FAP + KFs at 72 h after IR **(C)**. Data are representative of three independent samples and are presented as the mean ± SD; $n = 6$; ****, $p < 0.001$. IR promoted FAP + KF proliferation **(D)** and increased intracellular ATP production **(E)**. Data from three experiments with essentially the same results were combined and are presented as the mean ± SD; $n = 3$; *, $p < 0.05$; **, $p < 0.01$; ****, $p < 0.001$.

induce FAP + cell proliferation, primary KFs were isolated from patient excisions and irradiated with 10 Gy electron beam therapy. Vimentin, a fibroblast biomarker, is also known as fibroblast intermediate filament in non-muscle cells. The flow cytometry data revealed that the isolated primary KFs were 99.5% vimentin positive. Surprisingly, radiation induced a significant increase in the FAP + KF population; the FAP + KF percentage in the irradiation group was 82.1%, while that in the non-irradiation group was 0.39% (Figure 5A). To determine the role of FAP in radiation-induced senescence, the FAP + KFs were sorted, and senescence-associated β-galactosidase (SA-β-gal) activity was measured at 72 h after irradiation. Irradiation clearly increased the percentages of SA-β-gal + cells among both types of KFs; however, the increase was markedly smaller in the FAP + group than in the FAP- group, and the percentage of SA-β-gal + cells was significantly lower in the FAP + group than in the FAP- group (Figures 5B,C). Although the numbers of viable cells were comparable between nonirradiated and irradiated KF cultures at 0 h, the irradiated cultures thereafter yielded significantly more viable cells (Figure 5D). The observation of rapid recurrence with increased FAP expression and cell proliferation after irradiation suggests the need for an adequate energy supply. Adenosine triphosphate (ATP), the most common cellular energy currency of intermediate metabolism, is used to sustain various cellular functions such as anabolic synthesis, molecular transport, cell motility, and cell proliferation. Thus, ATP levels were measured to compare FAP+ and FAP- KF cell viability (Figure 5E). FAP + KFs had significantly higher ATP concentrations and showed a significantly greater rate of ATP production from glycolysis (393.1 vs. 314.8 pmol/min) and mitochondrial oxidative phosphorylation than FAP- KFs (439.8 vs. 337.5 pmol/min). Taken together, our results demonstrate a strong association between FAP + KF abundance and radiation resistance through cell cycle progression and increased energy production.

Discussion

Keloid, a fibroproliferative disease and physiological phenomenon unique to humans, can occur in genetically susceptible individuals (Brown and Bayat, 2009). Thus, because keloid is unique to humans, it is difficult to conduct

in vivo studies through the use of animal models. Fortunately, the development of immunodeficient mice strains might provide a novel approach to investigate the pathological progression of KSs *in vivo* by establishing reliable patient-derived KS xenografts models that remain viable for several weeks to months after transplantation (Marttala et al., 2016; Shultz et al., 2007). In this study, we established a PDX model of human-derived KS tissue by using NCG mice, and the graft successfully survived *in vivo* for as long as 20 weeks. Although significant tissue loss was observed over time, all grafts retained their original histotypic and morphological characteristics for 20 weeks, providing a sufficiently long window to investigate preclinical therapies and molecular mechanisms.

Numerous studies have shown the favorable effects of electron beam radiotherapy for keloid treatment. For example, recent data revealed that surgical excision followed by electron beam radiation provides excellent local control of keloids and reduces the recurrence rate to 8.6% (Wang et al., 2020), while the recurrent rate for traditional keloid surgery alone is up to 45–100% (Lee and Jang, 2018). Regarding optimal irradiation timing, most studies recommended electron beam radiotherapy as an adjuvant therapy within 24–48 h after keloid revision surgery (Ogawa et al., 2003). Mechanistically, the fibroblasts that dominated the incisional granulation tissue at this time were found to be sensitive to irradiation. Therefore, this radiotherapy strategy can effectively suppress the cell proliferation and division of fibroblasts and reduce collagen deposition. However, no consensus for the optimal irradiation dose and fraction regimen has been reached. In previous studies, keloid treatment has tended to involve postoperative irradiation with a dose of 12–20 Gy over 3–5 fractions (Renz et al., 2018), (Bischof et al., 2007). Herein, radiation with 20 Gy over 5 fractions was confirmed to yield superior local control compared to the control achieved with lower-dose regimens (Renz et al., 2018). Recently, emerging studies have demonstrated that the use of hypofractionated postoperative radiotherapy with a high-energy electron beam for keloids is an excellent strategy and that initiating radiotherapy as soon as possible after surgery could improve the therapeutic regimen (Shen et al., 2015). Adjuvant single-fraction radiotherapy with a dose of 8–10 Gy from an electron beam was also confirmed to be effective and safe for treating keloids (Song et al., 2014), (Sruthi et al., 2018). Concerning unresectable keloids, previous data have demonstrated that radical radiotherapy can achieve satisfactory and similar efficacy (Malaker et al., 2004). As a result, postsurgical radiotherapy has become the most widely accepted method for the treatment of keloids.

Here, we attempted to irradiate our PDX model of human-derived KS tissue with an electron beam. The results revealed that irradiation quickly destroyed the neovascular system of the graft and significantly reduced levels of the KS-related factors FAP and vimentin (Figures 2, 3). Interestingly, similar changes in graft volume and in FAP and vimentin were observed, and KS relapse was accompanied by restored FAP and vimentin expression. FAP, a proline-selective serine protease, is overexpressed in hypertrophic/KS tissue and the tumor stroma (cancer/tumor-associated fibroblasts, CAFs/TAFs) but undetectable in most normal adult tissues (Kalluri and Zeisberg, 2006; Spaeth et al., 2009). FAP plays an important role in ECM remodeling via its serine protease activity (Kennedy et al., 2009). Tumor relapse is usually caused by radiation resistance, which is determined by both the intrinsic characteristics and external microenvironment of cancer cells (Wang et al., 2017; Wang et al., 2005). Accumulating evidence has revealed that FAP + CAFs might provide a more immunosuppressive microenvironment to resist damage from immunocytes/radiotherapy/chemotherapy, resulting in increased tumor survival (Yang et al., 2016; Lindner et al., 2018; Ansems and Span, 2020). Moreover, a similar result from a transplanted tumor model demonstrated that FAP + stromal cells could facilitate immunosuppression via ablation of T cell antitumor activity (Kraman et al., 2010). However, the mechanism of induction of FAP expression remains unclear. Here, our data revealed that irradiation by electron beam could promote the FAP level *in vitro* and *in vitro* for the first time, and the reduction of FAP + tissue in the control group was positively correlated with tissue loss (Figure 3A), while the rebound of FAP + tissue in the irradiated group was also proportional to graft volume. In addition, our transcriptome experiments revealed that irradiation significantly enhanced translational activity in the irradiated grafts, including the translation of cell cycle regulators. Cyclin D1 plays a key role in regulating the G1/S transition by activating CDKs, whereas CKIs, such as p21 and p16, inhibit the cyclin/CDK complex kinase activity. Our data revealed that irradiation promoted cell cycle progression in FAP + cells, accompanied by upregulation of Cyclin D1 and downregulation of the CKIs p53, p21 and p16. In this study, we discovered that the induction of FAP expression by electron beam only in the primary human keloid derived fibroblast, we also attempted to detect radiation-induced FAP expression in mouse fibroblast cell line, but the cell line displayed a poor radio-sensitivity (data not shown). The role of enzymatic activity and ablation of FAP in recurrence of KS will be further investigated.

Taken together, our findings revealed a prominent expression of FAP in KS recurrence after surgical resection and radiation therapy, indicating that irradiation might enhance FAP + cell abundance, which was associated with cell proliferation and delayed cellular senescence, accompanied by ATP production.

Data availability statement

The raw data supporting the conclusions of this article will be made available by the authors, without undue reservation.

Ethics statement

The animal study was reviewed and approved by Ethics Committee of the First Hospital of Jilin University.

Author contributions

XH and YG performed most of the experiments. XH and TY analyzed the IHC data. YD performed qPCR analysis. KC and YG conceived, designed, and supervised all studies. KC and YG wrote the manuscript.

Funding

This study was supported by the Natural Science Foundation from Jilin Provincial Department of Science and Technology (No. 20200404166YY, No.20210101448JC), the Natural Science Foundation from the Jilin Provincial Department of Education (JJKH20201035KJ and JJKH20201030KJ).

Conflict of interest

The authors declare that the research was conducted in the absence of any commercial or financial relationships that could be construed as a potential conflict of interest.

Publisher's note

All claims expressed in this article are solely those of the authors and do not necessarily represent those of their affiliated organizations, or those of the publisher, the editors and the reviewers. Any product that may be evaluated in this article, or claim that may be made by its manufacturer, is not guaranteed or endorsed by the publisher.

References

Ansems, M., and Span, P. N. (2020). The tumor microenvironment and radiotherapy response; a central role for cancer-associated fibroblasts. *Clin. Transl. Radiat. Oncol.* 22, 90–97. doi:10.1016/j.ctro.2020.04.001

Aratani, S., Tagawa, M., Nagasaka, S., Sakai, Y., Shimizu, A., and Tsuruoka, S. (2018). Radiation-induced premature cellular senescence involved in glomerular diseases in rats. *Sci. Rep.* 8 (1), 16812. doi:10.1038/s41598-018-34893-8

Bischof, M., Krempien, R., Debus, J., and Treiber, M. (2007). Postoperative electron beam radiotherapy for keloids: Objective findings and patient satisfaction in self-assessment. *Int. J. Dermatol.* 46 (9), 971–975. doi:10.1111/j.1365-4632.2007.03326.x

Broughton, G., Janis, J. E., and Attinger, C. E. (2006). Wound healing: An overview. *Plast. Reconstr. Surg.* 117 (7), 1e-S–32e-S. doi:10.1097/01.prs.0000222562.60260.f9

Brown, J. J., and Bayat, A. (2009). Genetic susceptibility to raised dermal scarring. *Br. J. Dermatol.* 161 (1), 8–18. doi:10.1111/j.1365-2133.2009.09258.x

Connell-Crowley, L., Harper, J. W., and Goodrich, D. W. (1997). Cyclin D1/Cdk4 regulates retinoblastoma protein-mediated cell cycle arrest by site-specific phosphorylation. *Mol. Biol. Cell* 8 (2), 287–301. doi:10.1091/mbc.8.2.287

Dienus, K., Bayat, A., Gilmore, B. F., and Seifert, O. (2010). Increased expression of fibroblast activation protein-alpha in keloid fibroblasts: Implications for development of a novel treatment option. *Arch. Dermatol. Res.* 302 (10), 725–731. doi:10.1007/s00403-010-1084-x

Hahn, J. M., McFarland, K. L., Combs, K. A., and Supp, D. M. (2016). Partial epithelial-mesenchymal transition in keloid scars: Regulation of keloid keratinocyte gene expression by transforming growth factor-β1. *Burns Trauma* 4 (1), 30. doi:10.1186/s41038-016-0055-7

Hogstrom, K. R., and Almond, P. R. (2006). Review of electron beam therapy physics. *Phys. Med. Biol.* 51 (13), R455–R489. doi:10.1088/0031-9155/51/13/R25

Hoppe, R. T. (2003). Mycosis fungoides: Radiation therapy. *Dermatol. Ther.* 16 (4), 347–354. doi:10.1111/j.1396-0296.2003.01647.x

Kalluri, R., and Zeisberg, M. (2006). Fibroblasts in cancer. *Nat. Rev. Cancer* 6 (5), 392–401. doi:10.1038/nrc1877

Kennedy, A., Dong, H., Chen, D., and Chen, W. T. (2009). Elevation of seprase expression and promotion of an invasive phenotype by collagenous matrices in ovarian tumor cells. *Int. J. Cancer* 124 (1), 27–35. doi:10.1002/ijc.23871

Kraman, M., Bambrough, P. J., Arnold, J. N., Roberts, E. W., Magiera, L., Jones, J. O., et al. (2010). Suppression of antitumor immunity by stromal cells expressing fibroblast activation protein-alpha. *Science* 330 (6005), 827–830. doi:10.1126/science.1195300

Lee, H. J., and Jang, Y. J. (2018). Recent understandings of biology, prophylaxis and treatment strategies for hypertrophic scars and keloids. *Int. J. Mol. Sci.* 19 (3), 711. doi:10.3390/ijms19030711

Lindner, T., Loktev, A., Altmann, A., Giesel, F., Kratochwil, C., Debus, J., et al. (2018). Development of quinoline-based theranostic ligands for the targeting of fibroblast activation protein. *J. Nucl. Med.* 59 (9), 1415–1422. doi:10.2967/jnumed.118.210443

Maarouf, M., Schleicher, U., Schmachtenberg, A., and Ammon, J. (2002). Radiotherapy in the management of keloids. Clinical experience with electron beam irradiation and comparison with X-ray therapy. *Strahlenther. Onkol.* 178 (6), 330–335. doi:10.1007/s00066-002-0935-6

Malaker, K., Vijayraghavan, K., Hodson, I., and Al Yafi, T. (2004). Retrospective analysis of treatment of unresectable keloids with primary radiation over 25 years. *Clin. Oncol.* 16 (4), 290–298. doi:10.1016/j.clon.2004.03.005

Mankowski, P., Kanevsky, J., Tomlinson, J., Dyachenko, A., and Luc, M. (2017). Optimizing radiotherapy for keloids: A meta-analysis systematic review comparing recurrence rates between different radiation modalities. *Ann. Plast. Surg.* 78 (4), 403–411. doi:10.1097/SAP.0000000000000989

Marttala, J., Andrews, J. P., Rosenbloom, J., and Uitto, J. (2016). Keloids: Animal models and pathologic equivalents to study tissue fibrosis. *Matrix Biol.* 51, 47–54. doi:10.1016/j.matbio.2016.01.014

Mustoe, T. A., Cooter, R. D., Gold, M. H., Hobbs, F. D., Ramelet, A. A., Shakespeare, P. G., et al. (2002). International clinical recommendations on scar management. *Plast. Reconstr. Surg.* 110 (2), 560–571. doi:10.1097/00006534-200208000-00031

O'Brien, P., and O'Connor, B. F. (2008). Seprase: An overview of an important matrix serine protease. *Biochim. Biophys. Acta* 1784 (9), 1130–1145. doi:10.1016/j.bbapap.2008.01.006

Ogawa, R. (2017). Keloid and hypertrophic scars are the result of chronic inflammation in the reticular dermis. *Int. J. Mol. Sci.* 18 (3), 606. doi:10.3390/ijms18030606

Ogawa, R., Mitsuhashi, K., Hyakusoku, H., and Miyashita, T. (2003). Postoperative electron-beam irradiation therapy for keloids and hypertrophic scars: Retrospective study of 147 cases followed for more than 18 months. *Plast. Reconstr. Surg.* 111 (2), 547–553. discussion 554-5. doi:10.1097/01.PRS.0000040466.55214.35

Park, T. H., Rah, D. K., Chang, C. H., and Kim, S. Y. (2016). Establishment of patient-derived keloid xenograft model. *J. Craniofac. Surg.* 27 (7), 1670–1673. doi:10.1097/SCS.0000000000002901

Reinke, J. M., and Sorg, H. (2012). Wound repair and regeneration. *Eur. Surg. Res.* 49 (1), 35–43. doi:10.1159/000339613

Renz, P., Hasan, S., Gresswell, S., Hajjar, R. T., Trombetta, M., and Fontanesi, J. (2018). Dose effect in adjuvant radiation therapy for the treatment of resected keloids. *Int. J. Radiat. Oncol. Biol. Phys.* 102 (1), 149–154. doi:10.1016/j.ijrobp.2018.05.027

Shen, J., Lian, X., Sun, Y., Wang, X., Hu, K., Hou, X., et al. (2015). Hypofractionated electron-beam radiation therapy for keloids: Retrospective study of 568 cases with 834 lesions. *J. Radiat. Res.* 56 (5), 811–817. doi:10.1093/jrr/rrv031

Shetlar, M. R., Shetlar, C. L., Hendricks, L., and Kischer, C. W. (1985). The use of athymic nude mice for the study of human keloids. *Proc. Soc. Exp. Biol. Med.* 179 (4), 549–552. doi:10.3181/00379727-179-rc3

Shultz, L. D., Ishikawa, F., and Greiner, D. L. (2007). Humanized mice in translational biomedical research. *Nat. Rev. Immunol.* 7 (2), 118–130. doi:10.1038/nri2017

Song, C., Wu, H. G., Chang, H., Kim, I. H., and Ha, S. W. (2014). Adjuvant single-fraction radiotherapy is safe and effective for intractable keloids. *J. Radiat. Res.* 55 (5), 912–916. doi:10.1093/jrr/rru025

Spaeth, E. L., Dembinski, J. L., Sasser, A. K., Watson, K., Klopp, A., Hall, B., et al. (2009). Mesenchymal stem cell transition to tumor-associated fibroblasts contributes to fibrovascular network expansion and tumor progression. *PloS one* 4 (4), e4992. doi:10.1371/journal.pone.0004992

Sruthi, K., Chelakkot, P. G., Madhavan, R., Nair, R. R., and Dinesh, M. (2018). Single-fraction radiation: A promising adjuvant therapy to prevent keloid recurrence. *J. Cancer Res. Ther.* 14 (6), 1251–1255. doi:10.4103/jcrt.JCRT_20_17

Wang, X. M., Yu, D. M., McCaughan, G. W., and Gorrell, M. D. (2005). Fibroblast activation protein increases apoptosis, cell adhesion, and migration by the LX-2 human stellate cell line. *Hepatology* 42 (4), 935–945. doi:10.1002/hep.20853

Wang, Y., Gan, G., Wang, B., Wu, J., Cao, Y., Zhu, D., et al. (2017). Cancer-associated fibroblasts promote irradiated cancer cell recovery through autophagy. *EBioMedicine* 17, 45–56. doi:10.1016/j.ebiom.2017.02.019

Wang, Y., Ma, J., Zhang, Z., and Shen, H. (2020). Combined surgical excision and electron external beam radiation improves the treatment of keloids: A descriptive study. *Dermatol. Ther.* 33 (4), e13494. doi:10.1111/dth.13494

Yan, L., Cao, R., Wang, L., Liu, Y., Pan, B., Yin, Y., et al. (2015). Epithelial-mesenchymal transition in keloid tissues and TGF-β1-induced hair follicle outer root sheath keratinocytes. *Wound Repair Regen.* 23 (4), 601–610. doi:10.1111/wrr.12320

Yang, X., Lin, Y., Shi, Y., Li, B., Liu, W., Yin, W., et al. (2016). FAP promotes immunosuppression by cancer-associated fibroblasts in the tumor microenvironment via STAT3-CCL2 signaling. *Cancer Res.* 76 (14), 4124–4135. doi:10.1158/0008-5472.CAN-15-2973

Yang, Y. G., and Sykes, M. (2007). Xenotransplantation: Current status and a perspective on the future. *Nat. Rev. Immunol.* 7 (7), 519–531. doi:10.1038/nri2099

frontiers | Frontiers in Oncology

TYPE Original Research
PUBLISHED 30 August 2022
DOI 10.3389/fonc.2022.978050

Check for updates

OPEN ACCESS

EDITED BY
Pranav Gupta,
Albert Einstein College of Medicine, United States

REVIEWED BY
Kun Wang,
Guangzhou University of Chinese Medicine, China
Qi Zhang,
Huazhong University of Science and Technology, China

*CORRESPONDENCE
Jiaping Li
lijiap@mail.sysu.edu.cn

†These authors have contributed equally to this work

SPECIALTY SECTION
This article was submitted to Molecular and Cellular Oncology, a section of the journal Frontiers in Oncology

RECEIVED 25 June 2022
ACCEPTED 09 August 2022
PUBLISHED 30 August 2022

CITATION
Zhang G, Xiao Y, Zhang X, Fan W, Zhao Y, Wu Y, Wang H and Li J (2022) Dissecting a Hypoxia-Related Angiogenic Gene Signature for Predicting Prognosis and Immune status in Hepatocellular Carcinoma. *Front. Oncol.* 12:978050. doi: 10.3389/fonc.2022.978050

COPYRIGHT
© 2022 Zhang, Xiao, Zhang, Fan, Zhao, Wu, Wang and Li. This is an open-access article distributed under the terms of the Creative Commons Attribution License (CC BY). The use, distribution or reproduction in other forums is permitted, provided the original author(s) and the copyright owner(s) are credited and that the original publication in this journal is cited, in accordance with accepted academic practice. No use, distribution or reproduction is permitted which does not comply with these terms.

Dissecting a hypoxia-related angiogenic gene signature for predicting prognosis and immune status in hepatocellular carcinoma

Guixiong Zhang[1†], Yitai Xiao[2†], Xiaokai Zhang[1], Wenzhe Fan[1], Yue Zhao[1], Yanqin Wu[1], Hongyu Wang[1] and Jiaping Li[1*]

[1]Department of Interventional Oncology, The First Affiliated Hospital, Sun Yat-Sen University, Guangzhou, China, [2]Guangdong Provincial Key Laboratory of Biomedical Imaging and Guangdong Provincial Engineering Research Center of Molecular Imaging, The Fifth Affiliated Hospital, Sun Yat-sen University, Zhuhai, China

Background: Hypoxia and angiogenesis, as prominent characteristics of malignant tumors, are implicated in the progression of hepatocellular carcinoma (HCC). However, the role of hypoxia in the angiogenesis of liver cancer is unclear. Therefore, we explored the regulatory mechanisms of hypoxia-related angiogenic genes (HRAGs) and the relationship between these genes and the prognosis of HCC.

Methods: The transcriptomic and clinical data of HCC samples were downloaded from public datasets, followed by identification of hypoxia- and angiogenesis-related genes in the database. A gene signature model was constructed based on univariate and multivariate Cox regression analyses, and validated in independent cohorts. Kaplan-Meier survival and time-dependent receiver operating characteristic (ROC) curves were generated to evaluate the model's predictive capability. Gene set enrichment analysis (GSEA) was performed to explore signaling pathways regulated by the gene signature. Furthermore, the relationships among gene signature, immune status, and response to anti-angiogenesis agents and immune checkpoint blockade (ICB) were analyzed.

Results: The prognostic model was based on three HRAGs (ANGPT2, SERPINE1 and SPP1). The model accurately predicted that low-risk patients would have longer overall survival than high-risk patients, consistent with findings in other cohorts. GSEA indicated that high-risk group membership was significantly associated with hypoxia, angiogenesis, the epithelial-mesenchymal transition, and activity in immune-related pathways. The high-risk group also had more immunosuppressive cells and higher expression of immune checkpoints such as PD-1 and PD-L1. Conversely, the low-risk group had a better response to anti-angiogenesis and ICB therapy.

Conclusions: The gene signature based on HRAGs was predictive of prognosis and provided an immunological perspective that will facilitate the development of personalized therapies.

KEYWORDS

hepatocellular carcinoma, hypoxia, angiogenesis, prognosis, immune status

Introduction

Globally, liver cancer was the sixth-most common cancer (accounting for 4.5% of all new tumors) and the third leading cause of cancer-related death (accounting for over 8.3% of all such deaths) in 2020 (1). Among the primary types of liver cancer, hepatocellular carcinoma (HCC) accounts for approximately 75–85% of all cases, and the 5-year survival rate of HCC in China is only 14.1% (1, 2). Ablative therapies, transarterial chemoembolization (TACE), and surgery are routine treatments for HCC (3). Because of the complex etiology and high heterogeneity of HCC, its treatments and prognosis are unsatisfactory, and prognosis prediction is challenging (4–6). To improve prognosis, identifying biomarkers for treatment and prognostic prediction of HCC is critical.

Due to tumor neovascularization and high metabolism, hypoxia is present in approximately half of solid tumors, including HCC (7–10). Hypoxia promotes tumor cell proliferation and tumor progression by initiating multiple adaptive behaviors, such as angiogenesis, proliferation, and invasion. Hypoxia reconstructs the tumor immune microenvironment (TIM) by promoting the recruitment of innate immune cells, and interfering with the differentiation and function of adaptive immune cells (11–13). As a solid tumor rich in blood vessels, tumor-driven hypoxia increases the expression of proangiogenic factors leading to abnormal vascular proliferation of HCC, which contributes to tumor growth, invasion, metastasis, and immunosuppression. Tumor susceptibility to angiogenesis has been a hot spot of research recently, and targeted drugs are in clinical use (14, 15). During cancer progression, several proangiogenic cytokines—such as vascular endothelial growth factor A (VEGFA), fibroblast growth factor (FGF) and hypoxia inducible factor-1 (HIF-1)—which contribute to neovasculature sprouting and formation in the tumor microenvironment (TME), are implicated in immune TME remodeling and direct or indirect immune cell regulation (16–18). Nevertheless, the role of hypoxia in liver cancer angiogenesis is unclear. Closely related to angiogenesis, hypoxia regulates a series of genes involved in tumor angiogenesis, leading to the epithelial-mesenchymal transition (EMT) and immune escape, rendering tumor cells more tolerant to the hypoxic microenvironment, and enhancing their proliferation, metastasis, and invasion. Therefore, we analyzed the effect of angiogenesis-related genes under hypoxic conditions on the survival and immune microenvironment of HCC.

We first downloaded mRNA expression profiles and the corresponding clinical data of patients with HCC from public databases. Second, we constructed a prognostic multigene signature based on hypoxia-related angiogenic genes (HRAGs) in The Cancer Genome Atlas (TCGA) cohort, and validated it in an independent cohort. Third, we performed functional enrichment analysis and immune infiltration, as well as anti-angiogenesis and immune checkpoint blockade (ICB) therapy response predictions, to provide guidance for precise and effective HCC treatment.

Abbreviations: AUC, Areas under the curve; CAFs, Cancer-associated fibroblasts; DEGs, Differentially expressed genes; DFS, disease free survival; FDG, false discovery rate; GEO, Gene-Expression Omnibus; GSEA, Gene Set Enrichment Analysis; HCC, hepatocellular carcinoma; HRAGs, Hypoxia-related angiogenesis genes; ICB, Immunological checkpoint blockade; ICGC, International Cancer Genome Consortium; MDSCs, Myeloid-derived suppressor cells; OS, overall survival; PCA, Principal component analysis; ROC, Receiver operator characteristic; ssGSEA, Single-sample gene-set enrichment analysis; TCGA, The Cancer Genome Atlas; TME, Tumor microenvironment; t-SNE, t-distributed stochastic neighborembedding.

Materials and methods

Patients and datasets

The mRNA expression profiles and corresponding clinical information of HCC patients were obtained from The Cancer Genome Atlas-Liver Hepatocellular Carcinoma dataset (TCGA-LIHC, https://portal.gdc.cancer.gov/, 370 HCC and 50 normal tissue samples), International Cancer Genome Consortium (ICGC, https://dcc.icgc.org/projects/LIRI-JP, 229 HCC tissue samples), and Gene Expression Omnibus (GEO, https://www.ncbi.nlm.nih.gov/geo/query/acc.cgi?acc=GSE14520, 220 HCC tissue samples). The inclusion criteria for the follow-up analysis were HCC confirmed by pathology, available RNA expression data, and complete clinical data (> 30 days of follow-up). In total, 337 hypoxia-related genes (HRGs) and 201 angiogenesis-related genes (ARGs) were acquired by gene set enrichment analysis (GSEA) (hallmark-hypoxia or hallmark-angiogenesis), as well as

from the GeneCards database (using the terms *hypoxia* and *angiogenesis*; relevance scores > 4) and from previous reports.

Development and validation of a prognostic gene signature

The R package limma was used to identify differentially expressed genes (DEGs) between tumor tissues and adjacent nontumorous tissues, according to the criteria of | log 2 (fold-change) | > 1 and false discovery rate (FDR)< 0.05. Next, hypoxia-related angiogenic DEGs (HRAGs) were identified. The Gene Ontology (GO) and Kyoto Encyclopedia of Genes and Genomes (KEGG) functional annotations of these HRAGs were analyzed and visualized using the R package clusterProfiler.

Univariate Cox regression analysis was performed using the R package survival to determine the prognostic value of the DEGs for OS; $P< 0.05$ was considered statistically significant. An interaction network for the prognostic DEGs was generated using the STRING database (https://www.string-db.org/) and entered into a stepwise multivariate Cox regression analysis to identify covariates with independent prognostic value for OS. The risk score was based on the expression of predictive genes and the multivariate Cox regression risk model coefficients, and was calculated as follows:

$$\text{Risk score} = \sum_{i=1}^{n}(GeneExpression i \times Coef i)$$

Based on the median risk score or optimal cut-off value, HCC patients were divided into high- and low-risk groups. A Kaplan–Meier (K-M) survival analysis was performed to compare the high- and low-risk groups according to predictive signatures. The utility of prognostic prediction models was evaluated by calculating the areas under the curve (AUC) values of the receiver operator characteristic (ROC) curve using the R package survivalROC. Principal component analysis (PCA) and t-distributed stochastic neighbor embedding (t-SNE) were used to examine the clustering of the signature genes with the prcomp function of the R package stats and Rtsne. The ICGC and GSE14520 cohorts were analyzed to verify the results.

Prognostic value of the gene signature and construction of a predictive nomogram

Univariate and multivariate Cox regression analyses were performed to identify factors independently associated with OS in the TCGA cohort. To predict the survival of HCC patients, a nomogram was established based on the risk score and other clinical parameters. Calibration curve and time-dependent ROC analyses were performed to assess the accuracy of the nomogram. The nomogram and calibration curves were plotted using the R package rms.

Molecular characteristics and biological function analysis

GSEA of the MSigDB Collection (h.all.v7.4.symbols.gmt) was performed using GSEA software (version 4.1.0) to detect the set of genes expressed difference between the high- and low-risk groups. For each analysis, 1,000 gene set permutations were performed.

Estimation of tumor immune microenvironment

xCell (https://xcell.ucsf.edu/), which is based on a deconvolution algorithm, was used to infer immune cell infiltration from RNA-sequencing data. The infiltration scores of 17 immune cells and activities of 13 immune-related pathways were evaluated by single sample gene set enrichment analysis (ssGSEA) using the R package gsva. The normalized gene expression data of the TCGA and ICGC cohorts were uploaded into Sangerbox tools (http://www.sangerbox.com/tool) for bioinformatics analysis. Next, infiltration of cancer-associated fibroblasts (CAFs) was estimated using the MCPcounter and EPIC algorithms.

Anti-angiogenesis and ICB therapy response prediction and validation

Sensitivity and resistance to anti-angiogenesis drugs were evaluated using the R package pRRophetic. ImmuCellAI was used to predict the response to Immune checkpoint blockade (ICB) therapy (http://bioinfo.life.hust.edu.cn/ImmuCellAI#!/) (19). Immunohistochemical staining was performed as described previously. Briefly, HCC sample slides were deparaffinized and dehydrated by serial immersion in xylene, ethanol, and distilled water. Antigen retrieval was performed using citrate buffer (10 mM, pH 9.0) in a microwave on medium power. After blocking with goat serum at room temperature for 1 h, the tissues were sequentially incubated with an anti-secreted phosphoprotein-1 (SPP1) antibody (1:100, 22952-1-AP; Proteintech, Rosemont, IL, USA) at 4°C overnight and a secondary antibody at room temperature for 1 hour. A slide scanner (3DHistech Ltd., Budapest, Hungary) was used to capture images. Staining intensity, expressed as the H-score (range: 0–300) was automatically quantified using Pannoramic Viewer software (3DHistech Ltd.). Approval was obtained from the Institutional Review Boards of the Research Institute and Hospital National Cancer Center and The First Affiliated Hospital, Sun Yat-Sen University.

Statistical analysis

Data management and statistical analysis were conducted using R (version 4.1.0; R Development Core Team, Vienna, Austria) and GraphPad Prism software (version 8.3.0; GraphPad Software Inc., San Diego, CA, USA). Student's *t*-test or the Wilcoxon rank-sum test was used to compare gene expression between two groups. The chi-squared test was used to compare differences in proportions. Survival curves were plotted using the K-M method and compared by log-rank test. A value of $P< 0.05$ was taken to indicate statistical significance.

Results

Datasets

The study flow chart is shown in Figure 1. A total of 343 HCC patients from TCGA cohort, 229 from the ICGC cohort, and 220 from the GSE14520 cohort were included in this study. The clinical characteristics of the patients are listed in Supplementary Table S1.

Identification of prognostic hypoxia-related angiogenic genes in the TCGA dataset

DEGs analysis of the 374 HCC samples and 50 normal liver samples from TCGA revealed 21 differentially expressed HRAGs (Figures 2A–C). GO and KEGG enrichment and functional analysis showed that these genes were enriched in epithelial cell migration, chemotaxis, PI3K-Akt signaling pathway, focal adhesion, MAPK signaling pathway, and HIF-1 signaling pathway (Figures 2D, E). The HRAGs were related to cancer proliferation and invasion. Univariate Cox regression analysis showed that nine prognostic HRAGs significantly correlated with OS were risk factors for a poor prognosis of HCC (Figure 3A). PPI and gene correlation networks suggested connections among the prognostic genes (Figures 3B, C).

Construction and validation of the prognostic model

Three of the nine prognostic HRAGs were used to construct a prognostic predictive model. The corresponding coefficients and gene expression levels were used to calculate the risk score as follows: (0.389932838 × expression level of ANGPT2 + 0.108256217 × expression level of SERPINE1 + 0.121709881 × expression level of SPP1). Patients in the TCGA, ICGC, and GSE14520 datasets were divided into high- and low-risk groups based on the median risk score or optimal cut-off value. Interestingly, K-M survival curves based on the three genes showed that the predicted OS of the low-expression group was significantly longer than that of the high-expression group (Supplementary Figure S1). A PPI network was generated based on coexpression information for the three candidate genes from the GeneMANIA database (http://genemania.org/) (Figure 3D). The expression of prognostic genes and risk scores were significantly higher for tumor stage III/IV compared with stage I/II patients (Supplementary Figure S2). Therefore, a higher risk score is associated with more malignant HCC.

Furthermore, the high-risk group membership was significantly associated with higher tumor grade and advanced tumor, node, metastasis (TNM) stage (Table 1). Patients with a

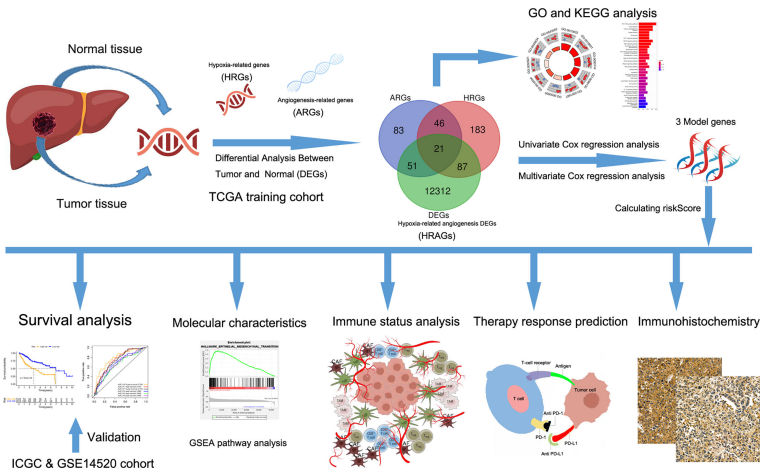

FIGURE 1
Flow chart of data collection and analysis.

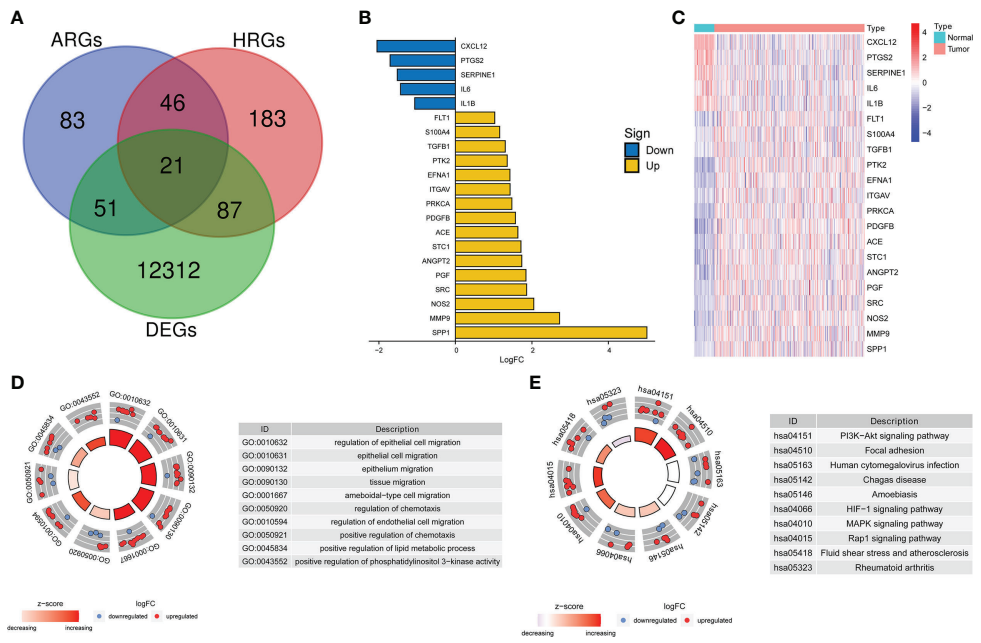

ID	Description
GO:0010632	regulation of epithelial cell migration
GO:0010631	epithelial cell migration
GO:0090132	epithelium migration
GO:0090130	tissue migration
GO:0001667	ameboidal-type cell migration
GO:0050920	regulation of chemotaxis
GO:0010594	regulation of endothelial cell migration
GO:0050921	positive regulation of chemotaxis
GO:0045834	positive regulation of lipid metabolic process
GO:0043552	positive regulation of phosphatidylinositol 3-kinase activity

ID	Description
hsa04151	PI3K-Akt signaling pathway
hsa04510	Focal adhesion
hsa05163	Human cytomegalovirus infection
hsa05142	Chagas disease
hsa05146	Amoebiasis
hsa04066	HIF-1 signaling pathway
hsa04010	MAPK signaling pathway
hsa04015	Rap1 signaling pathway
hsa05418	Fluid shear stress and atherosclerosis
hsa05323	Rheumatoid arthritis

FIGURE 2
Screening and enrichment analysis of hypoxia-related angiogenesis genes. **(A)** Venn diagram of 21 differentially expressed HRAGs in the TCGA cohort. **(B)** Deviation plot and **(C)** heatmap of 21 differentially expressed HRAGs in HCC and noncancerous tissues. **(D)** GO **(E)** and KEGG analyses revealed the most significantly enriched biological functions and pathways of the overlapping differentially expressed HRAGs.

high risk score had a higher mortality rate, shorter OS, and higher expression of the three model genes (Figure 4A). K-M survival curves indicated significantly longer survival time of the low-risk group, including OS (Figure 4B) and disease-free survival (DFS) (Supplementary Figure S3), compared to the high-risk group. The AUC of the time-dependent ROC curves was 0.783 at 0.5 years, 0.746 at 1 year, 0.733 at 1.5 years, 0.668 at 2 years, 0.648 at 3 years, and 0.669 at 5 years (Figure 4C). PCA (Figure 4D) and t-SNE (Figure 4E) confirmed risk profile differences between the two groups. To test the robustness of the gene signature model constructed based on the TCGA cohort, patients from the ICGC and GSE14520 cohorts were categorized into high- and low-risk groups according to the optimal cut-off value. The results for the ICGC (Figures 4G–J) and GSE14520 cohort (Supplementary Figure S4) were similar to those of TCGA cohort. Therefore, the prognostic model was predictive of the prognosis and progression of HCC.

Prognostic value of the gene signature

Univariate and multivariate Cox regression analyses showed that TNM stage and risk score were significantly associated with the prognosis of HCC in the TCGA cohort (Figures 5A, B). ROC curve analysis showed that the risk score was better for predicting prognosis than the other clinicopathological factors (Figure 5C). The risk scores and clinicopathological factors of 343 HCC patients with complete clinical information were used to create a prognostic nomogram for predicting survival (Figure 5D). The calibration curves of the prognostic nomogram showed good consistency between the predicted and actual 1-, 2-, 3-, and 5-year survival rates in the TCGA cohort (Figure 5E). The nomogram AUCs of the predicted 1-, 2-, 3-, and 5-year OS were 0.777, 0.712, 0.721, and 0.728, respectively (Figure 5F).

Molecular characteristics and biological function analysis

GSEA analysis revealed that high-risk group membership was significantly associated with angiogenesis, EMT, glycolysis and hypoxia. The immune-related pathways IL2/STAT5 and IL6/JAK/STAT3, as well as the inflammatory response, interferon (IFN)-γ/ response and tumor necrosis factor (TNF)-α signaling *via* NFKB were significantly enriched in the high-risk group ($P< 0.05$, FDR< 0.25) (Figure 6).

Tumor immune microenvironment analysis

xCell was used to evaluate the proportions of infiltrating immune cells. Patients in the high-risk group had higher

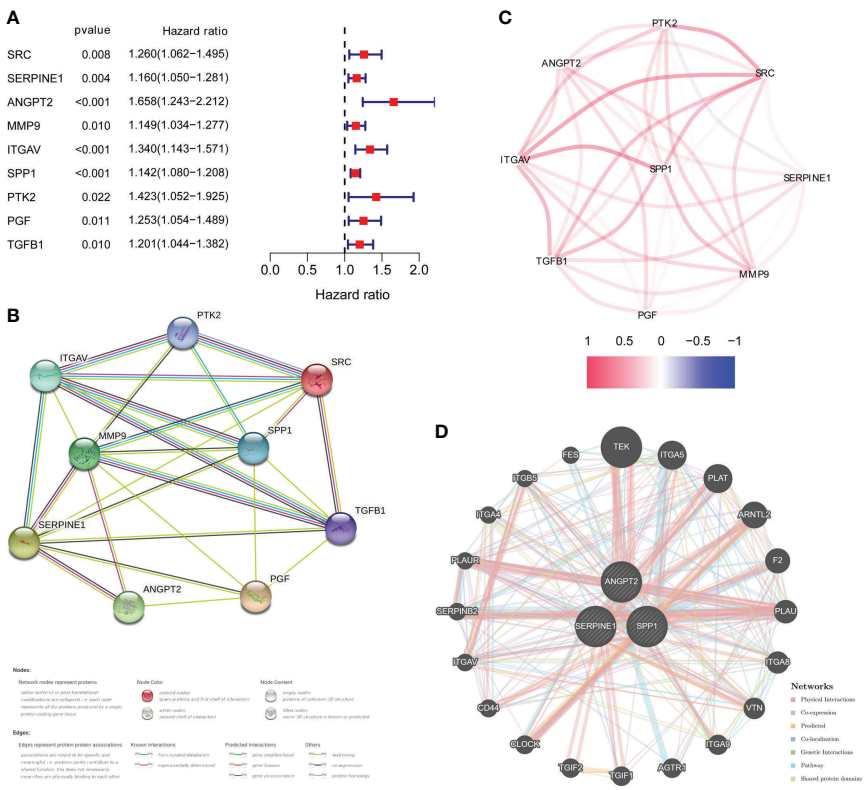

FIGURE 3
Identification of candidate genes related to the prognosis of HCC. **(A)** Forest plots of univariate Cox regression analysis of gene expression and OS in the TCGA cohort. **(B)** Protein–protein interaction (PPI) network and **(C)** correlated regulation network of prognostic HRAGs. **(D)** Correlation analysis of three model HRAGs from GeneMANIA.

proportions of macrophages and T regulatory cells (Tregs) than those in the low-risk group, but there was no difference in the proportions of other immune cell types (Supplementary Figures S5A, B). Next, the enrichment scores of immune cell subpopulations, related functions, and pathways were calculated by ssGSEA (Figure 7). Interestingly, dendritic cells (DCs), antigen-presenting cells (APCs), human leukocyte antigen (HLA), and major histocompatibility complex class I (MHC class I), which are involved in antigen presentation, were significantly elevated in the high-risk group. Furthermore, the activities of cytokine-cytokine receptors and immune checkpoints, and the enrichment scores for macrophages, myeloid-derived suppressor cells (MDSCs), and Tregs in the high-risk group were higher than in the low-risk group, whereas the type II IFN response showed the opposite trend. The risk score was significantly positively correlated with the proportion of cancer-associated fibroblasts (CAFs). The expression of immunosuppressive genes in the high-risk group was higher than in the low-risk group, in both the TCGA and ICGC cohorts (Supplementary Figures S5C, E). The expression of the pro-angiogenic factors, VEGFA and VEGFB, was significantly upregulated in the high-risk group (Figure S5D, F). However, there was no difference in the tumor mutation burden (TMB) or microsatellite instability (MSI) score (Supplementary Figures S5G, H). Therefore, the TME of patients in the high-risk group is in an immunosuppressive state.

Prediction and validation of the anti-angiogenesis and ICB responses

As shown in Figure 8A, the estimated IC_{50} showed that the low-risk group in both cohorts had a better response to sorafenib ($P< 0.05$). ImmuCellAI showed that the response rate to ICB therapy was higher in the group with a lower risk score (Figure 8B). The correlation heatmap indicated that SPP1 expression was most relevant to the risk score, and thus has great potential for predicting the response to anti-angiogenesis and ICB therapy (Figure 8C). Next, 19 Barcelona Clinic Liver Cancer (BCLC) C stage-HCC samples subjected to anti-angiogenesis treatment and immunotherapy after resection were further subjected to IHC staining. Follow-up information was collected from January 2015 to April 2022. Based on the H-scores, we divided the 19 patients into high- and low-expression

10.3389/fonc.2022.978050

TABLE 1 Baseline characteristics of the patients in different risk groups of three cohorts.

Variables	Group	TCGA cohort (n = 343)		P value	ICGC cohort (n = 229)		P value	GSE14520 cohort (n = 220)		P value
		High risk (n=125)	Low risk (n=218)		High risk (n=144)	Low risk (n=85)		High risk (n=108)	Low risk (n=112)	
median Survival time (days)		412	649		720	900		861	1635	
Survival status	Alive	63(50.4%)	161(73.85%)	**<0.0001**	110(76.39%)	79(92.94%)	**0.0011**	51(47.22%)	85(82.52%)	**<0.0001**
	Dead	62(49.6%)	57(26.15%)		34(23.61%)	6(7.06%)		57(52.78%)	18(17.48%)	
Gender	Female	45(36%)	65(29.82%)	0.2794	39(27.08%)	22(25.88%)	0.8782	12(11.11%)	18(16.07%)	0.3288
	Male	80(64%)	153(70.18%)		105(72.92%)	63(74.12%)		96(88.89%)	94(83.93%)	
Age	≤60	52(41.60%)	113(51.83%)	0.0732	30(20.83%)	19(22.35%)	0.8678	91(84.26%)	90(80.36%)	0.4839
	>60	73(58.40%)	105(48.17%)		114(79.17%)	66(77.65%)		17(15.74%)	22(19.64%)	
Grade	G1	7(5.6%)	46(21.1%)	**0.0009**	/	/		/	/	
	G2	67(53.6%)	94(43.1%)		/	/		/	/	
	G3	48(38.4%)	64(29.4%)		/	/			/	
	G4	2(1.6%)	10(4.6%)		/	/		/	/	
	unknown	1(0.8%)	4(1.8%)		/	/		/	/	
TNMstage	I	43(34.4%)	118(54.2%)	**0.0023**	17(11.8%)	19(22.4%)	**0.0012**	31(28.7%)	62(55.4%)	**<0.0001**
	II	32(25.6%)	45(21.0%)		58(40.3%)	47(55.3%)		39(36.1%)	38(33.9%)	
	III	42(33.6%)	38(17.8%)		53(36.8%)	16(18.8%)		37(34.3%)	11(9.8%)	
	IV	1(0.8%)	2(0.1%)		16(11.1%)	3(3.5%)		0	0	
	unknown	7(5.6%)	15(6.9%)		/	/		1(0.9%)	1(0.9%)	

groups. Representative immunohistochemically stained images are shown in Figure 8D. K-M curves showed that the OS of the low-expression group was trend longer than that of the high-expression group though not statistically significant (P = 0.1519, Figure 8E). In summary, the gene signature was predictive of the response to anti-angiogenesis treatment and ICB therapy.

Discussion

Predicting the effect of HCC treatment is challenging due to the paucity of useful biomarkers. The American Joint Committee on Cancer (AJCC) TNM staging system has long been considered reliable for predicting the prognosis of patients with HCC. However, it is based on macroscopic information, which does not reflect the biological features and heterogeneity of HCC. Integration of prognostic gene signatures and traditional parameters has advantages for predicting the prognosis of HCC. The importance of predicting the prognosis of HCC and administering treatments in a timely manner highlights the need to identify robust prognostic biomarkers for risk stratification.

Few studies have focused on the predictive value of hypoxia- or angiogenesis-related signatures. The complex regulatory mechanisms and effects of hypoxia-related angiogenesis genes (HRAGs) give rise to an ambiguous relationship with the prognosis of HCC. To our knowledge, this study is the first to develop a novel scoring system based on HRAGs. We investigated the expression of HRAGs in HCC tumor tissues, and their associations with survival, and constructed a novel prognostic model based on three HRAGs (ANGPT2, SERPINE1, and SPP1) to stratify HCC patients according to their estimated survival. The prognostic model showed good predictive power in both the training cohort and two external validation cohorts. Univariate and multivariate Cox regression analyses revealed the independent prognostic value of the three genes comprising the gene signature. A nomogram showed that the gene signature was predictive of 1-, 2-, 3-, and 5-year OS, and so may be useful when planning short-term follow-up. However, only three databases were used in this study, and the signature needs to be validated in an independent cohort.

The prognostic gene signature comprised three HRAGs (ANGPT2, SERPINE1, and SPP1). ANGPT2, which belongs to the angiopoietin family, is highly expressed in diverse tumor cells, and is implicated in tumor angiogenesis and inflammation (20, 21). ANGPT2 is highly expressed in, and closely related to, the development and prognosis of, HCC (15, 22). Increased expression of plasminogen activator inhibitor type 1 (also known as SERPINE1) was associated with tumor cell migration and invasion *via* activation of the PI3K-Akt pathway (23, 24). High expression of SERPINE1 in cancer tissues predicts a poor clinical outcome. In this study, SERPINE1 expression was lower in HCC tumor tissues than adjacent normal tissues in the TCGA dataset (Figure 2), possibly

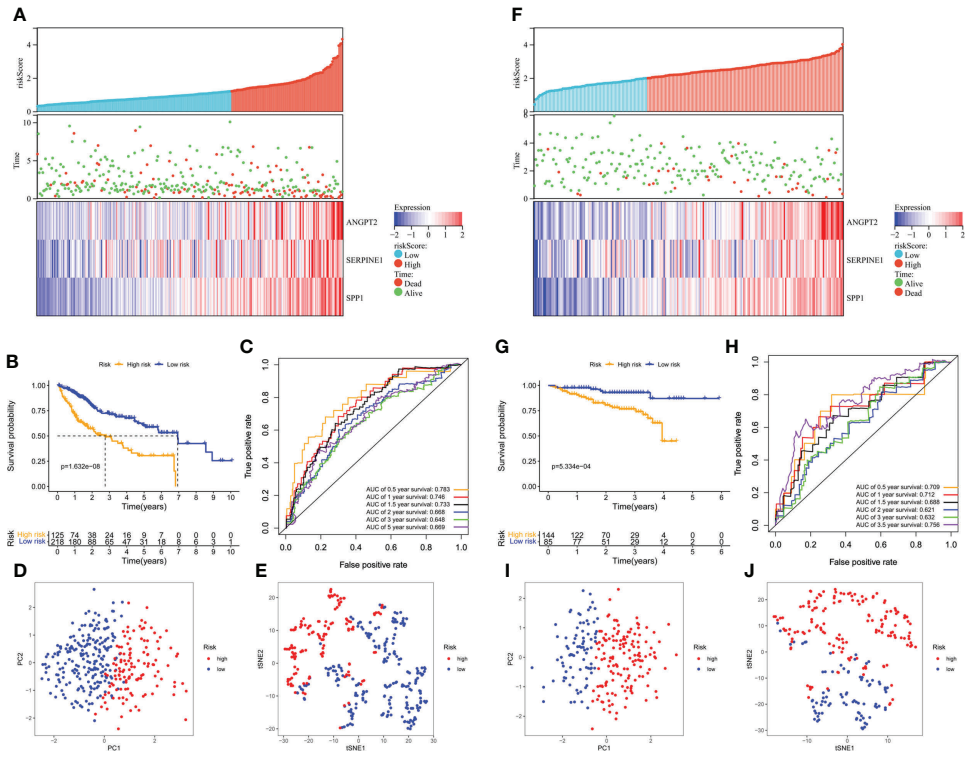

FIGURE 4
Survival analysis of HCC patients in the TCGA training and ICGC validation datasets. **(A, B)** Risk score distribution, survival status, and heatmap of the expression of the three HRAGs in the high- and low-risk groups in the training and validation cohorts. **(B, G)** Kaplan-Meier OS curve. **(C, H)** AUCs of time-dependent ROC curves. PCA **(D, I)** and t-SNE **(E, J)** analysis confirmed the clustering of the three genes comprising the HRAG signature. **(A–E)** TCGA cohort; **(F–J)** ICGC cohort.

because of the different roles SERPINE1 in tumor and normal tissues. SPP1, also called osteopontin, is an arginine-glycine-aspartate-containing phosphoprotein that is overexpressed in many cancers, including lung adenocarcinoma and HCC, and serves as a prognostic biomarker (25–27). SPP1 is involved in tumor immunosuppression and affects the TME (28). The expression of the three prognostic model genes, and the risk score, increased with increasing tumor stage, suggesting that they correlate with tumor malignancy and progression (Supplementary Figure S2).

To identify the pathway involved in hypoxia-related angiogenesis, HCC patients were divided into two groups according to the median risk score calculated by GSEA. Biological function analysis revealed greater activity not only in hypoxia- and angiogenesis-related pathways, but also in the EMT pathway (Figure 6). The EMT is a process of phenotypic plasticity that has roles in organ development, wound healing, tumor progression, and the response to therapeutics (29). Our findings suggest that HRAGs promote HCC progression by regulating the EMT pathway.

Because of its importance for immunotherapy and, potentially, precision therapy, the TME is a focus of research (30). In terms of predictive biomarkers, our high-risk group had higher proportions of macrophages, Tregs, and MDSCs (Figure 7). Higher proportions of tumor-associated macrophages and Tregs are associated with a poor prognosis of HCC (31). In addition, impairment of the type II IFN response and increased infiltration of MDSCs, Tregs, and macrophages, as in the high-risk group, is implicated in tumor immunological escape and tolerance, and impairs the antitumor T-cell response in HCC (32–34). Furthermore, the risk score was positively related to the proportion of CAFs in HCC. As a critical component of the TME, CAFs contribute to immune evasion and immunotherapy failure, and promote the proliferation and invasion of tumors, including HCC, by secreting growth factors and cytokines (35–37). The immune-related pathways IL2/STAT5 and IL6/JAK/STAT3, as well as the inflammatory response, IFN-γ response, and TNFα signaling *via* NFκB, were significantly enriched in the high-risk group (Figure 6). Cancer cells may drive the expression of immune checkpoints *via* these immune-related pathways (38). The expression of immune-related checkpoints (PD-L1, LAG3, CTLA4, TIM3, and TIGIT) in our high-risk group was higher than in the low-risk group, but the MSI and TMB, which indirectly reflect the ability

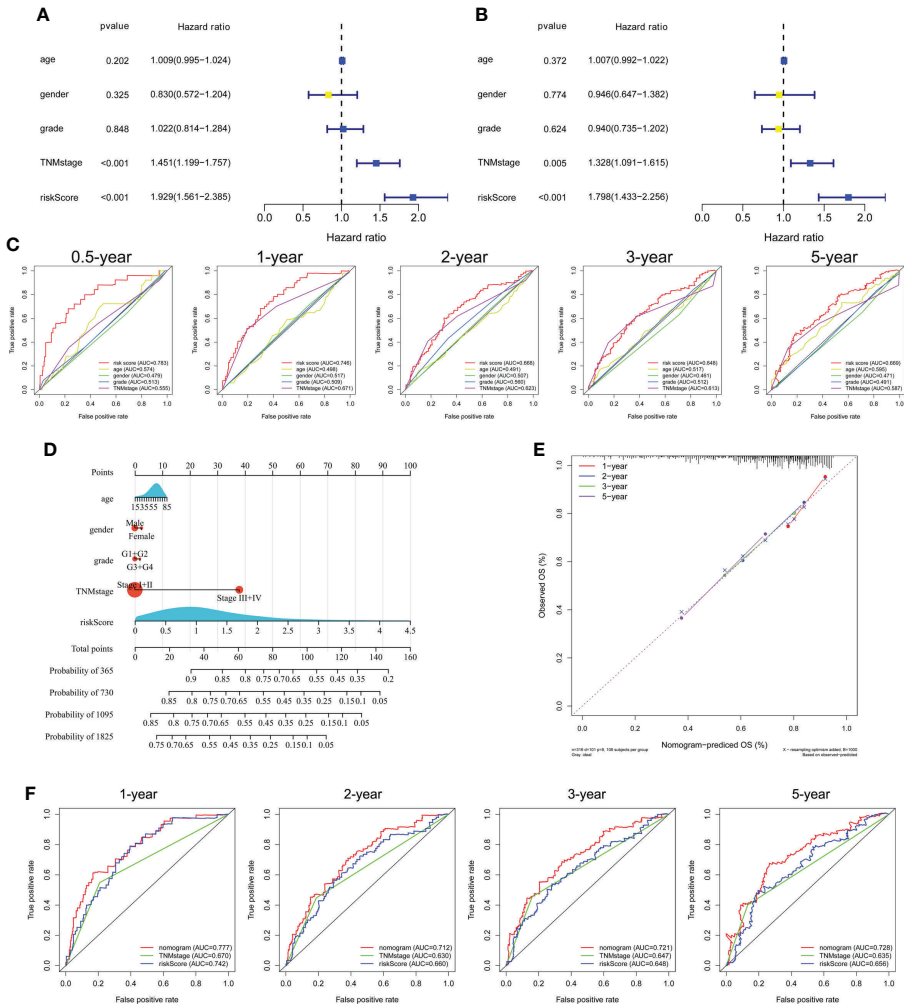

FIGURE 5
Independent prognostic power of the three genes comprising the signature in the TCGA cohort. **(A)** Univariate and **(B)** multivariate Cox regression analyses of the associations of the risk index (RI) and clinical parameters with OS. **(C)** ROC curve of the prognostic utility of the risk score, age, gender, grade, and TNM stage. **(D)** Nomogram for predicting 1-, 2-, 3-, and 5-year survival. **(E)** Calibration curves of the nomogram showed consistency in the predicted and observed 1-, 2-, 3-, and 5-year survival rates. **(F)** ROC curve analysis of the nomogram for 1-, 2-, 3-, and 5-year OS.

of a tumor to produce new antigens and predict the efficacy of immunotherapy for a variety of tumors, were not significantly different between the groups (Supplementary Figure S5). The expression of the pro-angiogenic factors VEGFA and VEGFB was significantly upregulated in the high-risk group in the ICGC and TCGA databases; these cytokines promote TME remodeling and directly or indirectly regulate immune cells (17). Therefore, in the high-risk group, anti-tumor immunity is probably attenuated; also, a high risk score may be correlated with immunosuppression in HCC, possibly explaining its poor prognosis. This may arise because the expression of angiogenesis-related genes under hypoxic conditions induces the production of myeloid suppressor cells, Tregs, and immunosuppression-related checkpoints, thereby disrupting the immune balance. In summary, tumor-driven hypoxia related angiogenesis plays a crucial role in modulating the tumor immune microenvironment.

In view of the fact that angiogenesis plays a central role in immunosuppression and can lead to resistance to ICBs, there is growing evidence to support a strategy combining anti-angiogenesis and ICBs with promising clinical activity. Due to the encouraging efficacy and safety findings of the IMbrave150 trial for atezolizumab plus bevacizumab, this novel anti-angiogenesis combined with immunotherapy has become the first-line treatment for patients with unresectable HCC (39, 40). The combination therapy can render the TME conducive to immune cell function. However, because angiogenesis and the TME have multiple roles, the mechanism underlying the effect of

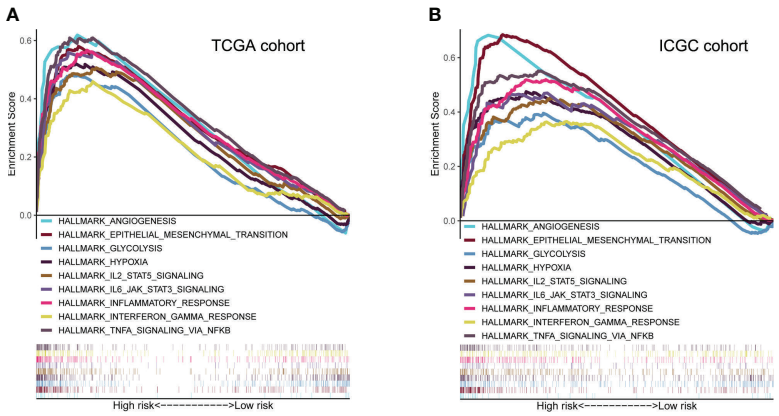

FIGURE 6
Molecular characteristics and biological function analysis. **(A, B)** Gene set enrichment analysis of biological functions and pathways in the risk score groups (P< 0.05, FDR< 0.25).

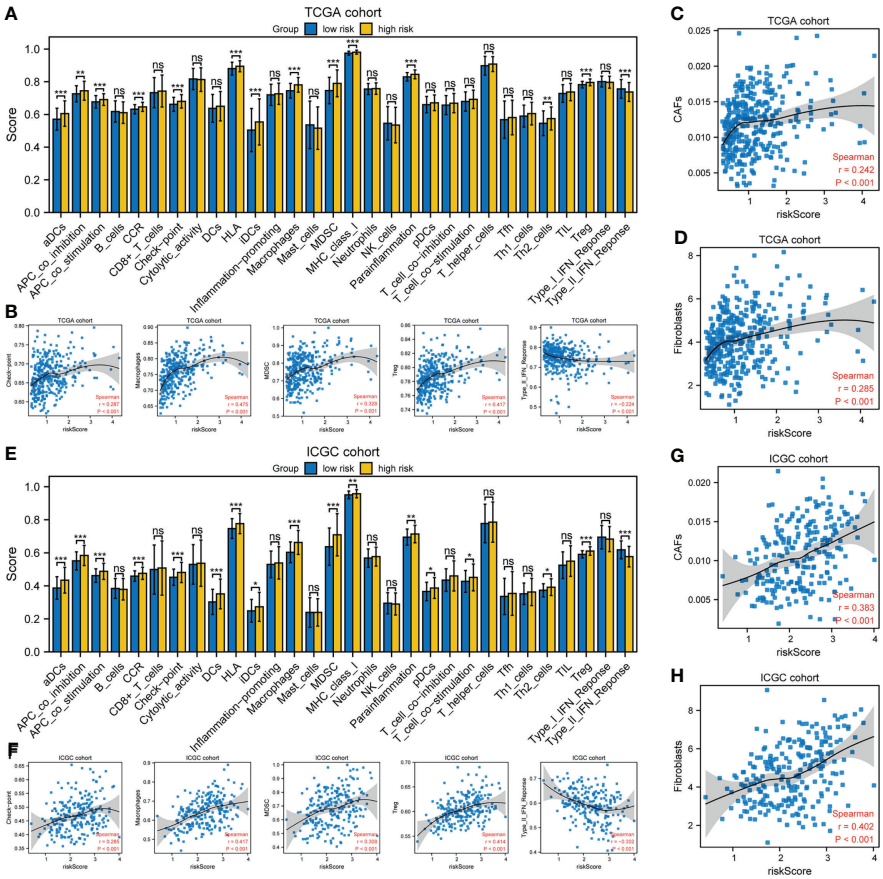

FIGURE 7
Tumor immune microenvironment analysis. **(A, E)** ssGSEA scores of 17 immune cells and 13 immune-related functions. ns: not significant; *P< 0.05; **P< 0.01; ***P< 0.001. **(B, F)** Spearman's rank correlation analysis between risk score and immune checkpoints, macrophages, MDSCs, Tregs, and type II IFN response. **(C, D, G, H)** Spearman's rank correlation analysis between risk score and CAFs according to the **(C, G)** EPIC and **(D, H)** MCPcounter algorithms. **(A–D)** TCGA cohort; **(E–H)** ICGC cohort.

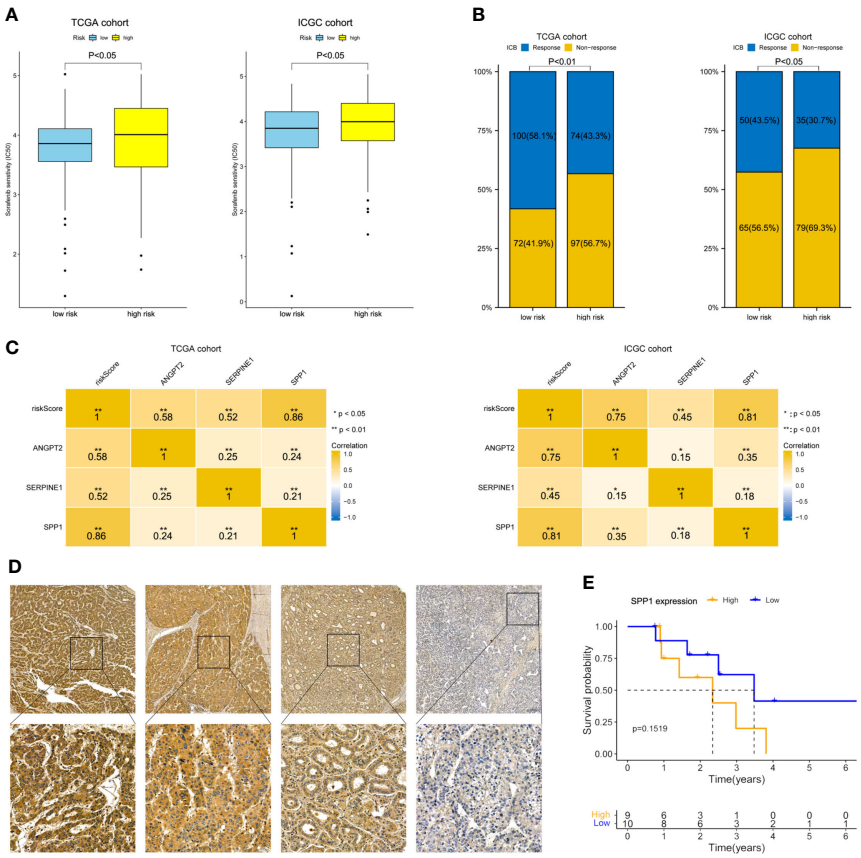

FIGURE 8
Therapeutic response prediction and immunohistochemistry of SPP1. **(A)** Sensitivity to sorafenib by risk group. **(B)** Response rate to ICB therapy. **(C)** Heatmap showing the correlation between risk score and the three model genes. **(D)** Representative immunohistochemically stained images of HCC tissues showing SPP1 expression (upper, 5.0×; lower, 20.0×). **(E)** K-M OS curves of 19 HCC patients with different SPP1 levels.

anti-angiogenesis combined with immunotherapy on liver cancer is unclear.

Our findings suggest that HRAGs not only contribute to tumor growth, metastasis, progression, and poor prognosis, but also to the infiltration of immunosuppressive cells and high expression of immune checkpoints. This could explain why anti-angiogenesis combined with immunotherapy is effective for unresectable HCC. The anti-angiogenesis and ICB therapy response rate was higher in the low-risk group. And SPP1 expression was most relevant to the risk score. Previous studies have illustrated that tumor-driven hypoxia promotes the expression of SPP1, which in turn promotes tumor angiogenesis and immunosuppressive microenvironment (28, 41, 42). SPP1 may be considered as a general marker of cancer progression, would be valuable in combination with other biomarkers to guide patient stratification and treatment strategies, and would be an attractive therapeutic target due to its multiple roles in promoting tumor aggressiveness. Our present study interestingly found that the OS of the low-SPP1-expression group of HCC patients who received anti-angiogenesis combined with immunotherapy after resection was trend longer than that of the high-SPP1-expression group (Figure 8). These findings may aid the development of comprehensive therapeutic strategies for HCC.

This study also had some limitations. First, the gene signature model was constructed and validated based on retrospective data from public databases. Second, the small sample size hampered statistical analysis. Third, a further study should investigate the biological mechanisms underlying the signature.

Conclusion

A novel gene signature model and HRAGs-based prognostic biomarker were developed and validated in an independent cohort. The gene signature may help identify immune infiltration and predict sensitivity to anti-angiogenesis and immunotherapy, and

the outcomes of HCC. The mechanism underlying the associations of HRAGs expression in HCC with the TME and sensitivity of anti-angiogenesis and immunotherapy are unclear, so further studies are needed.

Data availability statement

The datasets presented in this study can be found in online repositories. The names of the repository/repositories and accession number(s) can be found below: TCGA-LIHC: https://portal.gdc.cancer.gov/; ICGC: https://dcc.icgc.org/projects/LIRI-JP; GEO: https://www.ncbi.nlm.nih.gov/geo/query/acc.cgi?acc=GSE14520.

Ethics statement

The studies involving human participants were reviewed and approved by the Institutional Review Boards of the Research Institute and Hospital National Cancer Center and The First Affiliated Hospital, Sun Yat-Sen University. The patients/participants provided their written informed consent to participate in this study.

Author contributions

JL, GZ and YX conceived and designed the project. JL supervised the study. GZ and YX conducted and performed data collection and data analysis and interpretation. XZ, WF, YZ, YW, and HW contributed to discussion and reviewed and edited the manuscript. All authors read and approved the final version of the manuscript.

Funding

This research was supported by the National Natural Science Foundation of China (NSFC) (82172036, 81971719 and 81171441), and the Key Research and Development Project of Guangzhou City (202103000021), and the major scientific and technological project of Guangdong Province (2020B0101130016), and the National Natural Science Foundation of China (Youth Project, 82102161).

Conflict of interest

The authors declare that the research was conducted in the absence of any commercial or financial relationships that could be construed as a potential conflict of interest.

Publisher's note

All claims expressed in this article are solely those of the authors and do not necessarily represent those of their affiliated organizations, or those of the publisher, the editors and the reviewers. Any product that may be evaluated in this article, or claim that may be made by its manufacturer, is not guaranteed or endorsed by the publisher.

Supplementary material

The Supplementary Material for this article can be found online at: https://www.frontiersin.org/articles/10.3389/fonc.2022.978050/full#supplementary-material

References

1. Sung H, Ferlay J, Siegel RL, Laversanne M, Soerjomataram I, Jemal A, et al. Global cancer statistics 2020: Globocan estimates of incidence and mortality worldwide for 36 cancers in 185 countries. *CA Cancer J Clin* (2021) 71(3):209–49. doi: 10.3322/caac.21660

2. Allemani C, Matsuda T, Di Carlo V, Harewood R, Matz M, Niksic M, et al. Global surveillance of trends in cancer survival 2000-14 (Concord-3): Analysis of individual records for 37 513 025 patients diagnosed with one of 18 cancers from 322 population-based registries in 71 countries. *Lancet* (2018) 391(10125):1023–75. doi: 10.1016/S0140-6736(17)33326-3

3. Wang C, Vegna S, Jin H, Benedict B, Lieftink C, Ramirez C, et al. Inducing and exploiting vulnerabilities for the treatment of liver cancer. *Nature* (2019) 574 (7777):268–72. doi: 10.1038/s41586-019-1607-3

4. Cancer Genome Atlas Research Network. Electronic address wbe, cancer genome atlas research n. comprehensive and integrative genomic characterization of hepatocellular carcinoma. *Cell* (2017) 169(7):1327–41.e23. doi: 10.1016/j.cell.2017.05.046

5. Lin DC, Mayakonda A, Dinh HQ, Huang P, Lin L, Liu X, et al. Genomic and epigenomic heterogeneity of hepatocellular carcinoma. *Cancer Res* (2017) 77 (9):2255–65. doi: 10.1158/0008-5472.CAN-16-2822

6. Torrecilla S, Sia D, Harrington AN, Zhang Z, Cabellos L, Cornella H, et al. Trunk mutational events present minimal intra- and inter-tumoral heterogeneity in hepatocellular carcinoma. *J Hepatol* (2017) 67(6):1222–31. doi: 10.1016/j.jhep.2017.08.013

7. Brown JM, Wilson WR. Exploiting tumour hypoxia in cancer treatment. *Nat Rev Cancer* (2004) 4(6):437–47. doi: 10.1038/nrc1367

8. Jain RK. Normalization of tumor vasculature: An emerging concept in antiangiogenic therapy. *Science* (2005) 307(5706):58–62. doi: 10.1126/science.1104819

9. Wilson GK, Tennant DA, McKeating JA. Hypoxia inducible factors in liver disease and hepatocellular carcinoma: Current understanding and future directions. *J Hepatol* (2014) 61(6):1397–406. doi: 10.1016/j.jhep.2014.08.025

10. Lee SY, Jeong EK, Ju MK, Jeon HM, Kim MY, Kim CH, et al. Induction of metastasis, cancer stem cell phenotype, and oncogenic metabolism in cancer cells by ionizing radiation. *Mol Cancer* (2017) 16(1):10. doi: 10.1186/s12943-016-0577-4

11. Terry S, Buart S, Chouaib S. Hypoxic stress-induced tumor and immune plasticity, suppression, and impact on tumor heterogeneity. *Front Immunol* (2017) 8:1625. doi: 10.3389/fimmu.2017.01625

12. Zeng F, Zhang Y, Han X, Zeng M, Gao Y, Weng J. Employing hypoxia characterization to predict tumour immune microenvironment, treatment sensitivity and prognosis in hepatocellular carcinoma. *Comput Struct Biotechnol J* (2021) 19:2775–89. doi: 10.1016/j.csbj.2021.03.033

13. Palazon A, Goldrath AW, Nizet V, Johnson RS. Hif transcription factors, inflammation, and immunity. *Immunity* (2014) 41(4):518–28. doi: 10.1016/j.immuni.2014.09.008

14. Hilmi M, Neuzillet C, Calderaro J, Lafdil F, Pawlotsky JM, Rousseau B. Angiogenesis and immune checkpoint inhibitors as therapies for hepatocellular carcinoma: Current knowledge and future research directions. *J Immunother Cancer* (2019) 7(1):333. doi: 10.1186/s40425-019-0824-5

15. Morse MA, Sun W, Kim R, He AR, Abada PB, Mynderse M, et al. The role of angiogenesis in hepatocellular carcinoma. *Clin Cancer Res Off J Am Assoc Cancer Res* (2019) 25(3):912–20. doi: 10.1158/1078-0432.CCR-18-1254

16. Rahma OE, Hodi FS. The intersection between tumor angiogenesis and immune suppression. *Clin Cancer Res Off J Am Assoc Cancer Res* (2019) 25 (18):5449–57. doi: 10.1158/1078-0432.CCR-18-1543

17. Tian Y, Li Y, Shao Y, Zhang Y. Gene modification strategies for next-generation car T cells against solid cancers. *J Hematol Oncol* (2020) 13(1):54. doi: 10.1186/s13045-020-00890-6

18. Zhen Z, Shen Z, Hu Y, Sun P. Screening and identification of angiogenesis-related genes as potential novel prognostic biomarkers of hepatocellular carcinoma through bioinformatics analysis. *Aging (Albany NY)* (2021) 13(13):17707–33. doi: 10.18632/aging.203260

19. Miao YR, Zhang Q, Lei Q, Luo M, Xie GY, Wang H, et al. Immucellai: A unique method for comprehensive T-cell subsets abundance prediction and its application in cancer immunotherapy. *Adv Sci (Weinh)* (2020) 7(7):1902880. doi: 10.1002/advs.201902880

20. Scholz A, Plate KH, Reiss Y. Angiopoietin-2: A multifaceted cytokine that functions in both angiogenesis and inflammation. *Ann N Y Acad Sci* (2015) 1347:45–51. doi: 10.1111/nyas.12726

21. Akwii RG, Sajib MS, Zahra FT, Mikelis CM. Role of angiopoietin-2 in vascular physiology and pathophysiology. *Cells* (2019) 8(5):471. doi: 10.3390/cells8050471

22. Villa E, Critelli R, Lei B, Marzocchi G, Camma C, Giannelli G, et al. Neoangiogenesis-related genes are hallmarks of fast-growing hepatocellular carcinomas and worst survival. *Results Prospective Study Gut* (2016) 65(5):861–9. doi: 10.1136/gutjnl-2014-308483

23. Balsara RD, Castellino FJ, Ploplis VA. A novel function of plasminogen activator inhibitor-1 in modulation of the akt pathway in wild-type and plasminogen activator inhibitor-1-Deficient endothelial cells. *J Biol Chem* (2006) 281(32):22527–36. doi: 10.1074/jbc.M512819200

24. Li R, Li Y, Liang X, Yang L, Su M, Lai KP. Network pharmacology and bioinformatics analyses identify intersection genes of niacin and covid-19 as potential therapeutic targets. *Brief Bioinform* (2021) 22(2):1279–90. doi: 10.1093/bib/bbaa300

25. Shin HD, Park BL, Cheong HS, Yoon JH, Kim YJ, Lee HS. Spp1 polymorphisms associated with hbv clearance and hcc occurrence. *Int J Epidemiol* (2007) 36(5):1001–8. doi: 10.1093/ije/dym093

26. Shen XY, Liu XP, Song CK, Wang YJ, Li S, Hu WD. Genome-wide analysis reveals alcohol dehydrogenase 1c and secreted phosphoprotein 1 for prognostic biomarkers in lung adenocarcinoma. *J Cell Physiol* (2019) 234(12):22311–20. doi: 10.1002/jcp.28797

27. Song Z, Chen W, Athavale D, Ge X, Desert R, Das S, et al. Osteopontin takes center stage in chronic liver disease. *Hepatology* (2021) 73(4):1594–608. doi: 10.1002/hep.31582

28. Shurin MR. Osteopontin controls immunosuppression in the tumor microenvironment. *J Clin Invest* (2018) 128(12):5209–12. doi: 10.1172/JCI124918

29. Dongre A, Weinberg RA. New insights into the mechanisms of epithelial-mesenchymal transition and implications for cancer. *Nat Rev Mol Cell Biol* (2019) 20(2):69–84. doi: 10.1038/s41580-018-0080-4

30. Binnewies M, Roberts EW, Kersten K, Chan V, Fearon DF, Merad M, et al. Understanding the tumor immune microenvironment (Time) for effective therapy. *Nat Med* (2018) 24(5):541–50. doi: 10.1038/s41591-018-0014-x

31. Zhou SL, Zhou ZJ, Hu ZQ, Huang XW, Wang Z, Chen EB, et al. Tumor-associated neutrophils recruit macrophages and T-regulatory cells to promote progression of hepatocellular carcinoma and resistance to sorafenib. *Gastroenterology* (2016) 150(7):1646–58.e17. doi: 10.1053/j.gastro.2016.02.040

32. Lin Z, Xu Q, Miao D, Yu F. An inflammatory response-related gene signature can impact the immune status and predict the prognosis of hepatocellular carcinoma. *Front Oncol* (2021) 11:644416. doi: 10.3389/fonc.2021.644416

33. Chiu DK, Tse AP, Xu IM, Di Cui J, Lai RK, Li LL, et al. Hypoxia inducible factor hif-1 promotes myeloid-derived suppressor cells accumulation through Entpd2/Cd39l1 in hepatocellular carcinoma. *Nat Commun* (2017) 8(1):517. doi: 10.1038/s41467-017-00530-7

34. Lin Y, Yang X, Liu W, Li B, Yin W, Shi Y, et al. Chemerin has a protective role in hepatocellular carcinoma by inhibiting the expression of il-6 and gm-csf and mdsc accumulation. *Oncogene* (2017) 36(25):3599–608. doi: 10.1038/onc.2016.516

35. Kubo N, Araki K, Kuwano H, Shirabe K. Cancer-associated fibroblasts in hepatocellular carcinoma. *World J Gastroenterol* (2016) 22(30):6841–50. doi: 10.3748/wjg.v22.i30.6841

36. Chakravarthy A, Khan L, Bensler NP, Bose P, De Carvalho DD. Tgf-Beta-Associated extracellular matrix genes link cancer-associated fibroblasts to immune evasion and immunotherapy failure. *Nat Commun* (2018) 9(1):4692. doi: 10.1038/s41467-018-06654-8

37. Liu T, Han C, Wang S, Fang P, Ma Z, Xu L, et al. Cancer-associated fibroblasts: An emerging target of anti-cancer immunotherapy. *J Hematol Oncol* (2019) 12(1):86. doi: 10.1186/s13045-019-0770-1

38. Garcia-Diaz A, Shin DS, Moreno BH, Saco J, Escuin-Ordinas H, Rodriguez GA, et al. Interferon receptor signaling pathways regulating pd-L1 and pd-L2 expression. *Cell Rep* (2019) 29(11):3766. doi: 10.1016/j.celrep.2019.11.113

39. Finn RS, Qin S, Ikeda M, Galle PR, Ducreux M, Kim TY, et al. Atezolizumab plus bevacizumab in unresectable hepatocellular carcinoma. *N Engl J Med* (2020) 382(20):1894–905. doi: 10.1056/NEJMoa1915745

40. Casak SJ, Donoghue M, Fashoyin-Aje L, Jiang X, Rodriguez L, Shen YL, et al. Fda approval summary: Atezolizumab plus bevacizumab for the treatment of patients with advanced unresectable or metastatic hepatocellular carcinoma. *Clin Cancer Res Off J Am Assoc Cancer Res* (2021) 27(7):1836–41. doi: 10.1158/1078-0432.CCR-20-3407

41. Zhu Y, Yang J, Xu D, Gao XM, Zhang Z, Hsu JL, et al. Disruption of tumour-associated macrophage trafficking by the osteopontin-induced colony-stimulating factor-1 signalling sensitises hepatocellular carcinoma to anti-Pd-L1 blockade. *Gut* (2019) 68(9):1653–66. doi: 10.1136/gutjnl-2019-318419

42. Amilca-Seba K, Sabbah M, Larsen AK, Denis JA. Osteopontin as a regulator of colorectal cancer progression and its clinical applications. *Cancers* (2021) 13 (15):3793. doi: 10.3390/cancers13153793

frontiers | Frontiers in Oncology

TYPE Original Research
PUBLISHED 02 September 2022
DOI 10.3389/fonc.2022.956999

Check for updates

OPEN ACCESS

EDITED BY
Pranav Gupta,
Albert Einstein College of Medicine,
United States

REVIEWED BY
Yan Yang,
University College Dublin, Ireland
Xin You,
Goethe University Frankfurt, Germany

*CORRESPONDENCE
Nan Shao
shaon@mail.sysu.edu.cn
Ying Lin
linying3@mail.sysu.edu.cn

†These authors have contributed equally to this work and share first authorship

SPECIALTY SECTION
This article was submitted to Molecular and Cellular Oncology, a section of the journal Frontiers in Oncology

RECEIVED 30 May 2022
ACCEPTED 29 July 2022
PUBLISHED 02 September 2022

CITATION
Li Y, Li T, Zhai D, Xie C, Kuang X, Lin Y and Shao N (2022) Quantification of ferroptosis pathway status revealed heterogeneity in breast cancer patients with distinct immune microenvironment.
Front. Oncol. 12:956999.
doi: 10.3389/fonc.2022.956999

COPYRIGHT
© 2022 Li, Li, Zhai, Xie, Kuang, Lin and Shao. This is an open-access article distributed under the terms of the Creative Commons Attribution License (CC BY). The use, distribution or reproduction in other forums is permitted, provided the original author(s) and the copyright owner(s) are credited and that the original publication in this journal is cited, in accordance with accepted academic practice. No use, distribution or reproduction is permitted which does not comply with these terms.

Quantification of ferroptosis pathway status revealed heterogeneity in breast cancer patients with distinct immune microenvironment

Yuying Li[1,2†], Tianfu Li[1,2†], Duanyang Zhai[1,2], Chuanbo Xie[3], Xiaying Kuang[1], Ying Lin[1*] and Nan Shao[1*]

[1]Breast Disease Center, The First Affiliated Hospital, Sun Yat-sen University, Guangzhou, China, [2]Laboratory of Surgery, The First Affiliated Hospital, Sun Yat-sen University, Guangzhou, China, [3]Cancer Prevention Center, Sun Yat-sen University Cancer Center, State Key Laboratory of Oncology in South China, Collaborative Innovation Center for Cancer Medicine, Guangzhou, China

Clinical significance and biological functions of the ferroptosis pathway were addressed in all aspect of cancer regarding multi-omics level; however, the overall status of ferroptosis pathway alteration was hard to evaluate. The aim of this study is to comprehensively analyze the putative biological, pathological, and clinical functions of the ferroptosis pathway in breast cancer on a pathway level. By adopting the bioinformatic algorithm "pathifier", we quantified five programmed cell death (PCD) pathways (KO04210 Apoptosis; KO04216 Ferroptosis; KO04217 Necroptosis; GO:0070269 Pyroptosis; GO:0048102 Autophagic cell death) in breast cancer patients, and we featured the clinical characteristics and prognostic value of each pathway in breast cancer and found significantly activated PCD in cancer patients, among which ferroptosis demonstrated a significant correlation with the prognosis of breast cancer. Correlation analysis between PCD pathways identified intra-tumor heterogeneity of breast cancer. Therefore, clustering of patients based on the status of PCD pathways was done. Comparisons between subgroups highlighted specifically activated ferroptosis in cluster 2 patients, which showed the distinct status of tumor immunity and microenvironment from other clusters, indicating putative correlations with ferroptosis. NDUFA13 was identified and selected as a putative biomarker for cluster 2 patients. Experimental validations were executed on cellular level and NDUFA13 showed an important role in regulating ferroptosis activation and can work as a biomarker for ferroptosis pathway status. In conclusion, the status of the ferroptosis pathway significantly correlated with the clinical outcomes and intra-tumor heterogeneity of breast cancer, and NDUFA13 expression was identified as a positive biomarker for ferroptosis pathway activation in breast cancer patients.

KEYWORDS

programmed cell death, ferroptosis, tumor microenvironment, heterogeneity, NDUFA13

Introduction

Programmed cell death (PCD) has long-demonstrated significance in all aspect of life and keeps growing with the discovery of new functions and identification of new classifications (1). The newest subroutines were identified based on the molecular characteristics including apoptosis, necroptosis, pyroptosis, ferroptosis, entotic cell death, netotic cell death, parthanatos, lysosome-dependent cell death, autophagy-dependent cell death, alkaliptosis, and oxeiptosis, of which the molecular function and regulatory mechanism were summarized in a review done by Tang et al. (2).

Numerous reports were seen regarding the pathological alteration of PCD pathways in cancers. Several core genes were identified in the regulatory network of cell death. The caspases family plays a critical role in the regulation of cell death. PCD can be further categorized into two groups: caspase-dependent (e.g., apoptosis and pyroptosis) and caspase-independent (e.g., necroptosis, ferroptosis, parthanatos, alkaliptosis, and oxeiptosis) (3, 4). Studies focusing on the regulatory genes of PCD gave rise to the importance of each pathway in cancer; however, these studies can hardly reflect the overall status alteration of pathways. Quantifications of each pathways in patients were also rarely discussed.

The recent development of algorithms using sequencing data can transform gene-level data into pathway-level data. With considerations of regulatory information between genes, it can accurately reflect the status alteration of each pathway under different conditions and provide novel perspectives in the integration of multi-omics data on cancer (5, 6). Compared to R package "ssGSEA", which was developed using the annotated gene list of pathways, "pathifier" demonstrated better accuracy in a context-specific manner, especially with novel pathways or self-defined gene lists (7, 8), and was widely used in cancer studies focusing on pathway-based evaluations of pathological effects and identifications of testable biomarkers (6, 9, 10).

To fully understand the characteristics of ferroptosis pathway in breast cancer, we calculated a pathway deregulation score (PDS) of five PCD pathways by adopting "pathifier", a bioinformatic algorithm, using The Cancer Genome Atlas (TCGA) data. The aim of this study is to comprehensively analyze the putative biological, pathological, and clinical correlations of the ferroptosis pathway in breast cancer on a quantitative pathway level.

Materials and methods

Data accession

Expression data from TCGA breast invasive carcinoma (BRCA) dataset by RNA sequencing (RNAseq) (ployA+ IlluminaHiSeq, version 2017-10-13) and relative clinical phenotype information from TCGA Pan-Cancer (PANCAN) Clinical Data Resource (version 2019-12-06) were obtained from UCSC Xena data hub (https://xenabrowser.net/hub/). The expression value was shown as gene-level transcription estimates mean-normalized (per gene) across all TCGA cohorts [PANCAN normalized log2(norm_count+1)]. Four major clinical outcome endpoints were used as pre-described, namely, overall survival (OS), progression-free interval (PFI), disease-free interval (DFI), and disease-specific survival (DSS) (11). GTEx and TCGA PANCAN were also obtained from UCSC Xena data hub. Data from the Molecular Taxonomy of Breast Cancer International Consortium (METABRIC) project and the MSK-IMPACT project were downloaded from the cBioPortal for Cancer Genomics (http://www.cbioportal.org/) and were used as independent external validation datasets (12–14).

Generation of pathway deregulation score

To evaluate the biological status of PCD pathways in breast cancer, R package "pathifier" was used to transform gene-level information into pathway-level information on the basis of expression data, generating a compact and biologically relevant PDS of each sample (8). PDS ranged from 0 to 1. Tumor samples that got a higher score than the normal sample were deemed highly deregulated, whereas tumor samples with the lower score indicated an inactive status of a certain pathway. A gene list of PCD pathways was extracted from the Kyoto Encyclopedia of Genes and Genomes (KEGG) and Gene Ontology (GO) database (KO04210 Apoptosis; KO04216 Ferroptosis; KO04217 Necroptosis; GO:0070269 Pyroptosis; GO:0048102 Autophagic cell death). Each pathway was running for 1000 attempts with the minimal allowed standard deviation of 0.4. Illustration of clinical relevance was done with "pheatmap".

Evaluation of clinical significance

Prognostic value regarding the four clinical outcome endpoints enrolled was done using univariate and multivariate Cox regression. For multivariate Cox regression, PDS was enrolled and forward stepwise regression was done with the ER/PR/HER2 status, age, and T/N/M stage treated as confounders. R package "survival" was used for survival analyses of PDS with best separation cutoffs selected using "survminer". The minimal proportion of each group was no less than 10%. Further multivariance survival analyses and subgroup analyses were done as described and illustrated using "forestplot". Hazard ratio (HR) and 95% confidence interval (95%CI) were shown in the forest plot. The Kaplan–Meier plotter (KMplot; http://www.kmplot.com/analysis) was used to

evaluate the prognostic value of NDUFA13 in integrative breast patients on both RNA and protein levels. Distance metastasis-free survival was used as an endpoint.

To evaluate the predictive efficiency of PDS, R package "timeROC" was used to construct time-dependent ROC comparing survival data. Time points used include 0, 90, 180, 270, 365, 730, 1,095, 1,825, 2,920, 3,650, and 5,475 days. At each time points included, an AUC value was generated and compared across PCD pathways.

Decision curve analysis (DCA) was done to evaluate whether using the PDS of PCD pathways as prognostic factors would improve clinical decision-making for all decisions (15, 16). The "stdca.R" function was used to conduct DCA with prediction models compared to two default strategies: (1) assume that all patients are tested positive and therefore treat everyone (treat-all) or (2) assume that all patients are tested negative and offer treatment to no one (treat-none). Curves above the treat-none line and outdo treat-all line were deemed to gain benefit. The further assessment focused on the usefulness of the marker to identify patients with and without unnecessary treatment, and the net reduction plot was used to show the intervention avoided based on the prognostic value of the marker.

Clustering and principle components analysis (PCA)

Correlations between the PDS of PCD pathways were calculated and illustrated using R package "corrgram". Each pathway was distributed diagonally, with the correlation scatter diagram in the lower left corner and the correlation coefficients in the upper right corner. Further illustrations with circos plot were done using "circlize" (17). All analyses were done using Spearman's correlation tests.

Clustering of PDS of each PCD pathway was done with patients firstly being divided into "UP", "DOWN", and "NO CHANGE" groups using k.means, then clustered with ward.D. Illustrations were done using "pheatmap" and "ggplot2". PCA was done using "ggord" and illustrated with "yyplot".

Function enrichment

Clinical characteristics were compared between clusters using "pheatmap". Differential expression analyses were done between groups to identify genes that significantly deregulated between clusters using limma (18, 19). For gene set enrichment analysis (GSEA), we predefined the gene rank by expressional correlations. The h.all.v7.4.symbols.gmt and c2.cp.kegg.v7.4.symbols.gmt subsets were used to evaluate the relevant pathways and molecular mechanisms. Based on the predetermined gene rank, the minimum gene set was set to 5, the maximum gene was set to 5000, and 1,000 times of re-sampling. P-value < 0.05 and FDR < 0.25 were considered statistically significant.

Characterizing of tumor microenvironment

To fully present the correlation between PCD pathways and anti-cancer immune response process, cancer immunity was analyzed using the online tool TIP (Tracking Tumor Immunophenotype, http://biocc.hrbmu.edu.cn/TIP/), which integrates "ssGSEA" and "CIBERSORT" for tracking, analyzing, and visualizing the status of the seven-step Cancer-Immunity Cycle using RNAseq data (20). Detailed tumor-infiltrating immune cells were further calculated and characterized with clinical information and previously published TCGA immune subtypes.

Immune cell clustering within subgroups was done to feature the relationship among immune cells in a certain population. Spearman's correlations with P-value less than 0.0001 were left for clustering. Both k.means and hclust were used and integrated with recent studies to generate the final clustering results.

Selection of putative biomarkers

Exploration of putative biomarkers was first done with differentially expressed genes (DEGs). The calculation of DEGs was done using limma. Selection criteria were adjusted P-value < 0.05 and $|\log2FC| > 1$. For DEGs meeting the criteria, ROC was done to calculate the AUC, and genes were further ranged by AUC. Top genes were illustrated in heatmap. Further construction of selective panels was done using Lasso regression. Internal tests were done with patients in TCGA-BRCA 1:1 randomly assigned as a training set and a test set. External independent validations were done in the METABRIC and MSK-IMPACT projects.

Cell lines

Human breast cancer cell lines MDA-MB-231, SK-BR-3, MDA-MB-468, T-47D, ZR-75-1, and MCF-7 were obtained from American Type Culture Collection (ATCC; Manassas, VA, USA) and cultured in Dulbecco's modified Eagle's medium (DMEM; Gibco, New York, USA) or Roswell Park Memorial Institute 1640 (RPMI; Gibco, New York, USA), as required, with 10% fetal bovine serum (FBS; Gibco, New York, USA), and 1% penicillin and streptomycin (Gibco, New York, USA). All cells were cultured in the humidified incubator at 37°C with 5% CO_2.

Quantitative real-time polymerase chain reaction (qPCR)

MDA-MB-231 and ZR-75-1 cells were treated with DMSO or RSL3 (MedChemExpress, Monmouth Junction, NJ, USA; 10 μM) for 24 h. Total RNA was extracted through the RNA extraction kit (Promega, Beijing, China) and taken into reverse transcription using PrimeScript RT reagent Kit (Takara, Japan) to produce cDNA under the manufacturer's instructions. qPCR was conducted with SYBR Premix Ex Taq II (Takara) and LightCycler480 system (Roche, Switzerland). GAPDH was utilized as reference. Primers for NDUFA13 were listed as follow: forward primer: 5′- GGCCCATCGACTACAAACGG-3′; reversed primer: reverse primer: 5′- CGCTCACGGTTCCACTTCATT-3′.

Reactive oxygen species evaluation

The intracellular level of reactive oxygen species (ROS) was quantified by a Reactive Oxygen Species Assay Kit (Beyotime, China). This kit contains 2', 7'-dichlorofluorescein-diacetate (DCFH-DA), which is easily oxidized to fluorescent dichlorofluorescein (DCF) by intracellular ROS. Cells were seeded in six-well plates, stimulated with simvastatin for 24 h, then washed with PBS and treated with 10 μM DCFH-DA in the dark for 30 min at 37°C. The fluorescence was observed by fluorescence microscopy at 488-nm excitation and 525-nm emission after being washed three times with PBS.

Statistical analysis

All analyses were performed using RStudio version 1.2.5033 (R Core Team, Vienna, Austria) statistical software. PDS and gene data were presented as means ± SE unless otherwise indicated. Two group comparisons were made using Student's t-test, whereas multi-groups comparisons were done with one-way ANOVA. Further comparisons of numerous data were done using chi-square test. All analyses were done with missing sample excluded considering the large sample size. Correlation analyses were done using either Pearson's test or Spearman's test depending on parametric or non-parametric distribution of the data. Unless otherwise indicated, a two-sided *P*-value < 0.05 was considered significant. *P < 0.05; **P < 0.01; ***P < 0.001; ****P < 0.0001.

Results

Clinical characteristics and prognostic significance of PDS in breast cancer

To fully explore the clinical characteristics and prognostic significance of PCD pathway alterations in breast cancer, PDS of PCD pathways (KO04210 Apoptosis; KO04216 Ferroptosis; KO04217 Necroptosis; GO:0070269 Pyroptosis; GO:0048102 Autophagic cell death) for each patient was generated using "pathifier" to quantify the status alteration of each pathway based on RNAseq data from the TCGA-BRCA dataset with 1,091 tumor sample and 113 normal sample (Figure 1A). The final status of each PCD pathway was determined by comparing with normal samples (Figure 1B). Intriguingly, all PCD pathways were seen hyperactivated in tumor samples ($P < 0.0001$), demonstrating the significant role of PCD in breast cancer. Clinical characterization of PCD pathways was further explored. Among all clinical characteristics included, apoptosis, ferroptosis, and necroptosis pathways were activated in ER, PR-negative, and basal patients, whereas the autophagic cell death pathway was significantly suppressed (Figure A1A–C). Interestingly, despite no significant alteration being seen regarding HER2 status, comparisons between PAM50 subtypes showed significantly activated apoptosis, ferroptosis pathways, suppressed pyroptosis, and autophagic cell death pathway in HER2-positive subtype compared to hormone receptor-positive patients (Figure A1C). Furthermore, correlations between pathway alterations and vital status revealed significantly activated apoptosis, ferroptosis, necroptosis, and autophagic cell death pathways in living patients compared to deceased patients, demonstrating the putative prognostic significance of PCD in breast cancer (Figure A1D).

Given the status of PCD significantly altered between vital status, Cox regression and survival analyses were done to explore the prognostic values of PCD in breast cancer. As shown in Figure 1C, ferroptosis and necroptosis are significantly correlated with OS in univariate Cox regression, among which only ferroptosis was identified as an independent prognostic factor in multivariate analysis (HR 0.395, 95%CI 0.198–0.929, P = 0.033). Interestingly, apoptosis significantly correlated with DSS in multivariate analysis with the ER/PR/HER2 status, age, and T/N/M stage was treated as confounders; however, this was not seen in univariate Cox regression.

To validate the prognostic value of PCD, timeROCs were used to compare at a different time point (Figure A1E). In accordance with survival analysis, the ferroptosis pathway showed the highest AUC regarding OS, PFI, DFI, and DSS, especially in the first 3 years, with the highest AUC seen in the first year (OS: 0.68; PFI: 0.72; DFI: 0.66; DSS: 0.76) and declining ever after. The prognostic advantage of the ferroptosis pathway persisted in PFI and DSS up to the fifth year. Combined with the clinical significance seen in survival analyses, the ferroptosis pathway has demonstrated putative association with early recurrence and progression of breast cancer, and a certain hypothesis gave rise to the importance of the ferroptosis pathway in breast cancer in both pathogenetic and clinical ways. To further address the putative functions of ferroptosis in clinical decision-making, DCA was done comparing the instructive value of PCD regarding PFI, DFI, and DSS in the first 3 years. Intriguingly, in accordance with timeROC analyses, PDS of the ferroptosis pathway has shown the best efficacy as a risk score

for the early recurrence and progression of breast cancer in the first 3 years. In the prediction of PFI, an absolute gaining of Net Benefit (NB) in patients with a threshold probability ranged from 10% to 14%, whereas in DSS, significant gaining of NB was seen in patients with a probability ranging from 6% to 10% (Figure A1F). Moreover, evaluation of PDS as therapeutic indicators done in DCA also showed a good efficacy of the ferroptosis pathway regarding PFI and DFI. For patients with a threshold probability ranging from 9.5% to 14%, using PDS of ferroptosis as a biomarker for clinical intervention demonstrated the best efficacy, with a net reduction of 15 per 100 patients. Comparatively, prominent improvement was seen in ferroptosis as a biomarker for DSS in patients with a probability over 6%, with a net reduction of more than a quarter per 100 patients (Figure A1F).

Clustering of breast cancer patients based on PDS

Numerous works were done focusing on the crosstalk between PCD pathways on both biological and clinical levels; however, studies were done on the gene level, and by generating the PDS of PCD pathways, we tried to quantify the correlation on the pathway level (Figure 2A). Positive correlations were found between all PCD, except for autophagic cell death. However, scatter plots of pairwise comparisons between apoptosis, ferroptosis, necroptosis, and pyroptosis revealed underlying heterogeneity among breast cancer samples with the distribution of patients exhibiting distinct clusters. Therefore, clustering based on PDS was done. A total of five clusters were generated as shown in Figure 2B with sample types. Normal samples were seen mostly in cluster 1 (Normal = 88, Tumor = 13). PCA also identified a separated distribution between cluster 1 and other clusters (Figure 2C). Within tumor samples, PCA has seen a good separation between clusters 2, 3, and 5; however, there is cross-coverage between cluster 4 and other groups. For each pathway, comparisons were made to identify featured alterations in each cluster (Figure 2D; Table A1SF4), among which cluster 2 exhibited significantly hyperactivated ferroptosis and necroptosis pathways and autophagic cell death was significantly activated in cluster 3 and cluster 5. Detailed clinical characteristics were summarized in Table A2.

Survival analyses done in each cluster unraveled distinct results between clusters, but good consistency within each cluster (Figure A1G). In cluster 2, the activation of ferroptosis and autophagic cell death significantly correlated with better clinical outcomes, whereas cluster 5 has seen the activated PCD indicating worse clinical

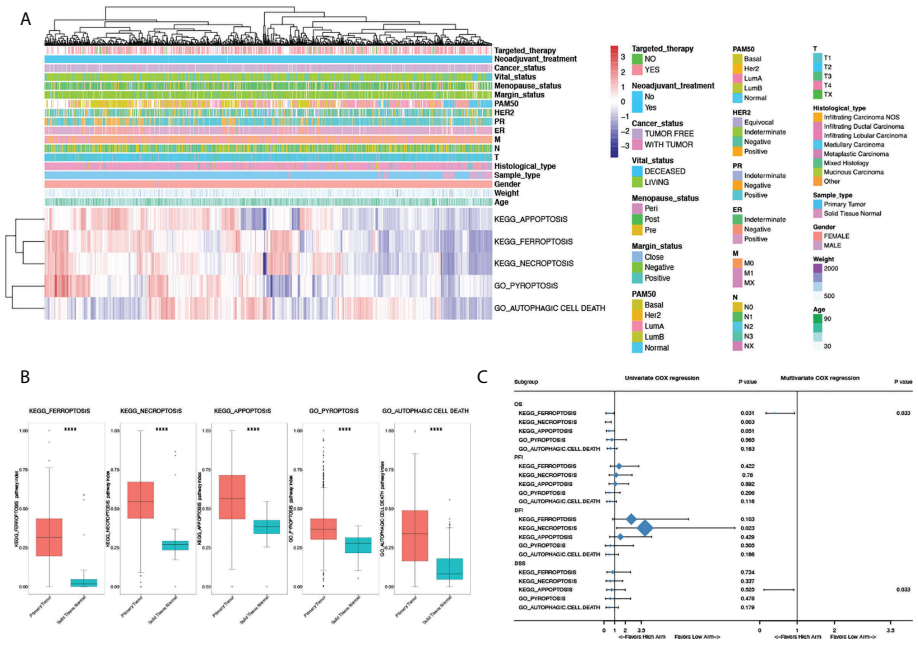

FIGURE 1
Clinical characteristics and prognostic significance of programmed cell death pathway alterations in breast cancer. **(A)** Heatmap illustrating pathway deregulation score (PDS) of PCD pathways in breast cancer generated with clinical annotations from TCGA BRCA data; colors were row-scaled and zero-centered. **(B)** Comparisons of PDS between sample types. **(C)** Univariate and multivariate Cox regression of PCD pathways in breast cancer regarding overall survival (OS), progression-free interval (PFI), disease-free interval (DFI), and disease-specific survival (DSS). Hazard ratio (HR) and 95% confidence interval (95%CI) were shown in the forest plot. For multivariate Cox regression, all pathway scores were enrolled and forward stepwise regression was done with the ER/PR/HER2 status, age, and T/N/M stage treated as confounders. *P*-value < 0.05 was considered significant. A two-sided *P*-value < 0.05 was considered significant. ****P < 0.0001.

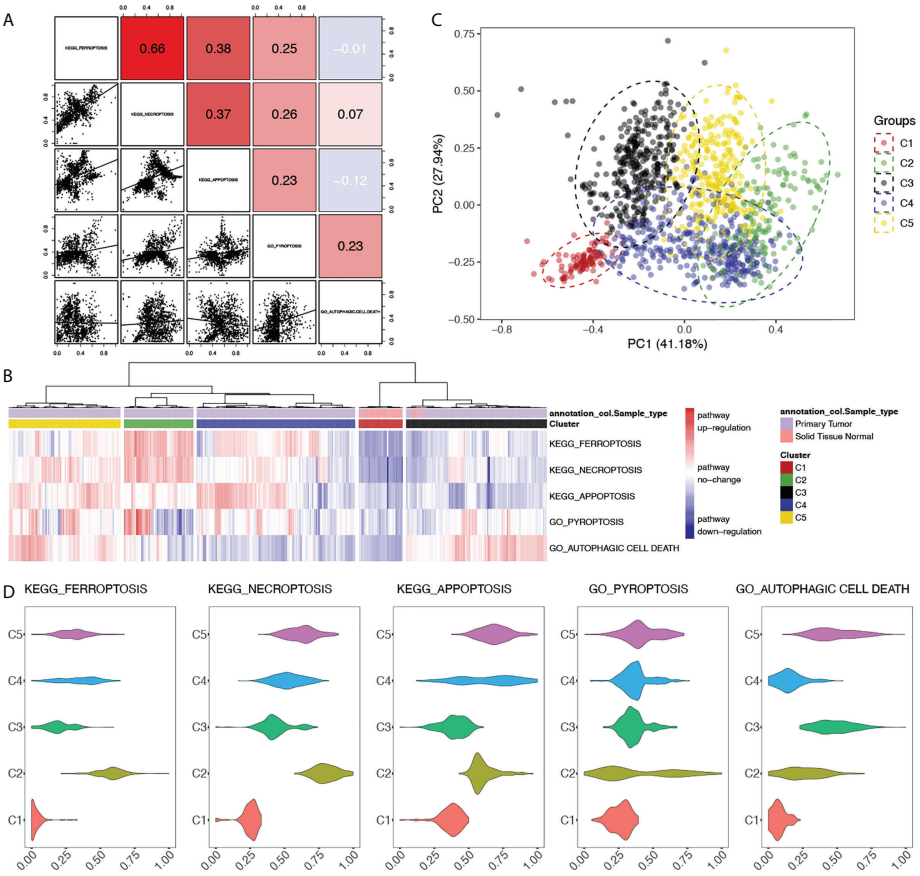

FIGURE 2
Clustering of breast cancer patients based on the alterations of programmed cell death pathways. **(A)** Correlations between PCD pathways in breast cancer. Correlational R-values between pathways were shown in the upper right with scatter plots in the bottom left. Color was illustrated according to the R-value. Red: R > 0, blue: R < 0. **(B)** Heatmap of clustering based on the PDS of PCD pathways of breast cancer patients with sample type annotation. **(C)** Principle components analysis (PCA) based on the PDS of PCD pathways with clusters of breast cancer patients illustrated with different colors. **(D)** Comparisons of PDS of each PCD pathways between clusters. *P*-value < 0.05 was considered significant.

outcomes. However, in either cluster 2 or cluster 5, identical clinical significance was seen regarding both OS and other outcomes. This suggested that our clustering results successfully eliminate heterogeneity within clusters. Among PCD pathways, ferroptosis showed significant clinical correlations in both cluster 2 and cluster 5 regarding OS, PFI, DFI, and DSS, which supported the clinical significance of ferroptosis in breast cancer addressed above. Furthermore, the different clinical relevance between cluster 2 and cluster 5 draws attention to the putative biological heterogeneity between these two clusters, which needs further exploration.

Functional enrichment between clusters

To fully explore the biological difference between clusters, clinical characteristics were first summarized and compared in Table A2. Clusters consist of different levels of sample type, histological type, ER/PR/HER2 status, M stage, marginal status, vital status, and history of targeted therapy. To explore the different biological characteristics between clusters, biomarkers for each cluster were enriched (Figure A2A). Top 100 biomarkers for each cluster were used for functional enrichments. Only specific biomarkers were enrolled for final analysis (Figure A2B, Table A3). Multi-group enrichments revealed common functions between clusters (Figures A2C, D), which mainly focus on the cell cycle pathway. Cluster-specific enrichments showed a distinct biological background of each cluster. Comparatively, cluster 2 specifically enriched in GO:0016579: protein deubiquitination, GO:0061756: leukocyte adhesion to vascular endothelial cell, GO:0046854: phosphatidylinositol phosphorylation, GO:0004842: ubiquitin-protein transferase activity, GO:1901699: cellular response to nitrogen compound, GO:0005667: transcription factor complex, and GO:0019902: phosphatase binding, among which GO:0061756 indicates a putative role in the infiltration of the tumor

microenvironment. The differentially enriched pathways provided novel perspectives on the difference between clusters and the intra-tumor heterogeneity, which was mainly discussed in the tumor microenvironment.

To explore the underlying correlation mentioned above, characterization of the microenvironment was depicted. A comprehensive heatmap of TILs was shown with patients scored by infiltration level of the 24 immune cells. Previously published immune indexes were also annotated to characterize tumor microenvironment (Figure 3A) (21). Leukocyte fraction, stromal fraction, and intra-tumor heterogeneity were used to quantify tumor purity. Comparisons of the overall infiltration score between clusters showed a significantly higher level of infiltration in cluster 2 than other clusters ($P < 0.001$, Figure 3B), which, in accordance with the functional enrichments, demonstrated an hyperactivated immune status in patients with activated ferroptosis pathway. However, compared to previously published immune subtypes and PAM50, cross-links were seen between subgroups and significant consistency was not seen (Figure 3C), which proved our clusters a novel classification, and the highlight of cluster 2 indicates a putative regulative role of ferroptosis in tumor immunity.

Given the theory of the seven-step Cancer-Immunity Cycle, clarification of correlations between PCD and specific steps contributes to the understanding of the specific underlying mechanism. Therefore, correlations were done with each step quantified using ssGSEA. As shown in Figure 3D, a general relationship was seen between PDC and the seven-step Cancer-Immunity Cycle, among which correlations were mainly found in steps 3, 4, and 5 (Table A4). Interestingly, negative correlations were found between pathways and trafficking of immune cells to tumors except for apoptosis, which implies a different biological function between apoptosis and other PCD pathways in immunity.

Distinct tumor microenvironment between patients with activated and inactivated ferroptosis pathway

Further exploration of the tumor microenvironment was done focusing on the different intercellular interactions of TILs. Correlations of each cell were calculated and clustered within each group. With the size of each dot representing the survival significance of each cell, cells clustered showed a comprehensive correlation and a different distribution between cluster 2 and cluster 5 (Figure 4A). Distinct interactions were seen with TILs clustered differently, demonstrating a distinct tumor microenvironment between clusters 2 and 5 caused by status alteration of ferroptosis. In summary, cluster 2 featured highly infiltrated immune cells that demonstrated anti-tumor efficacy, while cluster 5 exhibited a higher proportion of tumor-promoting cells.

Given the putative regulatory function of PCD mainly focuses on the immune infiltration process, comparisons of 24 tumor-infiltrating immune cells were done between cluster 2 and cluster 5 (Figure 4B), in which a lower level of type 1 regulatory T cells (Tr1), natural regulatory T cells (nT_{reg}), induced regulatory T cells (iT_{reg}), T helper cells 1 (T_H1), IL-17–producing effector T helper cells (T_H17), central memory T cell (T_{cm}), and effector memory T cell (T_{em}) were seen in cluster 2, whereas cytotoxic T cells (Tc), exhausted T cells (T_{ex}), natural killer T cells (NKT), follicular helper T cells (Tfh), NK cells, gammadelta T cells (γδT/Tgd), and $CD8^+$ T cells (CD8T) are highly infiltrated. The different levels of tumor-infiltrating immune cells indicate a distinct microenvironment between clusters 2 and 5 that may affect the biological functions of PCD.

Except for a significantly hyperactivated level of ferroptosis pathway, patients in cluster 2 showed a significantly higher proportion of ILC subtype, basal patients, and more metastasis ($P < 0.001$) compared to cluster 5 (Figure 4C). Functional enrichments were done between clusters 2 and 5 to explore the putative mechanism altered. PDS of all KEGG pathways was calculated and compared between clusters 2 and 5, among which the adipocytokine signaling pathway, T-cell receptor signaling pathway, TGF-beta signaling pathway, and leukocyte trans-endothelial migration pathway were found hyperactivated in cluster 2, whereas basal transcription factor pathway was significantly suppressed. For further validation, DEGs were calculated (Figure A3A) and used as an input for GSEA analyses of both GO and KEGG. The top 40 KEGG pathways and biological functions in GO were shown in Figures A3B, C. Intersections of the functional enrichments found immunological functions significantly altered between patients in clusters 2 and 5. In cluster 2, immune-related functions like antigen processing and presentation *via* MHC class Ib (NE: 0.97, NES: 1.46, *P*-value = 0.016), positive regulation of T-cell–mediated cytotoxicity (NE: 0.96, NES: 1.52, *P*-value = 0.010), and regulation of T-cell apoptotic process (NE: 0.93, NES: 1.49, *P*-value = 0.023) were significantly activated. This indicates that patients in cluster 2 are more immune-active compared to patients in cluster 5.

Given the opposed clinical significance of ferroptosis found in clusters 2 and 5, we hypothesized that ferroptosis may have a regulatory function on immunity. Therefore, correlations between ferroptosis pathway and tumor-infiltrating immune cells were explored in both cluster 2 and cluster 5, respectively. In cluster 2, Tgd, iT_{reg}, B cell, T_{cm}, and macrophage were found significantly correlated with ferroptosis (Figure 4D), whereas in cluster 5, significant correlations were seen in NKT, B cell, T_{ex}, iT_{reg}, T_H17, nT_{reg}, CD8.naive, DC, T_H1, and Tgd. Among cells that significantly correlated with ferroptosis in both clusters, reversed correlations were seen in Tgd, B cell, and iT_{reg} between the two clusters (Tgd: Rc2 = 0.25, Rc5 = −0.12; B cell: Rc2 = −0.18, Rc5 = 0.34; iT_{reg}: Rc2 = −0.23, Rc5 = 0.24). These results suggested that the different regulatory mechanisms of activated and inactivated ferroptosis between cluster 2 and cluster 5 mainly affect the infiltration, but not the function of immune cells.

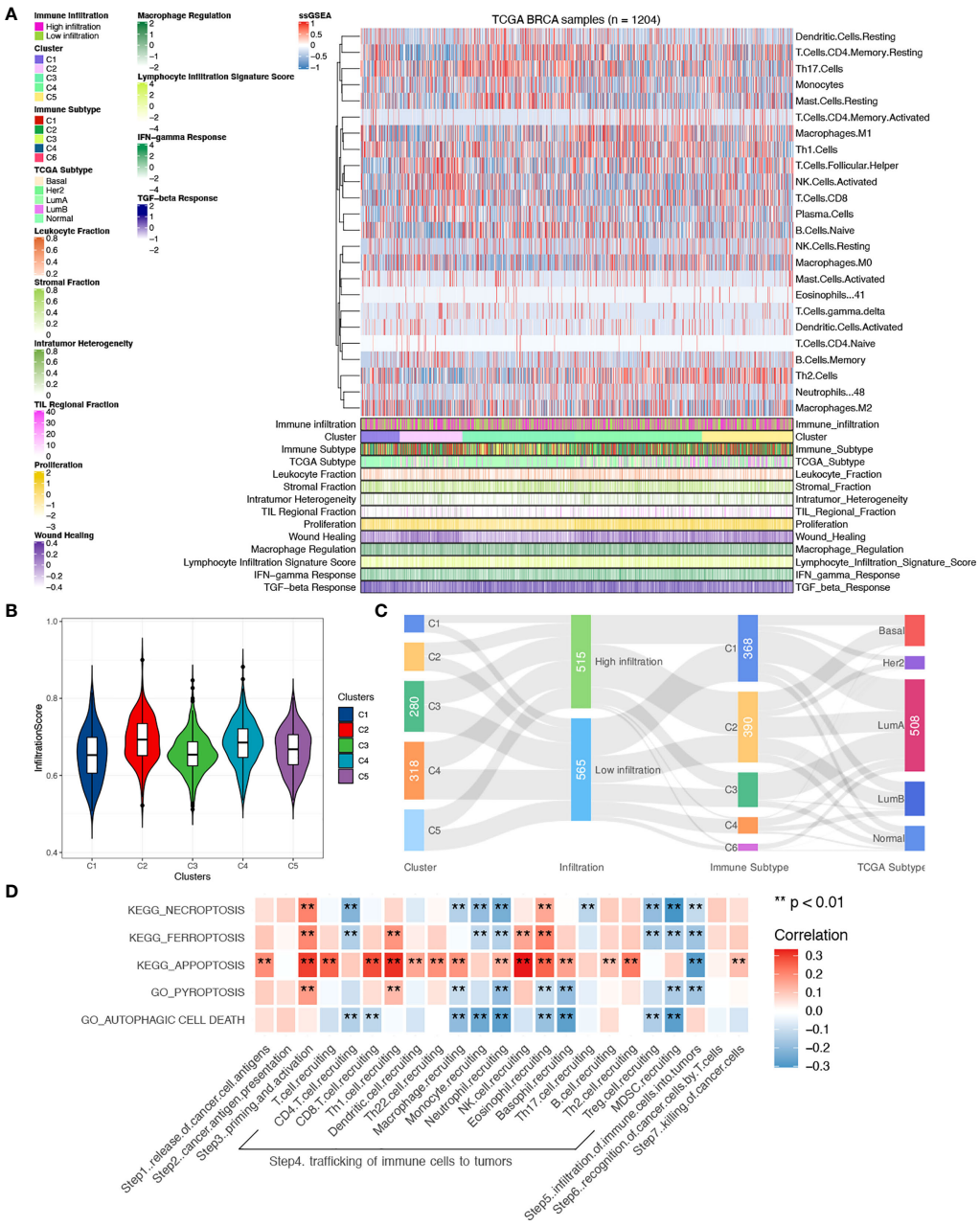

FIGURE 3
Comparisons of tumor microenvironment between clusters. **(A)** Heatmap of tumor-infiltrating immune cells between clusters with previously categorized immune subtypes information. **(B)** Comparisons of infiltration scores were done between clusters. **(C)** Correlations between clusters and immune subtypes, PAM50, and infiltration levels. **(D)** Correlations of PCD pathways and the seven-step Cancer-Immunity Cycle in all samples. A two-sided *P*-value < 0.05 was considered significant. **P < 0.01.

Selection of putative biomarker for ferroptosis-activated patients

Given the results presented above, patients in cluster 2 are characterized with the hyperactivated ferroptosis pathway and higher immune infiltration. Additional analyses were done to explore putative biomarker genes between the two clusters. DEGs were calculated between C2 and other patients and analyzed using ROC. Only the top 20 DEGs with the highest AUC were left for further comparison (Table A5), among which only three genes were significantly overexpressed in cluster 2 (namely, GADD45GIP1, NDUFA11, and NDUFA13; Figure 5A)

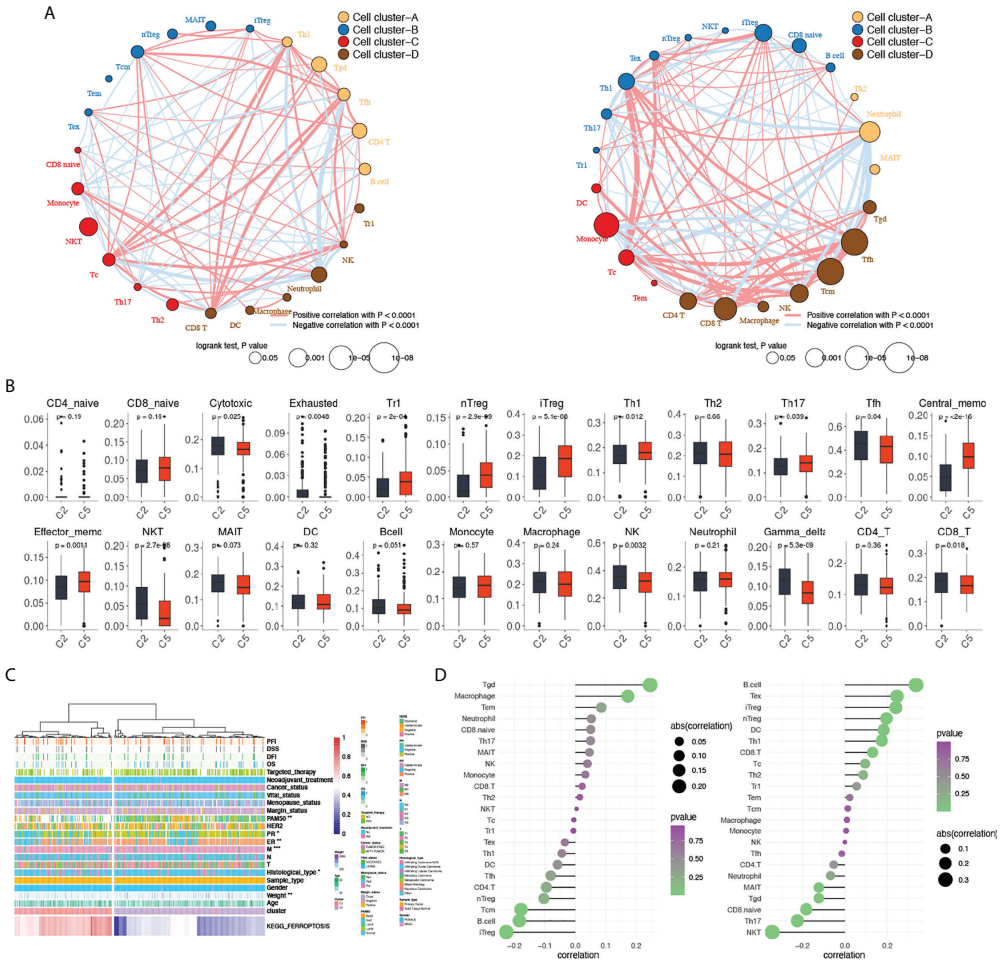

FIGURE 4
Comparisons of tumor-infiltrating immune cells between cluster 2 and cluster 5. **(A)** Clustering and correlations between tumor-infiltrating immune cells in cluster 2 (left) and cluster 5 (right). Red: positive correlation, blue: negative correlation. **(B)** Comparisons of tumor-infiltrating immune cells between cluster 2 and cluster 5. **(C)**. Heatmap of KEGG_FERROPTOSIS pathway alteration and clinical characteristics between clusters 2 and 5. **(D)** Correlations between KEGG_FERROPTOSIS and tumor-infiltrating immune cells between cluster 2 (left) and cluster 5 (right). A two-sided *P*-value < 0.05 was considered significant. *P < 0.05; **P < 0.01; ***P < 0.001.

and may work as putative biomarkers. A three-gene predictive model was generated by Lasso regression among the top 20 DEGs. Intriguingly, the predictive model constructed by Lasso only contains the three over-expressed genes. Evaluation of the three-gene index found stable and consistent predictive efficacy between the training cohort and test cohort [Train AUC: 0.929 (0.892–0.961); Test AUC: 0.936 (0.908–0.959); P = 0.810]. External validations were done in the METABRIC and MSK-IMPACT projects. The alterations of PCD were first quantified in both validation cohorts. Patients were clustered under the same criteria and the cluster 2 subset of patients was identified manually. The predictive efficacy of the three-gene predictive model was presented as ROC, and in both validation cohorts, the three-gene panel showed a good efficacy [validation 1: AUC 0.915 (0.889–0.942); validation 2: AUC 0.915 (0.893–0.935)] (Figure 5B). Furthermore, NDUFA13 demonstrated good efficacy compared to the three-gene predictive model (Figure 5B, AUC 0.919 (0.901–0.934) P = 0.101), suggesting that NDUFA13 can work as a single-gene biomarker for the selection of cluster 2 patients. Moreover, the correlation between NDUFA13 and ferroptosis pathway alteration was shown in Figure 5C with patients ranged by the expression of NDUFA13. Based on the results presented, overexpression of NDUFA13 strongly correlated with the status of ferroptosis (R = 0.53, P < 0.0001).

Given the positive correlation identified in our study, putative biological functions between NDUFA13 and ferroptosis may need further demonstration. Firstly, expression analysis revealed over-expression of NDUFA13 in breast cancer and several other cancers (Figure 5D), indicating putative oncogenic functions of NDUFA13 in tumors. Then, functional enrichments were done using GSEA, among which TOP 5 significantly enriched KEGG pathways and cancer hallmarks were shown in Figure 5E. Positive regulations of oxidative phosphorylation was enriched in both KEGG and

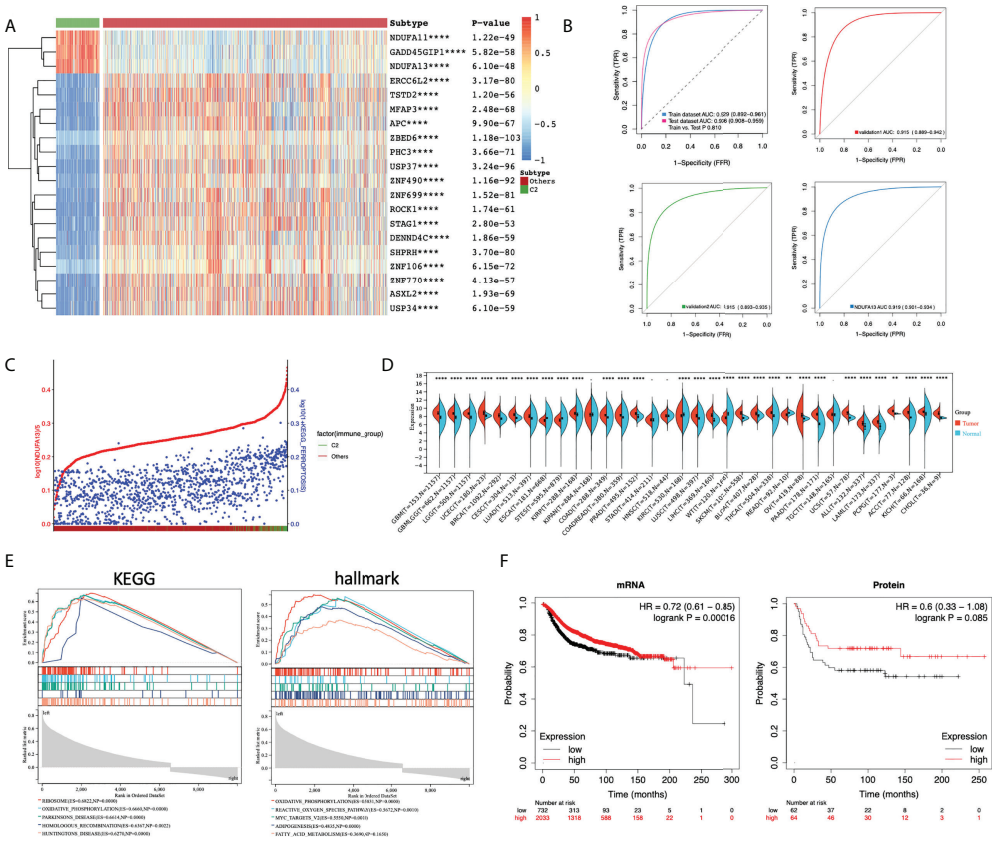

FIGURE 5
Selection of putative biomarker for cluster 2 patients. **(A)** Heatmap of the top 20 putative biomarkers between cluster 2 and other breast cancer patients. DEGs were calculated using limma; DEGs with adjusted *P*-value < 0.05 and |log2FC| > 1 were selected for ROC analysis. DEGs were ranged according to the AUC and only top 20 genes were illustrated. **(B)** ROC plot comparing the predictive value of the three over-expressed genes as biomarkers of cluster 2 patients. A three-gene index was generated using Lasso regression. The predicted value of the three-gene index generated was estimated with TCGA-BRCA patients divided equally into the training cohort and test cohort. Further validations were done using data from the METABRIC (validation 1) and MSK-IMPACT projects (validation 2). **(C)** Scatter plot showing the expression of NDUFA13 (red) and the PDS of ferroptosis pathway (blue) with patients annotated to cluster 2 or others. Patients were ranged by the expression of NDUFA13. **(D)** Pan-cancer expression analysis of NDUFA13 in 27 cancer types using TCGA PANCAN and GTEx dataset. **(E)** GSEA plots of NDUFA13-related pathways and cancer hallmarks. **(F)** Kaplan–Meier survival plots for NDUFA13 expression in breast cancer. Distant metastasis-free survival (DMFS) was used as an endpoint. A two-sided *P*-value < 0.05 was considered significant. **P < 0.01; ****P < 0.0001.

hallmark dataset (KEGG: ES = 0.6660, P = 0; HALLMARK: ES = 0.5831, P = 0). In the hallmark dataset, NDUFA13 was found positively correlated with ROS pathway (ES =0.5672, P = 0.001), adipogenesis (ES = 0.4835, P = 0), and fatty acid metabolism (ES = −0.3690,NES = −1.7, P = 0.1650), which were demonstrated factors associated with the occurrence of ferroptosis, indicating a biological correlation between NDUFA13 and ferroptosis. The KMplot was utilized to assess the prognostic effect of NDUFA13 on both mRNA and protein levels. A total of 2,765 breast cancer cases were available for distant metastasis-free survival (DMFS) analysis by mRNA and 126 cases by protein. Our study showed that the overexpression of NDUFA13 was correlated with a significant increase in the DMFS of breast cancer patients (Figure 5F, mRNA: P < 0.001, Protein: P = 0.085).

Validation of NDUFA13 as putative biomarker for ferroptosis

To fully validate the correlation between NDUFA13 and ferroptosis, the cellular expression level of NDUFA13 mRNA was first evaluated in order to provide the basic level of expression between subtypes. Comparatively, SK-BR-3 and MCF-7 exhibit a higher level of NDUFA13; nevertheless, a similar expression pattern was seen between cell lines (Figure 6A). MDA-MB-231 and ZR-75-1 were selected for further experimental demonstration considering the similar basic expression level and the molecular subtypes. After ferroptosis induced by 24-h incubation of RSL3 (10 μM), both cells showed significantly elevated levels of NDUFA13 compared to DMSO-treated groups (Figure 6B, P < 0.01).

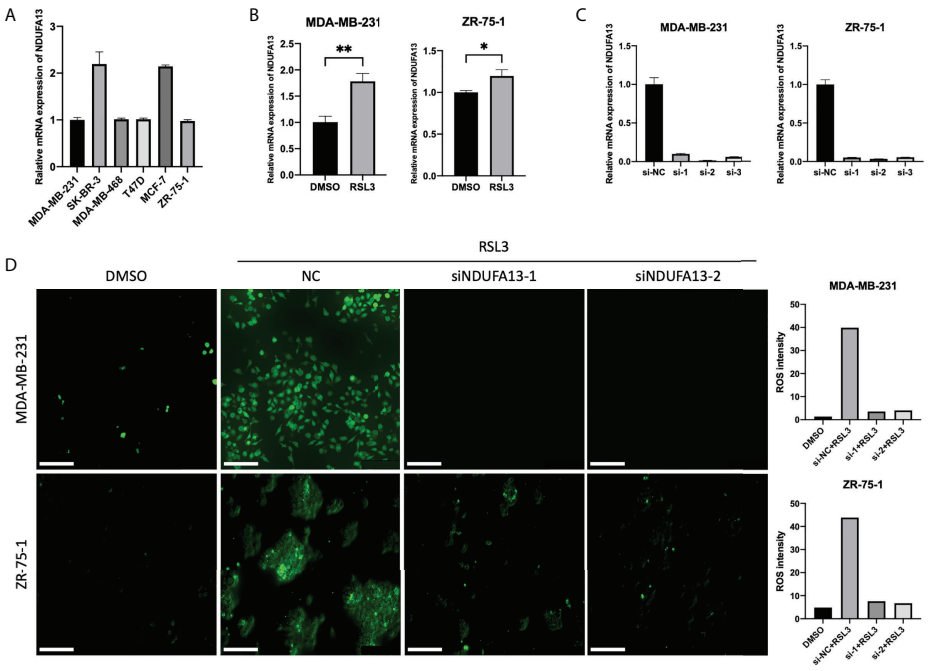

FIGURE 6
Validations of NDUFA13 as a biomarker for ferroptosis. **(A)** Expression of NDUFA13 in human breast cancer cell lines. **(B)** Expression of NDUFA13 mRNA in human breast cancer cell lines treated with DMSO or RSL3 (10 μM) for 24 h. **(C)** Efficiency test of NDUFA13 siRNA knockdown (KD). **(D)** Intracellular level of reactive oxygen species (ROS) in breast cancer cells treating with DMSO or RSL3 (10 μM) followed by NDUFA13 KD. A two-sided P-value < 0.05 was considered significant. *P < 0.05; **P < 0.01.

We then tested the intracellular level of ROS in MDA-MB-231 and ZR-75-1 after knocking down NDUFA13 (Figure 6C). Both cells showed a reduction of ROS in NDUFA13 knockdown (KD) groups compared with NC after treating with RSL3. These results indicated that NDUFA13 had a positive correlation with ferroptosis (Figure 6D).

Discussion

By adopting the bioinformatic algorithm "pathifier", we quantified five PCD pathways in breast cancer patients, so as to comprehensively analyze the putative biological, pathological, and clinical significance of PCD pathways in breast cancer on a pathway level. Given the results presented in our study, we found significantly activated PCD in cancer patients, among which ferroptosis demonstrated a significant correlation with the progression of breast cancer. Correlation analysis between PCD identified intra-tumor heterogeneity of breast cancer. Therefore, clustering of patients based on the PDS was done. Comparisons between subgroups highlighted specifically activated ferroptosis in cluster 2. Functional enrichment identified the distinct status of immunity and tumor microenvironment between patients with activated and inactivated ferroptosis pathways. To fulfill the clinical significance of ferroptosis, NDUFA13 was identified as a selective biomarker of ferroptosis activation and further demonstrated putative biological functions in the regulation of ferroptosis.

Previous works focusing on the pathway alterations in cancer were first seen in works done by Wang et al. regarding the Hippo signaling pathway (22). A comprehensive PANCAN analysis of 19 Hippo core genes across 33 cancer types using multi-omics data from TCGA was done and a YAP/TAZ transcriptional target signature of 22 genes was developed to characterize Hippo pathway activity. Another research focusing on the oncogenic pathways in human cancer was done by Li et al. (23). By reviewing literature published and further explored with TCGA data, multi-omics features of oncogenic pathways were summarized and restored as an online database. Despite the inspiring work done, all the discussion remained on the gene level, which hardly reflects the status of each pathway. Therefore, we used PDS generated by "pathifier" to reflect the pathway activity and further explore the clinical significance on a pathway level, which demonstrated more accurate efficacy than other methods.

Crosstalk between PCD pathways and immunity was previously summarized in a review done by Tang et al. (2), in which cell death was categorized into two kinds: immunogenic cell death (ICD) that alerts and triggers immunity against dead-cell antigens, including ferroptosis, necroptosis, pyroptosis, and autophagic cell death and tolerogenic cell death (TCD) that actively inhibits immune responses (24–27). Apoptosis was considered TCD mostly but grew an

importance in the activation of tumor immunity under certain conditions. The correlation between the ferroptosis pathway and tumor immunity identified in our study was previously demonstrated on a cellular level. Recent results done by Wang et al. reveal that $CD8^+$ T cells drive ferroptosis in tumor cells and the tumor suppressive function of interferon (IFN)-gamma secreted by $CD8^+$ T cells in response to immune checkpoint blockade meditated by ferroptosis, suggesting that the immune system may function in part through ferroptosis to prevent tumorigenesis, and ferroptosis may hold the key to tumor immunotherapy response (28, 29). Despite numerous works done, the immunological function of ferroptosis remained underestimated considering the result presented in our study. Intra-tumor heterogeneity contributes to the differential alteration of tumor immunity caused by ferroptosis. Here, we characterized a subset of breast cancer patients with hyperactivated status of ferroptosis and necroptosis pathway and overexpressed NDUFA13, in which activation of ferroptosis promoting the infiltration of anti-tumor cells like Tgd, therefore, might correlate with better responsiveness of immunotherapy in breast cancer. Previously reported biological functions of NDUFA13 mainly involved in the IFN/all-trans-retinoic acid (IFN/RA)–induced cell death and transfer of electrons from NADH to the respiratory chain, therefore, impacted the mitochondrial and cellular ROS production.

In conclusion, we quantified the status alteration of PCD pathways and highlighted the significant correlation of ferroptosis with early recurrence and progression of breast cancer. Intra-tumor heterogeneity of breast cancer was detected based on the status of the ferroptosis pathway. Mechanism analyses further revealed distinct tumor microenvironment and immunological function of ferroptosis between patients. NDUFA13 expression was identified as a positive biomarker for ferroptosis pathway activation in breast cancer patients.

Data availability statement

The original contributions presented in the study are included in the article/Supplementary Material. Further inquiries can be directed to the corresponding authors.

Author contributions

YYL and TL analyzed and interpreted the data and drafted the work. YYL and TL were major contributors in writing the manuscript. XK revised the manuscript. DZ helped with software used for analyses. NS was granted the funding. NS and YYL designed and corresponded for the work. All authors read and approved the final manuscript.

Funding

This research is funded by the Beijing Science And Technology Innovation Medical Development Foundation (KC2021-JX-0044-2) and Guangdong Health Management Society - Breast Disease Professional Committee Fund (2021001).

Conflict of interest

The authors declare that the research was conducted in the absence of any commercial or financial relationships that could be construed as a potential conflict of interest.

Publisher's note

All claims expressed in this article are solely those of the authors and do not necessarily represent those of their affiliated organizations, or those of the publisher, the editors and the reviewers. Any product that may be evaluated in this article, or claim that may be made by its manufacturer, is not guaranteed or endorsed by the publisher.

Supplementary material

The Supplementary Material for this article can be found online at: https://www.frontiersin.org/articles/10.3389/fonc.2022.956999/full#supplementary-material

References

1. Galluzzi L, Vitale I, Aaronson SA, Abrams JM, Adam D, Agostini P, et al. Molecular mechanisms of cell death: recommendations of the nomenclature committee on cell death 2018. *Cell Death Differ* (2018) 25(3):486–541. doi: 10.1038/s41418-017-0012-4

2. Tang D, Kang R, Berghe TV, Vandenabeele P, Kroemer G. The molecular machinery of regulated cell death. *Cell Res* (2019) 29(5):347–64. doi: 10.1038/s41422-019-0164-5

3. McIlwain DR, Berger T, Mak TW. Caspase functions in cell death and disease. *Cold Spring Harb Perspect Biol* (2015) 7(4):a008656. doi: 10.1101/cshperspect.a026716

4. Galluzzi L, Lopez-Soto A, Kumar S, Kroemer G. Caspases connect cell-death signaling to organismal homeostasis. *Immunity* (2016) 44(2):221–31. doi: 10.1016/j.immuni.2016.01.020

5. Kristensen VN, Lingjaerde OC, Russnes HG, Vollan HK, Frigessi A, Borresen-Dale AL. Principles and methods of integrative genomic analyses in cancer. *Nat Rev Cancer* (2014) 14(5):299–313. doi: 10.1038/nrc3721

6. Creixell P, Reimand J, Haider S, Wu G, Shibata T, Vazquez M, et al. Pathway and network analysis of cancer genomes. *Nat Methods* (2015) 12(7):615–21. doi: 10.1038/nmeth.3440

7. Hanzelmann S, Castelo R, Guinney J. GSVA: gene set variation analysis for microarray and RNA-seq data. *BMC Bioinf* (2013) 14:7. doi: 10.1186/1471-2105-14-7

8. Drier Y, Sheffer M, Domany E. Pathway-based personalized analysis of cancer. *Proc Natl Acad Sci U.S.A.* (2013) 110(16):6388–93. doi: 10.1073/pnas.1219651110

9. Haider S, Yao CQ, Sabine VS, Grzadkowski M, Stimper V, Starmans MHW, et al. Pathway-based subnetworks enable cross-disease biomarker discovery. *Nat Commun* (2018) 9(1):4746. doi: 10.1038/s41467-018-07021-3

10. Huang S, Chong N, Lewis NE, Jia W, Xie G, Garmire LX, et al. Novel personalized pathway-based metabolomics models reveal key metabolic pathways for breast cancer diagnosis. *Genome Med* (2016) 8(1):34. doi: 10.1186/s13073-016-0289-9

11. Liu J, Lichtenberg T, Hoadley KA, Poisson LM, Lazar AJ, Cherniack AD, et al. An integrated TCGA pan-cancer clinical data resource to drive high-quality survival outcome analytics. *Cell* (2018) 173(2):400–16 e11. doi: 10.1016/j.cell.2018.02.052

12. Razavi P, Chang MT, Xu G, Bandlamudi C, Ross DS, Vasan N, et al. The genomic landscape of endocrine-resistant advanced breast cancers. *Cancer Cell* (2018) 34(3):427–38 e6. doi: 10.1016/j.ccell.2018.08.008

13. Pereira B, Chin SF, Rueda OM, Vollan HK, Provenzano E, Bardwell HA, et al. The somatic mutation profiles of 2,433 breast cancers refines their genomic and transcriptomic landscapes. *Nat Commun* (2016) 7:11479. doi: 10.1038/ncomms11479

14. Curtis C, Shah SP, Chin SF, Turashvili G, Rueda OM, Dunning MJ, et al. The genomic and transcriptomic architecture of 2,000 breast tumours reveals novel subgroups. *Nature* (2012) 486(7403):346–52. doi: 10.1038/nature10983

15. Vickers AJ, Elkin EB. Decision curve analysis: a novel method for evaluating prediction models. *Med Decis Making* (2006) 26(6):565–74. doi: 10.1177/0272989X06295361

16. Vickers AJ, Cronin AM, Elkin EB, Gonen M. Extensions to decision curve analysis, a novel method for evaluating diagnostic tests, prediction models and molecular markers. *BMC Med Inform Decis Mak* (2008) 8:53. doi: 10.1186/1472-6947-8-53

17. Gu Z, Gu L, Eils R, Schlesner M, Brors B. Circlize implements and enhances circular visualization in r. *Bioinformatics* (2014) 30(19):2811–2. doi: 10.1093/bioinformatics/btu393

18. Yu G, Wang LG, Han Y, He QY. clusterProfiler: an r package for comparing biological themes among gene clusters. *OMICS* (2012) 16(5):284–7. doi: 10.1089/omi.2011.0118

19. Zhou Y, Zhou B, Pache L, Chang M, Khodabakhshi AH, Tanaseichuk O, et al. Metascape provides a biologist-oriented resource for the analysis of systems-level datasets. *Nat Commun* (2019) 10(1):1523. doi: 10.1038/s41467-019-09234-6

20. Xu L, Deng C, Pang B, Zhang X, Liu W, Liao G, et al. TIP: A web server for resolving tumor immunophenotype profiling. *Cancer Res* (2018) 78(23):6575–80. doi: 10.1158/0008-5472.CAN-18-0689

21. Zhang L, Zhao Y, Dai Y, Cheng JN, Gong Z, Feng Y, et al. Immune landscape of colorectal cancer tumor microenvironment from different primary tumor location. *Front Immunol* (2018) 9:1578. doi: 10.3389/fimmu.2018.01578

22. Wang Y, Xu X, Maglic D, Dill MT, Mojumdar K, Ng PK, et al. Comprehensive molecular characterization of the hippo signaling pathway in cancer. *Cell Rep* (2018) 25(5):1304–17 e5. doi: 10.1016/j.celrep.2018.10.001

23. Li F, Wu T, Xu Y, Dong Q, Xiao J, Xu Y, et al. A comprehensive overview of oncogenic pathways in human cancer. *Brief Bioinform* (2020) 21(3):957–69. doi: 10.1093/bib/bbz046

24. Johnson TS, McGaha T, Munn DH. Chemo-immunotherapy: Role of indoleamine 2,3-dioxygenase in defining immunogenic versus tolerogenic cell death in the tumor microenvironment. *Adv Exp Med Biol* (2017) 1036:91–104. doi: 10.1007/978-3-319-67577-0_7

25. Hannani D. Extracorporeal photopheresis: Tolerogenic or immunogenic cell death? beyond current dogma. *Front Immunol* (2015) 6:349. doi: 10.3389/fimmu.2015.00349

26. Green DR, Ferguson T, Zitvogel L, Kroemer G. Immunogenic and tolerogenic cell death. *Nat Rev Immunol* (2009) 9(5):353–63. doi: 10.1038/nri2545

27. Casares N, Pequignot MO, Tesniere A, Ghiringhelli F, Roux S, Chaput N, et al. Caspase-dependent immunogenicity of doxorubicin-induced tumor cell death. *J Exp Med* (2005) 202(12):1691–701. doi: 10.1084/jem.20050915

28. Sanmamed MF, Chen L. A paradigm shift in cancer immunotherapy: From enhancement to normalization. *Cell* (2019) 176(3):677. doi: 10.1016/j.cell.2019.01.008

29. Wang W, Green M, Choi JE, Gijon M, Kennedy PD, Johnson JK, et al. CD8 (+) T cells regulate tumour ferroptosis during cancer immunotherapy. *Nature* (2019) 569(7755):270–4. doi: 10.1038/s41586-019-1170-y

frontiers | Frontiers in Oncology

TYPE Original Research
PUBLISHED 06 September 2022
DOI 10.3389/fonc.2022.978921

Check for updates

OPEN ACCESS

EDITED BY
Shaoquan Zheng,
The First Affiliated Hospital of Sun Yat-sen University, China

REVIEWED BY
Yuzhen Gao,
Zhejiang University, China
Carmen Guerra,
Spanish National Cancer Research Center (CNIO), Spain

*CORRESPONDENCE
Sui-Cai Mi
boyuexinling@163.com

†These authors have contributed equally to this work

SPECIALTY SECTION
This article was submitted to Molecular and Cellular Oncology, a section of the journal Frontiers in Oncology

RECEIVED 27 June 2022
ACCEPTED 16 August 2022
PUBLISHED 06 September 2022

CITATION
Lu H, Zheng L-Y, Wu L-Y, Chen J, Xu N and Mi S-C (2022) The immune escape signature predicts the prognosis and immunotherapy sensitivity for pancreatic ductal adenocarcinoma. *Front. Oncol.* 12:978921. doi: 10.3389/fonc.2022.978921

COPYRIGHT
© 2022 Lu, Zheng, Wu, Chen, Xu and Mi. This is an open-access article distributed under the terms of the Creative Commons Attribution License (CC BY). The use, distribution or reproduction in other forums is permitted, provided the original author(s) and the copyright owner(s) are credited and that the original publication in this journal is cited, in accordance with accepted academic practice. No use, distribution or reproduction is permitted which does not comply with these terms.

The immune escape signature predicts the prognosis and immunotherapy sensitivity for pancreatic ductal adenocarcinoma

Hao Lu†, Li-Yan Zheng†, Ling-Yan Wu†, Jun Chen, Na Xu and Sui-Cai Mi*

Xiamen Hospital of Traditional Chinese Medicine, Xiamen Hospital, Beijing University of Chinese Medicine, Xiamen, China

Background: Pancreatic ductal adenocarcinoma (PDAC) is one of the deadliest malignancies worldwide. Immune escape is considered to be a reason for immunotherapy failure in PDAC. In this study, we explored the correlation between immune escape-related genes and the prognosis of PDAC patients.

Methods: 1163 PDAC patients from four public databases, including The Cancer Genome Atlas (TCGA), International Cancer Genome Consortium (ICGC), Array-express, and Gene Expression Omnibus (GEO), were included in our study. Cox regression analysis was used to identify the 182 immune genes which were significantly associated with overall survival (OS). And then we established an immune escape-related gene prognosis index (IEGPI) score using several datasets as the training cohort and validated it using the validation cohort. Kaplan-Meier (KM) and Cox regression analysis were used to detect the relationship of IEGPI score with OS. We further explored the relationship between the IEGPI and immune indexes. And the prediction value of response for immunotherapy in Tumor Immune Dysfunction and Exclusion (TIDE) dataset.

Results: We establish an IEGPI score based on 27 immune escape genes which were significantly related to the prognosis of OS in PDAC patients. Patients in the high-IEGPI group had a significantly worse overall survival rate compared with that in the low-IEGPI groups by KM curves and cox-regression. 5 of the 32 cancer types in TCGA could be significantly distinguished in survival rates through the low- and high-IEGPI groups. Moreover, the correlation between the IEGPI score was negatively correlated with an immune score in several datasets. And higher IEGPI better recurrence-free survival (RFS) and OS in the patients after patients were treated with both PD-1 and CTLA4 in the public datasets ($P<0.05$). Intriguingly, by using RT-PCR, we verified that the gene of PTPN2, CEP55, and JAK2 were all higher in the BxPC-3 and PANC-1 than HPDE5 cells. Lastly, we found that the IEGPI score was higher in K-

rasLSL.G12D/+, p53LSL.R172H/+, Pdx1Cre (KPC) mice model with anti-PD-L1 than that without anti-PD-L1.

Conclusion: Using the immune escape-related genes, our study established and validated an IEGPI score in PDAC patients from the public dataset. IEGPI score has the potential to serve as a prognostic marker and as a tool for selecting tumor patients suitable for immunotherapy in clinical practice.

KEYWORDS

Pancreatic ductal adenocarcinoma, immune escape, immune infiltration, prognosis, immunotherapy

Introduction

Pancreatic ductal adenocarcinoma (PDAC) is a highly malignant exocrine cancer with a dismal prognosis. Although PDAC has a relatively low incidence worldwide, it ranks the fourth leading cause of cancer-related death in the world (1). Radical surgery is the only effective treatment for the cure of PDAC. Unfortunately, most PDAC patients are present in advanced stages when they are diagnosed and not amenable for surgery. Even when PDACs undergo surgery, the 5-year postoperative survival rate is still not ideal. Despite great advances in chemotherapy for pancreatic cancer, chemo-resistance and toxic side effects also inhibited the improvement of PDAC patients' prognosis after treatment (2). Previous studies have demonstrated the 5-year survival rate of PDAC is less than 9%, which is far lower than that of other malignancies (3, 4).

Recent years, besides chemotherapy (5–7), immunotherapy has become a research hotspot in the treatment of malignances (8, 9), included pancreatic cancer. However, it has a poor effect on pancreatic cancer with PD-1/PD-L1 blockade monotherapy (10). Immune evasion might be the main cause of immunotherapy failure, which reflected in the resistance to immune checkpoint blockade (ICB) therapy (11, 12). More and more studies have disclosed the molecular mechanisms of immune evasion in pancreatic cancer (5, 13, 14), which increases the difficulty in the treatment of PDAC.

Considering the highly lethal characteristic and the poor effect of immunotherapy, PDAC patients' prognosis should be assessed for surgeons to evaluate the treatment benefits through some immune-related gene markers or signatures before surgery.

In this study, we developed and validated an immune escape-related prognostic signature (IEGPI score) with the whole genome expression data from several datasets for PDAC. More importantly, the IEGPI score could identify PDAC patients with an unfavorable prognostic outcome after surgery, and PDAC patients with a high sensitivity to immunotherapy after received with both PD-1 and CTLA4.

Materials and methods

Data source

The gene expression profiles and corresponding clinical data of PDAC were obtained from the TCGA (https://portal.gdc.cancer.gov), ICGC (https://dcc.icgc.org/), Arrayexpress (https://ebi.ac.uk/arrayexpress/), and GEO (GEO, http://www.ncbi.nlm.nih.gov/geo) databases. After we excluded some datasets 1) without overall survival (OS) and survival status; 2) sample size<50, a total of 1137 PDAC patients from seven datasets were enrolled in this study. Six datasets of TCGA-PAAD-US (n=146), ICGC-PACA-AU (n=267), E-MTAB-6134(n=288), GSE71729 (n=125) and GSE57495 (n=63) and GSE62452 (n=66) were used as the training cohorts; one other independent cohort, ICGC-PACA-CA (n=182) was served as an external validation cohort (Supplementary Table S1). The Single-cell dataset for PDAC was extracted from CRA001160. Lastly, the immunotherapy cohorts were downloaded from the TIDE (Tumor Immune Dysfunction and Exclusion, http://tide.dfci.harvard.edu/). The expression data of 6 pair KPC mice with PD-L1 and without PD-L1 were downloaded from GSE196435.

Processing of the immune escape-related genes

Totally, 182 immune escape genes were downloaded from previous study (Supplementary Table S1) (15). First, we stratified each immune escape gene into two groups by the median value in 7 datasets. Second, a univariate Cox regression analysis was

conducted to filter the 182 immune escape genes which are associated with OS in the PDAC patients. Finally, through the fixed-effects model based on meta-analysis, the pooled hazard ratio (HR) with 95% CI of immune escape gene was estimated.

Establishing the prognostic immune escape-related genes signature

For those immune escape genes, the pooled HRs with their standard estimates (SE) which were significantly related to prognosis were then integrated as the prognostic immune escape genes weight, and generated the immune escape-related gene prognosis index (IEGPI) score. In sum, IEGPI from a sample is given by:

$$\text{IEGPIscore} = \sum_{1}^{i}\left(\frac{HR-1}{SE}\right)*Gene(i)$$

In the aforementioned formula, gene (i) was the relative expression of OS-related immune escape genes, and n is the total number of OS-related immune escape genes based on the meta-analysis. In our analyses, the normalized Z-score was used to calculate the score.

Evaluation of tumor immune score

We utilized ESTIMATE (16) to evaluate tumor immune score based on immune gene expression signatures. The immune score, which represents the tumor immune infiltration level, is the fraction of immune cells in bulk tumor.

Estimation of immune cell infiltration

The single-sample gene set enrichment analysis (ssGSEA) (17) was introduced to quantify the relative infiltration of 28 immune cell types in the tumor microenvironment. Unique feature gene panels for each immune cell subset were obtained from the latest literature (18). An enrichment score in ssGSEA analysis represented the relative abundance of each immune cell type. The ssGSEA score was normalized to unity distribution, for which zero is the minimal and one is the maximal score for each immune cell type. The bio-similarity of the immune cell filtration was estimated by multidimensional scaling (MDS) and a Gaussian fitting model.

Evaluation of TMB

For each tumor sample, we determined its TMB as the total count of somatic mutations detected in the tumor. TMB was calculated by dividing the nonsynonymous mutations with 38 Mb as previously reported. In addition, we calculated Oncoplot, mutation landscape, and OncogenicPathways based on TCGAmutation and maftools R packages.

Functional and pathway enrichment analyses

By using the "clusterProfiler" R package (version 4.2.2) (19), the Kyoto Encyclopedia of Genes and Genomes (KEGG) enrichment analysis and Gene Ontology (GO) analysis were performed in our study. Gene Set Enrichment Analysis (GSEA) was used to explore the potential function and signaling pathway enrichment associated with the patients with high and low IEGPI Pancreatic ductal adenocarcinoma cancer.

RT-qPCR for gene expression study

To gain the insight of the characteristics of IEGIP score, we investigated PTPN2, CEP55 and JAK2 as the represented gene of IEGIP score in the cell lines. The sequences of Primer were set as following rules: PTPN2 Forward Primer was "GAAGAGTTGGATACTCAGCGTC", and Reverse Primer was set as "TGCAGTTTAACACGACTGTGAT". CEP55 Forward Primer was "CTTGAGGTTGAACGACAAACCA" and Reverse Primer was "AGCTCTTCGGATCTCTTCTTCTC". JAK2 Forward Primer was "ATCCACCCAACCATGTCTTCC", and Reverse Primer was "ATTCCATGCCGATAGGCTCTG". For cell lines, normal pancreatic ductal epithelial cell (HPDE6-C7 cell, BNCC338285) were purchased from Beijing Beina Chuanglian Institute of Biotechnology (Beijing, China), and PANC-1(GIBCO: 10566016) and BxPC-2(GIBCO: 11875093) were purchased from National Collection of Authenticated Cell Cultures. The condition of RT-qPCR was performed as the following: initial cDNA denaturation was at 95°C for 5 min, and 40 cycles at 95°C for 30s, and annealing temperatures were diversely set at 55°C, and extension at 72°C for 1 min.

Statistical analysis

Continuous variables were analyzed using the student's *t*-test or the Wilcoxon rank sum test, while the categorical variables were compared using the χ^2 or Fisher exact test. The Benjamini–Hochberg (FDR) was also used to adjust the P-values for the multiple comparisons. Immune escape genes with significant prognosis were selected according to the following criteria: meta-analysis, P<0.001, and FDR<0.001. Spearman correlation analysis was used to assess the potential relevance. Univariate and multivariate Cox regression analyses were performed to

explore the independent risk factors of OS and recurrence-free survival (RFS) in PDAC patients. Kaplan–Meier (KM) method and log-rank test were performed to compare the OS rates in each group. Time-dependent ROC curve was done to detect the prognostic value of IEGPI for PDAC patients. The area under the receiver operating characteristic curve (AUROC) was used to estimate the diagnostic value of IEGPI for chemosensitivity. All statistical analysis of all the clinical data was performed in R (version 3.6.2; https://www.r-project.org/). A two-sided P-value< 0.05 was considered statistically significant in all tests.

Results

Immune escape genes associated with prognosis of PDAC

First, in 7 datasets, we used the Cox regression analyses to uncover the 182 immune escape genes which were significantly associated with OS in PDAC patients. The detail information was list in Supplementary Table S1. Second, a meta-analysis (random effects model) was implemented among 7 datasets to harvest pooled HRs and the coefficients of significant genes associated with OS. Finally, we identified 27 immune escape genes which were significantly related to prognosis of OS in PDAC patients (Figures 1A). Of them, 13 were poor prognosis-related genes, and 14 were good prognosis-related genes. The forest plots in Figures 1B, C showed the pooled HRs and 95%CI of the above 27 immune escape genes after a meta-analysis (Supplementary Table S2).

According to the aforementioned formula, we used the 27 immune escape genes to establish an integrated score, namely IEGPI, for every patient in the seven datasets. Their KEGG pathway enrichment results showed in the Supplementary Table S3. Using the single-cell sequencing dataset of CRA001160, we found that IEGPI score was elevated in macrophages and tumor cells compared with other groups in a single-cell analysis (Figures 1D–F and Supplementary Table S4). Additionally, 27 immune escape genes were implemented into GO and KEGG analyses, and the results were illustrated in Figures 1G, H. We found some important items were enriched after GO analysis, such as response to endoplasmic reticulum stress, integral component of endoplasmic reticulum membrane, and cysteine-type peptidase activity. Moreover, some significant pathways such as antigen processing and presentation, JAK-STAT signaling pathway were enriched.

Prognosis estimation of IEGPI score

A correlation plot in Figure 2A demonstrated that there existed a strong correlation between the IEGPI score and most of the 27 immune escape-related genes in PDAC patients. Figures 2B, C showed relationship between HR value (Cox regression analysis of OS) and IEGPI score in the training cohort and validation cohort, respectively, which reflected a near-linear correlation overall.

More importantly, we merged six datasets of PDAC patients and then used the ROC curve finding the best cut-off value to divide patients into two groups (the high-IEGPI vs. low-IEGPI group). We make a KM curve to show the different OS rates between the high-IEGPI and low-IEGPI group (Figure 2D). Patients from the low-IEGPI group had a significantly better survival OS than those from the high-IEGPI group (P<0.001). Supplementary Figure 1 showed the survival differences between the high-and low-IEGPI groups in six different datasets, which also illustrated the same results with the Figure 2D. In addition, a validation cohort of PACA-CA was stratified into two groups used the above cut-off value. The KM curves in PACA-CA cohort also illustrated significantly different OS rates between the two groups (P=0.007) (Figure 2E). In addition, we analyzed the relationship between the IEGPI score and cell signaling pathways in five datasets through KEGG analysis (Figure 2F).

Furtherly, a forest figure in Figure 3A showed the multivariate Cox regression analysis results in seven PDAC datasets (Supplementary Tables S5, S6). We found that IEGPI score was an independent risk factor of OS in all datasets (all P< 0.05). Then we explored the impact of IEGPI score on tumor relapse of PDAC patients in four datasets (E-MTAB-6134, TCGA–PAAD, PACA_AU, and PACA_CA). the results in Figures 3B–E demonstrated that patients in the low-IEGPI group had significantly better relapse-free survival rates compared with those in the high-IEGPI groups (P<0.05).

At last, the TCGA pan-cancer analysis found that 5 types of 32 cancers could be significantly distinguished in survival through the low- and high-IEGPI groups (Figure 3F), suggesting the application potential of IEGPI score for prognostic prediction in other malignant diseases.

Relationship between the mutation genes and IEGPI

We explored the relationship between the IEGPI score and the TMB (tumor mutation burden) value. Figures 4A–C showed that in the PACA-AU cohort, PACA-CA cohort, and TCGA-PAAD cohort, the correlation between the IEGPI score TMB was not vary strong.

We then used the Oncoplot to illustrated the top 15 mutation genes in the High-and low-IEGPI score groups of PDAC, and the results included KRAS, TP53, SMAD4 and CDKN2A, etc. (Figure 4D). Notably, we observed that TP53 had a significantly higher mutation frequency in High-IEGPI group than in low-IEGPI group (Figure 4D). It could explain why High-IEGPI group had the worst prognosis among the two groups since TP53 mutations have been associated with unfavorable outcomes in various cancers.

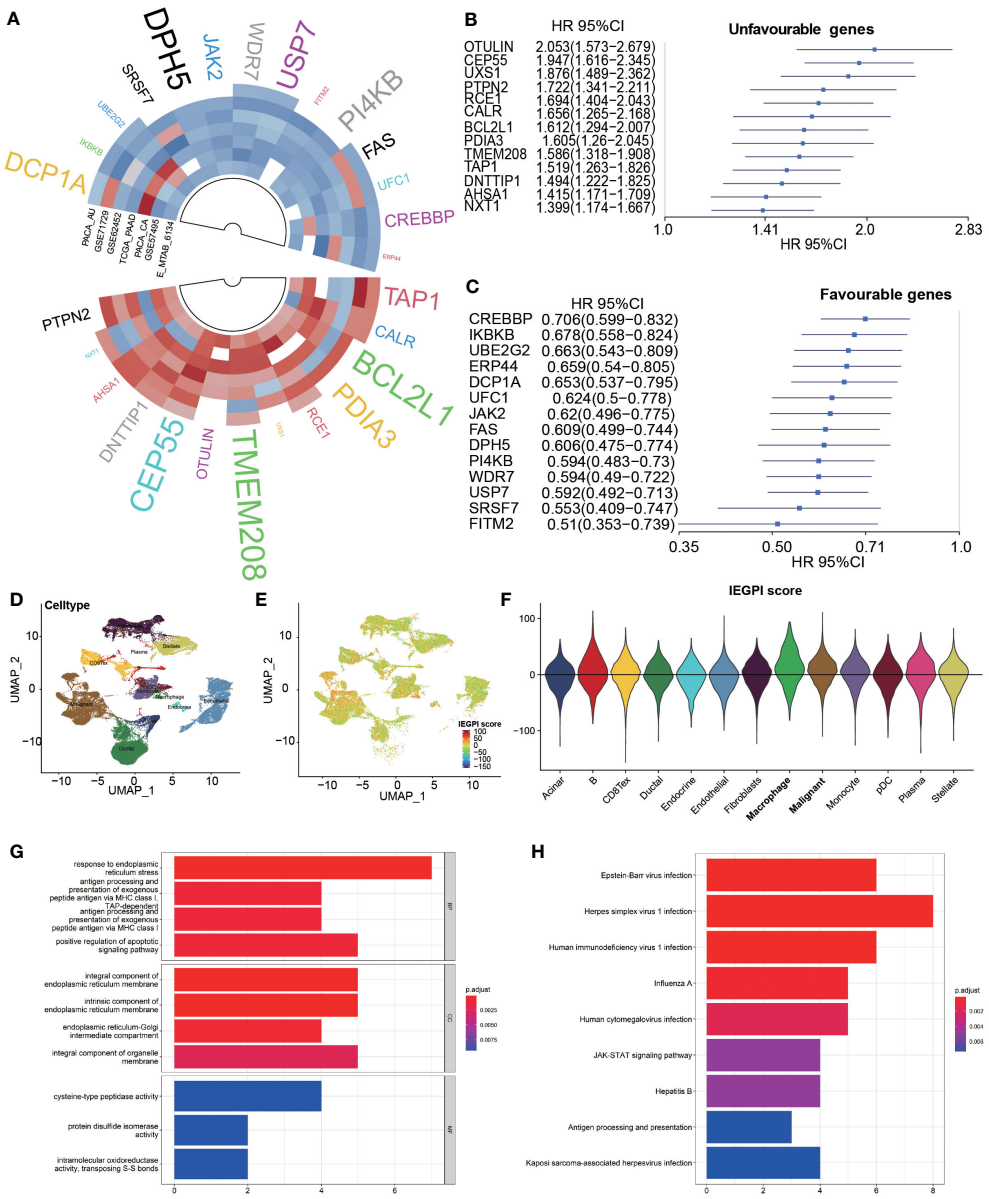

FIGURE 1
Construction of the IEGPI score. **(A–C)** 27 prognostic immune escape genes; **(D–F)** IEGPI score distribution in single-cell sequencing dataset of CRA001160; **(G)** 27 immune escape genes were implemented into GO analyses; **(H)** 27 immune escape genes were implemented into KEGG analyses.

Relationship between the immune infiltration and IEGPI

In order to explore the distribution of immune components in different IEGPI score patients, we used the Spearman correlative analysis to explore the relationship between the IEGPI score and the immune score. Figure 5A showed that in the PACA-AU cohort, TCGA-PADC cohort, E-MTAB cohort, and GSE62452 cohort, the correlation between the IEGPI score was negative linearly correlated with immune score.

In addition, we selected immune genes based on previous studies to study the relationship of the IEGPI score and immune functions (immune co-stimulation and check-point genes). Bubble plot of Figure 5B showed that in seven cohorts, immune genes had a huge-difference relationship with the IEGPI score. Moreover, a total of 28 infiltration immune cell

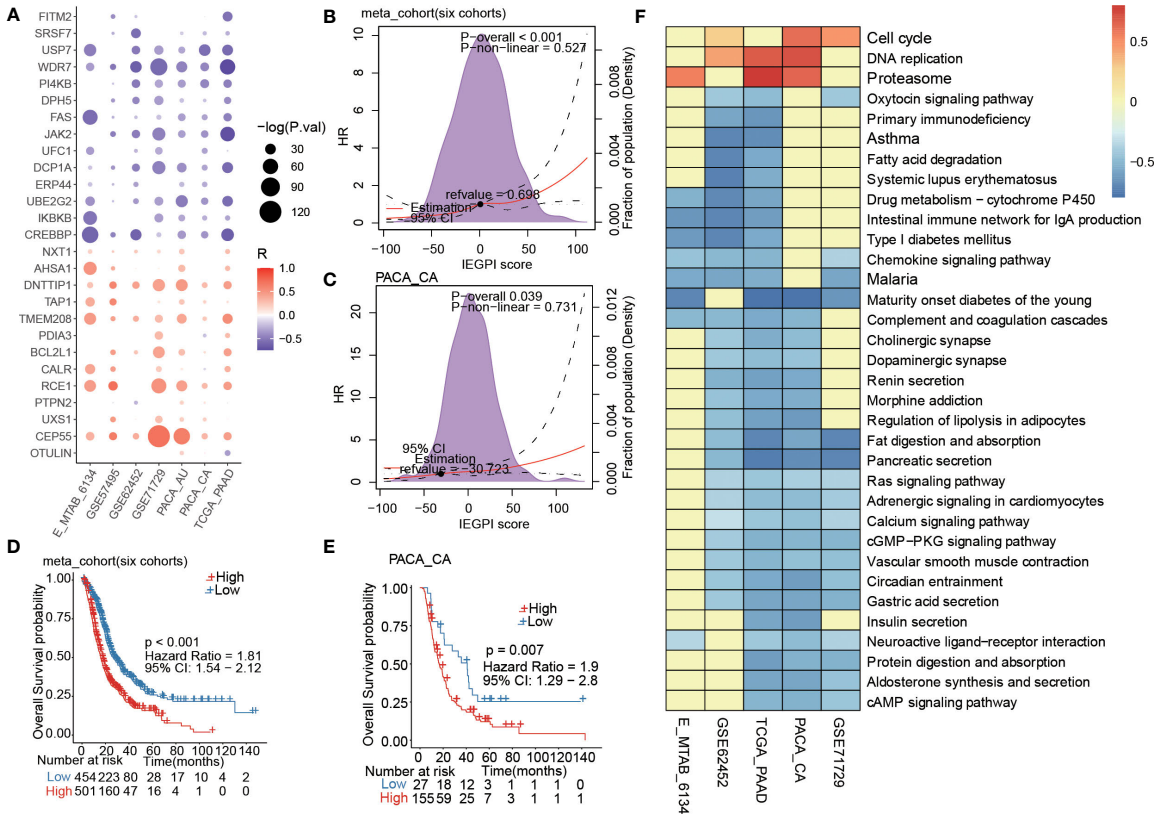

FIGURE 2
Prognostic estimation of IEGPI score. **(A)** Association of the IEGPI score with the 27 prognostic immune escape genes; **(B, C)** the HR value distribution with different IEGPI score in the training and validation cohorts; **(D, E)** Kaplan-Meier curves of IEGPI score in the training cohort and validation cohorts; **(F)** Relationship between the IEGPI score and cell signaling pathways *via* KEGG analyses.

were explored to show their negative relationship with the IEGPI score in in seven cohorts (Figure 5C).

IEGPI score for immunotherapy response prediction

First, using the TIDE dataset, we want to evaluate the IEGPI score's potential as a tool for immunotherapy response prediction in other tumors, such as melanoma, bladder cancer, and lung cancer (Figures 6A–E). We found that in the melanoma cohort treated with both PD1 and CTLA4, the likelihood of predicting a positive immunotherapy response is strong with AUC=0.800. Moreover, we also explored the distribution of IEGPI score in CR/PR and PD/SD, and the results showed that the patients with CR/PR had a higher IEGPI score (P<0.05) in melanoma patients receiving the both PD1 and CTLA4 treatment (Figure 6F). Additionally, the same trend was found in other tumors, although there were no significant differences between the high and low IEGPI score patients (Supplementary Figure S2). Noteworthy, Figures 6G, H showed that high-IEGPI score was associated with better RFS and OS in the melanoma patients treated with both PD-1 and CTLA4 (P<0.05).

Validation of IEGPI *in vitro* and vivo

To validate the reality of IEGPI score, we accessed the gene expression of PTPN2, CEP55 and JAK2 as the represented gene of IEGPI score by using RT-qPCR (Figures 7A–C). PTPN2, CEP55 and JAK2 were all higher in the PDAC related cell lines than normal cell lines *in vitro*. *In vivo*, we calculated the IEGPI in 12 samples of KPC mouse model and found that IEGPI score was higher in the s KPC mouse with PDL1 than that without PDL1 (Figure 7D, E).

Discussion

PDAC, as the most common type of pancreatic cancer, has an extremely poor survival (20). A mount of efforts has been

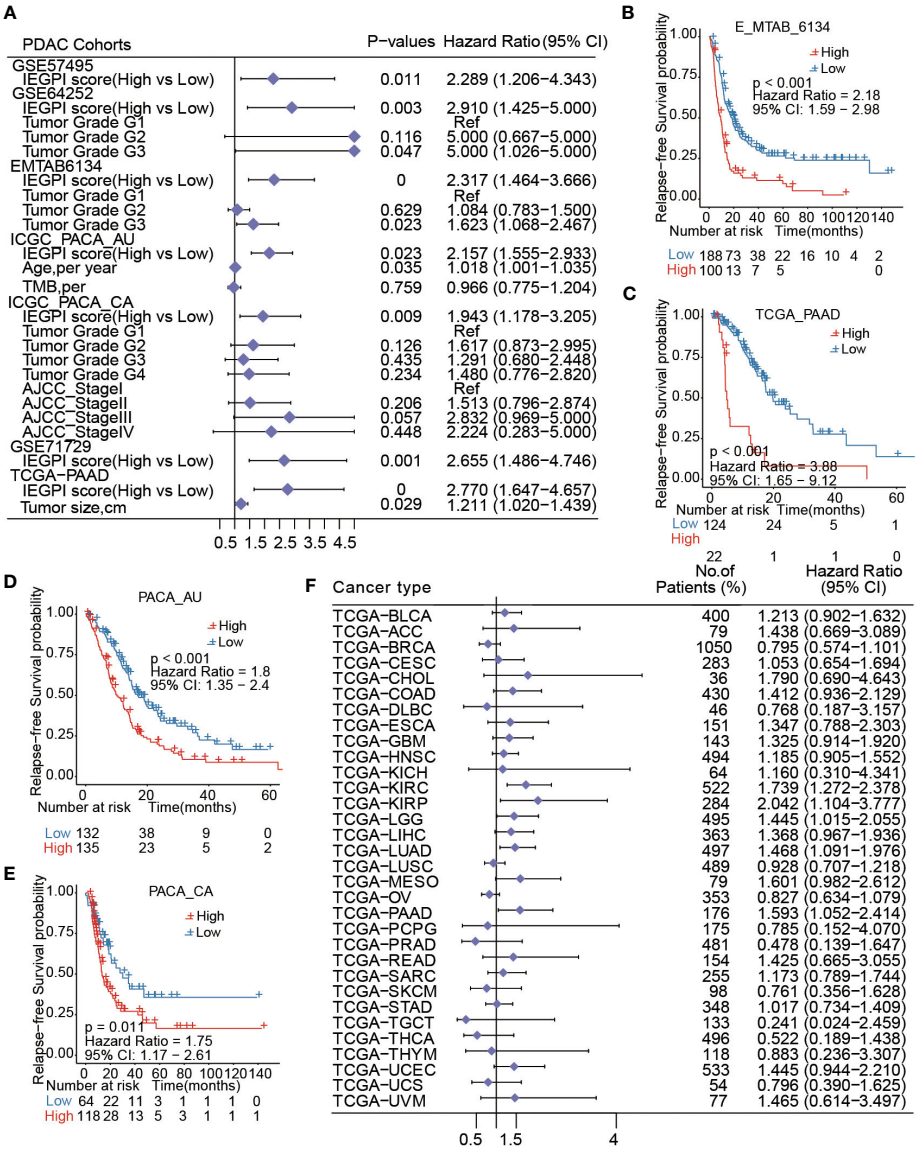

FIGURE 3
IEGPI score was an independent risk factor of OS in PDAC. **(A)** Multivariate Cox regression analysis results in seven PDAC datasets; **(B–E)** Kaplan-Meier curves of relapse-free survival in PDAC patients with different IEGPI score level in four public datasets; **(F)** the prognostic values of the IEGPI score in the Pan-cancer datasets.

underway to find an effective solution to improve the long-term prognosis. Blocking the immune checkpoints, such as targets programmed death 1 or programmed death 1 ligand 1 (PD-1/PD-L1) have been considered as a potential therapeutic target against PDAC. However, the treatment effect of pancreatic cancer is not promising with a single PD-1/PD-L1 blockade (21). Immune escape might be one of the reasons that impaired the PD-1/PD-L1 treatment effect of PDAC.

Recently, immune escape has been considered as an important factor which gives rise to immunotherapy failure in cancer therapy. A variety of factors, such as antigenic variation, lacking infiltration of T cells, and changes in tumor microenvironment, are all associated with immune escape (22). Although more and more mechanisms of immune escape have been found in studies for kinds of cancers recently, no study focus on the relationship of immune escape with the prognosis of cancers. In our study, we identified 27 immune escape-related genes which were significantly correlated with the OS in PDAC using the public datasets. More importantly, we selected the training cohort to establish a scoring system, namely IEGPI, which was used to stratify PDAC patients into two groups with significantly different survival outcomes. Then a

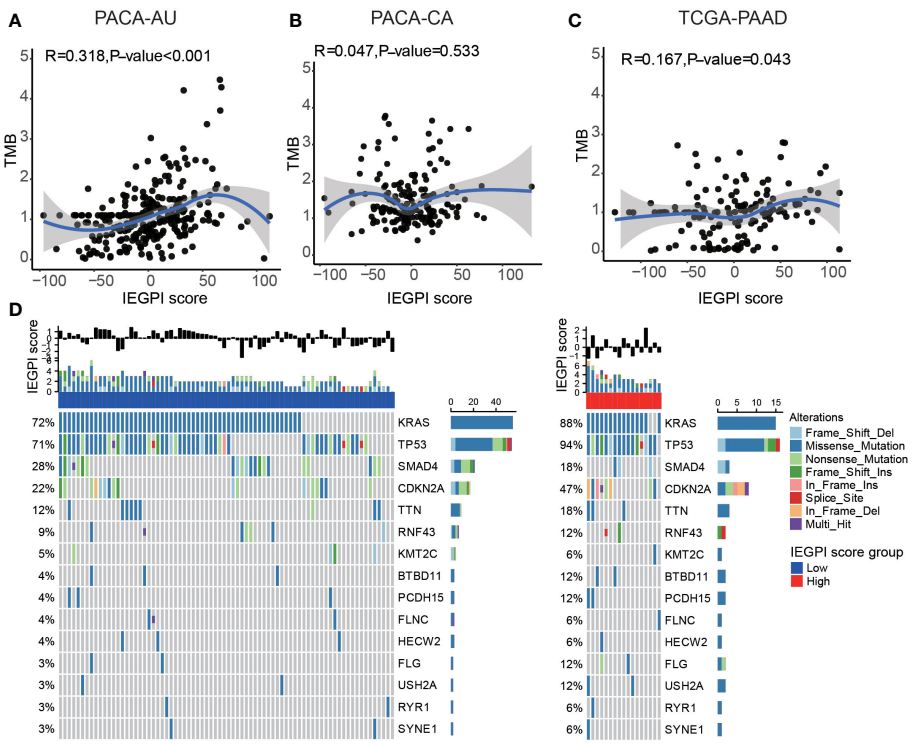

FIGURE 4
Relationship between the mutation genes and IEGPI score. **(A–C)** Relationship between the IEGPI score and TMB score in three public datasets; **(D)** the landscape of top 15-gene mutations in different IEGPI groups.

validation cohort was used to validated and evaluate the prognosis prediction of IEGPI score in PDAC, with a good survival prediction ability in PDAC. Interestingly, the elevated activities of antigen processing and presentation, JAK-STAT signaling pathways have potential contributions to the increased anti-tumor immunity in high-IEGPI score. In addition, we explored the relationship between the TMB, immune infiltration modules and the IEGPI score. Last but not least, we evaluated the ability of IEGPI score for the prediction of immunotherapy response in several cancers, and found that more patients harvested CR/PR have a high IEGPI score, suggesting they achieved a good survival outcome after immunotherapy.

The highlight of this study was that IEGPI score could predict the survival of PDAC patients after surgery, and also could be used as an indicator to reflect the sensibility and response of immunotherapy after receiving the PD-1 and CTLA4 treatments in tumors.

Previous reports have found that inherently immunosuppressive exists in PDAC which leading to a evasion from immune surveillance (23–27). Recently, Wang et al. concluded that the cancer Forkhead box protein 3 (C-FOXP3) can directly activates PD-L1 and mediate the immune escape of PDAC (28). In 2020, Yamamoto et al. identified NBR1-mediated selective macroautophagy/autophagy of MHC-I as a novel mechanism that facilitates immune evasion by PDAC cells (29). In our study, we found 27 immune escape-related genes which were significantly associated with OS in PDAC patients. Immune evasion leads to a poor response to immune checkpoint inhibitors and a poor survival in PDAC. Those genes might be the key genes on which the immunotherapy agents target in the future.

Identified the key immune escape-related genes which are significantly associated with PDAC patient's prognosis is an important method to assess and improve the effect of immunotherapy. In addition, molecular biomarkers based on immune escape-related genes has improved prognosis estimation for PDAC in daily clinical practice (30, 31).

In recent years, researchers have developed a series of evaluation systems used to assess or identify the progression or prognosis risk of pancreatic cancer using the gene expression datasets. For example, Using WGCNA, Giulietti et al. identified several genes (CEACAM1, MCU, VDAC1, CYCS, C15ORF52, TMEM51, LARP1 and ERLIN2) that appear to be critical to PDAC development, which might be potential therapeutic targets with clinical utility (32). In addition, a study built a prognostic score with 20 genes (PPS20) from high-throughput transcriptomic data in pancreatic cancer and found PPS20 was a

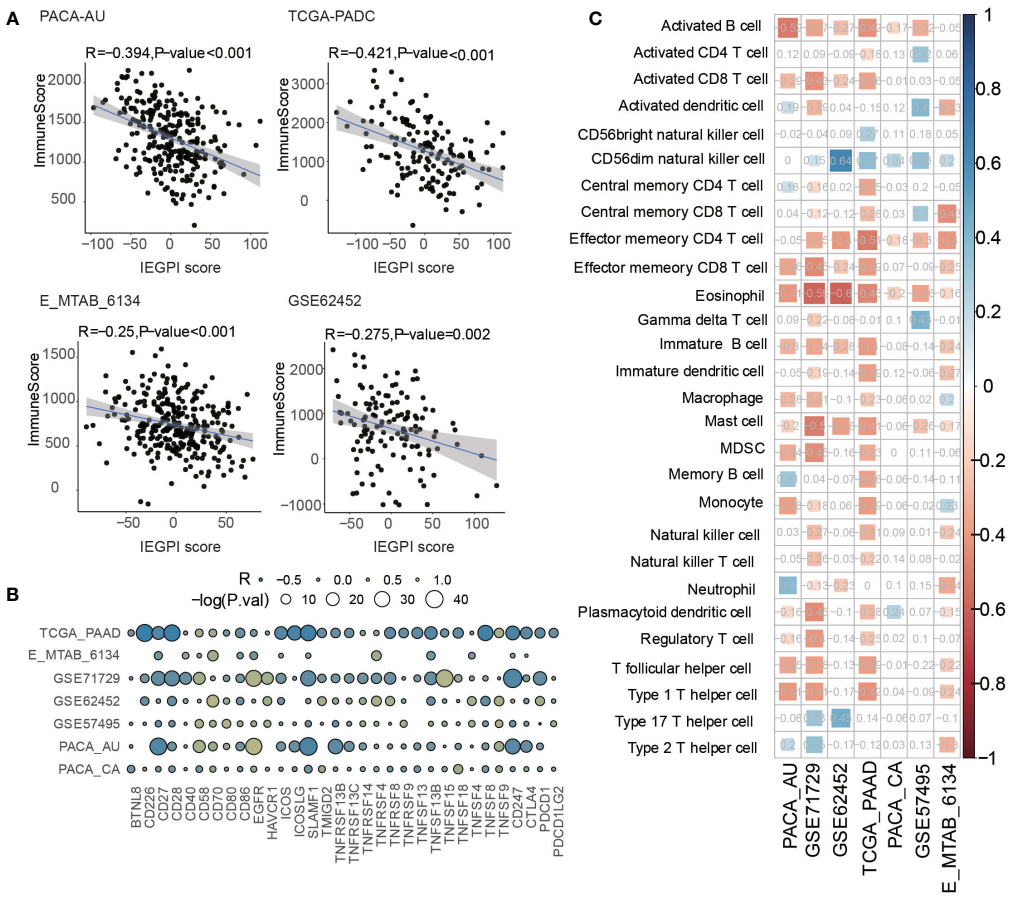

FIGURE 5
Relationship between the immune infiltration and IEGPI score. **(A)** Relationship between the IEGPI score and immune score in four public datasets; **(B)** correlation of the IEGPI score with immune co-stimulation and check-point genes in seven datasets; **(C)** Relationship between the expressions of 28 immune cells and IEGPI score in seven datasets.

more robust transcriptomic signature in prognostic prediction (33). Moreover, a robust 25-gene classifier associated with post-operative OS in pancreatic cancer was identified. It was proved to have a good prognostic value after multivariate analysis (34). However, aforesaid scores or systems don not pay attention to any genes related to immune escape in pancreatic cancer. In our study, we selected immune escape-related genes and developed an IEGPI score to predict the prognosis and distinguish the survival risk of patients.

Collectively, our study firstly integrated 27 prognostic immune escape genes to establish an IEGPI score and validated the expression of PTPN2, CEP55 and JAK2 in cell lines, which shows a good prediction in the prognosis of PDAC and immunotherapy response. The IEGPI might represent a potential prognostic biomarker as well as therapeutic targets of immunotherapy in the future. The higher the IEGPI score is, the higher the level of immune escape is, the worse the killing effect of the body's immune system on tumor cells is, and the worse the prognosis is. However, when patients received immunotherapy, patients with higher IEGPI score were more sensitive to immunotherapy. Because immunotherapy alters the tumor microenvironment, these individuals have a higher CR/PR ratio and better prognosis. Therefore, our IEGPI score also can be used to screen clinical PADC patients for immunotherapy, allowing them to achieve a better prognosis.

In conclusion, basing the public datasets, our study established and validated an IEGPI score which was an independent risk factor of OS in PDAC, and patients in the high-IEGPI group had a worse survival rate after surgery. Using the TIDE datasets, we also found that in melanoma patients who received the PD-L1 and CTLA4 treatments, high IEGPI-score patients had a better OS and RFS. Above results suggested that our IEGPI score has the potential to serve as a prognostic marker and as a tool for selecting tumor patients suitable for immunotherapy in clinical practice.

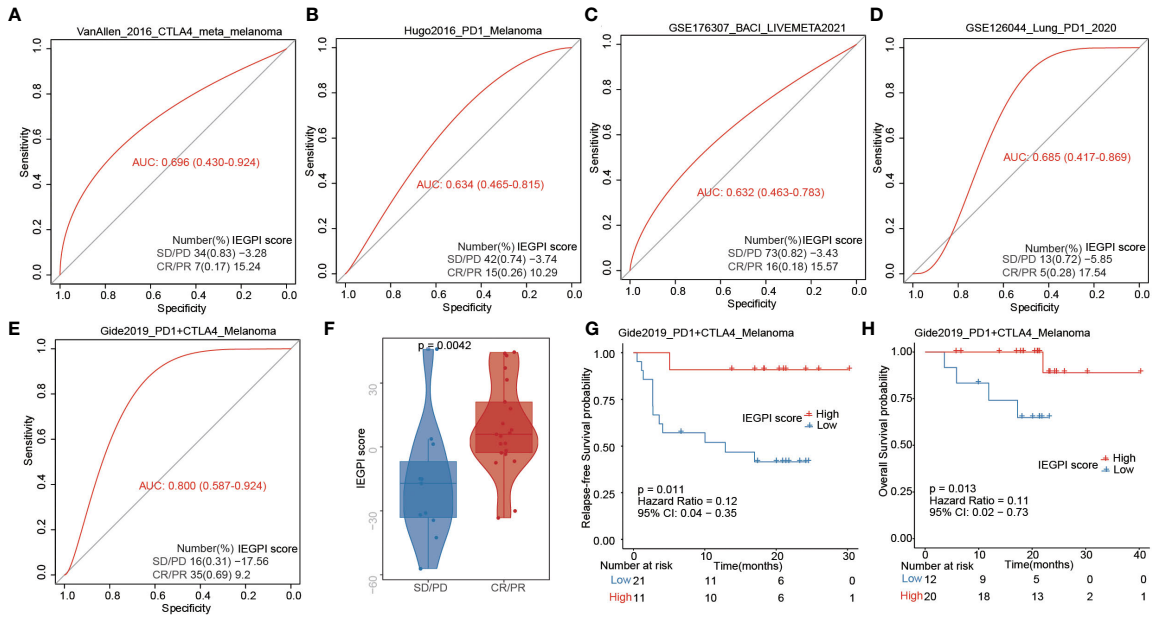

FIGURE 6
IEGPI score for immunotherapy response prediction. **(A–E)** IEGPI score's potential as a tool for immunotherapy response prediction in melanoma, bladder cancer, and lung cancer; **(F)** the distribution of IEGPI score in different immunotherapy response groups with both PD-1 and CTLA4 treatment; **(G, H)** Kaplan-Meier curves of patients with different IEGPI score.

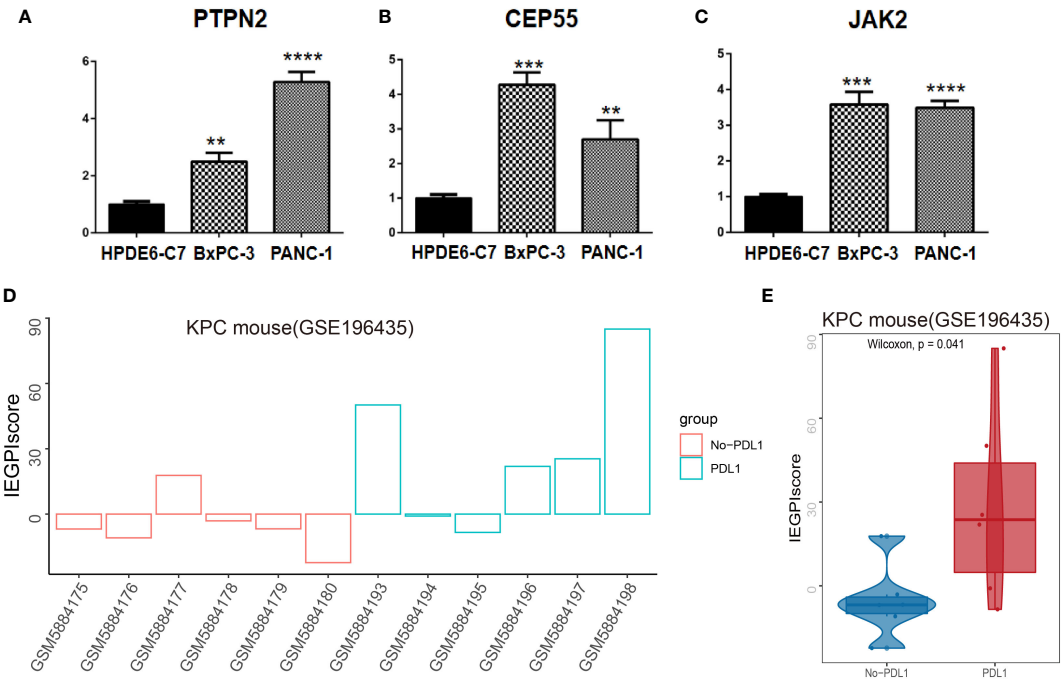

FIGURE 7
Validation of IEGPI score in cell lines and KPC mouse model. RT-PCR for represented IEGPI genes in HPDE6-C7, BxPC-3 and PANC-1. **(A)** PTPN2, **(B)** CEP55, **(C)** JAK2. **(D)** IEGPI score expression of each sample in the KPC mice model with and without PDL1.**(E)** differences of IEGPI score between the KPC mice model with and without PDL1. **P <0.01, ***P <0.001, ****P <0.0001.

Data availability statement

The original contributions presented in the study are included in the article/Supplementary Material. Further inquiries can be directed to the corresponding author.

Author contributions

HL, L-YZ, L-YW and S-CM performed the research. S-CM, and HL designed the research study. HL, L-YZ and L-YW contributed collection and assembly of data. HL, L-YZ and L-YW analysed the data. HL, L-YZ and L-YW wrote the paper. All authors contributed to the article and approved the submitted version.

Conflict of interest

The authors declare that the research was conducted in the absence of any commercial or financial relationships that could be construed as a potential conflict of interest.

Publisher's note

All claims expressed in this article are solely those of the authors and do not necessarily represent those of their affiliated organizations, or those of the publisher, the editors and the reviewers. Any product that may be evaluated in this article, or claim that may be made by its manufacturer, is not guaranteed or endorsed by the publisher.

Supplementary material

The Supplementary Material for this article can be found online at: https://www.frontiersin.org/articles/10.3389/fonc.2022.978921/full#supplementary-material

SUPPLEMENTARY FIGURE 1
Kaplan-Meier curves of IEGPI score in six datasets involving in the training cohort.

SUPPLEMENTARY FIGURE 2
The distribution of IEGPI score in different immunotherapy response groups.

References

1. Ferlay J, Colombet M, Soerjomataram I, Dyba T, Randi G, Bettio M, et al. Cancer incidence and mortality patterns in Europe: Estimates for 40 countries and 25 major cancers in 2018. *Eur J Cancer* (2018) 103:356–87. doi: 10.1016/j.ejca.2018.07.005

2. Merika EE, Syrigos KN, Saif MW. Desmoplasia in pancreatic cancer. can we fight it? *Gastroenterol Res Pract* (2012) 2012:781765. doi: 10.1155/2012/781765

3. Minicozzi P, Cassetti T, Vener C, Sant M. Analysis of incidence, mortality and survival for pancreatic and biliary tract cancers across Europe, with assessment of influence of revised European age standardisation on estimates. *Cancer Epidemiol* (2018) 55:52–60. doi: 10.1016/j.canep.2018.04.011

4. Rawla P, Sunkara T, Gaduputi V. Epidemiology of pancreatic cancer: Global trends, etiology and risk factors. *World J Oncol* (2019) 10:10–27. doi: 10.14740/wjon1166

5. Zhang XP, Chen Q, Liu Q, Wang Y, Wang F, Zhao ZM, et al. Development and validation of glycolysis-related prognostic score for prediction of prognosis and chemosensitivity of pancreatic ductal adenocarcinoma. *J Cell Mol Med* (2021) 25:5615–27. doi: 10.1111/jcmm.16573

6. Wang H, Gao Y, Vafaei S, Yu Q, Zhang J, Wang L, et al. A chemoresistance lncRNA signature for recurrence risk stratification of colon cancer patients with chemotherapy. *Mol Ther Nucleic Acids* (2022) 27:427–38. doi: 10.1016/j.omtn.2021.12.015

7. Gao Y, Chen S, Vafaei S, Zhong X. Tumor-infiltrating immune cell signature predicts the prognosis and chemosensitivity of patients with pancreatic ductal adenocarcinoma. *Front Oncol* (2020) 10:557638. doi: 10.3389/fonc.2020.557638

8. Gao Y, Wang H, Li H, Ye X, Xia Y, Yuan S, et al. Integrated analyses of m(1)A regulator-mediated modification patterns in tumor microenvironment-infiltrating immune cells in colon cancer. *Oncoimmunology* (2021) 10:1936758. doi: 10.1080/2162402X.2021.1936758

9. Chen S, Gao Y, Wang Y, Daemen T. The combined signatures of hypoxia and cellular landscape provides a prognostic and therapeutic biomarker in HBV-related hepatocellular carcinoma. *Int J Cancer* (2022) 151(5):809–24. doi: 10.1002/ijc.34045

10. Morrison AH, Byrne KT, Vonderheide RH. Immunotherapy and prevention of pancreatic cancer. *Trends Cancer* (2018) 4:418–28. doi: 10.1016/j.trecan.2018.04.001

11. Rooney MS, Shukla SA, Wu CJ, Getz G, Hacohen N. Molecular and genetic properties of tumors associated with local immune cytolytic activity. *Cell* (2015) 160:48–61. doi: 10.1016/j.cell.2014.12.033

12. McGranahan N, Rosenthal R, Hiley CT, Rowan AJ, Watkins TBK, Wilson GA, et al. Allele-specific HLA loss and immune escape in lung cancer evolution. *Cell* (2017) 171:1259–71.e1211. doi: 10.1016/j.cell.2017.10.001

13. Yamamoto K, Venida A, Yano J, Biancur DE, Kakiuchi M, Gupta S, et al. Autophagy promotes immune evasion of pancreatic cancer by degrading MHC-I. *Nature* (2020) 581:100–5. doi: 10.1038/s41586-020-2229-5

14. Lim SA, Kim J, Jeon S, Shin MH, Kwon J, Kim TJ, et al. Defective localization with impaired tumor cytotoxicity contributes to the immune escape of NK cells in pancreatic cancer patients. *Front Immunol* (2019) 10:496. doi: 10.3389/fimmu.2019.00496

15. Lawson KA, Sousa CM, Zhang X, Kim E, Akthar R, Caumanns JJ, et al. Functional genomic landscape of cancer-intrinsic evasion of killing by T cells. *Nature* (2020) 586:120–6. doi: 10.1038/s41586-020-2746-2

16. Yoshihara K, Shahmoradgoli M, Martinez E, Vegesna R, Kim H, Torres-Garcia W, et al. Inferring tumour purity and stromal and immune cell admixture from expression data. *Nat Commun* (2013) 4:2612. doi: 10.1038/ncomms3612

17. Hanzelmann S, Castelo R, Guinney J. GSVA: gene set variation analysis for microarray and RNA-seq data. *BMC Bioinf* (2013) 14:7. doi: 10.1186/1471-2105-14-7

18. Charoentong P, Finotello F, Angelova M, Mayer C, Efremova M, Rieder D. Pan-cancer immunogenomic analyses reveal genotype immunophenotype relationships and predictors of response to checkpoint blockade. *Cell Rep* (2017) 18:248–62. doi: 10.1016/j.celrep.2016.12.019

19. Yu G, Wang L-G, Han Y, He Q-Y. clusterProfiler: an r package for comparing biological themes among gene clusters. *OMICS* (2012) 16(5):284–7. doi: 10.1089/omi.2011.0118

20. Haj Mohammad N, Bernards N, Besselink MG, Busch OR, Wilmink JW, Creemers GJ, et al. Volume matters in the systemic treatment of metastatic pancreatic cancer: a population-based study in the Netherlands. *J Cancer Res Clin Oncol* (2016) 142:1353–60. doi: 10.1007/s00432-016-2140-5

21. Feng M, Xiong G, Cao Z, Yang G, Zheng S, Song X, et al. PD-1/PD-L1 and immunotherapy for pancreatic cancer. *Cancer Lett* (2017) 407:57–65. doi: 10.1016/j.canlet.2017.08.006

22. Kim JM, Chen DS. Immune escape to PD-L1/PD-1 blockade: seven steps to success (or failure). *Ann Oncol* (2016) 27:1492–504. doi: 10.1093/annonc/mdw217

23. Witkiewicz A, Williams TK, Cozzitorto J, Durkan B, Showalter SL, Yeo CJ, et al. Expression of indoleamine 2,3-dioxygenase in metastatic pancreatic ductal

adenocarcinoma recruits regulatory T cells to avoid immune detection. *J Am Coll Surg* (2008) 206:849–54. doi: 10.1016/j.jamcollsurg.2007.12.014

24. Crawford HC, Scoggins CR, Washington MK, Leach SD. Matrix metalloproteinase-7 is expressed by pancreatic cancer precursors and regulates acinar-to-ductal metaplasia in exocrine pancreas. *J Clin Invest* (2002) 109:1437–44. doi: 10.1172/JCI0215051

25. Dima SO, Tanase C, Albulescu R, Herlea V, Chivu-Economescu M, Purnichescu-Purtan R, et al. An exploratory study of inflammatory cytokines as prognostic biomarkers in patients with ductal pancreatic adenocarcinoma. *Pancreas* (2012) 41:1001–7. doi: 10.1097/MPA.0b013e3182546e13

26. Zhang H, Liu C, Kong Y, Huang H, Wang C, Zhang H. TGFbeta signaling in pancreatic ductal adenocarcinoma. *Tumour Biol* (2015) 36:1613–8. doi: 10.1007/s13277-014-2757-4

27. Farren MR, Mace TA, Geyer S, Mikhail S, Wu C, Ciombor K, et al. Systemic immune activity predicts overall survival in treatment-naive patients with metastatic pancreatic cancer. *Clin Cancer Res* (2016) 22:2565–74. doi: 10.1158/1078-0432.CCR-15-1732

28. Wang X, Li X, Wei X, Jiang H, Lan C, Yang S, et al. PD-L1 is a direct target of cancer-FOXP3 in pancreatic ductal adenocarcinoma (PDAC), and combined immunotherapy with antibodies against PD-L1 and CCL5 is effective in the treatment of PDAC. *Signal Transduct Target Ther* (2020) 5:38. doi: 10.1038/s41392-020-0144-8

29. Yamamoto K, Venida A, Perera RM, Kimmelman AC. Selective autophagy of MHC-I promotes immune evasion of pancreatic cancer. *Autophagy* (2020) 16:1524–5. doi: 10.1080/15548627.2020.1769973

30. Liang C, Shi S, Qin Y, Meng Q, Hua J, Hu Q, et al. Localisation of PGK1 determines metabolic phenotype to balance metastasis and proliferation in patients with SMAD4-negative pancreatic cancer. *Gut* (2020) 69:888–900. doi: 10.1136/gutjnl-2018-317163

31. Pupo E, Avanzato D, Middonti E, Bussolino F, Lanzetti L. KRAS-driven metabolic rewiring reveals novel actionable targets in cancer. *Front Oncol* (2019) 9:848. doi: 10.3389/fonc.2019.00848

32. Giulietti M, Occhipinti G, Principato G, Piva F. Weighted gene co-expression network analysis reveals key genes involved in pancreatic ductal adenocarcinoma development. *Cell Oncol (Dordr)* (2016) 39:379–88. doi: 10.1007/s13402-016-0283-27

33. Demirkol Canli S, Dedeoglu E, Akbar MW, Kucukkaraduman B, Isbilen M, Erdogan OS, et al. A novel 20-gene prognostic score in pancreatic adenocarcinoma. *PLoS One* (2020) 15:e0231835. doi: 10.1371/journal.pone.0231835

34. Birnbaum DJ, Bertucci F, Finetti P, Birnbaum D, Mamessier E. Molecular classification as prognostic factor and guide for treatment decision of pancreatic cancer. *Biochim Biophys Acta Rev Cancer* (2018) 1869:248–55. doi: 10.1016/j.bbcan.2018.02.001

frontiers | Frontiers in Cell and Developmental Biology

TYPE Original Research
PUBLISHED 13 September 2022
DOI 10.3389/fcell.2022.979262

Check for updates

OPEN ACCESS

EDITED BY
Shaoquan Zheng,
The First Affiliated Hospital of Sun Yat-sen University, China

REVIEWED BY
Yu-Gang Huang,
Hubei University of Medicine, China
Guangxi Wang,
Health Science Centre, Peking University, China

*CORRESPONDENCE
Jian Yang,
yangjian950910@126.com
Xin Tong,
txin@suda.edu.cn
Jun Zhao,
junzhao@suda.edu.cn

†These authors have contributed equally to this work

SPECIALTY SECTION
This article was submitted to Cancer Cell Biology, a section of the journal Frontiers in Cell and Developmental Biology

RECEIVED 27 June 2022
ACCEPTED 22 August 2022
PUBLISHED 13 September 2022

CITATION
Cui Y, Chen Z, Pan B, Chen T, Ding H, Li Q, Wan L, Luo G, Sun L, Ding C, Yang J, Tong X and Zhao J (2022), Neddylation pattern indicates tumor microenvironment characterization and predicts prognosis in lung adenocarcinoma.
Front. Cell Dev. Biol. 10:979262.
doi: 10.3389/fcell.2022.979262

COPYRIGHT
© 2022 Cui, Chen, Pan, Chen, Ding, Li, Wan, Luo, Sun, Ding, Yang, Tong and Zhao. This is an open-access article distributed under the terms of the Creative Commons Attribution License (CC BY). The use, distribution or reproduction in other forums is permitted, provided the original author(s) and the copyright owner(s) are credited and that the original publication in this journal is cited, in accordance with accepted academic practice. No use, distribution or reproduction is permitted which does not comply with these terms.

Neddylation pattern indicates tumor microenvironment characterization and predicts prognosis in lung adenocarcinoma

Yuan Cui[1,2†], Zhike Chen[1,2†], Bin Pan[1,2†], Tong Chen[3], Hao Ding[1,2], Qifan Li[1,2], Li Wan[4], Gaomeng Luo[1,2], Lang Sun[5], Cheng Ding[1,2], Jian Yang[1,2*], Xin Tong[1,2*] and Jun Zhao[1,2*]

[1]Department of Thoracic Surgery, The First Affiliated Hospital of Soochow University, Suzhou, China, [2]Institute of Thoracic Surgery, The First Affiliated Hospital of Soochow University, Suzhou, China, [3]Department of Orthopaedics, The First Affiliated Hospital of Nanjing Medical University, Nanjing, Jiangsu, China, [4]Soochow University Laboratory of Cancer Molecular Genetics, Medical College of Soochow University, Suzhou, China, [5]Department of Cardiovascular Surgery, The First Affiliated Hospital of Soochow University, Suzhou, China

Background: Lung adenocarcinoma (LUAD) is the most common type of lung cancer with a complex tumor microenvironment. Neddylation, as a type of post-translational modification, plays a vital role in the development of LUAD. To date, no study has explored the potential of neddylation-associated genes for LUAD classification, prognosis prediction, and treatment response evaluation.

Methods: Seventy-six neddylation-associated prognostic genes were identified by Univariate Cox analysis. Patients with LUAD were classified into two patterns based on unsupervised consensus clustering analysis. In addition, a 10-gene prognostic signature was constructed using LASSO-Cox and a multivariate stepwise regression approach.

Results: Substantial differences were observed between the two patterns of LUAD in terms of prognosis. Compared with neddylation cluster2, neddylation cluster1 exhibited low levels of immune infiltration that promote tumor progression. Additionally, the neddylation-related risk score correlated with clinical parameters and it can be a good predictor of patient outcomes, gene mutation levels, and chemotherapeutic responses.

Conclusion: Neddylation patterns can distinguish tumor microenvironment and prognosis in patients with LUAD. Prognostic signatures based on neddylation-associated genes can predict patient outcomes and guide personalized treatment.

KEYWORDS

lung adenocarcinoma, neddylation, tumor microenvironment, prognostic signature, therapeutic response

Introduction

Lung cancer is a malignant tumor with high morbidity and mortality worldwide (Ferlay et al., 2018; Cao et al., 2020). Histological subtypes of lung cancer can be classified into small cell lung cancer (SCLC) and non-small cell lung cancer (NSCLC). NSCLC can also be divided into lung squamous cell carcinoma (LUSC), lung adenocarcinoma (LUAD), and lung large cell carcinoma (Denisenko et al., 2018). Among them, LUAD is the most common histological subtype and patients with advanced LUAD often have poor prognoses (Hirsch et al., 2017). In addition, LUAD exhibits strong heterogeneity due to the complex tumor microenvironment (TME) and gene mutations (Wang et al., 2018; Jia et al., 2022). Therefore, early risk stratification and individualized treatment have a realistic value for patients with LUAD.

The pathogenesis of LUAD is complex and diverse. In recent years, the role of post-translational modification (PTM) in LUAD has been extensively studied (Park et al., 2020; Bajbouj et al., 2021; De et al., 2021). PTMs can affect the occurrence and development of LUAD by altering target protein activity, protein stability, protein interaction, and intracellular distribution (Stram and Payne, 2016). To date, more than 450 unique protein modifications have been identified (Chen et al., 2020). Like ubiquitination, neddylation can be divided into three steps. First, the neddylation E1 activating enzyme (NAE; a dimer of NAE1 and UBA3) activates the Neural Precursor Cell Expressed Developmentally Downregulated Protein 8 (NEDD8). The NEDD8 is then transferred to the neddylation E2 binding enzyme (UBE2M or UBE2F), and finally to the lysine residues of the target protein in the presence of neddylation E3 ligase which usually contains the cullin structure (Pellegrino et al., 2022). PTMs are involved in the activation of oncogenes, inactivation of tumor suppressor genes, and continuous activation of associated signaling pathways (Perkins, 2006; Han et al., 2018; Chen et al., 2020). Additionally, studies also have shown that many tumor-associated proteins have been reported to be neddylated, but the specific role of neddylation is unclear (Zhao et al., 2014).

The development of cancer is not only related to the characteristics of tumor cells but also linked to the TME. TME consists mainly of immune cells, such as T cells, B cells, and NK cells, and stromal cells, such as fibroblasts and endothelial cells (Domingues et al., 2016). The different immune cells play varied roles in tumor cell proliferation, apoptosis, and metastasis. Therefore, the number and proportion of immune cells in metastatic tissues play an important role in the classification of tumor subtypes (Hanahan and Coussens, 2012; Gambardella et al., 2020). For example, infiltration of $CD8^+$ T cells is often associated with a positive prognosis, whereas polarization of M2 macrophages is considered a negative prognostic marker (Petitprez et al., 2020). Numerous studies show that a wide range of proteins in immune and tumor cells undergo extensive neddylation, and high expression levels of many neddylation-associated proteins in tumors were indicative of poor patient outcomes (Chang et al., 2012; Li et al., 2013; Zhou L. et al., 2019). Therefore, by regulating the abundance of immune cells in TME, neddylation modification may provide new insights into the pathogenesis and treatment of LUAD.

Materials and methods

Data collection and processing

The LUAD expression profile, clinical information, and mutation data were downloaded from the TCGA (The Cancer Genome Atlas) database. After standardization and data collation, 500 tumor samples were eventually obtained from TCGA for further study. Expression profile and clinical information data from the GSE72094 dataset were obtained from the Gene Expression Omnibus (GEO) database. After standardization and data collation, 398 tumor samples from the GSE72094 dataset were finally obtained. Neddylation-associated genes were obtained from the Reactome database (https://reactome.org/). Genetic mutation data and Copy Number Variation (CNV) data were downloaded from the TCGA-LUAD. Public databases GeneMANIA (https://genemania.org/) and STRING (https://cn.string-db.org/) are used to analyze the protein-protein interactions.

Unsupervised consensus clustering

In this study, a Univariate Cox analysis of neddylation-associated genes was performed and 76 prognostic genes based on the clinical information and expression data were finally obtained from the TCGA database. Unsupervised consensus clustering analysis based on expression profile data from 76 prognostic genes was carried out using the R package "ConsensusClusterPlus" (Wilkerson and Hayes, 2010). The optimal clustering number was selected based on the Cumulative Distribution Curve. Principal Component Analysis (PCA) further confirmed the validity of clustering. Consensus clustering of differentially expressed core genes between two neddylation patterns used the same approach, and two genomic subtypes were eventually obtained.

Tumor immune microenvironment

In this study, ESTIMATE (Yoshihara et al., 2013), EPIC (Racle et al., 2017), TIMER (Li et al., 2016), and single-sample Gene Set Enrichment Analysis (ssGSEA) algorithms (Lin et al., 2021) were used to determine the TME. The ESTIMATE algorithm evaluated the ESTIMATE score, immune score, and stromal score, and analyzed tumor purity. The EPIC algorithm was used to demonstrate the infiltration abundance of seven immune cell types in the tumor. The

TIMER algorithm was applied to evaluate the infiltration abundance of six immune cell types. Additionally, the ssGSEA algorithm calculated the infiltration abundance of 24 immune cell types (Bindea et al., 2013).

Functional enrichment analysis and identification of core gene networks

The gene set variation analysis (GSVA) algorithm was used to analyze functional differences between two neddylation patterns (Hanzelmann et al., 2013). Hallmark gene sets were downloaded from the GSEA website (Liberzon et al., 2015). The enrichment score of each sample in the gene set was calculated using the R package "GSVA," resulting in enrichment score matrix. Mariathasan et al. (2018) compiled nine tumor-associated biological pathways. Differential genes between the two neddylation patterns were obtained using the R package "limma" (Ritchie et al., 2015). Kyoto Encyclopedia of Genes and Genomes (KEGG) and Gene Ontology (GO) databases were analyzed based on differentially expressed genes (FDR < 0.05, |log2FC| > 1) between the two patterns (The Gene Ontology, 2019; Kanehisa et al., 2021). KEGG analysis was performed using the R package "Cluster Profiler" (version 3.14.3). Metascape website was used to carry out GO analysis (Zhou Y. et al., 2019). The protein-protein interaction (PPI) network was constructed using the STRING database and the network connection type to "physical connection" with a confidence score of ≥0.4 was set (Szklarczyk et al., 2021). In addition, to build the network, Cytoscape software was used to calculate Degree scores and screen for core genes (Degree > 10) (Shannon et al., 2003).

Construction of neddylation score

In this study, R package "glmnet" was used to perform LASSO-Cox analysis (10-fold cross-validation). Multivariate stepwise regression was then performed on 17 genes obtained from LASSO. Finally, a prognostic signature consisting of 10 genes was developed. The formula for the signature was computed as follows: risk score = [Coef(1) × gene Exp(1)] + [Coef(2) × gene Exp(2)] + ... + [Coef(i) × gene Exp(i)] (Tibshirani, 1997; Wang et al., 2019). Prognostic analysis was performed by Kaplan-Meier curve using R packets "survival" and "survminer." The R packages "timeROC" and "survival" were used to assess 1-, 3-, and 5-year survival.

Prediction of chemotherapeutic drug sensitivity

R package "pRRophetic" was used to predict the efficacy of chemotherapy drugs (Geeleher et al., 2014). Minimum drug inhibition concentrations (IC_{50}) were calculated for each sample based on expression profile data from patients with LUAD. By comparing chemotherapeutic drug sensitivity between high- and low-risk groups, better personalization of LUAD treatment was possible by selecting specific drugs.

Results

Prognostic value and genetic variation of neddylation-associated genes in lung adenocarcinoma

Various types of PTMs include hydroxylation, lipidation, glycosylation, disulfide bond, ubiquitination, methylation, phosphorylation, acetylation, SUMOylation, lactylation, neddylation, etc. (Figure 1A). Studies have shown that protein PTMs play a crucial role in many biological processes in cancer malignancy. Neddylation is an important PTM, and a reversible process regulated by NEDD8, neddylation E1 activating enzymes (NAE1, UBA3), neddylation E2 binding enzymes (UBE2M, UBE2F), neddylation E3 ligases, de-neddylation proteins, etc. (Figure 1B). Neddylation affects the stability, conformation, and function of substrate proteins, which in turn regulate nuclear localization, intracellular signaling, DNA damage response, cell cycle, apoptosis, and the TME. Based on the role of neddylation in tumor progression, the gene set from the Reactome database was obtained, and neddylation-associated proteins were selected for further study. Figures 1C,D showed the flowchart of our study in LUAD. In this study, a Univariate Cox analysis of neddylation-associated genes was performed and 76 genes with prognostic values were identified (Figure 2A). To further explore the value of these 76 genes in tumors, their mutational status in LUAD was analyzed. A total of 135 samples were found to have mutations in these genes in 500 tumor samples, with an overall incidence of 27%, mainly in the form of missense mutations and nonsense mutations (Figure 2B). In addition, CNV analysis of the prognostic genes was also conducted. CNV amplifications were prevalent in many genes, especially PMD4 and PMB4, whereas CNV deletions mainly existed in PMA5, PMD13, and UBE2M (Figure 2C). CNV occurred on many chromosomes but was mainly concentrated on chromosomes 1, 2, 3, 7, 11, 12, 14, 15, 17, and 19 (Figure 2D). A PPI network of neddylation-related prognostic genes was also constructed. The protein network consisted of seven types of connections: physical interactions, predicted, co-expression, pathway, shared protein domains, co-localization, and genetic interactions. The neddylation-associated genes were found to have a common interaction and were predicted to play a synergistic role in tumors. To further explore the function of 76 prognostic genes, an enrichment analysis was performed using metascape (Supplementary Figures S1A,B). The results showed that these genes play an important role in biological processes such as neddylation, antigen processing, protein modification, and negative regulation of the immune system process.

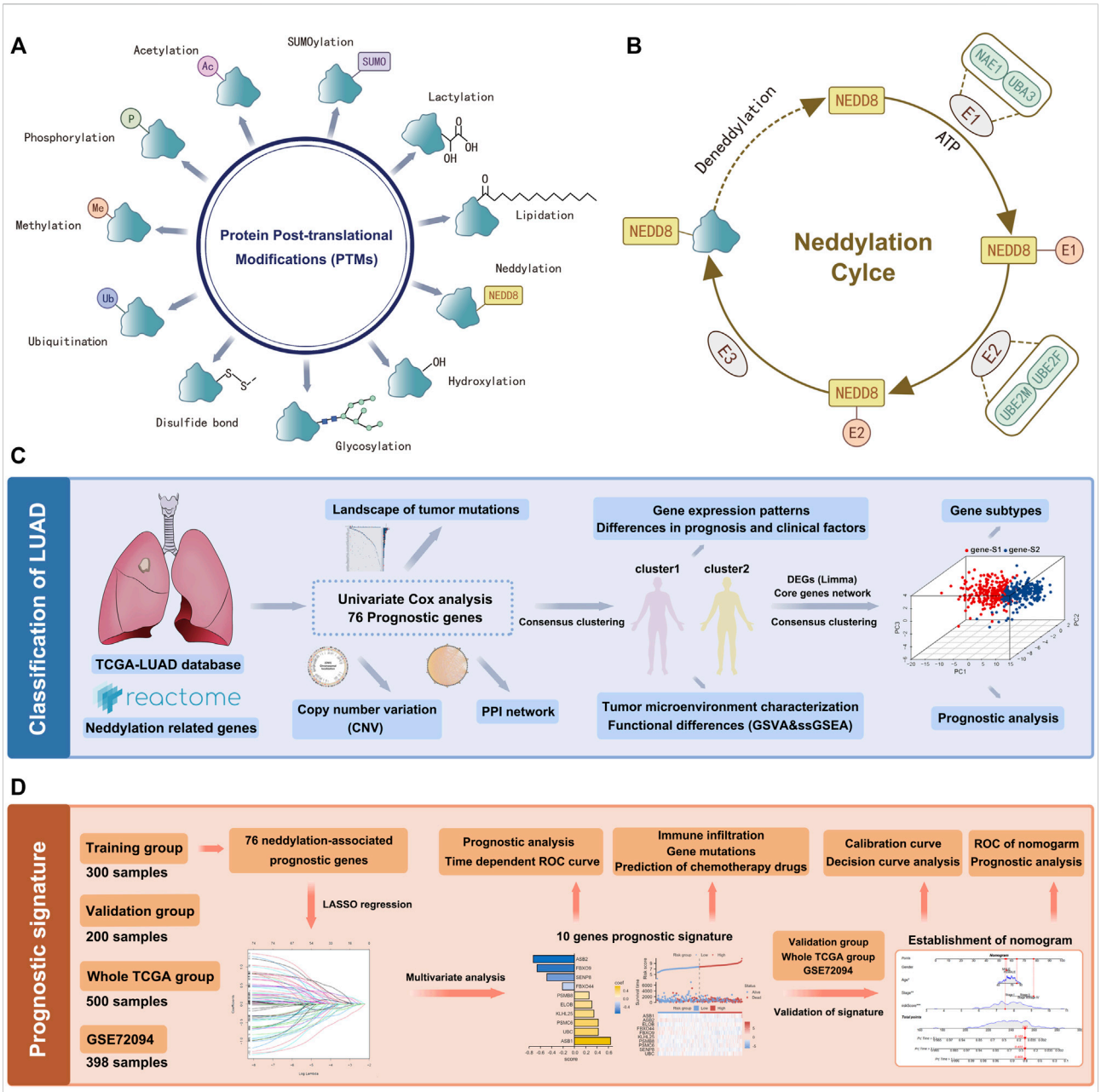

FIGURE 1
Flow chart of the data analysis. **(A)** PTMs of proteins. **(B)** Process of neddylation modification. **(C)** LUAD classification based on neddylation-related genes. **(D)** Prognosis signature based on neddylation-related genes.

Identification of two different molecular patterns of lung adenocarcinoma based on neddylation-related genes

Based on consensus clustering, the TCGA obtained LUAD samples were categorized into two patterns using neddylation-associated prognostic genes (Figure 3A). The highest stability between the two patterns existed when $k = 2$ (Figure 3B). Principal component analysis (PCA) further validated the significant differences between the two patterns (Figure 3C). The two patterns were labeled as neddylation cluster1 and neddylation cluster2, respectively. The two patterns differed in clinicopathologic factors in patients with LUAD (Figure 3D). Cluster1 had more male patients and also more patients aged ≤65 years compared with cluster2. Considering pathological stage, cluster1 had more patients with

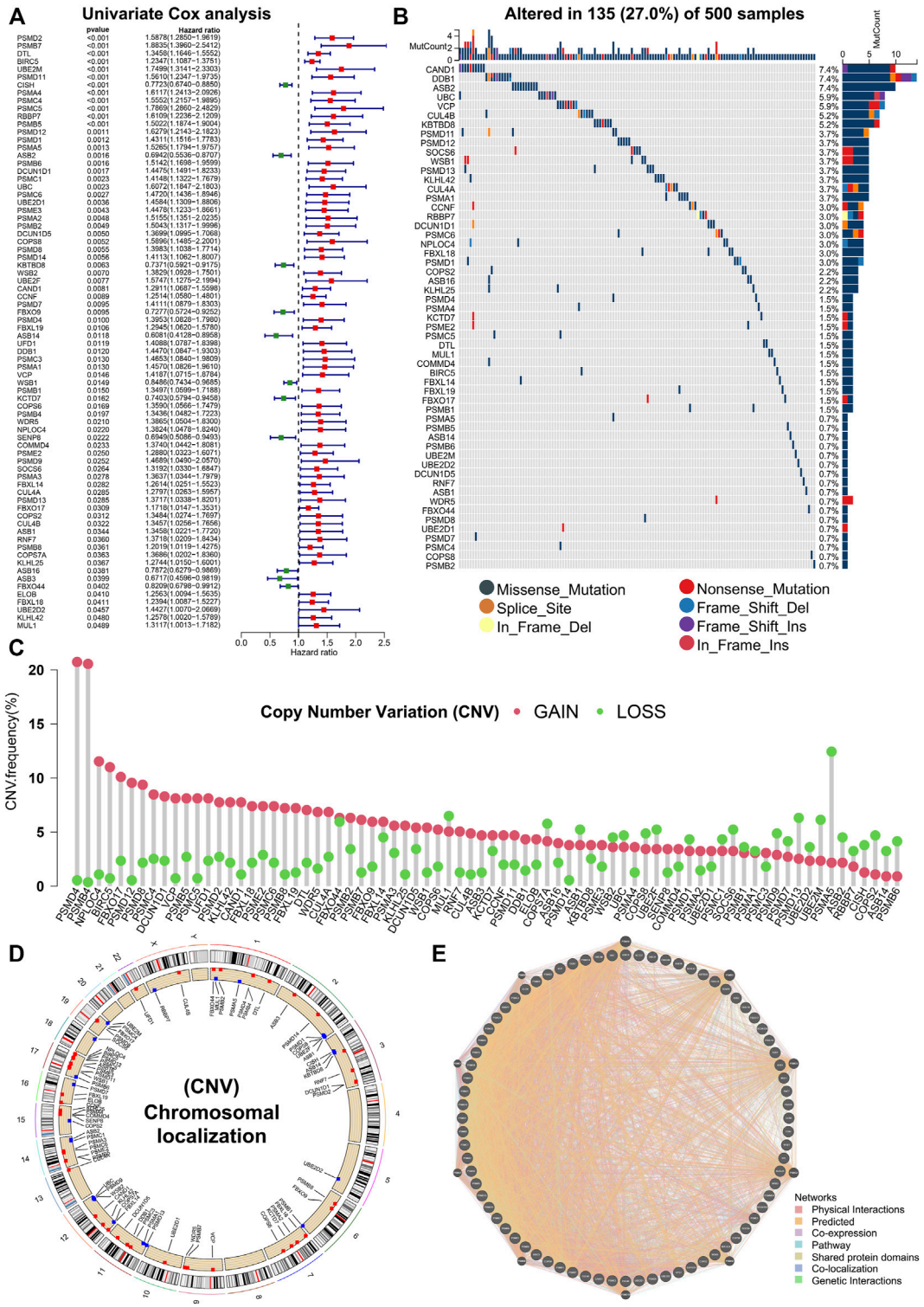

FIGURE 2
Genetic variants in 76 prognostic genes. **(A)** Univariate Cox analysis identifying 76 prognostic genes. **(B)** Mutation landscape of prognostic genes. **(C,D)** CNV in prognostic genes. **(E)** PPI network of prognostic genes.

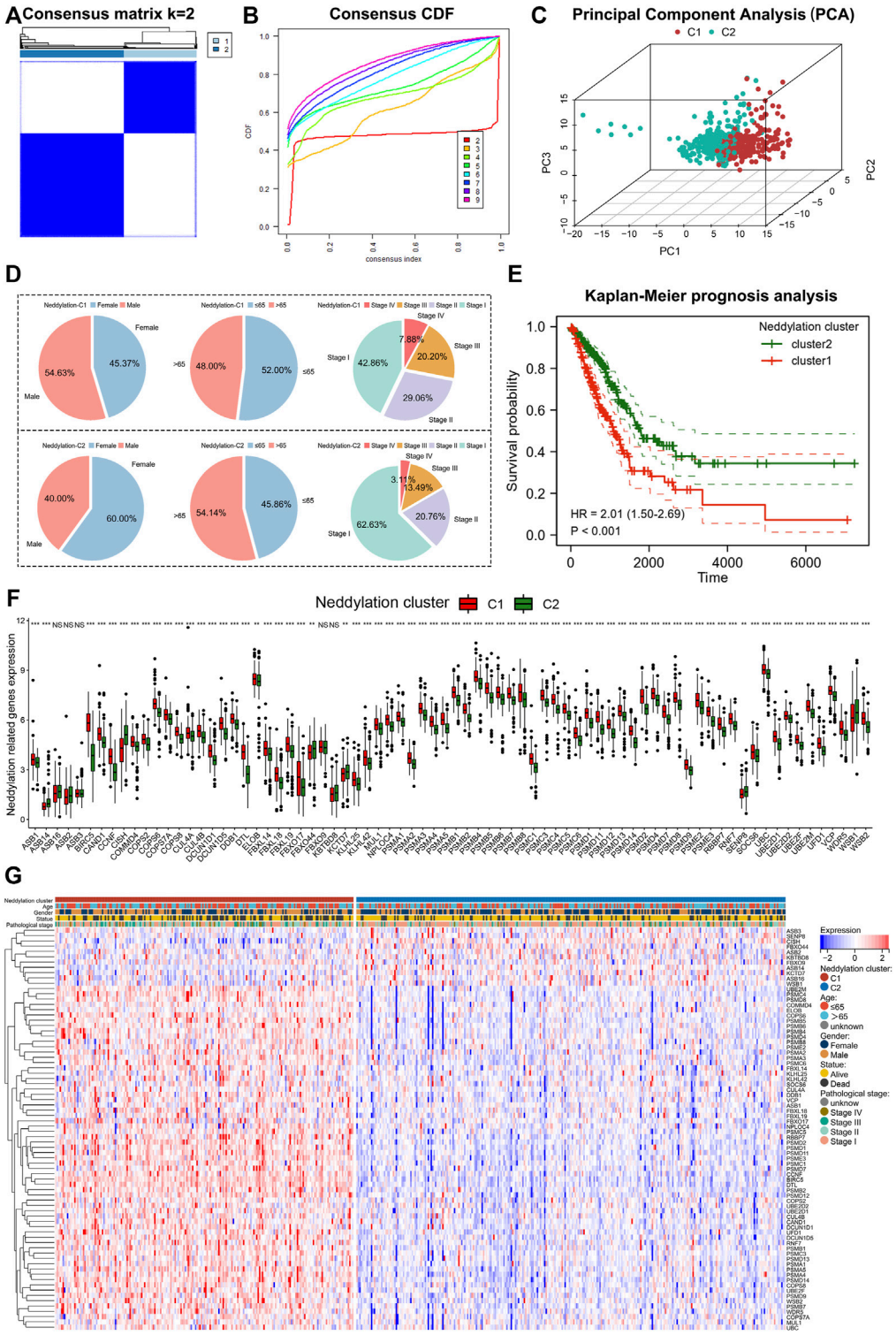

FIGURE 3
Identification of two patterns associated with neddylation. **(A,B)** Consensus clustering of 76 genes in LUAD. **(C)** PCA in two patterns. **(D)** Differences in clinical factors between the two patterns. **(E)** Differences in prognosis between the two patterns. **(F,G)** Expression of 76 prognostic-related genes in two patterns.

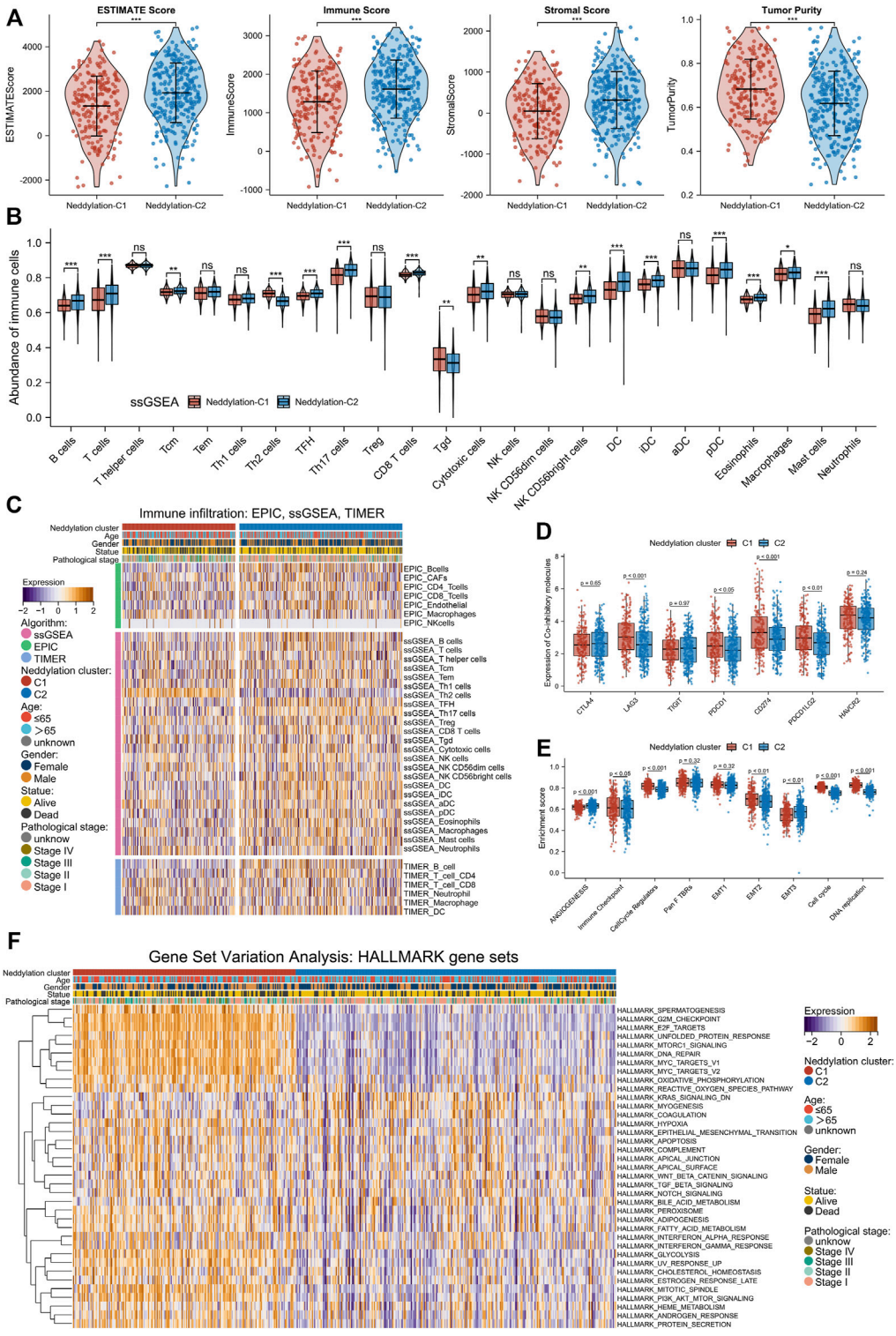

FIGURE 4
Two patterns revealed differences in TME and biological function. **(A)** ESTIMATE score, immune score, stromal score, and tumor purity of the two patterns. **(B)** Abundance of infiltration of 24 immune cells calculated by ssGSEA algorithm. **(C)** Differences in immune infiltration abundance between different patterns and clinical factors (EPIC, TIMER, ssGSEA algorithm). **(D)** Differences in expression of immune co-inhibitors between the two subtypes. **(E)** Calculation of enrichment scores of nine gene sets using ssGSEA algorithm. **(F)** Statistical differential pathways obtained by GSVA algorithm.

pathological stage III and stage IV tumors compared with cluster2. Cluster1 also demonstrated a worse prognosis than cluster2 using patient outcomes (Figure 3E). The expression of 76 prognostic genes between the two patterns was explored. The vast majority of neddylation-related genes are differentially expressed in both patterns (Figures 3F,G). Therefore, further exploring the two patterns of LUAD is of practical significance.

Immune landscape and functional differences between the two patterns

The immune infiltration abundance of TCGA samples was calculated using the ESTIMATE algorithm. By comparing the scores of cluster1 and cluster2, cluster1 was found to have higher tumor purity but conversely lower ESTIMATE, immune, and stromal scores (Figure 4A). These results were further validated by using ssGSEA, TIMER, and EPIC algorithms: results of the ssGSEA algorithm, which calculated enrichment scores for 24 immune cell types, revealed that cluster1 generally had a lower abundance of immune cells such as B cells, T cells, $CD8^+$ T cells, cytotoxic cells, dendritic cells (DC), and mast cells (Figure 4B); the TIMER and EPIC algorithms calculated enrichment scores for six and seven immune cell types, respectively, and results from both indicated that cluster1 had a lower abundance of $CD4^+$ T cells and B cells (Figure 4C). In short, these four algorithms suggested that cluster1 had lower levels of immune infiltration and was favorable for tumor escape. These findings were consistent with the prognostic results between the two patterns. Besides, immunotherapies targeting immune co-suppressor molecules have become a very important topic in the clinical treatment of lung cancer, particularly in treating adenocarcinoma. The differences in immune checkpoint expression levels between the two patterns were compared. As shown in Figure 4D, cluster1 had higher expression levels of LAG3, PDCD1, CD274, and PDCD1LG2 compared to cluster2, suggesting that patients in cluster1 may benefit from immunotherapies. To further investigate the differences in the functional mechanism between the two patterns, the ssGSEA method was used to compute nine gene sets reported by Mariathasan et al. (Angiogenesis, Immune checkpoint, Cell cycle regulators, Pan F TBRs, EMT1, EMT2, EMT3, Cell cycle, DNA replication). Results showed that cluster1 had higher levels of immune checkpoints, cell cycle regulators, EMT2, cell cycle, and DNA replication (Figure 4E). This meant that patients with LUAD in cluster1 had higher expression of immune checkpoints and also enhanced biological functions associated with cell proliferation and metastasis. In addition, the GSVA analysis was used to calculate scores for 50 gene sets from the Hallmark pathway and ultimately found statistical differences in 37 pathways between the two patterns (Figure 4F). Notably, cluster1 was significantly enriched at G2M checkpoints, DNA repair, E2F targets, MTORC1 signaling, MYC targets, Glycolysis, EMT, TGF-β signaling, PI3K-AKT-MTOR signaling, and many other tumor progression–related pathways (Supplementary Figure S2). Combining the results of ssGSEA and GSVA algorithms, cluster1 was found to exhibit a pro-tumor progression pattern in molecular mechanisms, which better explained the worse prognosis observed in the patients of this pattern.

Construction of two genomic subtypes based on differentially expressed genes

Using the R package "limma," differentially expressed genes between the two patterns ($|\log2FC| > 1$, FDR < 0.05) were identified. The red dots on the volcanic map were the upregulated genes and the blue dots were the downregulated genes (Figure 5A). Based on differentially expressed genes, KEGG and GO analyses were performed. Eight pathways were observed to be enriched by KEGG Figure 5B. Substantial enrichment of the cell cycle–related pathways was observed (Supplementary Table S1). Additionally, GO analysis was performed using metascape and enriched modules were exhibited in different color regions (Figure 5C). In these modules, many biological functions such as cell cycle, DNA replication, and cell cycle checkpoints were found to be involved; these results were consistent with the KEGG analysis. To further investigate the core genes that play a central role in these differentially expressed genes, constructed a core PPI network was constructed using the STRING database (network type: physical subnetwork, the minimum required interaction score: 0.4) and Cytoscape software (Cytohubba plugin, Degree > 10). Eventually, a core network of 62 genes was obtained (Figure 5D). A Univariate Cox analysis was performed on 62 core genes and all the core genes were found to be related to prognosis (Figure 5E). To further investigate the overall role of core genes, an unsupervised consensus clustering was used to classify the patients with LUAD obtained from the TCGA. Notably, patients with LUAD can be classified into two genomic subtypes, called genesubtype-S1 and genesubtype-S2 (Figures 5F,G). Results from the PCA showed significant differences between the two genomic subtypes (Figure 5H). It was observed that the prognosis of patients in genesubtype-S1 was worse (Figure 5I). A Sankey diagram was drawn to better understand the direct relationship between neddylation patterns and genomic subtypes and observed that the vast majority of neddylation cluster1 and a small fraction of neddylation cluster2 made up genesubtype-S1 (Figure 5J). Whereas the vast majority of neddylation cluster2 constituted genesubtype-S2. These results suggested that differential expressed genes obtained from neddylation patterns can identify two genomic subtypes with underlying differences in biological functions.

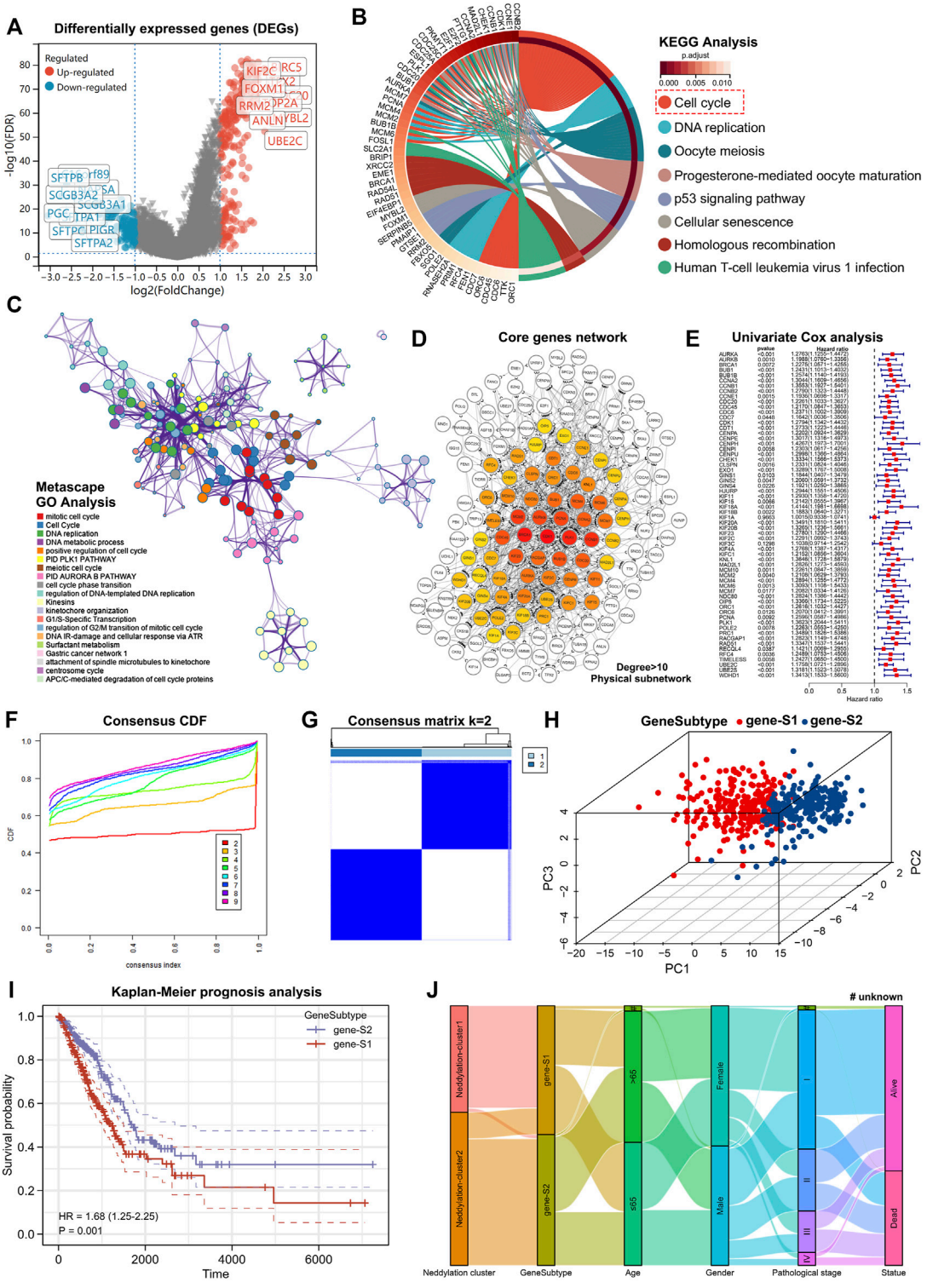

FIGURE 5
Identification of neddylation-associated gene subtypes based on differentially expressed genes. **(A)** Volcano map showed differentially expressed genes between two patterns (FDR < 0.05, |log2FC| > 1). **(B)** KEGG enrichment analysis of differentially expressed genes (FDR < 0.05, |log2FC| > 1). **(C)** GO enrichment analysis of differentially expressed genes (FDR < 0.05, |log2FC| > 1). **(D)** Construction of core gene network using STRING database and cytoscape software. **(E)** Univariate Cox analysis of core genes. **(F,G)** Consensus clustering based on core genes. **(H)** PCA of gene subtypes. **(I)** Prognostic differences between two gene subtypes. **(J)** Sankey diagram based on neddylation patterns, gene subtypes, age, gender, pathological stage, and survival status.

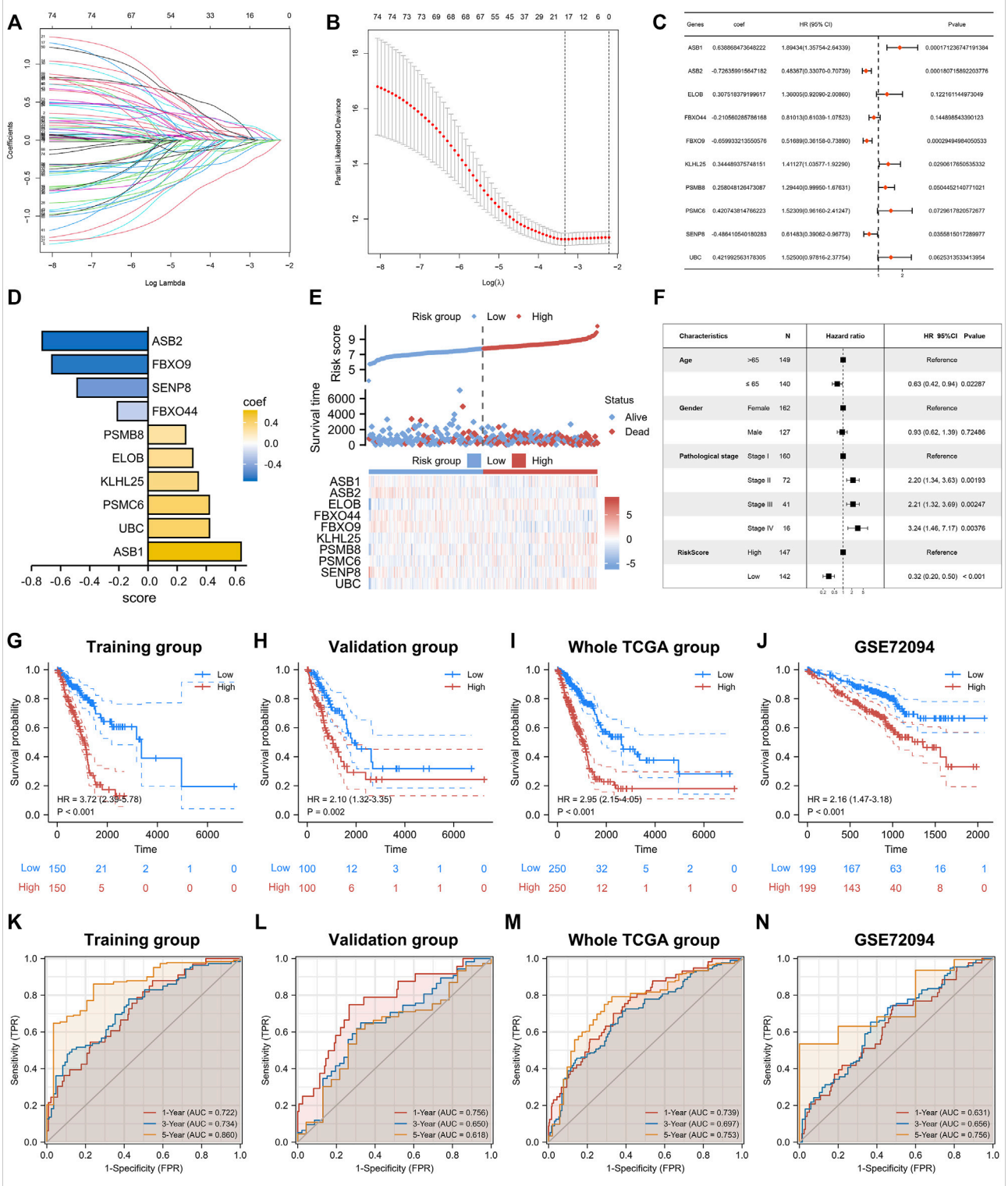

FIGURE 6
Construction of prognostic signature. **(A,B)** LASSO regression analysis based on 76 prognostic genes. **(C)** Multivariate Cox analysis was performed on genes obtained from LASSO. **(D)** The 10 genes that ultimately built the signature. **(E)** Differences in survival status and expression of 10 genes between high- and low-risk groups. **(F)** Multivariate Cox analysis of risk score and clinical factors. **(G–J)** Prognostic analysis of training set, validation set, whole TCGA Set, GSE72094. **(K–N)** Time-dependent ROC analysis of the training set, validation set, whole TCGA set, and GSE72094.

Construction of neddylation-associated prognostic signature

Based on the above analyses, we reconfirmed the biological functions of neddylation-associated genes in LUAD. Therefore, constructing a neddylation-associated prognostic signature was relevant for more accurate risk stratification and personalized treatment. First, conducted a LASSO-Cox regression analysis was conducted of the 76 prognostic genes to rule out co-linearity (Figures 6A,B). The obtained genes were then subjected to Multivariate stepwise regression analysis and 10 genes were ultimately obtained (Figures 6C,D). Based on the coefficients of these 10 genes, the following formula was computed: risk score = 0.638868474 * (ASB1 expression) + (−0.726359916) * (ASB2 expression) + 0.307518379 * (ELOB expression) + (−0.210560286) * (FBXO44 expression) + (−0.659933214) * (FBXO9 expression) + 0.344489376 * (KLHL25 expression) + 0.258048126 * (PSMB8 expression) + 0.420743815 * (PSMC6 expression) + (−0.48641054) * (SENP8 expression) + 0.421992563 * (UBC expression). Based on this formula, LUAD samples from the training set were classified into high- and low-risk groups. The heat map showed the expression of 10 genes in the high- and low-risk groups and a notably higher death rate was observed in the high-risk group (Figure 6E). Furthermore, a Multivariate Cox analysis was performed for patients with LUAD by risk score, age, gender, and pathological stage. The results showed that risk score can be an independent prognostic factor (Figure 6F). In addition, using the same formula, risk scores in the validation set, the entire TCGA database, and the external validation dataset GSE72094, were calculated. Prognostic analysis of four databases was conducted and significantly worse outcomes in all datasets for the high-risk group were observed Figures 6G–J. Additionally, a time-dependent receiver operating characteristic (ROC) analysis was performed on these four datasets to validate the predictive efficiency of signatures. The survival rates in the training set of 1, 3, and 5 years were 0.722, 0.734, and 0.860, respectively (Figure 6K). The validation sets also showed good predictive performance (Figures 6L–N). These results confirmed the accuracy of the 10-gene signature in determining patient risk stratification and prognosis. Moreover, to better investigate the relationship between risk scores and clinical parameters, a more refined examination was conducted. The results showed no statistically significant difference in risk scores between patients aged ≥65 years compared to those aged <65 years. However, in terms of gender, male patients had significantly higher risk scores than female patients. We also found that patients with pathological stage III and IV had higher risk scores than patients with pathological stage I and II (Supplementary Figures S3A–C). In addition, we performed prognostic analyses for patients with different clinical parameters. Excitingly, the results revealed that patients with high-risk scores in these clinical parameters all had a poorer prognosis (Supplementary Figures S3D–I).

Predicting immune infiltration, genetic mutations, and chemotherapeutic drug efficacy based on the risk score

As discussed earlier, two molecular patterns and two genomic subtypes associated with neddylation were identified. We further analyzed the relationship between risk scores and different subtypes. As shown in Figures 7A,B, neddylation cluster1 and genesubtype-S1 had a higher risk score; these findings were consistent with previous analysis. After confirming the prognostic efficacy of the signature, we further explored whether risk score can be used to determine immune infiltration, gene mutation status, and chemotherapeutic drug selection in patients with LUAD. The ESTIMATE algorithm helped identify the high-risk group with higher tumor purity and lower ESTIMATE, immune, and stromal scores. The high-risk group exhibited lower levels of immune infiltration (Figures 7C,D). To validate these results, ssGSEA analysis was performed on the training set. Interestingly, except for Th2 cells, the majority of immune cells exhibited a low abundance of immune infiltration (Figures 7E,F). These results suggested that the high-risk group had a negative TME that promotes tumor progression. Remarkably, the high-risk group also displayed notable differences in the extent of mutations compared to the low-risk group: mutations occurred in 145 of the 150 samples in the high-risk group, versus in 126 of the 150 samples in the low-risk group. Additionally, heat maps identified the 20 genes with the highest mutation rates in both groups, and significant differences were observed in the frequency of mutations in these genes (Figures 7G,H). Chemotherapeutic drug predictions were also performed for patients with LUAD in the high- and low-risk groups to provide options for personalized treatment. The high-risk group responded better with A.443654, GNF.2, Paclitaxel, Parthenolide, RO.3306, and Docetaxel, whereas the low-risk group responded better with ABT.263, AS601245, Axitinib, GDC.0449, MK.2206, PAC.1 (Figure 7I).

Building a more accurate nomogram that combines clinical factors with risk score

To improve the accuracy of the predictive effect of the risk score, the risk score was combined with clinical factors to construct a nomogram (Figure 8A). By establishing a calibration curve, the nomogram demonstrated good accuracy in predicting the 1-year, 3-year, and 5-year survival times (Figure 8B). The decision curve analysis (DCA) and ROC curves for 5-year survival revealed that nomo-scores and risk scores were better predictors for survival than in the pathological stage (Figures 8C,D). These findings confirmed that our signature has good prospects in clinical application. Additionally, we also constructed nomograms for the validation

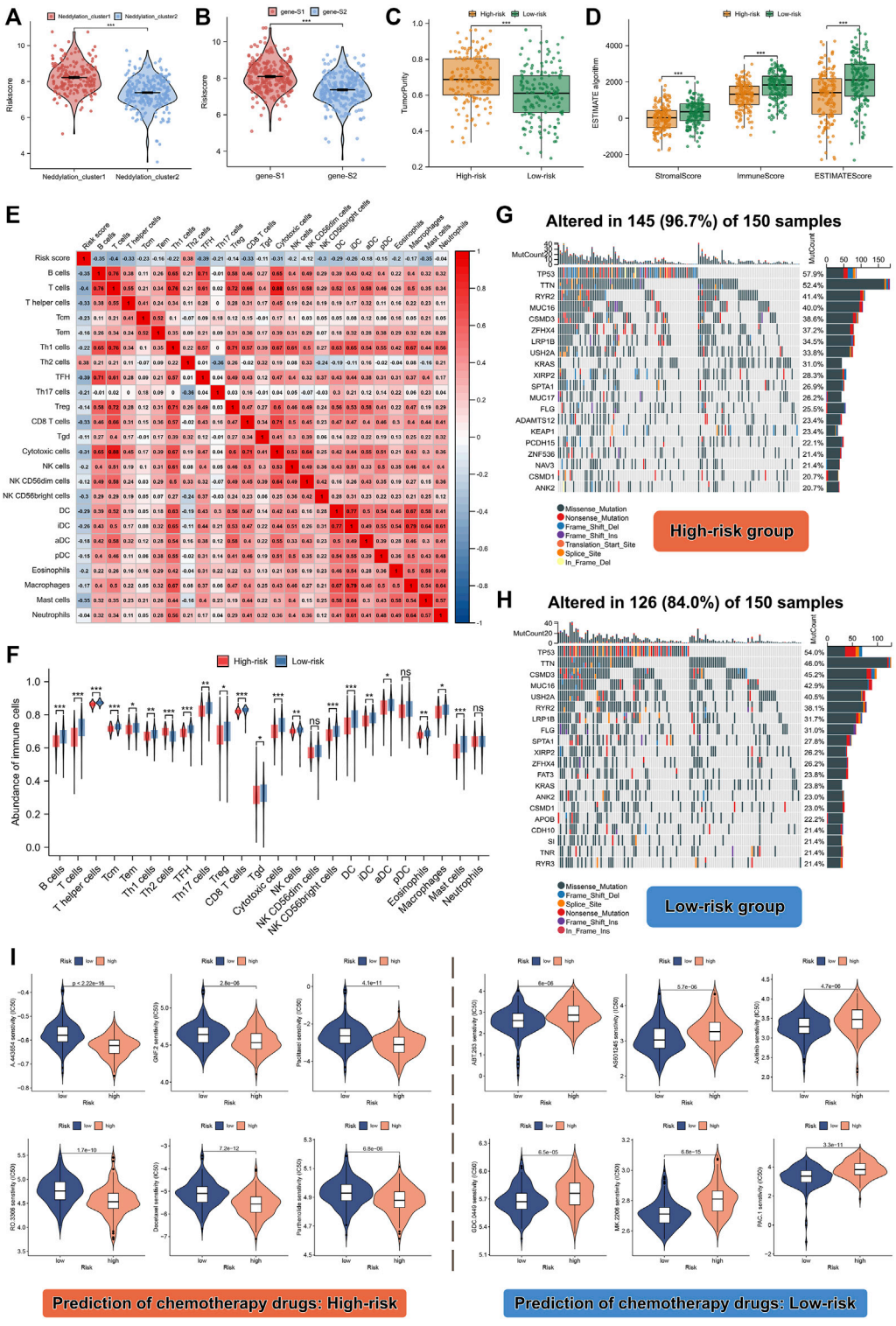

FIGURE 7
Differences in TME, mutation levels, and chemotherapeutic drug sensitivity among high- and low-risk patients. **(A)** Risk score between the two different neddylation patterns. **(B)** Risk score between the two different gene subtypes. **(C,D)** Tumor purity, estimate score, immune score, and stromal score between high- and low-risk groups. **(E,F)** Correlation between risk score and abundance of 24 immune cell types. **(G,H)** Correlation between risk score and genetic mutation. **(I)** Prediction of chemotherapeutic drugs in high- and low-risk groups.

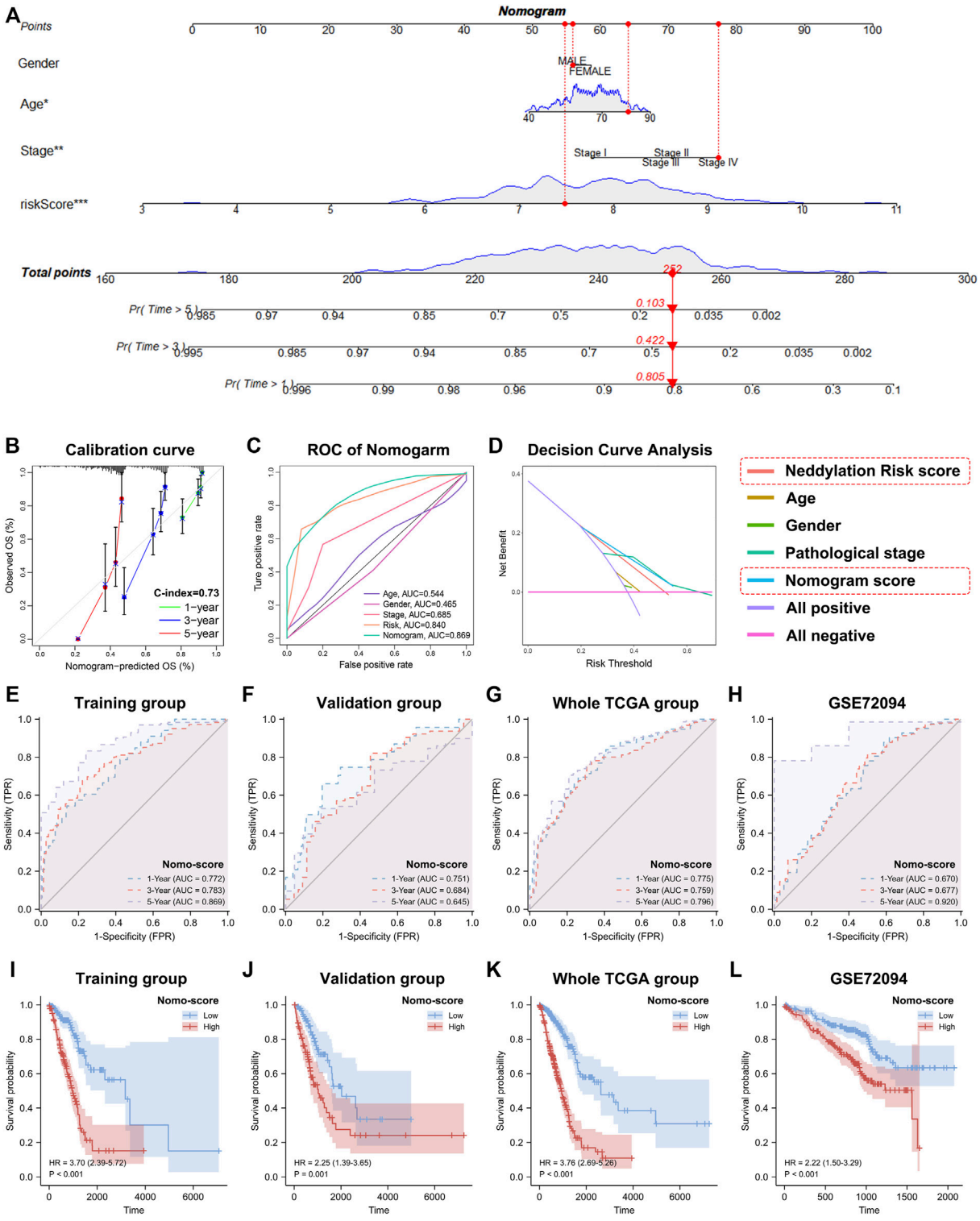

FIGURE 8
Construction of nomogram based on risk score and clinical factors. **(A)** A more predictive nomogram. **(B)** Calibration curve of 1-year, 3-year, and 5-year survival time. **(C)** Nomogram's 5-year survival time ROC curve. **(D)** Nomogram's 5-year survival time DCA curve. **(E–H)** Time-dependent ROC curves of the training set, validation set, entire TCGA set, and GSE72094 (based on nomo-score). **(I–L)** Kaplan-Meier analyses of the training set, validation set, entire TCGA set, and GSE72094 (based on nomo-score).

set, the entire TCGA dataset, and the external validation set GSE72094 to further confirm the validity of our nomogram and validated the prognosis accuracy across the four datasets (Figures 8E–H). The results revealed that the prognosis of patients with LUAD could be significantly distinguished based on the nomo-score: patients with a high nomo-score had a worse prognosis. Time-dependent ROC curves were also used to further validate the predictive efficiency of the nomogram and find that the nomo-score has higher AUC values than the risk score (Figures 8I–L). Taken together, these results further confirmed that risk score can be used not only as a prognostic factor alone but also in combination with other clinical factors to substantially improve the accuracy of prognosis determination in patients with LUAD.

Discussion

Cancer is an extremely complex entity. Many studies have shown that multiple factors are involved and controlled in tumorigenesis. Sustained growth signaling, unlimited replication potential, antiapoptotic factors, acquisition of invasive metastasis, reprogramming of cell metabolism, and TME are major hallmarks of cancer malignancy (Hanahan and Weinberg, 2011; Wong, 2011; Mossmann et al., 2018; Xiao and Yu, 2021; Yin et al., 2022). However, tumors exhibit extreme heterogeneity, which is characterized by mutations in genes and alterations in the TME (Paul et al., 2019; Zhang et al., 2022). Therefore, finely tailored therapeutic strategies are required for tumor treatment.

Neddylation is a type of protein PTM that increases proteomic diversity. Increasing evidence suggests that neddylation is aberrantly activated in a wide range of tumor types, consequently affecting tumor progression and altering the TME (Xie et al., 2021; Zhou et al., 2021). Further research on neddylation-related genes is warranted to provide new treatment strategies for cancer treatment (Zheng et al., 2021). Lung cancer is one of the leading causes of human death worldwide and has a high incidence and mortality rate. LUAD is the most common histological type of lung cancer and has a highly complex TME. Few studies have been conducted on neddylation modification in LUAD, and most of the existing literature focuses on the mechanisms and effects of one particular gene in the neddylation modifications (Zhou et al., 2017; Lee et al., 2018). Therefore, systematically investigating the role of neddylation-associated genes in predicting the prognosis of tumor progression and TME is of practical significance. Furthermore, using neddylation-associated tumor classification and risk stratification, determining the prognosis of LUAD and providing personalized treatment options might be possible.

In this study, 76 neddylation-associated prognostic genes in LUAD were first identified and their mutation frequency and CNV were analyzed. Based on prognostic genes, patients with LUAD were successfully classified into two patterns, viz., cluster1 and cluster2. Cluster1, when compared with cluster2, exhibited a higher proportion of patients with pathological stage III and IV LUAD, thus presenting a more pronounced malignant state with a worse prognosis. Using four immune infiltrating algorithms (ESTIMATE, EPIC, ssGSEA, and TIMER), it was noted that the levels of numerous immune cell types, including B cells, DC, mast cells, $CD4^+$ T cells, and $CD8^+$ T cells, were significantly lower in cluster1. Based on these results, we can conclude that the immune state in cluster1 promotes tumor progression and tumor escape, whereas, in cluster2, it showed inhibition of tumor progression. However, high levels of immune co-inhibitory molecules, such as LAG3, PDCD1, CD274, and PDCD1LG2, were also expressed in cluster1. This may be suggestive of a better response to immunotherapy among patients with LUAD in cluster1 (Schnell et al., 2020). To further investigate the potential mechanism of action of these two patterns in biological function, the ssGSEA algorithm was used to analyze the nine gene sets identified by Mariathasan et al. as well as Hallmark's 50 gene sets from the GSEA website. The ssGSEA algorithm analysis, and later confirmed by GSVA, showed that cluster1 demonstrated a tendency to favor tumor proliferation and metastasis, as evidenced by the higher enrichment scores for gene sets of cell cycle regulators, cell cycle, DNA replication, EMT2, immune checkpoints, etc. Cluster1 pattern shows activity across a wide range of pathways and demonstrated high enrichment scores for G2M checkpoints, E2F targets, unfolded protein responses, MYC targets, oxidative photography, mitotic spindle, DNA replay, glycolysis, and other tumor progression–associated biological functions. Notably, the cluster1 pattern was significantly enriched in the following signaling pathways: TNF-α, TGF-β, IL6-JAK-STAT3, PI3K-AKT-mTOR, and MTORC1. Numerous studies have shown that aberrant activation of these signaling pathways substantially contributes to growth, migration, and invasion of tumor cells, thus reshaping the TME and exhibiting worse prognosis (Kim et al., 2017; Johnson et al., 2018; Saito et al., 2018; Cruceriu et al., 2020; Iksen et al., 2021). Additionally, cluster1 also demonstrated notably increased adipogenesis, fatty acid metabolism, and cholesterol homeostasis; abnormal levels of metabolism play an important role in tumor progression as has been confirmed by previous studies (Li and Zhang, 2016; Ghaben and Scherer, 2019; Liu et al., 2021).

As there were differences in biological functions across the two neddylation patterns, differential expression analysis was performed which helped to further identify cell cycle-related genes that may play a central role in tumor progression and metastasis. Building and analysis of the core network helped to identify the 62 most critical genes. Additionally, through an unsupervised consensus clustering approach, LUAD was subdivided into two genomic subtypes, viz., genesubtype-S1 and genesubtype-S2. Genesubtype-S1 demonstrated a worse prognosis compared with genesubtype-S2, again demonstrating the importance of neddylation-associated genes in classifying patients with LUAD. Furthermore, for accurate risk stratification of patients with LUAD, a neddylation-associated prognostic signature was constructed. The signature was highly predictive: considerably worse outcomes were observed in patients with a high-risk score in the training set, validation set, whole TCGA

set, and GSE72094. The ROC analysis also showed high predictive accuracy. Notably, most immune cell types had low infiltration abundance in patients with LUAD with high-risk scores, suggesting tumorigenesis and tumor progression were favored in these patients. Genetic mutation analysis revealed that patients with high-risk scores had higher mutation frequency versus those with the low-risk score. Increased genetic mutations may lead to cellular physiological dysfunction and enhanced tumor metastasis. Finally, the sensitivity to chemotherapeutic agents was analyzed and appropriate chemotherapeutic agents were screened for both high- and low-risk groups of patients with LUAD to provide for a more refined treatment strategy.

Many LUAD-associated prognostic models have been made available previously; for example, an immune-related prognostic signature constructed by Yi et al. (2021), a ferroptosis-associated prognostic signature introduced by Wang et al. (2021), an autophagy-related prognostic signature developed by Li et al. (2022), and an inflammatory-associated prognostic signature identified by Zhai et al. (2021) have identified. Compared with these models, our study reported a prognostic model based on neddylation-associated genes which shows promising prognostic accuracy. To our knowledge, this study is the first of its kind. The 10-gene prognostic model constructed in this study aids in determining prognosis. Risk-score outperforms pathological stage in terms of predicting prognosis accurately. As an independent prognostic factor and clinically useful indicator, a risk score can be combined with other clinical factors to construct nomogram with increased accuracy and potential clinical application. However, this study has limitations. Our analysis was based primarily on TCGA and GEO databases, and further validation of the accuracy of our model in larger sample sizes observed in clinical studies would be required.

Conclusion

In summary, this study aimed to classify patients with LUAD into two patterns based on their neddylation-associated prognostic genes which potentially indicates the nature of TME. Significant differences were observed between the two patterns in the activation of the signaling pathways associated with tumor proliferation and metastasis. Prognostic signatures based on neddylation-related genes can help stratify patients with LUAD, guide personalized treatment, and provide a preliminary exploration for clinical use.

Data availability statement

The datasets presented in this study can be found in online repositories. The names of the repository/repositories and accession number(s) can be found in the article/Supplementary Material.

Author contributions

Conception and data analysis of the paper: YC and ZC. Drafting of the manuscript: JY and BP. Data collection and assistants in data analysis: TC, HD, and LW. Data visualization: QL, GL, and LS. Article revision: CD and XT. Funding and supervising: JZ. All authors participated in the work and agreed to take responsibility for all aspects of the work, thus ensuring that the research was accurate and that relevant issues were properly investigated and resolved.

Funding

This work was supported by the grants from Suzhou Science and Technology Bureau (LCZX2019002); Natural Science Foundation of Jiangsu province (BK20220250).

Acknowledgments

We thank Bullet Edits Limited for the linguistic editing. We are very grateful to JZ for his valuable guidance.

Conflict of interest

The authors declare that the research was conducted in the absence of any commercial or financial relationships that could be construed as a potential conflict of interest.

Publisher's note

All claims expressed in this article are solely those of the authors and do not necessarily represent those of their affiliated organizations, or those of the publisher, the editors and the reviewers. Any product that may be evaluated in this article, or claim that may be made by its manufacturer, is not guaranteed or endorsed by the publisher.

Supplementary material

The Supplementary Material for this article can be found online at: https://www.frontiersin.org/articles/10.3389/fcell.2022.979262/full#supplementary-material

References

Bajbouj, K., Al-Ali, A., Ramakrishnan, R. K., Saber-Ayad, M., and Hamid, Q. (2021). Histone modification in NSCLC: Molecular mechanisms and therapeutic targets. *Int. J. Mol. Sci.* 22, 11701. doi:10.3390/ijms222111701

Bindea, G., Mlecnik, B., Tosolini, M., Kirilovsky, A., Waldner, M., Obenauf, A. C., et al. (2013). Spatiotemporal dynamics of intratumoral immune cells reveal the immune landscape in human cancer. *Immunity* 39, 782–795. doi:10.1016/j.immuni.2013.10.003

Cao, M., Li, H., Sun, D., and Chen, W. (2020). Cancer burden of major cancers in China: A need for sustainable actions. *Cancer Commun.* 40, 205–210. doi:10.1002/cac2.12025

Chang, F. M., Reyna, S. M., Granados, J. C., Wei, S. J., Innis-Whitehouse, W., Maffi, S. K., et al. (2012). Inhibition of neddylation represses lipopolysaccharide-induced proinflammatory cytokine production in macrophage cells. *J. Biol. Chem.* 287, 35756–35767. doi:10.1074/jbc.M112.397703

Chen, L., Liu, S., and Tao, Y. (2020). Regulating tumor suppressor genes: Post-translational modifications. *Signal Transduct. Target. Ther.* 5, 90. doi:10.1038/s41392-020-0196-9

Cruceriu, D., Baldasici, O., Balacescu, O., and Berindan-Neagoe, I. (2020). The dual role of tumor necrosis factor-alpha (TNF-alpha) in breast cancer: Molecular insights and therapeutic approaches. *Cell. Oncol.* 43, 1–18. doi:10.1007/s13402-019-00489-1

De, S., Holvey-Bates, E. G., Mahen, K., Willard, B., and Stark, G. R. (2021). The ubiquitin E3 ligase FBXO22 degrades PD-L1 and sensitizes cancer cells to DNA damage. *Proc. Natl. Acad. Sci. U. S. A.* 118, e2112674118. doi:10.1073/pnas.2112674118

Denisenko, T. V., Budkevich, I. N., and Zhivotovsky, B. (2018). Cell death-based treatment of lung adenocarcinoma. *Cell Death Dis.* 9, 117. doi:10.1038/s41419-017-0063-y

Domingues, P., Gonzalez-Tablas, M., Otero, A., Pascual, D., Miranda, D., Ruiz, L., et al. (2016). Tumor infiltrating immune cells in gliomas and meningiomas. *Brain Behav. Immun.* 53, 1–15. doi:10.1016/j.bbi.2015.07.019

Ferlay, J., Colombet, M., Soerjomataram, I., Dyba, T., Randi, G., Bettio, M., et al. (2018). Cancer incidence and mortality patterns in Europe: Estimates for 40 countries and 25 major cancers in 2018. *Eur. J. Cancer* 103, 356–387. doi:10.1016/j.ejca.2018.07.005

Gambardella, V., Castillo, J., Tarazona, N., Gimeno-Valiente, F., Martinez-Ciarpaglini, C., Cabeza-Segura, M., et al. (2020). The role of tumor-associated macrophages in gastric cancer development and their potential as a therapeutic target. *Cancer Treat. Rev.* 86, 102015. doi:10.1016/j.ctrv.2020.102015

Geeleher, P., Cox, N., and Huang, R. S. (2014). pRRophetic: an R package for prediction of clinical chemotherapeutic response from tumor gene expression levels. *PLoS One* 9, e107468. doi:10.1371/journal.pone.0107468

Ghaben, A. L., and Scherer, P. E. (2019). Adipogenesis and metabolic health. *Nat. Rev. Mol. Cell Biol.* 20, 242–258. doi:10.1038/s41580-018-0093-z

Han, Z. J., Feng, Y. H., Gu, B. H., Li, Y. M., and Chen, H. (2018). The post-translational modification, SUMOylation, and cancer (Review). *Int. J. Oncol.* 52, 1081–1094. doi:10.3892/ijo.2018.4280

Hanahan, D., and Coussens, L. M. (2012). Accessories to the crime: Functions of cells recruited to the tumor microenvironment. *Cancer Cell* 21, 309–322. doi:10.1016/j.ccr.2012.02.022

Hanahan, D., and Weinberg, R. A. (2011). Hallmarks of cancer: The next generation. *Cell* 144, 646–674. doi:10.1016/j.cell.2011.02.013

Hanzelmann, S., Castelo, R., and Guinney, J. (2013). Gsva: Gene set variation analysis for microarray and RNA-seq data. *BMC Bioinforma.* 14, 7. doi:10.1186/1471-2105-14-7

Hirsch, F. R., Scagliotti, G. V., Mulshine, J. L., Kwon, R., Curran, W. J., Wu, Y.-L., et al. (2017). Lung cancer: Current therapies and new targeted treatments. *Lancet* 389, 299–311. doi:10.1016/S0140-6736(16)30958-8

Iksen, Pothongsrisit, S., and Pongrakhananon, V. (2021). Targeting the PI3K/AKT/mTOR signaling pathway in lung cancer: An update regarding potential drugs and natural products. *Molecules* 26, 4100. doi:10.3390/molecules26134100

Jia, Q., Wang, A., Yuan, Y., Zhu, B., and Long, H. (2022). Heterogeneity of the tumor immune microenvironment and its clinical relevance. *Exp. Hematol. Oncol.* 11, 24. doi:10.1186/s40164-022-00277-y

Johnson, D. E., O'Keefe, R. A., and Grandis, J. R. (2018). Targeting the IL-6/JAK/STAT3 signalling axis in cancer. *Nat. Rev. Clin. Oncol.* 15, 234–248. doi:10.1038/nrclinonc.2018.8

Kanehisa, M., Furumichi, M., Sato, Y., Ishiguro-Watanabe, M., and Tanabe, M. (2021). Kegg: Integrating viruses and cellular organisms. *Nucleic Acids Res.* 49, D545–D551. doi:10.1093/nar/gkaa970

Kim, L. C., Cook, R. S., and Chen, J. (2017). mTORC1 and mTORC2 in cancer and the tumor microenvironment. *Oncogene* 36, 2191–2201. doi:10.1038/onc.2016.363

Lee, G. W., Park, J. B., Park, S. Y., Seo, J., Shin, S. H., Park, J. W., et al. (2018). The E3 ligase C-CBL inhibits cancer cell migration by neddylating the proto-oncogene c-Src. *Oncogene* 37, 5552–5568. doi:10.1038/s41388-018-0354-5

Li, B., Severson, E., Pignon, J. C., Zhao, H., Li, T., Novak, J., et al. (2016). Comprehensive analyses of tumor immunity: Implications for cancer immunotherapy. *Genome Biol.* 17, 174. doi:10.1186/s13059-016-1028-7

Li, L., Liu, B., Dong, T., Lee, H. W., Yu, J., Zheng, Y., et al. (2013). Neddylation pathway regulates the proliferation and survival of macrophages. *Biochem. Biophys. Res. Commun.* 432, 494–498. doi:10.1016/j.bbrc.2013.02.028

Li, X., Dai, Z., Wu, X., Zhang, N., Zhang, H., Wang, Z., et al. (2022). The comprehensive analysis identified an autophagy signature for the prognosis and the immunotherapy efficiency prediction in lung adenocarcinoma. *Front. Immunol.* 13, 749241. doi:10.3389/fimmu.2022.749241

Li, Z., and Zhang, H. (2016). Reprogramming of glucose, fatty acid and amino acid metabolism for cancer progression. *Cell. Mol. Life Sci.* 73, 377–392. doi:10.1007/s00018-015-2070-4

Liberzon, A., Birger, C., Thorvaldsdottir, H., Ghandi, M., Mesirov, J. P., and Tamayo, P. (2015). The Molecular Signatures Database (MSigDB) hallmark gene set collection. *Cell Syst.* 1, 417–425. doi:10.1016/j.cels.2015.12.004

Lin, R., Fogarty, C. E., Ma, B., Li, H., Ni, G., Liu, X., et al. (2021). Identification of ferroptosis genes in immune infiltration and prognosis in thyroid papillary carcinoma using network analysis. *BMC Genomics* 22, 576. doi:10.1186/s12864-021-07895-6

Liu, W., Chakraborty, B., Safi, R., Kazmin, D., Chang, C. Y., and McDonnell, D. P. (2021). Dysregulated cholesterol homeostasis results in resistance to ferroptosis increasing tumorigenicity and metastasis in cancer. *Nat. Commun.* 12, 5103. doi:10.1038/s41467-021-25354-4

Mariathasan, S., Turley, S. J., Nickles, D., Castiglioni, A., Yuen, K., Wang, Y., et al. (2018). TGFβ attenuates tumour response to PD-L1 blockade by contributing to exclusion of T cells. *Nature* 554, 544–548. doi:10.1038/nature25501

Mossmann, D., Park, S., and Hall, M. N. (2018). mTOR signalling and cellular metabolism are mutual determinants in cancer. *Nat. Rev. Cancer* 18, 744–757. doi:10.1038/s41568-018-0074-8

Park, J. B., Seo, J., Park, J. W., and Chun, Y. S. (2020). Neddylation blockade induces HIF-1α driven cancer cell migration via upregulation of ZEB1. *Sci. Rep.* 10, 18210. doi:10.1038/s41598-020-75286-0

Paul, P., Malakar, A. K., and Chakraborty, S. (2019). The significance of gene mutations across eight major cancer types. *Mutat. Res.* 781, 88–99. doi:10.1016/j.mrrev.2019.04.004

Pellegrino, N. E., Guven, A., Gray, K., Shah, P., Kasture, G., Nastke, M. D., et al. (2022). The next frontier: Translational development of ubiquitination, SUMOylation, and NEDDylation in cancer. *Int. J. Mol. Sci.* 23, 3480. doi:10.3390/ijms23073480

Perkins, N. D. (2006). Post-translational modifications regulating the activity and function of the nuclear factor kappa B pathway. *Oncogene* 25, 6717–6730. doi:10.1038/sj.onc.1209937

Petitprez, F., Meylan, M., de Reynies, A., Sautes-Fridman, C., and Fridman, W. H. (2020). The tumor microenvironment in the response to immune checkpoint blockade therapies. *Front. Immunol.* 11, 784. doi:10.3389/fimmu.2020.00784

Racle, J., de Jonge, K., Baumgaertner, P., Speiser, D. E., and Gfeller, D. (2017). Simultaneous enumeration of cancer and immune cell types from bulk tumor gene expression data. *Elife* 6, e26476. doi:10.7554/eLife.26476

Ritchie, M. E., Phipson, B., Wu, D., Hu, Y., Law, C. W., Shi, W., et al. (2015). Limma powers differential expression analyses for RNA-sequencing and microarray studies. *Nucleic Acids Res.* 43, e47. doi:10.1093/nar/gkv007

Saito, A., Horie, M., and Nagase, T. (2018). TGF-Beta signaling in lung health and disease. *Int. J. Mol. Sci.* 19, E2460. doi:10.3390/ijms19082460

Schnell, A., Bod, L., Madi, A., and Kuchroo, V. K. (2020). The yin and yang of co-inhibitory receptors: Toward anti-tumor immunity without autoimmunity. *Cell Res.* 30, 285–299. doi:10.1038/s41422-020-0277-x

Shannon, P., Markiel, A., Ozier, O., Baliga, N. S., Wang, J. T., Ramage, D., et al. (2003). Cytoscape: A software environment for integrated models of biomolecular interaction networks. *Genome Res.* 13, 2498–2504. doi:10.1101/gr.1239303

Stram, A. R., and Payne, R. M. (2016). Post-translational modifications in mitochondria: Protein signaling in the powerhouse. *Cell. Mol. Life Sci.* 73, 4063–4073. doi:10.1007/s00018-016-2280-4

Szklarczyk, D., Gable, A. L., Nastou, K. C., Lyon, D., Kirsch, R., Pyysalo, S., et al. (2021). The STRING database in 2021: Customizable protein-protein networks, and functional characterization of user-uploaded gene/measurement sets. *Nucleic Acids Res.* 49, D605–D612. doi:10.1093/nar/gkaa1074

The Gene Ontology, C. (2019). The gene Ontology resource: 20 years and still GOing strong. *Nucleic Acids Res.* 47, D330–D338. doi:10.1093/nar/gky1055

Tibshirani, R. (1997). The lasso method for variable selection in the Cox model. *Stat. Med.* 16, 385–395. doi:10.1002/(sici)1097-0258(19970228)16:4<385::aid-sim380>3.0.co;2-3

Wang, D. C., Wang, W., Zhu, B., and Wang, X. (2018). Lung cancer heterogeneity and new strategies for drug therapy. *Annu. Rev. Pharmacol. Toxicol.* 58, 531–546. doi:10.1146/annurev-pharmtox-010716-104523

Wang, H., Lengerich, B. J., Aragam, B., and Xing, E. P. (2019). Precision lasso: Accounting for correlations and linear dependencies in high-dimensional genomic data. *Bioinformatics* 35, 1181–1187. doi:10.1093/bioinformatics/bty750

Wang, S., Xie, Z., and Wu, Z. (2021). Establishment and validation of a ferroptosis-related gene signature to predict overall survival in lung adenocarcinoma. *Front. Genet.* 12, 793636. doi:10.3389/fgene.2021.793636

Wilkerson, M. D., and Hayes, D. N. (2010). ConsensusClusterPlus: A class discovery tool with confidence assessments and item tracking. *Bioinformatics* 26, 1572–1573. doi:10.1093/bioinformatics/btq170

Wong, R. S. (2011). Apoptosis in cancer: From pathogenesis to treatment. *J. Exp. Clin. Cancer Res.* 30, 87. doi:10.1186/1756-9966-30-87

Xiao, Y., and Yu, D. (2021). Tumor microenvironment as a therapeutic target in cancer. *Pharmacol. Ther.* 221, 107753. doi:10.1016/j.pharmthera.2020.107753

Xie, P., Peng, Z., Chen, Y., Li, H., Du, M., Tan, Y., et al. (2021). Neddylation of PTEN regulates its nuclear import and promotes tumor development. *Cell Res.* 31, 291–311. doi:10.1038/s41422-020-00443-z

Yi, M., Li, A., Zhou, L., Chu, Q., Luo, S., and Wu, K. (2021). Immune signature-based risk stratification and prediction of immune checkpoint inhibitor's efficacy for lung adenocarcinoma. *Cancer Immunol. Immunother.* 70, 1705–1719. doi:10.1007/s00262-020-02817-z

Yin, J., Meng, X., Peng, L., Xie, W., Liu, X., He, W., et al. (2022). Ferroptosis and cancer immunotherapy. *Curr. Mol. Med.* 22, 467. doi:10.2174/1566524022666220509124608

Yoshihara, K., Shahmoradgoli, M., Martinez, E., Vegesna, R., Kim, H., Torres-Garcia, W., et al. (2013). Inferring tumour purity and stromal and immune cell admixture from expression data. *Nat. Commun.* 4, 2612. doi:10.1038/ncomms3612

Zhai, W. Y., Duan, F. F., Chen, S., Wang, J. Y., Lin, Y. B., Wang, Y. Z., et al. (2021). A novel inflammatory-related gene signature based model for risk stratification and prognosis prediction in lung adenocarcinoma. *Front. Genet.* 12, 798131. doi:10.3389/fgene.2021.798131

Zhang, A., Miao, K., Sun, H., and Deng, C. X. (2022). Tumor heterogeneity reshapes the tumor microenvironment to influence drug resistance. *Int. J. Biol. Sci.* 18, 3019–3033. doi:10.7150/ijbs.72534

Zhao, Y., Morgan, M. A., and Sun, Y. (2014). Targeting Neddylation pathways to inactivate cullin-RING ligases for anticancer therapy. *Antioxid. Redox Signal.* 21, 2383–2400. doi:10.1089/ars.2013.5795

Zheng, Y. C., Guo, Y. J., Wang, B., Wang, C., Mamun, M. A. A., Gao, Y., et al. (2021). Targeting neddylation E2s: A novel therapeutic strategy in cancer. *J. Hematol. Oncol.* 14, 57. doi:10.1186/s13045-021-01070-w

Zhou, L., Jiang, Y., Luo, Q., Li, L., and Jia, L. (2019a). Neddylation: A novel modulator of the tumor microenvironment. *Mol. Cancer* 18, 77. doi:10.1186/s12943-019-0979-1

Zhou, L., Zhang, L., Chen, S., Sun, D., and Qu, J. (2021). Elevated neddylation pathway promotes Th2 cells infiltration by transactivating STAT5A in hepatocellular carcinoma. *Front. Oncol.* 11, 709170. doi:10.3389/fonc.2021.709170

Zhou, W., Xu, J., Li, H., Xu, M., Chen, Z. J., Wei, W., et al. (2017). Neddylation E2 UBE2F promotes the survival of lung cancer cells by activating CRL5 to degrade NOXA via the K11 linkage. *Clin. Cancer Res.* 23, 1104–1116. doi:10.1158/1078-0432.CCR-16-1585

Zhou, Y., Zhou, B., Pache, L., Chang, M., Khodabakhshi, A. H., Tanaseichuk, O., et al. (2019b). Metascape provides a biologist-oriented resource for the analysis of systems-level datasets. *Nat. Commun.* 10, 1523. doi:10.1038/s41467-019-09234-6

frontiers | Frontiers in Oncology

TYPE Original Research
PUBLISHED 14 September 2022
DOI 10.3389/fonc.2022.958221

Check for updates

OPEN ACCESS

EDITED BY
Shaoquan Zheng,
The First Affiliated Hospital of Sun Yat-sen University, China

REVIEWED BY
Qian Long,
Second Xiangya Hospital, Central South University, China
Dan-Ping Huang,
Guangzhou University of Chinese Medicine, China

*CORRESPONDENCE
Qiusheng Xiong
283420533@qq.com

SPECIALTY SECTION
This article was submitted to Molecular and Cellular Oncology, a section of the journal Frontiers in Oncology

RECEIVED 31 May 2022
ACCEPTED 25 July 2022
PUBLISHED 14 September 2022

CITATION
Zou Z, Chai Y, Li Q, Lin X, He Q and Xiong Q (2022) Establishment of lactate-metabolism-related signature to predict prognosis and immunotherapy response in patients with colon adenocarcinoma. *Front. Oncol.* 12:958221. doi: 10.3389/fonc.2022.958221

COPYRIGHT
© 2022 Zou, Chai, Li, Lin, He and Xiong. This is an open-access article distributed under the terms of the Creative Commons Attribution License (CC BY). The use, distribution or reproduction in other forums is permitted, provided the original author(s) and the copyright owner(s) are credited and that the original publication in this journal is cited, in accordance with accepted academic practice. No use, distribution or reproduction is permitted which does not comply with these terms.

Establishment of lactate-metabolism-related signature to predict prognosis and immunotherapy response in patients with colon adenocarcinoma

Zhengrong Zou[1], Yongjie Chai[2], Qi Li[3], Xuan Lin[1], Qingfang He[4] and Qiusheng Xiong[4]*

[1]Department of Emergency Trauma Center, The First Affiliated Hospital of Gannan Medical University, Ganzhou, China, [2]Department of Anorectal Surgery, Zhucheng People's Hospital, Zhucheng, China, [3]Basic Medicine Department of Chuxiong Medical and Pharmaceutical College, Chuxiong, China, [4]Department of General Surgery, The First Affiliated Hospital of Gannan Medical University, Ganzhou, China

The outcome of colon adenocarcinoma (COAD) patients remains dismal, and lactate metabolism has been characterized to promote tumor development and immune evasion. Based on the above background, it is worthwhile to explore novel prognostic and therapeutic biomarkers for COAD patients from the aspect of lactate metabolism. Above all, 228 available lactate-metabolism-related genes (LMRGs) were acquired, and the landscape of copy number variation and the expression difference of mRNA levels between colon normal and tumor samples were investigated among these LMRGs. Importantly, eight overall survival (OS)-involved LMRGs were then distinguished by means of univariate Cox regression analysis in both GSE40967 and TCGA-COAD data sets. Subsequently, prognostic risk scores were established, integrating seven OS-related LMRGs by LASSO Cox regression analysis in the GSE40967 set, and then verified in the TCGA-COAD cohort. From the comprehensive analyses, COAD patients with high risk had comparatively more inferior survival probability in all populations of the study, and they tended to have more severe clinicopathological features with the risk score increasing. Moreover, by integrating age, AJCC T and pathological stage, and risk score, we constructed a prognostic nomogram that demonstrated great prediction effectiveness for OS of COAD patients. Furthermore, the potential effect of various risk score on tumor immune was assessed from enrichment of immune-related pathways, tumor-infiltrating immune cells, and expression levels of immune checkpoints separately. We could draw a conclusion that COAD patients with higher lactate-metabolism-related risk scores may acquire an immunosuppressive tumor microenvironment, which subsequently led to immune escapes and poor prognoses. Conclusively, all findings in the present study illustrate a great prognostic value of the lactate-metabolism-related risk signature, providing

more in-depth insights into the indispensable function of lactate metabolism in prognosis and tumor immunity of COAD.

KEYWORDS

colon adenocarcinoma, lactate metabolism, risk signature, tumor immune microenvironment, immunotherapy

Introduction

Colon adenocarcinoma (COAD) has been the third most common malignant tumor with 10% of all cancers and high mortality (1). Therapeutic advancements, including surgical technique, chemotherapy, and molecular targeted therapies, have greatly improved the outcome of patients with COAD (2). However, with the increases in incidence and drug resistance, the prognosis of some patients with COAD remains dismal (3). To further enhance the curative effect and survival of such population, more effective biomarkers and more accurate cancer identification are still urgent and worth exploring.

To date, there has been a general consensus that aerobic glycolysis (the Warburg effect) has emerged as a metabolic hallmark of cancers, and tumor cells secrete large amounts of lactate, which always results in lactate accumulation in the tumor microenvironment (TME) (4). Hence, lactate metabolism has attracted more attention in cancer metabolic research recently. A considerable amount of evidence has uncovered the nonnegligible role of lactate metabolism alterations as biomarkers of cancer prognoses (5–8). For COAD, lactate originated by the noncancer stem cells promoted self-renewal of cancer stem cells (CSCs) and consequently contributed to tumor progression (9). Besides this, meta-analyses revealed that high levels of lactate dehydrogenase were correlated with unfavorable overall survival (OS) in colorectal cancer (CRC) patients (10). Nonetheless, a full-scale landscape of the impact of lactate metabolism on prognosis of COAD still lacks.

COAD development is verified to be a complicated process involving the interactions between the tumor, TME, and host immune system (11). Accumulating evidence reveals that TME is closely related to the progression, relapse, metastasis, and therapeutic resistance of CRC (12). To be exact, the TME is especially lactate-enriched (13). For tumor-infiltrating immune cells, which are a part of the complex microenvironment, playing a leading role in the TME, lactate accumulation supported tumor immune escape by depressing the cytotoxic activities of T cells and connatural lymphocytes such as natural killer (NK) and natural killer T (NKT) cells (14, 15). In CRC, lactate-mediated acidification of TME is revealed to induce apoptosis of liver-resident NK cells in liver metastasis (16). In addition, decreasing lactate production in cancer cells is observed to synergize with immunotherapy by preventing the acidification of the TME in melanoma (17). On the whole, the effect of lactate metabolism on the TME cannot be underestimated. However, a comprehensive analysis of such influence in COAD has not yet been reached.

In this study, we identified prognostic lactate-metabolism-related genes (LMRGs) and establish a reliable nomogram model on the basis of LMRGs to predict the survival outcomes of COAD patients. Moreover, the potential relationship between the signature and the TME was further explored. Our study provides more evidence that lactate metabolism is strongly correlated with patient prognosis and tumor immunity in COAD.

Materials and methods

Data retrieval and collection of LMRGs

From The Cancer Genome Atlas (TCGA) database (41 normal colon samples and 473 COAD samples, https://portal.gdc.cancer.gov/repository) and GSE40967 in the Gene Expression Omnibus (GEO) database (585 COAD samples, https://www.ncbi.nlm.nih.gov/geo/), the public transcriptome expression matrices and clinical information of COAD patients were retrieved. Afterward, 573 COAD patients in GSE40967 were set to the training set, whereas 457 COAD samples of TCGA were selected as an external validation set after exclusion of patients with no OS information. From the Molecular Signature Database v7.5.1 (MSigDB), 284 LMRGs were downloaded (18). Furthermore, 228 overlapping LMRGs were collected for ulterior analyses after intersecting the aforementioned 284 LMRGs with all genes in GSE40967 and TCGA-COAD data sets (Supplementary Figure 1).

Verification of copy number variation (CNV) frequency and differentially expressed genes (DEGs) among LMRGs

The CNV data of patients from TCGA-COAD was attained in the UCSC Xena database (https://xenabrowser.net/datapages/).

Subsequently, the CNV frequency of the above 228 LMRGs was computed, and a bidirectional column chart was used to visualize the result. The DEGs within LMRGs were verified after comparing the normal and cancer samples in the TCGA-COAD data set when the threshold was set with false discovery rate (FDR)< 0.05 and |log2FC| > 1 using the "edgR" R package (19, 20). These significant DEGs were also described with a heat map and a volcano plot.

Acquisition of OS-related LMRGs in COAD

To demonstrate the profound prognostic significance of 228 LMRGs in COAD, Cox proportional hazards regression analyses were carried out for univariate analyses to obtain OS-related LMRGs with P<.05 in the GSE40967 (n = 573) and TCGA-COAD (n = 457) cohorts, respectively. Ulteriorly, the overlapping OS-related LMRGs were screened out for further research. Meanwhile, the relevant characteristics among the above LMRGs were illustrated in a correlation matrix plot, and the "RCircos" R package was utilized to display mRNA expressions and chromosomal positions of those candidate LMRGs (21).

Establishment and validation of lactate metabolism–correlated prognostic signature in COAD

To establish a statistically prognostic signature according to these eligible OS-related LMRGs, least absolute shrinkage and selection operator (LASSO) Cox regression analysis was accomplished in the training cohort. In addition, seven LMRGs were retrieved to construct a signature for COAD patients, whereas the prognostic significance of each LMRG included in the signature was portrayed, respectively. According to the predictive signature, the lactate-metabolism-related risk score of individual COAD patient would be calculated as follows:

$$\%\text{Risk Score} = \sum \text{Expression of Each LMRG} * \text{Corresponding Regression Coefficient}$$

Meanwhile, the risk score was adjusted by a linear transformation in every data set with the following formula:

$$\mathbf{adj.Risk\ score} = \frac{\text{Risk score} - \min(\text{Risk score})}{\max(\text{Risk score}) - \min(\text{Risk score})}$$

Subsequently, patients in each cohort were divided into high- and low-risk subgroups using the median cutoff value. To uncover the feasibility of the risk model, Kaplan–Meier survival analysis of OS difference was executed between high- and low-risk groups in two data sets separately, and Kaplan–Meier survival analyses of progression-free survival (PFS), disease-free survival (DFS), and disease-specific survival (DSS) were further performed between different risk groups in the TCGA-COAD cohort.

Completed investigation of risk score and clinical parameters in patients with COAD

To elucidate the availability of the risk signature based on LMRGs in clinical situations, we compared the distribution of adjusted risk values with different degrees of various clinicopathologic parameters using boxplots with the Kruskal test. Additionally, heat maps were plotted to decipher the correlation between each selected LMRG's expressions and important clinical indicators, comprising risk score, T, N, AJCC stage, and survival status in the training and validation sets.

Construction and evaluation of lactate-metabolism-related clinical nomogram in COAD

Furthermore, univariate and multivariate Cox regression analyses were delineated to explore whether the lactate-metabolism-related risk score could be an independent predictor of COAD. Based on the results presented, a lactate-metabolism-related nomogram, integrating risk score, age, T, and AJCC stage in the GSE40967 was constructed through the "rms" and "regplot" R packages (22, 23). In an effort to evaluate the predictive performance of the nomogram, we performed the calibration analysis and decision curve analysis (DCA) and plotted corresponding curves (24).

Identification of different biological functions within two risk subgroups

The "GSVA" R package was carried out to investigate the distinctions of biological processes and signaling pathways between high- and low-risk groups in the training and validation sets, respectively (25, 26). "c2.cp.kegg.v7.5.1.symbols.gmt" [KEGG] was dug out from MSigDB as the reference molecular signature database, and P values<.05 were deemed statistically significant after being adjusted. Ultimately, the top 20 significant KEGG pathways were displayed as heat maps.

Potential implications for TME landscape and immunotherapy based on the risk signature

To reveal the potential implications for immunotherapy based on lactate-metabolism-related risk score, different

expression levels of three immunologic checkpoints, namely PDCD1 (PD-1), CD274 (PD-L1), and CTLA4, were detected between high- and low-risk groups using the Wilcox test. To determine the relative tumor-infiltrating abundance of 22 immune cells in the two subgroups, the CIBERSORT deconvolution algorithm was employed in the training set (27, 28).

Statistical analysis

Statistical analyses were done with R software (Version 4.0.2, http://www.R-project.org). The log-rank test was applied to conduct the comparison between Kaplan–Meier curves in this study (29). The Kruskal test was utilized to uncover the differences of adjusted risk scores in various clinical parameters. The discrepancy of checkpoints in low- and high-risk groups was detected by the Wilcox test. The correlation matrix diagram was examined using Spearman's correlation test. All *P* values were bilateral, and statistical significances were set at $P<.05$.

Results

Identification of prognostic LMRGs in COAD

Initially, 228 common LMRGs were obtained through the intersection of two databases (GSE40967 and TCGA-COAD). We first assessed the global CNV alterations of 228 LMRGs in TCGA-COAD, which showed that there existed extensive CNV mutations among LMRGs. The top 20 genes in CNV amplification and deletion status are displayed in Figure 1A together. Then, the mRNA expression profiles of COAD samples in TCGA-COAD were analyzed to find differentially expressed LMRGs with the threshold of FDR< 0.05, |log2FC| > 1 and visualization of a heat map (Figure 1B) and a volcano plot (Figure 1C), respectively. Moreover, to identify prognostic candidate LMRGs in COAD for further research, univariate Cox regression analyses were performed to sift OS-related LMRGs in both TCGA-COAD and GSE40967 data sets (Figure 1D). In total, 22 and 98 significant OS-related genes were yielded, respectively, and eight equitant LMRGs (PLEC, BCS1L, CPT2, SDHB, COQ2, SLC39A8, PDSS2, and DLD) were factored into subsequent analyses (Figure 1E). Meanwhile, to obtain a more advanced understanding of these genes, a correlation network plot was presented to unravel the correlation features among eight eligible LMRGs (Figure 1F), and chromosomal positions and mRNA expression levels of these eight genes were illustrated by a circos plot (Figure 1G).

Establishment and validation of lactate-metabolism-related prognostic signature for patients with COAD

The above eight candidate LMRGs were subsequently analyzed through carrying out the LASSO Cox regression analysis in COAD patients of the GSE40967 training data set, and seven pivotal genes (PLEC, BCS1L, CPT2, SDHB, COQ2, SLC39A8, and PDSS2) were determined to build the prognostic signature (Figures 2A, B). In addition, Kaplan–Meier survival analyses were conducted to investigate the survival capability of every signature-contained gene in the training (Figure 2C) data set. From the results, we found that high expression of PLEC and low expressions of BCS1L, CPT2, SDHB, COQ2, SLC39A8, and PDSS2 were significantly correlated with more unfavorable OS in COAD, which further supports the effectiveness of the selected genes. At length, a risk signature was constructed as follows: risk score = Expression of PLEC * 0.265886 - Expression of CPT2 * 0.106776 - Expression of BCS1L * 0.196516 - Expression of SLC39A8 * 0.040630 - Expression of PDSS2 * 0.059233 - Expression of SDHB * 0.033911- Expression of COQ2 * 0.196516.

Then, to further test the prognostic value of our risk signature, patients of the TCGA-COAD training set and the GSE40967 validation set were independently segregated into high- and low-risk subgroups based on the median value of the risk score (Figure 3A). As we expected, patients of the high-risk group had higher incidence of deaths and shorter OS probability in both training and validation cohorts (Figure 3B). Meanwhile, the Kaplan–Meier survival analysis of OS indicated that high-risk COAD patients had considerably more unfavorable OS probability across all cohorts (Figure 3C, GSE40967, $p = .00044$ TCGA-COAD, $p = .0044$). Moreover, we performed survival analysis in patients of TCGA-COAD according to another survival index, and the results show that patients with high risk had similarly poorer PFS ($p = .00085$), DFS ($p = .0076$), and DSS ($p = .00056$), which strongly proves the above conclusions (Figure 3E). Additionally, we carried out time-dependent ROC curves to evaluate the performance of the risk prediction model, which depicted good predictive capability with AUCs in the training set as 0.606, 0.603, 0.643, 0.625, and 0.611 for 1-, 2-, 3-, 4-, and 5-year OS, and AUCs in the validation set were 0.613, 0.648, 0.615, 0.607, and 0.565 for 1-, 2-, 3-, 4-, and 5-year OS, respectively (Figure 3D).

Evaluation of the correlation between risk scores and clinicopathological indicators in COAD

Overall appraisal of the relationship between risk scores and common clinicopathological factors in COAD patients was then assessed. In the GSE40967 cohort, conspicuous discrepancies were observed between risk scores and clinical features, including survival status ($p<.0001$), T ($p<.05$), N ($p<.0001$),

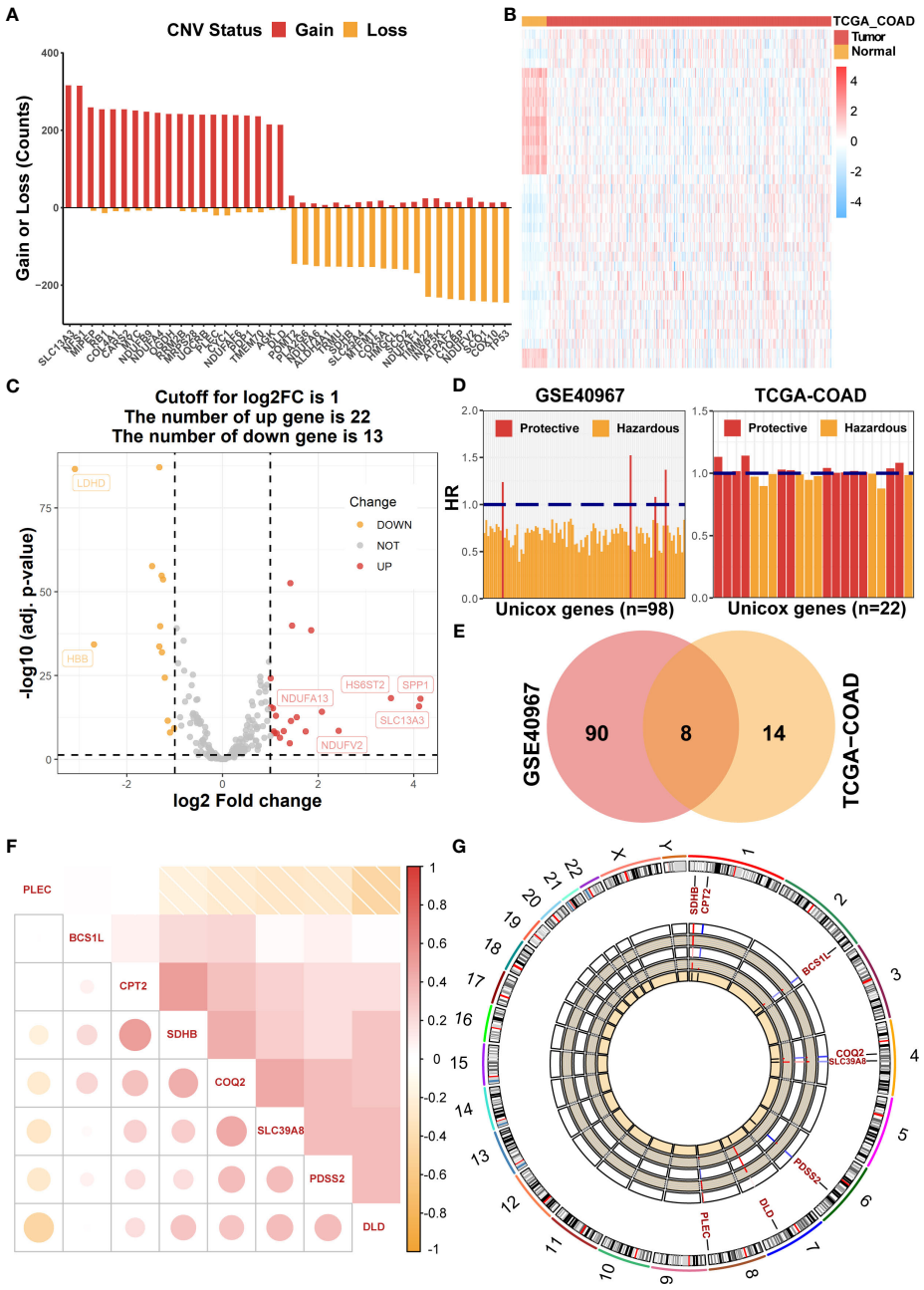

FIGURE 1
Identification of prognostic LMRGs in COAD patients. **(A)** The global CNV frequency of LMRGs in the TCGA-COAD cohort. **(B)** The heat map of differentially expressed LMRGs between adjacent and tumor samples in TCGA-COAD. **(C)** The volcano plot presenting differentially expressed genes among LMRGs. **(D)** OS-related LMRGs in GSE40967 and TCGA-COAD cohorts, respectively. **(E)** The Venn diagram to identify eight intersected prognostic LMRGs. **(F)** The correlation matrix plot exhibiting eight candidate LMRGs. **(G)** The Circos plot to illustrate regions on chromosomes and expressions of eight candidate LMRGs.

and AJCC stage (p<.0001) (Figure 4A). Similarly, significant correlations were also observed in the above indicators of the TCGA-COAD cohort (survival status, p<.05; N, p<.001; AJCC stage; p<.0001) except for T (Figure 4B). Of great interest, we noticed that the clinical features of COAD patients tended to be more severe as the risk scores increased, which reconfirmed the predictive value of the risk signature. Moreover, heat maps were also plotted to display the correlations between seven identified LMRGs and clinicopathological features in GSE40967 (Figure 4C) and TCGA-COAD (Figure 4D) data sets.

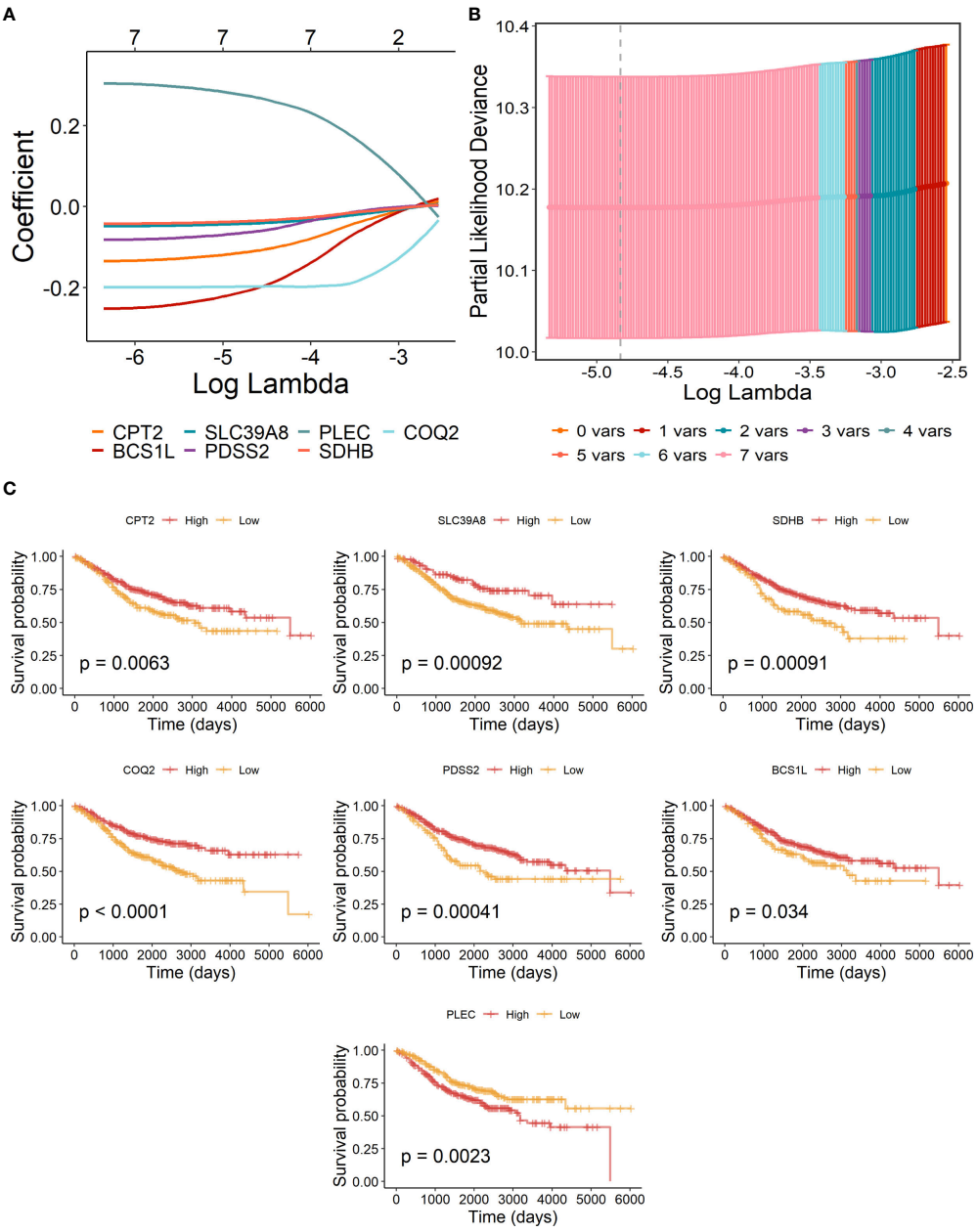

FIGURE 2
Construction of lactate-metabolism-related prognostic signature for COAD patients of the GSE40967 training group. **(A)** LASSO Cox regression analysis of the eight prognostic LMRGs. **(B)** Partial likelihood deviance for the LASSO regression to determine seven optimal prognostic LMRGs. **(C)** KM survival analyses of OS on the basis of mRNA expression levels of 7 LMRGs.

Construction and assessment of a prognostic nomogram based on the risk score signature

To further determine if the risk signature could serve as an independent prognostic indicator for COAD patients, we then conducted univariate and multivariate Cox regression analyses in GSE40967. The results disclosed that age, T, N, AJCC stage, and risk scores were all signally related to OS probability in the univariate Cox analysis (Figure 5A), whereas age, T, AJCC stage, and risk score remain independent prognostic factors after adjustment in the multivariate Cox analysis (Figure 5B). Subsequently, we developed a risk score–based nomogram to predict the individual OS probability of 2, 3, and 5 years according to the multivariate Cox analysis result (Figure 5C). Not surprisingly, the nomogram indicated that COAD patients with higher total points suffered a

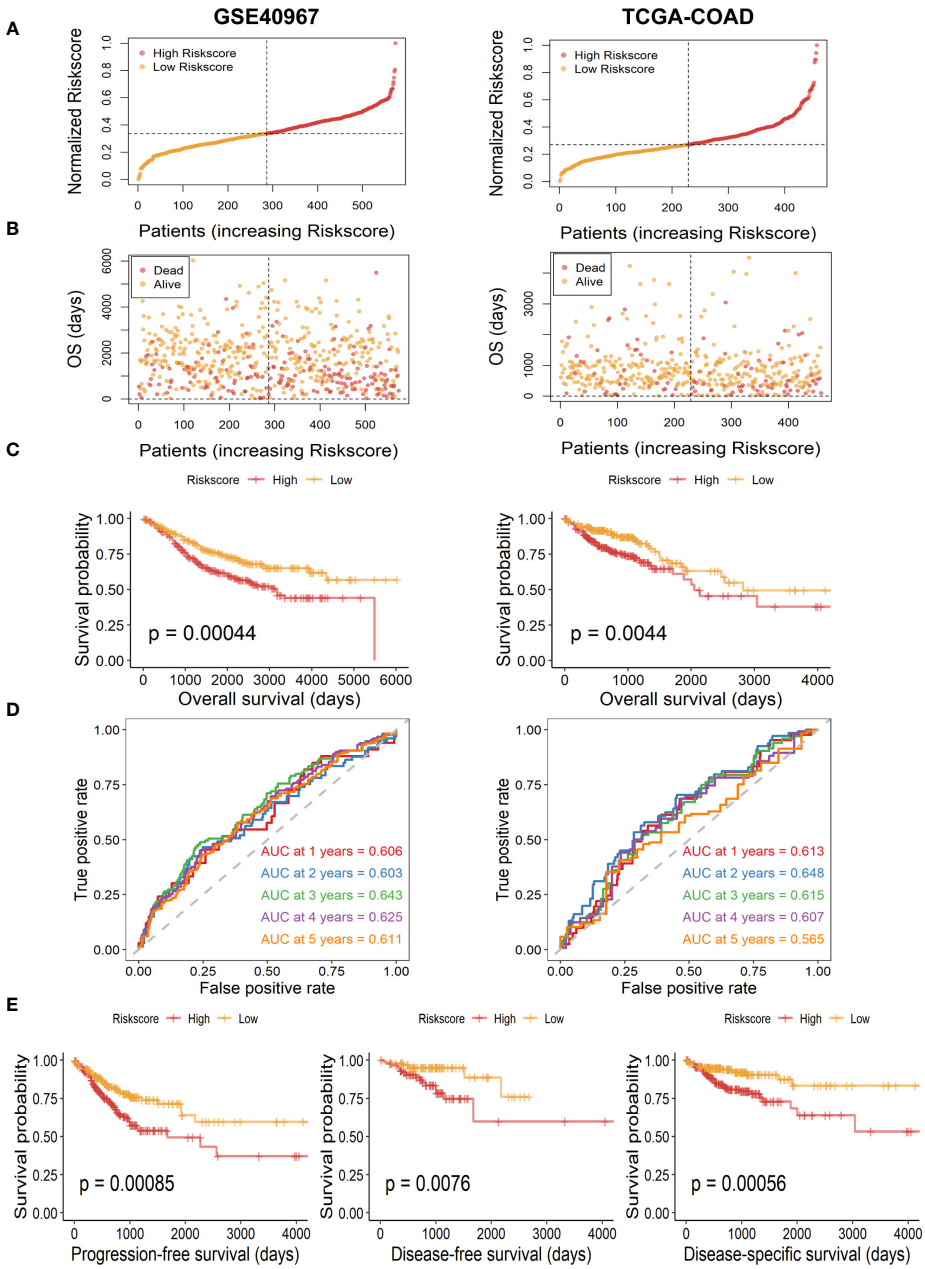

FIGURE 3
Assessment and validation of the availability of risk score in GSE40967 and TCGA-COAD sets. **(A)** Risk score distribution of COAD samples with different risks. **(B)** The distribution of risk score and OS time of COAD patients. **(C)** The Kaplan–Meier survival curves of OS according to high- and low-risk groups in patients with COAD. **(D)** The time-dependent ROC curves and AUC values for OS of the prognostic risk model. **(E)** The Kaplan–Meier survival curves of PFS, DFS, and DSS according to different risk groups.

lower survival chance. Moreover, calibration of the nomogram was assessed in a calibration plot, which displayed great fitness through comparing observed to predicted risk (Figure 5D). The DCA curve of the nomogram presented a more favorable clinical net benefit than any single factor (Figure 5E). Up to this point, the prognostic nomogram based on LMRG-related risk signature has been verified to have better OS prediction capability for COAD patients.

Evaluation of the correlation between risk score signature and immune landscape

As lactate metabolism has been recognized to play a vital role in TME, we first exploited "GSVA" enrichment analysis to unveil the discrepancy of immune-related pathways between high- and

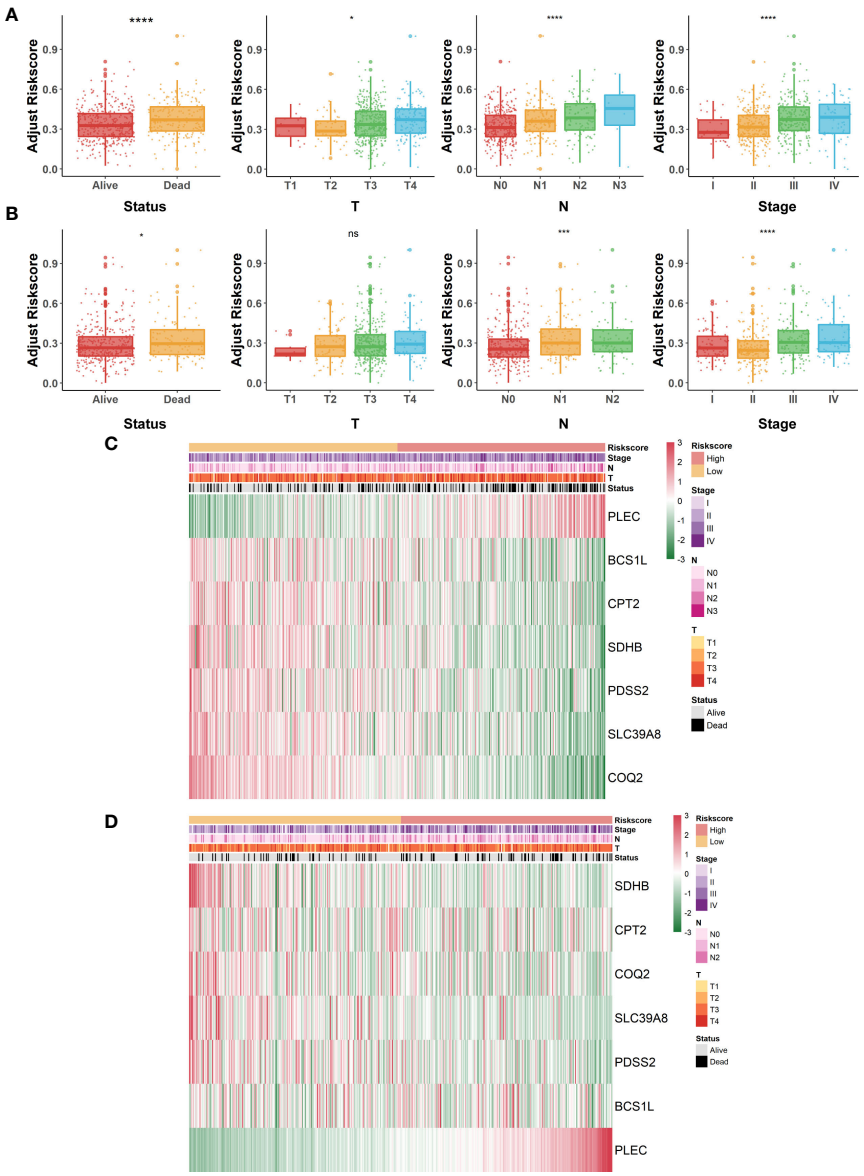

FIGURE 4
Correlation of lactate-metabolism-related risk signature and clinical indicators in COAD patients. **(A, B)** Box plots to present the relationship between different risk groups and clinicopathological characteristics of patients in GSE40967 **(A)** and TCGA-COAD **(B)**, respectively. **(C, D)** Correlation heat maps of risk signature-contained LMRGs and clinicopathological factors in GSE40967 **(C)** and TCGA-COAD **(D)** separately. *p < 0.05; ***p < 0.001; ****p < 0.0001; ns, not significant.

low-risk groups. As shown in Figure 6, neuroactive ligand receptor interaction, cytokine cytokine–receptor interaction, natural killer cell-mediated cytotoxicity, and chemokine signaling pathway were obviously enriched in the low-risk group of GSE40967 (Figure 6A), whereas neuroactive ligand receptor interaction, cytokine cytokine–receptor interaction, B-cell receptor signaling pathway, T-cell receptor signaling pathway, toll-like receptor signaling pathway, and chemokine signaling pathway were similarly enriched in the low-risk group of TCGA-COAD (Figure 6B). Then, we further compared the expression levels of common immune checkpoints within the two groups, and the results manifested that PD-1, PD-L1, and CTLA4 were all significantly augmented in the high-risk groups of both GSE40967 (Figure 6C) and TCGA-COAD data sets (Figure 6D), which unearthed the fact that COAD patients of high-risk groups may have an immunosuppressive TME and may also respond better to immunotherapy targeting the immune checkpoints.

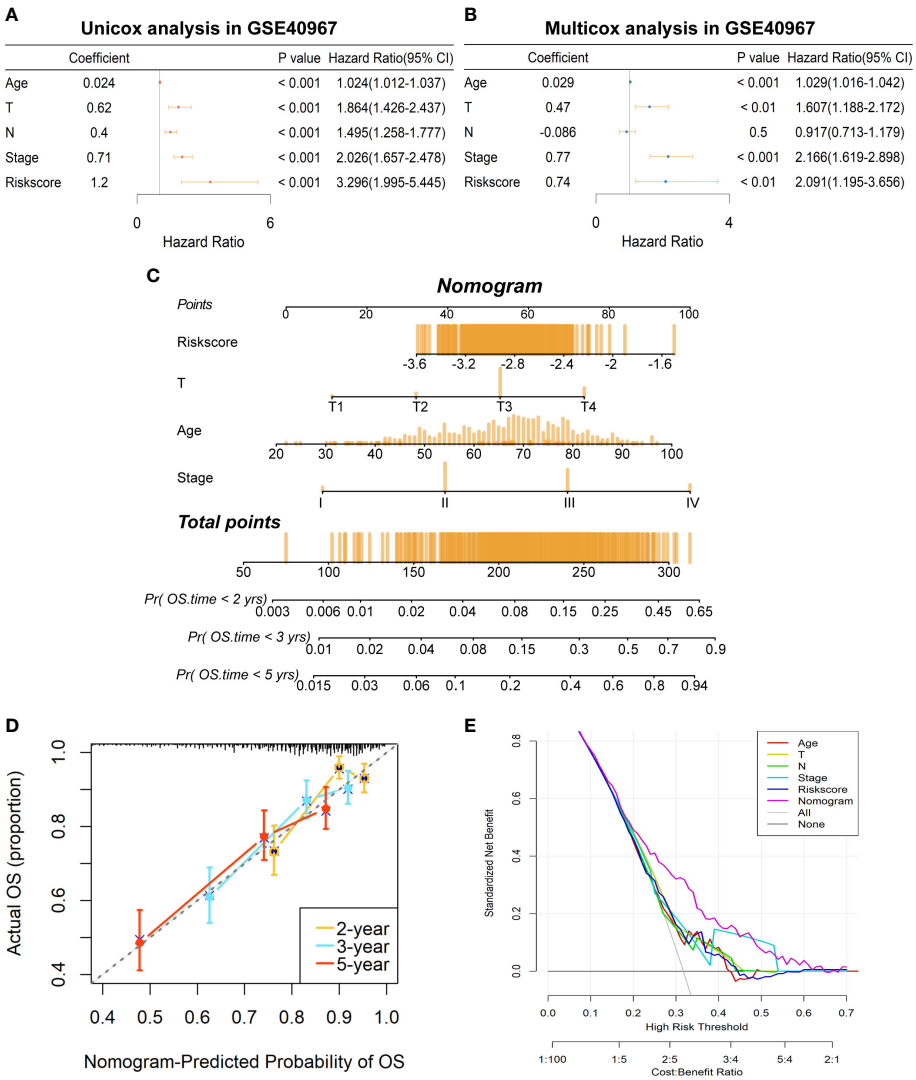

FIGURE 5
Establishment of a prognostic prediction nomogram based on the risk signature in GSE40967 training set. **(A)** The univariate Cox regression analysis of age, T, N, AJCC stage, and risk score for OS. **(B)** The multivariate Cox regression analysis of age, T, N, AJCC stage, and risk score for OS. **(C)** The prognostic nomogram was plotted to predict 2-, 3-, and 5-year survival probability of COAD patients. **(D)** The calibration plot was used to evaluate the prediction consistency of OS. **(E)** The DCA to assess clinical utility of the prognostic nomogram.

To more robustly demonstrate the effect of various risk scores on TME, the CIBERSORT algorithm was performed to estimate the infiltrating degree of immune cells in the TME of COAD in GSE40967. From the result, we found that naive B cells, resting memory CD4+ T cells, activated memory CD4+ T cells, and activated dendritic cells were markedly enriched in the TME of low-risk group, whereas macrophages M0 were notably strengthened in the high-risk group (Figure 6E). Judging from the results above, COAD patients with low risk might attain an immune-activated TME, which also supported that low-risk patients had more favorable prognoses.

Discussion

Although the treatment methods of COAD have been greatly improved, the prognoses of COAD patients remain dismal (30). Therefore, there is an urgent need to discover more accurate prognosis-related biomarkers and provide interventions as early as possible to improve the prognosis. Recently, it is worth drawing attention to the lactate metabolism, which has been reported to have played an unignorable role in tumorigenesis and progression, including COAD (10, 16). More strikingly, lactate was always produced by tumor cells and then accumulated in the

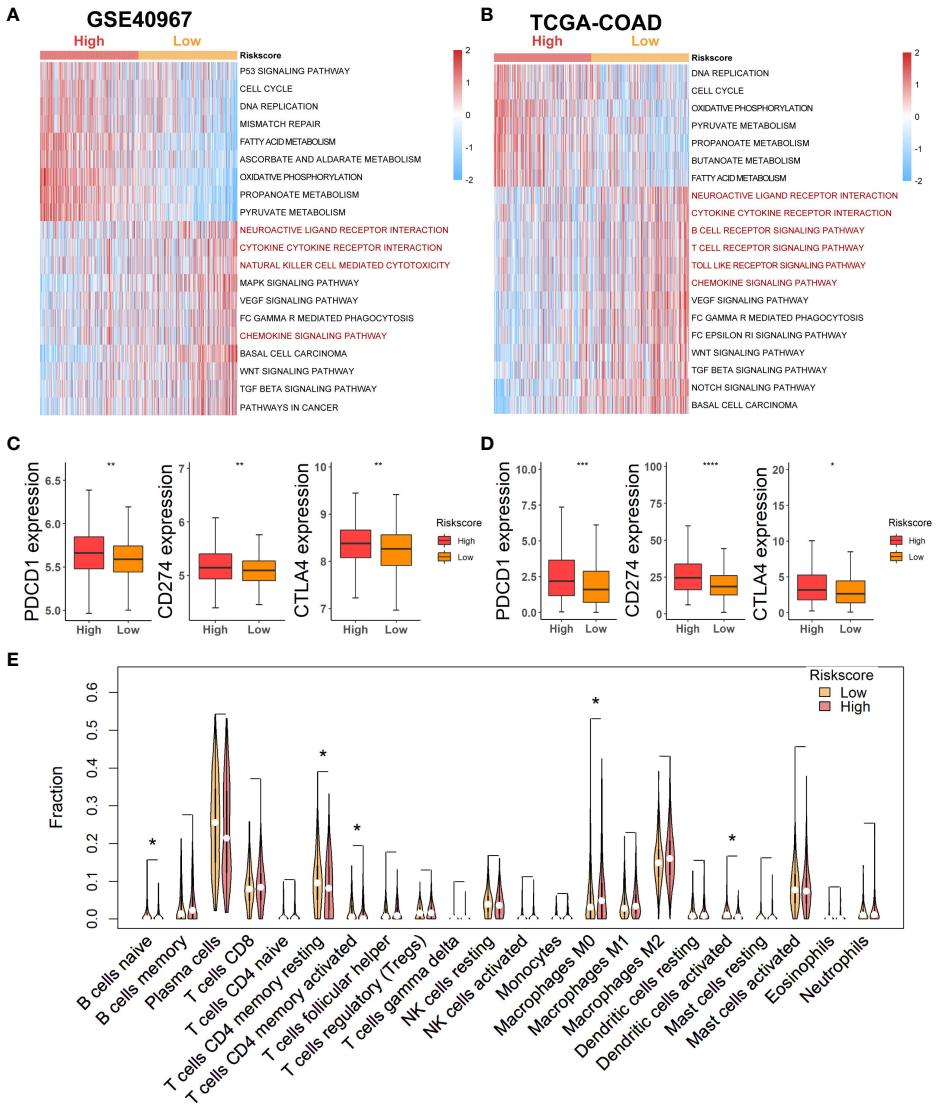

FIGURE 6
Estimation of potential relationship between various risk groups and immune landscape. **(A)** Results of GSVA analysis in GSE40967 to depict enriched immune-related pathways. **(B)** Results of GSVA analysis in TCGA-COAD to reveal enriched immune-related pathways. **(C, D)** Comparing expression levels of three classical markers of immune checkpoint between high- and low-risk groups in GSE40967 **(C)** and TCGA-COAD **(D)** separately. **(E)** Violin plots to show the relatively infiltrating abundances of 22 immune cells in COAD patients of GSE40967. *p < 0.05; **p < 0.01; ***p < 0.001; ****p < 0.0001.

TME, which subsequently generated some effects on tumor immune infiltrating cells, including inhibition of the functions of cytotoxic T, NK, and NKT cells (14, 15). Generally, the immunosuppressive role of lactate metabolism was associated with poorer response to immunotherapy of immune checkpoint inhibitors (ICIs). In several cancer types, high lactate dehydrogenase (LDH) levels have been verified to be independent biomarkers for predicting therapeutic response of ICIs (7, 8, 31). However, such research in COAD is still lacking. Based on the evidence above, we consolidated the mRNA expression profiles of LMRGs and the clinical data of COAD patients to explore novel prognosis-related biomarkers.

For searching the most effective LMRGs to construct the prognostic signature, we initially conducted univariate Cox regression analyses of OS in COAD patients of both GSE40967 and TCGA-COAD data sets. Furthermore, by optimization of eight available LMRGs with LASSO Cox regression analysis in GSE409678, seven pivotal genes were included to determine the risk signature, namely PLEC, BCS1L, CPT2, SDHB, COQ2, SLC39A8, and PDSS2.

Many studies have emerged implicating that PLEC (plectin) was a pro-tumorigenic regulator of tumor proliferation, migration, and invasion (32–34). Recent studies revealing the anticancer effect by directly targeting plectin have opened new avenues of research into plectin's role in cancer (35–37). For CRC, IHC analyses demonstrate increased expression of plectin in COAD and locally invasive nests compared with normal tissues (38). Suppression of plectin inhibited adhesion, migration, and invasion of colon carcinoma cells (39). Strikingly, knockout of plectin has also been implicated to reduce the motility of dermal fibroblasts and T cells *in vitro* as well as impaired the infiltration of macrophages and T cells during wound healing *in vivo* (40). Our study indicates that high expression of PLEC is related to poorer OS and clinicopathological features in COAD, which is consistent with the above evidence. However, more mechanisms to underpin these observations remain to be elucidated.

The carnitine palmitoyltransferase (CPT), including CPT1 and CPT2, are identified as important mediators of fatty acid oxidation (FAO) (41). CPT2 promotes the β-oxidation of fatty acids (FAs) through facilitating the conversion of acetyl-coenzyme A (CoA) to fatty acyl-CoA (42). CPT2 silencing is reported to facilitate the tumor progression of hepatocellular carcinoma, which is reconfirmed by our results (43). In addition, FAO mediated by CPTs also played an important role in tumor immunity (44).

SDHB was one of the four subunits comprising the succinate dehydrogenase (SDH) enzyme complex, which is related to the tricarboxylic acid (TCA) cycle and oxidative phosphorylation (45). The lack of SDHB function promotes the occurrence and development of several cancers, including liver and pancreatic cancer (46, 47). Similarly, the result of our analyses indicate that high expression of SDHB was related with better prognosis in COAD.

PDSS2 (prenyldiphosphate synthase subunit 2) was characterized as a tumor suppressor, and introduction of PDSS2 into cancer cells has been verified to inhibit tumor growth (48, 49). Likewise, the tumor suppressive role of PDSS2 was further strengthened with findings of COAD presented in our study. Regrettably, cancer-related studies of the other few candidate genes, including BCS1L, COQ2, and SLC39A8, are still absent, and we will seriously consider deeper research in our future studies.

The above seven LMRGs were selected to establish the prognostic signature, and then, prognosis and clinicopathological relevance of the risk signature were comprehensively evaluated. Based on the survival analyses, COAD patients of the high-risk group were confirmed to have shorter time of OS, PFS, DFS, and DSS. Moreover, the AUC values of ROC curves displayed good accuracy of the risk model in predicting 1-, 2-, 3-, 4-, and 5-year OS probability in both data sets independently. Furthermore, COAD patients of both training and validation cohorts were divided into different subgroups according to survival status, T, N, and AJCC stage. Not surprisingly, we found that with the risk score increasing, COAD patients tended to have worse clinical outcomes. Specifically, progressively higher risk scores were related to larger tumor size, more metastatic axillary lymph nodes, and more severe AJCC stage. Even more remarkably, through univariate and multivariate Cox regression analyses, the risk signature was considered as an independent prognostic factor when adjusted with clinical variables containing age, T, N, and AJCC stage. In addition, development of a prognostic nomogram also unfolded good prediction consistency and potential clinical feasibility of the risk score in COAD patients. Nevertheless, larger cohorts are needed to confirm the above results in prospective studies.

We have already mentioned that lactate metabolism was verified to play a significant role in the TME, and advancements in research on the TME and immunotherapy are expected to provide more valid improvements for the prognoses of CRC patients (50). Above all, we explored the difference of immune-related pathways between high- and low-risk groups using the "GSVA" enrichment analysis, and we found that some common immune-related pathways were enriched in the low-risk group of two data sets, including neuroactive ligand receptor interaction, cytokine cytokine–receptor interaction, and chemokine signaling pathway. Meanwhile, by comparing the expression differences of immune checkpoints, PD-1, PD-L1, and CTLA4 were all significantly upregulated in the high-risk group. Moreover, the result of the CIBERSORT algorithm also demonstrated that naive B cells, resting memory CD4+ T cells, activated memory CD4+ T cells, and activated dendritic cells were enriched in the TME of the low-risk group. Clues from the above three aspects implied that COAD with a higher risk value might be more likely to be immunosuppressed, which was consistent with the consensus that activated lactate metabolism usually promoted immune invasion and suppressed antitumor immune responses. As for the response to immunotherapy, we assumed that high-risk COAD patients would be more sensitive to ICIs as targeting immune checkpoints will transform the immune microenvironment of COAD with high risk from immunosuppression relative to immunoactivation.

Though all the conclusions in the present study should be further verified by experimental data, it primarily provides a comprehensive description of LMRGs in COAD and constructed a ponderable risk signature, which also has novel implications for immunotherapy in COAD patients.

Conclusion

In conclusion, our study establishes a reliable risk signature based on LMRGs for COAD patients. The signature was identified as an independent prognostic indicator through constructing a nomogram model that could accurately predict the survival probability of COAD patients. In addition, the potential relationship between different risk scores and tumor immune microenvironment was explored.

Broadly speaking, our study may provide important preclinical implications for cancer research about lactate metabolism and COAD.

Data availability statement

The original contributions presented in the study are included in the article/Supplementary Material. Further inquiries can be directed to the corresponding author.

Ethics statement

Ethical review and approval was not required for the study on human participants in accordance with the local legislation and institutional requirements. Written informed consent from the patients/participants or patients/participants' legal guardian/next of kin was not required to participate in this study in accordance with the national legislation and the institutional requirements.

Author contributions

All authors involved in the study have made a certain contribution, including designation (QX), data collection and analysis, manuscript drafting and revising (ZZ, YC, QL, XL, and QH) as well as study supervision (QX). All authors have read and approved the final manuscript submitted.

Acknowledgments

We are very grateful for the data support provided by public databases and constructive and helpful comments from the reviewers.

Conflict of interest

The authors declare that the research was conducted in the absence of any commercial or financial relationships that could be construed as a potential conflict of interest.

Publisher's note

All claims expressed in this article are solely those of the authors and do not necessarily represent those of their affiliated organizations, or those of the publisher, the editors and the reviewers. Any product that may be evaluated in this article, or claim that may be made by its manufacturer, is not guaranteed or endorsed by the publisher.

Supplementary material

The Supplementary Material for this article can be found online at: https://www.frontiersin.org/articles/10.3389/fonc.2022.958221/full#supplementary-material

References

1. Hao Y, Chen Y, He X, Yu Y, Han R, Li Y, et al. Polymeric nanoparticles with ROS-responsive prodrug and platinum nanozyme for enhanced chemophotodynamic therapy of colon cancer. *Adv Sci (Weinh)* (2020) 7(20):2001853. doi: 10.1002/advs.202001853

2. Ding D, Zhong H, Liang R, Lan T, Zhu X, Huang S, et al. Multifunctional nanodrug mediates synergistic photodynamic therapy and MDSCs-targeting immunotherapy of colon cancer. *Adv Sci (Weinh)* (2021) 8(14):e2100712. doi: 10.1002/advs.202100712

3. Palma S, Zwenger AO, Croce MV, Abba MC, Lacunza E. From molecular biology to clinical trials: Toward personalized colorectal cancer therapy. *Clin Colorectal Cancer* (2016) 15(2):104–15. doi: 10.1016/j.clcc.2015.11.001

4. Warburg O. On the origin of cancer cells. *Science* (1956) 123(3191):309–14. doi: 10.1126/science.123.3191.309

5. Chen P, Zuo H, Xiong H, Kolar MJ, Chu Q, Saghatelian A, et al. Gpr132 sensing of lactate mediates tumor-macrophage interplay to promote breast cancer metastasis. *Proc Natl Acad Sci U S A* (2017) 114(3):580–5. doi: 10.1073/pnas.1614035114

6. Walenta S, Wetterling M, Lehrke M, Schwickert G, Sundfor K, Rofstad EK, et al. High lactate levels predict likelihood of metastases, tumor recurrence, and restricted patient survival in human cervical cancers. *Cancer Res* (2000) 60(4):916–21.

7. Wang X, Zhang B, Chen X, Mo H, Wu D, Lan B, et al. Lactate dehydrogenase and baseline markers associated with clinical outcomes of advanced esophageal squamous cell carcinoma patients treated with camrelizumab (SHR-1210), a novel anti-PD-1 antibody. *Thorac Cancer* (2019) 10(6):1395–401. doi: 10.1111/1759-7714.13083

8. Zhang Z, Li Y, Yan X, Song Q, Wang G, Hu Y, et al. Pretreatment lactate dehydrogenase may predict outcome of advanced non small-cell lung cancer patients treated with immune checkpoint inhibitors: A meta-analysis. *Cancer Med* (2019) 8(4):1467–73. doi: 10.1002/cam4.2024

9. Zhao H, Yan C, Hu Y, Mu L, Liu S, Huang K, et al. Differentiated cancer cell-originated lactate promotes the self-renewal of cancer stem cells in patient-derived colorectal cancer organoids. *Cancer Lett* (2020) 493:236–44. doi: 10.1016/j.canlet.2020.08.044

10. Li G, Wang Z, Xu J, Wu H, Cai S, He Y. The prognostic value of lactate dehydrogenase levels in colorectal cancer: A meta-analysis. *BMC Cancer* (2016) 16:249. doi: 10.1186/s12885-016-2276-3

11. Lin S, Liu Q, Wen J, Bai K, Guo Y, Wang J. Mir-124 attenuates STAT3-mediated TH17 differentiation in colitis-driven colon cancer. *Front Oncol* (2020) 10:570128. doi: 10.3389/fonc.2020.570128

12. Tauriello DVF, Batlle E. Targeting the microenvironment in advanced colorectal cancer. *Trends Cancer* (2016) 2(9):495–504. doi: 10.1016/j.trecan.2016.08.001

13. Mercier-Letondal P, Marton C, Godet Y, Galaine J. Validation of a method evaluating T cell metabolic potential in compliance with ICH Q2 (R1). *J Transl Med* (2021) 19(1):21. doi: 10.1186/s12967-020-02672-7

14. Comito G, Iscaro A, Bacci M, Morandi A, Ippolito L, Parri M, et al. Lactate modulates CD4(+) T-cell polarization and induces an immunosuppressive environment, which sustains prostate carcinoma progression *via* TLR8/miR21 axis. *Oncogene* (2019) 38(19):3681–95. doi: 10.1038/s41388-019-0688-7

15. Husain Z, Huang Y, Seth P, Sukhatme VP. Tumor-derived lactate modifies antitumor immune response: effect on myeloid-derived suppressor cells and NK cells. *J Immunol* (2013) 191(3):1486–95. doi: 10.4049/jimmunol.1202702

16. Harmon C, Robinson MW, Hand F, Almuaili D, Mentor K, Houlihan DD, et al. Lactate-mediated acidification of tumor microenvironment induces apoptosis

of liver-resident NK cells in colorectal liver metastasis. *Cancer Immunol Res* (2019) 7(2):335–46. doi: 10.1158/2326-6066.CIR-18-0481

17. Daneshmandi S, Wegiel B, Seth P. Blockade of lactate dehydrogenase-a (LDH-a) improves efficacy of anti-programmed cell death-1 (PD-1) therapy in melanoma. *Cancers (Basel)* (2019) 11(4). doi: 10.3390/cancers11040450

18. Yang L, Tan P, Sun H, Zeng Z, Pan Y. Integrative dissection of novel lactate metabolism-related signature in the tumor immune microenvironment and prognostic prediction in breast cancer. *Front Oncol* (2022) 12:874731. doi: 10.3389/fonc.2022.874731

19. McCarthy DJ, Chen Y, Smyth GK. Differential expression analysis of multifactor RNA-seq experiments with respect to biological variation. *Nucleic Acids Res* (2012) 40(10):4288–97. doi: 10.1093/nar/gks042

20. Xie J, Tian W, Tang Y, Zou Y, Zheng S, Wu L, et al. Establishment of a cell necroptosis index to predict prognosis and drug sensitivity for patients with triple-negative breast cancer. *Front Mol Biosci* (2022) 9:834593. doi: 10.3389/fmolb.2022.834593

21. Zhang H, Meltzer P, Davis S. RCircos: an r package for circos 2D track plots. *BMC Bioinf* (2013) 14:244. doi: 10.1186/1471-2105-14-244

22. Zhang Z, Kattan MW. Drawing nomograms with r: applications to categorical outcome and survival data. *Ann Transl Med* (2017) 5(10):211. doi: 10.21037/atm.2017.04.01

23. Tang Y, Tian W, Xie J, Zou Y, Wang Z, Li N, et al. Prognosis and dissection of immunosuppressive microenvironment in breast cancer based on fatty acid metabolism-related signature. *Front Immunol* (2022) 13:843515. doi: 10.3389/fimmu.2022.843515

24. Alba AC, Agoritsas T, Walsh M, Hanna S, Iorio A, Devereaux PJ, et al. Discrimination and calibration of clinical prediction models: Users' guides to the medical literature. *JAMA* (2017) 318(14):1377–84. doi: 10.1001/jama.2017.12126

25. Hanzelmann S, Castelo R, Guinney J. GSVA: Gene set variation analysis for microarray and RNA-seq data. *BMC Bioinf* (2013) 14:7. doi: 10.1186/1471-2105-14-7

26. Zheng S, Zou Y, Tang Y, Yang A, Liang JY, Wu L, et al. Landscape of cancer-associated fibroblasts identifies the secreted biglycan as a protumor and immunosuppressive factor in triple-negative breast cancer. *Oncoimmunology* (2022) 11(1):2020984. doi: 10.1080/2162402X.2021.2020984

27. Newman AM, Liu CL, Green MR, Gentles AJ, Feng W, Xu Y, et al. Robust enumeration of cell subsets from tissue expression profiles. *Nat Methods* (2015) 12 (5):453–7. doi: 10.1038/nmeth.3337

28. Zheng S, Zou Y, Xie X, Liang JY, Yang A, Yu K, et al. Development and validation of a stromal immune phenotype classifier for predicting immune activity and prognosis in triple-negative breast cancer. *Int J Cancer* (2020) 147(2):542–53. doi: 10.1002/ijc.33009

29. Zou Y, Zheng S, Xie X, Ye F, Hu X, Tian Z, et al. N6-methyladenosine regulated FGFR4 attenuates ferroptotic cell death in recalcitrant HER2-positive breast cancer. *Nat Commun* (2022) 13(1):2672. doi: 10.1038/s41467-022-30217-7

30. Liang B, Shahbaz M, Wang Y, Gao H, Fang R, Niu Z, et al. Integrinbeta6-targeted immunoliposomes mediate tumor-specific drug delivery and enhance therapeutic efficacy in colon carcinoma. *Clin Cancer Res* (2015) 21(5):1183–95. doi: 10.1158/1078-0432.CCR-14-1194

31. Schouwenburg MG, Suijkerbuijk KPM, Koornstra RHT, Jochems A, van Zeijl MCT, van den Eertwegh AJM, et al. Switching to immune checkpoint inhibitors upon response to targeted therapy; the road to long-term survival in advanced melanoma patients with highly elevated serum LDH? *Cancers (Basel)* (2019) 11(12). doi: 10.3390/cancers11121940

32. Katada K, Tomonaga T, Satoh M, Matsushita K, Tonoike Y, Kodera Y, et al. Plectin promotes migration and invasion of cancer cells and is a novel prognostic marker for head and neck squamous cell carcinoma. *J Proteomics* (2012) 75 (6):1803–15. doi: 10.1016/j.jprot.2011.12.018

33. Buckup M, Rice MA, Hsu EC, Garcia-Marques F, Liu S, Aslan M, et al. Plectin is a regulator of prostate cancer growth and metastasis. *Oncogene* (2021) 40 (3):663–76. doi: 10.1038/s41388-020-01557-9

34. Shin SJ, Smith JA, Rezniczek GA, Pan S, Chen R, Brentnall TA, et al. Unexpected gain of function for the scaffolding protein plectin due to mislocalization in pancreatic cancer. *Proc Natl Acad Sci U S A* (2013) 110 (48):19414–9. doi: 10.1073/pnas.1309720110

35. Wernitznig D, Meier-Menches SM, Cseh K, Theiner S, Wenisch D, Schweikert A, et al. Plecstatin-1 induces an immunogenic cell death signature in colorectal tumour spheroids. *Metallomics* (2020) 12(12):2121–33. doi: 10.1039/d0mt00227e

36. Meier SM, Kreutz D, Winter L, Klose MHM, Cseh K, Weiss T, et al. An organoruthenium anticancer agent shows unexpected target selectivity for plectin. *Angew Chem Int Ed Engl* (2017) 56(28):8267–71. doi: 10.1002/anie.201702242

37. Meier-Menches SM, Zappe K, Bileck A, Kreutz D, Tahir A, Cichna-Markl M, et al. Time-dependent shotgun proteomics revealed distinct effects of an organoruthenium prodrug and its activation product on colon carcinoma cells. *Metallomics* (2019) 11(1):118–27. doi: 10.1039/C8MT00152A

38. Lee KY, Liu YH, Ho CC, Pei RJ, Yeh KT, Cheng CC, et al. An early evaluation of malignant tendency with plectin expression in human colorectal adenoma and adenocarcinoma. *J Med* (2004) 35(1-6). doi: 10.2147/OTT.S163266

39. McInroy L, Maatta A. Plectin regulates invasiveness of SW480 colon carcinoma cells and is targeted to podosome-like adhesions in an isoform-specific manner. *Exp Cell Res* (2011) 317(17):2468–78. doi: 10.1016/j.yexcr.2011.07.013

40. Abrahamsberg C, Fuchs P, Osmanagic-Myers S, Fischer I, Propst F, Elbe-Burger A, et al. Targeted ablation of plectin isoform 1 uncovers role of cytolinker proteins in leukocyte recruitment. *Proc Natl Acad Sci U S A* (2005) 102(51):18449–54. doi: 10.1073/pnas.0505380102

41. Foster DW. The role of the carnitine system in human metabolism. *Ann N Y Acad Sci* (2004) 1033:1–16. doi: 10.1196/annals.1320.001

42. McGarry JD, Brown NF. The mitochondrial carnitine palmitoyltransferase system. from concept to molecular analysis. *Eur J Biochem* (1997) 244(1):1–14. doi: 10.3390/cancers12010042

43. Lin M, Lv D, Zheng Y, Wu M, Xu C, Zhang Q, et al. Downregulation of CPT2 promotes tumorigenesis and chemoresistance to cisplatin in hepatocellular carcinoma. *Onco Targets Ther* (2018) 11:3101–10. doi: 10.2147/OTT.S163266

44. Hossain F, Al-Khami AA, Wyczechowska D, Hernandez C, Zheng L, Reiss K, et al. Inhibition of fatty acid oxidation modulates immunosuppressive functions of myeloid-derived suppressor cells and enhances cancer therapies. *Cancer Immunol Res* (2015) 3(11):1236–47. doi: 10.1158/2326-6066.CIR-15-0036

45. Rustin P, Munnich A, Rotig A. Succinate dehydrogenase and human diseases: new insights into a well-known enzyme. *Eur J Hum Genet* (2002) 10 (5):289–91. doi: 10.1038/sj.ejhg.5200793

46. Tseng PL, Wu WH, Hu TH, Chen CW, Cheng HC, Li CF, et al. Decreased succinate dehydrogenase b in human hepatocellular carcinoma accelerates tumor malignancy by inducing the warburg effect. *Sci Rep* (2018) 8(1):3081. doi: 10.1038/s41598-018-21361-6

47. Rahn S, Barbosa PD, Moller JL, Ammar N, Demetrowitsch T, Helm O, et al. Inflammation associated pancreatic tumorigenesis: Upregulation of succinate dehydrogenase (Subunit b) reduces cell growth of pancreatic ductal epithelial cells. *Cancers (Basel)* (2019) 12(1). doi: 10.3390/cancers12010042

48. Fung JM, Smith R, Brown MA, Lau SH, Xie D, Lau GK, et al. Identification and characterization of a novel melanoma tumor suppressor gene on human chromosome 6q21. *Clin Cancer Res* (2009) 15(3):797–803. doi: 10.1158/1078-0432.CCR-08-1472

49. Chen P, Zhao SH, Chu YL, Xu K, Zhu L, Wu Y, et al. Anticancer activity of PDSS2, prenyl diphosphate synthase, subunit 2, in gastric cancer tissue and the SGC7901 cell line. *Anticancer Drugs* (2009) 20(2):141–8. doi: 10.1097/CAD.0b013e32832016a9

50. Chen Y, Zheng X, Wu C. The role of the tumor microenvironment and treatment strategies in colorectal cancer. *Front Immunol* (2021) 12:792691. doi: 10.3389/fimmu.2021.792691

frontiers | Frontiers in Oncology

TYPE Original Research
PUBLISHED 16 September 2022
DOI 10.3389/fonc.2022.1000957

Check for updates

OPEN ACCESS

EDITED BY
Pranav Gupta,
Albert Einstein College of Medicine,
United States

REVIEWED BY
Xia Guo,
Sichuan University, China
HAO Xu,
Sichuan University, China

*CORRESPONDENCE
Indraneel Mittra
imittra@actrec.gov.in

SPECIALTY SECTION
This article was submitted to Molecular and Cellular Oncology, a section of the journal Frontiers in Oncology

RECEIVED 22 July 2022
ACCEPTED 31 August 2022
PUBLISHED 16 September 2022

CITATION
Pilankar A, Singhavi H, Raghuram GV, Siddiqui S, Khare NK, Jadhav V, Tandel H, Pal K, Bhattacharjee A, Chaturvedi P and Mittra I (2022) A pro-oxidant combination of resveratrol and copper down-regulates hallmarks of cancer and immune checkpoints in patients with advanced oral cancer: Results of an exploratory study (RESCU 004).
Front. Oncol. 12:1000957.
doi: 10.3389/fonc.2022.1000957

COPYRIGHT
© 2022 Pilankar, Singhavi, Raghuram, Siddiqui, Khare, Jadhav, Tandel, Pal, Bhattacharjee, Chaturvedi and Mittra. This is an open-access article distributed under the terms of the Creative Commons Attribution License (CC BY). The use, distribution or reproduction in other forums is permitted, provided the original author(s) and the copyright owner(s) are credited and that the original publication in this journal is cited, in accordance with accepted academic practice. No use, distribution or reproduction is permitted which does not comply with these terms.

A pro-oxidant combination of resveratrol and copper down-regulates hallmarks of cancer and immune checkpoints in patients with advanced oral cancer: Results of an exploratory study (RESCU 004)

Aishwarya Pilankar[1,2], Hitesh Singhavi[2,3], Gorantla V. Raghuram[1,2], Sophiya Siddiqui[1,2], Naveen Kumar Khare[1,2], Vishalkumar Jadhav[1,2], Harshali Tandel[1,2], Kavita Pal[1,2], Atanu Bhattacharjee[2,4], Pankaj Chaturvedi[2,3] and Indraneel Mittra[1,2*]

[1]Translational Research Laboratory, Tata Memorial Centre, Advanced Centre for Treatment, Research and Education in Cancer, Navi Mumbai, India, [2]Homi Bhabha National Institute, Mumbai, India, [3]Department of Head and Neck Surgery, Tata Memorial Centre, Tata Memorial Hospital, Mumbai, India, [4]Section of Biostatistics, Tata Memorial Centre, Centre for Cancer Epidemiology, Navi Mumbai, India

Background: Our earlier studies have shown that cell-free chromatin particles (cfChPs) that are released from dying cancer cells are readily internalised by bystander cells leading to activation of two hallmarks of cancer viz. genome instability and inflammation. These hallmarks could be down-regulated by deactivating cfChPs *via* medium of oxygen radicals generated upon admixing small quantities of the nutraceuticals resveratrol (R) and copper (Cu). In this exploratory study, we investigated whether oral administration of R and Cu (R-Cu) would down-regulate the hallmarks of cancer and immune checkpoints in advanced squamous cell carcinoma of oral cavity (OSCC).

Patients and methods: The study comprised of 25 patients divided into 5 equal groups. Five patients acted as controls; the remaining 20 were given R-Cu in four escalating doses. The lowest dose of R-Cu was 5.6mg and 560ng respectively, and the highest dose was 500mg and 5mg respectively. An initial biopsy was taken from patients at first presentation, and a second biopsy was taken 2 weeks later on the operating table. R-Cu was administered orally twice daily in the intervening period. Confocal microscopy was performed on tumour sections after fluorescent immuno-staining with anti-DNA and anti-histone antibodies to detect presence of cfChPs in the tumour micro-environment (TME). Immunofluorescence

analysis was performed for 23 biomarkers representing the 10 Hallmarks of cancer, including 5 immune checkpoints, defined by Hanahan and Weinberg.

Results: Confocal microscopy detected copious presence of cfChPs in TME of OSCC, which were eradicated/deactivated following two-week treatment with R-Cu. Eradication of cfChPs from TME was associated with marked down-regulation of 21/23 biomarkers, including the five immune checkpoints. The lower two doses of R-Cu were more effective than the higher doses. No adverse effects attributable to R-Cu were observed.

Conclusion: These results suggest that cfChPs released into TME from dying cancer cells are global instigators for cancer hallmarks and immune checkpoints in surviving cancer cells. The ability of R-Cu to deactivate cfChPs raises the prospect of a novel and non-toxic form of cancer treatment which sans killing of cancer cells, and instead induces healing by down-regulating cancer hallmarks and immune check-points.

Clinical Trial Registration: http://ctri.nic.in/Clinicaltrials/pmaindet2.php?trialid=19801&EncHid=&userName=CTRI/2018/03/012459.

KEYWORDS

tumour microenvironment, apoptosis, cell death, immune blockade, immunotherapy, stress

Introduction

Results of treatment of advanced squamous cell carcinoma of oral cavity (OSCC) continue to remain unsatisfactory, and is associated with considerable toxic side effects. Novel therapeutic approaches that are non-toxic are urgently needed. Our earlier studies have shown that cell-free chromatin particles (cfChPs) that are released from dying cancer cells can readily enter into surrounding bystander cells leading to activation of two critical hallmarks of cancer viz. dsDNA breaks (genome instability) and inflammation, which could lead to their oncogenic transformation (1). Activation of these cancer hallmarks could be abrogated by concurrent treatment with a combination of the nutraceuticals resveratrol (R) and copper (Cu) (1, 2). Fukuhara et al. were the first to demonstrate that oxygen radicals are generated upon admixing R and Cu (3). They showed that R acts as a catalyst to reduce Cu (II) to Cu (I) resulting in generation of oxygen radicals that are capable of cleaving plasmid pBR322 DNA (3, 4). We have extended these findings to show that oxygen radicals that are generated following admixture of R and Cu (R-Cu) can degrade genomic DNA and RNA (5), and can deactivate extra-cellular cfChPs by degrading their DNA component, both *in vitro* and *in vivo* (1, 2, 6–10).

Oxygen radicals are short lived molecular entities which contain an unpaired electron making them exceptionally reactive as they search for another electron to pair with, and in the process they can damage biomolecules such as DNA, proteins and lipids (11). Oxygen radical are normally generated by mitochondria (12); their over-production leads to oxidative stress which has several harmful effects on host cells (13). However, paradoxically, when oxygen radicals are artificially generated in the extracellular compartments of the body, such as by R-Cu, they can have wide ranging therapeutic effects in animal models and in human conditions that are associated with elevated levels of extracellular cfChPs (2, 6–10). These effects are mediated *via* the ability of oxygen radicals to deactivate extracellular cfChPs.

Oral administration of R-Cu leads to generation of oxygen radicals in the stomach, which are readily absorbed and have systemic effects in the form of deactivation of extracellular cfChPs. The cellular genomes are, however, protected from damage as the entry of oxygen radicals triggers the cells to activate their anti-oxidant defence mechanism which detoxifies the invading agents (8). Our pre-clinical studies have shown that oral administration of small quantities of R-Cu can have remarkable therapeutic effects in conditions associated with elevated levels of extracellular cfChPs (2, 6–8). For example, R-Cu administered orally can prevent toxic side effects of chemotherapy (6), and radiotherapy (2), and prevent fatality in mice following bacterial endotoxin induced sepsis (7). We

have also shown that prolonged oral administration of R-Cu to ageing mice can down-regulate several biological hallmarks of ageing and neurodegeneration (8). Our early results in patients receiving high dose chemotherapy and bone marrow transplantation for multiple myeloma have shown that orally administered R-Cu can significantly reduce Grade III-IV mucositis (9). Blood levels of inflammatory cytokines were also found to be significantly reduced following R-Cu treatment in that study (9). We have also shown in an observational study that oral administration of R-Cu to patients with severe Covid-19 reduced mortality by nearly 50% (10). Significantly, we have discovered that cfChPs deactivating activity of R-Cu is retained even when the molar concentration of Cu is reduced 10,000 fold with respect to that of R (2, 5–10). Consequently, in our pre-clinical and clinical studies, the molar ratio of R to Cu was maintained at $1{:}10^{-4}$ (2, 6–10).

In the present exploratory study, we investigated whether oral administration of R-Cu would lead to down-regulation of hallmarks of cancer and immune checkpoints in patients with OSCC. We show that cfChPs that were released from dying cancer cells are abundantly present in the tumour microenvironment (TME), and that orally administered R-Cu dramatically reduced cfChPs in TME. Elimination of cfChPs from TME was associated with significant down-regulation of 21/23 biomarkers representing the 10 hallmarks of cancer, including 5 immune check-points, that have been defined by Hanahan and Weinberg. These exploratory findings suggest that prolonged treatment with R-Cu may have the potential to induce healing without having to kill cancer cells.

Patients and methods

Ethics approval

This study was approved by Institutional Ethics Committee (IEC) of Advanced Centre for Treatment, Research and Education in Cancer, Tata Memorial Centre. A written informed consent was obtained from all study participants as stipulated by IEC. The trial was registered under Clinical Trial Registry of India (http://ctri.nic.in/Clinicaltrials/pmaindet2.php?trialid=19801&EncHid=&userName=CTRI/2018/03/012459).

Patients and R-Cu treatment

The study comprised of 25 patients with advanced OSCC who were divided into 5 groups of 5 patients each. Demographic details, histopathological type and grade, and tumour stage distribution of the 25 patients are given in Supplementary Table 1. All patients who were deemed to be suitable for surgery by the attending surgeon were included in this study. This being as exploratory study, no formal sample size calculation was undertaken; 25 seemed to us to be a feasible sample size since this number of patients could be recruited in 1 year to give us an inkling as to whether R-Cu was effective at all. A representative image of OSCC and H&E section of the tumour is given in Supplementary Figure 1. The first 5 patients acted as controls; the remaining 20 were given R-Cu orally, twice daily, in four escalating doses (Supplementary Table 2). Resveratrol (trade name TRANSMAX^{TM}) was procured from Biotivia, USA https://www.biotivia.com/product/transmax/); Chelated Copper was procured from Calrson Laboratories, USA (https://carlsonlabs.com/chelated-copper/). The lowest dose of R-Cu (Dose level I) comprised of 5.6mg of R and 560ng of Cu (molar ratio $1{:}10^{-4}$). This dose was arrived at by direct conversion of dose of R and Cu that we have used in our pre-clinical studies (R = 1mg/Kg and that of Cu 0.1μg/Kg) using a standard conversion formula (14). Dose levels II and III were approximately 10 fold and 100 fold higher than dose level I; dose level IV comprised of doses of R and Cu that have been recommended by the respective vendors for use as health supplements. Toxic side effects related to R-Cu treatment was monitored using CTCAE v3.03 guidelines.

R is supplied by the vendor as capsules containing 500mg of trans-resveratrol powder, and Cu is supplied as 5 mg tablets. For the purposes of this study, R powder was removed from the capsules and weighed as per requirement. Cu tablets were crushed in a pestle and mortar and the powder was weighed as per requirement. R powder being insoluble in water, and unpalatable at higher doses, was administered using honey as a vehicle (~15 mL). Cu, being soluble in water was administered as water based solution (20mL). R and Cu were administered orally, one after the other, twice daily for 2 weeks. The control group received vehicles (honey and water) alone. All above administrations were made on an empty stomach.

A diagnostic punch biopsy was taken from patients under local anaesthesia at the time of their first presentation to Tata Memorial Hospital, and a second biopsy was taken 2 weeks later at the time of surgery on the operating table under anaesthesia. In the intervening two weeks, R-Cu was administered orally in four escalating doses as described above (Supplementary Table 2). The control group received vehicles alone (~15mL honey followed by 20 mL of water). No adverse side effects attributable to R-Cu were recorded.

Fluorescence immune-staining and confocal microscopy

Formalin fixed paraffin embedded (FFPE) sections of tumour tissues were stained with fluorescent anti-DNA and anti-histone antibodies and examined by confocal microscopy, as described by us earlier (7). This was done to investigate the presence of cfChPs (if any) in TME. Fluorescence intensity was

quantified by randomly choosing five confocal fields (~ 50 cells per field), and calculating mean fluorescence intensity (MFI) which was expressed as mean ± S.E.M.

Immunofluorescence

Indirect immunofluorescence (IF) on FFPE sections of tumour tissues were performed according to the method described by us earlier (1). All IF analyses were performed in a blinded fashion such that the examiner was unaware of the identity of the slides being analysed. IF was used to assess the expression of 3 anti-oxidant enzymes viz. superoxide dismutase, catalase and glutathione peroxidase. Also examined by IF were 23 biomarkers representing 10 hallmarks of cancer, including 5 immune checkpoints (Supplementary Table 3). Source and catalogue numbers of antibodies used are given in (Supplementary Tables 4A–C). One thousand cells were analysed on each slide for all IF studies, and the number of positive cells was recorded. Results were expressed as mean number of positive cells (± SEM)/1000 cells.

Statistical analysis

Statistical comparison of pre versus post treatment values was performed in two ways: 1) combined comparison of all four treatment groups with the control group was performed applying two-way ANOVA using R software; 2) comparison of pre versus post treatment values within each treatment group was performed by paired Student's t-test using Graphpad Prism 6.0 software.

Results

R-Cu treatment up-regulates anti-oxidant enzymes in tumour cells

As an initial step, we examined whether oxygen radicals generated following oral administration of R-Cu might have diffused into the tumour tissue? This was indirectly examined by IF analysis of the three antioxidant enzymes mentioned above. We observed that R-Cu treatment had led to increased expression of all three enzymes within tumour cells (Figure 1 upper panels). This indicated that oxygen-radicals had entered into the tumour cells, and that the latter in an attempt to detoxify the offending oxygen-radicals, had up-regulated anti-oxidant enzymes as a cellular defence mechanism. Combined statistical comparison of pre versus post treatment values of the four treatment groups with the control group using two-way ANOVA showed that R-Cu treatment had led to a highly significant up-regulation of all three antioxidant enzymes

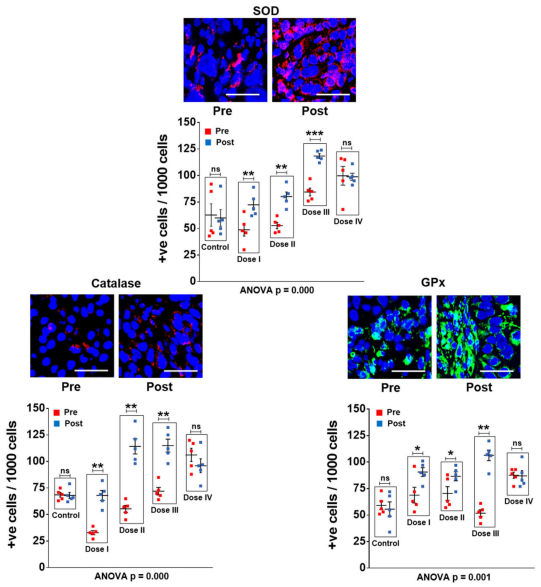

FIGURE 1
R-Cu treatment up-regulates anti-oxidant enzymes in OSCC tumour cells. FFPE sections of tumour tissues were stained with antibodies against superoxide dismutase (SOD), catalase and glutathione peroxidase (GPx), and examined under fluorescence microscopy. Upper panels provide representative images (scale bar 10μm); lower panels represent quantitative analysis of cells positive for respective anti-oxidant enzymes. One thousand cells were analysed in each case and the number of cells showing positive signals were recorded. Combined statistical comparison of pre versus post treatment values of all four treatment groups with the control group was done using two-way ANOVA; p values of which are given under each graph. Comparison of pre versus post treatment values within each treatment group was performed by paired Student's t-test. Results of the latter are represented as mean ± SEM of 5 patients in each treatment group. *< p < 0.05; **< p < 0.01; ***< p < 0.001; ns, not significant.

(Figure 1 lower panels). Individual comparison of pre and post treatment values within each treatment group using paired t test also showed significant increase in post R-Cu values for all three enzymes with respect to dose levels I – III. However, no significant difference between pre and post treatment values was seen in case of level IV for any of the three enzymes. No difference in antioxidant enzyme levels was seen between pre and post samples in the control group (Figure 1 lower panels).

R-Cu treatment eradicates/deactivates profusion of cfChPs present in TME

Confocal microscopy of FFPE sections of tumour tissues was performed after fluorescent immuno-staining with anti-DNA (red) and anti-histone (green) antibodies. Upon superimposing the fluorescent DNA and histone images, copious presence of yellow fluorescent signals, representing cfChPs, were detected in

TME (Figure 2A). The yellow cfChPs signals were virtually eliminated following two-week treatment with R-Cu. Mean fluorescent intensity (MFI) of yellow fluorescent cfChPs signals was quantitatively estimated and statistical analysis of the results was performed. Combined statistical comparison of pre versus post treatment MFI values of the four treatment groups with the control group using two-way ANOVA showed that treatment with R-Cu had led to a highly significant reduction in cfChPs in TME (Figure 2B). A significant reduction in post treatment values was also seen within each treatment group when analysed by paired t test. No difference in pre and post treatment MFI values was seen in the control group (Figure 2B). It should be noted that some of the red (DNA) and green (histone) fluorescent signals had not strictly co-localised. This is likely to be due to unevenness of cut surfaces of FFPE sections which prevented the respective antibodies to have access to some of the DNA and Histone epitopes on cfChPs.

R-Cu treatment down-regulates cancer hallmarks and immune checkpoints

Comparative results of IF analysis of pre and post R-Cu treatment values of the 10 hallmarks of cancer represented by 23 biomarkers, including 5 immune checkpoints, is given in Figure 3 (upper and lower panels). Combined statistical comparison of the four treatment groups with the control group using two-way ANOVA showed a highly significant reduction in biomarker expression in the post R-Cu treatment samples in 21/23 cases (Figure 3 lower panels). The exceptions

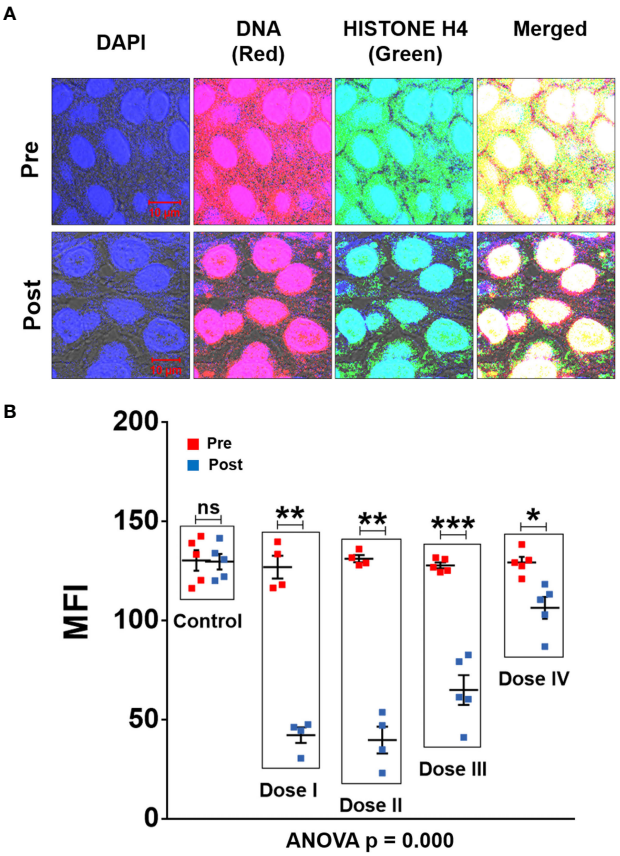

FIGURE 2
cfChPs are copiously present in TME of OSCC which are eradicated following treatment with R-Cu. **(A)** Representative confocal images of FFPE sections of tumour tissues immuno-stained with anti-DNA (red) and anti-histone (green) antibodies. Upon superimposing red and green fluorescence images, a profusion of cfCh particles in the form of yellow fluorescent signals is seen in TME. Yellow cfCh signals were markedly reduced following R-Cu treatment. **(B)** Quantitative analysis of MFI of yellow fluorescent signals representing C-cfChPs in five randomly chosen confocal fields (~50 cells per field). Combined statistical comparison of pre versus post treatment values of all four treatment groups with the control group was done using two-way ANOVA; p values of which are given under the graph. Comparison of pre versus post treatment values within each treatment group was performed by paired Student's t-test. Results of the latter are represented as mean ± SEM of tissue sections of 5 patients in each treatment group, except for pre and post values of dose levels I and II, wherein n was = 4. *< p < 0.05; **< p < 0.01, ***< p < 0.001; ns, not significant).

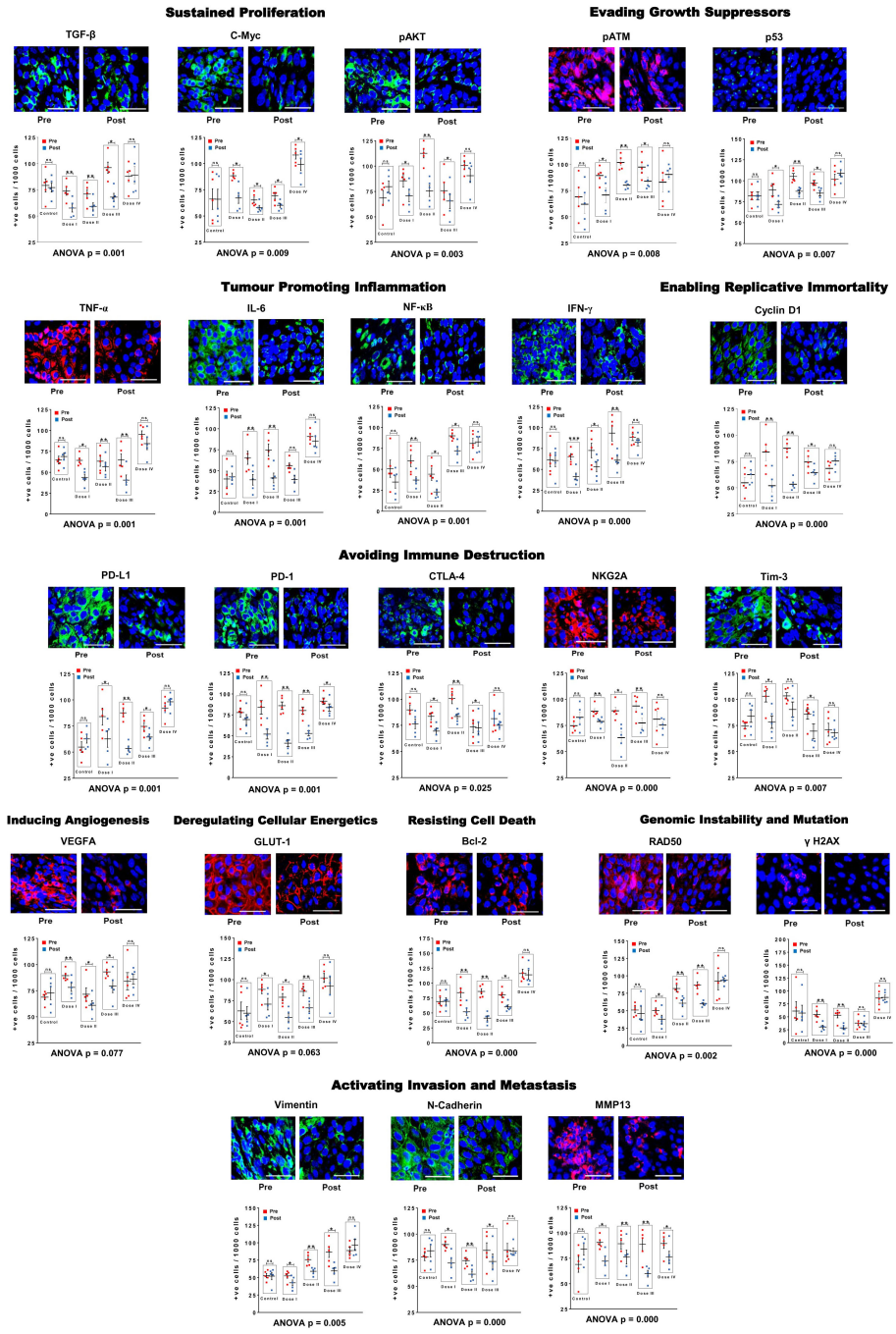

FIGURE 3
R-Cu treatment down-regulates cancer hallmark biomarkers, including five immune check-points, in OSCC. Upper panels are representative IF images (scale bar 10μm); lower panels represent results of quantitative analysis of various biomarkers. One thousand cells were analysed in each case and the number of cells showing positive fluorescent signals were recorded. Combined statistical comparison of pre versus post treatment values of all four treatment groups with the control group was done using two-way ANOVA; p values of which are given under each graph. Comparison of pre versus post treatment values within each treatment group was performed by paired Student's t-test. Results are represented as mean ± SEM of tissue sections of 5 patients in each treatment group. *< p < 0.05; **< p < 0.01; ***< p < 0.001). ns, not significant.

were VEGFA (angiogenesis) and Glut1 (cellular energetics), where difference between pre and post values did not reach statistical significance. We conclude from these exploratory results that eradication of cfChPs from TME following R-Cu treatment is associated with down-regulation of 21/23 biomarkers representing 10 cancer hallmarks, and 5 immune checkpoints, that we examined.

Comparison of pre versus post treatment values within each treatment group using paired t-test showed that, on the whole, the two lower dose levels (I and II) were more effective. In these two treatment groups, a statistically significant reduction in biomarker expression was seen in the post treatment samples in all 23 biomarkers examined (23/23) (Figure 3 lower panels). In case of dose level III, 20/23 and biomarkers showed statistical significant reduction in the post treatment samples. Dose level IV was least effective, with only 3/23 biomarkers showing significantly reduced values in the post R-Cu samples (Figure 3 lower panels).

Immune checkpoint proteins are expressed by lymphocytes present in TME

We were curious to find out whether the immune checkpoints PD-1, CTLA-4, Tim3 and NKG2A were being expressed by tumour infiltrating lymphocytes (TIL) present in TME. We performed dual IF analyses on tumour sections in which each checkpoint protein was simultaneously immune-stained for CD4 and CD8 lymphocytes (Supplementary Figures 2A–D). We found that all four immune checkpoint proteins co-localised with both types of immune lymphocytes. This finding confirmed that cfChPs released from the dying tumour cells had induced TIL present in TME to activate immune checkpoint proteins.

Discussion

Results of this exploratory study need to be confirmed in a larger series of patients, and in other tumour types. Nonetheless, several observations that we made may be worthy of note. For example, that 1) oxygen radicals generated following oral administration of R-Cu were ostensibly absorbed from the stomach to enter into systemic circulation and reach the tumour cells; 2) this led the latter to up-regulate anti-oxidant enzymes as a cellular defence mechanism; 3) cfChPs are copiously present in TME having been derived from dying tumour cells; 4) oxygen radicals that diffuse into the extracellular spaces of the tumour eradicate/deactivate the profusion of cfChPs present in TME; 5) eradication of cfChPs from TME is associated with down-regulation of 21/23 biomarkers representing the 10 hallmarks of cancer, including 5 immune checkpoints (15). The mechanistic steps involved in oxygen radical induced down-regulation of cancer hallmarks are graphically illustrated in Figure 4.

In spite of the fact that R-Cu generated oxygen radicals had diffused into the tumour cells, we did not observe any gross

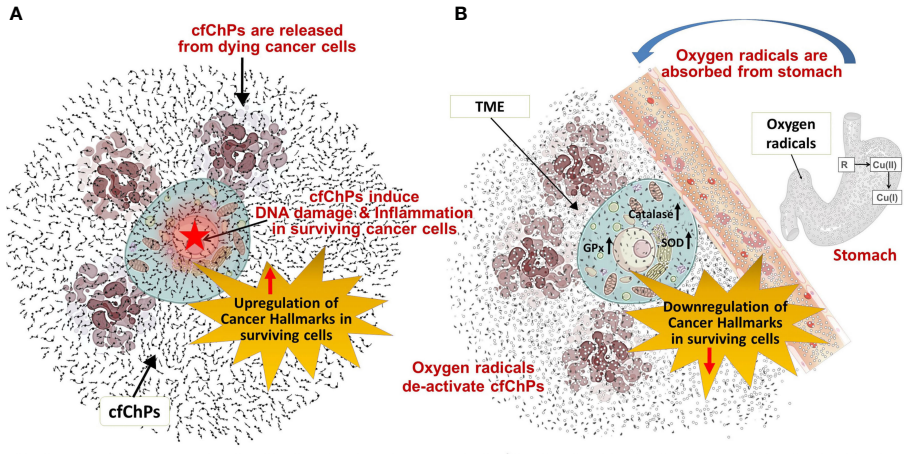

FIGURE 4
Graphical illustration of the mechanistic steps involved in oxygen radical induced down-regulation of cancer hallmarks. **(A)** cfChPs released from dying cancer cells induce DNA damage and inflammation, and up-regulate cancer hallmarks in surviving cancer cells. **(B)** Oxygen radicals generated upon oral ingestion of R-Cu are systemically absorbed from the stomach to reach TME leading to eradication of extra-cellular cfChPs and down-regulation of cancer hallmarks in surviving cells. Oxygen radicals also enter into the surviving cancer cells; but their cellular entry leads to activation of intracellular anti-oxidant enzymes which detoxify and eliminate the offending agents. SOD, superoxide dismutase; GPx, glutathione peroxidase; TME, tumour microenvironment.

damage to the tumour cell DNA following R-Cu treatment (Figure 2A). This suggested that the surviving tumour cells had protected themselves from damage by oxygen radical by up-regulating cellular anti-oxidant enzymes. No systemic toxic side effects were reported following R-Cu treatment for any of the dose levels administered; the up-regulated anti-oxidant enzymes had apparently protected all cells of the body from oxidative damage in a similar manner.

Results of our study suggest that cfChPs from dying cancer cells released into TME aggravate the oncogenic constitution of surviving cancer cells by activating cancer hallmarks in the tumour cells, and by activating immune checkpoint proteins in TIL. TME is known to play a critical role in all stages of tumour progression and metastases (16). It has been proposed that therapeutic targeting of constituents of TME could be a promising approach to controlling cancer (17). Our exploratory results presented herein suggest that treatment with R-Cu may be one such therapeutic approach which targets cfChPs present in TME *via* medium of oxygen radicals, and eradicates them to have potential therapeutic effects.

Our earlier results had shown, and which are confirmed in the current study, that cellular uptake of cfChPs leads to activation of two critical hallmarks of cancer viz. dsDNA breaks (genomic instability) and inflammation (1). These two hallmarks are also crucial sensors of cellular stress triggering widespread physiological and cellular responses, which also include cancer hallmarks (18, 19). This leads us to hypothesize that cfChPs from dying cancer cells trigger a stress response in surviving cells leading to global activation of cancer hallmarks and immune checkpoints.

We observed that the two lower dose levels of R-Cu were more effective than the higher ones. It is noteworthy that the amount of R present in the lowest dose (level I) was ~90 times less, and that of Cu ~4500 times less, than those that are recommended by the respective vendors for use as health supplements. Thus, small quantities of a combination of R and Cu can generate sufficient oxygen radicals to have profound effects in terms of down-regulation of cancer hallmarks and immune checkpoints by targeting a hitherto unknown constituent of TME.

Our analysis showed that R-Cu treatment led to down-regulation of all five immune check-points viz. PDL-1, PD-1, CTLA-4, TIM-3, and NKG2A that we examined. Targeted therapy of immune checkpoints has drawn much recent attention, and is beginning to show promising results in cancer treatment (20). However, what triggers activation of immune checkpoints has remained known. Our exploratory results suggest that cfChPs released from dying cancer cells into TME may be global activators of immune checkpoint proteins, and that they can be down-regulated by two-week treatment with small quantities of orally administered R-Cu. If the role of cfChPs in checkpoint activation is further confirmed, a new form of cancer immunotherapy might emerge whereby all known immune checkpoints are simultaneously down-regulated by small quantities of R-Cu.

Conclusion and future prospects

Our results suggest that cfChPs released from dying cancer cells are global instigators of cancer hallmarks and immune checkpoints. That cfChPs can be deactivated by small quantities of R-Cu raise the prospect of a novel and non-toxic form of cancer treatment which sans killing of cancer cells, and instead, induces healing by down-regulating hallmarks of cancer and immune checkpoint proteins. It has been argued that cancer is akin to a non-healing wound (21), and that hallmarks of cancer are also the hallmarks of wound healing (22). This being so, it is possible that cancer may be healed, like a wound, without having to be killed, and that oxygen radicals generated upon oral administration of R-Cu may prove to be a novel cancer healing agent of the future.

Data availability statement

The original contributions presented in the study are included in the article/Supplementary Material. Further inquiries can be directed to the corresponding author.

Ethics statement

The studies involving human participants were reviewed and approved by Tata Memorial Center Institutional Ethics Committee. The patients/participants provided their written informed consent to participate in this study.

Author contributions

AP, SS, HT, and VJ: Investigation, Visualisation Methodology; HS, PC, and NK: Investigation, methodology, project administration and supervision; GR and KP: Data curation, formal analysis, investigation, software, supervision, validation, visualisation and writing of the original draft; AB: Statistical analysis; IM: Conceptualisation, funding acquisition, methodology, project administration, resources, overall supervision, writing original draft, writing –review and editing. All authors contributed to the article and approved the submitted version.

Funding

This study was funded by Department of Atomic Energy, Government of India through its grant CTCTMC to Tata Memorial Centre awarded to IM. The study funders had no role in the conduct, design and interpretation of results in this study.

Acknowledgments

The authors sincerely thank Dr. Snehal Shabrish for preparing the infographic. Thanks are also due to Mr. Ashish Pawar and Mr. Roshan Shaikh for their help in preparing the manuscript.

Conflict of interest

The authors declare that the research was conducted in the absence of any commercial or financial relationships that could be construed as a potential conflict of interest.

Publisher's note

All claims expressed in this article are solely those of the authors and do not necessarily represent those of their affiliated organizations, or those of the publisher, the editors and the reviewers. Any product that may be evaluated in this article, or claim that may be made by its manufacturer, is not guaranteed or endorsed by the publisher.

Supplementary material

The Supplementary Material for this article can be found online at: https://www.frontiersin.org/articles/10.3389/fonc.2022.1000957/full#supplementary-material

SUPPLEMENTARY FIGURE 1
A representative photograph of advanced OSCC **(A)**, and its squamous cell phenotype as seen on H&E section **(B)**.

SUPPLEMENTARY FIGURE 2
Representative images showing expression of various immune checkpoint proteins by CD4 and CD8 lymphocytes. FFPE sections of OSCC tumour tissues were simultaneously immune-stained with antibodies against various immune-checkpoint proteins and those against CD4 and CD8 lymphocytes (scale bar 10μm). Co-localisation of all four immune checkpoint proteins and CD4 and CD8 lymphocytes is clearly seen.

References

1. Mittra I, Samant U, Sharma S, Raghuram GV, Saha T, Tidke P, et al. Cell-free chromatin from dying cancer cells integrate into genomes of bystander healthy cells to induce DNA damage and inflammation. *Cell Death Discov* (2017) 3(1):1–14. doi: 10.1038/cddiscovery.2017.15

2. Kirolikar S, Prasannan P, Raghuram GV, Pancholi N, Saha T, Tidke P, et al. Prevention of radiation-induced bystander effects by agents that inactivate cell-free chromatin released from irradiated dying cells. *Cell Death Dis* (2018) 9(12):1–16. doi: 10.1038/s41419-018-1181-x

3. Fukuhara K, Miyata N. Resveratrol as a new type of DNA-cleaving agent. *Bioorg Med Chem Lett* (1998) 8(22):3187–92. doi: 10.1016/S0960-894X(98)00585-X

4. Fukuhara K, Nagakawa M, Nakanishi I, Ohkubo K, Imai K, Urano S, et al. Structural basis for DNA-cleaving activity of resveratrol in the presence of Cu(II). *Bioorg Med Chem* (2006) 14(5):1437–43. doi: 10.1016/j.bmc.2005.09.070

5. Subramaniam S, Vohra I, Iyer A, Nair NK, Mittra I. A paradoxical synergism between resveratrol and copper (II) with respect to degradation of DNA and RNA. *F1000Research* (2015) 4:1145. doi: 10.12688/f1000research.7202.1

6. Mittra I, Pal K, Pancholi N, Shaikh A, Rane B, Tidke P, et al. Prevention of chemotherapy toxicity by agents that neutralize or degrade cell-free chromatin. *Ann Oncol* (2017) 28(9):2119–27. doi: 10.1093/annonc/mdx318

7. Mittra I, Pal K, Pancholi N, Tidke P, Siddiqui S, Rane B, et al. Cell-free chromatin particles released from dying host cells are global instigators of endotoxin sepsis in mice. *PloS One* (2020) 15(3):1–22. doi: 10.1371/journal.pone.0229017

8. Pal K, Gorantla RV, D'souza J, Mehta S, Jadhav V, Shaikh A, et al. A pro-oxidant combination of resveratrol and copper down-regulates multiple biological hallmarks of ageing and neurodegeneration. *bioRxiv* (2022). doi: 10.1101/2022.05.04.489500

9. Agarwal A, Khandelwal A, Pal K, Khare NK, Jadhav V, Gurjar M, et al. A novel pro-oxidant combination of resveratrol and copper reduces transplant related toxicities in patients receiving high dose melphalan for multiple myeloma (RESCU 001). *PloS One* (2022) 17(2):1–9. doi: 10.1371/journal.pone.0262212

10. Mittra I, de Souza R, Bhadade R, Madke T, Shankpal PD, Joshi M, et al. Resveratrol and copper for treatment of severe COVID-19: an observational study (RESCU 002). *medRxiv* (2020) 6(165):1–13. doi: 10.1101/2020.07.21.20151423

11. Halliwell B, Gutteridge JMC. Role of free radicals and catalytic metal ions in human disease: An overview. *Methods Enzymol* (1990) 186:1–85. doi: 10.1016/0076-6879(90)86093-B

12. Ray PD, Huang BW, Tsuji Y. Reactive oxygen species (ROS) homeostasis and redox regulation in cellular signaling. *Cell Signal* (2012) 24(5):981–90. doi: 10.1016/j.cellsig.2012.01.008

13. Pizzino G, Irrera N, Cucinotta M, Pallio G, Mannino F, Arcoraci V, et al. Oxidative stress: Harms and benefits for human health. *Oxid Med Cell Longev* (2017) 2017:1–13. doi: 10.1155/2017/8416763

14. Reagan-Shaw S, Nihal M, Ahmad N. Dose translation from animal to human studies revisited. *FASEB J* (2008) 22(3):659–61. doi: 10.1096/fj.07-9574LSF

15. Hanahan D, Weinberg RA. Hallmarks of cancer: The next generation. *Cell* (2011) 144(5):646–74. doi: 10.1016/j.cell.2011.02.013

16. Whiteside TL. The tumor microenvironment and its role in promoting tumor growth. *Oncogene* (2008) 27(45):5904–12. doi: 10.1038/onc.2008.271

17. Roma-Rodrigues C, Mendes R, Baptista PV, Fernandes AR. Targeting tumor microenvironment for cancer therapy. *Int J Mol Sci* (2019) 20(4):1–31. doi: 10.3390/ijms20040840

18. Sato H, Niimi A, Yasuhara T, Permata TBM, Hagiwara Y, Isono M, et al. DNA Double-strand break repair pathway regulates PD-L1 expression in cancer cells. *Nat Commun* (2017) 8(1):1–11. doi: 10.1038/s41467-017-01883-9

19. Liu YZ, Wang YX, Jiang CL. Inflammation: the common pathway of stress-related diseases. *Front Hum Neurosci* (2017) 11(316):1–11. doi: 10.3389/fnhum.2017.00316

20. Gong J, Chehrazi-Raffle A, Reddi S, Salgia R. Development of PD-1 and PD-L1 inhibitors as a form of cancer immunotherapy: A comprehensive review of registration trials and future considerations. *J Immunother Cancer* (2018) 6(1):1–18. doi: 10.1186/s40425-018-0316-z

21. Schäfer M, Werner S. Cancer as an overhealing wound: An old hypothesis revisited. *Nat Rev Mol Cell Biol* (2008) 9(8):628–38. doi: 10.1038/nrm2455

22. MacCarthy-Morrogh L, Martin P. The hallmarks of cancer are also the hallmarks of wound healing. *Sci Signal* (2020) 13(648):1–13. doi: 10.1126/scisignal.aay8690

frontiers | Frontiers in Oncology

TYPE Mini Review
PUBLISHED 23 September 2022
DOI 10.3389/fonc.2022.961637

Check for updates

OPEN ACCESS

EDITED BY
Shaoquan Zheng,
The First Affiliated Hospital of Sun Yat-sen University, China

REVIEWED BY
Ouyang Chen,
Duke University, United States
Jing Mu,
Shenzhen Hospital, Peking University, China

*CORRESPONDENCE
Demeng Xia
demengxia@163.com
Tianlin He
skyrainhe@163.com

†These authors have contributed equally to this work

SPECIALTY SECTION
This article was submitted to Molecular and Cellular Oncology, a section of the journal Frontiers in Oncology

RECEIVED 05 June 2022
ACCEPTED 01 September 2022
PUBLISHED 23 September 2022

CITATION
Chen G, Wu K, Li H, Xia D and He T (2022) Role of Hypoxia in the Tumor Microenvironment and Targeted Therapy.
Front. Oncol. 12:961637.
doi: 10.3389/fonc.2022.961637

COPYRIGHT
© 2022 Chen, Wu, Li, Xia and He. This is an open-access article distributed under the terms of the Creative Commons Attribution License (CC BY). The use, distribution or reproduction in other forums is permitted, provided the original author(s) and the copyright owner(s) are credited and that the original publication in this journal is cited, in accordance with accepted academic practice. No use, distribution or reproduction is permitted which does not comply with these terms.

Role of hypoxia in the tumor microenvironment and targeted therapy

Gaoqi Chen[1†], Kaiwen Wu[2†], Hao Li[3], Demeng Xia[4*] and Tianlin He[1*]

[1]Department of Hepatobiliary Pancreatic Surgery, Changhai Hospital, Second Military Medical University (Naval Medical University), Shanghai, China, [2]Department of Gastroenterology, The Third People's Hospital of Chengdu, The Affiliated Hospital of Southwest Jiaotong University, Chengdu, China, [3]Deparment of Neurology, Affiliated Hospital of Jiangsu University, Jiang Su University, Zhenjiang, China, [4]Luodian Clinical Drug Research Center, Shanghai Baoshan Luodian Hospital, Shanghai University, Shanghai, China

Tumor microenvironment (TME), which is characterized by hypoxia, widely exists in solid tumors. As a current research hotspot in the TME, hypoxia is expected to become a key element to break through the bottleneck of tumor treatment. More and more research results show that a variety of biological behaviors of tumor cells are affected by many factors in TME which are closely related to hypoxia. In order to inhibiting the immune response in TME, hypoxia plays an important role in tumor cell metabolism and anti-apoptosis. Therefore, exploring the molecular mechanism of hypoxia mediated malignant tumor behavior and therapeutic targets is expected to provide new ideas for anti-tumor therapy. In this review, we discussed the effects of hypoxia on tumor behavior and its interaction with TME from the perspectives of immune cells, cell metabolism, oxidative stress and hypoxia inducible factor (HIF), and listed the therapeutic targets or signal pathways found so far. Finally, we summarize the current therapies targeting hypoxia, such as glycolysis inhibitors, anti-angiogenesis drugs, HIF inhibitors, hypoxia-activated prodrugs, and hyperbaric medicine.

KEYWORDS

Tumor microenvironment, immunity, metabolism, hypoxia, targeted therapy

Abbreviations: TME, tumor microenvironment; NK cells, natural killer cells; TAMs, tumor-associated macrophages; IFN-γ, interferon-gamma; DCs, dendritic cells; MHC, Major histocompatibility complex; IL-6, interleukin-6; IL-10, interleukin-10; VEGF, vascular endothelial growth factor; HIF-1α, hypoxia-inducible factor-alpha; BNIP3, BCL2 and adenovirus E1B19 kDa interacting protein 3; PI3K, phosphatidylinositol 3 kinase; MMP10, metalloproteinase 10; VISTA, V-domain Ig suppressor of T cell activation; HLA-G, Human leukocyte antigen G; CAFs, Cancer-associated fibroblasts; TGF-β, tumor growth factor-beta; MDSCs, marrow-derived suppressor cells; Tregs, regulatory T cells; Foxp3, forkhead box P3; ROS, reactive oxygen species; HIFs, Hypoxia-Inducible Factors; PHD, prolyl hydroxylase; HRE, hypoxia response element; P-gp, p-glycoprotein; ETC, electron transport chain; HBO, Hyperbaric oxygen; HK2, Hexokinase 2; 3-BP, 3-bromopyruvic acid; CDT, chemical dynamic therapy; LDHA, lactate dehydrogenase A; αKGDH, α- Ketoglutarate dehydrogenase; ctDNA, circulating tumor DNA; PET-CT, positron emission tomography and computed tomography; ADC, antibody drug conjugate; NSCLC, non-small cell lung cancer.

Introduction

A recent study shows that the global cancer burden is increasing (1). The research on the molecular mechanism and target of the occurrence and development of malignant tumors may be a breakthrough to solve this problem. Recently, it has been proved that TME is a key factor in the occurrence and development of malignant tumors, which is being the well-known hotspot. However, due to the influence of tumor cells and abnormal vascular structure, TME often shows the characteristics of hypoxia, especially in solid tumors.

Under the condition of hypoxia, the expression of HIF increases, and a series of changes have taken place in the metabolic mode and immune function of TME. In order to adapt to the influence of hypoxia, tumor cells have changed their metabolic mode and obtained energy through glycolysis. Meanwhile, immune cells are regulated by hypoxia and have different effects. Among them, the function of immune cells that play an anti-tumor role is inhibited, such as cytotoxic T cells, B cells, and natural killer (NK) cells. However, the expression of immunosuppressive cells such as marrow-derived suppressor cells (MDSC) and regulatory (Treg) T cells is up-regulated. The changes of metabolism and immune effect provide an excellent living environment for tumor cells and hinder the effect of anti-tumor treatment. In addition, while providing survival conditions for tumor cells, TME under hypoxia obstructs the effect of antitumor drugs by hindering drug delivery (2–4). Therefore, traditional chemotherapy and single dose immunotherapy cannot achieve satisfactory results, which makes the treatment of malignant tumors challenging (5, 6).

In conclusion, hypoxia, as an independent prognostic indicator related to poor survival rate of cancer patients, is expected to become an effective target for fighting tumor and alleviating drug resistance (7). After summarizing, we found that people are increasingly interested in the field of hypoxia in TME, and hundreds of relevant academic papers in this field have been published (8). Among the published studies, research targeting metabolic enzymes, HIF, and angiogenesis related factors have made breakthroughs to varying degrees. Currently, what's exciting is more than 500 clinical trials have been adopt. In this review, we describe the effects of hypoxia on the proliferation, metastasis, and drug resistance of tumor cells in the TME from the perspectives of immunity, metabolism and HIF, and summarize the different treatment strategies targeting hypoxia. Finally, we summarized the current measures to combat drug resistance and the prospects for future research in this field.

Effects of hypoxia on TME

TME is a cellular environment that harbors the tumor, composed of tumor cells, fibroblasts, immune cells (T cells, B cells, natural killer (NK) cells, and tumor-associated macrophages (TAMs)), blood vessels, signaling molecules, and extracellular matrix (9, 10). Hypoxia is ubiquitous property in the TME, especially in solid tumors. Abnormal blood vessels in the tumor tissue cannot meet the excessive oxygen and nutrient demand for its rapid growth, leading to uneven hypoxia. Thus, the area away from the blood vessels was anoxic, while the adjacent tumor tissue was hyper-oxygenated. A recent study suggested that hypoxia affects the immune microenvironment and makes tumor cells escape from immune monitoring and killing (11). As shown in Figure 1, the anoxic area in tumor tissue hinders the infiltration of immune cells and promotes the growth of tumor cells (12).

Hypoxia inhibits the function of immune cells

Effector T cells are the main components of immune response in the tumor immune microenvironment, for example, the proliferation and differentiation of T cells determine the strength of the antitumor immune response. Several studies have confirmed that hypoxia is a major regulatory factor that inhibits the function and proliferation of T cells (11, 13). A2A receptor (A2AR) is a kind of G protein coupled receptor with high affinity for adenosine, which is expressed on T cells, NK cells, macrophages, and other immune cells (14). Tumor cells can inhibit the response of immune cells through adenosine-a2ar pathway and promote tumor cells to escape immune surveillance (14). Under hypoxic conditions, tumor cells exploit the glycolytic process to accumulate metabolites, such as lactic acid and adenosine, in the TME. The accumulation of lactic acid and adenosine inhibits T cell effector function and proliferation by blocking the Sirolimus pathway and interacting with the A2AR on the T cell surface (15, 16). On the other hand, hypoxia promotes the apoptosis of T lymphocytes, delays the differentiation of effector cells, and reduces the production of effector T cells and interferon-gamma (IFN-γ) (17). In order to inhibit T cell proliferation, differentiation, and other functional cells, such as dendritic cells (DCs) that present antigens to T cells and activate the Hapten response, which also affected by hypoxia.

B cells, as the main carrier of humoral immunity, play a key role in the production of antibodies. Therefore, the functional defect of B cells will lead to the decline of immune effect. In the hypoxic tumor microenvironment, the transcription and metabolism of B cells are mainly affected by hypoxia inducible factor-alpha (HIF-1α) and myelocytomatosis virus oncogene cellular homolog (MYC) (18, 19). Myc gene specifically regulates the growth and metabolism of these various types of cells and has the potential to cause cancer (19, 20). To meet the energy demand of proliferation, B cells with malignant tendency show high metabolic behavior different from normal cells

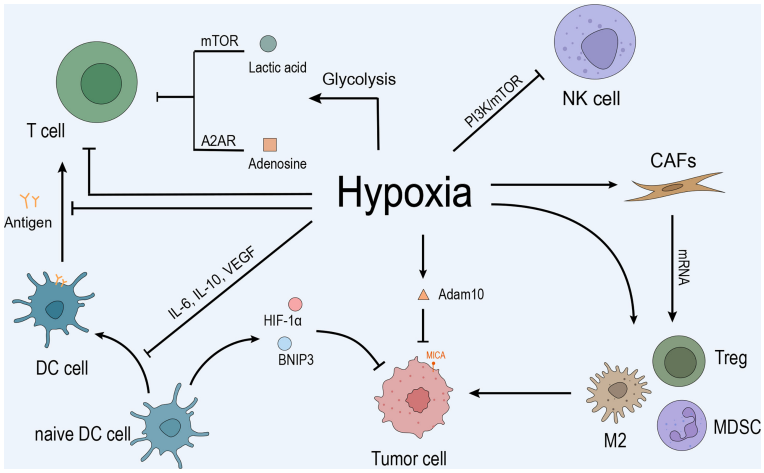

FIGURE 1
Hypoxia inhibits the immune response by inhibiting immune cells, recruiting immunosuppressive cells, regulating CAFs, promoting tumor cell growth, and mediating immune escape. **(A)** Anoxic metabolites, lactic acid, and adenosine inhibit T cell effector function and proliferation by blocking the mTOR pathway and interacting with the A2A receptor on the T cell surface. Hypoxia promotes T cell apoptosis and directly inhibits T cell proliferation and differentiation. Hypoxia upregulates IL-10, VEGF, and other cytokines through HIF-1α and inhibits the differentiation and maturation of DCs, leading to the inhibition of T cell function. Moreover, hypoxia-induced high levels of HIF-1α and BNIP3 promote programmed cell death in tumor cells captured by DC. In addition, hypoxia inhibits NK cell function by activating the PI3K/mTOR signaling pathway. **(B)** Hypoxia induced the mRNA expression of *TGF-β*, *VEGF*, *IL-6*, *IL-10*, and *PD-L1* and promoted CAF participation in the recruitment of MDSCs, Tregs, and type 2 TAMs to maintain the immunosuppressive state of the microenvironment, promoting tumor cells to evade immune surveillance. **(C)** Hypoxia upregulates the expression of MMP adam10 and induces the immune escape of tumor cells.

and show a vicious cycle. However, this differential performance still needs further research, and may become a treatment strategy in the future (19).

DCs are immune cells that capture and present antigens through major histocompatibility complex (MHC) glycoproteins. Many studies have shown that interleukin-6 (IL-6), IL-10, vascular endothelial growth factor (VEGF), and the other cytokines are upregulated by hypoxia, which inhibits the differentiation and maturation of DCs and T cell function (21, 22). *BCL2* gene, as a key gene regulating apoptosis, is up-regulated in tumor cells. The BCL2 encoded protein can achieve programmed cell death by regulating proteolytic caspase activation (23, 24). Immature DCs express high levels of HIF-1α and upregulated BCL2 and adenovirus E1B19 kDa interacting protein 3 (BNIP3), inducing programmed cell death in captured cells (25). Yang et al. found that the phagocytic capacity of DCs was lower than normal under hypoxia (26). In addition, hypoxia-stimulated DCs induce the differentiation of naive T cells into the Th2 phenotype, which in turn inhibits T cell proliferation (27). Hypoxia affects the function and differentiation ability of DCs, indicating that the activation ability of DCs to T cells. After that, the effect of T cell immunity on tumor cells is reduced, promoting the immune escape of tumor cells (26, 28).

NK cells constitute a class of naturally occurring cytotoxic lymphocytes. The ability of NK cells to kill tumor cells is inhibited under hypoxia (29) *via* the activated phosphatidylinositol 3 kinase (PI3K)-mTOR signaling pathway. In addition, hypoxia decreases the expression of the tumor cell surface recognition molecule MICA by upregulating the expression of metalloproteinase 10 (MMP10), thus downregulating the expression of NK and Natural killer group 2 member D (NKG2D) on T cells and inducing the immune escape of tumor cells (30). NKG2D is an activated receptor of immune cells such as T cells and NK cells, which could turn on the immune effect function. The upregulation of its ligand MCIA/MCIB on the surface of tumor cells is conducive to the continuous development of anti-tumor immunity (31). Therefore, the NKG2D ligand (NKG2DL) as a therapeutic target has become a research hotspot in recent years, in which the research progress in the fields of tumor vaccines has made exciting results (32, 33).

Immune checkpoint refers to the ligand-receptor pairs that stimulate or inhibit the immune response, which also affected by hypoxia (34). Hypoxia modulates PD-L1, human leukocyte antigen g (HLA-G), CD47, and the immune checkpoint V-domain IG suppressor of T cell activation (VISTA) to form an inhibitory immune microenvironment, promoting immune escape of tumor cells. PD-1 is widely distributed on the surface of lymphocytes. Under hypoxic conditions, the level of PD-L1 protein on the tumor cell surface is enhanced, and it combines with the PD-1 receptor on the activated T cell surface to produce the immunosuppressive effect (28, 35). Presently, antibodies against PD-1 and PD-L1 have achieved preliminary

success in the clinic (36). Human leukocyte antigen G (HLA-G) is another checkpoint molecule involved in tumor immune escape and is strongly associated with increased tumor invasiveness and suppression of immune cell function (37, 38). In addition, the immune checkpoint molecules involved in the inhibition of T cell proliferation and activity under hypoxia conditions include VISTA (11).

Hypoxia modulates immunosuppression

Cancer-associated fibroblasts (CAFs) are similar to inflammation-associated fibroblasts, and participate in tumor cell progression and immune cell regulation during the antitumor immune response (39). Ziani et al. demonstrated that the mRNA expression of CAF-related immunosuppressive modulators, such as tumor growth factor-beta (TGF-β), VEGF, IL6, IL10, and PD-L1 increased significantly under hypoxia (40). CAFs are involved in the collection and differentiation of marrow-derived suppressor cells (MDSCs), regulatory T cells (Tregs), and type 2 TAMs in TME (41, 42). In addition to the recruitment of immunosuppressive cells, CAFs inhibit T cell immune response and enhance the tumor cell immunosuppressive response in the TME, which might be related to the inhibition of CAF, DC, and NK cell functions (43, 44). Under hypoxia, $CD4^+$ T cells differentiate into Tregs by promoting Foxp3 transcription. Tregs are a subset of CD4 T cells and contribute to immunosuppression and tumor tolerance by producing TGF-β and suppressive effector T cells (21). MDSCs are immature myeloid cells that directly inihibit T cells, NK cells, and dendritic cells and promote angiogenesis in tumor tissue (45, 46). Chiu et al. demonstrated that under the influence of hypoxia, the differentiation of MDSCs was inhibited, but its immunosuppressive function was maintained (47). TAM is a major component of the solid TME (48). The two phenotypes of TAMs are M1-like and M2-like phenotypes (48). Type M2 TAMs are detected in anoxic regions and associated with immunosuppression, angiogenesis, tumor cell activation, and metastasis (49). Another study showed that prostaglandin E2, TGF-β, VEGF, IL-4, IL-6, and reactive oxygen species (ROS) were the major factors that induced TAMs to M2-type TAMs (29). In addition, hypoxia-mediated lactic acid accumulation under HIF-1α regulation increases the expression of VEGF and M2-like polarization of TAMs to maintain the immunosuppressive status of the TME (47, 50).

Changes in tumor metabolism caused by hypoxia

Hypoxia affects the TME and alters the tumor and the surrounding tissue metabolism. With the progress of TME studies, metabolic reprogramming has been recognized as a hallmark behavior of malignant tumors. As shown in Figure 2, metabolic reprogramming is the metabolic modification of tumor cells to maintain growth and resist treatment. This reprogramming includes aerobic glycolysis and L-glutamine metabolism et al (51). Thus, it could be deduced that hypoxia inhibits the apoptosis of tumor cells by promoting the metabolic reprogramming of tumor cells.

Glucose metabolism

Under aerobic conditions, cells produce pyruvic acid through the glycolytic process, which is oxidized in the mitochondria to produce energy. Under anoxic conditions, the energy of normal cells is mainly provided by glycolysis. However, most tumor cells tend to produce energy by glycolysis even under aerobic conditions. This phenomenon is known as the "Warburg effect" (52, 53). Through this phenomenon, tumor cells use glycolysis for energy and produce lactic acid. The lactic acid accumulates outside the tumor cell *via* activated monocarboxylic acid transporters, causing a low pH in the extracellular matrix. Some studies have shown that a low pH environment enhances the invasiveness of tumor cells and inhibits the cytotoxicity and proliferation of lymphocytes, which inhibits the functioning of immune effector cells in the TME (54). Nonetheless, as the acidic environment is corrected, the T cell effector function is restored (55). In addition, tumor cells use glycolytic metabolic intermediates to synthesize fats and proteins. The metabolic way of aerobic glycolysis weans the tumor cells off oxygen dependence, which is beneficial to the growth and proliferation of tumor cells in a hypoxic environment (56). Also, the multidrug resistance of tumor cells is closely related to the reprogramming of glucose metabolism. A current study suggested that this process is influenced by a combination of mechanisms, including "ion capture," decreased apoptotic potential, gene changes (such as p53 mutation), and increased activity of P-gp, a multidrug transporter.

Glutamine metabolism

Except for glycolysis, cancer cells under hypoxic conditions tend to choose an alternative substrate for energy metabolism, such as L-glutamine. Some studies have shown the critical role of L-glutamine plays in tumor cell proliferation as an alternative energy source for tumor metabolism (57). L-Glutamine is synthesized as glutamate, which is then converted into α-ketoglutaric acid through transamination and into the tricarboxylic acid cycle for energy metabolism to compensate for the reduced energy production from glycolysis (58, 59). In addition, glutamate provides nitrogen and carbon sources for tumor cells and participates in the synthesis of amino acids and nucleotides, which promotes the development of

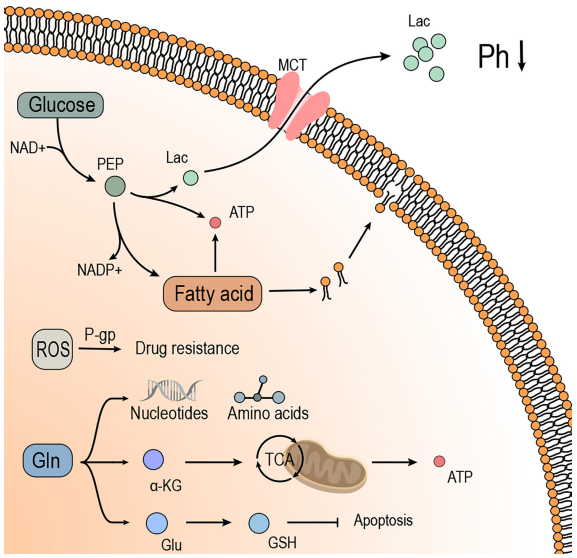

FIGURE 2
Hypoxia induces metabolic reprogramming of tumor cells, which provides energy and substrates for tumor cell growth and promotes drug resistance. I. Glucose provides energy to the tumor cells in the form of glycolysis, of which the metabolite Lac is transported to the outside of tumor cells through MCT, effectuating low pH and suppressing the immune effects. The intermediate products in glycolysis contribute to the synthesis of fatty acids and promote the growth and proliferation of tumor cells. II. Gln is broken down into a-KG in tumor cells to provide energy through the TCA cycle or raw materials to synthesize amino acids and nucleic acids in tumor cells. In addition, GLN expresses antioxidant ability by synthesizing GSH, which promotes drug resistance and anti-apoptosis in tumor cells. III. Fatty acids provide materials for the synthesis of biomembranes to meet the growth needs of tumor cells. The synthesis of fatty acids consumes PEP, which relieves the build-up of Lac from glycolysis. The breakdown of fatty acids produces large amounts of ATP, which provides energy for the growth and proliferation of tumor cells. IV. ROS induces drug resistance in tumor cells, associated with the P-gp.

malignant tumors (60). On the other hand, L-glutamine could be used to synthesize glutathione, a crucial antioxidant that maintains the redox balance and prevents oxidative damage to cells (61, 62). Friesen et al. suggested that glutathione, a metabolite of L-glutamine, is involved in mediating drug resistance and anti-apoptosis in cancer cells which may be related to the antioxidant capacity of glutathione. Strikingly, when glutathione levels are decreased, drug and apoptosis resistance of tumor cells is restored (63).

Fatty acid metabolism

The synthesis of biomembranes and signaling molecules is essential for the rapid proliferation and growth of tumor cells. Fatty acid is a critical raw material. Therefore, tumor cells have high levels of fatty acid synthesis. On the other hand, the synthesis consumes pyruvic acid, which slows the synthesis of lactic acid and prevents the excessive build-up of lactic acid. In addition, the decomposition of fatty acids provides energy for tumor cells and the free fatty acids of metabolic products act as signal molecules that activate various signaling pathways (64, 65). Hypoxia and fatty acid metabolism studies have shown that the occurrence of tumors is closely related to β-oxidation. The enzymes FASN, ACC, and ACLY involved in fatty acid metabolism are upregulated in tumors (66, 67). Another study showed that the efficacy of immunotherapy, T cell longevity, and antitumor effects are also affected by lipid metabolism (68).

The role of HIF

HIF is a major factor that mediates tumor cells to adapt to hypoxia (69). HIF-1α transcription factor directly targets *VEGF*, *TGF-β*, *IL-10*, and *PD-L1* genes and regulates the tumor immunosuppressive response to CAFs (70–72). HIF is a heterodimer helical-loop protein consisting of an O_2-sensitive α-subunit (including HIF-1α, HIF-2α, and HIF-3α) and a constitutive β-subunit (16). HIF-1α plays a key role in several steps of hypoxia induction (73). In case of hypoxia, HIF-1α breakdown is reduced and transferred to the nucleus when the function of prolyl hydroxylase (PHD-RRB is inhibited. In the cell nucleus, HIF-1α binds to HIF-1β to form heterodimers. HIF-1α/1β heterodimer activates the HIF target gene and promotes HIF expression by combining the HIF-1α/1β

heterodimer with p300/CBP and hypoxia response element (HRE), thus regulating various biological processes of tumor cells, including metabolic reprogramming, immunoregulation, angiogenesis, tumor cell invasion, and drug resistance (74, 75).

Among them, HIF could inhibit the immune response by promoting the up regulation of immune checkpoints, apoptosis of cytotoxic T cells and blocking phagocytosis, which is conducive to the occurrence and development of tumor cells. Studies have reported that the up-regulated immune checkpoint PD-L1 in tumor cells presents HIF-1α dependence, promote the apoptosis of cytotoxic T cells, and participate in the immune escape of tumor cells (76, 77). Similarly, the expression of CD47 protein on the surface of tumor cells is also affected by HIF-1α, and hinder the phagocytic ability of phagocytes to tumor cells through phosphorylation of signal regulatory proteins on the surface of macrophages α (SIRP α) (78). In recent years, the research results of CD47 protein showed that the expression of CD47 protein also inhibited the function of cytotoxic T cells and NK cells. Therefore, a series of clinical studies targeting CD47 protein are expected to bring new hope to the field of tumor therapy (79, 80). In addition, vascular endothelial growth factor (VEGF) is up-regulated affected by HIF-1α, which could promote metastasis and immune escape by inducing tumor angiogenesis. It is believed that the disorder of TGF-β is related to the occurrence and development of tumors, and enhances the invasive ability of tumor cells by inducing epithelial to mesenchymal transition (EMT) (81, 82). The research of Huang et al. showed that the HIF-1α regulate the function of TGF-β by forming Smad-HIF-1α complex under hypoxia, and then regulate the progress of tumor cells (83).

In addition to the inhibition of immune effects in TME, HIF-1 activates or inhibits the genes of key proteins in glycolysis pathway to regulate the metabolic process of tumor cells in hypoxic environment. Proteins or genes involved in the regulation of glycolysis pathway and regulated by HIF-1 include those involved in encoding glucose transporters (GLUT1 and GLUT3), hexokinases (HK1 and hK2), lactate dehydrogenase A (LDHA), etc (84–88). At the same time, oxidative phosphorylation related genes and proteins are negatively regulated by HIF-1. The differential regulation of proteins or genes relating glycolysis and oxidative phosphorylation by HIF-1 is conducive to the adaptation of tumor cells to achieve glucose metabolism reorganization. In addition, tumor cells reprogrammed by glucose metabolism have higher "competitiveness" to glucose in the microenvironment, so T cell apoptosis is induced by inhibition of energy metabolism, which aggravates the inhibition of T cell function. Except the glycolysis, HIF, as a major regulator, is involved in regulating glutamine metabolism in tumor cells (89). Under the condition of hypoxia, HIF-2α causes the change in *SLC1A5* gene encoding neutral amino acid transporter, which mediates the reprogramming of glutamine metabolism and the resistance to gemcitabine in tumor cells (90). Moreover, HIF inhibit α- Ketoglutarate participates in the tricarboxylic acid cycle by promoting α- Ketoglutarate dehydrogenase (αKGDH) degradation (91). In addition, HIF is also involved in regulating many metabolic pathways, such as fatty acids, pentose phosphate and adenosine, so as to provide a metabolic basis for the progression and metastasis of tumor cells.

In summary, the important role of HIF in tumor progression and its potential mechanism have been widely concerned by researchers. Further research in this field in the future is expected to help us have a deeper understanding of hypoxic TME, and bring new hope to the research of tumor targeted therapy (92).

Effect of hypoxia on tumor oxidative stress

ROS are the main molecules produced by oxidative stress and have been considered major factors in the tumor occurrence, development, and recurrence. The ROS in tumor cells originate from mitochondria (93). Under the influence of hypoxia, the oxygen utilization efficiency of tumor cells is decreased. Therefore, electron transport efficiency through the mitochondrial complexes in the electron transport chain (ETC) is reduced, resulting in abundant ROS in cells (94, 95). Notably, various concentrations of ROS exert different effects on tumor cell production (96). High concentrations of ROS disrupt the proteins and nucleic acids and induce apoptosis of tumor cells through oxidative stress (97). A low concentration of ROS can promote the development and metastasis of tumor cells (98). In addition, the concentration of ROS affects the sensitivity and resistance of tumor cells to chemotherapeutic drugs, which might be related to the level of p-glycoprotein (P-gp) in drug resistance (99) (Figure 2).

Effect of hypoxia on drug resistance of tumor

To date, chemotherapy is the cornerstone of cancer treatment. Anoxic metabolic disorders and changes in the microenvironment severely inhibit the efficacy of drugs such as Bleomycin. This could be because the oxygen-dependent chemotherapy drugs are more active when oxygen is available (100), while hypoxia directly inhibits the antitumor function of oxygen-dependent chemotherapeutic drugs (101). In addition, hypoxia indirectly reduces the efficacy of the drugs by interfering with the cell cycle, promoting DNA repair, and reducing the sensitivity of p53-mediated apoptosis (29, 102). Intriguingly,

immunotherapy has developed rapidly in the past decade and has produced significant clinical results. However, the current studies have suggested that hypoxic stimulation significantly limits the effectiveness of immunotherapy (21, 103, 104). About 33% of patients who responded to immunotherapy suffered resistance again (6). Hypoxia effectuates metabolic changes in tumor cells, including low pH, high ROS, abnormal blood vessels, and proliferating fibrous tissue. These changes are beneficial to tumor cell survival, provide anti-apoptosis advantages, inhibit drug penetration, and promote the development of cancer and drug resistance (105).

To confront the challenge of drug resistance, the main methods include early diagnosis, combined multi drug therapy, and adaptive therapy (106). Effective evaluation molecules could provide a good reference for the early diagnosis and progress of malignant tumors. Quantitative monitoring of circulating tumor DNA (ctDNA) is expected to become an important means of early diagnosis and dynamic monitoring of cancer, which will help to improve the overall survival rate and guide individualized treatment (107). Combined with positron emission tomography and computed tomography (PET-CT) imaging results, evaluate the curative effect. And then adjust the drugs, so as to avoid the emergence of drug resistance and achieve better curative effect (108). Meanwhile, precise drug delivery methods such as antibody drug conjugate (ADC) could increase the curative effect by increasing the local drug concentration (109). In addition, multi drug combination therapy is still an effective measure to combat drug resistance at present. The research of Niu et al. shows that the combined application of vibostolimab (anti-TIGIT humanized IgG1 monoclonal antibody) and pembrolizumab can significantly inhibit and improve the drug resistance of non-small cell lung cancer (NSCLC) (110).

Strategies for targeting hypoxic microenvironments

Bibliometric research published on *Frontiers in oncology* shows that researchers' interest in the research of tumor microenvironment is continuously rising from 2011 to 2021 (8). Moreover, the current research hotspot in this field focuses on the energy metabolism, oxidative phosphorylation, liposomes and other new drug delivery routes in TME (8). Therefore, in order to facilitate readers to understand the progress in this field, we summarize the treatment strategies that targeted at hypoxia. It is gratifying that several potential anti-tumor targets have been found (Table 1), including targeting hypoxia, glycolytic drugs, abnormal angiogenesis, and HIF drugs.

The energy metabolism of tumor microenvironment is a current research hotspot, and researchers have carried out a series of studies with it. A current study showed that glycolytic inhibitors effectively kill tumor cells that are not sensitive to chemotherapy drugs, even when they were present in multiple drug resistance cells (161, 162). Hexokinase 2 (HK2) plays a critical role in regulating aerobic glycolysis in tumor cells and has become one of the main targets of tumor therapy. A previous study showed that HK2 inhibitor 3-bromopyruvic acid (3-BP) significantly inhibits the progression and proliferation of tumor cells in HK2- expressing colorectal cancer. Moreover, apoptosis of tumor cells was induced by the signaling pathway of mitochondrial apoptosis (163). In recent years, the emergence of chemical dynamic therapy (CDT)

TABLE 1 Target drugs for metabolism, HIF, and other pathways.

Category	Pathway/Target	Drugs	Reference
HIF	HIF-1α/VEGF	PKM2, benzofuran, derivatives, BITC, VHH212, P-AscH, Alpha-solanine, TX-2098	(111–117)
	Others	USP25	(118)
Metabolism	Glycolysis	MIR210HG, UHRF1,2-deoxyglucose (2-DG),3-bromopyruvate (3-BP), UBR5, MTAP, CPI-613, ERO1L, BZW1	(119–127)
	Glutamine metabolism	CB-839 mTORC1, EGFR-Pak, SUCLA2, SLC1A5	(128–132)
	Pentose phosphate pathway	PRLR, p16, KRT6A	(133–135)
	Hexosamine biosynthesis pathway	GFAT1, PMG3, NAGK, NF-κB	(136–139)
	Branched chain amino acid (BCAA) metabolism	BCAT2, BCKDHA, BCAT1	(140–142)
	OXPHOS	UQCRC1, metformin, 64 (DX3-234), ONC212, Phenformin	(143–147)
Others	Autophagy	Hydroxychloroquine, BML-275, MEKINIST, SEMA3A	(148–151)
	Antiangiogenic agents	Sunitinib, ceritinib, EndoTAG-1, bevacizumab	(152–155)
	Hypoxia-activated prodrug	TH-302, Evofosfamide, YME1L, HMGCR inhibitors, SQLE	(155–160)

Summary of the current therapeutic pathway and targets related to hypoxia, such as HIF and metabolism, and the drugs corresponding to each approach and target.

has provided a new solution for cancer treatment (164). Interestingly, the amount of glutathione in the tumor cells directly affects the efficacy of chemotherapy. Glycolytic inhibitors could reduce the tumor's glycolytic process and enhance CDT selectivity to tumor cells, thereby exploiting metabolic differences to achieve the specific treatment for tumor cells (165). In addition, OXPHOS inhibitors, such as metformin, improve hypoxia in the microenvironment by inhibiting the mitochondrial complex I, which reduces oxygen consumption in cells and corrects the hypoxic TME. Besides, OXPHOS also inhibits the upregulation of cancer subtypes, such as ovarian cancer, prostate cancer, and thyroid cancer (166, 167).

Abnormal tumor blood vessels are major factors in the continuous hypoxia of TME that hinder drug delivery (168). In the hypoxic TME, angiogenesis-promoting cytokines, such as VEGF and TGF-β, impede the differentiation and maturation of endothelial cells in neovascularization. As a result, malformed and poorly permeable new blood vessels aggravate the anoxic state of the tumor, making it difficult to deliver drugs effectively to the tumor (169). Antiangiogenic drugs, such as anti-VEGF antibodies, correct the abnormal blood vessels and promote the normalization of tumor blood vessels, which in turn alleviates hypoxia and improves the efficacy of conventional antitumor drugs (170, 171). However, angiogenesis inhibitors alone do not receive ideal therapeutic results, which might be related to the complex mechanisms of angiogenesis compensation (172). Therefore, VEGF inhibitors need to be used in combination with chemotherapy or immunotherapy, which has achieved satisfactory results in solid tumors, such as ovarian and breast cancer (173, 174).

HIF activity is mainly dependent on HIF-1α and plays a critical role in the regulation of hypoxic TME. Presently, studies on targeting HIF-1α are being widely carried out. Targeting the HIF-1α signaling pathway is effective in the treatment of solid tumors, such as pancreatic cancer (175, 176). Ubiquitin carboxy-terminal hydrolase L 1(UCHL1) is a ubiquitin-free enzyme that stabilizes its α-subunit (HIF-1α). UCHL1 inhibitors promote the degradation of HIF-1α and inhibit the activity of its downstream genes. Li et al. showed that the inhibition of the UCHL1-HIF-1 pathway decreases the expression of malignant tumor-related factors and eliminates UCHL1-mediated tumor cell proliferation and metastasis (177). In addition, Nelson et al. found that in the hypoxic microenvironment of pancreatic cancer, downregulation of USP25 reduced the transcriptional activity of HIF-1α, leading to cell death in the hypoxic core of the tumor without normal tissue affected (118). In another mouse model of pancreatic cancer, Xu et al. demonstrated that the Benzofuran derivative inhibited tumor growth by acting on the HIF-1α/VEGF pathway under hypoxia (111). In addition, the combination of the HIF-1α inhibitor px-478 and the immune-checkpoint inhibitor enhances the cytotoxicity of T cells against tumor cells, which might be related to the blocking of the HIF-1α/LOXL2 signaling pathway (178). Currently, clinical trials of combined therapy with HIF-1α inhibitors are underway. Thus, HIF-1α inhibitors seem to be a promising cancer therapy in the future.

Of note, the selective is not negligible for drug development, anoxic prodrug is an inactive compound that could be activated automatically in a specific anoxic region. This exploits the selective metabolism of precursor drugs in an anoxic environment, diffuses the killing compounds to the whole TME, and realizes the selective killing of tumor cells (179). A randomized controlled trial for the treatment of advanced pancreatic cancer showed that hypoxia-activated prodrug TH-302 combined with GissiTabine drug yields promising results; the combination group achieved more median progression-free survival than the single Gissi treatment group (180). In addition, TH-302 combined immune checkpoint blocking therapy cured >80% of the tumors in a mouse model of prostate cancer, which prolongs the suppression of bone MDSCs and relieves the inhibition of T cell proliferation (181). Another study showed that CP-506, an anoxic prodrug of nitrogen mustard, also yielded satisfactory effects in tumor tissue (182).

Hyperbaric medicine improves hypoxia in the TME by increasing the amount of dissolved oxygen in the blood (183). In previous studies, hyperbaric medicine has shown a satisfactory excellent curative effect in some cancers (breast and ovarian cancer) (184, 185). Hyperbaric oxygen (HBO) can be used as an adjuvant therapy to inhibit tumors by improving the hypoxic microenvironment (186). A recent study showed that hyperbaric medicine in mice with lung cancer improves the anoxic state of tumors, promotes tumor cell apoptosis, and inhibits tumor growth (187).

Conclusion

Hypoxia is the key factor regulating TME, which mediates the occurrence, development, and drug resistance of tumor cells. Under the condition of hypoxia, TME show immunosuppression and metabolic reprogramming. Therefore, the proliferation and differentiation of immune cells were inhibited. Immunosuppressive cells such as MDSCs, TAM and Tregs are recruited to the hypoxic zone to promote the escape of tumor cells. The metabolic reprogramming of tumor cells is conducive to obtaining energy in a hypoxic environment while maintaining an acidic microenvironment. In addition, glutamine metabolism and fatty acid metabolism have made great contributions to the balanced redox, anti-apoptosis, growth promotion and drug resistance of tumor cells. More importantly, while the hypoxia inhibits the function of PHD, HIF-1α will be activated and promotes the expression of downstream target genes, which further promotes

the formation of hypoxic microenvironment and the progress of tumor cells. Therefore, anti-tumor therapy targeting hypoxia and related factors has attracted many researchers' exploration. Finally, drug resistance induced by hypoxia still plays an important role in the process of anti-tumor treatment, which significantly affects the outcome of treatment. In this review, we summarize the treatment schemes for hypoxia, such as glycolysis inhibitors, anti-angiogenesis drugs, HIF inhibitors, hypoxia-activated prodrugs, and hyperbaric medicine, and finally the found targets and signal pathways in the form of table.

In conclusion, hypoxia is still the key to fight against malignant tumors. It is very necessary to clarify the molecular mechanism of hypoxia on the formation of tumor microenvironment and drug resistance, which will contribute to the breakthrough of tumor targeted therapy in the following work.

Author contributions

(I) Conception and design: TH, DX. (II) Searching literature and led the writing of the review: DX, GC. (III) Making figures and table: GC, KW, HL. (IV) Final approval of manuscript: All authors.

Funding

This work was supported in part by the Shanghai "Rising Stars of Medical Talent" Youth Development Program, Outstanding Youth Medical Talents.

Conflict of interest

The authors declare that the research was conducted in the absence of any commercial or financial relationships that could be construed as a potential conflict of interest.

Publisher's note

All claims expressed in this article are solely those of the authors and do not necessarily represent those of their affiliated organizations, or those of the publisher, the editors and the reviewers. Any product that may be evaluated in this article, or claim that may be made by its manufacturer, is not guaranteed or endorsed by the publisher.

References

1. Sung H, Ferlay J, Siegel RL, Laversanne M, Soerjomataram I, Jemal A, et al. Global cancer statistics 2020: Globocan estimates of incidence and mortality worldwide for 36 cancers in 185 countries. *CA Cancer J Clin* (2021) 71(3):209–49. doi: 10.3322/caac.21660

2. Castells M, Thibault B, Delord J-P, Couderc B. Implication of tumor microenvironment in chemoresistance: Tumor-associated stromal cells protect tumor cells from cell death. *Int J Mol Sci* (2012) 13(8):9545–71. doi: 10.3390/ijms13089545

3. Khalaf K, Hana D, Chou JT-T, Singh C, Mackiewicz A, Kaczmarek M. Aspects of the tumor microenvironment involved in immune resistance and drug resistance. *Front Immunol* (2021) 12:656364. doi: 10.3389/fimmu.2021.656364

4. Seebacher NA, Krchniakova M, Stacy AE, Skoda J, Jansson PJ. Tumour microenvironment stress promotes the development of drug resistance. *Antioxidants (Basel)* (2021) 10(11):1801. doi: 10.3390/antiox10111801

5. Sanmamed MF, Chen L. A paradigm shift in cancer immunotherapy: From enhancement to normalization. *Cell* (2018) 175(2):313–26. doi: 10.1016/j.cell.2018.09.035

6. Hegde PS, Chen DS. Top 10 challenges in cancer immunotherapy. *Immunity* (2020) 52(1):17–35. doi: 10.1016/j.immuni.2019.12.011

7. McDonald P, Chafe S, Dedhar S. Overcoming hypoxia-mediated tumor progression: Combinatorial approaches targeting ph regulation, angiogenesis and immune dysfunction. *Front Cell Dev Biol* (2016) 4:27. doi: 10.3389/fcell.2016.00027

8. Wu K, Liu Y, Liu L, Peng Y, Pang H, Sun X, et al. Emerging trends and research foci in tumor microenvironment of pancreatic cancer: A bibliometric and visualized study. *Front In Oncol* (2022) 12:810774. doi: 10.3389/fonc.2022.810774

9. Quail DF, Joyce JA. Microenvironmental regulation of tumor progression and metastasis. *Nat Med* (2013) 19(11):1423–37. doi: 10.1038/nm.3394

10. Junttila MR, de Sauvage FJ. Influence of tumour micro-environment heterogeneity on therapeutic response. *Nature* (2013) 501(7467):346–54. doi: 10.1038/nature12626

11. Noman MZ, Hasmim M, Lequeux A, Xiao M, Duhem C, Chouaib S, et al. Improving cancer immunotherapy by targeting the hypoxic tumor microenvironment: New opportunities and challenges. *Cells* (2019) 8(9):1083. doi: 10.3390/cells8091083

12. Wan M, Ding Y, Li Z, Wang X, Xu M. Metabolic manipulation of the tumour immune microenvironment. *Immunology* (2022) 165(3):290–300. doi: 10.1111/imm.13444

13. Vuillefroy de Silly R, Dietrich P-Y, Walker PR. Hypoxia and antitumor Cd8 T cells: An incompatible alliance? *Oncoimmunology* (2016) 5(12):e1232236. doi: 10.1080/2162402X.2016.1232236

14. Leone RD, Emens LA. Targeting adenosine for cancer immunotherapy. *J For Immunotherapy Cancer* (2018) 6(1):57. doi: 10.1186/s40425-018-0360-8

15. Payen VL, Porporato PE, Baselet B, Sonveaux P. Metabolic changes associated with tumor metastasis, part 1: Tumor ph, glycolysis and the pentose phosphate pathway. *Cell Mol Life Sci CMLS* (2016) 73(7):1333–48. doi: 10.1007/s00018-015-2098-5

16. Vito A, El-Sayes N, Mossman K. Hypoxia-driven immune escape in the tumor microenvironment. *Cells* (2020) 9(4):992. doi: 10.3390/cells9040992

17. Mpekris F, Voutouri C, Baish JW, Duda DG, Munn LL, Stylianopoulos T, et al. Combining microenvironment normalization strategies to improve cancer immunotherapy. *Proc Natl Acad Sci United States America* (2020) 117(7):3728–37. doi: 10.1073/pnas.1919764117

18. Burrows N, Maxwell PH. Hypoxia and b cells. *Exp Cell Res* (2017) 356 (2):197–203. doi: 10.1016/j.yexcr.2017.03.019

19. Franchina DG, Grusdat M, Brenner D. B-cell metabolic remodeling and cancer. *Trends Cancer* (2018) 4(2):138–50. doi: 10.1016/j.trecan.2017.12.006

20. Sander S, Calado DP, Srinivasan L, Köchert K, Zhang B, Rosolowski M, et al. Synergy between Pi3k signaling and myc in burkitt lymphomagenesis. *Cancer Cell* (2012) 22(2):167–79. doi: 10.1016/j.ccr.2012.06.012

21. Noman MZ, Hasmim M, Messai Y, Terry S, Kieda C, Janji B, et al. Hypoxia: A key player in antitumor immune response. a review in the theme: Cellular responses to hypoxia. *Am J Physiol Cell Physiol* (2015) 309(9):C569–C79. doi: 10.1152/ajpcell.00207.2015

22. Chang WH, Lai AG. The hypoxic tumour microenvironment: A safe haven for immunosuppressive cells and a therapeutic barrier to overcome. *Cancer Lett* (2020) 487:34–44. doi: 10.1016/j.canlet.2020.05.011

23. Edlich F. Bcl-2 proteins and apoptosis: Recent insights and unknowns. *Biochem Biophys Res Commun* (2018) 500(1):26–34. doi: 10.1016/j.bbrc.2017.06.190

24. Radha G, Raghavan SC. Bcl2: A promising cancer therapeutic target. *Biochim Biophys Acta Rev Cancer* (2017) 1868(1):309–14. doi: 10.1016/j.bbcan.2017.06.004

25. Daniel SK, Sullivan KM, Labadie KP, Pillarisetty VG. Hypoxia as a barrier to immunotherapy in pancreatic adenocarcinoma. *Clin Transl Med* (2019) 8(1):10. doi: 10.1186/s40169-019-0226-9

26. Yang M, Ma C, Liu S, Sun J, Shao Q, Gao W, et al. Hypoxia skews dendritic cells to a T helper type 2-stimulating phenotype and promotes tumour cell migration by dendritic cell-derived osteopontin. *Immunology* (2009) 128(1 Suppl):e237–e49. doi: 10.1111/j.1365-2567.2008.02954.x

27. Weigert A, Weichand B, Sekar D, Sha W, Hahn C, Mora J, et al. Hif-1α is a negative regulator of plasmacytoid dc development *in vitro* and *in vivo*. *Blood* (2012) 120(15):3001–6. doi: 10.1182/blood-2012-03-417022

28. Labiano S, Palazon A, Melero I. Immune response regulation in the tumor microenvironment by hypoxia. *Semin Oncol* (2015) 42(3):378–86. doi: 10.1053/j.seminoncol.2015.02.009

29. Chouaib S, Noman MZ, Kosmatopoulos K, Curran MA. Hypoxic stress: Obstacles and opportunities for innovative immunotherapy of cancer. *Oncogene* (2017) 36(4):439–45. doi: 10.1038/onc.2016.225

30. Torres N, Regge MV, Secchiari F, Friedrich AD, Spallanzani RG, Raffo Iraolagoitia XL, et al. Restoration of antitumor immunity through anti-mica antibodies elicited with a chimeric protein. *J immunotherapy Cancer* (2020) 8(1):e000233. doi: 10.1136/jitc-2019-000233

31. Fuertes M, Domaica C, Zwirner N. Leveraging Nkg2d ligands in immuno-oncology. *Front Immunol* (2021) 12:713158. doi: 10.3389/fimmu.2021.713158

32. Badrinath S, Dellacherie M, Li A, Zheng S, Zhang X, Sobral M, et al. A vaccine targeting resistant tumours by dual T cell plus nk cell attack. *Nature* (2022) 606(7916):992–8. doi: 10.1038/s41586-022-04772-4

33. Ferrari de Andrade L, Tay R, Pan D, Luoma A, Ito Y, Badrinath S, et al. Antibody-mediated inhibition of mica and micb shedding promotes nk cell-driven tumor immunity. *Sci (New York NY)* (2018) 359(6383):1537–42. doi: 10.1126/science.aao0505

34. Zhang Y, Zheng J. Functions of immune checkpoint molecules beyond immune evasion. *Adv Exp Med Biol* (2020) 1248:201–26. doi: 10.1007/978-981-15-3266-5_9

35. Noman MZ, Desantis G, Janji B, Hasmim M, Karray S, Dessen P, et al. Pd-L1 is a novel direct target of hif-1α, and its blockade under hypoxia enhanced mdsc-mediated T cell activation. *J Exp Med* (2014) 211(5):781–90. doi: 10.1084/jem.20131916

36. Kalbasi A, Ribas A. Tumour-intrinsic resistance to immune checkpoint blockade. *Nat Rev Immunol* (2020) 20(1):25–39. doi: 10.1038/s41577-019-0218-4

37. Curigliano G, Criscitiello C, Gelao L, Goldhirsch A. Molecular pathways (Hla-G). *Clin Cancer Res an Off J Am Assoc Cancer Res* (2013) 19(20):5564–71. doi: 10.1158/1078-0432.CCR-12-3697

38. Garziera M, Scarabel L, Toffoli G. Hypoxic modulation of hla-G expression through the metabolic sensor hif-1 in human cancer cells. *J Immunol Res* (2017) 2017:4587520. doi: 10.1155/2017/4587520

39. Sahai E, Astsaturov I, Cukierman E, DeNardo DG, Egeblad M, Evans RM, et al. A framework for advancing our understanding of cancer-associated fibroblasts. *Nat Rev Cancer* (2020) 20(3):174–86. doi: 10.1038/s41568-019-0238-1

40. Ziani L, Buart S, Chouaib S, Thiery J. Hypoxia increases melanoma-associated fibroblasts immunosuppressive potential and inhibitory effect on T cell-mediated cytotoxicity. *Oncoimmunology* (2021) 10(1):1950953. doi: 10.1080/2162402X.2021.1950953

41. Kuen J, Darowski D, Kluge T, Majety M. Pancreatic cancer Cell/Fibroblast Co-culture induces M2 like macrophages that influence therapeutic response in a 3d model. *PloS One* (2017) 12(7):e0182039. doi: 10.1371/journal.pone.0182039

42. Comito G, Giannoni E, Segura CP, Barcellos-de-Souza P, Raspollini MR, Baroni G, et al. Cancer-associated fibroblasts and M2-polarized macrophages synergize during prostate carcinoma progression. *Oncogene* (2014) 33(19):2423–31. doi: 10.1038/onc.2013.191

43. Freeman P, Mielgo A. Cancer-associated fibroblast mediated inhibition of Cd8+ cytotoxic T cell accumulation in tumours: Mechanisms and therapeutic opportunities. *Cancers* (2020) 12(9):2687. doi: 10.3390/cancers12092687

44. Li T, Yang Y, Hua X, Wang G, Liu W, Jia C, et al. Hepatocellular carcinoma-associated fibroblasts trigger nk cell dysfunction *Via* Pge2 and ido. *Cancer Lett* (2012) 318(2):154–61. doi: 10.1016/j.canlet.2011.12.020

45. Dysthe M, Parihar R. Myeloid-derived suppressor cells in the tumor microenvironment. *Tumor Microenviron* (2020) 1224:117–40.

46. Hou A, Hou K, Huang Q, Lei Y, Chen W. Targeting myeloid-derived suppressor cell, a promising strategy to overcome resistance to immune checkpoint inhibitors. *Front Immunol* (2020) 11:783. doi: 10.3389/fimmu.2020.00783

47. Chiu DK-C, Tse AP-W, Xu IM-J, Di Cui J, Lai RK-H, Li LL, et al. Hypoxia inducible factor hif-1 promotes myeloid-derived suppressor cells accumulation through Entpd2/Cd39l1 in hepatocellular carcinoma. *Nat Commun* (2017) 8(1):517. doi: 10.1038/s41467-017-00530-7

48. Vitale I, Manic G, Coussens LM, Kroemer G, Galluzzi L. Macrophages and metabolism in the tumor microenvironment. *Cell Metab* (2019) 30(1):36–50. doi: 10.1016/j.cmet.2019.06.001

49. Komohara Y, Fujiwara Y, Ohnishi K, Takeya M. Tumor-associated macrophages: Potential therapeutic targets for anti-cancer therapy. *Adv Drug Delivery Rev* (2016) 99(Pt B):180–5. doi: 10.1016/j.addr.2015.11.009

50. Colegio OR, Chu N-Q, Szabo AL, Chu T, Rhebergen AM, Jairam V, et al. Functional polarization of tumour-associated macrophages by tumour-derived lactic acid. *Nature* (2014) 513(7519):559–63. doi: 10.1038/nature13490

51. Schiliro C, Firestein BL. Mechanisms of metabolic reprogramming in cancer cells supporting enhanced growth and proliferation. *Cells* (2021) 10(5):1056. doi: 10.3390/cells10051056

52. Vander Heiden MG, Cantley LC, Thompson CB. Understanding the warburg effect: The metabolic requirements of cell proliferation. *Sci (New York NY)* (2009) 324(5930):1029–33. doi: 10.1126/science.1160809

53. Urbano AM. Otto Warburg: The journey towards the seminal discovery of tumor cell bioenergetic reprogramming. *Biochim Biophys Acta Mol Basis Dis* (2021) 1867(1):165965. doi: 10.1016/j.bbadis.2020.165965

54. Kobliakov AV. Hypoxia and glycolysis as factors determining the malignant phenotype. *Tsitologiia* (2018) 58(7):499–506.

55. Sgarbi G, Gorini G, Liuzzi F, Solaini G, Baracca A. Hypoxia and If_1 expression promote ros decrease in cancer cells. *Cells* (2018) 7(7):64. doi: 10.3390/cells7070064

56. Rob A, Cairns I, , Harris S. Regulation of cancer cell metabolism. *Nat Rev Cancer* (2012) 11(2):85–95.

57. Yuneva M, Zamboni N, Oefner P, Sachidanandam R, Lazebnik Y. Deficiency in glutamine but not glucose induces myc-dependent apoptosis in human cells. *J Cell Biol* (2007) 178(1):93–105

58. Zhang J, Pavlova NN, Thompson CB. Cancer cell metabolism: The essential role of the nonessential amino acid, glutamine. *EMBO J* (2017) 36(10):1302–15. doi: 10.15252/embj.201696151

59. Zhdanov AV, Waters AHC, Golubeva AV, Dmitriev RI, Papkovsky DB. Availability of the key metabolic substrates dictates the respiratory response of cancer cells to the mitochondrial uncoupling. *Biochim Biophys Acta* (2014) 1837(1):51–62. doi: 10.1016/j.bbabio.2013.07.008

60. Kodama M, Oshikawa K, Shimizu H, Yoshioka S, Takahashi M, Izumi Y, et al. A shift in glutamine nitrogen metabolism contributes to the malignant progression of cancer. *Nat Commun* (2020) 11(1):1320. doi: 10.1038/s41467-020-15136-9

61. Matés JM, Campos-Sandoval JA, JdL Santos-Jiménez, Márquez J. Dysregulation of glutaminase and glutamine synthetase in cancer. *Cancer Lett* (2019) 467:29–39. doi: 10.1016/j.canlet.2019.09.011

62. Matés JM, Segura JA, Alonso FJ, Márquez J. Oxidative stress in apoptosis and cancer: An update. *Arch Toxicol* (2012) 86(11):1649–65. doi: 10.1007/s00204-012-0906-3

63. Friesen C, Kiess Y, Debatin KM. A critical role of glutathione in determining apoptosis sensitivity and resistance in leukemia cells. *Cell Death Differ* (2004) 11 Suppl 1:S73–85.

64. Domblides C, Lartigue L, Faustin B. Metabolic stress in the immune function of T cells, macrophages and dendritic cells. *Cells* (2018) 7(7):68. doi: 10.3390/cells7070068

65. Cheng C, Geng F, Cheng X, Guo D. Lipid metabolism reprogramming and its potential targets in cancer. *Cancer Commun (Lond)* (2018) 38(1):27. doi: 10.1186/s40880-018-0301-4

66. Menendez JA, Lupu R. Fatty acid synthase and the lipogenic phenotype in cancer pathogenesis. *Nat Rev Cancer* (2007) 7(10):763–77.

67. Pike LS, Smift AL, Croteau NJ, Ferrick DA, Wu M. Inhibition of fatty acid oxidation by etomoxir impairs nadph production and increases reactive oxygen species resulting in atp depletion and cell death in human glioblastoma cells. *Biochim Biophys Acta* (2011) 1807(6):726–34.

68. Xiao L, Ma X, Ye L, Su P, Xiong W, Bi E, et al. Il-9/Stat3/Fatty acid oxidation-mediated lipid peroxidation contributes to Tc9 cell longevity and enhanced antitumor activity. *J Clin Invest* (2022) 132(7):e153247. doi: 10.1172/JCI153247

69. Semenza GL. Hypoxia-inducible factors: Mediators of cancer progression and targets for cancer therapy. *Trends Pharmacol Sci* (2012) 33(4):207–14. doi: 10.1016/j.tips.2012.01.005

70. Jiang BH, Zheng JZ, Leung SW, Roe R, Semenza GL. Transactivation and inhibitory domains of hypoxia-inducible factor 1alpha. modulation of transcriptional activity by oxygen tension. *J Biol Chem* (1997) 272 (31):19253–60.

71. Deng B, Zhu J-M, Wang Y, Liu T-T, Ding Y-B, Xiao W-M, et al. Intratumor hypoxia promotes immune tolerance by inducing regulatory T cells *Via* tgf-β1 in gastric cancer. *PloS One* (2013) 8(5):e63777. doi: 10.1371/journal.pone.0063777

72. Meng X, Grötsch B, Luo Y, Knaup KX, Wiesener MS, Chen X-X, et al. Hypoxia-inducible factor-1α is a critical transcription factor for il-10-Producing b cells in autoimmune disease. *Nat Commun* (2018) 9(1):251. doi: 10.1038/s41467-017-02683-x

73. Semenza GL. Oxygen sensing, hypoxia-inducible factors, and disease pathophysiology. *Annu Rev Pathol* (2014) 9:47–71. doi: 10.1146/annurev-pathol-012513-104720

74. Bosco MC, D'Orazi G, Del Bufalo D. Targeting hypoxia in tumor: A new promising therapeutic strategy. *J Exp Clin Cancer Res CR* (2020) 39(1):8. doi: 10.1186/s13046-019-1517-0

75. Qiu G-Z, Jin M-Z, Dai J-X, Sun W, Feng J-H, Jin W-L. Reprogramming of the tumor in the hypoxic niche: The emerging concept and associated therapeutic strategies. *Trends Pharmacol Sci* (2017) 38(8):669–86. doi: 10.1016/j.tips.2017.05.002

76. Barsoum IB, Smallwood CA, Siemens DR, Graham CH. A mechanism of hypoxia-mediated escape from adaptive immunity in cancer cells. *Cancer Res* (2014) 74(3):665–74. doi: 10.1158/0008-5472.CAN-13-0992

77. Shen D-D, Bi Y-P, Pang J-R, Zhao L-J, Zhao L-F, Gao Y, et al. Generation, secretion and degradation of cancer immunotherapy target pd-L1. *Cell Mol Life Sci CMLS* (2022) 79(8):413. doi: 10.1007/s00018-022-04431-x

78. Logtenberg MEW, Scheeren FA, Schumacher TN. The Cd47-sirpα immune checkpoint. *Immunity* (2020) 52(5):742–52. doi: 10.1016/j.immuni.2020.04.011

79. Samanta D, Park Y, Ni X, Li H, Zahnow CA, Gabrielson E, et al. Chemotherapy induces enrichment of Cd47/Cd73/Pdl1 immune evasive triple-negative breast cancer cells. *Proc Natl Acad Sci United States America* (2018) 115 (6):E1239–E48. doi: 10.1073/pnas.1718197115

80. Jia X, Yan B, Tian X, Liu Q, Jin J, Shi J, et al. Cd47/Sirpα pathway mediates cancer immune escape and immunotherapy. *Int J Biol Sci* (2021) 17(13):3281–7. doi: 10.7150/ijbs.60782

81. Bachman KE, Park BH. Duel nature of tgf-beta signaling: Tumor suppressor vs. tumor promoter. *Curr Opin Oncol* (2005) 17(1):49–54.

82. Syed V. Tgf-β signaling in cancer. *J Cell Biochem* (2016) 117(6):1279–87. doi: 10.1002/jcb.25496

83. Huang Y, Chen Z, Lu T, Bi G, Li M, Liang J, et al. Hif-1α switches the functionality of tgf-β signaling *Via* changing the partners of smads to drive glucose metabolic reprogramming in non-small cell lung cancer. *J Exp Clin Cancer Res CR* (2021) 40(1):398. doi: 10.1186/s13046-021-02188-y

84. Massari F, Ciccarese C, Santoni M, Iacovelli R, Mazzucchelli R, Piva F, et al. Metabolic phenotype of bladder cancer. *Cancer Treat Rev* (2016) 45:46–57. doi: 10.1016/j.ctrv.2016.03.005

85. Sampedro-Núñez M, Bouthelier A, Serrano-Somavilla A, Martínez-Hernández R, Adrados M, Martín-Pérez E, et al. Lat-1 and glut-1 carrier expression and its prognostic value in gastroenteropancreatic neuroendocrine tumors. *Cancers* (2020) 12(10):2968. doi: 10.3390/cancers12102968

86. Zhang J, Zhang Y, Mo F, Patel G, Butterworth K, Shao C, et al. The roles of hif-1α in radiosensitivity and radiation-induced bystander effects under hypoxia. *Front Cell Dev Biol* (2021) 9:637454. doi: 10.3389/fcell.2021.637454

87. Scarini J, Rosa L, Souza R, Egal E, Tincani A, Martins A, et al. Gene and immunohistochemical expression of hif-1α, glut-1, fasn, and adipophilin in carcinoma ex pleomorphic adenoma development. *Oral Dis* (2020) 00:1–10. doi: 10.1111/odi.13332

88. Wu Z, Wu J, Zhao Q, Fu S, Jin J. Emerging roles of aerobic glycolysis in breast cancer. *Clin Trans Oncol Off Publ Fed Spanish Oncol Societies Natl Cancer Institute Mexico* (2020) 22(5):631–46. doi: 10.1007/s12094-019-02187-8

89. Samanta D, Semenza G. Metabolic adaptation of cancer and immune cells mediated by hypoxia-inducible factors. *Biochim Biophys Acta Rev Cancer* (2018) 1870(1):15–22. doi: 10.1016/j.bbcan.2018.07.002

90. Yoo H, Park S, Nam M, Kang J, Kim K, Yeo J, et al. A variant of Slc1a5 is a mitochondrial glutamine transporter for metabolic reprogramming in cancer cells. *Cell Metab* (2020) 31(2):267–83.e12. doi: 10.1016/j.cmet.2019.11.020

91. Sun R, Denko N. Hypoxic regulation of glutamine metabolism through Hif1 and Siah2 supports lipid synthesis that is necessary for tumor growth. *Cell Metab* (2014) 19(2):285–92. doi: 10.1016/j.cmet.2013.11.022

92. Infantino V, Santarsiero A, Convertini P, Todisco S, Iacobazzi V. Cancer cell metabolism in hypoxia: Role of hif-1 as key regulator and therapeutic target. *Int J Mol Sci* (2021) 22(11):5703. doi: 10.3390/ijms22115703

93. Weinberg F, Ramnath N, Nagrath D. Reactive oxygen species in the tumor microenvironment: An overview. *Cancers* (2019) 11(8):1191. doi: 10.3390/cancers11081191

94. Zhu X, Zuo L. Characterization of oxygen radical formation mechanism at early cardiac ischemia. *Cell Death Dis* (2013) 4:e787. doi: 10.1038/cddis.2013.313

95. Guzy RD, Hoyos B, Robin E, Chen H, Liu L, Mansfield KD, et al. Mitochondrial complex iii is required for hypoxia-induced ros production and cellular oxygen sensing. *Cell Metab* (2005) 1(6):401–8.

96. Sk UH, Bhattacharya S. Oxidative stress in cancer. (2021) doi: 10.1007/978-981-15-4501-6_126-1.

97. Bridge G, Rashid S, Martin SA. DNA Mismatch repair and oxidative DNA damage: Implications for cancer biology and treatment. *Cancers* (2014) 6(3):1597–614. doi: 10.3390/cancers6031597

98. Liao Z, Chua D, Tan NS. Reactive oxygen species: A volatile driver of field cancerization and metastasis. *Mol Cancer* (2019) 18(1):65. doi: 10.1186/s12943-019-0961-y

99. Galadari S, Rahman A, Pallichankandy S, Thayyullathil F. Reactive oxygen species and cancer paradox: To promote or to suppress? *Free Radic Biol Med* (2017) 104:144–64. doi: 10.1016/j.freeradbiomed.2017.01.004

100. Rockwell S. Hypoxia and drug resistance. *Encyclopedia Cancer (Second Edition)* (2002), 461–7.

101. Minassian LM, Cotechini T, Huitema E, Graham CH. Hypoxia-induced resistance to chemotherapy in cancer. *Adv Exp Med Biol* (2019) 1136:123–39.

102. Phung CD, Tran TH, Pham LM, Nguyen HT, Jeong J-H, Yong CS, et al. Current developments in nanotechnology for improved cancer treatment, focusing on tumor hypoxia. *J Control Release* (2020) 324:413–29. doi: 10.1016/j.jconrel.2020.05.029

103. Chouaib S, Janji B, Tittarelli A, Eggermont A, Thiery JP. Tumor plasticity interferes with anti-tumor immunity. *Crit Rev Immunol* (2014) 34(2):91–102.

104. Hasmim M, Messai Y, Ziani L, Thiery J, Bouhris J-H, Noman MZ, et al. Critical role of tumor microenvironment in shaping nk cell functions: Implication of hypoxic stress. *Front Immunol* (2015) 6:482. doi: 10.3389/fimmu.2015.00482

105. Jain RK. Antiangiogenesis strategies revisited: From starving tumors to alleviating hypoxia. *Cancer Cell* (2014) 26(5):605–22. doi: 10.1016/j.ccell.2014.10.006

106. Sharma M, Bakshi AK, Mittapelly N, Gautam S, Marwaha D, Rai N, et al. Recent updates on innovative approaches to overcome drug resistance for better outcomes in cancer. *J Control Release* (2022) 346:43–70. doi: 10.1016/j.jconrel.2022.04.007

107. Baylin SB, Jones PA. Epigenetic determinants of cancer. *Cold Spring Harb Perspect Biol* (2016) 8(9):a019505. doi: 10.1101/cshperspect.a019505

108. Ansell SM, Armitage JO. Positron emission tomographic scans in lymphoma: Convention and controversy. *Mayo Clin Proc* (2012) 87(6):571–80. doi: 10.1016/j.mayocp.2012.03.006

109. Baah S, Laws M, Rahman KM. Antibody-drug conjugates-a tutorial review. *Molecules* (2021) 26(10):2943. doi: 10.3390/molecules26102943

110. Attili I, Passaro A, de Marinis F. Anti-tigit to overcome resistance to immune checkpoint inhibitors in lung cancer: Limits and potentials. *Ann Oncol* (2022) 33(2):119–22. doi: 10.1016/j.annonc.2021.11.008

111. Xu X-L, Yang Y-R, Mo X-F, Wei J-L, Zhang X-J, You Q-D. Design, synthesis, and evaluation of benzofuran derivatives as novel anti-pancreatic carcinoma agents *Via* interfering the hypoxia environment by targeting hif-1α pathway. *Eur J Med Chem* (2017) 137:45–62. doi: 10.1016/j.ejmech.2017.05.042

112. Azoitei N, Becher A, Steinestel K, Rouhi A, Diepold K, Genze F, et al. Pkm2 promotes tumor angiogenesis by regulating hif-1α through nf-κb activation. *Mol Cancer* (2016) 15:3. doi: 10.1186/s12943-015-0490-2

113. Hu X, Xiao Y, Sun J, Ji B, Luo S, Wu B, et al. New possible silver lining for pancreatic cancer therapy: Hydrogen sulfide and its donors. *Acta Pharm Sin B* (2021) 11(5):1148–57. doi: 10.1016/j.apsb.2020.10.019

114. Kang G, Hu M, Ren H, Wang J, Cheng X, Li R, et al. Vhh212 nanobody targeting the hypoxia-inducible factor 1α suppresses angiogenesis and potentiates gemcitabine therapy in pancreatic cancer. *Cancer Biol Med* (2021) 18(3):772–87. doi: 10.20892/j.issn.2095-3941.2020.0568

115. Cho I-R, Kaowinn S, Moon J, Soh J, Kang HY, Jung C-R, et al. Oncotropic h-1 parvovirus infection degrades hif-1α protein in human pancreatic cancer cells independently of vhl and Rack1. *Int J Oncol* (2015) 46(5):2076–82. doi: 10.3892/ijo.2015.2922

116. Wen Z, Huang C, Xu Y, Xiao Y, Tang L, Dai J, et al. α-solanine inhibits vascular endothelial growth factor expression by down-regulating the Erk1/2-Hif-1α and Stat3 signaling pathways. *Eur J Pharmacol* (2016) 771:93–8. doi: 10.1016/j.ejphar.2015.12.020

117. Miyake K, Nishioka M, Imura S, Batmunkh E, Uto Y, Nagasawa H, et al. The novel hypoxic cytotoxin, tx-2098 has antitumor effect in pancreatic cancer;

possible mechanism through inhibiting vegf and hypoxia inducible factor-1α targeted gene expression. *Exp Cell Res* (2012) 318(13):1554–63. doi: 10.1016/j.yexcr.2012.03.013

118. Nelson JK, Thin MZ, Evan T, Howell S, Wu M, Almeida B, et al. Usp25 promotes pathological hif-1-Driven metabolic reprogramming and is a potential therapeutic target in pancreatic cancer. *Nat Commun* (2022) 13(1):2070. doi: 10.1038/s41467-022-29684-9

119. Yu T, Li G, Wang C, Gong G, Wang L, Li C, et al. Mir210hg regulates glycolysis, cell proliferation, and metastasis of pancreatic cancer cells through mir-125b-5p/Hk2/Pkm2 axis. *RNA Biol* (2021) 18(12):2513–30. doi: 10.1080/15476286.2021.1930755

120. Hu Q, Qin Y, Ji S, Xu W, Liu W, Sun Q, et al. Uhrf1 promotes aerobic glycolysis and proliferation *Via* suppression of Sirt4 in pancreatic cancer. *Cancer Lett* (2019) 452:226–36. doi: 10.1016/j.canlet.2019.03.024

121. Halbrook CJ, Lyssiotis CA. Employing metabolism to improve the diagnosis and treatment of pancreatic cancer. *Cancer Cell* (2017) 31(1):5–19. doi: 10.1016/j.ccell.2016.12.006

122. Chapiro J, Sur S, Savic LJ, Ganapathy-Kanniappan S, Reyes J, Duran R, et al. Systemic delivery of microencapsulated 3-bromopyruvate for the therapy of pancreatic cancer. *Clin Cancer Res an Off J Am Assoc Cancer Res* (2014) 20(24):6406–17. doi: 10.1158/1078-0432.CCR-14-1271

123. Chen L, Yuan R, Wen C, Liu T, Feng Q, Deng X, et al. E3 ubiquitin ligase Ubr5 promotes pancreatic cancer growth and aerobic glycolysis by downregulating Fbp1 *Via* destabilization of C/Ebpα. *Oncogene* (2021) 40(2):262–76. doi: 10.1038/s41388-020-01527-1

124. Hu Q, Qin Y, Ji S, Shi X, Dai W, Fan G, et al. Mtap deficiency-induced metabolic reprogramming creates a vulnerability to cotargeting purine synthesis and glycolysis in pancreatic cancer. *Cancer Res* (2021) 81(19):4964–80. doi: 10.1158/0008-5472.CAN-20-0414

125. Vasan K, Werner M, Chandel NS. Mitochondrial metabolism as a target for cancer therapy. *Cell Metab* (2020) 32(3):341–52.

126. Zhang J, Yang J, Lin C, Liu W, Huo Y, Yang M, et al. Endoplasmic reticulum stress-dependent expression of Ero1l promotes aerobic glycolysis in pancreatic cancer. *Theranostics* (2020) 10(18):8400–14. doi: 10.7150/thno.45124

127. Li Z, Ge Y, Dong J, Wang H, Zhao T, Wang X, et al. Bzw1 facilitates glycolysis and promotes tumor growth in pancreatic ductal adenocarcinoma through potentiating Eif2α phosphorylation. *Gastroenterology* (2022) 162(4):1256–1271.e14. doi: 10.1053/j.gastro.2021.12.249

128. Hamada S, Matsumoto R, Tanaka Y, Taguchi K, Yamamoto M, Masamune A. Nrf2 activation sensitizes K-ras mutant pancreatic cancer cells to glutaminase inhibition. *Int J Mol Sci* (2021) 22(4):1870. doi: 10.3390/ijms22041870

129. Tsai P-Y, Lee M-S, Jadhav U, Naqvi I, Madha S, Adler A, et al. Adaptation of pancreatic cancer cells to nutrient deprivation is reversible and requires glutamine synthetase stabilization by Mtorc1. *Proc Natl Acad Sci United States America* (2021) 118(10):e2003014118. doi: 10.1073/pnas.2003014118

130. Lee S-W, Zhang Y, Jung M, Cruz N, Alas B, Commisso C. Egfr-pak signaling selectively regulates glutamine deprivation-induced macropinocytosis. *Dev Cell* (2019) 50(3):381–392.e5. doi: 10.1016/j.devcel.2019.05.043

131. Tong Y, Guo D, Lin S-H, Liang J, Yang D, Ma C, et al. Sucla2-coupled regulation of gls succinylation and activity counteracts oxidative stress in tumor cells. *Mol Cell* (2021) 81(11):2303–2316.e8. doi: 10.1016/j.molcel.2021.04.002

132. Yoo HC, Park SJ, Nam M, Kang J, Kim K, Yeo JH, et al. A variant of Slc1a5 is a mitochondrial glutamine transporter for metabolic reprogramming in cancer cells. *Cell Metab* (2020) 31(2):267–283.e12. doi: 10.1016/j.cmet.2019.11.020

133. Nie H, Huang P-Q, Jiang S-H, Yang Q, Hu L-P, Yang X-M, et al. The short isoform of prlr suppresses the pentose phosphate pathway and nucleotide synthesis through the Nek9-hippo axis in pancreatic cancer. *Theranostics* (2021) 11(8):3898–915. doi: 10.7150/thno.51712

134. Buj R, Chen C-W, Dahl ES, Leon KE, Kuskovsky R, Maglakelidze N, et al. Suppression of P16 induces Mtorc1-mediated nucleotide metabolic reprogramming. *Cell Rep* (2019) 28(8):1971–1980.e8. doi: 10.1016/j.celrep.2019.07.084

135. Che D, Wang M, Sun J, Li B, Xu T, Lu Y, et al. Krt6a promotes lung cancer cell growth and invasion through myc-regulated pentose phosphate pathway. *Front Cell Dev Biol* (2021) 9:694071. doi: 10.3389/fcell.2021.694071

136. Sharma NS, Gupta VK, Garrido VT, Hadad R, Durden BC, Kesh K, et al. Targeting tumor-intrinsic hexosamine biosynthesis sensitizes pancreatic cancer to anti-Pd1 therapy. *J Clin Invest* (2020) 130(1):451–65. doi: 10.1172/JCI127515

137. Ricciardiello F, Gang Y, Palorini R, Li Q, Giampà M, Zhao F, et al. Hexosamine pathway inhibition overcomes pancreatic cancer resistance to gemcitabine through unfolded protein response and egfr-akt pathway modulation. *Oncogene* (2020) 39(20):4103–17. doi: 10.1038/s41388-020-1260-1

138. Campbell S, Mesaros C, Izzo L, Affronti H, Noji M, Schaffer BE, et al. Glutamine deprivation triggers nagk-dependent hexosamine salvage. *Elife* (2021) 10:e62644. doi: 10.7554/eLife.62644

139. Ma Z, Vocadlo DJ, Vosseller K. Hyper-O-Glcnacylation is anti-apoptotic and maintains constitutive nf-κb activity in pancreatic cancer cells. *J Biol Chem* (2013) 288(21):15121–30. doi: 10.1074/jbc.M113.470047

140. Li J-T, Yin M, Wang D, Wang J, Lei M-Z, Zhang Y, et al. Bcat2-mediated bcaa catabolism is critical for development of pancreatic ductal adenocarcinoma. *Nat Cell Biol* (2020) 22(2):167–74. doi: 10.1038/s41556-019-0455-6

141. Lee JH, Cho Y-R, Kim JH, Kim J, Nam HY, Kim SW, et al. Branched-chain amino acids sustain pancreatic cancer growth by regulating lipid metabolism. *Exp Mol Med* (2019) 51(11):1–11. doi: 10.1038/s12276-019-0350-z

142. Zhu Z, Achreja A, Meurs N, Animasahun O, Owen S, Mittal A, et al. Tumour-reprogrammed stromal Bcat1 fuels branched-chain ketoacid dependency in stromal-rich pdac tumours. *Nat Metab* (2020) 2(8):775–92. doi: 10.1038/s42255-020-0226-5

143. Wang Q, Li M, Gan Y, Jiang S, Qiao J, Zhang W, et al. Mitochondrial protein Uqcrc1 is oncogenic and a potential therapeutic target for pancreatic cancer. *Theranostics* (2020) 10(5):2141–57. doi: 10.7150/thno.38704

144. Ashton TM, McKenna WG, Kunz-Schughart LA, Higgins GS. Oxidative phosphorylation as an emerging target in cancer therapy. *Clin Cancer Res an Off J Am Assoc Cancer Res* (2018) 24(11):2482–90. doi: 10.1158/1078-0432.CCR-17-3070

145. Xue D, Xu Y, Kyani A, Roy J, Dai L, Sun D, et al. Discovery and lead optimization of benzene-1,4-Disulfonamides as oxidative phosphorylation inhibitors. *J Med Chem* (2022) 65(1):343–68. doi: 10.1021/acs.jmedchem.1c01509

146. Ferrarini I, Louie A, Zhou L, El-Deiry WS. Onc212 is a novel mitocan acting synergistically with glycolysis inhibition in pancreatic cancer. *Mol Cancer Ther* (2021) 20(9):1572–83. doi: 10.1158/1535-7163.MCT-20-0962

147. Masoud R, Reyes-Castellanos G, Lac S, Garcia J, Dou S, Shintu L, et al. Targeting mitochondrial complex I overcomes chemoresistance in high oxphos pancreatic cancer. *Cell Rep Med* (2020) 1(8):100143. doi: 10.1016/j.xcrm.2020.100143

148. Bigelsen S. Evidence-based complementary treatment of pancreatic cancer: A review of adjunct therapies including paricalcitol, hydroxychloroquine, intravenous vitamin c, statins, metformin, curcumin, and aspirin. *Cancer Manag Res* (2018) 10:2003–18. doi: 10.2147/CMAR.S161824

149. Duong H-Q, Hwang JS, Kim HJ, Seong Y-S, Bae I. Bml-275, an ampk inhibitor, induces DNA damage, G2/M arrest and apoptosis in human pancreatic cancer cells. *Int J Oncol* (2012) 41(6):2227–36. doi: 10.3892/ijo.2012.1672

150. Zhu X, Cao Y, Liu W, Ju X, Zhao X, Jiang L, et al. Stereotactic body radiotherapy plus pembrolizumab and trametinib versus stereotactic body radiotherapy plus gemcitabine for locally recurrent pancreatic cancer after surgical resection: An open-label, randomised, controlled, phase 2 trial. *Lancet Oncol* (2021) 22(8):1093–102. doi: 10.1016/S1470-2045(21)00286-2

151. Gioelli N, Maione F, Camillo C, Ghitti M, Valdembri D, Morello N, et al. A rationally designed Nrp1-independent superagonist Sema3a mutant is an effective anticancer agent. *Sci Transl Med* (2018) 10(442):eaah4807. doi: 10.1126/scitranslmed.aah4807

152. Martínez-Bosch N, Guerrero PE, Moreno M, José A, Iglesias M, Munné-Collado J, et al. The pancreatic niche inhibits the effectiveness of sunitinib treatment of pancreatic cancer. *Oncotarget* (2016) 7(30):48265–79. doi: 10.18632/oncotarget.10199

153. Jamshed MB, Munir F, Shahid N, Sadiq U, Muhammad SA, Ghanem NB, et al. Antitumor activity and combined inhibitory effect of ceritinib with gemcitabine in pancreatic cancer. *Am J Physiol Gastrointest Liver Physiol* (2020) 318(1):G109–G19. doi: 10.1152/ajpgi.00130.2019

154. Zhang Z, Song J, Xie C, Pan J, Lu W, Liu M. Pancreatic cancer: Recent progress of drugs in clinical trials. *AAPS J* (2021) 23(2):29. doi: 10.1208/s12248-021-00556-2

155. Miller AL, Garcia PL, Yoon KJ. Developing effective combination therapy for pancreatic cancer: An overview. *Pharmacol Res* (2020) 155:104740. doi: 10.1016/j.phrs.2020.104740

156. Sun JD, Liu Q, Ahluwalia D, Li W, Meng F, Wang Y, et al. Efficacy and safety of the hypoxia-activated prodrug Th-302 in combination with gemcitabine and nab-paclitaxel in human tumor xenograft models of pancreatic cancer. *Cancer Biol Ther* (2015) 16(3):438–49. doi: 10.1080/15384047.2014.1003005

157. Kishimoto S, Brender JR, Chandramouli GVR, Saida Y, Yamamoto K, Mitchell JB, et al. Hypoxia-activated prodrug evofosfamide treatment in pancreatic ductal adenocarcinoma xenografts alters the tumor redox status to potentiate radiotherapy. *Antioxid Redox Signal* (2021) 35(11):904–15. doi: 10.1089/ars.2020.8131

158. MacVicar T, Ohba Y, Nolte H, Mayer FC, Tatsuta T, Sprenger H-G, et al. Lipid signalling drives proteolytic rewiring of mitochondria by Yme1l. *Nature* (2019) 575(7782):361–5. doi: 10.1038/s41586-019-1738-6

159. Zhou L, Wang Q, Zhang H, Li Y, Xie S, Xu M. Yap inhibition by nuciferine *Via* ampk-mediated downregulation of hmgcr sensitizes pancreatic cancer cells to gemcitabine. *Biomolecules* (2019) 9(10):620. doi: 10.3390/biom9100620

160. Bian X, Liu R, Meng Y, Xing D, Xu D, Lu Z. Lipid metabolism and cancer. *J Exp Med* (2021) 218(1):e20201606. doi: 10.1084/jem.20201606

161. Reyes R, Wani NA, Ghoshal K, Jacob ST, Motiwala T. Sorafenib and 2-deoxyglucose synergistically inhibit proliferation of both sorafenib-sensitive and -resistant hcc cells by inhibiting atp production. *Gene Expr* (2017) 17(2):129–40. doi: 10.3727/105221616X693855

162. Yoo J-J, Yu SJ, Na J, Kim K, Cho YY, Lee YB, et al. Hexokinase-ii inhibition synergistically augments the anti-tumor efficacy of sorafenib in hepatocellular carcinoma. *Int J Mol Sci* (2019) 20(6):1292. doi: 10.3390/ijms20061292

163. Zhong J, Lu S, Jia X, Li Q, Liu L, Xie P, et al. Role of endoplasmic reticulum stress in apoptosis induced by Hk2 inhibitor and its potential as a new drug combination strategy. *Cell Stress Chaperones* (2022) 27(3):273–83. doi: 10.1007/s12192-022-01267-z

164. Zhou Y, Fan S, Feng L, Huang X, Chen X. Manipulating intratumoral fenton chemistry for enhanced chemodynamic and chemodynamic-synergized multimodal therapy. *Adv Mater* (2021) 33(48):e2104223. doi: 10.1002/adma.202104223

165. Huang Y, Wu S, Zhang L, Deng Q, Ren J, Qu X. A metabolic multistage glutathione depletion used for tumor-specific chemodynamic therapy. *ACS Nano* (2022) 16(3):4228–38. doi: 10.1021/acsnano.1c10231

166. Reznik E, Miller ML, Şenbabaoğlu Y, Riaz N, Sarungbam J, Tickoo SK, et al. Mitochondrial DNA copy number variation across human cancers. *Elife* (2016) 5:e10769. doi: 10.7554/eLife.10769

167. Zannella VE, Dal Pra A, Muaddi H, McKee TD, Stapleton S, Sykes J, et al. Reprogramming metabolism with metformin improves tumor oxygenation and radiotherapy response. *Clin Cancer Res an Off J Am Assoc Cancer Res* (2013) 19 (24):6741–50. doi: 10.1158/1078-0432.CCR-13-1787

168. Choueiri TK, Kaelin WG. Targeting the Hif2-vegf axis in renal cell carcinoma. *Nat Med* (2020) 26(10):1519–30. doi: 10.1038/s41591-020-1093-z

169. Akman M, Belisario DC, Salaroglio IC, Kopecka J, Donadelli M, De Smaele E, et al. Hypoxia, endoplasmic reticulum stress and chemoresistance: Dangerous liaisons. *J Exp Clin Cancer Res CR* (2021) 40(1):28. doi: 10.1186/s13046-020-01824-3

170. Pietrobon V, Marincola FM. Hypoxia and the phenomenon of immune exclusion. *J Transl Med* (2021) 19(1):9. doi: 10.1186/s12967-020-02667-4

171. Jain RK. Normalization of tumor vasculature: An emerging concept in antiangiogenic therapy. *Sci (New York NY)* (2005) 307(5706):58–62.

172. Augustin HG, Koh GY. Antiangiogenesis: Vessel regression, vessel normalization, or both? *Cancer Res* (2022) 82(1):15–7. doi: 10.1158/0008-5472.CAN-21-3515

173. Li Q, Wang Y, Jia W, Deng H, Li G, Deng W, et al. Low-dose anti-angiogenic therapy sensitizes breast cancer to pd-1 blockade. *Clin Cancer Res an Off J Am Assoc Cancer Res* (2020) 26(7):1712–24. doi: 10.1158/1078-0432.CCR-19-2179

174. Klemba A, Bodnar L, Was H, Brodaczewska KK, Wcislo G, Szczylik CA, et al. Hypoxia-mediated decrease of ovarian cancer cells reaction to treatment: Significance for chemo- and immunotherapies. *Int J Mol Sci* (2020) 21(24):9492. doi: 10.3390/ijms21249492

175. Lu X, Kang Y. Hypoxia and hypoxia-inducible factors: Master regulators of metastasis. *Clin Cancer Res an Off J Am Assoc Cancer Res* (2010) 16(24):5928–35. doi: 10.1158/1078-0432.CCR-10-1360

176. Tao J, Yang G, Zhou W, Qiu J, Chen G, Luo W, et al. Targeting hypoxic tumor microenvironment in pancreatic cancer. *J Hematol Oncol* (2021) 14(1):14. doi: 10.1186/s13045-020-01030-w

177. Li X, Hattori A, Takahashi S, Goto Y, Harada H, Kakeya H. Ubiquitin carboxyl-terminal hydrolase L1 promotes hypoxia-inducible factor 1-dependent tumor cell malignancy in spheroid models. *Cancer Sci* (2020) 111(1):239–52. doi: 10.1111/cas.14236

178. Luo F, Lu F-T, Cao J-X, Ma W-J, Xia Z-F, Zhan J-H, et al. Hif-1α inhibition promotes the efficacy of immune checkpoint blockade in the treatment of non-small cell lung cancer. *Cancer Lett* (2022) 531:39–56. doi: 10.1016/j.canlet.2022.01.027

179. Denny WA. Hypoxia-activated prodrugs in cancer therapy: Progress to the clinic. *Future Oncol* (2010) 6(3):419–28. doi: 10.2217/fon.10.1

180. Borad MJ, Reddy SG, Bahary N, Uronis HE, Sigal D, Cohn AL, et al. Randomized phase ii trial of gemcitabine plus Th-302 versus gemcitabine in patients with advanced pancreatic cancer. *J Clin Oncol* (2015) 33(13):1475–81. doi: 10.1200/JCO.2014.55.7504

181. Jayaprakash P, Ai M, Liu A, Budhani P, Bartkowiak T, Sheng J, et al. Targeted hypoxia reduction restores T cell infiltration and sensitizes prostate cancer to immunotherapy. *J Clin Invest* (2018) 128(11):5137–49. doi: 10.1172/JCI96268

182. Jackson-Patel V, Liu E, Bull MR, Ashoorzadeh A, Bogle G, Wolfram A, et al. Tissue pharmacokinetic properties and bystander potential of hypoxia-activated prodrug cp-506 by agent-based modelling. *Front Pharmacol* (2022) 13:803602. doi: 10.3389/fphar.2022.803602

183. Moen I, Stuhr LEB. Hyperbaric oxygen therapy and cancer–a review. *Target Oncol* (2012) 7(4):233–42. doi: 10.1007/s11523-012-0233-x

184. Selvendiran K, Kuppusamy ML, Ahmed S, Bratasz A, Meenakshisundaram G, Rivera BK, et al. Oxygenation inhibits ovarian tumor growth by downregulating Stat3 and cyclin-D1 expressions. *Cancer Biol Ther* (2010) 10(4):386–90.

185. Batenburg MCT, Maarse W, van der Leij F, Baas IO, Boonstra O, Lansdorp N, et al. The impact of hyperbaric oxygen therapy on late radiation toxicity and quality of life in breast cancer patients. *Breast Cancer Res Treat* (2021) 189(2):425–33. doi: 10.1007/s10549-021-06332-2

186. Li YC, Chen CH, Chang CL, Chiang JY, Chu CH, Chen HH, et al. Melatonin and hyperbaric oxygen therapies suppress colorectal carcinogenesis through pleiotropic effects and multifaceted mechanisms. *Int J Biol Sci* (2021) 17 (14):3728–44. doi: 10.7150/ijbs.62280

187. Chen S-Y, Tsuneyama K, Yen M-H, Lee J-T, Chen J-L, Huang S-M. Hyperbaric oxygen suppressed tumor progression through the improvement of tumor hypoxia and induction of tumor apoptosis in A549-Cell-Transferred lung cancer. *Sci Rep* (2021) 11(1):12033. doi: 10.1038/s41598-021-91454-2

frontiers | Frontiers in Oncology

TYPE Original Research
PUBLISHED 10 November 2022
DOI 10.3389/fonc.2022.963896

Check for updates

OPEN ACCESS

EDITED BY
Zhe-Sheng Chen,
St. John's University, United States

REVIEWED BY
Jean Chiou,
Academia Sinica, Taiwan
Frank Aboubakar Nana,
Université catholique de Louvain, Belgium

*CORRESPONDENCE
Kang-Yun Lee
leekangyun@tmu.edu.tw
Sheng-Ming Wu
chitosan@tmu.edu.tw

SPECIALTY SECTION
This article was submitted to Molecular and Cellular Oncology, a section of the journal Frontiers in Oncology

RECEIVED 08 June 2022
ACCEPTED 27 October 2022
PUBLISHED 10 November 2022

CITATION
Van Hiep N, Sun W-L, Feng P-H, Lin C-W, Chen K-Y, Luo C-S, Dung LN, Van Quyet H, Wu S-M and Lee K-Y (2022) Heparin binding epidermal growth factor–like growth factor is a prognostic marker correlated with levels of macrophages infiltrated in lung adenocarcinoma. *Front. Oncol.* 12:963896. doi: 10.3389/fonc.2022.963896

COPYRIGHT
© 2022 Van Hiep, Sun, Feng, Lin, Chen, Luo, Dung, Van Quyet, Wu and Lee. This is an open-access article distributed under the terms of the Creative Commons Attribution License (CC BY). The use, distribution or reproduction in other forums is permitted, provided the original author(s) and the copyright owner(s) are credited and that the original publication in this journal is cited, in accordance with accepted academic practice. No use, distribution or reproduction is permitted which does not comply with these terms.

Heparin binding epidermal growth factor–like growth factor is a prognostic marker correlated with levels of macrophages infiltrated in lung adenocarcinoma

Nguyen Van Hiep[1,2,3], Wei-Lun Sun[4,5,6], Po-Hao Feng[4,5,6], Cheng-Wei Lin[1,6,7], Kuan-Yuan Chen[4,5,6,8], Ching-Shan Luo[1,4,6], Le Ngoc Dung[3], Hoang Van Quyet[3], Sheng-Ming Wu[4,5,6]* and Kang-Yun Lee[1,4,5,6,8]*

[1]International Ph.D. Program in Medicine, College of Medicine, Taipei Medical University, Taipei, Taiwan, [2]Oncology Center, Bai Chay Hospital, Quang Ninh, Ha Long, Vietnam, [3]Department of Thoracic and Neurological Surgery, Bai Chay Hospital, Quang Ninh, Ha Long, Vietnam, [4]Division of Pulmonary Medicine, Department of Internal Medicine, Shuang Ho Hospital, Taipei Medical University, New Taipei City, Taiwan, [5]Division of Pulmonary Medicine, Department of Internal Medicine, School of Medicine, College of Medicine, Taipei Medical University, Taipei, Taiwan, [6]TMU Research Center for Thoracic Medicine, Taipei Medical University, Taipei, Taiwan, [7]Department of Biochemistry and Molecular Cell Biology, School of Medicine, College of Medicine, Taipei Medical University, Taipei, Taiwan, [8]Graduate Institute of Clinical Medicine, College of Medicine, Taipei Medical University, Taipei, Taiwan

Background: The interactions between tumor cells and the host immune system play a crucial role in lung cancer progression and resistance to treatment. The alterations of EGFR signaling have the potential to produce an ineffective tumor-associated immune microenvironment by upregulating a series of immune suppressors, including inhibitory immune checkpoints, immunosuppressive cells, and cytokines. Elevated Heparin-binding EGF-like growth factor (HB-EGF) expression, one EGFR ligand correlated with higher histology grading, worse patient prognosis, and lower overall survival rate, acts as a chemotactic factor. However, the role of heparin-binding epidermal growth factor-like growth factor (HB-EGF) in the accumulation of immune cells in the tumor microenvironment remains unclear.

Methods: The clinical association of HB-EGF expression in lung cancer was examined using the Gene Expression Omnibus (GEO) repository. HB-EGF expression in different cell types was determined using single-cell RNA sequencing (scRNA-seq) dataset. The correlation between HB-EGF expression and cancer-immune infiltrated cells was investigated by performing TIMER and ClueGo pathways analysis from TCGA database. The chemotaxis of HB-EGF and macrophage infiltration was investigated using migration and immunohistochemical staining.

Results: The high HB-EGF expression was significantly correlated with poor overall survival in patients with lung adenocarcinoma (LUAD) but not lung squamous cell carcinoma (LUSC). Moreover, HB-EGF expression was correlated with the infiltration of monocytes, macrophages, neutrophils, and dendritic cells in LUAD but not in LUSC. Analysis of scRNA-seq data revealed high HB-EGF expression in lung cancer cells and myeloid cells. Results from the pathway analysis and cell-based experiment indicated that elevated HB-EGF expression was associated with the presence of macrophage and lung cancer cell migration. HB-EGF was highly expressed in tumors and correlated with M2 macrophage infiltration in LUAD.

Conclusions: HB-EGF is a potential prognostic marker and therapeutic target for lung cancer progression, particularly in LUAD.

KEYWORDS

heparin-binding EGF-like growth factor (HBEGF), bioinformatics, biomarker, immune infiltration, macrophage chemotaxis, non-small cell lung cancer

Introduction

Lung cancer has the highest incidence among various types of cancer and is the leading cause of mortality worldwide. Despite advancements in screening, diagnostic, and therapeutic approaches, the overall survival (OS) of patients with lung cancer remains low (1). Immune checkpoint inhibitors, particularly those blocking cytotoxic T-lymphocyte–associated protein 4 (CTLA4) and programmed death-1 (PD-1)/programmed death-ligand 1 (PD-L1), have exhibited promising efficacy against lung cancer, with long-term survival benefits. However, less than 20% of patients respond to those agents, and acquired resistance is observed in many patients (2). Complex networks among tumor cells and the tumor microenvironment (TME) promote cancer progression and chemoresistance (3). The TME consists of cancer cells, associated fibroblasts, tumor vasculature, lymphoid tissue, adipocytes, cytokines, exosomes, and tumor-infiltrating immune cells (TIILs) such as T cells, B cells, dendritic cells (DC), myeloid-derived suppressor cells (MDSCs), and tumor-associated macrophages (TAMs) (4). Gaining insights into these networks can guide the development of current immunotherapies.

Aberrant signaling of ERBB family members plays an important role in tumorigenesis, particularly the epidermal growth factor (EGF) receptor (EGFR) in lung cancer. EGFR ligands that bind to their receptors mediate downstream signaling pathways, including RAS (rat sarcoma)/RAF (rapidly accelerating fibrosarcoma), phosphatidylinositol 3-kinase (PI3K)/AKT (the serine/threonine protein kinase) pathway contributes to lung tumor growth and metastasis (5). Activation of downstream signaling pathways of EGFR may also play an important role in evading antitumor immune responses (6). EGFR ligands, such as EGF and transforming growth factor [TGF]α, reduce tumor antigen presentation through MHC class I and II expression, while EGF promotes M2 polarization of macrophages (7, 8). Approximately 10-30% of patients with NSCLC harbor EGFR mutations, mainly in exons 18-21, which are considered to be oncogenic drivers and highly promote EGFR downstream signaling pathways (9). In addition, EGFR-mutated cancer cells can cause an anti-immune response in the TME by inducing a series of immunosuppressive events, including recruitment of immunosuppressive cells such as macrophages and Tregs, overexpression of suppressive immune checkpoints such as PD-1 and CTLA-4, induction of cytokines and TGF-β, and reduction of anti-tumor immune cells such as cytotoxic T lymphocytes (10, 11). In addition to its role in cancer cells, EGFR is expressed on several immune cells, including macrophages (12, 13), monocytes (14), plasma cells (15), and Tregs (16). Notably, macrophages constitute the bulk of the cells in the immune infiltrate of tumors, and their impact on cancer progression is extremely variable depending on their phenotype in the TME (17). Briefly, M1 and M2 macrophages in the TME can be divided into pro- and anti-inflammatory phenotypes, respectively (18). In lung cancer, M2 macrophage infiltration into tumor islets was associated with poor prognosis of NSCLC patients (19). CD204-positive TAM is the preferred marker for prognostic prediction in LUAD (20). NSCLC patients with EGFR mutations exhibit high triggering receptor expressed on myeloid cells 2 (TREM2)-positive (+) TAM infiltrations with unique NSCLC molecular features and advanced cancer progression (21). Additionally, TREM2+ TAMs are enriched in multiple anti-inflammatory cytokines, exhibit an M2-like

immunosuppressive phenotype, and enhance T cell dysfunction. TAM polarization leading to M2 macrophage prevalence in the TME can confer drug resistance (22). M2 type TAM-derived exosomes also contribute to irreversible tyrosine kinase inhibitor (TKI) of EGFR, osimertinib resistance in NSCLC by modulating the MSTRG.292666.16/miR-6386-5p/MAPK8IP3 axis (23). Remarkably, a cannabinoid receptor 2 agonist, JWH-015, inhibits M2 macrophage-induced epithelial-mesenchymal transition (EMT) in NSCLC cells by downregulating the EGFR signaling pathway (24). Furthermore, reprogramming of TAMs from M2 to M1 phenotype overcomes EGFRT790M-mediated drug resistance by dual targeting mannose receptor-overexpressing TAMs and HER-2+ NSCLC cells (25).

Heparin-binding EGF-like growth factor (HB-EGF), which is a high-affinity EGFR ligand, is involved in lung development and plays a vital role in the differentiation of alveolar epithelial type II cells (26). HB-EGF was first found in a conditional medium derived from macrophages. The soluble form of HB-EGF serves as a paracrine and autocrine mitogen factor for fibroblasts (27), smooth muscle cells (28), keratinocytes (29), and some cancer cells such as ovarian (30), cervical (31), and breast cancer cells (32). HB-EGF induces the chemotaxis and recruitment of cells expressing EGFR and human EGF receptor 4, which is associated with PI3K activity (33). HB-EGF cleavage by matrix metalloproteinase 14 may enhance the EGFR signaling pathway to increase cancer cell growth in NSCLC (34) and promotes lung cancer cell proliferation through the signal transducer and activator of transcription 3 (STAT3) signaling pathway (35). High level of HB-EGF in the TME is associated with the activation and accumulation of macrophages, which may promote cancer progression (31). In cervical cancer, HB-EGF is produced primarily in the tumor cell compartment, not in the stroma. Remarkably, TAMs also mediates the expression of HB-EGF and other EGFR ligands to activate EGFR signaling and subsequent tumor cell proliferation (31). CXCL12-driven stimulation of cervical and colon cancer cells and macrophages may initiate and promote the granulocyte-macrophage colony-stimulating factor/HB-EGF paracrine loop, followed by macrophages leading to cancer cell survival (36). Furthermore, elevated HB-EGF expression in lung cancer is correlated with cancer cell growth, higher histology grading, and poor prognosis (35). Apart from tumor growth-promoting effects, the detailed role of HB-EGF in the TME in lung cancer remains largely unknown. Notably, TAM infiltrations and its polarization are associated with lung cancer progression and drug resistance (19–21, 23–25). The autocrine and paracrine actions of HB-EGF derived from TME cancer cells and tumor-infiltrating immune cells (TIICs) may lead to lung cancer progression. Thus, we would further explore whether high HB-EGF expression promotes the tumor progression associated with infiltrating immune cells.

We hypothesized that HB-EGF is part of the immune TME and is associated with poor survival outcomes in patients with lung cancer. We comprehensively analyzed its expression and role in the prognosis of patients with non–small-cell lung cancer (NSCLC), including LUAD and LUSC, in the GEO datasets. Moreover, we evaluated the association of HB-EGF with TIICs in the TCGA NSCLC and Tumor Immune Estimation Resource (TIMER) and verified the role of HB-EGF in TAM migration by using our cohort of patients and *in vitro* studies.

Materials and methods

Survival analysis in GEO datasets

Three microarray data sets of NSCLC (GSE30219, GSE3141, and GSE50081) were obtained from the GEO database by using the R package "GEOquery" (37). The differential expression levels of EGFR ligands, namely HB-EGF, EGF, TGF-α, betacellulin [BTC], amphiregulin [AREG], and epiregulin [EREG], were analyzed using the Mann–Whitney–Wilcoxon test. From each database, the data of LUAD and LUSC were selected for survival analysis. The cutoff value for the high and low HB-EGF groups was determined as the median. The survival curves were fitted and visualized using two packages: "survival" and "survminer" in R studio.

Gene expression and correlation analysis in TCGA database

The mRNA sequencing data of LUAD and LUSC from TCGA were downloaded to investigate the association between the gene of HB-EGF and the gene of immune infiltration. The specific gene markers of each immune cell were referred from the CellMarker database (38). To assess the relationship between HB-EGF and other genes, Spearman's R correlation coefficient was calculated.

Analysis of single-cell RNA-sequencing

The single-cell RNA sequencing LUAD data were downloaded from GEO datasets (GSE131907). From expression matrix data, all 15 tumor samples—11 early stages and 4 late stages—were selected (Supplementary Table 1; extracted from the original paper) (39). Three quality filter criteria were applied to each cell: mitochondrial gene percentage (≤20%), unique molecular identifiers (100 to 150,000), and gene count (200 to 10,000). The 2000 highest variable genes were identified and used for principal component analysis (PCA)-based dimension reduction. Uniform Manifold Approximation and Projection (UMAP) were used to visualize clusters. Following the original paper, 60,924 cells were clustered into eight major cell lineages by using specific markers: epithelial cells, endothelial cells, fibroblasts,

myeloid cells, B lymphocytes, T lymphocytes, NK cells, and mast cells (39) (Supplementary Table 2).

Immune infiltration analysis by TIMER2.0

The correlation between HB-EGF expression and the number of immune infiltrates, including those of T cells, B cells, NK cells, neutrophils, monocytes, macrophages, dendritic cells, myeloid-derived suppressive cells, mast cells, and cancer-associated fibroblasts, were analyzed across the LUAD and LUSC databases. We adjusted for Spearman's correlations and purity. The algorithms TIMER, EPIC, MCP-COUNTER, CIBERSORT, CIBERSORT-ABS, XCELL, and QUANTISEQ provided by TIMER 2.0 (http://timer.cistrome.org/) were applied to evaluate immune infiltration.

Pathway analysis

We analyzed 576 samples from LUAD and evaluated the correlation with HB-EGF. The RNA-seq data (Level 3) were normalized with the Log2 (RSEM+1) method. The most correlated genes (n = 182) were used for pathway analysis performed using ClueGo software (Supplementary Table 3). The strength of the association between the terms was determined using kappa statistics. The network was generated and visualized using the Cytoscape yFiles radial layout.

Cell culture and differentiation

The human monocytic THP-1 and U-937 cells (ATCC, Manassas, VA, USA) were suspension cultured in RPMI 1640 medium (Gibco-11875) containing 10% fetal bovine serum and supplemented with 100 U/mL penicillin, 100 µg/mL streptomycin, and 50 µM β-mercaptoethanol. For stimulating the differentiation of THP-1 cells into macrophages, 10 ng/mL phorbol 12-myristate 13-acetate (PMA; Sigma-Aldrich, St. Louis, MO, USA) was added in culture medium for 48 h.

Migration assay

A monocyte migration assay was performed to investigate the chemotactic function of HB-EGF. First, 200 µL of serum-free RPMI 1640 containing 5×10^5 THP-1 cells were added to the upper chamber (24-transwell inserts, pore size of 8 µm, Corning, NY, USA). Subsequently, 600 µL of serum-free RPMI 1640 medium containing 100 ng/mL HB-EGF (Peprotech, Rocky Hill, NJ, USA) was loaded into the bottom chamber. The migrated cells were observed using an inverted microscope and counted in four fields (200× magnification) at 2, 4, and 8 h. This experiment was repeated three times.

After 10^5 THP-1 cells were differentiated into macrophages in the upper chamber for 48 h, the medium was discarded, and the cells were washed twice with phosphate-buffered saline (PBS) before using them in the migration assay. The same dose of HB-EGF was used in the bottom chamber to attract macrophages for 8 h. The non-migrated cells were gently scraped and washed with PBS. The migrated cells were fixed in ethanol and stained with crystal violet. At least four pictures of the migrated cells were obtained at 200× magnification and quantified using FIJI software. The experiments were repeated three times.

Macrophages cocultured with lung cancer cells

The macrophage-mediated cell proliferation of lung cancer was performed using a coculture assay. To stimulate differentiation into macrophages, 2×10^5 U-937 monocytes were seeded into the upper chamber of the transwell (porous with 0.4-µm pores; Corning, NY, USA) and treated with 10 ng/mL PMA for 24 h. Subsequently, cells were cultured in a medium with 20 ng/mL interleukin-4 (IL-4) and IL-13 for an additional 48 h to induce M2 macrophages. Cells were then washed with PBS and incubated with RPMI medium containing 2 µg/ml control IgG or HB-EGF antibodies (AB clonal, A16365) for 24 h. On the same day, 2×10^5 A549 cells were cultured in the lower chamber and incubated for 24 h to allow attachment. The subsequent coculture cells were incubated in a 6-well plate for 24–72 h. To assess M2 macrophage (ϕ)-mediated cancer cell migration, 1×10^5 U-937 monocytes were seeded in the 24-well plate. Similarly, cells were treated with PMA and M2 macrophage differentiation was subsequently applied. Then, M2 macrophages were washed with PBS and incubated with control or HB-EGF antibodies containing medium for 24 h. Subsequently, 1×10^5 A549 cells were seeded in the upper chamber (8-µm pore size) and placed on top of the 24-well plate containing M2 macrophages or a regular RPMI medium-only control. After 24 h of stimulation, migrated cells were stained, counted, and compared with control cells.

Immunohistochemistry

We obtained 30 tissue specimens of LUAD from the biobank at Taipei Medical University–Shuang Ho Hospital. Supplementary Table 4 lists clinical information. Immunohistochemical (IHC) staining was performed using 4-µm tissue sections. The tissues were deparaffinized and rehydrated by immersing them in a series of xylene and graded alcohol. Antigen retrieval was applied using Tris-EDTA buffer (pH 9.0) by pressuring cooking the tissue slides for 10 minutes. Endogenous peroxidase activity was blocked with 0.3% H_2O_2 for 15 min, and the tissues were incubated for 1 h in

10% bovine serum albumin to prevent nonspecific conjugation. For HB-EGF staining, the slides were incubated for 1 h at room temperature with the HB-EGF rabbit polyclonal antibody (AB clonal, A16365, 1:200 dilution). The slides were washed three times with PBS-T and incubated with the secondary antibody for 20 min. The color was developed using alkaline phosphatase (AP, EnzoBioscience). For the macrophage phenotype, double staining was performed using the mouse anti-CD68 monoclonal antibody (Proteintech, 66231-2-Ig, 1000 μg/mL, 1:1000) and rabbit anti-iNOS polyclonal antibody (Proteintech, 18985-1-AP, 267 μg/mL, 1:500) for M1 macrophage staining and the CD68 antibody (Proteintech, 66231-2-Ig, 1000 μg/mL, 1:1000) and CD163 polyclonal antibody (Proteintech, 16646-1-AP, 500 μg/mL, 1:200) for M2 macrophage staining. The primary antibodies were incubated for 1 h at room temperature, and the color was developed using AP and diaminobenzidine (Enzo, polyview, ADI-950-100) for 20 and 5 min, respectively. The single staining and negative control were performed but not shown in the context. CD68 is a pan-macrophage marker and CD163 is a M2 macrophage marker. M1-like macrophages, characterized by CD68 expression. iNOS is a M1 macrophage marker. The polarization macrophage can be categorized as: $CD68^+/CD163^-/iNOS^-$ (M0); $CD68^+/CD163^+$ cells (M2) and $CD68^+/iNOS^+$ (M1). The negative control was performed with the secondary antibodies (mouse and rabbit isotope controls). Negative control was always performed along with each experiment. Hematoxylin was applied as a counterstain for 5 min before dehydrating and covering the slides.

IHC quantification

HB-EGF expression was semi-quantitatively evaluated using the H-score (40), which was calculated by multiplying the percentage of positive cells with different staining intensity values (0: no signal, 1: weak, 2: moderate, and 3: strong). The proportion of positive cells was calculated using FIJI software, with double-stained cells identified using the Trainable Weka Segmentation, an integrated machine learning tool in FIJI (41). The percentage of double-positive cells represented the macrophage fraction in the tumor. At least four fields at 200× magnification from each slide were used for macrophage quantification.

Results

Higher HB-EGF gene expression predicted poor prognosis in LUAD

Activation of EGFR ligands and their downstream signaling pathways play a critical role in lung cancer progression (42). First, we compared the mRNA levels of common EGFR ligands in lung cancer (HB-EGF, EGF, TGF-α, BTC, AREG, and EREG) by using the gene expression dataset GSE30219, GSE3141, and GSE50081. HB-EGF exhibited the highest expression among the examined EGFR ligands (Figure 1A and Supplementary Figure 1A). Moreover, among the distinct subtypes of lung cancer cells, the HB-EGF mRNA level was highly expressed in NSCLC, especially in LUAD, LUSC, and basaloid squamous cell carcinoma (BAS), compared with small-cell lung cancer (SCLC; Figure 1B). In addition, the dot plot revealed a positive correlation between HB-EGF and EGFR gene expression levels in NSCLC ($r = 0.470$, $p < 0.0001$; Figure 1C and Supplementary Figures 1B–D). These results suggest that higher HB-EGF expression may play a vital role in lung cancer progression, particularly in NSLC.

To investigate the prognostic role of HB-EGF, we performed Kaplan–Meier survival analysis for determining the relationship between HB-EGF expression and OS in patients with NSCLC, particularly LUAD and LUSC. Among the patients with LUAD, those with higher HB-EGF expression had poorer OS in several GEO datasets, including GSE30219 (HR and 95% CI = 2.548 [1.284–5.059], $p = 0.008$), GSE3141 (HR = 2.301 [1.118–4.734], $p = 0.024$), and GSE32019 (HR = 1.883 [1.062–3.337], $p = 0.030$) (Figure 1D). No significant correlations were observed between HB-EGF expression and OS in patients with LUSC in these datasets (GSE30219: HR = 1.294 [0.698–2.401], $p = 0.413$; GSE3141: HR = 1.113 [0.514–2.411], $p = 0.786$; and GSE50081: HR = 1.449 [0.539–3.900], $p = 0.463$) (Figure 1E). Interestingly, by analyzing 4 GEO data including GSE29013, GSE31210, GSE50081, GSE8894, we found that the high HB-EGF expression relate with shorter progression free survival time in both LUAD and LUSC (Supplementary Figure 2). Collectively, our results indicated that the patients with higher HB-EGF expression had poorer prognosis, specially in LUAD.

HB-EGF expression was associated with tumor immune infiltration cell

To determine whether poor OS in patients with LUAD is attributable to higher HB-EGF levels affecting TIIC involvement in cancer progression, we explore the correlation between the expression of HB-EGF and the marker gene sets of diverse immune cells, namely cytotoxic T cells, Tregs, T helper cells, exhausted T cells, B cells, mast cells, NK cells, neutrophils, classical monocytes, nonclassical monocytes, M1/M2 macrophages, and plasmacytoid and conventional DCs. Analysis of TCGA gene expression in lung cancer revealed that HB-EGF expression in LUAD and LUSC had no or negative correlation with the markers of T cells, B cells, mast cells, and NK cells (Figures 2A–D) and are mostly positively correlated with the markers of neutrophils, monocytes, and DCs (Figures 2E–H). Furthermore, stronger correlations were observed in LUAD than in LUSC. These results (Figures 1, 2) revealed that higher HB-EGF expression might correlate with an

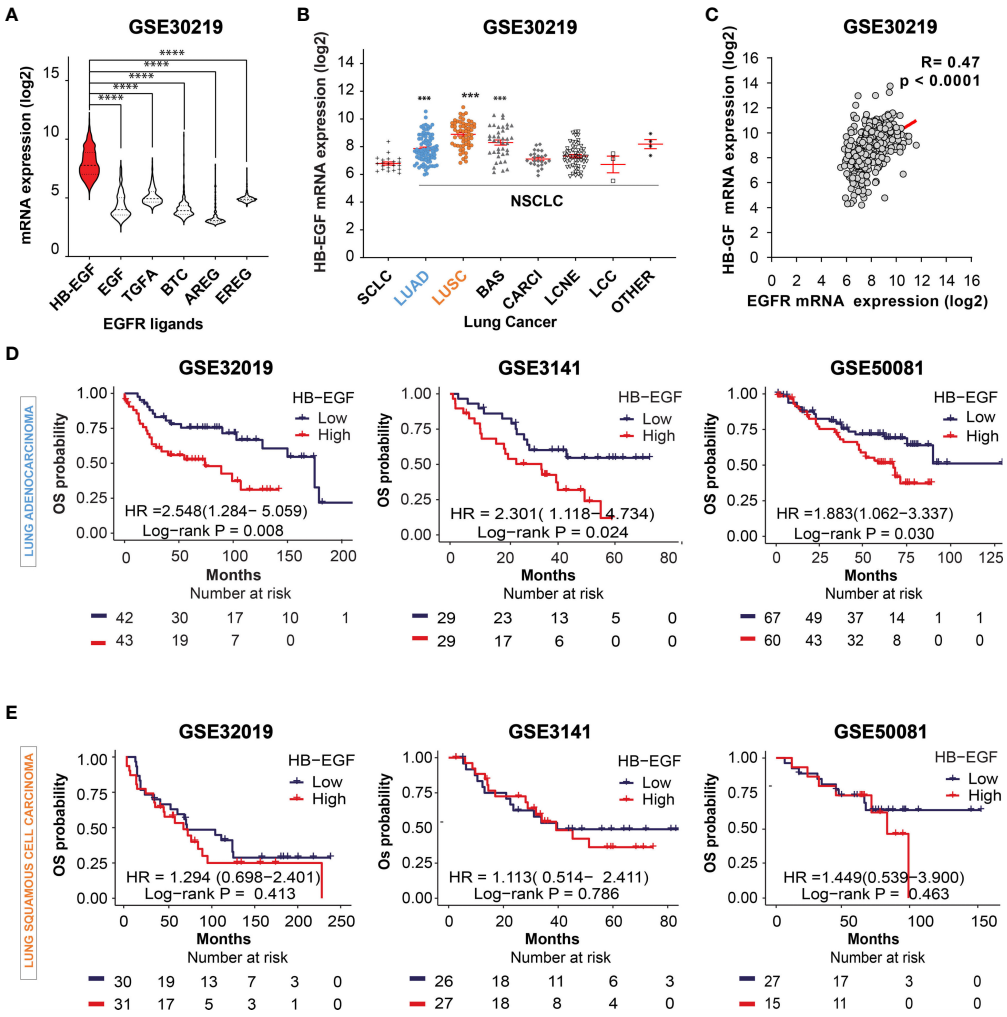

FIGURE 1
Prognostic potential of HB-EGF expression in LUAD **(A)** The gene expression levels of EGFR ligands, namely heparin-binding EGF-like growth factor (HB-EGF), epidermal growth factor (EGF), transforming growth factor-α (TGF-α), betacellulin (BTC), amphiregulin (AREG), and epiregulin (EREG), in lung cancer were analyzed using the GSE30219 dataset. The levels of HB-EGF were compared with those of other ligands by using the Wilcoxon rank-sum test, ****P < 0.0001. **(B)** Expression of the HB-EGF mRNA level across different types of lung cancer, including lung small cell carcinoma (SCLC), lung adenocarcinoma (LUAD), lung squamous cell carcinoma (LUSC), lung cancer basaloid (BAS), lung cancer carcinoid (CARCI), lung cancer large cell neuroendocrine (LCNE), and large cell carcinoma (LCC) in GSE 30219 ***p < 0.001. **(C)** The correlation between the gene expression of HB-EGF and EGFR in GSE30219 was determined by performing Spearman's rank correlation analysis. **(D, E)** Kaplan–Meier plot analysis of overall survival (OS) according to the HB-EGF mRNA expression level in patients with LUAD and LUSC in different GEO datasets (GSE30219, GSE3141, and GSE50081). We calculated p values by using the log-rank test.

increase in neutrophils, monocytes, and DCs in the TME, particularly in patients with LUAD with poor prognosis.

HB-EGF expression was correlated with myeloid cells infiltration in LUAD

The TIICs is an independent prognosis parameter in NSCLC (43, 44). Thus, the TIMER platform was used to determine the correlation between HB-EGF expression and TIICs in patients with NSCLC. Spearman's rank correlation indicated that high HB-EGF expression was associated with CD8+ T cells (r = 0.244, p = 4.29e-08), macrophages (r = 0.305, p = 4.05e-12), neutrophils (r = 0.361, p = 1.29e-16), and DCs (r = 0.337, p = 1.49e-14) in LUAD (Figures 3A, B). Consistent with the results of the TCGA data analysis (Figure 2), no significant correlation was observed between HB-EGF and TIICs in LUSC.

To identify the types of cells expressing HB-EGF, we used all 15 lung tumor samples of single-cell RNA sequencing data GSE131907. We used a canonical marker set to classify 60,924

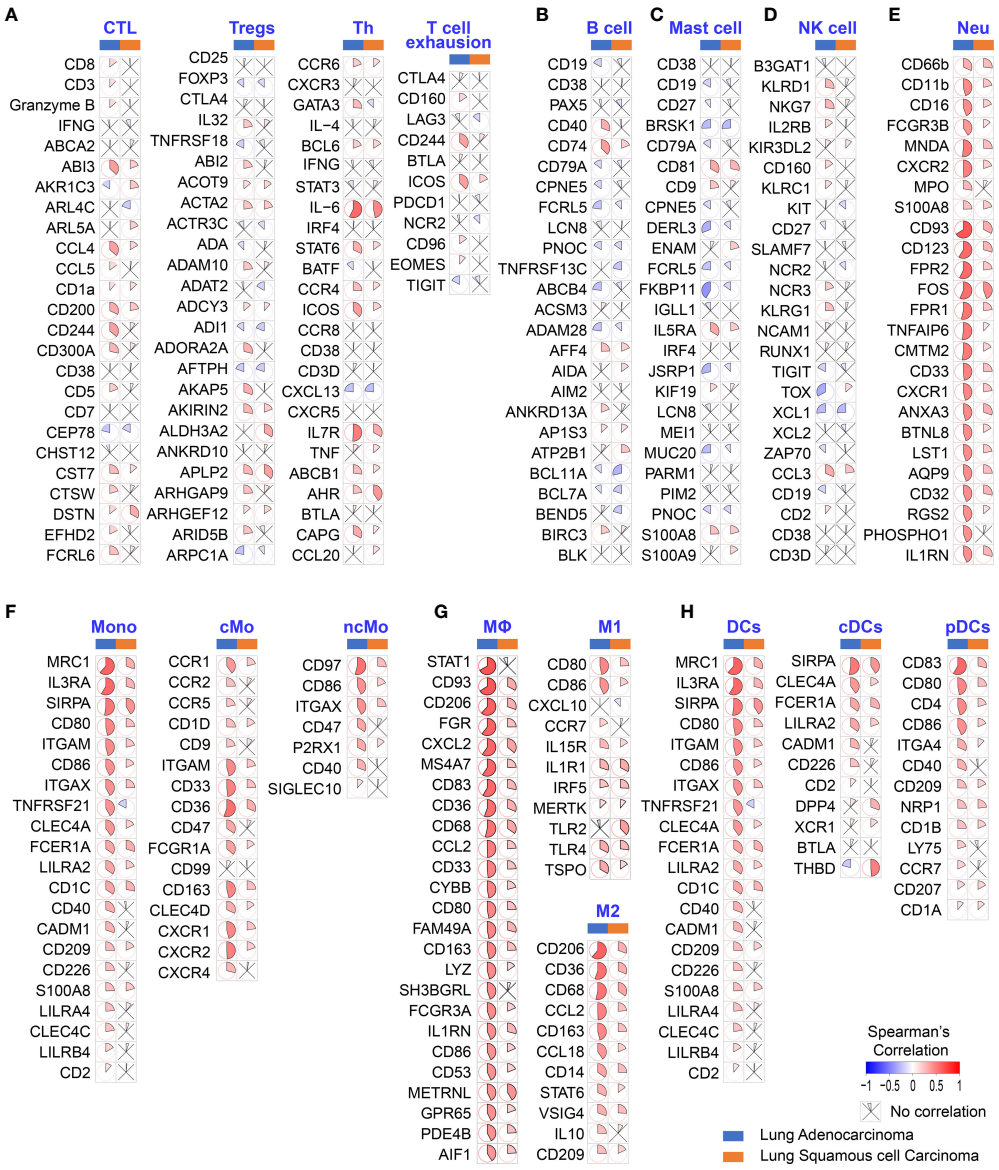

FIGURE 2
Correlation between HB-EGF expression level and immune gene markers in the lung cancer TGCA database. The color and sector represent Spearman's correlation between HB-EGF and immune gene markers: **(A)** T lymphocyte markers (CTC: cytotoxic T cells, Treg: regulatory T cells, and Th: T helper cells); **(B)** B lymphocyte markers; **(C)** Mast cell markers; **(D)** Natural killer (NK) cell markers; **(E)** Neutrophil markers (Neu); **(F)** Monocyte markers; **(G)** Macrophage markers (M1 and M2 subtypes); and **(H)** Dendritic cell markers (DC, dendritic cell; cDCs, conventional dendritic cells; and pDCs, plasmacytoid dendritic cells). (LUAD, lung adenocarcinoma; LUSC, lung squamous cell carcinoma).

cells into eight major cell lineages (Figure 3C and Supplementary Figure 3), and the lung epithelium (e.g., alveoli and cancer cells), stroma (e.g., endothelial cells and fibroblasts), and immune cells (e.g., T, NK, B, bone marrow and mast cells) were identified as common cell types. HB-EGF was particularly highly expressed in myeloid and epithelial cells (Figure 3D), suggesting that these cells are the main sources of HB-EGF secretion in the lung TME.

In addition, the correlation between HB-EGF and TIICs was determined using other algorithms to estimate immune cell types, namely TIMER, XCELL, MEPCOUNTER, CIBERSORT, QUANTISEQ, and EPIC (Supplementary Table 5). The results showed a significantly positive correlation between HB-EGF with DCs, monocytes, M2 macrophages, and neutrophils in LUAD but not in LUSC.

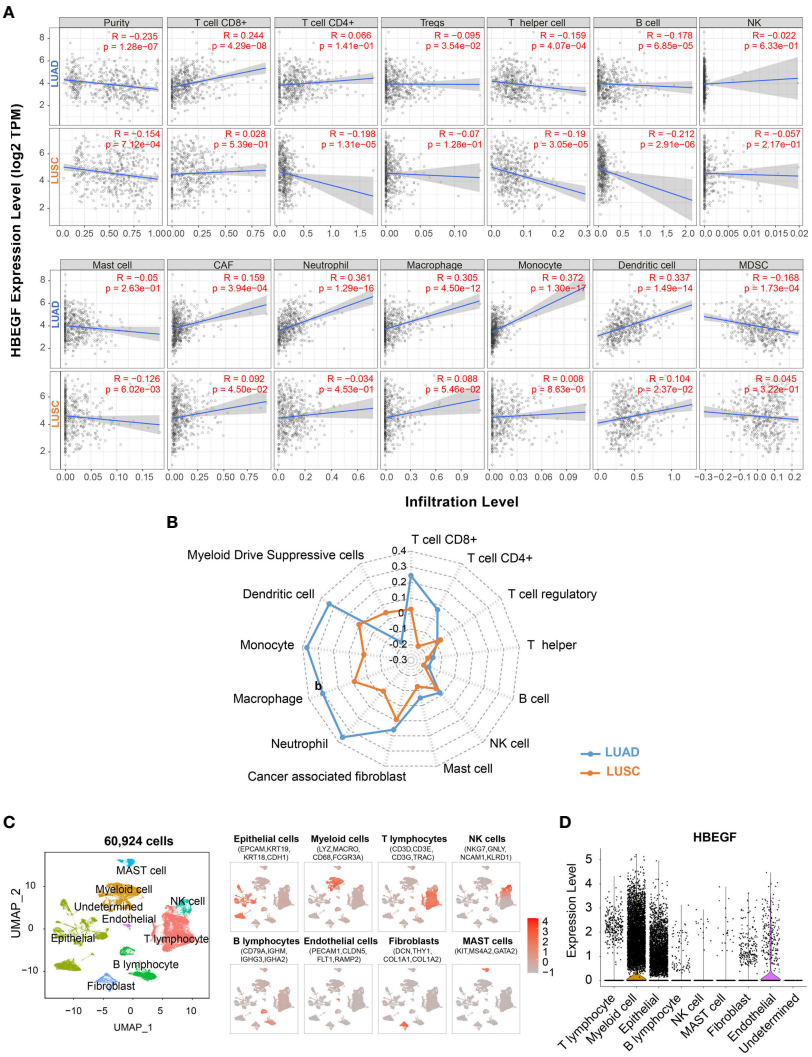

FIGURE 3
Correlation of the HB-EGF expression level with immune infiltration cells: **(A, B)** Spearman's correlation between HB-EGF and immune infiltration cells in LUAD and LUSC using TIMER2. **(C)** UMAP plot of 60,924 cells in 15 LUAD tumor samples using single-cell RNA-seq data GSE131907, colored by eight types of major cell lineages including epithelial cells, myeloid cells, T lymphocytes, natural killer cell, B lymphocytes, endothelial cells, fibroblast, and mast cells. **(D)** The violin plot indicated HB-EGF expression across cell types in figure **(C)**.

HB-EGF relevant co-expressed genes were involved in chemotaxis and activation of myeloid cells

To investigate the role of HB-EGF in promoting LUAD progression, we annotated the cellular functions of HB-EGF-related genes in the TCGA-LUAD cohort by using ClueGo. We used 182 genes highly related to HB-EGF ($r > 0.55$, $p < 0.001$) for functional analysis and determined that HB-EGF may participate in various processes of the immune response, including the regulation of monocyte and macrophage migration, macrophage–monocyte chemotaxis, macrophage activation, cytokine production, neutrophil chemotaxis, and leucocyte degranulation (Figure 4). Most HB-EGF-related genes were associated with monocyte-macrophage chemotaxis and macrophage activation, indicating their potential role in macrophage recruitment to the TME in LUAD.

HB-EGF promoted macrophage and lung cancer cell migration *in vitro*

To confirm the monocyte and macrophage chemotactic function of HB-EGF, we examined the migration ability of THP-1 monocytes and macrophages after HB-EGF treatment in the transwell migration assay. We observed that the number

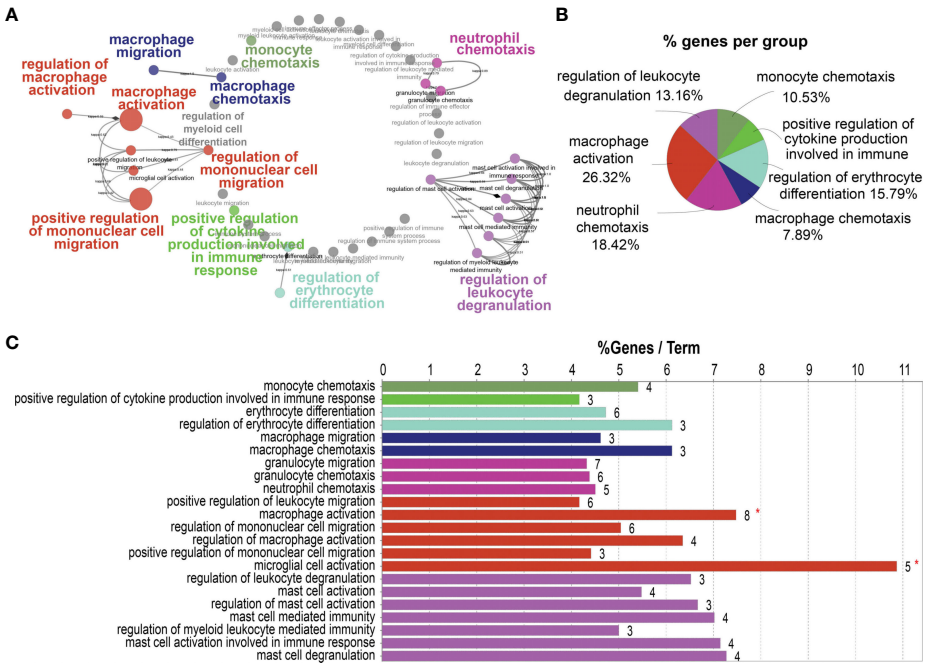

FIGURE 4
Potential pathways correlated with high HB-EGF-related genes using TCGA-LUAD: 182 genes exhibiting the highest correlation with HB-EGF were used for pathway analysis in ClueGO software. **(A)** Functionally grouped networks with terms as nodes linked based on their κ score level (≥0.3). **(B)** An overview chart with functional groups, including specific terms related to high HB-EGF expression. **(C)** The chart presents specific terms in **(B)**. The bars represent the number of genes from the analyzed cluster found to be associated with the term, and the label displayed on the bars is the percentage of identified genes compared with all genes associated with the term.

of migrating cells increased as early as 2 h following HB-EGF treatment (Figure 5A). Notably, at 8 h, we observed that cell migration increased by 6.36 times than that without HB-EGF. Consistent with our functional pathway analysis, HB-EGF significantly enhanced macrophage migration at 8 h (Figure 5B).

HB-EGF is secreted in U-937 cells and may be involved in macrophage-mediated cellular proliferation (45). We created a coculture system of U-937-derived macrophages and A549 cells to explore whether macrophage-derived HB-EGF affects the proliferation of lung cancer cells. The proliferation of lung cancer cells increased after coculturing with M2 macrophages (Figure 5C). Notably, the increase in cancer cell proliferation was significantly reduced when cocultured with macrophages treated with neutralizing HB-EGF antibodies but not reduced when cocultured with control IgG antibodies. HB-EGF secreted by TAM is closely related to primary tumor growth and promotes breast tumor migration (46). We then determined whether HB-EGF derived from macrophages-mediated lung cancer cell migration. The migration of cancer cells was significantly increased in coculture with M2 macrophages compared with the medium-only controls (Figure 5D). Additionally, the treatment of macrophages with anti-HB-EGF antibodies markedly diminished lung cancer cell migration compared with the control IgG. Collectively, macrophage-derived HB-EGF promoted cell proliferation and migration of lung cancer cells. Furthermore, these findings indicate that HB-EGF may increase the recruitment of TAMs and promote cancer progression.

HB-EGF was upregulated as tumor progression and associated with the amount of M2 macrophages in a validated cohort

HB-EGF protein expression was examined in the lung tissue sections derived from 30 patients with stage 1- 4 LUAD through IHC. The patients with stage 3/4 LUAD had higher tumor HB-EGF expression than did those with stage 1/2 LUAD (Figures 6A, B). Moreover, the patients with metastasis had higher tumor HB-EGF expression than did those without metastasis (Figure 6B). To evaluate the chemotactic role of HB-EGF in macrophages, M1 and M2 macrophages were stained with CD68/CD163 and CD68/iNOS, respectively (Figure 6C). Compared with the adjacent tissue, tumors had higher HB-EGF expression, higher M2 macrophage infiltration (Figure 6D), and similar M1 macrophage infiltration. Notably, HB-EGF protein expression was strongly positively correlated with M2 macrophage markers ($r = 0.706$, $p < 0.0001$) and not correlated with M1 macrophage markers (Figure 6E).

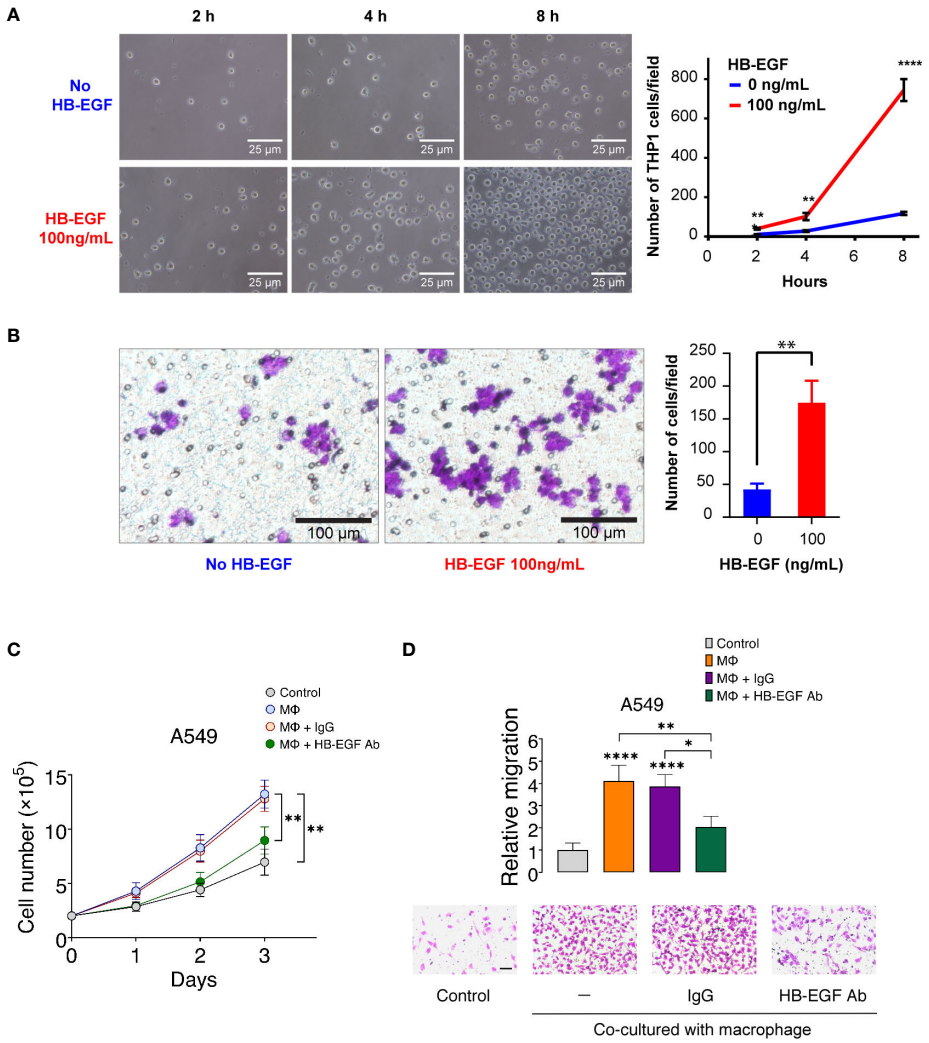

FIGURE 5
HB-EGF promotes monocyte and macrophage migration: **(A)** The short-term effect of HB-EGF mediated monocyte migration. A total of 5 × 10^5 THP-1 cells were used in a transwell migration assay. HB-EGF was added to the lower well at a concentration of 100 ng/mL. The migration cells were observed at 2, 4, and 8 h. The right panels present representative images (magnification, 200×), the left panel shows the quantification of migrated cells, and the bar presents the mean and SD. **(B)** HB-EGF mediated macrophage migration. A total of 10^5 THP-1 cells were differentiated into macrophages in PMA (10 ng/mL) for 48 h in the insert well of a 24-well Transwell plate prior to Transwell migration with 100 ng/mL HB-EGF for 8 h. The left panel shows representative images (magnification, 200×); the right panel presents the quantification of migrated cells, and the bar shows the standard deviation. Wilcoxon rank-sum tests were used to compare the number of migrated cells in two groups at each time point. **p < 0.01, ****p < 0.0001. **(C)** Effects of U-937-derived HB-EGF mediated the proliferation of A549 cells. U-937-derived M2 macrophages (Mϕ) were pretreated with anti-HB-EGF antibodies or control IgG for 24 h and then cocultured with A549 cells. The number of cancer cells was tracked for 1–3 days. Cell proliferation of A549 cells cocultured with Mϕ was assessed after treatment with an anti-HB-EGF neutralizing antibody. **(D)** U-937-derived HB-EGF-mediated cancer cell migration was measured. A549 cells (upper chamber) were cocultured with M2 Mϕ pretreated with anti-HB-EGF or control antibodies in transwell plates for 24 h. *p < 0.05, **p < 0.01, ****p < 0.0001.

Collectively, our findings supported a chemotactic role of tumor-expressing HB-EGF in attracting protumor M2 macrophages.

Discussion

The cancer hallmarks include sustaining proliferative signaling, evading growth suppressors, resisting cell death, enabling replicative immortality, inducing angiogenesis, and activating invasion and metastasis (47). The ability of cancer cells to evade immune destruction is significantly associated with worse OS. By "immunoediting," such as creating an inflammatory milieu or recruiting immunosuppressive cells to the TME, solid tumors can avoid detection and limit immune killing. Thus, immune-based therapies have the potential as cancer treatments. Since the early 2010s, the exploration of

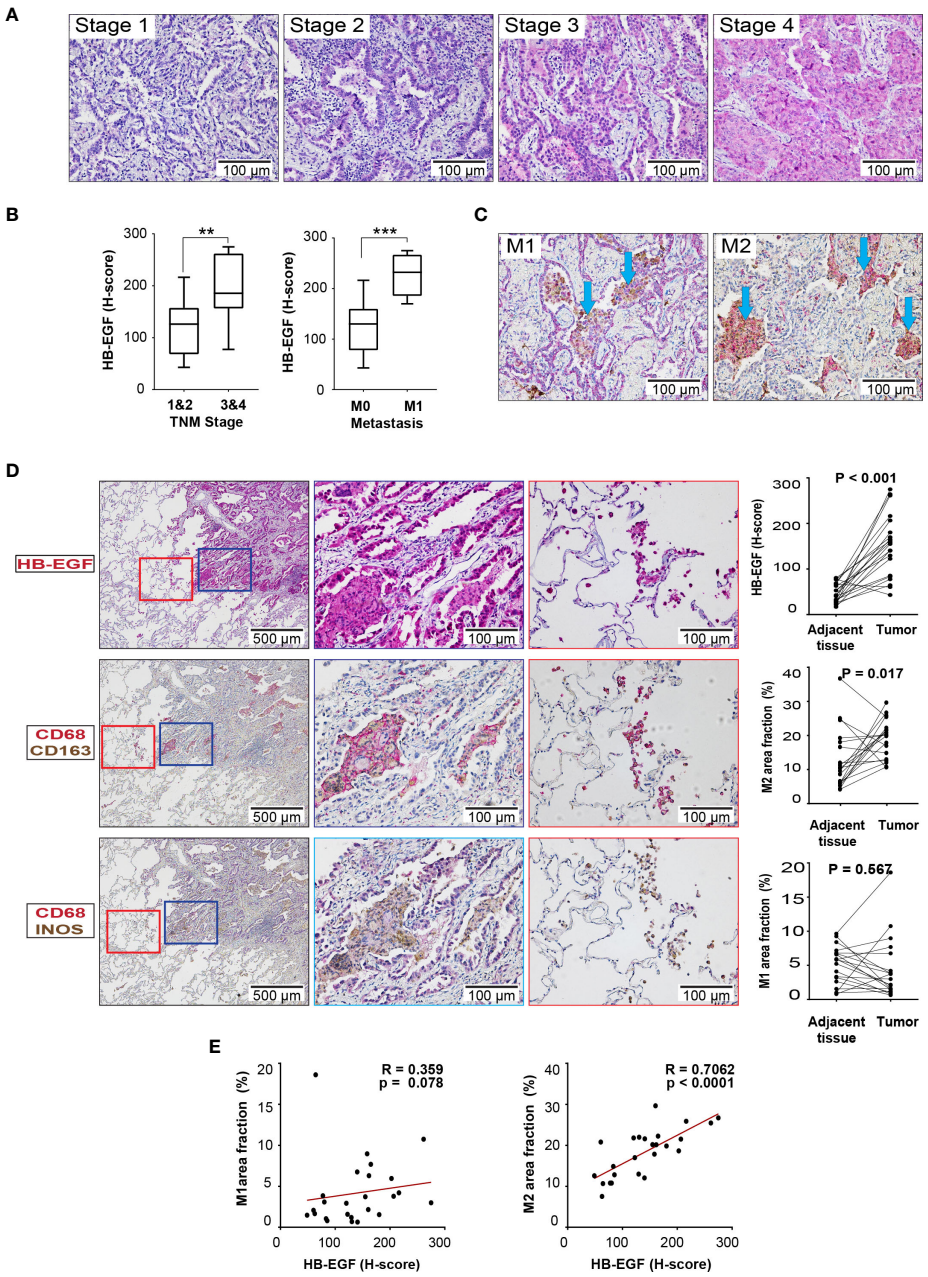

FIGURE 6
HB-EGF is highly expressed in lung cancer and positively correlated with M2 macrophages in LUAD: **(A)** Representative immunohistochemical images for HB-EGF in different stages of lung adenocarcinoma (magnification, 200×). **(B)** Semiquantitative expression of HB-EGF by stage and metastasis status. The whisker shows the standard deviation, and the Wilcoxon rank-sum test was used. **(C)** Representative immunohistochemical images for macrophage M1 and M2 double positive in lung tumor (CD68 (brown) and iNOS (red) for M1; CD68 (brown) and CD163 (red) for M2, magnification x20). **(D)** HB-EGF, M1, and M2 IHC images (magnification, 5× and 20×) and quantification for lung cancer and adjacent lung tissues. The Wilcoxon signed-rank test was used. **(E)** The dot plot shows Spearman's correlation between HB-EGF and the fraction of M1/M2 macrophages. ** mean $p < 0.01$, *** mean $p < 0.001$.

potential target-mediated cancer hallmarks through analyses of multiple transcriptional datasets has yielded powerful predictors of cancer signatures in the study of immune profiles, diagnosis, and prognosis. In our study, we used comprehensive computational methods to estimate the levels of HB-EGF expression and TIICs in lung cancer tissues by using gene expression datasets, which were validated by our independent cohort and *in vitro* experiments. The results revealed that higher

HB-EGF expression in the patients with LUAD was associated with poor prognosis and an increased TIICs level, particularly in neutrophils, monocyte, macrophages, and dendritic cells. HB-EGF is mainly expressed in epithelial and myeloid cells and partly in other types of cells in the TME. Furthermore, HB-EGF was noted to promote macrophage and lung cancer migration in cell-based experiments. IHC analysis findings indicated that HB-EGF protein levels in the lung cancer tissues were significantly correlated with M2 macrophage markers. Collectively, these results illustrated that HB-EGF is markedly increased in LUAD cancer cells and may promote TIICs recruitment, particularly M2 macrophages.

In this study, six common EGFR ligands, namely TGFA, HB-EGF, AREG, EREG, EGF, and BTC, were analyzed using the gene expression datasets. Among them, HB-EGF was the most significantly expressed in NSCLC, particularly in LUAD, LUSC, and BAS. A similar result for HB-EGF expression was observed in cervical cancer (31). Our results revealed that the patients with LUAD with higher HB-EGF expression had poor OS. However, we cannot exclude the importance of other EGFR ligands in the development of LUAD. Our previous findings revealed that higher EREG expression in LUAD but not LUSC was correlated with shorter OS (48). In addition, EREG produced by TAMs causes NSCLC cell EGFR-tyrosine kinase inhibitor resistance in the TME (49). EREG and HB-EGF may mediate signaling activation through the same corresponding receptor (11). However, whether HB-EGF mediates drug resistance through TIICs, such as TAMs, remains unclear. Notably, EGFR expression is lower in LUSC than in LUAD (50), possibly cause that HB-EGF overexpression is associated with poorer prognosis in LUAD but not LUSC. Remarkably, stage-dependent TIICs in the TME may have prognostic utility for lung cancer progression (51, 52). Our analysis of the gene expression datasets revealed that HB-EGF expression in LUAD was markedly correlated with the immune marker sets of TIICs, namely monocytes, TAMs, M1/M2 macrophages, neutrophils, and DCs, but not general T cells, CD8+ T cells, Th1, Th2, Th17, or B cells. TAMs is a TIICs in the TME, and TAM-derived HB-EGF mediates cancer cell migration (46). However, M1 and M2 TAMs play tumor-suppressing and tumor/metastasis-promoting roles, respectively (53). In our study, high HB-EGF expression indicated a significant association with most M2 TAM markers and poor prognosis in patients with LUAD, indicating the role of HB-EGF in recruiting M2 TAMs in the TME. Moreover, HB-EGF expression was significantly correlated with the markers of DCs and neutrophils. DCs in the TME of lung cancer tissues derived from mice and human patients exhibited high HB-EGF levels (54). In addition, DCs in the TME not only suppress T-cell-based anticancer immune responses but also promote cancer progression, including cancer cell growth, invasion, and pro-angiogenesis (55–57). Tumor-associated neutrophils may play a tumor-promoting role in the TME in cancer progression (58). Collectively, high HB-EGF expression may play tumor-promoting roles in the TME by increasing TIICs recruitment (e.g., DCs, monocytes, macrophages, and neutrophils) in LUAD but not in LUSC.

The cross-talk between cancer and the host immune system plays a crucial role in cancer initiation and progression. HB-EGF is a chemokine for a variety of cells, such as fibroblasts (27), smooth muscle cells (28), and cancer cells (59). An analysis of single-cell RNA-seq datasets revealed a higher HB-EGF expression in myeloid and lung epithelial cancer cells. Therefore, HB-EGF secretion in cancer cells may also affect the surrounding cells by changing the TME. Consistent with the findings of IHC analysis, HB-EGF protein expression was significantly increased in lung cancer tissues compared with normal tissues. Moreover, we explored mechanisms through which HB-EGF promotes LUAD progression. ClueGo functional analysis of 182 HB-EGF highly correlated genes indicated that HB-EGF may be involved in main processes including macrophage activation, macrophage–monocyte and neutrophil chemotaxis, leukocyte degranulation, and cytokine production. Activation of the EGFR signaling in monocytes is required for cell activation and migration (14). The effect of HB-EGF expression may increase the recruitment of monocytes and macrophages and further increase cell proliferation through the MEK/ERK signaling pathway (60). Our results demonstrated the chemotactic function of HB-EGF to promote monocyte or macrophage migration following short-term HB-EGF treatment. The higher expression of HB-EGF in LUAD may be related to the accumulation of immune cells, such as TAMs, in the TME. HB-EGF released by TAMs has a strong correlation with primary tumor growth and lymph node dissemination in breast cancer (46). In addition, TAMs may increase cancer growth through the GM-CSF/HB-EGF paracrine loop (14). Similarly, our results indicated that M2 macrophage-derived HB-EGF promotes lung cancer cell proliferation and migration. Furthermore, HB-EGF also significantly enhanced macrophage migration. These findings suggest that HB-EGF may increase TAM recruitment and promote lung cancer progression. However, further studies are required to clarify the mechanisms through which the excessive accumulation of HB-EGF in the TME causes different cellular interactions.

Macrophages may play key roles in inflammation promotion and resolution, cellular damage, and tissue remodeling because M1/M2 macrophages change their functional characteristics in response to alterations in the TME (31, 57). Notably, the alteration in the immune response from the M1 to M2 phenotype may be crucial for developing new lung cancer therapeutic strategies. Macrophage activation is the pathway with the highest gene expression and is significantly associated with HB-EGF expression. In our validation cohort, we observed a significant increase in M2 macrophages in tumors compared with adjacent normal tissues. In addition, HB-EGF protein levels were significantly correlated with M2 macrophage markers. HB-EGF stimulates the repolarization of the M1 to M2 phenotype by

inhibiting the STAT3 signaling pathway of LPS-mediated intestinal cell apoptosis (61). The interaction of HB-EGF with EGFR activates downstream STAT3 in the nucleus (62). Therefore, EGFR/STAT3 may be a key downstream signaling pathway for HB-EGF for promoting M2 macrophage polarization. However, whether HB-EGF promotes M2 polarization during lung cancer progression, particularly in LUAD, remains unknown.

TAMs may directly suppress cytotoxic T lymphocyte responses by upregulating immune checkpoint molecules, such as PD-L1, and inhibitory cytokine production (63). Thus, the macrophage activation status is critical in cancer progression and therapy. M2 TAMs promote tumor progression in the TME by recruiting immunosuppressive Tregs and inhibiting the remodeling of DCs in the ECM and altering the expression of numerous cytokines. Thus, HB-EGF increases M2 macrophage recruitment and may promote M2 macrophage proliferation and polarization, eventually impairing patient prognosis. Accordingly, HB-EGF suppression may be a new strategy for the treatment of certain cancers, such as LUAD.

Conclusions

In summary, HB-EGF is highly expressed in lung cancer cells, especially LUAD, which leads to poor prognosis and is correlated with increased TIICs, including monocytes, macrophages, neutrophils, and DCs. Furthermore, the high HB-EGF expression in the TME may play a tumor-promoting role by recruiting immune cells, particularly M2 macrophages. Therefore, HB-EGF can serve as a prognostic marker and therapeutic target in patients with LUAD.

Data availability statement

The original contributions presented in the study are included in the article/Supplementary Material. Further inquiries can be directed to the corresponding authors.

Ethics statement

The study protocol was approved by the Joint Institutional Review Board of Taipei Medical University (IRB no. N202103013). The patients/participants provided their written informed consent to participate in this study.

Author contributions

K-YL, S-MW, and NH conceptualized the study and reviewed the entire project and manuscript. NH and S-WL performed most experiments and wrote the manuscript. P-HF, S-WL, and S-MW designed the research and conducted experiments. NH, LD, and HQ performed the database collection and analysis and reviewed the manuscript. C-WL and C-SL provided expertise in statistical and figure analyses. P-HF, C-WL, and K-YC collected tumor tissue samples, conducted patient information analyses, and reviewed the manuscript. S-MW assumes responsibility for the content of the manuscript, including the data and analysis. All authors contributed to the critical revision of the manuscript for important intellectual content. All authors contributed to the article and approved the submitted version.

Funding

This study was funded by the Ministry of Science and Technology of Taiwan (MOST: 108-2314-B-038-111-MY3, 108-2314-B-038-063-MY3, 111-2314-B-038-150-MY3, and 111-2314-B-038-152-MY3), Ministry of Education of the Republic of China (DP2-111-21121-01-T-01-01), and Taipei Medical University and Shuang Ho Hospital (110TMU-SHH-19).

Conflict of interest

The authors declare that the research was conducted in the absence of any commercial or financial relationships that could be construed as a potential conflict of interest.

Publisher's note

All claims expressed in this article are solely those of the authors and do not necessarily represent those of their affiliated organizations, or those of the publisher, the editors and the reviewers. Any product that may be evaluated in this article, or claim that may be made by its manufacturer, is not guaranteed or endorsed by the publisher.

Supplementary material

The Supplementary Material for this article can be found online at: https://www.frontiersin.org/articles/10.3389/fonc.2022.963896/full#supplementary-material

SUPPLEMENTARY FIGURE 1
Overexpression of HB-EGF in lung cancer. **(A)** The mRNA expression levels of the EGFR ligands, including heparin-binding EGF-like growth factor (HB-EGF), epidermal growth factor (EGF), transforming growth factor-a (TGFA), betacellulin (BTC), amphiregulin (AREG), and epiregulin (EREG) in lung cancer were analyzed by using GSE3141 and GSE50081 dataset. The levels of HB-EGF were compared with other ligands by using Wilcoxon rank-sim test, ***$P<0.001$; **(B–D)** The dot-plot showed

Spearman's correlation between EGFR and its ligands in GSE30219, GSE3141, and GSE50081 datasets.

SUPPLEMENTARY FIGURE 2
Kaplan–Meier plot analysis of Progression free survival (PFS) according to the HB-EGF mRNA expression level in patients with LUAD **(A)** and LUSC **(B)** using combine 4 GEO datasets including GSE29013, GSE31210, GSE50081 and GSE8894. We calculated p values by using the log-rank test.

SUPPLEMENTARY FIGURE 3
The dot-plot of selected marker for 8 cell types using single-cell RNA sequencing data GSE131907. Epithelial cells markers: EPICAM, KTR18/19, CDH1; Fibroblast cells markers: DCN, THY1, COL1A1/2; Endothelial markers: PECAM1, CLDN5, FLT1, RAMP2, T cell's markers: CD3D/E/G, TRAC; Natural killer cells markers: NKG7, GNLY, NCAM1, KLRD1; B cells markers: CD79A, IGHM, IGHG3, IGHA2; Myeloid cells markers: LYZ, MARCO, CD68, FCGR3A; Mast cells markers: KIT, MS4A2, GATA2.

References

1. Siegel RL, Miller KD, Fuchs HE, Jemal A. Cancer statistics, 2022. *CA: A Cancer J Clin* (2022) 72(1):7–33. doi: 10.3322/caac.21708

2. Borghaei H, Paz-Ares L, Horn L, Spigel DR, Steins M, Ready NE, et al. Nivolumab versus docetaxel in advanced nonsquamous non-Small-Cell lung cancer. *N Engl J Med* (2015) 373(17):1627–39. doi: 10.1056/NEJMoa1507643

3. O'Donnell JS, Teng MWL, Smyth MJ. Cancer immunoediting and resistance to T cell-based immunotherapy. *Nat Rev Clin Oncol* (2019) 16(3):151–67. doi: 10.1038/s41571-018-0142-8

4. Madeddu C, Donisi C, Liscia N, Lai E, Scartozzi M, Maccio A. EGFR-mutated non-small cell lung cancer and resistance to immunotherapy: Role of the tumor microenvironment. *Int J Mol Sci* (2022) 23(12):6489. doi: 10.3390/ijms23126489

5. Marmor MD, Skaria KB, Yarden Y. Signal transduction and oncogenesis by ErbB/HER receptors. *Int J Radiat Oncol Biol Phys* (2004) 58(3):903–13. doi: 10.1016/j.ijrobp.2003.06.002

6. Concha-Benavente F, Ferris RL. Reversing EGFR mediated immunoescape by targeted monoclonal antibody therapy. *Front Pharmacol* (2017) 8:332. doi: 10.3389/fphar.2017.00332

7. Lian G, Chen S, Ouyang M, Li F, Chen L, Yang J. Colon cancer cell secretes EGF to promote M2 polarization of TAM through EGFR/PI3K/AKT/mTOR pathway. *Technol Cancer Res Treat* (2019) 18:1533033819849068. doi: 10.1177/1533033819849068

8. Pollack BP. EGFR inhibitors, MHC expression and immune responses : Can EGFR inhibitors be used as immune response modifiers? *Oncoimmunology* (2012) 1(1):71–4. doi: 10.4161/onci.1.1.18073

9. Mansuet-Lupo A, Alifano M, Pecuchet N, Biton J, Becht E, Goc J, et al. Intratumoral immune cell densities are associated with lung adenocarcinoma gene alterations. *Am J Respir Crit Care Med* (2016) 194(11):1403–12. doi: 10.1164/rccm.201510-2031OC

10. Wang F, Wang S, Zhou Q. The resistance mechanisms of lung cancer immunotherapy. *Front Oncol* (2020) 10:568059. doi: 10.3389/fonc.2020.568059

11. Cheng W-L, Feng P-H, Lee K-Y, Chen K-Y, Sun W-L, Van Hiep N, et al. The role of EREG/EGFR pathway in tumor progression. *Int J Mol Sci* (2021) 22(23):12828. doi: 10.3390/ijms222312828

12. Scholes AG, Hagan S, Hiscott P, Damato BE, Grierson I. Overexpression of epidermal growth factor receptor restricted to macrophages in uveal melanoma. *Arch Ophthalmol* (2001) 119(3):373–7. doi: 10.1001/archopht.119.3.373

13. Lanaya H, Natarajan A, Komposch K, Li L, Amberg N, Chen L, et al. EGFR has a tumour-promoting role in liver macrophages during hepatocellular carcinoma formation. *Nat Cell Biol* (2014) 16(10):972–7. doi: 10.1038/ncb3031

14. Chan G, Nogalski MT, Yurochko AD. Activation of EGFR on monocytes is required for human cytomegalovirus entry and mediates cellular motility. *Proc Natl Acad Sci U S A.* (2009) 106(52):22369–74. doi: 10.1073/pnas.0908787106

15. Mahtouk K, Hose D, Rème T, De Vos J, Jourdan M, Moreaux J, et al. Expression of EGF-family receptors and amphiregulin in multiple myeloma. amphiregulin is a growth factor for myeloma cells. *Oncogene* (2005) 24(21):3512–24. doi: 10.1038/sj.onc.1208536

16. Zaiss DM, van Loosdregt J, Gorlani A, Bekker CP, Gröne A, Sibilia M, et al. Amphiregulin enhances regulatory T cell-suppressive function *via* the epidermal growth factor receptor. *Immunity* (2013) 38(2):275–84. doi: 10.1016/j.immuni.2012.09.023

17. Mantovani A, Sozzani S, Locati M, Allavena P, Sica A. Macrophage polarization: Tumor-associated macrophages as a paradigm for polarized M2 mononuclear phagocytes. *Trends Immunol* (2002) 23(11):549–55. doi: 10.1016/S1471-4906(02)02302-5

18. Enderlin Vaz da Silva Z, Lehr HA, Velin D. *In vitro* and *in vivo* repair activities of undifferentiated and classically and alternatively activated macrophages. *Pathobiology* (2014) 81(2):86–93. doi: 10.1159/000357306

19. Cao L, Che X, Qiu X, Li Z, Yang B, Wang S, et al. M2 macrophage infiltration into tumor islets leads to poor prognosis in non-small-cell lung cancer. *Cancer Manag Res* (2019) 11:6125–38. doi: 10.2147/CMAR.S199832

20. Li Z, Maeda D, Yoshida M, Umakoshi M, Nanjo H, Shiraishi K, et al. The intratumoral distribution influences the prognostic impact of CD68- and CD204-positive macrophages in non-small cell lung cancer. *Lung Cancer* (2018) 123:127–35. doi: 10.1016/j.lungcan.2018.07.015

21. Zhang H, Liu Z, Wen H, Guo Y, Xu F, Zhu Q, et al. Immunosuppressive TREM2(+) macrophages are associated with undesirable prognosis and responses to anti-PD-1 immunotherapy in non-small cell lung cancer. *Cancer Immunol Immunother* (2022) 71(10):2511–22. doi: 10.1007/s00262-022-03173-w

22. Son B, Lee S, Youn H, Kim E, Kim W, Youn B. The role of tumor microenvironment in therapeutic resistance. *Oncotarget* (2017) 8(3):3933–45. doi: 10.18632/oncotarget.13907

23. Wan X, Xie B, Sun H, Gu W, Wang C, Deng Q, et al. Exosomes derived from M2 type tumor-associated macrophages promote osimertinib resistance in non-small cell lung cancer through MSTRG.292666.16-miR-6836-5p-MAPK8IP3 axis. *Cancer Cell Int* (2022) 22(1):83. doi: 10.1186/s12935-022-02509-x

24. Ravi J, Elbaz M, Wani NA, Nasser MW, Ganju RK. Cannabinoid receptor-2 agonist inhibits macrophage induced EMT in non-small cell lung cancer by downregulation of EGFR pathway. *Mol Carcinog* (2016) 55(12):2063–76. doi: 10.1002/mc.22451

25. Peng H, Chen B, Huang W, Tang Y, Jiang Y, Zhang W, et al. Reprogramming tumor-associated macrophages to reverse EGFR(T790M) resistance by dual-targeting codelivery of Gefitinib/Vorinostat. *Nano Lett* (2017) 17(12):7684–90. doi: 10.1021/acs.nanolett.7b03756

26. Wang Y, Maciejewski BS, Soto-Reyes D, Lee HS, Warburton D, Sanchez-Esteban J. Mechanical stretch promotes fetal type II epithelial cell differentiation via shedding of HB-EGF and TGF-alpha. *J Physiol* (2009) 587(Pt 8):1739–53. doi: 10.1021/acs.nanolett.7b03756

27. Besner G, Higashiyama S, Klagsbrun M. Isolation and characterization of a macrophage-derived heparin-binding growth factor. *Cell Regul* (1990) 1(11):811–9. doi: 10.1091/mbc.1.11.811

28. Higashiyama S, Abraham JA, Klagsbrun M. Heparin-binding EGF-like growth factor stimulation of smooth muscle cell migration: dependence on interactions with cell surface heparan sulfate. *J Cell Biol* (1993) 122(4):933–40. doi: 10.1083/jcb.122.4.933

29. Hashimoto K, Higashiyama S, Asada H, Hashimura E, Kobayashi T, Sudo K, et al. Heparin-binding epidermal growth factor-like growth factor is an autocrine growth factor for human keratinocytes. *J Biol Chem* (1994) 269(31):20060–6. doi: 10.1016/S0021-9258(17)32127-0

30. Shen Y, Ruan L, Lian C, Li R, Tu Z, Liu H. Discovery of HB-EGF binding peptides and their functional characterization in ovarian cancer cell lines. *Cell Death Discovery* (2019) 5:82. doi: 10.1038/s41420-019-0163-9

31. Schrevel M, Osse EM, Prins FA, Trimbos J, Fleuren GJ, Gorter A, et al. Autocrine expression of the epidermal growth factor receptor ligand heparin-binding EGF-like growth factor in cervical cancer. *Int J Oncol* (2017) 50(6):1947–54. doi: 10.3892/ijo.2017.3980

32. Zhou ZN, Sharma VP, Beaty BT, Roh-Johnson M, Peterson EA, Van Rooijen N, et al. Autocrine HBEGF expression promotes breast cancer intravasation, metastasis and macrophage-independent invasion in vivo. *Oncogene* (2014) 33(29):3784–93. doi: 10.1038/onc.2013.363

33. Elenius K, Paul S, Allison G, Sun J, Klagsbrun M. Activation of HER4 by heparin-binding EGF-like growth factor stimulates chemotaxis but not proliferation. *EMBO J* (1997) 16(6):1268–78. doi: 10.1093/emboj/16.6.1268

34. Stawowczyk M, Wellenstein MD, Lee SB, Yomtoubian S, Durrans A, Choi H, et al. Matrix metalloproteinase 14 promotes lung cancer by cleavage of heparin-binding EGF-like growth factor. *Neoplasia (New York NY).* (2017) 19(2):55–64. doi: 10.1016/j.neo.2016.11.005

35. Hsieh CH, Chou YT, Kuo MH, Tsai HP, Chang JL, Wu CW. A targetable HB-EGF-CITED4 axis controls oncogenesis in lung cancer. *Oncogene* (2017) 36 (21):2946–56. doi: 10.1038/onc.2016.465

36. Rigo A, Gottardi M, Zamò A, Mauri P, Bonifacio M, Krampera M, et al. Macrophages may promote cancer growth *via* a GM-CSF/HB-EGF paracrine loop that is enhanced by CXCL12. *Mol Cancer* (2010) 9:273. doi: 10.1186/1476-4598-9-273

37. Davis S, Meltzer PS. GEOquery: a bridge between the gene expression omnibus (GEO) and BioConductor. *Bioinformatics* (2007) 23(14):1846–7. doi: 10.1093/bioinformatics/btm254

38. Zhang X, Lan Y, Xu J, Quan F, Zhao E, Deng C, et al. CellMarker: a manually curated resource of cell markers in human and mouse. *Nucleic Acids Res* (2019) 47 (D1):D721–D8. doi: 10.1093/nar/gky900

39. Kim N, Kim HK, Lee K, Hong Y, Cho JH, Choi JW, et al. Single-cell RNA sequencing demonstrates the molecular and cellular reprogramming of metastatic lung adenocarcinoma. *Nat Commun* (2020) 11(1):2285. doi: 10.1038/s41467-020-16164-1

40. Avilés-Salas A, Muñiz-Hernández S, Maldonado-Martínez HA, Chanona-Vilchis JG, Ramírez-Tirado LA, HernáNdez-Pedro N, et al. Reproducibility of the EGFR immunohistochemistry scores for tumor samples from patients with advanced non-small cell lung cancer. *Oncol Lett* (2017) 13(2):912–20. doi: 10.3892/ol.2016.5512

41. Arganda-Carreras I, Kaynig V, Rueden C, Eliceiri KW, Schindelin J, Cardona A, et al. Trainable weka segmentation: a machine learning tool for microscopy pixel classification. *Bioinformatics* (2017) 33(15):2424–6. doi: 10.1093/bioinformatics/btx180

42. Liu T-C, Jin X, Wang Y, Wang K. Role of epidermal growth factor receptor in lung cancer and targeted therapies. *Am J Cancer Res* (2017) 7(2):187–202.

43. Barnes TA, Amir E. HYPE or HOPE: the prognostic value of infiltrating immune cells in cancer. *Br J Cancer* (2017) 117(4):E833-E835. doi: 10.1038/bjc.2017.220

44. Reynders K, Ruysscher DD. Tumor infiltrating lymphocytes in lung cancer: a new prognostic parameter. *J Thorac Dis* (2016) 8(8):E833–5. doi: 10.21037/jtd.2016.07.75

45. Higashiyama S, Abraham JA, Miller J, Fiddes JC, Klagsbrun M. A heparin-binding growth factor secreted by macrophage-like cells that is related to EGF. *Science* (1991) 251(4996):936–9. doi: 10.1126/science.1840698

46. Vlaicu P, Mertins P, Mayr T, Widschwendter P, Ataseven B, Högel B, et al. Monocytes/macrophages support mammary tumor invasivity by co-secreting lineage-specific EGFR ligands and a STAT3 activator. *BMC Cancer* (2013) 13:197. doi: 10.1186/1471-2407-13-197

47. Hanahan D, Weinberg RA. Hallmarks of cancer: the next generation. *Cell* (2011) 144(5):646-74. doi: 10.1016/j.cell.2011.02.013

48. Chen K-Y, Tseng C-H, Feng P-H, Sun W-L, Ho S-C, Lin C-W, et al. 3-nitrobenzanthrone promotes malignant transformation in human lung epithelial cells through the epiregulin-signaling pathway. *Cell Biol Toxicol* (2021). doi: 10.1007/s10565-021-09612-1

49. Ma S, Zhang L, Ren Y, Dai W, Chen T, Luo L, et al. Epiregulin confers EGFR-TKI resistance *via* EGFR/ErbB2 heterodimer in non-small cell lung cancer. *Oncogene* (2021) 40(14):2596–609. doi: 10.1038/s41388-021-01734-4

50. Joshi A, Zanwar S, Noronha V, Patil VM, Chougule A, Kumar R, et al. EGFR mutation in squamous cell carcinoma of the lung: does it carry the same connotation as in adenocarcinomas? *OncoTargets Ther* (2017) 10:1859–63. doi: 10.2147/OTT.S125397

51. Banat GA, Tretyn A, Pullamsetti SS, Wilhelm J, Weigert A, Olesch C, et al. Immune and inflammatory cell composition of human lung cancer stroma. *PloS One* (2015) 10(9):e0139073. doi: 10.1371/journal.pone.0139073

52. Kargl J , Busch SE, Yang GHY, Kim K-H, Hanke ML, Metz HE, Hubbard JJ, et al. Neutrophils dominate the immune cell composition in non-small cell lung cancer. *Nat Commun* (2017) 8:14381 doi: 10.1038/ncomms14381

53. Petty AJ, Yang Y. Tumor-associated macrophages: implications in cancer immunotherapy. *Immunotherapy* (2017) 9(3):289–302. doi: 10.2217/imt-2016-0135

54. Kuo P-L, Huang M-S, Cheng D-E, Hung J-Y, Yang C-J, Chou S-H. Lung cancer-derived galectin-1 enhances tumorigenic potentiation of tumor-associated dendritic cells by expressing heparin-binding EGF-like growth factor *. *J Biol Chem* (2012) 287(13):9753–64. doi: 10.1074/jbc.M111.321190

55. Eikawa S, Ohue Y, Kitaoka K, Aji T, Uenaka A, Oka M, et al. Enrichment of Foxp3+ CD4 regulatory T cells in migrated T cells to IL-6- and IL-8-expressing tumors through predominant induction of CXCR1 by IL-6. *J Immunol (Baltimore Md: 1950)* (2010) 185(11):6734–40. doi: 10.4049/jimmunol.1000225

56. Domínguez-Soto A, Sierra-Filardi E, Puig-Kröger A, Pérez-Maceda B, Gómez-Aguado F, Corcuera MT, et al. Dendritic cell-specific ICAM-3-grabbing nonintegrin expression on M2-polarized and tumor-associated macrophages is macrophage-CSF dependent and enhanced by tumor-derived IL-6 and IL-10. *J Immunol (Baltimore Md: 1950)* . (2011) 186(4):2192–200. doi: 10.4049/jimmunol.1000475

57. Mantovani A, Savino B, Locati M, Zammataro L, Allavena P, Bonecchi R. The chemokine system in cancer biology and therapy. *Cytokine Growth Factor Rev* (2010) 21(1):27–39. doi: 10.1016/j.cytogfr.2009.11.007

58. Mishalian I, Bayuh R, Levy L, Zolotarov L, Michaeli J, Fridlender ZG. Tumor-associated neutrophils (TAN) develop pro-tumorigenic properties during tumor progression. *Cancer Immunol. Immunother.* (2013) 62(11):1745–56. doi: 10.1007/s00262-013-1476-9

59. Peoples GE, Blotnick S, Takahashi K, Freeman MR, Klagsbrun M, Eberlein TJ. T Lymphocytes that infiltrate tumors and atherosclerotic plaques produce heparin-binding epidermal growth factor-like growth factor and basic fibroblast growth factor: a potential pathologic role. *Proc Natl Acad Sci United States America* (1995) 92(14):6547–51. doi: 10.1073/pnas.92.14.6547

60. Hyder A, Ehnert S, Hinz H, Nüssler AK, Fändrich F, Ungefroren H. EGF and HB-EGF enhance the proliferation of programmable cells of monocytic origin (PCMO) through activation of MEK/ERK signaling and improve differentiation of PCMO-derived hepatocyte-like cells. *Cell Commun Signaling* (2012) 10(1):23. doi: 10.1186/1478-811X-10-23

61. Wei J, Besner GE. M1 to M2 macrophage polarization in HB-EGF therapy for NEC. *J Surg Res* (2015) 197(1):126–38. doi: 10.1016/j.jss.2015.03.023

62. Lo H-W, Hsu S-C, Ali-Seyed M, Gunduz M, Xia W, Wei Y, et al. Nuclear interaction of EGFR and STAT3 in the activation of the iNOS/NO pathway. *Cancer Cell* (2005) 7(6):575–89. doi: 10.1016/j.ccr.2005.05.007

63. Jayasingam SD, Citartan M, Thang TH, Mat Zin AA, Ang KC, Ch'ng ES. Evaluating the polarization of tumor-associated macrophages into M1 and M2 phenotypes in human cancer tissue: Technicalities and challenges in routine clinical practice. *Front Oncol* (2019) 9:1512. doi: 10.3389/fonc.2019.01512

frontiers | Frontiers in Oncology

TYPE Original Research
PUBLISHED 23 December 2022
DOI 10.3389/fonc.2022.964508

Check for updates

OPEN ACCESS

EDITED BY
Shaoquan Zheng,
The First Affiliated Hospital of Sun Yat-sen University, China

REVIEWED BY
Kailin Xu,
Guangdong University of Technology, China
Yu Cai,
Jinan University, China

*CORRESPONDENCE
Zhiyu Wang
wangzhiyu@gzucm.edu.cn
Cheng Peng
pengchengchengdu@126.com
Neng Wang
ellen0000@gzucm.edu.cn

†These authors have contributed equally to this work

SPECIALTY SECTION
This article was submitted to Molecular and Cellular Oncology, a section of the journal Frontiers in Oncology

RECEIVED 08 June 2022
ACCEPTED 21 November 2022
PUBLISHED 23 December 2022

CITATION
Zhong Y, Peng F, Luo X, Wang X, Yang B, Tang X, Xu Z, Ren L, Wang Z, Peng C and Wang N (2022) A pyroptosis-related gene signature for prognostic and immunological evaluation in breast cancer. *Front. Oncol.* 12:964508. doi: 10.3389/fonc.2022.964508

COPYRIGHT
© 2022 Zhong, Peng, Luo, Wang, Yang, Tang, Xu, Ren, Wang, Peng and Wang. This is an open-access article distributed under the terms of the Creative Commons Attribution License (CC BY). The use, distribution or reproduction in other forums is permitted, provided the original author(s) and the copyright owner(s) are credited and that the original publication in this journal is cited, in accordance with accepted academic practice. No use, distribution or reproduction is permitted which does not comply with these terms.

A pyroptosis-related gene signature for prognostic and immunological evaluation in breast cancer

Yue Zhong[1†], Fu Peng[2,3†], Xiaoru Luo[1], Xuan Wang[4,5,6], Bowen Yang[4,5,6], Xinglinzi Tang[1], Zheng Xu[1], Linlin Ren[1], Zhiyu Wang[4,5,6*], Cheng Peng[2*] and Neng Wang[1*]

[1]Integrative Medicine Research Center, School of Basic Medical Sciences, Guangzhou University of Chinese Medicine, Guangzhou, Guangdong, China, [2]State Key Laboratory of Southwestern Chinese Medicine Resources, Chengdu University of Traditional Chinese Medicine, Chengdu, Sichuan, China, [3]Key Laboratory of Drug-Targeting and Drug Delivery System of the Education Ministry and Sichuan Province, West China School of Pharmacy, Sichuan University, Chengdu, China, [4]State Key Laboratory of Dampness Syndrome of Chinese Medicine, The Second Affiliated Hospital of Guangzhou University of Chinese Medicine, Guangzhou, Guangdong, China, [5]Guangdong Provincial Key Laboratory of Clinical Research on Traditional Chinese Medicine Syndrome, Guangdong Provincial Academy of Chinese Medical Sciences, Guangdong Provincial Hospital of Chinese Medicine, Guangzhou, Guangdong, China, [6]Guangdong-Hong Kong-Macau Joint Lab on Chinese Medicine and Immune Disease Research, Guangzhou University of Chinese Medicine, Guangzhou, Guangdong, China

Purpose: Pyroptosis exerts an undesirable impact on the clinical outcome of breast cancer. Since any single gene is insufficient to be an appropriate marker for pyroptosis, our aim is to develop a pyroptosis-related gene (PRG) signature to predict the survival status and immunological landscape for breast cancer patients.

Methods: The information of breast cancer patients was retrieved from The Cancer Genome Atlas (TCGA) and the Gene Expression Omnibus (GEO) databases. Quantitative real-time polymerase chain reaction (qRT-PCR) was performed to verify the gene expressions of this signature in breast cancer. Its prognostic value was evaluated by univariate Cox analysis, least absolute shrinkage and selection operator (LASSO) regression analysis, receiver operating characteristics (ROCs), univariate/multivariate analysis, and nomogram. Analyses of Gene Ontology (GO) and Kyoto Encyclopedia of Genes and Genomes (KEGG) were performed to explore its potential biological function in breast cancer. The potential correlation between this signature and tumor immunity was revealed based on single sample gene set enrichment analysis (ssGSEA), ESTIMATE and CIBERSORT algorithms.

Results: A PRG signature containing GSDMC, GZMB, IL18, and TP63 was created in a TCGA training cohort and validated in two validation GEO cohorts GSE58812 and GSE37751. Compared with a human mammary epithelial cell line MCF-10A, the expression levels of GSDMC, GZMB and IL18 were upregulated, while TP63 was found with lower expression level in breast cancer cells SK-BR-3, BT-549, MCF-7, and MDA-MB-231 using RT-qPCR

assay. Based on univariate and multivariate Cox models, ROC curve, nomogram as well as calibration curve, it was revealed that this signature with high-risk score could independently predict poor clinical outcomes in breast cancer. Enrichment analyses demonstrated that the involved mechanism was tightly linked to immune-related processes. SsGSEA, ESTIMATE and CIBERSORT algorithms further pointed out that the established model might exert an impact on immune cell abundance, immune cell types and immune-checkpoint markers. Furthermore, individuals with breast cancer responded differently to these therapeutic agents based on this signature.

Conclusions: Our data suggested that this PRG signature with high risk was tightly associated with impaired immune function, possibly resulting in an unfavorable outcome for breast cancer patients.

KEYWORDS

breast cancer, pyroptosis, 4-gene signature, survival status, immunological landscape

1 Introduction

Breast cancer belongs to one of the most common cancer diseases and ranks first or second in mortality rates among women worldwide, with approximately 2,260,000 increasing cases and almost 685,000 deaths according to the GLOBOCAN 2020 estimation (1). At present, a variety of anti-breast cancer treatments are available, including surgical operations, chemotherapeutic options, radiotherapeutic plans, hormone-based strategies, targeted therapies and others. Appropriate therapeutic measures are taken based on different breast cancer subtypes, such as HR+/ERBB2− (seven-tenths of the total), ERBB2 + (one-fifth of the total) as well as triple-negative (one-tenth of the total). The median overall survival (OS) for the first two subtypes is 5 years in comparison with approximately 1 year for the triple-negative phenotype. Accordingly, the main goal for treating the first two subtypes is eradication of local breast tumors/regional lymph nodes to prevent increasing risks of recurrence, while the therapeutic value in treating triple-negative phenotype is to prolong life span and alleviate patients' suffering (2). Although more than 90% breast cancer patients are initially diagnosed as non-metastatic phenotypes, 20–50% of them eventually develop into advanced stages or distant recurrent phenotypes of breast cancer (3). In addition, tumor progression is highly dependent on the tumor niche or tumor microenvironment (TME). Immune dysregulation always leads to ineffectiveness and even multidrug resistance of clinical agents in cancer modality therapies (4). TME-associated oncogenes and/or tumor suppressor genes have potential value in determining tumor typing, gene sets, and pathways as well as phenotype modeling for research into breast cancer (5). Hence, it is urgent and essential to develop and validate a prognostic model to predict OS and immunological landscape in patients with breast cancer.

Pyroptosis is a certain kind of programmable cell death mediated by inflammasomes. It has been characterized by the formation of inflammasomes, the activation of caspase and gasdermin, as well as the release of pro-inflammatory cytokines (5). In the canonical pathway, pyrolytic cells appear light swelling with many bubble-like inflammasomes. The inflammasomes then join together and recruit caspase-1 to activate GSDMD within its N-terminal domain, and trigger the abnormal expressions of IL1β, IL18, high mobility group

Abbreviations: TCGA, The Cancer Genome Atlas; GEO, Gene Expression Omnibus; qRT-PCR, Quantitative real-time polymerase chain reaction; LASSO, Least absolute shrinkage and selection operator; ROCs, Receiver operating characteristics; GO, Gene ontology; KEGG, Kyoto Encyclopedia of Genes and Genomes; ssGSEA, Single sample gene set enrichment analysis; OS, Overall survival; TME, Tumor microenvironment; HMGB1, High mobility group box 1; NK cells, Natural killer cells; PRGs, Pyroptosis-related genes; DEGs, Differential expression genes; PPI, Protein-protein interaction; PCA, Principal component analysis; t-SNE, T-distributed stochastic neighbor embedding; CSCs, Cancer stem cells; IC50, Half maximal inhibitory concentration; ARGs, Autophagy-related genes; HRs, Hazard ratios; AUC, Area under curve; aDCs, Active DCs; DCs, Dendritic cells; iDCs, Immature dendritic cells; pDCs, Plasmacytoid DCs; Tfh, T follicular helper; TIL, Tumor infiltrating lymphocyte; Treg, Regulatory cell; APC, Antigen presenting cell; HLA, Human leukocyte antigen; MHC, Major histocompatibility complex; IFN, Type I interferon; IFNγ, type II interferon; ICB, Immune checkpoint block; EGFR/ErbB1, Epidermal growth factor receptor; TOP1, Topoisomerase I.

box 1 (HMGB1) and others through necrotic membrane pores formed by GSDMD-N. Alternatively, both pyroptosis initiation and GSDMD cleavage are caspase 4, 5, 11-dependent by combining with cellular lipopolysaccharides rather than recruiting inflammasomes in the non-canonical pathway (6). A variety of inflammatory factors are released into TME and blood circulation to promote systemic inflammation during pyroptosis. Therefore, a number of pilot studies have been focused on pyroptosis to comprehend its association with infectious diseases, nervous system disorders, and atherosclerosis-associated diseases (7). Of note, it has also been demonstrated that pyroptosis displays dichotomous behaviors during oncogenesis possibly due to different cell types, genetics and tumor stages. On one hand, tumors with abnormal GSDMD expression, activated inflammasomes, and enhanced pro-inflammatory cytokines belong to a more aggressive phenotype by maintaining immunosuppressive cells, facilitating stromal cell transformation from epithelial cells, and up-regulating matrix metalloproteinases for extracellular matrix remodeling (6). On the other hand, pyroptosis exerts anti-tumor function. For instance, pyroptosis induced by NLRP3-mediated inflammasomes could significantly delay the growth and metastasis of hepatocellular carcinoma (7). Thus, it is necessary to establish diagnostic and prognostic signatures for pyroptosis in order to clarify its significance in breast cancer.

It appears that pyroptosis holds promise as a potential adjuvant in tumor immunotherapy with a good prospect. According to clinical findings, different tumor types respond differently to immunotherapy. Tumors sensitive to immunotherapy are classified as "hot tumors", while tumors with poor reactivity are called "cold tumors" (8). Thus, different treatment strategies should be adopted for different tumors, and how to transform "cold tumors" into "hot tumors" to improve the curative effect is particularly critical. An exciting research reported the synergistic effect of pyroptosis induction and PD-1 inhibitor could turn the tumor from immune-silent "cold tumors" to "hot tumors" with immune stimulation, suggesting the great potential of this combination (9). Moreover, pyroptosis contributes to tumor inhibition by stimulating anti-tumor immune response. Activating GSDME could promote macrophage phagocytosis and enhance the function of natural killer (NK) cells and CD8+ T cells (10). The study of Tan et al. revealed that DRD2 polarized macrophages to M1 by restricting NF-κB signaling, subsequently resulting in GSDME-induced pyroptosis in breast cancer (11). Overall, investigating the association between pyroptosis and tumor immunity can bring new insights into the prognosis and treatment of breast cancer.

Given the strong correlation between pyroptosis and cancer diseases, it is worth investigating the specific functions of PRGs (12). However, breast cancer-associated PRGs have not been fully explored yet. Herein, this study described a comprehensive analysis of breast cancer-associated PRGs, including their prognostic value, biological function and pathways, immunological characterization, drug sensitivity as well as genomic information. In particular, we developed a PRG-based signature to evaluate its prognostic value for breast cancer patients based on Kaplan-Meier and ROC methods. Subsequently, ssGSEA, ESTIMATE and CIBERSORT algorithms were also applied to clarify the relationship between PRGs and immune cell infiltration in TME, which would provide new targets for breast cancer immunotherapy.

2 Materials and methods

2.1 Data source and collection

We downloaded the RNA sequencing data of 1109 breast cancer tumor tissues as well as 113 adjacent tissues, and the related clinical information in the TCGA dataset (https://portal.gdc.cancer.gov/repository). Counts value matrix was utilized to screen out differentially expressed genes (DEGs) involved in pyroptosis, while TPM value matrix was used for the rest of analyses. Breast cancer patients with missing OS values or OS ≤30 days were excluded from the analysis to avoid statistical bias. We also used the GEO database (GSE58812 and GSE37751) (https://www.ncbi.nlm.nih.gov/geo/) to retrieve gene expression data and clinical data.

2.2 Identification of differentially expressed PRGs

The involved 52 PRGs were obtained from previous studies (13) (Table S1). The DEG identification between tumor tissues and adjacent tissues was conducted by the R package "edgeR" (14). Adjusted P-value < 0.05 and |log2 (fold change) | (log2 FC) > 1 were defined as the threshold. Protein-protein interaction (PPI) networks were set up using screened DEGs with the Retrieval of Interacting Genes (STRING) (https://string-db.org/).

2.3 Construction of the PRG model in breast cancer

To evaluate the prognostic value of this PRG model, both Cox regression analysis and LASSO regression analysis were utilized to evaluate the relationship between PRGs and the survival status in the TCGA cohort. For Cox regression analysis, genes that met P-value < 0.05 were further analyzed, and 4 survival-related genes were found. A prognostic model was then constructed using R package "glmnet" based on the LASSO regression. Finally, 4 genes were maintained. The penalty parameter (λ) was determined by applying minimum criteria. The risk score was calculated by the following formula:

$$\text{Riskscore} = \sum_{i=1}^{n} \text{Coef}(\text{Xi}) * \text{Exp}(\text{Xi})$$

For each gene Xi, coef (Xi) represented the coefficient, and Exp (Xi) represented gene expression. Breast cancer patients were classified into two groups (the high- and low-risk groups) based on the median risk score. We used principal component analysis (PCA) with "prcomp" R package and t-distributed stochastic neighbor embedding (t-SNE) test using "Rtsne" R package (15) to analyze two groups' distribution. Then, Kaplan-Meier analysis was applied to examine the interactions between risk value and the survival time using R packages of "survival" (16) and "survminer" (17), and ROC curve analysis was performed to evaluate their diagnosis index with "timeROC" R package (18).

2.4 Validation of PRG signature

To further test and verify the 4-gene signature model based on TCGA, its prediction accuracy was re-evaluated in the GEO pool (GSE58812 and GSE37751). Kaplan-Meier curves implied significant discrepancies between the two risk groups of patients. Then ROC curves analysis was used to confirm the robustness of our PRG prognostic model.

2.5 Cell culture

MCF-10A, BT-549, MCF-7 and MDA-MB-231 were purchased from the American Type Culture Collection (ATCC, Manassas, VA, United States). SK-BR-3 was obtained from Jiangsu Kaiji Biotechnology Co., Ltd (Nanjing, Jiangsu, China). The cells were cultured in medium (DMEM for SK-BR-3 and MDA-MB-231 cells; RPMI-1640 for BT-549 and MCF-7 cells) and were added with 10% fetal bovine serum (Gibco, Nork York, NY, United States) as well as 1% penicillin and streptomycin (Gibco, Nork York, NY, United States). Both DMEM and RPMI-1640 were purchased from Gibco company (Gibco, Nork York, NY, United States). MCF-10A was maintained in DMEM/F12 (Gibco, New York, NY, United States) supplemented with 5% horse serum (Hyclone, Logan, UT, United States), 20 ng/ml epidermal growth factor (BD Bioscience, Bedford, MA, United States), 10 μg/ml insulin (Sigma, St. Louis, MO, United States), 0.5 μg/ml hydrocortisone (StemCell Technologies, Vancouver, BC, Canada), 100 ng/ml cholera toxin (Macgene, Beijing, China) and 1% penicillin and streptomycin (Gibco, New York, NY, United States). All these cell lines were kept at 37°C, with a humidified atmosphere of 5% CO2.

2.6 RNA isolation and qRT-PCR analysis

The primer sequences of GSDMC, GZMB, IL18, and TP63 were synthesized by WcGene Biotech (Shanghai, China), and β-actin was synthesized by Sangon Biotech (Shanghai, China) (listed in Table S2). Total RNA was extracted with an RNA extraction kit (DP419, Tiangen Biotech Beijing Co., Ltd., Beijing, China), followed by reverse transcription reaction using TAKARA reverse transcription kit (RR047A, Takara, Shiga, Japan). Following qRT-PCR analysis was performed with TB Green® Premix Ex Taq™ II (RR820A, Takara, Shiga, Japan) in Bio-Rad CFX96. A comparative Ct method ($2^{-\Delta\Delta CT}$) was used to calculate the expression level of RNA normalized to β-actin.

2.7 Independent prognostic analysis

Univariate and multivariate Cox regression was conducted to investigate whether the risk score could be an independent prognostic factor. TCGA was used to obtain the clinical information (age, T stage, N stage, and M stage) of breast patients.

2.8 A predictive nomogram construction

A nomogram was established to predict the 1-, 3-, or 5-year survival probability and accuracy performance of the model assessed by calibration curves.

2.9 Functional enrichment analysis of PRGs

Patients with breast cancer were stratified by a median risk score into low- and high-risk groups from the TCGA and GEO cohorts. The DEG analysis was performed between two groups using the "limma" package (19). The threshold was set as follows: FDR < 0.05, | log2 FC | > 1. GO (20, 21) and KEGG (22) were performed by using "clusterProfiler" (23), and "ggplot2" (24) R package. The venn diagram was drawn by "VennDiagram" R package (25).

2.10 Assessment of immune status and CSC index between two subgroups

SsGSEA was performed to calculate the immune cell infiltration based on "GSVA" R package (26). The R package "ESTIMATE" was utilized to count the scores (immune/stromal/estimate score) and tumor purity in TME (27). R package "CIBERSORT" was used to reveal the intrinsic links between PRG score and immune cells abundance in TCGA (28). Subsequently, we used Spearman's correlation analysis to analyze the relationship between the risk score and the index of immune cells/cancer stem cells (CSCs). Threshold P-value < 0.05 was considered significant.

2.11 Drug sensitivity evaluation

An analysis of half inhibitory concentrations (IC50) of common drugs was performed using "pRRophetic" R software in TCGA (29). And we applied the Wilcoxon signed-rank test to detect IC50 between two subgroups.

2.12 Data analysis using cBioPortal

cBioPortal (www.cbioportal.org) is a comprehensive web resource for collection and analysis of cancer genomics data, such as copy number alterations, DNA methylation and so on (30). 2509 samples [Breast Cancer (METABRIC, Nature 2012 & Nat Commun 2016)] were explored, and mRNA expression z-scores (log microarray) were acquired using a z-score threshold of ± 2.0. We also used cBioPortal web platform to analyze the relationship between the TP63 gene expression and its methylation level.

2.13 Analysis of common genes between pyroptosis and autophagy

The autophagy-related genes (ARGs) were collected from Human Autophagy Database (http://www.autophagy.lu/) (Table S3). An intersection was acquired by ARGs and PRGs. The effects of high and low gene expression on OS were investigated by Kaplan–Meier curves using R packages of "survival" and "survminer" (17).

2.14 Statistical analysis

Data analyses were completed by R software (v4.0.1) and SPSS software (version 26). Statistical significance was defined by $P < 0.05$.

3 Results

3.1 Identification of pyroptosis-related DEGs in breast cancer

Figure 1 illustrated the flowchart of this study, including PRG signature construction, validation and functional analysis as well as response evaluation to therapies. We compared expression levels of 52 PRGs with DEGs from 1109 breast tumors and 113 adjacent tissues in TCGA, and identified 16 pyroptosis-related DEGs in breast cancer. Among them, 12 genes were significantly upregulated (BAX, BAK1, PYCARD, NOD2, GSDMD, IL18, AIM2, NLRP7, NLRP6, GSDMC, GZMB, NLRP2), while 4 other genes were obviously downregulated (IL6, TP63, ELANE, NLRP1) according to volcanoes ($P < 0.05$, Figure 2A). The differential PRG expressions were visualized by heatmaps in Figure 2B. To further investigate their intricate correlation with each other, a PPI-associated analysis was established in the light of a minimum interaction score of 0.4 (Figure 2C), and their interactions were also shown in a pyroptosis-based network (Figure 2D).

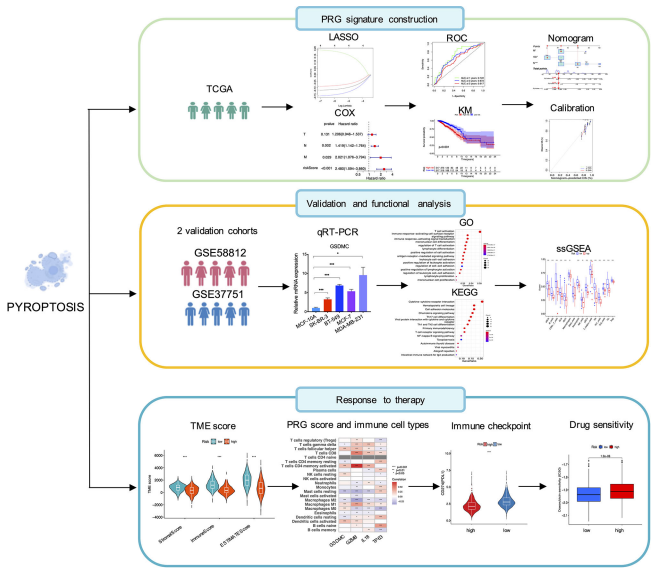

FIGURE 1
Schematic illustration of the study design, including PRG signature construction, validation and functional analysis and response evaluation to therapies.

3.2 Construction of a PRG-based prognostic model in TCGA

In the search for the survival-related PRGs, a univariate Cox regression analysis was conducted based on a threshold of $P < 0.05$. As shown, 4 out of 16 aforementioned DEGs were selected as the appropriate candidates for constructing a pyroptosis-related risk signature. In particular, 3 genes TP63, IL18, and GZMB were shown as protective genes with hazard ratios (HRs) < 1, while GSDMC was regarded as a risk gene with HRs >1 (Figure 2E). In the following LASSO regression analysis, a 4-gene risk model was built based on the LASSO optimal λ regression (Figure 2F). Accordingly, the risk score was calculated as indicated: Risk score = (−0.120 * TP63 Exp.) + (−0.090 * IL18

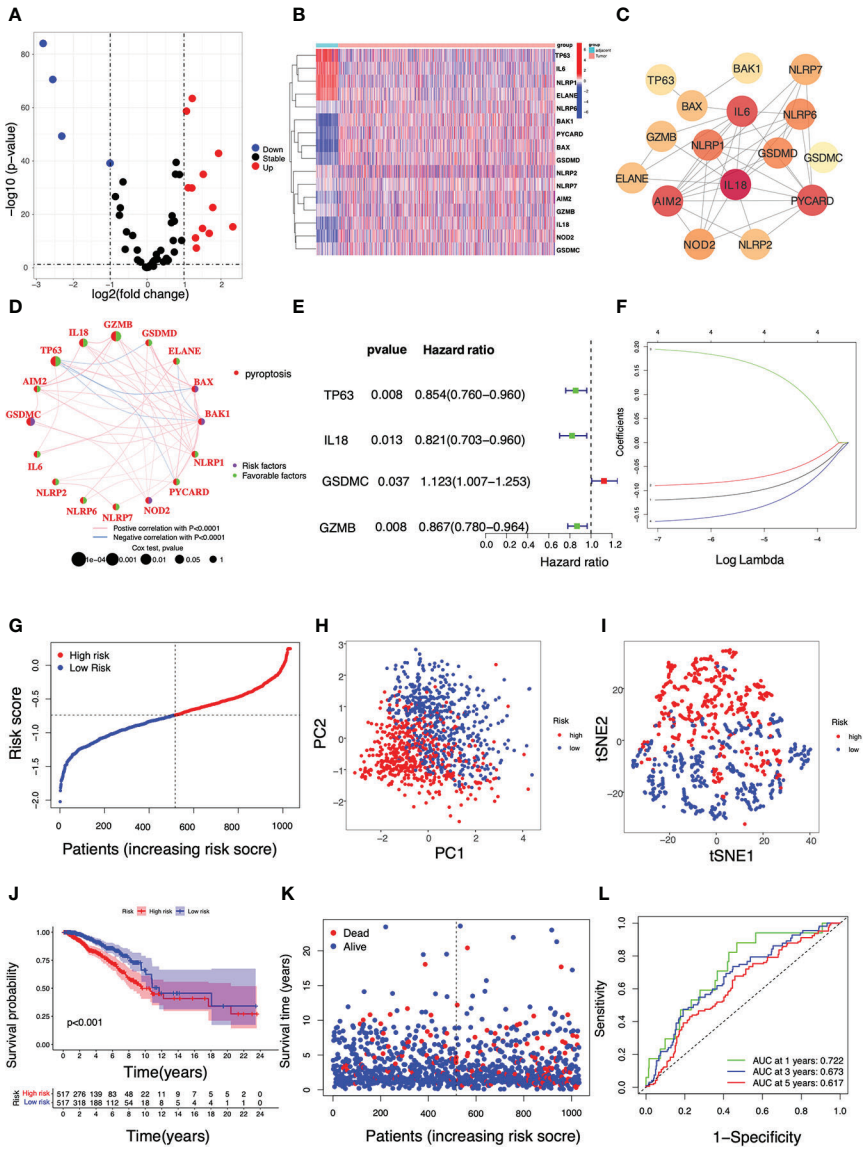

FIGURE 2
Identification of pyroptosis-related DEGs and construction of a PRG-based prognostic model using the TCGA cohort in breast cancer. **(A)** A volcano plot displaying pyroptosis-related DEGs in breast cancer ($P < 0.05$, *red*: up-regulated genes; *blue*: down-regulated genes); **(B)** A heatmap of the 16 differential PRG expressions between breast tumors and adjacent tissues ($P < 0.05$, *blue*: decreased expression; *red*: increased expression); **(C)** A PPI network indicating the intricate interactions of the 16 PRGs (interaction score = 0.4); **(D)** The connection network among PRGs (*Pink*: a positive association; *blue:* a negative association. *Green*: a favorable factor; *purple*: a risk factor). **(E)** Univariate Cox regression analysis of survival-related PRGs ($P < 0.05$); **(F)** A 4-gene risk model was built based on LASSO regression analysis; **(G)** The breast cancer patient distribution based on the median value of the risk score; **(H)** PCA plot and **(I)** T-SNE analysis in the TCGA cohort; **(J)** Kaplan–Meier curve analysis for the OS of patients with either high or low risk; **(K)** The survival status of each breast cancer patient (*left dotted line*: low-risk; *right dotted line*: high-risk); **(L)** ROC analysis curve for the signature of this 4-gene set.

Exp.) + (0.194 * GSDMC Exp.) + (−0.164 * GZMB Exp.). Patients with breast cancer were divided into two subgroups *i.e.* one with high risk (n = 517) and the other with low risk (n = 517) distinguished by the median risk score in TCGA (Figure 2G). In addition, the PCA and t-SNE analysis showed a high-quality separation between the two subgroups (Figures 2H, I). The Kaplan-Meier curve was used to reveal the discrepancies between the two risk groups, and it was found that breast cancer patients with high risk had shorter survival periods than those with low risk (Figures 2J, K). ROC analysis was then performed to validate the sensitivity and specificity of this signature, and the areas under curve (AUC) were 0.722 (1-year), 0.673 (3-year) and 0.617 (5-year), respectively (Figure 2L).

3.3 Signature validation with the GEO cohorts and qRT-PCR assay

Data from GSE58812 and GSE37751 were utilized as two independent validation sets to verify the prognostic value of this model. In GSE58812, 58 breast cancer patients were annotated as the low-risk populations and 49 were characterized by high risk based on the median risk score in the TCGA cohort (Figure 3A). In Kaplan–Meier analysis, a significantly lower survival rate was observed in the high-risk group compared to the low-risk group (P = 0.005, Figure 3B). The survival status in the indicated groups was presented in Figure 3C. The 1-, 3-, and 5-year AUC values were 0.720, 0.722, and 0.704 in GSE58812 (Figure 3D). Furthermore, patients with different risks (27 in the high-risk subgroup *v.s.* 34 in the low-risk subgroup) were assigned to two clusters in GSE37751 (Figure 3E). In GSE37751, patients in the high-risk group had shorter survival than those patients in the low-risk group (P = 0.029, Figure 3F). Also, the survival status was shown in Figure 3G, and the 1-, 3-, and 5-year AUC values were 0.636, 0.702, and 0.738 (Figure 3H). We additionally compared expressions of key genes between human breast cancer cells and a human mammary epithelial cell line MCF-10A using RT-qPCR assay. As shown, compared with MCF-10A, the expression levels of GSDMC, GZMB and IL18 were upregulated, while TP63 was found with lower expression level in breast cancer cells SK-BR-3, BT-549, MCF-7, and MDA-MB-231 (Figures 3I–L, P < 0.05).

3.4 Analysis of clinicopathological relevance and functional enrichment

Both univariate (Figure 4A) and multivariate (Figure 4B) Cox regression analyses proved that the PRG-based signature, as well as N stage and M stage, were independent predictors for poor prognosis of breast cancer patients (P < 0.05), demonstrating the robustness and accuracy of our method. The calibration curve for OS probability at 1, 3, and 5 years also suggested satisfactory consistency between the predicted and actual survival probabilities (C-index value=0.69, Figures 4C, D). Next, we continued to investigate the clinicopathological correlation of breast cancer with this PRG risk model in TCGA. As shown, the PRG signature in the high-risk group was significantly correlated with poor survival in older (≥ 40 years), M0 or M1, N1-N3, and T1-T2 or T3-T4 populations (P < 0.05; Figures 4E–H). Taken together, this PRG signature with high-risk score was possibly an independent prognostic marker linking to a poor clinical outcome for breast cancer patients.

In addition, enrichment analyses were carried out to reveal the molecular functions and underlying mechanisms associated with pyroptosis in breast cancer. For GO functional analysis, the terms existing in both the TCGA and GSE58812 cohorts included T cell activation, regulation of T cell activation, mononuclear cell differentiation, positive regulation of cell activation, lymphocyte differentiation, immune response minus;activating cell surface receptor signaling pathway, immune response–activating signal transduction, positive regulation of leukocyte activation, leukocyte cell–cell adhesion, positive regulation of lymphocyte activation, antigen receptor–mediated signaling pathway and regulation of leukocyte cell–cell adhesion (Figures 5A–C). For KEGG analysis, bubble charts demonstrated that the involved pathways co-existing in both cohorts were mainly associated with immunological modulation and cancer interference, including cytokine–cytokine receptor interaction, cell adhesion molecules, hematopoietic cell lineage, Th17 cell differentiation, chemokine signaling pathway, viral protein interaction with cytokine and cytokine receptor, Th1 and Th2 cell differentiation, primary immunodeficiency, T cell receptor signaling pathway, intestinal immune network for IgA production, allograft rejection, and autoimmune thyroid disease (Figures 5D–F).

3.5 Analysis of immunological status and TME characterization

On this basis, ssGSEA was then performed to evaluate the impact of this signature on immunological status, particularly immune cell types and functions. As shown, high-risk score led to lower levels of infiltrating immune cells, including active DCs (aDCs), B cells, CD8+T cells, dendritic cells (DCs), immature dendritic cells (iDCs), macrophages, neutrophils, natural killer (NK) cells, plasmacytoid DCs (pDCs), T helper cells, T follicular helper (Tfh) cells, Th1 cells, Th2 cells, tumor infiltrating lymphocyte (TIL), and regulatory cell (Treg) in two datasets (Figures 6A, B). In addition, the high-risk individuals presented lower activities in 13 immune-related pathways, including Antigen presenting cell (APC) co-inhibition, APC co-stimulation, C-C chemokine receptor (CCR), check-point, cytolytic activity, human leukocyte antigen (HLA),

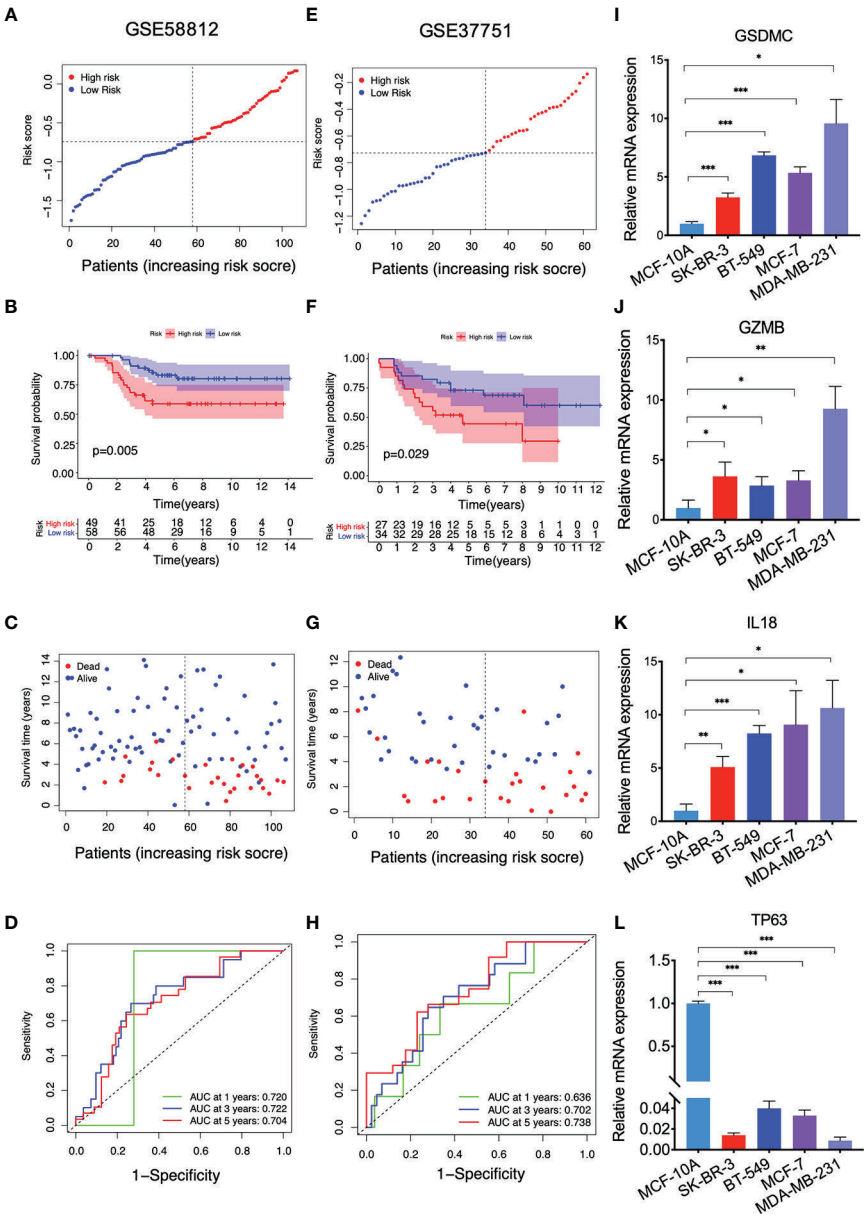

FIGURE 3
Validation of the PRG model with the GEO cohorts and qRT-PCR results. **(A)** The distribution of breast cancer patients based on the risk score in GSE58812; **(B)** Kaplan-Meier curves for OS in the low and high-risk groups in GSE58812; **(C)** The survival status for each breast cancer patient in GSE58812; **(D)** ROC curve analysis in GSE58812; **(E)** The distribution of breast cancer patients based on the risk score in GSE37751; **(F)** Kaplan-Meier curves for OS in the low and high-risk groups in GSE37751; **(G)** The survival status for each breast cancer patient in GSE37751; **(H)** ROC curve analysis in GSE37751; **(I–L)** qRT-PCR results indicating the expressions of GSDMC, GZMB, IL18, and TP63 in the indicated cell lines, values represented the mean ± SD. n=3, *P<0.05; **P<0.01; ***P<0.001.

inflammation-promoting, major histocompatibility complex (MHC) class I, parainflammation, T cell co-inhibition, T cell co-stimulation, type I interferon (IFN) response, and type II interferon (IFNγ) response (Figures 6C, D). Overall, these data suggested that high-risk conditions were largely associated with impaired immune function in breast cancer, possibly resulting in unfavorable outcomes for those patients.

Moreover, we also investigated whether and how risk score affected immune activities in TME. Firstly, CSCs are the roots of breast cancer (31). In this investigation, breast cancer cells with higher PRG score also yielded a higher CSC index, indicating that it might be possible to eliminate CSCs through the use of pyroptosis-related therapies by targeting these 4 PRGs ($P < 0.001$, Figure 7A). Next, we estimated TME score of breast

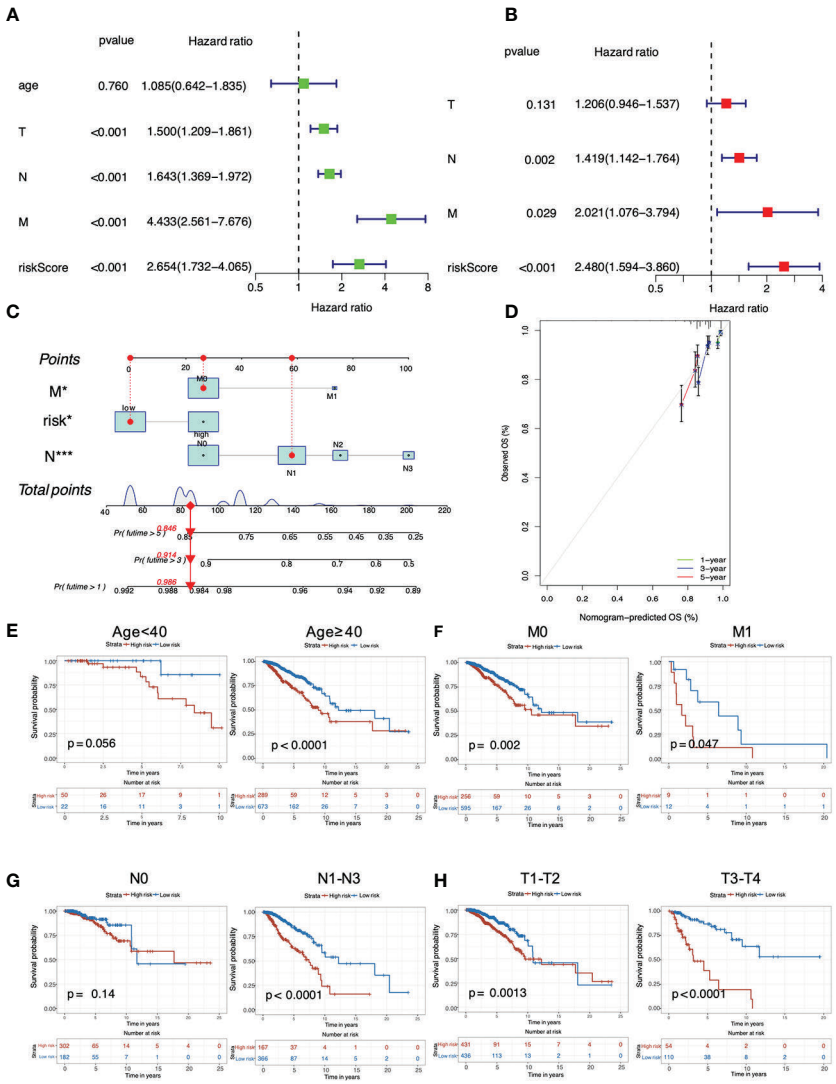

FIGURE 4
Analysis of predictive independency and clinicopathological relevance of the PRG signature in breast cancer. **(A)** Univariate Cox regression analysis; **(B)** Multivariate Cox regression analysis; **(C)** The nomogram for predicting OS probabilities for breast cancer patients with either high or low risk; **(D)** The 1-, 3- and 5-year nomogram calibration curves; Subgroup analysis of **(E)** age (< 40 years and ≥ 40 years), **(F)** M stage (M0 and M1), **(G)** N stage (N0 and N1-N3) and **(H)** T stage (T1-T2 and T3-T4).

cancer samples with R package "ESTIMATE" in TCGA. The goal of this algorithm was to retrieve stromal, immune and estimate scores. In particular, both stromal and immune scores were positively correlated to infiltration of stromal and immune cells, while the estimate score (the sum of the stromal and immune scores) was a negative indicator of purity of tumor cells (32). Compared with the low-risk group, the high-risk group with lower immune/stromal/estimate score exhibited higher tumor purities (Figure 7B). Further analysis revealed that most immune cells exhibited significant correlations with the four PRGs GSDMC, GZMB, IL18, and TP63 (Figures 7C, D). Also, the risk signature had a direct bearing on immune cell types determined by CIBERSORT algorithm. In particular, the PRG score was negatively correlated with T cells CD4 memory activated, T cells CD8, T cells CD4 memory resting, T cells gamma delta, Macrophages M1, B cells naïve and Plasma cells, while positively related to Macrophages M0, Macrophages M2, Mast cells activated and NK cells resting (Figure 7E). We also compared the immune-checkpoint markers between two subgroups. As shown, patients in the low-risk group expressed significantly higher levels of PD-1, PD-L1, PDL-2, CD80, CD86, and CTLA-4, implying that immune checkpoint blockade (ICB) therapies might be effective for the low-risk patients ($P < 0.001$, Figure 7F).

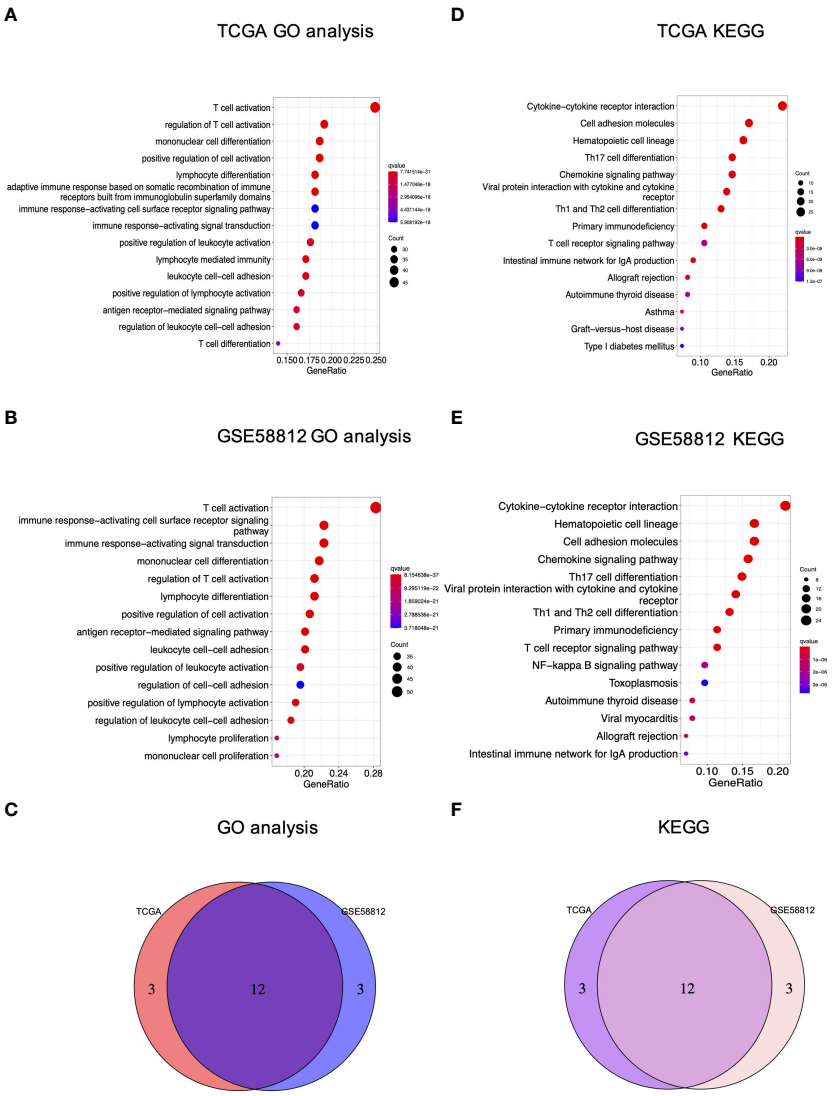

FIGURE 5
GO and KEGG analyses of the PRG signature in breast cancer. **(A)** GO analysis of the TCGA cohort; **(B)** GO analysis of GSE58812; **(C)** The Venn diagram of GO terms between the TCGA and GEO cohorts; **(D)** KEGG analysis of the TCGA cohort; **(E)** KEGG analysis of GSE58812; **(F)** The Venn diagram of KEGG terms between the TCGA and GEO cohorts.

3.6 Evaluation of drug sensitivity and genetic regulation

The risk signature was then used to predict whether breast cancer patients could benefit from chemotherapeutic treatments or targeted therapies. Wilcoxon's ranked-rank test was utilized to compare IC50 values between the high-risk and low-risk groups. As shown, the low-risk individuals with breast cancer had lower IC50 values for doxorubicin (Figure 8A), docetaxel (Figure 8B), paclitaxel (Figure 8C), lapatinib (Figure 8D), while IC50 values of drugs such as camptothecin (Figure 8E), embelin (Figure 8F) were obviously lower in breast cancer patients with high PRG risk (all $P < 0.001$). Overall, it was suggested that this signature was related to drug sensitivity and might provide guidance for treating breast cancer in the clinical setting.

In addition, we also investigated the genetic regulation of the four PRGs. An analysis of its molecular characteristics was conducted by searching the dataset of Breast Cancer (METABRIC, Nature 2012 & Nat Commun 2016) in cBioPortal. In particular, the OncoPrint tab summarized genomic alterations (including amplification, deletion, upregulation, and *etc.*) of TP63, IL18, GZMB, GSDMC were 8%, 0.2%, 5%, and 26%, respectively (Figure S1A). Of note, it was demonstrated that autophagy might play a crucial role in

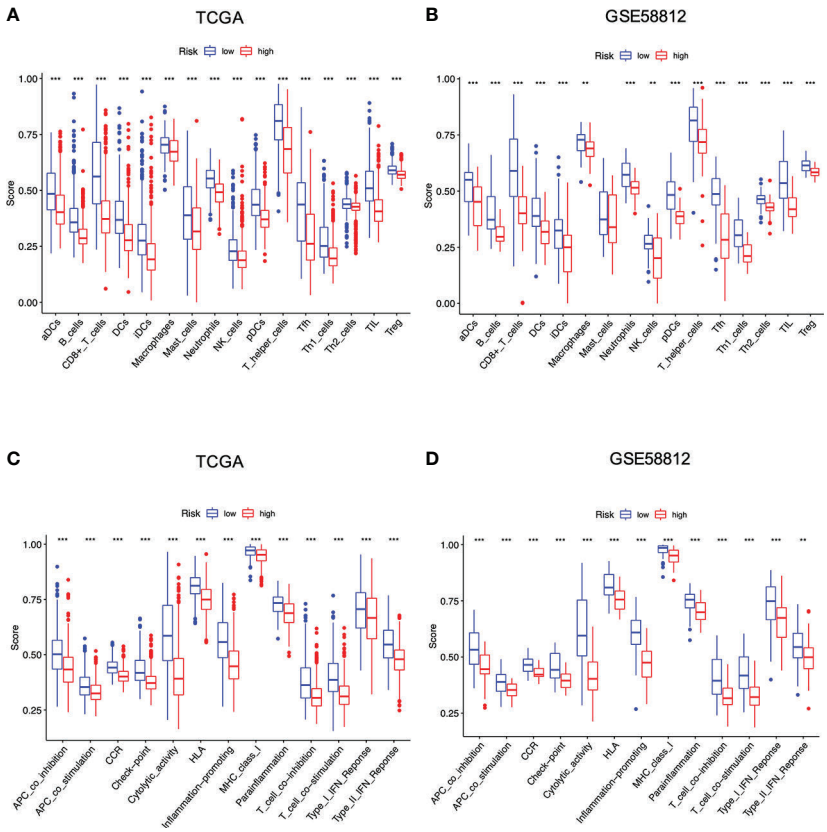

FIGURE 6
Differences of infiltrating immune cells and immune-related pathways between different risk groups based on the TCGA and GEO cohort. **(A, B)** Infiltrating immune cells between two risk groups; **(C, D)** Immune-related pathways between two risk groups (all **P < 0.01; ***P < 0.001).

keeping intracellular homeostasis by regulating pyroptosis (33). By comparing 52 PRGs with 222 ARGs, 11 common genes TP53, NLRC4, BAK1, CASP1, CASP4, CASP8, BAX, CHMP4B, TP63, CASP3, and CHMP2B were identified, among which only TP63 exhibited further interactions with the established 4-gene signature (Figure S1B). According to both the TCGA and GEO cohorts, a decrease of TP63 level was an indicator for poor survival status for breast cancer patients (Figure S1C–E). In addition, a comparison between N0 and N1-N3 status of breast cancer patients demonstrated that cases with lymph-node metastasis had lower TP63 mRNA expression (P = 0.017, Figure S1F), which might be due to its hypomethylation (Figure S1G).

4 Discussion

It is always important to seek and decipher pyroptosis-associated targets in breast cancer. For instance, GSDME methylation at high frequency contributed to lymph node metastasis and a poor prognosis for breast cancer patients (34, 35). Pizato et al. revealed that omega-3 docosahexaenoic acid had robust facilitation of pyroptosis-mediated cell death in triple-negative breast cancer, improving the understanding of DHA as nutriment and adjuvant treatment against breast cancer (36). The study from Liang et al. pointed out that trichlorobendazole triggered GSDME-dependent pyroptosis of breast cancer cells and clarified the involved mechanism was associated with augment of ROS/JNK/Bax-mitochondrial signal, suggesting the potential therapeutic use of this drug for treating breast cancer patients with high GSDME expression (37). Cisplatin induced anti-breast cancer effects at least partly by activating MEG3/NLRP3/caspase-1/GSDMD pathway (38). In light of these findings, it is crucial to develop a PRG-based prognostic signature to clarify the significance of pyroptosis in breast cancer. Herein, the PRG-based risk model containing GSDMC, GZMB, IL18, and TP63 was established in the TCGA cohort, followed by further validation with the GEO cohorts and qRT-PCR assay. Retrospectively, these targets could affect cancer progression by regulating pyroptosis directly or indirectly. For instance, GSDMC was initially recognized as an oncogene in metastatic mouse melanoma. Pyroptosis could be induced by

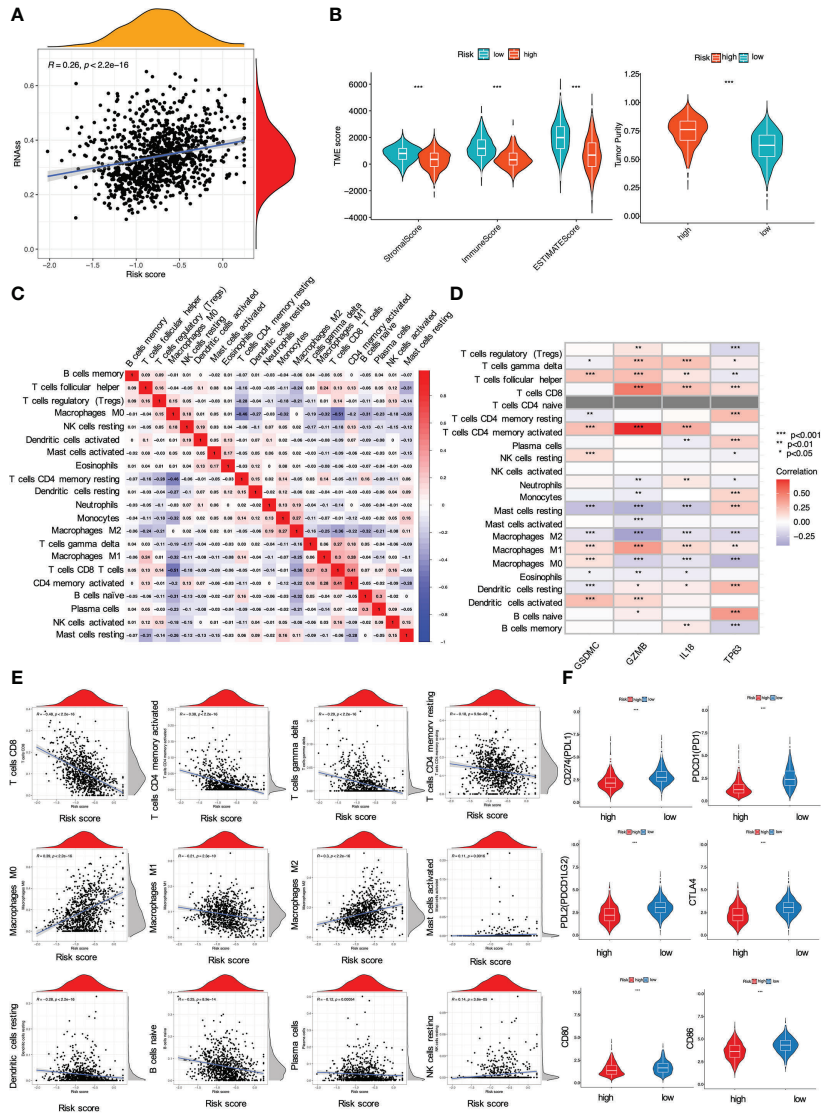

FIGURE 7
Impact of the risk signature on immune activities in TME. **(A)** Relationship between PRG score and cancer stem cells; **(B)** Analysis of PRGs related to immune/stromal/estimate score and tumor purity. The PRG signature correlated with **(C, D)** immune cell abundance, **(E)** immune cell types, and **(F)** checkpoints (all *P < 0.05; **P < 0.01; ***P < 0.001).

artificially truncated N-terminal GSDMC (GSDMC^{NT}), but the upstream signaling of GSDMC still remained unclear. A recent study by Hou et al. supplied one possible explanation for such a research gap. They demonstrated that tumor hypoxia induced PD-L1 nuclear translocation, accompanied by activation of GSDMC expression and pyroptosis induction (39). In addition, GSDMC overexpression might be related to lung cancer progression and poor survival (40). It was also worth mentioning that TP63 was identified as a core target in various cancer diseases. Lin et al. revealed that increased expression of TP63 isoform TAp63 abrogated the invasive abilities of colon cancer cells HT-29 and SW-620 (41). In murine model, TP63 loss led to activation of MAPK-P-STAT3 (Ser727)-MMP15 axis, resulting in metastatic spread of head and neck squamous cell carcinoma (42). A decline in TP63 expression was related to shorter survival times of patients with breast cancer, bladder cancer, and lung cancer (43–45). However, the influence of TP63 on pyroptosis as a single gene was not well understood. Wang et al. identified TP63 as an autophagy-related gene in breast cancer (45). Given that pyroptosis could be controlled by autophagy (33), TP63 might be an indirect factor affecting pyroptosis. In addition, TP63 has two isoforms *i.e.* TAp63 and ΔNp63 (46), making it hard for clarifying its specified role in breast cancer. Breast cancer also contains several molecular

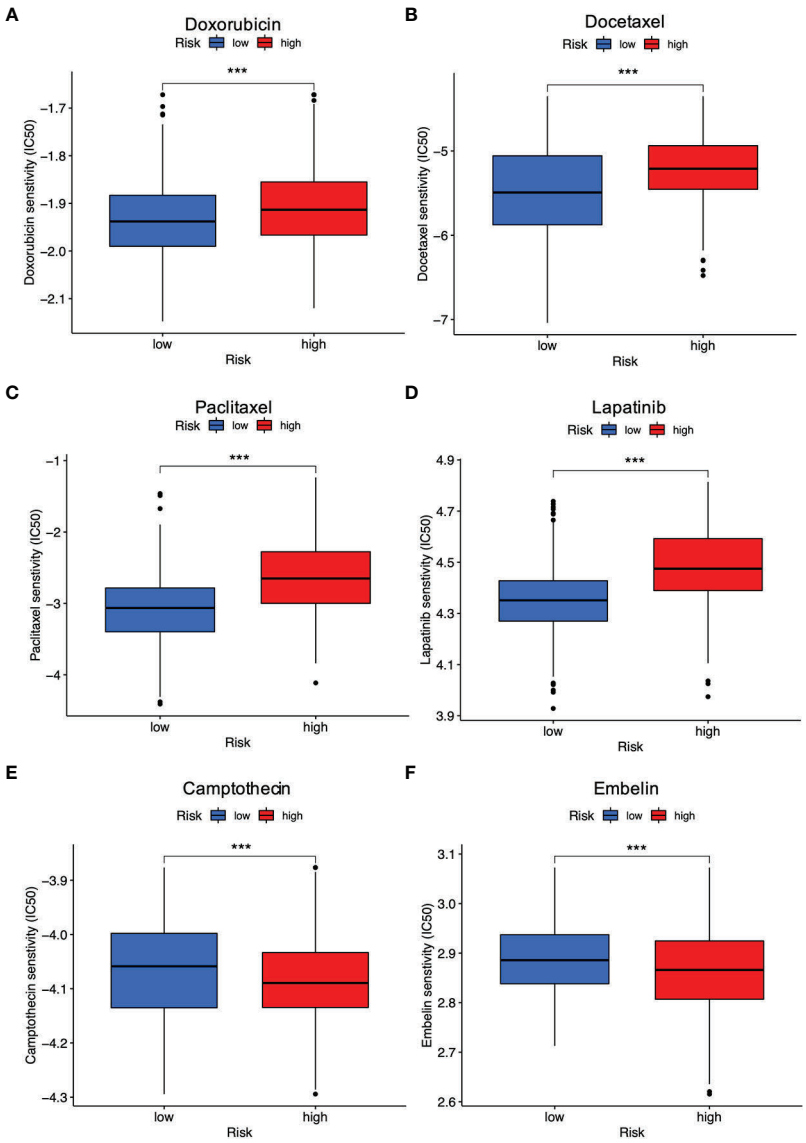

FIGURE 8
Evaluation of drug response between different risk groups. **(A)** Doxorubicin; **(B)** Docetaxel; **(C)** Paclitaxel; **(D)** Lapatinib; **(E)** Camptothecin; **(F)** Embelin (all ***P < 0.001).

subtypes, including HR+/ERBB2−, ERBB2+ as well as triple-negative (2). As such, it is not clear to identify which subtype of TP63 exerts a dominant role based on the present information retrieved from the bioinformatics database, and we will address this frustrating issue in our future study.

Since any single gene was insufficient to be an appropriate marker for pyroptosis, we investigated the 4 aforementioned PRGs as a whole for breast cancer prognostic and immunological evaluation in this study. Several studies also reported similar pyroptosis-related models for breast cancer. The study of Wu et al. retrieved 33 PRGs to evaluate their relation to breast cancer progression (47). On this basis, our investigation expanded the number to 52 PRGs for initiating our model, and 4 out of the 52 PRGs were selected as the appropriate candidates for constructing a pyroptosis-related risk signature. Of note, our study was partly consistent with the findings of Wu et al., revealing the supporting role of IL18 in breast cancer progression (47). In addition, Yu et al. incorporated 15 candidate genes i.e. NLRC4, IRF3, ANO6, GSDMC, TP53, FGF21, IL36B, DHX9, FOXO3, IL36G, IL18, GJA1, MST1, GZMB and GBP1 for the development of a PRG model related to breast cancer (48). Although several of these single hub genes were indirectly related to pyroptosis, their combination was demonstrated to be an accurate predictor of breast cancer survival. Compared to the study of Yu et al., our predictive

signature had fewer genes, which might save costs for the development of a corresponding diagnostic kit in future clinical applications (48). Beyond the above findings, we additionally revealed that TP63 was the common gene to associate pyroptosis with autophagy. The decreased expression of TP63 might have potential relation to hypomethylation, and predicted a poor OS rate for breast cancer patients. Since autophagy contributed to intracellular homeostasis by modulating pyroptosis (33), it is interesting to investigate the role of methylation-induced TP63 reduction in breast cancer and whether the involved mechanisms will be related to autophagic regulation by interfering with pyroptosis in the next study.

Our study further indicated that the obtained signature was highly relevant to immune response based on a combined analysis of GO, KEGG, ssGSEA and CIBERSORT, indicating the profound implication of pyroptosis in tumor immunity. In particular, GO and KEGG analysis revealed the low-risk group was featured by enhancement of T cell function and regulation of cytokine-cytokine receptor interaction. Then, ssGSEA and CIBERSORT methods were to analyze the association between the PRG signature and immune cell infiltration. According to the results of ssGSEA, the low risk led to greater quantities of immune cells, including B cells, T cells, dendritic cells, macrophages and so on. These results were consistent with the findings of CIBERSORT algorithm, showing that the low risk was correlated with subtypes of immune-stimulating cells, such as activated T cells, M1 macrophages, and dendritic cells, as well as B cells. In most cases, these cells might activate the immune system, leading to a positive prognosis of cancer diseases (49). Herein, it was confirmed by our results showing that T cells, M1 macrophages, dendritic cells and B cells were enriched in the low-risk group with a favorable prognosis in breast cancer. Furthermore, blockage of the immune checkpoint has become a trend in immunotherapy for breast cancer. Breast cancer patients have greatly benefited from immune checkpoint inhibitors by targeting PD-1 and PD-L1. A clinical trial revealed that atezolizumab, targeting PD-L1 protein, combined with nab-paclitaxel could be used to treat patients with metastatic triple-negative breast cancer (50). Also, KEYNOTE-012 and KEYNOTE-086 trials indicated that pembrolizumab was a PD-1 targeted immune checkpoint blocker for TNBC (51). In our study, it was shown that the low-risk patients had significantly higher levels of PD-1, PD-L1, PD-L2, CD80, CD86, and CTLA-4 than the high-risk patients, suggesting this low-risk subpopulation of breast cancer patients might benefit more from immune checkpoint blockade therapy. The above data suggested that the established PRG-related signature was tightly related to immune activation and tolerance.

Clinical outcomes and efficacy are hampered by acquired drug resistance in cancer diseases. In this study, it was found that the low-risk breast cancer patients were more sensitive to doxorubicin, docetaxel, paclitaxel, as well as lapatinib, whereas the high-risk populations were more responsive to camptothecin and embelin. Among the above therapeutic agents, doxorubicin, docetaxel and paclitaxel are common chemotherapeutic agents for breast cancer (52). There was evidence showing that paclitaxel could induce pyroptosis by activating Caspase-3/GSDME (53). Lapatinib is one of tyrosine kinase inhibitors targeting epidermal growth factor receptor (EGFR/ErbB1) as well as HER2/ErbB2 specifically for treating HER2+ subtypes of breast cancer (54). Moreover, camptothecin targets the nuclear enzyme topoisomerase I (TOP1) to treat endocrine-resistant breast cancer (55), and embelin is capable of inducing apoptosis in MCF-7 breast cancer cells (56). Individuals with breast cancer responded differently to these therapeutic agents on the basis of our PRG-based signature, and such prediction is aimed to decide which patients would benefit most from certain treatments. In other words, we hope to be capable of predicting novel drugs, identifying new therapeutic targets, and providing individualized treatment to breast cancer patients with such a model in the future.

5 Conclusion

Taken together, our study identified a 4-gene PRG signature tightly associated with survival status and immunological landscape, providing basic guidance for immunotherapy and individualized treatment in breast cancer.

Data availability statement

The datasets presented in this study can be found in online repositories. The names of the repository/repositories and accession number(s) can be found in the article/ Supplementary Material.

Author contributions

YZ and NW designed the study and wrote the first draft. ZW and CP revised the manuscript. YZ and FP conducted the bioinformatic analysis. YZ and XL conducted biological experiments for further validation. XL, XW and BY participated in data interpretation. XT, ZX and LR contributed to data collection and discussion. This manuscript has been approved by all authors for publication.

Funding

This study was supported by the National Natural Science Foundation of China [81973526; 81873306; 82004132]; Guangdong Traditional Chinese Medicine Bureau Project (20211114); the State Key Laboratory of Dampness Syndrome of Chinese Medicine [SZ2021ZZ19]; the 2020 Guangdong Provincial Science and Technology Innovation Strategy Special Fund (Guangdong-Hong Kong-Macau Joint Lab) [2020B1212030006]; the

Science and Technology Planning Project of Guangdong Province [2017B030314166]; Guangdong Science and Technology Department [2021A0505030059]; Guangzhou Science and Technology Project [202102010316]; Open Research Fund of Chengdu University of Traditional Chinese Medicine State Key Laboratory of Characteristic Chinese Medicine Resources in Southwest China [XZYZ-20201224-1945] and Funding for Young Scholars of Guangzhou University of Chinese Medicine [QNYC20190101].

Conflict of interest

The authors declare that the research was conducted in the absence of any commercial or financial relationships that could be construed as a potential conflict of interest.

Publisher's note

All claims expressed in this article are solely those of the authors and do not necessarily represent those of their affiliated organizations, or those of the publisher, the editors and the reviewers. Any product that may be evaluated in this article, or claim that may be made by its manufacturer, is not guaranteed or endorsed by the publisher.

Supplementary material

The Supplementary Material for this article can be found online at: https://www.frontiersin.org/articles/10.3389/fonc.2022.964508/full#supplementary-material

References

1. Sung H, Ferlay J, Siegel RL, Laversanne M, Soerjomataram I, Jemal A, et al. Global cancer statistics 2020: Globocan estimates of incidence and mortality worldwide for 36 cancers in 185 countries. *CA Cancer J Clin* (2021) 71(3):209–49. doi: 10.3322/caac.21660

2. Waks AG, Winer EP. Breast cancer treatment: A review. *JAMA* (2019) 321 (3):288–300. doi: 10.1001/jama.2018.19323

3. Lu J, Steeg PS, Price JE, Krishnamurthy S, Mani SA, Reuben J, et al. Breast cancer metastasis: Challenges and opportunities. *Cancer Res* (2009) 69(12):4951–3. doi: 10.1158/0008-5472.CAN-09-0099

4. Roma-Rodrigues C, Mendes R, Baptista PV, Fernandes AR. Targeting tumor microenvironment for cancer therapy. *Int J Mol Sci* (2019) 20(4):840. doi: 10.3390/ijms20040840

5. Luo J, Lai J. Pyroptosis-related molecular classification and immune microenvironment infiltration in breast cancer: A novel therapeutic target. *J Cell Mol Med* (2022) 26(8):2259–72. doi: 10.1111/jcmm.17247

6. Loveless R, Bloomquist R, Teng Y. Pyroptosis at the forefront of anticancer immunity. *J Exp Clin Cancer Res* (2021) 40(1):264. doi: 10.1186/s13046-021-02065-8

7. Yu P, Zhang X, Liu N, Tang L, Peng C, Chen X. Pyroptosis: Mechanisms and diseases. *Signal Transduct Target Ther* (2021) 6(1):128. doi: 10.1038/s41392-021-00507-5

8. Galon J, Bruni D. Approaches to treat immune hot, altered and cold tumours with combination immunotherapies. *Nat Rev Drug Discovery* (2019) 18(3):197–218. doi: 10.1038/s41573-018-0007-y

9. Gerard CL, Delyon J, Wicky A, Homicsko K, Cuendet MA, Michielin O. Turning tumors from cold to inflamed to improve immunotherapy response. *Cancer Treat Rev* (2021) 101:102227. doi: 10.1016/j.ctrv.2021.102227

10. Zhang Z, Zhang Y, Xia S, Kong Q, Li S, Liu X, et al. Gasdermin e suppresses tumour growth by activating anti-tumour immunity. *Nature* (2020) 579 (7799):415–20. doi: 10.1038/s41586-020-2071-9

11. Tan Y, Sun R, Liu L, Yang D, Xiang Q, Li L, et al. Tumor suppressor Drd2 facilitates M1 macrophages and restricts nf-kappab signaling to trigger pyroptosis in breast cancer. *Theranostics* (2021) 11(11):5214–31. doi: 10.7150/thno.58322

12. Song W, Ren J, Xiang R, Kong C, Fu T. Identification of pyroptosis-related subtypes, the development of a prognosis model, and characterization of tumor microenvironment infiltration in colorectal cancer. *Oncoimmunology* (2021) 10 (1):1987636. doi: 10.1080/2162402X.2021.1987636

13. Chen H, Luo H, Wang J, Li J, Jiang Y. Identification of a pyroptosis-related prognostic signature in breast cancer. *BMC Cancer* (2022) 22(1):429. doi: 10.1186/s12885-022-09526-z

14. Robinson MD, McCarthy DJ, Smyth GK. Edger: A bioconductor package for differential expression analysis of digital gene expression data. *Bioinformatics* (2010) 26(1):139–40. doi: 10.1093/bioinformatics/btp616

15. Maaten LVD. Accelerating t-SNE using tree-based algorithms. *J Mach Learn Res* (2014) 15(1):3221–45. doi: 10.5555/2627435.2697068

16. Auton T. Modelling survival data: Extending the cox model by t. m. therneau; p. m. grambsch. *J R Stat Soc Ser D (The Statistician)* (2001) 50:558–9. doi: 10.2307/2681246

17. Kassambara A, Kosinski M, Biecek P. *Drawing survival curves using 'Ggplot2' [R package survminer version 0.4.8]*. (2020).

18. Blanche P, Dartigues JF, Jacqmin-Gadda H. Estimating and comparing time-dependent areas under receiver operating characteristic curves for censored event times with competing risks. *Stat Med* (2013) 32(30):5381–97. doi: 10.1002/sim.5958

19. Ritchie ME, Phipson B, Wu D, Hu Y, Law CW, Shi W, et al. Limma powers differential expression analyses for rna-sequencing and microarray studies. *Nucleic Acids Res* (2015) 43(7):e47. doi: 10.1093/nar/gkv007

20. Ashburner M, Ball CA, Blake JA, Botstein D, Butler H, Cherry JM, et al. Gene ontology: Tool for the unification of biology. *Gene Ontol Consortium Nat Genet* (2000) 25(1):25–9. doi: 10.1038/75556

21. Gene Ontology C. The gene ontology resource: Enriching a gold mine. *Nucleic Acids Res* (2021) 49(D1):D325–D34. doi: 10.1093/nar/gkaa1113

22. Kanehisa M, Furumichi M, Sato Y, Ishiguro-Watanabe M, Tanabe M. Kegg: Integrating viruses and cellular organisms. *Nucleic Acids Res* (2021) 49(D1):D545–D551. doi: 10.1093/nar/gkaa970

23. Yu G, Wang LG, Han Y, He QY. Clusterprofiler: An r package for comparing biological themes among gene clusters. *OMICS* (2012) 16(5):284–7. doi: 10.1089/omi.2011.0118

24. Ginestet C. Ggplot2: Elegant graphics for data analysis. *J R Stat Society: Ser A (Statistics Society)* (2011) 174(1):245–6. doi: 10.1111/j.1467-985X.2010.00676_9.x

25. Chen H, Boutros PC. Venndiagram: A package for the generation of highly-customizable Venn and Euler diagrams in r. *BMC Bioinf* (2011) 12:35. doi: 10.1186/1471-2105-12-35

26. Hanzelmann S, Castelo R, Guinney J. Gsva: Gene set variation analysis for microarray and rna-seq data. *BMC Bioinf* (2013) 14:7. doi: 10.1186/1471-2105-14-7

27. Yoshihara K, Shahmoradgoli M, Martinez E, Vegesna R, Kim H, Torres-Garcia W, et al. Inferring tumour purity and stromal and immune cell admixture from expression data. *Nat Commun* (2013) 4:2612. doi: 10.1038/ncomms3612

28. Newman AM, Liu CL, Green MR, Gentles AJ, Feng W, Xu Y, et al. Robust enumeration of cell subsets from tissue expression profiles. *Nat Methods* (2015) 12 (5):453–7. doi: 10.1038/nmeth.3337

29. Geeleher P, Cox N, Huang RS. Prrophetic: An r package for prediction of clinical chemotherapeutic response from tumor gene expression levels. *PloS One* (2014) 9(9):e107468. doi: 10.1371/journal.pone.0107468

30. Gao J, Aksoy BA, Dogrusoz U, Dresdner G, Gross B, Sumer SO, et al. Integrative analysis of complex cancer genomics and clinical profiles using the cbioportal. *Sci Signal* (2013) 6(269):pl1. doi: 10.1126/scisignal.2004088

31. Chang CC. Recent translational research: Stem cells as the roots of breast cancer. *Breast Cancer Res* (2006) 8(1):103. doi: 10.1186/bcr1385

32. Ning X, Li R, Zhang B, Wang Y, Zhou Z, Ji Z, et al. Immune score indicator for the survival of melanoma patients based on tumor microenvironment. *Int J Gen Med* (2021) 14:10397–416. doi: 10.2147/IJGM.S336105

33. Guo R, Wang H, Cui N. Autophagy regulation on pyroptosis: Mechanism and medical implication in sepsis. *Mediators Inflammation* (2021) 2021:9925059. doi: 10.1155/2021/9925059

34. Kim MS, Lebron C, Nagpal JK, Chae YK, Chang X, Huang Y, et al. Methylation of the Dfna5 increases risk of lymph node metastasis in human breast cancer. *Biochem Biophys Res Commun* (2008) 370(1):38–43. doi: 10.1016/j.bbrc.2008.03.026

35. Croes L, Beyens M, Fransen E, Ibrahim J, Vanden Berghe W, Suls A, et al. Large-Scale analysis of Dfna5 methylation reveals its potential as biomarker for breast cancer. *Clin Epigenet* (2018) 10:51. doi: 10.1186/s13148-018-0479-y

36. Pizato N, Luzete BC, Kiffer L, Correa LH, de Oliveira Santos I, Assumpcao JAF, et al. Omega-3 docosahexaenoic acid induces pyroptosis cell death in triple-negative breast cancer cells. *Sci Rep* (2018) 8(1):1952. doi: 10.1038/s41598-018-20422-0

37. Yan L, Liu Y, Ma XF, Hou D, Zhang YH, Sun Y, et al. Triclabendazole induces pyroptosis by activating caspase-3 to cleave gsdme in breast cancer cells. *Front Pharmacol* (2021) 12:670081. doi: 10.3389/fphar.2021.670081

38. Yan H, Luo B, Wu X, Guan F, Yu X, Zhao L, et al. Cisplatin induces pyroptosis *Via* activation of Meg3/Nlrp3/Caspase-1/Gsdmd pathway in triple-negative breast cancer. *Int J Biol Sci* (2021) 17(10):2606–21. doi: 10.7150/ijbs.60292

39. Hou J, Zhao R, Xia W, Chang CW, You Y, Hsu JM, et al. Pd-L1-Mediated gasdermin c expression switches apoptosis to pyroptosis in cancer cells and facilitates tumour necrosis. *Nat Cell Biol* (2020) 22(10):1264–75. doi: 10.1038/s41556-020-0575-z

40. Wei J, Xu Z, Chen X, Wang X, Zeng S, Qian L, et al. Overexpression of gsdmc is a prognostic factor for predicting a poor outcome in lung adenocarcinoma. *Mol Med Rep* (2020) 21(1):360–70. doi: 10.3892/mmr.2019.10837

41. Lin CW, Li XR, Zhang Y, Hu G, Guo YH, Zhou JY, et al. Tap63 suppress metastasis *Via* mir-133b in colon cancer cells. *Br J Cancer* (2014) 110(9):2310–20. doi: 10.1038/bjc.2014.118

42. Lakshmanachetty S, Balaiya V, High WA, Koster MI. Loss of Tp63 promotes the metastasis of head and neck squamous cell carcinoma by activating mapk and Stat3 signaling. *Mol Cancer Res* (2019) 17(6):1279–93. doi: 10.1158/1541-7786.MCR-18-1355

43. Bankhead A3rd, McMaster T, Wang Y, Boonstra PS, Palmbos PL. Tp63 isoform expression is linked with distinct clinical outcomes in cancer. *EBioMedicine* (2020) 51:102561. doi: 10.1016/j.ebiom.2019.11.022

44. Ma Y, Fan M, Dai L, Kang X, Liu Y, Sun Y, et al. Expression of P63 and Ck5/6 in early-stage lung squamous cell carcinoma is not only an early diagnostic indicator but also correlates with a good prognosis. *Thorac Cancer* (2015) 6(3):288–95. doi: 10.1111/1759-7714.12181

45. Wang Y, Lu H, Wang Z, Li Y, Chen X. Tgf-Beta1 promotes autophagy and inhibits apoptosis in breast cancer by targeting Tp63. *Front Oncol* (2022) 12:865067. doi: 10.3389/fonc.2022.865067

46. Wu G, Nomoto S, Hoque MO, Dracheva T, Osada M, Lee CC, et al. Deltanp63alpha and Tap63alpha regulate transcription of genes with distinct biological functions in cancer and development. *Cancer Res* (2003) 63(10):2351–7.

47. Wu J, Zhu Y, Luo M, Li L. Comprehensive analysis of pyroptosis-related genes and tumor microenvironment infiltration characterization in breast cancer. *Front Immunol* (2021) 12:748221. doi: 10.3389/fimmu.2021.748221

48. Yu H, Fu Y, Tang Z, Jiang L, Qu C, Li H, et al. A novel pyroptosis-related signature predicts prognosis and response to treatment in breast carcinoma. *Aging (Albany NY)* (2022) 14(2):989–1013. doi: 10.18632/aging.203855

49. Liao D, Liu Z, Wrasidlo WJ, Luo Y, Nguyen G, Chen T, et al. Targeted therapeutic remodeling of the tumor microenvironment improves an her-2 DNA vaccine and prevents recurrence in a murine breast cancer model. *Cancer Res* (2011) 71(17):5688–96. doi: 10.1158/0008-5472.CAN-11-1264

50. Schmid P, Adams S, Rugo HS, Schneeweiss A, Barrios CH, Iwata H, et al. Atezolizumab and nab-paclitaxel in advanced triple-negative breast cancer. *N Engl J Med* (2018) 379(22):2108–21. doi: 10.1056/NEJMoa1809615

51. Isaacs J, Anders C, McArthur H, Force J. Biomarkers of immune checkpoint blockade response in triple-negative breast cancer. *Curr Treat Opt Oncol* (2021) 22(5):38. doi: 10.1007/s11864-021-00833-4

52. Rajappa S, Joshi A, Doval DC, Batra U, Rajendranath R, Deo A, et al. Novel formulations of docetaxel, paclitaxel and doxorubicin in the management of metastatic breast cancer. *Oncol Lett* (2018) 16(3):3757–69. doi: 10.3892/ol.2018.9057

53. Zhang CC, Li CG, Wang YF, Xu LH, He XH, Zeng QZ, et al. Chemotherapeutic paclitaxel and cisplatin differentially induce pyroptosis in A549 lung cancer cells *Via* caspase-3/Gsdme activation. *Apoptosis* (2019) 24(3-4):312–25. doi: 10.1007/s10495-019-01515-1

54. Moreira C, Kaklamani V. Lapatinib and breast cancer: Current indications and outlook for the future. *Expert Rev Anticancer Ther* (2010) 10(8):1171–82. doi: 10.1586/era.10.113

55. Tesauro C, Simonsen AK, Andersen MB, Petersen KW, Kristoffersen EL, Algreen L, et al. Topoisomerase I activity and sensitivity to camptothecin in breast cancer-derived cells: A comparative study. *BMC Cancer* (2019) 19(1):1158. doi: 10.1186/s12885-019-6371-0

56. Li Y, Li D, Yuan S, Wang Z, Tang F, Nie R, et al. Embelin-induced mcf-7 breast cancer cell apoptosis and blockade of mcf-7 cells in the G2/M phase *Via* the mitochondrial pathway. *Oncol Lett* (2013) 5(3):1005–9. doi: 10.3892/ol.2012.1084

Frontiers in Oncology

Advances knowledge of carcinogenesis and tumor progression for better treatment and management

The third most-cited oncology journal, which highlights research in carcinogenesis and tumor progression, bridging the gap between basic research and applications to imrpove diagnosis, therapeutics and management strategies.

Discover the latest Research Topics

See more →



Frontiers

Avenue du Tribunal-Fédéral 34
1005 Lausanne, Switzerland
frontiersin.org

Contact us

+41 (0)21 510 17 00
frontiersin.org/about/contact